

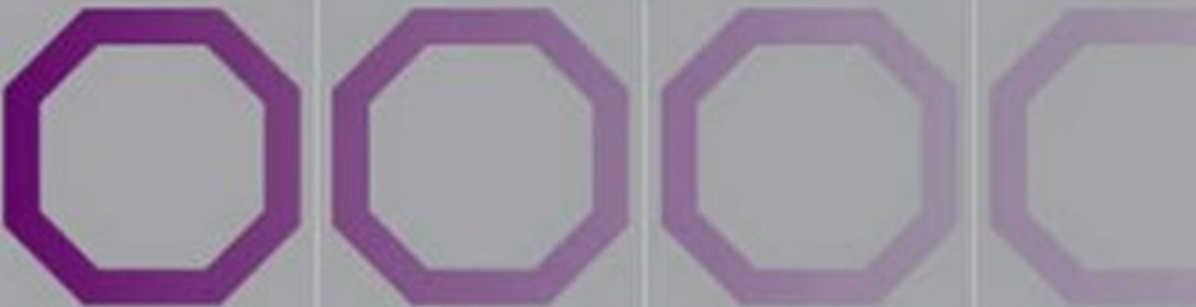


K.A. Gschneidner, Jr.,  
J.-C.G. Bünzli and V.K. Pecharsky  
Editors

HANDBOOK ON THE  
PHYSICS AND CHEMISTRY OF  
**RARE EARTHS**

Volume 38

North-Holland



## PREFACE

**Karl A. Gschneidner Jr., Jean-Claude G. Bünzli,  
Vitalij K. Pecharsky**

---

*These elements perplex us in our rearches [sic], baffle us in our speculations, and haunt us in our very dreams. They stretch like an unknown sea before us – mocking, mystifying, and murmuring strange revelations and possibilities.*

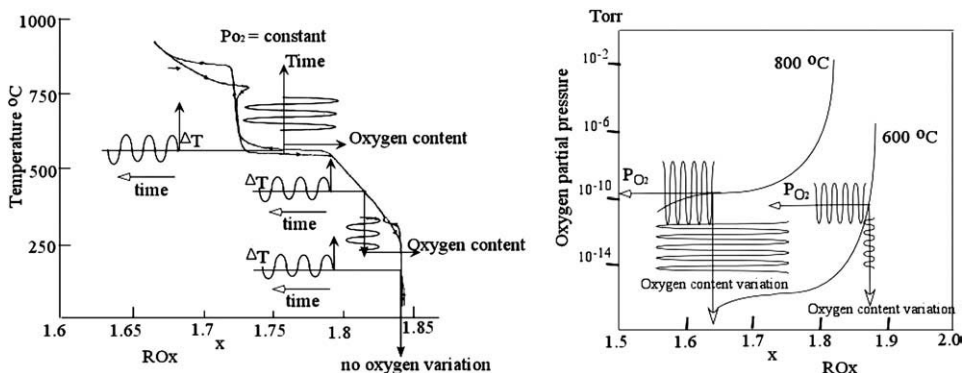
Sir William Crookes (February 16, 1887)

---

The first chapter (236) in this volume of the *Handbook on the Physics and Chemistry of Rare Earth* is a recapitulation of the scientific achievements and contributions made by the late Professor LeRoy Eyring (1919–2005) to the science of the lanthanide oxides in which the lanthanide element has a valence equal to or greater than three. Although LeRoy had a broad range of interests in the chemistry of the rare earths and actinides the main focus of his outstanding scientific career was concerned with the lanthanide higher oxides. This chapter was written by Dr. Zhenchuan Kang his last post doctoral associate. Professor Eyring was a co-editor of the first 32 volumes of the *Handbook*.

The remaining four chapters of volume 38 describe rare earth compounds which have three or more chemical constituents. Chapters 237 through 239 deal with metallic-like systems/compounds, while the last one (240) is concerned with discrete anionic assemblies intermediate in size between a molecule and a bulk solid—the polyoxometalates. Chapter 237, which reviews the rare earth–transition metal–plumbides, is a continuation of reviews on ternary rare earth–transition metal–nontransition elements (such as silicon, germanium, tin and indium) systems and covers phase relationships, crystallography and physical properties. The higher borides, i.e. compounds with boron contents greater than 6 for every metal atom, both binary and ternary systems are examined in chapter 238. The boron atoms form cages in which the rare earth metals reside and a number of unusual phenomena have been discovered in these covalently bonded atomic networks. The magnetic and superconducting behaviors of the quaternary rare earth–nickel–boron–carbon compounds,  $\text{RNi}_2\text{B}_2\text{C}$ , is the main topic covered in chapter 239, with the emphasis being the interplay between co-existing magnetism and superconductivity. The last, chapter 240, covers the structures, photophysical properties, catalytic behaviors and biological applications of the complex rare earth compounds formed with hexavalent molybdenum- or tungsten-containing metalate anions.

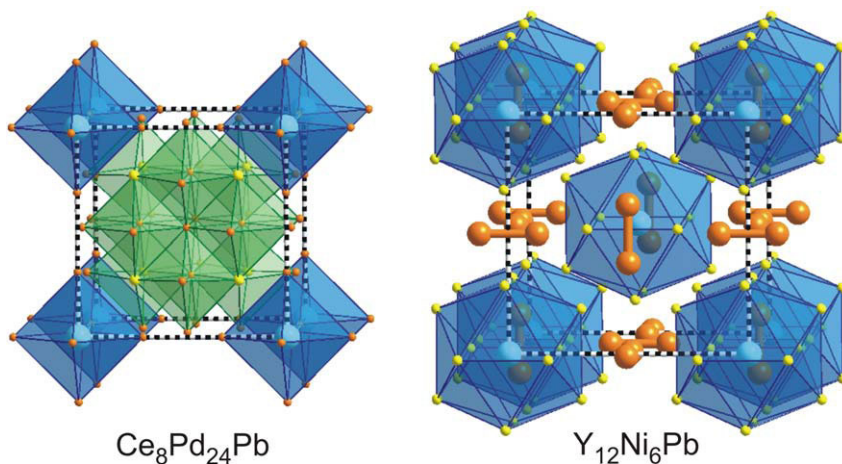
**CHAPTER 236. LANTHANIDE HIGHER OXIDES: THE CONTRIBUTIONS OF LEROY EYRING BY Z.C. KANG RARE EARTH HIGHER OXIDE DEVICES CONSULTING, STOW, MASSACHUSETTS, USA**



The first chapter of volume 38 pays tribute to Prof. LeRoy Eyring for his scientific contributions to the knowledge and understanding of the physical chemistry of the rare earth oxides, especially the higher valence lanthanide oxides,  $CeO_x$ ,  $PrO_x$  and  $TbO_x$ , where  $x \geq 1.5$ . These higher oxides are unique systems in which the oxygen content varies with both oxygen partial pressure and temperature. The range of non-stoichiometry of the higher oxides is tunable from narrow regions to a broad range, up to a maximum range from  $RO_{1.5}$  to  $RO_2$ . The  $RO_2$  fluorite structure is the fundamental basis of these systems, and the metal sublattice does not change until the temperature exceeds 1200 °C. The oxygen anions, however, can be absent as a single anion vacancy or as an oxygen vacancy pair. The Eyring's module theory is discussed in detail. Kang notes that the module theory can be utilized to elucidate the thermodynamic properties, hysteresis, fast anion migration, structures, and the redox reactions of the oxygen deficient fluorite related homologous series of the lanthanide higher oxides. The applications of these oxides are briefly discussed and include: redox catalysis, oxygen sensors, mixed conductors, intermediate temperature solid oxide fuel cells, as well as oxygen and hydrogen production.

**CHAPTER 237. RARE EARTH–TRANSITION METAL–PLUMBIDES BY RAINER PÖTTGEN AND UTE CH. RODEWALD WESTFÄLISCHE WILHELMS-UNIVERSITÄT MÜNSTER, GERMANY**

This chapter is dedicated to ternary intermetallic rare earth–transition metal–lead phases (plumbides). Compared to related compounds with silicon (see Rogl in chapter 51, volume 7), germanium (Salamaha, Sologub and Bodak, chapters 173



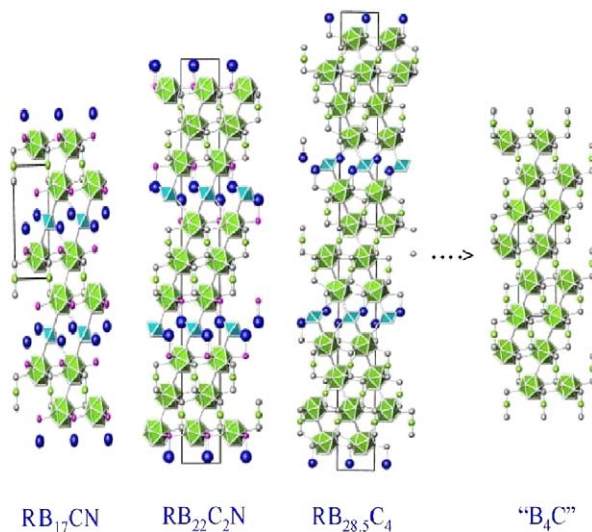
and 174, volume 27), tin (Skolozdra, chapter 164, volume 24), and indium (Kalychak, Zaremba, Pöttgen, Lukachuk and Hoffman, chapter 218, volume 34), much less is known about the intermetallics containing lead. Pöttgen and Rodewald begin by describing the few isothermal sections of ternary phase diagrams, which have been determined to date. Then they consider the crystal chemistry of this family, discussing in detail some 180 compounds crystallizing in about 20 types of crystal structures. A brief description of known chemical and physical properties of ternary plumbides (mostly magnetism and electronic transport) concludes the chapter. To date, the majority of known phases are lead-poor, i.e. they contain no more than 1/3 (atomic fraction) of lead. This may be partially due to high reactivity of rare earth lead-rich phases in air. The story of ternary rare earth plumbides is far from complete, and this class of materials is poised to become a vibrant area of research for the condensed matter community in the near future.

## CHAPTER 238. HIGHER BORIDES

BY TAKAO MORI

NATIONAL INSTITUTE FOR MATERIALS SCIENCE, TSUKUBA, JAPAN

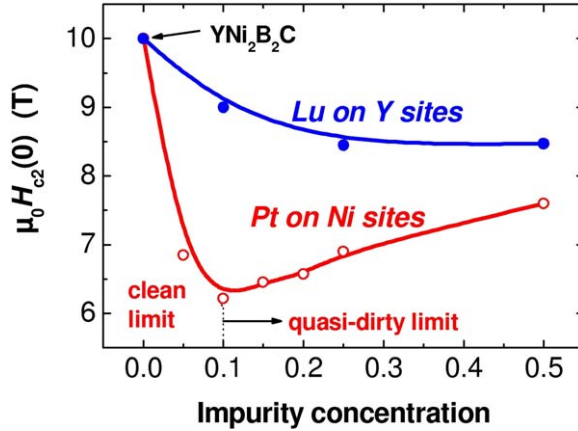
Although boride research has been extensively carried out for over half a century, many of the new higher boride compounds with boron to metal ratios exceeding 6 have been discovered in the past decade and attractive physical properties are starting to emerge. Recent advancements in the chemistry and physics of higher borides are reviewed in this chapter. Boron tends to form two dimensional atomic nets and clusters in compounds. It has one less electron than carbon and thus is electron deficient when forming atomic networks, but this causes it to have a special affinity for the rare earth elements leading to a myriad of compounds. The rare earth atoms supply electrons to stabilize the boron atomic framework and form intriguing novel structures, while the f electrons cause interesting and unusual behaviors. The strong covalent boron cluster framework supplies a light,



robust “armor” which is acid resistant and can withstand high temperatures. Attractive electronic, magnetic, and thermal behaviors can be developed from the “inside” to utilize the protective properties of this network for applications. For example, a new series of homologous rare earth boron cluster compounds have been found to unexpectedly exhibit n-type electrical conductivity. This is an exciting development for high temperature thermoelectric research since such behavior in higher borides has never been realized before without extreme doping, and since boron carbide is a well established p-type material. Recent intriguing findings have revealed that the boron “armor” is not simply docile, but that the boron clusters can mediate magnetic interactions in the solid to cause surprisingly strong and flexible magnetism in what are relatively dilute f-electron insulators. The addition of small amounts of a third element, such as carbon, nitrogen, and silicon, results in the formation of novel and varied rare earth boron cluster structures.

**CHAPTER 239. RARE-EARTH NICKEL BOROCARBIDES**  
**BY K.-H. MÜLLER, M. SCHNEIDER, G. FUCHS, AND S.L. DRECHSLER**  
**LEIBNIZ-INSTITUT FÜR FESTKÖRPER- UND WERKSTOFFFORSCHUNG**  
**DRESDEN, GERMANY**

A striking feature distinguishing the superconducting  $\text{RT}_2\text{B}_2\text{C}$  compounds from other R containing superconductors (i.e., Chevrel phases,  $\text{RRh}_4\text{B}_4$ , and  $\text{RBa}_2\text{Cu}_3\text{O}_{7-\delta}$  systems) known before 1994 is that for certain combinations of R and transition metals, T, superconductivity and antiferromagnetic order coexist in  $\text{RT}_2\text{B}_2\text{C}$  with the Neel temperature  $T_N$  being comparable with the superconducting critical temperature  $T_c$  i.e. the magnetic energy is comparable with the superconducting condensation energy. This chapter sheds new insights into the



interplay of superconductivity and magnetism. In the  $RT_2B_2C$  compounds a rich variety of magnetic structures have been observed due to the combined influence of RKKY-type exchange interaction and strong tetragonal crystalline electric fields. Other special features of these materials include Fermi surface nesting, multi-band superconductivity and a remarkable anisotropy of the superconducting gap. Due to the strong spin-orbit interaction of the 4f electrons, the magnetic order of the R magnetic moments in  $RT_2B_2C$  is often connected with 4f orbital ordering (also called quadrupolar ordering), observed as a tetragonal-to-orthorhombic lattice distortion below  $T_N$ . On the other hand, a square symmetry of single vortices and a square vortex lattice are observed in the non-magnetic and some magnetic  $RNi_2B_2C$  compounds due to the four-fold symmetry of the Fermi velocity. The pseudoquaternary compounds obtained from  $RNi_2B_2C$  by either partially substituting R by some other element R' or Ni by another transition metal represent a large class of materials with a rich variety of properties whose systematic investigation results in better understanding of superconductivity and magnetism and their interplay in the  $RNi_2B_2C$  compounds.

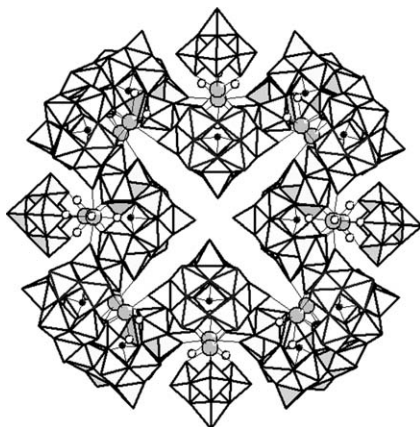
## CHAPTER 240. POLYOXOMETALATES

BY MICHAEL T. POPE

GEORGETOWN UNIVERSITY, WASHINGTON, DC, USA

Polyoxometalates (POMs), also known as heteropolyanions, are metal containing anions consisting of transition metal ions bonded to other ligands, mostly oxygen atoms, and generally, although not exclusively, based upon  $MoO_6$  or  $WO_6$  octahedra. While some POMs are polymeric, others appear as discrete entities.

Polyoxometalate anions, especially those of hexavalent molybdenum and tungsten interact with rare-earth cations to generate a seemingly endless variety of complexes in which the rare earths function as encrypted cations, as core heteroatoms, or as linkers of polyoxometalate fragments to yield discrete anionic assemblies currently incorporating as few as 8 and as many as 164 metal centers,



as well as materials based on infinite 1-, 2-, or 3-dimensional lattices. This review systematically describes the various solid state and solution structures observed for the polyoxometalates of the trivalent and tetravalent rare earths, including hollow structures that contain encapsulated alkali metal cations. The author then briefly evokes the interesting photophysical properties of these materials due to the presence of ligand-to-metal-charge transfer states which efficiently sensitize the luminescence of Ln(III) ions. Applications of the rare earth POMs in chemistry, as oxidation catalysts, and in medicine, as antitumor and anti-HIV agents are illustrated and perspectives for future research directions are presented.

# CONTENTS

<i>Preface</i>	v
<i>Contents</i>	xi
<i>Contents of Volumes 1–37</i>	xiii
<i>Index of Contents of Volumes 1–38</i>	xxiii
<b>236. Lanthanide Higher Oxides: The Contributions of Leroy Eyring</b>	<b>1</b>
Z.C. Kang	
<b>237. Rare Earth–Transition Metal–Plumbides</b>	<b>55</b>
Rainer Pöttgen and Ute Ch. Rodewald	
<b>238. Higher Borides</b>	<b>105</b>
Takao Mori	
<b>239. Rare-Earth Nickel Borocarbides</b>	<b>175</b>
K.-H. Müller, M. Schneider, G. Fuchs and S.-L. Drechsler	
<b>240. Polyoxometalates</b>	<b>337</b>
Michael T. Pope	
<i>Author index</i>	383
<i>Subject index</i>	431

# CONTENTS OF VOLUMES 1–37

## VOLUME 1: Metals

1978, 1st repr. 1982, 2nd repr. 1991; ISBN 0-444-85020-1

1. Z.B. Goldschmidt, *Atomic properties (free atom)* 1
  2. B.J. Beaudry and K.A. Gschneidner Jr, *Preparation and basic properties of the rare earth metals* 173
  3. S.H. Liu, *Electronic structure of rare earth metals* 233
  4. D.C. Koskenmaki and K.A. Gschneidner Jr, *Cerium* 337
  5. L.J. Sundström, *Low temperature heat capacity of the rare earth metals* 379
  6. K.A. McEwen, *Magnetic and transport properties of the rare earths* 411
  7. S.K. Sinha, *Magnetic structures and inelastic neutron scattering: metals, alloys and compounds* 489
  8. T.E. Scott, *Elastic and mechanical properties* 591
  9. A. Jayaraman, *High pressure studies: metals, alloys and compounds* 707
  10. C. Probst and J. Wittig, *Superconductivity: metals, alloys and compounds* 749
  11. M.B. Maple, L.E. DeLong and B.C. Sales, *Kondo effect: alloys and compounds* 797
  12. M.P. Dariel, *Diffusion in rare earth metals* 847
- Subject index 877

## VOLUME 2: Alloys and intermetallics

1979, 1st repr. 1982, 2nd repr. 1991; ISBN 0-444-85021-X

13. A. Iandelli and A. Palenzona, *Crystal chemistry of intermetallic compounds* 1
  14. H.R. Kirchmayr and C.A. Poldy, *Magnetic properties of intermetallic compounds of rare earth metals* 55
  15. A.E. Clark, *Magnetostrictive RFe<sub>2</sub> intermetallic compounds* 231
  16. J.J. Rhyne, *Amorphous magnetic rare earth alloys* 259
  17. P. Fulde, *Crystal fields* 295
  18. R.G. Barnes, *NMR, EPR and Mössbauer effect: metals, alloys and compounds* 387
  19. P. Wachter, *Europium chalcogenides: EuO, EuS, EuSe and EuTe* 507
  20. A. Jayaraman, *Valence changes in compounds* 575
- Subject index 613

## VOLUME 3: Non-metallic compounds – I

1979, 1st repr. 1984; ISBN 0-444-85215-8

21. L.A. Haskin and T.P. Paster, *Geochemistry and mineralogy of the rare earths* 1
  22. J.E. Powell, *Separation chemistry* 81
  23. C.K. Jørgensen, *Theoretical chemistry of rare earths* 111
  24. W.T. Carnall, *The absorption and fluorescence spectra of rare earth ions in solution* 171
  25. L.C. Thompson, *Complexes* 209
  26. G.G. Libowitz and A.J. Maeland, *Hydrides* 299
  27. L. Eyring, *The binary rare earth oxides* 337
  28. D.J.M. Sevan and E. Summerville, *Mixed rare earth oxides* 401
  29. C.P. Khattak and F.F.Y. Wang, *Perovskites and garnets* 525
  30. L.H. Brixner, J.R. Barkley and W. Jeitschko, *Rare earth molybdates (VI)* 609
- Subject index 655

**VOLUME 4: Non-metallic compounds – II**

1979, 1st repr. 1984; ISBN 0-444-85216-6

31. J. Flahaut, *Sulfides, selenides and tellurides* 1
32. J.M. Haschke, *Halides* 89
33. F. Hulliger, *Rare earth pnictides* 153
34. G. Blasse, *Chemistry and physics of R-activated phosphors* 237
35. M.J. Weber, *Rare earth lasers* 275
36. F.K. Fong, *Nonradiative processes of rare-earth ions in crystals* 317
- 37A. J.W. O’Laughlin, *Chemical spectrophotometric and polarographic methods* 341
- 37B. S.R. Taylor, *Trace element analysis of rare earth elements by spark source mass spectroscopy* 359
- 37C. R.J. Conzemius, *Analysis of rare earth matrices by spark source mass spectrometry* 377
- 37D. E.L. DeKalb and V.A. Fassel, *Optical atomic emission and absorption methods* 405
- 37E. A.P. D’Silva and V.A. Fassel, *X-ray excited optical luminescence of the rare earths* 441
- 37F. F.W.V. Boynton, *Neutron activation analysis* 457
- 37G. S. Schuhmann and J.A. Philpotts, *Mass-spectrometric stable-isotope dilution analysis for lanthanides in geochemical materials* 471
38. J. Reuben and G.A. Elgavish, *Shift reagents and NMR of paramagnetic lanthanide complexes* 483
39. J. Reuben, *Bioinorganic chemistry: lanthanides as probes in systems of biological interest* 515
40. T.J. Haley, *Toxicity* 553
- Subject index 587

**VOLUME 5**

1982, 1st repr. 1984; ISBN 0-444-86375-3

41. M. Gasgnier, *Rare earth alloys and compounds as thin films* 1
42. E. Gratz and M.J. Zuckermann, *Transport properties (electrical resistivity, thermoelectric power thermal conductivity) of rare earth intermetallic compounds* 117
43. F.P. Netzer and E. Bertel, *Adsorption and catalysis on rare earth surfaces* 217
44. C. Boulesteix, *Defects and phase transformation near room temperature in rare earth sesquioxides* 321
45. O. Greis and J.M. Haschke, *Rare earth fluorides* 387
46. C.A. Morrison and R.P. Leavitt, *Spectroscopic properties of triply ionized lanthanides in transparent host crystals* 461
- Subject index 693

**VOLUME 6**

1984; ISBN 0-444-86592-6

47. K.H.J. Buschow, *Hydrogen absorption in intermetallic compounds* 1
48. E. Parthé and B. Chabot, *Crystal structures and crystal chemistry of ternary rare earth–transition metal borides, silicides and homologues* 113
49. P. Rogl, *Phase equilibria in ternary and higher order systems with rare earth elements and boron* 335
50. H.B. Kagan and J.L. Namy, *Preparation of divalent ytterbium and samarium derivatives and their use in organic chemistry* 525
- Subject index 567

**VOLUME 7**

1984; ISBN 0-444-86851-8

51. P. Rogl, *Phase equilibria in ternary and higher order systems with rare earth elements and silicon* 1
52. K.H.J. Buschow, *Amorphous alloys* 265
53. H. Schumann and W. Genthe, *Organometallic compounds of the rare earths* 446
- Subject index 573

**VOLUME 8**

1986; ISBN 0-444-86971-9

54. K.A. Gschneidner Jr and F.W. Calderwood, *Intra rare earth binary alloys: phase relationships, lattice parameters and systematics* 1
55. X. Gao, *Polarographic analysis of the rare earths* 163
56. M. Leskelä and L. Niinistö, *Inorganic complex compounds I* 203
57. J.R. Long, *Implications in organic synthesis* 335
- Errata 375
- Subject index 379

**VOLUME 9**

1987; ISBN 0-444-87045-8

58. R. Reisfeld and C.K. Jørgensen, *Excited state phenomena in vitreous materials* 1
59. L. Niinistö and M. Leskelä, *Inorganic complex compounds II* 91
60. J.-C.G. Bünzli, *Complexes with synthetic ionophores* 321
61. Zhiquan Shen and Jun Ouyang, *Rare earth coordination catalysis in stereospecific polymerization* 395
- Errata 429
- Subject index 431

**VOLUME 10: High energy spectroscopy**

1988; ISBN 0-444-87063-6

62. Y. Baer and W.-D. Schneider, *High-energy spectroscopy of lanthanide materials – An overview* 1
63. M. Campagna and F.U. Hillebrecht, *f-electron hybridization and dynamical screening of core holes in intermetallic compounds* 75
64. O. Gunnarsson and K. Schönhammer, *Many-body formulation of spectra of mixed valence systems* 103
65. A.J. Freeman, B.I. Min and M.R. Norman, *Local density supercell theory of photoemission and inverse photoemission spectra* 165
66. D.W. Lynch and J.H. Weaver, *Photoemission of Ce and its compounds* 231
67. S. Hüfner, *Photoemission in chalcogenides* 301
68. J.F. Herbst and J.W. Wilkins, *Calculation of 4f excitation energies in the metals and relevance to mixed valence systems* 321
69. B. Johansson and N. Mårtensson, *Thermodynamic aspects of 4f levels in metals and compounds* 361
70. F.U. Hillebrecht and M. Campagna, *Bremsstrahlung isochromat spectroscopy of alloys and mixed valent compounds* 425
71. J. Röhrler, *X-ray absorption and emission spectra* 453
72. F.P. Netzer and J.A.D. Matthew, *Inelastic electron scattering measurements* 547
- Subject index 601

**VOLUME 11: Two-hundred-year impact of rare earths on science**

1988; ISBN 0-444-87080-6

- H.J. Svec, *Prologue* 1
73. F. Szabadváry, *The history of the discovery and separation of the rare earths* 33
74. B.R. Judd, *Atomic theory and optical spectroscopy* 81
75. C.K. Jørgensen, *Influence of rare earths on chemical understanding and classification* 197
76. J.J. Rhyne, *Highlights from the exotic phenomena of lanthanide magnetism* 293
77. B. Bleaney, *Magnetic resonance spectroscopy and hyperfine interactions* 323
78. K.A. Gschneidner Jr and A.H. Daane, *Physical metallurgy* 409
79. S.R. Taylor and S.M. McLennan, *The significance of the rare earths in geochemistry and cosmochemistry* 485
- Errata 579
- Subject index 581

**VOLUME 12**

1989; ISBN 0-444-87105-5

80. J.S. Abell, *Preparation and crystal growth of rare earth elements and intermetallic compounds* 1  
 81. Z. Fisk and J.P. Remeika, *Growth of single crystals from molten metal fluxes* 53  
 82. E. Burzo and H.R. Kirchmayr, *Physical properties of  $R_2Fe_{14}B$ -based alloys* 71  
 83. A. Szytuła and J. Leciejewicz, *Magnetic properties of ternary intermetallic compounds of the  $RT_2X_2$  type* 133  
 84. H. Maletta and W. Zinn, *Spin glasses* 213  
 85. J. van Zytveld, *Liquid metals and alloys* 357  
 86. M.S. Chandrasekharaiah and K.A. Gingerich, *Thermodynamic properties of gaseous species* 409  
 87. W.M. Yen, *Laser spectroscopy* 433  
 Subject index 479

**VOLUME 13**

1990; ISBN 0-444-88547-1

88. E.I. Gladyshevsky, O.I. Bodak and V.K. Pecharsky, *Phase equilibria and crystal chemistry in ternary rare earth systems with metallic elements* 1  
 89. A.A. Eliseev and G.M. Kuzmichyeva, *Phase equilibrium and crystal chemistry in ternary rare earth systems with chalcogenide elements* 191  
 90. N. Kimizuka, E. Takayama-Muromachi and K. Siratori, *The systems  $R_2O_3$ – $M_2O_3$ – $M'O$*  283  
 91. R.S. Houk, *Elemental analysis by atomic emission and mass spectrometry with inductively coupled plasmas* 385  
 92. P.H. Brown, A.H. Rathjen, R.D. Graham and D.E. Tribe, *Rare earth elements in biological systems* 423  
 Errata 453  
 Subject index 455

**VOLUME 14**

1991; ISBN 0-444-88743-1

93. R. Osborn, S.W. Lovesey, A.D. Taylor and E. Balcar, *Intermultiplet transitions using neutron spectroscopy* 1  
 94. E. Dormann, *NMR in intermetallic compounds* 63  
 95. E. Zirngiebl and G. Güntherodt, *Light scattering in intermetallic compounds* 163  
 96. P. Thalmeier and B. Lüthi, *The electron–phonon interaction in intermetallic compounds* 225  
 97. N. Grewe and F. Steglich, *Heavy fermions* 343  
 Subject index 475

**VOLUME 15**

1991; ISBN 0-444-88966-3

98. J.G. Sereni, *Low-temperature behaviour of cerium compounds* 1  
 99. G.-y. Adachi, N. Imanaka and Zhang Fuzhong, *Rare earth carbides* 61  
 100. A. Simon, Hj. Mattausch, G.J. Miller, W. Bauhofer and R.K. Kremer, *Metal-rich halides* 191  
 101. R.M. Almeida, *Fluoride glasses* 287  
 102. K.L. Nash and J.C. Sullivan, *Kinetics of complexation and redox reactions of the lanthanides in aqueous solutions* 347  
 103. E.N. Rizkalla and G.R. Choppin, *Hydration and hydrolysis of lanthanides* 393  
 104. L.M. Vallarino, *Macrocyclic complexes of the lanthanide(III) yttrium(III) and dioxouranium(VI) ions from metal-templated syntheses* 443  
 Errata 513  
 Subject index 515

**MASTER INDEX, Vols. 1–15**

1993; ISBN 0-444-89965-0

**VOLUME 16**

1993; ISBN 0-444-89782-8

105. M. Loewenhaupt and K.H. Fischer, *Valence-fluctuation and heavy-fermion 4f systems* 1  
 106. I.A. Smirnov and V.S. Oskotski, *Thermal conductivity of rare earth compounds* 107  
 107. M.A. Subramanian and A.W. Sleight, *Rare earths pyrochlores* 225  
 108. R. Miyawaki and I. Nakai, *Crystal structures of rare earth minerals* 249  
 109. D.R. Chopra, *Appearance potential spectroscopy of lanthanides and their intermetallics* 519  
 Author index 547  
 Subject index 579

**VOLUME 17: Lanthanides/Actinides: Physics – I**

1993; ISBN 0-444-81502-3

110. M.R. Norman and D.D. Koelling, *Electronic structure, Fermi surfaces, and superconductivity in f electron metals* 1  
 111. S.H. Liu, *Phenomenological approach to heavy-fermion systems* 87  
 112. B. Johansson and M.S.S. Brooks, *Theory of cohesion in rare earths and actinides* 149  
 113. U. Benedict and W.B. Holzapfel, *High-pressure studies – Structural aspects* 245  
 114. O. Vogt and K. Mattenberger, *Magnetic measurements on rare earth and actinide monopycnitides and monochalcogenides* 301  
 115. J.M. Fournier and E. Gratz, *Transport properties of rare earth and actinide intermetallics* 409  
 116. W. Potzel, G.M. Kalvius and J. Gal, *Mössbauer studies on electronic structure of intermetallic compounds* 539  
 117. G.H. Lander, *Neutron elastic scattering from actinides and anomalous lanthanides* 635  
 Author index 711  
 Subject index 753

**VOLUME 18: Lanthanides/Actinides: Chemistry**

1994; ISBN 0-444-81724-7

118. G.T. Seaborg, *Origin of the actinide concept* 1  
 119. K. Balasubramanian, *Relativistic effects and electronic structure of lanthanide and actinide molecules* 29  
 120. J.V. Beitz, *Similarities and differences in trivalent lanthanide- and actinide-ion solution absorption spectra and luminescence studies* 159  
 121. K.L. Nash, *Separation chemistry for lanthanides and trivalent actinides* 197  
 122. L.R. Morss, *Comparative thermochemical and oxidation – reduction properties of lanthanides and actinides* 239  
 123. J.W. Ward and J.M. Haschke, *Comparison of 4f and 5f element hydride properties* 293  
 124. H.A. Eick, *Lanthanide and actinide halides* 365  
 125. R.G. Haire and L. Eyring, *Comparisons of the binary oxides* 413  
 126. S.A. Kinkad, K.D. Abney and T.A. O'Donnell, *f-element speciation in strongly acidic media: lanthanide and mid-actinide metals, oxides, fluorides and oxide fluorides in superacids* 507  
 127. E.N. Rizkalla and G.R. Choppin, *Lanthanides and actinides hydration and hydrolysis* 529  
 128. G.R. Choppin and E.N. Rizkalla, *Solution chemistry of actinides and lanthanides* 559  
 129. J.R. Duffield, D.M. Taylor and D.R. Williams, *The biochemistry of the f-elements* 591  
 Author index 623  
 Subject index 659

**VOLUME 19: Lanthanides/Actinides: Physics – II**

1994; ISBN 0-444-82015-9

130. E. Holland-Moritz and G.H. Lander, *Neutron inelastic scattering from actinides and anomalous lanthanides* 1
131. G. Aeppli and C. Broholm, *Magnetic correlations in heavy-fermion systems: neutron scattering from single crystals* 123
132. P. Wachter, *Intermediate valence and heavy fermions* 177
133. J.D. Thompson and J.M. Lawrence, *High pressure studies – Physical properties of anomalous Ce, Yb and U compounds* 383
134. C. Colinet and A. Pasturel, *Thermodynamic properties of metallic systems* 479
- Author index 649
- Subject index 693

**VOLUME 20**

1995; ISBN 0-444-82014-0

135. Y. Onuki and A. Hasegawa, *Fermi surfaces of intermetallic compounds* 1
136. M. Gasgnier, *The intricate world of rare earth thin films: metals, alloys, intermetallics, chemical compounds, ...* 105
137. P. Vajda, *Hydrogen in rare-earth metals, including  $RH_{2+x}$  phases* 207
138. D. Gignoux and D. Schmitt, *Magnetic properties of intermetallic compounds* 293
- Author index 425
- Subject index 457

**VOLUME 21**

1995; ISBN 0-444-82178-3

139. R.G. Bautista, *Separation chemistry* 1
140. B.W. Hinton, *Corrosion prevention and control* 29
141. N.E. Ryan, *High-temperature corrosion protection* 93
142. T. Sakai, M. Matsuoka and C. Iwakura, *Rare earth intermetallics for metal–hydrogen batteries* 133
143. G.-y. Adachi and N. Imanaka, *Chemical sensors* 179
144. D. Garcia and M. Faucher, *Crystal field in non-metallic (rare earth) compounds* 263
145. J.-C.G. Bünzli and A. Milicic-Tang, *Solvation and anion interaction in organic solvents* 305
146. V. Bhagavathy, T. Prasada Rao and A.D. Damodaran, *Trace determination of lanthanides in high-purity rare-earth oxides* 367
- Author index 385
- Subject index 411

**VOLUME 22**

1996; ISBN 0-444-82288-7

147. C.P. Flynn and M.B. Salamon, *Synthesis and properties of single-crystal nanostructures* 1
148. Z.S. Shan and D.J. Sellmyer, *Nanoscale rare earth–transition metal multilayers: magnetic structure and properties* 81
149. W. Suski, *The  $ThMn_{12}$ -type compounds of rare earths and actinides: structure, magnetic and related properties* 143
150. L.K. Aminov, B.Z. Malkin and M.A. Teplov, *Magnetic properties of nonmetallic lanthanide compounds* 295
151. F. Auzel, *Coherent emission in rare-earth materials* 507
152. M. Dolg and H. Stoll, *Electronic structure calculations for molecules containing lanthanide atoms* 607
- Author index 731
- Subject index 777

**VOLUME 23**

1996; ISBN 0-444-82507-X

153. J.H. Forsberg, *NMR studies of paramagnetic lanthanide complexes and shift reagents* 1  
154. N. Sabbatini, M. Guardigli and I. Manet, *Antenna effect in encapsulation complexes of lanthanide ions* 69  
155. C. Görller-Walrand and K. Binnemans, *Rationalization of crystal-field parameterization* 121  
156. Yu. Kuz'ma and S. Chykhrij, *Phosphides* 285  
157. S. Boghosian and G.N. Papatheodorou, *Halide vapors and vapor complexes* 435  
158. R.H. Byrne and E.R. Sholkovitz, *Marine chemistry and geochemistry of the lanthanides* 497  
Author index 595  
Subject index 631

**VOLUME 24**

1997; ISBN 0-444-82607-6

159. P.A. Dowben, D.N. McIlroy and Dongqi Li, *Surface magnetism of the lanthanides* 1  
160. P.G. McCormick, *Mechanical alloying and mechanically induced chemical reactions* 47  
161. A. Inoue, *Amorphous, quasicrystalline and nanocrystalline alloys in Al- and Mg-based systems* 83  
162. B. Elschner and A. Loidl, *Electron-spin resonance on localized magnetic moments in metals* 221  
163. N.H. Duc, *Intersublattice exchange coupling in the lanthanide–transition metal intermetallics* 339  
164. R.V. Skolozdra, *Stannides of rare-earth and transition metals* 399  
Author index 519  
Subject index 559

**VOLUME 25**

1998; ISBN 0-444-82871-0

165. H. Nagai, *Rare earths in steels* 1  
166. R. Marchand, *Ternary and higher order nitride materials* 51  
167. C. Görller-Walrand and K. Binnemans, *Spectral intensities of f–f transitions* 101  
168. G. Bombieri and G. Paolucci, *Organometallic  $\pi$  complexes of the f-elements* 265  
Author index 415  
Subject index 459

**VOLUME 26**

1999; ISBN 0-444-50815-1

169. D.F. McMorro, D. Gibbs and J. Bohr, *X-ray scattering studies of lanthanide magnetism* 1  
170. A.M. Tishin, Yu.I. Spichkin and J. Bohr, *Static and dynamic stresses* 87  
171. N.H. Duc and T. Goto, *Itinerant electron metamagnetism of Co sublattice in the lanthanide–cobalt intermetallics* 177  
172. A.J. Arko, P.S. Riseborough, A.B. Andrews, J.J. Joyce, A.N. Tahvildar-Zadeh and M. Jarrell, *Photoelectron spectroscopy in heavy fermion systems: Emphasis on single crystals* 265  
Author index 383  
Subject index 405

**VOLUME 27**

1999; ISBN 0-444-50342-0

173. P.S. Salamakha, O.L. Sologub and O.I. Bodak, *Ternary rare-earth–germanium systems* 1  
174. P.S. Salamakha, *Crystal structures and crystal chemistry of ternary rare-earth germanides* 225  
175. B. Ya. Kotur and E. Gratz, *Scandium alloy systems and intermetallics* 339  
Author index 535  
Subject index 553

**VOLUME 28**

2000; ISBN 0-444-50346-3

176. J.-P. Connerade and R.C. Karnatak, *Electronic excitation in atomic species* 1  
 177. G. Meyer and M.S. Wickleder, *Simple and complex halides* 53  
 178. R.V. Kumar and H. Iwahara, *Solid electrolytes* 131  
 179. A. Halperin, *Activated thermoluminescence (TL) dosimeters and related radiation detectors* 187  
 180. K.L. Nash and M.P. Jensen, *Analytical separations of the lanthanides: basic chemistry and methods* 311  
 Author index 373  
 Subject index 401

**VOLUME 29: The role of rare earths in catalysis**

2000; ISBN 0-444-50472-9

- P. Maestro, *Foreword* 1  
 181. V. Paul-Boncour, L. Hilaire and A. Percheron-Guégan, *The metals and alloys in catalysis* 5  
 182. H. Imamura, *The metals and alloys (prepared utilizing liquid ammonia solutions) in catalysis II* 45  
 183. M.A. Ulla and E.A. Lombardo, *The mixed oxides* 75  
 184. J. Kašpar, M. Graziani and P. Fornasiero, *Ceria-containing three-way catalysts* 159  
 185. A. Corma and J.M. López Nieto, *The use of rare-earth-containing zeolite catalysts* 269  
 186. S. Kobayashi, *Triflates* 315  
 Author index 377  
 Subject index 409

**VOLUME 30: High-Temperature Superconductors – I**

2000; ISBN 0-444-50528-8

187. M.B. Maple, *High-temperature superconductivity in layered cuprates: overview* 1  
 188. B. Raveau, C. Michel and M. Hervieu, *Crystal chemistry of superconducting rare-earth cuprates* 31  
 189. Y. Shiohara and E.A. Goodilin, *Single-crystal growth for science and technology* 67  
 190. P. Karen and A. Kjekshus, *Phase diagrams and thermodynamic properties* 229  
 191. B. Elschnner and A. Loidl, *Electron paramagnetic resonance in cuprate superconductors and in parent compounds* 375  
 192. A.A. Manuel, *Positron annihilation in high-temperature superconductors* 417  
 193. W.E. Pickett and I.I. Mazin, *RBa<sub>2</sub>Cu<sub>3</sub>O<sub>7</sub> compounds: electronic theory and physical properties* 453  
 194. U. Staub and L. Soderholm, *Electronic 4f state splittings in cuprates* 491  
 Author index 547  
 Subject index 621

**VOLUME 31: High-Temperature Superconductors – II**

2001; ISBN 0-444-50719-1

195. E. Kaldis, *Oxygen nonstoichiometry and lattice effects in YBa<sub>2</sub>Cu<sub>3</sub>O<sub>x</sub>. Phase transitions, structural distortions and phase separation* 1  
 196. H.W. Weber, *Flux pinning* 187  
 197. C.C. Almasan and M.B. Maple, *Magnetoresistance and Hall effect* 251  
 198. T.E. Mason, *Neutron scattering studies of spin fluctuations in high-temperature superconductors* 281  
 199. J.W. Lynn and S. Skanthakumar, *Neutron scattering studies of lanthanide magnetic ordering* 315  
 200. P.M. Allenspach and M.B. Maple, *Heat capacity* 351  
 201. M. Schabel and Z.-X. Shen, *Angle-resolved photoemission studies of untwinned yttrium barium copper oxide* 391  
 202. D.N. Basov and T. Timusk, *Infrared properties of high-T<sub>c</sub> superconductors: an experimental overview* 437

203. S.L. Cooper, *Electronic and magnetic Raman scattering studies of the high- $T_c$  cuprates* 509  
 204. H. Sugawara, T. Hasegawa and K. Kitazawa, *Characterization of cuprate superconductors using tunneling spectra and scanning tunneling microscopy* 563  
 Author index 609  
 Subject index 677

**VOLUME 32**

2001; ISBN 0-444-50762-0

205. N.H. Duc, *Giant magnetostriction in lanthanide–transition metal thin films* 1  
 206. G.M. Kalvius, D.R. Noakes and O. Hartmann,  *$\mu$ SR studies of rare-earth and actinide magnetic materials* 55  
 207. Rainer Pöttgen, Dirk Johrendt and Dirk Kußmann, *Structure–property relations of ternary equiatomic YbTX intermetallics* 453  
 208. Kurima Kobayashi and Satoshi Hirose, *Permanent magnets* 515  
 209. I.G. Vasilyeva, *Polysulfides* 567  
 210. Dennis K.P. Ng, Jianzhuang Jiang, Kuninobu Kasuga and Kenichi Machida, *Half-sandwich tetrapyrrole complexes of rare earths and actinides* 611  
 Author index 655  
 Subject index 733

**VOLUME 33**

2003; ISBN 0-444-51323-X

211. Brian C. Sales, *Filled skutterudites* 1  
 212. Oksana L. Sologub and Petro S. Salamakha, *Rare earth – antimony systems* 35  
 213. R.J.M. Konings and A. Kovács, *Thermodynamic properties of the lanthanide(III) halides* 147  
 214. John B. Goodenough, *Rare earth – manganese perovskites* 249  
 215. Claude Piguet and Carlos F.G.C. Geraldes, *Paramagnetic NMR lanthanide induced shifts for extracting solution structures* 353  
 216. Isabelle Billard, *Lanthanide and actinide solution chemistry as studied by time-resolved emission spectroscopy* 465  
 217. Thomas Tröster, *Optical studies of non-metallic compounds under pressure* 515  
 Author index 591  
 Subject index 637

**VOLUME 34**

2004; ISBN 0-444-51587-9

218. Yaroslav M. Kalychak, Vasyl' I. Zaremba, Rainer Pöttgen, Mar' yana Lukachuk and Rolf-Dieter Hoffman, *Rare earth–transition metal–indides* 1  
 219. P. Thalmeier and G. Zwicknagl, *Unconventional superconductivity and magnetism in lanthanide and actinide intermetallic compounds* 135  
 220. James P. Riehl and Gilles Muller, *Circularly polarized luminescence spectroscopy from lanthanide systems* 289  
 221. Oliver Guillou and Carole Daguebonne, *Lanthanide-containing coordination polymers* 359  
 222. Makoto Komiyama, *Cutting DNA and RNA* 405  
 Author index 455  
 Subject index 493

**VOLUME 35**

2006; ISBN 0-444-52028-7

223. Natsuko Sakai, Katsuhiko Yamaji, Teruhisa Horita, Yue Ping Xiong and Harumi Yokokawa, *Rare-earth materials for Solid Oxide Fuel Cells (SOFC)* 1

224. Mathias S. Wickleder, *Oxo-selenates of rare earth elements* 45  
 225. Koen Binnemans, *Rare-earth beta-diketonates* 107  
 226. Satoshi Shinoda, Hiroyuki Miyake and Hiroshi Tsukube, *Molecular recognition and sensing via rare earth complexes* 273  
 Author index 337  
 Subject index 377

**VOLUME 36**

2006; ISBN 0-444-52142-9

227. Arthur Mar, *Bismuthides* 1  
 228. I. Aruna, L.K. Malhotra and B.R. Mehta, *Switchable metal hydride films* 83  
 229. Koen Binnemans, *Applications of tetravalent cerium compounds* 281  
 230. Robert A. Flowers II and Edamana Prasad, *Samarium (II) based reductants* 393  
 Author index 475  
 Subject index 511

**VOLUME 37: Optical Spectroscopy**

2007; ISBN 978-0-444-52144-6

231. Kazuyoshi Ogasawara, Shinta Watanabe, Hiroaki Toyoshima and Mikhail G. Brik, *First-principles calculations of  $4f^n \rightarrow 4f^{n-1}5d$  transition spectra* 1  
 232. Gary W. Burdick and Michael F. Reid,  *$4f^n-4f^{n-1}5d$  transitions* 61  
 233. Guokui Liu and Xueyuan Chen, *Spectroscopic properties of lanthanides in nanomaterials* 99  
 234. Takuya Nishioka, Kôichi Fukui and Kazuko Matsumoto, *Lanthanide chelates as luminescent labels in biomedical analyses* 171  
 235. Steve Comby and Jean-Claude G. Bünzli, *Lanthanide near-infrared luminescence in molecular probes and devices* 217  
 Author index 471  
 Subject index 503

## INDEX OF CONTENTS OF VOLUMES 1–38

- 4f excitation energies, calculations of **10**, ch. 68, p. 321
- 4f levels, thermodynamic aspects **10**, ch. 69, p. 361
- 4f state splittings in cuprates **30**, ch. 194, p. 491
- $4f^n-4f^{n-1}5d$  transitions **37**, ch. 231, p. 1; **37**, ch. 232, p. 61
  
- ab-initio calculation of energy levels **37**, ch. 231, p. 1
- absorption spectra of ions in solution **3**, ch. 24, p. 171; **18**, ch. 120, p. 150
- actinide concept, origin of **18**, ch. 118, p. 1
- activated phosphors **4**, ch. 34, p. 237
- activated thermoluminescence **28**, ch. 179, p. 187
- amorphous alloys **7**, ch. 52, p. 265
  - Al- and Mg-based **24**, ch. 161, p. 83
  - magnetic **2**, ch. 16, p. 259
- anion interaction in organic solvents **21**, ch. 145, p. 305
- antimony alloy systems **33**, ch. 212, p. 35
- atomic properties (free atom) **1**, ch. 1, p. 1
- atomic theory **11**, ch. 74, p. 81
  
- Belousov-Zhabotinsky reactions **36**, ch. 229, p. 281
- beta-diketonates **35**, ch. 225, p. 107
- biochemistry **18**, ch. 129, p. 591
- bioinorganic chemistry **4**, ch. 39, p. 515
- biological systems **13**, ch. 92, p. 423
- bismuth alloy systems **36**, ch. 227, p. 1
- borides **6**, ch. 48, p. 113; **6**, ch. 49, p. 335; **38**, ch. 238, p. 105; **38**, ch. 239, p. 175
  
- carbides **15**, ch. 99, p. 61; **38** ch. 239, p. 175
- Carnall, William T. **37**, dedication, p. xiii
- catalysis **29**, foreword, p. 1
  - ceria-containing three-way **29**, ch. 184, p. 159
  - metals and alloys **29**, ch. 181, p. 5
  - metals and alloys in liquid ammonia solutions **29**, ch. 182, p. 45
  - mixed oxides **29**, ch. 183, p. 75
  - zeolites **29**, ch. 185, p. 269
- cerimetry **36**, ch. 229, p. 281
- cerium **1**, ch. 4, p. 337
- cerium compounds
  - low-temperature behavior **15**, ch. 98, p. 1
  - tetravalent **36**, ch. 229, p. 281
- cerium(IV)
  - catalysts **36**, ch. 229, p. 281
  - mediated reactions **36**, ch. 229, p. 281
  - redox properties **36**, ch. 229, p. 281
- chalcogenides, magnetic measurements on mono- **17**, ch. 114, p. 301
- chemical analysis by
  - atomic emission with inductively coupled plasmas **13**, ch. 91, p. 385
  - mass spectrometry, *see* spectroscopy, mass
  - neutron activation **4**, ch. 37E, p. 457
  - optical absorption **4**, ch. 37D, p. 405
  - optical atomic emission **4**, ch. 37D, p. 405
  - polarography **4**, ch. 37A, p. 341; **8**, ch. 55, p. 163
  - spectrophotometry **4**, ch. 37A, p. 341
  - trace determination in high-purity oxides **21**, ch. 146, p. 367
  - X-ray excited optical luminescence **4**, ch. 37E, p. 441
- chemical sensors **21**, ch. 143, p. 179
- chemical understanding and classification **11**, ch. 75, p. 197
- chirality sensing **35**, ch. 226, p. 273
- coherent emission **22**, ch. 151, p. 507
- cohesion, theory of **17**, ch. 112, p. 149
- complexes **3**, ch. 25, p. 209
  - antenna effect **23**, ch. 154, p. 69
  - beta-diketonates **35**, ch. 225, p. 107
  - half-sandwich tetrapyrrole **32**, ch. 210, p. 611
  - inorganic **8**, ch. 56, p. 203; **9**, ch. 59, p. 91
  - macrocycles **15**, ch. 104, p. 443
  - molecular recognition in **35**, ch. 226, p. 273
  - organometallic  $\pi$  type **25**, ch. 168, p. 265
  - polyoxometalates **38**, ch. 240, p. 337
  - sensing in **35**, ch. 226, p. 273

- with synthetic ionophores 9, ch. 60, p. 321
- coordination catalysis in stereospecific polymerization 9, ch. 61, p. 395
- coordination in organic solvents 21, ch. 145, p. 305
- coordination polymers 34, ch. 221, p. 359
- corrosion prevention and control 21, ch. 140, p. 29
- corrosion protection 21, ch. 141, p. 93
- cosmochemistry 11, ch. 79, p. 485
- crystal chemistry
  - of higher borides 38, ch. 238, p. 105
  - of intermetallic compounds 2, ch. 13, p. 1
  - of ternary germanides 27, ch. 174, p. 225
  - of ternary systems with chalcogenides 13, ch. 89, p. 191
  - of ternary systems with metallic elements 13, ch. 88, p. 1
  - of ternary transition metal borides 6, ch. 48, p. 113
  - of ternary transition metal plumbides 38, ch. 237, p. 55
  - of ternary transition metal silicides 6, ch. 48, p. 113
  - of ThMn<sub>12</sub>-type compounds 22, ch. 149, p. 143
- crystal field 2, ch. 17, p. 295
  - in non-metallic compounds 21, ch. 144, p. 263
  - parametrization, rationalization of 23, ch. 155, p. 121
- crystal structures, *see* crystal chemistry
- cuprates
  - 4f state splittings 30, ch. 194, p. 491
  - crystal chemistry 30, ch. 188, p. 31
  - electron paramagnetic resonance (EPR) 30, ch. 191, p. 375
  - electronic theory 30, ch. 193, p. 453
  - flux pinning 31, ch. 196, p. 187
  - Hall effect 31, ch. 197, p. 251
  - heat capacity 31, ch. 200, p. 351
  - infrared properties 31, ch. 202, p. 437
  - magnetoresistance 31, ch. 197, p. 251
  - neutron scattering
    - magnetic ordering 31, ch. 199, p. 315
    - spin fluctuations 31, ch. 198, p. 281
  - overview 30, ch. 187, p. 1
  - oxygen nonstoichiometry and lattice effect 31, ch. 195, p. 1
  - phase equilibria 30, ch. 190, p. 229
  - phase transitions, structural distortions and phase separation 31, ch. 195, p. 1
  - photoemission, angle-resolved studies 31, ch. 201, p. 391
  - physical properties 30, ch. 193, p. 453
  - positron annihilation 30, ch. 192, p. 417
  - Raman scattering 31, ch. 203, p. 509
  - scanning tunneling microscopy 31, ch. 204, p. 563
  - single crystals, growth of 30, ch. 189, p. 67
  - superconductivity 30; 31
  - thermochemical properties 30, ch. 190, p. 229
  - tunneling spectra 31, ch. 204, p. 563
- dedications
  - F.H. Spedding 11, p. 1
  - Friedrich Hund 14, p. ix
  - LeRoy Eyring 36, p. xi
  - William T. Carnall 37, p. xiii
- diffusion in metals 1, ch. 12, p. 847
- diketonates, *see* beta-diketonates
- divalent samarium in organic chemistry 6, ch. 50, p. 525; 36, ch. 230, p. 393
- divalent ytterbium derivatives in organic chemistry 6, ch. 50, p. 525
- DNA, cutting of 34, ch. 222, p. 405
- dynamical screening of core holes in intermetallic compounds 10, ch. 63, p. 75
- elastic and mechanical properties of metals 1, ch. 8, p. 591
- electron paramagnetic resonance (EPR) 2, ch. 18, p. 387; 24, ch. 162, p. 221
  - in cuprate superconductors 30, ch. 191, p. 375
- electronic excitation in atomic species 28, ch. 176, p. 1
- electronic structure
  - calculations for molecules 22, ch. 152, p. 607
  - of metals 1, ch. 3, p. 233; 17, ch. 110, p. 1
- electronic theory of cuprates 30, ch. 193, p. 453
- electron-phonon interaction in intermetallic compounds 14, ch. 96, p. 225
- electron-spin resonance, *see* electron paramagnetic resonance
- emission spectra 10, ch. 71, p. 453
- europium chalcogenides 2, ch. 19, p. 507
- exchange coupling in transition metal intermetallics 24, ch. 163, p. 339
- excited state phenomena in vitreous materials 9, ch. 58, p. 1
- Eyring, L.
  - dedication 36, p. xi
  - contributions of, higher oxides 38, ch. 236, p. 1

- f-electron hybridization in intermetallic compounds 10, ch. 63, p. 75
- f-element speciation in strongly acidic media (superacids) 18, ch. 126, p. 507
- f–f transitions, spectral intensities 25, ch. 167, p. 101
- Fermi surfaces
  - of intermetallic compounds 20, ch. 135, p. 1
  - of metals 17, ch. 110, p. 1
- fluorescence spectra of ions in solution 3, ch. 24, p. 171
- fluoride glasses 15, ch. 101, p. 287
- fluorides 5, ch. 45, p. 387
- flux pinning in cuprates 31, ch. 196, p. 187
- garnets 3, ch. 29, p. 525
- geochemistry 3, ch. 21, p. 1; 11, ch. 79, p. 485; 23, ch. 158, p. 497
- germanium, ternary systems 27, ch. 173, p. 1
- halides 4, ch. 32, p. 89; 18, ch. 124, p. 365
  - metal-rich 15, ch. 100, p. 191
  - simple and complex 28, ch. 177, p. 53
  - thermodynamic properties 33, ch. 213, p. 147
  - vapors and vapor complexes 23, ch. 157, p. 435
- Hall effect in cuprates 31, ch. 197, p. 251
- heat capacity
  - of cuprates 31, ch. 200, p. 351
  - of metals 1, ch. 5, p. 379
- heavy fermions 14, ch. 97, p. 343; 16, ch. 105, p. 1; 19, ch. 132, p. 177
  - phenomenological approach 17, ch. 111, p. 87
  - photoelectron spectroscopy 26, ch. 172, p. 265
- high pressure studies 1, ch. 9, p. 707
  - anomalous Ce, Yb and U compounds 19, ch. 133, p. 383
  - optical studies of non-metallic compounds 33, ch. 217, p. 515
  - structural aspects 17, ch. 113, p. 245
- high temperature superconductors 30; 31
- history of the discovery and separation 11, ch. 73, p. 33
- Hund, F. 14, dedication, p. ix
- hydration 15, ch. 103, p. 393; 18, ch. 127, p. 529
- hydrides 3, ch. 26, p. 299; 18, ch. 123, p. 293
  - switchable films 36, ch. 228, p. 83
- hydrogen absorption in intermetallic compounds 6, ch. 47, p. 1
- hydrogen in metals, including  $RH_{2+x}$  phases 20, ch. 137, p. 207
- hydrolysis 15, ch. 103, p. 393; 18, ch. 127, p. 529
- hyperfine interactions 11, ch. 77, p. 323
- inelastic electron scattering 10, ch. 72, p. 547
- infrared properties of cuprates 31, ch. 202, p. 437
- inorganic complex compounds 8, ch. 56, p. 203; 9, ch. 59, p. 91
- intermediate valence 19, ch. 132, p. 177
- itinerant electron metamagnetism in cobalt intermetallics 26, ch. 171, p. 177
- kinetics of complexation in aqueous solutions 15, ch. 102, p. 347
- Kondo effect 1, ch. 11, p. 797
- lanthanide-induced shifts 4, ch. 38, p. 483; 23, ch. 153, p. 1; 33, ch. 215, p. 353
- lanthanide chelates
  - for sensitizing NIR luminescence 37, ch. 234, p. 171
  - in biomedical analyses 37, ch. 235, p. 217
- laser spectroscopy 12, ch. 87, p. 433
- lasers 4, ch. 35, p. 275
- light scattering in intermetallic compounds 14, ch. 95, p. 163
- liquid metals and alloys 12, ch. 85, p. 357
- LIS, *see* lanthanide-induced shifts
- luminescence
  - in biomedical analyses 37, ch. 234, p. 171
  - in NIR molecular probes and devices 37, ch. 235, p. 217
  - studies of ions 18, ch. 120, p. 150
  - spectra of ions in solution 3, ch. 24, p. 171
- $\mu$ SR studies of magnetic materials, 32, ch. 206, p. 55
- magnetic and transport properties of metals 1, ch. 6, p. 411
- magnetic correlations in heavy-fermion systems 19, ch. 131, p. 123
- magnetic properties (also *see* physical properties)
  - of borides 38, ch. 238, p. 105
  - of intermetallic compounds 2, ch. 14, p. 55; 20, ch. 138, p. 293
  - of nickel borocarbides 38, ch. 239, p. 175
  - of nonmetallic compounds 22, ch. 150, p. 295
  - of ternary  $RT_2X_2$  type intermetallic compounds 12, ch. 83, p. 133
  - of  $ThMn_{12}$ -type compounds 22, ch. 149, p. 143

- magnetic structures 1, ch. 7, p. 489
- magnetism 34, ch. 219, p. 135
- exotic phenomena 11, ch. 76, p. 293
  - surface 24, ch. 159, p. 1
- magnetoconductance in cuprates 31, ch. 197, p. 251
- magnetostriction
- RFe<sub>2</sub> 2, ch. 15, p. 231
  - transition metal thin films 32, ch. 205, p. 1
- marine chemistry 23, ch. 158, p. 497
- mechanical alloying 24, ch. 160, p. 47
- mechanically induced chemical reactions 24, ch. 160, p. 47
- metal–hydrogen batteries 21, ch. 142, p. 133
- mineralogy 3, ch. 21, p. 1
- minerals, crystal structures 16, ch. 108, p. 249
- mixed valence systems
- bremsstrahlung isochromat spectroscopy 10, ch. 70, p. 425
  - calculation of 4f excitation energies 10, ch. 68, p. 321
  - many-body formulation of spectra 10, ch. 64, p. 103
- molecular recognition 35, ch. 226, p. 273
- molybdates (VI) 3, ch. 30, p. 609
- Mössbauer effect 2, ch. 18, p. 387
- of intermetallic compounds 17, ch. 116, p. 539
- nanostructures and nanomaterials
- Al- and Mg-based systems 24, ch. 161, p. 83
  - properties 22, ch. 147, p. 1
  - spectroscopic properties 37, ch. 233, p. 99
  - synthesis 22, ch. 147, p. 1
  - transition metal multilayers 22, ch. 148, p. 81
- neutron scattering
- elastic 17, ch. 117, p. 635
  - in heavy-fermion systems 19, ch. 131, p. 123
  - inelastic 1, ch. 7, p. 489
  - inelastic of anomalous lanthanides 19, ch. 130, p. 1
  - intermultiple transitions 14, ch. 93, p. 1
  - of magnetic ordering in cuprates 31, ch. 199, p. 315
  - of spin fluctuations in cuprates 31, ch. 198, p. 281
- near-infrared luminescence in molecular probes and devices 37, ch. 235, p. 217
- nitride materials, ternary and higher order 24, ch. 166, p. 51
- NMR 2, ch. 18, p. 387
- in intermetallic compounds 14, ch. 94, p. 63
  - lanthanide induced shifts for extracting solution structures 33, ch. 215, p. 353
  - of complexes 23, ch. 153, p. 1
  - of paramagnetic complexes 4, ch. 38, p. 483
  - solution structure by paramagnetic NMR analysis 33, ch. 215, p. 353
- nonradiative processes in crystals 4, ch. 36, p. 317
- nuclear magnetic resonance, *see* NMR
- organic synthesis 8, ch. 57, p. 335
- organometallic compounds 7, ch. 53, p. 446
- oxidation–reduction properties 18, ch. 122, p. 239
- oxides
- binary 3, ch. 27, p. 337; 18, ch. 125, p. 413
  - higher 38, ch. 236, p. 1
  - mixed 3, ch. 28, p. 401
  - sesqui, defects in 5, ch. 44, p. 321
  - sesqui, phase transformation in 5, ch. 44, p. 321
  - ternary systems, R<sub>2</sub>O<sub>3</sub>–M<sub>2</sub>O<sub>3</sub>–M'O 13, ch. 90, p. 283
- oxo-selenates 35, ch. 224, p. 45
- oxygen nonstoichiometry and lattice effect in YBa<sub>2</sub>Cu<sub>3</sub>O<sub>x</sub> 31, ch. 195, p. 1
- permanent magnets 32, ch. 208, p. 515
- perovskites 3, ch. 29, p. 525
- manganese 33, ch. 214, p. 249
- phase equilibria
- in cuprates 30, ch. 190, p. 229
  - in ternary systems with boron 6, ch. 49, p. 335; 38, ch. 238, p. 105
  - in ternary systems with chalcogenides 13, ch. 89, p. 191
  - in ternary systems with metallic elements 13, ch. 88, p. 1
  - in ternary systems with lead 38, ch. 237, p. 55
  - in ternary systems with silicon 7, ch. 51, p. 1
  - intra rare earth binary alloys 8, ch. 54, p. 1
- phase transitions, structural distortions and phase separation in YBa<sub>2</sub>Cu<sub>3</sub>O<sub>x</sub> 31, ch. 195, p. 1
- phosphides 23, ch. 156, p. 285
- photoemission
- angle-resolved studies of untwinned YBa<sub>2</sub>Cu<sub>3</sub>O<sub>x</sub> 31, ch. 201, p. 391
  - in chalcogenides 10, ch. 67, p. 301

- inverse spectra, local density supercell theory **10**, ch. 65, p. 165
- of Ce and its compounds **10**, ch. 66, p. 231
- spectra, local density supercell theory **10**, ch. 65, p. 165
- physical metallurgy **11**, ch. 78, p. 409
- physical properties (also see magnetic properties)
  - of cuprates **30**, ch. 193, p. 453
  - of metals **1**, ch. 2, p. 173
  - of R<sub>2</sub>Fe<sub>14</sub>B-based alloys **12**, ch. 82, p. 71
  - pnictides **4**, ch. 33, p. 153
  - magnetic measurements on mono- **17**, ch. 114, p. 301
- polyoxometalates **38**, ch. 240, p. 337
- positron annihilation in high-temperature superconductors **30**, ch. 192, p. 417
- preparation and purification of metals **1**, ch. 2, p. 173
- pyrochlores **16**, ch. 107, p. 225
  
- quasicrystalline, Al- and Mg-based systems **24**, ch. 161, p. 83
  
- Raman scattering of cuprates **31**, ch. 203, p. 509
- redox reactions
  - in aqueous solutions **15**, ch. 102, p. 347
  - Ce(IV)/Ce(III) **36**, ch. 229, p. 347
- relativistic effects and electronic structure **18**, ch. 119, p. 29
- RNA, cutting of **34**, ch. 222, p. 405, **36**, ch. 229, p. 392
  
- samarium(II) reductants **36**, ch. 230, p. 393
- scandium alloy systems and intermetallics **27**, ch. 175, p. 339
- scanning tunneling microscopy of cuprates **31**, ch. 204, p. 563
- selenates **35**, ch. 224, p. 45
- selenides **4**, ch. 31, p. 1
- selenites **35**, ch. 224, p. 45
- separation chemistry **3**, ch. 22, p. 81; **18**, ch. 121, p. 197; **21**, ch. 139, p. 1
  - analytical, basic chemistry and methods **28**, ch. 180, p. 311
- shift reagents **4**, ch. 38, p. 483; **23**, ch. 153, p. 1; **33**, ch. 215, p. 353; **35**, ch. 225, p. 107
- single crystals
  - growth from molten metal fluxes **12**, ch. 81, p. 53
  - growth of cuprates **30**, ch. 189, p. 67
  - growth of metals and intermetallic compounds **12**, ch. 80, p. 1
- skutterudites, filled **33**, ch. 211, p. 1
- solid electrolytes **28**, ch. 178, p. 131; **35**, ch. 223, p. 1
- solid oxide fuel cells (SOFC) **35**, ch. 223, p. 1
- solution chemistry **15**, ch. 103, p. 393; **18**, ch. 127, p. 529; **18**, ch. 128, p. 559; **21**, ch. 145, 305
- solvation in organic solvents **21**, ch. 145, p. 305
- spectroscopic properties in transparent crystals **5**, ch. 46, p. 461
  - nanomaterials **37**, ch. 233, p. 99
- spectroscopy
  - appearance potential **16**, ch. 109, p. 519
  - bremsstrahlung isochromat **10**, ch. 70, p. 425
  - circularly polarized luminescence **34**, ch. 220, p. 289
  - high-energy **10**, ch. 62, p. 1
  - magnetic resonance **11**, ch. 77, p. 323
  - mass
    - – spark source matrices **4**, ch. 37C, p. 377
    - – spark source trace element analysis **4**, ch. 37B, p. 359
    - – stable-isotope dilution analysis **4**, ch. 37G, p. 471
    - – with inductively coupled plasmas analysis **13**, ch. 91, p. 385
  - optical **11**, ch. 74, p. 81; **37**, ch. 233, p. 99; ch. 234, p. 171; **37**, ch. 235, p. 217
  - photoelectron in heavy fermion systems **26**, ch. 172, p. 265
  - time-resolved emission in solution chemistry **33**, ch. 216, p. 465
- Spedding, F.H., **11**, prologue, p. 1
- spin glasses **12**, ch. 84, p. 213
- stannides, transition metal ternary systems **24**, ch. 164, p. 399
- steels **25**, ch. 165, p. 1
- stresses, static and dynamic **26**, ch. 170, p. 87
- sulfides **4**, ch. 31, p. 1
  - poly **32**, ch. 209, 567
- superconductivity **1**, ch. 10, p. 749; **34**, ch. 219, p. 135
  - crystal chemistry of cuprates **30**, ch. 188, p. 31
  - in metals **17**, ch. 110, p. 1
  - high-temperature layered cuprates: overview **30**, ch. 187, p. 1
  - nickel borocarbides **38**, ch. 239, p. 175
  - unconventional and magnetism **34**, ch. 219, p. 135
- surfaces
  - adsorption on **5**, ch. 43, p. 217
  - catalysis on **5**, ch. 43, p. 217

- switchable metal hydride films 36, ch. 228,  
p. 83
- systematics, intra rare earth binary alloys 8,  
ch. 54, p. 1
- tellurides 4, ch. 31, p. 1
- ternary equiatomic YbTX intermetallics 32,  
ch. 207, p. 453
- tetravalent cerium compounds 36, ch. 229,  
p. 281
- theoretical chemistry 3, ch. 23, p. 111
- thermal conductivity of compounds 16,  
ch. 106, p. 107
- thermochemical properties 18, ch. 122,  
p. 239
- of cuprates 30, ch. 190, p. 229
- of gaseous species 12, ch. 86, p. 409
- of metallic systems 19, ch. 134, p. 479
- thin films 5, ch. 41, p. 1; 20, ch. 136, p. 105
- switchable metal hydrides 36, ch. 228,  
p. 83
- toxicity 4, ch. 40, p. 553
- transition metal-indides 34, ch. 218, p. 1
- transport properties of intermetallics 5,  
ch. 42, p. 117; 17, ch. 115, p. 409
- triflates 29, ch. 186, p. 315
- tunneling spectra of cuprates 31, ch. 204,  
p. 563
- valence fluctuations 2, ch. 20, p. 575; 16,  
ch. 105, p. 1
- X-ray absorption spectra 10, ch. 71, p. 453
- X-ray scattering 26, ch. 169, p. 1

# Lanthanide Higher Oxides: The Contributions of Leroy Eyring

**Z.C. Kang\***

---

<b>Contents</b>	List of Symbols	2
	1. Introduction	2
	2. Historical Overview of the Lanthanide Higher Oxides	3
	3. Intrinsic Features of the Lanthanide Higher Oxides	6
	4. Thermodynamic Properties of the Lanthanide Higher Oxides	8
	4.1 Phase diagrams with bi-variant parameters: temperature and oxygen partial pressure	8
	4.2 Hysteresis and composition domains	12
	4.3 Oxygen releasing features of the binary and ternary oxides containing Ce, Pr, Tb	14
	5. Structural Characteristics of the Lanthanide Higher Oxides	18
	5.1 Experimental electron diffraction data of the lanthanide higher oxides	20
	5.2 Refined structures of the five homologous phases of the lanthanide higher oxides from experimental neutron diffraction data	20
	5.3 Fluorite-type module theory	23
	5.4 Rationalization of homologous series of oxygen-deficient fluorite-related lanthanide higher oxides and their compositional formula	27
	5.5 Coordination number of the lanthanide metal in the lanthanide higher oxides	27
	5.6 Module type and average valence state of the lanthanide higher oxides	29
	5.7 Composition domains in the lanthanide higher oxides	29
	5.8 Surface character and oxygen migration	33
	5.9 Structural modeling the undetermined structure of the lanthanide higher oxides	36
	5.9.1 Proposed structure of the Pr <sub>88</sub> O <sub>160</sub> phase	37
	5.9.2 Proposal structure of the Ce <sub>19</sub> O <sub>34</sub> phase	39

\* RE Power-Tech, P.O. Box 163, Stow, MA 01775, USA

5.10 From the binary oxide to the ternary oxide	41
6. Conductivity and Catalytic Properties of the Lanthanide Higher Oxides	42
6.1 Electrical conductivity of the lanthanide higher oxides	42
6.2 Conductivity of the ternary lanthanide higher oxides	44
6.3 Catalytic properties of the lanthanide higher oxides	45
6.4 Solvolytic disproportionation of the lanthanide higher oxides	49
7. Summary	50
Acknowledgements	51
Appendix A: Conversion Table for the Modular Designations	51
References	51

### List of Symbols

$E_F$	Fermi energy	<i>List of acronyms</i>
$F$	fluorite-type module without any oxygen vacancies	EELs electron energy loss spectroscopy
$t_0$	transference number	HREM high resolution electron microscopy
$U$	fluorite-type module having an oxygen vacancy	OBC oxygen buffer capacity
$U^i$ and $V^j$	two separated oxygen sublattices	IT-SOFC intermediate-temperature solid oxide fuel cell
$V$	fluorite-type module having an oxygen vacancy	TPD temperature-programmed desorption
$W$	fluorite-type module having two oxygen vacancies	TPR temperature-programmed reduction
$\beta$	Seebeck coefficient	
$\sigma_v$	oxygen anion conductivity	

## 1. INTRODUCTION

When Professor Leroy Eyring won the Spedding award he said that “As an alternative to being brilliant, one way to win the Spedding Award is to spend a lifetime focusing your own interest and that of your students on rare earth science. That is true in my case” (Eyring, 1994).

The lanthanide higher oxides are a paradise of solid state chemistry. Since Professor Leroy Eyring discovered the mysterious non-stoichiometry and homologous series of the black oxide of praseodymium in 1954 (Ferguson et al., 1954; Guth et al., 1954), he spent his lifetime to understand the thermodynamic, hysteresis, homologous series phases, reactions between the homologous phases, structures of the homologous phases and intrinsic principle of the structures of oxygen-deficient fluorite-related homologous series of the lanthanide higher oxides. Fortunately his indefatigable efforts have achieved his aim of understanding

the relationship between the properties and structures of the lanthanide higher oxides. Before Professor Leroy Eyring passed away he changed the content of his interest at his home pages of the Internet web site to “oxygen and hydrogen source for hydrogen economy”. The lanthanide higher oxides, as he expected, have and will have significant applications as a redox catalyst, mixed conductor, sensor, oxygen separation, intermediate temperature solid oxide fuel cell (IT-SOFC), catalyst for hydrogen production from methane and water and so on.

In this article I will elaborate on the knowledge, which was obtained by Professor Leroy Eyring and his colleagues in more than 50 years of research on the lanthanide higher oxides and their ideas for the applications of these oxides. Also the unique non-stoichiometric characteristics of the lanthanide higher oxides are emphasized and the intrinsic relationship between the macroscopic properties and nano-scale structures is demonstrated.

## 2. HISTORICAL OVERVIEW OF THE LANTHANIDE HIGHER OXIDES

In 1923  $\text{CeO}_2$  was found to have the fluorite structure (Goldschmidt and Thomsen, 1923), and in 1926  $\text{PrO}_2$  was found to have the same structure (Goldschmidt, 1926). In 1950 the intermediate compositions in the  $\text{PrO}_x$  system were reported to have the fluorite structure of variable lattice parameters (the superstructure reflections were not observed). In 1951  $\text{TbO}_2$  was also shown to have the fluorite structure (Gruen et al., 1951). By this time the basic fluorite structure had been established for all the known higher oxides of cerium, praseodymium and terbium.

In 1954 Leroy Eyring published the mysterious phenomenon of wide-range non-stoichiometric phases, and a homologous series of ordered intermediate oxides with a narrow composition range (Guth et al., 1954; Ferguson et al., 1954). These striking characteristics are the behaviors of the binary, oxygen-deficient, fluorite-type higher oxides of the lanthanide (Hyde et al., 1966; Hyde and Eyring, 1965; Bevan, 1955; Bevan and Kordis, 1964). Non-stoichiometric and homologous series phases are exhibited by the oxides of Ce, Pr, and Tb which equilibrated under various oxygen pressures up to one atmosphere under either isobaric or isothermal conditions at temperatures between 200 and 1200 °C. The oxygen contents of the particular stable phases that occur in these systems individually vary widely as the temperature and/or oxygen partial pressure are changed. In spite of these differences the three oxides can be individually understood through their common fluorite-related structures.

Careful analyses of the thermodynamic data of the praseodymium and terbium oxides led to the construction of their  $\text{RO}_x\text{-O}_2$  phase diagrams (Hyde et al., 1966; Hyde and Eyring, 1965). The cerium oxides were studied by means of X-ray powder diffraction (Bevan, 1955) and the  $\text{CeO}_x\text{-O}_2$  phase diagram was constructed from equilibrium reaction studies at oxygen pressures down to  $10^{-24}$  atm and temperatures up to 1200 °C (Bevan and Kordis, 1964; Ricken et al., 1984). It is worth to notice that the phase diagrams of  $\text{CeO}_x\text{-O}_2$ ,  $\text{PrO}_x\text{-O}_2$ , and  $\text{TbO}_x\text{-O}_2$  systems

**TABLE 1** Summary of the oxygen-deficient fluorite-related lanthanide higher oxides of the  $R_nO_{2n-2m}$  series

Phase designation and cations	Formula, unit cell content	$n$	$m$	O/R ratio	Space group
$l$ Ce, Pr, Tb	$R_7O_{12}$	7	1	1.714	$R\bar{3}$
$\zeta$ Ce(?) Pr	$R_9O_{16}$	9	1	1.778	$P\bar{1}$
$\delta(1)$ Ce, Tb	$R_{11}O_{20}$	11	1	1.818	$P\bar{1}$
$\beta(0)$ Pr	$R_{12}O_{22}$	12	1	1.833	
$\pi$ Ce(?), Pr, Tb	$R_{16}O_{30}$	16	1	1.875	
M19 Ce	$R_{19}O_{34}$	19	2	1.789	
$\beta(1)$ Pr	$R_{24}O_{44}$	24	2	1.833	$P2_1/c$
$\beta(2)$ Pr	$R_{24}O_{44}$	24	2	1.833	
M29 Ce	$R_{29}O_{52}$	29	3	1.793	
M39 Ce	$R_{39}O_{70}$	39	4	1.795	
$\varepsilon$ Ce(?), Pr	$R_{40}O_{72}$	40	4	1.800	$P2_1/c$
$\beta(3)$ Tb	$R_{48}O_{88}$	48	4	1.833	
$\delta'$ Ce, Pr, Tb	$R_{62}O_{112}$	62	6	1.806	
$\delta(2)$ Pr	$R_{88}O_{160}$	88	8	1.818	
$\delta$ Ce, Pr	$RO_{1.5-1.7}$				
$\alpha$ Ce, Pr	$RO_{1.7-2.0}$				

Notes: 1. Preparation: All preparations are by equilibration of the oxide with oxygen at temperatures and oxygen pressure predetermined from experimental data. 2. The diffraction patterns all show strong face-center-cubic reflections with commensurate, weak, superstructure reflections by whatever means they are taken.

are constructed under different oxygen partial pressure, in other words they are bi-variant systems.

Establishment of the structures of the lanthanide higher oxides, finding the structural principles involved, and attempts at understanding the relationship between their structures and properties have been under way for five decades.

Between 1951 and 1996 numerous studies utilizing X-ray, electron, and neutron diffraction and high-resolution electron microscopic techniques revealed an increasing number of ordered intermediate phases of the higher oxides of the lanthanide (Baenziger et al., 1960; Brauer and Gradinger, 1954; Brauer and Gengerich, 1957; Sawyer et al., 1965; Bartram, 1966; Von Dreele et al., 1975; Kunzmann and Eyring, 1975; Ray et al., 1975; Skarnulis et al., 1978; Summerville et al., 1978; Tuenge and Eyring, 1979, 1982; Knappe and Eyring, 1985; Schweda et al., 1991; Kang et al., 1992; Otsuka et al., 1986). All these phases were found to be commensurate superstructures of the fluorite substructure. The transformation matrices establishing the relationship between the fluorite subcells and the fluorite-related supercells for most of the new phases were found. Finally, the refined structures of five members of the homologous series had been published (Zhang et al., 1993a, 1993b, 1993c, 1995). Table 1 summarizes these results.

Attempts have been made to determine the structures of some members of the series by X-ray methods with little success. The properties of these oxides make

them difficult to prepare as single crystals or powders with precise composition suitable for X-ray structure determination partly because of the rapid exchange of oxygen between the crystal and its environment. Twinning, intergrowth between the phases, and absorption also contribute to this problem. Beyond this, the structure depends on the vacant oxygen site arrangement, which is of low symmetry in some case and is embedded within a close packing of much heavier atoms. Conveniently, and in contrast, the electron microscope using a small beam size can provide a diffraction pattern from a crystalline nanoparticle of a prepared powder. Furthermore, it can exhibit a real-space image showing the structure of the nanoparticle at atomic resolution (Cowley and Moodie, 1957; Cowley, 1981; Buseck et al., 1988).

During the 1960s, the structure of binary  $Tb_7O_{12}$  was predicted (Baenziger et al., 1960) and the structure of ternary  $M_{7-x}M'_xO_{12}$  phases  $UY_6O_{12}$  (Bartram, 1966) and  $Zr_3Sc_4O_{12}$  (Thornber et al., 1968) were determined by X-ray diffraction and shown to possess the predicted structure of  $Tb_7O_{12}$ . Because of this, two unsuccessful proposals were made in an effort to establish the structure principle for the series; one postulate identified strings of vacant oxygen sites (Hyde and Eyring, 1965; Hyde et al., 1965) along  $\langle 111 \rangle_F$  in the  $R_7O_{12}$  structure, and the other on the existence of slabs of edge-sharing, oxygen-centered tetrahedral,  $(MO)_n^{n+}$  separated by oxygen layers containing vacant sites (Caro, 1968, 1972).

In the 1970's, based on this same structural information the so-called "coordinated defect" (or c.d.) was proposed as a building block of these structures (Martin, 1974; Hoskins and Martin, 1975, 1976, 1977). This concept focused on the coordination of the vacant oxygen site with its nearest oxygen neighbors,  $\square O_6$  ( $\square$  is an oxygen vacancy). There are also four cations in tetrahedral coordination around the vacant site. The six nearest oxygen neighbors are essentially in octahedral positions with respect to the vacant oxygen site. The nearest and next-nearest atoms of a vacant oxygen site have the largest displacements from their ideal positions in the real fluorite unit cell due to the Coulomb interaction (four cations move 0.2 Å away from and the six oxygens move 0.3 Å toward the vacant site). These displacements, which are expected from the c.d. theory and are also consistent with the fluorite-type module theory, are observed in the refined structures (Zhang et al., 1993a; Von Dreele et al., 1975).

One year after the c.d. was suggested as the entity responsible for the stable structures of the series, the electron diffraction patterns and the transformation matrices of the supercells, in terms of the fluorite subcell of the intermediate phases,  $R_7O_{12}$ ,  $R_9O_{16}$ ,  $R_{40}O_{72}$ , and  $R_{24}O_{44}$  were published (Kunzmann and Eyring, 1975; Eyring, 1979). (In those days the even n compositions in the list were assigned the compositions  $R_{10}O_{18}$  and  $R_{12}O_{22}$ , respectively.) These diffraction patterns exhibited the reciprocal space structures and the relationship between the fluorite f.c.c. lattice and the superstructure lattices. They also gave information about the "building blocks" and their assembly, but unfortunately, the deeper meaning of this information was not appreciated at the time. In the same year, 1975, the structure of  $Pr_7O_{12}$  was determined from neutron powder diffraction data (Von Dreele et al., 1975). This confirmed the structure of  $Pr_7O_{12}$  to be the same structure as predicted for  $Tb_7O_{12}$  and found for  $UY_6O_{12}$  and  $Zr_3Sc_4O_{12}$ .

From thermodynamic insights won in the late 1970's new attempts to craft general structural principles by expanding the basic ideas of the c.d. model were attempted by incorporating additional coordination defects of greater complexity (Manes et al., 1980; Sorensen, 1981).

Until recently the intermediate phases were considered as being divided into an odd-family; for example,  $R_7O_{12}$ ,  $R_9O_{16}$ ,  $R_{11}O_{20}$ , and an even-family; such as  $R_{40}O_{72}$ ,  $R_{24}O_{44}$ , and  $R_{48}O_{88}$ . Beyond the large differences in unit cell volumes, the basis of this distinction was the relationship between the fluorite f.c.c. diffraction spots and the superstructure spots of the intermediate phases. The odd-family had an odd number of superstructure intervals along the  $\langle 135 \rangle_F$  direction, while the even-family had an even number of intervals along the  $\langle 220 \rangle_F$  direction. (There are some exceptions, for example, in the electron diffraction pattern of the smallest of the  $\beta$ -phase homologous,  $Pr_{12}O_{22}$ , the superstructure spots lie along the  $\langle 135 \rangle_F$  direction as is found for the odd numbers).

There are numerous examples of phases that do not conform to the expression,  $R_nO_{2n-2}$ , originally advanced (Hyde and Eyring, 1965) as the generic formula for the homologous series. For example, the polymorphs of  $Pr_{12}O_{22}$ ,  $Pr_{24}O_{44}$ ,  $Tb_{24}O_{44}$ , and  $Tb_{48}O_{88}$  exist, as listed in Table 1. For the  $\delta'$  phase it is even difficult to determine the number of the oxygen atoms in the unit cell or the relationship between the fluorite f.c.c. lattice and the superstructure since the superstructure spots are neither along the  $\langle 135 \rangle_F$  nor  $\langle 220 \rangle_F$ , instead there are 62 intervals along  $\langle -12, 6, 26 \rangle_F$  and  $\langle 22, 20, 4 \rangle_F$ . However, the composition of this phase was found gravimetrically to be  $TbO_{1.806}$  (Kunzmann and Eyring, 1975), which requires the formula to be  $Tb_{62}O_{112}$ . In the same way the  $n = 19$  phase ( $Ce_{19}O_{34}$ ) in the  $CeO_x$  system did not belong.

In 1996, after five homologous series,  $Pr_7O_{12}$ ,  $Pr_9O_{16}$ ,  $Tb_{11}O_{20}$ ,  $Pr_{40}O_{72}$ , and  $Pr_{24}O_{44}$ , were determined by refined neutron diffraction data, the fluorite-type module theory and principles integrated all of the known phases in the Ce, Pr, and Tb oxides into a single series,  $R_nO_{2n-2m}$ , where  $m$  follows directly from the equal probability that any of the eight oxygen sites in the fluorite-type module could be vacant. This equal probability of vacant anion sites demands rapid flexibility in the valence variation of the cation sublattice, which is characteristic of Ce, Pr, and Tb due to electron hopping (Kang et al., 1996; Kang and Eyring, 1997a, 1997b).

Based on the fluorite-type module theory the thermodynamic properties, hysteresis, and reactions between the homologous series can be elucidated and the structures of homologous series experimentally discovered may be modeled. Using these principles a wide range of non-stoichiometric ternary lanthanide higher oxides from  $RO_2$  to  $R_2O_3$  were founded.

### 3. INTRINSIC FEATURES OF THE LANTHANIDE HIGHER OXIDES

The striking characteristics of the lanthanide higher oxides are rooted in the electronic structure of Ce, Pr, and Tb atoms. The lanthanide elements located in the third group of the periodic table have a normal  $3+$  valence state and the normal oxides have the  $R_2O_3$  formula. Due to the special electron configurations of Ce

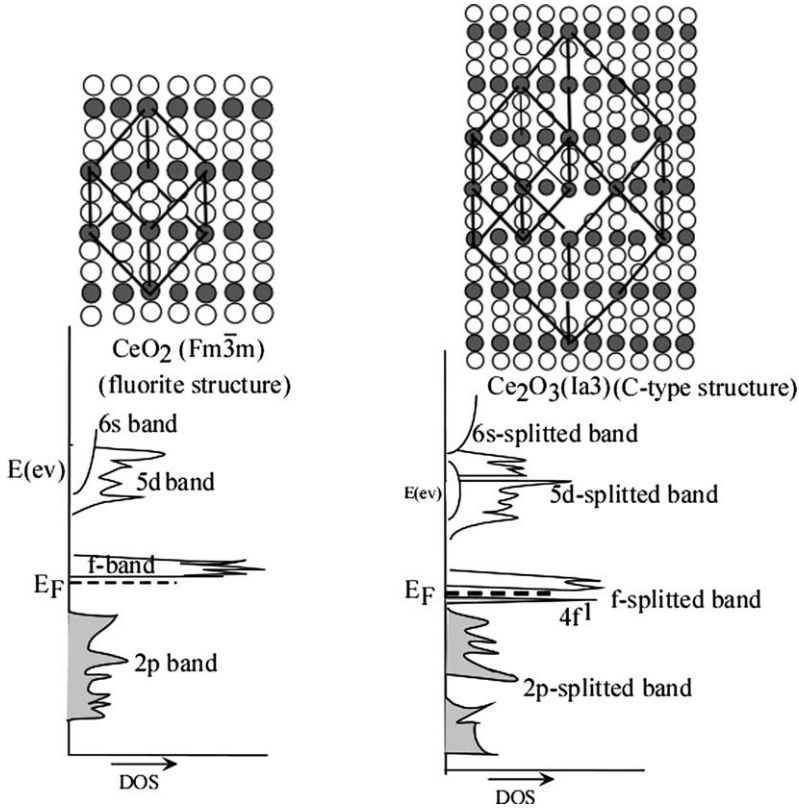


**FIGURE 1** Sketch of the electronic density of states of CeO<sub>2</sub> and Ce<sub>2</sub>O<sub>3</sub>.

([Xe]4f<sup>1</sup>5d<sup>1</sup>6s<sup>2</sup>), Pr ([Xe]4f<sup>3</sup>6s<sup>2</sup>), Tb([Xe]4f<sup>9</sup>6s<sup>2</sup>), Ce<sup>4+</sup>, Pr<sup>4+</sup>, and Tb<sup>4+</sup> can exist. But at one atmosphere pressure the valence states of Ce, Pr, and Tb elements in their oxides are always a mixture of both 3+ and 4+ and the average valence in the binary oxides of Ce, Pr and Tb is greater than 3+, and therefore, they are called higher oxides.

The electron structures of CeO<sub>2</sub>, PrO<sub>2</sub>, and Ce<sub>2</sub>O<sub>3</sub> have been calculated (Koelling et al., 1983; Hill and Catlow, 1991; Skorodumova et al., 2002). However, the “intermediate valence” has been studied for decades (Wachter, 1994). In CeO<sub>2</sub> the Ce<sup>4+</sup> ion has the electron configuration of the Xenon core, [Xe], and the empty 4f<sup>1</sup> state lies about 1.5 eV above Fermi level, E<sub>F</sub>. Therefore, CeO<sub>2</sub> is an insulator with large-gap and there is strong p-f hybridization between the 2p electron of oxygen and the 4f electron of Ce. On the other hand, the Ce<sup>3+</sup> ion has the 4f<sup>1</sup> electron localized in the 4f orbit. As a result the unit cell of Ce<sub>2</sub>O<sub>3</sub> is twice the size of the fluorite phase and the symmetry is changed from Fm-3m. into Ia-3; the bandwidth of the CeO<sub>2</sub> is narrowed by nesting; and the Fermi level is also modified. The calculated results (Koelling et al., 1983; Hill and Catlow, 1991; Skorodumova et al., 2002; Yang et al., 2004; Jiang et al., 2005a, 2005b) show that the energy level of the 4f<sup>1</sup> (of Ce<sup>3+</sup>) is located just a few eV below the Fermi en-

ergy,  $E_F$ , and the  $4f^1$  electron is localized around the  $Ce^{3+}$  cation instead of being delocalized into the f-p hybridization band. Figure 1 is a sketch of the electronic density state of  $CeO_2$  and  $Ce_2O_3$ .

The properties of the lanthanide higher oxides may depend on relationship between the Fermi energy,  $E_F$ , and 4f level. If the  $E_{4f}$  is close to Fermi energy, the cations become intermediate valent. Because hybridization will mix the originally localized 4f states with the 5d conduction band electrons and the 4f states acquire narrow width and dispersion. These partially filled narrow bands at  $E_F$  act like a sink for other conduction electrons. This leads the crystal to minimize its energy. The originally localized 4f state, being filled with an integer number of electrons, is now filled, in the narrow band case, with a non-integer number of electrons per cation. In the lanthanide higher oxides it is hard to say that the cations nearest to an oxygen vacancy have valence  $3+$ . The number of electrons in the narrow 4f band is dominated by the electron band structure, which depends on the oxygen vacancy content and unit cell dimension of structure of the ordered intermediate phases. The mysterious non-stoichiometric characteristics of the lanthanide higher oxides are related to these intrinsic features of the 4f electron band structures. Unfortunately, at present time only the electron band structures of  $CeO_2$ ,  $Ce_2O_3$ , and  $PrO_2$  have been calculated.

## 4. THERMODYNAMIC PROPERTIES OF THE LANTHANIDE HIGHER OXIDES

Several review articles and books on the lanthanide higher oxides, which include thermodynamic properties, have been published (Eyring, 1979; Haire and Eyring, 1994; Trovarelli, 2002; Adachi and Imanaka, 1998; Adachi et al., 2005). The systematic thermodynamic data of the cerium, praseodymium, and terbium oxides can be found in Bevan's and Eyring's papers (Hyde et al., 1966; Hyde and Eyring, 1965; Bevan and Kordis, 1964).

### 4.1 Phase diagrams with bi-variant parameters: temperature and oxygen partial pressure

The binary phase diagrams of  $CeO_x-O_2$ ,  $PrO_x-O_2$ , and  $TbO_x-O_2$  system can be found, for example, in Haire and Eyring review article (Haire and Eyring, 1994). For the convenience of the reader the modified phase diagram of  $CeO_x-O_2$ ,  $PrO_x-O_2$ , and  $TbO_x-O_2$  systems are given in Figures 2-4, respectively. These phase diagrams were constructed under different oxygen partial pressure, which is not same as for standard binary phase diagrams, which are normally under a constant oxygen pressure. For a better understanding of the relationship between temperature and composition it is better to utilize the isobaric data.

Figure 5 shows the isobar data of  $CeO_x-O_2$  system. At one atmosphere with a 150 torr oxygen partial pressure, the cerium oxide almost is dioxide,  $CeO_2$ , and there is no phase transition until the temperature increases up 1200 °C. However, when the oxygen partial pressure is about  $10^{-9}$  torr the oxygen content of the

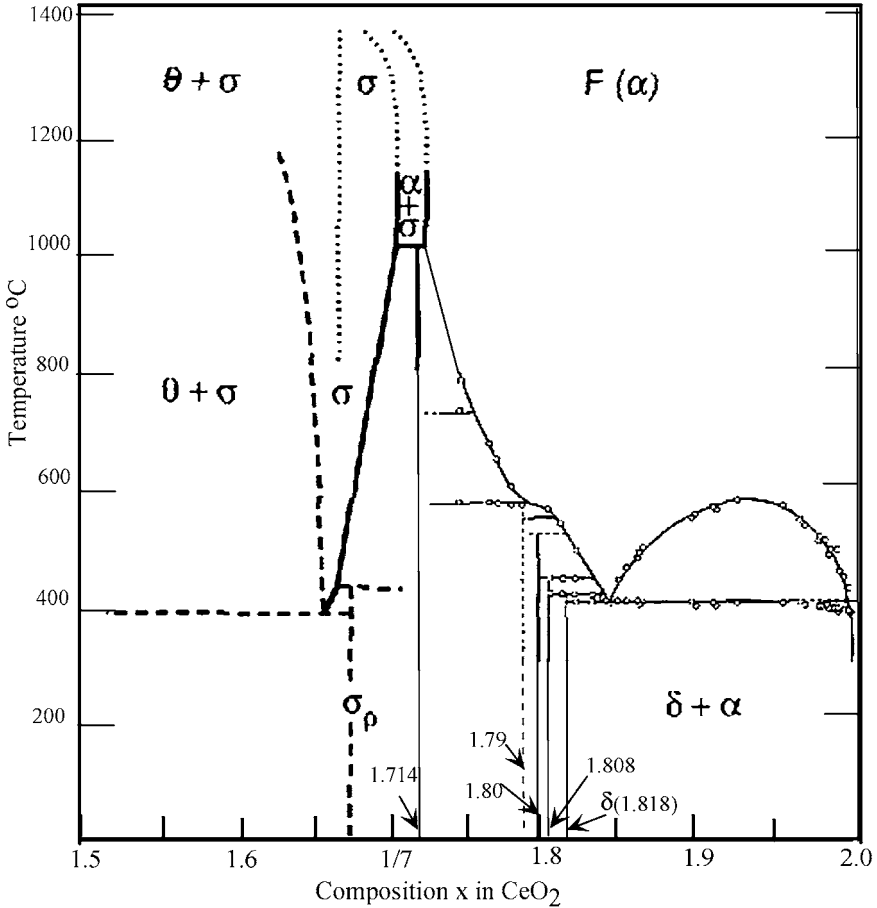


**FIGURE 2** Phase diagram for the CeO<sub>x</sub>-O<sub>2</sub> system (modified from Haire and Eyring, 1994).

cerium dioxide start to obviously decrease at 900 °C and rapid reduces to CeO<sub>1.8</sub> at 1150 °C. While the oxygen partial pressure is about 10<sup>-17</sup> torr the cerium oxide consists of two phases,  $\delta$  (CeO<sub>1.818</sub>) and  $\alpha$  (CeO<sub>1.98</sub>) at 900 °C. If the sample is cool down to room temperature, the  $x$  in CeO<sub>x</sub> may have different values depending on the cooling rate and the variation of oxygen partial pressures in the vicinity of the sample.

The  $x$  in PrO<sub>x</sub> is more sensitive to the oxygen partial pressure in comparison with CeO<sub>x</sub>. Figure 6 shows an isobaric data for PrO<sub>x</sub> system at 199 torr, which is almost same as in one atmosphere air. As temperature is increased up to 450 °C the oxygen content of the normal commercial grade of praseodymium oxides,  $x = 1.833$  (usually expressed as Pr<sub>6</sub>O<sub>11</sub>), starts to change and at 700 °C it become PrO<sub>1.714</sub>. Between 450 and 700 °C the oxygen content of the praseodymium oxide changes linearly with temperature. In other words the rate of change of the oxygen content is constant. Usually it is called as  $\alpha$ -phase with wide non-stoichiometry. At

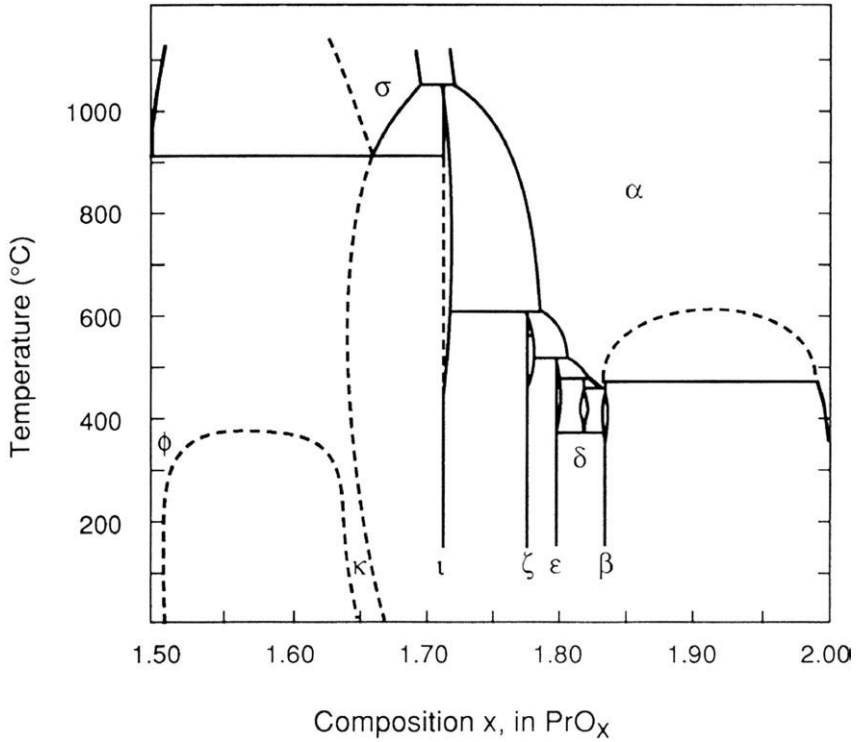


**FIGURE 3** Phase diagram for the  $\text{PrO}_x\text{-O}_2$  system (after Turcotte et al., 1971).

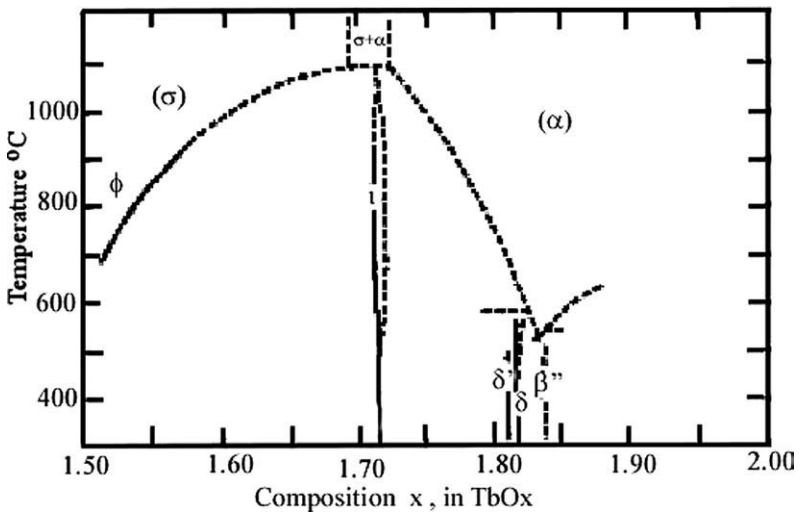


**FIGURE 4** Phase diagram for the  $\text{TbO}_x\text{-O}_2$  system (after Tuenge and Eyring, 1982).

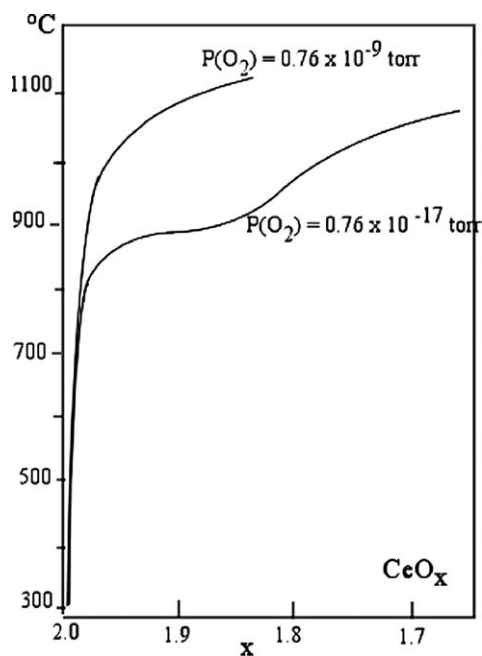


FIGURE 5 Isobaric data of the  $\text{CeO}_x$ - $\text{O}_2$  system.

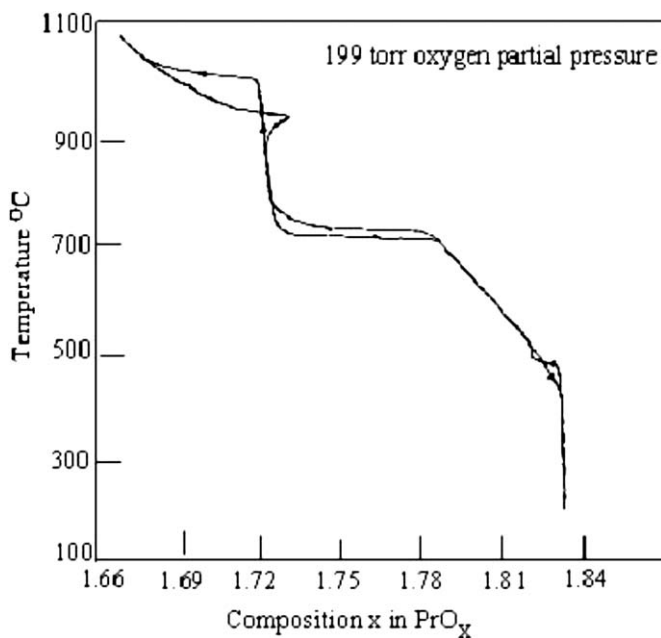
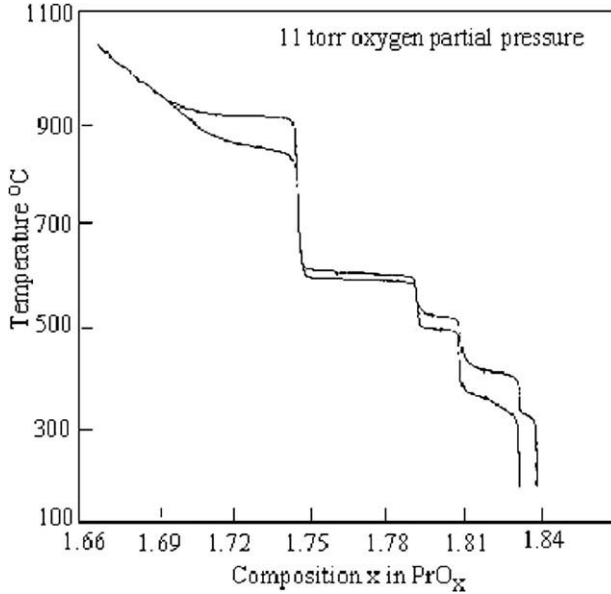


FIGURE 6 Isobaric data of the  $\text{PrO}_x$ - $\text{O}_2$  system at 199 torr oxygen partial pressure.



**FIGURE 7** Isobaric data of the  $\text{PrO}_x\text{-O}_2$  system at 11 torr oxygen partial pressure.

above  $700^\circ\text{C}$  the rate of changing oxygen content of the oxide is non-linear, which is a feature of a two phase system. If the oxygen partial pressure is 11 torr (as shown in the Figure 7), the oxygen content of the praseodymium higher oxide varies not only with temperature but also with the history of heating and cooling process. This means that when you heat up the praseodymium oxide sample and cooling it back to same temperature under 11 torr oxygen partial pressure, the sample will have different oxygen content than that of the original sample. This feature for  $\text{PrO}_x$  system is very obvious, but for  $\text{CeO}_x$  and  $\text{TbO}_x$  also have similar characteristics. The oxygen content of the lanthanide higher oxides always varies with temperature and the oxygen partial pressure. This is peculiar characteristic of the lanthanide higher oxides. Without carefully consideration of this characteristics of the lanthanide higher oxides the measured macroscopic properties (for examples, conductivity, oxygen storage capacity, so on) may be meaningless because the composition of the measured sample is different as the temperature and oxygen partial pressure minor variation during the measuring process.

## 4.2 Hysteresis and composition domains

As noted in the previous section the heat treatment history will strongly determine the oxygen content of the lanthanide higher oxides. In the two phase region of the  $\text{TbO}_{1.714}$  and  $\text{TbO}_{1.818}$  phases, as shown in Figure 8, when the heating process starts from the  $\text{TbO}_{1.818}$  phases it changes to  $\text{TbO}_{1.714}$  about  $580^\circ\text{C}$ . Then, when it cool to  $530^\circ\text{C}$  and heated back to  $600^\circ\text{C}$  the oxygen follows the path shown in the Figure 8, That is, the oxygen content of the sample as it is cooled does not

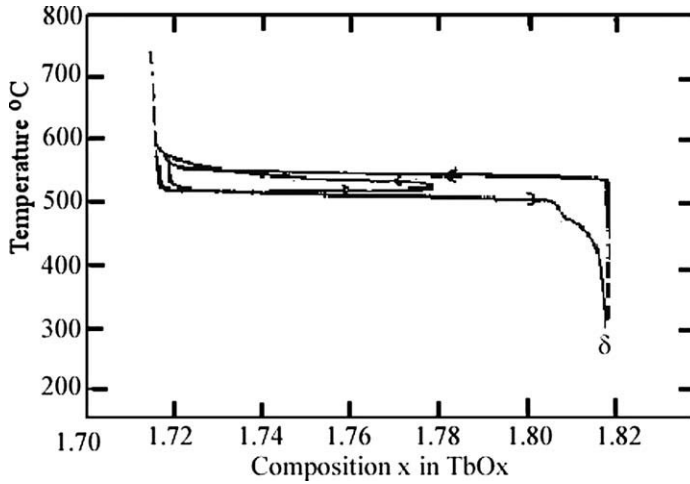


**FIGURE 8** Isobaric hysteresis loop of the  $\text{TbO}_x$  system for different heating and cooling processes (after Eyring, 1979).

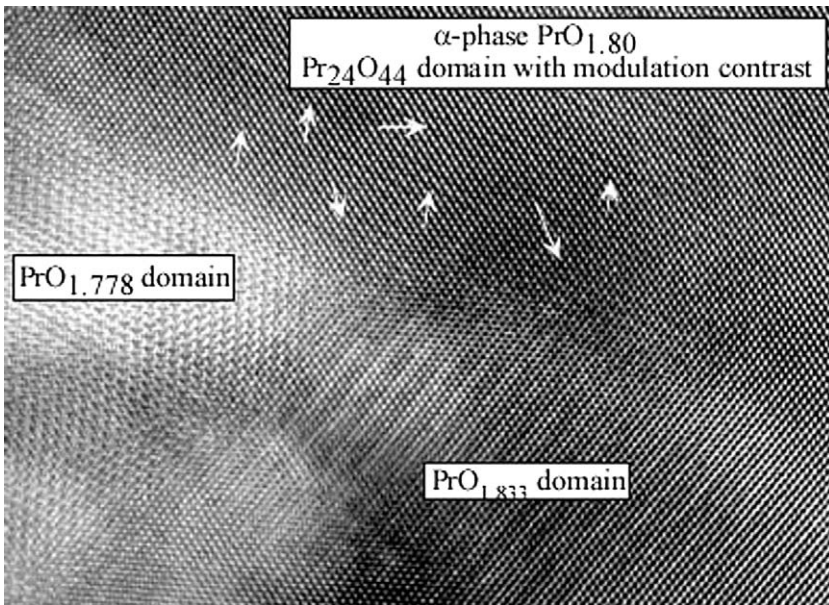


**FIGURE 9** Domain structure in a  $\alpha$ -phase with a nominal composition  $\text{PrO}_{1.82}$ .

follows same route as during the initial heating of the sample. As the sample is cooling down directly from 600 to 200 °C, then, the oxygen content of the sample goes through  $\delta'$  phase,  $\text{TbO}_{1.806}$ , before reaching the  $\text{TbO}_{1.818}$  composition. This is a memory effect of the composition domains, which is similar to that observed in ferromagnetism.

In the lanthanide higher oxides the composition hysteresis is due to composition domains (Boulesteix and Eyring, 1987; Kang, 2001). Figure 9 shows the composition domain in a  $\alpha$  phase with the nominal composition  $\text{PrO}_{1.82}$ . The arrows in the Figure 9 indicate the modulation waves having composition  $\text{PrO}_{1.80}$ . As ferromagnetic domains determine the hysteresis loop of the magnetization, the composition domains in the lanthanide higher oxides define the hysteresis loop of the oxygen content of the oxides (also see the module theory of the lanthanide higher oxides in Sections 5.3 and 5.7).

### 4.3 Oxygen releasing features of the binary and ternary oxides containing Ce, Pr, Tb

It is useful to know the differential of the oxygen content of the lanthanide higher oxides against the temperature,  $d(x \text{ in } \text{RO}_x)/dT$  under a given oxygen partial pressure and the oxygen partial pressure,  $d(x \text{ in } \text{RO}_x)/dp$  under a given temperature. These parameters demonstrate the oxygen releasing characters of the lanthanide higher oxides. They are related to the TPD (Temperature-Programmed Desorption), TPR (Temperature-Programmed Reduction) process and OBC (Oxygen Buffer Capacity) in the catalyst field.

Figure 10 demonstrates that the oxygen-releasing peak of the  $\text{CeO}_2$  shifts to higher temperature as oxygen partial pressure is increased to higher values.

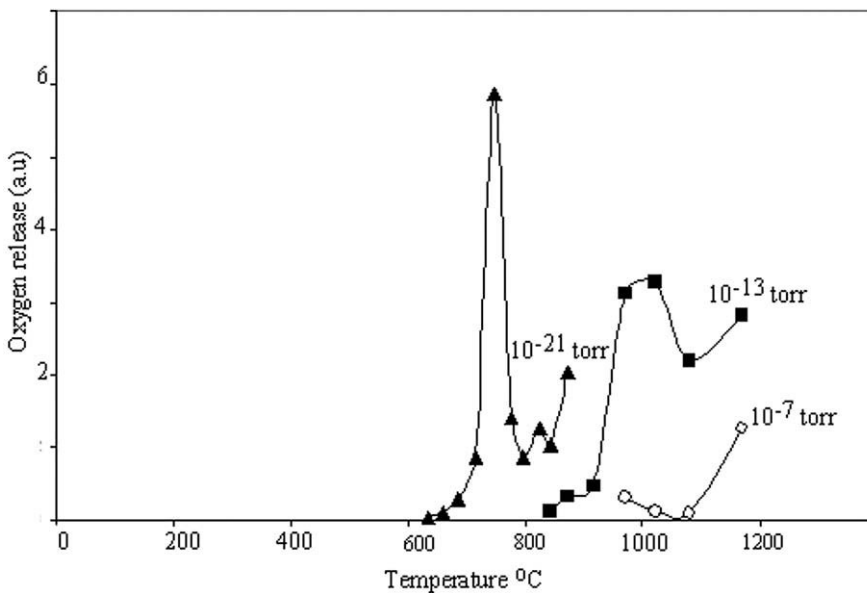


**FIGURE 10** Oxygen releasing process of  $\text{CeO}_2$  under  $10^{-7}$ ,  $10^{-13}$ , and  $10^{-21}$  torr oxygen partial pressure.

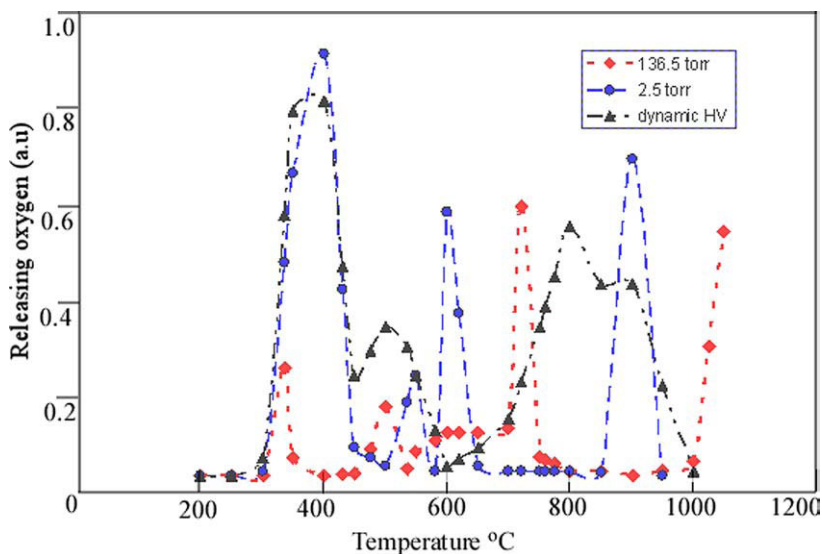


**FIGURE 11** Oxygen releasing of  $\text{PrO}_x$  under dynamic high vacuum, 2.5, and 136.5 torr oxygen partial pressures.

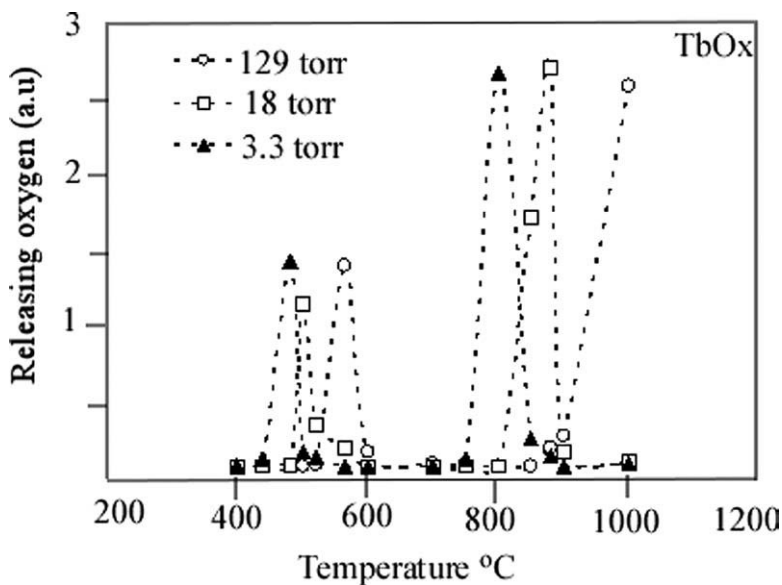


**FIGURE 12** Oxygen releasing of  $\text{TbO}_x$  under 3, 18, and 129 torr oxygen partial pressures.

Figures 11 and 12 show that the oxygen-releasing peaks of  $\text{PrO}_{2-\delta}$  and  $\text{TbO}_{2-\delta}$  have lower temperatures as the oxygen partial pressure is decreased, but the peaks values exhibit a mixed behavior.

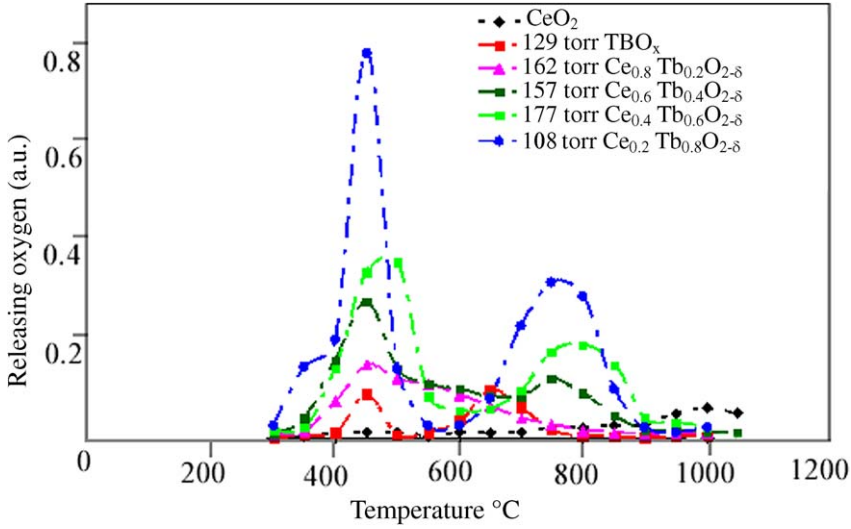


**FIGURE 13** Oxygen releasing of  $\text{Ce}_x\text{Tb}_{1-x}\text{O}_{2-\delta}$  oxides ( $x = 0.2, 0.4, 0.6, 0.8$ ) under oxygen partial pressure  $2 \times 10^{-4}$  torr.

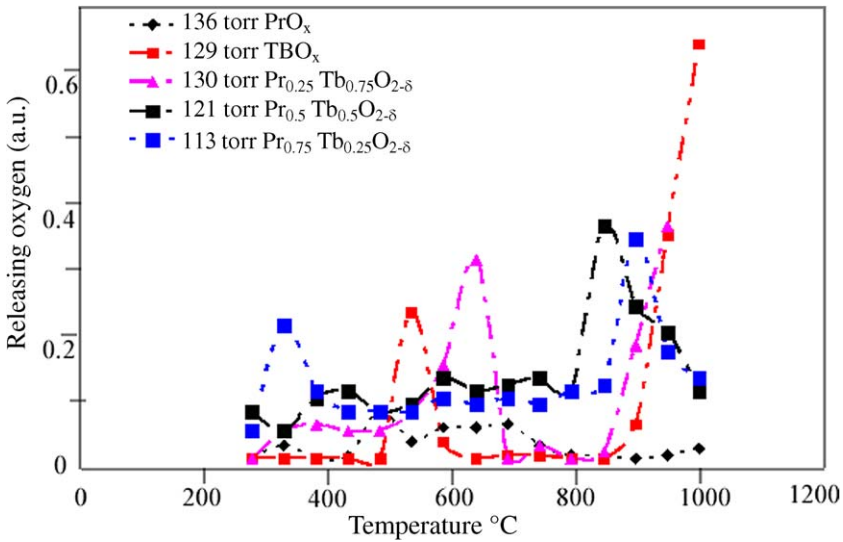


**FIGURE 14** Oxygen releasing of  $\text{Pr}_x\text{Tb}_{1-x}\text{O}_{2-\delta}$  oxides ( $x = 0.25, 0.5, 0.75$ ) under 113–136 torr oxygen partial pressure.

When a mixture of the Ce, Pr, and Tb oxides forms a solid solution of ternary oxides the oxygen-releasing peak is modified as shown in Figures 13 and 14 (Turcotte et al., 1973). In Figure 13 the mixture ratio of Ce and Tb elements is 8:2, 6:4, 4:6, and 2:8.

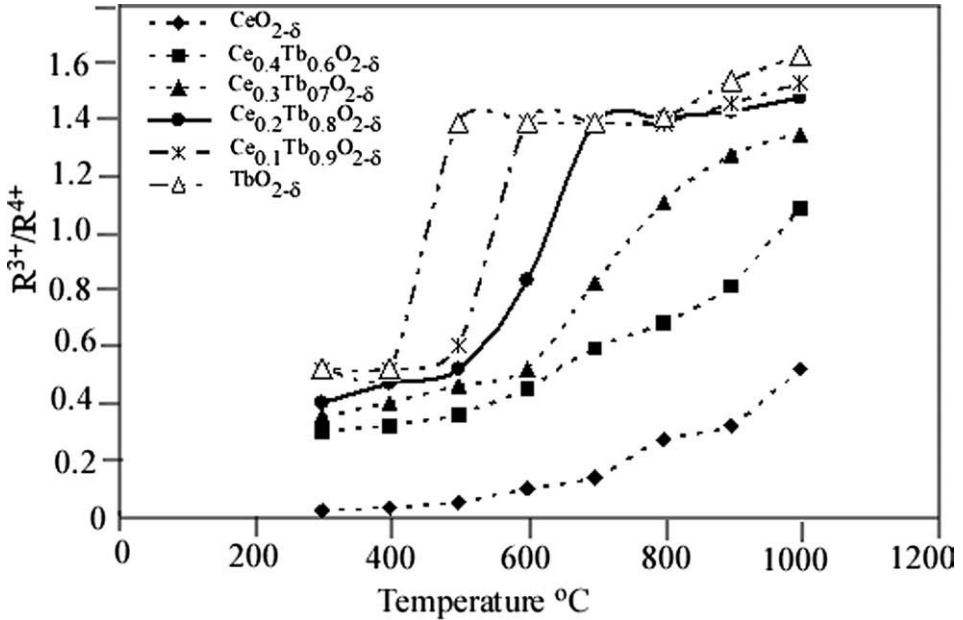


**FIGURE 15** The relationship between the valence ratio of  $\text{Ce}_x\text{Tb}_{1-x}\text{O}_{2-\delta}$  oxides ( $x = 0.1, 0.2, 0.3, 0.4$ ) and temperature under 55 torr oxygen partial pressure.

When the terbium content in the ternary oxides is increased, the oxygen-releasing peaks of these oxides move to lower temperatures and higher values. This shows that doping Tb into  $\text{CeO}_2$  will make  $\text{CeO}_2$  systems more easily reduced.

Under higher oxygen pressures, 113–136 torr, Pr doping into the  $\text{TbO}_{2-\delta}$  promotes the oxygen-releasing peaks to shift to lower temperatures, and even at 300 °C there is an oxygen releasing peak. For individual Ce, Pr, and Tb binary oxides there exist mixed valence state,  $\text{R}^{3+}/\text{R}^{4+}$ , which is controlled by the temperature and oxygen partial pressure. By varying the valence ratio would cause the oxygen releasing, a mixture of Ce, Pr, and Tb cations should influence the ratio of the  $\text{R}^{3+}/\text{R}^{4+}$  ions in ternary lanthanide higher oxides. Figure 15 is a plot of the valence ratio change of the  $\text{Ce}_x\text{Tb}_{1-x}\text{O}_{2-\delta}$  ternary oxides vs. the temperature, and indicates that as the Ce composition is increased the same valence ratio value moved to higher temperatures. This means that Ce promotes the Tb ions to preferring the  $\text{R}^{3+}$  state. Based on the knowledge of the Ce, Pr, and Tb mixed oxides it is possible to design a new oxides having a constant rate of releasing oxygen as the temperature is increased from room temperature to 1000 °C. In other words the oxide has widest non-stoichiometric range without any oxygen vacancy ordering in this temperature range (Kang and Eyring, 2000, 2001a, 2001b). Figure 16 shows that the oxygen content of  $\text{Ce}_{0.6}\text{Tb}_{0.2}\text{Zr}_{0.2}\text{O}_x$ , changes linearly from near  $\text{MO}_2$  to  $\text{M}_2\text{O}_3$  when the temperature increased from 200 to 1100 °C under 11 and 152 torr oxygen partial pressure. The oxygen releasing behavior of the  $\text{Ce}_{0.6}\text{Tb}_{0.2}\text{Zr}_{0.2}\text{O}_x$

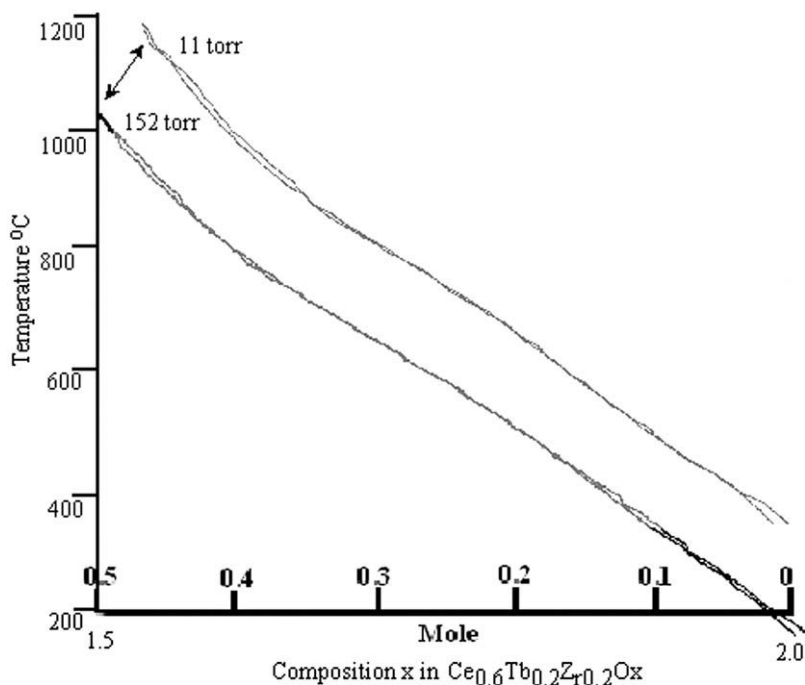


**FIGURE 16** Isobar data of the  $\text{Ce}_{0.6}\text{Tb}_{0.2}\text{Zr}_{0.2}\text{O}_x$  oxide under 11 and 152 torr oxygen partial pressure.

demonstrates the tunable feature of the valence variation and large oxygen storage capacity of the lanthanide higher oxides.

The oxygen releasing features of the lanthanide higher oxides is demonstrated in Figure 17, which shows the oxygen content changes with temperature or oxygen partial pressure swings. A temperature swing, for example of about  $\pm 20^\circ\text{C}$ , can induce a large or a small variation of the oxygen content of  $\text{RO}_x$  depended on the isobaric curve of the oxides. The oxygen partial pressure swing, for example  $\pm P_{\text{O}_2} = 10^{-2}$  torr, can also result in small and large variations of the oxygen content of  $\text{RO}_x$  based on the isotherm curve of the oxide. The oxygen partial pressure swing has been used in catalyst field as an Oxygen Buffer Capacity (OBC) (Bernal et al., 1997), and the temperature swing has been used to produce pure oxygen and hydrogen from methane and water (Otsuka-Yao-Matsuo et al., 1998; Kang and Eyring, 2000, 2001a, 2001b).

## 5. STRUCTURAL CHARACTERISTICS OF THE LANTHANIDE HIGHER OXIDES

Establishment of the structures of the lanthanide higher oxides, enabled scientists to find the structural principles involved, and this led to understand the relationships between the structures and properties over the past five decades. There

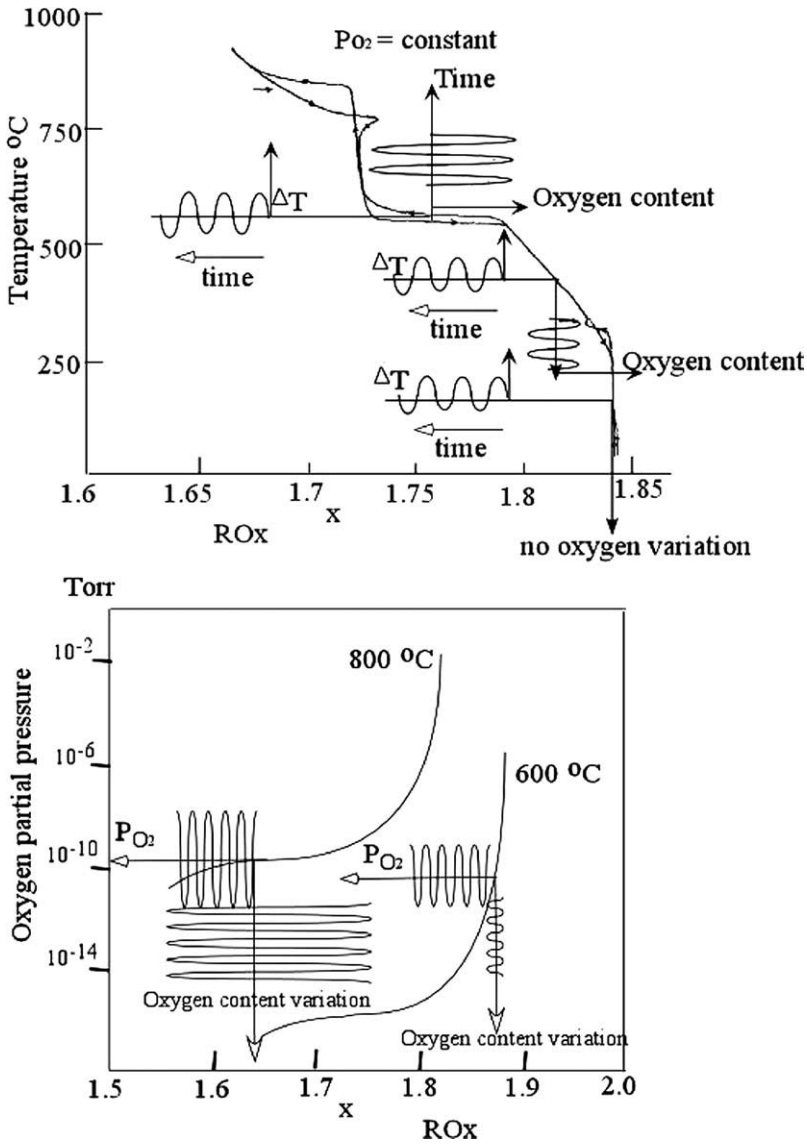


**FIGURE 17** A sketch of the oxygen content changes with temperature and oxygen partial pressure swings for the lanthanide higher oxides.

are number reasons why it has taken 50 years to achieve this knowledge. These include: (a) the synthesis of well ordered crystals of these higher oxides is inhibited by the extraordinary ease of transfer of oxygen between the higher oxides and the gas phase environment. (b) Although small crystals have been grown by hydrothermal techniques, large absorption errors and the formation of many superstructures of low symmetry have all combined to make definitive structural

studies a formidable task. (c) Twinning, and intergrowth between the phases (i.e. composition domains) contained in the tiny crystals make the collection of the diffraction data to be extremely difficult. Fortunately, the debate concerning the relationship between non-stoichiometry and structures promoted the achievement of the direct observation of the atomic arrangements in certain non-stoichiometric compounds. Cowley and Moodie's phase-grating theory and high-resolution electron microscopy (HREM) disclosed the relationship between the block structures and non-stoichiometry in the transition metal oxides (Cowley and Moodie, 1957; Cowley, 1981). Micro-diffraction techniques revealed structural information on the multi-twinning of the "linear phases", the "crystallographic shear" process, and "chemical/unit cell twinning" in many transition metal oxides (Bursill and Hyde, 1972; Buseck et al., 1988). HREM became a powerful tool and a "chemical laboratory" for obtaining the unit cell dimensions, space group, transformation matrices defining the unit cell, and the atomic arrangement of the lanthanide higher oxides.

## 5.1 Experimental electron diffraction data of the lanthanide higher oxides

Figure 18 gives the electron diffraction patterns of the oxygen-deficient fluorite-related homologous series of the lanthanide higher oxides. The diffraction patterns of the wide non-stoichiometric  $\alpha$ -phase also given in Figure 19. Based on the data of the experimental electron diffraction patterns the following points can be made: (1) the diffraction pattern of the lanthanide higher oxides, whether the oxygen vacancy is ordered or disordered, always has strong f.c.c. spots coming from the fluorite sublattice. (2) The superstructure spots always are running through the fluorite spots and have commensurate intervals between the fluorite spots along  $\langle 135 \rangle_F$  or  $\langle 220 \rangle_F$  direction except the  $n = 62$  phase. (3) The diffusion streaks of the non-stoichiometric phase are along  $\langle 220 \rangle_F$  direction. These intrinsic characteristics of the structures of the homologous series of the lanthanide higher oxides divulge the distributing rule of the oxygen vacancies in the fluorite sublattice of the homologous phases. A deep understand of this information will led to discovery of the structural principles of the homologous series of the lanthanide higher oxides.

## 5.2 Refined structures of the five homologous phases of the lanthanide higher oxides from experimental neutron diffraction data

By using the Rietveld refinements of the data obtained from neutron powder diffraction experiments of careful prepared  $\text{Pr}_7\text{O}_{12}$ ,  $\text{Pr}_9\text{O}_{16}$ ,  $\text{Tb}_{11}\text{O}_{20}$ ,  $\text{Pr}_{40}\text{O}_{72}$ , and  $\text{Pr}_{24}\text{O}_{44}$  samples, the structures of these phases have been determined. Figure 20 presents the structures in a  $\langle 211 \rangle_F$  projection corresponding to common  $[100]$  direction for almost all the phases. The locations for oxygen vacancy are marked by a vacancy centered tetrahedron. To assist the reader in understanding these tetrahedra, Figure 21 shows the relationship between the fluorite unit cell and the oxygen centered tetrahedron. The displacements of the metal and oxygen atoms also can

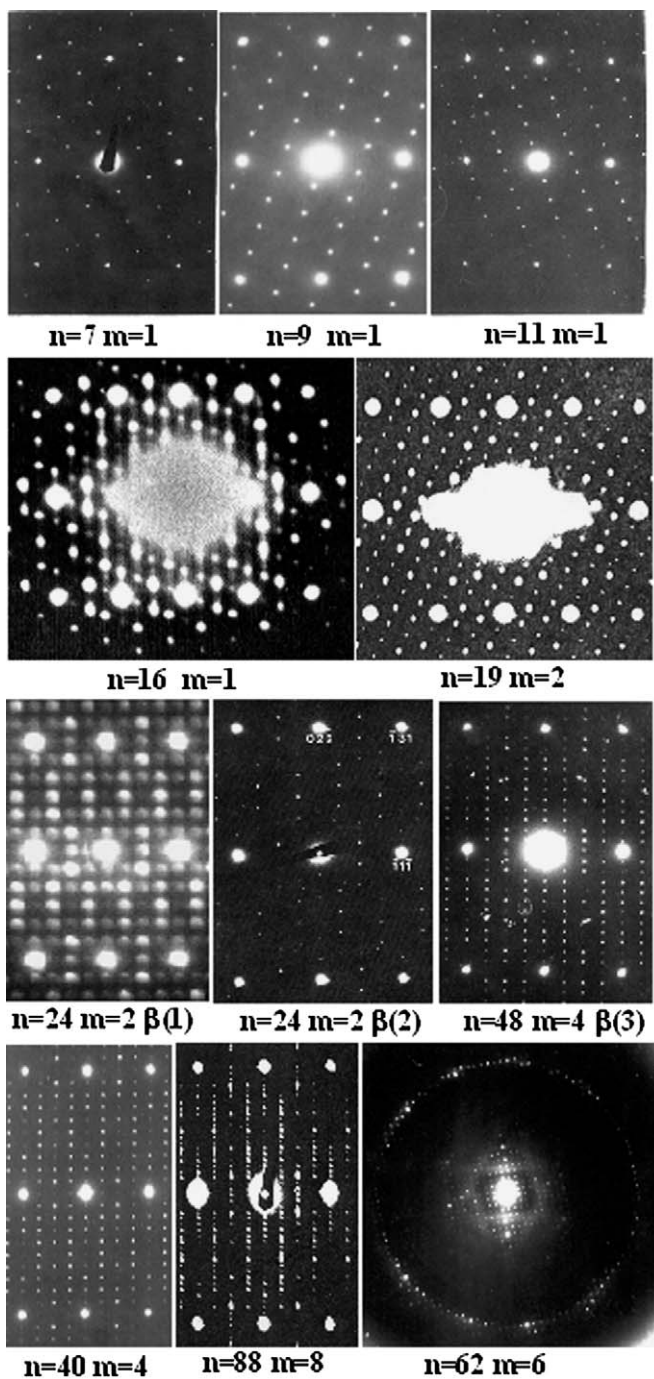


**FIGURE 18** Electron diffraction patterns of the homologous series phases of the lanthanide higher oxides.

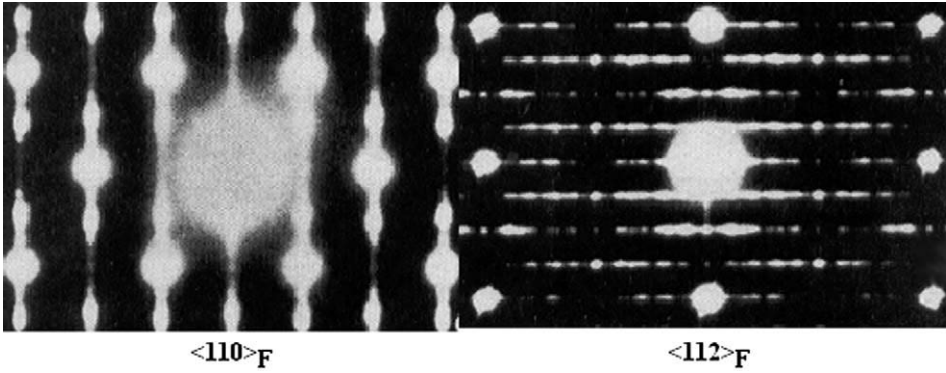


**FIGURE 19** Diffraction patterns of the  $\alpha$ -phase of the lanthanide higher oxides.

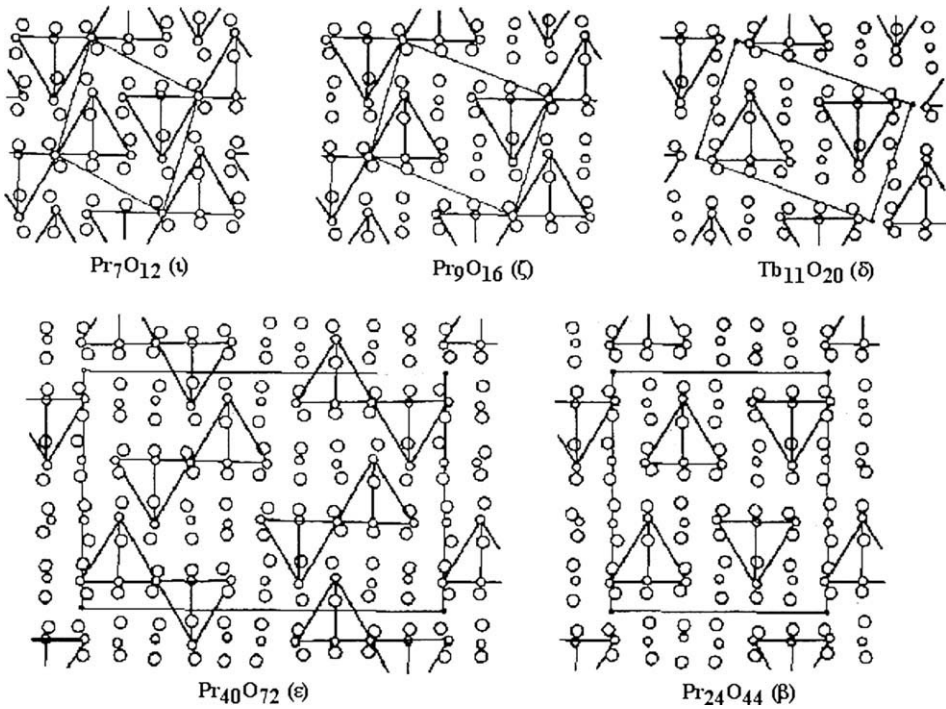


**FIGURE 20** The five structures of  $\text{Pr}_7\text{O}_{12}$ ,  $\text{Pr}_9\text{O}_{16}$ ,  $\text{Tb}_{11}\text{O}_{20}$ ,  $\text{Pr}_{40}\text{O}_{72}$ , and  $\text{Pr}_{24}\text{O}_{44}$  phases.

be seen in Figure 20. In Figure 21 the fluorite unit cell is outlined and the relationship between the eight tetrahedra and the fluorite structure can be clearly seen. The relationship between the structures and its electron diffraction patterns may be figured out.

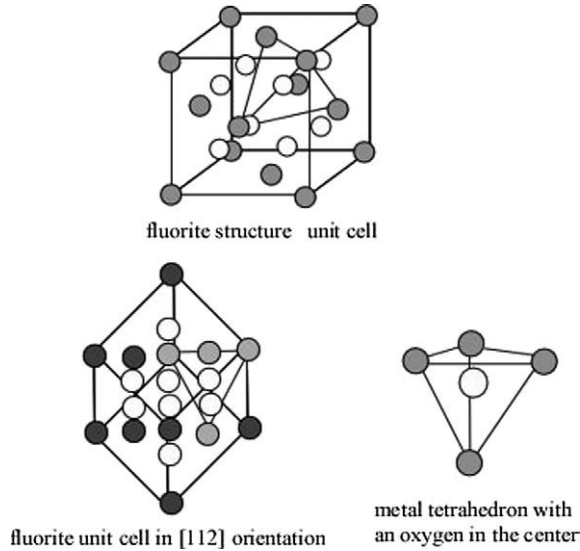


**FIGURE 21** Relationship between the fluorite structure and oxygen centered tetrahedron.

### 5.3 Fluorite-type module theory

In metals and alloys point defects generally obey statistical thermodynamics. In a binary oxide, of course, there are two elements: metal atoms and oxygen. The combination of metal and oxygen induces an interaction between the metal and oxygen atoms, which dominates the bonding as well as the distributing behavior of the atoms and the defects. For the lanthanide higher oxides the fluorite structure is the common relationships between the metal and oxygen atoms, which has been established by electron diffraction patterns. This fact means that oxygen vacancy is statistically distributed in the fluorite unit. The statistical rule: *the same circumstance should have the same possibility* guides us to analyze what is the "same circumstance" in fluorite unit cell. As Figure 21 shows, the eight oxygens are located in the center of the cation tetrahedron, and the cations have same valence flexibility. Therefore, each of the eight oxygen atom should have a statistically equal probability to be vacant. For the lanthanide higher oxides, the interaction between the metal and oxygen atoms is mainly ionic, but the valence state dominated by the relative position between the special narrow 4f band and Fermi level as mentioned above. In the binary lanthanide higher oxides each cation has same valence flexibility when the distance between cation–cation and cation–oxygen is modified. This special capability of mixed valences of the Ce, Pr, and Tb cations provide the electron hopping processes required to balance the electric charge due to an oxygen omission (vacancy). The neutralization of the electric charges can be achieved by the electron hopping.

Based on these fundamental rules *the eight oxygen atoms of a fluorite unit cell should have an a priori equal possibility to be vacant*. This implies that if there were only one oxygen vacancy in the system each site would have statistically a 1/8

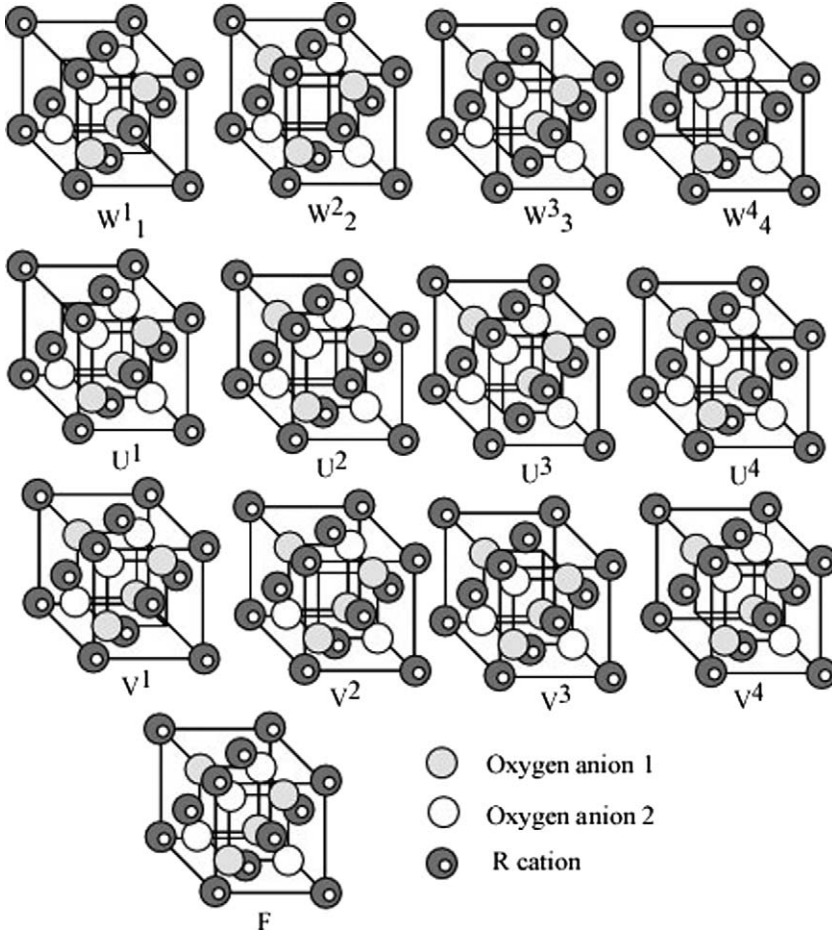


**FIGURE 22** Thirteen fluorite-type modules.

probability of being vacant. If eight oxygen vacancies exist in the system then there should be eight fluorite unit cells with a different oxygen site being vacant in each. This is why the fluorite-type module theory (Kang et al., 1996; Kang and Eyring, 1997a, 1997b) proposes 13 different fluorite-type modules as shown in Figure 22. (Previously  $U^i$  and  $D_j$  were used to denote the oxygen position at the oppositely orientated tetrahedra of an oxygen cube in a fluorite unit cell. Here we use  $U^i$  and  $V^j$  denote these two oxygen type sublattices. Although, the choice of either designation will yield the same structure model and are interchangeable in this respect.) It is expected that the new set of module designations will facilitate future discussions of the structure-property relationships such as the kinetics and mechanisms of structural changes and reactions as well as the compositional width of the stable phases. (Appendix A is a conversion table for transforming the earlier designations into the new set of modular names. These changes nothing in the

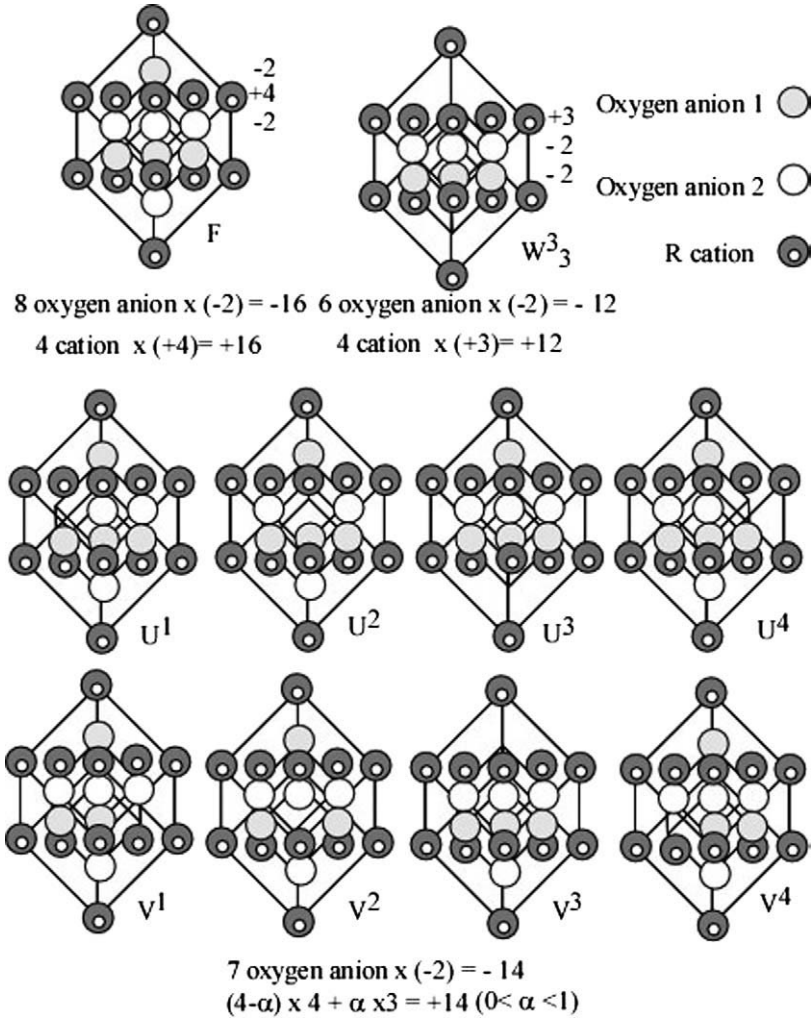


**FIGURE 23** The possible dipoles of the fluorite-type modules.

modeling procedure or the results described before.) The module ideas have been extended to the wide range of fluorite-related structures with vacancies in both anion and cation sites by Krivovichev (1999a, 1999b).

Figure 23 shows the charge distribution in the three types of modules. If we focus on a fluorite-type module, the missing oxygen atom in the fluorite unit cell induces an electric dipole in the fluorite-type module. The known structures of the lanthanide higher oxides show that the four cations surrounding an oxygen vacancy move away from the defect center by 0.2 Å while the six oxygen anions located in the immediate vicinity of the vacant oxygen site move toward the center by 0.3 Å. An oxygen vacancy belongs to one oxygen sublattice (for example  $U^i$ ), but the six oxygen atoms, which move toward the vacancy, belong to another oxy-

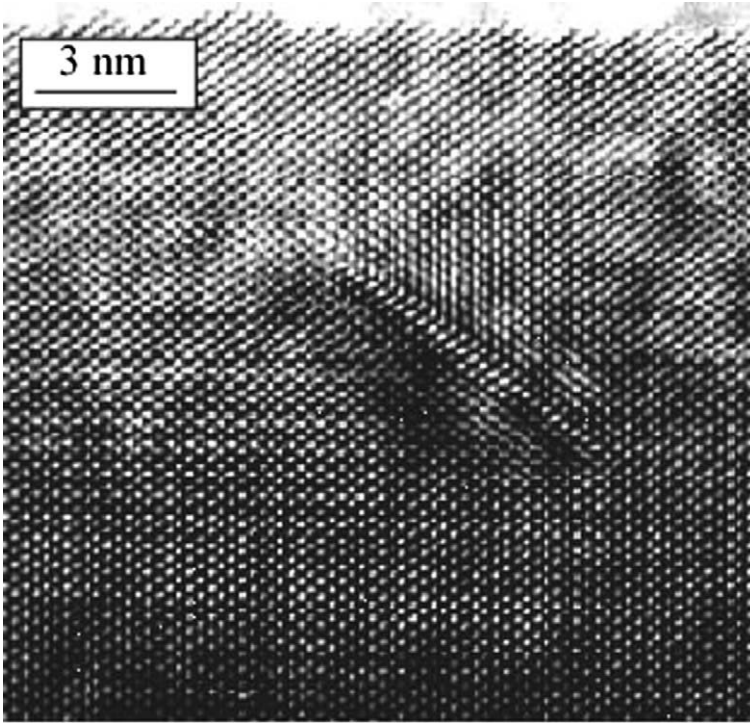


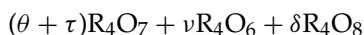
**FIGURE 24** The modulation contrast formed by the displacement of the cation and oxygen in PrO<sub>x</sub>.

gen sublattice ( $V^j$ ). These processes tend to neutralize the local charge and cause a distortion of the fluorite-type module. The symmetry of the f.c.c structure is broken thereby and an electron dipole must be created even though it may be small. The dipole direction is likely along  $\langle 111 \rangle_f$  of the fluorite structure. The interaction between the dipoles will increase the system energy. If the modules with a dipole can be stacked as sequences in which the dipoles are distributed sinusoidally the dipoles will cancel each other. A sinusoidal distribution may be the lowest energy configuration of these dipoles and can be related to the wave-type of the distortion distribution of the fluorite-type modules. From the point view of close-packing layers of the lanthanide cations and oxygen anions the sinusoidal distribution of the modules with an oxygen vacancy will cause the packing layers to be wrinkled. The wrinkling may become waves with a definite periodicity if the oxygen vacancies are ordered. The determined structures and HREM observation of the lanthanide higher oxides indicate that the modulation waves always exist in these systems as shown in Figure 24. When the modulation waves are swing away, then, one homologous phase changes to another homologous phase (Eyring and Kang, 1991). The distribution of "wave length" of the modulation would determine the normal oxygen content of a lanthanide higher oxide particle and this distribution

curve would be changed and result the oxygen content change as the temperature and oxygen partial pressure, where the oxide exist, vary.

#### 5.4 Rationalization of homologous series of oxygen-deficient fluorite-related lanthanide higher oxides and their compositional formula

If any phases of the lanthanide higher oxides are assembled by stacking the thirteen fluorite-type modules, then the composition of the oxide should have the compositional formula as follows:



in which  $R_4O_7$ ,  $R_4O_6$ , and  $R_4O_8$  are the compositions of modules with one, two, or none oxygen atoms missing respectively.  $\theta$ , and  $\tau$  are the numbers of the U and V type module with one oxygen missing.  $\nu$  and  $\delta$  are the numbers of modules with two or no oxygen missing, respectively.

If  $n$  designates the number of the fluorite-type modules in a unit cell of the homologous series phase and  $m$  is the number of times the eight oxygen sites have equally been vacant, then the composition of the homologous series is  $R_{4n}O_{8n-8m}$  where  $n = (\theta + \tau + \nu + \delta)$  and  $8m = (\theta + \tau + 2\nu)$ . This is called the modular generic formula and composition. If we use the number of each type of atom contained in a crystallographic unit cell as the generic chemical formula it would be  $R_nO_{2n-2m}$  since there are four atoms in each f.c.c. unit cell.

This formula rationalizes all of the experimentally discovered homologous phases. For example  $Pr_{88}O_{160}$  would have 88 modules and  $m = 8$ , which means it contains 16 oxygen vacancies in a crystallographic unit cell. Table 1 lists the values of  $n$  and  $m$  for all of the experimentally discovered phases in the lanthanide higher oxides.

#### 5.5 Coordination number of the lanthanide metal in the lanthanide higher oxides

The coordination number of a cation in a solid phase is an important parameter. It is well known that in the lanthanide higher oxides the coordination number of the lanthanide cation is 6, 7, or 8. Why do they have these numbers?

The coordination numbers of the lanthanide cation in these higher oxides depend on the type and numbers of the modules assembled in the phase. When one module is stacked upon another, then a cation located on the interface would be in both modules. The type of stacked module, as shown in Figure 25, determines the coordination number of the cation. The separation distance between the two oxygen vacancies dominates the Coulomb interaction energy of the system; the largest separation should be favorable since the shorter one has a higher Coulomb interaction energy.

Based on an analysis of the coordination number by assembling different type of modules, the stacking rules of the fluorite-type modules may be deduced. It appears that forming 8 and 7 coordinations is favorable energetically when any

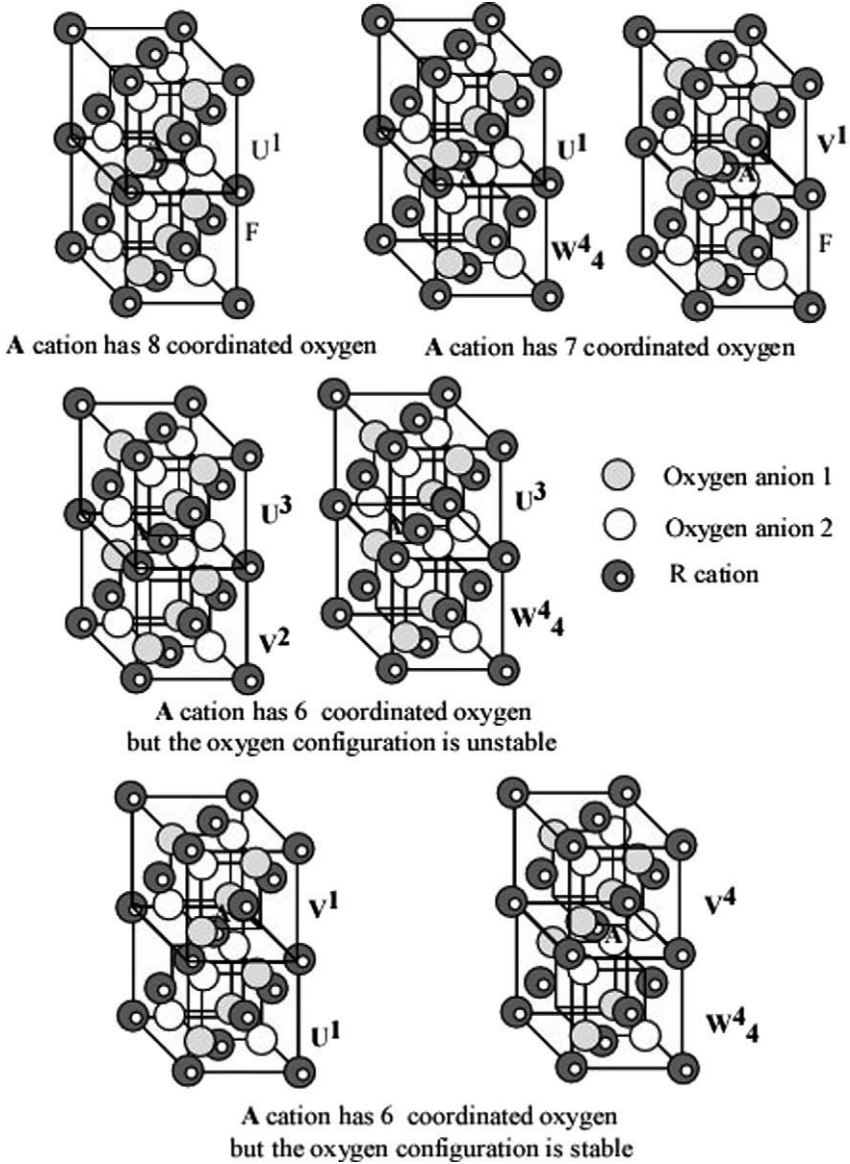


**FIGURE 25** Coordination number of the cation for various types of the module stacking.

two modules are connected to each other, but having coordination of 6 involves two extreme situations: one is unstable because it has high Coulomb interaction energy, but other is a low energy configuration.

Type of fluorite-type module can be easily changed by oxygen migration in the local oxygen sublattice. During such a process the eight possible oxygen sites are always held because the two oxygen sublattices should have equal charges to neu-

tralize system. The coordination number of a cation can be changed as the vacancy migrates from one site to another. Changing the coordination number should be related the valence variation of the cation due to the electron band structure modified by symmetry and the separation between the cation and the oxygen anion. The special electron configurations of Ce, Pr, and Tb atoms provide the ability to match with the coordination number variation.

## 5.6 Module type and average valence state of the lanthanide higher oxides

In the lanthanide higher oxides the most reduced phase is the sesquioxide and most oxidized one is the dioxide, the fluorite-type module W has 6 oxygen and 4 metal atoms (see Figure 23), which means the metal has a valence of 3+. If only W modules are stacked together, the cations can have only a coordination of 6, as occurs in the C-type structure of the lanthanide oxides. The cations in the F module obviously have a coordination of 8 and a valence of 4+. Therefore, the number of F, U, V, and W modules determines the average valence state of a lanthanide higher oxide. The more reduced phases would have more W modules and a less reduced phase would contain more F modules. The most oxidized phase would contain only F modules. For example, the  $R_7O_{12}$  ( $RO_{1.714}$ ) phase contains only one W module and the rest are U and V, but there is no F module. The  $R_9O_{16}$  only has one F module, but the  $R_{24}O_{44}$  contain 8 F modules. The oxidation reaction between the homologous phases can be written as module formula, and this formula may demonstrate the oxidation process in terms of the structural transformation. For example, the oxidation reaction,  $9Pr_7O_{12} + 2O_2 = 7Pr_9O_{16}$ , may be written as  $9(W3U3V) + 8O_2 = 7(F4U4V)$ , or  $9W + 8O_2 = 7FUV$ . This indicates that each of the 7W modules have to obtain 2 oxygen anions forming 7F, and the other 2W modules will each catch one oxygen anion forming UV. The reaction may be seen in a structural model shown in Figure 26. This structural model of the oxidation reaction of  $Pr_7O_{12}$  reveals that the elemental processes of the oxidation are the absorption of oxygen in the fluorite module at the surface of the crystal and the oxygen migration in the crystal. In the catalyst field, people talk about the surface and body oxygen of  $CeO_2$ , and that is the reason why the oxygen released from the surface and interstices of the  $CeO_2$  crystal required different energies. The energy barrier for oxygen migration is smaller than that for the oxygen escaping from an F module on the surface. The experimental and calculated data for the formation of an oxygen vacancy in the 111 facet of  $CeO_2$  is about 1.2 eV, but the energy barrier for the migration of an oxygen vacancy in  $CeO_2$  is about 0.7 eV. However, the energy barrier for the migration of an oxygen vacancy in  $CeO_x$  may be as small as 0.1 eV depending on the value of  $x$ .

## 5.7 Composition domains in the lanthanide higher oxides

The hysteresis loop of the oxygen content of the  $PrO_x$  and  $TbO_x$  is a obvious peculiar characteristic of the lanthanide higher oxides, but the hysteresis of the oxygen content of the  $CeO_x$  is difficult to observe directly in the isobaric curves because

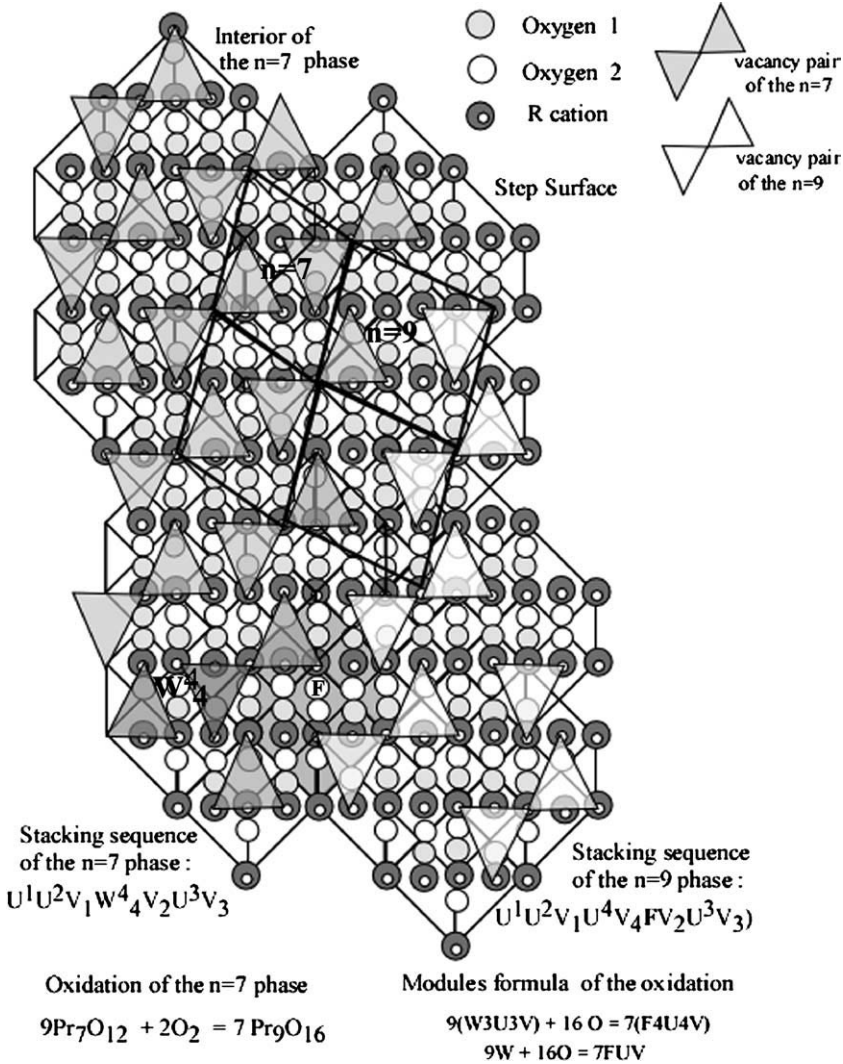
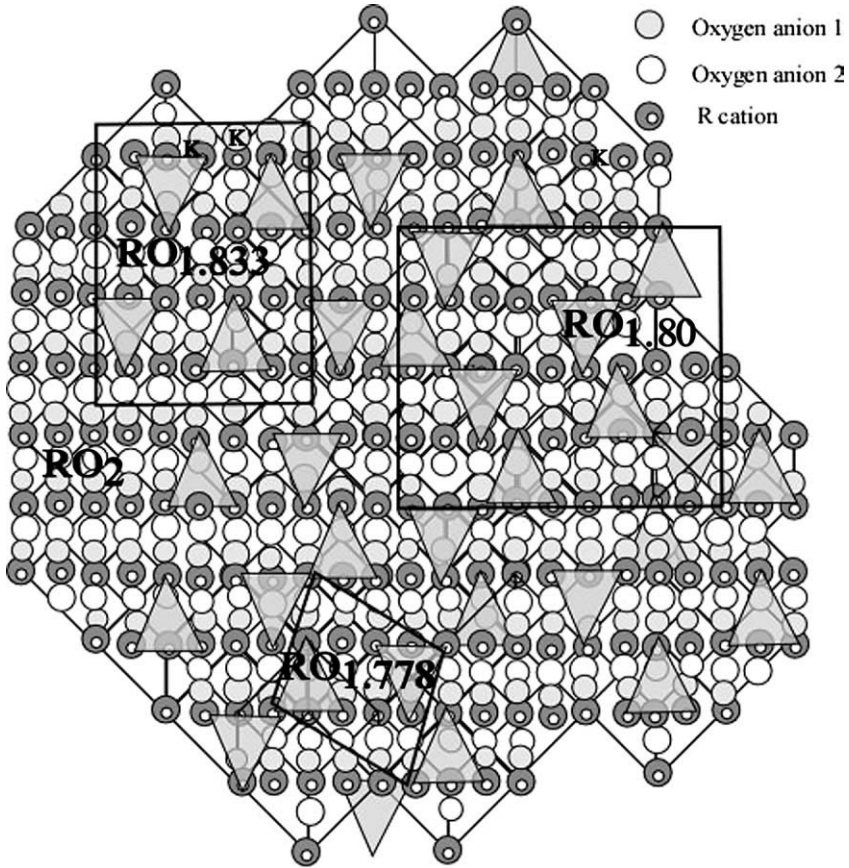


**FIGURE 26** The structural model of the reaction process between  $Pr_7O_{12}$  and  $Pr_9O_{16}$ .

the subtle differences in very low oxygen partial pressures (for example  $10^{-21}$  atm) and temperature changes will cause distinct variations of the oxygen content of the  $CeO_x$ . However, the hysteresis of the oxygen content of the  $CeO_x$  definitely exists (Bernal et al., 2005a, 2005b). The EEELs data from an E-cell HREM examinations also reveals this hysteresis (Sharma et al., 2004). The compositional domain structure is responsible for this phenomenon. As discussed in the module theory the composition of the lanthanide higher oxides depends on the number of different type of the modules. From structural view the cation sublattice is not changed eas-



**Compositional domains:  $RO_{1.778}$ ,  $RO_{1.80}$ ,  $RO_{1.833}$ ,  $RO_2$**

**FIGURE 27** Modules model of the compositional domains of  $RO_2$ ,  $RO_{1.833}$ ,  $RO_{1.80}$ ,  $RO_{1.778}$ .

ily until temperature exceeds to more than 1200 °C. But for the oxygen sublattice the oxygen vacancy content can be changed by the oxygen partial pressure in the vicinity of the oxide phase. The ordered oxygen vacancies in the oxygen sublattice may have different configurations in the different homologous phases with different oxygen content. Therefore a compositional domain can be formed. At certain oxygen partial pressure a definite configuration of the oxygen vacancies in the oxide can be established, forming a homologous phase. At other oxygen pressures and temperatures it is possible that there are several configurations of the oxygen vacancies, which existed simultaneously. Therefore the nominal composition would be the average oxygen content of the component ordered phases. This is how the wide non-stoichiometry of the lanthanide higher oxides can be formed. [Figure 27](#) illustrates this situation in the module model. It is clear that the cation sublattice is concreted with some distortion, but the oxygen vacancies on the oxy-

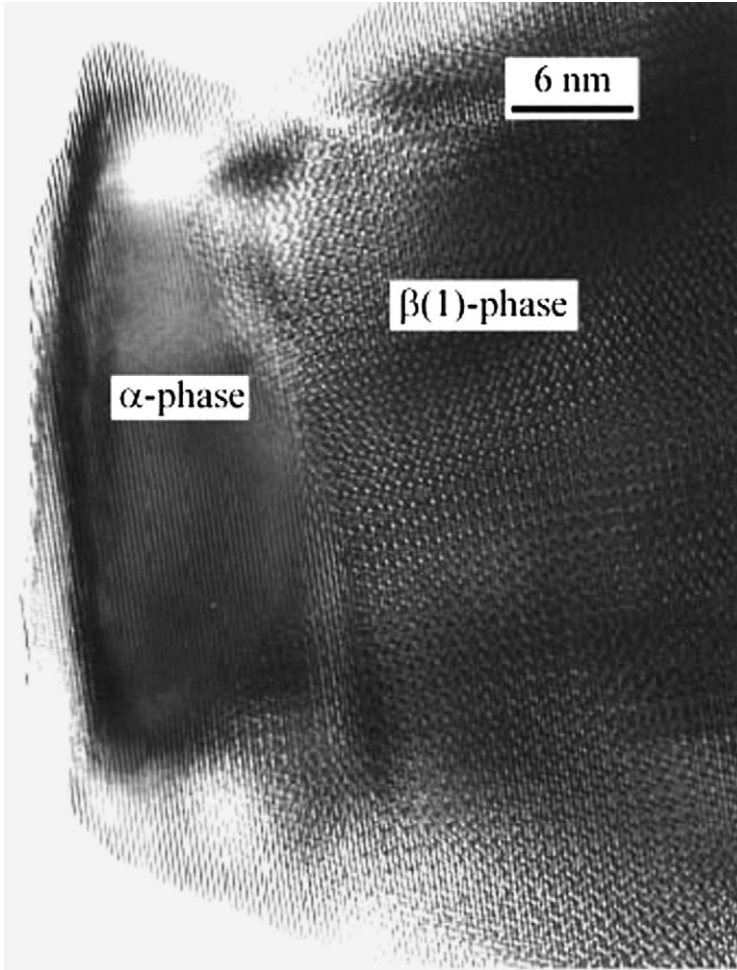


**FIGURE 28** Composition domains of  $\alpha$ -phase and  $\beta(1)$  phase ( $\alpha$ -phase is  $\text{PrO}_2$ , and  $\beta(1)$  phase is  $\text{PrO}_{1.833}$ ).

gen sublattice have different configurations, which induce different distortions. These distortions cause the superstructures of the different homologous series of the lanthanide higher oxides, if they are ordered. Figure 28 shows the composition domains of co-existing  $\text{PrO}_2$  and  $\text{Pr}_{24}\text{O}_{44}$ . The fluorite lattice is continuous in both phases, but the superstructures have different characteristic configurations of the oxygen vacancies.  $\text{PrO}_2$  domain does not have any oxygen vacancy, and only the fluorite lattice exists. The phase boundary between the homologous series is coherent and there is a vacancy concentration gradient between both sides of the phases. The driving forces for the phase boundary change are the chemical potential of the enthalpy and the configuration entropy of the oxygen vacancies.

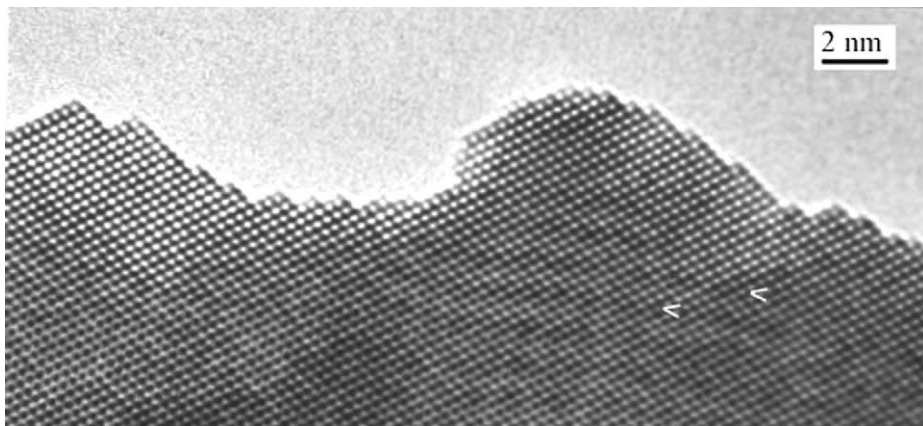


**FIGURE 29** Steps surface profile of a  $\text{TbO}_{1.833}$  crystal particles.

## 5.8 Surface character and oxygen migration

The lanthanide higher oxides have very good redox catalysis characteristic and a fast oxygen migration rate. The calculated surface energy of  $\text{CeO}_2$  indicates that the low energy (about 1.2 eV) surface is the  $\{111\}_F$  face (Sayle et al., 1992; Jiang et al., 2004, 2005a, 2005b). For the dissociation energy of oxygen molecule and the  $\text{Ce}^{4+}$  reduction on the  $\{111\}$  and  $\{110\}$  surfaces are same. High-resolution electron microscopy images (Figure 29) reveal that the surface with steps of the  $\{111\}$  facet is the surface characteristic of the lanthanide higher oxides (Kang et al., 1986, 1987; Kang and Eyring, 1992). The atoms on the  $\{110\}$  surface are more active than on the  $\{111\}$  surface. On the  $\{111\}$  surface the oxygen molecules on the outside are more easily dissociated to single atom, which is absorbed into an oxygen vacancy site, or an oxygen anion on an oxygen sublattice site is desorbed. Figure 30 demonstrates the atom movement of a nano-crystal with a twin-relationship to the bulk crystal. The columns of Tb atoms in the image are the black dots. The black arrows indicate the corners of the tiny twin, and the atoms on the up right corner of the twin are jumping as the time changes. The surface to the right side of the twin is a  $\{100\}$  type surface having a high energy and the atoms on this surface are more active and always try to be on the lower energy  $\{111\}$  facet as seen in these images.

The fast migration of oxygen in the lanthanide higher oxides is due to the characteristics of the fluorite structure and the valence variation of Ce, Pr, and Tb. The refined structures indicate that the four cations surrounding an oxygen vacancy move away from the defect center by 0.2 Å while the six oxygen anions located in the immediate vicinity of the vacant oxygen site move toward the center by 0.3 Å. That opens up the metal atom tetrahedron allowing the oxygen anions to move into the vacant site. If the oxygen vacancy is located underneath the surface, the relaxation of the metal atoms has larger value and the tetrahedron should be more opened up. Thus the site on the surface would have a higher activity for reaction.

Figure 31 shows a possible process of oxygen migration accompanying the valence variation due to the modification of the electron band structure and the

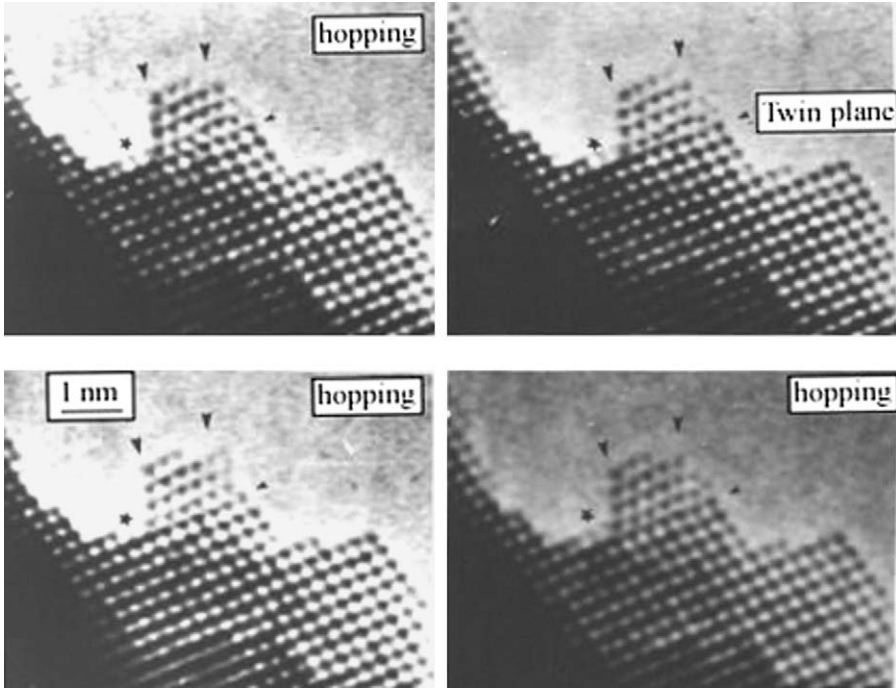


**FIGURE 30** The activity of the Tb atoms on the surface of {111} facets of  $\text{TbO}_x$ . The four arrows indicate the nano-twin crystal. The atoms at the right upper corner are very active during the electron beam radiation. Its temperature is about 600 °C. The left surface of this nano-twin is the {111} surface which has a low energy, and atoms at this surface are not active.

location of Fermi level (Jiang et al., 2005a, 2005b). The electrons in the narrow f band are favorable to become itinerant electrons when the distance between the two cations of a tetrahedron is increased due to the presence of an oxygen vacancy, while the distance between the shifted cations and the neighboring oxygen anions, which move toward the vacancy resulting in a regular tetrahedron, is decreased forming a p-f hybridized band. This exchange of the cerium atom f electron between the f orbit and p-f hybridized bands accounts for the valence flexibility of cerium. This valence flexibility promotes the oxygen migration process. In other words, the chemical potential of redox reaction causes the oxygen migration to be faster than the normal thermal diffusion.

If the lanthanide higher oxides, especially the cerium higher oxides,  $\text{CeO}_{2-\delta}$ , are used as an electrolyte in the intermediate-temperature solid oxide fuel cell (IT-SOFC), the driving force for the migration of the oxygen anion in the electrolyte are both the potentials of the oxygen concentration gradient and the redox reaction between the anode and cathode as shown in Figure 32. At the cathode side the oxygen partial pressure is 1 atmosphere (atm) and at the anode side the oxygen pressure is  $10^{-21}$  atm. The oxygen partial pressure (L) of the  $\text{CeO}_{2-\delta}$  electrolyte decreased as the curve shown in the Figure 32. The oxygen

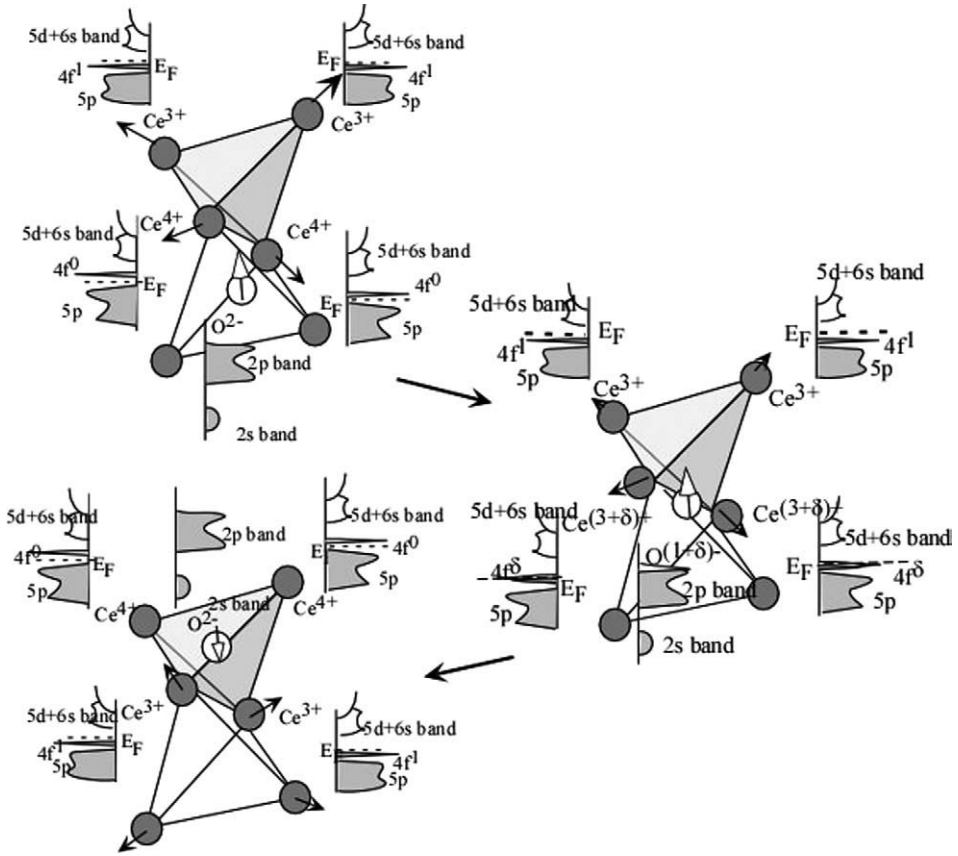


**FIGURE 31** The oxygen migration and the valence variation of the Ce cations.

content and possible phases of the electrolyte in the cross section of the electrolyte of the  $\text{CeO}_{2-\delta}$  at  $600^\circ\text{C}$  are shown in the Figure 32. The oxygen partial pressure dramatically falls near the cathode side and the oxygen vacancy concentration in this narrow region is small. The driving force for oxygen migration is mainly the potential of concentration gradient of the oxygen, and it is n-type conductor. In the center part of the electrolyte the oxygen partial pressure is low and it determines the compositional domains with different oxygen content (i.e. the corresponding homologous phases) in this region. The oxygen content is even lower near the anode side and correspondingly, the component homologous phases also vary. The most reduced phases existed beneath the surface of the anode depending upon the oxygen partial pressure near the surface of the anode. Usually it is  $\text{Ce}_{24}\text{O}_{44}$  ( $\text{CeO}_{1.833}$ ) or  $\text{Ce}_7\text{O}_{12}$  ( $\text{CeO}_{1.714}$ ).  $\text{Ce}_7\text{O}_{12}$  is a p-type conductor. The greater the reduced phase is, the easier it is to form carbon deposit on the anode.

The driving force of the migration of the oxygen anion is both the potential of the concentration gradient and the redox reaction between the homologous phases having different oxygen vacancy concentration. The migrating oxygen anion may

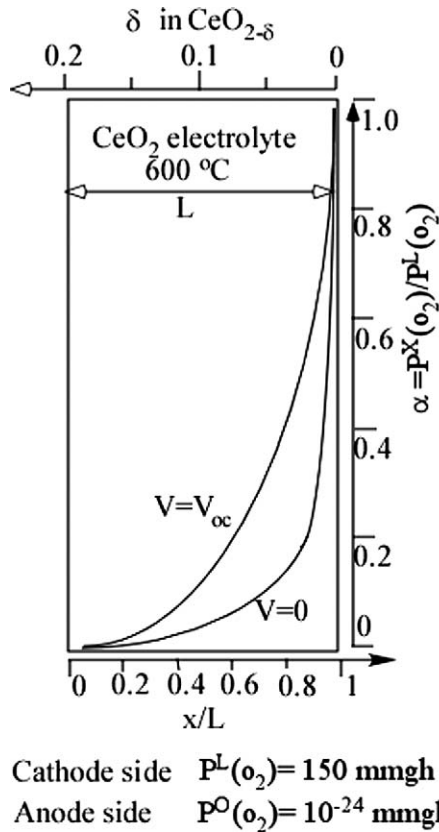


**FIGURE 32** The homologous phase of the  $\text{CeO}_{2-\delta}$  electrolyte between the cathode and anode as the oxygen partial pressure decreases from the cathode to the anode.

be trapped in some composition domain because it was oxidized under a certain condition, but in other regions the migration of the oxygen anion may be faster than thermal diffusion because the reduction reaction is underway. Therefore, the ionic conduction is higher in the lanthanide higher oxide.

### 5.9 Structural modeling the undetermined structure of the lanthanide higher oxides

Of the 15 experimentally known phases of the higher oxides only five of them have been determined by X-ray and neutron diffraction using the Rietveld refinements method. To understand the thermodynamic behavior and phase reactions it is helpful to have a model of the undetermined structures. Using the experimental electron diffraction data it is possible to determine the symmetry of the unit cell and develops a transformation matrix between the fluorite and ten of the intermediate phases as shown in Table 2. The module theory provides a method for modeling the unknown structures of the homologous series of the lanthanide

**TABLE 2** Homologous phases, space groups, and transformation matrix

Homologous phase	Space group	Transformation matrix
Ce <sub>7</sub> O <sub>12</sub>	R $\bar{3}$	2 $\bar{1}$ 1
Pr <sub>7</sub> O <sub>12</sub>		1 2 $\bar{1}$
Tb <sub>7</sub> O <sub>12</sub>		$\bar{1}$ 1 2
Pr <sub>9</sub> O <sub>16</sub>	P $\bar{1}$	2 0 1
		1 3 $\bar{1}$
		$\bar{1}$ 1 2
Ce <sub>19</sub> O <sub>34</sub>	P $\bar{1}$	2 $\bar{1}$ 2
		1 4 $\bar{1}$
		$\bar{1}$ 1 3
Pr <sub>40</sub> O <sub>72</sub>	P2 <sub>1</sub> /c	1 0 2
		1 5 $\bar{3}$
		$\bar{1}$ 5 3
Ce <sub>11</sub> O <sub>20</sub>	P $\bar{1}$	2 $\bar{1}$ 1
Tb <sub>11</sub> O <sub>20</sub>		1 3 $\bar{1}$
		$\bar{1}$ 2 2
Pr <sub>24</sub> O <sub>44</sub>	P2 <sub>1</sub> /c	1 0 2
		1 3 $\bar{3}$
		$\bar{1}$ 3 3
Tb <sub>48</sub> O <sub>88</sub>	P2 <sub>1</sub> /c(?)	2 0 2
		1 6 $\bar{3}$
		$\bar{1}$ $\bar{6}$ 3

higher oxides when electron diffraction data are available as is described below for two examples.

### 5.9.1 Proposed structure of the Pr<sub>88</sub>O<sub>160</sub> phase

In 1966 Hyde et al., showed that the tensimetric isobaric data for the praseodymium oxides indicated a stable phase with a composition PrO<sub>1.818</sub> at oxygen partial pressures of 30–205 torr in the temperature range 420–450 °C. This composition has not been prepared as a single phase because it easily decomposes to the  $\epsilon$ -phase, PrO<sub>1.778</sub>, during heating from the  $\alpha$ -phase, PrO<sub>1.833</sub>, or on cooling down from PrO<sub>1.80</sub>. The eutectoid reaction of PrO<sub>1.818</sub> always occurs and thus this phase co-exists with the other phases (Hyde et al., 1966).

The structural information had been reported by Turcotte et al. (1973), using high temperature X-ray diffraction. The electron diffraction pattern of the PrO<sub>1.818</sub> phase is completely different from those of CeO<sub>1.818</sub> and TbO<sub>1.818</sub> phases (see Figure 33) (Tuenge and Eyring, 1982).

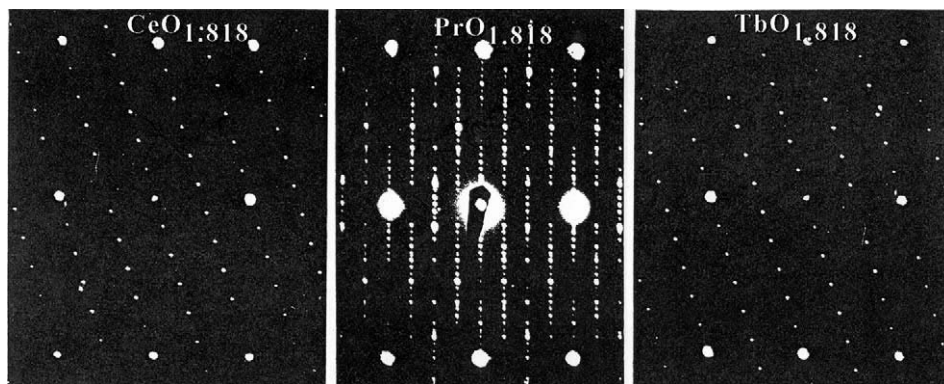


**FIGURE 33** Electron diffraction patterns of  $\text{Ce}_{11}\text{O}_{20}$ ,  $\text{Pr}_{88}\text{O}_{160}$ , and  $\text{Tb}_{11}\text{O}_{20}$ .

The known structures of the  $\text{Pr}_7\text{O}_{12}$  ( $\text{PrO}_{1.714}$ ),  $\text{Pr}_9\text{O}_{16}$  ( $\text{PrO}_{1.778}$ ), and  $\text{Pr}_{40}\text{O}_{72}$  ( $\text{PrO}_{1.800}$ ) phases indicate that pairs of oxygen vacancies may be favorable in forming the structures of the  $\text{PrO}_x$  phases, even though the  $\text{Pr}_{24}\text{O}_{44}$  phase ( $\text{PrO}_{1.833}$ ) has an isolated oxygen vacancy configuration. Based on the electron diffraction and module theory mentioned before,  $\text{PrO}_{1.818}$  should have 88 modules ( $n = 88$ ) and 8 times the eight oxygen sites to be equally vacant ( $m = 8$ ). The module content would be  $24\text{F}32\text{U}32\text{V}$ . It is impossible for  $\text{PrO}_{1.818}$  to contain any  $W$  modules because this phase is more oxidized than the  $\varepsilon$ -phase,  $\text{PrO}_{1.778}$ , which has no  $W$  modules in its structure. The  $W$  module, however, may appear because it is directly related to the  $\iota$ -phase  $\text{Pr}_7\text{O}_{12}$  ( $\text{PrO}_{1.714}$ ), for example  $n = 19$  and  $62$ . All of this information should be kept in mind as well as the unstable stacking of a pair of oxygen vacancies, which should be avoided.

To build a structural model is important to have the space group information. The known structure of  $\text{Pr}_{40}\text{O}_{72}$  has the space group,  $P2_1/c$ . The electron diffraction patterns of the  $\text{Pr}_{40}\text{O}_{72}$  and  $\text{Pr}_{88}\text{O}_{160}$  phases are almost same except of the numbers of the superstructure spots. Therefore, using the space group,  $P2_1/c$  and the 88 modules was constructed to a model fit the unit cell obtained from the experimental electron diffraction pattern. Figure 34 shows the proposal structure for this phase.

A comparison of the calculated and the experimental diffraction patterns seem to agree with each other (Kang and Eyring, 2006).

The proposed structure contains both the single and pair oxygen vacancies. The arrangement of the isolated oxygen vacancy is similar to observed in the  $\text{Tb}_{11}\text{O}_{20}$  phase, but the configuration of the pair oxygen vacancies are similar to those found in the structure of  $\text{Pr}_{40}\text{O}_{72}$  ( $\text{PrO}_{1.800}$ ). This structural feature may be the reason having the eutectoid reactions of the  $\text{PrO}_{1.818}$  between the  $\text{Pr}_{40}\text{O}_{72}$  (1.80) and  $\text{Pr}_{24}\text{O}_{44}$  (1.833). When the oxygen partial pressure is increased the pair oxygen vacancies become an isolated single vacancy in  $\text{Pr}_{24}\text{O}_{44}$ . But when the oxygen partial pressure is decreased the isolated single oxygen vacancy will become a pair

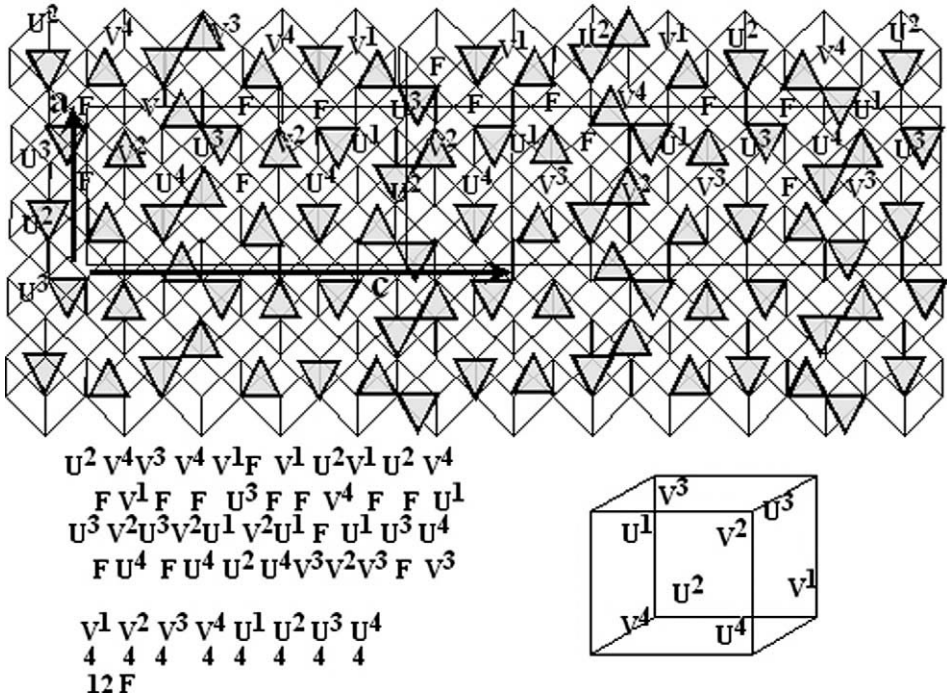


**FIGURE 34** The proposed structure of the  $Pr_{88}O_{160}$  phase (after Kang and Eyring, 2006).

configuration as in  $Pr_{40}O_{72}$ . This structure is extremely sensitive to the variation of oxygen partial pressure.

### 5.9.2 Proposal structure of the $Ce_{19}O_{34}$ phase

The  $Ce_{19}O_{34}$  phase was found when cerium dioxide was reduced by hydrogen in electron microscope. The diffraction pattern in the  $[211]_F$  direction is given in Figure 35. There are 19 superstructure spots along the direction  $[4-21]_F$ , and the electron diffraction pattern has the symmetry of the space group,  $P\bar{1}$ . The unit cell is a triclinic with an inversion center as shown in Figure 35.

At the time the  $Ce_{19}O_{34}$  phase was discovered the homologous formula in use was as  $R_nO_{2n-2}$ , and therefore, a contraction between the experimental composition and the calculated one existed, that is, the composition calculated from the formula  $R_nO_{2n-2}$  is  $CeO_{1.895}$ , but the experimental composition was close to  $CeO_{1.714}$ . This contraction remained for decades. But by utilizing the module theory, this contraction was solved (Kang and Eyring, 1997a, 1997b). Using  $m = 2$ , the module theory indicates the composition should be  $Ce_{19}O_{34}$  or  $CeO_{1.789}$ , which is close to  $CeO_{1.714}$ . Based on this result the structure of this phase should have 19 modules as  $3F8U8V$ . Because this phase is close to  $n = 7$  phase there are two possible solutions: one does not contain a  $W$  module (i.e.  $3F8U8V$ ), while the other one has a  $W$  (i.e.  $4FW7U7V$ ). The proposal structure is shown in Figure 36. The structure, however, contains a  $W$  module and it indicates the  $W$

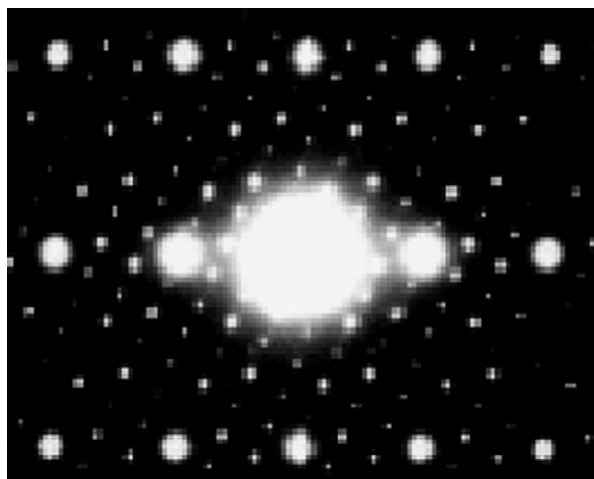


**FIGURE 35** Electron diffraction pattern of the  $Ce_{19}O_{34}$  phase.

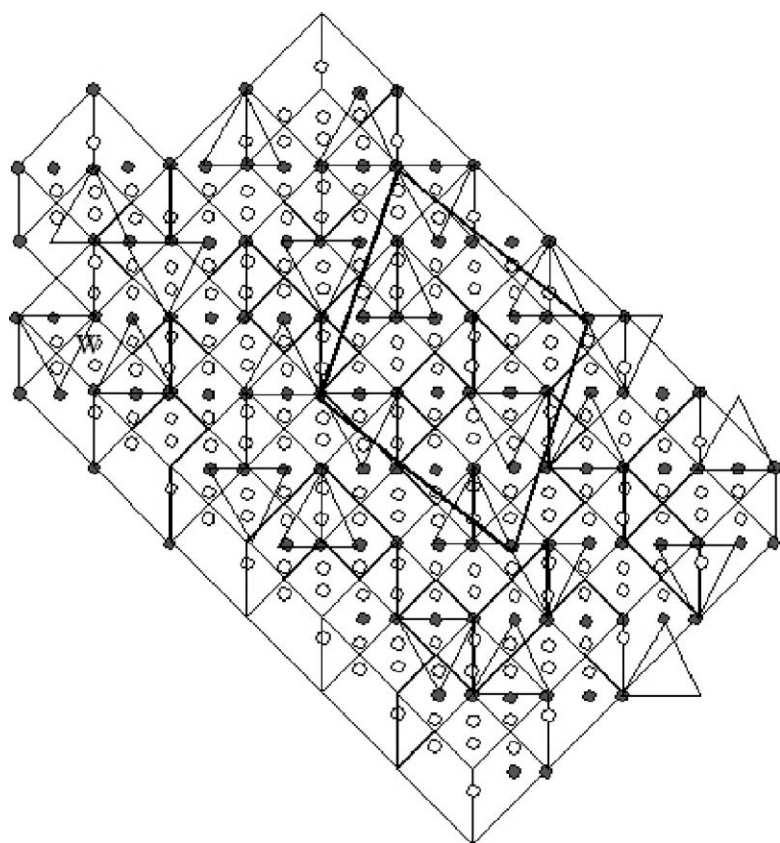


**FIGURE 36** The proposed structure of the  $Ce_{19}O_{34}$  phase.

modules in the  $n = 7$  phases are not completely dissociated (Kang and Eyring, 1997a, 1997b).

### 5.10 From the binary oxide to the ternary oxide

The binary lanthanide higher oxides,  $\text{CeO}_x$ ,  $\text{PrO}_x$ , and  $\text{TbO}_x$  have oxygen-deficient, fluorite-related structures. In these structures the cations occupy the same positions in the structure, and they have same valence flexibility. For the anion the coordinated environment for every oxygen site is same. Therefore, the entropy and the Coulomb interaction energy dominate the oxygen vacancy distribution. The subtle differences of the electron configurations between Ce, Pr, and Tb lead to the formation of oxides with a Ce, Pr Tb mixture having a wide range of non-stoichiometry. This means that the ordering process is probably hindered by the subtle difference of the valence flexibility of the Ce, Pr, and Tb (Sovestnov et al., 1994).

Doping with a fixed valence element, for example Zr, would limit the occupation possibilities of an oxygen vacancy on the fluorite sites also. For example,  $\text{Zr}_{0.5}\text{Ce}_{0.5}\text{O}_{2-\delta}$  has an oxygen vacancy ordered phase with the pyrochlore-type structure shown in Figure 37. Figure 37 shows the electron diffraction pattern and the module model for this phase. The Zr cations have fixed valence 4+ and they are not ordered. The oxygen vacancies in this oxide are distributed around the reduced cerium cations. Therefore, the probability of an oxygen site being vacant for the tetrahedron with Zr should be different, and then the modules for constructing the structure are limited. The composition domains are inevitable. Figure 38 is the high resolution electron microscopic image of this phase (Kang, 2006).

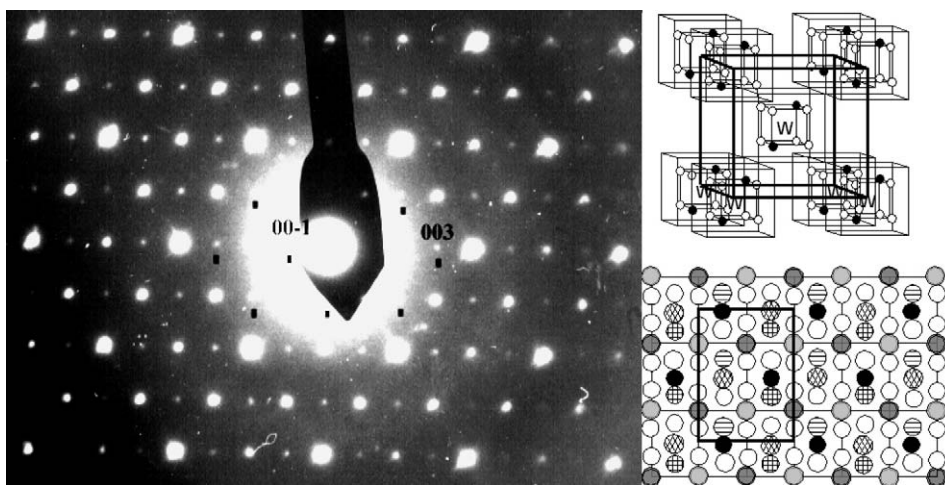


**FIGURE 37** The electron diffraction pattern of the pyrochlore-type phase and the module model.

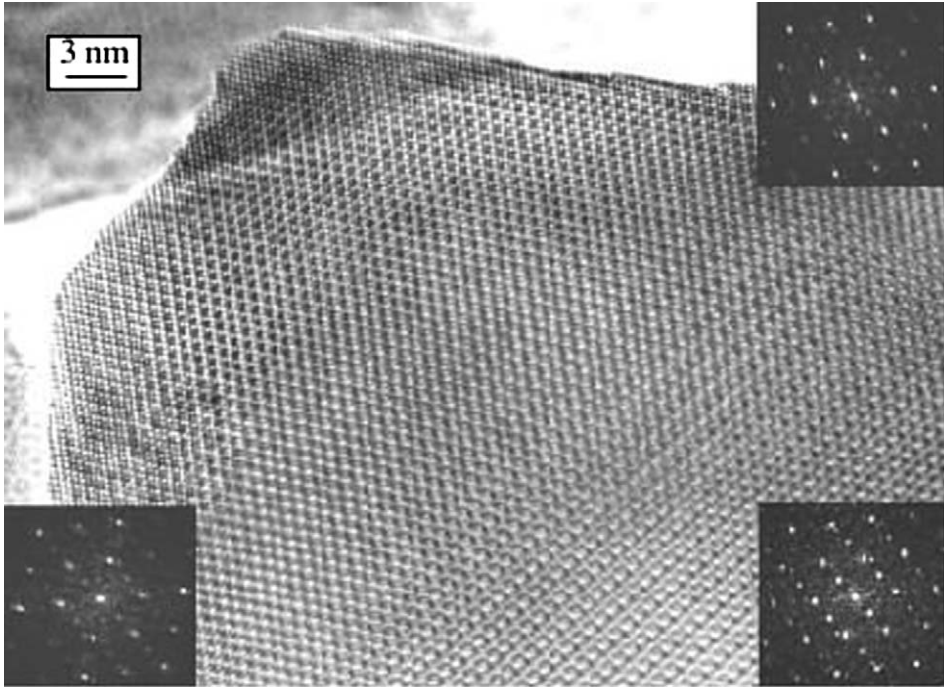


**FIGURE 38** The high resolution electron microscopic image of the pyrochlore-type phase of  $\text{Ce}_{0.5}\text{Zr}_{0.5}\text{O}_{2-\delta}$ .

## 6. CONDUCTIVITY AND CATALYTIC PROPERTIES OF THE LANTHANIDE HIGHER OXIDES

The lanthanide higher oxides have not only peculiar thermodynamic properties, but also unique physical and chemical properties. The physical and chemical properties are presented as a macroscopic parameter, such as the electrical conductivity, the coefficient of expansion, and the conversion rate of a catalysis process. Due to the lack of knowledge of the wide range of non-stoichiometry of the oxygen-deficient fluorite-related homologous series of the lanthanide higher oxides, the macroscopically measured data of the physical and chemical properties are scattered, and therefore, based on the structural principle of the module ideas a deep understanding the relationship between the properties and structures is needed.

### 6.1 Electrical conductivity of the lanthanide higher oxides

As discussed in previous sections the phase relationships in the lanthanide higher oxides of Ce, Pr, and Tb are quite complex and sensitive to environmental conditions, especially the oxygen partial pressures. Unless extreme care is taken, the property measurements will be on inadequately characterized materials.

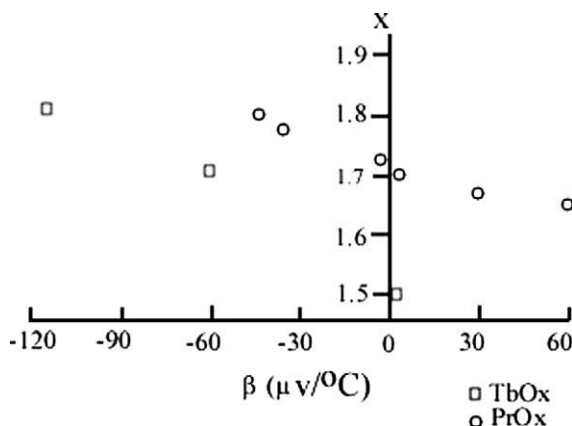


**FIGURE 39** The Seebeck coefficient,  $\beta$ , vs.  $x$  for  $\text{TbO}_x$  and  $\text{PrO}_x$ . It indicates that  $\text{Tb}_2\text{O}_3$ , and  $\text{PrO}_x$  ( $x < 1.728$ ) are  $p$ -type ( $\beta > 0$ ), and  $\text{Tb}_7\text{O}_{12}$ ,  $\text{Tb}_{11}\text{O}_{20}$ , and  $\text{PrO}_x$  ( $x \geq 1.728$ ) are  $n$ -type ( $\beta < 0$ ) conductors. (The data are from Honig et al., 1964; Rao et al., 1970).

The lanthanide higher oxides exhibit mixed conduction with electron hopping. The conductivity of the binary higher oxides in the composition range between  $\text{RO}_{1.5}$  and  $\text{RO}_{1.75}$  is  $p$ -type, but in the range  $\text{RO}_{1.75}$ – $\text{RO}_{2.0}$  it is  $n$ -type (Honig et al., 1964; Rao et al., 1970). Based on the data of Honig et al. and Rao et al., the Seebeck coefficient,  $\beta$ , vs.  $x$  of  $\text{RO}_x$  (Figure 39) indicates that  $\text{Tb}_2\text{O}_3$ ,  $\text{Pr}_7\text{O}_{12}$ , are  $p$ -type ( $\beta > 0$ ), but  $\text{Tb}_7\text{O}_{12}$ ,  $\text{PrO}_x$  and  $\text{TbO}_x$  ( $x > 1.714$ ) are  $n$ -type ( $\beta < 0$ ) conductors. Because the oxygen content of the higher oxides is dominated by the oxygen partial pressure, the conductivity of the lanthanide higher oxide has to be measured as a function of the oxygen partial pressure. The conductivity is sensitive to the structure of the solid, and based on the conductivity change the transition process between the homologous series of the lanthanide higher oxides can be monitored (Inaba and Naito, 1983a, 1983b; Inaba et al., 1980; Inaba et al., 1980, 1981a, 1981b, 1981c).

Figure 40 presents the conductivity of  $\alpha$ -phase of  $\text{PrO}_x$  oxides, which varies as a linear function of the oxygen partial pressure. This indicates that the lanthanide higher oxides with disordered oxygen vacancies are  $n$ -type conductors.

In the IT-SOFC the electrolyte of  $\text{CeO}_{2-\delta}$  has different homologous phases distributed in its cross section due to the oxygen partial pressure decreasing from 1 atm to  $10^{-21}$  atm from the cathode to the anode (see Figure 32). Beneath the anode surface the most reduced phase, usually  $\text{Ce}_{24}\text{O}_{44}$ ,  $\text{Ce}_{19}\text{O}_{34}$ , and/or  $\text{Ce}_7\text{O}_{12}$ , may exist, but at cathode side the disordered  $\alpha$ -phase  $\text{CeO}_x$  with  $x \approx 1.98$  may occur. This indicates that the intrinsic conductivity of the electrolyte of  $\text{CeO}_{2-\delta}$  varies from  $n$ -type to  $p$ -type with the oxygen partial pressure change from the cathode to the anode side. The configuration of the oxygen vacancies in the  $\text{CeO}_{2-\delta}$  electrolyte is modified from the isolated single vacancies near the cathode to the oxygen vacancy pairs at the anode side. If the temperature and/or oxygen partial pressure is changed an oxygen vacancy pair may dissociate to an isolated single vacancy. There are two activation energies for the migration of an oxygen anion

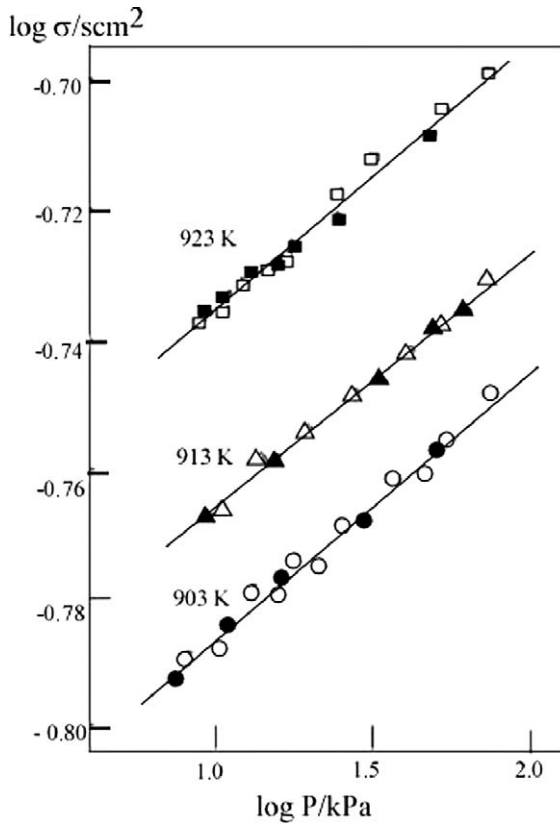


**FIGURE 40** The conductivity of the  $\alpha$ -phase of  $\text{PrO}_x$  as a function of the oxygen partial pressure at three different temperatures (after Inaba et al., 1981a, 1981b, 1981c).

in this electrolyte: one corresponding to the isolated oxygen vacancy and other to the oxygen vacancy pair. The electric conductivity is negligible near the cathode side, but measurable near the anode surface. The conductivity, including ionic and electronic, in the  $\text{CeO}_{2-\delta}$  electrolyte depends on both temperature and the oxygen partial pressure. A lack of knowledge of either the temperature or the oxygen partial pressure will lead to incomprehensive data.

## 6.2 Conductivity of the ternary lanthanide higher oxides

In oxygen-ionic conductors the conduction occurs by the transfer of anion vacancies such as  $\sigma_v = C_v q_v \mu_v$  ( $C_v$  is the number of anion vacancies per unit volume ( $\text{cm}^3$ );  $q_v$  is charge of a vacancy, and  $\mu_v$  is the mobility of charge carriers), and it is related to the diffusivity of the oxygen vacancy. The configuration of the oxygen vacancies determines the diffusivity of the oxygen vacancy (Shuk and Greenblatt, 1999). In the lanthanide higher oxides the configuration of the oxygen vacancies is closely related to its non-stoichiometry, which determined by the oxygen partial

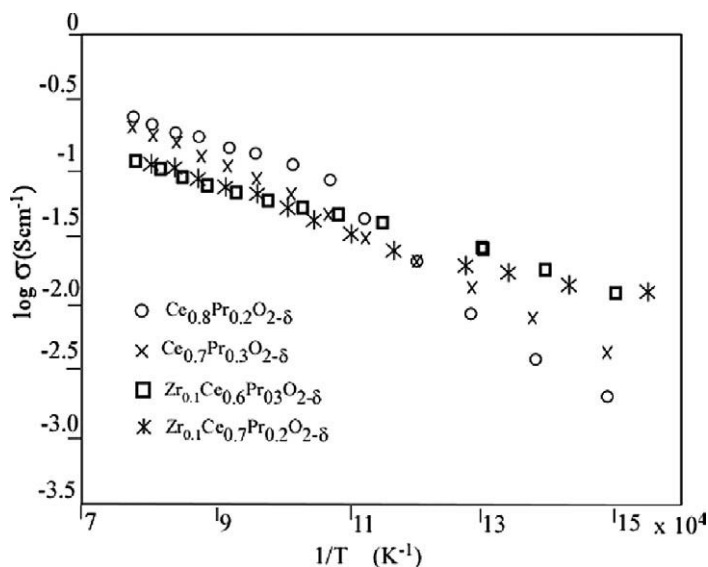


**FIGURE 41** The total conductivity of  $\text{Ce}_{0.8}\text{Pr}_{0.2}\text{O}_{2-\delta}$ ,  $\text{Ce}_{0.7}\text{Pr}_{0.3}\text{O}_{2-\delta}$ ,  $\text{Ce}_{0.6}\text{Pr}_{0.3}\text{Zr}_{0.1}\text{O}_{2-\delta}$ , and  $\text{Ce}_{0.7}\text{Pr}_{0.2}\text{Zr}_{0.1}\text{O}_{2-\delta}$  under one atmosphere pressure (after Fagg et al., 2005).

pressure and the electron structure of Ce, Pr, and Tb. There are many reports on the ionic conductivity of the doped  $\text{CeO}_2$ , but only a few publications demonstrate the ionic conductivity of the oxides with a mixture of Ce, Pr, and Tb. Takasu et al. (1984) reported the ionic conductivity and the transference number,  $t_o$ , of the oxygen ions in the  $\text{Ce}_x\text{Pr}_{1-x}\text{O}_{2-\delta}$  oxides. They demonstrate that as the praseodymium content is increased,  $t_o$  decreases and the conductivity dominated by electrons. Fagg et al. (2005) recently reported that doping Zr in the  $\text{Ce}_x\text{Pr}_{1-x}\text{O}_{2-\delta}$  oxides might improve the conductivity of  $\text{Ce}_x\text{Pr}_{1-x}\text{O}_{2-\delta}$  oxides as shown in Figure 41. They also indicated that both the ionic and electric conductivities decreased with decreasing oxygen partial pressure,  $p(\text{O}_2)$  and attributed this to the increase of the associated oxygen vacancies and the decrease of the mobile electronic charge carriers. As mentioned above when the concentration of the oxygen vacancies is high the pair oxygen vacancies configuration is favorable in  $\text{PrO}_x$  higher oxides, and thus the experimental data is understandable. Fagg et al. (2005) also indicated the ion transference number increased with increasing temperature and but is not influence significantly by decreasing the oxygen chemical potential.

### 6.3 Catalytic properties of the lanthanide higher oxides

The lanthanide higher oxides can easily release the lattice oxygen at lower oxygen partial pressures. Methane and carbon monoxide can be oxidized by the released oxygen from the higher oxides. Figure 42 shows the oxidation process of the carbon monoxide by the cerium higher oxide as the temperature is increased. As seen in Figure 43 the reduced cerium higher oxides is more efficient in oxidizing the

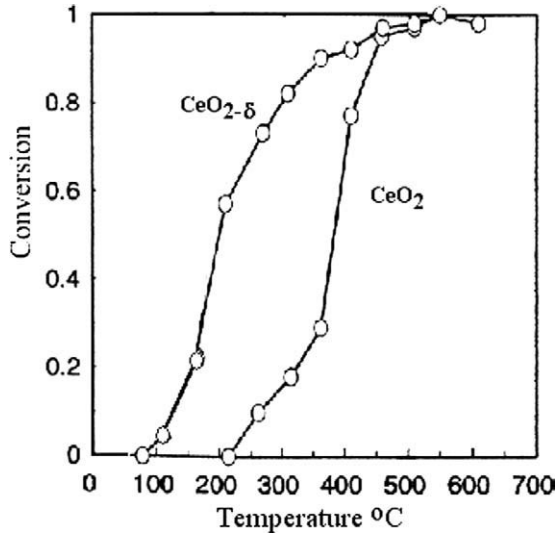


**FIGURE 42** Oxidation of carbon monoxide by cerium dioxide and a reduced cerium higher oxide as a function of temperature.

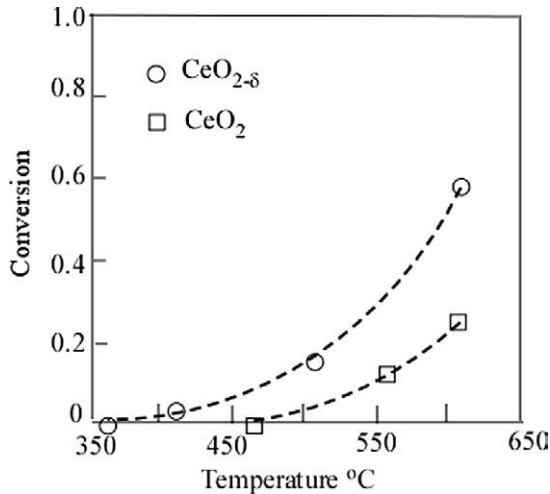


**FIGURE 43** Methane oxidation by CeO<sub>2</sub> and a reduced cerium higher oxide vs. temperature.

monoxide. A similar situation also occurs in the oxidation of methane as shown in Figure 43.

Doping Tb into CeO<sub>2</sub> can move the oxygen releasing peaks into lower temperature (see Section 5.1) and that may promote the oxidation methane. Figure 44 demonstrates the catalytic result of the methane oxidation by Ce<sub>0.8</sub>Tb<sub>0.2</sub>O<sub>2-δ</sub> oxide. The Ce<sub>0.8</sub>Tb<sub>0.2</sub>O<sub>2-δ</sub> oxide has better catalytic behavior than pure CeO<sub>2</sub>.

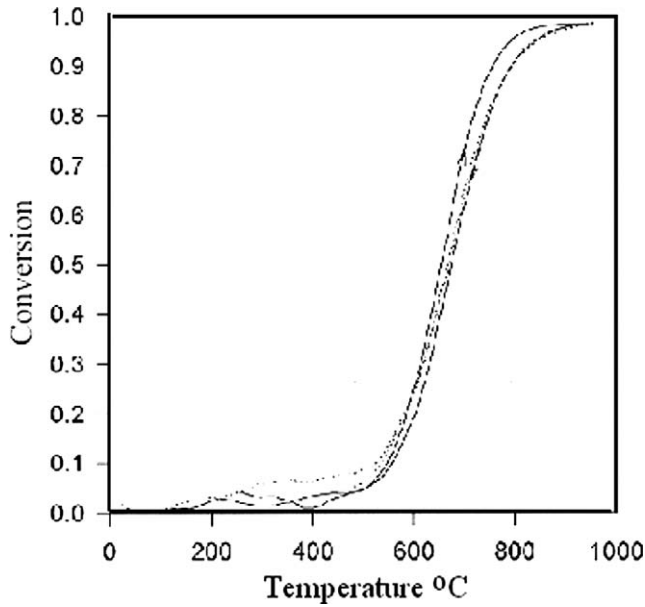


**FIGURE 44** Methane oxidation by the  $\text{Ce}_{0.8}\text{Tb}_{0.2}\text{O}_{2-\delta}$  oxide vs. temperature.

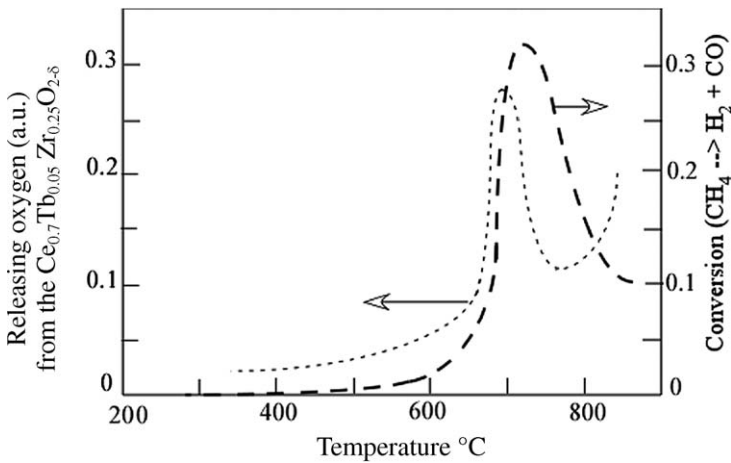
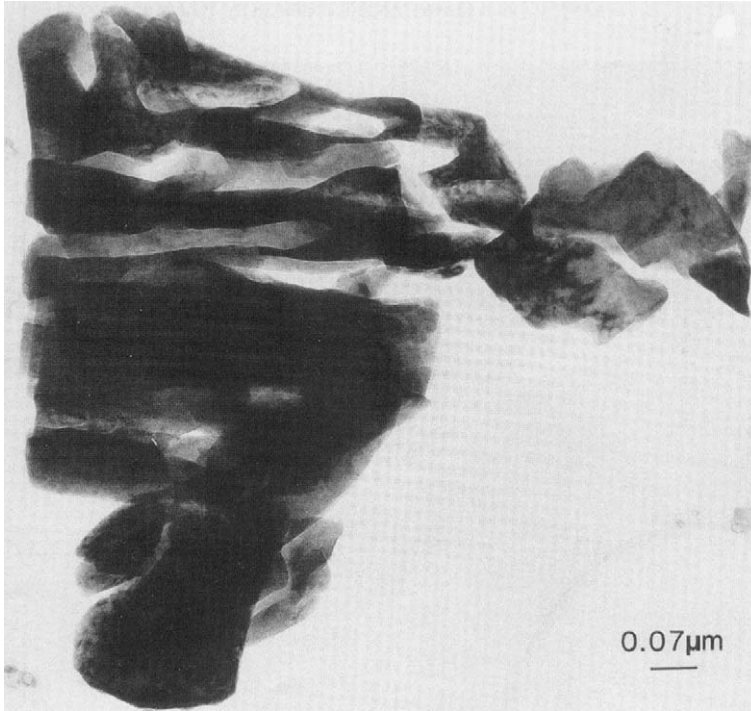
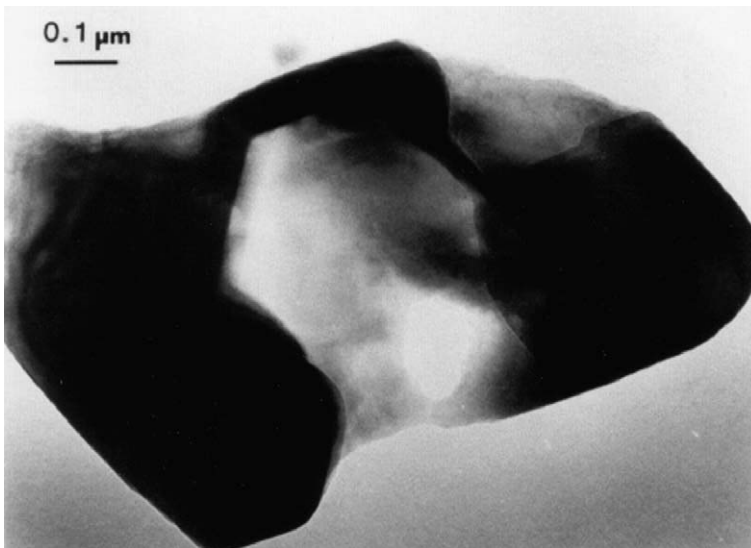


**FIGURE 45** Methane oxidation by the  $\text{Ce}_{0.7}\text{Tb}_{0.05}\text{Zr}_{0.25}\text{O}_{2-\delta}$  oxide as a function of temperature.

Otsuka et al. (1985) clearly demonstrated the relationship between the oxidation and reduction capacity and the reduced fraction of the cerium higher oxides. Using the releasing and absorbing oxygen properties of the lanthanide higher oxides at high and low temperatures, hydrogen can be produced using methane and water alternatively (Otsuka-Yao-Matsuo et al., 1998).



(a)



(b)

**FIGURE 46** The leaching product: (a) PrO<sub>2</sub> "Swedish cheese" and (b) the reacted site of leached TbO<sub>2</sub>.

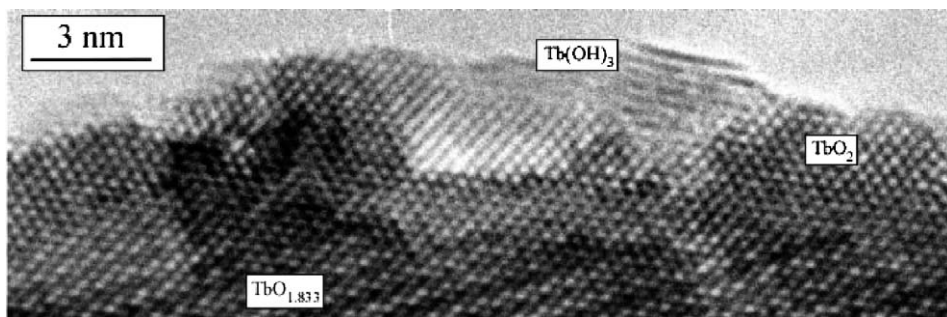


**FIGURE 47** A small amount of the hydroxide on the surface of  $\text{TbO}_2$ .

The ternary and quaternary of the lanthanide higher oxides also have redox catalytic ability. As mentioned before, the ternary and quaternary of the lanthanide higher oxides can release the lattice oxygen at constant rate over a wide temperature range as shown in Figure 16. Using temperature swings one can oxidize the methane and reduce water to produce hydrogen. Figure 45 shows the methane oxidation into hydrogen and carbon monoxide by the  $\text{Ce}_{0.7}\text{Tb}_{0.05}\text{Zr}_{0.25}\text{O}_{2-\delta}$  oxide (Kang and Eyring, 2000).

It appears that the ternary and quaternary of the lanthanide higher oxides have potential applications in catalyst field (Bernal et al., 2005a, 2005b).

#### 6.4 Solvolytic disproportionation of the lanthanide higher oxides

$\text{PrO}_2$  and  $\text{TbO}_2$  can only be prepared by a leaching process. If the  $\text{R}^{3+}$  and  $\text{R}^{4+}$  ions in the lanthanide higher oxides are distributed statistically in the fluorite lattice, and their valences are fixed, then as a result of leaching one should obtain a solid of  $\text{PrO}_2$  and  $\text{TbO}_2$  having many holes on the atomic scale. A HREM study of the leached crystals of  $\text{Pr}_7\text{O}_{12}$  and  $\text{Tb}_{11}\text{O}_{20}$  show many voids (like “Swiss cheese”) as shown in Figure 46. This indicates that the leaching process is a solvolytic disproportionation of the mixed valences oxide (Kang and Eyring, 1988a, 1988b). The valence state of cation in the higher oxides is flexible and it is hard to be sure which cation is trivalent and which is tetravalent. Because the  $\text{R}^{3+}$  can be dissolved in an acid, but  $\text{R}^{4+}$  is not dissolvable, when the  $\text{H}^+$  ion attacks the oxygen ion on the surface of the lanthanide higher oxides it forms an  $\text{OH}^-$  ion group. This process promotes electron hopping from  $\text{R}^{3+}$  to  $\text{R}^{4+}$  and creates the more  $\text{R}^{3+}$ , but simultaneously produces more  $\text{R}^{4+}$  inside the solid. The  $\text{R}(\text{OH})_3$  dissolves into the acid solution and leaves behind an emptied site. This process continues until a large number of the  $\text{R}^{4+}$  cations are formed in a region of the oxide and the electrons are hard to be supplied to the reaction site. The dissolved regions create large voids. Figure 46(a) shows the “Swiss cheese” of  $\text{PrO}_2$ . Defects, such as a dislocation, a stacking fault and a grain boundary, may be a site, which reacted with the acid as shown in Figure 46(b). Figure 47 shows a small amount of  $\text{Tb}(\text{OH})_3$  located on the surface of  $\text{TbO}_2$ . This fact divulges indirect evidence of the valence flexibility of the Ce, Pr, and Tb cations.

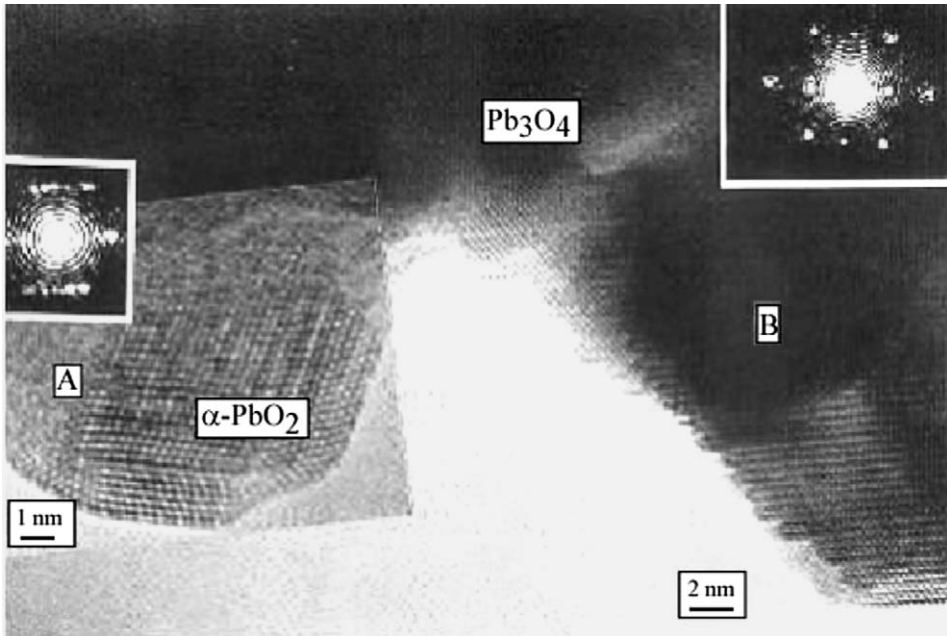


**FIGURE 48** Leaching process of  $\text{Pb}_3\text{O}_4$  shows dissolution of  $\text{Pb}^{2+}$  and precipitation of  $\text{Pb}^{4+}$  cations from the  $\text{Pb}_3\text{O}_4$  (after Kang et al., 1988c).

The “Swiss cheese” shows the difference between the lanthanide higher oxides and a mixed valent transition metal oxide, for example  $\text{Pb}_3\text{O}_4$ . In  $\text{Pb}_3\text{O}_4$ , the  $\text{Pb}^{2+}$  ion can be dissolved in a mineral acid but  $\text{Pb}^{4+}$  ion is not. When leaching the  $\text{Pb}^{2+}$  from the  $\text{Pb}_3\text{O}_4$  one obtain a solid crystal of  $\text{PbO}_2$  without any voids. The  $\text{PbO}_2$  crystal formed by leaching  $\text{Pb}_3\text{O}_4$  is crystallized from the solution in which the dissolved  $\text{Pb}^{2+}$  reacts with  $\text{H}_2\text{O}$  forming  $\text{Pb}^{4+}$  and precipitating a crystal of  $\text{PbO}_2$  (Kang et al., 1988c). Figure 48 shows the leaching process of  $\text{Pb}_3\text{O}_4$ . This behavior indicates that electron hopping does not occur in the transition metal oxide  $\text{Pb}_3\text{O}_4$ .

## 7. SUMMARY

The lanthanide higher oxides are unique systems in which the oxygen content of the higher oxides varies with both oxygen partial pressure and temperature. The range of non-stoichiometry of the lanthanide higher oxides is tunable from narrow regions to wide a range, even from  $\text{RO}_{1.5}$  to  $\text{RO}_2$ . The fluorite structure is fundamental basis and metal sublattice does not change until the temperature increases over  $1200^\circ\text{C}$ . But the oxygen anions can be absent as a single anion vacancy or as an oxygen vacancy pairs. The oxygen content of the lanthanide higher oxides closely related to both the temperature and the oxygen partial pressure, and correspondingly, the valence of the cations varies between the 3+ and 4+ depending on the position of the Fermi energy, whether it is higher or lower than the narrow

4f-band. The module theory, which was developed by Professor LeRoy Eyring, can be utilized to elucidate the thermodynamic properties, hysteresis, fast anion migration, the structures, and the redox reactions of the oxygen deficient fluorite related homologous series of the lanthanide higher oxides. Professor Leroy Eyring's contributions will promote the applications in redox catalysis, oxygen sensor, and mixed conductor, IT-SOFC, oxygen and hydrogen production.

## ACKNOWLEDGEMENTS

Author express heartfelt thanks to Professor Leroy Eyring for inviting me to join his research group to work on these exciting and mysterious compounds. It has been a wonderful experience and a deep pleasure working with him for more than 20 years. Author also greatly appreciates Professor C. Boulesteix at University of Marseille III in France, Professor E. Schweda at University of Tübingen in Germany, and Professor S. Bernal at University of Cadiz in Spain for fruitful discussions, communications, and cooperation over many years.

Author also greatly appreciates the financial supports of the U.S. National Science Foundation, Arizona State University, and Rhodia Inc.

## APPENDIX A: CONVERSION TABLE FOR THE MODULAR DESIGNATIONS

$$\begin{array}{lll} \mathbf{U}^1 = \mathbf{U}^1 & \mathbf{V}^1 = \mathbf{D}_3 & \mathbf{W}_1^1 = \mathbf{W}_3^1 \\ \mathbf{U}^2 = \mathbf{D}_2 & \mathbf{V}^2 = \mathbf{U}^4 & \mathbf{W}_2^2 = \mathbf{W}_2^4 \\ \mathbf{U}^3 = \mathbf{D}_4 & \mathbf{V}^3 = \mathbf{U}^2 & \mathbf{W}_3^3 = \mathbf{W}_4^2 \\ \mathbf{U}^4 = \mathbf{U}^3 & \mathbf{V}^4 = \mathbf{D}_1 & \mathbf{W}_4^4 = \mathbf{W}_1^3 \end{array}$$

Note: The integers 1, 2, 3, 4, are used as sub or superscripts in the U and D system, and designate successive corners, up and down, respectively, in the cubic module in a clockwise direction.

## REFERENCES

- Adachi, G.-y., Imanaka, N. *Chem. Rev.* 1998, **98**, 1479.  
 Adachi, G.-y., Imanaka, N., Kang, Z.C. *Binary Rare Earth Oxides*, Norwell, USA: Kluwer Academic; 2005.  
 Baenziger, N.C., Eick, H.A., Schuldt, H.S., Eyring, L. *J. Am. Chem. Soc.* 1960, **83**, 2219.  
 Bartram, S.F. *Inorg. Chem.* 1966, **5**, 749.  
 Bernal, S., Blanco, G., Cauqui, M.A., Corchado, P., Pintado, J.M., Rodríguez-Izquierdo, J.M. *Chem. Commun.* 1997, 1545.  
 Bernal, S., Blanco, G., Gatica, J.M., Pérez Omil, J.A., Pintado, J.M., Vidal, H. Chemical reactivity of binary rare earth oxides, in: Adachi, G.Y., Imanaka, N., Kang, Z.C., editors. *Binary Rare Earth Oxides*. Amsterdam: Kluwer Academic; 2005a, chap. 2.  
 Bernal, S., Blanco, G., Pintado, J.M., Rodríguez-Izquierdo, J.M., Yeste, M.P. *Catal. Commun.* 2005b, **6**, 582.

- Bevan, D.J.M. *J. Inorg. Nucl. Chem.* 1955, **1**, 49.
- Bevan, D.J.M., Kordis, J. *J. Inorg. Nucl. Chem.* 1964, **26**, 1509.
- Boulesteix, C., Eyring, L. *J. Solid State Chem.* 1987, **66**, 125.
- Brauer, G., Gingerich, K. *Anorg. Chem.* 1957, **69**, 460.
- Brauer, G., Gradinger, H. *Z. Anorg. Allg. Chem.* 1954, **277**, 90.
- Bursill, L.A., Hyde, B.G. *Prog. Solid State Chem.* 1972, **7**, 177.
- Buseck, P.R., Cowley, J.M., Eyring, L., editors. *High-Resolution Transmission Electron Microscopy and Associated Techniques*. Oxford: Oxford Univ. Press; 1988.
- Caro, P.E. *J. Less-Common Met.* 1968, **16**, 367.
- Caro, P.E. *Solid State Chemistry*, NBS Special Publication 1972, **364**, 367.
- Cowley, J.M. *Diffraction Physics* second ed., Amsterdam: North-Holland; 1981.
- Cowley, J.M., Moodie, A.F. *Acta Crystallogr.* 1957, **10**, 609.
- Eyring, L. The binary rare earth oxides, in: Gschneidner Jr., K.A., Eyring, L., editors. *Handbook on the Physics and Chemistry of Rare Earths*. Amsterdam: North-Holland; 1979, chap. 27.
- Eyring, L. *J. Alloys Compd.* 1994, **207–208**, 1.
- Eyring, L., Kang, Z.C. *Eur. J. Solid State Inorg. Chem.* 1991, **28**, 459.
- Fagg, D.P., Kharton, V.V., Shaula, A., Marozau, I.P., Frade, J.R. *Solid State Ionics* 2005, **176**, 1723.
- Ferguson, R.E., Guth, E.D., Eyring, L. *J. Am. Chem. Soc.* 1954, **76**, 3890.
- Goldschmidt, V.M. *Skrifter Norske Videnskaps-Akad. Oslo I, Mat.-Naturv. Kl.* 1926, **1/2**.
- Goldschmidt, V.M., Thomassen, L. *Skrifter Norske Videnskaps-Akad. Oslo I, Mat.-Naturv. Kl.* 1923, **2**.
- Gruen, D.M., Koehler, W.C., Katz, J.J. *J. Am. Chem. Soc.* 1951, **73**, 1475.
- Guth, E.D., Holden, J.R., Baenziger, N.C., Eyring, L. *J. Am. Chem. Soc.* 1954, **76**, 5239.
- Haire, R.G., Eyring, L. Comparisons of the binary oxides, in: Gschneidner Jr., K.A., Eyring, L., editors. *Handbook on the Physics and Chemistry of Rare Earths*. Amsterdam: North-Holland Publishing Company; 1994, chap. 125.
- Hill, S.E., Catlow, C.R.A. *J. Phys. Chem. Solid* 1991, **54**, 411.
- Honig, J.M., Cella, A.A., Cornwell, J.C. *Rare Earth Res.* 1964, **2**, 555.
- Hoskins, B.F., Martin, R.L. *J. Chem. Soc. Dalton* 1975, 576.
- Hoskins, B.F., Martin, R.L. *J. Chem. Soc. Dalton* 1976, 676.
- Hoskins, B.F., Martin, R.L. *J. Chem. Soc. Dalton* 1977, 320.
- Hyde, B.G., Bevan, D.J.M., Eyring, L. 1965, *Int. Conf. Electron Diffraction and Crystal Defects*, Austral. Acad. Sci., p. 11, C-4.
- Hyde, B.G., Bevan, D.J.M., Eyring, L. *Philos. Trans. R. Soc. London* 1966, **259**, 583.
- Hyde, B.G., Eyring, L., in: Eyring, L., editor. *Rare Earth Research III*. New York: Gordon & Breach; 1965, p. 623.
- Inaba, H., Lin, S.H., Eyring, L. *J. Solid State Chem.* 1981a, **37**, 58.
- Inaba, H., Naito, K. *J. Solid State Chem.* 1983a, **50**, 100.
- Inaba, H., Naito, K. *J. Solid State Chem.* 1983b, **50**, 111.
- Inaba, H., Navrotsky, A., Eyring, L. *J. Solid State Chem.* 1981c, **37**, 77.
- Inaba, H., Pack, S.P., Lin, S.H., Eyring, L. *J. Solid State Chem.* 1980, **33**, 295.
- Inaba, H., Pack, S.P., Lin, S.H., Eyring, L. *J. Solid State Chem.* 1981b, **37**, 67.
- Jiang, Y., Adams, J.B., Van Schilfgaarde, M. *J. Chem. Phys.* 2005a, **123**, 64701.
- Jiang, Y., Adams, J.B., Van Schilfgaarde, M., Sharma, R., Crozier, P.A. *Appl. Phys. Lett.* 2005b, **87**, 141917.
- Kang, Z.C. *Ferroelectrics* 2001, **251**, 21.
- Kang, Z.C. *J. Alloys Compd.* 2006, **408–412**, 1103.
- Kang, Z.C., Eyring, L. *J. Solid State Chem.* 1988a, **75**, 52.
- Kang, Z.C., Eyring, L. *J. Solid State Chem.* 1988b, **75**, 60.
- Kang, Z.C., Eyring, L. *J. Alloys Compd.* 1992, **181**, 483.
- Kang, Z.C., Eyring, L. *J. Alloys Compd.* 1997a, **249**, 206.
- Kang, Z.C., Eyring, L. *Aust. J. Chem.* 1997b, **49**, 981.
- Kang, Z.C., Eyring, L. *J. Solid State Chem.* 2000, **155**, 129.
- Kang, Z.C., Eyring, L. 2001a, Report for Fubright foundation.
- Kang, Z.C., Eyring, L. *J. Alloys Compd.* 2001b, **323–324**, 97.
- Kang, Z.C., Eyring, L. *J. Alloys Compd.* 2006, **408–412**, 1123.
- Kang, Z.C., Machesky, L., Eick, H.A., Eyring, L. *J. Solid State Chem.* 1988c, **75**, 73.

- Kang, Z.C., Smith, D.J., Eyring, L. *Surf. Sci.* 1986, **175**, 684.
- Kang, Z.C., Smith, D.J., Eyring, L. *Ultramicroscopy* 1987, **22**, 71.
- Kang, Z.C., Zhang, J., Eyring, L. *Aust. J. Chem.* 1992, **45**, 1499.
- Kang, Z.C., Zhang, J., Eyring, L. *Z. Anorg. Allg. Chem.* 1996, **622**, 465.
- Knappe, P., Eyring, L. *J. Solid State Chem.* 1985, **58**, 312.
- Koelling, D.D., Boring, A.M., Wood, J.H. *Solid State Commun.* 1983, **47**, 227.
- Krivovichev, S.V. *Solid State Sci.* 1999a, **1**, 211.
- Krivovichev, S.V. *Solid State Sci.* 1999b, **1**, 221.
- Kunzmann, P., Eyring, L. *J. Solid State Chem.* 1975, **14**, 229.
- Manes, L., Sørensen, O.T., Mari, C.M., Roy, I., in: *Thermodynamics of Nuclear Materials*, vol. 1. Vienna: IAEA; 1980, p. 405.
- Martin, R.L. *J. Chem. Soc. Dalton* 1974, 1335.
- Otsuka, K., Hatano, M., Morikawa, A. *Inorg. Chim. Acta* 1985, **109**, 193.
- Otsuka, K., Kunitomi, M., Saito, T. *Inorg. Chim. Acta* 1986, **115**, L31.
- Otsuka-Yao-Matsuo, S., Izu, N., Omata, T., Ikeda, K. *J. Electrochem. Soc.* 1998, **145**, 1406.
- Rao, G.V.R., Ramdas, S., Mehrotra, P.N., Rao, C.N.R. *J. Solid State Chem.* 1970, **2**, 377.
- Ray, S.P., Nowick, A.S., Cox, D.E. *J. Solid State Chem.* 1975, **15**, 344.
- Ricken, J., Nölting, J., Riess, I. *J. Solid State Chem.* 1984, **54**, 89.
- Sawyer, J.O., Hyde, B.G., Eyring, L. *Bull. Soc. Chim. France* 1965, 1190.
- Sayle, T.X., Parker, T.S.C., Catlow, C.R.A. *J. Chem. Soc. Chem. Commun.* 1992, 977.
- Schweda, E.D., Bevan, J.M., Eyring, L. *J. Solid State Chem.* 1991, **90**, 109.
- Sharma, R., Crozier, P., Kang, Z.C., Eyring, L. *Philos. Mag.* 2004, **84**, 2731.
- Shuk, P., Greenblatt, M. *Solid State Ionics* 1999, **116**, 217.
- Skarnulis, A.J., Summerville, E., Eyring, L. *J. Solid State Chem.* 1978, **23**, 59.
- Skorodumova, N.V., Simak, S.I., Lundqvist, B.I., Abrikosov, I.A., Johansson, B. *Phys. Rev. Lett.* 2002, **89**, 166601-1.
- Sovestnov, A.E., Shaburov, V.A., Melekh, B.T., Smirnov, I.A., Smirnov, Yu.P., Tyunis, A.V., Egorov, A.I. *Phys. Solid State* 1994, **36**, 620.
- Sorensen, O.T., editor. *Nonstoichiometric Oxides*. New York: Academic Press; 1981.
- Summerville, E., Tuege, R.T., Eyring, L. *J. Solid State Chem.* 1978, **24**, 21.
- Takasu, Y., Sugino, T., Matsuda, Y. *J. Appl. Electrochem.* 1984, **14**, 79.
- Thorner, M.R., Bevan, D.J.M., Graham, J. *Acta Crystallogr. B* 1968, **24**, 1183.
- Trovarelli, A. *Catalysis by Ceria and Related Materials*, London: Imperial College Press; 2002.
- Tuege, R.T., Eyring, L. *J. Solid State Chem.* 1979, **29**, 165.
- Tuege, R.T., Eyring, L. *J. Solid State Chem.* 1982, **41**, 75.
- Turcotte, R.A., Warmkessel, J.M., Tilley, R.J.D., Eyring, L. *J. Solid State Chem.* 1971, **3**, 265.
- Turcotte, R.P., Jenkins, M.S., Eyring, L. *J. Solid State Chem.* 1973, **7**, 454.
- Von Dreele, R.B., Eyring, L., Bowman, A.L., Yarnell, J.L. *Acta Crystallogr. B* 1975, **31**, 971.
- Wachter, P. Intermediate valence and heavy fermions, in: Gschneidner Jr., K.A., Eyring, L., editors. *Handbook on the Physics and Chemistry of Rare Earths*. Amsterdam: North-Holland Publishing Company; 1994, chap. 132.
- Yang, Z., Woo, T.K., Baudin, M., Hermansson, K. *J. Chem. Phys.* 2004, **120**, 7741.
- Zhang, J.R., Von Dreele, B., Eyring, L. *J. Solid State Chem.* 1993a, **104**, 21.
- Zhang, J.R., Von Dreele, B., Eyring, L. *J. Solid State Chem.* 1993b, **118**, 141.
- Zhang, J.R., Von Dreele, B., Eyring, L. *J. Solid State Chem.* 1993c, **122**, 53.
- Zhang, J.R., Von Dreele, B., Eyring, L. *J. Solid State Chem.* 1995, **118**, 133.

## Rare Earth–Transition Metal– Plumbides

**Rainer Pöttgen\*** and **Ute Ch. Rodewald\***

<b>Contents</b>	Symbols and abbreviations	56
	1. Introduction	56
	2. Synthesis	57
	3. Phase Diagrams	57
	4. Crystal Chemistry	62
	4.1 Lattice parameters	63
	4.2 The structure types $\text{Mo}_2\text{FeB}_2$ , $\text{Er}_2\text{Au}_2\text{Sn}$ and $\text{Mn}_2\text{AlB}_2$	63
	4.3 The structure types $\text{CaIn}_2$ , $\text{ZrBeSi}$ , $\text{NdPtSb}$ , $\text{LiGaGe}$ , $\text{CaLiSn}$ , and $\text{YbAgPb}$	78
	4.4 The structure types $\text{KHg}_2$ and $\text{TiNiSi}$	81
	4.5 The structure type $\text{ZrNiAl}$	82
	4.6 The structure type $\text{Ho}_6\text{Co}_2\text{Ga}$	83
	4.7 The structure types $\text{AuBe}_5$ and $\text{Cu}_3\text{Au}$	84
	4.8 The structure types $\text{Ce}_8\text{Pd}_{24}\text{Sb}$ and $\text{Sm}_{12}\text{Ni}_6\text{In}$	86
	4.9 The structure type $\text{Hf}_5\text{CuSn}_3$	87
	4.10 The structure type $\text{La}_6\text{Co}_{11}\text{Ga}_3$	88
	4.11 The structure types $\text{MnCu}_2\text{Al}$ and $\text{MgAgAs}$	89
	4.12 The structure type $\text{Yb}_3\text{Rh}_4\text{Sn}_{13}$	90
	4.13 The structure type $\text{La}_4\text{Ni}_3\text{Pb}_4$	91
	5. Chemical and Physical Properties	93
	5.1 Ternary equiatomic plumbides RTPb	93
	5.2 Ternary plumbides $\text{R}_2\text{T}_2\text{Pb}$	95
	5.3 Ternary plumbides $\text{R}_6\text{T}_{13}\text{Pb}$	96
	5.4 Ternary plumbides $\text{R}_4\text{Ni}_3\text{Pb}_4$	98
	5.5 The plumbide $\text{Ce}_8\text{Pd}_{24}\text{Pb}$	98
	5.6 The plumbide $\text{Dy}_5\text{CuPb}_3$	99
	6. Summary and Outlook	99
	Acknowledgements	100
	References	100

\* Institut für Anorganische und Analytische Chemie, Westfälische Wilhelms-Universität Münster, Corrensstrasse 30, D-48149 Münster, Germany  
E-mail: [pottgen@uni-muenster.de](mailto:pottgen@uni-muenster.de)

### Symbols and abbreviations

A	resistivity coefficient	T	transition metal
bcc	body centered cubic	TB-LMTO-ASA	tight-binding linear muffin tin-orbital atomic sphere approximation
CN	coordination number	$T_C$	magnetic Curie temperature, superconducting transition temperature
fcc	face centered cubic	$T_N$	magnetic Néel temperature
$J$	magnetic exchange parameter	$\rho$	resistivity
$k$	<i>klassengleiche</i> symmetry reduction	$\gamma$	electronic specific heat coefficient
$M$	mixed occupied position, magnetization	$\chi$	magnetic susceptibility
R	rare earth metal	X	main group element
SG	space group	$\mu_B$	Bohr magneton
$t$	<i>translationengleiche</i> symmetry reduction		

## 1. INTRODUCTION

Ternary intermetallic compounds  $R_xT_yX_z$  ( $R$  = rare earth element,  $T$  = transition metal;  $X$  = element of the 3rd, 4th, or 5th main group) have been intensively investigated over the last 50 years with respect to their extremely broad crystal chemistry and their greatly varying physical properties. Much of the data have been summarized in review articles, mostly in the *Handbook on the Physics and Chemistry of Rare Earths* (Parthé and Chabot, 1984; Rogl, 1984a, 1984b; Gladyshevsky et al., 1990; Grin and Gladyshevskii, 1989; Adachi et al., 1991; Kuz'ma and Chykhrij, 1996; Niewa and Jacobs, 1996; Skolozdra, 1997; Niewa and DiSalvo, 1998; Salamakha et al., 1999c; Salamakha, 1999b; Niewa, 2002; Sologub and Salamakha, 2003; Kalychak et al., 2005; Mar, 2006).

The crystal chemistry of the  $R_xT_yX_z$  borides, carbides, and nitrides differs significantly from that of the higher congeners. Only a few examples exist for isotypic compounds between the 2p and 3p systems. This seems to be mainly a result of the small size of these elements. The other main group elements ( $Al \rightarrow Tl$ ,  $Si \rightarrow Pb$ ,  $P \rightarrow Bi$ ) often show similar crystal chemistry. This is a very interesting situation, since for a given structure type, it is possible to vary the valence electron concentration through substitution of the  $X$  or  $T$  component. Thus, one can effectively modify the chemical bonding and the physical properties. This fascinating situation makes the  $R_xT_yX_z$  intermetallics a vivid research field in solid state chemistry and solid state physics.

While the systems with the 3p, 4p, and 5p main group elements have been investigated in detail, less information is available for the thallides, plumbides, and bismuthides. This is largely due to synthesis problems, since these elements

have comparatively low boiling temperatures, thus complicating the preparation of pure materials. Also the toxicity of thallium and lead might be a reason. Nevertheless, these intermetallics show highly interesting magnetic behaviors.

Herein we review the crystal chemistry, physical properties and structure–property relationships of known plumbides in the R–T–Pb systems. The latter have not been investigated as detailed as the tin based systems. So far, the studies mainly focussed on the 3d transition metals.

## 2. SYNTHESIS

The rare earth–transition metal–plumbides have all been prepared from pure elements. Although lead has relatively low melting (600 K) and boiling (2010 K) points, most of these plumbides have been synthesized via arc-melting. This simple technique allows for reactions at high temperatures in relatively short reaction times (Pöttgen et al., 1999b). The arc-melted buttons are always flipped over and remelted two or three times to ensure homogeneity. In many cases (e.g., Gordon et al., 1995; Cho et al., 1998), the authors added 1–2% excess lead in order to compensate for the loss of lead through evaporation. Usually the arc-melted ingots are sealed in evacuated silica ampoules and annealed at temperatures between 670 and 870 K depending on the composition of the compounds. The typical annealing times are up to four weeks. In some cases it was possible to brake off high-quality single crystal platelets (a few mm<sup>2</sup> in area) out of the solidified buttons (Chinchure et al., 2002). Such “selfgrowth” processes are often observed under metal flux condition (Kanatidis et al., 2005). Movshovich et al. (1996) obtained crystals (typical dimensions 2 × 2 × 10 mm<sup>3</sup>) of ZrNiAl type LaPtPb and CePtPb from a lead flux and they removed the excess lead in a centrifuge.

A different synthesis strategy was used by Iandelli (1994) for the preparation of the RPdPb (R = Y, La, Ce, Pr, Sm, Gd, Dy, Er, Yb) plumbides. Here, the elements were sealed in tantalum crucibles under argon, induction heated to ca. 1470 K and annealed for another 10–12 days at 1020 K. Similar technique was also used for the ytterbium based materials YbLiPb (Fornasini et al., 2001b), Yb<sub>2</sub>Au<sub>2</sub>Pb (Fornasini et al., 2001a), and Yb<sub>2</sub>Pt<sub>2</sub>Pb (Pöttgen et al., 1999a). A special, water-cooled sample chamber (Kußmann et al., 1998; Pöttgen et al., 1999d) has been constructed for the high-frequency annealing.

A method that has so far only scarcely been used for the synthesis of the R<sub>x</sub>T<sub>y</sub>Pb<sub>z</sub> plumbides is the lead flux. The latter has successfully been used for the growth of phosphide crystals (Kanatidis et al., 2005). This technique has certainly a great potential, especially for lead-rich R<sub>x</sub>T<sub>y</sub>Pb<sub>z</sub> compounds.

## 3. PHASE DIAGRAMS

Among the many R–T–Pb systems, only seven systems with copper (i.e. for R = Y, La, Ce, Nd, Sm, Gd, Dy) (Salamakha and Zaplatynsky, 1997; Gulay, 2000, 2002, 2003a, 2003b; Gulay and Wołczyrz, 2001a) and six with nickel (i.e. R = Y, La, Ce, Sm,

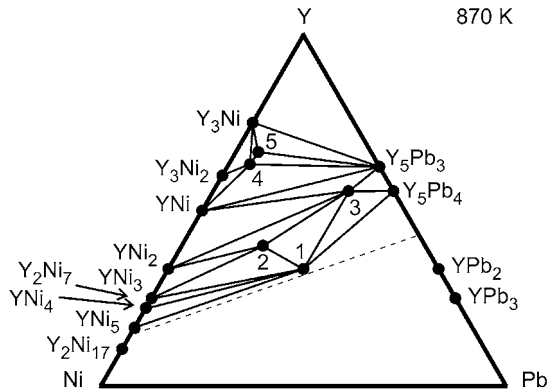


**FIGURE 1** Isothermal section of the phase diagram in the Y–Ni–Pb system at 870 K. 1—YNiPb; 2— $\text{Y}_2\text{Ni}_2\text{Pb}$ ; 3— $\text{Y}_5\text{NiPb}_3$ ; 4— $\text{Y}_{12}\text{Ni}_6\text{Pb}$ ; 5— $\text{Y}_6\text{Ni}_{2.5}\text{Pb}_{0.5}$ .

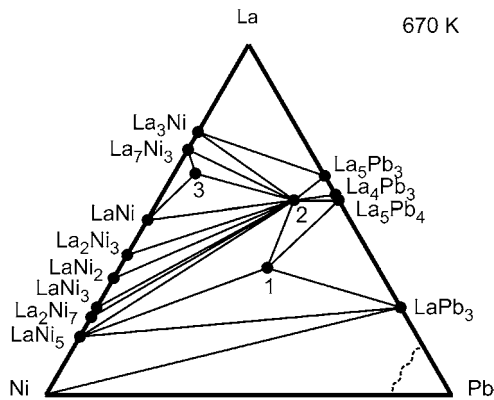


**FIGURE 2** Isothermal section of the phase diagram in the La–Ni–Pb system at 670 K. 1— $\text{La}_4\text{Ni}_3\text{Pb}_4$ ; 2— $\text{La}_5\text{NiPb}_3$ ; 3— $\text{La}_{12}\text{Ni}_6\text{Pb}$ .

Gd, Dy) (Gulay, 2003a, 2003b, 2005) have been investigated in detail. The isothermal sections of these systems have been studied for samples annealed at 670 or 870 K for 720 h (Figures 1–13).

The Nd–Ag–Pb phase diagram has only been studied for the 0–33 at% Nd range at 870 K (Salamakha et al., 1996). Only the equiatomic plumbide NdAgPb has been reported. Similar behavior has been observed for the Nd–Zn–Pb system at 870 K (Salamakha et al., 1999a). Both systems reveal a liquidus range in the lead rich region at 870 K. Probably the isothermal sections at lower temperatures will reveal the existence of lead rich compounds.

There is a distinct difference for these fifteen plumbide systems when compared with the stannide systems (Skolozdra, 1997). This difference becomes already evident when looking at the binary Ni–Sn(Pb) and Cu–Sn(Pb) systems (Massalski, 1986). While binary stannides like  $\text{Ni}_3\text{Sn}$ ,  $\text{Ni}_3\text{Sn}_2$ ,  $\text{NiSn}$ ,  $\text{Ni}_3\text{Sn}_4$ ,  $\text{Cu}_3\text{Sn}$ ,

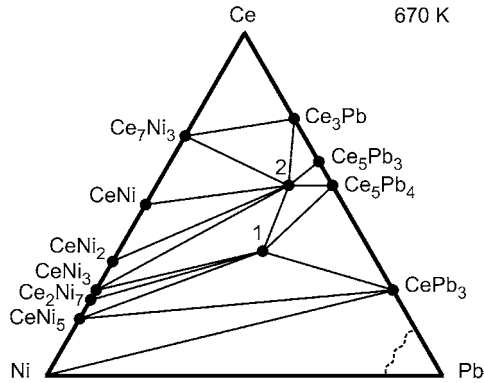


**FIGURE 3** Isothermal section of the phase diagram in the Ce–Ni–Pb system at 670 K. 1— $\text{Ce}_4\text{Ni}_3\text{Pb}_4$ ; 2— $\text{Ce}_5\text{NiPb}_3$ .

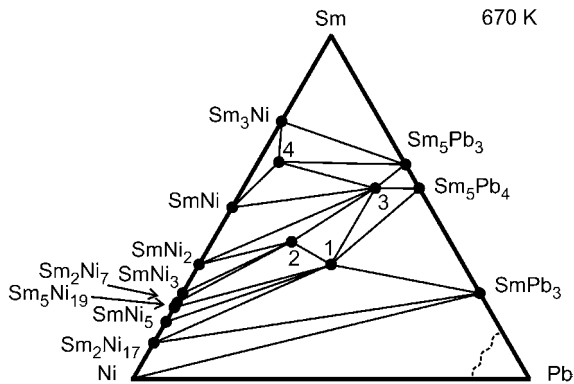


**FIGURE 4** Isothermal section of the phase diagram in the Sm–Ni–Pb system at 670 K. 1— $\text{SmNiPb}$ ; 2— $\text{Sm}_2\text{Ni}_2\text{Pb}$ ; 3— $\text{Sm}_5\text{NiPb}_3$ ; 4— $\text{Sm}_2\text{Ni}_6\text{Pb}$ .

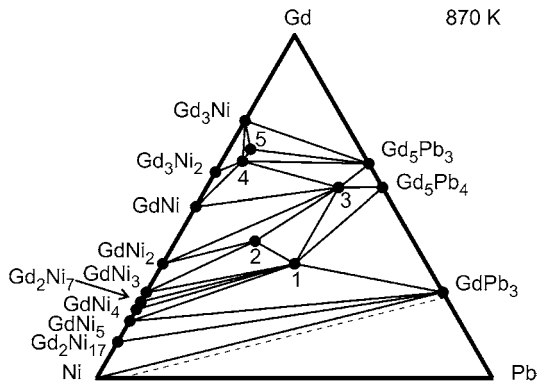


**FIGURE 5** Isothermal section of the phase diagram in the Gd–Ni–Pb system at 870 K. 1— $\text{GdNiPb}$ ; 2— $\text{Gd}_2\text{Ni}_2\text{Pb}$ ; 3— $\text{Gd}_5\text{NiPb}_3$ ; 4— $\text{Gd}_{12}\text{Ni}_6\text{Pb}$ ; 5— $\text{Gd}_6\text{Ni}_{2.5}\text{Pb}_{0.5}$ .

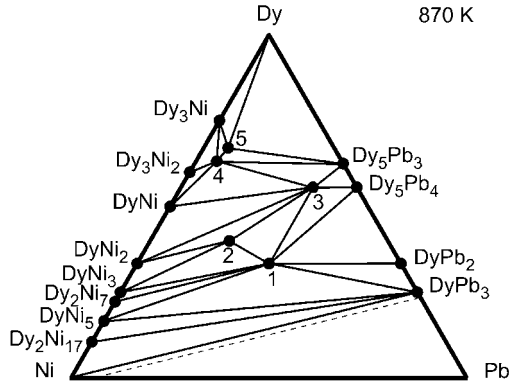


**FIGURE 6** Isothermal section of the phase diagram in the Dy–Ni–Pb system at 870 K. 1—DyNiPb; 2—Dy<sub>2</sub>Ni<sub>2</sub>Pb; 3—Dy<sub>5</sub>NiPb<sub>3</sub>; 4—Dy<sub>12</sub>Ni<sub>6</sub>Pb; 5—Dy<sub>6</sub>Ni<sub>2.39</sub>Pb<sub>0.55</sub>.

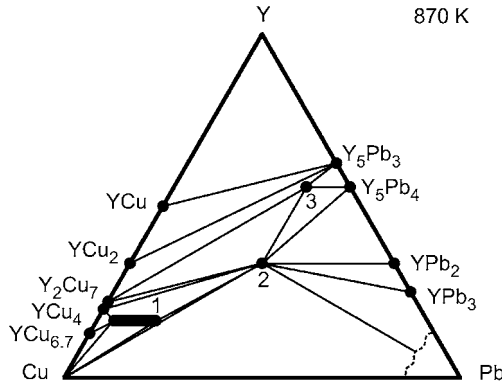


**FIGURE 7** Isothermal section of the phase diagram in the Y–Cu–Pb system at 870 K. 1—YCu<sub>5-x</sub>Pb<sub>x</sub> ( $x = 0.26-0.89$ ); 2—YCuPb; 3—Y<sub>5</sub>CuPb<sub>3</sub>.

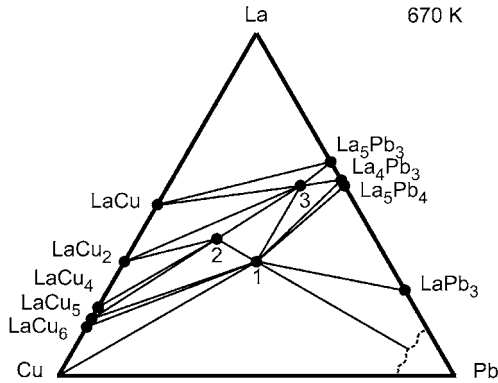


**FIGURE 8** Isothermal section of the phase diagram in the La–Cu–Pb system at 670 K. 1—LaCuPb; 2— $\sim$ La<sub>2</sub>Cu<sub>2</sub>Pb; 3—La<sub>5</sub>CuPb<sub>3</sub>.

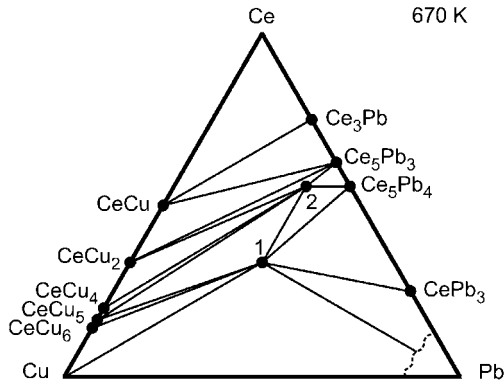


**FIGURE 9** Isothermal section of the phase diagram in the Ce–Cu–Pb system at 670 K. 1—CeCuPb; 2—Ce<sub>5</sub>CuPb<sub>3</sub>.

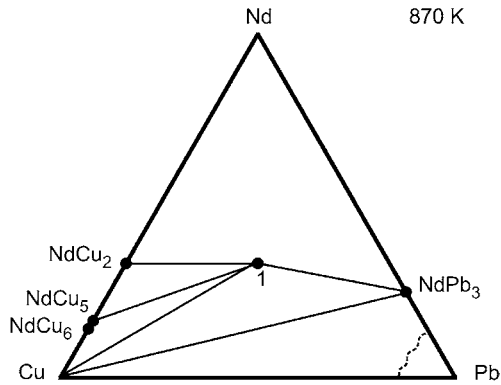


**FIGURE 10** Isothermal section of the phase diagram in the Nd–Cu–Pb system at 870 K. 1—NdCuPb.

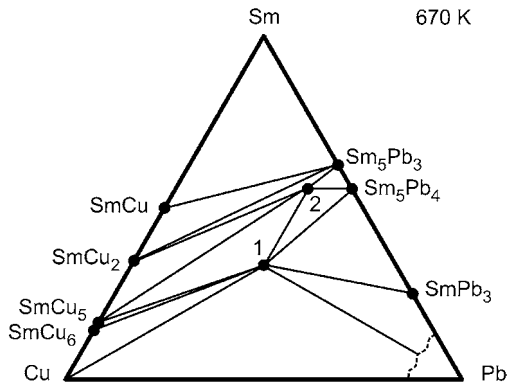


**FIGURE 11** Isothermal section of the phase diagram in the Sm–Cu–Pb system at 670 K. 1—SmCuPb; 2—Sm<sub>5</sub>CuPb<sub>3</sub>.

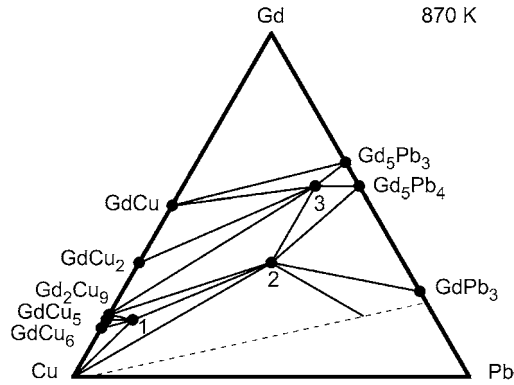


**FIGURE 12** Isothermal section of the phase diagram in the Gd–Cu–Pb system at 870 K. 1— $\text{GdCu}_{4.60}\text{Pb}_{0.40}$ ; 2— $\text{GdCuPb}_3$ ; 3— $\text{Gd}_5\text{CuPb}_3$ .

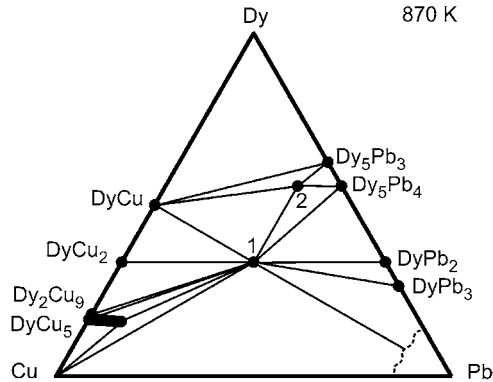


**FIGURE 13** Isothermal section of the phase diagram in the Dy–Cu–Pb system at 870 K. 1— $\text{DyCuPb}$ ; 2— $\text{Dy}_5\text{CuPb}_3$ .

$\text{Cu}_{10}\text{Sn}_3$ , and  $\text{Cu}_6\text{Sn}_5$  (Villars and Calvert, 1991, 1997) exist, no binary nickel and copper plumbides are known. This fact is transferred to the ternary R–Ni(Cu)–Pb systems. The plumbides systems contain fewer ternary compounds when compared to the stannide ones. To give an example, 15 stannides have been reported for the Gd–Ni–Sn system (Skolozdra, 1997), while only five plumbides exist in the related system with lead (Gulay, 2003b). This empirical rule is observed for many other ternary systems.

#### 4. CRYSTAL CHEMISTRY

In the following section we list and discuss the crystal chemical data of many  $\text{R}_x\text{T}_y\text{Pb}_z$  plumbides. The basic crystallographic data, lattice parameters, space

group symmetry and atomic positions (for one selected compound of each structure type) are listed first and the crystal chemistry is then discussed.

#### 4.1 Lattice parameters

Table 1 lists the lattice parameters of the  $R_xT_yPb_z$  plumbides in the order of the periodic table, i.e. from the yttrium to the lutetium compounds. For each compound also the structure type is listed.

#### 4.2 The structure types $Mo_2FeB_2$ , $Er_2Au_2Sn$ and $Mn_2AlB_2$

Structure type  $Mo_2FeB_2$  (Rieger et al., 1964) (Figure 14). SG  $P4/mbm$ ;  $Z = 2$ ,  $a = 780.84(4)$ ,  $c = 375.82(3)$  pm for  $Sm_2Pd_2Pb$  (Melnyk et al., 2004).  $4Sm$ :  $4h\ x\ x\ +\ 1/2\ 1/2$  ( $x = 0.1760$ ),  $4Pd$ :  $4g\ x\ x\ +\ 1/2\ 0$  ( $x = 0.3745$ );  $2Pb$ :  $2a\ 0\ 0\ 0$ .

Structure type  $Er_2Au_2Sn$  (Pöttgen, 1994) (Figure 14). SG  $P4_2/mnm$ ,  $Z = 4$ ,  $a = 776.0(1)$ ,  $c = 701.8(2)$  pm, for  $Yb_2Pt_2Pb$  (Pöttgen et al., 1999a).  $4Yb1$ :  $4f\ x\ x\ 0$  ( $x = 0.1801$ );  $4Yb2$ :  $4g\ x\ -x\ 0$  ( $x = 0.3414$ );  $8Pt$ :  $8j\ x\ x\ z$  ( $x = 0.37274$ ,  $z = 0.2717$ );  $4Pb$ :  $4d\ 0\ 1/2\ 1/4$ .

Structure type  $Mn_2AlB_2$  (Becher et al., 1966) (Figure 14). SG  $Cmmm$ ,  $Z = 2$ ,  $a = 400.34(9)$ ,  $b = 1391.7(3)$ ,  $c = 361.5(1)$  pm for  $Ho_2Ni_2Pb$  (Prokeš et al., 2005).  $4Ho$ :  $4j\ 0\ y\ 1/2$  ( $y = 0.3649$ );  $4Ni$ :  $0\ y\ 0$  ( $y = 0.1990$ );  $2Pb$ :  $2a\ 0\ 0\ 0$ .

Some plumbide structures can be considered as intergrowth variants of smaller slabs. In Figure 14 we present projections of the  $Sm_2Pd_2Pb$  ( $Mo_2FeB_2$  type, space group  $P4/mbm$ ) (Melnyk et al., 2004),  $Yb_2Pt_2Pb$  ( $Er_2Au_2Sn$  type, space group  $P4_2/mnm$ ) (Pöttgen et al., 1999a) and  $Ho_2Ni_2Pb$  ( $Mn_2AlB_2$  type, space group  $Cmmm$ ) (Prokeš et al., 2005) structures. The  $Mo_2FeB_2$  type is a ternary ordered version of the  $U_3Si_2$  structure (Zachariasen, 1949; Remschnig et al., 1992).

The  $R_2T_2Pb$  structures are 1:1 intergrowth variants of slightly distorted CsCl and  $AlB_2$  related slabs of compositions  $RPb$  and  $RT_2$ . In  $Sm_2Pd_2Pb$  and  $Yb_2Pt_2Pb$ , four  $AlB_2$  slabs are connected to one CsCl slab via the rectangular faces within the  $ab$  plane. The connectivity of the slabs is different in the  $Ho_2Ni_2Pb$  structure. Here blocks of the CsCl slabs are condensed in the  $a$  and  $c$  direction and are surrounded by the blocks of the  $AlB_2$  slabs along the  $b$  axis. It is interesting to note that, only in the series  $R_2Ni_2Cd$  dimorphism has been observed (Fickenscher et al., 2005). The  $Mn_2AlB_2$  type forms at high temperatures while the  $Mo_2FeB_2$  type is stable upon annealing the samples at low temperatures. Most of the  $R_2T_2Pb$  plumbides crystallize with these two structure types.

At this point we need to comment on the different sets of lattice parameters reported for the  $R_2Ni_2Pb$  plumbides (Table 1). The data reported by Gulay et al. (2000a) and Gulay and Hiebl (2003) are consistent, while larger differences occur for the lattice parameters given for  $Ho_2Ni_2Pb$  and  $Er_2Ni_2Pb$ . The nature of these inconsistencies remains unclear.

The situation is different for  $Yb_2Pt_2Pb$  (Pöttgen et al., 1999a) and  $Yb_2Au_2Pb$  (Fornasini et al., 2001a). These plumbides form superstructures and the space group symmetry is reduced from  $P4/mbm$  to  $P4_2/mnm$  via a *klassengleiche* transition of index 2 ( $k_2$ ) upon doubling the subcell  $c$  axis. The  $Pt_2$  and  $Au_2$  pairs

**TABLE 1** Crystallographic data for ternary rare–earth transition metal–plumbides. If listed in the literature, standard deviations are given in parentheses

Compound	Structure type	Space group	Lattice parameters (pm)			Reference(s)
			<i>a</i>	<i>b</i>	<i>c</i>	
Y <sub>6</sub> Co <sub>2.23</sub> Pb <sub>0.57</sub>	Ho <sub>6</sub> Co <sub>2</sub> Ga	<i>Immm</i>	944.49(4)	947.27(5)	992.76(5)	Gulay and Wolcyrz, 2001a
Y <sub>12</sub> Co <sub>6</sub> Pb	Sm <sub>12</sub> Ni <sub>6</sub> In	<i>Im</i> $\bar{3}$	968.6(1)	–	–	Gulay et al., 2000b
Y <sub>12</sub> Ni <sub>6</sub> Pb	Sm <sub>12</sub> Ni <sub>6</sub> In	<i>Im</i> $\bar{3}$	971.49(2)	–	–	Gulay et al., 2000b
Y <sub>6</sub> Ni <sub>2.5</sub> Pb <sub>0.5</sub>	Ho <sub>6</sub> Co <sub>2</sub> Ga	<i>Immm</i>	946.2(1)	960.5(1)	989.1(1)	Gulay, 2005
Y <sub>2</sub> Ni <sub>2</sub> Pb	Mn <sub>2</sub> AlB <sub>2</sub>	<i>Cmmm</i>	401.9(1)	1400.8(3)	367.9(1)	Gulay et al., 2000a
			401.85(4)	1402.6(1)	368.26(4)	Gulay and Hiebl, 2003
			400.9(1)	1396.6(3)	369.7(2)	Chinchure et al., 2003
			715.90(4)	451.76(2)	776.10(4)	Gulay et al., 2000c
YNiPb	TiNiSi	<i>Pnma</i>	716.21(1)	451.90(1)	775.88(2)	Gulay and Hiebl, 2002
			899.1(1)	–	663.93(4)	Gulay, 2005
Y <sub>5</sub> NiPb <sub>3</sub>	Hf <sub>5</sub> CuSn <sub>3</sub>	<i>P</i> 6 <sub>3</sub> / <i>mcm</i>	905.09(6)	–	662.95(3)	Gulay et al., 2001c;
Y <sub>5</sub> CuPb <sub>3</sub>	Hf <sub>5</sub> CuSn <sub>3</sub>	<i>P</i> 6 <sub>3</sub> / <i>mcm</i>				Gulay, 2000
YCuPb	LiGaGe	<i>P</i> 6 <sub>3</sub> <i>mc</i>	455.85(1)	–	733.28(2)	Gulay et al., 2001b;
YCu <sub>4.74–4.11</sub> Pb <sub>0.26–0.89</sub>	AuBe <sub>5</sub>	<i>F</i> $\bar{4}3m$	709.93(2)–	–	–	Gulay, 2001a;
			714.48(2)			Gulay, 2000
Y <sub>~4</sub> Rh <sub>6</sub> Pb <sub>~19</sub>	?	<i>cubic</i>	1419(1)	–	–	Venturini et al., 1986
YPdPb	ZrNiAl	<i>P</i> $\bar{6}2m$	771.7(1)	–	385.4(1)	Iandelli, 1994
			772.2	–	383.7	Marazza et al., 1995
			772.62(2)	–	367.79(2)	Melnyk et al., 2004
Y <sub>2</sub> Pd <sub>2</sub> Pb	Mo <sub>2</sub> FeB <sub>2</sub>	<i>P</i> 4/ <i>mbm</i>	678.6	–	–	Marazza et al., 1995
YPd <sub>2</sub> Pb	MnCu <sub>2</sub> Al	<i>Fm</i> $\bar{3}m$	748.26(9)	–	442.47(3)	Gulay, 2001b
YAgPb	ZrNiAl	<i>P</i> $\bar{6}2m$				

TABLE 1 (continued)

Compound	Structure type	Space group	Lattice parameters (pm)			Reference(s)
			<i>a</i>	<i>b</i>	<i>c</i>	
Y(Ag <sub>0.39</sub> Pb <sub>0.61</sub> ) <sub>2</sub>	CaIn <sub>2</sub>	<i>P6<sub>3</sub>/mmc</i>	474.14(2)	–	743.46(4)	Gulay and Wołczyrz, 2001d
Y(Ag <sub>0.23(8)</sub> Pb <sub>0.77(8)</sub> ) <sub>3</sub>	AuCu <sub>3</sub>	<i>Pm<math>\bar{3}m</math></i>	465.71(2)	–	–	Gulay and Wołczyrz, 2001c
YAuPb	MgAgAs	<i>F<math>\bar{4}3m</math></i>	672.9	–	–	Marazza et al., 1988
La <sub>5</sub> CrPb <sub>3</sub>	Ti <sub>5</sub> Ga <sub>4</sub>	<i>P6<sub>3</sub>/mcm</i>	954.7(1)	–	701.2(2)	Guloy and Corbett, 1994
La <sub>5</sub> MnPb <sub>3</sub>	Ti <sub>5</sub> Ga <sub>4</sub>	<i>P6<sub>3</sub>/mcm</i>	954.3(1)	–	701.0(1)	Guloy and Corbett, 1994
La <sub>5</sub> FePb <sub>3</sub>	Ti <sub>5</sub> Ga <sub>4</sub>	<i>P6<sub>3</sub>/mcm</i>	954.3(1)	–	700.8(2)	Guloy and Corbett, 1994
La <sub>6</sub> Fe <sub>13</sub> Pb	La <sub>6</sub> Co <sub>11</sub> Ga <sub>3</sub>	<i>I4/mcm</i>	815.5(2)	–	2412.3(7)	Weitzer et al., 1993
La <sub>6</sub> Co <sub>13</sub> Pb	La <sub>6</sub> Co <sub>11</sub> Ga <sub>3</sub>	<i>I4/mcm</i>	810.1(1)	–	2353.3(8)	Weitzer et al., 1993
La <sub>5</sub> CoPb <sub>3</sub>	Ti <sub>5</sub> Ga <sub>4</sub>	<i>P6<sub>3</sub>/mcm</i>	954.2(1)	–	700.9(1)	Guloy and Corbett, 1994
La <sub>12</sub> Co <sub>6</sub> Pb	Sm <sub>12</sub> Ni <sub>6</sub> In	<i>Im<math>\bar{3}</math></i>	1016.1(2)	–	–	Gulay et al., 2000b
La <sub>12</sub> Ni <sub>6</sub> Pb	Sm <sub>12</sub> Ni <sub>6</sub> In	<i>Im<math>\bar{3}</math></i>	1023.3(2)	–	–	Gulay et al., 2000b
La <sub>4</sub> Ni <sub>3</sub> Pb <sub>4</sub>	La <sub>4</sub> Ni <sub>3</sub> Pb <sub>4</sub>	<i>R3</i>	1003.67(7)	–	955.58(8)	Gulay, 2005
			1002.7(1)	–	955.4(1)	Kaczorowski and Gulay, 2007
La <sub>5</sub> NiPb <sub>3</sub>	Hf <sub>5</sub> CuSn <sub>3</sub>	<i>P6<sub>3</sub>/mcm</i>	948.67(4)	–	698.39(4)	Gulay, 2005
La <sub>5</sub> NiPb <sub>3</sub>	Ti <sub>5</sub> Ga <sub>4</sub>	<i>P6<sub>3</sub>/mcm</i>	954.5(1)	–	701.1(2)	Guloy and Corbett, 1994
La <sub>5</sub> CuPb <sub>3</sub>	Ti <sub>5</sub> Ga <sub>4</sub>	<i>P6<sub>3</sub>/mcm</i>	955.0(1)	–	702.6(2)	Guloy and Corbett, 1994
La <sub>5</sub> CuPb <sub>3</sub>	Hf <sub>5</sub> CuSn <sub>3</sub>	<i>P6<sub>3</sub>/mcm</i>	956.0(2)	–	702.3(2)	Gulay et al., 2001c
LaCuPb	CaIn <sub>2</sub>	<i>P6<sub>3</sub>/mmc</i>	467.6(3)	–	796.4(5)	Mazzone et al., 1982
			467.0	–	797.1	Dhar et al., 1995
			466.74(4)	–	796.63(5)	Gulay, 2002
La <sub>5</sub> ZnPb <sub>3</sub>	Ti <sub>5</sub> Ga <sub>4</sub>	<i>P6<sub>3</sub>/mcm</i>	955.1(1)	–	702.8(2)	Guloy and Corbett, 1994

(continued on next page)

TABLE 1 (continued)

Compound	Structure type	Space group	Lattice parameters (pm)			Reference(s)
			<i>a</i>	<i>b</i>	<i>c</i>	
La <sub>5</sub> RuPb <sub>3</sub>	Ti <sub>5</sub> Ga <sub>4</sub>	<i>P6<sub>3</sub>/mcm</i>	955.8(1)	–	703.5(1)	Gulay and Corbett, 1994
La <sub>3</sub> Rh <sub>4</sub> Pb <sub>13</sub>	Yb <sub>3</sub> Rh <sub>4</sub> Sn <sub>13</sub>	<i>Pm<math>\bar{3}n</math></i>	1003.1(5)	–	–	Venturini et al., 1986
LaPdPb	ZrNiAl	<i>P<math>\bar{6}2m</math></i>	778.9(5)	–	417.8(4)	Iandelli, 1994
			778.8	–	414.6	Marazza et al., 1995
La <sub>2</sub> Pd <sub>2</sub> Pb	Mo <sub>2</sub> FeB <sub>2</sub>	<i>P4/mbm</i>	795.11(2)	–	393.37(1)	Melnyk et al., 2004
La <sub>5</sub> AgPb <sub>3</sub>	Ti <sub>5</sub> Ga <sub>4</sub>	<i>P6<sub>3</sub>/mcm</i>	956.0(1)	–	703.7(2)	Gulay and Corbett, 1994
LaAgPb	CaIn <sub>2</sub>	<i>P6<sub>3</sub>/mmc</i>	487.2(3)	–	785.0(5)	Mazzone et al., 1983
LaAgPb	LiGaGe	<i>P6<sub>3</sub>mc</i>	485.95(3)	–	784.84(4)	Gulay and Wołczyrz, 2001b
LaPtPb	ZrNiAl	<i>P<math>\bar{6}2m</math></i>	777	–	416	Movshovich et al., 1996
LaAuPb	CaIn <sub>2</sub>	<i>P6<sub>3</sub>/mmc</i>	482.0	–	784.2	Marazza et al., 1988
Ce <sub>5</sub> NiPb <sub>3</sub>	Hf <sub>5</sub> CuSn <sub>3</sub>	<i>P6<sub>3</sub>/mcm</i>	938.39(4)	–	679.22(4)	Gulay, 2005
Ce <sub>4</sub> Ni <sub>3</sub> Pb <sub>4</sub>	La <sub>4</sub> Ni <sub>3</sub> Pb <sub>4</sub>	<i>R3</i>	994.7(1)	–	946.04(9)	Gulay, 2005
			994.3(2)	–	945.9(2)	Kaczorowski and Gulay, 2007
			993.1	–	946.4	Shigetoh et al., 2006
Ce <sub>5</sub> CuPb <sub>3</sub>	Hf <sub>5</sub> CuSn <sub>3</sub>	<i>P6<sub>3</sub>/mcm</i>	955.1(2)	–	677.6(2)	Gulay et al., 2001c
Ce <sub>5</sub> CuPb <sub>3</sub>	Ti <sub>5</sub> Ga <sub>4</sub>	<i>P6<sub>3</sub>/mcm</i>	954.2(6)	–	677.2(6)	Rieger and Parthé, 1968
CeCuPb	CaIn <sub>2</sub>	<i>P6<sub>3</sub>/mmc</i>	465.8(3)	–	777.2(5)	Mazzone et al., 1982
			466.1	–	777.3	Dhar et al., 1995
			465.81(4)	–	777.93(6)	Gulay, 2002
Ce <sub>2</sub> Rh <sub>2</sub> Pb	U <sub>3</sub> Si <sub>2</sub>	<i>P4/mbm</i>	768.03(3)	–	374.78(2)	Strydom, 2005
Ce <sub>3</sub> Rh <sub>4</sub> Pb <sub>13</sub> (623 K)	Yb <sub>3</sub> Rh <sub>4</sub> Sn <sub>13</sub>	<i>Pm<math>\bar{3}n</math></i>	999.4(5)	–	–	Venturini et al., 1986

**TABLE 1** (continued)

Compound	Structure type	Space group	Lattice parameters (pm)			Reference(s)
			<i>a</i>	<i>b</i>	<i>c</i>	
Ce <sub>3</sub> Rh <sub>4</sub> Pb <sub>13</sub> (723 K)	Yb <sub>3</sub> Rh <sub>4</sub> Sn <sub>13</sub>	<i>Pm</i> $\bar{3}n$	1001.1(5)	–	–	Venturini et al., 1986
Ce <sub>8</sub> Pd <sub>24</sub> Pb	Ce <sub>8</sub> Pd <sub>24</sub> Sb	<i>Pm</i> $\bar{3}m$	846.05(8)	–	–	Gordon et al., 1996
			846.0(2)	–	–	Jones et al., 1999
Ce <sub>2</sub> Pd <sub>2</sub> Pb	U <sub>3</sub> Si <sub>2</sub>	<i>P4/mbm</i>	791.5(1)	–	387.2(2)	Gordon et al., 1995
			791.12(5)	–	386.67(3)	Melnyk et al., 2004
CePdPb	ZrNiAl	<i>P</i> $\bar{6}2m$	775.0(5)	–	414.0(4)	Iandelli, 1994
			774.2	–	413.8	Marazza et al., 1995
CeAgPb	LiGaGe	<i>P6<sub>3</sub>mc</i>	484.39(3)	–	773.41(3)	Gulay and Wolcyrz, 2001b
CeAgPb	CaIn <sub>2</sub>	<i>P6<sub>3</sub>/mmc</i>	483.6(3)	–	767.0(5)	Mazzone et al., 1983
Ce <sub>5</sub> AgPb <sub>3</sub>	Ti <sub>5</sub> Ga <sub>4</sub>	<i>P6<sub>3</sub>/mcm</i>	964.3(6)	–	677.0(8)	Rieger and Parthé, 1968
CePtPb	ZrNiAl	<i>P</i> $\bar{6}2m$	774	–	413	Movshovich et al., 1996
Ce <sub>2</sub> Pt <sub>2</sub> Pb	U <sub>3</sub> Si <sub>2</sub>	<i>P4/mbm</i>	794.63(7)	–	381.50(6)	Pöttgen et al., 2000
CeAuPb	CaIn <sub>2</sub>	<i>P6<sub>3</sub>/mmc</i>	480.2	–	773.9	Marazza et al., 1988
Ce <sub>2</sub> Au <sub>2</sub> Pb	U <sub>3</sub> Si <sub>2</sub>	<i>P4/mbm</i>	810.70(7)	–	394.85(7)	Pöttgen et al., 2000
Pr <sub>6</sub> Fe <sub>13</sub> Pb	La <sub>6</sub> Co <sub>11</sub> Ga <sub>3</sub>	<i>I4/mcm</i>	810.6(1)	–	2356.5(9)	Weitzer et al., 1993
			811.8(2)	–	2357.4(9)	Leithe-Jasper et al., 1996
Pr <sub>12</sub> Co <sub>6</sub> Pb	Sm <sub>12</sub> Ni <sub>6</sub> In	<i>Im</i> $\bar{3}$	993.0(2)	–	–	Gulay et al., 2000b
Pr <sub>5</sub> NiPb <sub>3</sub>	Hf <sub>5</sub> CuSn <sub>3</sub>	<i>P6<sub>3</sub>/mcm</i>	933.7(1)	–	679.27(6)	Gulay, 2005
Pr <sub>4</sub> Ni <sub>3</sub> Pb <sub>4</sub>	La <sub>4</sub> Ni <sub>3</sub> Pb <sub>4</sub>	<i>R</i> 3	988.9(1)	–	941.7(1)	Gulay, 2005
			988.6(1)	–	941.9(1)	Kaczorowski and Gulay, 2007
Pr <sub>12</sub> Ni <sub>6</sub> Pb	Sm <sub>12</sub> Ni <sub>6</sub> In	<i>Im</i> $\bar{3}$	995.4(1)	–	–	Gulay et al., 2000b

(continued on next page)

TABLE 1 (continued)

Compound	Structure type	Space group	Lattice parameters (pm)			Reference(s)
			<i>a</i>	<i>b</i>	<i>c</i>	
Pr <sub>5</sub> CuPb <sub>3</sub>	Hf <sub>5</sub> CuSn <sub>3</sub>	<i>P6<sub>3</sub>/mcm</i>	938.4(1)	–	677.34(7)	Gulay et al., 2001c
PrCuPb	CaIn <sub>2</sub>	<i>P6<sub>3</sub>/mmc</i>	464.6(3)	–	769.2(5)	Mazzone et al., 1982
Pr <sub>3</sub> Rh <sub>4</sub> Pb <sub>13</sub> (623 K)	Yb <sub>3</sub> Rh <sub>4</sub> Sn <sub>13</sub>	<i>Pm<math>\bar{3}n</math></i>	998.7(5)	–	–	Venturini et al., 1986
Pr <sub>3</sub> Rh <sub>4</sub> Pb <sub>13</sub> (723 K)	Yb <sub>3</sub> Rh <sub>4</sub> Sn <sub>13</sub>	<i>Pm<math>\bar{3}n</math></i>	1002.1(5)	–	–	Venturini et al., 1986
PrPdPb	ZrNiAl	<i>P<math>\bar{6}2m</math></i>	772.8(1)	–	410.6(1)	Iandelli, 1994
			773.4	–	411.4	Marazza et al., 1995
Pr <sub>2</sub> Pd <sub>2</sub> Pb	Mo <sub>2</sub> FeB <sub>2</sub>	<i>P4/mbm</i>	787.75(3)	–	383.62(2)	Melnyk et al., 2004
PrPd <sub>2</sub> Pb	MnCu <sub>2</sub> Al	<i>Fm<math>\bar{3}m</math></i>	694.7	–	–	Marazza et al., 1995
PrAgPb	LiGaGe	<i>P6<sub>3</sub>mc</i>	482.67(4)	–	767.45(5)	Gulay and Wołczyrz, 2001b
PrAuPb	CaIn <sub>2</sub>	<i>P6<sub>3</sub>/mmc</i>	478.5	–	768.1	Marazza et al., 1988
Nd <sub>6</sub> Fe <sub>13</sub> Pb	La <sub>6</sub> Co <sub>11</sub> Ga <sub>3</sub>	<i>I4/mcm</i>	809.2(1)	–	2345.2(8)	Weitzer et al., 1993
			808.8(1)	–	2341.7(9)	Leithe-Jasper et al., 1996
Nd <sub>12</sub> Co <sub>6</sub> Pb	Sm <sub>12</sub> Ni <sub>6</sub> In	<i>Im<math>\bar{3}</math></i>	987.7(2)	–	–	Gulay et al., 2000b
Nd <sub>5</sub> NiPb <sub>3</sub>	Hf <sub>5</sub> CuSn <sub>3</sub>	<i>P6<sub>3</sub>/mcm</i>	928.0(1)	–	677.67(5)	Gulay and Wołczyrz, 2001e
Nd <sub>12</sub> Ni <sub>6</sub> Pb	Sm <sub>12</sub> Ni <sub>6</sub> In	<i>Im<math>\bar{3}</math></i>	993.2(2)	–	–	Gulay et al., 2000b
Nd <sub>2</sub> Ni <sub>2</sub> Pb	Mn <sub>2</sub> AlB <sub>2</sub>	<i>Cmmm</i>	413.44(7)	1428.3(1)	374.59(6)	Gulay and Wołczyrz, 2001e
NdNiPb	TiNiSi	<i>Pnma</i>	742.49(3)	461.16(1)	782.38(3)	Gulay et al., 2000c
Nd <sub>5</sub> CuPb <sub>3</sub>	Hf <sub>5</sub> CuSn <sub>3</sub>	<i>P6<sub>3</sub>/mcm</i>	930.9(1)	–	675.23(6)	Gulay et al., 2001c
NdCuPb	CaIn <sub>2</sub>	<i>P6<sub>3</sub>/mmc</i>	461.8(4)	–	759.4(8)	Salamakha and Zaplatynsky, 1997
						Salamakha et al., 1999a, 1999c
NdZnPb	CaIn <sub>2</sub>	<i>P6<sub>3</sub>/mmc</i>	458.8(2)	–	817.9(5)	

TABLE 1 (continued)

Compound	Structure type	Space group	Lattice parameters (pm)			Reference(s)
			<i>a</i>	<i>b</i>	<i>c</i>	
Nd <sub>4</sub> Rh <sub>6</sub> Pb <sub>19</sub> (623 K)	?	<i>cubic</i>	1422(1)	–	–	Venturini et al., 1986
Nd <sub>4</sub> Rh <sub>6</sub> Pb <sub>19</sub> (723 K)	?	<i>tetragonal</i>	1415(1)	–	2877(2)	Venturini et al., 1986
Nd <sub>2</sub> Pd <sub>2</sub> Pb	Mo <sub>2</sub> FeB <sub>2</sub>	<i>P4/mbm</i>	784.8(2)	–	379.8(1)	Melnyk et al., 2004
NdPdPb	ZrNiAl	<i>P6̄2m</i>	771.1	–	407.2	Marazza et al., 1995
NdAgPb	LiGaGe	<i>P6<sub>3</sub>mc</i>	480.98(3)	–	762.43(3)	Gulay and Wołczyrz, 2001b
NdAgPb	CaIn <sub>2</sub>	<i>P6<sub>3</sub>/mmc</i>	481.6(3)	–	761.1(5)	Mazzone et al., 1983
			479.94(2)	–	767.35(1)	Zaplatsinskii et al., 1996; Salamakha et al., 1996
NdAuPb	CaIn <sub>2</sub>	<i>P6<sub>3</sub>/mmc</i>	476.4	–	762.8	Marazza et al., 1988
Sm <sub>6</sub> Fe <sub>13</sub> Pb	La <sub>6</sub> Co <sub>11</sub> Ga <sub>3</sub>	<i>I4/mcm</i>	806.5(1)	–	2326.5(9)	Weitzer et al., 1993
Sm <sub>12</sub> Co <sub>6</sub> Pb	Sm <sub>12</sub> Ni <sub>6</sub> In	<i>Im̄3</i>	978.0(1)	–	–	Gulay et al., 2000b
Sm <sub>12</sub> Ni <sub>6</sub> Pb	Sm <sub>12</sub> Ni <sub>6</sub> In	<i>Im̄3</i>	982.5(2)	–	–	Gulay et al., 2000b
Sm <sub>2</sub> Ni <sub>2</sub> Pb	Mn <sub>2</sub> AlB <sub>2</sub>	<i>Cmmm</i>	408.7(1)	1418.7(3)	371.6(1)	Gulay et al., 2000a
			409.18(5)	1418.2(1)	371.87(4)	Gulay and Hiebl, 2003
SmNiPb	TiNiSi	<i>Pnma</i>	731.99(3)	457.69(2)	780.15(3)	Gulay et al., 2000c
			731.67(1)	457.55(1)	779.63(1)	Gulay and Hiebl, 2002
Sm <sub>5</sub> NiPb <sub>3</sub>	Hf <sub>5</sub> CuSn <sub>3</sub>	<i>P6<sub>3</sub>/mcm</i>	917.1(2)	–	671.0(1)	Gulay, 2003a
Sm <sub>5</sub> CuPb <sub>3</sub>	Hf <sub>5</sub> CuSn <sub>3</sub>	<i>P6<sub>3</sub>/mcm</i>	931.6(1)	–	668.81(4)	Gulay et al., 2001c
SmCuPb	LiGaGe	<i>P6<sub>3</sub>mc</i>	459.65(2)	–	747.69(2)	Gulay et al., 2001b
SmCuPb	CaIn <sub>2</sub>	<i>P6<sub>3</sub>/mmc</i>	460.9(3)	–	749.6(5)	Mazzone et al., 1982
Sm <sub>4</sub> Rh <sub>6</sub> Pb <sub>19</sub> (623 K)	?	<i>cubic</i>	1421(1)	–	–	Venturini et al., 1986
Sm <sub>4</sub> Rh <sub>6</sub> Pb <sub>19</sub> (723 K)	?	<i>tetragonal</i>	1413(1)	–	2873(2)	Venturini et al., 1986

(continued on next page)

TABLE 1 (continued)

Compound	Structure type	Space group	Lattice parameters (pm)			Reference(s)
			<i>a</i>	<i>b</i>	<i>c</i>	
SmPdPb	ZrNiAl	$P\bar{6}2m$	769.1(1) 770.1	–	401.6(2) 400.1	Iandelli, 1994 Marazza et al., 1995
Sm <sub>2</sub> Pd <sub>2</sub> Pb	Mo <sub>2</sub> FeB <sub>2</sub>	$P4/mbm$	780.84(4)	–	375.82(3)	Melnyk et al., 2004
SmPd <sub>2</sub> Pb	MnCu <sub>2</sub> Al	$Fm\bar{3}m$	686.9	–	–	Marazza et al., 1995
SmAgPb	CaIn <sub>2</sub>	$P6_3/mmc$	478.2(3)	–	755.7(5)	Mazzone et al., 1983
SmAgPb	LiGaGe	$P6_3mc$	477.97(4)	–	753.50(5)	Gulay and Wołczyrz, 2001b
Sm(Ag <sub>0.29(8)</sub> Pb <sub>0.71(8)</sub> ) <sub>3</sub>	AuCu <sub>3</sub>	$Pm\bar{3}m$	470.66(1)	–	–	Gulay and Wołczyrz, 2001c
SmAuPb	CaIn <sub>2</sub>	$P6_3/mmc$	474.2	–	757.5	Marazza et al., 1988
EuMgPb	TiNiSi	$Pnma$	811.7(2)	486.7(1)	889.0(2)	Merlo et al., 1993
EuAgPb	CeCu <sub>2</sub>	$Imma$	495.1(2)	766.8(4)	855.6(4)	Merlo et al., 1996
EuZnPb	CeCu <sub>2</sub>	$Imma$	482.7(1)	796.8(2)	823.7(2)	Merlo et al., 1991
EuCdPb	LiGaGe	$P6_3mc$	492.9(1)	–	790.0(3)	Merlo et al., 1991
Eu <sub>3</sub> Rh <sub>4</sub> Pb <sub>13</sub>	Yb <sub>3</sub> Rh <sub>4</sub> Sn <sub>13</sub>	$Pm\bar{3}n$	1005.0(5)	–	–	Venturini et al., 1986
EuPdPb	TiNiSi	$Pnma$	751.9(1)	475.8(1)	827.1(1)	Sendlinger, 1993
EuAuPb	KHg <sub>2</sub>	$Imma$	487.0(1)	763.3(3)	841.2(3)	Arpe, 1998
EuHgPb	LiGaGe	$P6_3mc$	499.6(3)	–	778.7(6)	Merlo et al., 1993
Gd <sub>6</sub> Co <sub>2.37</sub> Pb <sub>0.56</sub>	Ho <sub>6</sub> Co <sub>2</sub> Ga	$Immm$	948.24(5)	951.61(5)	999.22(6)	Gulay and Wołczyrz, 2001a
Gd <sub>12</sub> Co <sub>6</sub> Pb	Sm <sub>12</sub> Ni <sub>6</sub> In	$Im\bar{3}$	972.7(2)	–	–	Gulay et al., 2000b
Gd <sub>12</sub> Ni <sub>6</sub> Pb	Sm <sub>12</sub> Ni <sub>6</sub> In	$Im\bar{3}$	977.0(2)	–	–	Gulay et al., 2000b

**TABLE 1** (continued)

Compound	Structure type	Space group	Lattice parameters (pm)			Reference(s)
			<i>a</i>	<i>b</i>	<i>c</i>	
Gd <sub>2</sub> Ni <sub>2</sub> Pb	Mn <sub>2</sub> AlB <sub>2</sub>	<i>Cmmm</i>	406.19(9)	1410.7(2)	369.42(9)	Gulay et al., 2000a
			405.97(5)	1411.2(1)	369.73(4)	Gulay and Hiebl, 2003
			403.6(2)	1402.8(3)	366.9(6)	Chinchure et al., 2003
GdNiPb	TiNiSi	<i>Pnma</i>	724.81(9)	454.28(6)	777.01(9)	Gulay et al., 2000c
			724.37(2)	454.76(1)	777.72(2)	Gulay and Hiebl, 2002
Gd <sub>5</sub> NiPb <sub>3</sub>	Hf <sub>5</sub> CuSn <sub>3</sub>	<i>P6<sub>3</sub>/mcm</i>	909.4(1)	–	664.27(7)	Gulay, 2003b
Gd <sub>6</sub> Ni <sub>2.5</sub> Pb <sub>0.5</sub>	Ho <sub>6</sub> Co <sub>2</sub> Ga	<i>Immm</i>	948.7(1)	967.3(1)	1003.2(1)	Gulay, 2003b
GdCuPb	LiGaGe	<i>P6<sub>3</sub>mc</i>	458.59(3)	–	741.69(3)	Gulay et al., 2001b
GdCuPb	CaIn <sub>2</sub>	<i>P6<sub>3</sub>/mmc</i>	459.0(3)	–	741.8(5)	Mazzone et al., 1982
			459.6	–	742.5	Dhar et al., 1995
Gd <sub>5</sub> CuPb <sub>3</sub>	Hf <sub>5</sub> CuSn <sub>3</sub>	<i>P6<sub>3</sub>/mcm</i>	913.5(3)	–	665.8(2)	Gulay et al., 2001c
GdCu <sub>4.60</sub> Pb <sub>0.40</sub>	AuBe <sub>5</sub>	<i>F43m</i>	712.88(5)	–	–	Gulay, 2001a
GdPdPb	ZrNiAl	<i>P62m</i>	771.5(2)	–	392.5(1)	Iandelli, 1994
			772.0	–	392.1	Marazza et al., 1995
Gd <sub>2</sub> Pd <sub>2</sub> Pb	Mo <sub>2</sub> FeB <sub>2</sub>	<i>P4/mbm</i>	778.29(3)	–	372.07(2)	Melnyk et al., 2004
GdPd <sub>2</sub> Pb	MnCu <sub>2</sub> Al	<i>Fm3m</i>	683.5	–	–	Marazza et al., 1995
GdAgPb	CaIn <sub>2</sub>	<i>P6<sub>3</sub>/mmc</i>	476.9(3)	–	747.5(5)	Mazzone et al., 1983
GdAgPb	LiGaGe	<i>P6<sub>3</sub>mc</i>	476.51(3)	–	747.39(4)	Gulay and Wołczyrz, 2001b
Gd(Ag <sub>0.26(7)</sub> Pb <sub>0.74(7)</sub> ) <sub>3</sub>	AuCu <sub>3</sub>	<i>Pm3m</i>	465.82(1)	–	–	Gulay and Wołczyrz, 2001c
GdAuPb	MgAgAs	<i>F43m</i>	677.5	–	–	Marazza et al., 1988
Tb <sub>6</sub> Co <sub>2.35</sub> Pb <sub>0.61</sub>	Ho <sub>6</sub> Co <sub>2</sub> Ga	<i>Immm</i>	940.95(6)	943.38(6)	991.01(6)	Gulay and Wołczyrz, 2001a
Tb <sub>6</sub> Ni <sub>2.38</sub> Pb <sub>0.63</sub>	Ho <sub>6</sub> Co <sub>2</sub> Ga	<i>Immm</i>	935.92(6)	955.03(6)	994.43(7)	Gulay and Wołczyrz, 2001a

(continued on next page)

TABLE 1 (continued)

Compound	Structure type	Space group	Lattice parameters (pm)			Reference(s)
			<i>a</i>	<i>b</i>	<i>c</i>	
Tb <sub>12</sub> Ni <sub>6</sub> Pb	Sm <sub>12</sub> Ni <sub>6</sub> In	<i>Im</i> $\bar{3}$	970.7(2)	–	–	Gulay et al., 2000b
Tb <sub>5</sub> NiPb <sub>3</sub>	Hf <sub>5</sub> CuSn <sub>3</sub>	<i>P6</i> <sub>3</sub> / <i>mcm</i>	904.48(7)	–	661.01(3)	Gulay, 2005
Tb <sub>2</sub> Ni <sub>2</sub> Pb	Mn <sub>2</sub> AlB <sub>2</sub>	<i>Cmmm</i>	404.3(1)	1405.5(4)	367.0(1)	Gulay et al., 2000a
			403.96(5)	1405.0(1)	367.20(5)	Gulay and Hiebl, 2003
			398.5(1)	1382.2(3)	357.0(1)	Chinchure et al., 2003
TbNiPb	TiNiSi	<i>Pnma</i>	718.67(4)	453.31(2)	776.18(5)	Gulay et al., 2000c
			718.82(1)	453.39(1)	776.05(2)	Gulay and Hiebl, 2002
TbCuPb	LiGaGe	<i>P6</i> <sub>3</sub> <i>mc</i>	457.17(1)	–	735.37(3)	Gulay et al., 2001b
Tb <sub>5</sub> CuPb <sub>3</sub>	Hf <sub>5</sub> CuSn <sub>3</sub>	<i>P6</i> <sub>3</sub> / <i>mcm</i>	906.80(6)	–	659.62(3)	Gulay et al., 2001c
TbCu <sub>5-4.44</sub> Pb <sub>0-0.56</sub>	AuBe <sub>5</sub>	<i>F</i> $\bar{4}$ <i>3m</i>	704.1–	–	–	Gulay, 2001a
			715.55(2)	–	–	
Tb <sub>2</sub> Pd <sub>2</sub> Pb	Mo <sub>2</sub> FeB <sub>2</sub>	<i>P4/mbm</i>	775.03(3)	–	368.83(2)	Melnyk et al., 2004
TbPd <sub>2</sub> Pb	MnCu <sub>2</sub> Al	<i>Fm</i> $\bar{3}$ <i>m</i>	680.5	–	–	Marazza et al., 1995
TbPdPb	ZrNiAl	<i>P</i> $\bar{6}$ <i>2m</i>	772.3	–	386.1	Marazza et al., 1995
TbAgPb	LiGaGe	<i>P6</i> <sub>3</sub> <i>mc</i>	475.24(3)	–	743.22(3)	Gulay and Wołczyrz, 2001b
Tb(Ag <sub>0.23(9)</sub> Pb <sub>0.77(9)</sub> ) <sub>3</sub>	AuCu <sub>3</sub>	<i>Pm</i> $\bar{3}$ <i>m</i>	463.96(2)	–	–	Gulay and Wołczyrz, 2001c
TbAuPb	MgAgAs	<i>F</i> $\bar{4}$ <i>3m</i>	674.7	–	–	Marazza et al., 1988
Dy <sub>6</sub> Co <sub>2.37</sub> Pb <sub>0.53</sub>	Ho <sub>6</sub> Co <sub>2</sub> Ga	<i>Immm</i>	937.54(3)	939.76(3)	988.01(4)	Gulay and Wołczyrz, 2001a
Dy <sub>6</sub> Ni <sub>2.39</sub> Pb <sub>0.55</sub>	Ho <sub>6</sub> Co <sub>2</sub> Ga	<i>Immm</i>	937.48(3)	954.27(3)	988.23(3)	Gulay and Wołczyrz, 2001a
Dy <sub>12</sub> Ni <sub>6</sub> Pb	Sm <sub>12</sub> Ni <sub>6</sub> In	<i>Im</i> $\bar{3}$	966.2(1)	–	–	Gulay et al., 2000b
Dy <sub>2</sub> Ni <sub>2</sub> Pb	Mn <sub>2</sub> AlB <sub>2</sub>	<i>Cmmm</i>	402.6(1)	1399.4(4)	365.1(1)	Gulay et al., 2000a
			402.65(4)	1401.1(1)	365.15(4)	Gulay and Hiebl, 2003

**TABLE 1** (continued)

Compound	Structure type	Space group	Lattice parameters (pm)			Reference(s)
			<i>a</i>	<i>b</i>	<i>c</i>	
DyNiPb	TiNiSi	<i>Pnma</i>	714.85(5) 714.09(2)	452.19(3) 452.16(1)	774.81(6) 774.62(5)	Gulay et al., 2000c Gulay and Hiebl, 2002
Dy <sub>5</sub> NiPb <sub>3</sub>	Hf <sub>5</sub> CuSn <sub>3</sub>	<i>P6<sub>3</sub>/mcm</i>	895.6(1)	–	657.33(7)	Gulay, 2005
DyCuPb	CaIn <sub>2</sub>	<i>P6<sub>3</sub>/mmc</i>	456.2(3)	–	732.0(5)	Mazzone et al., 1982
DyCuPb	LiGaGe	<i>P6<sub>3</sub>mc</i>	455.85(3)	–	732.60(3)	Gulay et al., 2001a; Gulay et al., 2001b
Dy <sub>5</sub> CuPb <sub>3</sub>	Hf <sub>5</sub> CuSn <sub>3</sub>	<i>P6<sub>3</sub>/mcm</i>	900.4(2)	–	657.0(2)	Gulay et al., 2001a
Dy <sub>5</sub> CuPb <sub>3</sub>	Hf <sub>5</sub> CuSn <sub>3</sub>	<i>P6<sub>3</sub>/mcm</i>	906.0(3)	–	657.8(2)	Tran and Gulay, 2006
DyCu <sub>5–4.47</sub> Pb <sub>0–0.53</sub>	AuBe <sub>5</sub>	<i>F43m</i>	702.7– 714.52(2)	–	–	Gulay, 2001a; Gulay et al., 2001a
DyPdPb	ZrNiAl	<i>P6̄2m</i>	771.3(2) 772.3	– –	385.3(2) 383.0	Iandelli, 1994 Marazza et al., 1995
Dy <sub>2</sub> Pd <sub>2</sub> Pb	Mo <sub>2</sub> FeB <sub>2</sub>	<i>P4/mbm</i>	774.95(2)	–	365.67(1)	Melnyk et al., 2004
DyPd <sub>2</sub> Pb	MnCu <sub>2</sub> Al	<i>Fm3̄m</i>	679.9	–	–	Marazza et al., 1995
DyAgPb	CaIn <sub>2</sub>	<i>P6<sub>3</sub>/mmc</i>	474.4(3)	–	741.5(5)	Mazzone et al., 1983
DyAgPb	LiGaGe	<i>P6<sub>3</sub>mc</i>	474.22(3)	–	741.01(3)	Gulay and Wołczyrz, 2001b
Dy(Ag <sub>0.30(9)</sub> Pb <sub>0.70(9)</sub> ) <sub>3</sub>	AuCu <sub>3</sub>	<i>Pm3̄m</i>	465.14(2)	–	–	Gulay and Wołczyrz, 2001c; Gulay et al., 2001c
DyAuPb	MgAgAs	<i>F43m</i>	672.8	–	–	Marazza et al., 1988
Ho <sub>6</sub> Co <sub>2.20</sub> Pb <sub>0.59</sub>	Ho <sub>6</sub> Co <sub>2</sub> Ga	<i>Immm</i>	931.46(5)	935.44(6)	980.39(6)	Gulay and Wołczyrz, 2001a
Ho <sub>6</sub> Ni <sub>2.41</sub> Pb <sub>0.53</sub>	Ho <sub>6</sub> Co <sub>2</sub> Ga	<i>Immm</i>	927.72(4)	946.61(4)	983.91(5)	Gulay and Wołczyrz, 2001a
Ho <sub>5</sub> NiPb <sub>3</sub>	Hf <sub>5</sub> CuSn <sub>3</sub>	<i>P6<sub>3</sub>/mcm</i>	893.15(6)	–	656.49(2)	Gulay, 2005

(continued on next page)

TABLE 1 (continued)

Compound	Structure type	Space group	Lattice parameters (pm)			Reference(s)
			<i>a</i>	<i>b</i>	<i>c</i>	
Ho <sub>12</sub> Ni <sub>6</sub> Pb	Sm <sub>12</sub> Ni <sub>6</sub> In	<i>Im</i> $\bar{3}$	960.4(2)	–	–	Gulay et al., 2000b
Ho <sub>2</sub> Ni <sub>2</sub> Pb	Mn <sub>2</sub> AlB <sub>2</sub>	<i>Cmmm</i>	401.72(4)	1396.95(6)	363.36(3)	Gulay et al., 2000a
			401.39(7)	1397.6(2)	363.62(7)	Gulay and Hiebl, 2003
			402	1394	363	Chinchure et al., 2002
			405.6(2)	1410.4(2)	369.7(2)	Chinchure et al., 2003
HoNiPb	TiNiSi	<i>Pnma</i>	711.35(3)	451.54(2)	773.86(3)	Gulay et al., 2000c
			710.43(1)	451.11(6)	773.23(1)	Gulay and Hiebl, 2002
HoCuPb	CaIn <sub>2</sub>	<i>P6<sub>3</sub>/mmc</i>	455.1(3)	–	728.7(5)	Mazzone et al., 1982
HoCuPb	LiGaGe	<i>P6<sub>3</sub>mc</i>	454.58(3)	–	729.34(3)	Gulay et al., 2001b
Ho <sub>5</sub> CuPb <sub>3</sub>	Hf <sub>5</sub> CuSn <sub>3</sub>	<i>P6<sub>3</sub>/mcm</i>	895.6(1)	–	656.01(6)	Gulay et al., 2001c
HoCu <sub>5–4.50</sub> Pb <sub>0–0.50</sub>	AuBe <sub>5</sub>	<i>F</i> $\bar{4}3m$	701.6–	–	–	Gulay, 2001a
			709.65(2)			
Ho <sub>2</sub> Pd <sub>2</sub> Pb	Mo <sub>2</sub> FeB <sub>2</sub>	<i>P4/mbm</i>	773.77(3)	–	363.50(2)	Melnyk et al., 2004
HoPd <sub>2</sub> Pb	MnCu <sub>2</sub> Al	<i>Fm</i> $\bar{3}m$	678.1	–	–	Marazza et al., 1995
HoPdPb	ZrNiAl	<i>P</i> $\bar{6}2m$	772.0	–	381.5	Marazza et al., 1995
HoAgPb	LiGaGe	<i>P6<sub>3</sub>mc</i>	472.97(3)	–	737.98(3)	Gulay and Wołczyrz, 2001b
Ho(Ag <sub>0.26(6)</sub> Pb <sub>0.74(6)</sub> ) <sub>3</sub>	AuCu <sub>3</sub>	<i>Pm</i> $\bar{3}m$	461.75(2)	–	–	Gulay and Wołczyrz, 2001c
HoAuPb	MgAgAs	<i>F</i> $\bar{4}3m$	671.8	–	–	Marazza et al., 1988
Er <sub>6</sub> Co <sub>2.08</sub> Pb <sub>0.63</sub>	Ho <sub>6</sub> Co <sub>2</sub> Ga	<i>Immm</i>	928.53(5)	928.40(5)	979.62(6)	Gulay and Wołczyrz, 2001a
Er <sub>6</sub> Ni <sub>2.22</sub> Pb <sub>0.54</sub>	Ho <sub>6</sub> Co <sub>2</sub> Ga	<i>Immm</i>	925.42(4)	943.12(5)	981.14(5)	Gulay and Wołczyrz, 2001a
Er <sub>5</sub> NiPb <sub>3</sub>	Hf <sub>5</sub> CuSn <sub>3</sub>	<i>P6<sub>3</sub>/mcm</i>	890.65(7)	–	656.31(3)	Gulay, 2005

TABLE 1 (continued)

Compound	Structure type	Space group	Lattice parameters (pm)			Reference(s)
			<i>a</i>	<i>b</i>	<i>c</i>	
Er <sub>2</sub> Ni <sub>2</sub> Pb	Mn <sub>2</sub> AlB <sub>2</sub>	<i>Cmmm</i>	400.8(1)	1393.1(4)	361.7(1)	Gulay et al., 2000a
			400.82(3)	1392.89(8)	361.77(3)	Gulay and Hiebl, 2003
			400.80(7)	1389.97(4)	360.31(2)	Chinchure et al., 2001
			401.6(1)	1402.1(3)	368.5(2)	Chinchure et al., 2003
ErNiPb	TiNiSi	<i>Pnma</i>	707.56(7)	450.28(4)	772.27(7)	Gulay et al., 2000c
			707.10(2)	450.37(1)	772.36(2)	Gulay and Hiebl, 2002
ErCuPb	LiGaGe	<i>P6<sub>3</sub>mc</i>	452.83(2)	–	725.46(3)	Gulay et al., 2001b
ErCuPb	CaIn <sub>2</sub>	<i>P6<sub>3</sub>/mmc</i>	454.1(3)	–	726.1(5)	Mazzone et al., 1982
Er <sub>5</sub> CuPb <sub>3</sub>	Hf <sub>5</sub> CuSn <sub>3</sub>	<i>P6<sub>3</sub>/mcm</i>	891.43(5)	–	653.19(2)	Gulay et al., 2001c
ErCu <sub>5–4.34</sub> Pb <sub>0–0.66</sub>	AuBe <sub>5</sub>	<i>F4̄3m</i>	700.3–	–	–	Gulay, 2001a
			711.29(4)			
ErPdPb	ZrNiAl	<i>P6̄2m</i>	771.4(1)	–	379.8(2)	Iandelli, 1994
			770.4	–	379.4	Marazza et al., 1995
Er <sub>2</sub> Pd <sub>2</sub> Pb	Mo <sub>2</sub> FeB <sub>2</sub>	<i>P4/mbm</i>	771.57(4)	–	361.57(3)	Melnyk et al., 2004
ErPd <sub>2</sub> Pb	MnCu <sub>2</sub> Al	<i>Fm3̄m</i>	673.9	–	–	Marazza et al., 1995
ErAgPb	CaIn <sub>2</sub>	<i>P6<sub>3</sub>/mmc</i>	472.1(3)	–	738.0(5)	Mazzone et al., 1983
ErAgPb	ZrNiAl	<i>P6̄2m</i>	740.62(7)	–	445.96(2)	Gulay, 2001b
Er(Ag <sub>0.35</sub> Pb <sub>0.65</sub> ) <sub>2</sub>	CaIn <sub>2</sub>	<i>P6<sub>3</sub>/mmc</i>	471.70(2)	–	737.11(4)	Gulay and Wołczyrz, 2001d
Er(Ag <sub>0.24(9)</sub> Pb <sub>0.76(9)</sub> ) <sub>3</sub>	AuCu <sub>3</sub>	<i>Pm3̄m</i>	462.44(2)	–	–	Gulay and Wołczyrz, 2001c
ErAuPb	MgAgAs	<i>F4̄3m</i>	669.4	–	–	Marazza et al., 1988
Tm <sub>6</sub> Co <sub>2.17</sub> Pb <sub>0.59</sub>	Ho <sub>6</sub> Co <sub>2</sub> Ga	<i>Immm</i>	924.78(4)	923.74(4)	975.83(4)	Gulay and Wołczyrz, 2001a
Tm <sub>6</sub> Ni <sub>2.22</sub> Pb <sub>0.57</sub>	Ho <sub>6</sub> Co <sub>2</sub> Ga	<i>Immm</i>	919.71(5)	935.53(6)	973.73(6)	Gulay and Wołczyrz, 2001a

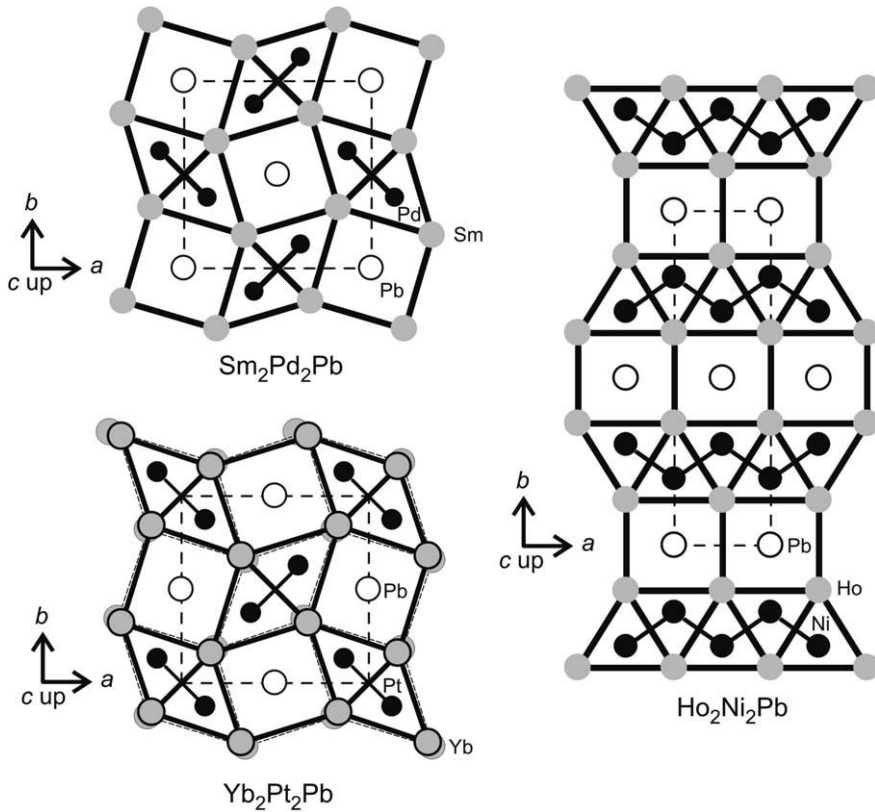
(continued on next page)

TABLE 1 (continued)

Compound	Structure type	Space group	Lattice parameters (pm)			Reference(s)
			<i>a</i>	<i>b</i>	<i>c</i>	
Tm <sub>5</sub> NiPb <sub>3</sub>	Hf <sub>5</sub> CuSn <sub>3</sub>	<i>P6<sub>3</sub>/mcm</i>	886.55(8)	–	653.02(3)	Gulay, 2005
Tm <sub>2</sub> Ni <sub>2</sub> Pb	Mn <sub>2</sub> AlB <sub>2</sub>	<i>Cmmm</i>	399.10(3)	1389.52(6)	359.92(2)	Gulay et al., 2000a
			399.35(5)	1389.2(1)	360.81(5)	Gulay and Hiebl, 2003
TmNiPb	TiNiSi	<i>Pnma</i>	703.49(5)	449.24(3)	770.76(6)	Gulay et al., 2000c
			703.09(2)	449.37(1)	770.85(2)	Gulay and Hiebl, 2002
TmCuPb	LiGaGe	<i>P6<sub>3</sub>mc</i>	452.56(1)	–	723.49(2)	Gulay et al., 2001b
Tm <sub>5</sub> CuPb <sub>3</sub>	Hf <sub>5</sub> CuSn <sub>3</sub>	<i>P6<sub>3</sub>/mcm</i>	890.04(8)	–	651.42(4)	Gulay et al., 2001c
TmCu <sub>5-4.55</sub> Pb <sub>0-0.45</sub>	AuBe <sub>5</sub>	<i>F4<sub>3</sub>m</i>	699.1–	–	–	Gulay, 2001a
			709.30(4)			
Tm <sub>2</sub> Pd <sub>2</sub> Pb	Mo <sub>2</sub> FeB <sub>2</sub>	<i>P4/mbm</i>	770.21(3)	–	359.00(2)	Melnyk et al., 2004
TmPdPb	ZrNiAl	<i>P6<sub>2</sub>m</i>	771.0	–	375.4	Marazza et al., 1995
TmAgPb	ZrNiAl	<i>P6<sub>2</sub>m</i>	737.14(7)	–	445.69(2)	Gulay, 2001b
Tm(Ag <sub>0.31</sub> Pb <sub>0.69</sub> ) <sub>2</sub>	CaIn <sub>2</sub>	<i>P6<sub>3</sub>/mmc</i>	470.35(2)	–	735.64(5)	Gulay and Wołczyrz, 2001d
Tm(Ag <sub>0.22(8)</sub> Pb <sub>0.78(8)</sub> ) <sub>3</sub>	AuCu <sub>3</sub>	<i>Pm3̄m</i>	460.56(2)	–	–	Gulay and Wołczyrz, 2001c
YbLiPb	YbAgPb	<i>P6̄m2</i>	491.8(1)	–	1092.1(3)	Fornasini et al., 2001b
YbMgPb	ZrNiAl	<i>P6<sub>2</sub>m</i>	771.9(1)	–	472.8(1)	Merlo et al., 1993
YbCuPb	CaIn <sub>2</sub>	<i>P6<sub>3</sub>/mmc</i>	455.7(3)	–	733.1(5)	Mazzone et al., 1982
YbZnPb	LiGaGe	<i>P6<sub>3</sub>mc</i>	471.6(1)	–	762.5(1)	Merlo et al., 1991
Yb <sub>~4</sub> Rh <sub>6</sub> Pb <sub>~19</sub>	?	<i>cubic</i>	1418(1)	–	–	Venturini et al., 1986

TABLE 1 (continued)

Compound	Structure type	Space group	Lattice parameters (pm)			Reference(s)
			<i>a</i>	<i>b</i>	<i>c</i>	
YbPd <sub>2</sub> Pb	MnCu <sub>2</sub> Al	<i>Fm</i> $\bar{3}m$	673.3	–	–	Marazza et al., 1995
YbAgPb	CaIn <sub>2</sub>	<i>P</i> 6 <sub>3</sub> / <i>mmc</i>	489	–	723	Mazzone et al., 1983
YbAgPb	YbAgPb	<i>P</i> $\bar{6}m2$	487.3(1)	–	1101.7(3)	Merlo et al., 1996
YbCdPb	ZrNiAl	<i>P</i> $\bar{6}2m$	770.4(1)	–	471.9(1)	Merlo et al., 1991
Yb <sub>2</sub> Pt <sub>2</sub> Pb	Er <sub>2</sub> Au <sub>2</sub> Sn	<i>P</i> 4 <sub>2</sub> / <i>mnm</i>	776.0(1)	–	701.8(2)	Pöttgen et al., 1999a
Yb <sub>2</sub> Au <sub>2</sub> Pb	Er <sub>2</sub> Au <sub>2</sub> Sn	<i>P</i> 4 <sub>2</sub> / <i>mnm</i>	803.7(2)	–	746.5(2)	Fornasini et al., 2001a
YbHgPb	ZrBeSi	<i>P</i> 6 <sub>3</sub> / <i>mmc</i>	492.2(2)	–	723.1(5)	Merlo et al., 1993
Lu <sub>6</sub> Co <sub>2.07</sub> Pb <sub>0.61</sub>	Ho <sub>6</sub> Co <sub>2</sub> Ga	<i>I</i> <i>mmm</i>	919.96(4)	918.04(5)	968.92(5)	Gulay and Wołczyrz, 2001a
Lu <sub>6</sub> Ni <sub>2.10</sub> Pb <sub>0.56</sub>	Ho <sub>6</sub> Co <sub>2</sub> Ga	<i>I</i> <i>mmm</i>	911.70(4)	927.15(4)	967.44(5)	Gulay and Wołczyrz, 2001a
Lu <sub>5</sub> NiPb <sub>3</sub>	Hf <sub>5</sub> CuSn <sub>3</sub>	<i>P</i> 6 <sub>3</sub> / <i>mcm</i>	877.5(1)	–	651.16(6)	Gulay, 2005
Lu <sub>2</sub> Ni <sub>2</sub> Pb	Mn <sub>2</sub> AlB <sub>2</sub>	<i>C</i> <i>mmm</i>	398.44(9)	1385.1(2)	358.01(9)	Gulay et al., 2000a
LuNiPb	TiNiSi	<i>P</i> <i>nma</i>	698.52(6)	448.05(3)	769.08(6)	Gulay et al., 2000c
LuCuPb	LiGaGe	<i>P</i> 6 <sub>3</sub> / <i>mc</i>	450.52(1)	–	720.02(2)	Gulay et al., 2001b
Lu <sub>5</sub> CuPb <sub>3</sub>	Hf <sub>5</sub> CuSn <sub>3</sub>	<i>P</i> 6 <sub>3</sub> / <i>mcm</i>	876.0(1)	–	646.51(5)	Gulay et al., 2001c
LuCu <sub>5-4.42</sub> Pb <sub>0-0.58</sub>	AuBe <sub>5</sub>	<i>F</i> $\bar{4}3m$	697.0– 711.40(1)	–	–	Gulay, 2001a
Lu <sub>2</sub> Pd <sub>2</sub> Pb	Mo <sub>2</sub> FeB <sub>2</sub>	<i>P</i> 4/ <i>mbm</i>	769.30(2)	–	355.99(1)	Melnyk et al., 2004
LuAgPb	ZrNiAl	<i>P</i> $\bar{6}2m$	737.23(5)	–	441.18(2)	Gulay, 2001b



**FIGURE 14** Projections of the  $\text{Sm}_2\text{Pd}_2\text{Pb}$ ,  $\text{Yb}_2\text{Pt}_2\text{Pb}$ , and  $\text{Ho}_2\text{Ni}_2\text{Pb}$  structures along the shortest unit cell axes. The rare earth metal, transition metal, and lead atoms are drawn as medium gray, black filled, and open circles, respectively. The distorted  $\text{AlB}_2$  and  $\text{CsCl}$  related slabs are emphasized.

dislocate from the subcell mirror planes, leading to distortions for the trigonal and the square prisms. This kind of superstructure has first been observed for  $\text{Er}_2\text{Au}_2\text{Sn}$  (Pöttgen, 1994). Since the crystal chemistry of the  $\text{R}_2\text{T}_2\text{X}$  intermetallics has recently been reviewed (Lukachuk and Pöttgen, 2003), for further details we refer to this overview.

### 4.3 The structure types $\text{CaIn}_2$ , $\text{ZrBeSi}$ , $\text{NdPtSb}$ , $\text{LiGaGe}$ , $\text{CaLiSn}$ , and $\text{YbAgPb}$

Structure type  $\text{CaIn}_2$  (Iandelli, 1964) (Figure 15). SG  $P6_3/mmc$ ;  $Z = 2$ ,  $a = 455.7$ ,  $c = 733.1$  pm for  $\text{YbCuPb}$  (Mazzone et al., 1982).  $2\text{Yb}$ :  $2b\ 0\ 0\ 1/4$ ,  $4\text{M}$ :  $4f\ 1/3\ 2/3\ z$  ( $\text{M} = \text{Cu}_{0.5}\text{Pb}_{0.5}$ ,  $z = 0.04$ ).

Structure type  $\text{NdPtSb}$  (Wenski and Mewis, 1986) (Figure 15). SG  $P6_3mc$ ,  $Z = 2$ ,  $a = 466.74(4)$ ,  $c = 796.63(5)$  pm for  $\text{LaCuPb}$  (Gulay, 2002).  $2\text{La}$ :  $2a\ 0\ 0\ 0$ ;  $2\text{Cu}$ :  $2b\ 1/3\ 2/3\ z$  ( $z = 0.808$ );  $2\text{Pb}$ :  $2b\ 1/3\ 2/3\ z$  ( $z = 0.2499$ ).

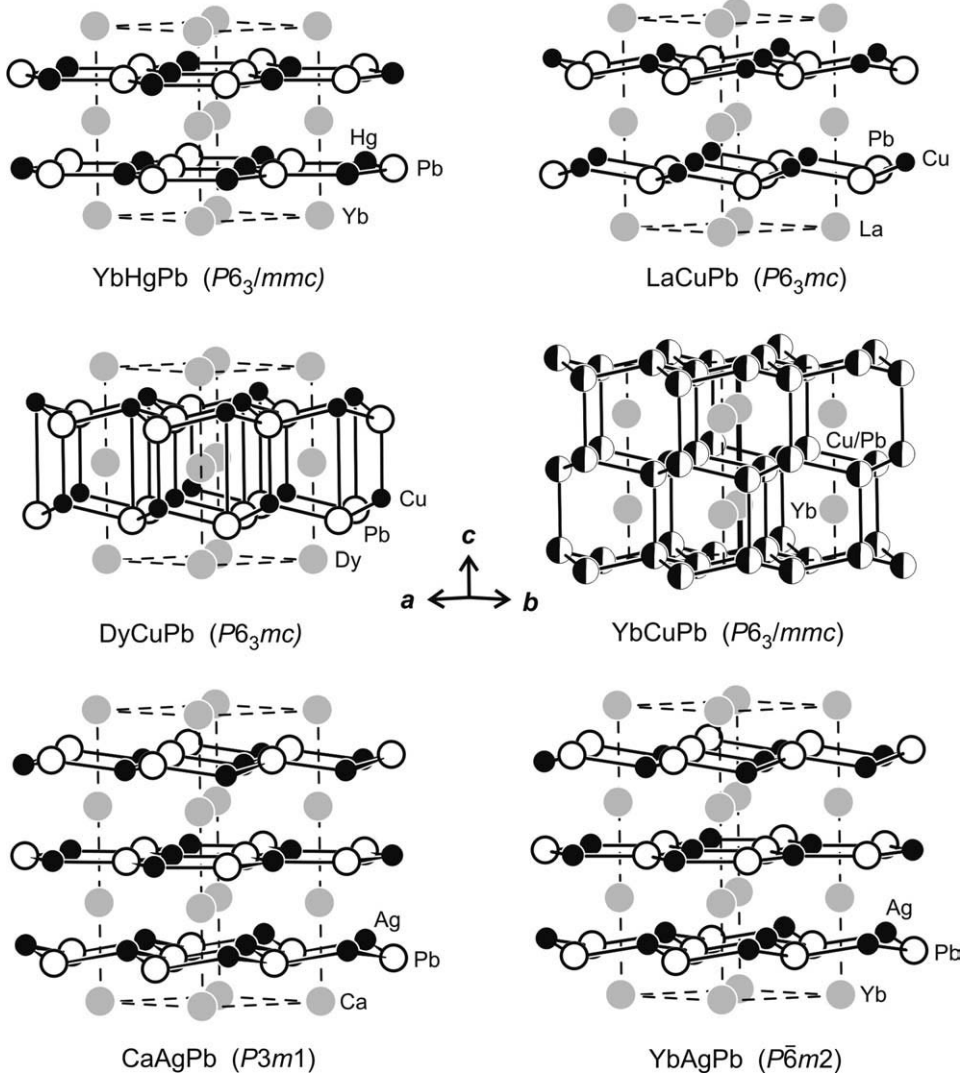


**FIGURE 15** The crystal structures of YbHgPb, LaCuPb, DyCuPb, YbCuPb, CaAgPb, and YbAgPb. The rare earth (alkaline earth), transition metal (T), and lead atoms are drawn as medium gray, black filled, and open circles, respectively. The mixed-occupied site in the YbCuPb structure is shown with segments. The two- and three-dimensional [TPb] networks are emphasized.

Structure type LiGaGe (Bockelmann et al., 1970; Bockelmann and Schuster, 1974) (Figure 15). SG  $P6_3mc$ ,  $Z = 2$ ,  $a = 457.1(1)$ ,  $c = 734.5(1)$  pm for DyCuPb (Gulay et al., 2001a).  $2Dy: 2a\ 0\ 0\ 0$ ;  $2Cu: 2b\ 1/3\ 2/3\ z$  ( $z = 0.8153$ );  $2Pb: 2b\ 1/3\ 2/3\ z$  ( $z = 0.2278$ ).

Structure type CaLiSn (Müller and Voltz, 1974) (Figure 15). SG  $P3m1$ ,  $Z = 3$ ,  $a = 487.9(1)$ ,  $c = 1112.1(2)$  pm for CaAgPb (Merlo et al., 1996).  $1Ca1: 1a\ 0\ 0\ z$

( $z = 0.337$ ); 1Ca2:  $1a\ 0\ 0\ z$  ( $z = 0.669$ ); 1Ca3:  $1a\ 0\ 0\ z$  ( $z = 0.000$ ); 1Ag1:  $1b\ 1/3\ 2/3\ z$  ( $z = 0.1917$ ); 1Ag2:  $1b\ 1/3\ 2/3\ z$  ( $z = 0.8110$ ); 1Ag3:  $1c\ 2/3\ 1/3\ z$  ( $z = 0.499$ ); 1Pb1:  $1b\ 1/3\ 2/3\ z$  ( $z = 0.4976$ ); 1Pb2:  $1c\ 2/3\ 1/3\ z$  ( $z = 0.1488$ ); 1Pb3:  $1c\ 2/3\ 1/3\ z$  ( $z = 0.8464$ ).

Structure type ZrBeSi (Nielsen and Baenziger, 1954) (Figure 15). SG  $P6_3/mmc$ ,  $Z = 2$ ,  $a = 492.2(2)$ ,  $c = 723.1(5)$  pm for YbHgPb (Merlo et al., 1993). 2Yb:  $2a\ 0\ 0\ 0$ ; 2Hg:  $2c\ 1/3\ 2/3\ 1/4$ ; 2Pb:  $2d\ 1/3\ 2/3\ 3/4$ .

Structure type YbAgPb (Merlo et al., 1996) (Figure 15). SG  $P\bar{6}m2$ ,  $Z = 3$ ,  $a = 487.3(1)$ ,  $c = 1101.7(3)$  pm. 2Yb1:  $2g\ 0\ 0\ z$  ( $z = 0.3341$ ); 1Yb2:  $1a\ 0\ 0\ 0$ ; 2Ag1:  $2h\ 1/3\ 2/3\ z$  ( $z = 0.1937$ ); 1Ag2:  $1f\ 2/3\ 1/3\ 1/2$ ; 2Pb1:  $2i\ 2/3\ 1/3\ z$  ( $z = 0.1522$ ); 1Pb2:  $1d\ 1/3\ 2/3\ 1/2$ .

The basic structural units in the six structure types presented in Figure 15 are planar or slightly puckered  $T_3Pb_3$  hexagons. These hexagons show different stacking sequences and they are separated by the rare earth atoms. These arrangements resemble the well known  $AlB_2$  type, and indeed, these structure types can be considered as superstructures of the anisotype  $AlB_2$ . The group-theoretical description of these superstructures was given recently by Hoffmann and Pöttgen (2001).

Some of the equiatomic plumbides, e.g. the series  $RCuPb$  (Mazzone et al., 1982) have been described with the  $CaIn_2$  type (space group  $P6_3/mmc$ ), with a random distribution of the copper and lead atoms in the indium sublattice. Later it has been shown that these plumbides indeed exhibit an ordering between the transition metal and lead atoms (Gulay et al., 2001b). The ordering results in a *translationengleiche* symmetry reduction of index 2 ( $t_2$ ) from space group  $P6_3/mmc$  to  $P6_3mc$ . This way we obtain separate two-fold positions for T and X. Depending on the degree of puckering one has to assign different structure types. If the layers are only weakly puckered, the intralayer T–Pb distances are much smaller than the interlayer ones and the [TPb] networks are two-dimensional. This branch is assigned to the  $NdPtSb$  type (Wenski and Mewis, 1986). If the puckering is pronounced, one observes a transition towards a tetrahedral network, similar to the  $LiGaGe$  type (Bockelmann et al., 1970; Bockelmann and Schuster, 1974). Within a series of RTX compounds, the puckering increases with decreasing the size of the rare earth atom (Sebastian et al., 2006, and ref. therein).

Some plumbides, i.e.  $YAg_{0.78}Pb_{1.22}$ ,  $ErAg_{0.70}Pb_{1.30}$ , and  $TmAg_{0.62}Pb_{1.38}$  (Gulay and Wołczyrz, 2001d) have compositions that deviate from the ideal 1:1:1 composition. Consequently, such plumbides show no structural long-range order and they crystallize with a  $CaIn_2$  type structure with a random distribution of silver and lead in the indium sites.

If the  $T_3Pb_3$  layers are planar, e.g. YbHgPb (Merlo et al., 1993), the ZrBeSi type (Nielsen and Baenziger, 1954) occurs. This structure type mostly occurs when the rare earth atoms have a large radius. The stacking sequence of the  $T_3Pb_3$  hexagons is similar in the three structure types, i.e. AB AB.

Tripling of the  $AlB_2$  subcells occurs in the structures of  $CaLiSn$  (Müller and Voltz, 1974) and YbAgPb (Merlo et al., 1996). Here, one observes a stacking sequence ABC ABC. In the higher symmetry YbAgPb structure (space group  $P6m2$ ) we observe one planar and two puckered  $Ag_3Pb_3$  hexagons (Figure 15). Between

the puckered hexagons, the lead atoms move towards each other and  $\text{Pb}_2$  pairs with a Pb–Pb distance on 335 pm result. Chemical bonding was investigated for isotopic  $\text{YbAgSn}$  (Pöttgen et al., 1999a) on the basis of TB-LMTO-ASA band structure calculations. They clearly reveal strong Ag–Sn bonding within the three networks and also Sn1–Sn1 between the puckered layers. This model of chemical bonding can, to a first approximation, be applied to  $\text{YbAgPb}$ . The silver site can also be occupied by lithium, leading to the plumbide  $\text{YbLiPb}$  (Fornasini et al., 2001b). Here one observes intralayer Li–Pb distances of 284 pm in the planar and 288 pm in the puckered  $\text{Li}_3\text{Pb}_3$  hexagons.

There exists also a lower symmetry variant, the  $\text{CaLiSn}$  type, space group  $P3m1$ , where also the B layer is puckered (Figure 15). So far, no rare earth containing compound has been observed with this structure type, however, this arrangement is realized for the plumbide  $\text{CaAgPb}$  (Merlo et al., 1996).

#### 4.4 The structure types $\text{KHg}_2$ and $\text{TiNiSi}$

Structure type  $\text{KHg}_2$  (Duwell and Baenziger, 1955) (Figure 16). SG  $Imma$ ,  $Z = 4$ ,  $a = 487.0(1)$ ,  $b = 763.3(3)$ ,  $c = 841.2(3)$  pm for  $\text{EuAuPb}$  (Arpe, 1998).  $4\text{Eu}$ :  $4e\ 0\ 1/4\ z$  ( $z = 0.5304$ );  $8\text{M}$ :  $8h\ 0\ y\ z$  ( $\text{M} = \text{Au}_{0.5}\text{Pb}_{0.5}$ ,  $y = 0.9607$ ,  $z = 0.1678$ ).

Structure type  $\text{TiNiSi}$  (Shoemaker and Shoemaker, 1965) (Figure 16). SG  $Pnma$ ,  $Z = 4$ ,  $a = 742.49(3)$ ,  $b = 461.16(1)$ ,  $c = 782.38(3)$  pm for  $\text{NdNiPb}$  (Gulay et al., 2000c).  $4\text{Nd}$ :  $4c\ x\ 1/4\ z$  ( $x = 0.9848$ ,  $z = 0.7142$ );  $4\text{Ni}$ :  $4c\ x\ 1/4\ z$  ( $x = 0.190$ ,  $z = 0.088$ );  $4\text{Pb}$ :  $4c\ x\ 1/4\ z$  ( $x = 0.3026$ ,  $z = 0.4198$ ).

The plumbides with the  $\text{KHg}_2$  type (space group  $Imma$ ) (Duwell and Baenziger, 1955) and the  $\text{TiNiSi}$  type (space group  $Pnma$ ) (Shoemaker and Shoemaker, 1965) belong to the  $\text{AlB}_2$  structural family. These two structure types are orthorhombically distorted variants of the parent  $\text{AlB}_2$  (Hoffmann and Pöttgen, 2001). At this point we need to note that also the related  $\text{CeCu}_2$  type (Larson and Cromer, 1961)

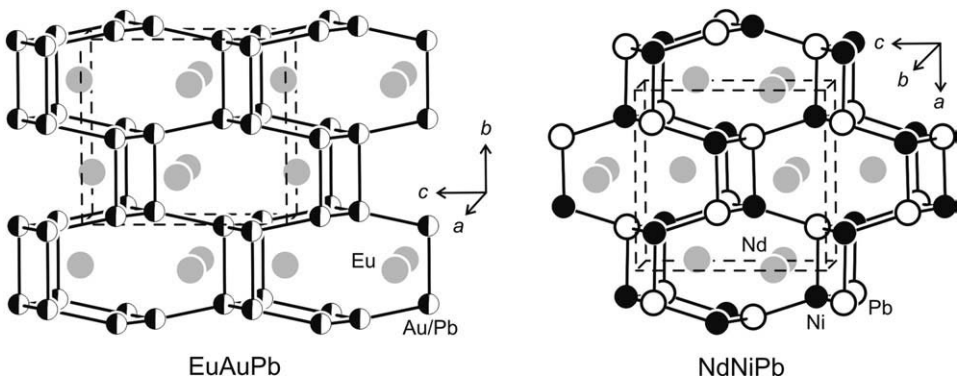


**FIGURE 16** The crystal structures of  $\text{EuAuPb}$  and  $\text{NdNiPb}$ . The europium (neodymium), nickel, and lead atoms are drawn as medium gray, black filled, and open circles, respectively. The mixed-occupied Au/Pb site in the  $\text{EuAuPb}$  structure is shown with segments. The three-dimensional [TPb] networks are emphasized.

is often listed in literature. CeCu<sub>2</sub> and KHg<sub>2</sub> are isopointal structures (Gelato and Parthé, 1987; Parthé and Gelato, 1984). Since the KHg<sub>2</sub> structure has been determined earlier, we consequently call it the KHg<sub>2</sub> type.

EuAuPb (Arpe, 1998) is an example for a KHg<sub>2</sub> type plumbide. The gold and lead atoms are randomly distributed on the mercury site. A serve problem for this compound is the almost identical scattering power of gold and lead for X-rays. It is thus not possible to determine whether the Au and Pb are ordered. The structure refinement, however, revealed a higher U<sub>22</sub> displacement parameter for the mixed occupied Au/Pb site, indicating a significant degree of short-range ordering as expected, since gold and lead have different chemical potentials. The [AuPb] network is three-dimensional (Figure 16) and leaves larger channels that are filled by the europium atoms.

The TiNiSi structure is a superstructure of the KHg<sub>2</sub> type. The space group symmetry is reduced from *Imma* to *Pnma* via a *klassengleiche* symmetry reduction of index 2 (*k*2). Thus, we observe superstructure reflections which indicate the ordering of the transition metal and lead atoms. The eightfold mercury site in the KHg<sub>2</sub> type splits into two independent fourfold sites which allow the ordering. As an example, the structure of NdNiPb is shown in Figure 16. Within the three-dimensional [NiPb] network, the nickel and lead atoms both have strongly distorted tetrahedral coordination. The network shows a stronger distortion than in the KHg<sub>2</sub> type. Again, the neodymium atoms fill channels within the network. Overviews on the crystal chemistry and chemical bonding in TiNiSi related intermetallics have been published by Bojin and Hoffmann (2003a, 2003b), Landrum et al. (1998) and Nuspl et al. (1996).

#### 4.5 The structure type ZrNiAl

Structure type ZrNiAl (Krypyakevich et al., 1967; Dwight et al., 1968; Zumdick et al., 1999) (Figure 17). SG  $P\bar{6}2m$ ,  $Z = 3$ ,  $a = 737.23(5)$ ,  $c = 441.18(2)$  pm for LuAgPb (Gulay, 2001b). 3Lu:  $3g \ x \ 0 \ 1/2$  ( $x = 0.5746$ ); 3Ag:  $3f \ x \ 0 \ 0$  ( $x = 0.2496$ ); 1Pb1:  $1b \ 0 \ 0 \ 1/2$ ; 2Pb2:  $2c \ 1/3 \ 2/3 \ 0$ .

The plumbides RAgPb with R = Y, Er, Tm, Lu adopt the hexagonal ZrNiAl type structure (Zumdick et al., 1999), space group  $P\bar{6}2m$ . As an example we present the LuAgPb structure in Figure 17. LuAgPb contains two crystallographically independent lead sites, both in trigonal prismatic coordination. The Pb1 atoms have six nearest silver neighbours at Pb1–Ag distances of 287 pm and the Pb2 atoms are located in a trigonal prism formed by the lutetium atoms. Both types of trigonal prisms are capped on the rectangular faces leading to coordination number 9, i.e. [Pb1Ag<sub>6</sub>Lu<sub>3</sub>] and [Pb2Ag<sub>3</sub>Lu<sub>6</sub>]. The silver atoms have a distorted tetrahedral lead coordination with Ag–Pb distances ranging from 282 to 287 pm, close to the sum of the covalent radii (Emsley, 1999) of 288 pm. We can thus assume a considerable degree of Ag–Pb bonding within the LuAgPb structure. Together, the silver and lead atoms build up a three-dimensional [AgPb] network in which the lutetium atoms fill distorted hexagonal channels. The various facets of the crystal chemistry of ZrNiAl related intermetallics had been described pre-

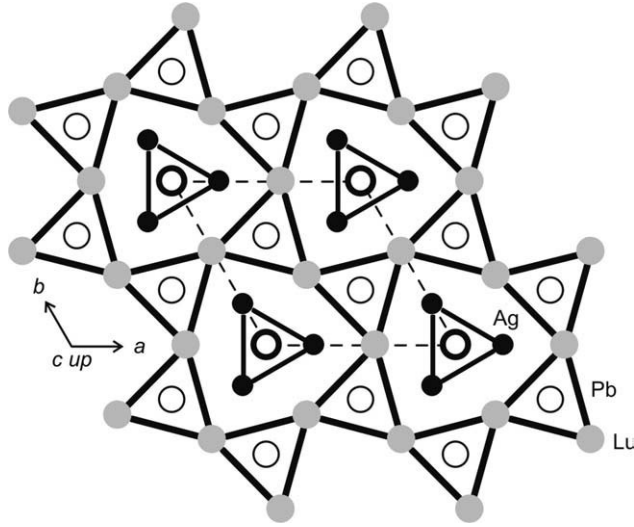


**FIGURE 17** Projection of the LuAgPb structure onto the  $ab$  plane. Lutetium, silver, and lead atoms are drawn as medium gray, black filled, and open circles, respectively. All atoms lie on mirror planes at  $z = 0$  (thin lines) and  $z = 1/2$  (thick lines). The trigonal prismatic coordination of the two crystallographically independent tin atoms is emphasized.

viously. For more details we refer to the previous work (Hovestreydt et al., 1982; Zumdick and Pöttgen, 1999).

For the RAgPb series it is interesting to note that the plumbides with the early rare earth metals adopt the NdPtSb type structure up to Dy as rare earth metal. This change in structure type is driven by the size of the rare earth elements. A comparison with the series RCuPb and RAuPb is given by Marazza et al. (1988).

#### 4.6 The structure type $\text{Ho}_6\text{Co}_2\text{Ga}$

Structure type  $\text{Ho}_6\text{Co}_2\text{Ga}$  (Gladyshevsky et al., 1983) (Figure 18).  $SG\ Immm$ ,  $Z = 4$ ,  $a = 927.72(4)$ ,  $b = 946.61(4)$ ,  $c = 983.91(5)$  pm for  $\text{Ho}_6\text{Ni}_{2.41}\text{Pb}_{0.53}$  (Gulay and Wołczyrz, 2001a).  $8\text{Ho}1: 8n\ x\ y\ 0$  ( $x = 0.2909$ ,  $y = 0.1795$ );  $8\text{Ho}2: 8m\ x\ 0\ z$  ( $x = 0.3025$ ,  $z = 0.3196$ );  $8\text{Ho}3: 8l\ 0\ y\ z$  ( $y = 0.1946$ ,  $z = 0.2127$ );  $3.76\text{Ni}1: 4j\ 1/2\ 0\ z$  ( $z = 0.122$ );  $4\text{Ni}2: 4g\ 0\ y\ 0$  ( $y = 0.361$ );  $2\text{Pb}: 2c\ 1/2\ 1/2\ 0$ ;  $2\text{M}: 2a\ 0\ 0\ 0$  ( $\text{M} = \text{Ni}_{0.94}\text{Pb}_{0.06}$ ).

The  $\text{Ho}_6\text{Co}_2\text{Ga}$  type intermetallics form for several series of gallides, indides, stannides and plumbides. The structure of  $\text{Ho}_6\text{Ni}_{2.41}\text{Pb}_{0.53}$  is given as an example in Figure 18. A common feature of the indides and plumbides is the mixed transition metal/indium (lead) occupancy at the origin of the unit cell ( $2a$  site). However, there is a significant new feature in the plumbides (Gulay and Wołczyrz, 2001a). Most Co1 and Ni1 sites of these compounds reveal defects of up to 34%. This has not been observed for the indium based single crystals.

The Pb2 atoms have distorted icosahedral holmium coordination. These icosahedra show an orthorhombic body-centered packing. All three crystallographically independent holmium atoms are in the coordination sphere of the Pb2 atoms.

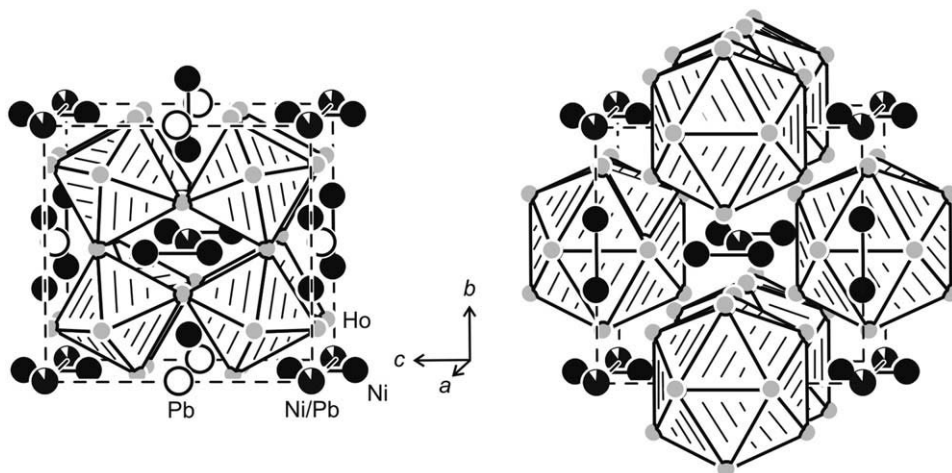


**FIGURE 18** The crystal structure of  $\text{Ho}_6\text{Ni}_{2.41}\text{Pb}_{0.53}$ . Holmium, nickel, and lead atoms are drawn as medium gray, black filled, and open circles, respectively. The mixed occupied Ni/Pb site is drawn with segments. The left-hand drawing emphasizes the empty  $\text{Ho}_6$  octahedra, while the icosahedral coordination of the lead atoms is shown in the right-hand drawing. The nickel dumb-bells are emphasized.

The Ni1 and Ni2 atoms build up  $\text{Ni}_2$  dumb-bells at Ni–Ni distances of 240 and 263 pm, respectively. The  $\text{Ni}_{12}$  dumb-bells are oriented parallel to the  $c$  direction, while the  $\text{Ni}_{22}$  dumb-bells run parallel to  $b$ . Both dumb-bells are located between the  $\text{Pb}_2\text{Ho}_{12}$  icosahedra. An interesting feature of the  $\text{Ho}_6\text{Ni}_{2.41}\text{Pb}_{0.53}$  structure is the formation of empty  $\text{Ho}_6$  octahedra as emphasized in the left-hand drawing of Figure 18. For further crystal chemical details we refer to recent work on the indide phases (Zaremba et al., 2006, 2007).

#### 4.7 The structure types $\text{AuBe}_5$ and $\text{Cu}_3\text{Au}$

Structure type  $\text{AuBe}_5$  (Misch, 1935) (Figure 19). SG  $F\bar{4}3m$ ,  $Z = 4$ ,  $a = 709.93(2)$  pm for  $\text{YCu}_{4.74}\text{Pb}_{0.26}$  (Gulay, 2001a). 4Y:  $4a\ 0\ 0\ 0$ ; 16Cu:  $16e\ x\ x\ x$  ( $x = 0.625$ ); 4M:  $4c\ 1/4\ 1/4\ 1/4$  ( $M = \text{Cu}_{0.74}\text{Pb}_{0.26}$ ).

Structure type  $\text{Cu}_3\text{Au}$  (Owen and Liu, 1947) (Figure 19). SG  $Pm\bar{3}m$ ,  $Z = 1$ ,  $a = 465.71(2)$  pm for  $\text{Y}(\text{Ag}_{0.23}\text{Pb}_{0.77})_3$  (Gulay and Wołczyrz, 2001c). 1Y:  $1a\ 0\ 0\ 0$ ; 3M:  $3c\ 0\ 1/2\ 1/2$  ( $M = \text{Ag}_{0.23}\text{Pb}_{0.77}$ ).

In the R–Cu–Pb systems many solid solutions  $\text{RCu}_{5-x}\text{Pb}_x$  with cubic  $\text{AuBe}_5$  type structure have been observed. This structure is formed with yttrium and the late rare earth elements Gd–Lu. The  $\text{AuBe}_5$  type (Misch, 1935) belongs to the family of structures that are related with the cubic Laves phase  $\text{MgCu}_2$  (Müller, 1996; Wells, 1990). The latter is centrosymmetric, space group  $Fd\bar{3}m$ .  $\text{MgCu}_4\text{Sn}$  (Gladyshevskii et al., 1952; Osamura and Murakami, 1978) is a non-centrosymmetric variant of the  $\text{MgCu}_2$  type that allows an ordering of magnesium and tin in 1:1 ratio. The eight-fold magnesium site of  $\text{MgCu}_2$  splits into two four-

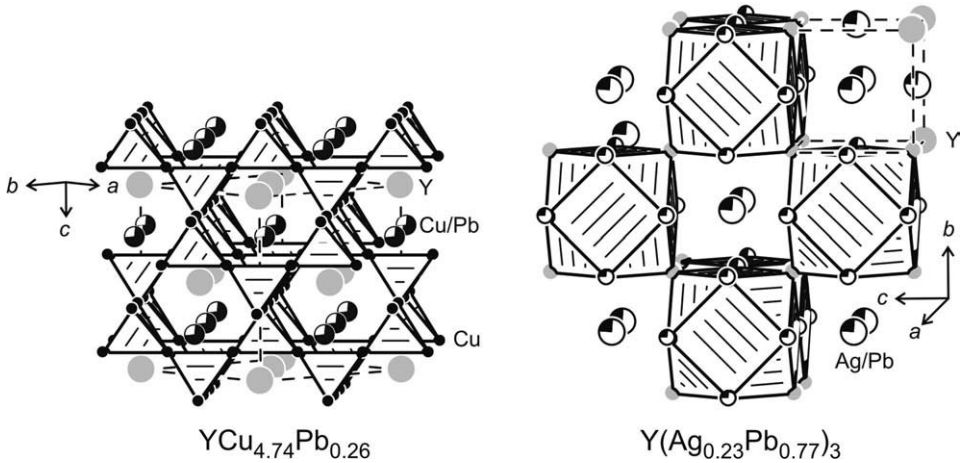


**FIGURE 19** The crystal structures of  $\text{YCu}_{4.74}\text{Pb}_{0.26}$  and  $\text{Y}(\text{Ag}_{0.23}\text{Pb}_{0.77})_3$ . Yttrium, transition metal, and lead atoms are drawn as medium gray, black filled, and open circles, respectively. The mixed occupied sites are drawn with segments. The network of condensed tetrahedra in  $\text{YCu}_{4.74}\text{Pb}_{0.26}$  and the cuboctahedral coordination in  $\text{Y}(\text{Ag}_{0.23}\text{Pb}_{0.77})_3$  are emphasized.

fold sites upon reducing the space group symmetry from  $Fd\bar{3}m$  to  $F\bar{4}3m$  via a *translationengleiche* symmetry reduction of index 2 (t2). The  $\text{AuBe}_5$  structure is an occupation variant of the  $\text{MgCu}_4\text{Sn}$  type, where the magnesium site is occupied by the gold atoms, while the beryllium atoms occupy the copper and the tin sites. In the plumbides  $\text{RCu}_{5-x}\text{Pb}_x$  most solid solutions show only a small degree of Cu–Pb mixing. The yttrium compound with 15 at% Pb shows the largest lead content. As a consequence of the larger size of the lead atoms, the Cu–Pb mixing is different on the two crystallographically independent sites 16e and 4c. Up to 57% Pb can occupy the 4c site in the yttrium compound, while all 16e sites have less than 10% lead occupancy.

The structure of  $\text{YCu}_{4.74}\text{Pb}_{0.26}$  is shown as an example in Figure 19. The copper atoms on the 16e site build up a three-dimensional network of corner-sharing tetrahedra. This network leaves voids of coordination number 16 which are filled by the rare earth and Pb/Cu atoms on the four-fold sites. The large coordination number of this void readily explains the higher lead content on this site. The atoms occupying the 16e site (mainly copper in the  $\text{RCu}_{5-x}\text{Pb}_x$  series) have coordination number 12 in the form of a distorted icosahedron. For more crystal chemical details on the Laves phases and related compounds we refer to review articles (Simon, 1983; Nesper, 1991; Johnston and Hoffmann, 1992; Nesper and Miller, 1993).

The plumbides  $\text{R}(\text{Ag}, \text{Pb})_3$  with  $\text{R} = \text{Y}, \text{Sm}, \text{Gd–Tm}$  crystallize with a very simple structure type, i.e.  $\text{Cu}_3\text{Au}$ , an ordered version of the cubic close packing. The rare earth atoms fill Wyckoff position 1a (the origin of the unit cell, see Figure 19), while the silver and lead atoms show random distribution on the 3c site. The phase analytical investigations reveal that up to 78% lead can occupy that site. Both sites have cuboctahedral coordination (CN 12).

#### 4.8 The structure types $\text{Ce}_8\text{Pd}_{24}\text{Sb}$ and $\text{Sm}_{12}\text{Ni}_6\text{In}$

Structure type  $\text{Ce}_8\text{Pd}_{24}\text{Sb}$  (Gordon and DiSalvo, 1996) (Figure 20). SG  $Pm\bar{3}m$ ,  $Z = 1$ ,  $a = 846.05(8)$  pm for  $\text{Ce}_8\text{Pd}_{24}\text{Pb}$  (Gordon et al., 1996). 8Ce:  $8g \ x \ x \ x$  ( $x = 0.25140$ ); 6Pd1:  $6f \ x \ 1/2 \ 1/2$  ( $x = 0.25552$ ); 6Pd2:  $6e \ x \ 0 \ 0$  ( $x = 0.31118$ ); 12Pd3:  $12h \ x \ 1/2 \ 0$  ( $x = 0.26675$ ); 1Pb:  $1a \ 0 \ 0 \ 0$ .

Structure type  $\text{Sm}_{12}\text{Ni}_6\text{In}$  (Kalychak et al., 1998) (Figure 20). SG  $Im\bar{3}$ ,  $Z = 2$ ,  $a = 971.49(2)$  pm for  $\text{Y}_{12}\text{Ni}_6\text{Pb}$  (Gulay et al., 2000b). 24Y:  $24g \ 0 \ y \ z$  ( $y = 0.1888$ ,  $z = 0.6986$ ); 12Ni:  $12e \ x \ 0 \ 1/2$  ( $x = 0.1200$ ); 2Pb:  $2a \ 0 \ 0 \ 0$ .

The cerium intermetallics  $\text{Ce}_8\text{Pd}_{24}\text{X}$  ( $X = \text{Ga}, \text{In}, \text{Sn}, \text{Pb}, \text{Sb}, \text{Bi}$ ) (Gordon et al., 1996; Cho et al., 1998) crystallize with a superstructure of the  $\text{Cu}_3\text{Au}$  type discussed in Section 4.7. This structure type has first been refined for  $\text{Ce}_8\text{Pd}_{24}\text{Sb}$  (Gordon and DiSalvo, 1996). For description of the structure we start with the  $\text{Cu}_3\text{Au}$  type compound  $\text{CePd}_3$  (Harris and Norman, 1968), where the palladium atoms leave one undistorted octahedral void. For electronegativity reasons, the  $M$  atoms listed above fill only the  $\text{Pd}_6$  octahedra, while the  $\text{Ce}_2\text{Pd}_4$  octahedra remain empty, similar to the perovskite structure.

The crystal chemical investigations revealed superstructure reflections for the  $\text{Ce}_8\text{Pd}_{24}\text{X}$  compounds, leading to a doubling of the  $\text{CePd}_3$  unit cell in all three directions. This corresponds to two steps of symmetry reduction and leaves a free positional parameter for the palladium atoms. One can then generate larger (filled) and smaller (empty)  $\text{Pd}_6$  octahedra. The latter occur in 1:7 ratio leading to the composition  $\text{Ce}_8\text{Pd}_{24}\text{X}$  (Figure 20).

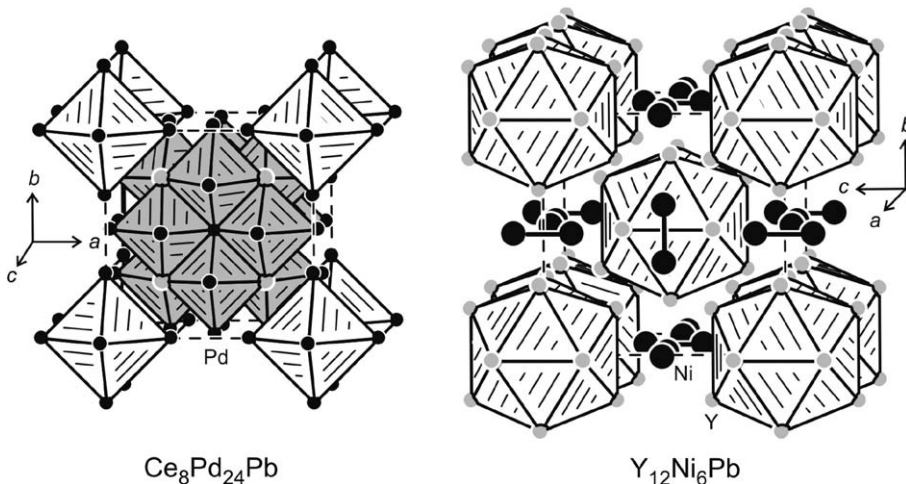


**FIGURE 20** The structures of  $\text{Ce}_8\text{Pd}_{24}\text{Pb}$  and  $\text{Y}_{12}\text{Ni}_6\text{Pb}$ . Cerium (yttrium), palladium (nickel), and lead atoms are drawn as medium gray, black filled, and open circles, respectively. The lead filled  $\text{Pd}_6$  (white) and the empty  $\text{Ce}_2\text{Pd}_4$  (gray) octahedra of the  $\text{Ce}_8\text{Pd}_{24}\text{Pb}$  structure are emphasized. In the  $\text{Y}_{12}\text{Ni}_6\text{Pb}$  structure, the main structural motifs are lead centered icosahedra and  $\text{Ni}_2$  dumb-bells.

The change of the X component allows for a change of the valence electron concentration and one can thus modify the separation between the Fermi energy and the 4f energy levels. The ternary compounds  $\text{Ce}_8\text{Pd}_{24}\text{X}$  have significantly different properties than binary  $\text{CePd}_3$  (see Section 5.5).

Another cubic structure type occurs for the series of  $\text{R}_{12}\text{Ni}_6\text{Pb}$  ( $\text{R} = \text{Y, La, Pr, Nd, Sm, Gd–Ho}$ ) and  $\text{R}_{12}\text{Co}_6\text{Pb}$  compounds (Gulay et al., 2000b). The plumbides adopt the  $\text{Sm}_{12}\text{Ni}_6\text{In}$  type, space group  $Im\bar{3}$  (Kalychak et al., 1998). The  $\text{Y}_{12}\text{Ni}_6\text{Pb}$  structure has been refined from powder X-ray diffractometer data. In Figure 20 we present the different coordination environments in that structure. The yttrium atoms in this rare earth metal rich compound have coordination number 15 with yttrium, nickel, and lead atoms in their coordination shell. The lead atoms have icosahedral yttrium coordination and these icosahedra show a cubic body-centered packing. The most peculiar structural feature concerns the nickel atoms. The latter form dimers at a short Ni–Ni distance of 233 pm, even slightly shorter than in fcc nickel (249 pm) (Donohue, 1974). Similar segregation of the transition metal atoms has also been observed for the  $\text{Ho}_6\text{Co}_2\text{Ga}$  type plumbides (Section 4.6) and the  $\text{Pr}_5\text{Ni}_6\text{In}_{11}$  type indides (Kalychak et al., 1987; Tang et al., 1995; Pöttgen et al., 1999c).

Each nickel atom has trigonal prismatic yttrium coordination. Due to formation of the  $\text{Ni}_2$  pairs, these trigonal prisms are condensed via one rectangular side leading to distorted  $\text{AlB}_2$  related units. The remaining rectangular faces of these subunits are further capped by yttrium atoms. Also these units show the bcc packing. The nickel atoms show strong bonding to yttrium. There is one short Y–Ni contact at 268 pm, even shorter than the sum of the covalent radii of 277 pm (Emsley, 1999). There are no Ni–Pb contacts in the  $\text{Y}_{12}\text{Ni}_6\text{Pb}$  structure.

#### 4.9 The structure type $\text{Hf}_5\text{CuSn}_3$

Structure type  $\text{Hf}_5\text{CuSn}_3$  (Rieger et al., 1965) (Figure 21). SG  $P6_3/mcm$ ,  $Z = 2$ ,  $a = 909.4(1)$ ,  $c = 664.27(7)$  pm for  $\text{Gd}_5\text{NiPb}_3$  (Gulay, 2003b).  $6\text{Gd}: 6g \times 0 1/4 (x = 0.2306)$ ;  $4\text{Gd}: 4d 1/3 2/3 0$ ;  $2\text{Ni}: 2b 0 0 0$ ;  $6\text{Pb}: 6g \times 0 1/4 (x = 0.5999)$ .

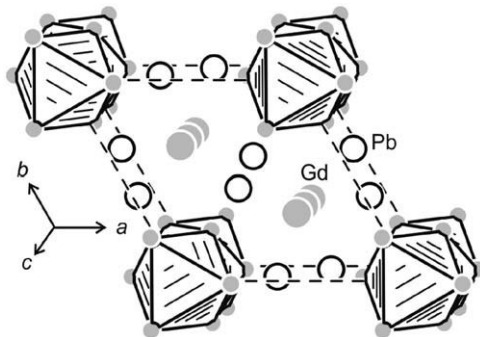


**FIGURE 21** View of the  $\text{Gd}_5\text{NiPb}_3$  structure approximately along the  $c$  axis. Gadolinium, nickel, and lead atoms are drawn as medium gray, black filled, and open circles, respectively. The rows of face-sharing  $\text{NiGd}_6$  octahedra are emphasized.

The  $\text{Hf}_5\text{CuSn}_3$  structure (Rieger et al., 1965) is a filled version of the binary  $\text{Mn}_5\text{Si}_3$  type (Aronsson, 1960). It is also possible, that the X component fills the octahedral void. This has first been observed for  $\text{Ti}_5\text{Ga}_4$  (Schubert et al., 1962; Pötzschke and Schubert, 1962) and often, the ternary filled versions are referred to this structure type in the literature.

These structures crystallize with space groups  $P6_3/mcm$  with two formula units per cell. The binary variant has empty  $\text{Mn}_6$  octahedra which are partially or completely filled in the ternary versions. As an example, we present the  $\text{Gd}_5\text{NiPb}_3$  structure in Figure 21. The  $\text{NiGd}_6$  octahedra are condensed via common triangular faces along the  $c$  axis. These rows form the motif of a hexagonal rod packing. Similar to the  $\text{Y}_{12}\text{Ni}_6\text{Pb}$  structure discussed above, short Ni–Gd1 distances of 268 pm, close to the sum of the covalent radii of 276 pm are observed (Emsley, 1999). The Gd2 and Pb atoms are located between the rods. Again, no Ni–Pb contacts are observed.

The octahedral voids in the  $\text{Mn}_5\text{Si}_3$  type structure can be filled not only by a late transition metal. As an example Guloy and Corbett (1994) have tested this possibility for  $\text{La}_5\text{Pb}_3$ . The voids could be filled with P, S, Cl, As, Se, Sb, Cr, Mn, Fe, Co, Ni, Cu, Zn, Ru, and Ag atoms and also partially with boron or carbon. Filling of the voids leads to a small increase of the lattice parameters. On the other hand, lead can also act as the interstitial element on the octahedral site. The structural relationships of various  $\text{M}_5\text{X}_4$  structures have recently been discussed by Guloy and Corbett (2005).

#### 4.10 The structure type $\text{La}_6\text{Co}_{11}\text{Ga}_3$

Structure type  $\text{La}_6\text{Co}_{11}\text{Ga}_3$  (Sichevich et al., 1985) (Figure 22). SG  $I4/mcm$ ,  $Z = 4$ ,  $a = 810.6(1)$ ,  $c = 2356.5(9)$  for  $\text{Pr}_6\text{Fe}_{13}\text{Pb}$  (Weitzer et al., 1993). 16Pr1:  $16l \ x \ 1/2 + x \ z$  ( $x = 0.1627$ ,  $z = 0.1857$ ); 8Pr2:  $8f \ 0 \ 0 \ z$  ( $z = 0.8944$ ); 16Fe1:  $16l \ x \ 1/2 + x \ z$  ( $x = 0.1795$ ,  $z = 0.0585$ ); 16Fe2:  $16k \ x \ y \ 0$  ( $x = 0.0659$ ,  $y = 0.2103$ ); 16Fe3:  $16l \ x \ 1/2 + x \ z$  ( $x = 0.3856$ ,  $z = 0.0936$ ); 4Fe4:  $4d \ 0 \ 1/2 \ 0$ ; 4Pb:  $4a \ 0 \ 0 \ 1/4$ .

The  $\text{Pr}_6\text{Fe}_{13}\text{Pb}$  structure is presented in Figure 22. Although the unit cell is rather large, there are simple building groups in  $\text{Pr}_6\text{Fe}_{13}\text{Pb}$ . The lead atoms are located on the mirror planes at  $z = 1/4$  and  $3/4$ . Each lead atom has a bicapped square antiprismatic (CN 10) praseodymium coordination almost equal Pr–Pb distances of 339 and 340 pm. These antiprisms share four common edges with each other, leading to a layer around  $z = 1/4$  and  $3/4$ , respectively.

These layers of condensed antiprisms are well separated from each other by two-dimensional layers formed by the four crystallographically independent iron atoms. The shortest Pr–Pr distance between the layers is at 498 pm. The motif of the iron layer is also simple. The Fe4 atoms on the mirror planes at  $z = 0$  and  $1/2$  have a tetragonally distorted icosahedral iron coordination (CN 12) at Fe–Fe distances between 241 and 257 pm, close to the Fe–Fe distance of 248 pm in *bcc* iron (Donohue, 1974). The remaining Fe1, Fe2, and Fe3 atoms build up the ligands for the icosahedra around Fe4. The  $\text{Fe}_4\text{Fe}_{12}$  icosahedra are connected with each other via many Fe–Fe bonds with Fe–Fe distances in the range of 249–276 pm.

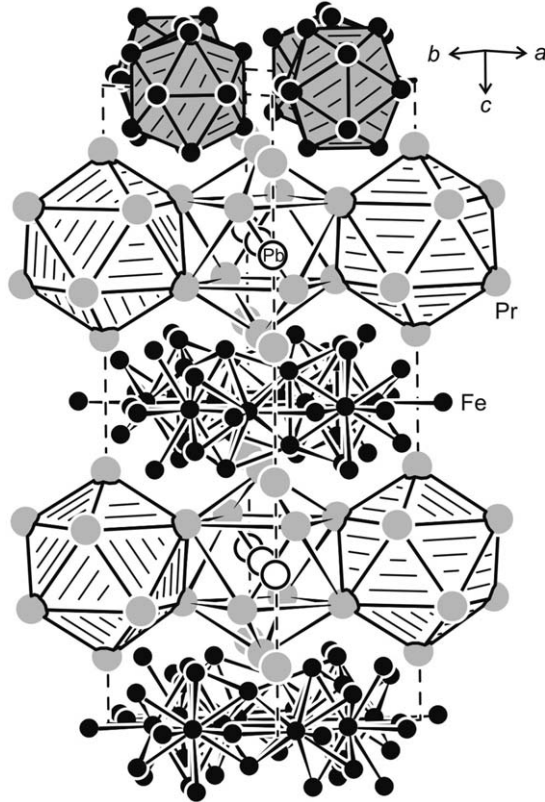


**FIGURE 22** The structure of  $\text{Pr}_6\text{Fe}_{13}\text{Pb}$ . Praseodymium, iron, and lead atoms are drawn as medium gray, black filled, and open circles, respectively. The layers of edge-sharing  $\text{PbPr}_{10}$  polyhedra are separated by the iron cluster units. For details see text.

The structural features of  $\text{Pr}_6\text{Fe}_{13}\text{Pb}$  are similar to the stannide  $\text{Th}_4\text{Fe}_{13}\text{Sn}_5$  (Manfrinetti et al., 1997; Moze et al., 2000; Principi et al., 2001), where a two-dimensional  $\text{Fe}_{13}$  cluster unit (243–268 pm Fe–Fe) is separated by layers of condensed  $\text{SnTh}_6$  octahedra. In both iron-rich compounds, the iron sublattices give a magnetic contribution.

$\text{Pr}_6\text{Fe}_{13}\text{Pb}$  and  $\text{Nd}_6\text{Fe}_{13}\text{Pb}$  can be loaded with up to 13.1 hydrogen atoms per formula unit within tetrahedral sites, leading to an increase of the cell volume by 10% (Leithe-Jasper et al., 1996), leading to drastic changes in the magnetic properties.

#### 4.11 The structure types $\text{MnCu}_2\text{Al}$ and $\text{MgAgAs}$

Structure type  $\text{MnCu}_2\text{Al}$  (Heusler, 1934). SG  $Fm\bar{3}m$ ,  $Z = 4$ ,  $a = 678.6$  pm for  $\text{YPd}_2\text{Pb}$  (Marazza et al., 1995). 4Y:  $4b\ 1/2\ 1/2\ 1/2$ ; 8Pd:  $8c\ 1/4\ 1/4\ 1/4$ ; 4Pb:  $4a\ 0\ 0\ 0$  (Figure 23).

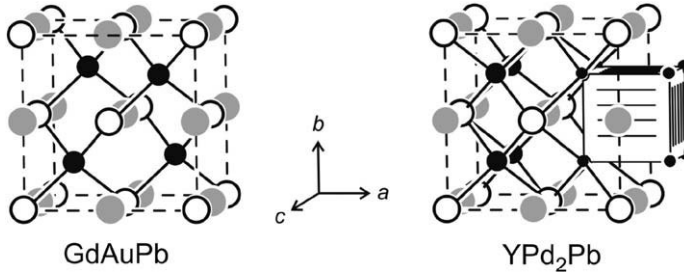


**FIGURE 23** The crystal structures of GdAuPb and YPd<sub>2</sub>Pb. Gadolinium (yttrium), gold (palladium), and lead atoms are drawn as medium gray, black filled, and open circles, respectively. The three-dimensional [AuPb] and [Pd<sub>2</sub>Pb] networks and one PbPd<sub>8</sub> cube in YPd<sub>2</sub>Pb are emphasized.

Structure type MgAgAs (Nowotny and Sibert, 1941). SG  $F\bar{4}3m$ ,  $Z = 4$ ,  $a = 677.5$  pm for GdAuPb (Marazza et al., 1988). 4Gd:  $4d \ 3/4 \ 3/4 \ 3/4$ ; 4Au:  $4c \ 1/4 \ 1/4 \ 1/4$ ; 4Pb:  $4a \ 0 \ 0 \ 0$  (Figure 23).

The famous Heusler type structure can be considered as a ternary ordered variant of the BiF<sub>3</sub> type. On the other hand, the YPd<sub>2</sub>Pb structure can also be derived from a cubic closest packing of the lead atoms, where the octahedral voids are filled with yttrium (rocksalt substructure) and the tetrahedral voids are filled by the palladium atoms.

The structure of the MgAgAs type plumbides RAuPb (R = Y, Gd–Er) is closely related to the Heusler type structure. The lead atoms have tetrahedral gold coordination and vice versa. Also the rare earth atoms fill tetrahedral voids. Geometrically this structure can be derived from the fluorite type, where the gold atoms occupy the calcium positions and the gold and lead atoms are ordered on the fluorite sites, thus causing the symmetry reduction from  $Fm\bar{3}m$  to  $F\bar{4}3m$ .

#### 4.12 The structure type Yb<sub>3</sub>Rh<sub>4</sub>Sn<sub>13</sub>

Structure type Yb<sub>3</sub>Rh<sub>4</sub>Sn<sub>13</sub> (Hodeau et al., 1980). SG  $Pm\bar{3}n$ ,  $Z = 2$ ,  $a = 999.4(5)$  pm for Ce<sub>3</sub>Rh<sub>4</sub>Pb<sub>13</sub> (Venturini et al., 1986). 6Ce:  $6d \ 1/4 \ 1/2 \ 0$ ; 8Rh:  $8e \ 1/4 \ 1/4 \ 1/4$ ; 2Sn1:  $2a \ 0 \ 0 \ 0$ ; 24Sn2:  $24k \ 0 \ y \ z$  ( $y = 0.30570$ ;  $z = 0.15333$ ) (Figure 24).

The striking structural features of the Ce<sub>3</sub>Rh<sub>4</sub>Pb<sub>13</sub> structure are condensed distorted RhPb<sub>6</sub> trigonal prisms (Figure 24). This polyhedral network leaves two different cages which are occupied by cerium and lead. The Pb1 atoms have an icosahedral lead coordination as emphasized at the left-hand part of Figure 20. The cerium atoms have coordination number 16 by twelve lead and four rhodium atoms. The  $2a$  site in the Yb<sub>3</sub>Rh<sub>4</sub>Sn<sub>13</sub> type structure needs some attention. Some structures reveal occupancy of that site with the main group element, while others show mixed occupancy with a rare earth or alkaline earth metal (Schreyer and Fässler, 2006). Some compounds show even full occupancy with a rare earth metal (Eisenmann and Schäfer, 1986; Galadzhun and Pöttgen, 1999). Furthermore, several materials show a strong rattling of the atoms on these positions, a structural

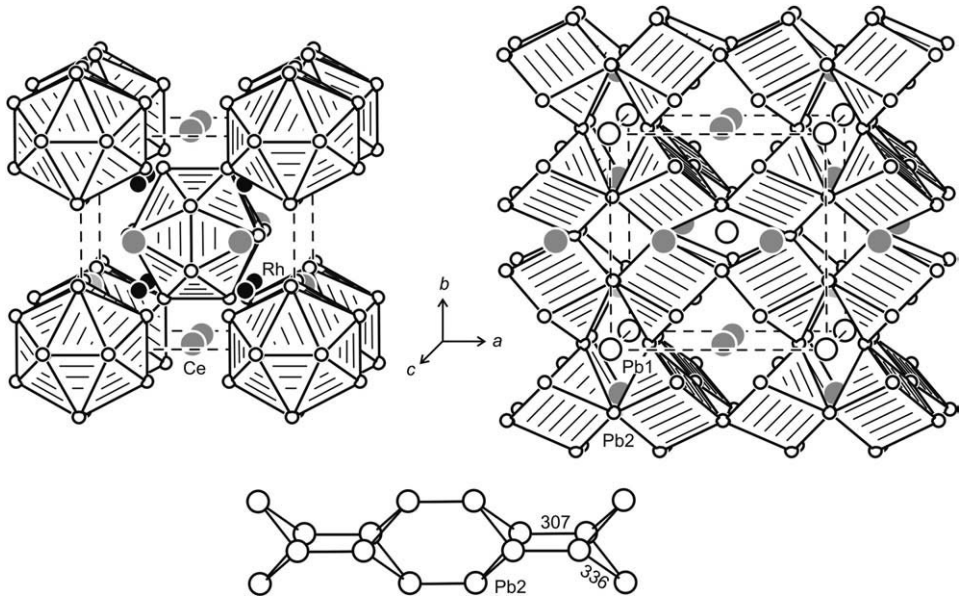


**FIGURE 24** The structure of  $\text{Ce}_3\text{Rh}_4\text{Pb}_{13}$ . Cerium, rhodium, and lead atoms are drawn as medium gray, black filled, and open circles, respectively. The icosahedral lead coordination (left-hand part) and the condensed trigonal  $\text{RhPb}_6$  prisms (right-hand drawing) are emphasized. The bottom drawing shows a cutout of the lead sublattice. For details see text.

feature that is related to the skutterudite family (Sales, 2003). The most important difference between the  $\text{Yb}_3\text{Rh}_4\text{Sn}_{13}$  and the filled skutterudite structure is in the transition metal coordination, i.e. trigonal prisms in the  $\text{Yb}_3\text{Rh}_4\text{Sn}_{13}$  type and octahedra in the filled skutterudite structures.

Now we return to the lead sublattice in  $\text{Ce}_3\text{Rh}_4\text{Pb}_{13}$ . As outlined in the lower part of Figure 24, the Pb2 atoms form one-dimensional chains which are composed of  $\text{Pb}_6$  rings. The chains then form a rod-packing like in the well-known  $\text{Cr}_3\text{Si}$  (A15) type structure. For details on these rod-packings we refer to Hyde and Andersson (1989).

Some of the plumbides within the  $\text{Yb}_3\text{Rh}_4\text{Sn}_{13}$  family show complex superstructures. They have the compositions  $\text{R}_{\sim 4}\text{Rh}_6\text{Pb}_{\sim 19}$  ( $\text{R} = \text{Y}, \text{Pr}, \text{Nd}, \text{Sm}, \text{Yb}$ ) (Venturini et al., 1986) and the structure is closely related with the  $\text{Er}_{1-x}\text{Sn}_x\text{Er}_4\text{Rh}_6\text{Sn}_{18}$  structure (Hodeau et al., 1984; Vandenberg, 1980). This complex structure type crystallizes in space group  $I4_1/acd$ . All investigated stannide crystals are twinned by recticular pseudomerohedry. So far, the corresponding plumbides have only been studied by X-ray powder diffraction.

#### 4.13 The structure type $\text{La}_4\text{Ni}_3\text{Pb}_4$

Structure type  $\text{La}_4\text{Ni}_3\text{Pb}_4$  (Gulay, 2005) (Figure 25). SG  $R\bar{3}$ ,  $Z = 3$ ,  $a = 1003.67(6)$  pm,  $c = 955.58(8)$  pm.  $9\text{La}1: 9b \ x \ y \ z$  ( $x = 0.332, y = 0.050, z = 0.763$ );  $3\text{La}2: 3a \ 0 \ 0 \ z$

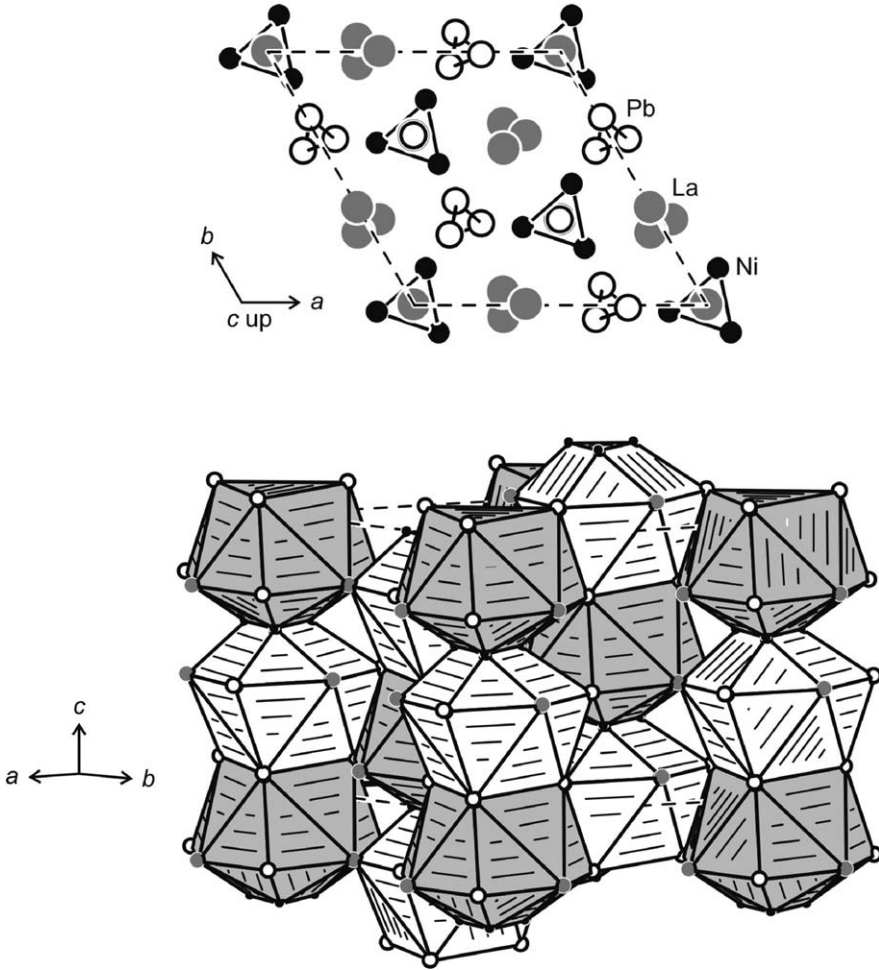


**FIGURE 25** Projection of the  $\text{La}_4\text{Ni}_3\text{Pb}_4$  structure onto the  $ab$  plane. Lanthanum, nickel, and lead atoms are drawn as medium gray, black filled, and open circles, respectively. The lead chains and the triangular nickel units are emphasized. The bottom drawing shows the polyhedra of coordination number 12 for the  $\text{La}_2$  (gray shading) and  $\text{Pb}_2$  atoms.

( $z = 0.880$ );  $9\text{Ni}$ :  $9b\ x\ y\ z$  ( $x = 0.696$ ,  $y = 0.222$ ,  $z = 0.937$ );  $9\text{Pb}_1$ :  $9b\ x\ y\ z$  ( $x = 0.5937$ ,  $y = 0.9407$ ,  $z = 0.762$ );  $3\text{Pb}_2$ :  $3a\ 0\ 0\ z$  ( $z = 0.333$ ).

Besides the  $\text{YbAgPb}$  type (Section 4.3),  $\text{La}_4\text{Ni}_3\text{Pb}_4$  is the only structure type that has so far exclusively been observed for rare earth–transition metal–plumbides. A view of the  $\text{La}_4\text{Ni}_3\text{Pb}_4$  structure is presented in Figure 25. There are two peculiar features: (i)  $\text{Ni}_3$  triangles with an extremely short Ni–Ni distance of 223 pm, and (ii) chains (spirals) of the  $\text{Pb}_1$  atoms at  $\text{Pb}_1$ – $\text{Pb}_1$  of 339 pm. Both of these distances are shorter than the Ni–Ni (249 pm) and Pb–Pb (350 pm) distances in the elements (Donohue, 1974). One can thus safely assume significant Ni–Ni and Pb–

Pb bonding in these structural units. Similar short Ni–Ni distances have also been observed in the structures of  $\text{Y}_{12}\text{Ni}_6\text{Pb}$  (233 pm) (Section 4.8) and  $\text{Ho}_6\text{Ni}_{2.41}\text{Pb}_{0.53}$  (240 pm) (Section 4.6).

The La2 and Pb2 atoms both have coordination number 12. These two polyhedra include all other atoms in their coordination shells. They are connected into columns via triangular faces in the form of an AB AB stacking along the  $c$  axis (Figure 25). Neighboring columns are shifted with respect to each other by one third of the translation period  $c$ , and the polyhedra of different columns are connected with each other via common edges.

## 5. CHEMICAL AND PHYSICAL PROPERTIES

Although more than 180 rare earth–transition metal plumbides have been structurally characterized, only a few of them have been studied with respect to their chemical and physical properties. The available data are discussed in this section. Most of the plumbides are light gray in polycrystalline form. Single crystals have metallic lustre. In contrast to the majority rare earth–transition metal–stannides (Skolozdra, 1997) and indides (Kalychak et al., 2005), many of the plumbides are sensitive to moisture. Handling and storage of the compounds should be performed in argon-filled glove boxes or Schlenk tubes.

In the following subsections we first discuss the properties of the equiatomic plumbides RTPb and those with  $\text{Mn}_2\text{AlB}_2$  type structure. The latter have intensively been investigated with respect to their magnetic and electrical properties since they have comparably simple crystal structures. This facilitates the calculation of the electronic structure and various properties. Finally we focus on  $\text{Ce}_8\text{Pd}_{24}\text{Pb}$  (Gordon et al., 1996; Gordon and DiSalvo, 1996; Cho et al., 1998; Jones et al., 1999) and  $\text{Pr}_6\text{Fe}_{13}\text{Pb}$  (Weitzer et al., 1993).

### 5.1 Ternary equiatomic plumbides RTPb

Among the equiatomic plumbides, the series of  $\text{RNiPb}$  ( $R = \text{Y, Sm, Gd–Tm}$ ) (Gulay and Hiebl, 2002) have intensively been investigated.  $\text{YNiPb}$  with the diamagnetic yttrium atoms behaves like a Pauli paramagnet. All other  $\text{RNiPb}$  plumbides show Curie–Weiss behavior above 50 K with experimental effective magnetic moments of 1.0, 8.0, 9.9, 11.1, 10.8, 9.7, and 7.9  $\mu_{\text{B}}/R$  for the Sm, Gd, Tb, Dy, Ho, Er, and Tm compound, respectively.  $\text{SmNiPb}$  shows the typical Van Vleck type behavior and ferromagnetic ordering around  $T_{\text{C}} = 8$  K.  $\text{GdNiPb}$ ,  $\text{TbNiPb}$ , and  $\text{DyNiPb}$  reveal antiferromagnetic ordering below  $T_{\text{N}} = 16, 14,$  and 9 K, respectively.  $\text{HoNiPb}$  again orders ferromagnetically at 4 K, but no hint for magnetic ordering was detected for  $\text{ErNiPb}$  and  $\text{TmNiPb}$  in the temperature range  $>4$  K.

All  $\text{RNiPb}$  plumbides are metallic conductors which show a weak curvilinear temperature dependence above 100 K. Due to the microcracks in the samples and the difficulty in cutting regularly-shaped bars, only normalized resistivity data could be measured. For  $\text{YNiPb}$  the resistivity curve could be fitted with the Bloch–

Grüneisen relation. Some of the magnetically ordering plumbides, i.e. SmNiPb, GdNiPb, and TbNiPb show a change in slope at the ordering temperature, indicating strong decrease of spin disorder scattering in the magnetically ordered state.

Within the RCuPb series, NdCuPb (Öner et al., 1999) and LaCuPb, CeCuPb, and GdCuPb (Dhar et al., 1995) have been studied. The non-magnetic ground state of LaCuPb was evident from temperature dependent heat capacity data. CePtSb is a Curie–Weiss paramagnet above 45 K with an experimental effective magnetic moment of  $2.89 \mu_B/\text{Ce}$  atom, slightly higher than expected for  $\text{Ce}^{3+}$  ( $2.54 \mu_B$ ). This can be explained by a contribution from the conduction-band polarization. The negative Weiss constant ( $-8.1$  K) was indicative for antiferromagnetic ordering ( $T_N = 8.3$  K) as proven by heat capacity measurements. Magnetization measurements reveal that the antiferromagnetic ground state is stable. At 2 K the magnetization increases linearly up to 5.5 T. Resistivity data of CeCuPb and GdCuPb reveal metallic behavior. A change in slope near 38 K is indicative for magnetic ordering in GdCuPb.

The neodymium based plumbides NdCuPb, NdAgPb, and NdAuPb (Öner et al., 1999) show antiferromagnetic ordering at  $T_N = 14.6$ , 12.6, and 18.9 K, respectively. These samples revealed an additional transition to a superconducting state at transition temperatures of 7.25, 7.00, and 6.85 K, respectively. The nature of these transitions is still not clear. Due to hysteresis behavior of the magnetization of NdAgPb at 5 K, the authors claimed that NdAgPb is a type II superconductor.

The magnetic properties of LaPtPb and CePtPb with hexagonal ZrNiAl type structure (Movshovich et al., 1996) have been investigated on small single crystals grown from a lead flux. Again, LaPtPb shows a non-magnetic ground state and CePtPb is paramagnetic. Axis dependent measurements revealed strong anisotropy with a ratio  $\chi_{ab}/\chi_{ac}$  extrapolating to a value of 65 at the Néel temperature ( $T_N = 0.9$  K). Also the low-temperature magnetization shows strong anisotropy. The moment at 5 T is  $0.92 \mu_B/\text{Ce}$  within the  $ac$  plane, but  $M_c$  is five times smaller. Specific heat measurements revealed a  $\gamma$  value of  $300 \text{ mJ}/(\text{mol K}^2)$ , classifying CePtSb as a heavy Fermion system. The low-temperature resistivity shows a temperature dependence of the form  $\rho = \rho_0 + AT^2$  with  $A = 0.24 \mu\Omega \text{ cm}/\text{K}^2$ . CePtSb shows interesting behavior under applied hydrostatic pressure. The  $ac$  susceptibility measurements reveal an increase of the Néel temperature with increasing pressure at a rate of 20 mK/kbar.

EuAuPb (Arpe, 1998; Pöttgen and Johrendt, 2000) shows a magnetic moment of  $6.8 \mu_B/\text{Eu}$  atom in the paramagnetic range and antiferromagnetic ordering at 7 K. The stable antiferromagnetic ground state was also evident from the negative Weiss constant of  $-14$  K and the monotonically increasing magnetization curve with a value of  $2.8 \mu_B/\text{Eu}$  at 2 K and 5.5 T.  $^{151}\text{Eu}$  Mössbauer spectroscopic studies confirmed the divalent nature of europium in EuAuPb with an isomer shift value of  $-10.9 \text{ mm/s}$  at 78 K. Line broadening in the Mössbauer spectra occurred around 8 K in agreement with the susceptibility measurements, however, no full magnetic hyperfine field splitting was evident at 4.2 K.

## 5.2 Ternary plumbides $R_2T_2Pb$

Among the magnetically characterized  $R_2T_2Pb$  plumbides, only  $Ce_2Pd_2Pb$  (Gordon et al., 1995) crystallizes with the tetragonal  $Mo_2FeB_2$  type, while all other  $R_2T_2Pb$  plumbides adopt the orthorhombic  $Mn_2AlB_2$  type structure.  $Ce_2Pd_2Pb$  exhibits Curie–Weiss behavior. A fit in the temperature region 140–300 K resulted in an experimental effective magnetic moment of  $2.70 \mu_B/Ce$  atom and a strongly negative Weiss constant of  $-30$  K. Antiferromagnetic ordering has been observed at  $T_N = 6.2$  K. Temperature dependent resistivity data show metallic behavior and a clear change in slope at the Néel temperature. A broad bump in the resistivity curve is indicative for crystal field splitting of the  $J = 5/2$  ground state. A clear minimum above the Néel temperature manifests the Kondo type behavior.  $Ce_2Rh_2Pb$  (Strydom, 2005) is a reasonable metallic conductor. The resistivity data could be fitted to a Grüneisen–Bloch model. No evidence for magnetic ordering was evident down to 4 K.

$Yb_2Pt_2Pb$  (Pöttgen et al., 1999a) adopts a superstructure of the  $Mo_2FeB_2$  type (see Section 4.2). This plumbide shows Curie–Weiss behavior in the temperature range 100–300 K with an experimental effective moment of  $4.3 \mu_B/Yb$  atom, indicating essentially trivalent ytterbium. The negative paramagnetic Curie temperature of  $-21$  K points towards antiferromagnetic interactions at low temperatures.

The whole series of  $R_2Ni_2Pb$  plumbides with orthorhombic  $Mn_2AlB_2$  type structure has intensively been studied with respect to the outstanding magnetic properties. Gulay and Hiebl (2003) gave an overview on the magnetic and electrical properties of the  $R_2Ni_2Pb$  plumbides with  $R = Y, Sm, Gd-Tm$ .  $Y_2Ni_2Pb$  behaves like a Pauli paramagnet (non-magnetic ground state) and  $Sm_2Ni_2Pb$  shows the typical features of Van Vleck paramagnetism. All paramagnetic  $R_2Ni_2Pb$  plumbides undergo transitions to ferromagnetically ordered states. The highest ordering temperature of 40 K was observed for the terbium compound.

These compounds are metallic conductors, and similar to  $YNiPb$ , the Bloch–Grüneisen relation is also valid for  $Y_2Ni_2Pb$ . The magnetic ordering manifests in the temperature dependence of the resistivities through abrupt changes in the slopes (decrease of spin-disorder scattering).

Most of the  $R_2Ni_2Pb$  plumbides have been grown in the form of single crystal platelets either via a lead flux or by special annealing procedures (Chinchure et al., 2003). The surfaces of such crystals show terrace-like structures. The single crystals then allow direction dependent magnetic measurements.

$Er_2Ni_2Pb$  reveals antiferromagnetic ordering below 3.5 K and the specific heat data indicate further magnetic transitions 3.2 and 2.0 K (Chinchure et al., 2001). The experimental effective magnetic moment of  $9.5 \mu_B/Er$  atom is in good agreement with the free ion value for  $Er^{3+}$  ( $9.58 \mu_B/Er$ ). The magnetic ordering is also evident in the resistivity plot. Furthermore, the magnetization curve at 1.8 K points to complex field induced spin reorientations. Gulay and Hiebl (2003) reported a discrepancy concerning the magnetic behavior of  $Er_2Ni_2Pb$ . The ordering temperature (6 K) and the nature of magnetic ordering (ferromagnetism) reported by Gulay and Hiebl (2003) are in contrast to the data by Chinchure et al. (2001).

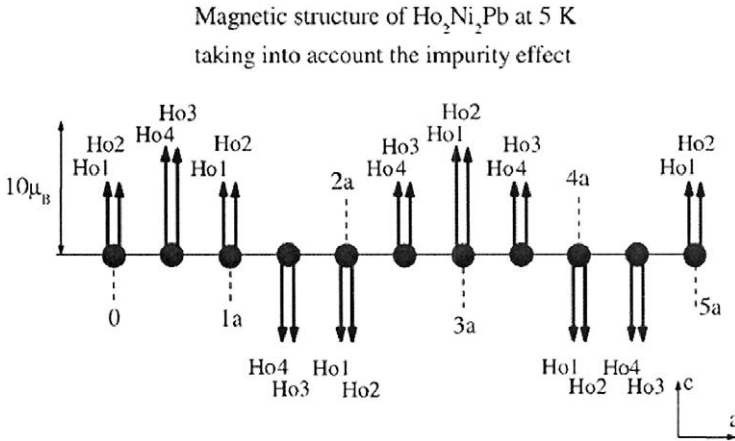


**FIGURE 26** Schematic representation of the magnetic structure of  $\text{Ho}_2\text{Ni}_2\text{Pb}$  at 5 K projected onto the  $ac$  plane. From Prokeš et al. (2005).

The magnetic behavior of  $\text{Ho}_2\text{Ni}_2\text{Pb}$  is even more complex (Muñoz-Sandoval et al., 2001; Chinchure et al., 2002, 2003; Prokeš et al., 2005). Bulk magnetic measurements revealed two distinct magnetic transitions at 7.0 and 4.8 K (Prokeš et al., 2005) and the magnetization curve shows a pronounced metamagnetic transition (Muñoz-Sandoval et al., 2001) with a large hysteresis at 1.8 K, most likely resulting from the strongly anisotropic crystal structure. The uncompensated antiferromagnetic structure of  $\text{Ho}_2\text{Ni}_2\text{Pb}$  has been determined from neutron powder diffraction experiments. The collinear magnetic structure shows an unequal number of up and down magnetic moments with a magnetic unit cell of  $5a \times b \times c$  (Figure 26).

The magnetization data of  $\text{Gd}_2\text{Ni}_2\text{Pb}$  and  $\text{Tb}_2\text{Ni}_2\text{Pb}$  (Muñoz-Sandoval et al., 2004) reveal clear metamagnetic transitions at 1.8 K with moderate critical fields of 3 and 4 T, respectively. Interestingly, pronounced square loop hysteresis has been observed for  $\text{Tb}_2\text{Ni}_2\text{Pb}$ , similar to  $\text{Pr}_2\text{Pd}_2\text{Mg}$  (Kraft et al., 2003). These changes in magnetization have a pronounced effect on the magnetoresistance properties. At the metamagnetic transition sharp changes up to 30% occur in  $\Delta\rho/\rho_0$  for  $\text{Dy}_2\text{Ni}_2\text{Pb}$ ,  $\text{Ho}_2\text{Ni}_2\text{Pb}$ , and  $\text{Er}_2\text{Ni}_2\text{Pb}$  (Figure 27).

Neutron diffraction and bulk magnetic measurements of  $\text{Dy}_2\text{Ni}_2\text{Pb}$  (Prokeš et al., 2003) reveal two distinct magnetic ordering regimes with  $T_N = 14.5$  K and  $T_C = 3.5$  K, respectively. The complicated non-collinear antiferromagnetic spin structure can be described by two commensurate propagation vectors  $q_1 = (0, 0, 0)$  and  $q_2 = (1/3, 0, 0)$  and the dysprosium magnetic moments confined in the  $ac$  plane.

### 5.3 Ternary plumbides $\text{R}_6\text{T}_{13}\text{Pb}$

Within the series of  $\text{La}_6\text{Co}_{11}\text{Ga}_3$  type compounds the plumbides  $\text{La}_6\text{Fe}_{13}\text{Pb}$ ,  $\text{La}_6\text{Co}_{13}\text{Pb}$ ,  $\text{Pr}_6\text{Fe}_{13}\text{Pb}$ ,  $\text{Nd}_6\text{Fe}_{13}\text{Pb}$ , and  $\text{Sm}_6\text{Fe}_{13}\text{Pb}$  are known (Weitzer et al.,

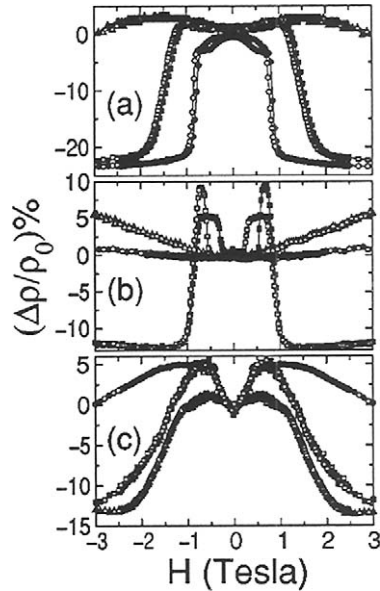


**FIGURE 27** Normalized (percent) change in magnetoresistance vs field  $H$  at 1.8 K for (a)  $\text{Dy}_2\text{Ni}_2\text{Pb}$ , (b)  $\text{Ho}_2\text{Ni}_2\text{Pb}$ , and (c)  $\text{Er}_2\text{Ni}_2\text{Pb}$ . Close (open) symbols stand for increasing (decreasing) field. From Chinchure et al. (2002).

1993). A severe problem in the preparation of these iron and cobalt rich materials is the occurrence of iron-rich impurity phases like  $\text{Sm}_2\text{Fe}_{17}$  and/or  $\text{SmFe}_3$  that can irreversibly affect the property measurements. For that reason, magnetic data are only accessible for  $\text{La}_6\text{Co}_{13}\text{Pb}$ ,  $\text{Pr}_6\text{Fe}_{13}\text{Pb}$ , and  $\text{Nd}_6\text{Fe}_{13}\text{Pb}$ .

The  $\text{R}_6\text{T}_{13}\text{Pb}$  plumbides consist of two different magnetic sublattices build up by the rare earth metal and iron (cobalt) atoms. Measurement of the lanthanum compound with the diamagnetic  $\text{La}^{3+}$  species allows the determination of the cobalt spin structure.  $\text{La}_6\text{Co}_{13}\text{Pb}$  orders ferromagnetically at  $T_C = 140$  K with a saturation moment of  $12.3 \mu_B/\text{f.u.}$  and a moment of  $0.9 \mu_B/\text{Co atom}$ .  $\text{Pr}_6\text{Fe}_{13}\text{Pb}$  and  $\text{Nd}_6\text{Fe}_{13}\text{Pb}$  have much higher ordering temperatures of 420 and 330 K, respectively with saturation magnetizations of 2.3 and  $9.5 \mu_B/\text{f.u.}$  Lead can be substituted by indium, thallium, tin, arsenic, antimony, and bismuth. This substitution has drastic influences on the ordering temperatures which rise up to 550 K for  $\text{Nd}_6\text{Fe}_{13}\text{Sb}$ .

The magnetic ordering was also monitored via  $^{57}\text{Fe}$  Mössbauer spectra at 4.2 and 295 K. The four crystallographically independent iron sites could be distinguished in the Mössbauer spectra. The isomer shifts at 4.2 and 295 K are similar for the four iron sites. As expected, the hyperfine fields detected at the iron nuclei are about 20% larger at 4.2 K. They range between 23.5 and 36.3 T.

In the hydrides  $\text{Pr}_6\text{Fe}_{13}\text{PbH}_{13.1}$  and  $\text{Nd}_6\text{Fe}_{13}\text{PbH}_{13.1}$  (Leithe-Jasper et al., 1996) the magnetization behavior changes drastically. Ferromagnetic ordering with a moment of 23–27  $\mu_B/\text{formula unit}$  occurs at room temperature.

## 5.4 Ternary plumbides $R_4Ni_3Pb_4$

The magnetic and electrical transport properties of the plumbides  $R_4Ni_3Pb_4$  ( $R = La, Ce, Pr$ ) have been investigated in detail (Kaczorowski and Gulay, 2007; Shigetoh et al., 2006).  $La_4Ni_3Pb_4$  is a Pauli paramagnet with an almost temperature independent susceptibility of  $1.3 \times 10^{-4}$  emu/mol La. Resistivity measurements reveal simple metallic behavior with specific resistivities of 240 and 103  $\mu\Omega$  cm at room temperature and 4.2 K, respectively, resulting in a residual resistivity ratio of only 2.3.  $Ce_4Ni_3Pb_4$  shows Curie–Weiss behavior above 50 K with an experimental effective magnetic moment of  $2.56 \mu_B/Ce$  and a Weiss constant of  $-57.3$  K, indicative for antiferromagnetic ordering (Kaczorowski and Gulay, 2007). Shigetoh et al. (2006) reported a slightly higher moment of  $2.80 \mu_B/Ce$  and a more negative Weiss constant of  $-69.7$  K. The large negative value of the Weiss constant is often observed for cerium intermetallics with rather high Kondo temperature.

Magnetization measurements of  $Ce_4Ni_3Pb_4$  at 1.72 K (Kaczorowski and Gulay, 2007) show a metamagnetic transition at a critical field strength of 1.5 T. At 5 T, the magnetic moment per cerium atoms is only  $0.4 \mu_B$ . In the low temperature region two distinct magnetic transitions occur at  $T_M = 4$  K and  $T_N = 3$  K. These two transitions have been ascribed to the two crystallographically independent cerium sites. They are clearly resolved in the specific heat data. The electronic specific heat coefficient of  $\gamma = 200$  mJ/(Ce mol K<sup>2</sup>) classifies  $Ce_4Ni_3Pb_4$  as system where the heavy fermion state survives in the weak ferromagnetic state (Shigetoh et al., 2006).

Resistivity data of  $Ce_4Ni_3Pb_4$  show a sudden drop near the Néel temperature of 3 K (Kaczorowski and Gulay, 2007). The negative temperature coefficient of the electrical resistivity, the largely negative paramagnetic Curie temperature and the reduced magnetic moment in the magnetically ordered region are the characteristic features for a Kondo system. In parallel to this behavior, magnetoresistivity measurements at 4.2 K and 8 T reveal a value of  $-17\%$ .

$Pr_4Ni_3Pb_4$  remains paramagnetic over the whole temperature range investigated (Kaczorowski and Gulay, 2007). The experimental magnetic moment and the Weiss constant are  $3.58 \mu_B/Pr$  and  $-16.5$  K. The absence of long-range magnetic ordering in  $Pr_4Ni_3Pb_4$  is also evident from magnetization data at 1.72 K. Resistivity measurements show a residual resistivity ratio of ca. 3 and the crystal electrical field interactions are found to be relatively weak.

## 5.5 The plumbide $Ce_8Pd_{24}Pb$

$Ce_8Pd_{24}Pb$  (Gordon et al., 1996) shows stable trivalent cerium. Susceptibility data reveal an effective magnetic moment of  $2.48 \mu_B/Ce$  atom in the paramagnetic range, close to the free ion value of  $2.54 \mu_B$  for  $Ce^{3+}$ . Already the negative Weiss constant of  $-10(2)$  K was indicative for the antiferromagnetic ordering ( $T_N = 6$  K) at low temperature. Resistivity data show a strong drop at the Néel temperature, indicating decrease of spin disorder scattering. The high-temperature part of the susceptibility reveals the influence of crystal field splitting. The magnetic ordering was clearly detected also in the specific heat measurements (Cho et al., 1998). The

high electronic specific heat coefficient of  $1160 \text{ mJ}/(\text{mol K}^2)$  classifies  $\text{Ce}_3\text{Pd}_{24}\text{Pb}$  as a heavy Fermion system. Thermopower measurements (Jones et al., 1999) show a moderate decrease of the Seebeck coefficient from  $8.5 \mu\text{V}/\text{K}$  at  $297 \text{ K}$  to  $4.0 \mu\text{V}/\text{K}$  at  $78 \text{ K}$ .

## 5.6 The plumbide $\text{Dy}_5\text{CuPb}_3$

In the large series of  $\text{R}_5\text{TPb}_3$  plumbides, so far only magnetic data of  $\text{Dy}_5\text{CuPb}_3$  have been reported (Tran and Gulay, 2006).  $\text{Dy}_5\text{CuPb}_3$  shows Curie–Weiss behavior above  $80 \text{ K}$  with an experimental magnetic moment of  $10.84 \mu_{\text{B}}/\text{Dy}$  and a Weiss constant of  $50.5(5) \text{ K}$ , indicative for ferri- or ferromagnetic ordering. Magnetization and magnetoresistance measurements reveal that there are two distinct magnetic transitions, i.e. ferromagnetic ordering at  $T_{\text{C}} = 45.0 \pm 0.5 \text{ K}$  and anti-ferromagnetic ordering at  $T_{\text{N}} = 6.5 \pm 0.5 \text{ K}$ . It is supposed that the change in the magnetic structure with decreasing temperature from  $T_{\text{C}}$  to  $T_{\text{N}}$  is accompanied by an enhancement of fluctuation of the magnetic moments and this behavior can most likely be attributed to the two crystallographically independent dysprosium sites.  $\text{Dy}_5\text{CuPb}_3$  shows a significant magnetoresistance value of  $-24\%$  in the temperature range between  $T_{\text{C}}$  and  $T_{\text{N}}$ . At  $300 \text{ K}$  a negative thermoelectric power of  $-17 \mu\text{V}/\text{K}$  is observed. The magnetic transitions are also evident in the resistivity data of this metallic plumbide.

## 6. SUMMARY AND OUTLOOK

So far more than 180 rare earth–transition metal–plumbides have been reported. They crystallize with 23 different structure types. Apart from the few lead rich plumbides with  $\text{Yb}_3\text{Rh}_4\text{Sn}_{13}$  and related structures, only plumbides with 33 at% or even lower lead content have been reported. Some ternary systems exhibit large liquidus ranges in the lead rich regions at  $870 \text{ }^\circ\text{C}$ . Through phase analytical investigations at lower temperatures one will certainly get access to new lead rich phases. In view of the more than 500 and 850 rare earth–transition metal–stannides and indides, respectively, the lead based systems certainly have a great potential for many more phases to be discovered.

Only  $\text{YbAgPb}$  and  $\text{La}_4\text{Ni}_3\text{Pb}_4$  show peculiar structure types, which have first been observed for a plumbide. All other plumbides exhibit relatively simple structure types, which have been observed also for silicides, germanides, stannides, gallides, or indides. We expect that lead characteristic structures will form in the lead rich parts of the ternary systems, similar to the gallium and indium based phase diagrams.

A few  $\text{RTPb}$  and  $\text{R}_2\text{T}_2\text{Pb}$  plumbides that have been characterized with respect to their magnetic behavior show very interesting properties. Also in this field, the plumbides exhibit a large potential for new phenomena and can thus be considered a vivid area of research for the future.

## ACKNOWLEDGEMENTS

This work was financially supported by the Deutsche Forschungsgemeinschaft.

## REFERENCES

- Adachi, G.-Y., Imanaka, N., Zhang, F. Rare earth carbides, in: Gschneidner Jr., K.A., Eyring, L., editors. Handbook on the Physics and Chemistry of Rare Earths, vol. 15. Amsterdam: North-Holland; 1991, chap. 99.
- Aronsson, B. *Acta Chem. Scand.* 1960, **14**, 1414.
- Arpe, P.E. *Synthese und strukturchemische Untersuchungen an ternären Plumbiden des Ytterbiums*, Universität Münster: Staatsexamensarbeit; 1998.
- Becher, H.J., Krogmann, K., Peisker, E. *Z. Anorg. Allg. Chem.* 1966, **344**, 140.
- Bockelmann, W., Schuster, H.-U. *Z. Anorg. Allg. Chem.* 1974, **410**, 233.
- Bockelmann, W., Jacobs, H., Schuster, H.-U. *Z. Naturforsch.* 1970, **25b**, 1305.
- Bojin, M.D., Hoffmann, R. *Helv. Chim. Acta* 2003a, **86**, 1653.
- Bojin, M.D., Hoffmann, R. *Helv. Chim. Acta* 2003b, **86**, 1683.
- Chinchure, A.D., Muñoz-Sandoval, E., Gortemulder, T.J., Hendrikx, R.W.A., Mydosh, J.A. *J. Alloys Compd.* 2003, **359**, 5.
- Chinchure, A.D., Muñoz-Sandoval, E., Mydosh, J.A. *Phys. Rev. B* 2001, **64**, 020404.
- Chinchure, A.D., Muñoz-Sandoval, E., Mydosh, J.A. *Phys. Rev. B* 2002, **66**, 020409.
- Cho, B.K., Gordon, R.A., Jones, C.D.W., DiSalvo, F.J., Kim, J.S., Stewart, G.R. *Phys. Rev. B* 1998, **57**, 15191.
- Dhar, S.K., Manfrinetti, P., Palenzona, A. *Phys. Rev. B* 1995, **51**, 12464.
- Donohue, J. *The Structures of the Elements*, New York: Wiley; 1974.
- Duwell, E.J., Baenziger, N.C. *Acta Crystallogr.* 1955, **8**, 705.
- Dwight, A.E., Mueller, M.H., Conner Jr., R.A., Downey, J.W., Knott, H. *Trans. Met. Soc. AIME* 1968, **242**, 2075.
- Eisenmann, B., Schäfer, H. *J. Less-Common Met.* 1986, **123**, 89.
- Emsley, J. *The Elements*, Oxford: Oxford Univ. Press; 1999.
- Fickenscher, Th., Rodewald, U.Ch., Niepmann, D., Mishra, R., Eschen, M., Pöttgen, R. *Z. Naturforsch.* 2005, **60b**, 271.
- Fornasini, M.L., Merlo, F., Pani, M. *Z. Kristallogr. NCS* 2001a, **216**, 24.
- Fornasini, M.L., Merlo, F., Pani, M. *Z. Kristallogr. NCS* 2001b, **216**, 173.
- Galadzhun, Ya.V., Pöttgen, R. *Z. Anorg. Allg. Chem.* 1999, **625**, 481.
- Gelato, M.L., Parthé, E. *J. Appl. Crystallogr.* 1987, **20**, 139.
- Gladyshevskii, E.I., Kripiakevich, P.I., Tesliuk, M.J. *Dokl. Akad. Nauk SSSR* 1952, **85**, 81.
- Gladyshevsky, E.I., Bodak, O.I., Pecharsky, V.K. Phase equilibria and crystal chemistry in ternary rare earth systems with metallic elements, in: Gschneidner Jr., K.A., Eyring, L., editors. Handbook on the Physics and Chemistry of Rare Earths, vol. 13. Amsterdam: North-Holland; 1990, chap. 88.
- Gladyshevsky, R.E., Grin, Yu.N., Yarmolyuk, Ya.P. *Dopov. Akad. Nauk Ukr. RSR, Ser. A* 1983, **45**, 67.
- Gordon, R.A., DiSalvo, F.J. *Z. Naturforsch.* 1996, **51b**, 52.
- Gordon, R.A., Ijiri, Y., Spencer, C.M., DiSalvo, F.J. *J. Alloys Compd.* 1995, **224**, 101.
- Gordon, R.A., Jones, C.D.W., Alexander, M.G., DiSalvo, F.J. *Physica B* 1996, **225**, 23.
- Grin, Yu.N., Gladyshevskii, R.E. *Gallides Handbook*, Moscow: Metallurgy; 1989, in Russian.
- Gulay, L.D. *J. Alloys Compd.* 2000, **313**, 144.
- Gulay, L.D. *J. Alloys Compd.* 2001a, **314**, 206.
- Gulay, L.D. *J. Alloys Compd.* 2001b, **314**, 219.
- Gulay, L.D. *J. Alloys Compd.* 2002, **347**, 124.
- Gulay, L.D. *J. Alloys Compd.* 2003a, **348**, 146.
- Gulay, L.D. *J. Alloys Compd.* 2003b, **349**, 201.
- Gulay, L.D. *J. Alloys Compd.* 2005, **392**, 165.
- Gulay, L.D., Hiebl, K. *J. Alloys Compd.* 2002, **339**, 46.

- Gulay, L.D., Hiebl, K. J. *Alloys Compd.* 2003, **351**, 35.
- Gulay, L.D., Wołczyrz, M. J. *Alloys Compd.* 2001a, **315**, 164.
- Gulay, L.D., Wołczyrz, M. J. *Alloys Compd.* 2001b, **316**, 209.
- Gulay, L.D., Wołczyrz, M. J. *Alloys Compd.* 2001c, **319**, 218.
- Gulay, L.D., Wołczyrz, M. J. *Alloys Compd.* 2001d, **325**, 201.
- Gulay, L.D., Wołczyrz, M. *Polish J. Chem.* 2001e, **75**, 1073.
- Gulay, L.D., Kalychak, Ya.M., Wołczyrz, M. J. *Alloys Compd.* 2000a, **311**, 228.
- Gulay, L.D., Kalychak, Ya.M., Wołczyrz, M., Łukaszewicz, K. J. *Alloys Compd.* 2000b, **311**, 238.
- Gulay, L.D., Kalychak, Ya.M., Wołczyrz, M., Łukaszewicz, K. J. *Alloys Compd.* 2000c, **313**, 42.
- Gulay, L.D., Stępień-Damm, J., Wołczyrz, M. J. *Alloys Compd.* 2001a, **314**, 209.
- Gulay, L.D., Stępień-Damm, J., Wołczyrz, M. J. *Alloys Compd.* 2001b, **315**, 169.
- Gulay, L.D., Stępień-Damm, J., Wołczyrz, M. J. *Alloys Compd.* 2001c, **319**, 148.
- Guloy, A.M., Corbett, J.D. *J. Solid State Chem.* 1994, **109**, 352.
- Guloy, A.M., Corbett, J.D. *J. Solid State Chem.* 2005, **178**, 1112.
- Harris, I.R., Norman, M. J. *Less-Common Met.* 1968, **15**, 285.
- Heusler, O. *Ann. Phys.* 1934, **19**, 155.
- Hodeau, J.L., Chenavas, J., Marezio, M., Remeika, J.P. *Solid State Commun.* 1980, **36**, 839.
- Hodeau, J.L., Marezio, M., Remeika, J.P. *Acta Crystallogr. B* 1984, **40**, 26.
- Hoffmann, R.-D., Pöttgen, R. Z. *Kristallogr.* 2001, **216**, 127.
- Hovestreydt, E., Engel, N., Klepp, K., Chabot, B., Parthé, E. J. *Alloys Compd.* 1982, **85**, 247.
- Hyde, B.G., Andersson, S. *Inorganic Crystal Structures*, New York: Wiley; 1989.
- Iandelli, A. Z. *Anorg. Allg. Chem.* 1964, **330**, 221.
- Iandelli, A. J. *Alloys Compd.* 1994, **203**, 137.
- Johnston, R.L., Hoffmann, R. Z. *Anorg. Allg. Chem.* 1992, **616**, 105.
- Jones, C.D.W., Gordon, R.A., Cho, B.K., DiSalvo, F.J., Kim, J.S., Stewart, G.R. *Physica B* 1999, **262**, 284.
- Kaczorowski, D., Gulay, L.D. J. *Alloys Compd.* 2007, **436**, 9.
- Kalychak, Ya.M., Zaremba, V.I., Pöttgen, R., Lukachuk, M., Hoffmann, R.-D. Rare earth–transition metal–indides, in: Gschneidner Jr., K.A., Bünzli, J.-C.G., Pecharsky, V.K., editors. *Handbook on the Physics and Chemistry of Rare Earths*, vol. 34. Amsterdam: Elsevier; 2005, chap. 218.
- Kalychak, Ya.M., Zaremba, V.I., Stępień-Damm, J., Galadzhun, Ya.V., Aksel'rud, L.G. *Krystallografiya* 1998, **43**, 17, in Russian.
- Kalychak, Ya.M., Zavaliiy, Yu.P., Baranyak, V.M., Dmytrakh, O.V., Bodak, O.I. *Krystallografiya* 1987, **32**, 1021, in Russian.
- Kanatzidis, M.G., Pöttgen, R., Jeitschko, W. *Angew. Chem. Int. Ed.* 2005, **44**, 6996.
- Kraft, R., Fickenscher, Th., Kotzyba, G., Hoffmann, R.-D., Pöttgen, R. *Intermetallics* 2003, **11**, 111.
- Krypyakevich, P.I., Markiv, V.Ya., Melnyk, E.V. *Dopov. Akad. Nauk Ukr. RSR Ser. A* 1967, 750.
- Kußmann, D., Hoffmann, R.-D., Pöttgen, R. Z. *Anorg. Allg. Chem.* 1998, **624**, 1727.
- Kuz'ma, Yu., Chykhrij, S. Phosphides, in: Gschneidner Jr., K.A., Eyring, L., editors. *Handbook on the Physics and Chemistry of Rare Earths*, vol. 23. Amsterdam: North-Holland; 1996, chap. 156.
- Landrum, G.A., Hoffmann, R., Evers, J., Boysen, H. *Inorg. Chem.* 1998, **37**, 5754.
- Larson, A.C., Cromer, D.T. *Acta Crystallogr.* 1961, **14**, 73.
- Leithe-Jasper, A., Skomski, R., Qui, Q., Coey, J.M.D., Weitzer, F., Rogl, P. *J. Phys.: Condens. Matter* 1996, **8**, 3453.
- Lukachuk, M., Pöttgen, R. Z. *Kristallogr.* 2003, **218**, 767.
- Manfrinetti, P., Canepa, F., Palenzona, A., Fornasini, M.L., Giannini, E. J. *Alloys Compd.* 1997, **247**, 109.
- Mar, A. Bismuthides, in: Gschneidner Jr., K.A., Bünzli, C.G., Pecharsky, V.K., editors. *Handbook on the Physics and Chemistry of Rare Earths*, vol. 36. Amsterdam: Elsevier; 2006, chap. 227.
- Marazza, R., Rossi, D., Ferro, R. J. *Less-Common Met.* 1988, **138**, 189.
- Marazza, R., Mazzone, D., Riani, P., Zanicchi, G. J. *Alloys Compd.* 1995, **220**, 241.
- Massalski, T.B., editor. *Binary Alloy Phase Diagrams*. Metals Park, OH: Amer. Soc. Metals; 1986.
- Mazzone, D., Rossi, D., Marazza, R., Ferro, R. J. *Less-Common Met.* 1982, **84**, 301.
- Mazzone, D., Borzone, G., Rossi, D., Ferro, R. J. *Less-Common Met.* 1983, **94**, L5.
- Melnyk, G., Kandpal, H.C., Gulay, L.D., Tremel, W. J. *Alloys Compd.* 2004, **370**, 217.
- Merlo, F., Pani, M., Fornasini, M.L. J. *Less-Common Met.* 1991, **171**, 329.
- Merlo, F., Pani, M., Fornasini, M.L. J. *Alloys Compd.* 1993, **196**, 145.

- Merlo, F., Pani, M., Fornasini, M.L. *J. Alloys Compd.* 1996, **232**, 289.
- Misch, L. *Metallwirtschaft, Metallwissenschaft Metalltechnik* 1935, **14**, 897.
- Movshovich, R., Lawrence, J.M., Hundley, M.F., Neumeier, J., Thompson, J.D., Lacerda, A., Fisk, Z. *Phys. Rev. B* 1996, **53**, 5465.
- Moze, O., Manfrinetti, P., Canepa, F., Palenzona, A., Fornasini, M.L., Rodriguez-Carvajal, J.R. *Intermetallics* 2000, **8**, 273.
- Müller, U. *Anorganische Strukturchemie*, 3. Auflage, Stuttgart: Teubner; 1996.
- Müller, W., Voltz, R. *Z. Naturforsch.* 1974, **29b**, 163.
- Muñoz-Sandoval, E., Chinchure, A.D., Hendriks, R.W.A., Mydosh, J.A. *Europhys. Lett.* 2001, **56**, 302.
- Muñoz-Sandoval, E., Diaz-Ortiz, A., Chinchure, A.D., Mydosh, J.A. *J. Alloys Compd.* 2004, **369**, 260.
- Nesper, R. *Angew. Chem.* 1991, **103**, 805.
- Nesper, R., Miller, G.J. *J. Alloys Compd.* 1993, **197**, 109.
- Nielsen, J.W., Baenziger, N.C. *Acta Crystallogr.* 1954, **7**, 132.
- Niewa, R. *Z. Kristallogr.* 2002, **217**, 8.
- Niewa, R., DiSalvo, F.J. *Chem. Mater.* 1998, **10**, 2733.
- Niewa, R., Jacobs, H. *Chem. Rev.* 1996, **96**, 2053.
- Nowotny, H., Sibert, W. *Z. Metallkd.* 1941, **33**, 391.
- Nuspl, G., Polborn, K., Evers, J., Landrum, G.A., Hoffmann, R. *Inorg. Chem.* 1996, **35**, 6922.
- Öner, Y., Senoussi, S., Sologub, O., Salamakha, P. *Physica B* 1999, **259–261**, 887.
- Osamura, K., Murakami, Y. *J. Less-Common Met.* 1978, **60**, 311.
- Owen, E.A., Liu, Y.H. *Philos. Mag.* 1947, **38**, 354.
- Parthé, E., Chabot, B. Crystal structures and crystal chemistry of ternary rare earth–transition metal borides, silicides and homologues, in: Gschneidner Jr., K.A., Eyring, L., editors. *Handbook on the Physics and Chemistry of Rare Earths*, vol. 6. Amsterdam: North-Holland; 1984, chap. 48.
- Parthé, E., Gelato, M.L. *Acta Crystallogr. A* 1984, **40**, 169.
- Pöttgen, R. *Z. Naturforsch.* 1994, **49b**, 1309.
- Pöttgen, R., Johrendt, D. *Chem. Mater.* 2000, **12**, 875.
- Pöttgen, R., Arpe, P.E., Felser, C., Kußmann, D., Müllmann, R., Mosel, B.D., Künnen, B., Kotzyba, G. *J. Solid State Chem.* 1999a, **145**, 668.
- Pöttgen, R., Gulden, T., Simon, A. *GIT Labor-Fachzeitschrift* 1999b, **43**, 133.
- Pöttgen, R., Hoffmann, R.-D., Kremer, R.-K., Schnelle, W. *J. Solid State Chem.* 1999c, **142**, 180.
- Pöttgen, R., Lang, A., Hoffmann, R.-D., Künnen, B., Kotzyba, G., Müllmann, R., Mosel, B.D., Rosenhahn, C. *Z. Kristallogr.* 1999d, **214**, 143.
- Pöttgen, R., Fugmann, A., Hoffmann, R.-D., Rodewald, U.Ch., Niepmann, D. *Z. Naturforsch.* 2000, **55b**, 155.
- Pötzschke, M., Schubert, K. *Z. Metallkd.* 1962, **53**, 474.
- Principi, G., Spataru, T., Maddalena, A., Palenzona, A., Manfrinetti, P., Blaha, P., Schwarz, K., Kuncser, V., Filoti, G. *J. Alloys Compd.* 2001, **317**, 567.
- Prokeš, K., Muñoz-Sandoval, E., Chinchure, A.D., Mydosh, J.A. *Phys. Rev. B* 2003, **68**, 134427.
- Prokeš, K., Muñoz-Sandoval, E., Chinchure, A.D., Mydosh, J.A. *Eur. Phys. J. B* 2005, **43**, 163.
- Remschnig, K., Le Bihan, T., Noël, H., Rogl, P. *J. Solid State Chem.* 1992, **97**, 391.
- Rieger, W., Parthé, E. *Monatsh. Chem.* 1968, **99**, 291.
- Rieger, W., Nowotny, H., Benesovsky, F. *Monatsh. Chem.* 1964, **95**, 1502.
- Rieger, W., Nowotny, H., Benesovsky, F. *Monatsh. Chem.* 1965, **96**, 98.
- Rogl, P. Phase equilibria in ternary and higher order systems with rare earth elements and boron, in: Gschneidner Jr., K.A., Eyring, L., editors. *Handbook on the Physics and Chemistry of Rare Earths*, vol. 6. Amsterdam: North-Holland; 1984a, chap. 49.
- Rogl, P. Phase equilibria in ternary and higher order systems with rare earth elements and silicon, in: Gschneidner Jr., K.A., Eyring, L., editors. *Handbook on the Physics and Chemistry of Rare Earths*, vol. 7. Amsterdam: North-Holland; 1984b, chap. 51.
- Salamakha, P., Zaplatynsky, O. *J. Alloys Compd.* 1997, **260**, 127.
- Salamakha, P., Zaplatynsky, O., Sologub, O., Bodak, O. *J. Alloys Compd.* 1996, **239**, 94.
- Salamakha, P., Demchenko, P., Sologub, O., Bodak, O. *Polish J. Chem.* 1999a, **73**, 885.
- Salamakha, P.S. Crystal structures and crystal chemistry of ternary rare-earth germanides, in: Gschneidner Jr., K.A., Eyring, L., editors. *Handbook on the Physics and Chemistry of Rare Earths*, vol. 27. Amsterdam: North-Holland; 1999b, chap. 174.

- Salamakha, P.S., Sologub, O.L., Bodak, O.I. Ternary rare-earth-germanium systems, in: Gschneidner Jr., K.A., Eyring, L., editors. Handbook on the Physics and Chemistry of Rare Earths, vol. 27. Amsterdam: North-Holland; 1999c, chap. 173.
- Sales, B.C. Filled Skutterudites, in: Gschneidner Jr., K.A., Bünzli, C.G., Pecharsky, V.K., editors. Handbook on the Physics and Chemistry of Rare Earths, vol. 33. Amsterdam: North-Holland; 2003, chap. 211.
- Schreyer, M., Fässler, Th.F. *Solid State Sci.* 2006, **8**, 793.
- Schubert, K., Meissner, H.G., Pötzschke, M., Rossteutscher, W., Stolz, E. *Naturwissenschaften* 1962, **49**, 57.
- Sebastian, C.P., Eckert, H., Rayaprol, S., Hoffmann, R.-D., Pöttgen, R. *Solid State Sci.* 2006, **8**, 560.
- Sendlinger, B. Hochdruck-Untersuchungen an den ambivalenten Verbindungen MTX (M = Yb, Ca, Eu, Sr, Ba; T = Pd, Pt; X = Si, Ge, Sn, Pb), Dissertation: Universität München; 1993.
- Shigetoh, K., Sasakawa, T., Umeo, K., Takabatake, T. *J. Phys. Soc. Jpn.* 2006, **75**, 33701.
- Shoemaker, C.B., Shoemaker, D.P. *Acta Crystallogr.* 1965, **18**, 900.
- Sichevich, O.M., Lapunova, R.V., Sobolev, A.N., Grin, Yu.N., Yarmolyuk, Ya.P. *Sov. Phys. Crystallogr.* 1985, **30**, 627.
- Simon, A. *Angew. Chem.* 1983, **95**, 94.
- Skolozdra, R.V. Stannides of rare-earth and transition metals, in: Gschneidner Jr., K.A., Eyring, L., editors. Handbook on the Physics and Chemistry of Rare Earths, vol. 24. Amsterdam: North-Holland; 1997, chap. 164.
- Sologub, O.L., Salamakha, P.S. Rare earth-antimony systems, in: Gschneidner Jr., K.A., Bünzli, C.G., Pecharsky, V.K., editors. Handbook on the Physics and Chemistry of Rare Earths, vol. 33. Amsterdam: North-Holland; 2003, chap. 212.
- Strydom, A.M. *J. Alloys Compd.* 2005, **394**, 152.
- Tang, J., Gschneidner Jr., K.A., White, S.J., Roser, M.R., Goodwin, T.J., Corrucini, L.R. *Phys. Rev. B* 1995, **52**, 7328.
- Tran, V.H., Gulay, L.D. *J. Solid State Chem.* 2006, **179**, 646.
- Vandenberg, J.M. *Mater. Res. Bull.* 1980, **15**, 835.
- Venturini, G., Kamta, M., McRae, E., Maréché, J.F., Malaman, B., Roques, B. *Mater. Res. Bull.* 1986, **21**, 1203.
- Villars, P., Calvert, L.D. *Pearson's Handbook of Crystallographic Data for Intermetallic Phases* Desk Edition, Materials Park, OH: ASM International; 1991, 1997.
- Weitzer, F., Leithe-Jasper, A., Rogl, P., Hiebl, K., Noël, H., Wiesinger, G., Steiner, W. *J. Solid State Chem.* 1993, **104**, 368.
- Wells, A.F. *Structural Inorganic Chemistry*, fifth edn., Oxford: Clarendon Press; 1990.
- Wenski, G., Mewis, A. *Z. Kristallogr.* 1986, **176**, 125.
- Zachariasen, W.H. *Acta Crystallogr.* 1949, **2**, 94.
- Zaplatinskii, O.V., Salamakha, P.S., Muratova, L.A. *Inorg. Mater.* 1996, **32**, 734.
- Zaremba, R.I., Kalychak, Ya.M., Rodewald, U.Ch., Pöttgen, R., Zaremba, V.I. *Z. Naturforsch.* 2006, **61b**, 942.
- Zaremba, V.I., Kalychak, Ya.M., Dzevenko, M.V., Rodewald, U.Ch., Hoffmann, R.-D., Pöttgen, R. *Monatsh. Chem.* 2007, **138**, 101.
- Zumdick, M.F., Pöttgen, R. *Z. Kristallogr.* 1999, **214**, 90.
- Zumdick, M.F., Hoffmann, R.-D., Pöttgen, R. *Z. Naturforsch.* 1999, **54b**, 45.

## Higher Borides

Takao Mori\*

<b>Contents</b>	List of Symbols and Acronyms	106
	1. Introduction	107
	2. Synthesis Techniques	108
	3. Bonding in Higher Borides	109
	4. Dodecaborides $RB_{12}$	111
	4.1 Structure	111
	4.2 Physical properties	111
	4.2.1 Electrical properties	111
	4.2.2 Magnetic properties	113
	4.2.3 $YbB_{12}$ ; a Kondo insulator	114
	4.2.4 Recent developments regarding magnetism of $RB_{12}$	114
	5. Nomenclature/Notation of the Higher Borides	116
	6. $RB_{66}$	116
	6.1 Structure of $RB_{66}$	117
	6.2 Physical properties of $RB_{66}$	119
	7. $RB_{50}$ (and $RB_{44}Si_2$ )	120
	7.1 Magnetic properties of $TbB_{50}$	120
	7.2 Crystal growth realized through addition of Si, and $GdB_{44}Si_2$	120
	7.3 Structure of $RB_{50}$ -type compounds	123
	7.4 Substitution of magnetic atoms	127
	7.5 The ytterbium phase	127
	7.6 Electrical resistivity of $RB_{50}$ -type compounds	129
	7.7 Application of high fields	130
	7.8 Nature of the antiferromagnetic transition of $RB_{50}$ -type compounds	130
	7.9 ESR of $GdB_{44}Si_2$ : indications of one dimensionality	132
	7.10 Mechanism of the magnetic interaction in $RB_{50}$ -type compounds	132
	7.11 Magnetic structure of $RB_{50}$ -type compounds	134
	7.12 Summary of magnetism of $RB_{50}$ -type compounds	135
	8. $RB_{25}$ and $RAlB_{14}$	136

\* National Institute for Materials Science, Namiki 1-1, Tsukuba, 305-0044, Japan  
E-mail: [mori.takao@nims.go.jp](mailto:mori.takao@nims.go.jp)

8.1	Structures of $\text{RB}_{25}$ and $\text{RAlB}_{14}$	136
8.2	Bonding in $\text{RB}_{25}$ and $\text{RAlB}_{14}$	136
8.3	Electrical properties of $\text{RB}_{25}$ and $\text{RAlB}_{14}$	138
8.4	Magnetic properties of $\text{RB}_{25}$	139
8.5	Magnetic properties of $\text{RAlB}_{14}$	139
9.	Homologous R–B–C(N) Compounds: $\text{RB}_{15,5}\text{CN}$ , $\text{RB}_{22}\text{C}_2\text{N}$ , $\text{RB}_{28,5}\text{C}_4$	140
9.1	Crystal structures	142
9.2	Magnetic properties: spin glass behavior	143
9.3	Dynamical properties: indication of 2 dimensionality	145
9.4	Comparison of magnetic properties	147
9.5	Summary of the spin glass behavior	149
10.	$\text{RB}_{18}\text{Si}_5$ ( $\text{R}_{1,8}\text{B}_{36}\text{C}_2\text{Si}_8$ )	149
10.1	Structures of $\text{RB}_{18}\text{Si}_5$ and $\text{R}_{1,8}\text{B}_{36}\text{C}_2\text{Si}_8$	150
10.2	Electrical properties of $\text{RB}_{18}\text{Si}_5$	150
10.3	Magnetic properties of $\text{RB}_{18}\text{Si}_5$ and $\text{R}_{1,8}\text{B}_{36}\text{C}_2\text{Si}_8$	152
10.4	Field dependence	154
11.	Sc Higher Borides	157
12.	Thermoelectric Properties of Higher Borides	158
12.1	$\text{RB}_{66}$	158
12.2	Doping of $\text{YB}_{66}$	159
12.3	$\text{RB}_{44}\text{Si}_2$ ( $\text{RB}_{50}$ -type) compounds	161
12.4	Homologous R–B–C(N) compounds: $\text{RB}_{15,5}\text{CN}$ , $\text{RB}_{22}\text{C}_2\text{N}$ , $\text{RB}_{28,5}\text{C}_4$	165
13.	Summary/Conclusion and Outlook	168
	References	170

### List of Symbols and Acronyms

1D	one dimensional	$I_m$	isothermal remanent magnetizations
2D	two dimensional	$J$	total angular momentum
3D	three dimensional	$k_B$	Boltzmann factor
$C$	specific heat	$N$	number of spins
$d$	density	$N_A$	Avogadro number
$D_t$	thermal diffusivity constant	$R$	rare earth (metal, element)
$D(E_F)$	density of states at the Fermi energy	RKKY	Ruderman–Kittel–Kanamori–Yoshida
$E_F$	Fermi energy	$T$	temperature
ESR	electron spin resonance	$T_0$	characteristic temperature of variable range hopping
FC	field cooling	$T_f$	peak temperature of the zero field cooled susceptibility in spin glasses
FZ	floating zone	$T_N$	Neel temperature
$g$	Lande factor	VRH	variable range hopping
$g(\tau)$	distribution function of relaxation time		
$H_{C_2}(T)$	upper critical field		

XRD	X-ray diffraction	$\rho_0$	prefactor of the resistivity
Z, ZT	figure of merit	$\sigma_{\text{TRM}}$	thermal remanent magnetization
ZFC	zero field cooling		
$\alpha$	Seebeck coefficient	$\tau_C$	median relaxation time
$\beta$	width parameter	$\chi'$	in-phase susceptibility
$\theta$	Curie–Weiss temperature	$\chi''$	out-of-phase susceptibility
$\kappa$	thermal conductivity	$\chi_0$	isothermal susceptibility
$\lambda$	magnetic penetration depth	$\chi_s$	adiabatic susceptibility
$\mu_B$	Bohr magneton	$\omega$	frequency
$\xi$	localization length	$\Delta$	superconducting energy gap
$\rho$	resistivity		

## 1. INTRODUCTION

Boron is inclined to form strong covalent bonds, but since it has only three valence electrons, it is electron deficient to form a three dimensional network with conventional electron pair bonding. To overcome this circumstance, boron-rich compounds tend to form boron clusters which have “economic” bonding. In particular, compounds which are especially boron-rich typically have the B<sub>12</sub> icosahedra cluster as a basic building block of the structure. Because of the strong covalent bonds, such boron cluster compounds generally possess attractive properties, such as high melting points, high hardness, light weight, acid resistance, and small compressibility. Compounds like  $\beta$ -boron, boron carbide, MgAlB<sub>14</sub>, and YB<sub>66</sub> have been well researched over the years. There have been review articles dealing with these B<sub>12</sub> icosahedra compounds and general interesting features derived from the particular/unique bonding of boron and of boron icosahedra (e.g. Matkovich et al., 1965; Hoard and Hughes, 1967; Naslain et al., 1976; Matkovich and Economy, 1977; Etourneau, 1985; Higashi, 1986; Golikova, 1987; Werheit, 1999; Aselage and Emin, 2003; Emin, 2004).

Boron has a particular affinity with rare earth elements, and forms rare earth borides which are of particular interest. The rare earth atoms supply electrons to the boron atomic framework to stabilize and form novel structures, while the shell of f electrons supplies further attractive properties like magnetism. Borides with lower boron content, like the hexaborides RB<sub>6</sub> and tetraborides RB<sub>4</sub> are well known metallic compounds and have been studied throughout the years, revealing interesting magnetic properties (e.g. Gignoux and Schmitt, 1997).

Up to the early 1990s, the only rare earth boride known with RB<sub>n</sub> ( $n > 12$ ) was RB<sub>66</sub>. These compounds have been primarily studied for their interesting structure and structurally derived features like the amorphous behavior of thermal properties. However, in a recent development, new higher borides have been discovered like the RB<sub>25</sub> and RB<sub>50</sub> compounds. Furthermore, with addition of small amounts of 3rd elements like C, N, Si, the boron cluster framework was found to arrange

itself in new structures, and new compounds like  $\text{RB}_{15.5}\text{CN}$ ,  $\text{RB}_{22}\text{C}_2\text{N}$ ,  $\text{RB}_{28.5}\text{C}_4$ ,  $\text{RB}_{18}\text{Si}_5$ , were also discovered.

The structures of these new compounds are of interest and furthermore, exciting physical properties have been found. For example, a surprisingly strong magnetic coupling is found, despite the fact that they are insulating dilute f-electron systems. A wide variation of the magnetic behavior has also been observed, ranging from a 1D dimer-like transition, 2D spin glass behavior, and 3D long range ordering. Recently, in a development for high temperature thermoelectrics, the homologous R–B–C(N) compounds have been discovered to display n-type behavior. n-type behavior had previously never been observed for boron icosahedra compounds unless they had been extremely doped with transition metals.

This review will cover the synthesis, structure, and physical (especially the magnetic, thermoelectric) properties of the rare earth higher borides  $\text{RB}_n$  ( $n \geq 12$ ). The dodecaborides  $\text{RB}_{12}$  will also be included. Although  $\text{RB}_{12}$  are a different class of materials compared to the icosahedra-containing borides in the sense that they are metallic compounds (with the exception of  $\text{YbB}_{12}$ ) and have the cubooctahedron as a structural unit, they are also referred to as “higher borides” and recently interesting variations are being discovered in their magnetic behavior.

It is noted here that the term “higher borides” has not been well defined and it has occasionally been used to describe any boron-containing compound which is simply boron-rich. However, in those cases, it can be said that the “higher” is not treated fairly since the simple word “borides” by itself indicates that the main player is indeed boron, and therefore refers to a boron-rich compound. In this review the term “higher borides” is used to point to the rare earth borides which are distinguished by having a particularly lot of boron in them, namely, (ignoring any minor additions of 3rd elements), borides which have  $\text{RB}_n$  with  $n \geq 12$ . Borides not making the cut in terms of this defined boron content like the previously mentioned hexaborides  $\text{RB}_6$ , tetraborides  $\text{RB}_4$ , and diborides  $\text{RB}_2$  are well known metallic compounds and have been the topic of previous reviews (e.g. Etourneau, 1985; Gignoux and Schmitt, 1997). The higher borides have  $\text{B}_{12}$  icosahedra clusters (cubooctahedra clusters in the case of the dodecaborides  $\text{RB}_{12}$ ) as basic building blocks of the structure, and while they have that basic tenement in common, we find a rich variety of structures and intriguing physical properties manifesting in this family of compounds.

As noted above, recently a flood of new compounds have been brought to the light and one of the purposes of this review is to make them more familiar to the reader.

## 2. SYNTHESIS TECHNIQUES

There are basically three synthesis methods to obtain higher borides.

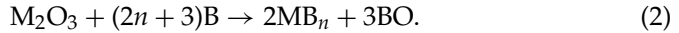
(1) Direct reaction of the elements:

Metals and amorphous boron powder are mixed and then heated and reacted under vacuum or inert gas,



## (2) Borothermal reduction method:

Metal oxides and amorphous boron powder are mixed and then heated and reacted under vacuum, e.g. for trivalent rare earth borides:



## (3) Flux method:

This is a method solely used to obtain crystals of the borides. The raw materials of the borides are mixed into large amount of a low melting metal (e.g. Al, Cu, Sn) which will function in the role of the flux for the crystal growth, and then the mixture is heated. The flux is removed by an acid or alkali leaving the crystals as a solid residue.

Boride crystals can also, of course, be obtained by other methods, for example, by preparing feed rods, using methods (1) and (2) above, for the floating zone method to grow crystals.

In the above methods, the borides are notated in the form of a simple binary boride  $MB_n$ . However, we have discovered that small additions of 3rd elements like carbon, nitrogen, and silicon can lead to the formation of new higher borides, and this will be presented in detail in the appropriate sections. For the synthesis of such compounds, it has been found to be expedient to first obtain  $MB_n$  ( $n > 10$ ) and then add the desired amounts of carbon powder, or BN powder, or Si powder plus additional B powder if necessary to react again to obtain the desired compounds.

With regard to the heating, it can be accomplished by (a) using commercial furnaces; (b) heating components like graphite wool wrapped around BN crucibles which are inductively heated; and (c) for borides which can be arc melted. We note that for preparing carbon-free higher borides (e.g.  $RB_{50}$ ) by method (b), it is preferable to use a heating component which does not contain carbon, such as a  $TiB_2/AlN/BN$  composite.

### 3. BONDING IN HIGHER BORIDES

The bonding in higher borides has been the origin of a complex variation in the structures which has not been observed in any other element. The unique bonding and electronic structural features of boron have been described in many works and reviews (e.g. Longuet and Roberts, 1955; Lipscomb and Britton, 1960; Hoard and Hughes, 1967; Naslain et al., 1976; Matkovich and Economy, 1977; Naslain, 1977; Bambakidis and Wagner, 1981; Bullett, 1982; Golikova, 1987; Shirai and Nakamatsu, 1994; Emin, 2004). Similar to carbon, boron tends to form covalent bonds. However, since it only has 3 valence electrons available, there is a deficiency in trying to form a three-dimensional network of conventional two electron covalent bonds. This particular circumstance gives rise to the fascinating variety of clusters and structures which are found in boron-rich compounds. In particular, the boron icosahedron (Figure 1) functions as a basic building block. The icosahedron obviously has many symmetry elements. Most notable are the

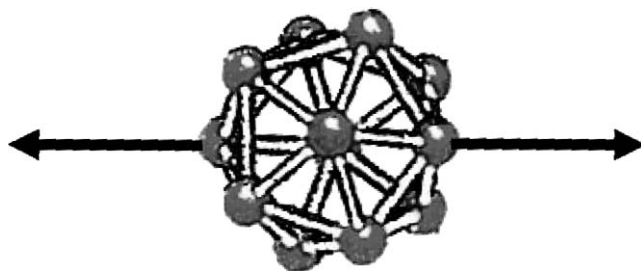


**FIGURE 1** Boron icosahedron. The arrows indicate one of the six five-fold axes.

six five-fold axes (one of which is depicted in [Figure 1](#)) around which each boron atom is linked to five other boron atoms in the icosahedron. An outward pointing bond to connect the icosahedron with other structural elements can easily be imagined, and [Hoard and Hughes \(1967\)](#) have indicated that this bond is preferentially aligned along the five fold axes. However, the five-fold axes obviously cannot be used as symmetry operators in a three dimensional network. As [Naslain et al. \(1976\)](#) have pointed out, the wide variation of structures occurs because of the necessary distortion of the icosahedra arrangement, and furthermore, voids in which other structural elements (atoms, i.e. rare earth atoms) can be occupied are created. One way of viewing the structure of the higher rare earth borides is that the boron atoms form electron deficient clusters which are arranged into a three dimensional framework. Metal atoms occupy the voids created among the clusters and supply electrons to the electron deficient boron framework, stabilizing the structure.

Regarding the electronic structure, various molecular orbital calculations on a single boron icosahedron have been performed ([Longuet and Roberts, 1955](#); [Bambakidis and Wagner, 1981](#); [Bullett, 1982](#); [Shirai and Nakamatsu, 1994](#)).

There are 12 outward-pointing radial hybrids and 13 bonding molecular orbitals for intra-cluster bonding. Therefore, the boron icosahedron within a structure is two-electron-deficient:  $36 - (12 + 13 \times 2) = -2$ . This can be well understood by considering  $(\text{B}_{12}\text{H}_{12})^{-2}$ , for example. It should be noted that the formation of the boron cluster is extremely “economic” in terms of electrons, since conventional pair bonding would require 60 electrons, rather than 26.

Incidentally, the  $\text{B}_6$  octahedron ([Longuet and Roberts, 1955](#)) and  $\text{B}_{12}$  cubooctahedron ([Lipscomb and Britton, 1960](#)) are also found to be two-electron deficient. This electron deficiency of the clusters leads to dramatically different physical properties for trivalent and divalent metal borides as illustrated for example in the next section on the dodecaborides. More on the bonding requirements in the higher borides will be discussed in later sections.

Finally, the framework formed by the boron clusters is relatively rigid and therefore, there are constraints on the size of the metal atoms/ions which can occupy the voids. That is why there are different boundaries regarding which rare earth atoms can form each particular higher boride (as will be seen in the following sections). A rare earth existence diagram for all the higher borides will be presented at the end of this review, see [Section 13](#).

## 4. DODECABORIDES $RB_{12}$

Although they are “higher borides” according to our definition above, strictly speaking, the dodecaborides are in a different class of compounds compared to the other higher borides which will be discussed in this review. The rare earth dodecaborides  $RB_{12}$  (with the exception of ytterbium) are good metals and in this sense similar to  $RB_6$ ,  $RB_4$ , while the other higher borides with  $RB_n$  ( $n > 12$ ) are all insulators. This stark boundary is interesting but reasonable when considering the bonding. As discussed in the previous section, the boron  $B_{12}$  cubooctahedra and icosahedra are electron deficient by two electrons. Therefore, in the case of  $RB_{12}$ , since the trivalent rare earth atoms can supply three electrons, straightforwardly thinking, they have one excess conduction electron per unit cell and are all metals (except for  $YbB_{12}$ , where ytterbium takes an intermediate valence state and therefore it shows anomalous properties, i.e. a Kondo insulator). If  $n > 12$  for  $RB_n$ , and considering that the boron atoms are electron deficient, there is no assurance that there will be excess electrons even for a trivalent rare earth. This is illustrated in an actual example later in Section 8.2.

$RB_{12}$  forms for the rare earth elements of  $R = Gd, Tb, Dy, Y, Ho, Er, Tm, Yb, Lu, Zr,$  and  $Sc$ , but not the light lanthanides,  $R = La, Ce, Pr, Nd, Sm,$  and  $Eu$ , because these metals are too large.

### 4.1 Structure

The  $RB_{12}$  phases are isostructural with the cubic  $UB_{12}$ -type structure (space group  $Fm\bar{3}m$ ) with the rare earth atoms and the boron  $B_{12}$  cubooctahedra being the basic structural units (Bertaut and Blum, 1949). The structure is depicted in Figure 2. It is interesting that the 12 boron atoms form a cubooctahedron in  $RB_{12}$  in contrast to the icosahedron cluster which is predominant in the higher borides. The lattice constant, for example, for  $TbB_{12}$  is  $a = 7.4959 \text{ \AA}$ .

It has been reported that  $ScB_{12}$  has a tetragonal modification of the  $UB_{12}$ -type structure with lattice parameters of  $a = 5.22 \text{ \AA}$  and  $c = 7.35 \text{ \AA}$  with the space group of  $I4/mmm$  (Hamada et al., 1993; Paderno and Shitsevalova, 1995). Due to the small size of scandium as compared to the other rare earth atoms, scandium phases have been observed to form anomalous higher boride structures compared to the heavy lanthanides and yttrium, as will be discussed later in Sections 9 and 11. Small amounts of metal replacement for  $Sc$  in  $Sc_{1-x}M_xB_{12}$  ( $x$  as small as 0.1,  $M = Y, Tm, Lu$ ) have been reported to stabilize the structure in the normal cubic  $UB_{12}$ -type.

### 4.2 Physical properties

#### 4.2.1 Electrical properties

Johnson and Daane (1963) grew a polycrystal of  $YB_{12}$  in their early systematic work on yttrium borides and alkaline hexaborides. Paderno et al. (1995) have reported on the single crystal growth of the rare earth series of the dodecaborides. Single crystals of  $ScB_{12}$ ,  $HoB_{12}$ ,  $TmB_{12}$ ,  $ErB_{12}$ , and  $LuB_{12}$  were successfully grown, but crystals containing the larger size rare earth elements  $Dy$  and  $Tb$  were found

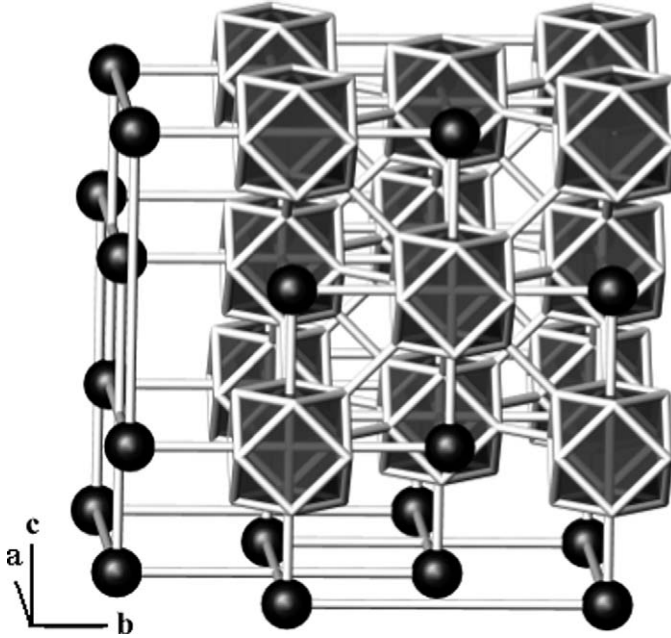


**FIGURE 2** The structure of the cubic dodecaborides  $RB_{12}$  ( $UB_{12}$ -type). The polyhedra are  $B_{12}$  cubooctahedra, while circles depict the rare earth atoms.

to be more difficult to grow. A  $DyB_{12}$  crystal could only be obtained as a polycrystal and for  $TbB_{12}$  it was only possible to obtain single phase samples by sintering. The  $RB_{12}$  compounds are all good metals, typically they have electrical resistivities of  $\sim 100 \mu\Omega \text{ cm}$  or lower at room temperature (Johnson and Daane, 1963; Paderno et al., 1995; Gabani et al., 1999), with the exception of  $YbB_{12}$ .

In an early paper, Matthias et al. (1968) report superconductivity to occur for all the non-magnetic dodecaborides; namely,  $ScB_{12}$ ,  $YB_{12}$ ,  $LuB_{12}$ , and  $ZrB_{12}$ , with transition temperatures of  $T_C = 0.39, 4.7, 0.48,$  and  $5.8$  K, respectively. However, they note that the transition for  $YB_{12}$  did not show the full volume fraction, and Czopnik et al. (2005) have recently reported that the specific heat of a  $YB_{12}$  zone melted tricrystal did not show any clear superconductivity transition above the lowest measuring temperature of  $2.5$  K. The transition temperature  $T_C = 4.7$  K initially reported is different from that of simple  $YB_6$  ( $T_C = 6.5\text{--}7.1$  K, Matthias et al., 1968) which would be a typically surmised impurity. An inclusion of  $YB_6$  in solid solution form may be a possible origin for the behavior initially observed (Matthias et al., 1968) since the  $T_C$  of  $YB_6$  can be expected to vary in such a case (Fisk et al., 1974), however, further investigation on the  $YB_{12}$  system is merited.

Detailed measurements on  $LuB_{12}$  have made it clear that it is a simple BCS-type weak-coupling superconductor with an energy gap of  $2\Delta = 3.52 k_B T_C$  and a very small critical field of  $1$  mT (Flachbart et al., 2005).

The isotope effect on  $T_C$  of  $ZrB_{12}$  was investigated and a much larger value of  $d(\log T_C)/d(\log m) = -0.32$  obtained for Zr from measurements of Zr isotope 90,

91, 92, and 94 samples (Fisk et al., 1971) compared to  $-0.09$  determined for B from B isotope 10, 11, and naturally occurring samples (Chu and Hill, 1968). It is noted that there is no isotope effect for elemental Zr (Bucher et al., 1965). This indicates that the superconductivity in  $\text{ZrB}_{12}$  is Zr-derived, and caused by phonon modes associated with the internal motion of Zr atoms inside the boron framework (Fisk et al., 1971).

Conflicting reports as to the exact nature of the superconductivity in  $\text{ZrB}_{12}$  have been made as described in the following:

Daghero et al. (2004) conclude that  $\text{ZrB}_{12}$  is a conventional BCS-type s-wave weak-coupling superconductor. However, interestingly, from point contact spectroscopy measurements they obtain an energy gap of  $2\Delta = 4.8 k_{\text{B}}T_{\text{C}}$ , which value is typical of a strong-coupling superconductor. Tsindlekht et al. (2004) explain the divergence by concluding it was due to enhanced surface superconducting characteristics for  $\text{ZrB}_{12}$ . Khasanov et al. (2005) propose that the coupling of the charge carriers to the lattice in  $\text{ZrB}_{12}$  has nonadiabatic character near the surface.

In contrast to the conventional s-wave superconductor picture above, Gasparov et al. (2006) report unusual temperature dependence of the magnetic penetration depth  $\lambda(T)$  and upper critical field  $H_{\text{C}2}(T)$  and propose that  $\text{ZrB}_{12}$  has an unconventional two-gap superconductivity.

Some controversy also exists whether  $\text{ZrB}_{12}$  is actually a type-II superconductor (Daghero et al., 2004; Gasparov et al., 2006). Tsindlekht et al. (2004) conclude that it is an unusual marginal superconductor near the border between type-I and type-II, while Wang and coworkers (Wang et al., 2005) report that there is a crossover from type-I superconductivity near  $T_{\text{C}}$  to type-II/I (as defined by Auer and Ullmaier (1973)) below  $\sim T_{\text{C}}/2$ .

Further work will no doubt be done on this intriguing system.

Regarding the electrical properties of other dodecaborides, interestingly, Hamada et al. have reported that  $\text{ScB}_{12}$  has p-type conduction (Hamada et al., 1993) in contrast to the n-type behavior observed for the other trivalent  $\text{RB}_{12}$  compounds and which is expected for these metals with excess electrons in the bonding as noted above.

The resistivities of the magnetic borides  $\text{DyB}_{12}$ ,  $\text{HoB}_{12}$ ,  $\text{ErB}_{12}$ , and  $\text{TmB}_{12}$ , have been carefully measured by Gabani et al. (1999) for good quality crystals with low room temperature resistivities ( $10\text{--}30 \mu\Omega \text{ cm}$ ) compared to the early work. Near the antiferromagnetic transition temperatures  $T_{\text{N}}$ , the resistivities all show small increases in the form of humps and then rapid drops as the temperature is lowered. This behavior can be explained as an initial increase in the resistivity attributed to the appearance of superzone boundaries within the Brillouin zone, followed by a decrease due to a reduction in spin scattering (Taylor and Darby, 1972; Fournier and Gratz, 1993).

#### 4.2.2 Magnetic properties

An early paper by Matthias et al. (1968) deals with the three compounds  $\text{HoB}_{12}$ ,  $\text{ErB}_{12}$ , and  $\text{TmB}_{12}$ , and reports antiferromagnetic transitions at  $T_{\text{N}} = 6.5, 6.5,$  and  $4.2 \text{ K}$ , respectively. The magnetic properties of the whole series of rare earth phases for  $\text{RB}_{12}$  were measured by Moiseenko and Odintsov (1979). However, the mea-

measurements were only performed down to liquid nitrogen temperature and magnetic transitions were not observed. Lower temperature measurements were made substantially later for the compounds which were not included in Matthias et al.'s work like  $\text{TbB}_{12}$  and  $\text{DyB}_{12}$ , and higher transition temperatures were obtained, namely,  $T_N = 19.2$  and  $16.5$  K for  $\text{TbB}_{12}$  and  $\text{DyB}_{12}$ , respectively (Paderno et al., 1995; Gabani et al., 1999). This is an interesting feature common to some of the well known borides. While for many of the relatively metal-rich borides (e.g.  $\text{RB}_4$ ,  $\text{RB}_6$ ,  $\text{RB}_{12}$ ) it is generally not so difficult to grow good crystals, sample preparation is sometimes more difficult for some of the particular rare earth/metal phases of the compound, as noted above. Even so, the synthesis/crystal chemistry/structural aspects of these compounds became well advanced at an early date, while low temperature physical properties measurements were not always so widely and readily available. And therefore, in some cases, the attractive exciting properties have lain unnoticed for the less easily prepared phases, until discovered relatively recently to cause some excitement. And nowhere was this demonstrated more vividly than for the metallic boride compound  $\text{MgB}_2$  in which relatively high  $T_C$  superconductivity was discovered half a century after the compound was first synthesized (Nagamatsu et al., 2001).

To summarize the basic magnetism of  $\text{RB}_{12}$ ; antiferromagnetic transitions were found to occur (Matthias et al., 1968; Paderno et al., 1995; Gabani et al., 1999) for  $\text{TbB}_{12}$ ,  $\text{DyB}_{12}$ ,  $\text{HoB}_{12}$ ,  $\text{ErB}_{12}$ , and  $\text{TmB}_{12}$  at  $T_N = 19.2, 16.5, 7.5, 6.7,$  and  $3.4$  K, respectively, and this trend is consistent with the deGennes factor (deGennes, 1958).

#### 4.2.3 $\text{YbB}_{12}$ ; a Kondo insulator

Cerium-containing compounds like  $\text{CeB}_6$ ,  $\text{Ce}_3\text{Bi}_4\text{Pt}_3$ ,  $\text{CeNiSn}$ , etc. have sometimes been found to embody a fascinating playground for heavy fermion physics (for reviews see: Hundley et al., 1990; Kasuya, 1992; Tsunetsugu et al., 1997; Degiorgi, 1999; Hanzawa, 2002; Vidhyadhiraja et al., 2003). Accordingly, ytterbium compounds have also been studied with interest since ytterbium is the hole analog of cerium. Strikingly, it has been discovered (Kasaya et al., 1983; Iga et al., 1984) that  $\text{YbB}_{12}$  exhibits anomalous behavior among the magnetic rare earth dodecaborides and is a Kondo insulator system. The unusual resistivity behavior of  $\text{YbB}_{12}$  had also been conjectured previously by Fisk et al. (1969) from a study of the  $\text{Sc}_{1-x}\text{Yb}_x\text{B}_{12}$  system. The success of preparing single crystals of  $\text{YbB}_{12}$  enabled discovery and detailed study of its interesting properties (Kasaya et al., 1983; Iga et al., 1984). The origin of the anomalous behavior in  $\text{YbB}_{12}$  is the mixed valency of Yb in the dodecaborides, in contrast to the trivalent behavior of the other lanthanide ions. However, since this topic has been previously reviewed excellently in detail (e.g. Kasuya, 1992) in the context of heavy fermion physics, we will not go into detail here.

#### 4.2.4 Recent developments regarding magnetism of $\text{RB}_{12}$

Recently, further detailed investigations have been carried out on the magnetic  $\text{RB}_{12}$  compounds and despite the simple structure of the systems, exciting new results are being obtained (e.g. Kohout et al., 2004; Siemsmeyer et al., 2006). Incidentally, it should be noted that the metallic "lower borides"  $\text{RB}_4$  tetraborides

**TABLE 1** Basic magnetic transition ( $T_N$  = Neel temperature) and superconducting transition ( $T_C$ ) temperatures of  $RB_{12}$  ( $R = \text{Gd, Tb, Dy, Ho, Er, Tm, Yb, Lu, Zr, Y, and Sc}$ ).  $\text{YbB}_{12}$  is a Kondo insulator (e.g., Kasuya, 1992)

	$T_C$ (K)	$T_N$ (K)	Reference	Updated information	Reference
$\text{TbB}_{12}$	–	19.2	Paderno et al. (1995)	Additional trans. 18.2 K, 14.6 K	Murasik et al. (2002)
$\text{DyB}_{12}$	–	16.5 <sup>a</sup>	Paderno et al. (1995)	–	–
$\text{HoB}_{12}$	–	6.5 <sup>a</sup>	Matthias et al. (1968)	Incomm. mag. struct., amp. modulated	Kohout et al. (2004)
$\text{ErB}_{12}$	–	6.5 <sup>a</sup>	Matthias et al. (1968)	Incomm. mag. struct.	Siemensmeyer et al. (2006)
$\text{TmB}_{12}$	–	4.2 <sup>a</sup>	Matthias et al. (1968)	Incomm. mag. struct.	Siemensmeyer et al. (2006)
$\text{LuB}_{12}$	0.48	–	Matthias et al. (1968)	$2\Delta = 3.52 k_B/T_C$ , $B_C \sim 1 \text{ mT}$	Flachbart et al. (2005)
$\text{ZrB}_{12}$	5.8	–	Matthias et al. (1968)	Zr, $d(\log T_C)/d(\log m) = -0.32$	Fisk et al. (1971)
$\text{ZrB}_{12}$				s-wave weak-coupling (bulk) <sup>b</sup>	e.g., Daghero et al. (2004)
$\text{ZrB}_{12}$				s-wave strong-coupling (surface) <sup>b</sup>	e.g., Tsindlekht et al. (2004)
$\text{ZrB}_{12}$				Two-gap superconductor <sup>c</sup>	Gasparov et al. (2006)
$\text{YB}_{12}$	4.7	–	Matthias et al. (1968)	$T_C < 2.5 \text{ K}$	Czopnik et al. (2005)
$\text{ScB}_{12}$	0.39	–	Matthias et al. (1968)	–	–

<sup>a</sup> Gabani et al. (1999) have determined refined  $T_N$  from resistivity measurements of 16.44, 7.36, 6.65, and 3.28 K, for  $\text{DyB}_{12}$ ,  $\text{HoB}_{12}$ ,  $\text{ErB}_{12}$ , and  $\text{TmB}_{12}$ , respectively.

<sup>b</sup> Not compatible with <sup>c</sup>.

<sup>c</sup> Not compatible with <sup>b</sup>.

and  $\text{RB}_6$  hexaborides are also being reexamined carefully, and as a result, yielding some intriguing new information on their physics. For example,  $\text{RB}_4$  ( $R = \text{Dy, Er}$ ) has been found to embody a frustrated Shastry–Sutherland-type magnetic spin system (Watanuki et al., 2005; Michimura et al., 2006). A possible transition

through a quantum critical point was observed by applying pressure to  $\text{SmB}_6$  (Gabani et al., 2003).

Going back to the dodecaborides, recent neutron diffraction measurements have revealed that  $\text{HoB}_{12}$ ,  $\text{TmB}_{12}$ , and  $\text{ErB}_{12}$  are found to have incommensurate magnetic structures (Kohout et al., 2004; Siemensmeyer et al., 2006). In the case of  $\text{HoB}_{12}$  it was also shown that the structure is amplitude modulated. Furthermore, field-induced phases were also discovered to exist in these compounds. For  $\text{TbB}_{12}$  it has also recently been reported to show two first order transitions in the specific heat at 18.2 and 14.6 K, below the Neel temperature of  $T_N$  (Murasik et al., 2002). The magnetic phase diagrams of the dodecaborides appear to be far more complicated than previously imagined and one idea (Kohout et al., 2004; Siemensmeyer et al., 2006) has been to attribute this behavior to an interesting interplay between RKKY interaction and dipole interaction and also possible frustration effects from the fcc symmetry.

An updated/refined list of the respective superconducting and antiferromagnetic transition temperatures for the  $\text{RB}_{12}$  phases is given in Table 1.

## 5. NOMENCLATURE/NOTATION OF THE HIGHER BORIDES

Among the higher borides there are two different philosophies in the nomenclature/notation, due to the fact that some of the compounds intrinsically have partial occupancies of the rare earth sites (and incidentally, for some compounds partially occupied boron interstitial sites). One nomenclature is writing something close to the actual chemical composition, for example  $\text{RB}_{25}$ . The other is to ignore the partial occupancy when writing the formula of the compound, e.g.  $\text{RB}_{15.5}\text{CN}$ ,  $\text{RB}_{22}\text{C}_2\text{N}$ ,  $\text{RB}_{28.5}\text{C}_4$ . Since the R site is not fully occupied, the actual chemical composition for  $\text{RB}_{22}\text{C}_2\text{N}$ , for example, is approximately  $\text{RB}_{30}\text{C}_3\text{N}_{1.5}$ .

This can lead to some confusion regarding the actual composition of the samples and is inconvenient in the latter case when trying to mix elements and do synthesis just looking at the face values. However, the latter case is more expressive of the crystal structure.

Examination of the literature shows that the notations have been mixed, and we select as notation here that what we judge has generally been used. However, we will make note of the actual chemical composition in some cases of the latter notation where it is not so clear. For some compounds, the partial occupancy and also some width in the homogeneity range led to further scattering in the notation (as will be seen in following sections, e.g. Section 7.2 on  $\text{RB}_{44}\text{Si}_2$ ).

The following sections on higher borides are arranged in the approximate order of their discovery.

## 6. $\text{RB}_{66}$

Seyboldt (1960) first discovered an extremely boron-rich rare earth cubic compound with only 1–2 atomic percent of rare earth. Early notations of this compound have varied from  $\text{RB}_{\sim 100}$  to  $\text{RB}_{\sim 70}$  to  $\text{RB}_{\sim 50}$  (an early review of the Y–B

phase diagram is given by Gschneidner (1961)), but the composition and structure of this yttrium phase were finally well characterized by Richards and Kasper in 1969 (Richards and Kasper, 1969), and the notation generally unified as “YB<sub>66</sub>”. Beautiful single crystals of this compound can be grown (e.g. Oliver and Brower, 1971). The RB<sub>66</sub> compound forms for R = Pr, Nd, Sm, Gd, Tb, Dy, Y, Ho, Er, Tm, Yb, and Lu.

### 6.1 Structure of RB<sub>66</sub>

The structure of YB<sub>66</sub> is cubic (space group *Fm3c*) with  $a = 23.44 \text{ \AA}$ . It has been studied extensively. As noted above, Richards and Kasper (1969) solved the detailed structure first and Higashi for example, has re-examined the structure by investigating crystals with different stoichiometries of the YB<sub>66</sub> phase within the

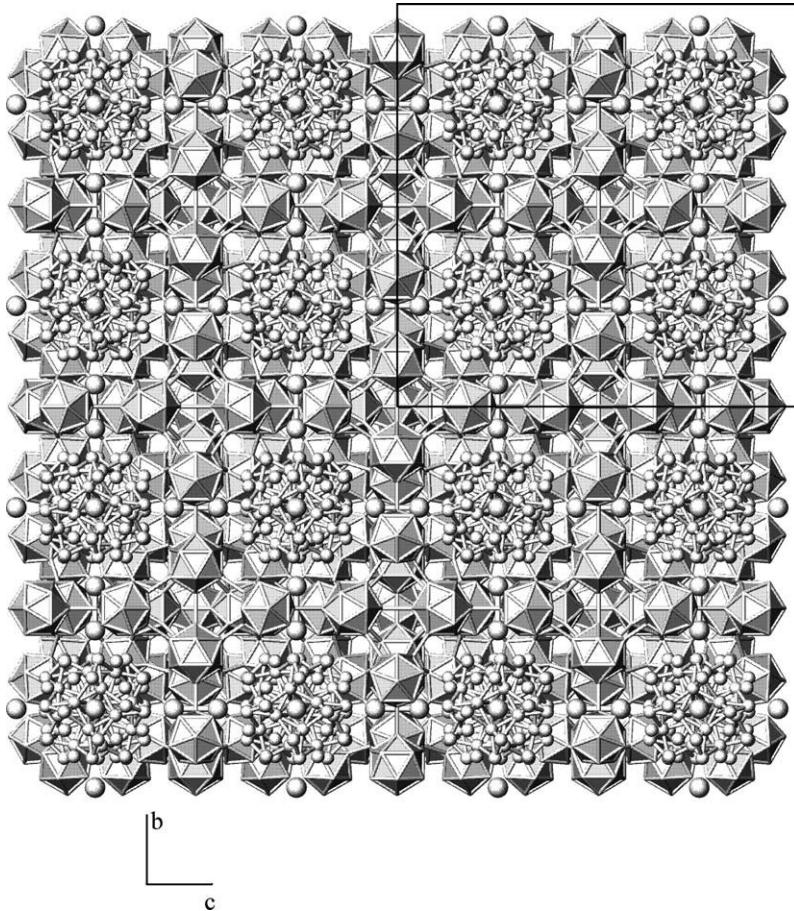


**FIGURE 3** The structure of cubic RB<sub>66</sub> viewed along one of the axes. The polyhedra are B<sub>12</sub> icosahedra, while small and large circles depict boron and rare earth sites, respectively.

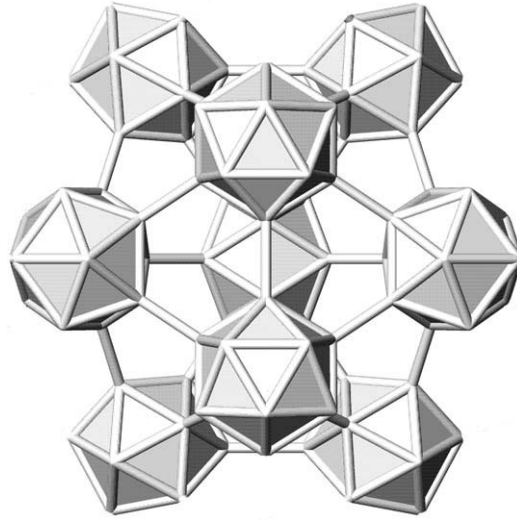


**FIGURE 4** The “supericosahedron”  $B_{12}(B_{12})_{12}$ .

homogeneity range, namely,  $YB_{56}$  and  $YB_{62}$  (Higashi et al., 1997b). The basic  $YB_{66}$  structure is depicted in Figure 3. The boron framework is formed by eight so-called super-icosahedra  $B_{12}(B_{12})_{12}$ , each of which is comprised of thirteen  $B_{12}$  icosahedra (Figure 4). A central icosahedron is bonded to and surrounded by twelve icosahedra. The super-icosahedra in the  $RB_{66}$  structure have two different orientations and form two cubic sublattices. So called  $B_{80}$  clusters occupy the holes created by the arrangement of the super-icosahedra. The  $B_{80}$  cluster has 80 boron sites, which are partially occupied by only about 42 boron atoms. Yttrium atoms occupy peanut shaped holes with centers at  $(0.05789, 1/4, 1/4)$  and  $(0.05629, 1/4, 1/4)$  which have an expected occupancy of around 0.5. Due to the close distance of the yttrium sites in the peanut and the occupancy, it was initially thought that yttrium atoms cannot simultaneously occupy both sites. When depicting the basic structure of  $YB_{66}$  in Figure 3, the yttrium atom was drawn as a single site with a coordinate of  $(0.0545, 1/4, 1/4)$ . However,  $YB_{66}$  has a homogeneity region and it is possible to grow crystals with a composition of  $YB_{56}$ , for example. In this case, the yttrium occupancy is 57.5% and inevitably there must exist pairs where yttrium has simultaneous occupancy, thus forming a dumbbell of yttrium atoms. Indeed, the thermal displacement and Y–Y distance is actually found to be larger for  $YB_{56}$  compared to  $YB_{66}$ , indicating the double occupancy. Taking this into account, a schematic view of the  $YB_{66}$  structure is given in Figure 5 (Higashi et al. 1997b).

A striking feature of the  $YB_{66}$  cubic structure is that the unit cell contains more than 1600 atoms due to the large lattice parameter. Related to this, a novel application for  $YB_{66}$  was discovered and will be described in the next section.

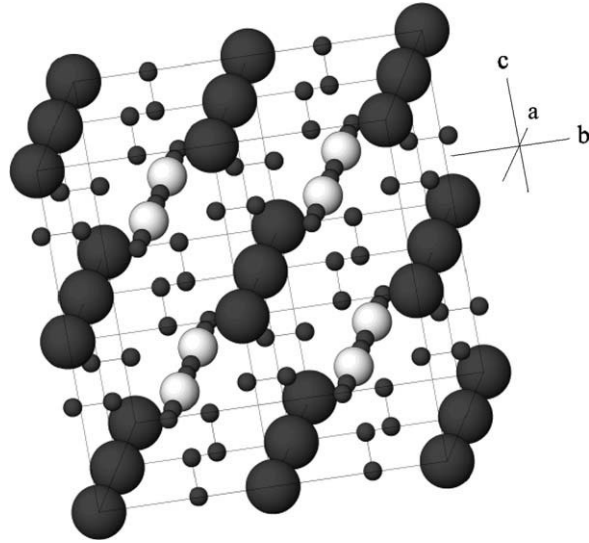


**FIGURE 5** A schematic view of the  $\text{YB}_{66}$  structure, with the large circles indicating  $(\text{B}_{12})_{13}$  supericosahedra, the medium-sized circles representing  $\text{B}_{80}$  clusters, and the small dumbbells indicating rare earth sites.

## 6.2 Physical properties of $\text{RB}_{66}$

As the first insulating/semiconducting higher boride series, the electrical transport of these compounds has been carefully investigated (e.g. Slack et al., 1977; Golikova, 1987; Werheit et al., 1991). The temperature dependence of the resistivity  $\rho$  follows the dependency of Mott's variable range hopping (VRH) model for 3 dimensional systems (Mott, 1968; Efros and Shklovskii, 1985), where

$$\rho = \rho_0 \exp[(T_0/T)^{0.25}]. \quad (3)$$

Room temperature resistivities of  $\text{YB}_{66}$  and  $\text{GdB}_{66}$  take values of  $3 \times 10^2$  and  $5 \times 10^2 \Omega \text{ cm}$ , respectively (Golikova, 1987) and the  $\text{RB}_{66}$  phases can be considered as insulators. The characteristic temperature of the VRH  $T_0$  for example for  $\text{GdB}_{66}$  was determined as  $4 \times 10^7 \text{ K}$ . The conductivity is p-type. The thermal conductivity and thermopower of  $\text{RB}_{66}$ , will be discussed in Section 12 on "Thermoelectrics in higher borides".

Infrared spectroscopy measurements on  $\text{YB}_{66}$  reveal a strong absorption band around  $130 \text{ cm}^{-1}$  which is thought to be due to the local vibration of yttrium atoms (Werheit et al., 1991).

A novel application for the  $\text{YB}_{66}$  compound was discovered by Wong et al. (1990). They focused on the unusually large lattice constant of  $\text{YB}_{66}$  which results in a strong XRD peak reflection at  $2d = 11.76 \text{ \AA}$  (the 400 index), and the fact that high quality single crystals of this refractory compound can be grown. Therefore,  $\text{YB}_{66}$  crystals can be used as a soft X-ray (1–2 keV) monochromator for dispersing synchrotron radiation. An  $\text{YB}_{66}$  monochromator was first successfully installed at

the Stanford Synchrotron Radiation Laboratory (Wong et al., 1999) and has since been installed in other facilities.

The magnetic properties of  $\text{RB}_{66}$  have not revealed any magnetic transitions above 1.8 K.

## 7. $\text{RB}_{50}$ (AND $\text{RB}_{44}\text{Si}_2$ )

$\text{RB}_{50}$  was the first icosahedra-containing higher boride system in which a magnetic transition was discovered.  $\text{YB}_{50}$  was first synthesized in 1994 (Tanaka et al., 1994), and the magnetic transitions were discovered some years later when Mori and coworkers synthesized the magnetic lanthanide phases of  $\text{RB}_{50}$  and investigated their properties (Mori and Tanaka, 1999a). The discovery of a transition was of interest because  $\text{RB}_{50}$  is a relatively dilute magnetic system which was furthermore found to be an insulator (Mori and Tanaka, 2001a), but despite this, the magnetic interaction manifested was surprisingly strong. It is also unusual among the recently discovered higher boride phases in that large size crystals can be grown. As a result of all the above and because magnetism of insulating higher borides was a new field, especially detailed investigations have been carried out on this system and will be described (in exploratory order) in the following sections.

$\text{RB}_{50}$  forms for the rare earth elements of Tb, Dy, Y, Ho, Er, Tm, Yb, and Lu. As will be noted later, it was also discovered that addition of Si which creates the pseudo-isostructural  $\text{RB}_{44}\text{Si}_2$  compound enables the realization of the Gd phase.

### 7.1 Magnetic properties of $\text{TbB}_{50}$

$\text{TbB}_{50}$  was found to exhibit the first magnetic transition ever observed in a boron icosahedra boride (Mori and Tanaka, 1999a). The transition temperature was  $T_N \sim 17$  K (Figure 6). At 2 K the antiferromagnetic phase undergoes a metamagnetic transition at  $\sim 30$  kG. (Figure 7). From a detailed comparison with other terbium higher borides such as  $\text{TbB}_{66}$  and  $\text{Tb}_{25}$ , a hypothesis was made that the shortness of the  $B_{12}$  icosahedral lattice constant in the  $\text{RB}_{50}$  structure was the critical factor in determining the magnetic ordering temperature. This indirectly pointed to the  $B_{12}$  icosahedra as the mediator of magnetic interactions (Mori et al., 2001; Mori and Tanaka, 1999a, 1999b, 2001a). This interaction will be discussed in detail in Section 7.10.

### 7.2 Crystal growth realized through addition of Si, and $\text{GdB}_{44}\text{Si}_2$

$\text{RB}_{50}$  starts to decompose above 2100 K into phases like  $\text{RB}_6$  and  $\text{RB}_{66}$  without melting. Tanaka et al. (1997a) first demonstrated that it was possible to grow a yttrium borosilicide crystal isostructural to  $\text{YB}_{50}$  by adding a small amount of silicon. It was further shown that the addition of silicon has another interesting function in that it expands the lattice constants (Mori and Tanaka, 1999b, 2001b) and thus makes possible the realization of a Gd higher boride with a structure related to the  $\text{RB}_{50}$ -type compound. This is a simple example of so-called material design. Due

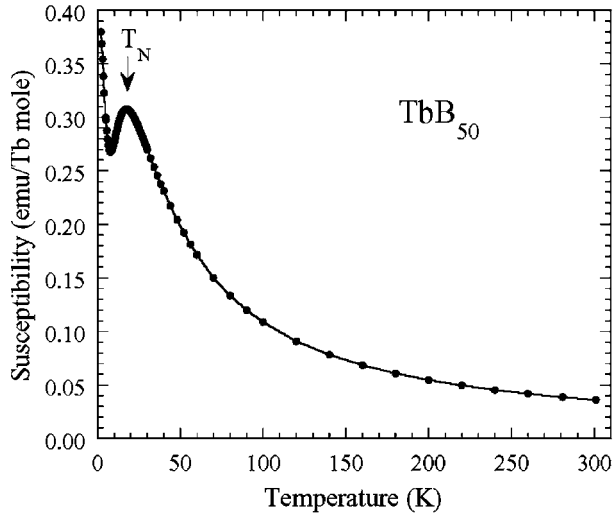


**FIGURE 6** The magnetic susceptibility of TbB<sub>50</sub>. The arrow indicates the antiferromagnetic transition at  $T_N = 17$  K (Mori and Tanaka, 1999a).

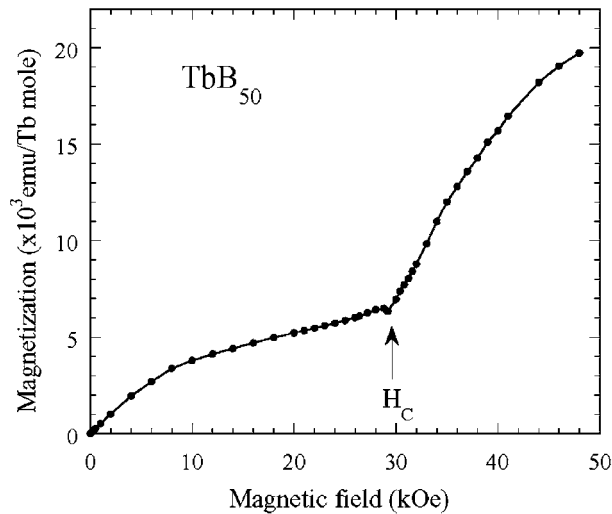


**FIGURE 7** The magnetization curve of TbB<sub>50</sub> at 2 K. A metamagnetic transition occurs at a critical field of  $H_C = 30$  kOe (Mori and Tanaka, 1999a).

to the large radius of the gadolinium atom, GdB<sub>50</sub> will not form, despite the fact the synthesis of such a compound would be desirable in light of the magnetic transition discovered in TbB<sub>50</sub> and the large deGennes factor of Gd (albeit the detailed magnetic interaction mechanism was unknown). However, with the addition of



**FIGURE 8** A photograph of a floating zone (FZ) grown  $\text{TmB}_{44}\text{Si}_2$  crystal (Mori, 2006a). The scale is in centimeters.

silicon, the lattice constants were expanded and as a result it became possible to obtain samples of a Gd-like  $\text{RB}_{50}$ -type compound (Mori and Tanaka, 2001b).

The structure of  $\text{RB}_{44}\text{Si}_2$  is closely related to  $\text{RB}_{50}$  with Si partially replacing some boron sites. The structure will be described in detail in Section 7.3, however, the difference in the nominal stoichiometry is assumed to be due to a lower occupancy of Si compared to boron because of Si's larger size. We note that up to now, various notations of this rare earth borosilicide phase have been used, e.g.  $\text{YB}_{41}\text{Si}_{1.2}$  (Higashi et al., 1997b),  $\text{YB}_{41}\text{Si}_{1.0}$  (Tanaka et al., 1997a),  $\text{TbB}_{44}\text{Si}_{0.7}$  (Mori and Tanaka, 2001a),  $\text{YbB}_{45.6}\text{Si}_{1.0}$  (Mori and Tanaka, 2003). These variations reflect the difference in the actual chemical compositions of the samples, which can be ascribed to differences in the various partially occupied sites of boron and silicon which exist in this phase (Higashi et al., 1997a). An important point is that differences in silicon or boron content do not have a significant effect on the magnetic properties beyond the obvious differences due to the slightly varying lattice constants (i.e. compounds with more silicon content generally have larger lattice constants) (Mori and Tanaka, 1999b, 2000; Mori, 2006a). To avoid confusion, some researchers have started to use the unified notation " $\text{RB}_{44}\text{Si}_2$ " to represent this borosilicide phase, and this will be the notation generally used in this chapter.

While large-sized crystals of  $\text{RB}_{44}\text{Si}_2$  can be grown by the floating zone (FZ) method and an example is shown in Figure 8 (Mori, 2006a), the crystals are not single crystals but are polycrystals with large grains (Mori, 2006a). To date it has not been possible to determine the crystal orientation to perform measurements on any crystalline  $\text{RB}_{44}\text{Si}_2$  compound. This has been attributed to the difficulty of effectively using the Laue technique because of the complicated structure and weakness of reflections from the boron-rich compound. However, the existence of a large magnetic anisotropy has been observed (Mori and Tanaka, 2001a; Mori et al., 2002) and it has been determined that the  $b$ -axis is the easy axis of magnetization (Mori et al., 2001).

**TABLE 2** Lattice parameters of orthorhombic RB<sub>50</sub> (R = Tb, Dy, Ho, Er, Y)

	<i>a</i> (Å)	<i>b</i> (Å)	<i>c</i> (Å)	Volume (Å <sup>3</sup> )	Reference
TbB <sub>50</sub>	16.609(3)	17.619(3)	9.477(3)	2773.3	Mori and Tanaka (1999a)
DyB <sub>50</sub>	16.608(3)	17.623(2)	9.472(2)	2772.3	Mori and Tanaka (2000)
HoB <sub>50</sub>	16.599(3)	17.609(2)	9.470(2)	2768.0	Mori and Tanaka (2000)
ErB <sub>50</sub>	16.603(2)	17.611(2)	9.469(2)	2768.7	Mori and Tanaka (2000)
YB <sub>50</sub>	16.625(1)	17.620(1)	9.480(1)	2777.0	Tanaka et al. (1994)

**TABLE 3** Lattice parameters of orthorhombic RB<sub>44</sub>Si<sub>2</sub> (R = Gd, Tb, Dy, Ho, Er, Tm, Yb, Y). The structure is pseudo-isostructural to RB<sub>50</sub>

	<i>a</i> (Å)	<i>b</i> (Å)	<i>c</i> (Å)	Volume (Å <sup>3</sup> )	Reference
GdB <sub>44</sub> Si <sub>2</sub> <sup>a</sup>	16.746(3)	17.731(3)	9.565(3)	2793.7	Mori (2006a)
TbB <sub>44</sub> Si <sub>2</sub>	16.651(5)	17.661(2)	9.500(2)	2793.7	Mori (2006a)
DyB <sub>44</sub> Si <sub>2</sub>	16.658(8)	17.655(6)	9.508(6)	2796.3	Mori (2006a)
HoB <sub>44</sub> Si <sub>2</sub>	16.608(9)	17.578(7)	9.492(6)	2771.1	Mori (2006a)
ErB <sub>44</sub> Si <sub>2</sub>	16.600(8)	17.621(7)	9.485(5)	2774.4	Mori (2006a)
TmB <sub>44</sub> Si <sub>2</sub>	16.655(4)	17.667(4)	9.494(2)	2793.6	Mori (2006a)
YbB <sub>44</sub> Si <sub>2</sub>	16.636(4)	17.644(2)	9.488(2)	2785.0	Mori (2006a)
YB <sub>44</sub> Si <sub>2</sub>	16.674(1)	17.667(1)	9.511(1)	2793.7	Higashi et al. (1997a)

<sup>a</sup> Data for GdB<sub>44</sub>Si<sub>2</sub> are for a sintered polycrystalline sample. The data for the other rare earth phases are for crystals grown by the floating zone method.

### 7.3 Structure of RB<sub>50</sub>-type compounds

The structure of the RB<sub>50</sub>-type compounds was determined by Higashi et al. from an analysis of a single crystal of YB<sub>41</sub>Si<sub>1.2</sub> which is nearly isostructural with the RB<sub>50</sub> phase, as noted above (Higashi et al., 1997a). The structure for both phases is orthorhombic (space group *Pbam*) with similar lattice constants, for example, for TbB<sub>50</sub> and TbB<sub>44</sub>Si<sub>2</sub>, the lattice constants are: *a* = 16.609 Å, *b* = 17.619 Å, *c* = 9.477 Å and *a* = 16.651 Å, *b* = 17.661 Å, *c* = 9.500 Å, respectively (Mori and Tanaka, 2000). Lattice parameters reported for the series of RB<sub>50</sub> and RB<sub>44</sub>Si<sub>2</sub> are given in Table 2 and 3, respectively. Similar to other higher borides, boron clusters form the basic framework, with metal atoms occupying the voids. A particular feature of this structure is that the rare earth atoms form infinite ladders in the direction of the *c*-axis along which there is also an infinite B<sub>12</sub> icosahedra chain. This is depicted in a view of the structure given in Figure 9. Within the ladder the chains have alternating bonds, with separations of 4.36 and 5.14 Å in the case of TbB<sub>44</sub>Si<sub>2</sub>. These chains are separated from one another in the *a*-*b* plane by 3.96 Å to form the ladder. The *c*-axis lattice constant appears to reflect the differences

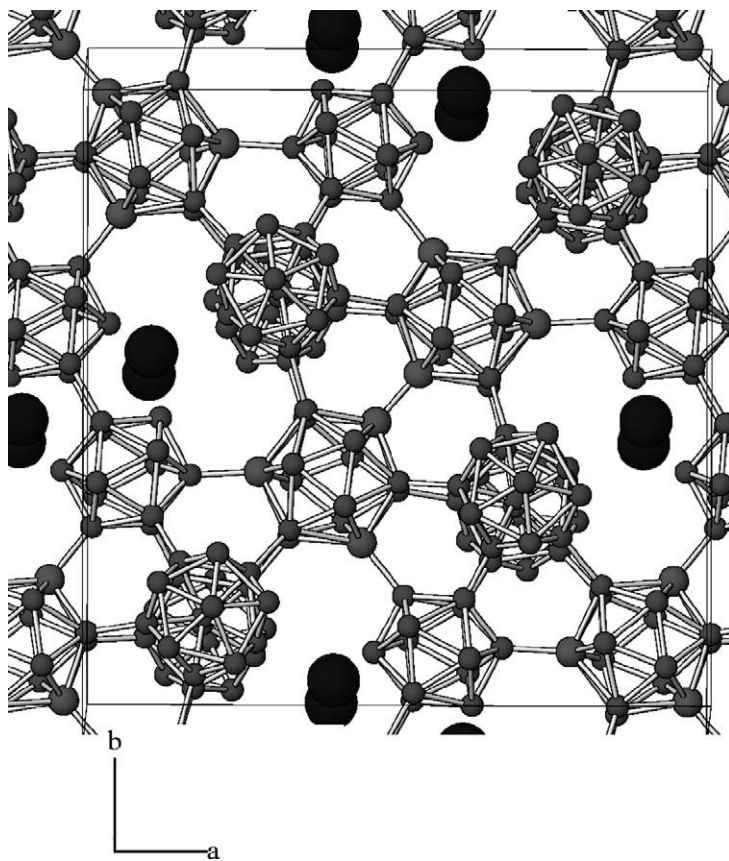


**FIGURE 9** A view of the structure of  $\text{RB}_{44}\text{Si}_2$  ( $\text{RB}_{50}$ -type) along a slight tilt from the  $c$ -axis. Small circles indicate boron atoms, medium sized circles are silicon atoms of the  $\text{B}_{12}\text{Si}_3$  polyhedron, and the large circles indicate rare earth atoms. For clarity, only two of the five structurally independent  $\text{B}_{12}$  icosahedra are plotted together with the  $\text{B}_{12}\text{Si}_3$  polyhedron (Mori, 2006a).

in size of the rare earth ions compared to the other two axes (Mori and Tanaka, 2000; Mori, 2006a). We note that an error was reported for the  $x$  coordinate of the rare earth site (0.29628, 0.05199, 0.22964) in Higashi's paper; the correct value is (0.39628, 0.05199, 0.22964).

It was noted earlier that the unit cell for  $\text{YB}_{66}$  has a very large number of atoms, over 1600. The  $\text{RB}_{50}$ -type compounds have a smaller unit cell but still, a large number of more than 330 atoms reside therein. There are five structurally independent  $\text{B}_{12}$  icosahedra and the  $\text{B}_{12}\text{Si}_3$  polyhedron. The formal atomic composition within a single unit cell of the borosilicide compound can be written as  $\text{Tb}_8(\text{B}_{12})_{22}(\text{B}_{12}\text{Si}_3)_4\text{Si}_4\text{B}_{36}$ . Namely, it has 8 Tb atoms, 22  $\text{B}_{12}$  icosahedra, 4  $\text{B}_{12}\text{Si}_3$  polyhedra, and 4 Si and 36 B interstitial sites. As noted before, the Si sites and B interstitial sites have a partial occupancy. A partial view of the structure was given in Figure 9 by considering only a minority number of the polyhedron clus-

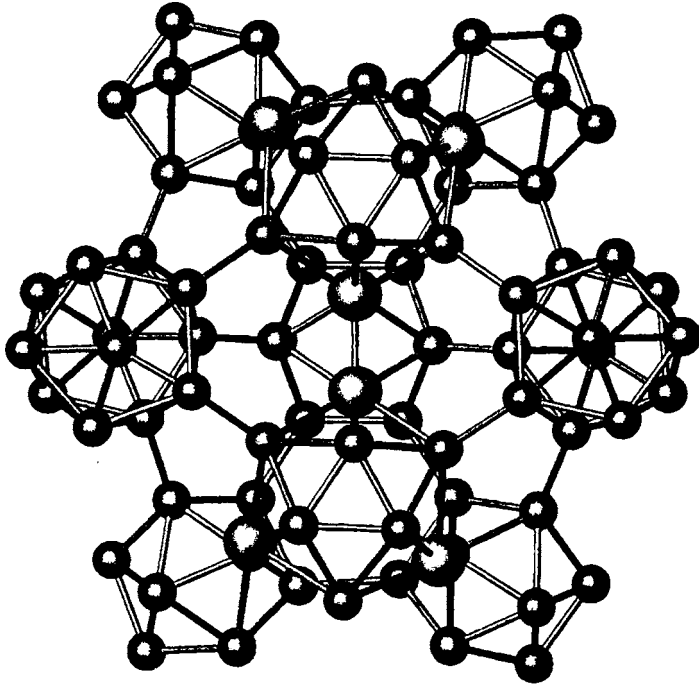
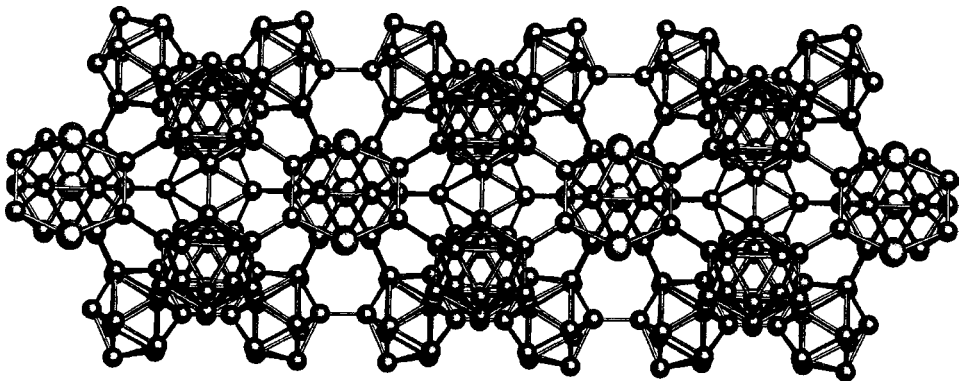


**FIGURE 10** A view of a  $B_{12}(B_{12})_8(B_{12}Si_3)_4$  super-cluster (Higashi et al., 2002).



(a)

**FIGURE 11** Views of the  $RB_{44}Si_2$  structure showing the arrangement of the  $B_{12}(B_{12})_8(B_{12}Si_3)_4$  super-clusters (a) along the  $B_{12}Si_3-B_{12}Si_3$  direction (b) along the  $c$ -axis. The small circles indicate boron atoms, medium sized circles are silicon atoms of the  $B_{12}Si_3$  polyhedron. Voids are created by the super-clusters, as seen in (b) which are occupied by  $B_{12}-B_{12}$  pairs and rare earth atoms which form alternating infinite chains along the  $c$ -axis (Higashi et al., 2002).

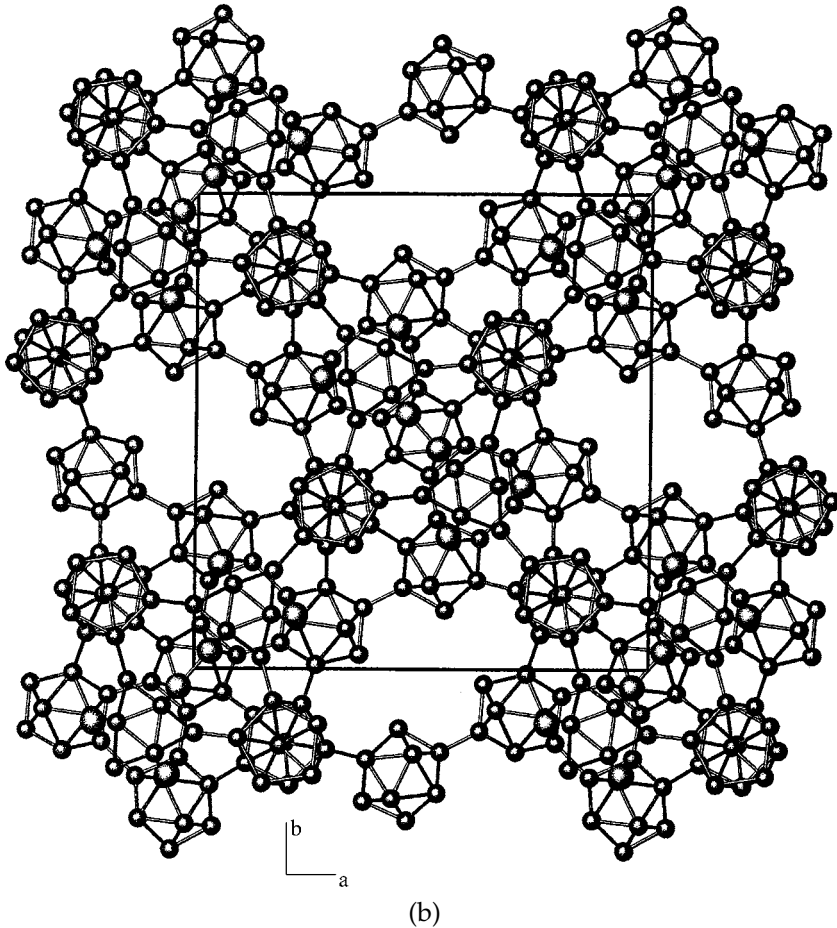


FIGURE 11 (Continued.)

ters. The full structure is actually much more complicated, however, similar to the case of  $\text{YB}_{66}$ , the arrangement of the boron clusters becomes easier to understand when so called super-clusters are considered. In the  $\text{RB}_{66}$  structure, there were the  $\text{B}_{12}(\text{B}_{12})_{12}$  super-icosahedra, and for  $\text{RB}_{44}\text{Si}_2$ , as discussed by Higashi,  $\text{B}_{12}(\text{B}_{12})_8(\text{B}_{12}\text{Si}_3)_4$  super-clusters (Figure 10) can be seen to form the basic structure (Higashi et al., 2002). The  $\text{B}_{12}(\text{B}_{12})_8(\text{B}_{12}\text{Si}_3)_4$  clusters are centered at the origin and the C-face center of the orthorhombic unit cell. Two dimensional networks of these super-clusters extend in the basal plane and form infinite pillars along the  $c$ -axis direction at  $(x, y) = (0, 0)$  and  $(1/2, 1/2)$  connected by  $\text{B}_{12}\text{Si}_3$ – $\text{B}_{12}\text{Si}_3$  edges. This arrangement of the super-clusters create large voids which are occupied by  $\text{B}_{12}$ – $\text{B}_{12}$  pairs and rare earth atoms which form alternating infinite chains along the  $c$ -axis. Two different views of the structure formed by the  $\text{B}_{12}(\text{B}_{12})_8(\text{B}_{12}\text{Si}_3)_4$  super-clusters are given in Figure 11.

**TABLE 4** Magnetic properties of the  $RB_{50}$  compounds ( $R = Tb, Dy, Ho, Er$ ) (Mori and Tanaka, 2000)

	$C_1$ (emu/R mol)	$\mu_{\text{eff}}$ ( $\mu_B$ /R atom)	$\mu_{\text{eff}}^{\text{free ion}}$ ( $\mu_B$ /R atom)	$\theta$ (K)	$T_N$ (K)	$H_C$ (kG)
TbB <sub>50</sub>	-0.007	10.3	9.72	-15.3	17.5	30.0
DyB <sub>50</sub>	-0.013	11.9	10.65	-13.7	6.2	18.0
HoB <sub>50</sub>	-0.017	11.5	10.62	-13.7	7.5	16.0
ErB <sub>50</sub>	-0.004	9.74	9.58	-5.4	4.6	8.0

## 7.4 Substitution of magnetic atoms

As an initial step for further studying the magnetic transition in TbB<sub>50</sub>, the magnetic atoms were substituted for Tb along the lanthanide series which form RB<sub>50</sub>; dysprosium to thulium (Mori and Tanaka, 2000). A transition was not observed for TmB<sub>50</sub> above 1.8 K, but the other phases exhibit antiferromagnetic transitions at (including the terbium phase)  $T_N = 17.5, 6.2, 7.5,$  and  $4.6$  K for TbB<sub>50</sub>, DyB<sub>50</sub>, HoB<sub>50</sub>, and ErB<sub>50</sub>, respectively. The corresponding magnetic critical fields,  $H_C$ , were 30, 18, 16, and 8 kG. The magnitude of  $H_C$  is approximately proportional to  $T_N$  or the Curie–Weiss temperature  $\theta$ .

It was noted that the  $T_N$ /Curie–Weiss temperatures did not have a simple dependence on the  $B_{12}$  icosahedral lattice constant, but seemed to scale with the deGennes factor (deGennes, 1958) similar to the RKKY mechanism (Mori and Tanaka, 2000). The magnetic parameters for the RB<sub>50</sub> series are given in Table 4. Later a comprehensive investigation of the whole series of lanthanide RB<sub>44</sub>Si<sub>2</sub> compounds (Mori, 2006a) reveal significant deviations from this behavior (see Section 7.10).

## 7.5 The ytterbium phase

As discussed in Section 4 on the RB<sub>12</sub> dodecaborides, the ytterbium phase sometimes displays anomalous physical properties among a series of heavy lanthanide compounds (Kasaya et al., 1983; Iga et al., 1984; Kasuya, 1992). However, due to the high vapor pressure of ytterbium it is generally difficult to prepare single crystals of ytterbium containing borides. Using the floating zone, FZ, method, single crystals of RB<sub>50</sub>-type YbB<sub>44</sub>Si<sub>2</sub> were successfully grown (Mori and Tanaka, 2003). From physical property measurements, it was found that the compound shows antiferromagnetic behavior similar to the other phases, and that specific heat results suggest that the ground state is a Kramer's doublet, see Figure 12 where the magnetic entropy is plotted as a function of temperature. This was the first information obtained on the ground state in these compounds. The broad peak in the specific heat (Figure 12) indicates that the transition in these compounds is of short range order.

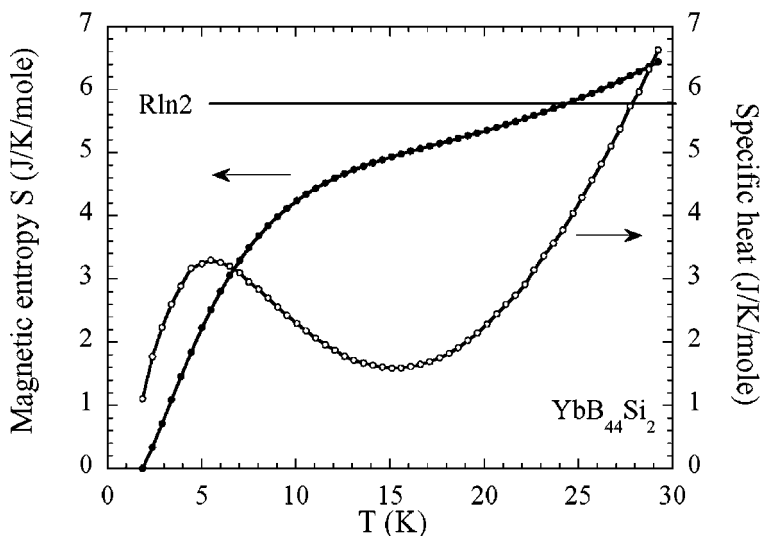


**FIGURE 12** The temperature dependence of the magnetic entropy  $S$  (●) and specific heat (○) of  $\text{YbB}_{44}\text{Si}_2$  (Mori and Tanaka, 2003).

The state of Yb in  $\text{YbB}_{44}\text{Si}_2$  was shown to be trivalent (Mori and Tanaka, 2003) and in this regard it is different from  $\text{YbB}_{12}$  which exhibited mixed valency (Kasaya et al., 1983; Iga et al., 1984; Kasuya, 1992). We observe that some of the higher borides form trivalent ytterbium borides which show no apparent anomalous behavior (e.g.  $\text{YbB}_{44}\text{Si}_2$ ,  $\text{YbB}_{18}\text{Si}_5$ ,  $\text{YbB}_{66}$ ), while for some phases like  $\text{RB}_{15.5}\text{CN}$ ,  $\text{RB}_{22}\text{C}_2\text{N}$ , and  $\text{RB}_{28.5}\text{C}_4$  (Section 9) the ytterbium compound does not form in the first place, even although the surrounding erbium and lutetium compounds do. Gschneidner (1969) has carried out a detailed study into the general mechanism for valence determination in ytterbium and europium compounds. In this work, he points out that an extra energy of promotion is necessary for trivalent ytterbium and europium compounds to form compared to stable divalent ones, and that the magnitude of the heat of formation becomes a critical factor in determining in which compounds, ytterbium and erbium take the trivalent state (see also Gschneidner and Daane, 1988). With this in mind, we speculate that the reason for the differences noted above in the existence of the ytterbium phase of the higher borides, may be, that while it is not energetically favorable for the trivalent ytterbium phase to form in  $\text{RB}_{15.5}\text{CN}$ ,  $\text{RB}_{22}\text{C}_2\text{N}$ , and  $\text{RB}_{28.5}\text{C}_4$ , at the same time, the size requirements of the rare earth site inside the boron frameworks may preclude the divalent or intermediate valence ytterbium compound from forming. As for why so many of the ytterbium higher borides have a tendency to form small trivalent states whereas the divalent state is in general predominant, the size constraint may be playing a role, as conjectured in the case of  $\text{RBe}_{13}$  (Gschneidner, 1969).

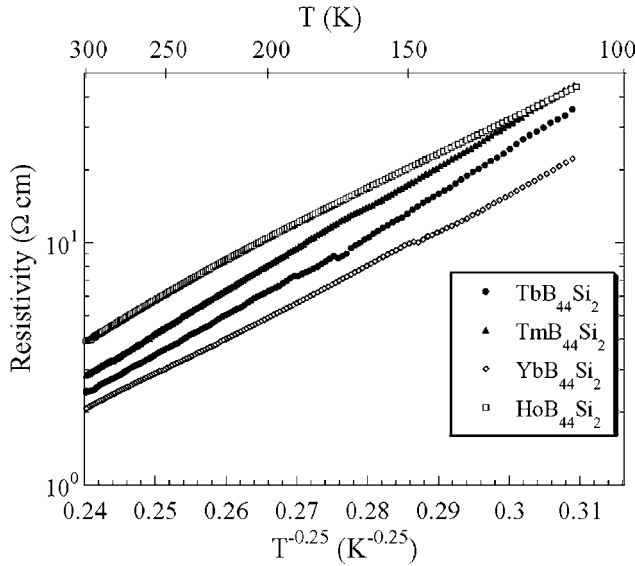


**FIGURE 13** The temperature dependence of the resistivity  $\rho$  of  $\text{RB}_{44}\text{Si}_2$  crystals. R = Tb (●), Ho (□), Tm (▲), and Yb (○). The lines indicate the fit to  $\rho = \rho_0 \exp[(T_0/T)^{1/4}]$  (Mori, 2006a).

**TABLE 5** Parameters of the resistivity of  $\text{RB}_{44}\text{Si}_2$  (Mori, 2006a)

	$\rho_0$ ( $\times 10^{-4}$ $\Omega$ cm)	$T_0$ ( $\times 10^6$ K)
$\text{TbB}_{44}\text{Si}_2$	2.2	2.2
$\text{HoB}_{44}\text{Si}_2$	9.6	1.5
$\text{TmB}_{44}\text{Si}_2$	2.0	2.5
$\text{YbB}_{44}\text{Si}_2$	5.8	1.4

## 7.6 Electrical resistivity of $\text{RB}_{50}$ -type compounds

The electrical resistivities of  $\text{RB}_{44}\text{Si}_2$  crystals were found to follow the 3D variable range hopping law described above, as shown in Figure 13 (Mori, 2006a). The room temperature resistivity of  $\text{TbB}_{44}\text{Si}_2$  for example is  $\sim 35$   $\Omega$  cm while the characteristic temperature  $T_0 = 2.2 \times 10^6$  K. The resistivity results indicate that the conductivity carriers do not contribute strongly to the magnetism like is the case for the lanthanide metallic compounds. The characteristic temperatures  $T_0$  (see Table 5) are similar for the different lanthanide phases and the values are sizably smaller than those observed for the  $\text{RB}_{66}$  compounds described above.

The characteristic temperature  $T_0$  follows the relationship

$$k_B T_0 = 18.1 / [D(E_F) \xi^3], \quad (4)$$

where  $D(E_F)$  is the density of states at the Fermi energy,  $E_F$ , and  $\xi$  is the localization length at  $E_F$  (Mott, 1968; Efros and Shklovskii, 1985). Therefore, these data indicate

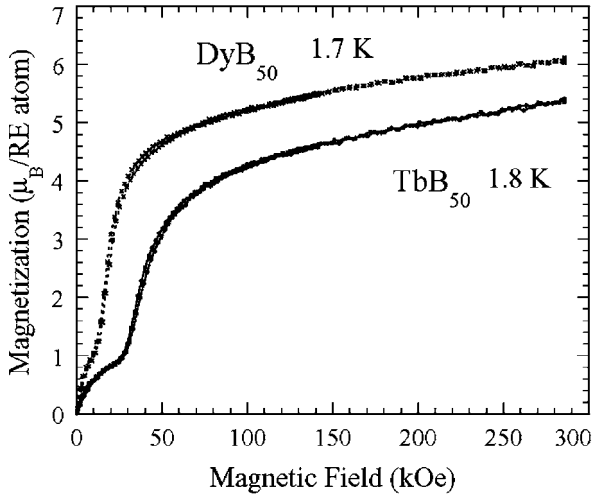


**FIGURE 14** The high field magnetization of  $RB_{50}$  ( $R = \text{Tb, Dy}$ ) (Mori et al., 2002).

that  $RB_{44}\text{Si}_2$  has a higher density of localized states at the Fermi level, or longer localization lengths compared to  $RB_{66}$  indicating that the carrier wave functions are less localized.

As noted in Section 7.2, the  $RB_{44}\text{Si}_2$  samples that can be grown are not single crystals but are polycrystalline. Therefore, we note that there is sample/measurement (configuration of electrodes and preferred orientation) dependence and this is reflected in differences in the absolute values of the resistivity for the different lanthanide phases. However, the  $T_0$  of crystals are similar and should be considered to be close to the intrinsic values. That is,  $T_0$  is a microscopic parameter reflective of the localization length which is dependent on intrinsic disorder throughout the compound, while  $\rho_0$  in Eq. (3) will cumulatively reflect contributions from the grain boundaries. The values of  $\rho_0$  and  $T_0$  are listed in Table 5.

## 7.7 Application of high fields

Below fields of up to 55 kG, the magnetization of the  $RB_{50}$  compounds universally appeared to nearly saturate at around just half the saturation magnetization value of free lanthanide ions (Mori and Tanaka, 2000). This behavior was interesting since the structure of  $RB_{50}$  has one-dimensional features analogous to some Haldane compounds (Haldane, 1983). Measurements up to 280 kG (Figure 14) showed no further transition to a higher field state and it was revealed that a sizable magnetic anisotropy exists in this system (Mori et al., 2002).

## 7.8 Nature of the antiferromagnetic transition of $RB_{50}$ -type compounds

The intrinsic nature of the transition in the  $RB_{50}$ -type compounds was further investigated through a non-magnetic doping effect (Mori, 2004). The lanthanide sites

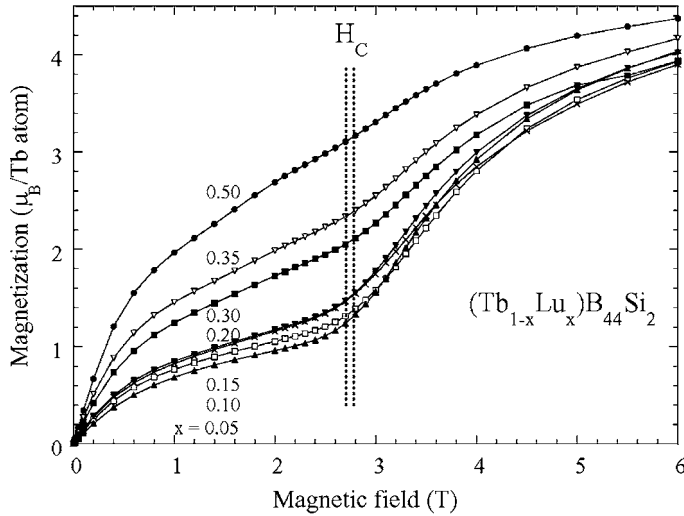


**FIGURE 15** The magnetization curves of  $\text{Tb}_{1-x}\text{Lu}_x\text{B}_{44}\text{Si}_2$  at 2 K for  $x = 0.05, 0.10, 0.15, 0.20, 0.3, 0.35, 0.5$ . The dotted lines indicate the range of the critical field  $H_C$ , from 2.7 to 2.8 T, which is defined as the peak of the derivative of the derivative of the magnetization curves (Mori, 2004).

in  $\text{RB}_{44}\text{Si}_2$  have full occupancy and non-magnetic Lu was substitutionally doped ( $x = 0.05\text{--}0.50$ ) into the terbium phase. Sintered polycrystalline  $(\text{Tb}_{1-x}\text{Lu}_x)\text{B}_{44}\text{Si}_2$  samples were prepared and measured. The most striking result is observed in the magnetization curves.  $\text{TbB}_{44}\text{Si}_2$  exhibits a metamagnetic transition at high fields, where the critical field  $H_C$  is a measure of the strength of the magnetic coupling. Figure 15 shows that despite dilution up to 50%  $(\text{Tb}_{0.5}\text{Lu}_{0.5})\text{B}_{44}\text{Si}_2$ ,  $H_C$  does not vary. The doping has also been observed to result in a correlated increase of free Tb spins. Analysis of the  $M\text{--}H$  curves showed that the lower field part below the metamagnetic transition can be fit well with a Brillouin function:

$$M = N g \mu_B \left\{ (2J + 1) / 2 \coth \left[ (2J + 1) g \mu_B B / 2 k_B T \right] - 1 / 2 \coth (g \mu_B B / 2 k_B T) \right\},$$

where  $J = 6$ ,  $g = 1.5$  for the Tb ions and  $N$  is the number of spins. Dependence of  $N$  on the doping level  $x$  corresponds well with the dependence of the magnitude of the low temperature Curie tail which increases with the non-magnetic doping.

These results indicate that the antiferromagnetic transition in  $\text{TbB}_{44}\text{Si}_2$  is actually of dimer-like nature, where non-magnetic substitution leads to broken pairs resulting in free spins (Mori, 2004). The antiferromagnetically coupled pairs do not feel the effects of dilution of other terbium sites, and therefore, are stable below  $H_C$  which is a unique value regardless of the doping content.

$N$  is plotted versus the doping concentration  $x$  in Figure 16. The solid line shows the expected  $2N_A x(1 - x)$  curve for a dimer-like scenario as described above. No fitting parameters were used in this theoretical curve, and despite some scattering of the data, the general agreement with the experimental results is close, supporting the dimer-like picture of the transition.

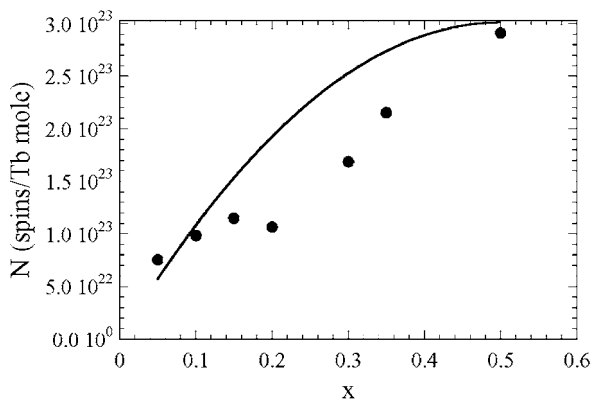


**FIGURE 16** The number of free spins  $N$  versus the doping level  $x$ . The line indicates the  $2NAx(1-x)$  curve expected for a dimer-like behavior. No fitting parameters were used (Mori, 2004).

There are two likely configurations for the magnetic pairs to be formed. Looking at close metal–metal separations, pairs are likely to be formed between the rungs of the lanthanide ladder (3.96 Å metal–metal separation) or along the ladder and the  $c$ -axis (an alternating 4.36 and 5.14 Å metal–metal separation). Other possible pairings were disregarded since the distances are sizably larger. The former situation is persuasive due to the short separation of the lanthanide atoms, but the latter is also likely since the lanthanide atoms form an alternating-bond chain along the  $c$ -axis which would be favorable for forming dimers. ESR measurements should yield further insight, and is discussed in the next section.

### 7.9 ESR of $GdB_{44}Si_2$ : indications of one dimensionality

As a microscopic probe to investigate the magnetism of  $RB_{50}$ -type systems, the ESR of the  $GdB_{44}Si_2$   $^8S_{7/2}$  system was investigated (Mori, 2006b). The ESR linewidth followed behavior expected for a one-dimensional antiferromagnet with classical spins (Cheung et al., 1978). There was no divergence as the transition temperature was approached but rather a peak/drop in the magnitude of linewidth. The indicated one-dimensionality points to the latter scenario described above in Section 7.8, with the magnetic ions forming pairs along the  $c$ -axis in a one dimensional arrangement. This picture is also consistent with the idea that the  $B_{12}$  icosahedra clusters are mediating the interaction in some way, since these one-dimensional lanthanide chains are aligned alongside infinite  $B_{12}$  icosahedra chains.

### 7.10 Mechanism of the magnetic interaction in $RB_{50}$ -type compounds

We consider the mechanism of the magnetic interaction in these  $B_{12}$  icosahedra cluster-containing compounds. Magnetic properties of the whole series of  $RB_{44}Si_2$  ( $R = Gd, Tb, Dy, Ho, Er, Tm, Yb$ ) were investigated (Mori, 2006a), and information is gained from the  $f$ -electron dependence of  $\theta$ , which is a measure of the strength

**TABLE 6** Magnetic properties of  $RB_{44}Si_2$  ( $R = Gd, Tb, Dy, Ho, Er, Tm, Yb$ ).  $T_N$  is the transition temperature estimated from the magnetic susceptibility, while  $T^*$  is the peak in the specific heat

	$C_1 \times 10^6$ (emu/g)	$\mu_{\text{eff}}$ ( $\mu_B/R$ atom)	$\mu_{\text{eff}}^{\text{free ion}}$ ( $\mu_B/R$ atom)	$\theta$ (K)	$T_N$ (K)	$T^*$ (K)	References
$GdB_{44}Si_2^a$	-2.5	7.87	7.94	-7.2	7	4	Mori (2006b)
$TbB_{44}Si_2$	-5.0	10.4	9.72	-19.9	17.5	~10	Mori (2006a)
$DyB_{44}Si_2$	2.2	9.34	10.63	-8.6	~7	~5	Mori (2006a)
$HoB_{44}Si_2$	-1.1	10.3	10.60	-7.8	~7	~6	Mori (2006a)
$ErB_{44}Si_2$	1.5	8.87	9.59	-5.0	4.5	2.9	Mori (2006a)
$TmB_{44}Si_2$	11	6.85	7.57	-1.6	<1.8	18.0	Mori (2006a)
$YbB_{44}Si_2$	0.4	4.48	4.54	-10.6	~8	16.0	Mori (2006a)

*a* Data for  $GdB_{44}Si_2$  are for a sintered polycrystalline sample. The data for the other rare earth phases are for crystals grown by the floating zone method.

of the magnetic coupling. The obtained magnetic parameters for  $RB_{44}Si_2$  are given in Table 6. Two conventional f-electron magnetic coupling mechanisms were considered. First, the RKKY mechanism (Ruderman and Kittel, 1954; Kasuya, 1956; Yoshida, 1957) was considered. Since this mechanism is dependent on the conduction electrons it is not normally expected to be effective for a variable range hopping system like  $RB_{44}Si_2$ , but because the mechanism of the interaction in the higher borides is not clear, it was at least worthwhile to evaluate it. The interaction due to the RKKY mechanism is expected to scale with the de Gennes factor (deGennes, 1958)

$$\theta_{\text{RKKY}} \propto (g - 1)^2 J(J + 1), \quad (5)$$

where  $g$  is the Lande factor and  $J$  the total angular momentum.

Another conventional mechanism is the dipole-dipole interaction, which can be approximately expressed as;

$$\theta_{\text{dipole}} \propto g^2 \mu_B^2 J(J + 1). \quad (6)$$

The expected f-electron dependence for these two conventional mechanisms versus the experimental values obtained for  $\theta$  of  $RB_{44}Si_2$  are plotted in Figure 17. As can be seen, the f-electron dependence observed for  $RB_{44}Si_2$  does not match either mechanism and it suggests another model is responsible for the observed results (Mori, 2006a).

It should also be stressed that in addition to the difference in f-electron dependence, the magnitude of magnetic coupling observed for  $RB_{50}$ -type compounds is much stronger (e.g. for  $TbB_{44}Si_2$ ,  $\theta = -19.9$  K) than would typically be expected from the simple dipole-dipole interaction, because the lanthanide  $B_{12}$  icosahedral borides are relatively magnetically dilute compounds and have relatively large metal-metal spacings.

As will also be seen in later sections on other higher borides, the experimental results indicated that the  $B_{12}$  icosahedra clusters are functioning to mediate the

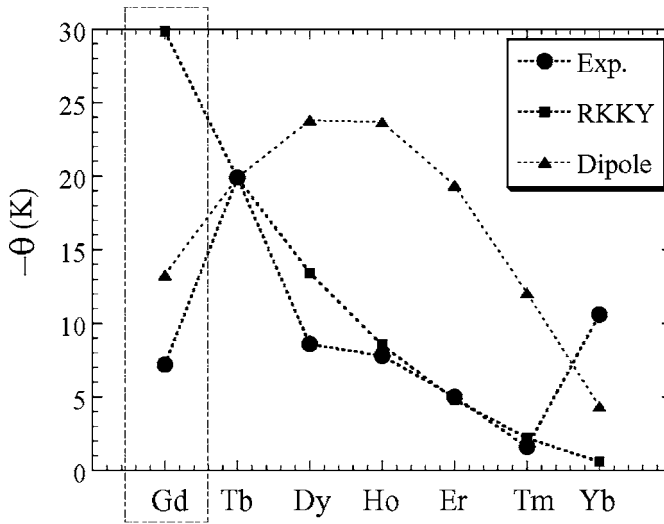


**FIGURE 17** The experimental values (●) and calculated values of the Curie–Weiss temperature  $\theta$  scaled with the de Gennes factor (■) and  $g_J^2 \mu_B^2 J(J+1)$  (▲) which are then normalized to the experimental value of  $\text{TbB}_{44}\text{Si}_2$ . Data for  $\text{RB}_{44}\text{Si}_2$  with  $R = \text{Tb, Dy, Ho, Er, Tm, Yb}$  were obtained for FZ grown crystals while Gd data was obtained for arc melted  $\text{GdB}_{44}\text{Si}_2$  polycrystalline samples (Mori, 2006a).

interaction, which is a new phenomena (Mori and Tanaka, 1999a, 2001a; Mori et al., 2001, 2004b; Mori and Zhang, 2002; Mori and Leithe-Jasper, 2002; Mori, 2004, 2006a, 2006b). Theoretical work remains to solve the explicit mechanism of magnetic interaction mediated by the boron clusters.

## 7.11 Magnetic structure of $\text{RB}_{50}$ -type compounds

In an attempt to further elucidate the nature of the  $\text{RB}_{50}$ -type magnetic transition the magnetic structure of the  $\text{TbB}_{44}\text{Si}_2$  compound was investigated. Neutron diffraction measurements were carried out at 300 and 4 K. Because this is such a boron-rich system, special care was taken in preparing the  $^{11}\text{B}$  isotope compound (Mori et al., 2004a). To prevent infiltration of normal boron into the sample during synthesis, the usual method involving borothermal reduction of terbium oxides in BN crucibles was not used, but rather, the sample was synthesized from terbium metal using the arc melt method. While isotopically pure  $\text{Tb}^{11}\text{B}_{44}\text{Si}_2$  samples were successfully synthesized, a drawback was that a  $\text{B}_2\text{O}$  impurity appeared in the sample. A peculiar phenomenon was observed in that the  $\text{B}_2\text{O}$  impurity peaks in the neutron diffraction patterns disappeared for some reason at low temperatures.  $\text{B}_2\text{O}$  should not normally be expected to be removed from the sample by cooling and the reason for this behavior is not known yet. Neutron diffraction pattern is shown in Figure 18. Regardless of the behavior of the  $\text{B}_2\text{O}$  peaks, it can clearly be seen that a lack of magnetic ordering is observed (Mori et al., 2004a), indicating that the magnetic transitions in these  $\text{RB}_{50}$ -type systems are of short range order

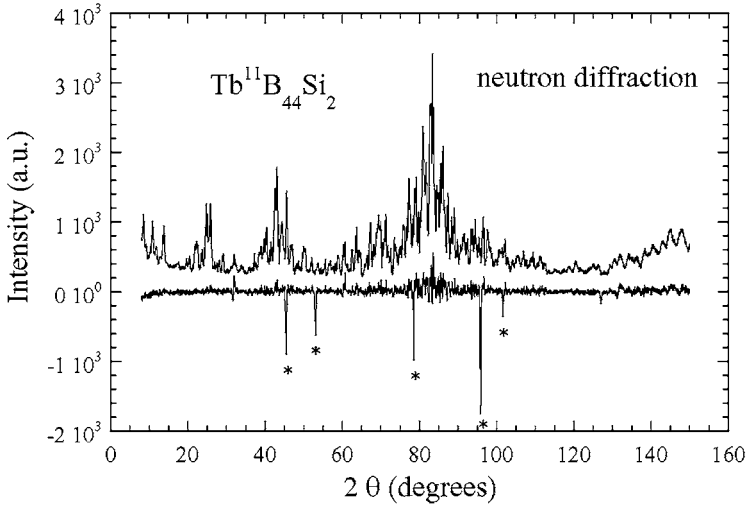


**FIGURE 18** The neutron diffraction pattern of  $\text{Tb}^{11}\text{B}_{44}\text{Si}_2$  at 4 K (top) together with the difference pattern (bottom) which was obtained by subtracting the intensities of the 300 K pattern from those of the 4 K pattern. The asterisks indicate the strong peak positions of  $\text{B}_2\text{O}$  (Mori et al., 2004a).

character. This behavior is thought to originate from the one-dimensional structural aspects of the compound and is consistent with the picture of the magnetic interaction being dominant between the rare earth pairs along the  $c$ -axis chain.

## 7.12 Summary of magnetism of $\text{RB}_{50}$ -type compounds

$\text{RB}_{50}$  compounds are the first boron icosahedra compounds in which magnetic transitions were reported to exist (Mori and Tanaka, 1999a, 2000). It is possible to synthesize the pseudo-isostructural  $\text{RB}_{44}\text{Si}_2$  compounds (Tanaka et al., 1997a; Mori and Tanaka, 1999b, 2001b; Mori, 2006a).  $\text{TbB}_{50}$  has a transition temperature of  $T_N = 17$  K, which is surprisingly high considering that these are magnetically dilute insulating  $f$ -electron compounds. Investigation of the rare earth series indicates that the magnetic coupling mechanism is different from that of conventional  $f$ -electron systems (Mori, 2006a) and including results from investigations on other  $\text{B}_{12}$  icosahedra systems. It has been proposed that the  $\text{B}_{12}$  icosahedron are playing a role to mediate the interaction (Mori and Tanaka, 1999a, 2001a; Mori et al., 2001, 2004b; Mori and Zhang, 2002; Mori and Leithe-Jasper, 2002; Mori, 2004, 2006a, 2006b). The invariance of the critical magnetic field with regards to non-magnetic dilution, indicates that the transition is dimer-like with magnetic ions forming pairs (Mori, 2004). ESR results support one dimensionality of the system which indicates that magnetic dimer pairs are formed along a bond alternating chain parallel to the  $c$ -axis (Mori, 2006b).

To conclude,  $\text{RB}_{50}$ -type compounds are found to be one dimensional dimer-like magnetic systems with surprisingly strong magnetic interaction for a dilute, localized  $f$ -electron insulator.

## 8. RB<sub>25</sub> AND RAlB<sub>14</sub>

### 8.1 Structures of RB<sub>25</sub> and RAlB<sub>14</sub>

Similar to the YB<sub>50</sub> compound described in the previous section, discovery of the YB<sub>25</sub> compound (Tanaka et al., 1997b) was quite recent, compared to the less boron-containing YB<sub>12</sub> and the high boron YB<sub>66</sub> phases, because it does not melt stably and cannot be prepared by arc melt.

Since the unit cell dimensions were close to that of the YAlB<sub>14</sub> compound previously discovered by Korsukova et al. (1989, 1992) and because the actual [B]/[Y] ratio in the YAlB<sub>14</sub> compound was nearly 25, it was speculated that the crystal structure of YB<sub>25</sub> is close to that of YAlB<sub>14</sub>. These are good examples of the different nomenclatures used in borides, which were noted above in Section 5. The notation YAlB<sub>14</sub> is made ignoring the partial occupancies of the rare earth and aluminum sites. YB<sub>25</sub> is representative of the actual chemical composition which takes into account the partial occupancy of the rare earth site which is around 60%.

YAlB<sub>14</sub> has the orthorhombic MgAlB<sub>14</sub>-type structure (Matkovich and Economy, 1970; Higashi and Ito, 1983) with space group of *Imma*. A later refinement of the crystal structure for TbB<sub>25</sub> (Mori et al., 2001) confirmed that the RB<sub>25</sub> structure is a monoclinic distortion of the MgAlB<sub>14</sub>-type structure. The space group was determined to be *I12/m1* (Mori et al., 2001). For example, for TbB<sub>25</sub>, the crystallographic parameters are:  $a = 5.855 \text{ \AA}$ ,  $b = 10.3354 \text{ \AA}$ ,  $c = 8.2808 \text{ \AA}$ , and  $\beta = 89.512^\circ$ . The crystal structure of RB<sub>25</sub> is shown in Figure 19.

Since the RB<sub>25</sub> and RAlB<sub>14</sub> structures are very similar, their basic characteristics can be described together. Lattice parameters for the rare earth series of both compounds are listed in Table 7. Infinite B<sub>12</sub> icosahedra chains run along the *b*-axis direction, with two icosahedra occupying the length of 10.335 Å. Infinite zigzag chains of rare earth sites with occupancy of approximately 60% run along the direction of the *a*-axis. The spacing of the rare earth sites within the chain is 3.48 Å, for example in the case of TbB<sub>25</sub>. The separation between terbium chains along the *b*-axis, which is importantly the axis along the B<sub>12</sub> chains, is 5.73 Å. The reported rare earth phases for RB<sub>25</sub> have been R = Gd, Tb, Dy, Ho, Er, and Y. The RAlB<sub>14</sub> phase has been obtained for Tb, Dy, Ho, Er, Yb, Lu, and Y.

### 8.2 Bonding in RB<sub>25</sub> and RAlB<sub>14</sub>

RB<sub>25</sub> is a notation based on the actual chemical composition, but it can be expressed as R<sub>~0.6</sub>B<sub>14</sub>. The absence of the aluminum atoms in RB<sub>25</sub>, compared to the R<sub>0.62</sub>Al<sub>0.73</sub>B<sub>14</sub> (RAlB<sub>14</sub>) compound is noteworthy. As previously discussed, many researchers have investigated the bonding and electronic structure of boron icosahedra-containing compounds. The bonding in compounds such as LiAlB<sub>14</sub> and Mg<sub>2</sub>B<sub>14</sub> has been discussed (Bullett, 1982), and since the boron icosahedra is "2 electron deficient", "B<sub>14</sub>", i.e. B·B<sub>12</sub>·B can be considered to be 4 electron deficient. Therefore, the compounds LiAlB<sub>14</sub> and Mg<sub>2</sub>B<sub>14</sub> with the metal atoms supplying 4 electrons each, nicely fill this electron requirement. And it is interesting how in the case of R<sub>0.62</sub>Al<sub>0.73</sub>B<sub>14</sub>, where the metal sites are partially occupied,

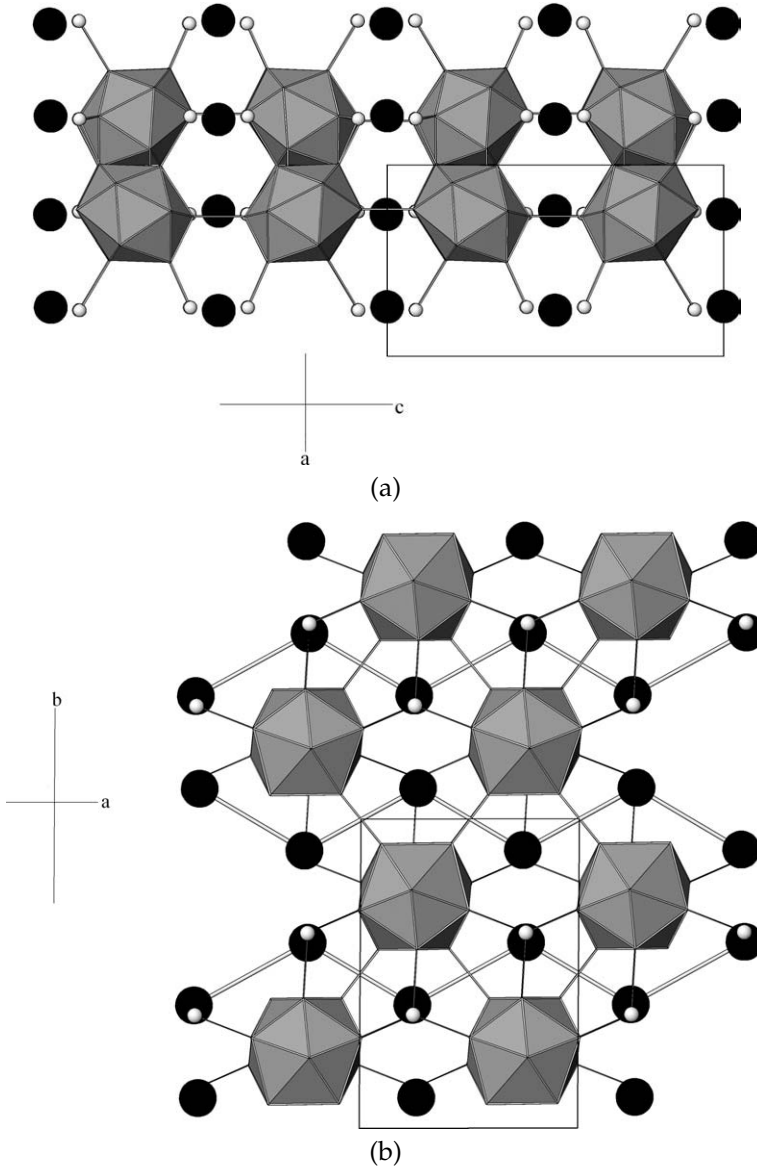


**FIGURE 19** The crystal structure of  $RB_{25}$ : (a) view along the  $b$ -axis, and (b) a view along the  $c$ -axis. The polyhedra are  $B_{12}$  icosahedra, small circles indicate boron atoms, while the large circles indicate rare earth atoms (Mori et al., 2001).

that just enough amounts of rare earth and aluminum occupy the sites to supply approximately 4 electrons. It is difficult to add more rare earth or aluminum to these phases to give more than 4 electrons which would have resulted in a metal. This appears to be a general tendency of the boron icosahedra compounds, as none

**TABLE 7** Lattice parameters of  $RB_{25}$  and  $RAIB_{14}$  phases.  $RB_{25}$  is monoclinic and  $RAIB_{14}$  is orthorhombic. The lattice parameters of  $MgAlB_{14}$  are also included as reference

	$a$ (Å)	$b$ (Å)	$c$ (Å)	$\beta$ (°)	Reference
GdB <sub>25</sub>	5.853	10.339	8.313	89.58	Mori et al. (2001)
TbB <sub>25</sub>	5.855	10.335	8.281	89.512	Mori et al. (2001)
DyB <sub>25</sub>	5.856	10.325	8.277	89.56	Mori et al. (2001)
HoB <sub>25</sub>	5.858	10.319	8.271	89.54	Mori et al. (2001)
ErB <sub>25</sub>	5.856	10.309	8.262	89.54	Mori et al. (2001)
YB <sub>25</sub>	5.857	10.320	8.284	89.60	Tanaka et al., 1997a)
TbAlB <sub>14</sub>	5.836	10.419	8.189	(90)	Korsukova et al. (1989)
DyAlB <sub>14</sub>	5.846	10.420	8.198	(90)	Korsukova et al. (1989)
HoAlB <sub>14</sub>	5.841	10.410	8.188	(90)	Korsukova et al. (1989)
ErAlB <sub>14</sub>	5.842	10.406	8.186	(90)	Korsukova et al. (1989)
YbAlB <sub>14</sub>	5.860	10.439	8.222	(90)	Korsukova et al. (1989)
LuAlB <sub>14</sub>	5.867	10.364	8.157	(90)	Korsukova et al. (1989)
YAlB <sub>14</sub>	5.821	10.395	8.183	(90)	Korsukova et al. (1989)
MgAlB <sub>14</sub>	5.848	10.313	8.115	(90)	Matkovich and Economy (1970)

of the compounds have experimentally been found to be metallic. They are all insulators/semiconductors, unless doped with extremely large amounts of transition metals as in the case of doped beta-boron (e.g. Slack et al., 1987). As noted before in Section 4, in the case of  $RB_{12}$ , which is necessarily a metal for trivalent rare earth atoms, the “B<sub>12</sub>” does not form an icosahedra but a cubooctahedra.

This gives rise to the question of the origin of this behavior. Whether the boron icosahedra framework naturally has a tendency to “repel”/reject the accommodation of an abundance of electrons, or whether the presence of a relatively electron-rich environment is detrimental to the formation of boron icosahedra. The dodecaboride case may indicate the latter, but this is not clear at the present time. In any case, the contrast of  $RB_{25}$  ( $R_{\sim 0.6}B_{14}$ ) with its lack of aluminum atoms, to  $R_{0.62}Al_{0.73}B_{14}$  is intriguing and further comparative investigations, for example, on the band structure, should be worthwhile.

### 8.3 Electrical properties of $RB_{25}$ and $RAIB_{14}$

For reference, polycrystalline  $MgAlB_{14}$  has a room temperature resistivity of  $1 \times 10^2 \Omega \text{ cm}$  and is a p-type conductor (Prudenziati et al., 1973). Results on  $RB_{25}$ , which cannot be grown as large crystals, are not available. The resistance of an  $ErAlB_{14}$  single crystal was measured below room temperature and found to generally follow the 3D VRH dependence with  $T_0 = 670 \text{ K}$  (Korsukova et al., 1989). A deviation in the resistivity vs. temperature plot was observed at low temperatures below 16 K. The absolute values of the resistivity were not given. A large negative magnetoresistance is also observed. The characteristic temperature  $T_0$  reported for  $ErAlB_{14}$  is much smaller than those of  $RB_{66}$  and  $RB_{44}Si_2$  and is in line

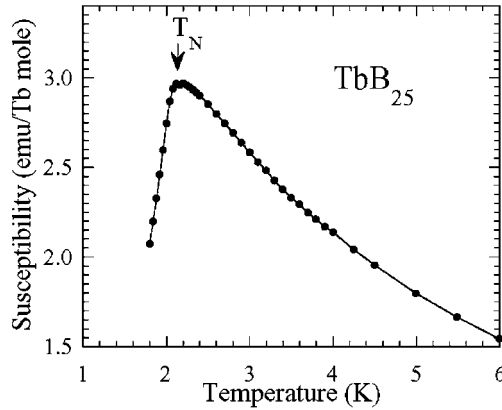


**FIGURE 20** The low temperature magnetic susceptibility of  $\text{TbB}_{25}$ . The arrow indicates the antiferromagnetic transition at  $T_N = 2.1$  K (Mori et al., 2001).

with the tendency for the more metal-rich samples being less localized (or having a larger density of states at the Fermi level).

#### 8.4 Magnetic properties of $\text{RB}_{25}$

The magnetic properties of the  $\text{RB}_{25}$  series were investigated (Mori et al., 2001).  $\text{RB}_{25}$  compounds are paramagnetic with no magnetic transitions observed down to 1.8 K for  $R = \text{Gd}, \text{Tb}, \text{Dy}, \text{Ho},$  and  $\text{Er}$ . However,  $\text{TbB}_{25}$  shows a drop in the susceptibility around 2.1 K, indicative of an antiferromagnetic-like transition (Figure 20). The transition temperature  $T_N$  of 2.1 K for  $\text{TbB}_{25}$  is almost one order lower than that for the more magnetically dilute  $\text{TbB}_{50}$ . A comparison of the two compounds was made (Mori et al., 2001). Although there are shorter metal–metal distances in  $\text{TbB}_{25}$  (3.48 Å within the zigzag chain along the  $a$ -axis), the metal–metal distances along the  $\text{B}_{12}$  icosahedra chain, which had been previously speculated to be the critical distance for magnetic interaction in these compounds (Mori and Tanaka, 1999a, 1999b, 2001a), are longer for  $\text{TbB}_{25}$  than  $\text{TbB}_{50}$ . The separations are 5.73 Å for  $\text{TbB}_{25}$  ( $T_N = 2.1$  K) compared to an alternating 5.12 Å and 4.36 Å separation for  $\text{TbB}_{50}$  ( $T_N = 17$  K). These results are consistent with the interaction along the  $\text{B}_{12}$  chain being important.

The effective magnetic moments of all the phases indicate trivalent states for the lanthanide ions.

#### 8.5 Magnetic properties of $\text{RAlB}_{14}$

From fits of the high temperature ( $150 \text{ K} < T < 250 \text{ K}$ ) magnetic susceptibilities of  $\text{RAlB}_{14}$  ( $\text{Tb}, \text{Dy}, \text{Ho}, \text{Er}$ ), relatively large Curie–Weiss temperatures of  $|\theta| \sim 10 \text{ K}$  were determined by Korsukova et al. (1989). However, the existence of magnetic transitions were not reported. An anomaly is that the  $\text{Tb}$  phase is reported to have  $\theta = 10 \text{ K}$ , which indicates ferromagnetic interaction.

The magnitudes of the reported Curie–Weiss temperatures are larger than  $\text{RB}_{25}$ . It is instructive to compare the behavior of the two series of compounds since their basic structural difference is the addition of Al occupying 4e sites in  $\text{RAlB}_{14}$  and a slight distortion from orthorhombic to monoclinic ( $\beta = 89.512^\circ$ ) structure for  $\text{RB}_{25}$ . The filling of the Al atoms might be having a beneficial effect on the magnetic interaction (although the detailed explicit mechanism is not known yet), but it still remains to be explained why magnetic transitions have not been observed for  $\text{RAlB}_{14}$  despite the reported large values of  $\theta$ , whereas one has been observed for  $\text{TbB}_{25}$  at  $T_N = 2.1$  K.

The magnetic susceptibility curves presented by [Korsukova et al. \(1989\)](#) show some unusual curvatures and it may be worthwhile to investigate the behavior in more detail, applying different magnetic fields.

## 9. HOMOLOGOUS R–B–C(N) COMPOUNDS: $\text{RB}_{15.5}\text{CN}$ , $\text{RB}_{22}\text{C}_2\text{N}$ , $\text{RB}_{28.5}\text{C}_4$

With the addition of small amounts of a third element (such as carbon, nitrogen, silicon) several new striking structures of the higher borides were found, leading to interesting properties.

The compounds discussed in this section were made by the addition of carbon and nitrogen, and they are a homologous layered series of rare earth boron carbonitrides. Serendipity was involved in the discovery of these compounds as traces of the phases were first found accidentally, due to the unintentional addition of small amounts of carbon originating from the graphite wool which is sometimes used as a heating element for synthesis; and also small amounts of nitrogen apparently coming from the BN crucibles heated in the graphite susceptors under Ar gas (in which there are trace amounts of oxygen which can act as a catalyzing agent) rather than a dynamical vacuum. The first compound in the series to be discovered was  $\text{RB}_{15.5}\text{CN}$  ([Leithe-Jasper et al., 2004](#)).

These compounds form for the heavy rare earth atoms with relatively small size, namely,  $R = \text{Ho, Er, Tm, Lu, Y, Sc}$ . Sc appears to be anomalous (again) because of its small size and only forms for the  $\text{RB}_{15.5}\text{CN}$  phase. Recently, careful synthesis has revealed that at least for the  $\text{RB}_{22}\text{C}_2\text{N}$  phase, the dysprosium phase can also be formed ([Mori et al., 2008b](#)). We note that nitrogen addition is absolutely essential for only forming the  $\text{RB}_{15.5}\text{CN}$  phase. It has been found possible to synthesize the  $\text{RB}_{22}\text{C}_2\text{N}$  phase with carbon replacing nitrogen. Incidentally, an excellent compilation and review on the phase diagrams, structures, and lattice parameters of all ternary metal boron carbon systems discovered before these new compounds has been made by [Rogl \(1998\)](#). A previous review has also been published by [Rogl \(1984\)](#) on the phase equilibria in ternary and higher order systems containing rare earth elements and boron. A comprehensive review and analysis has also been made by [J. Bauer et al. \(1998\)](#) on the formation of previously known rare earth borocarbide structure types from the viewpoint of the electron count, and they show how it is possible to regard these compounds as solid state coordination compounds.

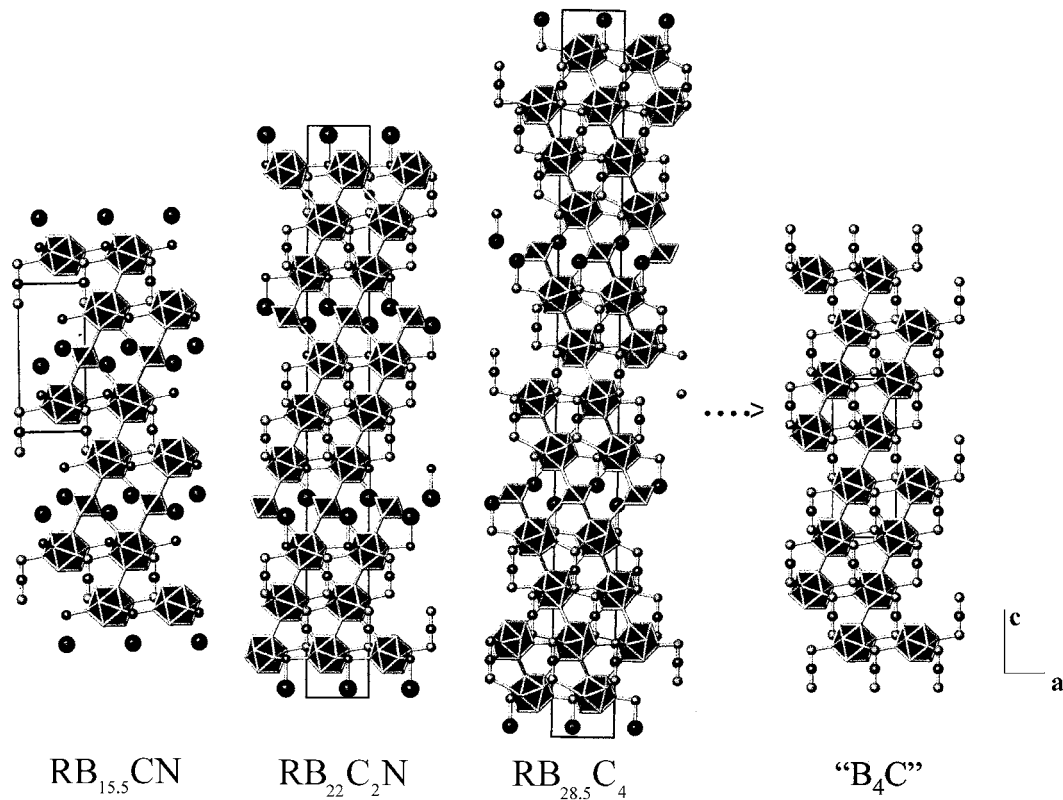


**FIGURE 21** The crystal structures of  $RB_{15.5}CN$ ,  $RB_{22}C_2N$ , and  $RB_{28.5}C_4$ , in views perpendicular to the  $c$ -axis. The large polyhedra are  $B_{12}$  icosahedra, smaller polyhedra indicate  $B_6$  octahedra, the three bonded atoms along  $[001]$  are three atom carbon–boron–carbon chains, where the open circles are carbon atoms and the medium sized dark circles are boron atoms. The large dark circles indicate rare earth atoms, while small dark circles individually connected to the  $B_{12}$  icosahedra (in the cases of  $RB_{15.5}CN$  and  $RB_{22}C_2N$ ) are nitrogen atoms. For comparison the structure of boron carbide “ $B_4C$ ” is also depicted.

**TABLE 8** Lattice parameters of the homologous R–B–C(N) compounds RB<sub>15.5</sub>CN, RB<sub>22</sub>C<sub>2</sub>N, and RB<sub>28.5</sub>C<sub>4</sub>. The structure of RB<sub>15.5</sub>CN is trigonal and those of RB<sub>22</sub>C<sub>2</sub>N and RB<sub>28.5</sub>C<sub>4</sub> are rhombohedral. The data of trigonal MgB<sub>9</sub>N is also included as reference

	<i>a</i> (Å)	<i>b</i> (Å)	Volume (Å <sup>3</sup> )	Reference
Sc <sub>15.5</sub> CN	5.568	10.756	288.8	Leithe-Jasper et al. (2004)
YB <sub>15.5</sub> CN	5.592	10.873	294.9	Leithe-Jasper et al. (2004)
HoB <sub>15.5</sub> CN	5.588	10.878	294.2	Leithe-Jasper et al. (2004)
ErB <sub>15.5</sub> CN	5.589	10.880	294.3	Leithe-Jasper et al. (2004)
TmB <sub>15.5</sub> CN	5.580	10.850	292.6	Leithe-Jasper et al. (2004)
LuB <sub>15.5</sub> CN	5.577	10.839	291.9	Leithe-Jasper et al. (2004)
YB <sub>22</sub> C <sub>2</sub> N	5.623	44.765	1226.9	Zhang et al. (2001a)
HoB <sub>22</sub> C <sub>2</sub> N	5.614	44.625	1248.4	Zhang et al. (2001a)
ErB <sub>22</sub> C <sub>2</sub> N	5.624	44.681	1224.9	Zhang et al. (2001a)
TmB <sub>22</sub> C <sub>2</sub> N	5.631	44.737	1228.7	Zhang et al. (2001a)
LuB <sub>22</sub> C <sub>2</sub> N	5.595	44.464	1205.7	Zhang et al. (2001a)
YB <sub>28.5</sub> C <sub>4</sub>	5.649	56.899	1572.7	Zhang et al. (2001b)
HoB <sub>28.5</sub> C <sub>4</sub>	5.638	56.881	1566.0	Zhang et al. (2001b)
ErB <sub>28.5</sub> C <sub>4</sub>	5.640	56.868	1566.5	Zhang et al. (2001b)
TmB <sub>28.5</sub> C <sub>4</sub>	5.622	56.649	1550.9	Zhang et al. (2001b)
B <sub>4</sub> C	5.601	12.073	328.03	Kirfel et al. (1979)
MgB <sub>9</sub> CN	5.496	20.087	525.5	Mironov et al. (2002)

## 9.1 Crystal structures

RB<sub>15.5</sub>CN is trigonal (space group *P*-3*m*1) (Leithe-Jasper et al., 2004) while RB<sub>22</sub>C<sub>2</sub>N and RB<sub>28.5</sub>C<sub>4</sub> are rhombohedral (space group *R*-3*m*) (Zhang et al., 2001a, 2001b). The structures are depicted in Figure 21, while lattice parameters are given in Table 8. The compounds have a layered structure along the *c*-axis. The rare earth and B<sub>6</sub> octahedral layers are separated by layers comprised of B<sub>12</sub> icosahedra and three atom chains of carbon–boron–carbon (C–B–C). The number of these B<sub>12</sub> icosahedra and C–B–C chain layers increases successively from two B<sub>12</sub> layers for the RB<sub>15.5</sub>CN compound to four layers for the RB<sub>28.5</sub>C<sub>4</sub> compound. The C–B–C chains link the boron icosahedra. The configuration of the rare earth atoms in respect to each other is the same for all the R–B–C(N) homologous compounds. The rare earth atoms form two regular triangular layers closely laid on top of one another in an AB stacking, which projected along the *c*-axis appear as a honeycomb array (Figure 24). In the nearest neighbor rare earth direction (indicated by the thick bonds), a rare earth atom in one layer is connected to three rare earth atoms in the adjacent layer forming corner-sharing deformed tetrahedra with a separation of 3.52 Å in the case of HoB<sub>22</sub>C<sub>2</sub>N for example. The separation of the rare earth atoms within the regular triangular layer (indicated by the thin bonds) is 5.62 Å in this case. The rare earth sites have partially occupancy, with occupancy

taking values for example, of around 91%, 74%, and 83% for  $\text{ScB}_{15.5}\text{CN}$ ,  $\text{YB}_{22}\text{C}_2\text{N}$ , and  $\text{YB}_{28.5}\text{C}_4$ , respectively.

Theoretically, since these are layered homologous compounds, a numerous/infinite number of compounds are possible in the family. However, realistically, we have been able to synthesize pure phases of only the three compounds. Compounds which contained more than four layers of the  $\text{B}_{12}$  icosahedral and C–B–C chain layers (which is the case for  $\text{RB}_{28.5}\text{C}_4$ ) always contained a mixture of other number layers also. In the limit of the boron icosahedra and C–B–C chain layers separating the metal layers reaching infinity (i.e. no rare earth layers) the compound is actually analogous to boron carbide. In the opposite limit, a compound with just one boron icosahedra layer is imaginable. And in actuality, such a  $\text{MgB}_9\text{N}$  compound was independently discovered by Mironov et al. (2002). However, such a compound with rare earth atoms has not yet been synthesized.

## 9.2 Magnetic properties: spin glass behavior

Spin glass behavior was observed for this series of compounds  $\text{RB}_{15.5}\text{CN}$ ,  $\text{RB}_{22}\text{C}_2\text{N}$ ,  $\text{RB}_{28.5}\text{C}_4$  ( $\text{R} = \text{Ho}, \text{Er}$ ) (Mori et al., 2002; Mori and Mamiya, 2003; Mori et al., 2004b). The Tm phases may also exhibit the same behavior, however, the magnetic interaction was not strong, and revealed only paramagnetic behavior above 1.8 K. The spin glass behavior is intriguing as these are non-doped, crystalline compounds. As far as we are aware, this is the first observation of spin glass behavior in a non-doped boride. For example, as characteristic physical properties, the relaxation of isothermal remanent magnetization was observed (Figure 22):

$$I_m = \sigma_{10} \exp[-C(\omega t)^{-(1-n)} / (1-n)] \quad (7)$$

(e.g.  $\text{HoB}_{22}\text{C}_2\text{N}$ ,  $C = 0.033$ ,  $1-n = 0.10$ ), and the existence of wait time effects (Figure 23). These data show that these quaternary phases are non-doped compounds composed of rare earth atoms configured in a boron framework exhibiting magnetic glassiness. The reason that spin glass behavior manifests in this particular series of compounds is considered to be due to a combination of disorder from partial occupancy of the rare earth atomic sites, and more importantly, also frustration of magnetic interactions, which arises due to the unique configuration of rare earth atoms (Mori and Leithe-Jasper, 2002; Mori and Mamiya, 2003).

The rare earth atomic layers are separated by large distances along the  $c$ -axis ( $\sim 15 \text{ \AA}$  for  $\text{RB}_{22}\text{C}_2\text{N}$ ), and therefore, it is indicated that any sizable magnetic interaction will be among rare earth atoms within the layers. As noted in the previous section, the rare earth atoms form two regular triangular layers closely laid on top of one another in AB stacking within the layers (Figure 24). In the nearest neighbor rare earth direction (indicated by the thick bonds), a rare earth atom in one layer is connected to three rare earth atoms in the adjacent layer forming corner-sharing deformed tetrahedral with a separation of  $3.52 \text{ \AA}$  (for  $\text{HoB}_{22}\text{C}_2\text{N}$  for example). The separation of the rare earth atoms within the regular triangular layer (indicated by the thin bonds) is  $5.62 \text{ \AA}$ . If the antiferromagnetic interaction along the nearest neighbor direction (thick bonds), which we label as  $J_0$ , was dominant then there would be no frustration, since a minimization of energy would be satisfied with

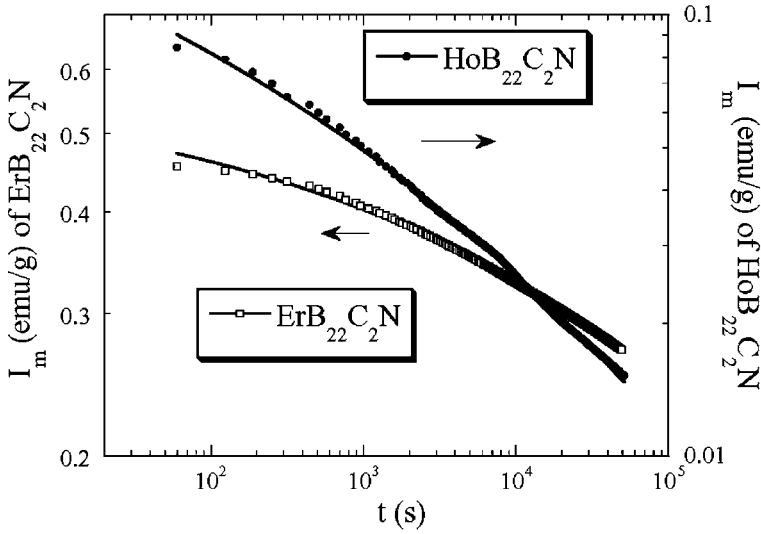


**FIGURE 22** The time decay of the isothermal remanent magnetizations  $I_m$  of  $\text{HoB}_{22}\text{C}_2\text{N}$  and  $\text{ErB}_{22}\text{C}_2\text{N}$  at 5 and 2 K, respectively. The lines depict the stretched exponential fit;  $I_m = \sigma_{10} \exp[-C(\omega t)^{-(1-n)} / (1-n)]$  (Mori and Leithe-Jasper, 2002).

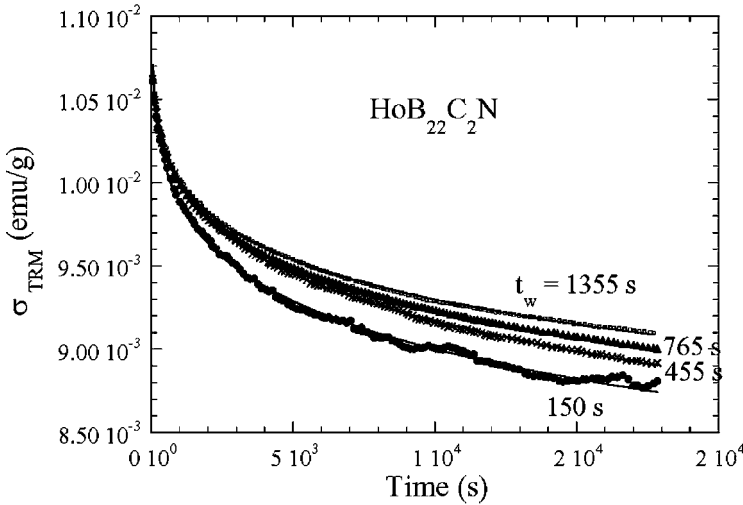


**FIGURE 23** The time decay of the thermal remanent magnetization  $\sigma_{\text{TRM}}$  of  $\text{HoB}_{22}\text{C}_2\text{N}$  at 10 K for different wait times of  $t_w$  of 150 s (●), 455 s (×), 765 s (▲), and 1355 s (■) (Mori and Leithe-Jasper, 2002).

a configuration where the spins are ferromagnetically aligned within the triangular layers and the layers themselves are antiferromagnetically ordered. However, since frustration of the magnetic interactions is indicated, therefore, this points to

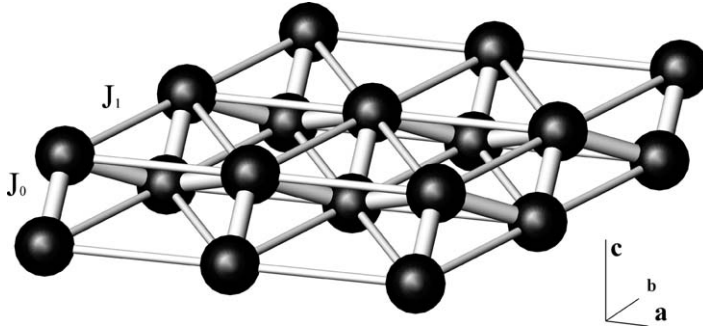


**FIGURE 24** The arrangement of the rare earth atoms in the R–B–C(N) homologous compounds.

the interaction within the triangular layers  $J_1$ , being stronger than  $J_0$  despite the longer distance. We note that the  $B_{12}$  icosahedra are situated along  $J_1$  in contrast to  $J_0$ , and this again supports the novel idea of the magnetic interaction being mediated by the boron icosahedra clusters.

### 9.3 Dynamical properties: indication of 2 dimensionality

AC susceptibility measurements can yield valuable information on the dynamical properties of a system. The ac susceptibility of  $HoB_{22}C_2N$  shows frequency dependence, but could not be analyzed satisfactorily by the dynamical scaling theory of a three dimensional spin glass (Mori and Mamiya, 2003). Therefore, a detailed investigation of the behavior of relaxation times by the Cole–Cole analysis (Cole and Cole, 1941) was performed. The complex susceptibility can be phenomenologically expressed as:

$$\chi = \chi_s + (\chi_0 - \chi_s) / (1 + (i\omega\tau_C)^{1-\beta}), \quad (8)$$

where  $\chi_0$  and  $\chi_s$  are the isothermal ( $\omega = 0$ ) and adiabatic ( $\omega \rightarrow \infty$ ) susceptibilities, respectively,  $\tau_C$  is the median relaxation time around which a distribution of relaxation times (symmetric on the logarithmic scale) is assumed, while  $\beta$  ( $0 < \beta < 1$ ) is representative of the width of the distribution.  $\beta = 1$  for a distribution of infinite width, while  $\beta = 0$  for the Debye form of a single relaxation time. Equation (8) can be decomposed into a relationship of  $\chi'$  and  $\chi''$  which is used to fit the Argand diagrams in Figure 25. The maxima of the diagrams give  $\omega\tau_C = 1$ , while the flatness of the arcs are a measure of the width of the distribution of relaxation times. The distribution function of relaxation times  $g(\tau)$  at each temperature can be determined from this analysis as plotted in Figure 26. As temperature is lowered, the distribution of relaxation times  $g(\tau)$  in  $HoB_{22}C_2N$  becomes very broad, indicating that the spins are frozen into “macroscopic” time scales. The qualitative behavior of  $HoB_{22}C_2N$  was similar to what has been observed for other spin glasses (e.g. Huser et al., 1986) and was obviously different from the blocking phenomena of

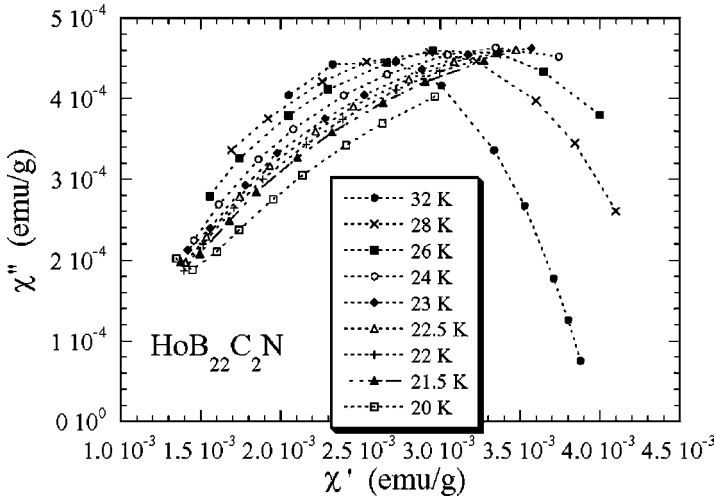


**FIGURE 25** The Argand diagrams of  $\text{HoB}_{22}\text{C}_2\text{N}$  for 32 K (●), 28 K (×), 26 K (■), 24 K (○), 23 K (◆), 22.5 K (△), 22 K (+), 21.5 K (▲), and 20 K (□) (Mori and Mamiya, 2003).

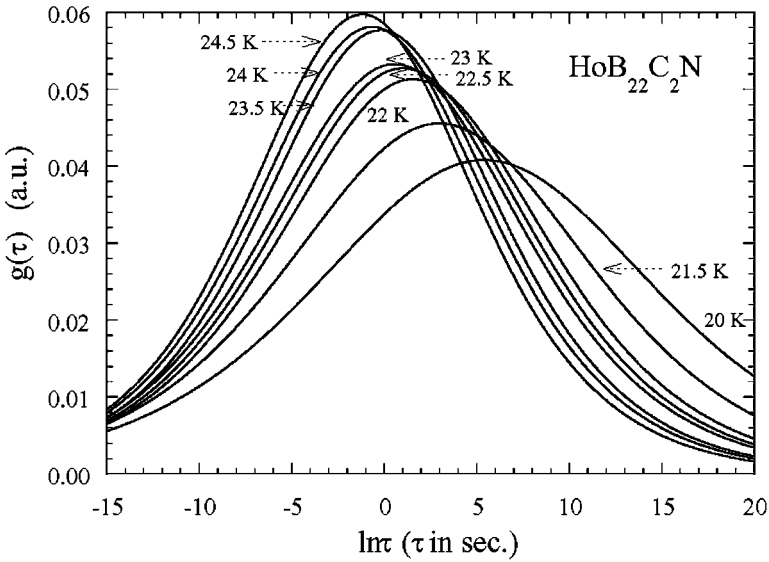


**FIGURE 26** The distribution of relaxation times  $g(t)$  of  $\text{HoB}_{22}\text{C}_2\text{N}$  for several selected temperatures from 24.5 to 20 K (Mori and Mamiya, 2003).

a typical superparamagnet in which the width parameter  $\beta$  has been observed to have little temperature dependence (e.g. Mydosh, 1993).

Analysis of the temperature dependence of the median relaxation time  $\tau_C$  shows that it can actually be described well in terms of a generalized Arrhenius

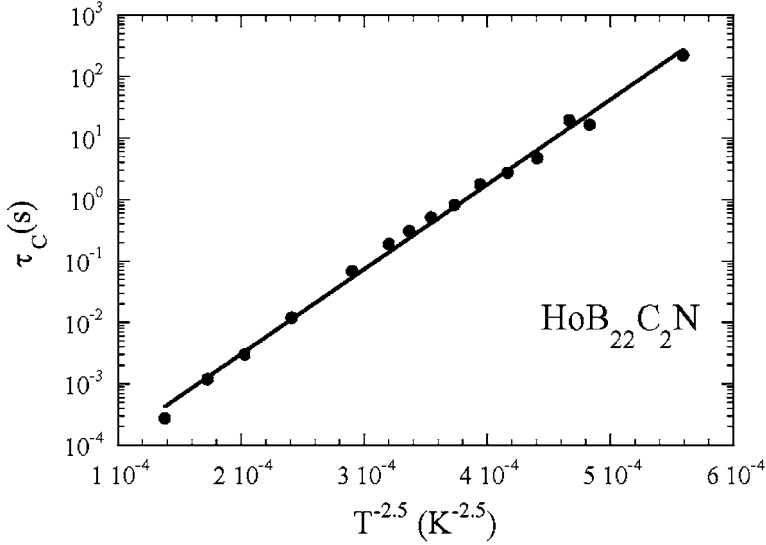


**FIGURE 27** The temperature dependence of the median relaxation time  $\tau_C$  of  $\text{HoB}_{22}\text{C}_2\text{N}$  plotted versus  $T^{-2.5}$ .  $\tau_C$  can be described well by the generalized Arrhenius law  $\ln(\tau_C/\tau_0) \propto T^{-(1+\phi\nu)}$ , with  $\tau_0 = 5.3 \times 10^{-6}$  s and  $1 + \phi\nu = 2.5$  (Mori and Mamiya, 2003).

law, as plotted in Figure 27 (Mori and Mamiya, 2003):

$$\ln(\tau_C/\tau_0) \propto T^{-(1+\phi\nu)}, \quad \tau_0 = 5.3 \times 10^{-6} \text{ s}, \quad 1 + \phi\nu = 2.5. \quad (9)$$

Monte Carlo simulations on 2D systems have given values of  $1 + \phi\nu \sim 2$  with the generalized Arrhenius dependence (Kinzel and Binder, 1984; Young, 1983). Theoretical calculations have also been made on a diluted triangular antiferromagnetic lattice model, which is similar to the system considered here, and the results have also yielded a generalized Arrhenius dependence with an exponent of 2 (Anderico et al., 1982).

To summarize, the analysis of dynamical properties have shown that the  $\text{HoB}_{22}\text{C}_2\text{N}$  system is not a simple superparamagnet, nor a typical 3D spin glass, but a new 2 dimensional spin glass system (Mori and Mamiya, 2003). In fact, a dilute triangular lattice magnetic system.

## 9.4 Comparison of magnetic properties

The configuration of the rare earth atoms in the basal planes of the three compounds  $\text{RB}_{15.5}\text{CN}$ ,  $\text{RB}_{22}\text{C}_2\text{N}$ ,  $\text{RB}_{28.5}\text{C}_4$  is similar. In Figure 28 it can be seen that they display basically the same spin glass behavior with some variations in the values of the peak temperatures  $T_f$ . Magnetic parameters of the homologous series are given in Table 9. The spacing of the rare earth layer pairs along the  $c$ -axis is approximately 10 Å, 15 Å, and 19 Å for  $\text{RB}_{15.5}\text{CN}$ ,  $\text{RB}_{22}\text{C}_2\text{N}$ , and  $\text{RB}_{28.5}\text{C}_4$ , respectively (see Figure 21). Considering that the spacing is much larger than the spacing within the layers and varies substantially among the homologous compounds, the

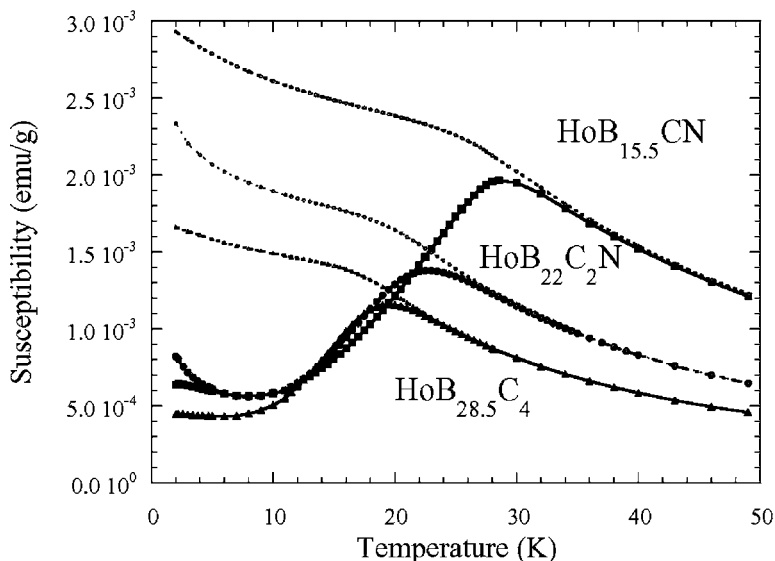


**FIGURE 28** The temperature dependence of the magnetic susceptibility of  $\text{HoB}_{15.5}\text{CN}$  (■),  $\text{HoB}_{22}\text{C}_2\text{N}$  (●), and  $\text{HoB}_{28.5}\text{C}_4$  (▲) for ZFC (large closed symbols) and FC curves (small open symbols) (Mori et al., 2004b).

**TABLE 9** Magnetic properties of the homologous R–B–C(N) compounds  $\text{RB}_{15.5}\text{CN}$ ,  $\text{RB}_{22}\text{C}_2\text{N}$ , and  $\text{RB}_{28.5}\text{C}_4$  (R = Er, Ho).  $T_f$  is defined as the peak temperature of the zero field cooled (ZFC) susceptibility

	$\mu_{\text{eff}}$ ( $\mu_{\text{B}}/\text{R atom}$ )	$\theta$ (K)	$T_f$ (K)	References
$\text{ErB}_{15.5}\text{CN}$	8.89	−4.0	6.1	Mori et al. (2004b)
$\text{ErB}_{22}\text{C}_2\text{N}$	9.02	−7.1	5.1	Mori and Zhang (2002)
$\text{ErB}_{28.5}\text{C}_4$	8.79	−7.5	4.5	Mori et al. (2004b)
$\text{HoB}_{15.5}\text{CN}$	9.84	15.6	28.8	Mori et al. (2004b)
$\text{HoB}_{22}\text{C}_2\text{N}$	10.1	−16.9	22.5	Mori and Zhang (2002)
$\text{HoB}_{28.5}\text{C}_4$	9.60	9.7	19.3	Mori et al. (2004b)

assumption that the magnetic interaction between different pairs of rare earth pair layers is smaller than the interaction among the layers appears to be sound. As can be seen from Tables 8 and 9,  $T_f$  monotonically decreases as the basal plane lattice constant  $a$  increases (corresponding to an increase in the separation of the rare earth atoms in the basal plane), which is reasonable with the magnetism being governed within the rare earth layers.

The results from the comparison of the magnetic properties between the different homologous compounds are consistent with the conclusions in the previous

section which indicate that the configuration of the 2D triangular rare earth layers dictate the physics of this system.

We note that anomalous ferromagnetic Curie–Weiss constants were observed for  $\text{HoB}_{15.5}\text{CN}$  and  $\text{HoB}_{28.5}\text{C}_4$  (Mori et al., 2004b). The reason for this is not clear at present and should be investigated further.

## 9.5 Summary of the spin glass behavior

The homologous R–B–C(N) compounds  $\text{RB}_{15.5}\text{CN}$ ,  $\text{RB}_{22}\text{C}_2\text{N}$ , and  $\text{RB}_{28.5}\text{C}_4$ , exhibit spin glass behavior (Mori and Leithe-Jasper, 2002; Mori et al., 2004b) and from a dynamical properties investigation of  $\text{HoB}_{22}\text{C}_2\text{N}$ , are found to actually indicated to be two dimensional spin glasses (Mori and Mamiya, 2003).

The configuration of the rare earth sites in the R–B–C(N) homologous compounds is notable as there are two flat two dimensional triangular lattices closely stacked upon one another in an AB stacking sequence. Antiferromagnetic interaction within the flat triangular layers is found to be dominant and the source of frustration in this system.

Making a comparison with some other  $\text{B}_{12}$  magnetic compounds, (1) the  $\text{RB}_{50}$ -type compounds have full occupancy of R sites and therefore no source of sizable disorder, (2)  $\text{GdB}_{18}\text{Si}_5$ , which is discussed in the next section, has partial occupancy of Gd sites but geometrically does not have frustration of the magnetic interactions, (3)  $\text{RB}_{66}$  has large disorder but only a small magnetic interaction. Therefore, it is indicated that the R–B–C(N) homologous compounds provide a unique system where there is both disorder originating from partial occupancy of rare earth sites and simultaneous frustration due to their particular configuration, which results in the spin glass behavior observed in the rare earth boron cluster systems.

Regarding the magnetic interaction, the strongest magnetic interaction is indicated to occur within the triangular lattice, i.e. along a metal–metal separation (5.62 Å in the case of e.g.  $\text{HoB}_{22}\text{C}_2\text{N}$ ) which is the second nearest separation, but is in proximity to  $\text{B}_{12}$  icosahedra. The shortest metal–metal separation which is not along  $\text{B}_{12}$  icosahedra is found to give a weaker coupling despite the much shorter distance (3.54 Å in the case of e.g.  $\text{HoB}_{22}\text{C}_2\text{N}$ ).

As was the case for  $\text{RB}_{50}$ -type compounds and  $\text{RB}_{25}$  compounds, this is further experimental evidence that the  $\text{B}_{12}$  icosahedra are functioning as a novel mediator of the magnetic interaction between the rare earth ions.

Finally, we would like to stress again that it was the addition of small amounts of C and N in the synthesis of higher borides which caused these new structures to form. As a result, hitherto unknown configurations of the rare earth atoms confined in the boron cluster network were observed to appear, leading to these interesting properties.

## 10. $\text{RB}_{18}\text{Si}_5$ ( $\text{R}_{1.8}\text{B}_{36}\text{C}_2\text{Si}_8$ )

The previous section dealt with new phases which were found to form with the small additions of carbon and nitrogen. In this section, we describe a new phase

which was formed with the addition of silicon (in addition to  $\text{RB}_{44}\text{Si}_2$  described previously, which is essentially a modification of the  $\text{RB}_{50}$  compound).

Crystals of the new compound  $\text{YB}_{17.6}\text{Si}_{4.6}$  were grown by using a silicon flux, which was afterwards removed by a mixture of  $\text{HNO}_3$  and  $\text{HF}$  (Zhang et al., 2002). The compound could also be synthesized by the solid state reaction method, sintering with an abundance of silicon. At a similar time, Kanatzidis's group reported the discovery of the compound  $\text{Tb}_{1.8}\text{B}_{36}\text{C}_2\text{Si}_8$  (Salvadore et al., 2002). Crystals of  $\text{Tb}_{1.8}\text{B}_{36}\text{C}_2\text{Si}_8$  were obtained by using a gallium flux.  $\text{Tb}_{1.8}\text{B}_{36}\text{C}_2\text{Si}_8$  and  $\text{YB}_{17.6}\text{Si}_{4.6}$  are basically the same structure. Salvador et al. have reported that the presence of carbon is absolutely necessary for the formation of this compound and that it is actually a quaternary compound.

Going back to the nomenclature of the borides, it is possible to notate this compound as  $\text{YB}_{17.6}\text{Si}_{4.6}$  (or  $\text{RB}_{18}\text{Si}_5$ ) or  $\text{R}_{1.8}\text{B}_{36}\text{C}_2\text{Si}_8$  which is approximately the chemical composition actually found for these compounds, or alternately, to express the partial occupancy of the rare earth sites as  $x$  or  $3 - y$ , notating the compound as  $\text{R}_x\text{B}_{12}\text{Si}_3$  or  $\text{R}_{3-y}\text{B}_{36}\text{C}_2\text{Si}_8$  with  $x$  taking a value of around 0.7 and  $y \sim 1.2$ . We note that the latter case is different from the notation of  $\text{RAlB}_{14}$  or  $\text{RB}_{22}\text{C}_2\text{N}$ , for example, since the partial occupancy in this case is explicitly expressed by  $x$  or  $3 - y$ .

$\text{RB}_{18}\text{Si}_5$  forms for  $\text{R} = \text{Gd}, \text{Tb}, \text{Dy}, \text{Ho}, \text{Er}, \text{Tm}, \text{Yb}, \text{Lu},$  and  $\text{Y}$ ,  $\text{R}_{1.8}\text{B}_{36}\text{C}_2\text{Si}_8$  was reported to form for at least  $\text{Tb}, \text{Dy}, \text{Er}, \text{Tm}, \text{Y},$  and  $\text{Sc}$ .

## 10.1 Structures of $\text{RB}_{18}\text{Si}_5$ and $\text{R}_{1.8}\text{B}_{36}\text{C}_2\text{Si}_8$

The basic framework of the  $\text{RB}_{18}\text{Si}_5$  ( $\text{R}_{1.8}\text{B}_{36}\text{C}_2\text{Si}_8$ ) structure, which is made up of boron icosahedra, is notable in that the boron clusters form two-dimensional layers. Within the layers, the boron icosahedra have a trigonal arrangement and hexagonal rings of icosahedra with holes in the middle. The boron cluster layers are separated from each other and linked by Si-Si bridges which interestingly, have a similar atomic separation to elemental cubic Si. The structure is rhombohedral (space group  $R\bar{3}m$ ) with lattice constants of  $a = b = 10.07 \text{ \AA}$ , and  $c = 16.45 \text{ \AA}$  in the hexagonal setting for  $\text{GdB}_{18}\text{Si}_5$ , and is depicted in Figure 29.

The rare earth sites have an occupancy of around 68% and a view of only the rare earth arrangement is given in Figure 30. As can be seen in the figure, the rare earth atoms, which form triangular and hexagonal arrangements, have the shortest metal-metal spacing ( $5.04 \text{ \AA}$  in the case of  $\text{GdB}_{18}\text{Si}_5$ ). The  $\text{R}_{1.8}\text{B}_{36}\text{C}_2\text{Si}_8$  structure described by Salvadore et al. (2002) is basically the same as that noted above for  $\text{RB}_{18}\text{Si}_5$ . The carbon atoms are located in the structure in the form of C-C pairs which are bonded to  $\text{B}_{12}$  icosahedra.

## 10.2 Electrical properties of $\text{RB}_{18}\text{Si}_5$

The resistivity of  $\text{GdB}_{18}\text{Si}_5$  measured along the  $[001]$  axis is plotted in Figure 31 (Mori and Zhang, 2002). Similar to other icosahedral borides, the resistivity follows the 3 dimensional VRH law, and the characteristic temperature is determined to be  $T_0 = 6.7 \times 10^6 \text{ K}$  which is slightly larger than the values observed for the  $\text{RB}_{44}\text{Si}_2$  phase (Table 9) which have a value of  $\sim 2 \times 10^6 \text{ K}$ . This would indicate

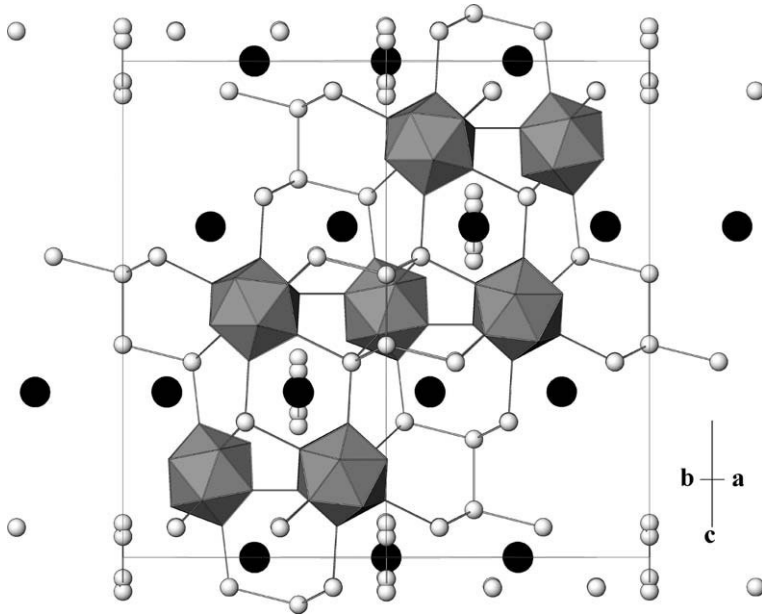


**FIGURE 29** The crystal structure of  $RB_{18}Si_5$ , projected onto the (110) plane. Polyhedra indicate  $B_{12}$  icosahedra, small gray circles are silicon atoms, and large black circles represent rare earth atoms.

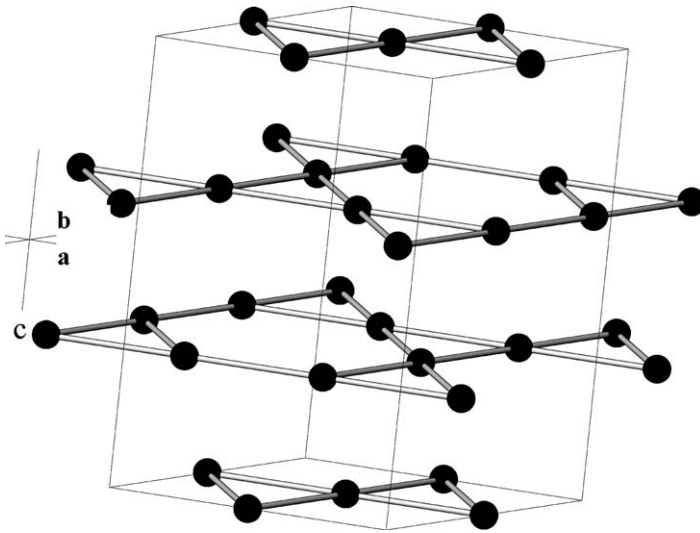


**FIGURE 30** The arrangement of the rare earth atoms in the  $RB_{18}Si_5$  structure.

that in the  $RB_{18}Si_5$  phase, the carriers are more localized than in  $RB_{44}Si_2$  which is interesting since, although the number of examples are small, there is a general tendency for the compound to be less localized as the higher borides became

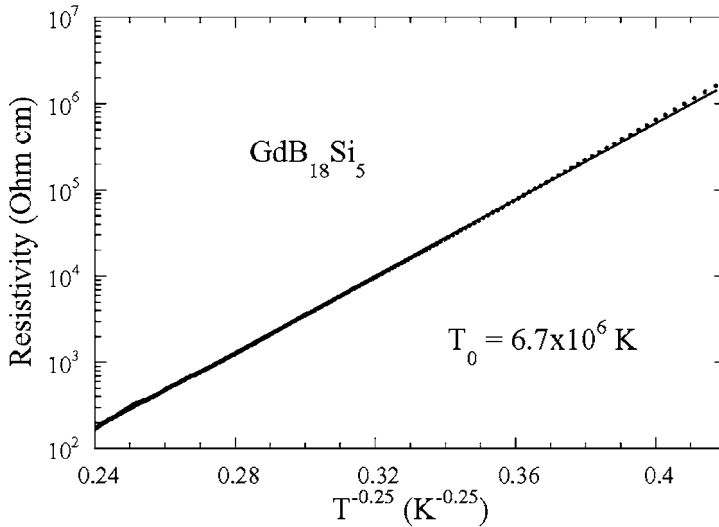


**FIGURE 31** The temperature dependence of the resistivity  $\rho$  of  $\text{GdB}_{18}\text{Si}_5$ . The line indicates the fit to  $\rho = \rho_0 \exp[(T_0/T)^{1/4}]$  (Mori and Zhang, 2002).

more metal rich (i.e.  $\text{RB}_{66}$  to  $\text{RB}_{44}\text{Si}_2$  to  $\text{RAIB}_{14}$ ).  $\text{GdB}_{66}$  having  $T_0 = 4 \times 10^7$  K (Section 6.2) and as noted in Section 8.3 an especially low value of  $T_0 = 670$  K was reported for  $\text{ErAlB}_{14}$  (Korsukova et al., 1989). Taking the  $\text{RB}_{18}\text{Si}_5$  result into account, the  $\text{RAIB}_{14}$  result may be anomalous because of the Al atoms which are incorporated into the structure. The values of  $T_0$  are in line for  $\text{RB}_{66}$  to  $\text{RB}_{18}\text{Si}_5$  to  $\text{RB}_{44}\text{Si}_2$  when we consider the occupation values of the rare earth sites which may be a large source of disorder (0.55 to 0.68 to 1.0, respectively). Of course,  $\text{RB}_{66}$  also contains the  $\text{B}_{80}$  cluster which has an occupancy of only 42 atoms as noted in Section 6.1 and the  $\text{RB}_{44}\text{Si}_2$  phase notably has a partial occupancy of the silicon sites (Section 7.3). Further systematic investigation into the conduction mechanisms of the higher borides should be interesting.

### 10.3 Magnetic properties of $\text{RB}_{18}\text{Si}_5$ and $\text{R}_{1.8}\text{B}_{36}\text{C}_2\text{Si}_8$

$\text{GdB}_{18}\text{Si}_5$  was discovered to exhibit interesting properties at low temperature (Mori and Zhang, 2002). The other lanthanide phases do not show any magnetic transitions above 1.8 K. A large Curie–Weiss temperature was reported for  $\text{Tb}_{1.8}\text{B}_{36}\text{C}_2\text{Si}_8$  by Salvadore et al. (2002), however, magnetic susceptibility curves were not given and the existence of a magnetic transition at low temperatures was not reported.

The magnetic properties of single crystals of  $\text{GdB}_{18}\text{Si}_5$  were measured (Mori and Zhang, 2002). The magnetic susceptibility is shown for two directions in Figure 32. A sharp drop in the in-plane susceptibility is observed at  $T_N = 3.2$  K indicating that an antiferromagnetic transition occurs at this temperature. The

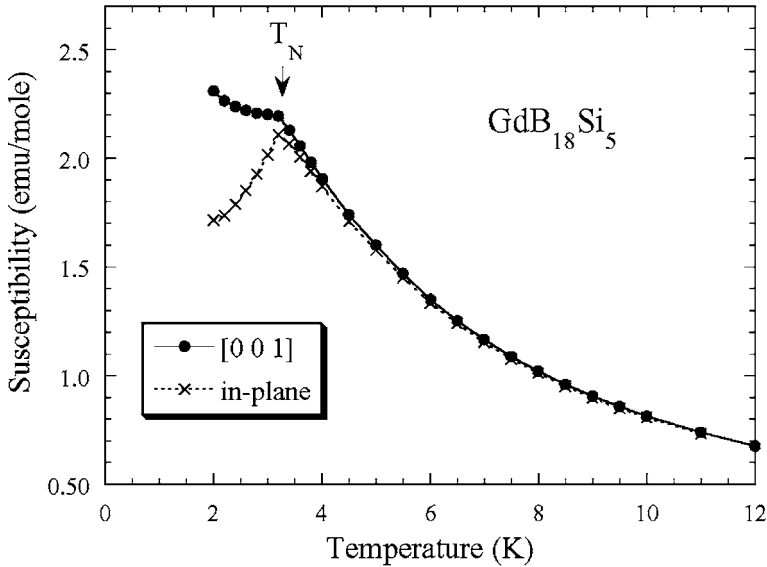


**FIGURE 32** The temperature dependence of the magnetic susceptibility of  $\text{GdB}_{18}\text{Si}_5$  along the [001] direction (●) and in-plane (×) (Mori and Zhang, 2002).

anisotropy between the in-plane and [001] susceptibility indicates that the spins are ordered in the  $a$ - $b$  plane.

A  $\lambda$ -type peak is observed in the magnetic specific heat at 3.2 K and supports a long range order antiferromagnetic transition occurring in this system (Figure 33). This behavior is in contrast to the behavior observed for  $\text{RB}_{50}$ -type compounds and  $\text{R-B-C(N)}$  homologous compounds which only had broad peaks in the specific heat due to the low dimensionality (Section 7) and spin glass behavior (Section 9), respectively.

The long range ordering in  $\text{GdB}_{18}\text{Si}_5$  is striking, since it is the first long range ordering ever discovered in the lanthanide boron icosahedra compounds, despite the fact that it has partial occupancy (68%) of the lanthanide sites. It should be worthwhile to attempt to determine exactly what kind of magnetic structure is taken by this compound. However, both natural boron and gadolinium have extremely large neutron cross sections. Isotope enrichment of the two elements in the sample is readily available for boron but not monetarily feasible for gadolinium. Using a hot neutron source or X-ray techniques should overcome this problem and enable an investigation into the magnetic structure.

The entropy  $S$  attains a value near 17 J/K mol at 18 K which is close to the full magnetic entropy of  $R \ln 8 = 17.3$  J/K mol expected in this case, since the  $^8\text{S}_{7/2}$  ground state of  $\text{Gd}^{3+}$  is spherically symmetric and degeneracy is not expected to be lifted by crystalline electric field CEF effects.

Regarding the mechanism of the magnetic interaction, the configuration of the lanthanide atoms in regard to the  $\text{B}_{12}$  icosahedra is again considered. The metal-metal spacing of the magnetic gadolinium atoms along the  $\text{B}_{12}$  icosahedra

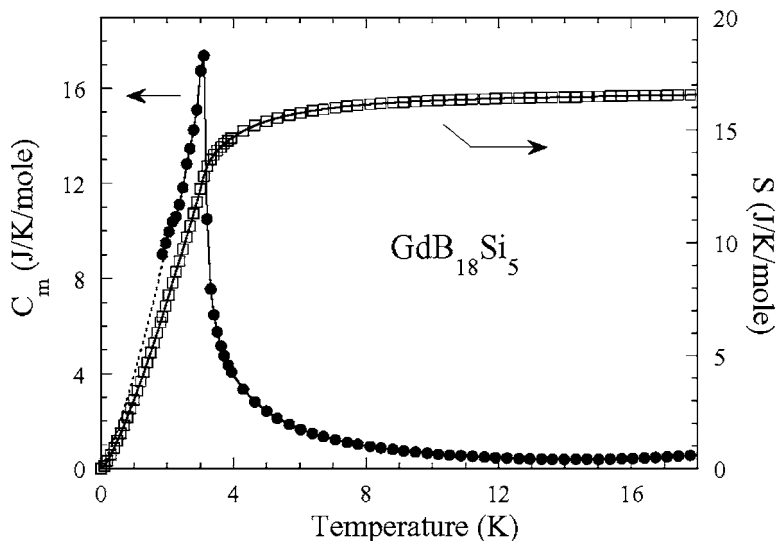


**FIGURE 33** The temperature dependence of the magnetic specific heat  $C_m$  (●) and entropy  $S$  (□) of  $\text{GdB}_{18}\text{Si}_5$  (Mori and Zhang, 2002).

is  $5.04 \text{ \AA}$  for  $\text{GdB}_{18}\text{Si}_5$  which has  $T_N = 3.2 \text{ K}$ . This is shorter than the spacing for  $\text{RB}_{25}$  of  $\sim 5.73 \text{ \AA}$  in which  $\text{GdB}_{25}$  does not have a transition down to  $1.8 \text{ K}$  and in which  $\text{TbB}_{25}$  has a transition at  $T_N = 2.1 \text{ K}$ . The spacing of the icosahedra in  $\text{GdB}_{18}\text{Si}_5$  is sizably longer than the shortest spacing along the  $B_{12}$  icosahedra for  $\text{RB}_{50}$  of  $\sim 4.31 \text{ \AA}$  where  $\text{TbB}_{50}$  has a transition at  $T_N = 17 \text{ K}$  (the  $\text{GdB}_{50}$  phase, unfortunately, does not exist). The transition temperature (magnitude of magnetic interaction) of  $\text{GdB}_{18}\text{Si}_5$  appears to be explainable with the picture where the  $B_{12}$  icosahedra are mediating the effective magnetic interaction. We note that this dependence is not followed by the  $\text{R-B-C(N)}$  compounds which have a separation of around  $5.6 \text{ \AA}$  in the 2D triangular layers, but exhibit the largest Curie-Weiss temperatures. However, frustration or some kind of anisotropic effect may be playing a role for these compounds. Further work to elucidate the mechanism of magnetic interaction in these lanthanide icosahedra borides is definitely necessary.

It is interesting that in the  $\text{RB}_{18}\text{Si}_5$  system, the Gd phase has a transition at  $3.2 \text{ K}$  with no transition above  $1.8 \text{ K}$  for the Tb phase, while the  $\text{RB}_{25}$  phase shows opposite behavior with a transition only observed for the Tb phase. This is an indication of the effect of the anisotropy of the lanthanide ions (in the Gd case, a lack of anisotropy) on the magnetic interaction and should be useful toward solving the explicit mechanism.

#### 10.4 Field dependence

The magnetic field dependence of the susceptibility of  $\text{GdB}_{18}\text{Si}_5$  was determined for the field applied along the  $c$ -axis, see Figure 34. As is typical for antiferromagnetic transitions, the transition temperature  $T_N$  shifts to lower temperatures as the

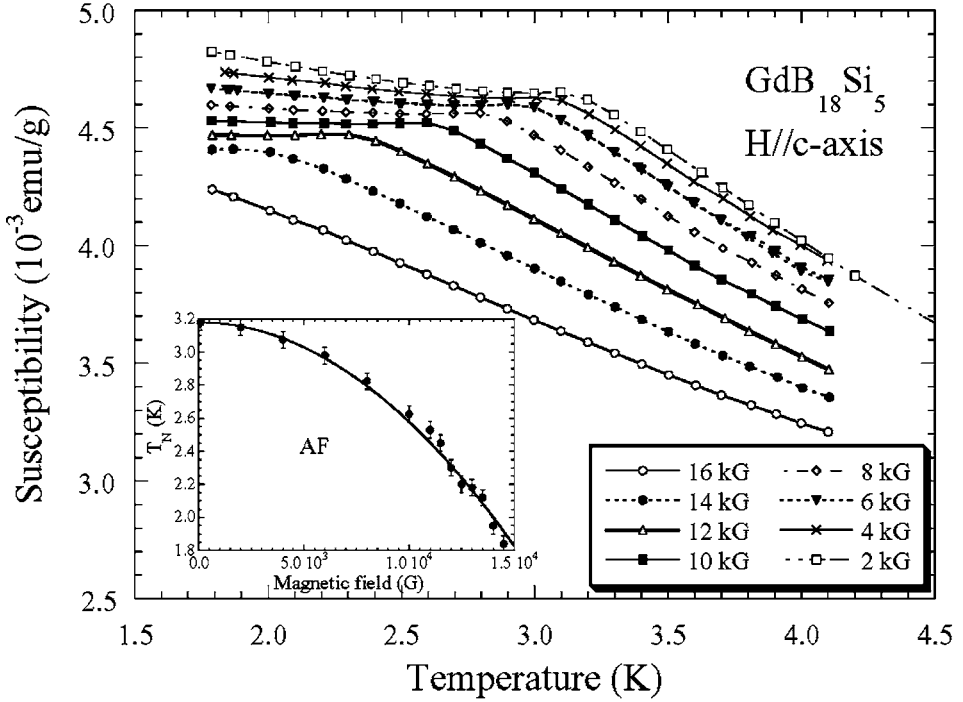


**FIGURE 34** The temperature dependence of the  $c$ -axis magnetic susceptibility of  $\text{GdB}_{18}\text{Si}_5$  for 16 kG (○), 14 kG (●), 12 kG (△), 10 kG (■), 8 kG (◇), 6 kG (▼), 4 kG (×), and 2 kG (□). The lines are guides to the eye. The inset shows the fit to Eq. (10),  $T = T_N(1 - (H/H_C)^2)$ , with  $T_N$  set as 3.18 K (determined from the low field measurement data) and the parameter  $H_C$  determined to be 23 kG (Mori, 2005a).

magnetic field is increased. The general magnitude of field corresponds to the temperature scale. If we assume a simple quadratic suppression of  $T_N$  due to magnetic fields as determined, for example, by Shapira and Foner (1970), we can obtain a fitting curve as given in the inset of Figure 34.

$$T = T_N(1 - (H/H_C)^2). \quad (10)$$

In this case, setting  $T_N$  as 3.18 K as determined from the low field measurements, the critical field  $H_C$  at which  $T_N$  goes to zero is estimated to be  $H_C = 23$  kG. This estimated absolute value of  $H_C$  matches the magnitude of order which is expected for local moment antiferromagnets:  $H_C \sim k_B T_N / \mu_B$ .

An interesting dependence at low magnetic fields was observed when the field was varied in-plane (Figures 35 and 36), with a reorientation of the spins, i.e. a spin flip appears to occur at fields below 300 G. The origin of this behavior is likely due to the spherical nature of the  $4f$  electrons cloud of the gadolinium ions, but the actual observation of a spin flip at such low magnetic fields is interesting and unusual (Mori, 2005a).

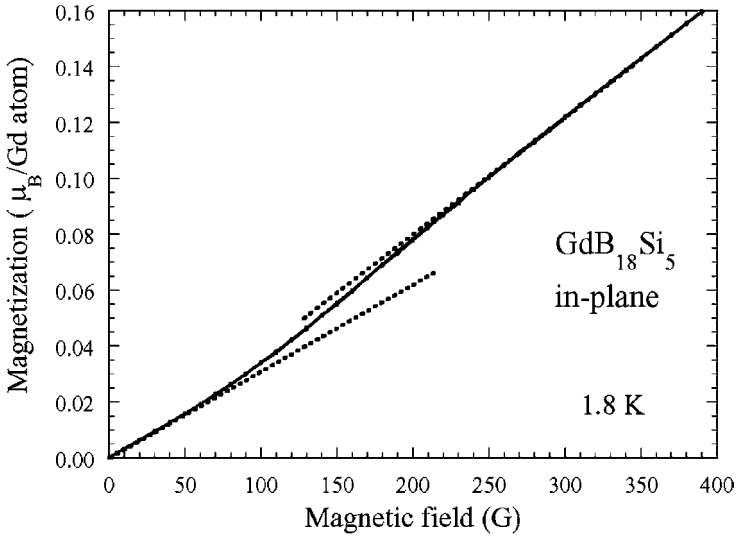


**FIGURE 35** The low field magnetization curve of GdB<sub>18</sub>Si<sub>5</sub> with the field applied in-plane at 1.8 K. The dotted lines are guides to the eye (Mori, 2005a).

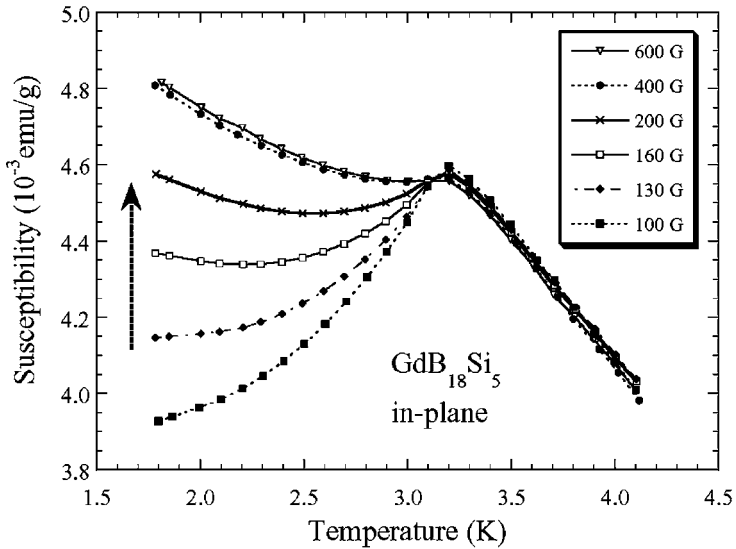


**FIGURE 36** The temperature dependence of the magnetic susceptibility of GdB<sub>18</sub>Si<sub>5</sub> with field applied in-plane for 600 G ( $\nabla$ ), 400 G ( $\bullet$ ), 200 G ( $\times$ ), 160 G ( $\square$ ), 130 G ( $\blacklozenge$ ), and 100 G ( $\blacksquare$ ) (Mori, 2005a).

To summarize the results of RB<sub>18</sub>Si<sub>5</sub> compounds, the addition of silicon lead to the formation of new B<sub>12</sub> icosahedra compounds, and as a result, the first 3 dimensional long range order in icosahedra borides was discovered. The rare earth sites

**TABLE 10** Crystallographic data of scandium higher borides

	Crystal system	Space group	<i>a</i> (Å)	<i>b</i> (Å)	<i>c</i> (Å)	References
ScB <sub>19</sub>	Tetragonal	<i>P4</i> <sub>1</sub> <i>2</i> <sub>1</sub> <i>2</i> or <i>P4</i> <sub>3</sub> <i>2</i> <sub>1</sub> <i>2</i>	10.292	–	14.246	Tanaka et al. (1998)
ScB <sub>17</sub> C <sub>0.25</sub>	Hexagonal	<i>P6/mmm</i>	14.550	–	8.954	Leithe-Jasper et al. (2000)
Sc <sub>4.5-x</sub> B <sub>57-y+z</sub> C <sub>3.5-z</sub> ( <i>x</i> = 0.27, <i>y</i> = 1.1, <i>z</i> = 0.2)	Orthorhombic	<i>Pbam</i>	17.304	10.325	14.483	Tanaka et al. (2002)
Sc <sub>3.67-x</sub> B <sub>41.4-y-z</sub> C <sub>0.67+z</sub> Si <sub>0.33-w</sub> ( <i>x</i> = 0.52, <i>y</i> = 1.42, <i>z</i> = 1.17, <i>w</i> = 0.02)	Hexagonal	<i>P6̄ma</i>	14.306	–	23.748	Tanaka et al. (2004)

have rather low occupancy in RB<sub>18</sub>Si<sub>5</sub>, and elucidation of the magnetic structure should be worthwhile. The magnitude of the magnetic interaction of RB<sub>18</sub>Si<sub>5</sub> in comparison with RB<sub>50</sub>-type compounds and RB<sub>25</sub> compounds is consistent with the picture of the B<sub>12</sub> icosahedra mediating the magnetic interaction. (The R–B–C(N) compounds do not follow this dependence, however, they are systems with a strong frustration.)

## 11. Sc HIGHER BORIDES

As noted in previous sections, the scandium phases of compounds have sometimes been observed to have different structures compared to the other rare earths, because of the relatively small size of scandium. The scandium higher borides have been found to be a particular fertile ground for the formation of new higher boride structures.

Compounds such as ScB<sub>19</sub>, ScB<sub>17</sub>C<sub>0.25</sub>, Sc<sub>4.5-x</sub>B<sub>57-y+z</sub>C<sub>3.5-z</sub>, and Sc<sub>3.67-x</sub>B<sub>41.4-y-z</sub>C<sub>0.67+z</sub>Si<sub>0.33-w</sub> have been discovered. ScB<sub>19</sub> is tetragonal (space group *P4*<sub>1</sub>*2*<sub>1</sub>*2* or *P4*<sub>3</sub>*2*<sub>1</sub>*2*) (Tanaka et al., 1998) and isotypic with the  $\alpha$ -AlB<sub>12</sub> structure type. ScB<sub>17</sub>C<sub>0.25</sub> is hexagonal (space group *P6/mmm*) and while the basic structure is formed by the boron icosahedra arrangement, an interesting tubular configuration of boron atoms along the *c*-axis was found (Leithe-Jasper et al., 2000). Sc<sub>4.5-x</sub>B<sub>57-y+z</sub>C<sub>3.5-z</sub> (*x* = 0.27, *y* = 1.1, *z* = 0.2) is orthorhombic (space group *Pbam*) (Tanaka et al., 2002) and Sc<sub>3.67-x</sub>B<sub>41.4-y-z</sub>C<sub>0.67+z</sub>Si<sub>0.33-w</sub> (*x* = 0.52, *y* = 1.42, *z* = 1.17, *w* = 0.02) is hexagonal (space group *P6̄ma*) (Tanaka et al., 2004). Both have complicated structures with six and seven structurally independent boron icosahedra, respectively, in addition to other kinds of boron polyhedra. The lattice constants for all these scandium higher borides are listed in Table 10.

Growing single crystals of any of these compounds in large size and good quality have proven to be difficult and the physical properties of these scandium higher borides have not been investigated in detail yet. Resistivity measurements on a  $\text{Sc}_{3.67-x}\text{B}_{41.4-y-z}\text{C}_{0.67+z}\text{Si}_{0.33-w}$  crystal which contained inclusions of impurities, showed variable range hopping behavior (Mori et al., unpublished), which is typically observed in boron icosahedra borides, as described in this review.

## 12. THERMOELECTRIC PROPERTIES OF HIGHER BORIDES

In recent years the search for new thermoelectric materials has been carried out with great intensity, not least because of the huge possibilities for useful energy conversion of waste heat, and the needs of modern society where the limits of classical energy resources are rapidly being reached (e.g. Kanatzidis, 2003; Nolas et al., 2001; Rowe, 1995).

There is obviously a particular need to develop materials which can function at high temperatures. Due to their strong covalent bonding, boron cluster compounds generally possess attractive mechanical properties as materials, e.g. stability under high temperature due to their high melting points (typically >2300 K), chemical stability, resistance to acidic conditions, and small compressibility. Furthermore, importantly, the  $\text{B}_{12}$  icosahedra compounds have also been found to have intrinsic low thermal conductivity, as will be discussed in detail in later sections, and which is desirable for thermoelectric applications.

Indeed, focusing on this low thermal conductivity, Slack et al. have investigated boron cluster compounds like beta boron,  $\text{YB}_{66}$  among others, as possible embodiments of the “electron crystal phonon glass” systems that they have proposed (Slack et al., 1971; Cahill et al., 1989).

Other boron cluster compounds like boron carbide (e.g. Wood and Emin, 1984) and doped  $\beta$ -boron (Werheit et al., 1981; Slack et al., 1987) have also been studied as possible thermoelectric materials. Boron carbide in particular has been discovered to be an exemplar p-type high temperature thermoelectric compound (see the review by Aselage and Emin, 2003). In the following sections, the thermoelectric properties (focusing on the high temperature) of some of the higher rare earth borides discussed in this review are presented. It is noted that the boron cluster compounds which contain the heavy lanthanide elements (i.e.  $\text{RB}_{66}$ ,  $\text{RB}_{44}\text{Si}_2$ ) appear to have a lower thermal conductivity than those that do not contain metal atoms (i.e. boron carbide,  $\beta$ -boron). This can be considered to be a good starting point for the development of thermoelectric properties.

### 12.1 $\text{RB}_{66}$

The thermal properties of  $\text{RB}_{66}$  were first measured by Slack et al. (1971). The thermal conductivity  $\kappa$  of  $\text{RB}_{66}$  takes low values (e.g.  $\sim 0.02$  W/(cm K) at room

temperature) and shows a behavior characteristic of amorphous solids at low temperatures, despite the fact that it is a crystalline compound (Slack et al., 1971; Cahill et al., 1989). A high Debye temperature of 1340 K has been determined for YB<sub>66</sub>. RB<sub>66</sub> is p-type and large Seebeck coefficients  $\alpha$  (e.g.  $\sim 600$   $\mu\text{V}/\text{K}$  for ErB<sub>66</sub>) have been observed at room temperature (Golikova, 1987) but the temperature dependence of  $\alpha$  shows a decrease at higher temperatures for RB<sub>66</sub> (Golikova, 1987; Mori, 2005b).

The power factors of RB<sub>66</sub> are not high because of the poor electrical conductivity of the compounds.

## 12.2 Doping of YB<sub>66</sub>

Doping has been investigated extensively for compounds like  $\beta$ -boron and boron carbide to try to modify their thermoelectric properties (e.g., Werheit et al., 1981; Slack et al., 1987; Aselage and Emin, 2003). There have not been as many attempts to dope the rare earth higher borides, we are only aware of transition metal doping into YB<sub>66</sub> (Tanaka et al., 2000, 2006; Mori and Tanaka, 2006).

The thermal conductivity (Tanaka et al., 2006) and thermoelectric properties (Mori and Tanaka, 2006) of Nb-doped YB<sub>66</sub> have particularly been investigated because good quality crystals can be grown for the dopant Nb. Doped Nb atoms replace a boron dumbbell pair in the B13 site of (0.235, 0.235, 0.235), following the numbering scheme of (Higashi et al., 1997b) which is located inside the B<sub>80</sub> cluster, see Section 6.1. The Nb-doping has been found to result in an increase of the thermal conductivity by around a factor of 2. The reason for the increase in  $\kappa$  is proposed to be due to the replacement of the boron pair site which is speculated to lower the thermal conductivity. The resistivities of the undoped and Nb-doped samples follow the 3D VRH law;  $\rho = \rho_0 \exp[(T_0/T)^{0.25}]$  as shown in Figure 37(a). The  $T_0$  values are lower for Nb-doped YB<sub>66</sub>, indicating that  $D(E_F)$  increases or the localization length  $\xi$  elongates with the doping.

Corresponding to the doping and the resistivity behavior, the Seebeck coefficients also undergo variation, as discussed in detail (Mori and Tanaka, 2006) and plotted in Figure 37(b). Regarding the thermoelectric power factor  $P = \alpha^2/\rho$ , the compound with 89% Nb dopant occupancy shows an increase by factor 3 over the non-doped sample at room temperature (Figure 38). However, in the high temperature region, which is the important temperature region for these compounds, the non-doped sample actually exhibits the highest power factor for  $T > 550$  K. This result is interesting insofar that it shows that in the case of these compounds it can actually be worth striving for a high  $T_0$  even at the price of a higher resistivity and thus a lower power factor at lower temperatures. Even though  $\rho_0$  is large, at high temperatures there can be reversals due to the large value of  $T_0$  and the variable range hopping mechanism.

The gauge of the attractiveness of a thermoelectric material is given by the figure of merit ZT;

$$ZT = \alpha^2/\rho/\kappa, \quad (11)$$

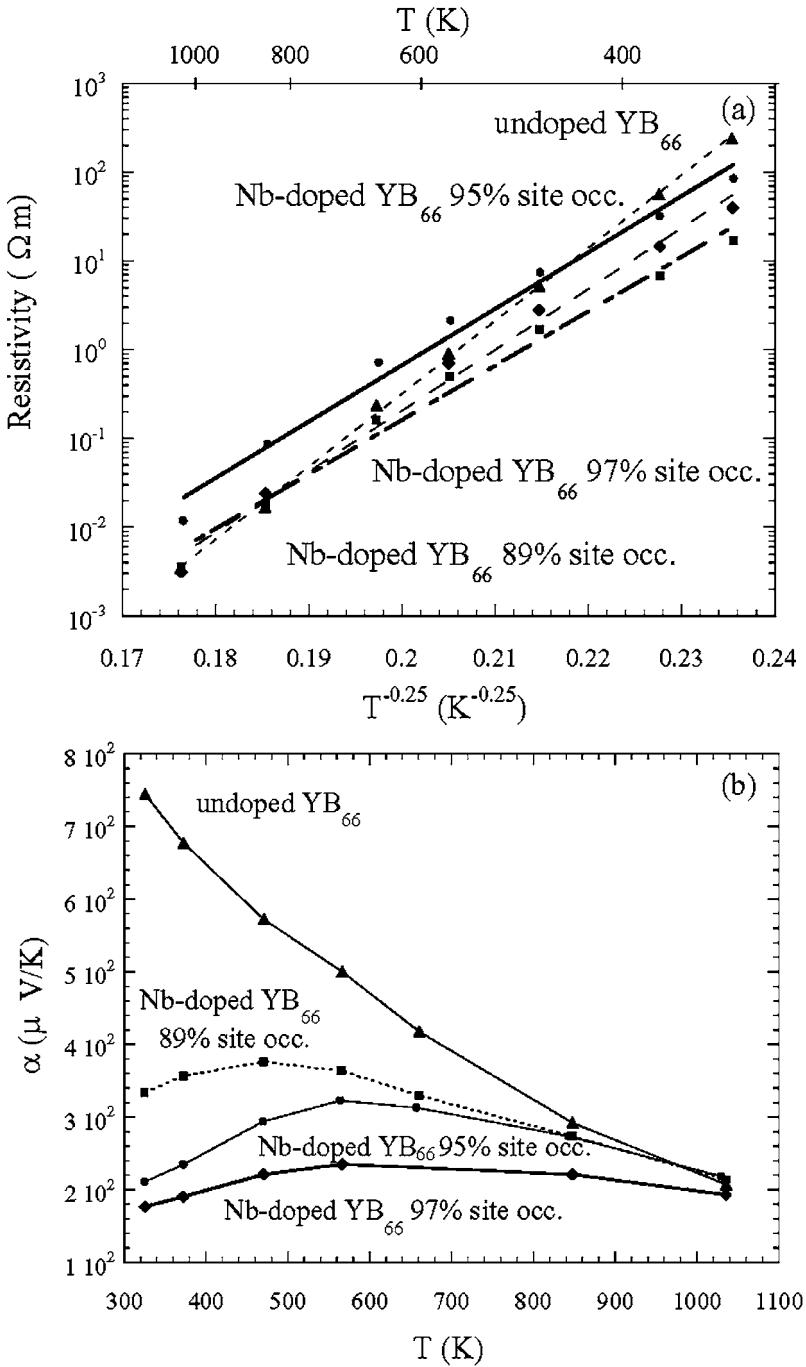


**FIGURE 37** The temperature dependence of the (a) resistivity  $\rho$  and (b) Seebeck coefficient  $\alpha$  of undoped (▲) and Nb-doped  $\text{YB}_{66}$  compounds; 89% occupancy (■), 95% occupancy (●), and 97% occupancy (◆) in the 3D VRH plot (Mori and Tanaka, 2006).

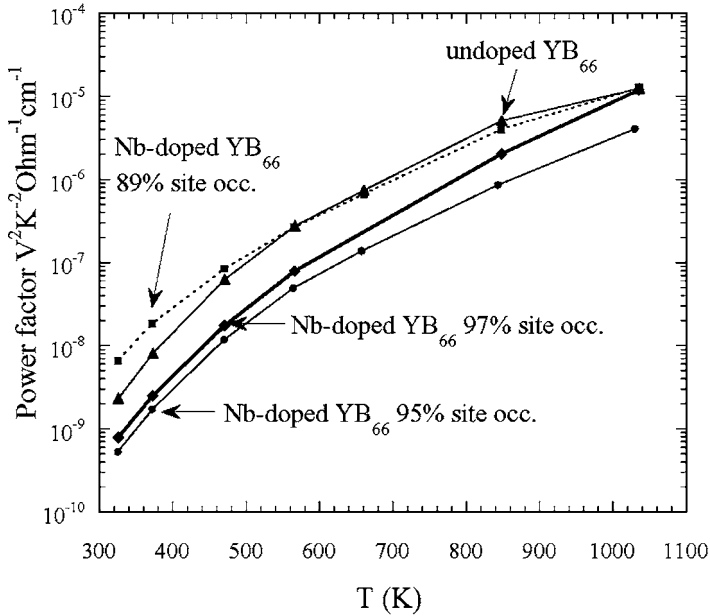


**FIGURE 38** The temperature dependence of the power factor of undoped ( $\blacktriangle$ ) and Nb-doped  $\text{YB}_{66}$  compounds; 89% occupancy ( $\blacksquare$ ), 95% occupancy ( $\bullet$ ), and 97% occupancy ( $\blacklozenge$ ) (Mori and Tanaka, 2006).

where  $\kappa$  is the thermal conductivity. The high temperature results for the power factor  $\alpha^2/\rho$  given above, together with the increase in the thermal conductivity in doped samples indicate that  $\text{YB}_{66}$  is not a feasible system to pursue among the rare earth boron cluster compounds for high temperature thermoelectric applications.

However, carbon doping was found to decrease the thermal conductivity of  $\text{YB}_{66}$  while not having a sizable detrimental effect on the other properties, and this could be a powerful method for improving the thermoelectric properties of higher borides in general (Mori and Tanaka, 2006).

### 12.3 $\text{RB}_{44}\text{Si}_2$ ( $\text{RB}_{50}$ -type) compounds

The low temperature thermoelectric properties of  $\text{YB}_{44}\text{Si}_2$  were first investigated by Ishizawa and Tanaka (2000), but were found not to be particularly attractive, because they were far from being competitive with good thermoelectric materials at these temperature ranges. The high temperature properties were investigated for a series of  $\text{RB}_{44}\text{Si}_2$  crystals (Mori, 2005b). The high temperature resistivities and thermopowers, i.e. Seebeck coefficients,  $\alpha$  of  $\text{RB}_{44}\text{Si}_2$  crystals are plotted in Figures 39 and 40, respectively. As noted before in Section 7.2, up to now, the  $\text{RB}_{44}\text{Si}_2$  crystals that have been grown are not single crystals but are crystals with grains. Therefore, a sample/measurement technique (i.e. configuration of electrodes) dependence is sometimes observed. Due to the polycrystalline nature of the samples, the presently obtained values can be considered to be a lower limit of the electrical

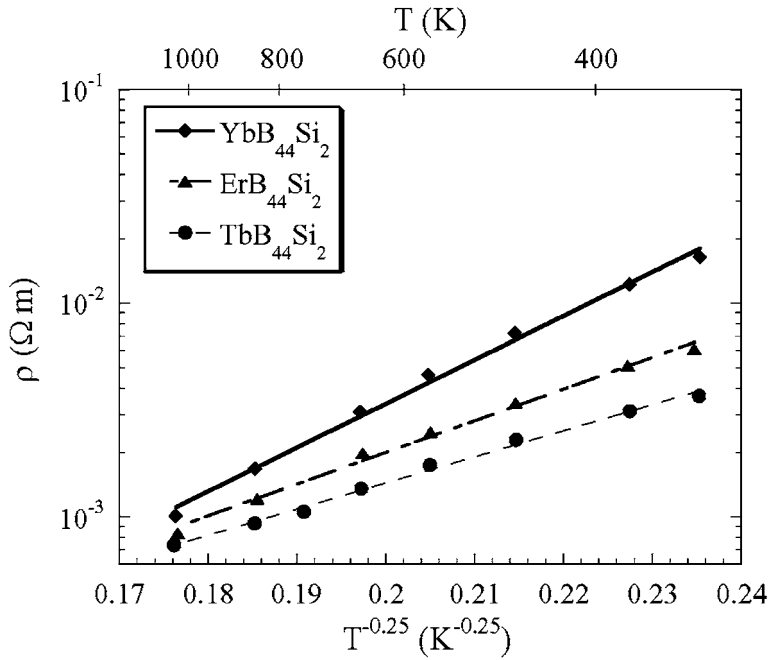


**FIGURE 39** The temperature dependence of the high temperature resistivity,  $\rho$ , of these  $RB_{44}Si_2$  crystals with  $R = Tb$  (●),  $Er$  (▲),  $Yb$  (◆) (Mori, 2005a).

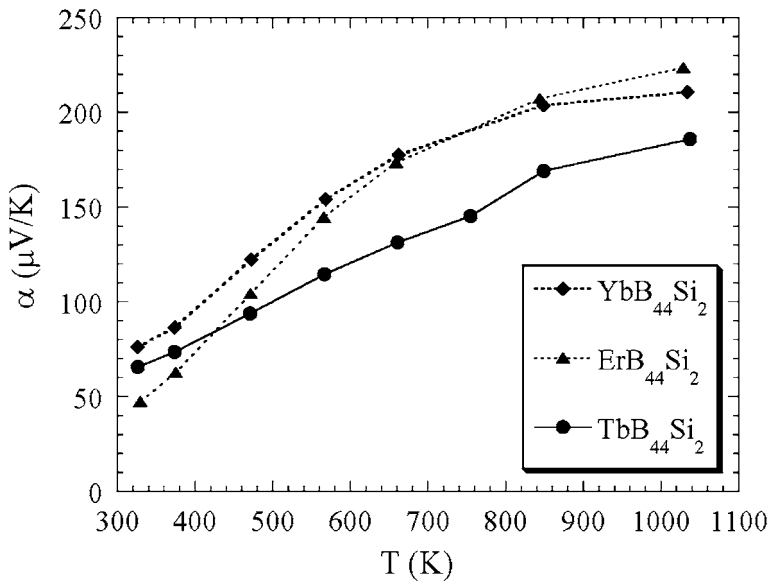


**FIGURE 40** The temperature dependence of the Seebeck coefficient,  $\alpha$ , of these  $RB_{44}Si_2$  crystals with  $R = Tb$  (●),  $Er$  (▲),  $Yb$  (◆) (Mori, 2005a).

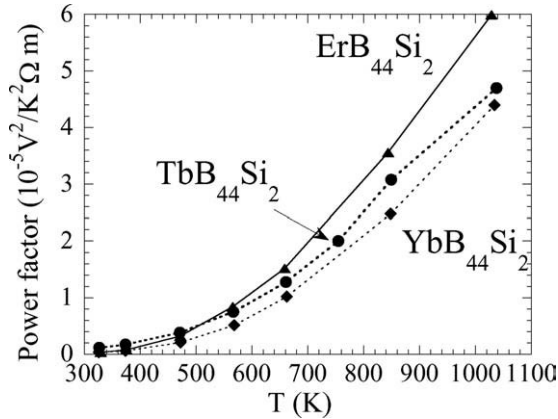


**FIGURE 41** The temperature dependence of the power factor of  $\text{RB}_{44}\text{Si}_2$  crystals with  $\text{R} = \text{Tb}$  (●),  $\text{Er}$  (▲),  $\text{Yb}$  (◆) (Mori, 2005a).

conductivity of these compounds and one can expect them to improve with the development of techniques for the successful growth of single crystals.

With regard to the Seebeck coefficient,  $\alpha$  increases monotonically as temperature is increased and takes on large values exceeding  $200 \mu\text{V}/\text{K}$  at  $1000 \text{ K}$  (see Figure 40). This temperature dependence is an attractive characteristic for high temperature use, since the  $\text{RB}_{44}\text{Si}_2$  compounds actually have high melting points of approximately  $2300 \text{ K}$ .  $\text{RB}_{44}\text{Si}_2$  is a p-type conductor which is the same as that of all the icosahedra borides unless they are highly doped with transition metal elements (Emin, 2004).

Figure 41 shows the temperature dependence of the power factor  $\alpha^2/\rho$  of  $\text{RB}_{44}\text{Si}_2$ . The power factor shows a sharp rise at the higher temperatures ( $>800 \text{ K}$ ). Although the absolute values are not large, it should be noted that these are relatively new compounds and attempts to improve the properties, i.e. doping optimization of composition, and improved sample preparation techniques, are yet to be explored. Being cluster compounds, boron cluster compounds typically have open spaces among the clusters and should relatively readily accommodate dopants. As noted above, transition metal doping has been a technique used to successfully modify the properties of  $\beta$ -boron (Werheit et al., 1981; Slack et al., 1987). In any case,  $\text{RB}_{44}\text{Si}_2$  is found to have a much higher power factor than  $\text{RB}_{66}$  (Mori, 2005b).

From Eq. (11), an obviously desirable characteristic for thermoelectric materials is to have low thermal conductivity  $\kappa$ . The thermal diffusivity constant,  $D_t$ , of  $\text{ErB}_{44}\text{Si}_2$  has been found to have small values of  $D_t \leq 1.1 \times 10^{-2} \text{ cm}^2/\text{s}$  (Mori, 2006c). These values are significantly smaller than what has been observed for boron carbide samples (Wood et al., 1985). Although no data exists for the sound velocities of  $\text{ErB}_{44}\text{Si}_2$ , the velocities are probably high since borides are typically hard materials. Therefore, the small values of  $D_t$  indicate extremely short phonon

mean free paths in this compound.  $\kappa$  can be determined from the relation

$$\kappa = C \cdot D_t \cdot d, \quad (12)$$

where  $d$  is the density and  $C$  is the specific heat. The thermal conductivity of  $\text{ErB}_{44}\text{Si}_2$  is low, having values of  $\kappa \sim 1.5 \times 10^{-2}$  W/(cm K). These values are even smaller than those obtained for  $\text{RB}_{66}$  and an order lower than  $\beta$ -boron (Cahill et al., 1989) and boron carbide (Wood et al., 1985) which are  $\text{B}_{12}$  compounds but do not contain heavy metal atoms. As noted in previous sections, the thermoelectric properties of  $\text{RB}_{66}$  have been found to be largely inferior to  $\text{RB}_{44}\text{Si}_2$ . Therefore, in  $\text{RB}_{44}\text{Si}_2$  we have a compound which retains the characteristic low thermal conductivity of the  $\text{B}_{12}$  icosahedral borides (e.g.  $\text{RB}_{66}$ ) while they have an improved resistivity and high temperature thermopower.

It has been proposed for skutterudite and clathrate compounds that the metal atoms in the light atomic matrix act as “rattlers” (Slack and Tsoukala, 1994), namely phonon scatterers, and result in a very low thermal conductivity, and this has actually been observed (e.g., Sales et al., 1997; Nolas et al., 2002). The apparent tendency among the boron cluster compounds containing rare earth atoms to have lower thermal conductivity than those that do not, has been noted. One wonders whether or not, the rare earth atoms in the higher borides are functioning as rattlers. The equivalent isotropic thermal parameter of the rare earth atoms in  $\text{RB}_{44}\text{Si}_2$ , for example, has a rather large value ( $B = 0.22 \text{ \AA}^2$ ), however, it is not especially large compared to the matrix boron atoms themselves.

Another factor, which should be taken into account for the higher borides, is the compositional disorder. As noted in previous sections, partially occupied boron sites typically exist in these compounds (albeit not in the icosahedra). Furthermore, the rare earth sites are also partially occupied for some compounds. In the case of  $\text{RB}_{44}\text{Si}_2$ , the rare earth sites have full occupancy, however, Si partially replaces B in the  $\text{B}_{12}\text{Si}_3$  polyhedron and causes additional disorder. The effects of compositional disorder on the thermal conductivity in a series of boron carbide samples with different carbon content have actually been observed (Wood et al., 1985). They observe that the thermal conductivity decreases as carbon content is reduced from 20 at%. Since the reduction of carbon translates to C–B–C chains being replaced in part by C–B–B chains, this is thought to introduce disorder into the system. Additional systematic studies into the thermal conductivity of other newly discovered rare earth boron icosahedra compounds should shed more light on the “rattler” question in higher borides. A recent study (Mori et al., 2007a) has evaluated the various mechanisms (i.e. disorder, “rattling”, crystal complexity) in a comparison of the low temperature thermal conductivities of  $\text{RB}_{66}$  and  $\text{RB}_{44}\text{Si}_2$  and concludes that disorder is having a dominant effect.

The figure of merit  $ZT$  of  $\text{ErB}_{44}\text{Si}_2$  which had the highest power factor among the investigated  $\text{RB}_{44}\text{Si}_2$  phases, is given in Figure 42. At 1000 K,  $ZT$  reaches a value of  $ZT \sim 0.04$ . Although this value is not high compared for example to  $ZT \sim 1$  for the well known thermoelectric material bismuth telluride at room temperature, the high temperature stability of borides should be noted, and attractively, the trend of the temperature dependence of  $ZT$  shows a sharp increase

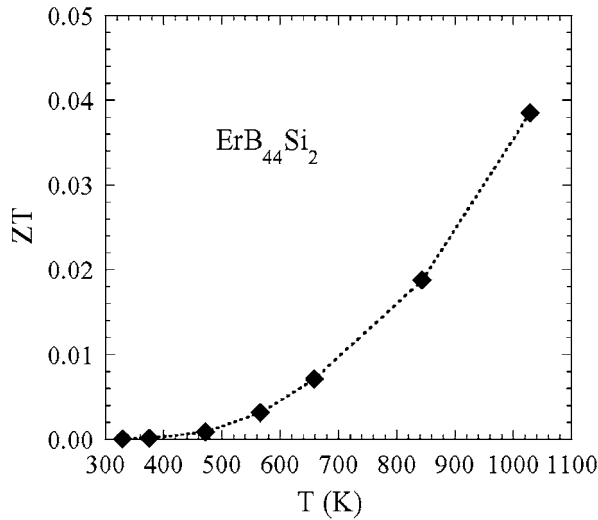


**FIGURE 42** The temperature dependence of the figure of merit, ZT, of  $\text{ErB}_{44}\text{Si}_2$  (Mori, 2006c).

with increasing temperatures, especially above 1000 K. This compound has a melting point of around 2300 K, and if we assume a simple polynomial extrapolation to 1500 K we obtain a ZT of  $\sim 0.12$  (Mori, 2006c). This is actually about half of the ZT value of an optimally carbon concentration controlled (“doped”) boron carbide compound (Aselage and Emin, 2003). Investigation on modifying/doping the  $\text{RB}_{44}\text{Si}_2$  compounds to improve their properties should be carried out, since  $\text{RB}_{44}\text{Si}_2$  may be a viable p-type replacement for boron carbide for high temperature thermoelectric applications, and it can be readily melted in the processing stage.

#### 12.4 Homologous R–B–C(N) compounds: $\text{RB}_{15.5}\text{CN}$ , $\text{RB}_{22}\text{C}_2\text{N}$ , $\text{RB}_{28.5}\text{C}_4$

As noted previously in Section 9, the homologous R–B–C(N) compounds are two dimensional magnetically frustrated systems (Mori and Leithe-Jasper, 2002; Mori and Mamiya, 2003; Mori et al., 2004b). Dresselhaus et al. (1999) have proposed that low dimensional systems can have enhanced thermoelectric properties. While the coupling between the transport properties and magnetic properties is not clear for this particular system, this was the motivation to investigate the thermoelectric properties of this series of compounds (Mori and Nishimura, 2006). The  $\text{RB}_{15.5}\text{CN}$ ,  $\text{RB}_{22}\text{C}_2\text{N}$ , and  $\text{RB}_{28.5}\text{C}_4$  compounds will not melt stably to form large size crystals. Therefore, polycrystalline powders were hot pressed for transport measurements. Although conventional hot press techniques may only yield a solid of a relatively low density of approximately 50% of the theoretical value, important features may be made clear. The temperature dependence of the thermopower  $\alpha$ , for some of the R–B–C(N) compounds are plotted in Figure 43. The most striking result is that n-type behavior is observed for  $\text{RB}_{22}\text{C}_2\text{N}$  and  $\text{RB}_{15.5}\text{CN}$  phases. Starting with boron carbide, the boron icosahedra com-

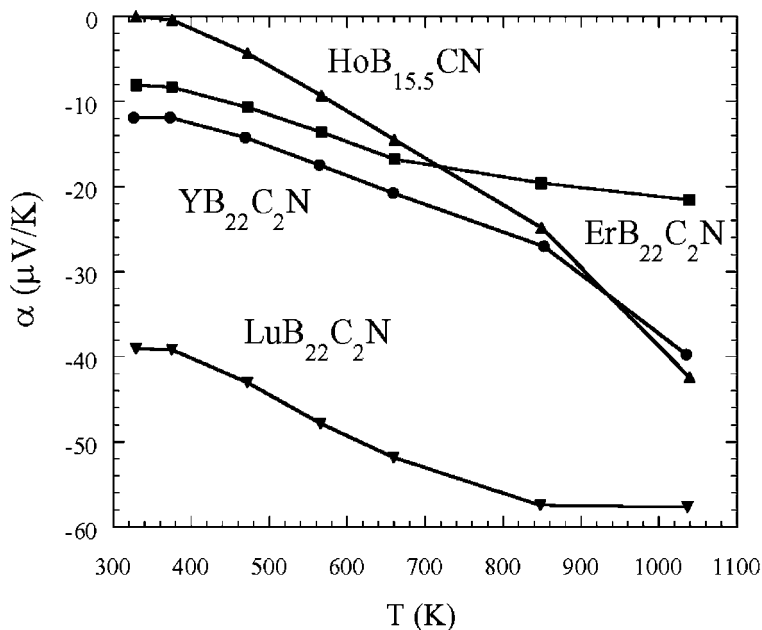


**FIGURE 43** The temperature dependence of the Seebeck coefficient,  $\alpha$ , for hot pressed  $\text{HoB}_{15.5}\text{CN}$  and  $\text{RB}_{22}\text{C}_2\text{N}$  ( $\text{R} = \text{Er}, \text{Lu}, \text{and } \text{Y}$ ) (Mori and Nishimura, 2006).

pounds previously discovered had all shown p-type behavior, unless doped with large amounts of foreign elements like transition metals (Werheit et al., 1981; Slack et al., 1987). The p-type behavior was shown to be an intrinsic characteristic in normal boron icosahedra compounds (Emin, 2004). The behavior reported for  $\text{RB}_{22}\text{C}_2\text{N}$  and  $\text{RB}_{15.5}\text{CN}$  was the first example of n-type behavior observed for a non-doped higher boride (Mori and Nishimura, 2006). The compounds are non-doped and therefore, leave open conventional avenues of doping to further improve the properties. The discovery of an n-type compound is extremely important in terms of the potential development of this class of compounds as viable thermoelectric materials. Thermoelectric devices will typically use p and n-type legs, and boron carbide has already been discovered to be an exemplar p-type high temperature thermoelectric compound.

As noted in Section 9, the structures of the R-B-C(N) compounds (Figure 21) are homologous to that of boron carbide which exhibits typical p-type characteristics. Boron carbide is the limit where the number of boron icosahedra and C-B-C chain layers separating the metal layers reaches infinity (i.e. no rare earth layers). It has been speculated that the 2 dimensional metal layers of these rare earth R-B-C(N) compounds are playing a role for the unusual n-type behavior, but the mechanism is not yet clear.

The absolute values of the thermopower of the R-B-C(N) phases are not as large as that of boron carbide (Wood and Emin, 1984) or  $\text{RB}_{44}\text{Si}_2$  (Mori, 2005b) but they appear to generally increase with increasing temperature up to temperatures

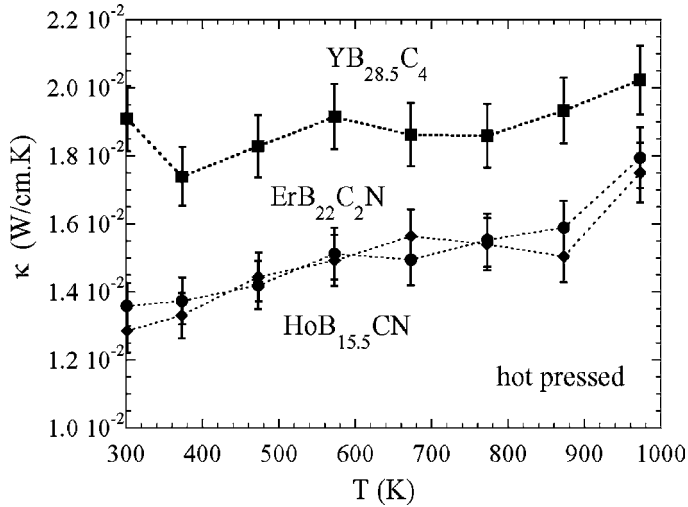


**FIGURE 44** The temperature dependence of the thermal conductivity,  $\kappa$ , for hot pressed HoB<sub>15.5</sub>CN, ErB<sub>22</sub>C<sub>2</sub>N, and YB<sub>28.5</sub>C<sub>4</sub> samples (Mori and Nishimura, 2006).

exceeding 1000 K. The conventionally hot pressed samples had a low density, and accordingly, a very high resistivity which led to a low power factor. It should be noted that the low density of the hot pressed samples will not be a factor in the intrinsic n-type behavior which was observed.

The thermal conductivities  $\kappa$  of the hot pressed HoB<sub>15.5</sub>CN, ErB<sub>22</sub>C<sub>2</sub>N, and YB<sub>28.5</sub>C<sub>4</sub> samples (see Figure 44) have quite low values (e.g. 0.013 W/(cm K) at room temperature for HoB<sub>15.5</sub>CN), but the low densities of the samples, of course, plays a role. However, measurements for denser compounds prepared by SPS (spark plasma synthesis) showed a relatively small increase of around factor 2, while exhibiting an improvement of the resistivity of close to 2 orders. This indicates that these phases are also basically low thermal conductivity compounds like the other rare earth boron cluster compounds. The hot pressed samples shown in Figure 44 have relatively low densities, but were all prepared by the same method and have similar percentage of the respective theoretical densities and therefore, this enables a comparison between the different homologous phases. Although the  $\kappa$  values for HoB<sub>15.5</sub>CN and ErB<sub>22</sub>C<sub>2</sub>N are close, it appears there is a dependence on the homologous series with the thermal conductivity increasing as the number of boron cluster layers increase, which is interesting since it could indicate that the metal atoms are playing a role to depress thermal conductivity (Mori and Nishimura, 2006). However, a dependence on the relative masses of the rare earth atoms may also exist, and it is necessary to make a comprehensive investigation on the rare earth series before a definite conclusion can be made.

As noted, the figures of merit of the conventionally hot pressed samples were not high, due to the high resistivity of the samples with relatively low density. However, the temperature dependence shows an attractive increase with increasing temperature above 1000 K similar to the other rare earth boron cluster com-

pounds. Furthermore, the initial results obtained were for compounds “as is” and properties are expected to improve with further research. The important result obtained was that an n-type higher boride compound was discovered for the first time without the need of aggressive doping, as a starting point for further investigations.

Indeed, recently two techniques were discovered for dramatically improving the thermoelectric properties of the first n-type boron cluster compounds;  $\text{RB}_{15.5}\text{CN}$  and  $\text{RB}_{22}\text{C}_2\text{N}$ . Spark plasma synthesis (SPS) was found to be an effective method to densify the samples compared to conventional hot pressing, while seeding the sample with small amounts of metal borides like  $\text{RB}_4$  and  $\text{RB}_6$  was also discovered to improve the properties (Mori et al., 2007b). Due to these improvements the power factor of some of these compounds improved by factors varying up to over two orders. The seeding method showed less increase in the thermal conductivity and appears to be a powerful processing technique. Furthermore, these preparation methods do not rely on the conventional transition metal doping-technique used for borides, and leaves room for further improvement since these are cluster compounds and readily accommodate foreign dopants on an atomic level in the voids.

Recent investigations have revealed that the intrinsic behavior of  $\text{RB}_{28.5}\text{C}_4$  is also n-type (Mori et al., 2008a). Very small inclusions of boron carbon “ $\text{B}_4\text{C}$ ” can cause the p-type behavior previously observed in some samples (Mori and Nishimura, 2006). The origin of the striking n-type behavior observed in the homologous R–B–C(N) compounds is not completely resolved yet but indicated to pertain to the two-dimensional rare earth layers (Mori et al., 2008a).

Although the presently obtained absolute values of power factors still need to be improved, these compounds may offer a n-type boride counterpart to the well known p-type boron carbide which is one of the few thermoelectric material viable for extremely high temperature use (1500 K), and further research on the R–B–C(N) compounds is merited.

### 13. SUMMARY/CONCLUSION AND OUTLOOK

First of all, a rare earth existence diagram is given in Figure 45 for all the higher boride compounds discussed in this review. As noted before, size constraints on the voids which are created among the boron cluster networks result in different ranges of possible rare earth elements for the different compounds.

An interesting aspect of these compounds is that a large variety of different structures/arrangements of boron clusters which have similar energies appear to exist. The small addition of non-metallic elements like carbon, nitrogen, and silicon, result in completely different structures being formed, despite having similar rare earth to network-constituent (B, C, N, Si) ratios. Novel structures formed, and thus, confined in the boron lattice/network new configurations of the rare earth atoms were observed, and as a result, particularly interesting properties were discovered.

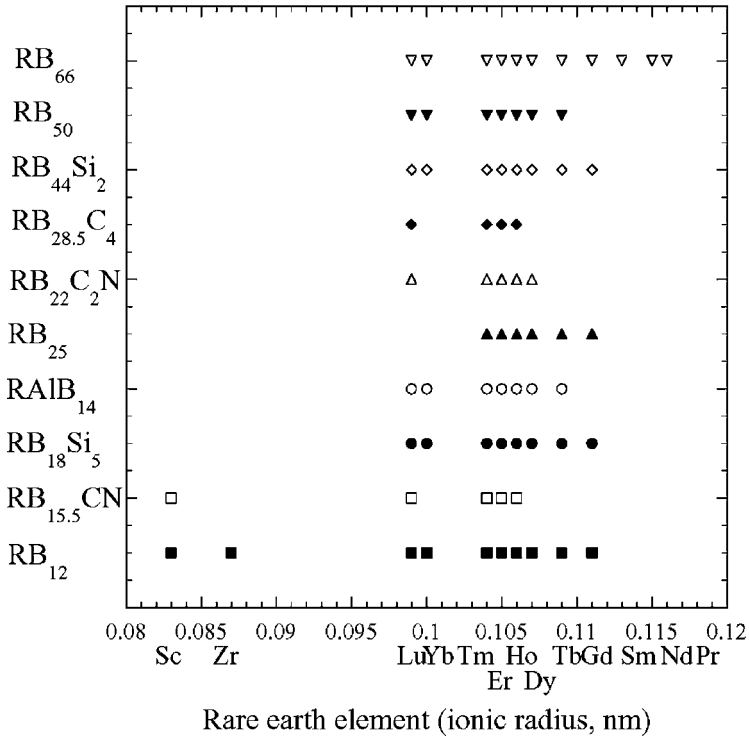


**FIGURE 45** Rare earth existence diagram for the higher borides:  $RB_{66}$  (▽),  $RB_{50}$  (▼),  $RB_{44}Si_2$  (◇),  $RB_{28.5}C_4$  (◆),  $RB_{22}C_2N$  (△),  $RB_{25}$  (▲),  $RAIB_{14}$  (○),  $RB_{18}Si_5$  (●),  $RB_{15.5}CN$  (□), and  $RB_{12}$  (■).

The higher borides covered in this review range from the dodecaborides  $RB_{12}$ , which are metals, to the  $RB_n$ ;  $n > 12$  (ignoring in this notation the additions of the third elements) borides which are all boron icosahedra compounds and are insulators. As metals, the dodecaborides have been known to exhibit attractive properties like magnetism and superconductivity and have been researched for over 40 years. However, new results are emerging, as the magnetism of these cubic compounds appears to be much more complicated than previously imagined.  $RB_{66}$  was the only rare earth higher boride ( $RB_n$ ;  $n > 12$ ) known until the early 1990s and while possessing interesting structural and mechanical features, it was not particularly noted for its physical properties besides from glass-like thermal conductivity. Non-melting sintering techniques and addition of small amounts of a third element resulted in a large number of novel boron icosahedra-containing higher borides being discovered. With new structures being realized, and also in some cases, novel configurations of the rare earth, a myriad of attractive physical properties such as one-dimensional dimer-like transition, two-dimensional spin glass, three-dimensional long range order, were discovered. The apparent function of the boron icosahedra clusters to mediate the unexpectedly large magnetic interaction was also brought to light. Furthermore, n-type electrical properties, which were thought to be non-existent in boron icosahedra compounds unless

highly doped with transition metals, were also realized in a R–B–C(N) homologous series of compounds which have a notable layered structure.

Interesting problems remain to be solved. Although the figure of merit is still quite low due to the poor density, can the homologous R–B–C(N) borides be densified and/or doped to become a viable n-type counterpart to boron carbide which is an exemplar n-type high temperature thermoelectric compound?

Other questions which need to be resolved are: why are the compounds n-type? What are their electronic structures? How anisotropic are their electrical and thermal properties?

What are the explicit mechanisms for the surprisingly strong magnetic interactions in the boron icosahedra-containing compounds, which are relatively dilute, f-electron insulators?

Most of the higher borides described in this work were discovered within the space of 10 years, yet what other new attractive cluster compounds are waiting to be discovered along with their exciting and unexpected magnetic, electrical, and thermal properties?

A lot of work remains to be done.

## REFERENCES

- Anderico, C.Z., Fernandez, J.F., Streit, T.S.J. *Phys. Rev. B* 1982, **26**, 3824.  
 Aselage, T.L., Emin, D., in: Kanatzidis, M.G., editor. *Chemistry, Physics and Materials Science of Thermoelectric Materials: Beyond Bismuth Telluride*. Dordrecht: Kluwer Academic; 2003, p. 55.  
 Auer, J., Ullmaier, H. *Phys. Rev. B* 1973, **7**, 136.  
 Bambakidis, G., Wagner, R.P. *J. Phys. Chem. Solids* 1981, **42**, 1023.  
 Bauer, J., Halet, J.F., Saillard, J.V. *Coord. Chem. Rev.* 1998, **178–180**, 723.  
 Bertaut, F., Blum, P. *C. R. Acad. Sci., Paris* 1949, **229**, 111.  
 Bucher, E., Muller, J., Olsen, J.L., Palmy, C. *Phys. Lett.* 1965, **15**, 303.  
 Bullett, D.W. *J. Phys. C* 1982, **15**, 415.  
 Cahill, D.G., Fischer, H.E., Watson, S.K., Pohl, R.O., Slack, G.A. *Phys. Rev. B* 1989, **40**, 3254.  
 Cheung, T.T.P., Soos, Z.G., Dietz, R.E., Merritt, F.R. *Phys. Rev. B* 1978, **17**, 1266.  
 Chu, C.W., Hill, H.H. *Science* 1968, **159**, 1227.  
 Cole, K.S., Cole, R.H. *J. Chem. Phys.* 1941, **9**, 341.  
 Czopnik, A., Shitsevalova, N., Pluzhnikov, V., Krivchikov, A., Paderno, Yu., Onuki, Y. *J. Phys.: Condens. Matter* 2005, **17**, 5971.  
 Daghero, D., Gonnelli, R.S., Ummarino, G.A., Calzolari, A., Dellarocca, V., Stepanov, V.A., Filip-pov, V.B., Paderno, Y.B. *Supercond. Sci. Technol.* 2004, **17**, S250.  
 deGennes, P.G. *Compt. Rend.* 1958, **247**, 1836.  
 Degiorgi, L. *Rev. Mod. Phys.* 1999, **71**, 687.  
 Dresselhaus, M.S., Dresselhaus, G., Sun, X., Zhang, Z., Cronin, S.B., Koga, T. *Phys. Solid State* 1999, **41**, 679.  
 Efros, A.L., Shklovskii, B.I., in: Efros, A.L., Pollak, M., editors. *Electron–Electron Interactions in Disordered Systems*. Amsterdam: North-Holland; 1985, p. 409.  
 Emin, D. *J. Solid State Chem.* 2004, **177**, 1619.  
 Etourneau, J. *J. Less Common Met.* 1985, **110**, 267.  
 Fisk, Z., Matthias, B.T., Corenzwit, E. *Proc. Nat. Acad. Sci.* 1969, **64**, 1151.  
 Fisk, Z., Lawson, A.C., Matthias, B.T., Corenzwit, E. *Phys. Lett.* 1971, **37A**, 251.  
 Fisk, Z., Lawson, A.C., Fitzgerald, R.W. *Mater. Res. Bull.* 1974, **9**, 633.  
 Flachbart, K., Gabani, S., Gloos, K., Meissner, M., Opel, M., Paderno, Y., Pavlik, V., Samuely, P., Schu-berth, E., Shitsevalova, N., Siemsmeyer, K., Szabo, P. *J. Low Temp. Phys.* 2005, **140**, 339.

- Fournier, J.M., Gratz, E., in: Gschneidner Jr., K.A., Eyring, L., Lander, G.H., Choppin, G.R., editors. Handbook on the Physics and Chemistry of Rare Earths, vol. 17. Amsterdam: North-Holland; 1993, p. 423.
- Gabani, S., Bat'ko, I., Flachbart, K., Herrmannsdoerfer, T., Koenig, Y., Paderno, R., Shitsevalova, N. J. Magn. Mater. 1999, **207**, 131.
- Gabani, S., Bauer, E., Berger, S., Flachbart, K., Paderno, Y., Paul, C., Pavlik, V., Shitsevalova, N. Phys. Rev. B 2003, **67**, 172406.
- Gasparov, V.A., Sidorov, N.S., Zver'kova, I.I. Phys. Rev. B 2006, **73**, 094510.
- Golikova, O.A. Phys. Status Solids A 1987, **101**, 277.
- Gignoux, D., Schmitt, D., in: Buschow, K.H.J., editor. Handbook of Magnetic Materials, vol. 10. Amsterdam: North-Holland; 1997, p. 239.
- Gschneidner Jr., K.A., in: Rare Earth Alloys. New York: D. Van Nostrand Co.; 1961, p. 127.
- Gschneidner Jr., K.A. J. Less Common Met. 1969, **17**, 13.
- Gschneidner Jr., K.A., Daane, A.H., in: Gschneidner Jr., K.A., Eyring, L., editors. Handbook on the Physics and Chemistry of Rare Earths, vol. 11. Amsterdam: North-Holland; 1988, p. 475.
- Haldane, F.D.M. Phys. Lett. 1983, **93A**, 464.
- Hamada, K., Wakata, M., Sugii, N., Matsuura, K., Kubo, K., Yamauchi, H. Phys. Rev. B 1993, **48**, 6892.
- Hanzawa, K. J. Phys. Soc. Jpn. 2002, **71**, 1481.
- Higashi, I. AIP Conf. Proc. 1986, **140**, 1.
- Higashi, I., Ito, T. J. Less Common Met. 1983, **92**, 239.
- Higashi, I., Tanaka, T., Kobayashi, K., Ishizawa, Y., Takami, M. J. Solid State Chem. 1997a, **133**, 11.
- Higashi, I., Kobayashi, K., Tanaka, T., Ishizawa, Y. J. Solid State Chem. 1997b, **133**, 16.
- Higashi, I., Ishii, T., Tanaka, T. 2002, unpublished.
- Hoard, J.L., Hughes, R.E., in: Muetterties, E.L., editor. The Chemistry of Boron and its Compounds. New York: Wiley; 1967, p. 25.
- Hundley, M.F., Canfield, P.C., Thompson, J.D., Fisk, Z., Lawrence, J.M. Phys. Rev. B 1990, **42**, 6842.
- Huser, D., van Duynveldt, A.J., Nieuwenhuys, G.J., Mydosh, J.A. J. Phys. C 1986, **19**, 3697.
- Iga, F., Takakuwa, Y., Takahashi, Y., Kasaya, M., Kasuya, T., Sagawa, T. Solid State Commun. 1984, **50**, 903.
- Ishizawa, Y., Tanaka, T. J. Solid State Chem. 2000, **154**, 229.
- Johnson, R.W., Daane, A.H. J. Chem. Phys. 1963, **38**, 425.
- Kanatzidis, M.G. Chemistry, Physics and Materials Science of Thermoelectric Materials: Beyond Bismuth Telluride, Kluwer; 2003.
- Kasaya, M., Iga, F., Negishi, K., Nakai, S., Kasuya, T. J. Magn. Mater. 1983, **31–34**, 437.
- Kasuya, T. Prog. Theor. Phys. 1956, **16**, 45.
- Kasuya, T. Prog. Theor. Phys. Suppl. 1992, **108**, 1.
- Khasanov, R., Di Castro, D., Belogolovskii, M., Paderno, Yu., Filippov, V., Brüttsch, R., Keller, H. Phys. Rev. B 2005, **72**, 224509.
- Kinzel, W., Binder, K. Phys. Rev. B 1984, **29**, 1300.
- Kirfel, A., Gupta, A., Will, G. Acta Crystallogr. B 1979, **35**, 1052.
- Kohout, A., Batko, I., Czopnik, A., Flachbart, K., Matas, S., Meissner, M., Paderno, Y., Shitsevalova, N., Siemensmeyer, K. Phys. Rev. B 2004, **70**, 224416.
- Korsukova, M.M., Gurin, V.N., Kuzma, B.Yu., Chaban, N.F., Chykhrii, S.I., Moshchalkov, V.V., Brandt, N.B., Gippius, A.A., Nyan, K.K. Phys. Status Solidi A 1989, **114**, 265.
- Korsukova, M.M., Lundstrom, T., Tergenius, L.E., Gurin, V.N. J. Alloys Compd. 1992, **187**, 39.
- Leithe-Jasper, A., Bourgeois, L., Michiue, Y., Shi, Y., Tanaka, T. J. Solid State Chem. 2000, **154**, 130.
- Leithe-Jasper, A.L., Tanaka, T., Bourgeois, L., Mori, T., Michiue, Y. J. Solid State Chem. 2004, **177**, 431.
- Lipscomb, W.N., Britton, D. J. Chem. Phys. 1960, **33**, 275.
- Longuet, H.C., Roberts, M. De V. Proc. Roy. Soc. A 1955, **230**, 110.
- Matkovich, V.I., Economy, J., in: Boron and Refractory Borides. Berlin, New York: Springer-Heidelberg; 1977, p. 78.
- Matkovich, V.I., Griese, R.F., Economy, J. Z. Kristallogr. 1965, **122**, 116.
- Matkovich, V.I., Economy, J. Acta Crystallogr. B 1970, **26**, 616.
- Matthias, B.T., Geballe, T.H., Andres, K., Corenzwit, E., Hull, G., Maita, P.J. Science 1968, **159**, 530.
- Michimura, S., Shigekawa, A., Iga, F., Sera, M., Takabatake, T., Ohoyama, K., Okabe, Y. Physica B 2006, **378–380**, 596.

- Mironov, A., Kazakov, S., Jun, J., Karpinski, J. *Acta Crystallogr. C* 2002, **58**, 195.
- Moiseenko, L.L., Odintsov, V.V. *J. Less Common Met.* 1979, **67**, 237.
- Mori, T. *J. Appl. Phys.* 2004, **95**, 7204.
- Mori, T. *Polyhedron* 2005a, **24**, 2803.
- Mori, T. *J. Appl. Phys.* 2005b, **97**, 093703.
- Mori, T. *Z. Kristallogr.* 2006a, **221**, 464.
- Mori, T. *J. Appl. Phys.* 2006b, **99**, 08J309.
- Mori, T. *Physica B* 2006c, **383**, 120.
- Mori, T., Leithe-Jasper, A. *Phys. Rev. B* 2002, **66**, 214419.
- Mori, T., Mamiya, H. *Phys. Rev. B* 2003, **68**, 214422.
- Mori, T., Nishimura, T. *J. Solid State Chem.* 2006, **179**, 2908.
- Mori, T., Tanaka, T. *J. Phys. Soc. Jpn.* 1999a, **68**, 2033.
- Mori, T., Tanaka, T. *J. Alloys Compd.* 1999b, **288**, 32.
- Mori, T., Tanaka, T. *J. Phys. Soc. Jpn.* 2000, **69**, 579.
- Mori, T., Tanaka, T. *IEEE Trans. Mag.* 2001a, **37**, 2144.
- Mori, T., Tanaka, T. *Mat. Res. Bull.* 2001b, **36**, 2463.
- Mori, T., Tanaka, T. *J. Alloys Compd.* 2003, **348**, 203.
- Mori, T., Tanaka, T. *J. Solid State Chem.* 2006, **179**, 2889.
- Mori, T., Zhang, F. *J. Phys.: Condens. Matter* 2002, **14**, 11831.
- Mori, T., Zhang, F., Tanaka, T. *J. Phys.: Condens. Matter* 2001, **13**, L423.
- Mori, T., Tanaka, T., Kitazawa, H., Abe, H., Tsujii, N., Kido, G. *Physica B* 2002, **312–313**, 870.
- Mori, T., Izumi, F., Ishii, Y. *J. Alloys Compd.* 2004a, **374**, 105.
- Mori, T., Zhang, F., Leithe-Jasper, A. *J. Solid State Chem.* 2004b, **177**, 444.
- Mori, T., Martin, J., Nolas, G. 2007a. *J. Appl. Phys.* 102, in press.
- Mori, T., Nishimura, T., Yamaura, K., Takayama-Muromachi, E. *J. Appl. Phys.* 2007b, **101**, 093714.
- Mori, T., Nishimura, T., Budnyk, S., Burkhardt, U., Grin, Yu. 2008a, submitted for publication.
- Mori, T., Takimoto, T., Grin, Yu. 2008b, to be submitted.
- Mott, N.F. *J. Non-Crystallogr. Solids* 1968, **1**, 1.
- Murasik, A., Czopnik, A., Keller, L., Zolliker, M., Shitsevalova, N., Paderno, Y. *Phys. Status Solidi B* 2002, **234**, R13.
- Mydosh, J.A. *Spin Glasses*, London: Taylor and Francis; 1993.
- Nagamatsu, J., Nakagawa, N., Muranaka, T., Zenitani, Y., Akimitsu, J. *Nature* 2001, **410**, 63.
- Naslain, R., in: *Boron and Refractory Borides*. Berlin, New York: Springer-Heidelberg; 1977, p. 139.
- Naslain, R., Guette, A., Hagenmuller, P. *J. Less Common Met.* 1976, **47**, 1.
- Nolas, G.S., Sharp, J., Goldsmid, H.J., editors. *Thermoelectrics: Basic Principles and New Materials Development*. Springer; 2001.
- Nolas, G.S., Cohn, J.L., Dyck, J.S., Uher, C., Yang, J. *Phys. Rev. B* 2002, **65**, 165201.
- Oliver, D.W., Brower, G.D. *J. Cryst. Growth* 1971, **11**, 185.
- Paderno, Y., Shitsevalova, N. *J. Alloys Compd.* 1995, **219**, 119.
- Paderno, Y., Shitsevalova, N., Batko, I., Flachbart, K., Misiorek, H., Mucha, J., Jezowski, A. *J. Alloys Compd.* 1995, **219**, 215.
- Prudenziati, M., Majni, G., Alberigi-Quaranta, A. *Solid State Commun.* 1973, **13**, 1927.
- Richards, S.M., Kasper, J.S. *Acta Crystallogr. B* 1969, **25**, 237.
- Rogl, P., in: *Gschneidner Jr., K.A., Eyring, L., editors. Handbook on the Physics and Chemistry of Rare Earths*, vol. 6. Amsterdam: North-Holland; 1984, p. 335.
- Rogl, P., in: *Effenberg, G., editor. Phase Diagrams of Ternary Metal–Boron–Carbon Systems*. Ohio: ASM International; 1998.
- Rowe, D.M. *CRC Handbook of Thermoelectrics*, CRC; 1995.
- Ruderman, M.A., Kittel, C. *Phys. Rev.* 1954, **96**, 99.
- Sales, B.C., Mandrus, D., Chakoumakos, B.C., Keppens, V., Thompson, J.R. *Phys. Rev. B* 1997, **56**, 15081.
- Salvadore, J.R., Bilc, D., Mahanti, S.D., Kanatzidis, M.G. *Angew. Chem. Int. Ed.* 2002, **41**, 844.
- Seyboldt, A.U. *Trans. Am. Soc. Metals* 1960, **52**, 971.
- Shapira, Y., Foner, S. *Phys. Rev. B* 1970, **1**, 3083.
- Shirai, K., Nakamatsu, H. *JJAP Series* 1994, **10**, 70.
- Siemensmeyer, K., Flachbart, K., Gabani, S., Mat'as, S., Paderno, Y., Shitsevalova, N. *J. Solid State Chem.* 2006, **179**, 2748.

- Slack, G.A., Rosolowski, J.H., Hejna, C., Garbaskas, M., Kasper, J.S. 1987, Proc. 9th Int. Symp. Boron, Borides and Related Compounds, Duisburg, Germany, 132.
- Slack, G.A., Tsoukala, V. J. Appl. Phys. 1994, **76**, 1635.
- Slack, G.A., Oliver, D.W., Horn, F.H. Phys. Rev. B 1971, **4**, 1714.
- Slack, G.A., Oliver, D.W., Brower, G.D., Young, J.D. J. Phys. Chem. Solids 1977, **38**, 45.
- Tanaka, T., Okada, S., Ishizawa, Y. J. Alloys Compd. 1994, **205**, 281.
- Tanaka, T., Okada, S., Ishizawa, Y. J. Solid State Chem. 1997a, **133**, 55.
- Tanaka, T., Okada, S., Yu, Y., Ishizawa, Y. J. Solid State Chem. 1997b, **133**, 122.
- Tanaka, T., Okada, S., Gurin, V.N. J. Alloys Compd. 1998, **267**, 211.
- Tanaka, T., Shi, Y., Mori, T., Leithe-Jasper, A. J. Solid State Chem. 2000, **154**, 54.
- Tanaka, T., Yamamoto, A., Sato, A. J. Solid State Chem. 2002, **168**, 192.
- Tanaka, T., Yamamoto, A., Sato, A. J. Solid State Chem. 2004, **177**, 476.
- Tanaka, T., Kamiya, K., Numazawa, T., Sato, A., Takenouchi, S. Z. Kristallogr. 2006, **221**, 472.
- Taylor, K.N.R., Darby, M.I. Physics of Rare Earth Solids, London: Chapman & Hall; 1972. p. 374.
- Tsindlekht, M.I., Leviev, G.I., Asulin, I., Sharoni, A., Millo, O., Felner, I., Paderno, Yu.B., Filippov, V.B., Belogolovskii, M.A. Phys. Rev. B 2004, **69**, 212508.
- Tsunetsugu, H., Sigrist, M., Ueda, K. Rev. Mod. Phys. 1997, **69**, 809.
- Vidhyadhiraja, N.S., Smith, V.E., Logan, D.E., Krishnamurthy, H.R. J. Phys.: Condens. Matter 2003, **15**, 4045.
- Wang, Y., Lortz, R., Paderno, Y., Filippov, V., Abe, S., Tutsch, U., Junod, A. Phys. Rev. B 2005, **72**, 024548.
- Watanuki, R., Sato, G., Suzuki, K., Ishihara, M., Yanagisawa, T., Nemoto, Y., Goto, T. J. Phys. Soc. Jpn. 2005, **74**, 2169.
- Werheit, H., deGroot, K., Malkemper, W., Lundstrom, T. J. Less Common Met. 1981, **82**, 163.
- Werheit, H., Kuhlmann, U., Tanaka, T. AIP Conf. Proc. 1991, **231**, 125.
- Werheit, H., in: Gogotsi, Y.G., Andrievski, R.A., editors. Materials Science of Carbides, Nitrides, and Borides. Dordrecht: Kluwer; 1999, p. 65.
- Wong, J., Shimkaveg, G., Goldstein, W., Eckart, M., Tanaka, T., Rek, Z.U., Tompkins, H. Nucl. Instrum. Methods A 1990, **291**, 243.
- Wong, J., Tanaka, T., Rowen, M., Schafers, F., Muller, B.R., Rek, Z.U. J. Synch. Rad. 1999, **6**, 1086.
- Wood, C., Emin, D. Phys. Rev. B 1984, **29**, 4582.
- Wood, C., Emin, D., Gray, P.E. Phys. Rev. B 1985, **31**, 6811.
- Yoshida, K. Phys. Rev. 1957, **106**, 893.
- Young, A.P. Phys. Rev. Lett. 1983, **50**, 917.
- Zhang, F.X., Leithe-Jasper, A., Xu, J., Mori, T., Matsui, Y., Tanaka, T., Okada, S. J. Solid State Chem. 2001a, **159**, 174.
- Zhang, F.X., Xu, F.F., Mori, T., Liu, Q.L., Sato, A., Tanaka, T. J. Alloys Compd. 2001b, **329**, 168.
- Zhang, F., Sato, A., Tanaka, T. J. Solid State Chem. 2002, **164**, 361.

## Rare-Earth Nickel Borocarbides

K.-H. Müller\*, M. Schneider\*, G. Fuchs\*, S.-L. Drechsler\*

Contents	List of Symbols	177
	1. Introduction	179
	1.1 The discovery of rare-earth nickel borocarbide superconductors	180
	1.2 Superconductors based on boron and carbon	181
	1.3 Interplay of superconductivity and magnetism	185
	1.3.1 Superconductivity and magnetic ordering as antagonistic phenomena	185
	1.3.2 Superconductors with magnetic impurities	186
	1.3.3 Superconductivity and local-magnetic-moment cooperative phenomena	187
	1.3.4 Superconductivity and itinerant-electron magnetism	191
	1.4 RNi <sub>2</sub> B <sub>2</sub> C compounds	192
	2. Crystal Structure and Chemical Composition	195
	2.1 LuNi <sub>2</sub> B <sub>2</sub> C-type-structure compounds	195
	2.2 Lattice distortions due to orbital ordering	198
	2.3 Single-, double- and triple-layer borocarbides (nitrides)	200
	2.4 Metastable and related R–T–B–C(N) phases	202
	3. Sample Preparation and Basic Properties	204
	3.1 Preparation of polycrystals, single crystals and thin films	204
	3.2 Electronic structure	209
	3.3 Superconducting coupling mechanism	212
	3.4 Transport properties	215
	3.4.1 Magnetoresistance	215
	3.4.2 Hall effect	217
	3.4.3 Thermoelectric power	218
	3.4.4 Thermal conductivity	219
	3.5 Symmetry of the superconducting gap	221
	3.5.1 The role of thermal conductivity and specific heat	224
	3.5.2 Tunneling and point-contact spectroscopy	227
	3.5.3 de Haas–van Alphen (dHvA) effect	229
	3.6 The upper critical field	232

\* Leibniz-Institut für Festkörper- und Werkstoffforschung Dresden, POB 270116, D-01171 Dresden, Germany

3.7	Effects of pressure	238
3.8	Superconducting-state characteristics of $\text{YNi}_2\text{B}_2\text{C}$ and $\text{LuNi}_2\text{B}_2\text{C}$	239
4.	Magnetic and Superconducting Properties of $\text{RNi}_2\text{B}_2\text{C}$ with $\text{R} = \text{Ce to Yb}$	241
4.1	Effects of the crystalline electric field on magnetic and orbital ordering	243
4.1.1	Magnetic order	243
4.1.2	Orbital order	246
4.2	$\text{CeNi}_2\text{B}_2\text{C}$	249
4.3	$\text{PrNi}_2\text{B}_2\text{C}$	250
4.4	$\text{NdNi}_2\text{B}_2\text{C}$	252
4.5	$\text{SmNi}_2\text{B}_2\text{C}$	253
4.6	$\text{GdNi}_2\text{B}_2\text{C}$	254
4.7	$\text{TbNi}_2\text{B}_2\text{C}$	256
4.8	$\text{DyNi}_2\text{B}_2\text{C}$	258
4.9	$\text{HoNi}_2\text{B}_2\text{C}$	260
4.9.1	Types of magnetic order in $\text{HoNi}_2\text{B}_2\text{C}$	262
4.9.2	Metamagnetic transitions and magnetoresistance	263
4.9.3	Reentrant and near-reentrant behavior	266
4.9.4	Interplay of superconductivity and magnetism in $\text{HoNi}_2\text{B}_2\text{C}$	268
4.9.5	Multiband coexistence of superconductivity and magnetism in $\text{HoNi}_2\text{B}_2\text{C}$	268
4.10	$\text{ErNi}_2\text{B}_2\text{C}$	271
4.10.1	Weak ferromagnetism in $\text{ErNi}_2\text{B}_2\text{C}$	272
4.10.2	Coexistence of ferromagnetism and superconductivity in $\text{ErNi}_2\text{B}_2\text{C}$	274
4.11	$\text{TmNi}_2\text{B}_2\text{C}$	276
4.12	$\text{YbNi}_2\text{B}_2\text{C}$	278
5.	Vortex Lattices in $\text{RNi}_2\text{B}_2\text{C}$ Superconductors	279
5.1	Non-magnetic borocarbides	279
5.1.1	Hexagonal and square vortex lattice	280
5.1.2	Size of the vortex cores	286
5.1.3	Vortex matter phase diagram	286
5.1.4	Vortex pinning	287
5.1.5	Dynamics of the vortex lattice	287
5.2	Magnetic borocarbides	289
5.2.1	$\text{ErNi}_2\text{B}_2\text{C}$	289
5.2.2	$\text{HoNi}_2\text{B}_2\text{C}$	291
5.2.3	$\text{TmNi}_2\text{B}_2\text{C}$	292
6.	Superconductivity in $\text{R}(\text{Ni},\text{T})_2\text{B}_2\text{C}$ and $(\text{R},\text{R}')\text{Ni}_2\text{B}_2\text{C}$	293
6.1	Partial substitution of Ni by $\text{T} = \text{Co, Cu, Pd, Pt, etc.}$	293
6.2	Effects of chemical pressure and disorder	295
6.3	Magnetic impurities in a non-magnetic superconductor	302
6.4	Non-magnetic impurities in an antiferromagnetic superconductor	306
6.5	$(\text{R},\text{R}')\text{Ni}_2\text{B}_2\text{C}$ superconductors with magnetic parent compounds	308
7.	Conclusions and Outlook	310

Acknowledgements

312

References

313

**List of Symbols**

$\alpha$	scaling exponent of the upper critical field	$\theta$	polar angle or paramagnetic Curie temperature
$\alpha_{I,C}$	isotope exponent (of constituent C)	$\theta_D$	Debye temperature
$\alpha_J$	second order Stevens coefficient	<b>H</b>	magnetic field
<b>A</b>	vector potential	$H_1$	lower vortex-structure transition field
$A_{nm}$	crystalline-electric-field coefficients	$H_2$	upper vortex-structure transition field
$\beta$	scaling exponent of the upper critical field	$H_c$	thermodynamic critical field
$\beta_L$	apex angle	$H_{c1}$	lower critical field
$\gamma(H)$	measure for the electronic mixed-state specific heat	$H_{c2}(T)$	upper critical field
$\gamma_{imp}$	impurity scattering rate	$H_{c2}^*$	fitting parameter of the upper critical field
$\gamma_m$	ratio of anisotropic effective masses	$H_{eff}$	effective magnetic field
$\gamma_N$	Sommerfeld coefficient	$H_M$	metamagnetic transition field
$c_{66}$	shear modulus	$H_N$	metamagnetic transition field
$c_s$	speed of sound	$H^*$	metamagnetic transition field
$C$	Curie constant	$H'$	metamagnetic transition field
$C_e$	electronic contribution to $C_p$	$H''$	metamagnetic transition field
$C_p$	specific heat	$I$	strength of the exchange interaction between 4f electrons and the conduction electrons
$\delta$	deviation from the stoichiometric composition	$j$	(electrical) current density
$\Delta, \Delta(T)$	energy gap	$j_c$	critical current density
$\Delta_0$	$\Delta(0)$	$J$	total angular momentum
$\Delta_c$	value of the energy gap outside the vortex core	$J_{\parallel}$	magnetic exchange constant parallel to <b>c</b>
$\Delta C_p$	jump in $C_p$ associated with the superconducting transition	$J_{\perp}$	magnetic exchange constant perpendicular to <b>c</b>
$\Delta E_Q$	nuclear quadrupole splitting	$\kappa$	thermal conductivity
$F_p$	pinning force	$\kappa_{GL}$	Ginzburg-Landau parameter
$\overline{DG}$	effective de Gennes factor		
$E$	energy		
$E_F$	Fermi level		
$g$	Landé factor		

$\mathbf{k}$	momentum	RRR	residual resistivity ratio
$k_B$	Boltzmann constant	$R_W$	Wilson ratio
$\lambda$	London penetration depth	$S$	spin
$\lambda_{ph}$	electron-phonon coupling constant	$S_Q$	thermoelectric power
$l$	mean free path	$\tau$	propagation wave vector
$L$	orbital momentum	$T$	temperature
$\langle \mu \rangle$	staggered magnetic moment	$T$	transition metal
$\mu_0$	vacuum permeability	$T_0$	(different types of) transition temperature
$\mu_B$	Bohr magneton	$T_c$	superconducting critical temperature
$\mu_p$	paramagnetic moment	$T_c^0$	superconducting critical temperature without magnetic impurities
$\mu_s$	saturation moment	$T_C$	Curie temperature
$\mu^*$	Coulomb pseudopotential	$T_D$	Dingle temperature
$m_{0,exp}$	observed orbitally-averaged mass	$T_K$	Kondo temperature
$m_{0,LDA}$	calculated orbitally-averaged mass	$T_M$	magnetic ordering temperature
$m_e$	bare electron mass	$T_N$	magnetic transition (into Néel state) temperature
$m_e^*$	effective band electron mass	$T_Q$	(antiferro-)quadrupolar ordering temperature
$M$	magnetization or mass of atoms	$T_R$	spin reorientation temperature
$M_s$	spontaneous magnetization	$T_{sf}$	fluctuation temperature
MR	magnetoresistance	$T_{WFM}$	transition temperature to weak ferromagnetism
$N(E)$	normal-state electron density of states	$T^*$	magnetic transition (between different magnetic states) temperature
$\xi, \xi(T)$	coherence length	$\phi$	azimuthal angle
$\xi_0$	BCS (also called Ginzburg-Landau) coherence length	$\phi_0$	flux quantum
$\xi_a$	$a$ -axis component of an incommensurate propagation vector	$v_F, v_{Fi}$	Fermi velocity (of the subgroup of electrons $i$ )
$\xi_{c2}$	coherence length derived from $H_{c2}(0)$	$V$	electron-phonon interaction strength
$P$	(hydrostatic) pressure	$\chi'$	ac susceptibility
$P_u$	uniaxial pressure	$\chi_D$	diamagnetic susceptibility
$\mathbf{q}$	nesting vector	$\chi_P$	paramagnetic susceptibility
$\rho$	electrical resistivity	$x, y$	dopant concentration
$\rho_0$	residual resistivity	$z$	coordinate of boron in the LuNi <sub>2</sub> B <sub>2</sub> C structure
$\rho_c$	size of the vortex core		
$\rho_N$	normal-state electrical resistivity		
$R$	electrical resistance		
R	rare earth		
$R_H$	Hall coefficient		

$\square_g$	square vortex lattice with nearest neighbors along [100]	LDA	local-density approximation
$\square_v$	square vortex lattice with nearest neighbors along [110]	MOI	magneto-optical imaging
<i>List of acronyms</i>		$\mu$ SR	muon-spin relaxation
AFM	(commensurate) antiferromagnetic	NMR	nuclear magnetic relaxation
AFQO	antiferroquadrupolar ordering	OO	orbital ordering
AG	Abrikosov–Gor’kov	PCS	point-contact spectroscopy
ARPES	angle-resolved photoemission spectroscopy	PES	photoemission spectroscopy
BCS	Bardeen–Cooper–Schrieffer	PLD	pulsed laser deposition
CEF	crystalline electric field(s)	QO	quadrupolar ordering
CJTE	cooperative Jahn–Teller effect	RKKY	Ruderman–Kittel–Kasuya–Yosida
CPA	coherent-potential approximation	SANS	small-angle neutron scattering
dHvA	de Haas–van Alphen	SDW	spin-density wave
DOS	electronic density of states	s.g.	space group
el–ph	electron–phonon	SL	spin–orbit
FC	field cooled	STM	scanning tunneling microscopy
FLL	flux-line lattice	STS	scanning tunneling spectroscopy
FODOS	field-orientational dependence of the density of states	SVS	spontaneous vortex state
FPLO	full potential-localized orbitals	TB-LMTO	tight binding–linear muffin tin orbitals
FP-LMTO	full potential-linear muffin tin orbitals	TEP	thermoelectric power
FQO	ferroquadrupolar ordering	VSM	vibrating sample magnetometer
FS	Fermi surface	WFM	weak ferromagnetism
FSS	Fermi surface sheet	XANES	X-ray absorption near-edge structure
GL	Ginzburg–Landau	XPS	X-ray photo-electron spectroscopy
ISB	isotropic single band	XRES	X-ray resonant exchange scattering
		ZFC	zero-field cooled

## 1. INTRODUCTION

Soon after the discovery of the quaternary borocarbide superconductors in 1994 a remarkable progress in the investigation of their physical properties could be asserted (Müller and Narozhnyi, 2001b). One reason for this rapid progress is the favorable synthesis properties of this class of materials, which resulted in high-quality polycrystalline samples over a wide range of compositions, as well as thin

films and single crystals early in the development of the field. Thus these borocarbides have been considered as “a toy box for solid-state physicists” (Canfield et al., 1998) and the study of them resulted in better understanding of superconductors in general and magnetic superconductors in particular. A typical example is the novel concept of strongly coupled two-band superconductivity introduced to explain the anomalous temperature dependence of the upper critical field of  $\text{YNi}_2\text{B}_2\text{C}$  and  $\text{LuNi}_2\text{B}_2\text{C}$  (Shulga et al., 1998) and now widely used for other superconductors such as  $\text{MgB}_2$ . Without doubt the most intriguing property of these materials is that they exhibit both superconductivity and exchange-coupled magnetic order, which compete and coexist. In virtue of the fact that a superconducting critical temperature  $T_c$  as high as 23 K has been achieved (in  $\text{YPd}_2\text{B}_2\text{C}$ ) they have been assigned to the class of high-temperature superconductors (Pickett, 2001).

After a short report on the discovery of the quaternary borocarbide superconductors in Section 1.1, for comparison a limited survey of other superconductors based on boron and/or carbon will be presented in Section 1.2 whereas the interplay of superconductivity and magnetism in other materials is discussed in Section 1.3. At the end of this section some special features of the  $\text{RNi}_2\text{B}_2\text{C}$  compounds and review articles in this field can be found in Section 1.4 as well as the further outline of this chapter.

## 1.1 The discovery of rare-earth nickel borocarbide superconductors

Superconductivity in quaternary rare-earth transition-metal borocarbides was discovered when, for seemingly single-phase polycrystalline samples of the hexagonal compound  $\text{YNi}_4\text{B}$ , a drop in the electrical resistivity and the magnetic susceptibility at about 12 K had been observed by Mazumdar et al. (1993). However, the superconducting phase in all investigated  $\text{YNi}_4\text{B}$  samples was a minor fraction of the material ( $\approx 2\%$ ). It had been suggested that the superconductivity in the  $\text{YNi}_4\text{B}$  samples may be due to a phase stabilized by the presence of an element other than Y, Ni and B. This was supported by the observation of bulk superconductivity in polycrystalline material with the nominal composition  $\text{YNi}_4\text{BC}_{0.2}$  (Nagarajan et al., 1994). At the same time Cava et al. (1994a, 1994b) reported results on superconductivity in multiphase  $\text{YPd}_5\text{B}_3\text{C}_{0.35}$  with a transition temperature  $T_c$  as high as 23 K and in single-phase materials of the composition  $\text{RNi}_2\text{B}_2\text{C}$  ( $R = \text{Y, Lu, Tm, Er, Ho}$  with  $T_c \approx 15.5 \text{ K, 16.5 K, 11 K, 10.5 K, 8 K}$ , respectively). It was found that the superconducting behavior of the  $\text{YNi}_4\text{B}$  and  $\text{YNi}_4\text{BC}_{0.2}$  samples mentioned above is caused by  $\text{YNi}_2\text{B}_2\text{C}$ . Consequently, this was the discovery of the first superconducting quaternary intermetallic compound. In the case of the Y-Pd-B-C system the classification of the phase being responsible for  $T_c \approx 23 \text{ K}$  was much more complicated because, so far, only multiphase superconducting material has been prepared for this system. Not all of the phases present in superconducting Y-Pd-B-C materials could be identified, and evidence for at least two superconducting phases has been reported (Hossain et al., 1994). Only a few years later it has finally been shown by a microanalysis technique that  $\text{YPd}_2\text{B}_2\text{C}$  is the 23 K superconducting phase (Dezaneti et al., 2000).

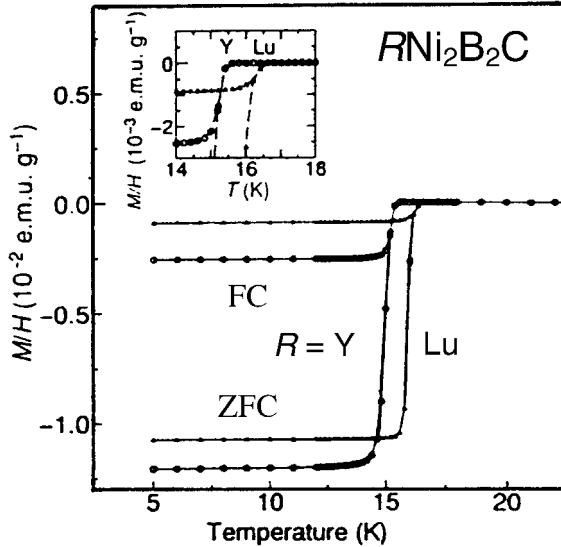


**FIGURE 1** Temperature dependence of the dc magnetic susceptibility of  $\text{LuNi}_2\text{B}_2\text{C}$  and  $\text{YNi}_2\text{B}_2\text{C}$  in a magnetic field of 20 Oe. ZFC and FC means zero-field cooling and field cooling, respectively (after Cava et al., 1994b).

A typical dc susceptibility-versus-temperature transition curve for polycrystalline  $\text{LuNi}_2\text{B}_2\text{C}$  and  $\text{YNi}_2\text{B}_2\text{C}$  with  $T_c \approx 16.5$  K and 15 K, respectively, is shown in Figure 1. The growth of very high-quality single crystals of nickel borocarbide superconductors (see, e.g., Xu et al., 1994) almost immediately after their discovery has had a profound impact on the quality of the work performed. Thus many of the pitfalls of the early research on other complex materials, such as high- $T_c$  superconductors, carried out on polycrystalline samples of variable quality, have essentially been avoided (Cava, 2001).

## 1.2 Superconductors based on boron and carbon

According to the BCS theory of superconductivity, the critical temperature

$$T_c \sim \theta_D \exp(-1/N(E_F)V) \quad (1)$$

is determined by the Debye temperature  $\theta_D$  representing the phonon spectrum, the normal state electron density of states  $N(E_F)$  at the Fermi level  $E_F$  and some measure  $V$  of the electron-phonon interaction (Bardeen, 1992). Although formula (1) had been derived for simple systems with the superconductivity driven by electron-phonon interaction, under the condition  $N(E_F)V \ll 1$ , it has been successfully applied to qualitatively describe superconductivity in a wide class of materials. The value of  $\theta_D$  monotonically increases with the inverse mass of the atoms participating in the lattice vibrations of the considered material. Therefore low-mass elements and their compounds are considered as candidates for superconductors with high critical temperature  $T_c$ . Thus, monatomic or diatomic forms of

metallic hydrogen are expected to exhibit superconductivity at quite high temperatures (Ashcroft, 1968; Richardson and Ashcroft, 1997). However, hydrogen-based superconductivity has not been found yet. The difficulty is to have, simultaneous with the large Debye temperature, conduction electrons with a large enough  $N(E_F)$  and a sufficiently large  $V$ . Besides hydrogen, lithium, and beryllium other light elements such as boron and carbon might be beneficial for increasing  $T_c$ . Examples for boron or (and) carbon containing superconductors are presented in Table 1. Contrary to boron, elemental carbon does not superconduct but intercalation compounds of graphite with alkali metals are superconductors with  $T_c < 1$  K (Hannay et al., 1965) and superconductivity with  $T_c$  as high as 11.5 K has been found in the intercalation compound  $\text{CaC}_6$  (see Table 1). Electron doping of carbon, resulting in superconductivity, has also been achieved in exohedral fullerenes. As an example,  $\text{Rb}_3\text{C}_{60}$  bulk material has  $T_c = 28$  K (Rosseinsky et al., 1991; Gunnarsson, 1997; see Table 1). Recently hole doped diamond has been prepared and shows a  $T_c$  of 4 K (Ekimov et al., 2004; see Table 1). Among the metal-carbon compounds  $\text{MgNi}_3\text{C}$  (see Table 1) is of particular interest because its superconducting ground state is close to a ferromagnetic instability and a two-band model is needed to describe its transport properties (Wälte et al., 2004, 2005). It can be considered as a three-dimensional analogue to the layered  $\text{RNi}_2\text{B}_2\text{C}$  compounds. Superconductors with remarkably high critical temperatures have also been found among organic compounds and inorganic carbides (see Table 1). Some carbon based superconductors recently have been reviewed by Kremer et al. (2007).

At ambient pressure boron is an insulator consisting of 12-atom icosahedral units. As reported by Eremets et al. (2001), under high pressure B becomes not only metallic, as predicted by Mailhot et al. (1990) but even superconducting and it has a positive pressure derivative of the critical temperature  $dT_c/dP$ . Pressure-induced superconductivity has also been found in organic compounds (e.g., BEDT-TTF in Table 1), doped spin-ladder cuprates (Uehara et al., 1996) and many other materials. Obviously pressure can cause, through various mechanisms, crystallographic and electronic structures that are favorable for superconductivity. On the other hand the electronic bands of a metal will broaden if the material is compacted, which is consistent with the fact that a negative  $dT_c/dP$  has been observed for many superconductors (Wijngaarden and Griessen, 1992). Therefore pressure-induced superconductivity, also in the case of boron, is expected to be characterized by a non-monotonic pressure dependence of  $T_c$  with a maximum value of  $T_c$  at a certain pressure. Such a behavior has been confirmed, e.g., for iron (Shimizu et al., 2001) and doped spin-ladder cuprates (Dagotto, 1999).

Superconductivity is also known for many borides (see Table 1). The most notable example is  $\text{MgB}_2$  a binary compound with a simple crystal structure, which was well known for many years (Russell et al., 1953). But, unbelievably, its transport and magnetic properties had not been investigated until quite recently although there was an intensive search, on a large international scale, for higher values of  $T_c$  in the family of binary compounds. The highest critical temperatures were achieved for A15-type compounds with a maximum value of about 23 K, which could not be improved since the early seventies until the discovery of the high- $T_c$  cuprate superconductors in 1986 (Bednorz and Müller, 1986;

**TABLE 1** Some boron and carbon containing superconductors. HP—under high pressure

Boron and borides			Carbon and carbides			Borocarbides		
	$T_c$ (K)	Space gr. structure		$T_c$ (K)	Space gr. structure		$T_c$ (K)	Space gr. structure
B	11.2 <sup>1</sup>	HP	Rb <sub>3</sub> C <sub>60</sub>	28 <sup>13</sup>	Fm $\bar{3}m$	LuB <sub>2</sub> C <sub>2</sub>	2.4 <sup>27</sup>	P4/mbm
YB <sub>12</sub>	4.7 <sup>2</sup>	Fm $\bar{3}m$	CaC <sub>6</sub>	11.5 <sup>14</sup>	BiF <sub>3</sub>	YB <sub>2</sub> C <sub>2</sub>	3.6 <sup>27</sup>	LaB <sub>2</sub> C <sub>2</sub>
ZrB <sub>12</sub>	5.8 <sup>2</sup>	UB <sub>12</sub>	(inter-cal. graph.)		CaC <sub>6</sub>	Mo <sub>2</sub> BC	7.5 <sup>28</sup>	Cmcm Mo <sub>2</sub> BC
YB <sub>6</sub>	7.1 <sup>2</sup>	Pm $\bar{3}m$	CB <sub>8</sub>	4 <sup>15</sup>	Fd $\bar{3}m$			
LaB <sub>6</sub>	5.7 <sup>2</sup>	CaB <sub>6</sub>			diamond	LuNi <sub>2</sub> B <sub>2</sub> C	16 <sup>29</sup>	I4/mmm
MgB <sub>2</sub>	39 <sup>3</sup>	P6/mmm	BEDT-TTF-	12.8 <sup>16</sup>	organic	ScNi <sub>2</sub> B <sub>2</sub> C	15 <sup>30</sup>	LuNi <sub>2</sub> B <sub>2</sub> C
MoB <sub>2.5</sub>	8.1 <sup>4</sup>	AlB <sub>2</sub>	based salt	HP		ThNi <sub>2</sub> B <sub>2</sub> C	8 <sup>31</sup>	
NbB	8.3 <sup>5</sup>	Cmcm	YC <sub>2</sub>	4.0 <sup>17</sup>	I $\bar{4}$ /mmm	YNi <sub>2</sub> B <sub>2</sub> C	15.5 <sup>29</sup>	
TaB	4.0 <sup>5</sup>	CrB			CaC <sub>2</sub>	YPd <sub>2</sub> B <sub>2</sub> C	23 <sup>32</sup>	
Mo <sub>2</sub> B	5.1 <sup>6</sup>	I4/mcm	La <sub>2</sub> C <sub>3</sub>	11 <sup>18</sup>	I43d	YPt <sub>2</sub> B <sub>2</sub> C	10 <sup>33</sup>	
Re <sub>3</sub> B	4.7 <sup>4</sup>	CuAl <sub>2</sub>	(Y,Th) <sub>2</sub> C <sub>3</sub>	17 <sup>19</sup>	Pu <sub>2</sub> C <sub>3</sub>			
Li <sub>2</sub> Pd <sub>3</sub> B	8 <sup>7</sup>	Cmcm	Mo <sub>56</sub> C <sub>44</sub>	13 <sup>20</sup>	Fm $\bar{3}m$			
		Re <sub>3</sub> B	NbC <sub><i>y</i></sub>	11.8 <sup>21</sup>	NaCl			
		P4 <sub>3</sub> 32						
		Li <sub>2</sub> Pd <sub>3</sub> B <sup>34</sup>	Mo <sub>2</sub> C	12.2 <sup>5</sup>	orthorh.			
LuRuB <sub>2</sub>	10.0 <sup>8</sup>	Pnma						

*(continued on next page)*

**TABLE 1** (continued)

Boron and borides			Carbon and carbides			Borocarbides	
	$T_c$ (K)	Space gr. structure		$T_c$ (K)	Space gr. structure	$T_c$ (K)	Space gr. structure
YRuB <sub>2</sub>	7.8 <sup>8</sup>	LuRuB <sub>2</sub>	LaNiC <sub>2</sub> (La,Th)NiC <sub>2</sub>	2.7 <sup>22</sup> 7.9 <sup>23</sup>	Amm2 CeNiC <sub>2</sub>		
YOs <sub>3</sub> B <sub>2</sub>	6.0 <sup>8</sup>	P6/mmm					
LuOs <sub>3</sub> B <sub>2</sub>	4.7 <sup>9</sup>	CeCo <sub>3</sub> B <sub>2</sub>	LaBrC	7.1 <sup>24</sup>	C2/m		
			YIC	10.0 <sup>25</sup>	Gd <sub>2</sub> C <sub>2</sub> I <sub>2</sub>		
ErRh <sub>4</sub> B <sub>4</sub>	8–9 <sup>10,11</sup>	P4 <sub>2</sub> /nmc	Y(Br,I)C	11.6 <sup>25</sup>			
LuRh <sub>4</sub> B <sub>4</sub>	8–12 <sup>10,11</sup>	CeCo <sub>4</sub> B <sub>4</sub> <sup>12</sup>					
YRh <sub>4</sub> B <sub>4</sub>	10–11 <sup>10,11</sup>		Mo <sub>3</sub> Al <sub>2</sub> C	10 <sup>20</sup>	P4 <sub>1</sub> 32 $\beta$ -Mn		
			MgNi <sub>3</sub> C	8.5 <sup>26</sup>	Pm $\bar{3}$ m SrTiO <sub>3</sub>		

<sup>1</sup> Eremets et al., 2001. <sup>2</sup> Matthias et al., 1968. <sup>3</sup> Nagamatsu et al., 2001. <sup>4</sup> Cooper et al., 1970. <sup>5</sup> Savitskii et al., 1973. <sup>6</sup> Havinga et al., 1972. <sup>7</sup> Togano et al., 2004. <sup>8</sup> Ku and Shelton, 1980. <sup>9</sup> Lee et al., 1987. <sup>10</sup> Fischer and Maple, 1982. <sup>11</sup> Maple and Fischer, 1982. <sup>12</sup> The alternative types LuRu<sub>4</sub>B<sub>4</sub> (s.g. I4<sub>1</sub>/acd) and LuRh<sub>4</sub>B<sub>4</sub> (s.g. Ccca) have also been reported for the RRh<sub>4</sub>B<sub>4</sub> compounds (Rogl, 1984). <sup>13</sup> Rosseinsky et al., 1991. <sup>14</sup> Weller et al., 2005. <sup>15</sup> Ekimov et al., 2004. <sup>16</sup> Williams et al., 1991. <sup>17</sup> Gulden et al., 1997. <sup>18</sup> Giorgi et al., 1969. <sup>19</sup> Krupka et al., 1969. <sup>20</sup> Fink et al., 1965. <sup>21</sup> Gusev et al., 1996. <sup>22</sup> Lee et al., 1996. <sup>23</sup> Lee and Zeng, 1997. <sup>24</sup> Simon et al., 1991. <sup>25</sup> Henn et al., 2000. <sup>26</sup> He et al., 2001. <sup>27</sup> Sakai et al., 1982. <sup>28</sup> Lejay et al., 1981. <sup>29</sup> Cava et al., 1994b. <sup>30</sup> Ku et al., 1994. <sup>31</sup> Lai et al., 1995. <sup>32</sup> Tominez et al., 1998; Dezaneti et al., 2000; Cava et al., 1994a. <sup>33</sup> Cava et al., 1994d. <sup>34</sup> Eibenstein and Jung, 1997.

Wu et al., 1987). Nagamatsu et al. (2001) found a  $T_c$  as high as 40 K for  $MgB_2$ . Electronic structure calculations show that  $MgB_2$ , being essentially metallic boron held together by covalent B–B and ionic B–Mg bonding, is electronically a typical sp metal (Kortus et al., 2001). The crystal structure of  $MgB_2$  may be regarded as that of completely intercalated graphite with carbon replaced by boron. Thus the band structure of  $MgB_2$  is graphite-like, but with  $\pi$  bands lying deeper than in graphite, and two-dimensionality (2D) features are assumed to be important for the superconductivity in this compound (An and Pickett, 2001). Now it is well established that  $MgB_2$  is a multiband superconductor with two well distinguishable superconducting gaps (see, e.g., Wälte et al., 2006). A strong influence of 2D effects on  $T_c$  had been proposed by Ginzburg (1964, 2000) but these aspects are yet to be understood in more detail. On the other hand, the electronic structure of the quaternary borocarbides  $RNi_2B_2C$  is clearly three-dimensional (see Section 3.2). The lattice structure of  $LuB_2C_2$  and  $YB_2C_2$  (see Table 1) contains well-separated BC layers, suggesting 2D behavior. Anyhow, the electronic properties of these low- $T_c$  superconductors are not yet well investigated.

### 1.3 Interplay of superconductivity and magnetism

The discovery of the quaternary rare-earth transition-metal borocarbide (RTBC) superconductors generated great excitement for two reasons. First,  $T_c \approx 23$  K in the Pd-system was, at that time, the highest known transition temperature for bulk intermetallics. Such a high  $T_c$  had been reported for thin  $Nb_3Ge$ -films, two decades before (Gavaler et al., 1974). Apart from the relatively high values of their  $T_c$ , the RTBC have attracted a great deal of attention because some of them contain a high concentration of lanthanide magnetic moments, which are coupled by an exchange interaction. The interplay between the two collective phenomena magnetism and superconductivity has been an active area of interest for many years (see reviews by Fischer and Maple, 1982; Maple and Fischer, 1982; Bulaevskii et al., 1985; Fischer, 1990; Maple, 1995). In this section we will briefly review this problem starting with compounds where superconductivity and magnetism completely (to our present knowledge) exclude each other, then continuing with systems for which some kind of coexistence of these two phenomena was observed, and finishing with the recently discovered coexistence of superconductivity and weak itinerant ferromagnetism.

#### 1.3.1 Superconductivity and magnetic ordering as antagonistic phenomena

In the usual BCS theory of superconductivity electrons are paired with opposite spins (singlet pairing) and, obviously, they cannot give rise to magnetically ordered states. Hence magnetic order and superconductivity should be antagonistic. In high- $T_c$  cuprate materials, depending on the doping rate, the Cu-3d electrons (or holes) contribute to a localized antiferromagnetic (or spin glass) state or they participate in superconductivity, i.e. the two phenomena do not really coexist (Aharony et al., 1988; Luke et al., 1990).

Intriguing forms of competition between superconductivity and ferromagnetism have recently been reported for the element iron, where the two coop-

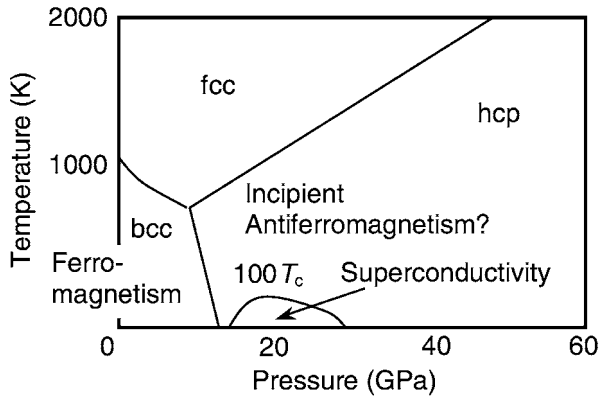


**FIGURE 2** Proposed temperature-pressure phase diagram of iron (after Saxena and Littlewood, 2001) with the ferromagnetic body-centered cubic (bcc) phase, the paramagnetic face-centered cubic phase (fcc) and the hexagonal close-packed phase (hcp).

erative phenomena are related to different crystallographic structures. It is well known that, at pressure above 10 GPa, Fe transforms from a ferromagnetic cubic phase into a non-ferromagnetic hexagonal one. Wohlfarth (1979) argued that the hexagonal iron might be a low-temperature superconductor. This prediction has now been confirmed by Shimizu et al. (2001) who found superconductivity in Fe below 2 K at pressures  $P$  between 15 and 30 GPa. An interesting open question is whether high-pressure iron is an unconventional superconductor with Cooper pairing mediated by magnetic fluctuations (as proposed by Fay and Appel, 1980) instead of phonons. At  $T = 0$  the superconductivity disappears at a quantum critical point ( $P \approx 30$  GPa; see Figure 2). This may be due to reduced magnetic fluctuations or to a reduced density of states  $N(E_F)$  caused by electron-band broadening at higher densities.

### 1.3.2 Superconductors with magnetic impurities

The superconducting state can coexist with magnetic moments of localized electrons (e.g., of 4f type). It was experimentally found by Matthias et al. (1958a) that for magnetic lanthanide impurities substituted into a superconductor,  $T_c$  rapidly decreases with increasing impurity concentration and that superconductivity is completely destroyed beyond a critical concentration of the order of one percent. This has been well understood by a theoretical approach of Abrikosov and Gor'kov (1960) who took into account that scattering by magnetic impurities leads to pair breaking. However, many systems with lanthanide magnetic moments show deviations from the behavior predicted by Abrikosov and Gor'kov (AG). As has been proven theoretically (Keller and Fulde, 1971; Fulde and Peschel, 1972) and confirmed by many experiments, the effects of crystalline electric fields on the magnetic moments result in a weaker decrease of  $T_c$  with increasing magnetic-impurity concentration compared to the AG prediction. On the other hand, it was demonstrated theoretically by Müller-Hartmann and Zittartz (1971) and experimentally by Riblet and Winzer (1971) that effects

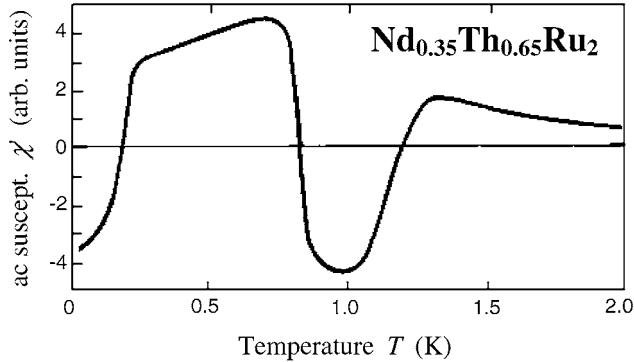


**FIGURE 3** Reentrant superconductivity in  $\text{Nd}_{0.35}\text{Th}_{0.65}\text{Ru}_2$  at zero applied magnetic field (after Hüser et al., 1983). Upon cooling, first, the real part of the ac susceptibility,  $\chi'$ , becomes negative, indicating superconductivity, then the material reenters the normal state ( $\chi' > 0$ ) and eventually reentrance of superconductivity occurs at even lower temperatures.

of hybridization and strong correlation (Kondo effect) may cause a considerably stronger reduction of  $T_c$  than predicted by AG. Furthermore the AG predictions will fail for higher concentrations of the lanthanide magnetic moments which are usually coupled by certain types of indirect exchange interaction and show cooperative magnetic phenomena.

The first example where such deviation from the AG behavior has been realized is  $\text{CeRu}_2$  where more than 30% of non-magnetic Ce can be replaced by Gd (Matthias et al., 1958b; Peter et al., 1971), Tb (Hillenbrand and Wilhelm, 1970; Fernandez-Baca and Lynn, 1981) or Ho (Lynn et al., 1980; Willis et al., 1980) before superconductivity is suppressed. The measurements of the susceptibility, the specific heat and the Mössbauer effect as well as neutron-scattering results clearly indicated that the ordering of the heavy-lanthanide magnetic moments in these materials is of spin-glass or, strictly speaking, cluster-glass type with short-range ferromagnetic order (Roth, 1978; Davidov et al., 1977). For the pseudobinary systems  $(\text{Gd},\text{La})\text{Ru}_2$  (Jones et al., 1978) and  $(\text{Nd},\text{Th})\text{Ru}_2$  (Hüser et al., 1983), which are superconducting spin glasses or cluster glasses similar to the  $(\text{R},\text{Ce})\text{Ru}_2$  systems mentioned above, even reentrant superconductivity occurs as shown in Figure 3 for the compound  $\text{Nd}_{0.35}\text{Th}_{0.65}\text{Ru}_2$ . The competition between superconductivity and ferromagnetic short-range order results in a complicated non-monotonic temperature dependence of the susceptibility, indicating two normal and two superconducting phases as a function of temperature.

### 1.3.3 Superconductivity and local-magnetic-moment cooperative phenomena

To understand the interplay of superconductivity and magnetism in systems containing localized magnetic moments in high concentration, Gor'kov and Rusinov (1964) extended the AG theory taking into account cooperative magnetic phenomena. They concluded that ferromagnetism would destroy superconductivity because the conduction electrons will be polarized by exchange interaction with the ordered magnetic moments. Ginzburg (1956) had pointed out, already before,

that superconductivity and ferromagnetism in (type-I) superconductors can only coexist if the magnetic field  $H_{\text{eff}} \approx M_s$  caused by the net spontaneous magnetization  $M_s$  in the material is smaller than the thermodynamic critical field  $H_c$  of the superconductor. Fulde and Ferrell (1964) and Larkin and Ovchinnikov (1964) demonstrated theoretically that, if in such cases  $H_{\text{eff}}$  is sufficiently large, the superconducting state will deviate from the BCS state in being spatially non-uniform. For type-II superconductors this conclusion has to be modified, as only states must be excluded which, at the same time, are homogeneously magnetized and homogeneously superconducting. This will be achieved if  $H_{\text{eff}}$  is smaller than the lower critical field  $H_{c1}$ . An alternative solution of the dilemma is the self-induced formation of vortex structures (see, e.g., Fulde and Keller, 1982). Such spontaneous vortex structures should occur for  $H_{c1} < M_s < H_{c2}$  (Chia et al., 2006) where this relation should not be taken too literally because actually more detailed information on  $H_{\text{eff}}$  and its relation to  $M_s$  would have to be taken into account. A further possibility is that the electromagnetic coupling of superconductivity and magnetism causes an oscillating magnetic order which coexists with a homogeneous superconducting state. The wavelength of the oscillations is governed by the penetration depth  $\lambda$  of the superconductor (Blount and Varma, 1979; Matsumoto et al., 1979). An alternative mechanism for oscillatory magnetic order has been proposed by Anderson and Suhl (1959): the strength of the exchange interaction between the lanthanide magnetic moments mediated by the conduction electrons (RKKY interaction) is changed in the superconducting state because the electron-spin susceptibility is reduced in the long-wavelength range. Consequently the effective exchange interaction in the superconducting state will have a maximum at a finite wavelength, leading to an oscillatory magnetic state, even if the material would be ferromagnetic in the absence of superconductivity. The wavelength of this state is controlled by the coherence length  $\xi$  of the superconductor.

It was predicted by Baltensperger and Strässler (1963) that antiferromagnetic order may coexist with superconductivity. The first examples of compounds where true long range magnetic order coexisting with superconductivity has been observed are ternary Chevrel phases  $\text{RMO}_6\text{S}_8$  and  $\text{RRh}_4\text{B}_4$  compounds (see Fischer and Maple, 1982; Maple and Fischer, 1982). It is assumed that the magnetic moments and the superconducting electrons in these compounds belong to different more or less "isolated" sublattices, supporting superconductivity to exist despite the high concentration of localized magnetic moments (Lynn, 2001). The magnetic ordering temperatures are low ( $\approx 1$  K) whereas  $T_c$  is considerably larger. Therefore it cannot be excluded that magnetostatic interaction dominates the energies in the magnetic subsystem. It was found that in  $\text{ErRh}_4\text{B}_4$  (Fertig et al., 1977) and  $\text{HoMo}_6\text{S}_8$  (Ishikawa and Fischer, 1977) superconductivity is in competition with long-range ferromagnetic order, which results in a reentrant behavior and in the coexistence of superconductivity with oscillatory magnetic states (Thomlinson et al., 1982; Lynn et al., 1984). For most of the superconducting  $\text{RMO}_6\text{S}_8$  and  $\text{RRh}_4\text{B}_4$  compounds the magnetic interactions favor antiferromagnetic order with a magnetic unit cell on a length scale small compared to coherence length  $\xi$  and penetration depth  $\lambda$ , which results in a relatively weak influence on the superconducting

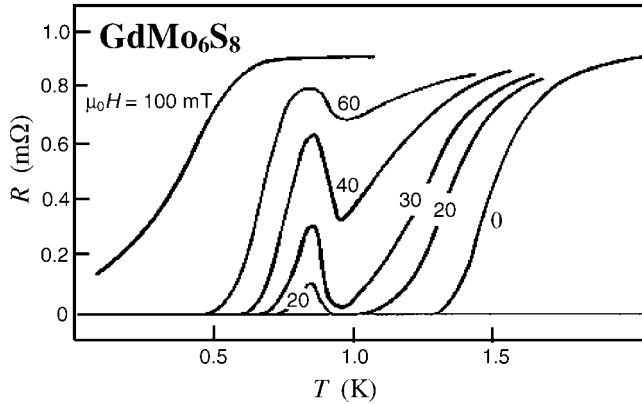


**FIGURE 4** Resistance- vs.-temperature curves of a  $\text{GdMo}_6\text{S}_8$  sample (nominal composition  $\text{Gd}_{1.2}\text{Mo}_6\text{S}_8$ ) for different values of the applied magnetic field, indicating near-reentrant superconductivity, i.e. reentrant behavior at a finite field only (after Ishikawa et al., 1982).

state i.e. antiferromagnetic order and superconductivity do readily accommodate one another. The antiferromagnetic transition in these materials has been confirmed by neutron scattering (see Thomlinson et al., 1982). Initially this transition had been observed as an anomaly in the upper critical field (Ishikawa et al., 1982). In particular, a near-reentrant behavior has been found for some of the antiferromagnetic ternary compounds i.e. reentrant behavior occurs if a sufficiently high magnetic field is applied, as shown in Figure 4 for  $\text{GdMo}_6\text{S}_8$ .

To explain this near-reentrant behavior it is usually argued (see Maple and Fischer, 1982) that, in the vicinity of the antiferromagnetic ordering temperature  $T_N$ , the applied field induces a remarkable degree of ferromagnetic order, which has been confirmed for various compounds.

In the case of  $\text{GdMo}_6\text{S}_8$ , additionally, large spin fluctuations below  $T_N$  have been assumed to enhance the near-reentrant behavior (Ishikawa et al., 1982). Machida et al. (1980b) extended the theory of antiferromagnetic superconductors (Baltensperger and Strässler, 1963), taking into account effects of the antiferromagnetic molecular field caused by aligned local magnetic moments in addition to spin fluctuations. Morozov (1980) as well as Zwicknagl and Fulde (1981) integrated the concept of Baltensperger and Strässler (1963) into the Eliashberg theory and they found that the influence of the antiferromagnetic staggered magnetization on the phonon-mediated quasiparticle attraction also results in anomalies of  $H_{c2}(T)$ , in particular, in its reduction below  $T_N$ .

The cuprates  $\text{RBa}_2\text{Cu}_3\text{O}_{7-\delta}$  with the orthorhombic (nearly tetragonal) R123-type structure exist for  $R = \text{Y}$  and all 4f elements with the exception of Ce and Tb. For  $0 < \delta < 0.6$  they are Cu-mixed-valence high- $T_c$  superconductors, with the exception of  $R = \text{Pr}$ . The value of  $T_c$  is about 90 K and it practically does not depend on the choice of R.  $\text{GdBa}_2\text{Cu}_3\text{O}_7$  shows three-dimensional antiferromagnetic ordering with  $T_N \approx 2.2$  K and a staggered magnetic moment of  $7.4\mu_B$  which is close to the Hund's rule  $\text{Gd}^{3+}$  free ion value (Paul et al., 1988). Since  $T_N$  does

not change much if  $\delta$  is increased from 0 to 1 and the material becomes a semiconductor with antiferromagnetic ordering of the  $\text{Cu}^{2+}$  magnetic moments (Dunlap et al., 1988), the Gd magnetic order cannot be dominantly governed by indirect exchange via conduction electrons (RKKY interaction) and the two antiferromagnetic structures on the R and the Cu sublattices are only weakly coupled to each other. On the other hand the value of  $T_N \approx 2.2$  K is too high to be explained by dipolar interactions only. Thus the type of magnetic coupling of the R magnetic moments is not yet fully understood. For R = Nd, Sm, Dy, Er, and Yb the single- $\text{R}^{3+}$ -ion crystal field splitting results in magnetic (doublet) ground states and the  $\text{RBa}_2\text{Cu}_3\text{O}_7$  compounds with these R elements show antiferromagnetic ordering with  $T_N \leq 1$  K. For R = Dy and Er the R magnetism (as well as the Cu magnetism) is two-dimensional (Lynn, 1992). For R = Ho the crystal field ground state in the R123 structure is a singlet. Nevertheless, antiferromagnetic ordering ( $T_N = 0.17$  K) has been observed also for this compound and the Ho magnetic moments have assumed to be induced in the electronic singlet ground state by nuclear hyperfine interaction (Dunlap et al., 1987). In these R123 superconductors the superconductivity persists below  $T_N$ . Hence there is no measurable effect of the ordered magnetic moments on superconductivity. This fact supports that exchange interaction between the conduction electrons and the lanthanide magnetic moments is minor and pair breaking due to exchange scattering is weak. On the other hand, the relatively high value of  $T_N \approx 2.2$  K (for Gd123) suggests that some small indirect exchange between the lanthanide magnetic moments operates across the  $\text{CuO}_2$  layers (Fischer, 1990). The situation is totally different for Pr123 where antiferromagnetic order of the Pr magnetic moments develops at  $T_N \approx 17$  K and superconductivity does not occur. The superconductivity in Pr123, which has been reported by Zou et al. (1998), is not yet understood. Probably it is connected with a modified occupation of the lattice sites by Pr and Ba ions (Narozhnyi and Drechsler, 1999; Blackstead et al., 2001). The anomalous behavior of Pr123 has been attributed to hybridization of Pr-4f states with O-2p states, dramatically increasing the exchange interactions between the Pr magnetic moments and completely disrupting the quasiparticles which form the Cooper pairs in the  $\text{CuO}_2$  planes (Fehrenbacher and Rice, 1993; Lynn, 1997; Skanthakumar et al., 1997). A further consequence of the hybridization of the Pr-4f electrons, besides the enhanced value of  $T_N$  and the absence of superconductivity, is a considerable interaction of the Cu magnetic subsystem with the Pr subsystem. This behavior is in contrast to that observed in the R123 materials mentioned above: Pr123 shows Cu antiferromagnetism over the whole range of  $\delta = 0$ –1 with an ordering temperature  $T_N[\text{Cu}]$  of about 300 K instead of  $T_N[\text{Cu}] \approx 410$  K for Y123 at  $\delta \approx 0.9$ . Furthermore, below  $T_N \approx 17$ –20 K an incommensurate magnetic structure develops involving both the Pr and the Cu moments where the Cu moments are found to be non-collinear (Boothroyd, 2000).

Coexistence of superconductivity and magnetic order has also been reported for ruthenocuprates with typical composition  $\text{RuSr}_2\text{RCu}_2\text{O}_8$  or  $\text{RuSr}_2(\text{R,Ce})_2\text{Cu}_2\text{O}_{10-\delta}$ , with R = Sm, Eu or Gd, where the magnetic-ordering temperature  $T_N = 100$ –180 K is much higher than  $T_c = 15$ –40 K (Bauernfeind et al., 1995; Felner et al., 1997c). Neutron diffraction experiments (Lynn et al., 2000) have shown that  $T_N$  is related to basically antiferromagnetically ordered magnetic mo-

ments in the Ru sublattices and, in the case of  $\text{RuSr}_2\text{GdCu}_2\text{O}_8$ , the Gd moments order independently antiferromagnetically at 2.5 K. The small ferromagnetic component reported for these materials for temperatures below  $T_N$  is possibly attributed to spin canting resulting in weak ferromagnetism of Dzyaloshinsky–Moriya type. To explain the coexistence of this type of magnetism with superconductivity it has been assumed that the magnetically ordered Ru sublattice is practically decoupled from the superconducting  $\text{CuO}_2$  planes (Bernhard et al., 1999; Felner, 1998; Felner et al., 1999; see also Braun, 2001; Awana, 2005; Chu et al., 2005; Felner et al., 2005; Williams, 2006).

True microscopic coexistence of superconductivity and localized-electron weak ferromagnetism has been found in  $\text{ErNi}_2\text{B}_2\text{C}$  (see Section 4.10.2).

In the Heusler alloy  $\text{ErPd}_2\text{Sn}$  superconductivity and antiferromagnetic order coexist although there is no clear separation between the superconducting and the magnetic sublattices and  $T_c \approx 1.17$  K is not much different from  $T_N \approx 1$  K (Shelton et al., 1986; Stanley et al., 1987). However, the focus on this interesting compound (Lynn, 2001) was short lived because of the discovery of the high- $T_c$  cuprate superconductors.

An interesting theoretical prediction is that, similarly as in the p-wave superconductors discussed in the next subsection, non-magnetic impurities in an antiferromagnetic superconductor cause pair breaking (Morozov, 1980; Zwicky and Fulde, 1981) whereas non-magnetic impurities in a non-magnetic superconductor are not expected to destroy superconductivity (Anderson, 1959).

### 1.3.4 Superconductivity and itinerant-electron magnetism

Fay and Appel (1980) predicted unconventional superconductivity (i.e. spin triplet pairing in particular p-wave pairing; see also Section 3.5) mediated by longitudinal spin fluctuations to coexist with itinerant ferromagnetism if the magnetization is small enough. These authors also declared  $\text{ZrZn}_2$  as a candidate for this phenomenon. For reasons of time-reversal symmetry, in p-wave superconductors all impurities are pair breakers (Foulkes and Gyorffy, 1977) and, therefore, superconductivity will be observed only in very clean samples. This behavior is different from that of BCS (s-wave) superconductors where non-magnetic impurities do not destroy superconductivity (Anderson, 1959). Matthias and Bozorth (1958) had found that  $\text{ZrZn}_2$  is ferromagnetic although both elements, Zr and Zn, are non-ferromagnetic. These authors also were the first who suggested that  $\text{ZrZn}_2$  could be a superconductor. Wohlfarth (1968) showed that  $\text{ZrZn}_2$  is a weak itinerant d-electron ferromagnet. However it has been demonstrated recently that  $\text{ZrZn}_2$  samples prepared so far do not superconduct (Yelland et al., 2005). Superconductivity coexisting with weak itinerant ferromagnetism has been reported for  $\text{UGe}_2$  (Saxena et al., 2000),  $\text{URhGe}$  (Aoki et al., 2001), and  $\text{Sr}_2\text{RuO}_4$  (Sudhakar Rao et al., 2006) and it has been assumed to be based on triplet pairing. In  $\text{UGe}_2$  the superconductivity is pressure induced and it disappears at the same pressure as the ferromagnetism. However, the nature of superconductivity in  $\text{UGe}_2$  is not yet really understood (Nakane et al., 2005). Since the 5f magnetic moments are expected to be partially localized, Suhl (2001) and Abrikosov (2001) developed an alternative pairing model based on interaction of the conduction electrons with

ferromagnetically ordered localized spins which can only lead to an s-wave order parameter. This concept is supported by experiments of Bauer et al. (2001) who showed that high-purity specimens with long mean free paths are not needed in the case of  $\text{UGe}_2$  in order to observe superconductivity near the critical pressure where the magnetic ordering temperature vanishes. Furthermore, for the s-wave superconductivity not to be destroyed by magnetism the metal has to be of heavy-fermion type, which also is supported by the experimental results of Bauer et al. (2001) (for the interplay of superconductivity and magnetism in heavy-fermion metals and quantum critical materials see also Steglich, 2007).

Superconductivity has also been found to coexist and to compete with itinerant-electron antiferromagnetism (spin-density waves), which has been extensively reviewed by Gabovich et al. (2001).

To summarize Section 1.3, there are various forms of the interplay of magnetism and superconductivity, which can be divided into competition and coexistence phenomena. In iron different types of crystal structure and bonding between the atoms, both varied by preparation routes or thermodynamic parameters such as pressure, result in one of the antagonistic cooperative phenomena ferromagnetism or superconductivity. Strong competition is found in high- $T_c$  cuprates where, depending on the doping rate, Néel-type antiferromagnetism (or spin glass) or superconductivity occur, both based on copper-d electrons. Coexistence of localized magnetic moments (e.g., from 4f elements) with superconductivity is known for systems where the concentration of these moments is small enough or they are antiferromagnetically ordered and only weakly coupled to the conduction electrons. Even weak ferromagnetism of such localized moments can coexist with superconductivity. In  $\text{RuSr}_2\text{GdCu}_2\text{O}_8$  and  $(\text{R,Ce})\text{RuSr}_2\text{Cu}_2\text{O}_{10-\delta}$ , probably, the Ru subsystem with weak ferromagnetism of Dzyaloshinsky–Moriya type is weakly coupled to and coexists with superconducting  $\text{CuO}_2$  layers. Most surprising are the coexistence of localized-electron weak ferromagnetism with superconductivity in  $\text{ErNi}_2\text{B}_2\text{C}$  (see Section 4.10.2) and the coexistence of weak itinerant ferromagnetism with triplet-pairing superconductivity in  $\text{UGe}_2$ ,  $\text{URhGe}$  and  $\text{Sr}_2\text{RuO}_4$ .

## 1.4 $\text{RNi}_2\text{B}_2\text{C}$ compounds

A striking feature distinguishing the superconducting  $\text{RT}_2\text{B}_2\text{C}$  compounds from other superconductors known until 1994 is that for certain combinations of elements R and T superconductivity and antiferromagnetic order have been found to coexist in  $\text{RT}_2\text{B}_2\text{C}$  with the values of the magnetic ordering temperature  $T_N$  being comparable with the  $T_c$  values (see Figure 5), i.e. the magnetic energy is comparable with the superconducting condensation energy. Therefore the investigation of these compounds is expected to result in new insights into the interplay of superconductivity and magnetism. In addition to many specific studies in this field published so far, there are various reports and review articles summarizing experimental and theoretical results on the superconducting and magnetic properties of these materials and comparing them with other superconductors, as, e.g., Canfield et al. (1997b), Lynn (1997), Takagi et al. (1997), Canfield et al. (1998), Felner (1998), Gupta (1998), Nagarajan and Gupta (1998), Schmidt and

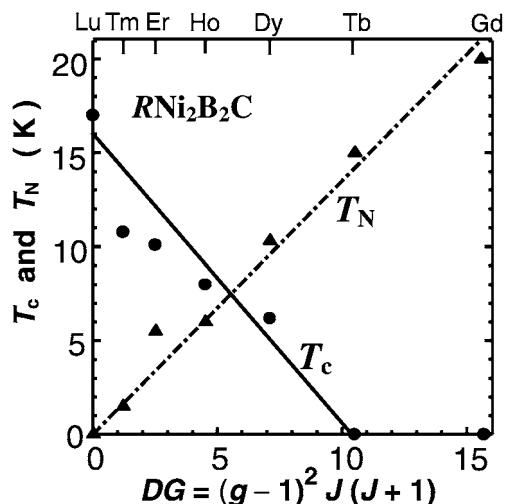


**FIGURE 5** Critical temperatures for superconductivity,  $T_c$ , and antiferromagnetic ordering,  $T_N$ , for  $RNi_2B_2C$  compounds with  $R = Lu, Tm, Er, Ho, Dy, Tb$  and  $Gd$  (for  $R = Tb$  the absence of superconductivity has been confirmed down to 300 mK by [Tomy et al., 1996a](#)).  $DG$  is the de Gennes factor,  $g$  the Landé factor, and  $J$  the total angular momentum of the  $R^{3+}$  Hund's rule ground state. The straight lines represent rough linear approximations.

Braun (1998), Paranthaman and Chakoumakos (1998), Hilscher and Michor (1999), Drechsler et al. (1999a), Gupta (2000), Schmiedeshoff et al. (2000), Tominez et al. (2000), Drechsler et al. (2001b), Müller and Narozhnyi (2001a), Müller et al. (2002), Hilscher et al. (2002), Wills et al. (2003), Thalmeier and Zwicky (2005), Mazumdar and Nagarajan (2005), Nagarajan et al. (2005), Bud'ko and Canfield (2006), Gupta (2006). Articles in this field are also collected in the Proceedings of the NATO Workshop "Rare Earth Transition Metal Borocarbides", held at Dresden, Germany, in June 2000 (Müller and Narozhnyi, 2001b; see also Drechsler and Mishonov, 2001).

The high values of  $T_N$  demand that in quaternary borocarbides, different from the situation in high- $T_c$  cuprates and the classical magnetic superconductors, the exchange coupling between the lanthanide magnetic moments is the dominant magnetic interaction rather than magnetostatic interaction. Obviously the exchange is mediated by conduction electrons. Consequently also the interaction between the magnetic moments and the conduction electrons must be relatively strong. Figure 5 shows a linear scaling of  $T_N$  and, roughly approximated, also of  $T_c$  with the de Gennes factor ( $DG$ ),

$$DG = (g - 1)^2 J(J + 1), \quad (2)$$

of the  $R^{3+}$  Hund's rule ground state where  $g$  is the Landé factor and  $J$  the total angular momentum (de Gennes, 1958). Such de Gennes scaling, at the same time for both  $T_N$  and  $T_c$ , is known for various isostructural metallic  $R$  compounds, which is due to the fact that both effects, antiferromagnetism and the suppression of super-

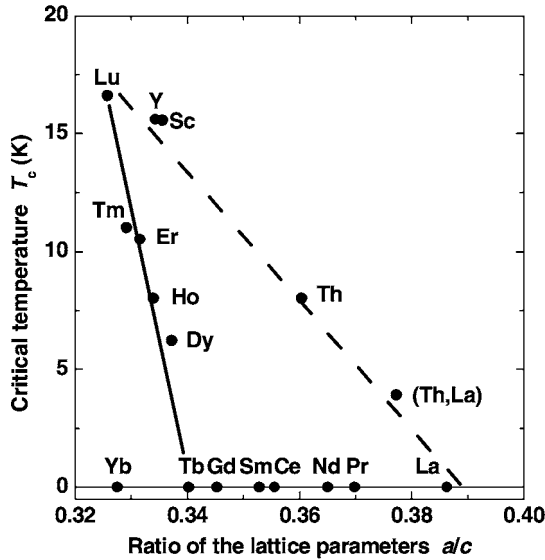


**FIGURE 6** Transition temperature vs. the  $a/c$  ratio of the lattice parameters for  $\text{RNi}_2\text{B}_2\text{C}$  compounds with the  $\text{LuNi}_2\text{B}_2\text{C}$ -type structure (see Section 2.1) for non-magnetic (after Lai et al., 1995) and magnetic R elements (based on the lattice parameters given in Figure 29). The absence of superconductivity,  $T_c \rightarrow 0$ , has been confirmed by low-temperature measurements, e.g. down to 340 mK and 20 mK for  $R = \text{Yb}$  and  $\text{La}$ , respectively (Yatskar et al., 1996; El Massalami et al., 1998a). Dashed line: series with strong variation of  $a/c$ ; solid line: series with weak variation of  $a/c$  (here de Gennes scaling works rather well according to Figure 5).

conductivity are governed by exchange interaction of conduction electrons with R-4f electrons. In some approximation both,  $T_N$  and the difference  $\Delta T_c$  of the critical temperature compared to that of a non-magnetic ( $DG = 0$ ) reference material, can be written as

$$T_N \sim -\Delta T_c \sim I^2 N(E_F) DG, \quad (3)$$

where  $I$  is the strength of the exchange interaction between 4f electrons and the conduction electrons and  $N(E_F)$  is the density of states at the Fermi level (Fischer, 1990). From Figure 5 it can be seen that both cases,  $T_N < T_c$  ( $R = \text{Tm}, \text{Er}, \text{Ho}$ ) and  $T_N > T_c$  ( $R = \text{Dy}$ ) occur in the series  $\text{RNi}_2\text{B}_2\text{C}$ . A similar phase diagram as that in Figure 5 had been predicted by Machida et al. (1980a) for a hypothetical system in which  $I$  varies instead of  $DG$ .

As can be seen in Figure 6,  $T_c$  of  $\text{RNi}_2\text{B}_2\text{C}$  compounds also much depends on the lattice parameters. As an example the dashed line represents the variation of  $T_c$  in a series with non-magnetic elements R. It should be noted that the effects of lattice parameters in Figure 6 cannot be explained by only taking into account the variation of  $N(E_F)$  in the expression (3), caused by the variation of the lattice parameters. In particular in  $\text{CeNi}_2\text{B}_2\text{C}$  and  $\text{YbNi}_2\text{B}_2\text{C}$  superconductivity is suppressed by strong hybridization of 4f electrons with conduction electrons (see Sections 4.2 and 4.12).

In this chapter we report on the current status of research on the quaternary borocarbide superconductors starting from their discovery. We will concentrate on the magnetic and superconducting properties of the  $\text{RNi}_2\text{B}_2\text{C}$  compounds. Section 2 is devoted to the typical crystal structure of the  $\text{RNi}_2\text{B}_2\text{C}$  phases and lattice distortions caused by magnetic ordering, but also to other compounds and crystal structures, which are related to those of  $\text{RNi}_2\text{B}_2\text{C}$ . Section 3 briefly summarizes the preparation of  $\text{RNi}_2\text{B}_2\text{C}$  compounds, and the electronic and superconducting properties of those compounds with non-magnetic R elements. Special features are Fermi surface nesting characterized by the nesting wave-vector ( $\approx 0.55, 0, 0$ ) and phonon softening at a certain wave vector (Section 3.3), and the positive curvature of the upper critical field as a function of temperature,  $H_{c2}(T)$ , near  $T_c$  (Section 3.6). The  $\text{RNi}_2\text{B}_2\text{C}$  compounds with 4f elements R are considered in Section 4. Among them, Ce and Yb are interesting because, in  $\text{RNi}_2\text{B}_2\text{C}$ , they show intermediate 4f valence and heavy fermion behavior, respectively.  $\text{DyNi}_2\text{B}_2\text{C}$  is outstanding because it is one of the exceptional superconducting antiferromagnets with  $T_N > T_c$ . In  $\text{HoNi}_2\text{B}_2\text{C}$  three different types of magnetic order occur and the competition between superconductivity and magnetism is most complex. An exciting feature of  $\text{ErNi}_2\text{B}_2\text{C}$  is the coexistence of superconductivity with a special type of weak ferromagnetism. Results on flux line lattices in the borocarbides, including the transformation from hexagonal to square vortex lattices, are presented in Section 5. The investigation of pseudoquaternary compounds  $(\text{R},\text{R}')\text{Ni}_2\text{B}_2\text{C}$ , reported in Section 6, provides more insight into the pair-breaking mechanisms in the quaternary borocarbides. A short summary and conclusions will be presented in Section 7.

## 2. CRYSTAL STRUCTURE AND CHEMICAL COMPOSITION

### 2.1 $\text{LuNi}_2\text{B}_2\text{C}$ -type-structure compounds

With the investigation of superconducting rare-earth transition-metal borocarbides the new  $\text{LuNi}_2\text{B}_2\text{C}$ -type structure, space group  $I4/mmm$ , has been discovered. This phase can be considered as the  $\text{ThCr}_2\text{Si}_2$ -type structure, which has the same space group, interstitially modified by carbon (Siegrist et al., 1994a, 1994b). Figure 7 shows the non-modified and the modified structures with  $\text{Th} \rightarrow \text{Gd}$ ,  $\text{Cr} \rightarrow \text{Co}$ ,  $\text{Si} \rightarrow \text{B}$  and  $\text{Lu} \rightarrow \text{Gd}$ ,  $\text{Ni} \rightarrow \text{Co}$ , respectively. The family of ternary rare-earth transition-metal metalloid compounds with the  $\text{ThCr}_2\text{Si}_2$ -type structure is very large (Just and Paufler, 1996) and a broad variety of magnetic and electronic properties has been observed in it. For example in  $\text{SmMn}_2\text{Ge}_2$ , both Sm and Mn carry a magnetic moment and two metamagnetic transitions occur connected with giant magnetoresistance effects (Brabers et al., 1993). Different collective phenomena as heavy-fermion behavior, superconductivity and magnetic order have been found in the exotic compound  $\text{CeCu}_2\text{Si}_2$  (Steglich et al., 1995). The  $\text{LuNi}_2\text{B}_2\text{C}$ -type structure has three open parameters, the two lattice constants  $a$  and  $c$  and the coordinate  $z$  of the boron atom. It has been pointed out by Godart et al. (1997) that the values of  $a$  and  $c$  of  $\text{RNi}_2\text{B}_2\text{C}$  compounds show a certain dispersion indicating a domain of existence which is in agreement with the variety of physical properties observed in many individual cases. The structure of the  $\text{RNi}_2\text{B}_2\text{C}$  compounds

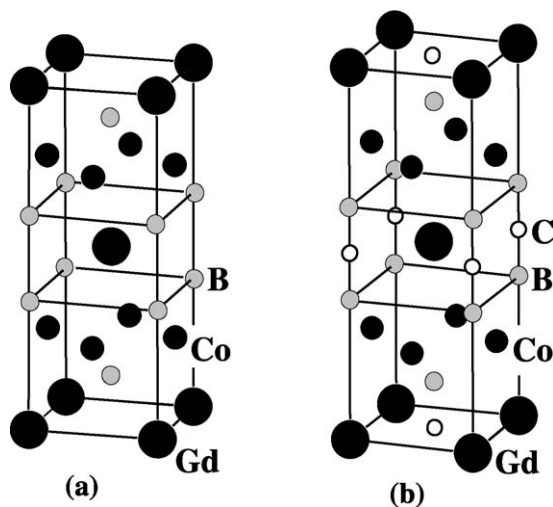


**FIGURE 7** (a)  $\text{GdCo}_2\text{B}_2$  has the  $\text{ThCr}_2\text{Si}_2$ -type structure, where Gd resides on the Th, Co on the Cr, and B on the Si sites, respectively. (b)  $\text{GdCo}_2\text{B}_2\text{C}$  has the  $\text{LuNi}_2\text{B}_2\text{C}$ -type structure, i.e. the  $\text{ThCr}_2\text{Si}_2$ -type interstitially modified with C atoms. The lattice constants are  $a = 3.575 \text{ \AA}$  and  $c = 9.561 \text{ \AA}$  for  $\text{GdCo}_2\text{B}_2$  (Felner, 1984),  $a = 3.548 \text{ \AA}$  and  $c = 10.271 \text{ \AA}$  for  $\text{GdCo}_2\text{B}_2\text{C}$  (Mulder et al., 1995), respectively.

is highly anisotropic with a ratio  $c/a$  of about 3. It has alternating sheets of  $\text{Ni}_2\text{B}_2$  tetrahedra and RC layers. In a good approximation, the parameters  $c$  and  $z$  linearly decrease with increasing radius of R (where R is assumed to be in the trivalent oxidation state) whereas  $a$  linearly increases with the radius of R, with the exception of Ce (see Section 4.2). Thus while going through the series of R elements from Lu to La, the structure shows a contraction along the tetragonal  $c$ -axis but an expansion perpendicular to it i.e. a decrease in the degree of anisotropy characterized by  $c/a$  and the boron shifts away from the RC layers more in the vicinity of the Ni layers. However, the radius variation of the rare earth does not much affect the B–C distance and the B–Ni distance. Consequently, there is a remarkable reduction of the B–Ni–B bonding angle from  $108.8^\circ$  for Lu to  $102^\circ$  for La, which is expected to influence the variation of the electronic structure within the series (Mattheiss et al., 1994). Baggio-Saitovitch et al. (2000), Loureiro et al. (2001) and D.R. Sánchez et al. (2005b) have also noted that the superconductivity and its suppression in the  $\text{RNi}_2\text{B}_2\text{C}$  series are structurally driven via the B–Ni–B bonding angle. A more detailed analysis of the influence of the crystal-chemical parameters of the  $\text{RNi}_2\text{B}_2\text{C}$  compounds on their properties has been presented by Volkova et al. (2002). The Ni–Ni distance in  $\text{LuNi}_2\text{B}_2\text{C}$  ( $2.449 \text{ \AA}$ ) is smaller than that in metallic Ni ( $2.492 \text{ \AA}$ ), confirming the metallic character of this compound.

Table 2 shows the known  $\text{RT}_2\text{B}_2\text{C}$  compounds (R: Sc, Y, La, Th, or 4f or 5f elements; T: 3d, 4d, or 5d elements). As many as six compounds of this type are known for R = Ce (Mazumdar and Nagarajan, 2005) as well as for La. Table 3 contains the superconducting compounds listed in Table 2 and their superconducting transition temperatures  $T_c$  and, if existing, the magnetic ordering tempera-

**TABLE 2** Known R–T–B–C compounds with the LuNi<sub>2</sub>B<sub>2</sub>C-type structure. Compounds printed in bold face are superconductors (see also Table 3)

CeCo <sub>2</sub> B <sub>2</sub> C	ErCo <sub>2</sub> B <sub>2</sub> C	LaIr <sub>2</sub> B <sub>2</sub> C	NdRh <sub>2</sub> B <sub>2</sub> C	TbCo <sub>2</sub> B <sub>2</sub> C	YCo <sub>2</sub> B <sub>2</sub> C
CeIr <sub>2</sub> B <sub>2</sub> C	<b>ErNi<sub>2</sub>B<sub>2</sub>C</b>	LaNi <sub>2</sub> B <sub>2</sub> C	PrCo <sub>2</sub> B <sub>2</sub> C	TbNi <sub>2</sub> B <sub>2</sub> C	<b>YNi<sub>2</sub>B<sub>2</sub>C</b>
<b>CeNi<sub>2</sub>B<sub>2</sub>C</b>	ErRh <sub>2</sub> B <sub>2</sub> C	<b>LaPd<sub>2</sub>B<sub>2</sub>C</b>	PrNi <sub>2</sub> B <sub>2</sub> C	TbRh <sub>2</sub> B <sub>2</sub> C	<b>YPd<sub>2</sub>B<sub>2</sub>C</b>
CePd <sub>2</sub> B <sub>2</sub> C	GdCo <sub>2</sub> B <sub>2</sub> C	<b>LaPt<sub>2</sub>B<sub>2</sub>C</b>	PrPd <sub>2</sub> B <sub>2</sub> C	<b>ThNi<sub>2</sub>B<sub>2</sub>C</b>	<b>YPt<sub>2</sub>B<sub>2</sub>C</b>
CePt <sub>2</sub> B <sub>2</sub> C	GdNi <sub>2</sub> B <sub>2</sub> C	LaRh <sub>2</sub> B <sub>2</sub> C	<b>PrPt<sub>2</sub>B<sub>2</sub>C</b>	<b>ThPd<sub>2</sub>B<sub>2</sub>C</b>	<b>YRu<sub>2</sub>B<sub>2</sub>C</b>
CeRh <sub>2</sub> B <sub>2</sub> C	GdRh <sub>2</sub> B <sub>2</sub> C	LuCo <sub>2</sub> B <sub>2</sub> C	PrRh <sub>2</sub> B <sub>2</sub> C	<b>ThPt<sub>2</sub>B<sub>2</sub>C</b>	YbNi <sub>2</sub> B <sub>2</sub> C
DyCo <sub>2</sub> B <sub>2</sub> C	HoCo <sub>2</sub> B <sub>2</sub> C	<b>LuNi<sub>2</sub>B<sub>2</sub>C</b>	<b>ScNi<sub>2</sub>B<sub>2</sub>C</b>	ThRh <sub>2</sub> B <sub>2</sub> C	
<b>DyNi<sub>2</sub>B<sub>2</sub>C</b>	<b>HoNi<sub>2</sub>B<sub>2</sub>C</b>	NdCo <sub>2</sub> B <sub>2</sub> C	SmCo <sub>2</sub> B <sub>2</sub> C	<b>TmNi<sub>2</sub>B<sub>2</sub>C</b>	
DyPt <sub>2</sub> B <sub>2</sub> C	HoRh <sub>2</sub> B <sub>2</sub> C	NdNi <sub>2</sub> B <sub>2</sub> C	SmNi <sub>2</sub> B <sub>2</sub> C	UNi <sub>2</sub> B <sub>2</sub> C	
DyRh <sub>2</sub> B <sub>2</sub> C	LaCo <sub>2</sub> B <sub>2</sub> C	<b>NdPt<sub>2</sub>B<sub>2</sub>C</b>	SmRh <sub>2</sub> B <sub>2</sub> C	URh <sub>2</sub> B <sub>2</sub> C	

**TABLE 3** Borocarbide superconductors with LuNi<sub>2</sub>B<sub>2</sub>C-type structure and their superconducting transition temperature  $T_c$  and magnetic ordering temperature  $T_N$ 

Compound	$T_c$ (K)	$T_N$ (K)	Compound	$T_c$ (K)	$T_N$ (K)
CeNi <sub>2</sub> B <sub>2</sub> C	0.1 <sup>1</sup> (?)	–	YRu <sub>2</sub> B <sub>2</sub> C	9.7 <sup>20</sup> (?)	–
DyNi <sub>2</sub> B <sub>2</sub> C	6.2 <sup>2</sup> , 6.4 <sup>3</sup>	11 <sup>2,18</sup>	LaPd <sub>2</sub> B <sub>2</sub> C	1.8 <sup>21</sup>	–
HoNi <sub>2</sub> B <sub>2</sub> C	8.8 <sup>24</sup> , 7.5 <sup>5</sup>	5–8 <sup>8,9,10</sup>	ThPd <sub>2</sub> B <sub>2</sub> C	14.5 <sup>15</sup>	–
ErNi <sub>2</sub> B <sub>2</sub> C	10.5 <sup>4,5</sup>	6.8 <sup>11,12</sup>	YPd <sub>2</sub> B <sub>2</sub> C <sup>m</sup>	23 <sup>4,16,19</sup>	–
TmNi <sub>2</sub> B <sub>2</sub> C	11 <sup>4,5</sup>	1.5 <sup>13,14</sup>	LaPt <sub>2</sub> B <sub>2</sub> C	10–11 <sup>17,22</sup>	–
LuNi <sub>2</sub> B <sub>2</sub> C	16.5 <sup>4,5</sup>	–	PrPt <sub>2</sub> B <sub>2</sub> C	6 <sup>17,22</sup>	–
YNi <sub>2</sub> B <sub>2</sub> C	15.5 <sup>4</sup>	–	NdPt <sub>2</sub> B <sub>2</sub> C	≈2 <sup>23</sup>	1.5 <sup>23</sup>
ScNi <sub>2</sub> B <sub>2</sub> C <sup>m</sup>	15 <sup>6</sup>	–	YPt <sub>2</sub> B <sub>2</sub> C	10–11 <sup>17,22</sup>	–
ThNi <sub>2</sub> B <sub>2</sub> C	8 <sup>7</sup>	–	ThPt <sub>2</sub> B <sub>2</sub> C	6.5 <sup>15</sup>	–

<sup>m</sup> Metastable. <sup>1</sup> El Massalami et al., 1998a. <sup>2</sup> Cho et al., 1995a. <sup>3</sup> Tomy et al., 1995. <sup>4</sup> Cava et al., 1994b. <sup>5</sup> Eisaki et al., 1994. <sup>6</sup> Ku et al., 1994. <sup>7</sup> Lai et al., 1995. <sup>8</sup> Grigereit et al., 1994. <sup>9</sup> Goldman et al., 1994. <sup>10</sup> Canfield et al., 1994. <sup>11</sup> Sinha et al., 1995. <sup>12</sup> Zarestky et al., 1995. <sup>13</sup> Cho et al., 1995b. <sup>14</sup> Lynn et al., 1997. <sup>15</sup> Sarrao et al., 1994. <sup>16</sup> Tominez et al., 1998. <sup>17</sup> Cava et al., 1994d. <sup>18</sup> Dervenagas et al., 1995a. <sup>19</sup> Dezaneti et al., 2000. <sup>20</sup> Hsu et al., 1998. <sup>21</sup> Jiang et al., 1995. <sup>22</sup> Buchgeister et al., 1995. <sup>23</sup> Paulose et al., 2003. <sup>24</sup> Rathnayaka et al., 1996.

tures  $T_N$ . Superconductivity in CeNi<sub>2</sub>B<sub>2</sub>C has been reported by El Massalami et al. (1998a) but has not been confirmed by further publications. If true, it would be exceptional in that this would be the only superconducting RNi<sub>2</sub>B<sub>2</sub>C compound with a light lanthanide R where Ce is in a mixed-valence state (see Section 4.2). Neither has the reported superconductivity in YRu<sub>2</sub>B<sub>2</sub>C (Hsu et al., 1998) been confirmed.

It should be noted that for RNi<sub>2</sub>B<sub>2</sub>C the counterpart without carbon does not exist. Cobalt is, so far, the only transition metal for which both the filled (with C) and the non-filled structures could be prepared (see Table 4). The examples of ferromagnetic GdCo<sub>2</sub>B<sub>2</sub> and antiferromagnetic GdCo<sub>2</sub>B<sub>2</sub>C show that the introduction of interstitial carbon has a remarkable effect on the magnetic and, consequently, electronic properties of these compounds.

**TABLE 4** Structural and magnetic properties of  $\text{RCo}_2\text{B}_2$  and  $\text{RCo}_2\text{B}_2\text{C}$  phases with the  $\text{ThCr}_2\text{Si}_2$  and  $\text{LuNi}_2\text{B}_2\text{C}$ -type structure, respectively. F—ferromagnetic; A—antiferromagnetic; P—paramagnetic; imp—impurity phase; SR—spin reorientation;  $T_C$ —Curie temperature;  $T_N$ —Néel temperature;  $a$  and  $c$ —tetragonal lattice parameters;  $z$ —coordinate of B with  $c$  as its unit

$\text{RCo}_2\text{B}_2$ $\text{RCo}_2\text{B}_2\text{C}$	$a$ (Å)	$c$ (Å)	$z$ of the B site (4e)	Type of magnetic order	$T_C$ (K)	$T_N$ (K)
$\text{YCo}_2\text{B}_2$	3.5598 <sup>2</sup>	9.342 <sup>2</sup>	0.3780 <sup>5</sup>	P <sup>2</sup>		
$\text{YCo}_2\text{B}_2\text{C}$	3.50 <sup>7</sup>	10.60 <sup>7</sup>		P (Pauli) <sup>1,6</sup>		
$\text{LaCo}_2\text{B}_2$	3.6186 <sup>2</sup>	10.223 <sup>2</sup>	0.3750 <sup>5</sup>	P <sup>2</sup>		
$\text{LaCo}_2\text{B}_2\text{C}$	3.63 <sup>7</sup>	10.38 <sup>7</sup>				
$\text{PrCo}_2\text{B}_2$	3.5985 <sup>2</sup>	9.951 <sup>2</sup>		F <sup>2</sup>	19.5 <sup>2</sup>	
$\text{PrCo}_2\text{B}_2\text{C}$	3.6156 <sup>8</sup>	10.3507 <sup>8</sup>	0.3506 <sup>8</sup>	A <sup>7,8</sup>		8.5 <sup>8</sup>
$\text{NdCo}_2\text{B}_2$	3.5920 <sup>1,5</sup>	9.8381 <sup>1,5</sup>	0.3750 <sup>5</sup>	F <sup>1,2</sup>	32 <sup>1</sup>	
$\text{NdCo}_2\text{B}_2\text{C}$	3.59 <sup>7</sup>	10.30 <sup>7</sup>		A <sup>6</sup>		≈3 <sup>6</sup>
$\text{SmCo}_2\text{B}_2$	3.5806 <sup>2</sup>	9.673 <sup>2</sup>		no (F imp <sup>2</sup> )		
$\text{SmCo}_2\text{B}_2\text{C}$	3.57 <sup>7</sup>	10.39 <sup>7</sup>		A <sup>6</sup>		≈6 <sup>6</sup>
$\text{GdCo}_2\text{B}_2$	3.575 <sup>1,5</sup>	9.561 <sup>1,5</sup>	0.3750 <sup>5</sup>	F <sup>1,2</sup>	26 <sup>1,2</sup>	
$\text{GdCo}_2\text{B}_2\text{C}$	3.548 <sup>3</sup>	10.271 <sup>3</sup>		A <sup>3</sup> A (helical) <sup>4</sup>		5.5 <sup>3</sup> ≈7 <sup>4</sup>
$\text{TbCo}_2\text{B}_2$	3.5670 <sup>5</sup>	9.4889 <sup>5</sup>	0.3750 <sup>5</sup>	?		
$\text{TbCo}_2\text{B}_2\text{C}$	3.53 <sup>7</sup>	10.52 <sup>7</sup>		A <sup>6</sup>		≈6 <sup>6</sup>
$\text{DyCo}_2\text{B}_2$	3.5548 <sup>2</sup>	9.331 <sup>2</sup>		A <sup>2</sup>		9.3 <sup>2</sup>
$\text{DyCo}_2\text{B}_2\text{C}$	3.51 <sup>7</sup>	10.54 <sup>7</sup>		A <sup>6</sup>		≈8 <sup>6</sup>
$\text{HoCo}_2\text{B}_2$	3.5517 <sup>2</sup>	9.251 <sup>2</sup>		A <sup>2</sup>		8.5 <sup>2</sup>
$\text{HoCo}_2\text{B}_2\text{C}$	3.500 <sup>6</sup>	10.590 <sup>6</sup>		A <sup>6</sup> , SR at 1.46 K		5.4 <sup>6</sup>
$\text{ErCo}_2\text{B}_2$	3.5450 <sup>2</sup>	9.161 <sup>2</sup>		A <sup>2</sup>		3.3 <sup>2</sup>
$\text{ErCo}_2\text{B}_2\text{C}$	3.48 <sup>7</sup>	10.60 <sup>7</sup>		A <sup>6</sup>		≈4 <sup>6</sup>

<sup>1</sup> Felner, 1984. <sup>2</sup> Rupp et al., 1987. <sup>3</sup> Mulder et al., 1995. <sup>4</sup> Bud'ko et al., 1995a. <sup>5</sup> Just and Paufler, 1996. <sup>6</sup> Rapp and El Massalami, 1999. <sup>7</sup> El Massalami et al., 2000. <sup>8</sup> Durán et al., 2006.

## 2.2 Lattice distortions due to orbital ordering

High-resolution neutron scattering on powder samples and high-resolution X-ray diffraction on single crystals revealed tetragonal-to-orthorhombic phase transitions in  $\text{ErNi}_2\text{B}_2\text{C}$  (Detlefs et al., 1997a; Kreyssig et al., 2001),  $\text{TbNi}_2\text{B}_2\text{C}$  (C. Song et al., 1999; Kreyssig et al., 2001; C. Song et al., 2001a),  $\text{DyNi}_2\text{B}_2\text{C}$  (Gasser et al., 1998a; Kreyssig et al., 2001), and  $\text{HoNi}_2\text{B}_2\text{C}$  (Kreyssig et al., 1999a). In the case of  $\text{HoNi}_2\text{B}_2\text{C}$  this transition has also been detected as a softening of the  $c_{66}$  elastic modulus, observed by sound experiments (Fil et al., 2004; Suzuki et al., 2004).

**TABLE 5** Magnetoelastic tetragonal-to-orthorhombic distortions at  $T = 1.5$  K (after Kreyssig et al., 2001) for  $\text{HoNi}_2^{11}\text{B}_2\text{C}$ ,  $\text{DyNi}_2^{11}\text{B}_2\text{C}$ ,  $\text{TbNi}_2^{11}\text{B}_2\text{C}$  and  $\text{ErNi}_2^{11}\text{B}_2\text{C}$  (direction of the distortion from Detlefs et al., 1999). The depicted direction for the distortion is the direction, in which the  $\mathbf{a}$ - $\mathbf{b}$ -basal plane is shortened. The distortion is quantified by the ratio of the side length of the orthorhombic  $\mathbf{a}$ - $\mathbf{b}$ -basal plane subtracted by 1. All directions are described in the tetragonal reference system

Compound	Propagation vector	Magnetic moment		Distortion	
		Value	Direction	Value	Direction
$\text{HoNi}_2^{11}\text{B}_2\text{C}$	(0 0 1)	$10.2\mu_{\text{B}}$	[1 1 0]	0.0019	[1 1 0]
$\text{DyNi}_2^{11}\text{B}_2\text{C}$	(0 0 1)	$8.0\mu_{\text{B}}$	[1 1 0]	0.0034	[1 1 0]
$\text{TbNi}_2^{11}\text{B}_2\text{C}$	(0.551 0 0)	$8.2\mu_{\text{B}}$	[1 0 0]	0.0062	[0 1 0]
$\text{ErNi}_2^{11}\text{B}_2\text{C}$	(0.554 0 0)	$8.2\mu_{\text{B}}$	[0 1 0]	0.0024	[0 1 0]

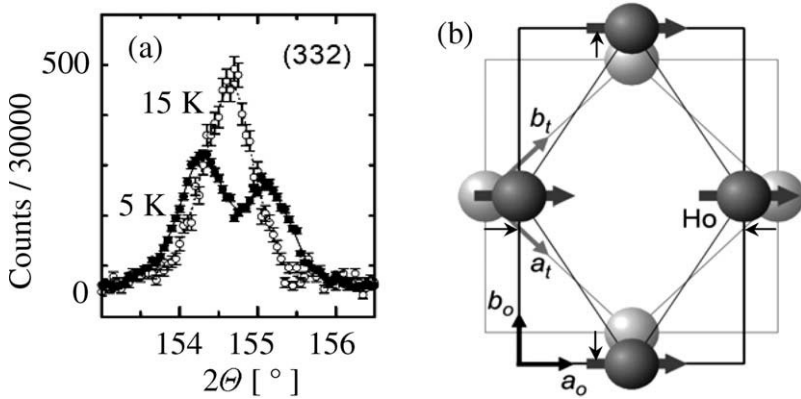


**FIGURE 8** Orthorhombic distortion of tetragonal  $\text{HoNi}_2\text{B}_2\text{C}$ . (a) Upon cooling from 15 K to 1.5 K the neutron-diffraction reflection (332) splits into two peaks (after Kreyssig, 2001).

(b) Schematic presentation of the distortion:  $a_t$ ,  $b_t$ —original tetragonal axes; large square: tetragonal basal plane;  $\rightarrow$ ,  $\uparrow$ : shift of the Ho atoms leading to the orthorhombic cell with the axes  $a_o$ ,  $b_o$ . Thick arrows: Ho magnetic moments in the commensurate  $c$ -axis modulated structure. Reused with permission from Kreyssig, A., Loewenhaupt, M., Freudenberger, J., Müller, K.-H., Ritter, C., *J. Appl. Phys.* 1999, **85**, 6058.

© 1999 American Institute of Physics

The results of some of these investigations are summarized in Table 5. Due to the different types of antiferromagnetic order occurring in these compounds (see Section 4) different types (directions) of the orthorhombic distortion develop in the magnetically ordered state. Such magnetoelastic distortions are common in rare-earth compounds and result from a competition of elastic, magnetic and crystalline-electric-field energy (Morin and Schmitt, 1990). They can be considered as the result of orbital ordering (or quadrupolar ordering; see Section 4.1) of the 4f electrons because the strong spin-orbit interaction couples the electric quadru-

pole moments to the ordered magnetic moments. In particular, in  $\text{HoNi}_2\text{B}_2\text{C}$  and  $\text{DyNi}_2\text{B}_2\text{C}$ , which exhibit collinear commensurate antiferromagnetic order at low temperatures, the magnetoelastic distortions can be approximately considered as the result of ferroquadrupolar ordering of the free-ion- $(J, J_z = J)$  quadrupole moments. It has been pointed out by [Detlefs et al. \(1999\)](#) that the lowering of lattice symmetry not only concerns the lattice structure but also has consequences for the detailed description of the magnetic structure. As an example, [Figure 8](#) shows the splitting of a certain neutron-diffraction reflection, caused by the distortion, and a schematic representation of the distortion, for  $\text{HoNi}_2\text{B}_2\text{C}$ . The distortion is a shortening of the tetragonal unit cell in  $[110]$  direction that coincides with the axes of the magnetic moments and of the negative free-ion- $(J, J_z = J)$  quadrupole moments.

Interestingly, the spontaneous magnetoelastic distortions in  $\text{ErNi}_2\text{B}_2\text{C}$  and  $\text{TbNi}_2\text{B}_2\text{C}$  are also commensurate although the underlying magnetic structures are incommensurate. The reason for this could be the observed so-called squaring-up of the staggered magnetic moments i.e. deviations of their magnitude from sinusoidal modulation. However small incommensurate lattice distortions in  $\text{TmNi}_2\text{B}_2\text{C}$  at temperatures below 13.5 K, in the non-magnetic orbitally ordered phase have been reported by [Andersen et al. \(2006a\)](#) (see also [Section 4.11](#)).

### 2.3 Single-, double- and triple-layer borocarbides (nitrides)

The  $\text{RNi}_2\text{B}_2\text{C}$  compounds can be considered as the  $n = 1$  variant of  $(\text{RC}/\text{N})_n\text{Ni}_2\text{B}_2$  structures where  $n$  RC or RN layers alternate with single  $\text{Ni}_2\text{B}_2$  layers (see [Figure 9](#)). Examples for the case  $n = 2$  are given by the compounds  $\text{YNiBC}$  ([Kitô et al., 1997](#)),  $\text{GdNiBC}$  ([El Massalami et al., 1995b](#)),  $\text{TbNiBC}$  ([El Massalami et al., 1998b](#)),  $\text{DyNiBC}$  ([El Massalami et al., 1998b](#)),  $\text{HoNiBC}$  ([El Massalami et al., 1995a](#)),  $\text{ErNiBC}$  ([Chang et al., 1996a](#)),  $\text{YbNiBC}$  ([Hossain et al., 1998](#)),  $\text{LuNiBC}$  ([Siegrist et al., 1994a](#)), and  $\text{LaNiBN}$  ([Cava et al., 1994c](#)). Among them only  $\text{LuNiBC}$  was reported to be superconducting ([Gao et al., 1994](#)) which, however, was questioned later on ([Cava, 2001](#)). Superconductivity was observed in  $\text{R}(\text{Ni},\text{Cu})\text{BC}$ , i.e. by the substitution of Cu for Ni, up to  $T_c = 8.9$  K for  $\text{R} = \text{Y}$  and up to  $T_c = 6.4$  K for  $\text{R} = \text{Lu}$  ([Gangopadhyay and Schilling, 1996](#)). Superconductivity has been also reported for various  $\text{RReBC}$  samples which, however, consisted of unknown phases ( $\text{R} = \text{Lu}, \text{Gd}, \text{Tb}$ ; [Chinchure et al., 1999, 2000](#)).  $\text{ErNiBC}$  is a ferromagnet ([Chang et al., 1996a](#)). Comparative studies on  $\text{RNiBC}$  compounds have been presented by [Fontes et al. \(1999\)](#), [Bourdarot et al. \(2001\)](#) and [Baggio-Saitovitch et al. \(2001, 2002a, 2002b\)](#). The latter authors found that  $\text{RNiBC}$ - and  $\text{RNi}_2\text{B}_2\text{C}$ -superconductors show the same dependence of  $T_c$  on structural features of the  $\text{NiB}_4$  tetrahedra in their lattice structure.

As a realization of the case  $n = 3$ , the superconductor  $\text{La}_3\text{Ni}_2\text{B}_2\text{N}_3$  has been prepared ([Cava et al., 1994c](#); [Zandbergen et al., 1994a](#); [Michor et al., 1996, 1998](#); [Blaschkowski et al., 2002](#)). Hydrogenation of this compound results in an increase of  $T_c$  by 0.5 K to 13.1 K ([Sieberer et al., 2006](#)). From results of electronic-structure calculations, [Verma et al. \(2005\)](#) predicted  $T_c \approx 30$  K for the hypothetical

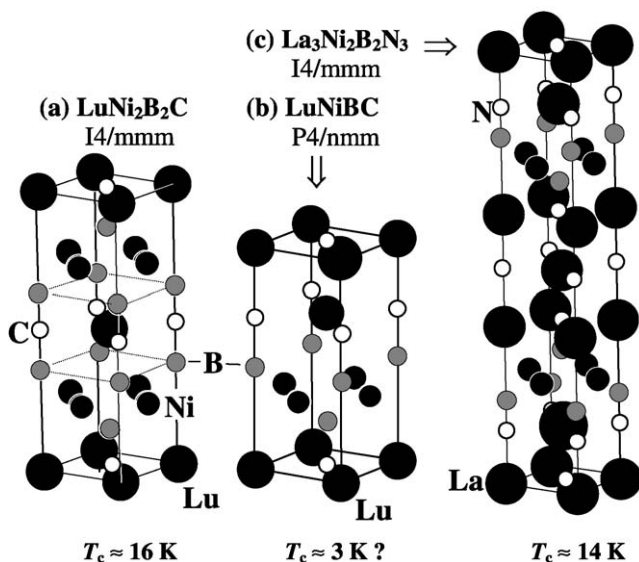


**FIGURE 9** Tetragonal rare-earth nickel borocarbides (nitrides) with (a) single, (b) double, and (c) triple RC(N)-layers and values of the superconducting transition temperature  $T_c$  (Cava et al., 1994c; Gao et al., 1994; and Blaschkowski et al., 2002, respectively).

$\text{Th}_3\text{Ni}_2\text{B}_2\text{N}_3$  compound.  $\text{Ce}_3\text{Ni}_2\text{B}_2\text{N}_3$  also exists but is not superconducting above 4 K (Cava, 2001). The case  $n = 4$  is realized in the non-superconducting compounds  $\text{Lu}_2\text{NiBC}_2$  (Zandbergen et al., 1994c) and  $\text{Y}_2\text{NiBC}_2$  (Rukang et al., 1995). However the relative positions of the layers do not appear to correlate over long distances and the 2:1:1:2 phase is subject to severe microtwinning. So far no detailed analysis on the crystal structure and physical properties of the  $n = 4$  compounds has been published.

The series  $(\text{RC})_n\text{Ni}_2\text{B}_2$  can be formally extended to  $(\text{RC})_n(\text{Ni}_2\text{B}_2)_m$  with  $m \neq 1$  and/or  $n \neq 1$ . Kitô et al. (1997) prepared the  $n = 3, m = 2$  quaternary borocarbide  $\text{Y}_3\text{Ni}_4\text{B}_4\text{C}_3$  which has a tetragonal layered structure (proposed space group I4) built up of a half  $\text{YNi}_2\text{B}_2\text{C}$  unit and a full  $\text{YNiBC}$  unit stacked along the  $c$ -axis. Measurements of resistance and susceptibility indicated a superconducting transition temperature of about 10 K (for a two-phase material containing the 3:4:4:3-phase together with the 1:1:1:1-phase). Yang-Bitterlich et al. (2002) detected  $\text{Y}_3\text{Ni}_4\text{B}_4\text{C}_3$ ,  $\text{Y}_5\text{Ni}_8\text{B}_8\text{C}_5$  and  $\text{Y}_5\text{Ni}_6\text{B}_6\text{C}_5$ .

A systematic investigation of the whole family of these multilayer compounds would be helpful for the understanding of the mechanisms for superconductivity and magnetism in the quaternary rare-earth transition-metal borocarbides. However this report will be restricted to magnetism and superconductivity in single-layer  $\text{RNi}_2\text{B}_2\text{C}$  borocarbides, i.e.  $(\text{RC}/\text{N})_n(\text{Ni}_2\text{B}_2)_m$  compounds with  $n \neq 1$  and  $m \neq 1$  will not be considered.

## 2.4 Metastable and related R–T–B–C(N) phases

Although some work on thermodynamics and phase diagrams of R–T–B–C(N) systems has been done (see e.g., Cava, 2001; Behr and Löser, 2005) the knowledge on R–T–B–C(N) phase diagrams and thermodynamic stability of the  $(RC)_n(Ni_2B_2)_m$  compounds, including the  $RNi_2B_2C$  compounds, is incomplete. In spite of the discovery of the  $LuNi_2B_2C$ -type structure, even the crystal structures of quaternary superconducting R–T–B–C phases and their stability in the composition range near the stoichiometry 1:2:2:1 are far from being completely determined. This is particularly true for R–Pd–B–C compounds where the highest value of  $T_c$ , 23 K for Y–Pd–B–C, had been reported (Cava et al., 1994a; Hossain et al., 1994). Pd-based borocarbides have been prepared by arc melting (Cava et al., 1994a; Sarrao et al., 1994) and also by non-equilibrium routes as rapid quenching (Ström et al., 1996; Freudemberger, 2000) or mechanical alloying (Gümbel et al., 2000a, 2000b). Although the superconducting phase with  $T_c = 23$  K has been identified as  $YPd_2B_2C$  with the  $LuNi_2B_2C$ -type structure (Dezaneti et al., 2000; Tominez et al., 2000) this compound turns out to be metastable and has never been prepared as a single phase. A stabilization of the pseudoquaternary compounds  $Y(Ni_yPd_{1-y})_2B_2C$  by the introduction of Ni is possible only for  $y \geq 0.62$  (Bitterlich et al., 2002b). As can be seen in Figure 10, in the multiphase sample of the original paper of Hossain et al. (1994) there is a second superconducting phase with  $T_c \approx 10$  K, whose composition and crystal structure is still unknown. Similarly, a non-identified superconducting phase, in addition to  $ThPd_2B_2C$ , has been seen in the Th–Pd–B–C system (Sarrao et al., 1994; see also Zandbergen et al., 1994b).

Superconductivity in  $ScNi_2B_2C$  is also based on a metastable phase (Ku et al., 1994) and single-phase samples could not be prepared. Tomilo et al. (2001b; see also 1999, 2001a) found two tetragonal phases in their samples with rather different values of the lattice constants  $a$  and  $c$  and unit cell volume  $V$  (phase 1:

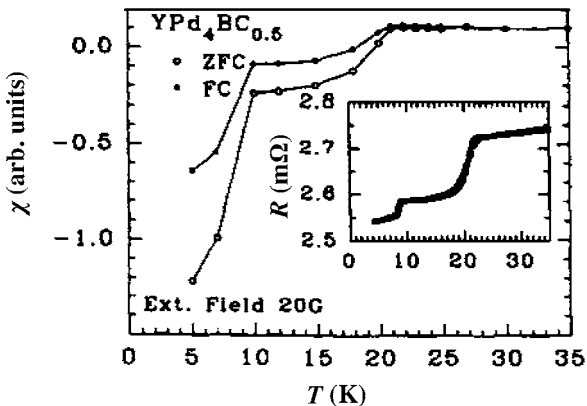


**FIGURE 10** Temperature dependence of the magnetic susceptibility  $\chi$  and the electrical resistance (inset) of a polycrystalline Y–Pd–B–C sample, indicating two superconducting phases with transition temperatures  $T_c$  of about 10 K and 23 K (Hossain et al., 1994).

0.332 nm, 1.004 nm, 0.1107 nm<sup>3</sup>; phase 2: 0.354 nm, 1.055 nm, 0.1320 nm<sup>3</sup>). These authors identified their phase 2 as the superconducting phase ScNi<sub>2</sub>B<sub>2</sub>C based on the data shown in Figure 6. However Kiruthika et al. (2004) found only one tetragonal ScNi<sub>2</sub>B<sub>2</sub>C phase in their as-cast samples and, interestingly, they could stabilize it by substituting Y for Sc in small amounts (of, e.g., 10 at%) and thereby increasing the average R size in the system.

The tendency of B–C disorder, i.e. mutual exchange of B and C atoms in the RNi<sub>2</sub>B<sub>2</sub>C compounds in not well heat-treated samples (see Section 3.1) is also an example for the formation of metastable phases in the R–T–B–C system.

Besides the quaternary intermetallic compounds discussed in the previous sections, there are many other binary, ternary and even quaternary compounds in the R–T–B–C systems which are more or less related to the quaternary borocarbide superconductors. The presence of such phases in the samples, even in small amounts, may lead to wrong conclusions concerning the superconducting or magnetic behavior of the main phase under investigation. For example, a ferromagnetic impurity phase may suggest weak ferromagnetism or reentrant superconductivity in the main phase. On the other hand superconducting impurity phases may simulate the superconducting behavior of the investigated main phase (see also Table 1). Of particular interest are phases, which form in thermodynamic equilibrium with the 1:2:2:1 borocarbide superconductors. Because the number of such related compounds is enormously large and their thermodynamic relations are far from being well investigated, in the following we will discuss only a few examples.

Among the quaternary R–T–B–C compounds the R<sub>4</sub>T<sub>2</sub>B<sub>3</sub>C<sub>4</sub> type being structurally related to the previously discussed R<sub>4</sub>T<sub>2</sub>B<sub>2</sub>C<sub>4</sub>-type structure (Section 2.3;  $n = 4$ ) is, by far, found for a wider range of transition metals T than any other quaternary structure type in the R–T–B–C systems, suggesting that it represents a stable intermetallic structure type (Link et al., 2002). So far no superconductor has been found in the R<sub>4</sub>T<sub>2</sub>B<sub>3</sub>C<sub>4</sub> family.

Among the numerous ternary rare-earth borocarbides, the RB<sub>2</sub>C<sub>2</sub> compounds with the LaB<sub>2</sub>C<sub>2</sub>-type structure (space group (s.g.) P4/mbm) consist of R layers and covalently bonded B–C networks alternatively stacked along the tetragonal *c*-axis (Bauer and Bars, 1980). This series is interesting because it contains superconductors, YB<sub>2</sub>C<sub>2</sub> and LuB<sub>2</sub>C<sub>2</sub> (see Table 1), as well as magnetically ordered compounds with relatively complicated magnetic structures affected by quadrupolar interactions and compounds with quadrupolar order (see Section 4.1). DyB<sub>2</sub>C<sub>2</sub> and HoB<sub>2</sub>C<sub>2</sub> show a small spontaneous magnetization below  $T_C \approx 15$  K (Yamauchi et al., 1999) and 5–7 K (Sakai et al., 1981; Onodera et al., 1999), respectively. The ternary compounds RNi<sub>4</sub>B with the CeCo<sub>4</sub>B-type structure (s.g. P6/mmm) are worth mentioning because YNi<sub>4</sub>B was the main phase on which trace superconductivity had been found leading to the discovery of the quaternary borocarbide superconductors (see Section 1.1). For R elements with partially filled 4f shells these 1:4:1 compounds are magnetically ordered with ordering temperatures of 10.5 K, 39 K, 36 K, 18.5 K, 12 K, 6 K, 8 K, and 3.5 K for R = Nd, Sm, Gd, Tb, Dy, Ho, Er, and Tm, respectively (Nagarajan et al., 1995). HoNi<sub>4</sub>B has a spontaneous magnetization below  $T_C \approx 6$  K (Alleno et al., 2001). Further ternary compounds possibly forming in equilibrium with RNi<sub>2</sub>B<sub>2</sub>C are

$\text{RNiC}_2$  (s.g. Amm2, Behr et al., 1999b) and  $\text{RNi}_2\text{C}_2$  (Takeya et al., 1996) as well as  $\text{R}_2\text{Ni}_3\text{B}_6$  (orthorhombic, s.g. Cmmm) where  $\text{Ho}_2\text{Ni}_3\text{B}_6$  has a spontaneous magnetization below  $T_C \approx 12$  K (Alleno et al., 2001). Veremchuk et al. (2006) found six ternary borides in the system Yb–Ni–B, Chen et al. (2000) reported on nine ternary borides in the system Gd–Ni–B and Ruiz et al. (2002) detected nine ternary Gd–B–C compounds. Bitterlich et al. (2001a) showed that the presence of small amounts of  $\text{YNi}_2\text{C}_2$  or  $\text{YNi}_4\text{C}$  or  $\text{YNiC}_2$  in equilibrium with  $\text{YNi}_2\text{B}_2\text{C}$  modifies the detailed composition of that main phase and, consequently, modifies its value of  $T_C$ .

There are also many binary compounds, which have to be considered as possible impurity phases in the quaternary borocarbides as, e.g.,  $\text{Ni}_2\text{B}$  (s.g. I4/mcm),  $\text{Ni}_3\text{B}$  and  $\text{Ni}_3\text{C}$  (both s.g. Pnma) or  $\text{RB}_2$  (s.g. P6/mmm),  $\text{RB}_4$  (s.g. P4/mbm),  $\text{RB}_6$  (s.g.  $\text{Pm}\bar{3}\text{m}$ ),  $\text{RB}_{12}$  (s.g.  $\text{Im}\bar{3}\text{m}$ ) and  $\text{R}_2\text{C}_3$  (s.g.  $\text{I}\bar{4}3\text{d}$ ) where  $\text{HoB}_2$  is a ferromagnet with  $T_C = 15$  K (Buschow, 1980) and  $\text{YB}_6$ ,  $\text{YB}_{12}$ ,  $\text{YC}_2$ ,  $\text{LuC}_2$ ,  $\text{Y}_2\text{C}_3$  are superconductors (see Table 1 and Godart et al., 1995). Furthermore, many binary R–Ni compounds with a broad range of magnetic transition temperatures (Buschow, 1980) have to be taken into account for the complete understanding of the phase diagrams.

### 3. SAMPLE PREPARATION AND BASIC PROPERTIES

In this section we will discuss some problems in the preparation of the  $\text{RNi}_2\text{B}_2\text{C}$  compounds and how certain details of the preparation procedure such as sample purity, heat-treatment regimes etc. can strongly modify the physical properties of these materials (Section 3.1). Furthermore, we will briefly report on basic properties of the  $\text{RNi}_2\text{B}_2\text{C}$  superconductors with R elements that have a zero total angular momentum in the Hund's rule ground state of  $\text{R}^{3+}$ , i.e.  $\text{R} = \text{Sc}, \text{Y}, \text{Lu}, \text{or } \text{Th}^{4+}$ . However, since  $\text{ScNi}_2\text{B}_2\text{C}$  is metastable and Th is radioactive, and thus are more difficult to handle, most studies on the non-magnetic  $\text{RNi}_2\text{B}_2\text{C}$  superconductors are concerned with  $\text{YNi}_2\text{B}_2\text{C}$  and  $\text{LuNi}_2\text{B}_2\text{C}$ . Some results on  $\text{ScNi}_2\text{B}_2\text{C}$  can be found in Section 2.4. Starting with the non-magnetic  $\text{RNi}_2\text{B}_2\text{C}$  it will be easier to understand the behavior of borocarbide superconductors with magnetic  $\text{R}^{3+}$  ions, considered in Sections 4 to 6. The superconducting transition temperatures of the  $\text{RNi}_2\text{B}_2\text{C}$  superconductors are presented in Figure 6 and Table 3.

#### 3.1 Preparation of polycrystals, single crystals and thin films

Soon after the discovery of the  $\text{RNi}_2\text{B}_2\text{C}$  compounds (see Section 1.1) high-quality polycrystalline samples and even single crystals could be prepared, thus enabling significant studies at an early stage. Some properties, however, sensitively depend on small stoichiometric variations or on atomic disorder in the samples. In this section, we focus on this problem including a short overview on preparation techniques. Studies on the deposition and on basic properties of thin films will also be reported.

Most of the single crystals used for physical investigations have been grown by the flux method (Xu et al., 1994; Canfield and Fisher, 2001). Single crystals with

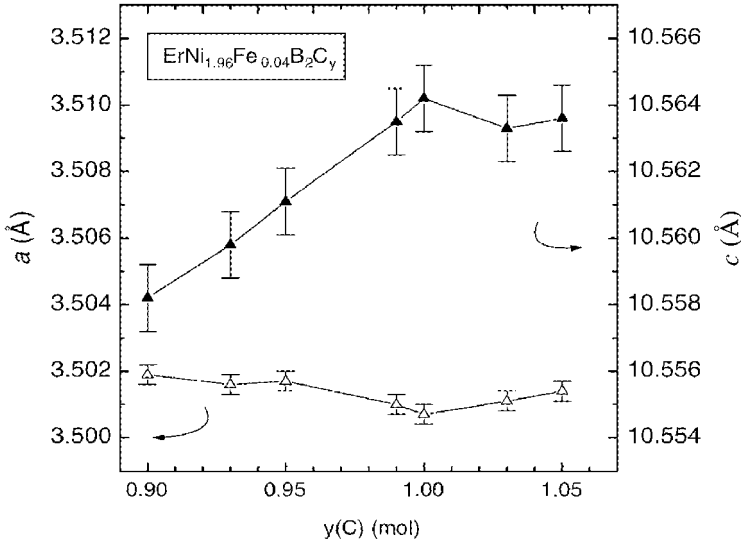


**FIGURE 11** The lattice constants,  $a$  (left axis) and  $c$  (right axis), dependence on the carbon content  $y$  of  $\text{ErNi}_{1.96}\text{Fe}_{0.04}\text{B}_2\text{C}_y$  (from Alleno et al., 2004b).

© 2004 Elsevier

larger dimension in  $c$  direction have been grown by floating-zone melting methods (Takeya et al., 1996; Behr et al., 1999a, 2000; Behr and Löser, 2005). Another growth technique for  $\text{RNi}_2\text{B}_2\text{C}$  single crystals is the cold copper crucible method (Durán et al., 2000). Various melting techniques such as arc melting (see, e.g., Mazumdar and Nagarajan, 2005; Freudenberger et al., 2001b) or rapid quenching (Ström et al., 1996) have been used to prepare polycrystalline materials. Powders, in particular of metastable 1:2:2:1 phases, have been produced by mechanical alloying (see Oertel et al., 2000; Gümbel et al., 2000a, 2000b). Some of the  $\text{RNi}_2\text{B}_2\text{C}$  compounds are rather stable. For example,  $\text{YNi}_2\text{B}_2\text{C}$  starts oxidizing and decomposing only above 850 °C (Buchgeister and Pitschke, 1996). The problems of preparing the metastable compounds  $\text{YPd}_2\text{B}_2\text{C}$  and  $\text{ScNi}_2\text{B}_2\text{C}$  have been discussed in Section 2.4.

As shown in Figure 6, the superconducting transition temperatures of  $\text{RNi}_2\text{B}_2\text{C}$  compounds are strongly correlated with their lattice parameters. Small values of  $a/c$  favor superconductivity, i.e. higher  $T_c$  values. On the other hand, the lattice parameters and their ratio are very sensitive to small deviations from the stoichiometric composition as can be seen in the example presented in Figure 11. The variation of the carbon content affects  $a$  and  $c$  in the opposite directions leading to a pronounced minimum of  $a/c$  just at the stoichiometric composition. This supports the detrimental role of deviations from the ideal formation of the 1:2:2:1 phases in their superconducting properties. Thus, for  $\text{HoNi}_2\text{B}_2\text{C}$ , even a loss of superconductivity has been observed for a deviation from the stoichiometric composition as small as 1% of C (Souptel et al., 2007). Interestingly, the situation is completely different to that of the double-layer borocarbides

(RNiBC; see Figure 9b), for which superconductivity only can be obtained in the case of the partial substitution of Ni by Cu (Gangopadhyay and Schilling, 1996; Graw et al., 2001) or if a significant B–C off-stoichiometry is realized (Kiruthika et al., 2005).

A number of studies are based on YNi<sub>2</sub>B<sub>2</sub>C samples with differing stoichiometry or homogeneity. Lipp et al. (2000) concluded from measurements of the electrical resistivity and the specific heat that both, the electron density of states and the phonon spectrum, change with the boron content. Yang-Bitterlich and Krämer (2000) found a connection between the sample homogeneity and the nature of the dislocations. Lascialfari et al. (2003) attributed the occurrence of superconducting fluctuations slightly above  $T_c$  to a spatial variation of the transition temperature due to microscopic defects. Bitterlich et al. (2000) and Souptel et al. (2005b) analyzed the influence of segregation phenomena on the spatial-dependent composition of float-zone grown RNi<sub>2</sub>B<sub>2</sub>C (R = Y, Ho, Tb) single crystals. The latter report also includes the crucial role of oxygen impurities.

A particularly careful preparation including “ideal” heat treatment is needed in the case of DyNi<sub>2</sub>B<sub>2</sub>C because the onset of superconductivity in this antiferromagnet is very sensitive to the presence of impurities (Ribeiro et al., 2003; see also Sections 4.8 and 6.4). Avila et al. (2002, 2004) reported a strong annealing dependence of the properties of the heavy-fermion superconductor YbNi<sub>2</sub>B<sub>2</sub>C (Section 4.12) and addressed this to ligand disorder. Such variations occur in the electrical resistivity and the thermoelectric power (Avila et al., 2002) as well as in the Hall coefficient (Bud’ko and Canfield, 2005). A strong influence of heat-treatment regimes on the superconducting properties has also been found for other RNi<sub>2</sub>B<sub>2</sub>C compounds (Miao et al., 2002). In particular the reentrant behavior of HoNi<sub>2</sub>B<sub>2</sub>C is very sensitive to details of the annealing procedure (Schmidt et al., 1997; Wagner et al., 1999; see also Section 4.9). Neutron diffraction data seemed to provide evidence that all the crystallographic sites in RNi<sub>2</sub>B<sub>2</sub>C are fully occupied and, in particular, there is no B ↔ Ni site mixing (Chakoumakos and Paranthaman, 1994). However, the conventional diffraction techniques are not sensitive enough to light elements to determine interchange or defects on the B and C sublattices, which possibly have substantial effects on the physical properties of these compounds. Even the concentration of the light elements has only been determined, e.g., by nuclear microanalysis, within 3–4% (Berger et al., 2000). First indications for a modification of the carbon site occupation in polycrystalline HoNi<sub>2</sub>B<sub>2</sub>C samples annealed at lower temperature (800 °C) were obtained by Dertinger et al. (2001) performing Fourier analysis of X-ray powder diffraction data. A subsequent study by Leisegang et al. (2006) on a floating-zone grown single crystal showed a smeared electron density in the B–C network of the as-grown crystal in contrast to a well localized distribution in the well-annealed single crystal (see Figure 12). A B–C site mixing of up to 8% and 2% was derived for the as-grown crystal and the well-annealed crystal, respectively.

In a systematic study of heat treatment for different RNi<sub>2</sub>B<sub>2</sub>C single crystals Miao et al. (2002) found the optimal annealing temperature and time to be 1000 °C and (at least) 75 h, respectively. Souptel et al. (2005b) showed that such heat treatment at 1000 °C eliminates precipitates. However, Hillier et al. (2002) determined

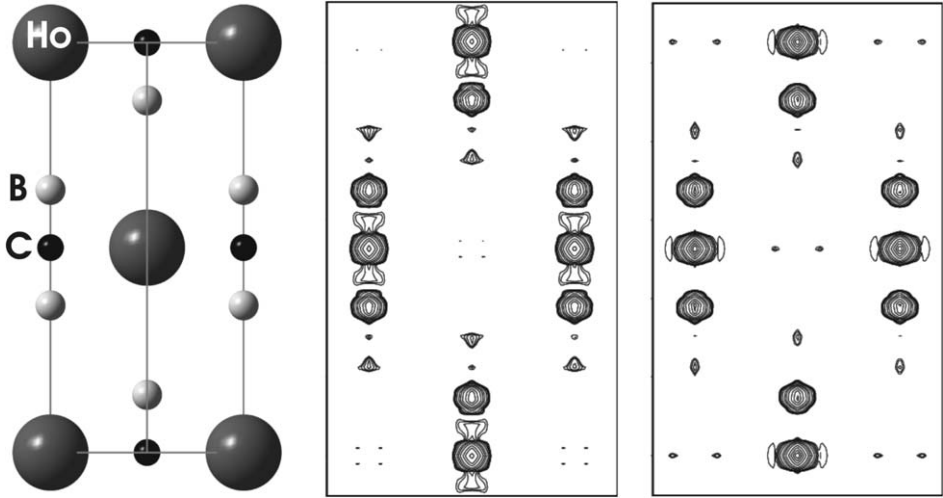


**FIGURE 12** Influence of annealing on the local electron density ED of B and C atoms in  $\text{HoNi}_2\text{B}_2\text{C}$  obtained by Fourier difference analysis of X-ray data (with  $\text{ED} = \text{ED}_{\text{exp}} - \text{ED}_{\text{calc}}$ , where  $\text{ED}_{\text{exp}}$  is the measured ED and  $\text{ED}_{\text{calc}}$  is the calculated ED without B and C atoms). The measurements were performed in the  $(1\bar{1}0)$  plane of the unit cell. This plane having dimensions of  $7 \times 12.5 \text{ \AA}^2$  is drawn in the left panel; the complete crystal structure of the  $\text{RNi}_2\text{B}_2\text{C}$  compounds can be found in Figure 9(a). From the ED maps shown for as-grown (middle) and annealed (last step:  $500^\circ\text{C}$  for 72 h; right panel) crystals, upper limits of 8% and 2% disorder in the B–C system were determined, respectively. The lines represent constant electron density of  $\Delta\rho_e = 1, 1.2, 1.5, 2, 3, 5, 7, 10, 15, 20, 30$  electrons per  $\text{\AA}^3$ . By courtesy of Leisegang et al. (2006).

the boron–carbon disorder by time-of-flight powder diffraction and found a surprisingly high site-disorder of 8.6% in  $\text{YNi}_2^{10}\text{B}_2\text{C}$  annealed at  $1000^\circ\text{C}$  even for 4 days. This may be the reason why optimal superconducting properties in a  $\text{HoNi}_2\text{B}_2\text{C}$  single crystal obtained by the float-zone technique have been achieved only after an additional annealing at a considerably lower temperature ( $500^\circ\text{C}$  for 72 h; Souptel, 2005; Leisegang et al., 2006; Müller et al., 2007).

A very subtle dependence of  $T_c$  on the carbon content has been shown by Alleno et al. (2004a) also for the  $\text{Er}_{1-x}\text{Tb}_x\text{Ni}_2\text{B}_2\text{C}$  system. For  $\text{ErNi}_2\text{B}_2\text{C}$ , some of the features associated with the weak ferromagnetism seem to depend on the sample quality (Chia et al., 2006; see Section 4.10). Moreover, in pseudoquaternary compounds different minority phases can cause a composition variation of the superconducting phase (Bitterlich et al., 1999) thus hampering the comparison of experimental results. Furthermore it has to be noted that in  $\text{R}_{1-x}\text{R}'_x\text{Ni}_2\text{B}_2\text{C}$  borocarbides with R and R' much differing in their atomic sizes (see Section 4.2, Figure 29) miscibility gaps have been observed. Thus for nominal values  $x$  around 0.5 these mixed systems are at most two-phase (Freudenberger et al., 2001b).

The preparation of c-axis aligned or even epitaxial  $\text{RNi}_2\text{B}_2\text{C}$  thin films has been performed using both, pulsed laser deposition (PLD; Cimberle et al., 1997; Häse et al., 1997) and magnetron sputtering technique (Arisawa et al., 1994; Andreone

et al., 1996). Furthermore, a preferred *a*-axis orientation can be realized by PLD with a lowered deposition temperature, which, however, also leads to unfavorable film quality due to a higher defect concentration (Wimbush et al., 2001; Reibold et al., 2002). In the following discussion, only *c*-axis oriented borocarbide thin films will be considered. Reviews of early studies in this field have been presented by Andreone et al. (1998), Grassano et al. (2001a) and Iavarone et al. (2001).

Challenging problems in the borocarbide thin-film growth are the absence of well-matching substrate materials and the occurrence of impurity phases. Most of the studied  $\text{RNi}_2\text{B}_2\text{C}$  thin films were grown on MgO substrates. An extensive study on the influence of different MgO cuts on the deposition of  $\text{LuNi}_2\text{B}_2\text{C}$  is given by Ferdeghini et al. (2003). Grassano et al. (2001b) present a detailed analysis on the use of different substrate materials and, additionally, on the PLD process parameters like substrate temperature, target-substrate distance, beam energy density, and film thickness. The ablated plume has been investigated by Y. Wang et al. (2002a, 2002b) showing relevant differences in the flow velocity of different ablated species and the presence of aggregation/fragmentation processes. X-ray diffraction revealed the presence of  $\text{Y}_2\text{O}_3$  in  $\text{YNi}_2\text{B}_2\text{C}$  thin films, which firstly was ascribed to the oxidation at the target surface (Andreone et al., 1996). However, Reibold et al. (2002) showed the formation of an interfacial  $\text{Y}_2\text{O}_3$ -rich layer, bordering on the substrate and being accompanied by further impurity phases. Cao et al. (2004, 2005) addressed the  $\text{Y}_2\text{O}_3$  phase to the chemical reaction of the deposited yttrium with oxygen released from the MgO substrate and, moreover, investigated the orientation relationships between  $\text{YNi}_2\text{B}_2\text{C}$  and the impurity phases. The deposition of an  $\text{Y}_2\text{O}_3$  buffer layer reduces the volume fraction of impurity phases and improves the superconducting properties of the films (Cao et al., 2004; Subba Rao et al., 2005).

Thin films have been successfully used to measure superconducting properties of  $\text{RNi}_2\text{B}_2\text{C}$  systems, in particular, to determine the anisotropy of the upper critical field of  $\text{YNi}_2\text{B}_2\text{C}$  (see Section 3.6) and of  $\text{HoNi}_2\text{B}_2\text{C}$  (Häse et al., 2000a, 2000b; Wimbush and Holzapfel, 2006; see also Section 4.9). Thin films have also been used for point-contact and scanning tunneling spectroscopy studies, which are powerful tools for the investigation of the superconducting gap in  $\text{RNi}_2\text{B}_2\text{C}$  (see Section 3.5.2). An interesting phenomenon, dendritic flux instabilities in an  $\text{YNi}_2\text{B}_2\text{C}$  thin film have been observed (Wimbush et al., 2004a; see Section 5.1.5).

Whereas the zero-field critical current density  $j_c$  in the first reports on  $\text{YNi}_2\text{B}_2\text{C}$  thin films was in the order of  $10^5$  A/cm<sup>2</sup> at 4 K (Arisawa et al., 1994; Andreone et al., 1996), improved preparation conditions now enable values of  $2.5 \times 10^6$  A/cm<sup>2</sup> at 2 K and, in the case of  $\text{HoNi}_2\text{B}_2\text{C}$ ,  $1.4 \times 10^6$  A/cm<sup>2</sup> at 2 K (Wimbush et al., 2003). These values exceed those measured on bulk samples (see e.g., James et al., 2000; Krutzler et al., 2005; and also Section 5.2.2) by nearly two orders of magnitude resembling the situation in the cuprates. Moreover, a comparably stronger anisotropy in  $j_c$  has been found in  $\text{YNi}_2\text{B}_2\text{C}$  and  $\text{HoNi}_2\text{B}_2\text{C}$  thin films with significantly higher current densities for  $\mathbf{H} \perp \mathbf{c}$  than for  $\mathbf{H} \parallel \mathbf{c}$  (Arisawa et al., 1994; Häse et al., 2001b; Wimbush et al., 2003). An orientation-dependent pinning, with weak pinning centres for flux penetrating perpendicular to the plane of the film and stronger pinning within the plane, was deduced.

Since the preparation of  $\text{RNi}_2\text{B}_2\text{C}$  thin films is now well established, it will be used in future work to prepare single-phase films and even textured films of systems that are difficult to produce as bulk materials, e.g., the metastable phase  $\text{YPd}_2\text{B}_2\text{C}$  (see Section 2.4) or  $\text{R}_{1-x}\text{R}'_x\text{Ni}_2\text{B}_2\text{C}$  mixed systems (see Section 6).

### 3.2 Electronic structure

Ni is different from the Cu in cuprates because it does not carry a local magnetic moment in the quaternary borocarbides (Lynn, 2001). For  $\text{YNi}_2\text{B}_2\text{C}$  this is in agreement with an analysis of both the susceptibility and NMR data, and is also consistent with electronic structure calculations (Suh et al., 1996). These authors also could exclude antiferromagnetic spin correlations on the Ni sublattice. In principle, the normal-state magnetic properties of this material can be well understood as contributions from core-electron diamagnetism, van Vleck paramagnetism and Pauli paramagnetism (Cho, 2000). However, the diamagnetic (Landau) contribution from the conduction electrons has so far been ignored in the studies on  $\text{RNi}_2\text{B}_2\text{C}$  compounds. (The Landau contribution has been shown to be very important, e.g., in PdH, Cu, Ag, and Au with a somewhat similar structure of the global density of states  $N(E)$  of a relative narrow special mixed-band complex above a broad complex dominated by d electrons, just as calculated for the transition-metal borocarbides under consideration (see Figure 13).) Unfortunately, at present the magnitude of such a diamagnetic contribution for borocarbides as well as for most other real metals and superconductors remains unknown (we remind the reader that in an isotropic electron gas it is:  $\chi_d = -(m_e/3m_e^*)\chi_p$ , where  $m_e$  and  $m_e^*$  are the bare and the effective band electron mass, respectively, and  $\chi_p$  is the paramagnetic (Pauli) spin susceptibility). Taking into account the experimental data of Cho (2000), from our estimated Wilson ratio  $R_w \approx 0.9$  to 1, the electron-phonon and electron-paramagnon renormalizations of the electronic density of states  $N(0)$  at the Fermi level (as seen in the magnetic-susceptibility and the specific-heat measurements) are expected to be comparable in size. The calculated sizable negative quadratic curvature of  $\chi_p(T) \sim N(0) - AT^2$  is in qualitative agreement with the experimental data for the measured powder-averaged susceptibility for  $\text{YNi}_2\text{B}_2\text{C}$  (Cho, 2000). The theoretical LDA value for the coefficient  $A$  for  $\text{LuNi}_2\text{B}_2\text{C}$  is of the same order as that obtained from an experimental fit to the susceptibility data, but for  $\text{YNi}_2\text{B}_2\text{C}$  the LDA value is approximately only half of that fitted to the experimental results. In contrast, for  $\text{ThNi}_2\text{B}_2\text{C}$  an almost negligible quadratic curvature has been predicted (see Drechsler et al., 2001b).

Although the isomer shift of the Dy nucleus, determined by Mössbauer studies on  $\text{DyNi}_2\text{B}_2\text{C}$ , suggested that the Dy-C plane is insulating and the electrical conduction seems to take place mainly in the Ni-B sheets (J.P. Sanchez et al., 1996), it is now generally accepted that the  $\text{RNi}_2\text{B}_2\text{C}$  compounds, despite their layered crystal structure, are three-dimensional in their electronic behavior, and hence they are quite different from the layered cuprates (Lynn et al., 1997). Three-dimensional, nearly isotropic metallic behavior was confirmed by measurements of the temperature dependence of the electrical resistivity,  $\rho(T)$ , on single-crystalline  $\text{YNi}_2\text{B}_2\text{C}$  and  $\text{LuNi}_2\text{B}_2\text{C}$  over the entire temperature range

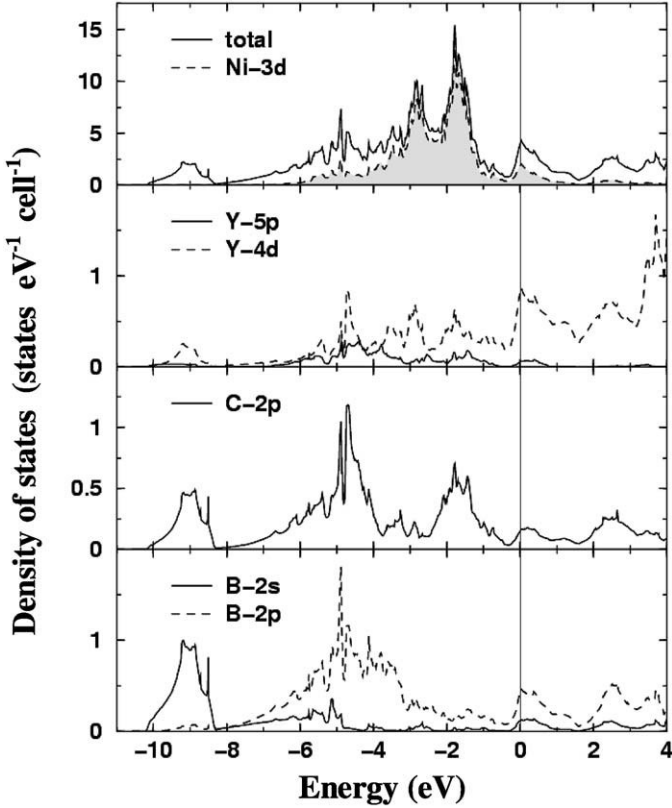


**FIGURE 13** Total and partial (concerning the different types of electrons) electronic density of states calculated for  $\text{YNi}_2\text{B}_2\text{C}$ , using the local density approximation. The Fermi level  $E_F$  is defined as zero energy (from Rosner et al., 2001).

$T_c < T < 300$  K (Fisher et al., 1997). Furthermore, a clearly three-dimensional, but strongly anisotropic electronic structure has also been observed in various experiments such as: the de Haas–van Alphen effect (Nguyen et al., 1996; Ignatchik et al., 2005), X-ray absorption spectroscopy (von Lips et al., 1999), electron-positron annihilation radiation technique (Dugdale et al., 1999; Hamid, 2003), or X-ray photo-electron spectroscopy—XPS (Kumari et al., 2003). The electronic structure of  $\text{RNi}_2\text{B}_2\text{C}$  compounds has been studied also by numerous first-principle calculations (e.g., Pickett and Singh, 1994; Mattheiss, 1994; Mattheiss et al., 1994; Coehoorn, 1994; Lee et al., 1994; Kim et al., 1995; Ravindran et al., 1998; Dugdale et al., 1999; Diviš et al., 2000; Rosner et al., 2001; Diviš et al., 2001; Felser, 2001; Rhee and Harmon, 2002; Youn et al., 2002; Drechsler et al., 2003; Yamauchi et al., 2004; Yamauchi and Harima, 2005; Shorikov et al., 2006). These calculations clearly confirmed that the 1:2:2:1 borocarbides are three-dimensional metals with all atoms contributing to the metallic character.

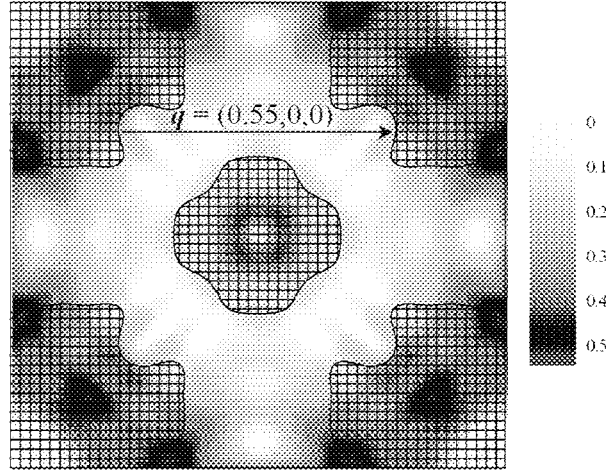


**FIGURE 14** A section of the Fermi surface of  $\text{LuNi}_2\text{B}_2\text{C}$  showing a nesting feature characterized by the wave vector  $\mathbf{q} \approx (0.55, 0, 0)$ , and contour plot of the magnitude of the Fermi velocity  $v_F$  (in  $10^6$  m/s) in the (001) plane through the  $\Gamma$  point (from Yamauchi and Harima, 2005).

© 2005 Elsevier

The main contribution to the density of states at the Fermi level,  $N(E_F)$ , arises from Ni-3d electrons. In particular the peak in the density of states near the Fermi level is attributed to the quasi-two dimensional network of Ni atoms. Nevertheless there is a considerable admixture of Y-4d as well as B-2p and C-2p electrons (see Figure 13). It has been concluded that the superconductivity in  $\text{RNi}_2\text{B}_2\text{C}$  is related to the relatively high density of states on the already mentioned narrow peak at the Fermi level shown in Figure 13 for  $\text{YNi}_2\text{B}_2\text{C}$  but also calculated for other  $\text{RNi}_2\text{B}_2\text{C}$  compounds and  $\text{YPd}_2\text{B}_2\text{C}$ . The experimental and theoretical investigation of the electronic structure showed that the Fermi surface (FS), in particular the Fermi velocity  $v_F$ , is strongly anisotropic and the FS consists of different sheets. Although the FSs of  $\text{RNi}_2\text{B}_2\text{C}$  for different R are similar, important differences can be recognized. Thus for all  $\text{RNi}_2\text{B}_2\text{C}$  superconductors the FS seems to have nested regions characterized by a (nearly) common nesting vector  $\mathbf{q} \approx (0.55, 0, 0)$ , as shown in Figure 14 for  $\text{LuNi}_2\text{B}_2\text{C}$ , whereas such nesting feature is absent in the non-superconductor  $\text{LaNi}_2\text{B}_2\text{C}$ . Also there are closed and open parts in the FS along  $\mathbf{k} \approx (0, 0, 0.5)$  for  $\text{YNi}_2\text{B}_2\text{C}$  and  $\text{LuNi}_2\text{B}_2\text{C}$ , respectively, which might explain the qualitative differences in the Hall-effect data reported for these compounds (Rosner et al., 2001). A complete analysis comparing the different FSs through the series of  $\text{RNi}_2\text{B}_2\text{C}$  compounds is still missing. Youn et al. (2002) and Rhee and Harmon (2002) derived the optical conductivity from their calculated electronic structures and confirmed the strong anisotropy in the optical properties of  $\text{YNi}_2\text{B}_2\text{C}$  and  $\text{LuNi}_2\text{B}_2\text{C}$  earlier observed experimentally (e.g., by Bommeli et al., 1997; Mun et al., 2001). The seeming discrepancy that some of the electronic properties of the  $\text{RNi}_2\text{B}_2\text{C}$  are strongly anisotropic (as the optical conductivity) and others are isotropic (as the normal-state resistivity  $\rho$ ) can be understood as the nearly

isotropic transport properties are mainly related to groups of electrons with relatively large  $v_F$  being less anisotropic and not associated with FS nesting. The optical conductivity consists of intra-band (Drude-like) and inter-band contributions. The latter ones are strongly weighted by transition-matrix elements reflected also by the so-called combined density of states. This way more local properties of the band structure *away* from the Fermi level  $E_F$  are probed. An example for probing a special subgroup of fast electrons is given by the isotropic superconducting effective mass in  $\text{YNi}_2\text{B}_2\text{C}$  as found by torque magnetometry (Johnston-Halperin et al., 1995).

In the Bardeen–Cooper–Schrieffer (BCS) theory of superconductivity the transition temperature  $T_c$  strongly increases with  $N(E_F)$ :

$$T_c = 1.13\theta_D \exp(-1/N(E_F)V), \quad (4)$$

where  $\theta_D$  is the Debye temperature characterizing the phonon spectrum of the material which limits the attractive range of the electron–phonon (el–ph) interaction,  $V$  is some measure of the electron–phonon interaction and  $N(E_F)V \ll 1$  (Bardeen et al., 1957a, 1957b). For  $\text{LaNi}_2\text{B}_2\text{C}$  the value of  $N(E_F)$  is about half of that for  $\text{LuNi}_2\text{B}_2\text{C}$  or  $\text{YNi}_2\text{B}_2\text{C}$  (Mattheiss et al., 1994; Diviš et al., 2000) and it has been argued that, according to Eq. (4), this is the main reason why  $\text{LaNi}_2\text{B}_2\text{C}$  is not superconducting. However, it has been pointed out by Drechsler et al. (1999a) that the superconductor  $\text{LaPt}_2\text{B}_2\text{C}$  with  $T_c \approx 11$  K has a similar or even lower value of  $N(E_F)$  compared to  $\text{LaNi}_2\text{B}_2\text{C}$  (Singh, 1994). Consequently, since  $\theta_D$  is similar for all  $\text{RNi}_2\text{B}_2\text{C}$  compounds, there must also be a considerable variation of the interaction strength  $V$  across the series of the quaternary borocarbides, which affects  $T_c$  according to Eq. (4) or these materials are not simple BCS-type superconductors. This will be further discussed in Section 3.3.

### 3.3 Superconducting coupling mechanism

In general it is a difficult task to elucidate unambiguously the pairing mechanism of a given novel superconducting material. As a rule after its discovery decades are necessary to settle this point. Historically, the observation of a sizable isotope effect for the critical temperature  $T_c$  is frequently regarded as evidence for a phonon mechanism. Also microscopically the symmetry and the anisotropy of the superconducting order parameter must be discussed in the context of the pairing mechanism and the symmetry and anisotropy of the underlying pairing and de-pairing interactions. However, in actuality, the observable physical properties are usually discussed on the basis of a phenomenological description (see Section 3.5). For the borocarbides under consideration, the interplay of superconductivity and magnetism as well as possible relations to unconventional superconductors play an important role in addressing the origin of the pairing.

A remarkable boron isotope effect has been observed for  $\text{YNi}_2\text{B}_2\text{C}$  as well as  $\text{LuNi}_2\text{B}_2\text{C}$  supporting the classification of these materials as phonon-mediated superconductors (Lawrie and Franck, 1995; Cheon et al., 1999; see Figure 15). The BCS theory predicts for the isotope effect  $T_c \sim M^{-\alpha_I}$  where  $M$  is the mass of the atoms which substantially participate in the lattice vibrations being relevant for

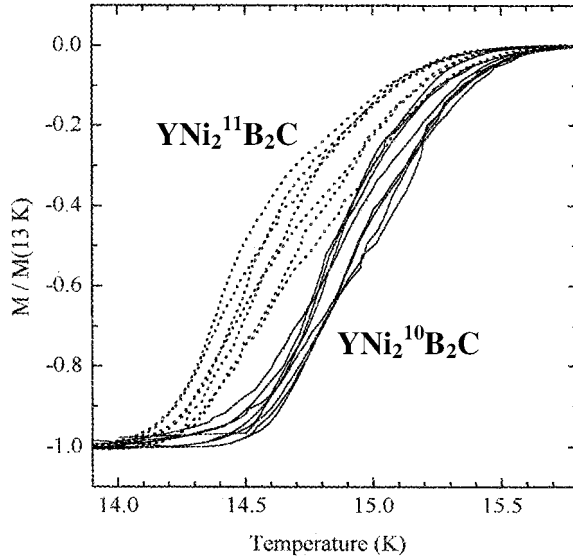


**FIGURE 15** Field-cooled magnetization measured for increasing temperature at  $\mu_0 H = 2.5$  mT on single crystalline  $\text{YNi}_2\text{B}_2\text{C}$  with the two isotopes  $^{10}\text{B}$  (solid lines) and  $^{11}\text{B}$  (dotted lines), clearly indicating a boron isotope effect (Cheon et al., 1999).

© 1999 Elsevier

the superconductivity, and  $\alpha_I = 0.5$  is the isotope exponent. For  $\text{YNi}_2\text{B}_2\text{C}$  and  $\text{LuNi}_2\text{B}_2\text{C}$  Cheon et al. (1999) found  $\alpha_{I,B} \approx 0.21$  and  $0.11$ , respectively, as the partial isotope exponents of boron. No carbon isotope effect could be observed in  $\text{YNi}_2\text{B}_2\text{C}$  i.e. no change of  $T_c$  when  $^{12}\text{C}$  is substituted by  $^{13}\text{C}$  (Lawrie and Franck, 1995). Although at first glance the observation of a clear B isotope effect seems to prove the electron–phonon (el–ph) mechanism and the special role of a high-frequency  $\text{B–A}_{1g}$  related phonon near 100 meV which strongly modulates the  $\text{NiB}_4$  tetrahedral bond as suggested by Mattheiss (1994), a more detailed analysis shows that this phenomenon is probably much more complex. In this context it is noteworthy that very recently Naidyuk et al. (2007b) succeeded to observe for the first time a weak coupling between conduction electrons and high-frequency B-related phonons near 100 meV in point-contact spectroscopy measurements on the closely related compound  $\text{HoNi}_2\text{B}_2\text{C}$ .

Thus, although according to the BCS theory,  $T_c$  should be proportional to the zero-temperature superconducting gap, a gap-like feature denoted as  $\Omega$  in  $\text{B}_{2g}$  symmetry, measured by electronic Raman scattering (Yang et al., 2002), shows a negative isotope effect, i.e.  $\Omega(^{10}\text{B}) < \Omega(^{11}\text{B})$ . A possible reason for such discrepancies might be that more electronic degrees of freedom are involved than taken into account in the BCS theory (Drechsler et al., 2001a, 2001b). In particular, the electronic structure and thus the electron–phonon interaction might be different for both isotopic compounds (Drechsler et al., 2004), provided there is a strongly asymmetric coupling of different bands to the high-frequency phonons (Morozov,

1977). In the present case with a very complex multiband electronic structure at the Fermi level, which exhibits bands having strongly different admixtures of Ni- and B-derived orbitals, such a scenario seems to be not unrealistic, although detailed quantitative studies are still missing. Any attempt to reproduce the isotope effect within the standard classical phonon scenario based on the Eliashberg theory (Shulga et al., 1998) requires a significant coupling to high-frequency modes, and limits in this way the total coupling strength to  $\lambda_{\text{ph}} < 0.7$ , which is at variance with the analysis of specific-heat data which gives a larger coupling strength, i.e.  $\lambda_{\text{ph}} \approx 1$ . Calculations within the framework of the LDA mixed-basis pseudopotential method result in  $\lambda_{\text{ph}} = 0.85$  (Reichardt et al., 2005). We would remind the reader that the Eliashberg and the BCS coupling constants are approximately related as  $\lambda_{\text{ph}} \sim (N(E_{\text{F}})V + \mu^*) / (1 - N(E_{\text{F}})V)$ , where  $\mu^* \sim 0.1$  is the Coulomb pseudopotential. In addition, possible strong anharmonicities especially for the low-frequency phonons near 7 meV suggest some B-admixture (Reichardt et al., 2005), which leads to still more difficult and subtle unsolved theoretical problems. Thus, the nearly twice as large isotope exponent observed for  $\text{YNi}_2\text{B}_2\text{C}$  in comparison with that of the closely related compound  $\text{LuNi}_2\text{B}_2\text{C}$  might be considered as a hint for a combination of the mentioned above non-classic scenarios.

Analyzing thermodynamic data and phonon densities of states, Hilscher and Michor (1999) concluded that for 1:2:2:1 borocarbides the BCS weak-coupling limit is not fulfilled and strong-coupling effects arise from the presence of particular low-frequency optical phonon modes. This is also supported by point-contact spectroscopy (Yanson et al., 1997). These effects can be well described by strong-coupling corrections within the framework of the standard Eliashberg theory (Carbotte, 1990). Hilscher et al. (2001) have shown that a strong drop of  $T_{\text{c}}$  from  $\text{LuNi}_2\text{B}_2\text{C}$  or  $\text{YNi}_2\text{B}_2\text{C}$  to  $\text{LaNi}_2\text{B}_2\text{C}$  can be predicted by using the formula of McMillan (1968) who calculated  $T_{\text{c}}$  in the framework of the Gor'kov–Eliashberg theory which takes into account strong coupling effects and details of the phonon spectrum and of the electron–phonon coupling (Allen, 1991). However in this approach, the electronic structure is described by an isotropic single band, which is expected to be the reason why some problems with the borocarbide superconductors remained unsolved despite the mentioned-above corrections to the BCS theory, e.g., the question why  $\text{LaPt}_2\text{B}_2\text{C}$  is superconducting but  $\text{LaNi}_2\text{B}_2\text{C}$  and  $\text{YCo}_2\text{B}_2\text{C}$  are not, or why there is an anisotropy and the unusual temperature dependence of  $H_{\text{c}2}$ . The latter has been treated by introducing a two-band structure in place of the single-band theory (see Section 3.6). The key to the mentioned problems is the complex Fermi surface (FS) of the quaternary borocarbides, discussed in Section 3.2, i.e. the fact that it consists of several sheets and is highly anisotropic with strongly varying values of the Fermi velocity  $v_{\text{F}}$  (Drechsler et al., 1999b, 2001a; Rosner et al., 2001). Therefore  $T_{\text{c}}$  will not be governed by the overall density of states  $N(E_{\text{F}})$  but by the partial density of states (DOS) of slow electrons that have been shown to stem from nested regions (see Section 3.2).

The nesting vector  $\mathbf{q} \approx (0.55, 0, 0)$  also appears in phonon softening at temperatures below  $T_{\text{c}}$ , observed in  $\text{LuNi}_2\text{B}_2\text{C}$  and  $\text{YNi}_2\text{B}_2\text{C}$  (Dervenagas et al., 1995b; Stassis et al., 1997; Bullock et al., 1998; Zarestky et al., 1999; Isida et al., 2001) as well as  $\text{ErNi}_2\text{B}_2\text{C}$  (Kawano-Furukawa et al., 2002b). The latter authors assume that the

phonon softening at the wave vector  $\mathbf{q}$  is a common phenomenon in all quaternary borocarbide superconductors (see also Kreyssig et al., 2004 for  $\text{HoNi}_2\text{B}_2\text{C}$ ). Using scanning tunneling spectroscopy and microscopy, Martínez-Samper et al. (2003) found that the FS nesting also causes a strong anisotropy in the electron–phonon interaction in  $\text{LuNi}_2\text{B}_2\text{C}$  and  $\text{YNi}_2\text{B}_2\text{C}$  (see also Section 3.5).

The behavior of superconductors in a magnetic field is usually analyzed using approaches on a phenomenological level, i.e. London theory and Ginzburg–Landau–Abrikosov theory. However, in the case of  $\text{RNi}_2\text{B}_2\text{C}$  superconductors these theories have to be extended taking into account non-locality in the relation between electric-current density and vector potential (Kogan et al., 1997b; Metlushko et al., 1997; Kogan et al., 2000; Gurevich and Kogan, 2001; Thompson et al., 2001; Bud’ko and Canfield, 2006; Kogan et al., 2006; see Sections 3.6 and 5).

### 3.4 Transport properties

Studies on the normal state magnetoresistance (MR; including the electrical resistivity  $\rho$ ), the Hall effect (Hall coefficient  $R_H$ ), the thermal conductivity  $\kappa$ , and the thermoelectric power (TEP;  $S_Q$ ) give important information on the charge carriers, the electronic structure, the scattering mechanisms, and the properties of the vortex lattice of the investigated materials. Effects of annealing on MR,  $R_H$ , and  $S_Q$  have been discussed in Section 3.1; the special heavy-fermion behavior of  $\text{YbNi}_2\text{B}_2\text{C}$  will be considered in Section 4.1.2.

#### 3.4.1 Magnetoresistance

The zero-field electrical resistivity  $\rho$  of  $\text{RNi}_2\text{B}_2\text{C}$  superconductors above the transition temperatures  $T_c$  exhibits a typically metallic behavior in the range up to 600 K (Fisher et al., 1995) with only small deviations between different crystallographic directions. The minor anisotropy was attributed to the influence of magnetic R ions (Fisher et al., 1997), whereas a recent study (Schneider, 2005) supports the description of a fundamentally isotropic resistivity but suggests possible crystal imperfections as origin for the small differences observed. The temperature dependence of  $\rho$  was found to follow perfectly the Bloch–Grüneisen law for an  $\text{YNi}_2\text{B}_2\text{C}$  single crystal (Gonnelli et al., 2000), whereas in a large number of reports, a power-law behavior  $\rho(T) = \rho_0 + AT^p$  at low temperatures with  $p$  in the range between 2.0 and 2.6 was observed for  $R = \text{Y, Lu, Ho, and Er}$  and  $p = 1.4$  ( $R = \text{Tm}$ ) as well as  $p = 3.0$  for  $R = \text{Dy}$  (see, e.g., Rathnayaka et al., 1997; Bhatnagar et al., 1997; Boaknin et al., 2001). The origin of this discrepancy remains to be solved although annealing effects or non-stoichiometric composition seem to significantly influence the resistivity (see Section 3.1). The impact of magnetic ordering on  $\rho$  has been studied by Hennings et al. (2002) for  $R = \text{Tb, Dy and Gd}$ . The electrical resistivity of  $\text{Ho}_{0.5}\text{Y}_{0.5}\text{Ni}_2\text{B}_2\text{C}$  decreases with increasing pressure (Oomi et al., 2003a). Using the electron–phonon spectral function as derived from the phonon density of states, da Rocha et al. (2003) could well describe the measured  $\rho$  data of a series of  $\text{Y}(\text{Ni}_{1-x}\text{Mn}_x)_2\text{B}_2\text{C}$  samples.

In  $\text{YNi}_2\text{B}_2\text{C}$ , just above  $T_c$ , positive and quite large values were found for both, the longitudinale magnetoresistance MR (i.e. applied field parallel to the current;

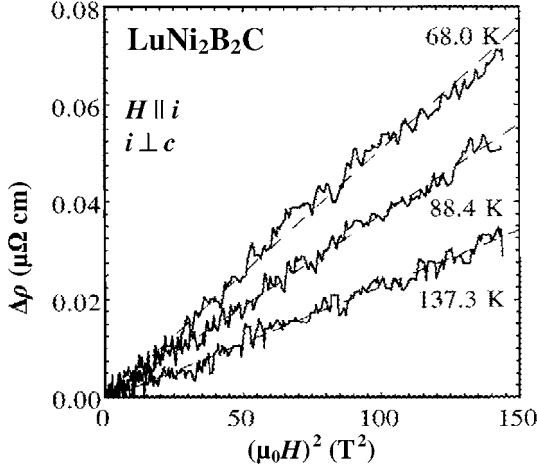


**FIGURE 16** Difference between the in-plane resistivity in magnetic fields and its zero-field value for  $\text{LuNi}_2\text{B}_2\text{C}$  at three different temperatures as a function of  $H^2$ .  $H$  is parallel to the electrical current. The dashed lines represent fits according to  $\Delta\rho \sim H^2$  (after Fisher et al., 1997).

Mazumdar et al., 1996; Narozhnyi et al., 1999a) and the transverse MR (i.e. field perpendicular to the current; Rathnayaka et al., 1997), where 8% for  $H = 50$  kOe might be considered as a characteristic value. An even larger transverse as well as longitudinal MR was observed for polycrystalline  $\text{LuNi}_2\text{B}_2\text{C}$  (Takagi et al., 1994; Narozhnyi et al., 1999a). The anisotropy (with respect to the crystal axes) in the transverse magnetoresistance of the non-magnetic  $\text{RNi}_2\text{B}_2\text{C}$  compounds was reported to be small (Rathnayaka et al., 1997). At higher temperatures, for  $\text{LuNi}_2\text{B}_2\text{C}$  a  $\text{MR} \sim H^2$  dependence describes the in-plane longitudinal MR quite well (Fisher et al., 1997; see Figure 16), and the coefficients of the magnetoresistance scale accordingly to Kohler's rule, i.e. the field dependence of MR for different scattering times (temperatures) can be rescaled by the temperature-dependent zero-field resistance. For  $\text{YNi}_2\text{B}_2\text{C}$ , a rather  $H$ -linear transverse MR was found at 25 K for higher fields (Rathnayaka et al., 1997). Moreover, this compound exhibits a change of sign of the transverse MR at 80 K for  $H = 4$  T with negative high-temperature values (Chu et al., 2000), which may possibly be connected with the occurrence of spin fluctuations. A possible reason for the different behavior of the magnetoresistance of  $\text{YNi}_2\text{B}_2\text{C}$  and  $\text{LuNi}_2\text{B}_2\text{C}$ , in particular for the large MR values of polycrystalline  $\text{LuNi}_2\text{B}_2\text{C}$ , is the formation of open orbits on the Fermi surface in certain field directions, which also suggests differences in the electronic structure (for a detailed discussion, see Narozhnyi et al., 1999a).

For the  $\text{RNi}_2\text{B}_2\text{C}$  compounds with  $R = \text{Pr, Tb, Dy, Ho, Er, and Tm}$ , the magnetoresistance provides insight into the scattering mechanisms due to the spin arrangement. This will be discussed together with the magnetic order in Section 4. Values of the transverse MR were also reported for the pseudoquaternary compounds  $\text{Er}_{0.8}\text{Tb}_{0.2}\text{Ni}_2\text{B}_2\text{C}$ ,  $\text{Er}_{0.8}\text{Lu}_{0.2}\text{Ni}_2\text{B}_2\text{C}$ , and  $\text{ErNi}_{1.9}\text{Co}_{0.1}\text{B}_2\text{C}$  (Takeya and El

Massalami, 2004) to be almost temperature independent in the range between the superconducting or magnetic transitions and 20 K.

### 3.4.2 Hall effect

There are only a small number of studies on the normal-state Hall coefficient  $R_H$  of  $RNi_2B_2C$ , including polycrystals of  $R = Y, Lu, La, Ho,$  and  $Gd$  (Fisher et al., 1995; Narozhnyi et al., 1996, 1999a; Mandal and Winzer, 1997; Freudenberger et al., 1999a). For all of these compounds, negative values of  $R_H$  were observed with a weak temperature dependence, confirming the electron-like character of the charge carriers. A surprising difference between the characteristics of  $YNi_2B_2C$  and  $LuNi_2B_2C$  was reported by Narozhnyi et al. (1999a) and Freudenberger et al. (1999a) (see Figure 17, note the absolute values of  $R_H$ ). The non-linearity in  $R_H(T)$  for  $LuNi_2B_2C$  below 60 K is in contrast to the linear behavior of  $YNi_2B_2C$  and all of the other  $RNi_2B_2C$  compounds investigated. Furthermore the  $R_H$  values, differing nearly by a factor of two over a wide temperature range, were confirmed by a study of the effective Magnus force using the acoustic Stewart–Tolman effect (Fil et al., 2006). A modified band structure due to the formation of open electron orbits (in a magnetic field) on the Fermi surface might explain the difference. On the other hand, an also sample-dependent thermoelectric power (see Section 3.4.3) points to a strong influence of impurities or sample imperfections.

Despite of its vanishing at low magnetic fields, the Hall resistivity in the vortex state of  $YNi_2B_2C$  and  $LuNi_2B_2C$  is negative and has no sign reversal below  $T_c$  (Narozhnyi et al., 1999a; Freudenberger et al., 1999a). For higher fields and annealed samples, it is approximately proportional to the square of the longitudinal component of the resistivity. The influence of pinning effects on the mixed-state Hall resistivity was discussed by Narozhnyi et al. (1999a). Thus, much information can be gained from both, normal-state and vortex-state Hall effect. Since now high-

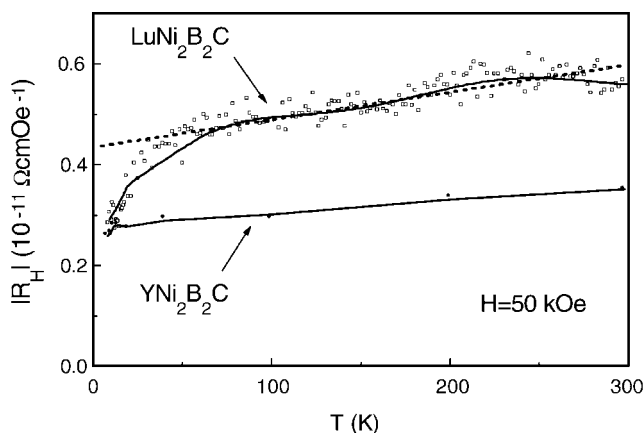


**FIGURE 17** Temperature-dependent magnitude of the Hall coefficient  $|R_H|$  (obtained at  $\mu_0 H = 5$  T) for annealed  $LuNi_2B_2C$  and  $YNi_2B_2C$  polycrystals. The dotted line represents a linear extrapolation of the high-temperature data for  $LuNi_2B_2C$ ; the solid lines are guides for the eye (after Narozhnyi et al., 1999a).

quality, well-characterized  $\text{RNi}_2\text{B}_2\text{C}$  single crystals are available, further studies of  $R_H$  should be performed. Moreover, since the measured values of  $R_H$ , as well as those of the thermoelectric power, deviate from results of band-structure calculations, these anomalies should motivate more detailed investigations.

### 3.4.3 Thermoelectric power

In agreement with band-structure calculations and with above discussed measurements of the Hall effect, the generally reported negative values for the normal-state thermoelectric power (TEP) of the  $\text{RNi}_2\text{B}_2\text{C}$  phases (Naugle et al., 1999a) indicate that the charge carriers are of electronic character. A comparison of the in-plane TEP (Rathnayaka et al., 1997; Bhatnagar et al., 1997; Hennings et al., 2002) with results on polycrystalline samples (Fisher et al., 1995) suggests large differences between the TEP values parallel and perpendicular to the  $c$ -axis. A recent study on single crystals of  $\text{YNi}_2\text{B}_2\text{C}$  and  $\text{HoNi}_2\text{B}_2\text{C}$  (Schneider, 2005), however, revealed a rather weak anisotropy. Thus, the influence of crystal imperfections has to be considered also in accordance with the annealing effects discussed in Section 3.1. The impact of the magnetic ordering on the TEP,  $S_Q$ , is shown in Figure 18 for three  $\text{RNi}_2\text{B}_2\text{C}$  compounds with  $T_c < T_N$  ( $R = \text{Dy}$ ) or without superconductivity ( $R = \text{Tb}, \text{Gd}$ ). Whereas in the case of  $\text{GdNi}_2\text{B}_2\text{C}$  very subtle changes in the slope of the  $S_Q$ -vs.- $T$  curve are observed at the magnetic ordering temperatures, the changes in  $S_Q(T)$  are more pronounced for  $\text{DyNi}_2\text{B}_2\text{C}$  and  $\text{TbNi}_2\text{B}_2\text{C}$  including the effect of weak ferromagnetism for the latter one (Hennings et al., 2002). The interplay between superconductivity and magnetic order in a series of  $\text{Ho}_x\text{Dy}_{1-x}\text{Ni}_2\text{B}_2\text{C}$  samples generates a rich variety of  $S_Q(T)$  dependencies (Naugle et al., 2000).

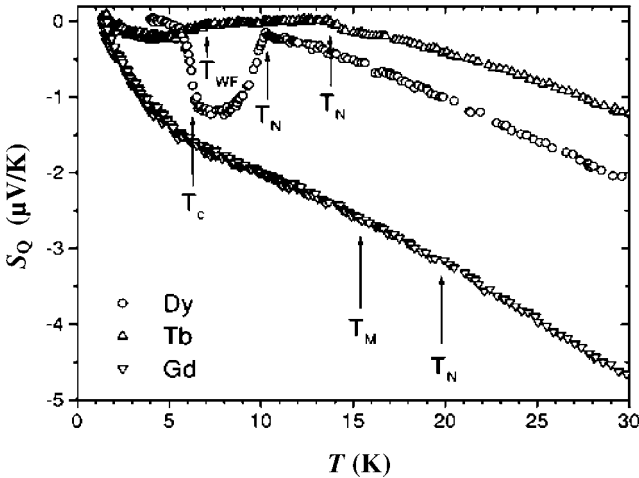


**FIGURE 18** Thermoelectric power  $S_Q$  for  $\text{RNi}_2\text{B}_2\text{C}$  ( $R = \text{Dy}, \text{Tb}, \text{Gd}$ ) measured perpendicular to the  $c$ -axis. The arrows indicate superconducting and different magnetic transition temperatures that are described in more detail in Sections 4.6, 4.7 (where  $T_{\text{WFM}}$  is used instead of  $T_{\text{WF}}$ ), and 4.8 (after Hennings et al., 2002).

The enhancement of the TEP below the magnetic transition temperatures has been explained by the magnon drag due to the electron–magnon interaction or, alternatively, by the loss of spin-flip scattering which influences the electron diffusion TEP (Hennings et al., 2002). There are discrepancies concerning the nature of the phonon-drag contribution. Whereas Fisher et al. (1995) assumed a standard peak-like behavior of the phonon drag, in some studies (Rathnayaka et al., 1997; Bhatnagar et al., 1997; Hennings et al., 2002) a model based on saturation effects was proposed similar to that for the cuprate superconductors. The high-temperature slope of  $S_Q(T)$  scales well with the de Gennes factor (Naugle et al., 2001), which is also supported by the smaller TEP in  $\text{Lu}_x\text{Gd}_{1-x}\text{Ni}_2\text{B}_2\text{C}$  ( $x = 0.88$ ) compared with that of  $\text{LuNi}_2\text{B}_2\text{C}$  (Rathnayaka et al., 2003). Schneider (2005) showed that the high-temperature approximation of the standard phonon-drag contribution connected with a usual electron diffusion term well describes the measured data on  $\text{YNi}_2\text{B}_2\text{C}$  single crystals over a wide temperature range. However, no pronounced phonon-drag peak is present, similar to results for  $\text{MgB}_2$  (Schneider et al., 2001). The magnitude of the diffusion TEP is sensitively affected by the phonon drag, whose nature requires further analysis. It is noted that the phonon-drag models result in diffusion TEP values differing by a factor of approximately two, whereas band-structure calculations (see Section 3.2) employing Mott’s formula and the calculated total density of states  $N(E)$  deviate from the experimental results by a factor of up to ten (Fisher et al., 1995). This discrepancy cannot be explained by renormalization due to electron–phonon interaction or similar effects. Possibly, multiband effects have to be taken into account. Therefore both, the experimental investigation of the TEP and the theoretical calculation of the partial (Fermi-surface sheet) densities of states are of interest since the diffusion TEP is quite sensitive to details of the band structure.

#### 3.4.4 Thermal conductivity

The in-plane thermal conductivity  $\kappa$  far above the superconducting or magnetic transition temperatures shows similar behavior for all investigated  $\text{RNi}_2\text{B}_2\text{C}$  compounds with the exception of  $\text{R} = \text{Gd}$ , which displays enhanced  $\kappa$  values and a remarkable phonon contribution to the heat conduction, whereas otherwise a prevailing electronic proportion of  $\kappa$  can be deduced from the comparison with the electrical resistivity (Hennings et al., 2002). A detailed review on thermal-conductivity studies including an analysis of the contributions to  $\kappa$  from electrons and phonons is given by Belevtsev et al. (2003). For  $\text{YNi}_2\text{B}_2\text{C}$  and  $\text{HoNi}_2\text{B}_2\text{C}$  the in-plane thermal conductivity is larger than that for the heat current parallel to  $c$  over a wide temperature range (Sera et al., 1996; Schneider, 2005). Whereas in the latter case a maximum in  $\kappa$  was observed in these studies for  $\text{YNi}_2\text{B}_2\text{C}$ , Hennings et al. (2002) found a constant increase of the in-plane thermal conductivity with increasing temperature above  $T_c$  (see the inset of Figure 19) as observed for all investigated borocarbides. Furthermore, from a comparison with specific-heat results, these authors derived strong evidence for enhanced scattering of phonons by electrons in  $\text{LuNi}_2\text{B}_2\text{C}$  at high temperatures, thus providing evidence for a strong electron–phonon interaction.

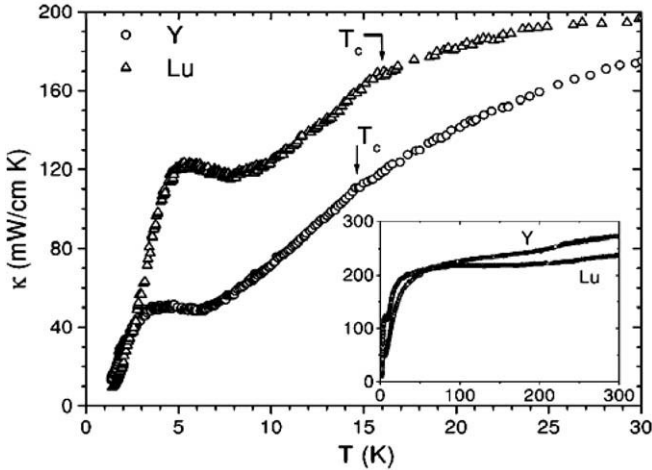


**FIGURE 19** Thermal conductivity of  $\text{RNi}_2\text{B}_2\text{C}$  ( $R = \text{Y}$  and  $\text{Lu}$ ) perpendicular to the  $c$ -axis for two temperature ranges. The arrows indicate the superconducting transition temperatures (reprinted figure with permission from Hennings, B.D., Naugle, D.G., Canfield, P.C., *Phys. Rev. B* 2002, **66**, 214512).

© 2002 by the American Physical Society

For  $\text{YNi}_2\text{B}_2\text{C}$  and  $\text{LuNi}_2\text{B}_2\text{C}$  a distinct change in the slope of  $\kappa(T)$  at  $T_c$  is observed by Hennings et al. (2002; Figure 19) in agreement with results of studies for different sample quality (Sera et al., 1996; Boaknin et al., 2000; Cao et al., 2001; Izawa et al., 2002; Schneider, 2005). The clear enhancement of  $\kappa$  at about 5 K is most probably due to the reduced scattering of phonons by electrons. However, Cao et al. (2001) and Izawa et al. (2002) did not observe such enhancement. Furthermore, all magnetic  $\text{RNi}_2\text{B}_2\text{C}$  superconductors investigated by Hennings et al. (2002) do not exhibit such enhanced  $\kappa$  values below  $T_c$ . In contrast, peaks or enhanced in-plane  $\kappa(T)$  just below the magnetic ordering temperatures presumably due to the loss of spin-flip scattering were reported for  $\text{RNi}_2\text{B}_2\text{C}$  single crystals with  $R = \text{Ho}$ ,  $\text{Tb}$ ,  $\text{Dy}$  and  $\text{Tm}$  (Sera et al., 1996; Hennings et al., 2002). In the case of  $\text{TmNi}_2\text{B}_2\text{C}$ , some other possible explanations for the strong increase in  $\kappa$  far below  $T_c$  were offered by Hennings et al. (2002), including additional heat conduction by magnons, the presence of uncondensed electrons in agreement with a two-band model, or gapless superconductivity (see also Section 4.11). More subtle changes in  $\kappa(T)$  connected with magnetic ordering were observed for  $R = \text{Gd}$  and  $\text{Er}$  whereas the transitions into the weak ferromagnetic state for  $R = \text{Tb}$  and  $\text{Er}$  could not be detected in  $\kappa$  (Hennings et al., 2002). Especially for  $R = \text{Gd}$  and  $\text{Er}$ , different results were found for polycrystalline samples (Cao et al., 2000, 2001); surprisingly featuring more pronounced variations in  $\kappa(T)$  for a lower sample quality. At  $T_c$ , the magnetic  $\text{RNi}_2\text{B}_2\text{C}$  compounds with  $R = \text{Er}$  and  $\text{Tm}$  exhibit distinct changes in the slope of  $\kappa(T)$  for both, polycrystalline samples and single crystals (Cao et al., 2000; Hennings et al., 2002). In contrast, the superconducting phase transition is not evident in the thermal conductivity for  $R = \text{Dy}$  and  $\text{Ho}$  (Cao et al., 2001; Hennings

et al., 2001, 2002). For  $\text{HoNi}_2\text{B}_2\text{C}$ , Hennings et al. (2002) proposed a possible gapless superconducting state between  $T_N$  and  $T_c$  caused by magnetic pair breaking. This is also supported by spectroscopic investigations (see Section 4.9). A study by Schneider (2005) showing a kink in  $\kappa(T)$  at  $T_c$ , however, is not consistent with this prediction, whereas an alternative mechanism leading to gapless superconductivity might be present. It is interesting to note that up to now there is no experimental evidence for an energy gap in this temperature range, thus leaving a puzzling situation for both, further experimental studies and theoretical description. The maximum in  $\kappa(T)$  at  $T_N$  points to an enhanced fraction of uncondensed electrons in one of the bands supporting the scenario of the coexistence of magnetism and superconductivity on *different* Fermi-surface pieces (see Sections 4.8 and 4.9).

The Lorenz number as derived from thermal conductivity and electrical resistivity has small values just above  $T_c$  indicating different scattering mechanisms being important in the heat and charge transport for  $\text{YNi}_2\text{B}_2\text{C}$ ,  $\text{LuNi}_2\text{B}_2\text{C}$ , and  $\text{HoNi}_2\text{B}_2\text{C}$  (Sera et al., 1996; Boaknin et al., 2000; Schneider, 2005). The shape of a typical minimum in the temperature dependence of the Lorenz number at about 40 K seems to be connected with the residual resistivity of the crystals (Boaknin et al., 2000).

Applying a magnetic field just above the lower critical field  $H_{c1}$  leads to a reduced thermal conductivity due to the scattering especially of phonons by vortices, whereas for  $H > H_{c2}$  a less field-dependent behavior of  $\kappa$  is expected. Thus, thermal-conductivity studies can be used to determine the critical fields as demonstrated by Cao et al. (2003) for  $\text{LuNi}_2\text{B}_2\text{C}$  (see Section 3.6). The field-induced suppression of enhanced contributions to  $\kappa$ , which are caused by superconducting or magnetic transitions, was reported for  $\text{RNi}_2\text{B}_2\text{C}$  with  $R = \text{Y}$  (Sera et al., 1996), Er, Dy, and Ho (Cao et al., 2000, 2001). Further published studies on the thermal conductivity in magnetic fields, at low temperatures, will be discussed in Section 3.5.1. Surprisingly, there are only a few reports on  $\kappa(H, T)$ . In particular, zero-field *c*-axis thermal-conductivity data are nearly completely missing. Nevertheless, rich and detailed information has been extracted from the few measurements of  $\kappa$  that have been performed up to now.

### 3.5 Symmetry of the superconducting gap

The symmetry of the superconducting order parameter is a fundamental property used to distinguish conventional from unconventional superconductors. In the latter case, it is lower than that of the crystal structure (the same as that of the Fermi surface). If pair-breaking impurities are absent (magnetic ones in the case of non-magnetic borocarbides and any kind of an impurity in the case of magnetic borocarbides), the quasiparticles in the superconducting state acquire a gap near the Fermi level. This gap can be identified with the superconducting order parameter. The gap of a superconductor (as a function in *k* space) reflects the symmetry of a Cooper pair. Ignoring the relative weak spin-orbit interaction in the non-magnetic  $\text{RNi}_2\text{B}_2\text{C}$  compounds under consideration, the Cooper pair's antisymmetric wave function is given by a product of an orbital and a spin part. In the case of singlet pairing with total spin  $S = 0$ , the orbital part must be of even parity

and can be classified by an even total angular momentum  $l = 0, 2, 4, \dots$  denoted as s-, d-, and g-wave states, respectively. Then, a pure s-wave state has no zeros (nodes), which is at variance with a pure d- or g-wave state. Finally, an (s+g)-wave state may exhibit point-like zeros for specially adjusted amplitudes of the s and g components as adopted by Maki et al. (2002) for  $\text{YNi}_2\text{B}_2\text{C}$  and  $\text{LuNi}_2\text{B}_2\text{C}$ . A simple s-wave state has a constant gap  $\Delta$  whereas in the more general and realistic extended s-wave state the gap  $\Delta(\mathbf{k})$  changes over the Fermi surface, in other words it becomes anisotropic. From a formal microscopic point of view this must be a consequence of the symmetry of the pairing electron–phonon interaction and/or the symmetry of the competing depairing interactions, i.e. an antiferromagnetic one, or the remaining screened Coulomb repulsion for which, however, almost nothing is known exactly. Anyhow, in our opinion a strong anisotropy of the latter seems to be unlikely whereas a strong anisotropy of the antiferromagnetic paramagnon interaction caused by the nesting properties of the Fermi surface (see Section 3.2) is rather natural. In principle, the anisotropy of the pairing and depairing interaction can be probed by the point-contact and the superconducting tunneling spectroscopy using differently oriented interfaces. However, the preparation of such high-quality interfaces changing their orientation in small angular steps is a difficult task. In addition, the inversion of the tunneling data in order to extract the spectral density of the pairing functions, the so-called Eliashberg functions  $\alpha^2F(\omega)$ , remains an unsolved mathematical (possibly even ill-defined) problem in the anisotropic and multiband case being relevant here. Furthermore, the underlying tunnel currents are affected by the anisotropic Fermi velocities. Therefore, at present only limited information has been extracted from tunneling data obtained in  $\mathbf{c}$  direction and  $\mathbf{a}$ – $\mathbf{b}$ -plane, i.e. the anisotropic gap structures (see Section 3.5.2). More information can be obtained by analyzing the orbit-averaged mass renormalization affecting the de Haas–van Alphen data in changing the magnetic-field orientation (see Section 3.5.3).

The nature of the quasiparticle energy gap is one of the most challenging questions in the research on  $\text{RNi}_2\text{B}_2\text{C}$ . A few years after their discovery these compounds were assumed to be conventional s-wave superconductors with an anisotropic gap (Müller et al., 2002) although an analysis of the upper critical field (Wang and Maki, 1998) and the field dependence of the specific heat suggested d-wave superconductivity (Nohara et al., 1997). However, the strong influence of Pt substitutions for Ni on the gap connected with a weakly reduced  $T_c$  (Nohara et al., 1999; Yokoya et al., 2000) quite certainly rules out such a line node scenario, even if d-wave pairing was favored in a study based on perturbation theory (Fukazawa et al., 2001). In the more recent investigations on non-magnetic borocarbides, a controversy has developed: (i) are the electrons from different bands involved in the pairing mechanism, as adopted for the explanation of the  $H_{c2}$  peculiarities by Shulga et al. (1998) (see Section 3.6), or (ii) does an extremely strong anisotropy in a single band, possibly including gap nodes, better describe the experimental data. For the latter case, a phenomenological model with an (s + g)-wave symmetry of the gap function was proposed by Lee and Choi (2002). In particular, Maki et al. (2002) used the form  $\Delta(\mathbf{k}) = 1/2\Delta(1 - \sin^4\theta \cos(4\phi))$ , where  $\theta$  and  $\phi$  are the polar and the azimuthal angle in the  $\mathbf{k}$  space, respectively. It leads to

four point nodes in the energy gap located regularly in the **a**–**b**-plane and predicts four-fold symmetry in the angular variation of both the **c**-axis component of the thermal conductivity and the specific heat in an in-plane magnetic field. The model takes into account the momentum- and position-dependent Doppler shift of the quasiparticle energies. A generalization for any direction of the applied field was given by Thalmeier and Maki (2003). The angle-dependent thermal conductivity was found to be strongly influenced by the presence of impurities (Won et al., 2003; Yuan et al., 2003; Maki et al., 2004). A theoretical study by Yuan and Thalmeier (2003) has confirmed the stability of the mixed gap function. The (s + g)-wave model is described in detail by Thalmeier and Zwicknagl (2005). The origin of the highly anisotropic s-wave gap has not yet been fully understood. Kontani (2004) proposed, in our opinion, a more convincing model based on strongly anisotropic and sharp antiferromagnetic spin fluctuations in YNi<sub>2</sub>B<sub>2</sub>C and LuNi<sub>2</sub>B<sub>2</sub>C related to the pronounced nesting properties of the Fermi surface although the strong-coupling gap calculations were performed for simplified Fermi surfaces. Anyhow, his main result, which is important in the present context, is that for the extended s-wave scenario depairing anisotropic antiferromagnetic fluctuations are much more effective in producing strongly anisotropic gaps than the anisotropic electron–phonon interaction.

The electronic Raman scattering data (Yang et al., 2000) with a remarkable scattering strength below the superconducting peak are well described theoretically assuming (s + g)-wave symmetry (Won et al., 2004) in the range of small Raman shift values, whereas the shape of the calculated B<sub>1g</sub> peak is not consistent with the experimental results. In a study by Lee and Choi (2002) this discrepancy was thought to be due to the possible influence of inelastic scattering. The ultrasonic attenuation in YNi<sub>2</sub>B<sub>2</sub>C shows significant deviations from the standard-BCS model (Watanabe et al., 2004). The (s + g)-wave model describes the results for some of the modes investigated but predicts a different behavior for two other ones (Won and Maki, 2004). The enhanced flux-flow resistivity is not consistent with the conventional normal-state vortex core model and indicates the influence of the gap anisotropy (Takaki et al., 2002). Angle-dependent in-plane values for the vortex-state magnetization of YNi<sub>2</sub>B<sub>2</sub>C and LuNi<sub>2</sub>B<sub>2</sub>C showing four-fold in-plane anisotropy were firstly interpreted within the non-local London theory (Civale et al., 1999; Kogan et al., 1999). This was questioned by Kusunose (2005) who suggested the influence of the anisotropic gap structure in agreement with the (s + g)-wave interpretation. However, a calculation based on the quasiclassical Eilenberger formalism, assuming such a gap function (Adachi et al., 2005), does not yield the four-fold anisotropy. A large number of studies on the gap symmetry of RNi<sub>2</sub>B<sub>2</sub>C including NMR results was summarized by Brandow (2003) who suggested strongly anisotropic s-wave superconductivity but also pointed out that a single-band description might oversimplify the interpretation due to the complex Fermi surface. It is noteworthy that the suppression of the Hebel–Slichter peak was observed by Iwamoto et al. (2000) and connected with possible unconventional superconductivity. This suppression also occurs in two-band superconductors with interband impurity scattering (Mitrović and Samokhin, 2006). Parker and Haas (2007) concluded from their theoretical analysis that the Hebel–Slichter peak in

the NMR signal should appear for any unconventional superconductor. A recent NMR study on  $\text{YNi}_2\text{B}_2\text{C}$  by Saito et al. (2007) suggested (s + g)-wave pairing. Analyzing  $\mu\text{SR}$  data for  $\text{YNi}_2\text{B}_2\text{C}$ , Landau and Keller (2007) found an indication on two-gap superconductivity but stressed that more experimental data are required for a definite conclusion. The possible interaction between the gap symmetry and the structure of the vortex lattice will be considered in Section 5. In the following subsections, further experimental results will be discussed with the focus on their agreement with the theoretical models.

### 3.5.1 The role of thermal conductivity and specific heat

The normal-state thermal conductivity  $\kappa$  has been analyzed in Section 3.4.4 including its changes at the transition to the superconducting state. The first study on  $\text{LuNi}_2\text{B}_2\text{C}$  extended to temperatures down to 50 mK (Boaknin et al., 2000) seemed to confirm a conventional s-wave pairing as indicated by the phononic  $T^3$  dependence of  $\kappa$  at these low temperatures in zero magnetic field. However, a subsequent investigation with applied field (Boaknin et al., 2001) revealed a large fraction of delocalized quasiparticles even at  $T = 70$  mK, which is in sharp contrast to the conventional superconductors Nb and  $\text{V}_3\text{Si}$ , but with some similarity with the behavior of the unconventional superconductor  $\text{UPt}_3$  which exhibits line nodes. Consequently, a highly anisotropic s-wave gap was derived including the possibility of nodes. A theoretical analysis for the case of s-wave symmetry showed a considerable thermal transport in the mixed state due to the creation of gapless excitations in the magnetic field (Dukan et al., 2002). More recently the  $\text{MgB}_2$  and  $\text{PrOs}_4\text{Sb}_{12}$  superconductors exhibited a significantly larger fraction of delocalized quasiparticles at comparable low temperatures, compared to that of the borocarbides. Although first studies suggested anisotropic s-wave superconductivity including point nodes in the latter case (Haas and Maki, 2002; Izawa et al., 2003), detailed investigations on the thermal conductivity (Sologubenko et al., 2002; Seyfarth et al., 2005, 2007) addressed the unusually enhanced  $\kappa$  values at low temperatures to multiband superconductivity in these compounds.

In a rotational-field study on  $\text{YNi}_2\text{B}_2\text{C}$ , by Izawa et al. (2002; for a recent review on such experiments see Matsuda et al., 2006) the  $\mathbf{c}$ -axis component of the thermal conductivity  $\kappa_{zz}$  ( $T = 0.43$  K,  $B = 1$  T,  $\theta = 90^\circ$ ,  $\phi$ ) (the definitions of  $\theta$  and  $\phi$  are given in the inset of Figure 20) exhibits four-fold in-plane oscillations with narrow cusps for an applied field in the  $\mathbf{a}$ - $\mathbf{b}$ -plane (see Figure 20). Their amplitude was strongly reduced if the magnetic field was rotated  $45^\circ$  away towards the  $\mathbf{c}$ -axis. The results for  $\theta = 90^\circ$  are in excellent agreement with the (s + g)-wave model described above suggesting the presence of point nodes along [100] and [010]. An alternative explanation of the cusp-like singularity in  $\kappa$  was given by Udagawa et al. (2005). They calculated the field-orientational dependence of the density of states (FODOS) based on the solution of the Eilenberger equation and found rather broad minima in the point-node case. The FODOS is strongly influenced by the local Fermi-surface part and its order parameter but not so strong by the entire global nodal structure. In  $\text{YNi}_2\text{B}_2\text{C}$ , the Fermi-surface nesting leads to a quasi two-dimensional nature of one of the conduction-electron bands. Assuming a two-band model with an isotropic superconducting coherence length,

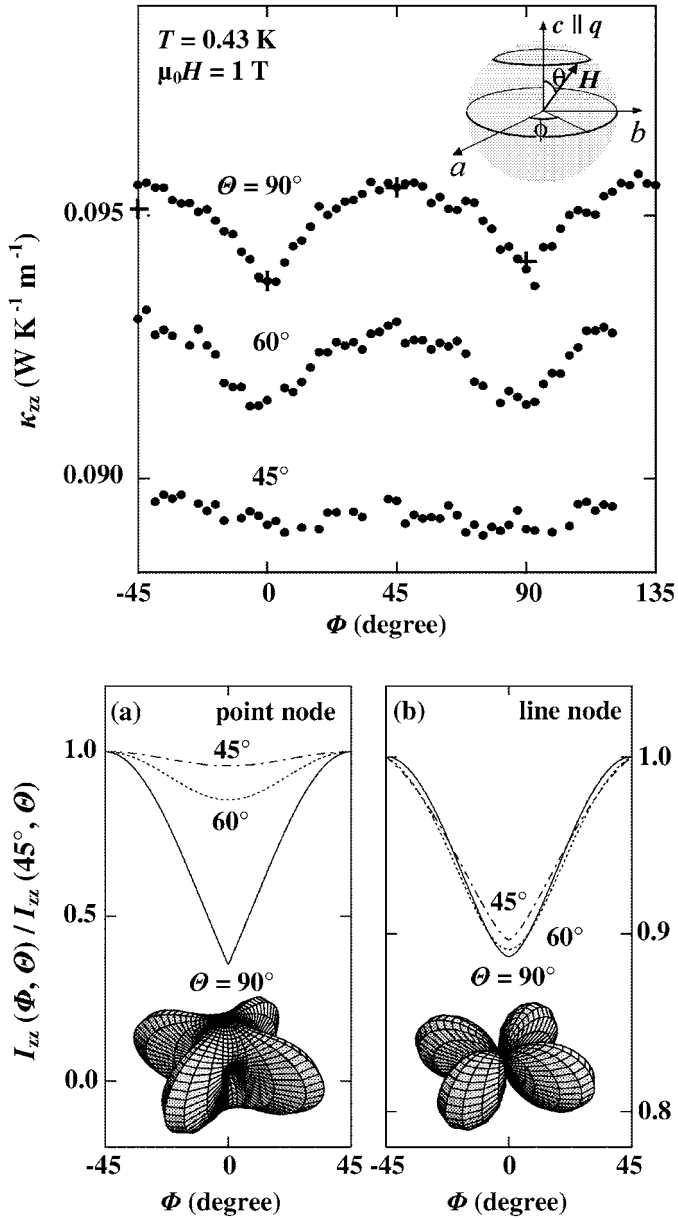


**FIGURE 20** Angle-dependent  $c$ -axis thermal conductivity of  $\text{YNi}_2\text{B}_2\text{C}$  (upper panel),  $\theta$  and  $\phi$  are defined in the inset. The lower pair of panels shows the gap symmetry in the case of (a) point nodes ( $(s+g)$  wave) and (b) line nodes and, additionally, the resulting angular variation of a quantity  $I_{zz}$ , related to its value for  $\phi = 45^\circ$ , that is proportional to the  $c$ -axis component of  $\kappa$  (reprinted figures with permission from Izawa, K., Kamata, K., Nakajima, Y., Matsuda, Y., Watanabe, T., Nohara, M., Takagi, H., Thalmeier, P., Maki, K., Phys. Rev. Lett. 2002, **89**, 137006).

cusplike minima are attributed to nesting effects rather than to a contribution from a nodal gap structure. However, considering the disappearance of those minima in  $Y(Ni_{0.95}Pt_{0.05})_2B_2C$  (not yet being in the dirty limit; see Section 6.2), Matsuda et al. (2006) concluded that a nesting scenario should be unlikely. The occurrence of Fermi-surface nesting in pseudoquaternary borocarbides and the effect of strong disorder, caused by doping in the Ni-B network, on nesting needs, however, further investigation.

Despite the previously debated d-wave symmetry of the superconducting gap in  $YNi_2B_2C$  as suggested from the interpretation of specific-heat ( $C_p$ ) data (Nohara et al., 1997), additional mechanisms for the  $T^3$  dependence of the electronic part of  $C_p$  and its unusual magnetic-field dependence were discussed, including the shrinking of the vortex core radius with increasing field (Nohara et al., 1999). The influence of disorder is discussed in Section 6.2. Measurements of the microwave

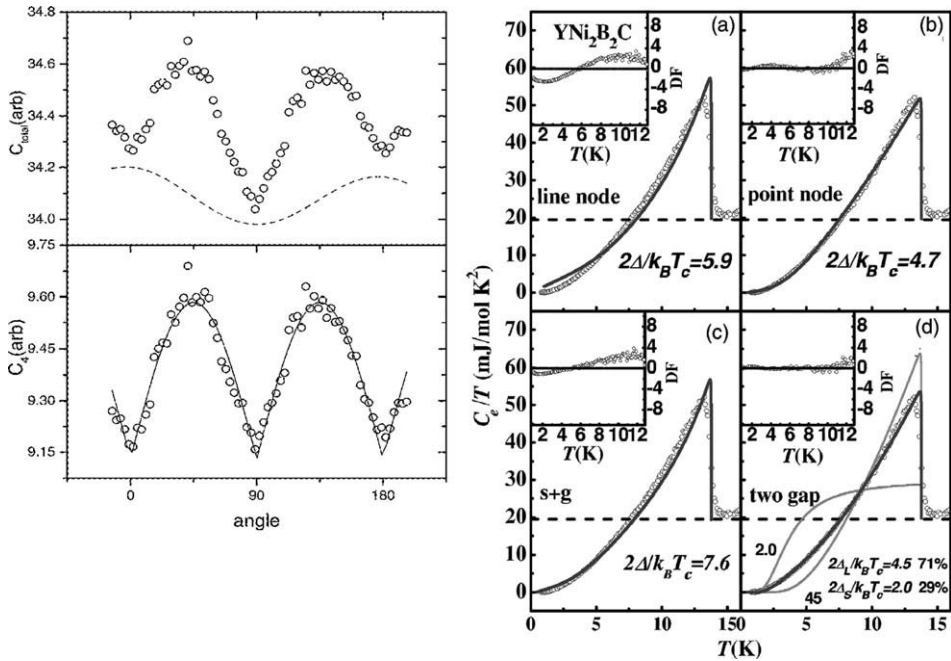


**FIGURE 21** Left panel: Angle-dependent heat capacity  $C_p$  of  $YNi_2B_2C$  (angle of the magnetic field with respect to the a-axis) at 2 K in a field of 1 T. Total contribution and two-fold component (dashed line) due to the experimental setup (top); four-fold component after subtraction of the background (bottom); the solid line describes a fit with a cusped function (reprinted figure with permission from Park, T., Salamon, M.B., Choi, E.M., Kim, H.J., Lee, S.-I., Phys. Rev. Lett. 2003, **90**, 177001). Right panel: symbols (circles) – temperature-dependent electronic contribution  $C_e$  to  $C_p$  and fits (thick lines) to various models: (a) line-node gap; (b) point-node gap with  $\Delta = \Delta_0 \sin n\theta$ ; (c) (s + g)-wave; (d) two-gap, where the thin lines show the  $C_e/T$  for the larger and the smaller gap. The respective insets show the absolute difference DF between calculation and measured data (after Huang et al., 2006).

surface impedance pointed to the importance of the delocalized quasiparticles around the vortex core (Izawa et al., 2001). A study of  $C_p$  on  $\text{YNi}_2\text{B}_2\text{C}$  with a magnetic field in the basal plane revealed four-fold oscillations (Park et al., 2003; see Figure 21, left panel). They were discussed as a variation of the quasiparticle density of states using Doppler shift arguments. Gap nodes along [100] are consistent with the thermal-conductivity results of Izawa et al. (2002) although a d-wave gap would also lead to four-fold oscillations. Similar observations were reported for  $\text{LuNi}_2\text{B}_2\text{C}$  by Park et al. (2004b). A slightly disordered sample, however, featured an eight-fold pattern at 2 K and 1.5 T. This has been ascribed to non-local effects in addition to the gap anisotropy. A theoretical study based on the quasi-classical Eilenberger formalism (Miranović et al., 2005) supported the interpretation of the rotational-field experiments. It was pointed out, however, that more detailed low-field data are required to distinguish between gap nodes and non-zero gap minima. A detailed analysis of the specific heat of  $\text{YNi}_2\text{B}_2\text{C}$  has been presented by Huang et al. (2006). The zero-field data were compared with the predictions of different theoretical models (Figure 21, right panel). Good agreement was found for a point-node scenario with  $\Delta = \Delta_0 \sin n\theta$ , where  $\theta$  is the polar angle in the  $\mathbf{k}$  space. Alternatively, an excellent description of the data is attained employing a two-band model, whereas an isotropic s-wave or line-node scenario can be ruled out. It is noted that the (s + g)-wave model results in  $C_p \sim T^2$  (Yuan et al., 2003), which is significantly different from the usually observed  $T^3$  dependence.

Thus, measurements of  $\kappa$  and  $C_p$  provided first hints for possible nodes in the energy gap. More detailed investigations, however, point to different scenarios, in particular those based on Fermi-surface nesting. Also there are discrepancies between experimental data and the (s + g)-wave description.

### 3.5.2 Tunneling and point-contact spectroscopy

Studies using point-contact spectroscopy (PCS), scanning tunneling spectroscopy (STS), photoemission spectroscopy (PES), or angle-resolved PES (ARPES) provide a local insight, especially into the structure of the superconducting gap. In this section, we will discuss the behavior of the non-magnetic borocarbides. Results on the magnetic ones are included in Section 4 and STS studies on the flux line lattice in Section 5. The early spectroscopic studies on borocarbides were reviewed by Andreone et al. (1998) and Yanson (2001). An overview of the recent progress in PCS of  $\text{RNi}_2\text{B}_2\text{C}$  was presented by Naidyuk et al. (2007a).

PES results on  $\text{YNi}_2\text{B}_2\text{C}$  (Yokoya et al., 2000; Baba et al., 2006a, 2006b) indicate an anisotropic s-wave pairing. A substitution of 20% Ni by Pt leads to a nearly isotropic behavior (see Figure 22, left panel). This smearing due to impurities clearly rules out a d-wave symmetry in the superconducting gap structure. The best fit to the experimental data of  $\text{YNi}_2\text{B}_2\text{C}$  is achieved assuming an anisotropic s-wave whereas an (s + g)-wave shows significant deviations. A study using ARPES (Yokoya et al., 2006) brought experimental evidence for the existence of three different Fermi-surface sheets. A gap anisotropy was observed even on a single Fermi-surface sheet.

PCS results on  $\text{YNi}_2\text{B}_2\text{C}$  (Raychaudhuri et al., 2004) showing a large anisotropy of the gap parameter were interpreted in terms of the (s + g)-wave model. A sub-

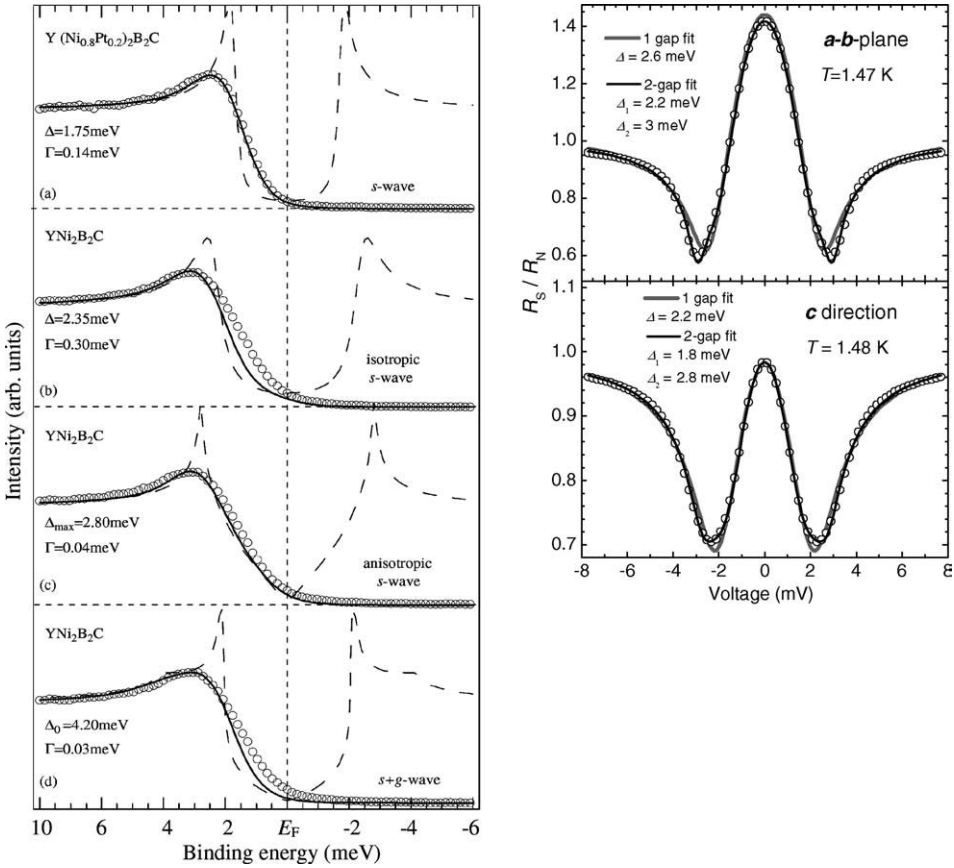


**FIGURE 22** Left panel: Photoemission spectra of  $Y(Ni_{0.8}Pt_{0.2})_2B_2C$  and  $YNi_2B_2C$  at 3.5 K (circles) and comparison with different theoretical models (see text; from [Baba et al., 2006a](#)). Broken lines are the Dynes functions before being multiplied by the Fermi–Dirac distribution function and convolved by the Gaussian; Dynes functions used for the fits (solid lines) to the data include a smearing parameter  $\Gamma$  additionally to the gap value  $\Delta$ . Right panel: Differential resistance  $R_S = dV/dI$  normalized by the normal-state value  $R_N$  of a  $LuNi_2B_2C$ –Ag point contact for measurements in the **a–b**-plane and, below, in **c** direction (solid circles; after [Bobrov et al., 2006](#)). Black lines represent a fit using a two-gap model, gray lines correspond to a one-gap approximation.

© 2006 Elsevier

sequent study ([Mukhopadhyay et al., 2005](#); see also [Raychaudhuri et al., 2007](#)) addressed the partially observed lowered  $T_c$  values to the difficulty of the experimental resolution of small gaps applying point contacts. It was pointed out that zero-field data are not sufficient to distinguish between nodal and multiband superconductivity. The extrapolated vanishing of the smaller gap much below the upper critical field and the BCS-like behavior of the larger one governing the values of  $T_c$  and  $H_{c2}$  were shown to be similar to the two-band superconductor  $MgB_2$ .

Similar gap structures were also obtained on an  $\text{YNi}_2\text{B}_2\text{C}$  thin film (Bashlakov et al., 2005). Maxima in the superconducting gap distribution for different point-contacts at 2.0 and 2.4 meV favor a possible two-band description also supported by the BCS-like behavior of the larger gap. For  $\text{LuNi}_2\text{B}_2\text{C}$ -based point contacts (Bobrov et al., 2005, 2006), the PCS results show no significant anisotropy of the energy gap in the basal plane and in the  $c$  direction, and they are well described by a two-band model (see Figure 22, right panel). The directional variation of the gap values obtained by PCS on  $\text{YNi}_2\text{B}_2\text{C}$  single crystals (Bashlakov et al., 2007) has been attributed to multiband superconductivity, which is also supported by the behavior of the excess current showing similarities with that in  $\text{MgB}_2$ .

Recent STS studies on  $\text{YNi}_2\text{B}_2\text{C}$  and  $\text{LuNi}_2\text{B}_2\text{C}$  (Martínez-Samper et al., 2003; Suderow et al., 2003) favor an anisotropic  $s$ -wave gap function, and show very different gap values over different parts of the Fermi surface, which is connected with an anisotropic electron–phonon interaction. Although STS should be able to resolve the exact gap symmetry and to distinguish between point nodes and line nodes (Pairor and Smith, 2003), the situation might be more complicated due to the presence of additional non-superconducting bands (Devereaux, 2000). Nishimori et al. (2004) observed a four-fold-symmetric star-shaped vortex core in  $\text{YNi}_2\text{B}_2\text{C}$  and derived an adequate symmetry for the energy gap. In a subsequent analysis of the tunneling spectra Nakai et al. (2006) pointed out that the resulting  $V$ -shaped density of states has to be considered in the interpretation of thermodynamic measurements, which agrees with the results of Udagawa et al. (2005).

### 3.5.3 de Haas–van Alphen (dHvA) effect

Quantum oscillations in the magnetization are obtained in both, normal and superconducting state, thus providing information about the Fermi surface (FS) and additionally about the superconducting gap via the damping of the dHvA oscillations. The early work on the dHvA effect in rare-earth nickel borocarbides was reviewed by Winzer and Krug (2001) especially focusing on the connection between experimentally observed frequencies and the special Fermi surface sheets as derived from band-structure calculations. Despite the attempts of several worldwide band-structure groups, so far not all of the observed dHvA-frequencies could be ascribed to one of the calculated extreme FS cross sections. Especially challenging is the missing assignment of the  $\beta$ -frequency whose FS cross section corresponds to 18% of the Brillouin zone. The reason for this long-standing discrepancy remains unclear at present. In our opinion it might be related to the above mentioned B–C disorder, and/or a non-classic electronic structure affected by the asymmetric electron–phonon coupling to high-frequency modes in the multiband picture (Drechsler et al., 2004). Anyhow, a complete understanding of the electronic structure in the normal state is a necessary prerequisite for a future consequent microscopic theory of the superconducting state. The comparison of the observed (extremal) orbitally-averaged masses  $m_{o,\text{exp}} = (1 + \lambda_o)m_{o,\text{LDA}}$  (with the calculated smaller ones  $m_{o,\text{LDA}}$ ) provides a valuable insight into the strength of the local electron–boson (phonon as well as paramagnon) interaction. Changing the direction of the applied external magnetic field, changes the perpendicular FS cross-section and the related FS orbit. Hence, even its anisotropy can be probed.

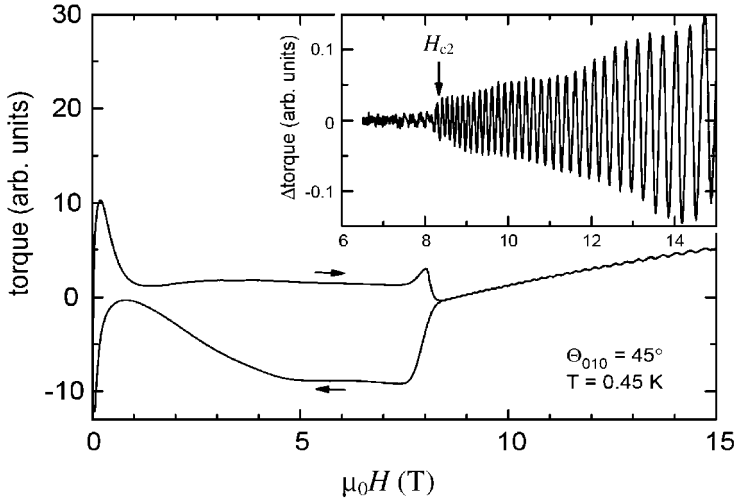


**FIGURE 23** de Haas–van Alphen effect in superconducting  $\text{YNi}_2\text{B}_2\text{C}$ . The field-dependent torque signal is observed at 0.45 K. The magnetic field is rotated  $45^\circ$  from [001] to [100], arrows indicate the field-sweep directions. In the inset, after background subtraction, dHvA oscillations can be seen more clearly (Ignatchik et al., 2005).

© 2005 Elsevier

Recent measurements and LDA–FPLO calculations performed by the groups of Wosnitzer and Rosner, respectively, (Bergk et al., 2007) showed such a large mass-enhancement anisotropy up to a factor of five for  $\text{YNi}_2\text{B}_2\text{C}$ .

In the following paragraphs, the discussion will be restricted to the behavior of the gap. An example for dHvA oscillations in  $\text{YNi}_2\text{B}_2\text{C}$  is shown in Figure 23; the peak seen in the increasing-field measurement at around 8 T will be discussed in Section 5.1.4.

Ignatchik et al. (2005) observed an abrupt damping of the oscillations below  $H_{c2}$  for any measured direction and concluded that gap nodes are unlikely but a strong anisotropy is possible. Terashima et al. (1997) found the damping to be much smaller than theoretically expected, and thus the gap in the corresponding sheet named  $\alpha$  is smaller than the gap on other Fermi surface parts, but noted that the  $\alpha$  part covers only small fraction of the whole Fermi surface. The damping factor for the measured frequency increases with the angle from [001] towards [110], which can be ascribed to a strongly anisotropic gap parameter, even of a single Fermi surface sheet (Bintley and Meeson, 2003). Noteworthy, similar discrepancies between theoretical isotropic single-band description and dHvA results in the superconducting state were also found for the well-known two-band superconductors  $\text{MgB}_2$  (Fletcher et al., 2004) and  $\text{NbSe}_2$  (Corcoran et al., 1994). One possible extension of the theory, including the peak-effect region was given by Maniv et al. (2006), who considered superconducting fluctuations. At high magnetic fields close to  $H_{c2}$  they obtained a large gap of 7.6 meV for a particular FS orbit on the FS, from analyzing the Dingle plot of the dHvA signal, which however is possi-

bly influenced by the peak effect. A band-structure calculation by Yamauchi et al. (2004) points to a saddle point singularity of the 17th band connected with larger electron–phonon coupling and a locally larger gap, which might cause a behavior similar to that expected for a gap-node function. Quantum oscillations were also found in the magnetostriction of  $\text{YNi}_2\text{B}_2\text{C}$  (Bud'ko et al., 2006a) consistent with dHvA data from magnetization.

To conclude the section on the gap symmetry, it is obvious that the situation remains quite intricate, but the d-wave pairing proposed in late nineties in connection with basal plane anisotropies of  $H_{c2}$  for  $\text{LuNi}_2\text{B}_2\text{C}$  and the field dependence of the specific heat in the superconducting state seems now to be quite unlikely. Most probably both, the (s + g)-wave approach to describe the field dependence of the thermal conductivity (as well as a huge gap anisotropy) and the earlier introduced isotropic two-band model set up to describe  $H_{c2}$  peculiarities, are too simple for a consistent description of the variety of the measured properties. Thus the general disadvantage of all these special models is that they were developed to explain certain experiments each of them probing *different subgroups of electrons* with large or small Fermi velocities, far away or close to the nesting regions, strongly or weakly coupled, etc.

Thus, a future improved general complex theory has to integrate all these different “snapshots” into a coherent picture where all these electrons and interactions will be treated on equal footing. It seems to be necessary to take into account the full multiband character and, furthermore, effects of additional anisotropy beyond the more or less anisotropic electron–phonon interaction. The itinerant-electron antiferromagnetic spin fluctuations related to the nesting of the Fermi surface and/or strongly anisotropic Coulomb scattering are possible candidates. These interactions being pair-breaking for an extended s-wave superconducting order parameter are probably not strong enough to cause unconventional superconductivity with an order parameter exhibiting real nodes as in the cuprate superconductors. The question about the presence of nodes has been one of the main points in the research on borocarbides during the last few years. An understanding of the superconducting gap in the non-magnetic  $\text{RNi}_2\text{B}_2\text{C}$  phases should be also helpful for the magnetic ones and vice versa. In particular, the suppression of superconductivity on most parts of the Fermi-surface pieces except a special one which shows nearly isotropic single-band superconductivity in  $\text{DyNi}_2\text{B}_2\text{C}$  and  $\text{HoNi}_2\text{B}_2\text{C}$  below  $T_N$  (where the magnetic structure is a simple commensurate antiferromagnetic type) is very instructive to understand the contributions of individual Fermi-surface pieces in the non-magnetic borocarbides (see Sections 4.8 and 4.9). Also, further theoretical studies and experimental data including the development of the superconducting properties in the presence of a small amount of magnetic lanthanide ions are required to elucidate which pairing state is realized in each of the borocarbides, which can be different for cases with different coexisting magnetic phases, depending on the specific lanthanide ion R. This includes additional methods such as the measurement of the Josephson effect as analyzed theoretically by Kolesnichenko and Shevchenko (2005). Moreover, significant information on the energy gaps and especially the contribution of electrons with small Fermi velocities is gained from the analysis of the upper critical field, e.g.,

for  $\text{YNi}_2\text{B}_2\text{C}$  (Shulga et al., 1998) and  $\text{HoNi}_2\text{B}_2\text{C}$  (Müller et al., 2007), as discussed in the following subsection and in Section 4.9.

### 3.6 The upper critical field

The upper critical field  $H_{c2}(T)$  as a fundamental quantity of type-II superconductors provides deep insight into (i) the coupling strength, (ii) the electronic structure, (iii) the symmetry and anisotropy of the order parameter, (iv) the presence of various disorder-related scattering processes, and, if magnetic lanthanide ions are present, into (v) effects of crystal fields and anisotropic exchange interaction. All these factors affect the magnitude, the shape and the anisotropy of  $H_{c2}(T)$ . Naturally, it is a difficult task to take all of them into account on equal footing within a consistent microscopic theory. In this respect borocarbide superconductors are complex systems, and quantitatively not yet well understood. However, due to the rich variety of possible isoelectronic chemical substitutions systematic investigations are possible and, as a consequence, much qualitative insight can be obtained.

The reported experimental data on the upper critical field  $H_{c2}$  of  $\text{YNi}_2\text{B}_2\text{C}$  and  $\text{LuNi}_2\text{B}_2\text{C}$  scatter considerably due to paramagnetic signals from impurities which are difficult to avoid in the nominally non-magnetic borocarbides (Mun et al., 1998). Nevertheless it has clearly been shown for both compounds that  $H_{c2}$  is anisotropic not only with respect to the tetragonal  $c$ -axis and the basal plane but also within that plane. The upper critical field has been determined from various measurements: of the magnetization (Xu et al., 1994; Metlushko et al., 1997) including those on randomly-oriented powder samples (Bud'ko et al., 2001b); of the electrical resistance of single crystals (Rathnayaka et al., 1997; Du Mar et al., 1998) and thin films (Grassano et al., 2001a; Häse et al., 2001a, 2001b; Wimbush et al., 2004b); of the magnetic quadrupole moment in a VSM (Jaiswal-Nagar et al., 2005); of the thermal conductivity (Cao et al., 2003); and of the specific heat (Huang et al., 2006), where the latter two studies do not provide information about the anisotropic behavior. An example of the  $H_{c2}$  anisotropy is shown in Figure 24. It is noteworthy that a finite slope for  $H_{c2}(T)$  as  $T \rightarrow 0$  was found for  $\text{LuNi}_2\text{B}_2\text{C}$ , see Schmiedeshoff et al. (2001). The out-of-plane anisotropy can be described within the phenomenological one-band GL theory of superconductivity (Ginzburg and Landau, 1950) or its microscopic derivation from the BCS theory (Gor'kov, 1959) by an effective mass anisotropy. In the case of  $\text{LuNi}_2\text{B}_2\text{C}$  the degree of the out-of-plane anisotropy of  $H_{c2}$  is nearly temperature independent and the resulting mass anisotropy,  $m_c^*/m_a^* \approx 1.35$ , is in good agreement with the Fermi surface anisotropy determined from band-structure calculations (Mattheiss, 1994).

On a phenomenological level the in-plane anisotropy of  $H_{c2}$  cannot be explained within the (local) GL theory. In principle, non-local extension introduced by Hohenberg and Werthamer (1967) might be helpful to overcome this difficulty. In this approach, which is valid for weak anisotropies, in addition to the second rank mass tensor, a fourth rank tensor is introduced. The non-local effects were predicted to be observable in sufficiently clean materials where the transport

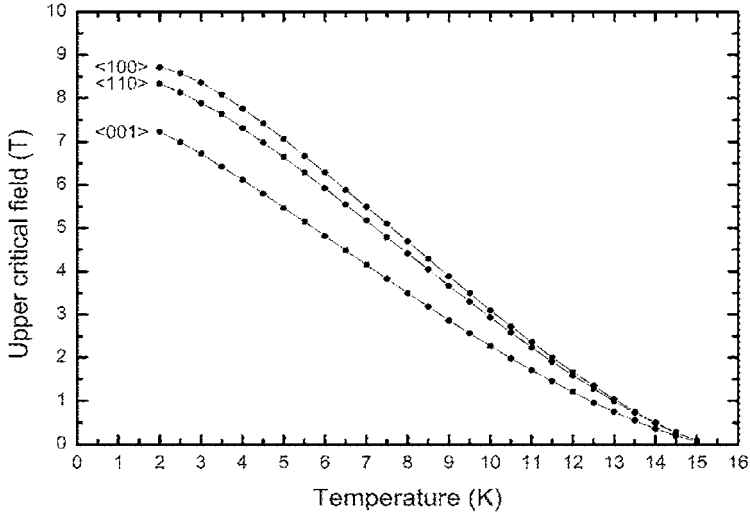


**FIGURE 24** The temperature dependence of the upper critical field of an  $\text{YNi}_2\text{B}_2\text{C}$  thin film, resistively measured in the principal crystallographic directions (from [Wimbush et al., 2004b](#)).

© 2004 Elsevier

mean free path  $l$  becomes larger than the coherence length  $\xi$ . Strictly speaking, the correct description of strongly anisotropic cases as the nested parts of the Fermi surface would require the introduction of a large number of higher order ranked tensors or a discrete description ([Maška and Mierzejewski, 2001](#)). Therefore, the frequently used simple non-local approaches mentioned below should be taken with some caution despite certain success they have in describing the physics of vortex lattices (see Section 5). At least the clear microscopic meaning of the effective quantities present in the weakly anisotropic case is lost in the strongly anisotropic one.

The non-local effects can result in an anisotropy of  $H_{c2}$  microscopically due to the anisotropy of the pairing state ([Shiraishi et al., 1999](#)) or directly to the anisotropy in the shape of the Fermi surface ([Metlushko et al., 1997](#)). The anisotropy of the Fermi surface sheets (see Section 3.2) has been assumed to cause the mentioned basal anisotropy of  $H_{c2}$  because the borocarbide superconductors are usually clean-limit type-II superconductors. In the clean limit for an anisotropic Fermi surface the non-local corrections to  $H_{c2}$  are given by

$$H_{c2}(T, \phi) = D[1 + (-3/2 + 0.34C)t + 0.34At \cos(4\phi)], \quad (5)$$

where  $t = 1 - T/T_c$ ,  $\phi$  is the angle in the basal plane, measured with respect to the tetragonal  $\mathbf{a}$ -axis,  $A$  and  $C$  contain averages of the Fermi velocity and can be estimated from electronic-structure calculations or taken, together with  $D$ , as fitting parameters ([Metlushko et al., 1997](#)). For  $\text{LuNi}_2\text{B}_2\text{C}$  these authors found  $C = 9.4$ ,  $A = 0.43$ , and excellent agreement of the experimentally determined dependence of  $H_{c2}$  on  $T$  and  $\phi$  using Eq. (5). Also the data of  $H_{c2}$  measured in  $c$  direction could very well be reproduced by the corresponding formula. A spe-

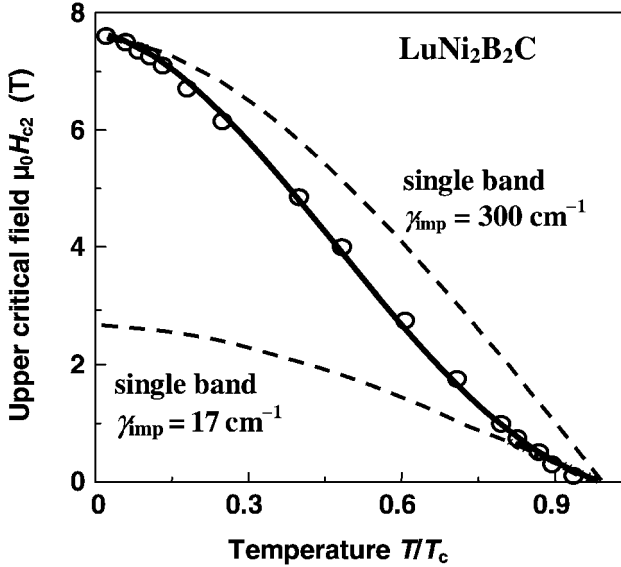


**FIGURE 25**  $H_{c2}(T)$  of a  $\text{LuNi}_2\text{B}_2\text{C}$  single crystal measured parallel to the tetragonal  $c$ -axis (circles). The solid curve was calculated using a two-band model (see text). Dashed lines: isotropic single-band (ISB) models with two values of  $\gamma_{\text{imp}}$  (see text; after Shulga et al., 1998).

cial feature of Eq. (5) is, for appropriate values of  $A$  and  $C$ , a positive curvature of the temperature dependence of  $H_{c2}$  near  $T_c$ , which does not occur in the standard BCS theory. Such an upward curvature has been observed in all crystal orientations, for both,  $\text{LuNi}_2\text{B}_2\text{C}$  and  $\text{YNi}_2\text{B}_2\text{C}$ . An example is shown in Figure 25. The anomalously curved shape of  $H_{c2}(T)$  as compared with the standard parabolic-like Werthamer–Helfand–Hohenberg (WHH) behavior is roughly characterized by three parameters, the two curvature exponents near  $T = 0$  and  $T = T_c$  and the inflection point in between. An empirically found simple expression (valid approximately at temperatures above the inflection point (Freudenberger et al., 1998a), which contains a single exponent  $\alpha$  only, is

$$H_{c2}(T) = H_{c2}^*(1 - T/T_c)^{1+\alpha}. \quad (6)$$

Usually  $H_{c2}^*$  does not exceed  $H_{c2}(0)$  by more than about 10 to 15%. Since experimentally it is somewhat inconvenient to perform measurements at very low temperatures and relatively high fields, high accuracies of extrapolations of  $H_{c2}(0)$  are impossible. For qualitative discussions  $H_{c2}(0)$  can often be replaced by  $H_{c2}^*$ , keeping in mind the uncertainty mentioned above.

It has been pointed out by Shulga et al. (1998) that the non-local approach leading to results as Eq. (5) does not cover all of the experimental results as, e.g., the fact that the reported anisotropy of  $H_{c2}$  of  $\text{YNi}_2\text{B}_2\text{C}$  is significantly smaller than that of  $\text{LuNi}_2\text{B}_2\text{C}$  but its positive curvature is even larger. Therefore these authors analyzed  $H_{c2}(T)$  within the microscopic Eliashberg theory of superconductivity (Eliashberg, 1960). First they tried to explain the experimen-

tal data on  $H_{c2}(T)$  taking into account only an isotropic single-band (ISB) effective electronic structure. The standard ISB approach (Carbotte, 1990) describes quantitatively the renormalization of the physical properties of metallic systems due to electron–phonon (el–ph) interaction. The input parameters are the density of states  $N(E_F)$ , the Fermi velocity  $v_F$ , the impurity scattering rate  $\gamma_{\text{imp}}$ , the Coulomb pseudopotential  $\mu^*$ , and the spectral function  $\alpha(\omega)^2F(\omega)$  of the el–ph interaction. These parameters can be determined from experimental data of the normal-state low-temperature electronic specific heat, the plasma frequency (from optical conductivity),  $H_{c2}(0)$ ,  $T_c$  and its isotope exponent  $\alpha_I$ , and the low- $T$  resistivity  $\rho(0)$  or the Dingle temperature  $T_D$  (from de Haas–van Alphen experiments). The el–ph coupling constant has been estimated to be  $\lambda_{\text{ph}} \approx 0.7$  using  $\lambda_{\text{ph}} = 2 \int d\omega \alpha(\omega)^2 F(\omega) / \omega$ , which indicates an intermediate coupling regime where  $H_{c2}(T)$  should be insensitive to details of  $\alpha(\omega)^2 F(\omega)$ . It was found that the ISB approach cannot reproduce the experimental  $H_{c2}(T)$  data of  $\text{LuNi}_2\text{B}_2\text{C}$  and  $\text{YNi}_2\text{B}_2\text{C}$ . In the example of Figure 25, not only is the positive curvature absent in the ISB results but, even more importantly, also the value  $H_{c2}(0)$  can only be achieved for the unrealistically high scattering rate  $\gamma_{\text{imp}} = 300 \text{ cm}^{-1}$  whereas realistic values  $\gamma_{\text{imp}} \leq 17 \text{ cm}^{-1}$  result in a too low ISB value of  $H_{c2}(0)$ . It should be noted that for weakly or moderately anisotropic systems in the clean limit, as is the situation for the non-magnetic borocarbides under consideration, the evaluation of a quantity  $Q \sim H_{c2}(0) \langle v_F^2 \rangle_{\text{FS}} / (1 + \lambda_{\text{ph}})^2 T_c^2$  (with  $\langle v_F^2 \rangle_{\text{FS}}$  as the Fermi velocity averaged over the whole Fermi surface) is helpful to classify them as pronounced multiband superconductors (for details see Shulga and Drechsler, 2001; Fuchs et al., 2002a). Superconductors with  $Q \approx 1$  can be described by the isotropic single-band model, e.g., Nb with  $Q \approx 1.4$ . If the value of  $Q$  departs significantly from 1, a multiband or unconventional description is required. For  $\text{YNi}_2\text{B}_2\text{C}$  a value  $Q \approx 4$  is obtained confirming the above mentioned discrepancies between the experimental  $H_{c2}(T)$  data and the standard ISB approach. Thus Shulga et al. (1998) extended their calculation considering two bands in the Eliashberg analysis where one of the two Fermi velocities,  $v_{F1}$ , is considerably smaller than the Fermi-surface average of  $v_F$ . These slow electrons have a strong el–ph coupling and are mainly responsible for the superconductivity. It is noteworthy that the slow electrons in  $\text{LuNi}_2\text{B}_2\text{C}$  and  $\text{YNi}_2\text{B}_2\text{C}$  stem from nested regions on the Fermi surface, whereas in the non-superconducting compound  $\text{LaNi}_2\text{B}_2\text{C}$  there is no nesting and, consequently, a smaller dispersion of  $v_F$  (Rosner et al., 2001).

The two-band description of  $H_{c2}$  has been confirmed by subsequent theoretical studies (Drechsler et al., 2001c; Askerzade, 2003a, 2003b; Nicol and Carbotte, 2005) that are also extended on further thermodynamic properties. A similar approach using an anisotropic electron–phonon interaction spectral function (Manalo and Schachinger, 2001) also leads to good agreement with the experimental data.

The dispersion of  $v_F$  in  $\text{YNi}_2\text{B}_2\text{C}$  has been confirmed by de Haas–van Alphen experiments (Goll et al., 1996). The values of  $H_{c2}(0)$  and  $T_c$  are reduced by the presence of the fast electrons that have only a moderate el–ph coupling. On the other hand, the positive curvature of  $H_{c2}(T)$  is caused by interband coupling between the slow and the fast electrons. In the example of Figure 25 the experimental

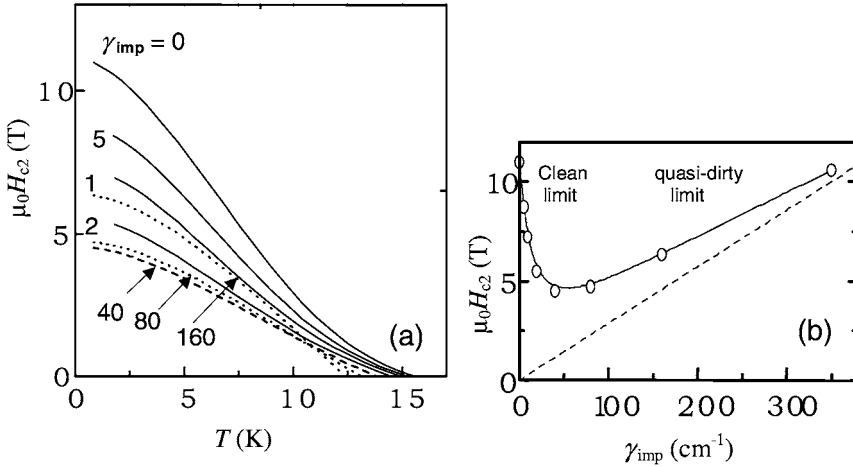


**FIGURE 26** (a) The temperature dependence of the upper critical field of LuNi<sub>2</sub>B<sub>2</sub>C calculated within a two-band model for several impurity-scattering rates  $\gamma_{\text{imp}}$  (cm<sup>-1</sup>). (b) The calculated  $H_{c2}(0)$ -vs.- $\gamma_{\text{imp}}$  curve illustrating the transition from the clean to the dirty limit. Dashed line:  $H_{c2}(0)$ - $\gamma_{\text{imp}}$  dependence in the dirty limit (Drechsler et al., 2000; see also Fuchs et al., 2001).

© 2000 Elsevier

$H_{c2}(T)$  curve can be well reproduced by taking the velocity ratio  $v_{F2}/v_{F1} \approx 4.5$  and adjusting the other input parameters of the two-band model to experimental data from the literature. Figure 26 shows that, within the two-band model, both, the value  $H_{c2}(0)$  and the degree of positive curvature, can be considerably varied by changing the scattering rate  $\gamma_{\text{imp}}$  (Shulga and Drechsler, 2001; Fuchs et al., 2001; Gurevich, 2003). As expected, in the clean limit  $H_{c2}$  decreases with increasing interband scattering  $\gamma_{\text{imp}}$ . This prediction has been experimentally confirmed for pseudoquaternary (Lu,Y)Ni<sub>2</sub>B<sub>2</sub>C compounds where an increase of substitutional disorder results in a decrease of  $H_{c2}(T)$  (see Section 6.2 and Fuchs et al., 2001). On the other hand, for large values of  $\gamma_{\text{imp}}$  (quasi-dirty limit)  $H_{c2}$  is predicted to increase with increasing  $\gamma_{\text{imp}}$ . Consequently  $H_{c2}$  has a minimum at a certain value of  $\gamma_{\text{imp}}$  if the other input parameters of the two-band model are kept constant (see Figure 26(b)).

The description of the upper critical field by the two-band model holds also for applied hydrostatic pressure (Suderow et al., 2004; see Figure 27).  $H_{c2}$  dramatically decreases under pressure (see also Oomi et al., 2003a and references cited therein as well as Section 3.7 for ErNi<sub>2</sub>B<sub>2</sub>C and TmNi<sub>2</sub>B<sub>2</sub>C). Furthermore, its positive curvature is weakened with increasing pressure pointing to a decreasing weight of the strongly-coupled subgroup of electrons by the enhancement of their Fermi velocities and the reduction of their individual coupling strength (Suderow et al., 2004), and/or an enhancement of the destructive interband scattering.

Similar effects have been obtained for the substitution of non-magnetic ions by magnetic ones. This concerns the strongly reduced  $H_{c2}$  due to magnetic pair breaking (see, e.g., Takeya and El Massalami, 2004) and, additionally, the decreased positive curvature (Lan et al., 2000, 2001; Rathnayaka et al., 2003; see also

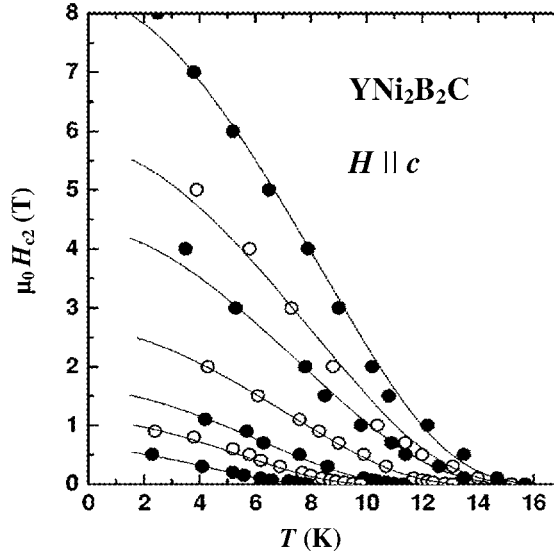


**FIGURE 27** The temperature dependence of the upper critical field of  $\text{YNi}_2\text{B}_2\text{C}$  measured by susceptibility with applied field parallel to  $c$  at ambient pressure, 2.3, 3.3, 5.4, 7.6, 9.0, and 11.7 GPa (from top to bottom). The solid lines correspond to two-band fits (after Suderow et al., 2004).

Ovchinnikov and Kresin, 2000 for a Green's functions approach to magnetic scattering in borocarbides). Due to the complex interplay between superconductivity and magnetism, the upper critical field of  $\text{RNi}_2\text{B}_2\text{C}$  with magnetic R ions will be discussed in Section 4 together with the specific localized-moment magnetic order in these compounds.

Concerning the interpretation of the anisotropy of  $H_{c2}$ , it should be noted that the large in-plane anisotropy reported by Metlushko et al. (1997) is correlated with the direction of the nesting vector (0.55, 0, 0). Another manifestation of strong local anisotropy effects is provided by deviations from the angular dependence due to anisotropic effective masses (Fermi velocities)

$$H_{c2}(\theta) = H_{c2}^{\text{ab}} (\sin^2 \theta + \gamma_m^2 \cos^2 \theta)^{-1/2}, \quad (7)$$

where  $\gamma_m^2 = m_c/m_{\text{ab}}$  and  $\theta$  measures the angle between the magnetic field and the tetragonal  $c$ -axis (see, e.g., Tinkham, 1994). Due to the interaction with the nearly isotropic weakly coupled electrons the strong anisotropy of the nested parts of the Fermi surface is washed out.

A positive curvature of  $H_{c2}(T)$  has been observed for a number of superconductors during recent years. In the exemplary case of  $\text{MgB}_2$ , this property was observed by Müller et al. (2001b) and Bud'ko et al. (2001a) and, in the former report, attributed to a two-band model supported by theoretical investigations (Shulga et al., 2001). This characterization has been further established through, e.g., specific-heat studies (Y. Wang et al., 2001) and is now well accepted. Also  $2\text{H-NbSe}_2$  (Suderow et al., 2005) and  $\text{ZrB}_{12}$  (Gasparov et al., 2006) have been described

as fully-gapped two-band superconductors. For the presumably unconventional superconductor  $\text{PrOs}_4\text{Sb}_{12}$ , a two-band model has been found applicable to  $H_{c2}(T)$  in the measured range  $T/T_c > 0.3$  (Measson et al., 2004).

### 3.7 Effects of pressure

There is no doubt that the zero-pressure equilibrium crystal structure of a material, including the values of its lattice constants, is governed by the electronic interaction between the involved atoms. However, there is no complete description of this mechanism and various auxiliary concepts have been introduced to explain the cohesion of atoms in the different types of solids, as, e.g., metallic bonding, ionic bonding, covalence, etc. Conversely, (even small) changes in the lattice structure, caused by application of uniaxial or isotropic (i.e. hydrostatic) pressure, have a strong influence on the electronic properties. Therefore studying the effects of pressure on superconducting and magnetic properties of  $\text{RNi}_2\text{B}_2\text{C}$  can help testing and improving the concepts presented in Sections 3 and 4.

The first results on the influence of hydrostatic pressure  $P$  on  $T_c$  of  $\text{RNi}_2\text{B}_2\text{C}$  ( $R = \text{Y, Lu, Tm, Er}$  and  $\text{Ho}$ ) were reported by Schmidt and Braun (1994). The results on the influence of  $P$  on  $T_c$  in non-magnetic borocarbides are contradictory. For example, Schmidt and Braun (1994) found that  $T_c(P)$  of  $\text{YNi}_2\text{B}_2\text{C}$  decreases linearly with pressure at rates of  $-0.058$  K/GPa. This is in agreement with the results of Murayama et al. (1994) and Looney et al. (1995), but is in contradiction with the data of Alleno et al. (1995b) who found a  $T_c(P)$  dependence with positive initial slope of  $+0.03$  K/GPa and with a maximum centered at  $P \approx 0.52$  GPa. These observations indicate that even the sign of the pressure dependence of  $T_c$  depends on the microstructure of the samples (Alleno et al., 1995b). Strongly scattering  $dT_c/dP$  values have been found also for  $\text{LuNi}_2\text{B}_2\text{C}$  with values of  $+0.188$  K/GPa (Schmidt and Braun, 1994) and  $-0.05$  K/GPa (Gao et al., 1994), whereas Murayama et al. (1994) observed a maximum in  $T_c(P)$  at  $P \approx 0.5$  GPa. A fast decrease of  $T_c$  with increasing pressure of  $-0.9$  K/GPa has been reported for  $\text{YPd}_2\text{B}_2\text{C}$ , which was explained by a dominating pressure-induced lattice stiffening rather than the shift in the electronic density of states (Murdoch et al., 1999; see also Murayama et al., 1994). This might also be connected with the metastability of this phase (see Section 2.4). Contrary to the behavior of  $T_c$ , the magnetic ordering temperature  $T_N$  has found to increase with increasing pressure for all  $\text{RNi}_2\text{B}_2\text{C}$  compounds investigated so far, i.e. for  $R = \text{Gd}$  (Bud'ko et al., 1996),  $\text{Ho}$  (Carter et al., 1995b; Uwatoko et al., 1996; Dertinger, 2001) and  $\text{Er}$  (Matsuda et al., 2000).

The effect of hydrostatic pressure on the interplay between superconductivity and magnetism in borocarbides has been discussed for  $R = \text{Tm}$  (Oomi et al., 1999),  $\text{Er}$  (Matsuda et al., 2000),  $\text{Ho}$  (Uwatoko et al., 1996; Carter et al., 1995b; Oomi et al., 2001; Dertinger, 2001; Jo et al., 2003; Akiyama et al., 2006; Section 4.9) and  $\text{Dy}$  (Falconi et al., 2002; Section 4.8). A much stronger suppression of the upper critical field  $H_{c2}$  under high pressure has been observed for  $\text{ErNi}_2\text{B}_2\text{C}$  and  $\text{TmNi}_2\text{B}_2\text{C}$ , compared to the  $\text{RNi}_2\text{B}_2\text{C}$  compounds with a non-magnetic  $R$ . The pressure dependence of  $H_{c2}$  in  $\text{YNi}_2\text{B}_2\text{C}$  (Suderow et al., 2004; Section 3.6) and of  $\text{Ho}_{1-x}\text{Dy}_x\text{Ni}_2\text{B}_2\text{C}$  (Choi et al., 2002; Kim et al., 2003; Section 6.5) supports the

scenario of multiband superconductivity. Also the puzzling  $dT_c/dP$  values for different  $RNi_2B_2C$  might be explained by a multiband approach as will be discussed in Section 4.8.

The pressure-dependent electrical resistivity of the heavy-fermion compound  $YbNi_2B_2C$  (see also Section 4.12) could be explained by competing contributions from crystal-electric-field splitting and Kondo effect (Oomi et al., 2006). The pressure-dependent room-temperature thermoelectric power of  $YNi_2B_2C$  exhibits a peak around 2 GPa, which was explained by changes in the Fermi-surface topology (Meenakshi et al., 1998). A possible correlation with a small peak in the temperature-dependent thermopower around 200 K (Fisher et al., 1995; Section 3.4.3) needs further investigation.

High-pressure studies on  $YNi_2B_2C$  at room temperature do not indicate any structural transition up to  $P = 16$  GPa (Meenakshi et al., 1996, 1998). The bulk modulus was found to be 200 GPa, and estimated to be 270 GPa or 208 GPa from calculations based on the TB-LMTO method (Meenakshi et al., 1996) and the FP-LMTO method (Cappannini et al., 1998), respectively. A similar value of 210 GPa has been obtained by Weht et al. (1996) for  $LuNi_2B_2C$  within the local-density approximation. For  $HoNi_2B_2C$ , a bulk modulus of 192 GPa has been measured by Oomi et al. (2003b; see also 2002), whereas Jaenicke-Rössler et al. (1998) have found a value of 130 GPa for  $TbNi_2B_2C$  at low pressure. Dertinger (2001) reports on a strong influence of the sample perfection (see Section 3.1) on the bulk modulus.

These effects of hydrostatic pressure can be related to and compared with the influence of uniaxial pressure  $P_u$  or substitution-induced internal strain (caused by so-called chemical pressure; Section 6.2). For the latter case, Sánchez et al. (2000) conclude from results on  $Y_{1-x}La_xNi_2B_2C$  that in  $YNi_2B_2C$  the positive in-plane pressure derivatives of  $T_c$  are accompanied by negative  $c$ -axis values. In contrast, reverse signs of the uniaxial pressure dependencies are derived from thermal-expansion measurements using thermodynamic relations (Bud'ko et al., 2006a). Direct investigations using uniaxial pressure are nearly completely missing. One study on  $YNi_2B_2C$  and  $HoNi_2B_2C$  shows a very weak in-plane  $dT_c/dP_u$  (Kobayashi et al., 2006). Beside the uniaxial-pressure dependence of  $T_c$ , the thermal expansion provides information about changes in the lattice constants as a function of temperature or magnetic field (magnetostriction; for a review, see Doerr et al., 2005; for recent thermal-expansion studies, see Bud'ko et al., 2006a, 2006b; Cura et al., 2004; Ma, Schneider et al., 2007). Thus, comparing results on the effects of pressure, temperature and magnetic field should enable additional insight not only into the behavior of the lattice structure, but also into the electronic properties.

### 3.8 Superconducting-state characteristics of $YNi_2B_2C$ and $LuNi_2B_2C$

Section 3 will close with a short summary of the important properties and parameters of the superconducting state of  $YNi_2B_2C$  and  $LuNi_2B_2C$  (see Table 6), including additional references to those cited in the previous subsections, but without an attempt of completeness. These best-studied non-magnetic borocarbides are type-II superconductors (as discovered by Schubnikow et al., 1936) in

**TABLE 6** Properties of  $\text{YNi}_2\text{B}_2\text{C}$  and  $\text{LuNi}_2\text{B}_2\text{C}$ .  $T_c$ —superconducting transition temperature,  $H_{c2}$ —upper critical field at  $T = 0$ ,  $H_{c1}$ —lower critical field at  $T = 0$ ,  $H_c$ —thermodynamical critical field at  $T = 0$ ,  $\xi(0)$ —coherence length at  $T = 0$ ,  $\lambda(0)$ —penetration depth at  $T = 0$ ,  $\kappa_{\text{GL}}(0)$ —Ginzburg–Landau parameter at  $T = 0$ ,  $\Delta C_p$ —specific heat jump at  $T_c$ ,  $\gamma_N$ —normal-state Sommerfeld constant,  $N(E_F)$ —density of states at the Fermi level in states per eV and unit cell,  $v_F$ —Fermi velocity,  $\lambda_{\text{ph}}$ —electron–phonon coupling constant,  $\mu^*$ —Coulomb pseudopotential,  $\theta_D$ —Debye temperature,  $\Delta(0)$ —quasiparticle energy gap at  $T = 0$ ,  $l$ —mean free path, RRR—residual resistivity ratio  $\rho(300\text{ K})/\rho(T \approx T_c)$ ,  $T_D$ —Dingle temperature. Ranges for the values of properties due to its multiband character are indicated by “..” whereas scattering experimental results are separated by a comma

Property	$\text{YNi}_2\text{B}_2\text{C}$	$\text{LuNi}_2\text{B}_2\text{C}$	Property	$\text{YNi}_2\text{B}_2\text{C}$	$\text{LuNi}_2\text{B}_2\text{C}$
$T_c$ (K)	15.5 <sup>1</sup>	16.5 <sup>1</sup>	$N(E_F)$ (1/eV)	4.31 <sup>13</sup>	4.05 <sup>13</sup>
$\mu_0 H_{c2}$ (T)	11 <sup>2</sup>	9 <sup>7</sup> , 12.1 <sup>10</sup>	$v_F$ ( $10^5$ m/s)	0.85..3.8 <sup>2</sup> , 4.2 <sup>8</sup>	0.96..3.7 <sup>2</sup> , 4.2 <sup>8</sup>
$\mu_0 H_{c1}$ (mT)	30 <sup>3</sup> , 8 <sup>4</sup>	30 <sup>3</sup> , 80 <sup>7</sup>	$\lambda_{\text{ph}}$	0.9 <sup>3</sup> , 1.02 <sup>11</sup>	0.75 <sup>3</sup> , 1.22 <sup>11</sup>
$\mu_0 H_c$ (T)	0.23 <sup>3</sup> , 0.26 <sup>5</sup>	0.31 <sup>3</sup> , 0.54 <sup>7</sup>	$\mu^*$	$\approx 0.1^2$ , 0.13 <sup>11</sup>	$\approx 0.1^2$ , 0.13 <sup>11</sup>
$\xi(0)$ (nm)	8 <sup>6</sup> , 10 <sup>4</sup> , 5.5 <sup>8</sup>	6 <sup>6,7</sup>	$\theta_D$ (K)	490 <sup>3</sup>	360 <sup>3</sup>
$\lambda(0)$ (nm)	120 <sup>6</sup> , 350 <sup>4</sup>	130 <sup>6</sup> , 71 <sup>7</sup>	$\Delta(0)$ (meV)	2.2 <sup>9</sup> , 1.5..3.1 <sup>14</sup>	2.2 <sup>9</sup> , 1.9..3.0 <sup>17</sup>
$\kappa_{\text{GL}}(0)$	15 <sup>6</sup> , 35 <sup>4</sup>	22 <sup>6</sup> , 12 <sup>7</sup>	$\Delta(0)/k_B T_c$	2.1 <sup>3</sup> , 1.7 <sup>9</sup>	2.2 <sup>3</sup> , 1.7 <sup>9</sup>
$\Delta C_p$ (mJ/(mol K))	460 <sup>3</sup>	695 <sup>3</sup>	$l$ (nm)	33 <sup>12</sup>	70 <sup>7</sup> , 29 <sup>12</sup>
$\gamma_N$ (mJ/(mol K <sup>2</sup> ))	18.5 <sup>3</sup>	19.5 <sup>3</sup> , 35 <sup>7</sup>	RRR	48 <sup>16</sup> , 63 <sup>18</sup>	27 <sup>2</sup> , 44 <sup>15</sup>
$\Delta C_p/\gamma_N T_c$	1.77 <sup>3</sup>	2.21 <sup>3</sup>	$T_D$ (K)	2.8 <sup>2</sup> , 0.6..2.2 <sup>14</sup>	4 <sup>2</sup>

<sup>1</sup> Cava et al., 1994b. <sup>2</sup> Shulga et al., 1998. <sup>3</sup> Michor et al., 1995. <sup>4</sup> Prozorov et al., 1994. <sup>5</sup> K.-J. Song et al., 2003. <sup>6</sup> Hilscher and Michor, 1999. <sup>7</sup> Takagi et al., 1994. <sup>8</sup> Heinecke and Winzer, 1995. <sup>9</sup> Ekino et al., 1996. <sup>10</sup> Schmiedeshoff et al., 2001. <sup>11</sup> Manalo et al., 2001. <sup>12</sup> Du Mar et al., 1998. <sup>13</sup> Diviš et al., 2000. <sup>14</sup> Bintley and Meeson, 2003; see text. <sup>15</sup> Fuchs et al., 2004. <sup>16</sup> Souptel et al., 2005a. <sup>17</sup> Bobrov et al., 2006. <sup>18</sup> Bud’ko et al., 2006a.

the clean limit. Substitutions on the rare-earth or the transition-metal site, however, can reduce both, the residual resistivity ratio and the normal-state electronic mean free path, due to disorder, thus moving the systems towards dirty-limit superconductivity (see Section 6). The three-dimensional globally isotropic electronic structure of  $\text{YNi}_2\text{B}_2\text{C}$  and  $\text{LuNi}_2\text{B}_2\text{C}$  is accompanied by a strong dispersion in the Fermi velocity caused by the complicated shape of the Fermi surface. The resulting positive curvature in the temperature dependence of the upper critical field near  $T_c$  can be explained phenomenologically by non-local corrections to the standard theories of London, Ginzburg, Landau and Abrikosov. On the microscopic level, the description of  $H_{c2}(T)$  requires a multiband (at least with two bands) electronic structure with different values of the Fermi velocity and the electron–phonon coupling constant as analyzed in the framework of the Eliashberg theory (Shulga et al., 1998; see Section 3.6). The anisotropic Fermi surface leads to anisotropy in  $H_{c2}(T)$ , in  $\xi(0)$  and, in particular, also in  $\Delta(0)$  as understood within the two-band model. Whereas maximum values for  $H_{c2}(0)$  and  $\xi(0)$  reported in the literature are given in Table 6, ranges of values are listed for  $v_F$ ,  $\Delta(0)$ , and  $T_D$ . In the case of  $\text{YNi}_2\text{B}_2\text{C}$ , the value for the energy gap given in Table 6 as derived from de Haas–van Alphen

measurements was confirmed by point-contact spectroscopy ( $\Delta(0) = 1.5\text{--}2.4$  meV; Bashlakov et al., 2005) but smaller gap values were obtained from the spectroscopic study by Mukhopadhyay et al. (2005) ( $\Delta(0) = 0.4\text{--}2.2$  meV).

The values of the BCS ratios  $\Delta C_p/\gamma T_c$  and  $\Delta(0)/k_B T_c$  and those of  $\lambda_{ph}$  indicate moderate electron–phonon coupling. However the Eliashberg analysis by Shulga et al. (1998, 2001) showed that this statement has to be modified as the different groups of electrons have different strengths of coupling: strong, intermediate and weak where the strongly coupled (near the nested regions of the Fermi surface) electrons are mainly responsible for superconductivity but the properties of the superconducting state are considerably affected by interaction of those strongly coupled with moderately coupled electrons (interband coupling). Thus, the interpretation of experimental results for  $YNi_2B_2C$  and  $LuNi_2B_2C$  needs more care than for the much simpler two-band systems such as  $MgB_2$ . The energy gap of these non-magnetic borocarbides is not yet fully understood. Seemingly, the influence of at least two different groups of electrons and also that of anisotropy within these bands has to be considered (see Section 3.5). Whether the gap is strongly anisotropic (without zeros in  $\mathbf{k}$  space) or has point nodes is one of the presently most controversial discussed issues in the field of borocarbide superconductivity. Thus, additional results also from different experimental techniques are highly desirable.

#### 4. MAGNETIC AND SUPERCONDUCTING PROPERTIES OF $RNi_2B_2C$ WITH $R = Ce$ TO $Yb$

In this section,  $RNi_2B_2C$  compounds will be considered where  $R$  are 4f elements with an incompletely filled f shell, which are sometimes called magnetic R elements because in these cases the  $R^{3+}$  ion carries a magnetic moment.  $EuNi_2B_2C$  does not exist and  $PmNi_2B_2C$  has not been investigated because Pm has no stable isotope (largest half-life is  $\approx 15$  years). From Figure 6 it can be clearly seen that the 4f electrons must have a considerable influence on the superconductivity in  $RNi_2B_2C$  because, for spacings in the crystal structure, which are comparable to those for non-magnetic R elements, the transition temperature  $T_c$  of  $RNi_2B_2C$  with magnetic R elements is considerably smaller or the superconductivity is even completely suppressed. The calculated density of states  $N(E_F)$  of  $RNi_2B_2C$  superconductors has nearly the same values for magnetic R elements (see Table 7) as for non-magnetic R elements (Diviš et al., 2000).

In order to investigate the 4f-electron magnetism in these compounds various measurements have been performed such as elastic (Skanthakumar and Lynn, 1999) and inelastic (Gasser et al., 1997) neutron scattering, muon-spin relaxation (Le et al., 1997), Mössbauer effect (Felner, 2001), X-ray resonant exchange scattering (Detlefs et al., 1997b), magnetization and magnetic susceptibility (Cho, 1998), resistivity and magnetoresistance (Fisher et al., 1997), specific heat (Hilscher and Michor, 1999), etc., where only one representative reference is given in each case. Results of such experiments are summarized in Figures 5, 6 and in Table 7. All  $RNi_2B_2C$  compounds which contain magnetic  $R^{3+}$  ions, with the exception

**TABLE 7** Type of the ground state of  $\text{RNi}_2\text{B}_2\text{C}$  compounds: SC—superconducting, AFM—commensurate antiferromagnetic order, SDW—incommensurate antiferromagnetic order (spin density wave), WFM—weak ferromagnetism;  $T_{\text{N}}$ —magnetic ordering temperature,  $T_{\text{c}}$ —superconducting transition temperature, and  $N(E_{\text{F}})$ —density of states at the Fermi level

Compound	Ground state	$T_{\text{N}}$ (K)	$T_{\text{c}}$ (K)	$N(E_{\text{F}})$
CeNi <sub>2</sub> B <sub>2</sub> C	Mixed valence <sup>16,17</sup> (SC <sup>1</sup> )	–	(0.1 <sup>1</sup> (?))	2.4 <sup>32</sup>
PrNi <sub>2</sub> B <sub>2</sub> C	AFM <sup>7</sup>	4.0 <sup>7</sup>	–	2.00 <sup>20</sup>
NdNi <sub>2</sub> B <sub>2</sub> C	AFM <sup>7,24</sup>	4.8 <sup>25</sup>	–	2.10 <sup>20</sup>
SmNi <sub>2</sub> B <sub>2</sub> C	AFM <sup>24</sup>	9.8 <sup>31,33</sup>	–	2.97 <sup>20</sup>
GdNi <sub>2</sub> B <sub>2</sub> C	SDW <sup>26</sup>	19.4 <sup>16,25,26,30</sup>	–	3.57 <sup>20</sup>
TbNi <sub>2</sub> B <sub>2</sub> C	SDW <sup>7,14</sup> /WFM <sup>14,19</sup>	15.0 <sup>7,14</sup>	–	4.11 <sup>20</sup>
DyNi <sub>2</sub> B <sub>2</sub> C	AFM <sup>2,6,7</sup> /SC <sup>2,3</sup>	11.0 <sup>2,6</sup>	6.2 <sup>2</sup> , 6.4 <sup>3</sup>	4.16 <sup>20</sup>
HoNi <sub>2</sub> B <sub>2</sub> C	AFM <sup>8,9</sup> /SC <sup>4,5</sup>	5...8 <sup>8,9,10</sup>	8.8 <sup>34</sup> , 7.5 <sup>5</sup>	4.04 <sup>20</sup>
ErNi <sub>2</sub> B <sub>2</sub> C	SDW <sup>11,12</sup> (WFM <sup>21,22</sup> ) /SC <sup>4,5</sup>	6 <sup>27</sup> ...6.8 <sup>11,12</sup>	10.5 <sup>4,5,27</sup>	4.32 <sup>20</sup>
TmNi <sub>2</sub> B <sub>2</sub> C	SDW <sup>7,18,29</sup> /SC <sup>4,5</sup>	1.5 <sup>28,13,7</sup>	11 <sup>4,5</sup>	4.02 <sup>20</sup>
YbNi <sub>2</sub> B <sub>2</sub> C	Heavy fermion <sup>23,15</sup>	–	–	–

<sup>1</sup> El Massalami et al., 1998a. <sup>2</sup> Cho et al., 1995a. <sup>3</sup> Tomy et al., 1995. <sup>4</sup> Cava et al., 1994b. <sup>5</sup> Eisaki et al., 1994. <sup>6</sup> Dervenagas et al., 1995a. <sup>7</sup> Lynn et al., 1997. <sup>8</sup> Grigereit et al., 1994. <sup>9</sup> Goldman et al., 1994. <sup>10</sup> Canfield et al., 1994. <sup>11</sup> Sinha et al., 1995. <sup>12</sup> Zarestky et al., 1995. <sup>13</sup> Cho et al., 1995b. <sup>14</sup> Dervenagas et al., 1996. <sup>15</sup> Yatskar et al., 1996. <sup>16</sup> Gupta et al., 1995. <sup>17</sup> Alleno et al., 1995a. <sup>18</sup> Chang et al., 1996b. <sup>19</sup> Cho et al., 1996a. <sup>20</sup> Diviš et al., 2000. <sup>21</sup> Canfield et al., 1996. <sup>22</sup> Kawano et al., 1999. <sup>23</sup> Dhar et al., 1996. <sup>24</sup> Detlefs et al., 1997b. <sup>25</sup> Nagarajan et al., 1995. <sup>26</sup> Detlefs et al., 1996. <sup>27</sup> Cho et al., 1995c. <sup>28</sup> Movshovich et al., 1994. <sup>29</sup> Sternlieb et al., 1997. <sup>30</sup> El Massalami et al., 1995c. <sup>31</sup> Prassides et al., 1995. <sup>32</sup> Diviš, 2001. <sup>33</sup> Hossain et al., 1995. <sup>34</sup> Rathnayaka et al., 1996.

of  $R = \text{Yb}$ , show antiferromagnetic (AFM) ordering in the temperature range  $1.5 \text{ K} < T < 20 \text{ K}$ . The relatively large values of the magnetic ordering temperature  $T_{\text{N}}$  and its approximate scaling with the de Gennes factor point to a strong interaction between the  $R$  magnetic moments which is clearly dominated by RKKY-type exchange rather than by dipolar interaction. Also crystalline electric fields have only minor effects on the magnetic ordering temperature in  $\text{RNi}_2\text{B}_2\text{C}$  compounds (Sok and Cho, 2005). Details of the AFM structure, in particular the local direction of the  $R$  magnetic moments, are the result of a competition between the exchange interaction and crystalline electric fields (which will be discussed in Section 4.1). In the cases  $R = \text{Tb}$  and  $\text{Er}$  weak ferromagnetism has been observed, i.e. a small net magnetic moment in addition to the main antiferromagnetic structure (see Sections 4.7 and 4.10). In other cases (e.g.,  $R = \text{Ho}$ , see Section 4.9), besides the ground-state magnetic structure other magnetic structures occur at elevated temperatures. The exchange interaction between the  $4f$  electrons and the conduction electrons in  $\text{RNi}_2\text{B}_2\text{C}$  seems not to induce  $\text{Ni}$  magnetic moments, i.e. as in the case of non-magnetic  $R$ -elements, no  $\text{Ni}$  magnetic moments have been detected in these compounds so far (Skanthakumar and Lynn, 1999).

As an interesting result (Baggio-Saitovitch et al., 2001, 2002b; D.R. Sánchez et al., 2005b) the quadrupole splitting  $\Delta E_{\text{Q}}$  observed by Mössbauer spectroscopy on the  $\text{Ni}$  site (diluted by <sup>57</sup>Fe) is strongly correlated with the  $\text{B-Ni-B}$  bonding angle which had been supposed to have a strong influence on the superconducting tran-

sition temperature  $T_c$  via the coupling to high-frequency phonons connected with boron (Mattheiss et al., 1994). However, as the result of the majority of investigations, now the role of these phonons is regarded as less important (see Section 3). Although the electronic structure, superconductivity and magnetism in  $\text{RNi}_2\text{B}_2\text{C}$  are three-dimensional phenomena, different types of large anisotropy have been reported. Thus the isomer shift in  $\text{DyNi}_2\text{B}_2\text{C}$  is significantly smaller than in metallic Dy or  $\text{DyM}_2\text{Si}_2$  (J.P. Sanchez et al., 1996), which has been assigned to relatively strong covalent bonds between the R and C atoms. A strong anisotropy concerning the dependence of the exchange interaction between the R magnetic moments on their *position* in the crystal structure has been reported by Cho et al. (1996b) who derived, from magnetization data, a ratio of the exchange constants between Ho magnetic moments in  $\text{HoNi}_2\text{B}_2\text{C}$  for the line connecting the two Ho atoms being parallel and perpendicular to the tetragonal *c*-axis,  $J_{\parallel}/J_{\perp}$ , of nearly  $-10$ . These authors used the misleading terms exchange anisotropy and anisotropic exchange interaction. One has to be careful in using such notations: exchange anisotropy, also called exchange biasing, is a totally different phenomenon discovered by Meiklejohn and Bean (1957) and anisotropic exchange interaction is used for cases where the interaction depends on the *direction* of the two interacting moments with respect to the lattice (see, e.g., Yosida, 1996). The exchange interaction considered by Cho et al. (1996b) is, however, isotropic.

In Section 4.1 we will discuss the influence of crystalline electric fields on the magnetic properties and the phenomenon of orbital ordering (also called quadrupolar ordering or hidden order) of the 4f electrons in  $\text{RNi}_2\text{B}_2\text{C}$  compounds. In the following sections we will briefly report on the behavior of the individual  $\text{RNi}_2\text{B}_2\text{C}$  compounds from  $\text{R} = \text{Ce}$  to  $\text{Yb}$ .

## 4.1 Effects of the crystalline electric field on magnetic and orbital ordering

### 4.1.1 Magnetic order

The ground-state magnetic structures of some borocarbides, including all magnetic  $\text{RNi}_2\text{B}_2\text{C}$  superconductors, are shown in Figure 28. These structures are characterized by the value of the ordered R magnetic moment ( $\mu$ ) and its direction with respect to the crystallographic axes and to the neighboring R magnetic moments. A further characteristic property of these structures is their propagation wave vector  $\tau$  which may be commensurate or incommensurate with respect to the lattice structure. In lanthanide materials the intraatomic correlation of the 4f electrons and their spin-orbit (SL) interaction are much stronger than the influence of the crystalline electric fields (CEF) and the interaction between the  $\text{R}^{3+}$  ions. Consequently the free-ion Hund's rule values of the spin ( $S$ ), the orbital momentum ( $L$ ) and the total angular momentum ( $J$ ) are good quantum numbers in such materials. However the CEF and the interatomic interactions modify the  $(2J + 1)$ -fold degenerated Hund's rule free-ion ground state and lift its degeneracy. Thus the magnetic properties of the  $\text{RNi}_2\text{B}_2\text{C}$  are the result of the interplay between the CEF and the RKKY exchange interaction between the  $\text{R}^{3+}$  ions. If the CEF interaction would be much stronger than the exchange interaction, the magnetic subsystem could

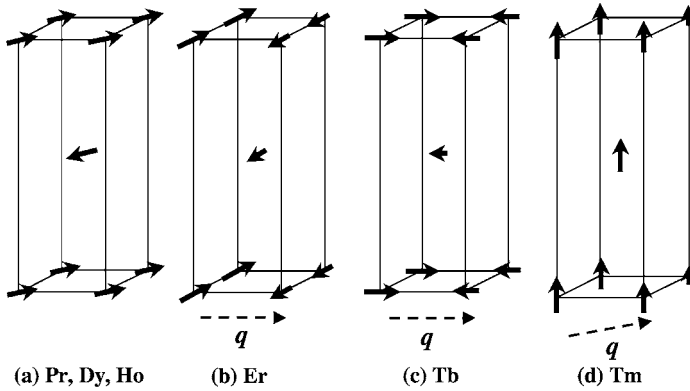


**FIGURE 28** Different types of magnetic structures in the ground state of  $\text{RNi}_2\text{B}_2\text{C}$  compounds. (a) For  $\text{R} = \text{Pr, Dy, Ho}$  commensurate antiferromagnetic structure. (b), (c) and (d): For  $\text{R} = \text{Er, Tb}$  and  $\text{Tm}$  incommensurate antiferromagnetic structures (spin-density waves) with a propagation vector  $\tau$  (in this figure denoted as  $q$ ) in the  $a$ - $b$ -plane; (b) moments in the  $a$ - $b$ -plane and  $\perp$  to  $\tau$ ; (c) moments in the  $a$ - $b$ -plane and  $\parallel \tau$ ; (d) moments  $\parallel c$  and  $\perp \tau$  (after Lynn et al., 1997).

be described, in zero approximation, by the single-ion CEF quantum states. The energy of the  $(2J + 1)$ -fold degenerated multiplet will split into CEF energy levels.

According to a theorem of Kramers (1930), in a system containing an odd number of electrons, all energy levels will keep an even degeneracy. Since  $\text{Ce}^{3+}$ ,  $\text{Nd}^{3+}$ ,  $\text{Sm}^{3+}$ ,  $\text{Gd}^{3+}$ ,  $\text{Dy}^{3+}$ ,  $\text{Er}^{3+}$  and  $\text{Yb}^{3+}$  have an odd number of electrons (see Table 8), the CEF ground state of these so-called Kramers ions is, at least, two-fold degenerated and consequently they will carry a magnetic moment i.e. this ground state will split in an external magnetic field. The CEF level schemes of the  $\text{RNi}_2\text{B}_2\text{C}$  compounds have been determined by various types of experiments as, e.g., inelastic neutron scattering (Gasser et al., 1997; Gasser and Allenspach, 2001) or Raman scattering (Rho et al., 2004).

Hybridization and correlation effects can suppress those 4f magnetic moments as, in particular, observed for  $\text{R} = \text{Ce}$  or  $\text{Yb}$ , i.e. for one electron or hole in the free  $\text{R}^{3+}$ -4f shell (see Tables 7 and 8). On the other hand the non-Kramers ions  $\text{Pr}^{3+}$ ,  $\text{Tb}^{3+}$ ,  $\text{Ho}^{3+}$  and  $\text{Tm}^{3+}$  contain an even number of electrons and consequently their CEF states can be singlet states which of course are non-magnetic. For  $\text{R} = \text{Pr}$  in  $\text{RNi}_2\text{B}_2\text{C}$  with point symmetry of  $\text{D}_{4h}$  at the R-site, indeed, the CEF ground state level is a singlet whereas that for  $\text{R} = \text{Tm}$  it is a magnetic doublet (Sierks et al., 2000; Rotter et al., 2001). For  $\text{R} = \text{Ho}$  and  $\text{Tb}$  the situation is more complicated because both, singlets and doublets are close to the CEF ground state level. As seen in Table 8, the  $\text{RNi}_2\text{B}_2\text{C}$  compounds show a staggered magnetic moment  $\langle \mu \rangle$  for all 4f elements but Ce and Yb. Consequently, the moment  $\langle \mu \rangle$  in  $\text{PrNi}_2\text{B}_2\text{C}$ , and probably in  $\text{HoNi}_2\text{B}_2\text{C}$ , is induced due to mixing of the CEF ground state with higher states through RKKY interaction which also causes cooperative ordering of the magnetic moments. The local directions of the ordered R magnetic moments are governed by single-ion anisotropy mainly due to CEF (with the ex-

**TABLE 8** Properties of free  $R^{3+}$  ions:  $n$ —number of 4f electrons,  $S$ —total spin,  $L$ —total orbital angular momentum,  $J$ —total angular momentum,  $g$ —Landé factor, DG—de Gennes factor,  $\alpha_J$ —second Stevens coefficient,  $\mu_p$ —paramagnetic moment,  $\mu_s$ —saturation moment;  $\langle\mu\rangle$ —staggered magnetic moment in  $RNi_2B_2C$  where the orientation of the moments with respect to the  $c$ -axis is given in the last column (Lynn et al., 1997; Skanthakumar and Lynn, 1999; Detlefs et al., 1996, 1997b; El-Hagary et al., 2000a; Allenspach and Gasser, 2000)

$R^{3+}$	$n$	Hund's rules quantum numbers			$g$	DG	$\alpha_J$ ( $10^{-2}$ )	$\mu_p$ ( $\mu_B$ )	$\mu_s$ ( $\mu_B$ )	$\langle\mu\rangle$ ( $\mu_B$ )	$\ \mu\ $ $\perp c$
		$S$	$L$	$J$							
Ce	1	1/2	3	5/2	6/7	0.18	-5.71	2.5	2.1	0	
Pr	2	1	5	4	4/5	0.80	-2.10	3.6	3.2	0.81	$\perp$
Nd	3	3/2	6	9/2	8/11	1.8	-0.64	3.6	3.3	2.10	$\perp$
Sm	5	5/2	5	5/2	2/7	4.56	4.13	0.85	0.7	?	$\parallel$
Gd	7	7/2	0	7/2	2	15.8	0	7.9	7	7	$\perp, \parallel$
Tb	8	3	3	6	3/2	10.5	-1.01	9.7	9	7.8	$\perp$
Dy	9	5/2	5	15/2	4/3	7.1	-0.64	10.7	10	8.5	$\perp$
Ho	10	2	6	8	5/4	4.5	-0.22	10.6	10	8.6	$\perp$
Er	11	3/2	6	15/2	6/5	2.6	0.25	9.6	9	7.2	$\perp$
Tm	12	1	5	6	7/6	1.2	1.01	7.6	7	3.4	$\parallel$
Yb	13	1/2	3	7/2	8/7	0.32	3.17	4.5	4	0	
Lu	14	0	0	0	-	0	0	0	0	0	

ception of the case  $R = Gd$ , see Section 4.6). There are two types of magnetic structures with the moments either parallel to the  $c$ -axis ( $R = Tm, Sm$ ; Table 8) or perpendicular to  $c$ . This different behavior can be explained, in most cases, by second-order CEF effects. The CEF are usually characterized by the CEF coefficients  $A_{nm}$  (Hutchings, 1964) which are approximately the same in all  $RNi_2B_2C$  compounds (Gasser et al., 1996). In lowest non-vanishing order the interaction of an  $R$  ion with the CEF is proportional to  $\alpha_J A_{20}$  with  $\alpha_J$  as the second order Stevens factor which roughly speaking characterizes the shape of the 4f ( $J, J_z = J$ ) free-ion ground-state charge density for the  $R^{3+}$  ion, where  $\alpha_J < 0$  characterizes a negative electric quadrupole moment (discus-like shape) and  $\alpha_J > 0$  a positive quadrupole moment (rugbyball-like shape). Table 8 shows that for all  $R^{3+}$  ions with  $\alpha_J < 0$  the moments are within the  $\mathbf{a-b}$ -plane, for  $\alpha_J > 0$  the moments are parallel to the  $c$ -axis, with the exception of Er. This case is more complicated and was discussed in detail by Cho et al. (1995c): in that case higher order CEF coefficients can not be neglected. On the other hand, the susceptibility  $\chi$  at higher temperatures is known to be determined by  $A_{20}$  and  $\alpha_J$  only. Measurements of  $\chi$  of  $ErNi_2B_2C$  single crystals at higher temperatures gave results which are compatible with Table 8, i.e.  $\chi$  measured perpendicular to  $c$  is smaller than measured parallel to  $c$  ( $\chi_{\perp} < \chi_p$ ). Only at temperatures below about 150 K Cho et al. (1995c) found  $\chi_p < \chi_{\perp}$  which is interpreted as being due to the influence of higher order CEF terms and is in accord with the structure shown in Figure 28(b). The

experimental values  $\langle \mu \rangle$  of the ordered R magnetic moments in  $\text{RNi}_2\text{B}_2\text{C}$  and their preferred directions, summarized in Table 8, could be well reproduced by a self-consistent mean-field approach taking into account some general assumptions on the RKKY interaction and experimental CEF data (Gasser et al., 1996; Gasser, 1999; Gasser and Allenspach, 2001; Rotter et al., 2001; Cavadini et al., 2002). The direction of the ordered R magnetic moments with respect to their R neighbors in the  $\text{RNi}_2\text{B}_2\text{C}$  lattice is dominated by the RKKY interaction and, due to the presence of the above mentioned magnetically easy axes, they usually are parallel or antiparallel. However in some cases small deviations from the strongly parallel or antiparallel alignment of neighbors have been reported. Examples are the spiral structure and the **a**-axis-modulated structure observed in  $\text{HoNi}_2\text{B}_2\text{C}$  at elevated temperatures (see Section 4.9.1). Whether the magnetic long-range order is commensurate or incommensurate is the result of the competition between CEF and RKKY interactions. Incommensurability is a typical effect of the RKKY interaction and, as expected, it occurs in the magnetic structures reported for  $\text{GdNi}_2\text{B}_2\text{C}$  (see Section 4.6). However incommensurate magnetic structures have been observed also for other  $\text{RNi}_2\text{B}_2\text{C}$  compounds in their ground states or metamagnetic states (see Figure 28 and Table 7 and the following subsections). Since the RKKY interaction is mediated by the conduction electrons, the incommensurate magnetization structures depend on details of the electronic structure of the conduction electrons. This is the reason why the nesting vector  $\mathbf{q} \approx (0.55, 0, 0)$  discussed in Section 3.2 manifests itself as a modulation wave vector of different incommensurate structures as found in various  $\text{RNi}_2\text{B}_2\text{C}$  compounds (see the following subsections). Wills et al. (2003) could show by group theory arguments why the ground-state magnetic structures of  $\text{HoNi}_2\text{B}_2\text{C}$  and  $\text{DyNi}_2\text{B}_2\text{C}$  do not have the incommensurate propagation vector  $\boldsymbol{\tau} \approx (0.55, 0, 0)$ : this propagation vector is not compatible with the CEF easy moment direction (110).

#### 4.1.2 Orbital order

The  $(2J + 1)$ -fold degenerated ground state of an  $\text{R}^{3+}$  ion has not only magnetic but also orbital degrees of freedom i.e. the charge distribution characterized by its tensor of electric quadrupole moment is not fixed. In the solid state, in many cases, this degeneracy is only partially lifted by the CEF and besides magnetic also orbital degrees of freedom of the  $\text{R}^{3+}$  can survive. As a simple example, the CEF ground state of  $\text{Pr}^{3+}$  in cubic  $\text{PrPb}_3$  is a  $\Gamma_3$  doublet that is non-magnetic but has an orbital degree of freedom by carrying two electric quadrupole moments. Now there is evidence that this material shows antiferroquadrupolar ordering (AFQO) at  $T_Q = 0.4$  K (Onimaru et al., 2005), i.e. below  $T_Q$  the quadrupole moments are long-range ordered in a staggered periodic arrangement. On the other hand, the electric quadrupole moment of  $\text{Pr}^{3+}$  in its  $\Gamma_3$ -doublet CEF ground state in cubic  $\text{PrOs}_4\text{Sb}_{12}$  has been considered to be involved in the heavy-fermion superconductivity of this compound (see Bauer et al., 2002; Sales, 2003) and field-induced AFQO has been reported (Kohgi et al., 2003).

In  $\text{HoB}_6$ , below  $T_Q = 6.1$  K, the  $\text{Ho}^{3+}$  quadrupole moments order in parallel (Yamaguchi et al., 2003). This is called ferroquadrupolar ordering (FQO). The cooperative phenomena AFQO and FQO are special types of quadrupolar order-

ing (QO) or orbital ordering (OO) where the latter term is usually preferred in cases of d-electron orbital degrees of freedom (van den Brink et al., 2004). They are caused by interactions between the individual quadrupole moments, where phonon-mediated interaction and different types of exchange interaction (akin to “magnetic” exchange) have been discussed as the most important mechanisms besides the direct electric quadrupole–quadrupole interaction (Levy et al., 1979; Kugel and Khomskii, 1982). The phonon-mediated interaction is the conventional mechanism of the cooperative Jahn–Teller effect (CJTE), i.e. lattice distortion due to lifting of orbital degeneracy by OO. However OO primarily caused by other mechanisms also results in CJTE-like lattice distortions. At the above-mentioned FQO transition in HoB<sub>6</sub> a homogeneous lattice distortion occurs, changing the lattice structure from cubic to trigonal. For AFQO transitions the lattice distortions are non-uniform and, in the case of R compounds, they are often small and difficult to observe. Therefore, sometimes such AFQO transitions are called hidden-order phase transitions (Mulders et al., 2007). Experimental methods that have been successfully used to determine orbital ordering are resonant X-ray scattering (Mulders et al., 2007), neutron diffraction in a magnetic field (Onimaru et al., 2005) and  $\mu$ SR (Schenck and Solt, 2004), complemented by ultrasonic, dilatometric, specific heat, thermal transport and magnetic measurements. In R compounds, due to the strong SL interaction, magnetic ordering automatically includes QO (see also Section 2.2). However even in materials with R<sup>3+</sup> ions that carry magnetic moments in their CEF ground state QO can occur without any magnetic ordering. Thus the above-mentioned HoB<sub>6</sub> shows antiferromagnetic order (AFMO) only below  $T_N = 5.6$  K, i.e. between  $T_N$  and  $T_Q$  it exhibits FQO but no magnetic ordering. The tetragonal compound DyB<sub>2</sub>C<sub>2</sub> has attracted much attention lately as its antiferroquadrupolar ordering temperature  $T_Q$  is as high as 24.7 K whereas AFMO is observed below  $T_N = 15.3$  K (Yamauchi et al., 1999). Here the AFMO has canted magnetic sublattices and a net magnetic moment because the Dy quadrupole moments of the AFQO sublattices represent different directions of strong uniaxial magnetic anisotropy, which is in competition with the antiferromagnetic exchange interaction. Interestingly the CEF ground state of Dy<sup>3+</sup> in DyB<sub>2</sub>C<sub>2</sub> is a Kramers doublet which has no orbital degrees of freedom. It has been concluded that the relatively strong RKKY-like quadrupole–quadrupole interaction is responsible for the ground state and the first excited doublets to form an effective quartet with orbital degrees of freedom (Staub et al., 2005). This phenomenon is similar to the above mentioned formation of induced magnetic moments in non-Kramers ions. On the other hand in HoB<sub>2</sub>C<sub>2</sub> which has the same LaB<sub>2</sub>C<sub>2</sub>-type lattice structure as DyB<sub>2</sub>C<sub>2</sub>, AFMO occurs below  $T_N = 5.8$  K and AFQO (similar to that in DyB<sub>2</sub>C<sub>2</sub>) only below  $T_Q = 6.1$  K (Onodera et al., 1999). In both materials the AFQO, in particular the value of  $T_Q$ , depends on the applied magnetic field  $H$  although the electric quadrupoles as well as the quadrupole–quadrupole interaction are time-even and, therefore, they should not couple to  $H$ . Possibly the observed dependence of the QO on  $H$  is mediated by the strong SL-interaction and the coupling of  $H$  to the (time-odd) magnetic moments. TbB<sub>2</sub>C<sub>2</sub> has also the LaB<sub>2</sub>C<sub>2</sub>-type lattice structure and shows AFMO below  $T_N = 21.7$  K but no AFQO. On the other hand an  $H$ -induced AFQO transition has been reported to occur in

the antiferromagnetic phase of  $\text{TbB}_2\text{C}_2$  (Kaneko et al., 2003). This has been refused by Mulders et al. (2007) who performed inelastic neutron scattering and resonant X-ray diffraction on  $\text{TbB}_2\text{C}_2$  and, for  $T < T_N$  and  $H = 0$ , they found FQO with the quadrupole moments rigidly coupled to the magnetic moments of the antiferromagnetic sublattices, similar to the phenomena observed in  $\text{DyNi}_2\text{B}_2\text{C}$  and  $\text{HoNi}_2\text{B}_2\text{C}$  (see Section 2.2). With increasing  $\mathbf{H}$  along [110] the magnetic moments rotate toward the field direction in a gradual manner and the quadrupole moments follow this rotation, steadily moving from parallel to perpendicular alignment, i.e. there is no field-induced QO phase transition in  $\text{TbB}_2\text{C}_2$ .

Effects of orbital ordering are well known also for 3d-electron systems (Kanamori, 1960; Kugel and Khomskii, 1982; Tokura and Nagaosa, 2000; van den Brink et al., 2004; Khomskii and Kugel, 2003; Hotta, 2006). Typical examples are cubic systems with one 2d-electron in the  $e_g$  orbital doublet. The manifold of the  $e_g$  states, usually designated as the  $(x^2 - y^2)$  and  $(3z^2 - r^2)$  type wave functions, can also be considered as the manifold of  $(3z^2 - r^2)$ ,  $(3y^2 - r^2)$  and  $(3x^2 - r^2)$  type wave functions (which of course are not independent of each other) with their elongated charge clouds being aligned along the  $z$ ,  $y$  and  $x$  axes, respectively. Typical examples of such systems are  $\text{LaMnO}_3$ , with AFQO below  $T_Q = 780$  K and so-called A-type AFMO below  $T_N = 140$  K (Goodenough, 1955; Murakami et al., 1998), and  $\text{Y}_{0.5}\text{Ba}_{0.5}\text{O}_3$  with FQO below  $T_Q \cong 500$  K and AFMO below  $T_N = 200$  K (Williams and Attfield, 2005). In both perovskite-like structures the  $e_g$  orbitals of the Jahn–Teller ion  $\text{Mn}^{3+}$  are involved in the OO which causes Jahn–Teller-like lattice distortions. However, in such perovskites additional distortions lifting the cubic symmetry are caused by non-ideal ratios of the sizes of the concerned ions and, in the case of  $\text{Y}_{0.5}\text{Ba}_{0.5}\text{O}_3$ , by effects of charge ordering. In the 3d-electron materials the CEF are considerably stronger than the SL interaction. Therefore the 3d electric quadrupole moments are not rigidly coupled to dominantly spin-based 3d magnetic moments. Nevertheless there is a strong interaction between the spin and the orbital degrees of freedom because the “magnetic” exchange interaction is very sensitive to orbital order. Thus the A-type magnetic structure in  $\text{LaMnO}_3$  consists of ferromagnetically ordered  $\text{Mn}^{3+}$  spins in the **a–b**-plane of an orthorhombic lattice structure and antiferromagnetically ordered ones along the **c**-axis which is the alignment axis of the spins. But the magnetic structure in  $\text{Y}_{0.5}\text{Ba}_{0.5}\text{O}_3$  is rather different from that of  $\text{LaMnO}_3$  due to the different type of orbital order resulting in different types of exchange interaction.

The discussed examples show that orbital ordering in 3d, 4f, and 5f electron systems is of much current interest. The orbital degrees of freedom are expected to yield a particularly rich variety of phenomena in cases where the quadrupole–quadrupole interaction and the dipolar interaction are similar in strength.

For  $\text{RNi}_2\text{B}_2\text{C}$  compounds little work has been done so far in order to investigate phenomena of QO. Lattice distortions induced by AFMO have been reported for some of these compounds and recently a quadrupolar (non-magnetic) phase has been discovered in  $\text{TmNi}_2\text{B}_2\text{C}$  (see Sections 2.2 and 4.11).

## 4.2 CeNi<sub>2</sub>B<sub>2</sub>C

The lattice parameters of CeNi<sub>2</sub>B<sub>2</sub>C do not fit the linear relationship found for the other RNi<sub>2</sub>B<sub>2</sub>C compounds (see Figure 29). Neither the trivalent nor the tetravalent radius for Ce falls on the corresponding straight lines. The approximate valence Ce<sup>+3.75</sup> obtained by interpolation points to an intermediate valence of cerium in this compound (Siegrist et al., 1994a, 1994b). However, X-ray absorption spectroscopy at the Ce-L<sub>III</sub> edge (Alleno et al., 1995a) yields a valence of Ce in CeNi<sub>2</sub>B<sub>2</sub>C of 3.26, which is slightly smaller than the well-known saturation value of 3.3 (Röhler, 1987). Magnetic susceptibility, specific heat and neutron diffraction experiments showed that Ce is essentially non-magnetic and there are no magnetic transitions in CeNi<sub>2</sub>B<sub>2</sub>C although, as discussed in Section 4.1, Ce<sup>3+</sup> is a Kramers ion and, therefore, it has a magnetic CEF ground state (Alleno et al., 1995a; Carter et al., 1995a; Lynn et al., 1997). Here “non-magnetic” essentially means that the susceptibility has no Curie-like singularity but remains finite at zero temperature, which can be roughly described by replacing  $T$  by  $(T + T_{sf})$ , i.e. considering the thermal fluctuations together with quantum interconfiguration fluctuations (Sales and Wohleben, 1975). The fluctuation temperature  $T_{sf} \approx 640$  K (Alleno et al., 1995a) is a measure of the hybridization interaction of the 4f electron with the conduction electrons. Interestingly, Ce is stably trivalent in the moderate heavy-fermion system CePt<sub>2</sub>B<sub>2</sub>C and also in CePd<sub>2</sub>B<sub>2</sub>C that orders antiferromagnetically at  $\approx 4.5$  K (Mazumdar et al., 2002; Hossain et al., 2002). From the variation of  $T_c$  as a function of the lattice-constant

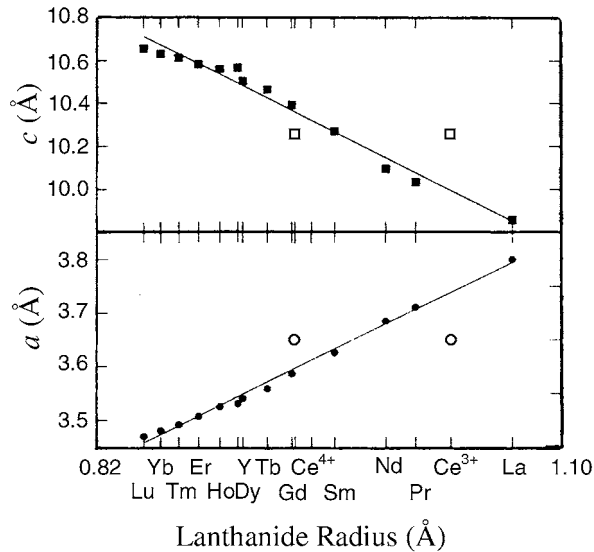


**FIGURE 29** Lattice constants  $a$  and  $c$  of RNi<sub>2</sub>B<sub>2</sub>C for various elements R versus the ionic radii of R<sup>3+</sup> ions, measured at 300 K. For R = Ce (open symbols) both Ce<sup>3+</sup> and Ce<sup>4+</sup> have been considered on the abscissa. Both the radii of Ce<sup>3+</sup> and Ce<sup>4+</sup> do not fit the curve observed for the other rare earths (from Siegrist et al., 1994b).

ratio  $a/c$  one would expect  $\text{CeNi}_2\text{B}_2\text{C}$  to be a superconductor (see Figure 6). The intermediate valence of Ce cannot be considered as the reason for the absence of superconductivity in  $\text{CeNi}_2\text{B}_2\text{C}$  because the intermediate-valence compounds  $\text{CeRu}_3\text{Si}_2$  and  $\text{CeRu}_2$  are superconductors as are their Ce  $\rightarrow$  La homologs (Rauchschwalbe et al., 1984). The change of electronic structure caused by the variation of lattice parameters and/or the distortion of the B–Ni–B tetrahedral angle may be one reason for the absence of superconductivity (Siegrist et al., 1994b; Mattheiss et al., 1994). Probably these phenomena cause the reduced density of states at the Fermi level  $N(E_F)$  (see Table 7) and the absence of Fermi surface nesting. The value of  $N(E_F)$  of  $\text{CeNi}_2\text{B}_2\text{C}$  in Table 7 was calculated assuming Ce to be trivalent, i.e. neglecting hybridization of the 4f electrons.

Based on ac magnetic susceptibility and specific heat measurements, El Massalami et al. (1998a) claimed that they observed superconductivity in  $\text{CeNi}_2\text{B}_2\text{C}$  with  $T_c$  of about 0.1 K, which, however, has never been reproduced.

### 4.3 $\text{PrNi}_2\text{B}_2\text{C}$

The lattice parameters of  $\text{PrNi}_2\text{B}_2\text{C}$  (Siegrist et al., 1994b; see Figure 29) fit well the linear relationship derived for the other  $\text{RNi}_2\text{B}_2\text{C}$ , which points to a valence of Pr in  $\text{PrNi}_2\text{B}_2\text{C}$  of close to 3. Neutron-diffraction measurements (Lynn et al., 1997) have shown that  $\text{PrNi}_2\text{B}_2\text{C}$  orders antiferromagnetically at  $T_N \approx 4$  K (see Table 7) in the same commensurate magnetic structure as observed in the ground states of  $\text{DyNi}_2\text{B}_2\text{C}$  and  $\text{HoNi}_2\text{B}_2\text{C}$  (Figure 28(a)). As discussed in Section 4.1, Pr has a singlet CEF ground state in  $\text{PrNi}_2\text{B}_2\text{C}$  and, therefore, its ordered magnetic moment is of an induced type. Its value of  $0.81\mu_B$  is considerably smaller than the free-ion value (Table 8).

Durán et al. (2002) report a second magnetic transition in a  $\text{PrNi}_2\text{B}_2\text{C}$  single crystal at 15 K resulting in ferromagnetic hysteresis at low temperatures. However it is questionable whether this is an intrinsic property of  $\text{PrNi}_2\text{B}_2\text{C}$  because these authors also found the splitting of the zero-field-cooling (ZFC) susceptibility curves from field-cooling (FC) ones in  $\text{HoNi}_2\text{B}_2\text{C}$  single crystals (Durán et al., 2000), which is definitely not an intrinsic property of  $\text{HoNi}_2\text{B}_2\text{C}$  as has been checked by the authors of this review article. May be, Durán et al. (2000, 2002) have not carried out the required heat-treatment procedure that is needed to exclude impurity phases and atomic disorder at the lattice sites (see Section 3.1). A similar splitting of ZFC and FC susceptibility curves at  $T_0 \approx 15$  K has been observed in polycrystalline  $\text{PrNi}_2\text{B}_2\text{C}$  (as well as  $\text{DyNi}_2\text{B}_2\text{C}$ ) by Takeya and Kuznietz (1999). Later  $T_0$  was considered a spin fluctuation temperature used to scale pressure dependent resistance-vs.-temperature curves of (Pr,Dy) $\text{Ni}_2\text{B}_2\text{C}$  polycrystals (El Massalami et al., 2004). But again these results must be doubted to be intrinsic properties because the investigated samples had not been annealed additionally at lower temperature and, in particular, for  $\text{DyNi}_2\text{B}_2\text{C}$  any intrinsic anomaly at about 15 K can be excluded (Ribeiro et al., 2003).

$\text{PrNi}_2\text{B}_2\text{C}$  does not exhibit superconductivity (Lynn et al., 1997, see Table 2). Although a detailed analysis of this behavior is still missing, various reasons are known that contribute to the suppression of superconductivity in this com-

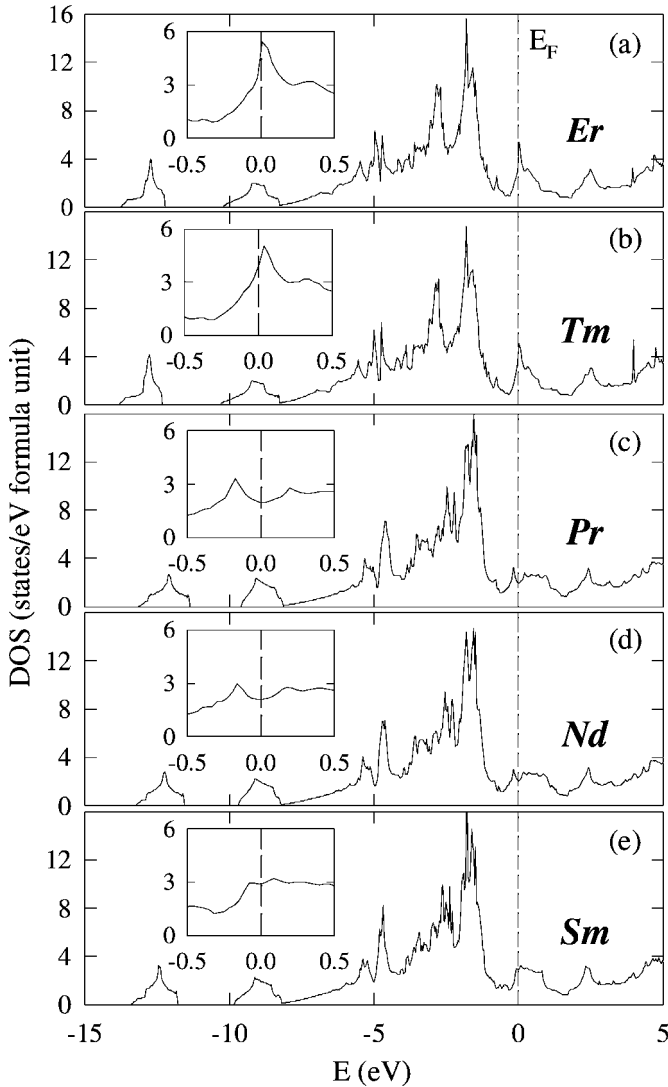


**FIGURE 30** Calculated electronic density of states (DOS) for different  $\text{RNi}_2\text{B}_2\text{C}$  compounds. For superconductors (here  $R = \text{Er}, \text{Tm}$ ) the DOS has a pronounced peak at the Fermi level ( $E = 0$ ) whereas for the non-superconductors, in particular for  $R = \text{Pr}$ , there is no peak at  $E = 0$ . The insets show details of the DOS around the Fermi level (Diviš et al., 2001).

pound. First of all, different from results on  $\text{RNi}_2\text{B}_2\text{C}$  superconductors (see, e.g., Coehoorn, 1994; Diviš et al., 2000, 2001), the electronic density of states in  $\text{PrNi}_2\text{B}_2\text{C}$  has no peak at the Fermi level (see Figure 30). Two, further mechanisms acting against superconductivity are magnetic pair breaking and hybridization of the 4f electrons with the itinerant (s, p, d) electrons. Magnetic pair breaking alone would reduce a fictitious  $T_c$  in  $\text{PrNi}_2\text{B}_2\text{C}$  from 6 K down to 4 K. In particular, in

$Y_{1-x}Pr_xNi_2B_2C$  the superconductivity suppression rate  $|\partial T_c/\partial x|$  is 35 K which is about 20 times larger than expected from de Gennes scaling for  $Y_{1-x}Gd_xNi_2B_2C$ . This can only partially be explained by the difference in the ionic radii of  $Y^{3+}$  and  $Pr^{3+}$  ions (Narozhnyi et al., 2001b). Thus the eventual suppression of superconductivity in  $PrNi_2B_2C$  is attributed to electronic hybridization, which is supported by numerous measurements of magnetic properties, specific heat, electrical resistivity and magnetoresistance on this compound (Narozhnyi et al., 1999c, 2000a, 2001a, 2001b).

There is an interesting analogy between the anomalous behavior of Pr in borocarbides with the well-known anomalous properties of Pr-containing cuprates (Lynn, 1997, see Section 1.3). For  $PrBa_2Cu_3O_{7-\delta}$ , e.g., it is widely accepted that the absence of superconductivity and the anomalously high  $T_N$  are connected with the increased hybridization of 4f levels with planar oxygen-derived states being important for superconductivity of doped holes.

#### 4.4 $NdNi_2B_2C$

This borocarbide is a non-superconducting antiferromagnet with the magnetic structure shown in Figure 31. According to the empirical curves of Figure 6 the absence of superconductivity in  $NdNi_2B_2C$  is expected to be mainly caused by two reasons. Firstly, the change of the lattice spacings is expected to cause the changed electronic structure compared to the cases  $R = Sc, Lu$  and  $Y$ , in particular the reduced density of states at the Fermi level  $N(E_F)$  (see Table 7 and Figure 30; Siegrist et al., 1994b; Mattheiss et al., 1994; Diviš et al., 2001). However these effects of the lattice structure are not sufficient to explain the absence of superconductivity for  $R = Nd$  since  $ThNi_2B_2C$  is a superconductor in spite of its relatively large lattice-constant ratio  $a/c$  (see Figure 6). The second mechanism suppressing superconductivity in  $NdNi_2B_2C$  is the lanthanide magnetism. As discussed in Section 4.1,  $Nd^{3+}$  is a Kramers ion whose individual magnetic moment cannot be quenched by crystalline electric fields (CEF). Magnetic ordering in  $NdNi_2B_2C$  at

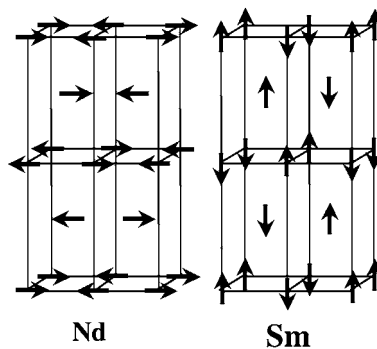


**FIGURE 31** Observed magnetic structures of  $NdNi_2B_2C$  and  $SmNi_2B_2C$  (Skanthakumar and Lynn, 1999).

$T_N = 4.8$  K had been reported by Nagarajan et al. (1995) and Gupta et al. (1995) who measured the magnetic susceptibility on polycrystalline samples and found a paramagnetic moment of  $3.6\mu_B$  per Nd ion which agrees with the free-ion value  $\mu_p$  in Table 8. The magnetic structure of NdNi<sub>2</sub>B<sub>2</sub>C (Figure 31), including the staggered Nd magnetic moment ( $2.1\mu_B$ , see Table 8) has been determined by Lynn et al. (1997) using elastic neutron diffraction. This structure has been confirmed by X-ray resonant exchange scattering (XRES; Detlefs et al., 1997b). So far no inelastic neutron scattering experiments have been performed to determine the CEF excitations. However Diviš and Rusz (2002) as well as Diviš et al. (2005) have calculated the CEF parameters from first principles, using density functional theory. Their results are in good agreement with experimental results on specific heat and magnetic susceptibility.

#### 4.5 SmNi<sub>2</sub>B<sub>2</sub>C

The fact that SmNi<sub>2</sub>B<sub>2</sub>C is not a superconductor can be understood by similar reasons as in the case of NdNi<sub>2</sub>B<sub>2</sub>C. Although the calculated density of states  $N(E_F)$  of SmNi<sub>2</sub>B<sub>2</sub>C is larger than that of NdNi<sub>2</sub>B<sub>2</sub>C, it is considerably smaller than that of the superconducting RNi<sub>2</sub>B<sub>2</sub>C compounds (see Table 7). Furthermore Sm<sup>3+</sup> is a Kramers ion (see Section 4.1) and therefore, the Sm magnetic moments will be present which also are unfavorable for superconductivity. Magnetic ordering in SmNi<sub>2</sub>B<sub>2</sub>C at about 9.8 K had been observed by Hossain et al. (1995) and Prassides et al. (1995) who measured magnetic susceptibility and muon spin relaxation, respectively. The paramagnetic moment has been determined by El-Hagary et al. (2000a) who analyzed the temperature dependence of magnetic susceptibility and found a modified Curie–Weiss law,  $\chi = \chi_0 + C/(T - \theta)$ , with a paramagnetic Curie temperature  $\theta = -23$  K and, resulting from the Curie constant  $C$ , a paramagnetic Sm moment of  $\mu_p = 0.6\mu_B$  which is relatively close to the Sm<sup>3+</sup> free-ion value  $0.85\mu_B$  (see Table 8). The constant term  $\chi_0 = 3.7 \times 10^{-6}$  cm<sup>3</sup>/g has been attributed to van Vleck paramagnetism due to  $J$  multiplet spacing and coupling of the  $J = 5/2$  ground state to the  $J = 7/2$  state. These authors also found an anomaly of the specific heat of SmNi<sub>2</sub>B<sub>2</sub>C at about 1 K below  $T_N$ , which they assumed to be associated with some spin reorientation transition. Since Sm is highly neutron absorbing, no neutron diffraction studies have been performed on SmNi<sub>2</sub>B<sub>2</sub>C. Fortunately the magnetic structure of this compound can be determined by the XRES technique mentioned in Section 4.4 (Detlefs et al., 1997b). It should be noted that the two magnetic structures of NdNi<sub>2</sub>B<sub>2</sub>C and SmNi<sub>2</sub>B<sub>2</sub>C in Figure 31 have the same modulation wave vector  $(1/2, 0, 1/2)$ , but the magnetic moments in the two compounds have different directions. In both cases, the magnetic unit cell is double the chemical unit cell along the **a** and **c** directions while it is the same along **b**. Typical XRES integrated-intensity curves from which the structures of Figure 31 could be derived are shown in Figure 32. Since the magnetic structure of NdNi<sub>2</sub>B<sub>2</sub>C has been independently determined by neutron diffraction, the XRES results for this material can be considered as a proof of the ability of X-ray resonant exchange scattering to determine moment directions with no *a priori* information.

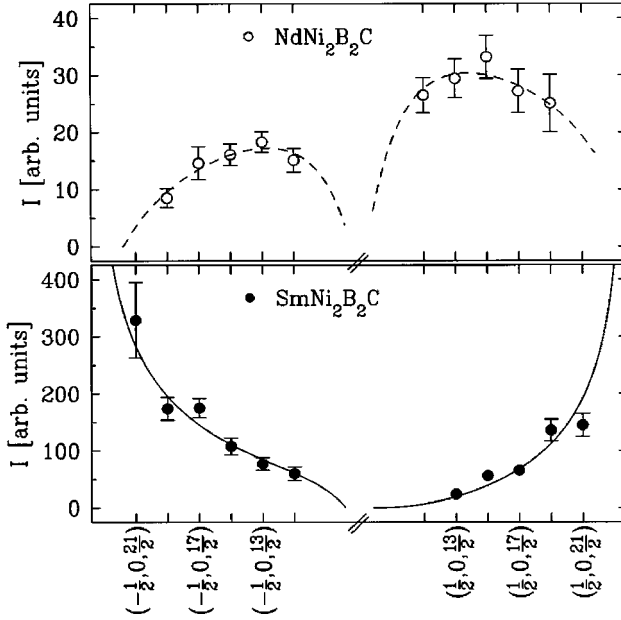


**FIGURE 32** The integrated intensity of magnetic reflections of X-ray resonant exchange scattering, measured for NdNi<sub>2</sub>B<sub>2</sub>C and SmNi<sub>2</sub>B<sub>2</sub>C. Dashed line and full line: model calculations for a magnetic moment parallel to the tetragonal a- and c-axes, respectively (after Detlefs et al., 1997b).

Unfortunately the staggered magnetic moment  $\langle \mu \rangle$  in SmNi<sub>2</sub>B<sub>2</sub>C cannot be determined by XRES. The CEF splitting of the  $J = 5/2$  ground-state multiplet of Sm<sup>3+</sup> in SmNi<sub>2</sub>B<sub>2</sub>C has been calculated by Diviš et al. (2002) from first principles, using density functional theory.

#### 4.6 GdNi<sub>2</sub>B<sub>2</sub>C

The absence of superconductivity in GdNi<sub>2</sub>B<sub>2</sub>C is understandable for various reasons. According to the tendency of the transition temperature  $T_c$  of RNi<sub>2</sub>B<sub>2</sub>C compounds with heavy R-elements to approximately follow de Gennes scaling (see Figure 5),  $T_c$  of GdNi<sub>2</sub>B<sub>2</sub>C should be zero. Furthermore, Gd<sup>3+</sup> has no orbital momentum  $L$  and, consequently, it has a spherical charge density resulting in a vanishing Stevens coefficient  $\alpha_J$  (see Table 8). Therefore the magnitude as well as the direction of the Gd magnetic moment in GdNi<sub>2</sub>B<sub>2</sub>C is nearly insensitive to crystalline electric fields (CEF) and Gd can be considered as the most effective magnetic pair breaker among the R elements in the magnetic-impurity picture (Cho et al., 1996c). Additionally, the lattice parameters of GdNi<sub>2</sub>B<sub>2</sub>C are different from those of superconducting RNi<sub>2</sub>B<sub>2</sub>C compounds and according to the  $T_c$ -vs.- $a/c$  curve in Figure 6(a) a hypothetically non-magnetic GdNi<sub>2</sub>B<sub>2</sub>C compound would have a reduced value of  $T_c$ , which also manifests itself in a reduced density of states at the Fermi level  $N(E_F)$  (see Table 7). Measurements of the mag-

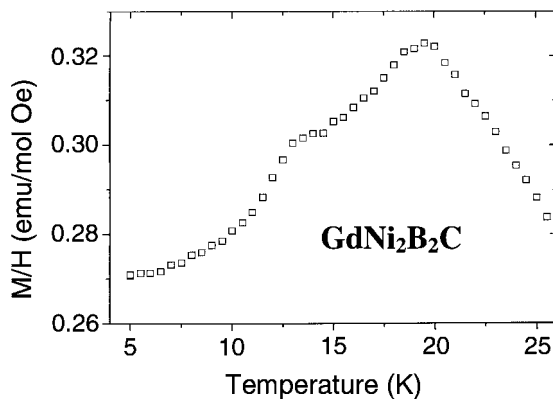


**FIGURE 33** Temperature dependence of the susceptibility of  $\text{GdNi}_2\text{B}_2\text{C}$  measured at 1 Tesla on an oriented powder, indicating the two magnetic phase transitions near 20 K and 14 K (after Felner, 2001).

netic susceptibility, at temperatures up to 300 K, on  $\text{GdNi}_2\text{B}_2\text{C}$  single crystals confirmed that this compound is nearly magnetically isotropic and yielded an effective paramagnetic moment  $\mu_p = 8.1\mu_B$  which is close to the  $\text{Gd}^{3+}$  free-ion value of  $7.9\mu_B$  (see Table 8) and agrees with the value measured by Gupta et al. (1995) on a powder sample, whereas measurements of the magnetization at low temperatures indicate a magnetic ordering temperature  $T_N \approx 20$  K and a spin reorientation transition temperature  $T_R \approx 14$  K (Canfield et al., 1995; see also Figure 33).

Due to the weak influence of the CEF in this compound its magnetic structure is expected to be governed by the RKKY exchange interaction and by the electronic structure including the shape of the Fermi surface. Since natural Gd strongly absorbs neutrons and non-absorbing Gd isotopes are expensive, neutron diffraction has not been used to determine the magnetic structure in  $\text{GdNi}_2\text{B}_2\text{C}$ . Combining resonant and non-resonant X-ray magnetic scattering Detlefs et al. (1996) confirmed the value of  $T_N = 19.4$  K and showed that below  $T_N$  this compound forms incommensurate antiferromagnetic states with a wave vector  $\tau \approx (0.55, 0, 0)$  which is close to the nesting vector discussed in Section 3.2. Between  $T_N$  and 13.6 K the magnetic structure is equivalent to that of  $\text{ErNi}_2\text{B}_2\text{C}$  in its ground state i.e. the ordered magnetic moment is along the **b**-axis (see Figure 28). Below  $T_R = 13.6$  K an additional ordered component of the magnetic moment develops along the **c** axis. According to Rotter et al. (2003) and El Massalami et al. (2003a) the microscopic mechanisms for the (weak) magnetic anisotropy favoring these magnetization directions are magnetostatic and, alternatively, anisotropic-exchange interactions. The two magnetic phase transitions have been observed also by  $^{155}\text{Gd}$  Mössbauer spectroscopy that reveals a bunched spiral-like low-temperature structure with the Gd magnetic moments rotating within the **b**-**c**-plane (Mulder et al., 1995; Tomala et al., 1998; see Figure 34). The value of  $T_R$  has also been confirmed by  $^{57}\text{Fe}$  Mössbauer spectroscopy, using a  $^{57}\text{Fe}$  probe on the Ni sites in  $\text{GdNi}_2\text{B}_2\text{C}$  (Baggio-Saitovitch et al., 2002a) and specific heat measurements (El Massalami et al., 2003b, 2003c). The value of the staggered Gd moment ( $\mu$ ) in  $\text{GdNi}_2\text{B}_2\text{C}$  has not yet been

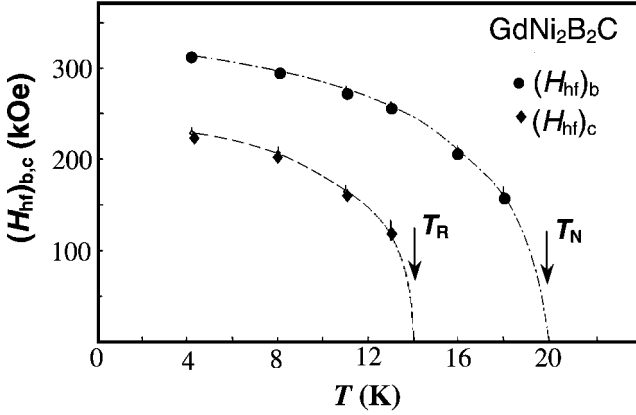


**FIGURE 34** Temperature dependence of the hyperfine field components along the tetragonal b- and c-axes,  $(H_{hf})_b$  and  $(H_{hf})_c$ , of a  $\text{GdNi}_2\text{B}_2\text{C}$  sample, reflecting the temperature dependence of the corresponding components of the Gd magnetic moment. The lines leading to the ordering temperature  $T_N = 20$  K and the spin-reorientation temperature  $T_R = 14$  K are guides for the eye (after Tomala et al., 1998).

experimentally determined. However, since  $\text{Gd}^{3+}$  is a spin-only ion with the spin  $S$  as large as  $7/2$  no remarkable deviations from the ideal value  $\langle \mu \rangle = \mu_s = 7\mu_B$  (see Table 8) are expected to be caused by crystalline electric fields or quantum fluctuations or effects of hybridization.

In  $\text{GdNi}_2\text{B}_2\text{C}$  weak spontaneous magnetostrictive effects have been observed for temperatures below  $T_N$  that have assumed to be caused by exchange magnetostriction (Doerr et al., 2005). However contrary to the predictions of the exchange magnetostriction model no change of the lattice symmetry occurs at  $T_N$ . This phenomenon is not yet understood, but it also appears in other Gd-based anti-ferromagnets and has been called the magnetoelastic paradox (Rotter et al., 2006).

#### 4.7 $\text{TbNi}_2\text{B}_2\text{C}$

As can be seen from Figures 5 and 6,  $\text{TbNi}_2\text{B}_2\text{C}$  shows magnetic ordering at  $T_N = 15$  K but it does not superconduct (Tomy et al., 1996c) and, as in the case of  $\text{GdNi}_2\text{B}_2\text{C}$ , the absence of superconductivity is thought to be mainly caused by the ordered 4f magnetic moments. The magnetic structure is a longitudinally polarized incommensurate spin-density wave along the **a**-axis with the magnetic moments parallel to the modulation vector of this SDW (see Figure 28 and Tables 7 and 8). The relation of this magnetic structure to the orthorhombic lattice distortion, as discussed in Section 2.2, has been determined by resonant magnetic X-ray scattering (C. Song et al., 2001a). The modulation vector  $\tau = (0.55, 0, 0)$  practically coincides with the nesting vector found in most of the quaternary borocarbide superconductors (see Section 3.2). This fact together with the high density of states at the Fermi level ( $N(E_F)$ )—see Table 7) suggests that without the 4f-local-moment magnetism  $\text{TbNi}_2\text{B}_2\text{C}$  would be a superconductor. Below  $T_{\text{WFM}} = 8$  K

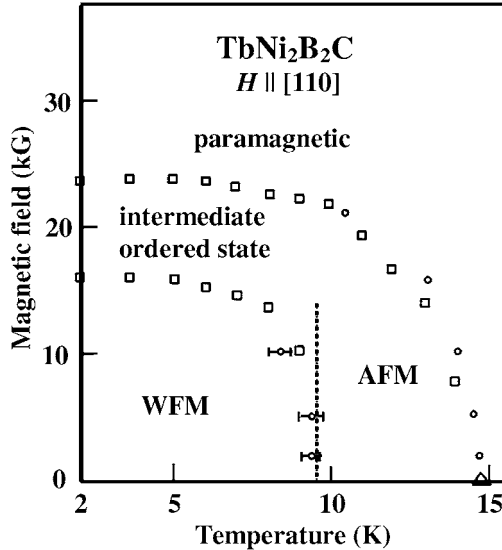


**FIGURE 35** Magnetic-field-vs.-temperature magnetic phase diagram for  $\text{TbNi}_2\text{B}_2\text{C}$  for  $H \parallel [110]$  proposed by Cho et al. (1996a). Data were taken from magnetization measurements at constant temperatures (squares) and constant fields (circles); triangle: from electrical resistivity. Error bars are shown for only a few data near 9 K. AFM: antiferromagnetic; WFM: weakly ferromagnetic. The dotted line marks the WFM-to-AFM transition at zero field. The nature of the ‘intermediate ordered state’ is not yet known.

Cho et al. (1996a) found a small ferromagnetic component within the  $\mathbf{a}$ - $\mathbf{b}$ -plane of a  $\text{TbNi}_2\text{B}_2\text{C}$  single crystal and, below this temperature, the magnetization-vs.-field curves show ferromagnetic hysteresis. These phenomena have been attributed to a similar type of weak ferromagnetism as in the case of  $\text{ErNi}_2\text{B}_2\text{C}$  (see Section 4.10.1) caused by squaring-up and locking-in of the SDW into commensurate structures. The latter mechanism has been analyzed in detail by Walker and Detlefs (2003). The onset of weak ferromagnetism has also been confirmed by X-ray magnetic circular dichroism measurements (C. Song et al., 2001b) and specific heat measurements (Tomy et al., 1996a; El Massalami et al., 2003b, 2003c). A magnetic phase diagram with a domain of a weak ferromagnetism, as proposed by Cho et al. (1996a), is shown in Figure 35. At temperatures where the weak ferromagnetism occurs the intensity of elastic neutron diffraction shows a weak anomaly (Dervenagas et al., 1996; Lynn et al., 1997). The presence of weak ferromagnetism has also been supported by Mössbauer spectroscopy and muon spin relaxation ( $\mu\text{SR}$ ; Sánchez et al., 1998). The  $M$ - $H$  isotherms at low temperatures show that for  $\mathbf{H}$  perpendicular to the  $\mathbf{c}$ -axis  $\text{TbNi}_2\text{B}_2\text{C}$  undergoes a series of metamagnetic transitions before finally saturating into a ferromagnetic state (Tomy et al., 1996a; Canfield and Bud’ko, 1997; see Figure 36). On the other hand, for  $\mathbf{H}$  parallel to  $\mathbf{c}$ , the  $M$ - $H$  isotherms (not shown here) are linear as in simple antiferromagnets. This indicates that the direction of the ordered Tb magnetic moments is strongly confined to the  $\mathbf{a}$ - $\mathbf{b}$ -plane in agreement with the negative sign of the

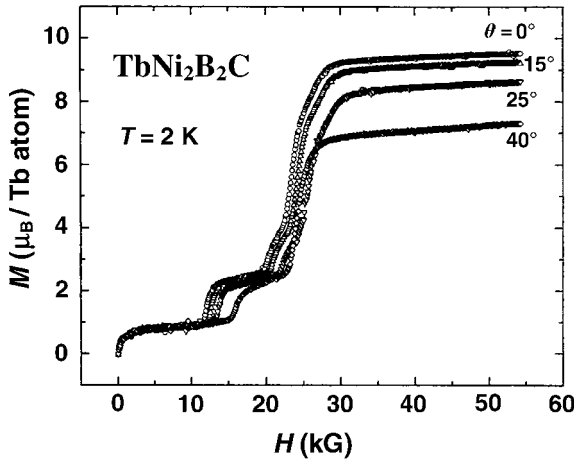


**FIGURE 36** Metamagnetic transitions measured on a  $\text{TbNi}_2\text{B}_2\text{C}$  single crystal, at 2 K. Field  $H$  and measured component of magnetization  $M$  are within the tetragonal basal plane.  $\theta$ -angle with respect to the  $a$ -axis (Canfield and Bud'ko, 1997).

© 1997 Elsevier

Stevens coefficient  $\alpha_J$  of  $\text{Tb}^{3+}$  (see Table 8). The metamagnetic transitions are accompanied by large values of magnetoresistance which remains considerably large even above the ordering temperature  $T_N \approx 15$  K (Tomy et al., 1996a; Müller et al., 1998). This points to strong spin-disorder scattering and possibly the reorientation of magnetic short-range order. So far no theoretical model has been published describing the magnetic structure in the ground state or the metamagnetic states of  $\text{TbNi}_2\text{B}_2\text{C}$ . Such a model would have to take into account Fermi surface nesting of the conduction electrons which mediate the exchange coupling of the Tb moments, the effects of the crystalline electric field and the magnetoelastic interaction.

#### 4.8 $\text{DyNi}_2\text{B}_2\text{C}$

This compound is unique in the  $\text{RNi}_2\text{B}_2\text{C}$  series insofar as the onset of superconductivity occurs in an antiferromagnetically ordered state, i.e.  $T_N = 11$  K  $>$   $T_c = 6.3$  K (see also Table 7). On the other hand, this is in agreement with the overall behavior of the  $\text{RNi}_2\text{B}_2\text{C}$  compounds with heavy 4f elements R, shown in Figure 5. It should be noted that in the ruthenocuprates, discussed in Section 1.3, antiferromagnetic order (and even weak ferromagnetism) coexists with superconductivity and  $T_N$  is considerably larger than  $T_c$ . An additional magnetic phase transition at  $\approx 16$  K in polycrystalline  $\text{DyNi}_2\text{B}_2\text{C}$  samples annealed at  $\approx 1373$  K has been reported by Takeya et al. (2005; and previous papers of this group, cited therein). However Ribeiro et al. (2003) concluded from data measured on heat-treated single crystals that such a transition is not an intrinsic feature of single-phase  $\text{DyNi}_2\text{B}_2\text{C}$ . Thus the origin of the observed transition at  $\approx 16$  K may be due

to the presence of impurity phases or to atomic disorder at certain lattice sites (e.g., B–C disorder; see Section 3.1).

The ground-state magnetic structure of DyNi<sub>2</sub>B<sub>2</sub>C shown in Figure 28(a) consists of ferromagnetic sheets, with the Dy magnetic moments parallel to the [110] direction, which are antiparallel in adjacent Dy planes. If a magnetic field is applied perpendicular to the *c*-axis on a DyNi<sub>2</sub>B<sub>2</sub>C single crystal, at temperatures below *T<sub>N</sub>* various metamagnetic transitions can be observed (Lin et al., 1995; Tomy et al., 1996b; Canfield and Bud'ko, 1997; Naugle et al., 1998; Winzer et al., 1999, 2001). A strength-of-field angle-of-field phase diagram of the metamagnetic states, derived from resistivity and magnetization data for *T* < 2 K has been constructed by Winzer et al. (1999). Hysteresis phenomena connected with these metamagnetic transitions have been considered to be the reason why, upon warming, field-cooled DyNi<sub>2</sub>B<sub>2</sub>C single crystals exhibit near-reentrant superconductivity. For a field **H** applied parallel to the *a*-axis, at temperatures below 2 K, resistivity  $\rho$ -versus-*H* curves show a strong hysteresis, i.e. upon decreasing *H* the onset of superconductivity occurs at a much lower value of *H* than the upper critical field obtained for increasing *H* (Peng et al., 1998). No hysteresis effects have been observed for **H**||*c* and the hysteresis in superconductivity is almost zero for **H**||[110]. Winzer et al. (1999) have also related this hysteresis of the  $\rho$ -vs.-*H* transition curves to the hysteresis in the metamagnetic transitions. The metamagnetic transitions result in a positive low-temperature magnetoresistance as large as 30% (Peng et al., 1998) similar to that observed in TbNi<sub>2</sub>B<sub>2</sub>C (Tomy et al., 1996a). It would be interesting to know whether at least one of the metamagnetic states has a modulation vector  $\tau$  close to the nesting vector (0.55, 0, 0) as observed for HoNi<sub>2</sub>B<sub>2</sub>C (see Section 4.9.2).

In the non-superconducting antiferromagnetic state the resistivity measured on single crystals in the *a*–*b*-plane (Cho et al., 1995a) and on polycrystalline samples (Lin et al., 1995) strongly decreases with decreasing temperature, resulting in a normal-state resistance ratio  $\rho(T_N)/\rho(T_c)$  of typically 2.5. This is attributed to reduced spin-disorder scattering due to magnetic ordering but is not yet really understood.

In a phenomenological Ginzburg–Landau approach based on the fact that different electron bands participate in the Fermi surface (Doh et al., 1999), and on a recent electron structure analysis (Shorikov et al., 2006) it has been found that in DyNi<sub>2</sub>B<sub>2</sub>C and in Dy<sub>*x*</sub>Ho<sub>1–*x*</sub>Ni<sub>2</sub>B<sub>2</sub>C certain parts of the Fermi surface are dominated by Ni-3d<sub>*xy*</sub> electrons that provide a basis for superconductivity and are rather insensitive to the antiferromagnetic order of the (Dy, Ho)-4f electrons. Thus, although the electronic properties at large are governed by a multi-sheet Fermi surface only those parts of it for which the magnetic order is “invisible” contribute to superconductivity. This approach is equivalent to the multiband scenario of coexisting magnetism and superconductivity on different Fermi surface sheets. According to it, superconductivity survives on the Fermi surface sheet which is free of R-5d states since they mediate the exchange interaction between the 4f-R electrons and the conduction-band electrons (Drechsler et al., 2001b, 2004; see also Shulga et al., 1998). Such effective single-band behavior is in perfect accord with point-contact spectroscopy on DyNi<sub>2</sub>B<sub>2</sub>C (Yanson et al., 2000a, 2000b) indicating

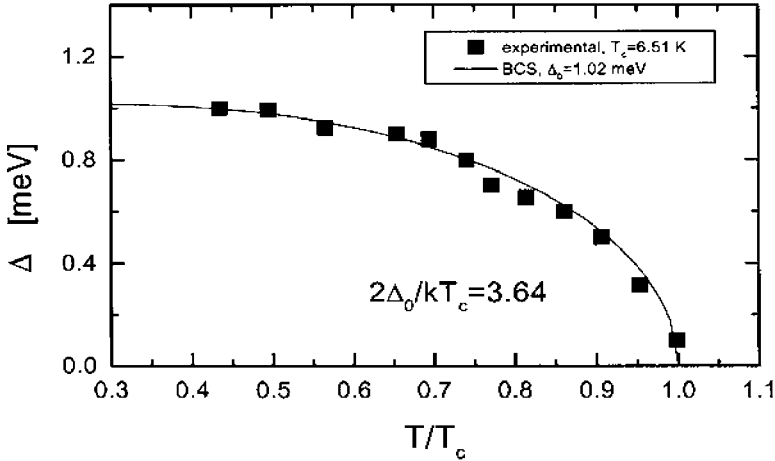


**FIGURE 37** Temperature dependence of the superconducting gap  $\Delta$  of  $\text{DyNi}_2\text{B}_2\text{C}$  obtained by point-contact spectroscopy (from Yanson et al., 2000a).

© 2000 Elsevier

one superconducting gap which is BCS-like in its magnitude and in its temperature dependence (see Figure 37). In principle, this approach might explain the different pressure dependencies of the magnetic and superconducting properties experimentally determined for the  $\text{RNi}_2\text{B}_2\text{C}$  family: For  $\text{DyNi}_2\text{B}_2\text{C}$  Falconi et al. (2002) found  $T_N$  to be nearly independent of pressure whereas  $dT_c/dP$  is large in magnitude ( $-0.7$  K/GPa) as compared to  $\text{YNi}_2\text{B}_2\text{C}$  (see Section 3.7), because completely different electronic states are responsible for the superconductivity around 6 K and 15 K, observed in  $\text{DyNi}_2\text{B}_2\text{C}$  and  $\text{YNi}_2\text{B}_2\text{C}$ , respectively (Drechsler et al., 2007). Consequently, a sizable group of uncondensed electrons (not involved in the pairing mechanism) should coexist with superconductivity in between  $\approx 6$  and 15 K in  $\text{YNi}_2\text{B}_2\text{C}$  and  $\text{LuNi}_2\text{B}_2\text{C}$ .

A particularly interesting manifestation of the anisotropy of the physical properties of  $\text{DyNi}_2\text{B}_2\text{C}$  is the paramagnetic Meissner effect reported by Tomy et al. (1996b), i.e. if a field  $H < 40$  Oe is applied parallel to the  $c$ -axis, in the field-cooling mode, the response of the sample is paramagnetic, similar as observed for high- $T_c$  cuprates (Braunisch et al., 1992). A systematic study of whether this effect also occurs in other  $\text{RNi}_2\text{B}_2\text{C}$  compounds and of its microscopic origin in  $\text{DyNi}_2\text{B}_2\text{C}$  is still missing, but such studies should be done.

## 4.9 $\text{HoNi}_2\text{B}_2\text{C}$

$\text{HoNi}_2\text{B}_2\text{C}$  is one of the most interesting compounds among the borocarbide superconductors. As can be seen in Figure 38, resistivity-vs.-temperature curves measured at zero magnetic field  $H$  show a sharp transition into the superconducting state at  $T_c \approx 8$  K. For relatively small fields (e.g., 0.13 T for the polycrystalline sample of Figure 38(a)) near-reentrant superconductivity similar to

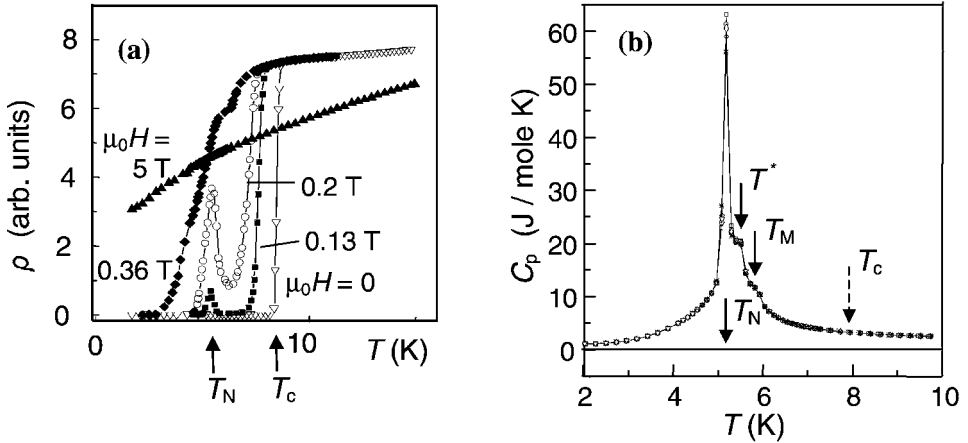


**FIGURE 38** (a) Resistivity vs. temperature measured at different magnetic fields  $H$  on a polycrystalline  $\text{HoNi}_2\text{B}_2\text{C}$  sample.  $T_c$  is the superconducting transition temperature at  $H = 0$ . A near-reentrant behavior occurs around a temperature  $T_N$ . (b) Temperature dependence of the specific heat  $C_p$  of a  $\text{HoNi}_2\text{B}_2\text{C}$  single crystal ( $2 \text{ mm} \times 3 \text{ mm} \times 0.1 \text{ mm}$  in size), measured at zero magnetic field. Above the main peak of  $C_p(T)$  at  $T_N$ , two additional features appear at  $T^*$  and  $T_M$ . No jump in  $C_p$  can be seen at  $T_c$ . Samples prepared by J. Freudenberger.

that in  $\text{GdMo}_6\text{S}_8$  (see Figure 4) is observed, which was first reported by Eisaki et al. (1994). Figure 38 also shows that the temperature range near  $T_N$  where the reentrant behavior occurs does not much depend on the value of  $H$ . Therefore  $T_N$  is considered to be some intrinsic temperature indicating a magnetic phase transition. This is supported also by measurements of the specific heat  $C_p$  (see Figure 38(b)) that shows a peak near  $T_N$ . Interestingly, two further features can be seen in Figure 38(b) at  $T^*$  and  $T_M$ , indicating two other magnetic-ordering phenomena, which will be discussed in Sections 4.9.1 to 4.9.5. On the other hand, no anomaly of  $C_p$  at  $T_c$  can be seen in Figure 38(b). This has been attributed to the fact that the high-temperature tails of the  $C_p$  anomalies at  $T_N$ ,  $T^*$ , and  $T_M$  are still higher at  $T_c$  than the expected jump in  $C_p$  associated with the superconducting transition (Canfield et al., 1994). An analysis of the specific heat near  $T_c$  on a finer  $C_p$  scale will be presented in Section 4.9.5. Special behaviors at temperatures near and above  $T_N$  were also observed for various other physical properties. Thus, the thermal conductivity shows a discontinuous increase at  $T_N$  (Sera et al., 1996; see Section 3.4.4). The temperature dependence of the microwave impedance has a maximum at  $T_N$ , which disagrees with single-band BCS calculations (Jacobs et al., 1995).

Investigating  $\text{HoNi}_2\text{B}_2\text{C}$  one has to consider that between  $T_N$  and  $T_c$  the magnetic and superconducting properties are quite sensitive to the details of the preparation procedure and to small deviations from the ideal stoichiometry (Wagner et al., 1999; Dertinger et al., 2001; Alleno et al., 2001; Behr and Löser, 2005; see also Sections 3.1 and 4.9.3).

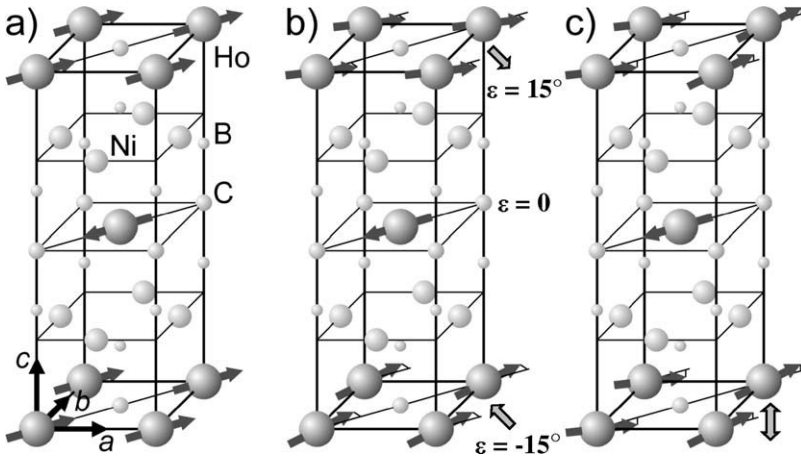


**FIGURE 39** The different magnetic structures of  $\text{HoNi}_2\text{B}_2\text{C}$  as determined by neutron scattering. (a) Commensurate antiferromagnetic. (b) Incommensurate  $c^*$  structure (spiral) with the modulation vector  $\tau_2 = (0, 0, 0.916)$ ; there  $\epsilon$  describes the deviation of the azimuth angle of the local magnetic moments with respect to the commensurate antiferromagnetic structure. (c) A proposed incommensurate  $a^*$  structure (after Kreyßig, 2001). Its modulation vector is  $\tau_3 = (0.585, 0, 0)$ . Its detailed deviations of the azimuth angle of the local magnetic moments are still unknown.

#### 4.9.1 Types of magnetic order in $\text{HoNi}_2\text{B}_2\text{C}$

It has been shown by elastic neutron diffraction that at zero magnetic field in  $\text{HoNi}_2\text{B}_2\text{C}$  three different types of antiferromagnetic order occur which, in a certain temperature range, even may coexist (Grigereit et al., 1994; Goldman et al., 1994; Kreyssig et al., 2005). Upon cooling, the commensurate structure of Figures 28(a) and 39(a) largely forms at  $T_N \approx 5.2$  K. This structure with its ferromagnetic sheets in the tetragonal basal plane is in accord with the results of Cho et al. (1996b) who analyzed the susceptibility of single crystals and found Ho–Ho nearest-neighbor exchange constants that are positive within the basal plane but negative and considerably weaker along the  $c$ -axis. As will be discussed in Section 4.9.4 significant neutron scattering intensity of this structure is also observed above  $T_N$ . Additionally, in the temperature range  $T_N < T < T_c$  there is an incommensurate spiral structure along the tetragonal  $c$ -axis with a modulation vector  $\tau_2 \approx (0, 0, 0.916)$  where, as in the ground state, the magnetic moments are ferromagnetically aligned in the  $\mathbf{a}$ – $\mathbf{b}$ -plane. The ferromagnetic sheets in adjacent layers have a relative orientation of about  $163.4^\circ$  instead of  $180^\circ$  for the ground state (see Figures 39(b) and 39(a)). Utilizing high-resolution X-ray scattering Hill et al. (1996) showed that this  $c$ -axis spiral is characterized by two wave vectors,  $\tau_1 = (0, 0, 0.906)$  and  $\tau_2 = (0, 0, 0.919)$ .

The  $c$ -axis spiral has been successfully described in a quasi-linear mean field model taking into account crystalline electric fields and the RKKY interaction and supposing the presence of the ferromagnetic sheets (Amici and Thalmeier, 1998). Furthermore, in a small temperature range above  $T_N$  an  $\mathbf{a}$ -axis modu-

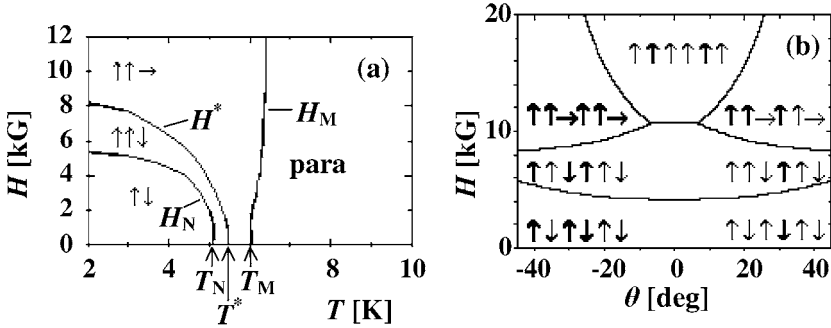


**FIGURE 40** Magnetic phase diagrams of  $\text{HoNi}_2\text{B}_2\text{C}$ . (a) Field  $H$  applied along the tetragonal  $a$ -axis (i.e.  $\theta = \pm 45$  deg; see panel (b)).  $\uparrow\downarrow$  is the antiferromagnetic phase corresponding to Figures 28(a) and 39(a). Here para means the paramagnetic phase steadily changing, with increasing  $H$ , into the saturated (ferromagnetic) state  $\uparrow\uparrow$  which, at low temperatures, is a metamagnetic phase. The metamagnetic phases  $\uparrow\uparrow\downarrow$  and  $\uparrow\uparrow\rightarrow$  are described in the text (after Rathnayaka et al., 1996; Detlefs et al., 2000). (b)  $H$ - $\theta$  phase diagram at  $T = 2$  K, where  $H$  is perpendicular to the  $c$ -axis and has an angle  $\theta$  with respect to the nearest magnetically easy  $[110]$  direction; the meanings of the arrows are as in (a) (after Canfield et al., 1997a).

lated incommensurate magnetization structure occurs with a modulation vector  $\tau_3 \approx (0.58, 0, 0)$  which is close to the nesting vector  $\mathbf{q} \approx (0.55, 0, 0)$  known from other borocarbide superconductors in particular  $\text{LuNi}_2\text{B}_2\text{C}$  and  $\text{YNi}_2\text{B}_2\text{C}$  (see Section 3.2). The exact form of this  $\mathbf{a}^*$  structure is still unknown. From results of neutron diffraction experiments on powder samples Loewenhaupt et al. (1997) and Kreyßig (2001) concluded that the  $\mathbf{a}^*$  structure has an oscillating component of magnetic moments in the  $\mathbf{a}$ - $\mathbf{b}$ -plane as outlined in Figure 39(c). Also a study by Detlefs et al. (2000) of metamagnetic phases suggests that the  $\mathbf{a}^*$  structure has only magnetic moments perpendicular to the  $c$ -axis (see Section 4.9.2). Experimental and theoretical work must be done to clarify the nature of the  $\mathbf{a}^*$  structure and its underlying mechanism which is obviously connected with Fermi surface nesting.

#### 4.9.2 Metamagnetic transitions and magnetoresistance

For magnetic fields  $H$  applied perpendicular to the tetragonal  $c$ -axis of  $\text{HoNi}_2\text{B}_2\text{C}$  single crystals, measurements of magnetization and elastic neutron diffraction show up to three metamagnetic transitions similar to those visible in Figure 36 for  $\text{TbNi}_2\text{B}_2\text{C}$  (Cho et al., 1996b; Rathnayaka et al., 1996; Canfield et al., 1997a; Campbell et al., 2000a; Detlefs et al., 2000; Krutzler et al., 2005). It was concluded that in a strength-of-field angle-of-field phase diagram, besides the paramagnetic phase at elevated temperatures and the simple antiferromagnetic phase ( $\uparrow\downarrow$ ) at low temperatures and low fields, three additional low-temperature phases occur for sufficiently high fields. These metamagnetic phases are denoted by the arrow combinations  $\uparrow\uparrow\downarrow$  and  $\uparrow\uparrow\rightarrow$  in Figure 40.

Here it is assumed that in all of the magnetically ordered phases the local magnetic moments are directed along those  $[110]$  axes that are either near parallel (arrow  $\uparrow$ ) or near antiparallel ( $\downarrow$ ) or near perpendicular ( $\rightarrow$ ) to the applied

field. As a very important result Detlefs et al. (2000 and 2001) found by elastic neutron diffraction at 2 K that the second metamagnetic phase ( $\uparrow\uparrow\rightarrow$ ) has a modulation vector  $\boldsymbol{\tau}_3 \approx (4/7, 0, 0)$  which is close to the nesting vector  $\mathbf{q} \approx (0.55, 0, 0)$  (see Section 3.2). In this experiment the angle  $\theta$  of  $\mathbf{H}$  with respect to the [110] direction was  $15^\circ$ . A similar result has been reported by Campbell et al. (2000a) who made measurements at  $\theta = 45^\circ$ , i.e. for  $\mathbf{H}$  parallel to [100], and found that the second metamagnetic transition results in a magnetic phase that is characterized by an incommensurate wave vector of about  $(0.61, 0, 0)$ . The presence of an  $\mathbf{a}^*$ -metamagnetic phase at 2 K is supported by results of Kreyssig et al. (1999b) who performed elastic neutron-diffraction experiments on  $\text{HoNi}_2\text{B}_2\text{C}$  powders and also detected three different metamagnetic phases.

The extension of the boundaries between the metamagnetic phases to the zero-field boundaries at  $T_N$ ,  $T^*$  and  $T_M$ , as shown in Figure 40, has also been supported by specific-heat measurements by J.-H. Choi et al. (2001) and Park et al. (2004a). The latter authors found a strong anisotropy of the  $H_M$ -vs.- $T$  curves: for fields parallel to the  $\mathbf{a}$ -axis  $H_M$  increases with increasing  $T$  (see Figure 40(a)), while it decreases for fields parallel to [110]. It has been assumed that, upon cooling, the  $\mathbf{a}^*$  phase develops at  $T_M$  and the in-plane anisotropy of  $H_M(T)$  is due to Fermi-surface nesting features. The transition at  $T_N$  is of first order. The commensurate antiferromagnetic low-temperature phase is connected with the lattice distortion described in Section 2.2. The magnetic phase transition at  $T^*$  is described as a change from an  $\mathbf{a}^*$ -dominant phase to a  $\mathbf{c}^*$ -dominant phase, and it cannot be excluded that it is also of first order (Park et al., 2004a). A first-order transition at  $T^*$  would explain the fact that both phases,  $\mathbf{a}^*$  and  $\mathbf{c}^*$  coexist above as well as below  $T^*$ , as has been confirmed in detail by Kreyssig et al. (2005) by elastic neutron diffraction experiments on a  $\text{HoNi}_2\text{B}_2\text{C}$  single crystal prepared by the floating-zone method. Finite neutron-diffraction peak intensities of the commensurate antiferromagnetic structure and of the incommensurate spiral  $\mathbf{c}^*$  appear even above  $T_M$  (Kreyssig et al., 1997; Mi. Schneider et al., 2006; see also Figure 43). These short-range-order or fluctuation phenomena have not yet been investigated in detail.

Further experimental work should be done in order to determine the complete region in the  $H$ - $T$ - $\theta$  space where the phase ( $\uparrow\uparrow\rightarrow$ ) of Figure 40 exists. Also it has to be clarified whether this phase in its whole range of existence is really characterized by an incommensurate propagation vector  $\boldsymbol{\tau}_3 = (\xi_a, 0, 0)$  and how much  $\xi_a$  varies across the phase diagram. It is interesting to note that in  $\text{Ho}_x\text{R}_{1-x}\text{Ni}_2\text{B}_2\text{C}$  compounds with  $\text{R} = \text{Y}$  or  $\text{Lu}$  and  $x \leq 0.25$  the value of  $\xi_a$  weakly increases with increasing  $x$  (Kreyssig et al., 2000). The wave vector  $\boldsymbol{\tau}_3$  is ubiquitous in the quaternary borocarbides (Canfield and Bud'ko, 2001) as: (i) the borocarbide superconductors show Fermi-surface nesting characterized by a nesting vector equal to  $\boldsymbol{\tau}_3$  (see Section 3.2); (ii) in some of the  $\text{RNi}_2\text{B}_2\text{C}$  compounds, in particular for  $\text{R} = \text{Y}$  and  $\text{Lu}$ , phonon softening is observed for a wave vector  $\boldsymbol{\tau}_3$  (see Section 3.3); (iii) zero-field incommensurate magnetization structures with  $\boldsymbol{\tau}_3$  as the modulation vector occur in  $\text{RNi}_2\text{B}_2\text{C}$  for  $\text{R} = \text{Gd}$ ,  $\text{Tb}$ ,  $\text{Ho}$  and  $\text{Er}$  (see Sections 4.6, 4.7, 4.9.1, and 4.10); and (iv) a metamagnetic phase with a modulation vector close to  $\boldsymbol{\tau}_3$  has been reported also for  $\text{TmNi}_2\text{B}_2\text{C}$  (see Section 4.11). Two microscopic approaches

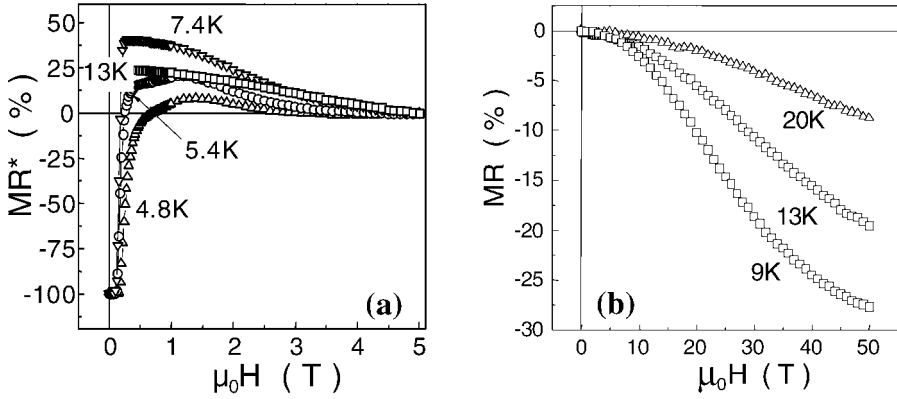


**FIGURE 41** Magnetoresistivity characterized by (a)  $\text{MR}^* = [R(H) - R(5 \text{ T})]/R(5 \text{ T})$ ; (b)  $\text{MR} = [R(H) - R(0)]/R(0)$  of polycrystalline  $\text{HoNi}_2\text{B}_2\text{C}$  as a function of the magnetic field  $H$  (applied parallel to the current), measured at different temperatures.

have been presented in literature, which, until recently, had been believed to reasonably describe the magnetic phase diagram of Figure 40(b).

Amici and Thalmeier (1998) used the quasi one-dimensional model mentioned in Section 4.9.1. In their approach the presence of ferromagnetically ordered Ho layers with the magnetic moments oriented perpendicular to the tetragonal  $c$ -axis is adopted and the competition of the RKKY interaction along the  $c$ -axis with the crystalline electric field is analyzed in order to determine the transition between the commensurate antiferromagnetic structure and the incommensurate  $c^*$  spiral shown in Figure 39.

The so-called clock model of Kalatsky and Pokrovsky (1998) is also a semiclassical approximation which starts with the assumption that the strong single-ion anisotropy confines the Ho magnetic moments to the four  $[110]$  directions. Both models predict the phase boundaries of Figure 40(b) and the temperature dependence of the  $c$ -axis commensurate-to-incommensurate transition surprisingly well. However both models cannot explain the nature and origin of the  $a^*$  phase observed at zero field (see Section 4.9.1) or at a finite field as reported by Detlefs et al. (2000). Possibly these problems can only be solved by a more detailed description of the RKKY interaction, taking into account the Fermi-surface-nesting features.

Abliz et al. (2003) report on S-shaped magnetization-vs.-field curves measured on a  $\text{HoNi}_2\text{B}_2\text{C}$  single crystal in high fields along  $[001]$ . These curves are characterized by a temperature-independent inflection point at about 25 T. The authors attributed this phenomenon to CEF level crossing.

Figure 41 shows that, in the normal state,  $\text{HoNi}_2\text{B}_2\text{C}$  has a considerably large magnetoresistance, MR, of a negative sign. (The positive sign of  $\text{MR}^*$  in Figure 41(a) is due to the alternative normalization of this quantity which has been introduced so that data from normal and superconducting states can be included in the same figure.) The normal-state MR of  $\text{HoNi}_2\text{B}_2\text{C}$  is isotropic concerning the direction of the applied field with respect to the measuring current and it

has been pointed out by Fisher et al. (1997) that the temperature and field dependence of MR can be attributed to spin-disorder scattering. However the large values of MR observed above the magnetic ordering temperature (Figure 41(b)) are not yet explained. May be they are related to magnetic short-range order or low-dimensionality magnetic ordering (Müller et al., 2001a). Such ordering effects at small length scales or in low dimensionality may also be the reason for the high-temperature tails observed for the specific heat (Figure 38(b)) and the neutron scattering intensity (see Section 4.9.4). The large normal-state values of MR\* (Figure 41(a)) may be connected with the reorientation of ordered magnetic moments, i.e. metamagnetic transitions as discussed above. Magnetoresistance measurements have also been successfully used to investigate the hydrostatic-pressure dependence of the metamagnetic transitions in HoNi<sub>2</sub>B<sub>2</sub>C (Oomi et al., 2003b). It was found that the metamagnetic transition fields increase with increasing pressure (of up to 2 GPa).

#### 4.9.3 Reentrant and near-reentrant behavior

Now it is generally accepted that single-phase stoichiometric HoNi<sub>2</sub>B<sub>2</sub>C exhibits the near-reentrant behavior presented in Figure 38(a) although some of the numerous investigated HoNi<sub>2</sub>B<sub>2</sub>C samples show a real reentrant behavior at zero field. It can be summarized that depending on details of the preparation route HoNi<sub>2</sub>B<sub>2</sub>C samples are found to be magnetically ordered superconductors with near-reentrant behavior or reentrant superconductors or even non-superconducting magnetically ordered materials (Schmidt et al., 1995). It has been pointed out by Alleno et al. (2001) that this variation in the superconducting properties may be due to the fact that HoNi<sub>2</sub>B<sub>2</sub>C forms in equilibrium with ferromagnetic phases in the Ho–Ni–B–C system, e.g., HoB<sub>2</sub>C<sub>2</sub> (≈7 K), Ho<sub>2</sub>Ni<sub>3</sub>B<sub>6</sub> (≈12 K), HoNi<sub>4</sub>B (≈6 K), etc. which have Curie temperatures (quoted in the brackets) in the temperature range of interest (4–8 K) and may coexist with HoNi<sub>2</sub>B<sub>2</sub>C microscopically. It is well known that ferromagnetism favors reentrant behavior (see Section 1.3). The formation of such secondary phases is supported by non-stoichiometry. Therefore the chemical characterization of the sample is of prime importance. However, due to the presence of the two light elements B and C the various classical characterization techniques as chemical analysis, intensity analysis of X-ray or neutron diffraction, transition electron microscopy, high-resolution electron microscopy, etc. are almost inefficient in determining composition and occupancy of lattice sites by B and C (see also Section 3.1). Recently the carbon content of the phases in HoNi<sub>2</sub>B<sub>2</sub>C samples could be successfully determined using nuclear- and electron-probe microanalysis (Alleno et al., 2001). Furthermore, it has been stressed by Wagner et al. (1999) and Schmidt and Braun (1998) that HoNi<sub>2</sub>B<sub>2</sub>C has a finite homogeneity range, which may result in a corresponding range of magnetic and superconducting properties. Schmidt et al. (1997), Wagner et al. (1999), Dertinger et al. (2001), and Behr and Löser (2005) could continuously (reversibly as well as irreversibly) change the superconducting properties of HoNi<sub>2</sub>B<sub>2</sub>C samples, in particular the transition temperature  $T_c$  and the reentrant behavior, by appropriate heat-treatment procedures (see also Section 3.1). Uwatoko et al. (1996) have shown that reentrant superconductivity in single-crystalline HoNi<sub>2</sub>B<sub>2</sub>C can also

be induced by hydrostatic pressure of 11 kbar. For increasing pressure they found an increase of  $T_N$  and a decrease of  $T_c$ . These authors attribute their results to an enhanced coupling of the conduction electrons to the Ho magnetic moments, due to the increased pressure. A more detailed investigation of the influence of hydrostatic pressure  $P$  on the superconducting and magnetic properties of  $\text{HoNi}_2\text{B}_2\text{C}$  was done by Dertinger (2001). He found  $dT_c/dP = -0.32 \text{ K/GPa}$  and, depending on whether or not the samples are superconducting (due to the chemical or microstructural variations discussed above),  $dT_N/dP = 0.2 \text{ K/GPa}$  or  $1.4 \text{ K/GPa}$ , respectively, with  $T_N$  as the temperature below which the commensurate antiferromagnetic structure shown in Figures 28(a) and 39(a) appears. Similar results have been reported by Jo et al. (2003) and Akiyama et al. (2006). The latter authors determined  $dT_c/dP = -0.6 \text{ K/GPa}$  and  $dT_N/dP = 0.4 \text{ K/GPa}$  and pointed out that  $T_c$  and  $T_N$  will coincide at a pressure near 3.2 GPa. Interestingly, uniaxial pressure along the [110] direction, up to 0.4 GPa, does not change  $T_c$  but, as expected taking into account the magnetoelastic distortions discussed in Section 2.2, it increases  $T_N$  by about  $dT_N/dP_u = 8 \text{ K/GPa}$  (Kobayashi et al., 2006). From thermal-expansion experiments Ma. Schneider et al. (2007) derived  $dT_c/dP_u = 0.1 \text{ K/GPa}$  for uniaxial pressures  $P_u$  applied along [001].

As a general empirical rule for  $\text{HoNi}_2\text{B}_2\text{C}$  samples, the appearance of reentrant behavior caused by stoichiometric effects, disorder, pressure, or magnetic field is always connected with a reduced value of  $T_c$ . Thus Schmidt (1997) could systematically reduce  $T_c$  and induce reentrant behavior in  $\text{HoNi}_2\text{B}_2\text{C}$  by the substitution of Ni by Co to a minor degree. An example for the influence of heat treatment is

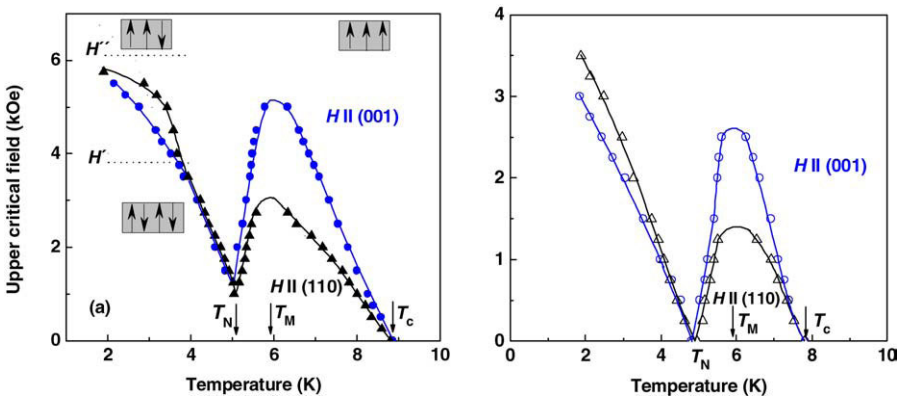


**FIGURE 42** Influence of annealing on the upper critical field  $H_{c2}$  of a  $\text{HoNi}_2\text{B}_2\text{C}$  single crystal (size:  $2 \times 2 \text{ mm}^2$  in the  $\mathbf{a-b}$ -plane, 4 mm in  $c$  direction, prepared by the floating-zone melting method), measured in the [110] and [001] directions. (a) Well-annealed sample (see Section 3.1): near-reentrant behavior, i.e.  $H_{c2}(T)$  has a pronounced minimum near  $T_N$  but it never disappears. The fields  $H'$  and  $H''$  and the arrows will be explained in Section 4.9.5; for  $T_M$ , see Figure 38. (b): As-grown crystal: reentrant behavior, i.e.  $H_{c2}(T) = 0$  at  $T \approx T_N$  (Müller et al., 2007).

shown in Figure 42. As expected the not well annealed sample has the lower  $T_c$  and exhibits reentrant behavior.

Dertinger (2001) also found that the  $\mathbf{a}^*$ -axis modulated structure  $\mathbf{a}^*$  of Figure 39 is much more sensitive to pressure, compared to the other two magnetic structures of Figure 39, and it even disappears at relatively low values of  $P$ . Interestingly he observed near-reentrant behavior also at temperatures and pressures where the  $\mathbf{a}^*$  structure had disappeared. Therefore he concluded that the near-reentrant behavior in  $\text{HoNi}_2\text{B}_2\text{C}$  cannot mainly be caused by the presence of the  $\mathbf{a}^*$  incommensurate magnetic structure. This problem will be further discussed in the next Section 4.9.4.

#### 4.9.4 Interplay of superconductivity and magnetism in $\text{HoNi}_2\text{B}_2\text{C}$

It is obvious that the commensurate antiferromagnetic structure of Figure 39(a) coexists with superconductivity in  $\text{HoNi}_2\text{B}_2\text{C}$ , as in  $\text{DyNi}_2\text{B}_2\text{C}$ . On the other hand, as can be seen in Figures 43(a) and 43(c) the superconductivity is suppressed over the small temperature range where the two incommensurate magnetic structures of Figures 39(b) and 39(c) occur. Now the question arises which of these two magnetic structures is more relevant for the near-reentrant behavior? In  $\text{Y}_{0.15}\text{Ho}_{0.85}\text{Ni}_2\text{B}_2\text{C}$  the situation is totally different (Figures 43(b) and 43(d)). Here the  $\mathbf{a}^*$  structure again is localized at the same temperatures as the reentrant behavior but the  $\mathbf{c}^*$  spiral exists over a broad range of temperature. Thus the  $\mathbf{a}^*$  structure is more closely related to the near-reentrant superconductivity in  $\text{Y}_{0.15}\text{Ho}_{0.85}\text{Ni}_2\text{B}_2\text{C}$  (as well as in  $\text{Lu}_{0.15}\text{Ho}_{0.85}\text{Ni}_2\text{B}_2\text{C}$ , Freudenberger et al., 1998b) than the  $\mathbf{c}^*$  spiral. This seems to be in contradiction to the results of Dertinger (2001) (discussed in Section 4.9.3) who found a near-reentrant behavior of a  $\text{HoNi}_2\text{B}_2\text{C}$  sample in which the  $\mathbf{a}^*$  structure had been suppressed by pressure.

Thus further experiments have to be done to elucidate the connection between the (near-)reentrant behavior and the various magnetic structures in  $\text{HoNi}_2\text{B}_2\text{C}$ . In a theoretical analysis the onset of the  $\mathbf{c}^*$  spiral was found to depress superconductivity (Amici et al., 2000). However this approach does not take into account the presence of the  $\mathbf{a}^*$  structure as well as the multiband electronic structure. As discussed in Section 4.9.1 the  $\mathbf{a}^*$  structure is related to Fermi surface nesting. It was theoretically shown by Machida et al. (1980b) that if antiferromagnetic ordering is connected with Fermi surface nesting the superconducting state may be heavily disturbed. For  $\text{HoNi}_2\text{B}_2\text{C}$  the strong correlation between the near-reentrant behavior and the  $\mathbf{a}^*$  magnetic ordering has first been emphasized by Müller et al. (1997) and has been confirmed also by Canfield and Bud'ko (2001). The crucial role of the  $\mathbf{a}^*$  structure manifests itself also in  $^{57}\text{Fe}$  Mössbauer spectra, which show a magnetic hyperfine field at the Ni-site in  $\text{HoNi}_2\text{B}_2\text{C}$  between  $T_N$  and  $T_c$  (D.R. Sánchez et al., 1996) and in enhanced vortex pinning found by local Hall-probe magnetization measurements (Dewhurst et al., 1999).

#### 4.9.5 Multiband coexistence of superconductivity and magnetism in $\text{HoNi}_2\text{B}_2\text{C}$

As has been shown in Sections 3.3–3.7, the superconducting properties, in particular the behavior of the upper critical field  $H_{c2}$ , of the non-magnetic borocarbides

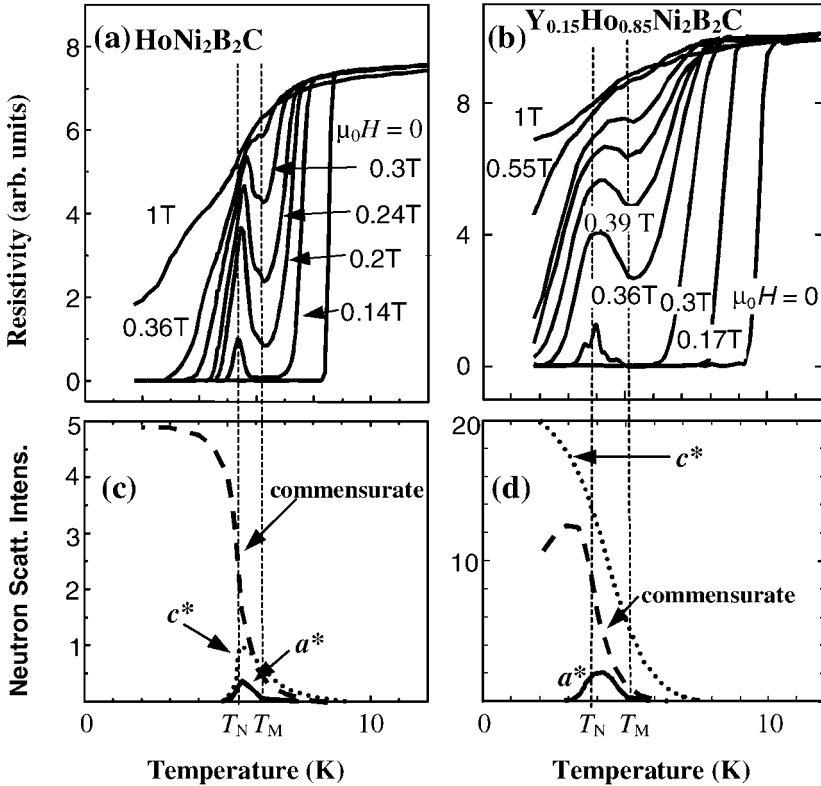


**FIGURE 43** (a) and (b): Resistivity vs. temperature curves for polycrystalline  $\text{HoNi}_2\text{B}_2\text{C}$  and  $\text{Y}_{0.15}\text{Ho}_{0.85}\text{Ni}_2\text{B}_2\text{C}$  samples, respectively, showing reentrant behavior in small magnetic fields. (c) and (d): The comparison with the neutron-diffraction peak intensities shows that the  $a^*$  structure is strongly related to the reentrant behavior (Eversmann et al., 1996; Müller et al., 1997; Kreyszig et al., 1997).  $T_N$  and  $T_M$  have been determined from the minima and the maxima, respectively, in (a) and (b); these values largely agree with  $T_N$  and  $T_M$  determined from specific-heat data (see Section 4.9.5).

$\text{YNi}_2\text{B}_2\text{C}$  and  $\text{LuNi}_2\text{B}_2\text{C}$  can only be understood by taking into account the fact that different (at least two) electron bands participate in the Fermi surface. Thus an interesting question is whether such multiband concept is needed also in the case of the local-moment antiferromagnetic superconductor  $\text{HoNi}_2\text{B}_2\text{C}$  and how it explains the interplay of magnetism and superconductivity in this compound (Müller et al., 2007). As can be seen in Figures 42 and 44, the transition temperature of a well prepared  $\text{HoNi}_2\text{B}_2\text{C}$  single crystal has been found to be as high as  $T_c = 8.8$  K. However, the energy gap determined by point-contact spectroscopy can be well fitted to a BCS gap function vanishing at  $T = T^* \approx 5.6$  K (Naidyuk et al., 2007b) where the specific heat has a special feature that has been attributed to a change, with increasing temperature, from a  $c^*$  dominated to an  $a^*$  dominant magnetic phase (see Section 4.9.2 and Park et al., 2004a). Although the magnitude

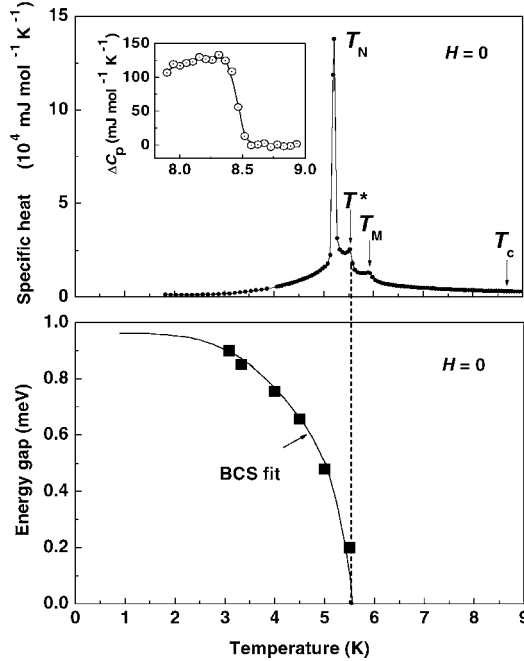


**FIGURE 44** High-quality  $\text{HoNi}_2\text{B}_2\text{C}$  single crystal of Figure 42(a) at zero magnetic field. Upper panel: specific heat with special features at temperatures  $T_N$ ,  $T^*$  and  $T_M$  (as in Figure 38); inset: specific-heat discontinuity at  $T_C$ . Lower panel: energy gap determined by point-contact spectroscopy and fitted to the BCS gap formula (after Müller et al., 2007).

and the temperature dependence of the (small) superconducting gap in the range  $T^* \leq T \leq T_C$  is not yet well investigated, gapless superconductivity (as proposed by Rybaltchenko et al., 1999; see also Section 3.4.4) cannot be excluded. The BCS-like gap together with the isotropy of  $H_{c2}$  observed below  $T_N$  (see Figure 42(a)) strongly suggests that superconductivity in the low-temperature antiferromagnetic phase survives at a pillow-like Fermi surface sheet (FSS; Drechsler et al., 2004) which is isolated from the influence of the lanthanide magnetism localized at other FSSs.

At lower temperatures the critical field  $H_{c2}(T)$  in Figure 42(a) shows some anisotropy in the field range between  $H'$  and  $H''$ . It has been found that the metamagnetic transition between the structures  $\uparrow\downarrow\uparrow\downarrow \dots$  and  $\uparrow\uparrow\downarrow \dots$  does not abruptly take place at a fixed field but is a steady change in the field range between  $H'$  and  $H''$  (Müller et al., 2007). It is not clear whether this is an intrinsic property of that metamagnetic transition for fields along [110] or that the single crystal was slightly misorientated. A similar misorientation of the investigated sample may also be the reason why Park et al. (2004a) determined, from their low-temperature specific heat data, three characteristic fields,  $H_N$ ,  $H^*$  and  $H_M$  (see Figure 40) for metamagnetic-like transitions although, according to Figure 40(b), only two metamagnetic transitions occur along [110] at low temperatures. Naugle et al. (2006)

confirmed that the characteristic fields of the metamagnetic transition crucially depend on the orientation of the sample. Studying  $H_{c2}$  of high-quality biaxially textured  $\text{HoNi}_2\text{B}_2\text{C}$  thin films, [Wimbush and Holzapfel \(2006\)](#) found that the complex magnetic phase diagram of this compound manifests itself in the temperature dependence and the anisotropy of  $H_{c2}$ .

A remarkable anisotropy in  $H_{c2}(T)$  can be seen in [Figures 42\(a\) and 42\(b\)](#), for both the well-annealed and the as-grown single crystal, at temperatures above  $T_N$  and even in the paramagnetic region above  $T_M$ . From a comparison of this phenomenon with the much weaker and opposite anisotropy of  $H_{c2}(T)$  in  $\text{YNi}_2\text{B}_2\text{C}$  (see [Section 3.6](#)) it can be concluded that  $H_{c2}(T)$  is smaller for  $\mathbf{H}$  parallel to  $[110]$  (compared to  $[001]$ ; see [Figure 42](#)) because, due to crystalline electric fields, the magnetic fluctuations have larger components in the tetragonal basal plane. Further contributions to the anisotropy of  $H_{c2}(T)$  may come from anisotropic FSSs possibly contributing to the small- (or even zero-) gap superconductivity in  $\text{HoNi}_2\text{B}_2\text{C}$  at temperatures above  $T^*$  as discussed above.

The inset of [Figure 44](#) shows a significant jump  $\Delta C_p$  of the specific heat  $C_p$  at  $T_c$ . [El-Hagary et al. \(1998\)](#) determined  $\Delta C_p \approx 140 \text{ mJ}/(\text{mol K})$  from  $C_p$  data measured at zero field and at 200 mT where, in the vicinity of  $T_c$ , the superconductivity is suppressed.

To summarize [Section 4.9](#), it can be concluded that a multiband scenario is indispensable for understanding the rich variety of superconducting and magnetic properties in  $\text{HoNi}_2\text{B}_2\text{C}$ . Many of these phenomena, in particular those occurring at temperatures between  $T_N$  and  $T_M$ , are not yet well understood.

#### 4.10 $\text{ErNi}_2\text{B}_2\text{C}$

[Figures 5 and 28](#) as well as [Tables 3 and 7](#) show that superconducting  $\text{ErNi}_2\text{B}_2\text{C}$  starts to order magnetically at 6.8 K in a transversely polarized spin-density wave (SDW) with the modulation vector  $\boldsymbol{\tau} \approx (0.55, 0, 0)$  parallel to the  $\mathbf{a}$ -axis and the Er magnetic moments parallel to  $\mathbf{b}$  (or vice versa; [Sinha et al., 1995](#); [Zarestky et al., 1995](#)). Thus, as already discussed in [Section 4.1](#), the case  $R = \text{Er}$  is the only exception from the simple rule relating the sign of the second Stevens coefficient  $\alpha_J$  with the direction of the staggered magnetization  $\langle \boldsymbol{\mu} \rangle$  with respect to the tetragonal  $\mathbf{c}$ -axis in  $\text{RNi}_2\text{B}_2\text{C}$ . The modulation vector  $\boldsymbol{\tau}$  is close to modulation vectors found in  $\text{GdNi}_2\text{B}_2\text{C}$ ,  $\text{TbNi}_2\text{B}_2\text{C}$ , and  $\text{HoNi}_2\text{B}_2\text{C}$  and to the nesting vector in the  $\text{RNi}_2\text{B}_2\text{C}$  superconductors (see [Section 3.2](#)). [Figure 45](#) shows that a series of up to three metamagnetic transitions occurs in  $\text{ErNi}_2\text{B}_2\text{C}$  if a magnetic field  $\mathbf{H}$  is applied perpendicular to the tetragonal  $\mathbf{c}$ -axis whereas the magnetization-vs.-field curve for  $\mathbf{H}$  parallel to  $\mathbf{c}$  is simply increasing, with a slightly negative curvature, as known for usual antiferromagnets ([Szymczak et al., 1996](#); [Canfield and Bud'ko, 1997](#)). It was shown by elastic neutron diffraction that the first two metamagnetic transitions are due to incommensurate antiferromagnetic states with different values of the  $\mathbf{a}$ -axis modulation, and the third transition is due to a state in which the Er moments are ferromagnetically aligned by the applied field ([Campbell et al., 2000b](#)). A detailed analysis of these transitions, based

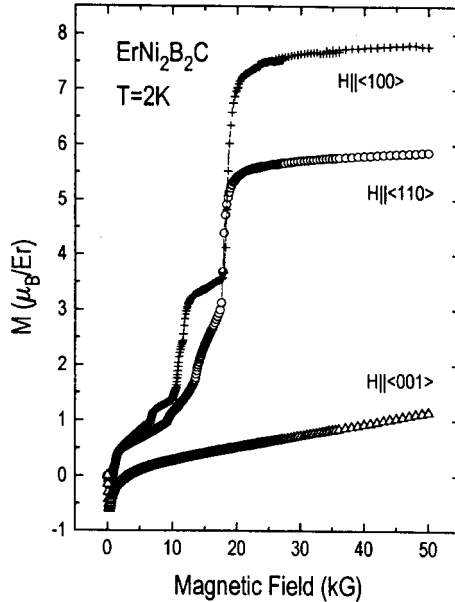


**FIGURE 45** Magnetization ( $M$ )-vs.-field ( $H$ ) curves for different directions of the field  $H$ , showing metamagnetic transitions in  $\text{ErNi}_2\text{B}_2\text{C}$  (from Canfield et al., 1996).

© 1996 Elsevier

on neutron-diffraction data and a mean-field model (J. Jensen, 2002) has been presented by A. Jensen et al. (2004).

#### 4.10.1 Weak ferromagnetism in $\text{ErNi}_2\text{B}_2\text{C}$

Measurements of the specific heat and extrapolation of magnetization-vs.-field curves to zero field indicate, at  $T_{\text{WFM}} = 2.3$  K, a second phase transition to an ordered state that has a net magnetization of roughly  $0.33\mu_{\text{B}}$  per Er atom. This phenomenon is similar to that observed in  $\text{TbNi}_2\text{B}_2\text{C}$  and has been denominated as weak ferromagnetism (WFM; Canfield et al., 1996; El Massalami et al., 2003b, 2003c). The three phase transitions in  $\text{ErNi}_2\text{B}_2\text{C}$  at  $T_{\text{N}}$ ,  $T_{\text{c}}$  and  $T_{\text{WFM}}$  could also be seen in thermal-expansion experiments (Bud'ko et al., 2006b). In using the term WFM one has to be careful because it has already been used for various different phenomena such as: (i) itinerant WFM where both types of itinerant electrons, spin up and spin down are at the Fermi level (examples:  $\text{ZrZn}_2$  and  $\alpha\text{Fe}$ ; Wohlfarth, 1968); (ii) the classical WFM of Dzyaloshinsky–Moriya-type (Dzyaloshinsky, 1957; Moriya, 1960) concerning the staggered localized magnetic moments in antiferromagnets as, e.g., in  $\text{NiF}_2$  or in the ruthenocuprates discussed in Section 1.3.3. Here the combination of exchange interaction, crystalline electric fields, and spin-orbit coupling can be regarded as an antisymmetric exchange interaction which, for sufficiently low lattice symmetry, can lead to spin canting that results in a finite net magnetization; and (iii) canting of the staggered magnetic moments in an antiferromagnet, resulting in a finite net magnetization can also be caused by or-

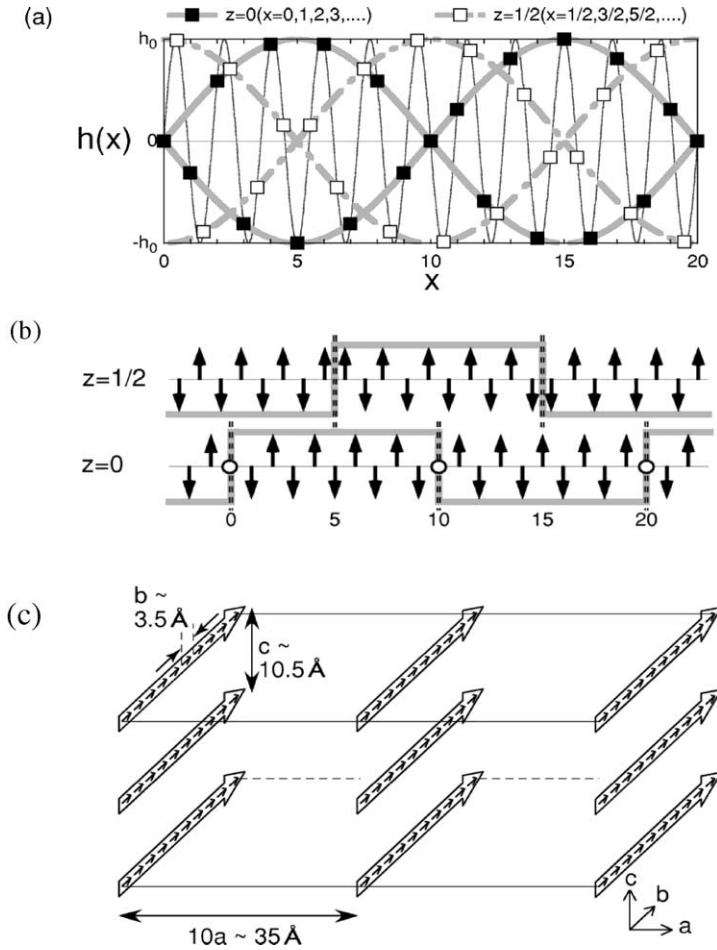


**FIGURE 46** WFM in  $\text{ErNi}_2\text{B}_2\text{C}$  (reprinted figure with permission from Kawano-Furukawa, H., Takeshita, H., Ochiai, M., Nagata, T., Yoshizawa, H., Furukawa, N., Takeya, H., Kadowaki, K., Phys. Rev. B 2002, **65**, 180508(R)). (a) Effective field  $h(x)$ , according to the RKKY interaction, with the wave vector  $\tau = 0.55a^*$ , experienced by Er atoms at the lattice sites characterized by their coordinates  $x$  and  $z$  with the lattice constants as units (thin line). Thick lines describe the long-wave modulation derived from the non-commensurate  $\tau$ . (b) Squared-up SDW in the  $x$ - $y$  plane with magnetic antiphase domain boundaries (dashed lines). In the  $z = 0$  layer the Er magnetic moments at  $x = 0, 10, \dots$  (marked by O) experience  $h(x) = 0$ . Thus they can order ferromagnetically. (c) Resulting overall WFM structure.

© 2002 American Physical Society

dering of electric quadrupolar moments, as observed in  $\text{DyB}_2\text{C}_2$  (see Section 4.1.2). In  $\text{ErNi}_2\text{B}_2\text{C}$  the “WFM” seems to be of totally different nature as Kawano et al. (1999), Kawano-Furukawa et al. (2002a, 2004) and S.-M. Choi et al. (2001) have shown by neutron diffraction: On lowering  $T$  from  $T_N$  the SDW shows squaring-up and finally it locks-in into commensurate antiferromagnetically ordered sec-

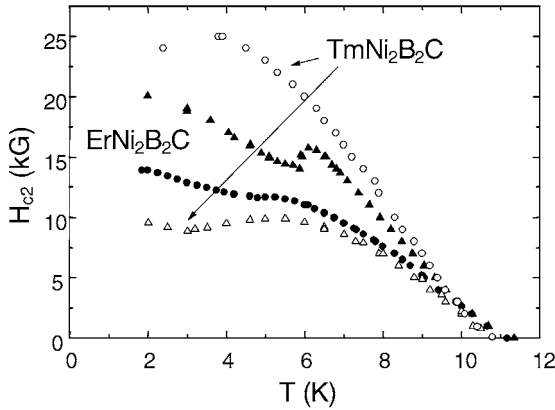


**FIGURE 47** Temperature dependence of the upper critical field  $H_{c2}$  for  $\text{TmNi}_2\text{B}_2\text{C}$  and  $\text{ErNi}_2\text{B}_2\text{C}$  single crystals. Circles:  $H \parallel a$ , triangles:  $H \parallel c$  (after Canfield and Bud'ko, 2001).

tions separated by antiphase boundaries in the magnetic structure, carrying ferromagnetically ordered magnetic moments that form a simple orthorhombic unit cell of  $10a \times b \times c$  (see Figure 46(c)). There it can be seen, that the “WFM” structure consists of ferromagnetic sheets in the  $\mathbf{b}$ - $\mathbf{c}$ -plane with  $\mathbf{b}$  as the magnetically easy axis, that are stacked along the  $\mathbf{a}$ -axis. Due to SDW-squaring-up the paramagnetic  $\text{Er}^{3+}$  moments are present already at temperatures above  $T_{\text{WFM}}$ . It is not yet well known what kind of magnetic interaction is responsible for the alignment of these moments at  $T_{\text{WFM}}$  (Kawano-Furukawa et al., 2002a). Walker and Detlefs (2003) have theoretically shown that certain types of the above mentioned locking-in of the SDW are necessary for WFM to occur. Schmiedeshoff et al. (2002) found a characteristic feature of the magnetoresistance of  $\text{ErNi}_2\text{B}_2\text{C}$  at a temperature  $T_0$  close to  $T_{\text{WFM}}$ . Since  $T_0$  is independent of applied fields up to 18 T these authors consider it unlikely that the WFM in  $\text{ErNi}_2\text{B}_2\text{C}$  is as simply coupled to the antiferromagnetic state as discussed above and suggested in Figure 46.

#### 4.10.2 Coexistence of ferromagnetism and superconductivity in $\text{ErNi}_2\text{B}_2\text{C}$

In  $\text{ErNi}_2\text{B}_2\text{C}$  the upper critical field  $H_{c2}$  is strongly anisotropic and has some irregularity at  $T_N$  (see Figure 47) but it shows a less pronounced near-reentrant behavior than  $\text{HoNi}_2\text{B}_2\text{C}$  (Cho et al., 1995c; Canfield et al., 1998; Bud'ko and Canfield, 2000a). To understand the anisotropy of  $H_{c2}$ , details of the incommensurate magnetic structures and features of the conduction-electron structure (e.g., Fermi surface nesting), which influence the 4f-moment magnetism via RKKY interaction, as well as crystalline electric fields resulting in anisotropy of magnetic and superconducting properties would have to be taken into account. A study of scanning tunneling spectroscopy (STS; Watanabe et al., 2000) showed a superconducting gap anomaly at the antiferromagnetic-ordering temperature. Its analysis suggested the influence of the spin ordering on the superconducting gap structure. These results have been confirmed by photoemission spectroscopy by Baba et al. (2006a) who observed strong magnetic pair breaking and a possible weakening of

the superconductivity by the antiferromagnetism. Crespo et al. (2006) explained STS results by a superconducting gap opening only on a fraction of the Fermi surface, which supports a multiband description, but could not completely rule out surface magnetic effects.

Even more exciting is that  $\text{ErNi}_2\text{B}_2\text{C}$  is the first example of true microscopic coexistence of ferromagnetism and superconductivity without any reentrant behavior. There is no doubt that, as in the case of other  $\text{RNi}_2\text{B}_2\text{C}$  superconductors (see Section 3.5), the superconductivity in  $\text{ErNi}_2\text{B}_2\text{C}$  is of singlet-pairing nature. Since the London penetration depth  $\lambda \approx 70$  nm in  $\text{ErNi}_2\text{B}_2\text{C}$  (Gammel et al., 1999a) is much larger than the spacing between the ferromagnetic layers (see Figure 46) it should be a good approximation considering the material homogeneously magnetized with a net magnetization  $\mu_0 M_s \approx 0.6$  T being equivalent to  $0.3\mu_B$  per Er atom (Bluhm et al., 2006), which is close to the lower critical field  $H_{c1}$  (Ng and Varma, 1997; Bud'ko and Canfield, 2006). Therefore an interesting question is whether a spontaneous vortex state (SVS) develops at  $T < T_{\text{WFM}}$  and in zero external field  $H$  (see Section 1.3.3). Reports on SVS in  $\text{ErNi}_2\text{B}_2\text{C}$  (e.g., Kawano-Furukawa et al., 2001) based on small-angle neutron scattering data turned out to be inconclusive. In these experiments, a magnetic field was applied to align ferromagnetic domains. After removing the field, the vortex lattice was found to persist below  $T_{\text{WFM}}$  but disappeared above it. However, in such an experiment trapped flux below  $T_{\text{WFM}}$  cannot be ruled out, remaining in the superconductor (as a metastable state) due to enhanced pinning below  $T_{\text{WFM}}$ . Recently, evidence for the existence of an SVS in  $\text{ErNi}_2\text{B}_2\text{C}$  has been provided by a penetration depth study (Chia et al., 2006). A maximum appearing in the in-plane penetration depth  $\Delta\lambda(T)$  at  $T = 0.45$  K was assigned to the proliferation and freezing of spontaneous vortices. However, no spontaneous vortex lattice could be found by scanning Hall probe imaging of  $\text{ErNi}_2\text{B}_2\text{C}$  down to 1.9 K (Bluhm et al., 2006). Instead of this, a weak, random magnetic signal was observed in the ferromagnetic phase below  $T_{\text{WFM}}$ . A reason for this discrepancy could be that the elastic properties of an SVS differ drastically from those of a conventional external-field-induced vortex lattice (Radzihovsky et al., 2001). Thus it is still an open question whether or not a spontaneous vortex state is the thermal-equilibrium state in  $\text{ErNi}_2\text{B}_2\text{C}$  below  $T_{\text{WFM}}$ .

The WFM is assumed to cause enhanced flux pinning in  $\text{ErNi}_2\text{B}_2\text{C}$  because, upon cooling, the critical current density  $j_c$  dramatically increases at  $T_{\text{WFM}}$  (Gammel et al., 2000a). Significant vortex pinning is also observed in the temperature range above 2.3 K and has been attributed to the formation of antiferromagnetic domain walls at  $T < T_N$  and pinning at the domain walls (Saha et al., 2001; Vinnikov et al., 2005). Saha et al. (2001) observed an enhanced magnetic stray field near the domain walls by magneto-optical investigations and concluded that localized ferromagnetic spin components at twin boundaries between antiferromagnetic domains cause enhanced flux pinning. Recent data for  $\text{ErNi}_2\text{B}_2\text{C}$  with single-vortex resolution obtained by scanning Hall probe imaging (Bluhm et al., 2006) and Bitter decoration (Vinnikov et al., 2005) strongly suggest that the variation of the observed stray field is due to a higher density of vortices at the twin boundaries. For sufficiently large fields  $\text{ErNi}_2\text{B}_2\text{C}$  shows a hexagonal-

to-square vortex lattice transition (Eskildsen et al., 1997b) similar as observed in non-magnetic RNi<sub>2</sub>B<sub>2</sub>C superconductors (see Section 5).

#### 4.11 TmNi<sub>2</sub>B<sub>2</sub>C

The temperature dependence of the specific heat  $C_p(T)$  of TmNi<sub>2</sub>B<sub>2</sub>C shows pronounced anomalies at the critical temperature  $T_c = 11$  K and the magnetic ordering temperature  $T_N = 1.5$  K. This is different from the behavior of HoNi<sub>2</sub>B<sub>2</sub>C where the magnetic contribution to  $C_p(T)$  dominates (Figure 38) due to the higher value of  $T_N$  and the smaller difference  $T_c - T_N$  in HoNi<sub>2</sub>B<sub>2</sub>C compared to TmNi<sub>2</sub>B<sub>2</sub>C. Neutron diffraction revealed a transversely polarized spin-density wave as the ground-state magnetic order in TmNi<sub>2</sub>B<sub>2</sub>C with magnetic moments parallel to  $c$  (see Figure 28 and Table 8) and a modulation vector  $\tau_F = (0.093, 0.093, 0)$  (Skanthakumar and Lynn, 1999). Thus TmNi<sub>2</sub>B<sub>2</sub>C is the only magnetic RNi<sub>2</sub>B<sub>2</sub>C superconductor with the magnetic moments parallel to the tetragonal  $c$ -axis, which, however, is a natural consequence of  $\alpha_j$  being positive for Tm<sup>3+</sup> (see Section 4.1, in particular Table 8). From crystal field excitations determined by inelastic neutron scattering the saturated magnetic moment of TmNi<sub>2</sub>B<sub>2</sub>C has been calculated to be  $4.7\mu_B$  per Tm site (Gasser et al., 1996) which is considerably larger than the mean staggered magnetic moment observed by elastic neutron diffraction (Table 8). Gasser et al. (1998b) explained this discrepancy by the presence of two different magnetic moments, one close to the calculated value and one of about  $0.1\mu_B$  as observed by Mulders et al. (1998) using Mössbauer spectroscopy and  $\mu$ SR, which may be due to boron-carbon disorder. For applied in-plane magnetic fields  $H$  above 0.9 T Nørgaard et al. (2000, 2004) found a low-temperature field-induced incommensurate antiferromagnetic order with a wave vector  $\tau_A = (0.48, 0, 0)$  which is relatively close to the nesting vector  $\mathbf{q} = (0.55, 0, 0)$  discussed in Section 3.2. The staggered magnetic moment of this structure is parallel to the tetragonal  $c$ -axis. Andersen et al. (2006a) report on an incommensurate quadrupole order for  $T < 13.5$  K,  $H = 0$ , which has the same propagation vector  $\tau_A$  as the low-temperature field-induced magnetic structure. Later they stated more precisely that long-range quadrupole order appears below  $T_Q \approx 8$  K whereas between 8 K and 13.5 K short-range quadrupole order is observed (see Figure 48). Furthermore these authors found that the  $\tau_A$  magnetic structure can also be field-induced in the quadrupolar phase, i.e. in the temperature range  $T_N < T < T_Q$ , and  $T_Q$  increases with increasing  $H$ . Both a field-induced antiferromagnetic structure with its staggered magnetic moment perpendicular to  $\mathbf{H}$  and an increase of  $T_Q$  with increasing  $H$  have also been found in other materials that exhibit quadrupolar ordering as, e.g., CeB<sub>6</sub>. There the effects of  $H$  have been attributed to the assistance of field-induced dipolar and octupolar moments and the suppression of competing quadrupolar fluctuations (see Goodrich et al., 2004, and references cited therein). An interesting question is whether the antiferromagnetic order develops steadily if  $H$  is increased in the temperature range  $T_N < T < T_Q$  or if there is a real field-induced phase transition from paramagnetism to antiferromagnetism as implied by Nørgaard et al. (2004).

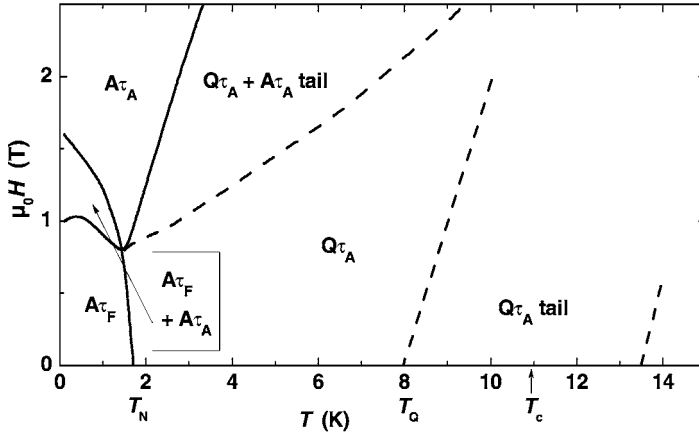


**FIGURE 48** Tentative temperature-field phase diagram (for  $\mathbf{H}||[100]$ ) of  $\text{TmNi}_2\text{B}_2\text{C}$  (after Andersen et al., 2006b). Here  $A\tau_F$  and  $A\tau_A$  are the antiferromagnetic phases with the wave vectors  $\tau_F = (0.093, 0.093, 0)$  and  $\tau_A = (0.48, 0, 0)$ , respectively, and  $Q\tau_A$  is the quadrupolar phase.  $A\tau_A$  tail and  $Q\tau_A$  tail denote phases with short-range ordered  $A\tau_A$ - and  $Q\tau_A$ -like phases, respectively. Dashed lines mark phase boundaries that are not yet well determined. Below  $T_Q$  and  $T_N$  long-range quadrupolar and antiferromagnetic order, respectively, occur at zero field,  $H = 0$ .  $T_c$  is the superconducting transition temperature.

From the temperature dependence of the superconducting gap in  $\text{TmNi}_2\text{B}_2\text{C}$  as observed by scanning tunneling spectroscopy (Suderow et al., 2001) a BCS-like superconductivity has been confirmed. A small gap anisotropy was found to be possible but gap nodes were ruled out. A fit using a two-band model agreed well with the spectroscopic data.

Figure 47 shows that, contrary to the case of  $\text{ErNi}_2\text{B}_2\text{C}$ ,  $H_{c2}$  of  $\text{TmNi}_2\text{B}_2\text{C}$  is larger for  $\mathbf{H}\perp\mathbf{c}$  than for  $\mathbf{H}||\mathbf{c}$ . This is in accord with results of Cho et al. (1995b) who found a larger paramagnetic susceptibility in  $\text{TmNi}_2\text{B}_2\text{C}$  for  $\mathbf{H}||\mathbf{c}$ , resulting in a larger Tm-sublattice magnetization. Consequently, a larger effective field acting on the conduction electrons via exchange interaction is expected for  $\mathbf{H}||\mathbf{c}$ . The non-monotonic  $H_{c2}(T)$  dependence has been described phenomenologically by Jensen and Hedegård (2007). Nagarajan et al. (1999) showed by muon spin relaxation ( $\mu\text{SR}$ ) that in  $\text{TmNi}_2\text{B}_2\text{C}$  quasistatic magnetic correlations persist up to 50 K which possibly represent magnetic short-range order along the magnetically easy  $\mathbf{c}$ -axis for  $T > T_N = 1.5$  K. This is also supported by a study by Naugle et al. (1999b) who found a negative transverse magnetoresistance for  $\mathbf{H}||\mathbf{c}$ , up to temperatures of at least 20 K.

For fields applied along the  $\mathbf{c}$ -axis several magnetic flux line lattice (FLL) symmetry transitions as well as transitions of the magnetic structure which are hysteretic have been observed by small-angle neutron scattering (Eskildsen et al., 1998, 1999; Paul et al., 2001). Results of neutron scattering experiments for both  $\mathbf{H}||\mathbf{a}$  and  $\mathbf{H}||\mathbf{c}$  have been summarized by Eskildsen et al. (2001a) in magnetic field-*vs.*-temperature FLL phase diagrams for  $\text{TmNi}_2\text{B}_2\text{C}$  (see also Section 5.2).

## 4.12 YbNi<sub>2</sub>B<sub>2</sub>C

The Yb atom is symmetric to the Ce atom insofar as it has one hole in its 4f electron shell instead of one electron. It is well known that many Ce- and Yb-based compounds show effects of hybridization of the f electrons with the (s, p, d) conduction electrons. Since the 4f shell is smaller in Yb than in Ce the degree of hybridization in Yb compounds is expected to be weaker than in their Ce homologs. Indeed, according to the lattice constants of YbNi<sub>2</sub>B<sub>2</sub>C (Siegrist et al., 1994b) Yb can be considered close to trivalent in this compound (see Figure 29), which is in agreement with the result of X-ray absorption L<sub>III</sub>-edge studies by Dhar et al. (1996). From de Gennes scaling roughly valid for heavy R elements in RNi<sub>2</sub>B<sub>2</sub>C (see Section 1.4) one would expect YbNi<sub>2</sub>B<sub>2</sub>C to be a magnetic superconductor with  $T_c$  of about 12 K and a magnetic ordering temperature of 0.4 K. However, no indications of a superconducting or a magnetic transition were observed down to  $\approx 0.05$  K (Lacerda et al., 1996; Bonville et al., 1999). These anomalies are connected with a heavy-fermion behavior of the system. Specific-heat measurements at low temperatures yield a Sommerfeld coefficient  $\gamma_N$  of 530 mJ/(mol K<sup>2</sup>) which is larger by a factor of 50 than  $\gamma_N$  for the non-magnetic LuNi<sub>2</sub>B<sub>2</sub>C and indicates an enhanced effective electron mass, due to the above mentioned effects of hybridization (Yatskar et al., 1996; Dhar et al., 1996; Beyermann et al., 1999). A Kondo temperature  $T_K \approx 11$  K has been derived from these specific-heat data by using a single-impurity approach. Resistivity-vs.-temperature measurements on Yb<sub>x</sub>Lu<sub>1-x</sub>Ni<sub>2</sub>B<sub>2</sub>C show that  $T_K$  only weakly varies with the concentration  $x$  (Bud'ko et al., 1997; see also S. Li et al., 2006). Inelastic neutron scattering (Sierks et al., 1999; Boothroyd et al., 2001, 2003; Rotter et al., 2001) yield nearly twice as high energy levels of the four Kramers doublets compared to a CEF approach valid for other RNi<sub>2</sub>B<sub>2</sub>C compounds (Gasser et al., 1996). From the width of the quasielastic neutron-diffraction peak the Kondo temperature has been estimated to be  $T_K \approx 25$  K (Boothroyd et al., 2003). The magnetic susceptibility shows a Curie-Weiss behavior above 150 K (Yatskar et al., 1996; Dhar et al., 1996) with the paramagnetic moment close to that of free Yb<sup>3+</sup> ions (see Table 8). Also <sup>11</sup>B-NMR data indicate that YbNi<sub>2</sub>B<sub>2</sub>C is non-magnetic for  $T < 5$  K but it has local Yb magnetic moments for higher temperatures (Sala et al., 1997). Microscopic evidence of zero Yb magnetic moments in YbNi<sub>2</sub>B<sub>2</sub>C at low temperatures is provided by <sup>170</sup>Yb Mössbauer spectroscopy (Bonville et al., 1999). Indication of 4f conduction-band hybridization in YbNi<sub>2</sub>B<sub>2</sub>C was also obtained from polarization-dependent X-ray-absorption near-edge structure (XANES) studies at the B-K, C-K, and Ni-L<sub>III</sub> thresholds (Mazumdar et al., 2001), and from studies of the thermal variation of the quadrupole hyperfine interaction using the <sup>172</sup>Yb perturbed angular correlation technique (Rams et al., 2000). In Yb<sub>x</sub>Lu<sub>1-x</sub>Ni<sub>2</sub>B<sub>2</sub>C a very rapid suppression of superconductivity with increasing  $x$  (much more rapid than in Gd<sub>x</sub>Lu<sub>1-x</sub>Ni<sub>2</sub>B<sub>2</sub>C) has been reported (Bud'ko et al., 1997; Rathnayaka et al., 1999) and has been attributed to pair breaking effects of Kondo impurities as described by Müller-Hartmann and Zittartz (1971).

The resistivity of YbNi<sub>2</sub>B<sub>2</sub>C decreases monotonically with decreasing temperature, but drops pronouncedly below  $\approx 50$  K (Yatskar et al., 1996; Dhar et al., 1996;

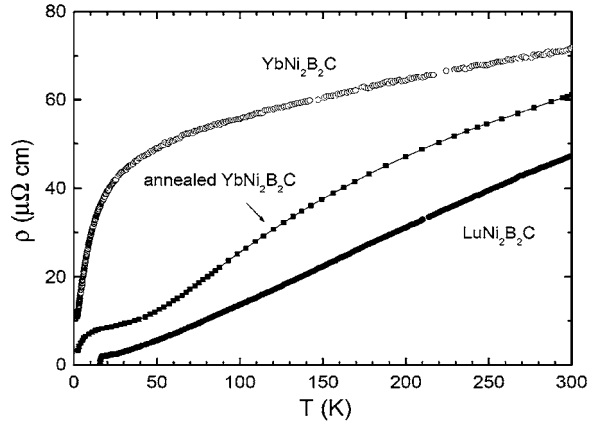


**FIGURE 49** Temperature dependence of the resistivity of different  $\text{YbNi}_2\text{B}_2\text{C}$  samples compared with that of  $\text{LuNi}_2\text{B}_2\text{C}$ . After Avila et al. (2004).

Avila et al., 2004). A quadratic temperature dependence of the resistivity was found below 1.5 K, which is a characteristic feature of strong electron correlation (Yatskar et al., 1996). Figure 49 shows that the resistivity-vs.-temperature curves can be drastically modified by annealing the  $\text{YbNi}_2\text{B}_2\text{C}$  samples, which has been explained by ligand disorder leading to local distributions of  $T_K$  (Avila et al., 2004).

A complicated behavior of the magnetoresistance MR was found by Lacerda et al. (1996), Yatskar et al. (1999) and Christianson et al. (2001). Above 5 K, the transverse MR is negative and approximately isotropic, whereas at low  $T$  it is strongly anisotropic with respect to the crystal axes and changes its sign below 1 K for  $\mathbf{H} \perp \mathbf{c}$ . A strong temperature dependence of the Hall coefficient  $R_H$  was reported by Narozhnyi et al. (1999b), which is in contrast with the weakly temperature-dependent  $R_H$  observed for several other borocarbides (see Section 3.4.2).

As has been pointed out by Boothroyd et al. (2003) a detailed analysis of the low-temperature thermodynamic, transport and magnetic data of  $\text{YbNi}_2\text{B}_2\text{C}$  shows significant deviations from Fermi-liquid behavior. Therefore these authors conjecture that  $\text{YbNi}_2\text{B}_2\text{C}$  is close to a quantum critical point on the non-magnetic side of a transition to a magnetic ground state, and that the mentioned deviations are due to corresponding quantum fluctuations. Such a transition is suggested by the fact that with increasing strength of the interaction between  $f$  and  $(s, p, d)$  electrons a regime of magnetic ground states will firstly be replaced by a heavy-fermion regime and then by a regime of intermediate valence (Grewe and Steglich, 1991).

## 5. VORTEX LATTICES IN $\text{RNi}_2\text{B}_2\text{C}$ SUPERCONDUCTORS

### 5.1 Non-magnetic borocarbides

According to Abrikosov (1957), magnetic flux penetrates type-II superconductors as a periodic arrangement of quantized magnetic flux lines or vortices, i.e. a vor-

tex lattice. An isolated vortex is characterized by two length scales, the coherence length  $\xi$  and the penetration depth  $\lambda$ , where  $\lambda > \xi$ . The coherence length is the distance over which the superconducting order parameter  $\Delta(r)$  rises from zero at  $r = 0$ , the center of the vortex, to its value  $\Delta_c$  outside the vortex core. Thus, the coherence length is related to the radius of the vortex core. The vortex core is surrounded by circulating supercurrents, which generate the magnetic field of the vortex. Both, supercurrents and field decay over the penetration depth  $\lambda$ .

In isotropic systems, the flux lines form a two-dimensional hexagonal lattice, which is favored by the repulsive nature of the vortex interaction because, for given flux-line density, the vortex spacing of a hexagonal lattice is larger than that of a square lattice. Hexagonal vortex lattices have been observed in many superconductors by small-angle neutron scattering (SANS), electron microscopy, magneto-optical or other techniques and, in recent years, also by scanning tunneling microscopy (STM; see Brandt, 1995). However, even in conventional type-II superconductors with an isotropic gap such as PbTl (Obst, 1969), Nb (Christen et al., 1980), and  $V_3Si$  (Yethiraj et al., 1999), a hexagonal-to-square vortex-lattice transition was found to occur when the magnetic field was applied along a four-fold symmetric axis of the crystal structure. This phenomenon has attracted large interest after similar transformations had been detected in a number of superconductors as the borocarbides  $RNi_2B_2C$  ( $R = Er, Y, Lu, Tm$ ; Yaron et al., 1996; Yethiraj et al., 1997; De Wilde et al., 1997; Eskildsen et al., 1998), the heavy-fermion compound  $CeCoIn_5$  (Eskildsen et al., 2003), the p-wave superconductor  $Sr_2RuO_4$  (Riseman et al., 1998), and several high- $T_c$  cuprates with d-wave pairing symmetry as  $La_{2-x}Sr_xCuO_4$  (Gilardi et al., 2002),  $YBa_2Cu_3O_7$  (Brown et al., 2004), and  $Nd_{1.85}Ce_{0.15}CuO_4$  (Gilardi et al., 2004). The transition from the hexagonal to the square vortex lattice is caused by the competition between certain sources of anisotropy and the repulsive vortex-vortex interaction. The competing anisotropy favoring a square vortex lattice may be due to the anisotropy of the Fermi surface or anisotropy in the superconducting order parameter, in particular in cases of unconventional superconductivity (d- or p-wave pairing).

### 5.1.1 Hexagonal and square vortex lattice

$RNi_2B_2C$  compounds are s-wave superconductors with some peculiarities pointing to a strongly anisotropic gap or a multiband scenario (see Section 3.5). The hexagonal-to-square transition of the vortex lattice in these compounds for applied fields along the  $c$ -axis was found to arise from the square cross-section of a single vortex. The square symmetry of a single vortex in  $YNi_2B_2C$  was proved by the strong in-plane anisotropy of the penetration depth of  $\lambda_{100}/\lambda_{110} = 1.45$  found in a SANS study (Yethiraj et al., 1998). The local field contour of a vortex in  $YNi_2B_2C$  for applied fields  $\mathbf{H}||c$  at a distance of  $\approx\lambda$  from the center of the vortex core is shown schematically in Figure 50(a). Later it was shown by scanning tunneling spectroscopy (STS; Nishimori et al., 2004) that the vortex cores in  $YNi_2B_2C$  have a corresponding four-fold symmetry. The star-shaped image of the vortex core shown in Figure 50(b) demonstrates that the quasiparticle density of states extends toward the  $a$ -axis, which is consistent with the shape of the field contour in Figure 50(a).

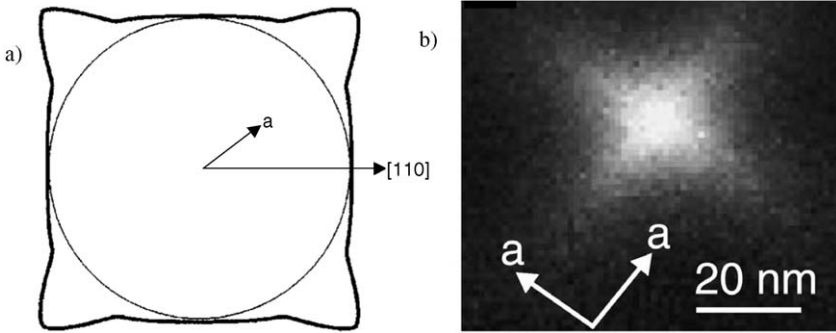


**FIGURE 50** Single vortex in  $\text{YNi}_2\text{B}_2\text{C}$ . (a) Constant local-field contour at a distance of  $\approx \lambda$  from the center of the vortex core (after Yethiraj et al., 1998). (b) Vortex core imaged by STS (from Nishimori et al., 2004).

© 2004 Physical Society of Japan

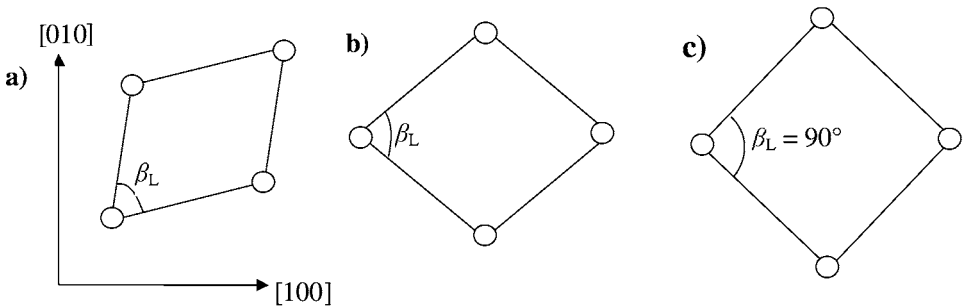


**FIGURE 51** Vortex lattice in  $\text{YNi}_2\text{B}_2\text{C}$  schematically derived from SANS investigations at 2 K in magnetic fields applied along the  $c$ -axis. (a)  $\mu_0 H = 0.1$  T; (b) 0.15 T; (c) 0.45 T (after Levett et al., 2002).

Because at low fields the distance between vortices is large, the hexagonal vortex lattice is not affected by the four-fold symmetry of vortices. However, the square lattice becomes energetically favorable at higher fields, when the intervortex distance becomes comparable to the penetration depth. In the non-magnetic compounds  $\text{YNi}_2\text{B}_2\text{C}$  and  $\text{LuNi}_2\text{B}_2\text{C}$ , a rhombically distorted vortex lattice was observed by SANS measurements at low magnetic fields, i.e. the apex angle  $\beta_L$  along the long diagonal of the unit cell of the vortex lattice is smaller than the usual  $60^\circ$  for a hexagonal vortex lattice. The diagonal of this unit cell is aligned with the crystallographic  $[110]$  axis as shown in Figure 51(a). Before the hexagonal-to-square lattice transition occurs, the rhombic vortex lattice undergoes a first-order jump in  $\beta_L$  to a value larger than  $60^\circ$  (see Figure 51(b)). With increasing applied field, the apex angle  $\beta_L$  continuously increases and, above a transition field  $H_2(T)$ , a square lattice is formed (see Figure 51(c)).

STS images of the vortex lattice in  $\text{YNi}_2\text{B}_2\text{C}$  corresponding to the configurations in Figures 51(b) and 51(c) are shown in Figure 52. The investigated  $\text{YNi}_2\text{B}_2\text{C}$

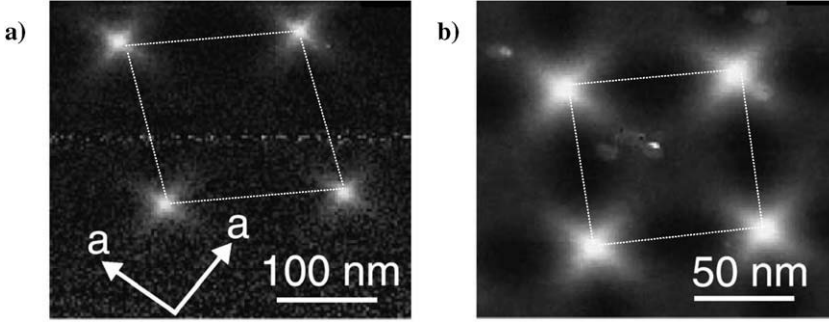


**FIGURE 52** Vortex lattice in  $\text{YNi}_2\text{B}_2\text{C}$  imaged by plotting the local quasiparticle density of states at 0.46 K in magnetic fields  $\mathbf{H}$  applied along the  $c$ -axis. (a)  $\mu_0 H = 0.07$  T; (b) 0.3 T (after Nishimori et al., 2004).

single crystal grown by the floating-zone method had a residual resistivity ratio of about 29 and a Ginzburg–Landau (GL) parameter  $\kappa_{\text{GL}} = \lambda/\xi = 17$  and was found to be in the clean limit. The crystal lattice of a clean  $\mathbf{a}$ – $\mathbf{b}$ -surface obtained by cracking the single crystal at 4.2 K was imaged in atomic resolution by scanning tunneling microscopy (STM). The low-field STS image of the vortex lattice obtained at  $\mu_0 H = 0.07$  T ( $T = 0.46$  K) shows a rhombic vortex lattice. The diagonal of the unit cell is aligned with the crystallographic  $\mathbf{a}$ -axis as in Figure 51(b). The square lattice of the high-field image was measured at  $\mu_0 H = 0.3$  T ( $T = 0.46$  K). Due to the high resolution of this image, the star-shaped cores of the vortices become nicely visible. The pronounced quasiparticle states extend towards the diagonal of the vortex-lattice unit cell or the crystallographic  $\mathbf{a}$ -axes. As a result, a square lattice with diagonals along the crystallographic  $\mathbf{a}$ -axes is formed as the minimum energy configuration at high magnetic fields.

As mentioned above, a square vortex lattice can arise from an underlying anisotropy of either the Fermi surface (via the Fermi velocity  $v_{\text{F}}$ ) or the superconducting energy gap. The reason is that in the region around the vortex core, the local relation between the current density  $\mathbf{j}(\mathbf{r})$  and the vector potential  $\mathbf{A}$  of the standard Ginzburg–Landau theory becomes non-local due to the finite spatial extent of the cooper pair (BCS coherence length)  $\xi_0 = \hbar v_{\text{F}}/\pi\Delta_0$  with  $\Delta_0$  as the superconducting gap at  $T = 0$ , i.e. the current density  $\mathbf{j}$  at each point is determined by the vector potential  $\mathbf{A}$  within a domain size of approximately  $\xi_0$  around the coordinates of this point. In the framework of a microscopic theory it was shown that quasiparticles with energies  $E > \Delta(0)$  contribute to the spatial structure of the core of an isolated vortex (Caroli et al., 1964; Gygi and Schlüter, 1991). Far from the vortex cores, the non-local corrections vanish. Using non-local corrections to the London model (London and London, 1935a, 1935b) which describes superconductors with large GL parameters  $\kappa_{\text{GL}}$ , Kogan et al. (1997a, 1997b) coupled in their non-local London model the vortex structure to the anisotropy of the Fermi surface. The relevant Fermi velocities were derived from band-structure calculations using Fermi-surface averaged higher momenta for  $v_{\text{F}}$ . This way the anisotropy of the fast electrons dominates. This model suc-

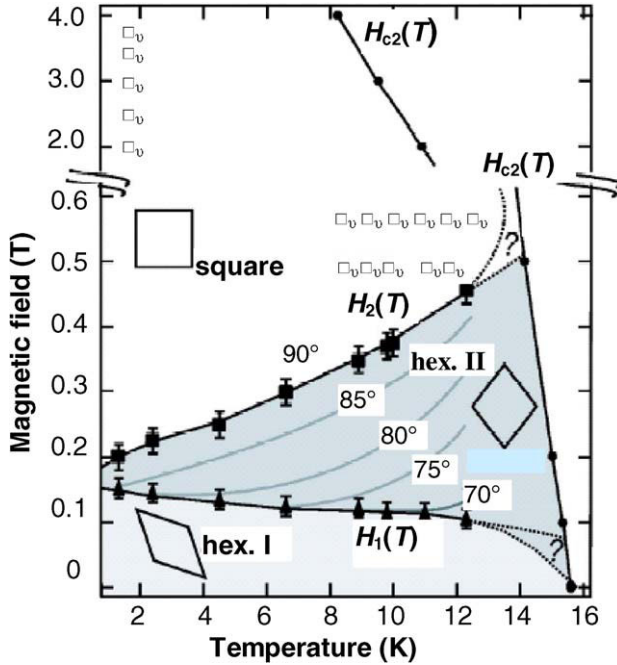


**FIGURE 53** Vortex phase diagram of  $\text{YNi}_2\text{B}_2\text{C}$  for  $\mathbf{H}||\mathbf{c}$  showing separated regions dominated by a hexagonal vortex lattice at low applied fields ( $H < H_1(T)$ ; hex. I), a reoriented hexagonal vortex lattice (hex. II) for applied fields between  $H_1(T)$  and  $H_2(T)$ , and a square vortex lattice at high applied fields ( $H > H_2(T)$ ). Contours of constant vortex-lattice angle  $\beta_L$  (see Figure 51) are shown schematically. The symbols  $\square_v$  indicate observations of a square vortex lattice arising from the four-fold in-plane anisotropy of the Fermi velocity  $v_F$ . For details see the text (after Dewhurst et al., 2005).

cessfully describes the structure, orientation and field dependence of the vortex lattice in non-magnetic rare-earth borocarbides.

Experimental data for the vortex lattice of  $\text{YNi}_2\text{B}_2\text{C}$  for  $\mathbf{H}||\mathbf{c}$  are summarized in the  $H$ - $T$  phase diagram (Dewhurst et al., 2005) of Figure 53. The first and second order transition curves  $H_1(T)$  and  $H_2(T)$ , respectively, were determined from SANS investigations; the upper critical field  $H_{c2}(T)$  was obtained from dc-magnetization measurements on the same  $\text{YNi}_2\text{B}_2\text{C}$  single crystal. The transition curves  $H_1(T)$  and  $H_2(T)$  divide the  $H$ - $T$  phase diagram into three separate regions: (i) a low-field region below  $H_1(T)$  where the hexagonal vortex lattice (with rhombic distortion) is not affected by the square symmetry of the vortices, (ii) the field region between  $H_1(T)$  and  $H_2(T)$  where the intervortex distance become comparable with the penetration depth so that the square symmetry of the vortex cores causes a  $45^\circ$  reorientation of the rhombic vortex lattice, and (iii) the high-field region above  $H_2(T)$  where a square vortex lattice becomes energetically favorable due to the strong interaction between vortices. It is clearly seen that with increasing temperature the high-field rhombic vortex lattice remains stable in an increasing field

range of the phase diagram. The determination of  $H_1(T)$  and  $H_2(T)$  is difficult at temperature close to  $H_{c2}(T)$  because there the diffraction intensity is weak. Therefore no  $H_1$  and  $H_2$  data are available close to  $H_{c2}(T)$ . Nevertheless, the  $H_2(T)$  curve in Figure 53 shows no indication of a reentrance of the rhombic vortex lattice near  $H_{c2}(T)$ , as it was earlier reported for  $\text{LuNi}_2\text{B}_2\text{C}$  (Eskildsen et al., 2001b). The behavior of  $\text{LuNi}_2\text{B}_2\text{C}$  had been explained by thermal fluctuations of vortices near  $H_{c2}(T)$ , which had been assumed to suppress the anisotropy induced by the non-locality (Gurevich and Kogan, 2001). However, it can not be excluded that the SANS data reported for  $\text{LuNi}_2\text{B}_2\text{C}$  were affected by strong disorder effects due to vortex pinning. It was pointed out that these investigations have been performed for a large mosaic of naturally-aligned  $\text{LuNi}_2\text{B}_2\text{C}$  crystallites. In contrast, a smaller and much more perfect  $\text{YNi}_2\text{B}_2\text{C}$  single crystal has been used for the SANS study reported by Dewhurst et al. (2005). In this case, the high resolution of the equipment used for the measurement has allowed them to work with a much smaller single crystal than the sample used for the SANS study on  $\text{LuNi}_2\text{B}_2\text{C}$ .

It was shown theoretically (D.P. Li et al., 2006) that the presence of quenched disorder might be responsible for the positive slope of the  $H_2(T)$  line in Figure 53, whereas in the clean case the hexagonal-to-square transition line would be parallel to the temperature axis if thermal fluctuations are neglected.

The square symbols  $\square_v$  in Figure 53 indicate where a square vortex lattice according to Figure 51(c) was identified. The nearest neighbors of the square lattice  $\square_v$  are found in the directions of the minima of the Fermi velocity  $v_F$  (see Figures 54(c) and 54(d)). It was shown by Nakai et al. (2002) that the four-fold gap anisotropy also would stabilize the formation of a square lattice, however the nearest neighbors of this square lattice  $\square_g$  are found in the directions of the minima of the energy gap, i.e. along the crystallographic **a**- and **b**-axes as shown in Figures 54(a) and 54(b). So far, only the square lattice  $\square_v$  was observed in  $\text{YNi}_2\text{B}_2\text{C}$  and  $\text{LuNi}_2\text{B}_2\text{C}$ . The square lattice  $\square_g$  is expected to appear at high magnetic fields where the intervortex distance becomes so small that the vortex–vortex interaction is dominated by the anisotropy of the vortex core. Note that the extended quasiparticle states of the vortex cores are expected to expand to the direction with the small energy gap (Nishimori et al., 2004). Therefore, the shape of the vortex cores with extended quasiparticle density of states toward the **a**- and **b**-axes (see Figure 50(b)) indicates that the superconducting energy gap in  $\text{YNi}_2\text{B}_2\text{C}$  is four-fold symmetric with the minima along the **a**- and **b**-axes as shown in Figure 54(a). This gap anisotropy is consistent with data obtained for  $\text{YNi}_2\text{B}_2\text{C}$  from specific heat (Park et al., 2003), thermal conductivity (Izawa et al., 2002), photoemission spectroscopy (Yokoya et al., 2000) and point-contact spectroscopy (Raychaudhuri et al., 2004). Based on the shape of the gap function,  $(s + g)$  symmetry of the order parameter has been proposed (Maki et al., 2002). Alternatively, the gap anisotropy can be also described in the frame of two-band superconductivity (Mukhopadhyay et al., 2005; Raychaudhuri et al., 2007) indicating that the unusual gap anisotropy might originate from different bands on the Fermi surface having different coupling strengths (see Section 3.5).

The anisotropy of the Fermi surface (with its four-fold symmetry of the Fermi velocity) is not only responsible for the square vortex lattice  $\square_v$ , but also for the

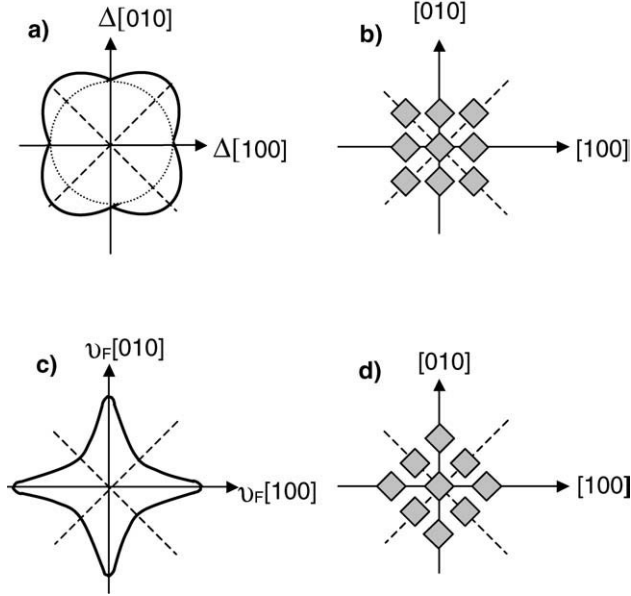


**FIGURE 54** Four-fold in-plane anisotropy of (a) the superconducting gap and (c) the Fermi velocity together with the orientations of the square lattice (b)  $\square_g$  and (d)  $\square_v$  relative to the crystal lattice (after Nakai et al., 2002).

anisotropy of the upper critical field  $H_{c2}$  in the basal plane of non-magnetic borocarbides. The in-plane anisotropy of  $H_{c2}$  of  $\text{LuNi}_2\text{B}_2\text{C}$  showing a four-fold symmetry in its angular dependence was found to decrease from  $H_{c2}^{[100]}/H_{c2}^{[110]} \approx 1.1$  at low temperatures to a value of 1.04 at 14 K (Metlushko et al., 1997). This anisotropy of  $H_{c2}$  in the tetragonal basal plane could be quantitatively described using a non-local extension (Hohenberg and Werthamer, 1967) of Gor'kov's derivation (Gor'kov, 1959) of the GL equations. The anisotropic Fermi velocity determined from the  $H_{c2}$  data (Metlushko et al., 1997) was found to agree with data derived from band-structure calculations (Mattheiss, 1994; Rhee et al., 1995; see Section 3.6 for some remaining puzzles of this approach).

It should be noted that non-local effects are restricted to the clean limit of type-II superconductivity. They are suppressed by scattering and vanish in the dirty limit. This suppression was investigated on  $\text{Lu}(\text{Ni}_{1-x}\text{Co}_x)_2\text{B}_2\text{C}$  compounds (Gammel et al., 1999b; Eskildsen et al., 2000). It is well known that  $\text{LuNi}_2\text{B}_2\text{C}$  which is in the clean limit can be changed into a dirty-limit superconductor by doping with 9% Co (Cheon et al., 1998). Cobalt doping results in a decrease of the mean free path and an increase of the coherence length. Thus, the field  $H_2$  at which the hexagonal-to-square transition of the vortex lattice occurs is shifted to higher values. In particular, at 2 K,  $H_2$  increases from  $\approx 2$  kOe (for  $x = 0$ ) to 10.2 kOe (for  $x = 4.5\%$ ) and to 14 kOe (for  $x = 6\%$ ). In the dirty limit (for  $x = 9\%$ ), no transition to a square vortex lattice was observed (Eskildsen et al., 2000).

### 5.1.2 Size of the vortex cores

Remarkably, not only the shape, but also the *size* of the vortex cores is affected by the quasiparticle states around the vortex cores. The vortex core size  $\rho_c$  which is of the order of the coherence length  $\xi$ , is defined by the slope,  $\Delta'(r) = d/dr \Delta(r)$ , of the order parameter  $\Delta(r)$  at the vortex axis  $r = 0$ , according to  $1/\rho_c = \Delta'(0)/\Delta(a/2)$  where  $\Delta(a/2)$  is the order parameter at half way between two neighboring vortices. The size of the vortex core in rare-earth borocarbides shows a significant dependence on temperature and magnetic field, whereas in a local model (without delocalized quasiparticles), the size  $\rho_c$  of the vortex core does not strongly depend on the magnetic field and temperature, deep in the superconducting state ( $T \ll T_c, H \ll H_{c2}$ ). For  $\text{LuNi}_2\text{B}_2\text{C}$ , a linear decrease of  $\rho_c$  with temperature from about 90 Å at 10 K to 64 Å at 1 K was found by muon spin rotation (Price et al., 2002). This was attributed to the Kramer–Pesch effect (Kramer and Pesch, 1974), where the shrinking of the cores is due to the depopulation of localized high-energy bound electron states in vortex cores. With increasing magnetic field, the core size  $\rho_c$  of  $\text{LuNi}_2\text{B}_2\text{C}$  and  $\text{YNi}_2\text{B}_2\text{C}$  was found strongly to decrease, following an  $H^{-0.5}$  dependence for large fields. It is worth mentioning that the same field dependence was observed also in other clean superconductors with high GL parameters  $\kappa_{GL}$ , as in  $\text{V}_3\text{Si}$ ,  $\text{CeRu}_2$ ,  $\text{YBa}_2\text{Cu}_3\text{O}_7$  and  $\text{NbSe}_2$  (Sonier, 2004). Remarkably, among these superconductors,  $\text{CeRu}_2$  and  $\text{NbSe}_2$  show no hexagonal-to-square transition of the vortex lattice. The existence of quasiparticle states inside and outside the cores is considered to be responsible for this behavior. It was found that the coherence length  $\xi$  calculated within the BCS theory for clean superconductors exhibits the same field dependence as the size  $\rho_c$  of the vortex cores (Kogan and Zhelezina, 2005). Thereby, the dimensionless coherence length  $\xi/\xi_{c2}$  (with  $\xi_{c2}$  from  $H_{c2} = \phi_0/(2\pi\xi_{c2}^2)$ ) should be a nearly universal function of the reduced field  $H/H_{c2}$  for clean materials in high fields and at low temperatures. Finally, it was shown that the field dependence of both,  $\rho_c$  and  $\xi$ , is weakened by impurity scattering and by increasing temperature (Kogan and Zhelezina, 2005). Therefore, this field dependence completely disappears in the dirty limit and at temperatures close to  $T_c$ .

### 5.1.3 Vortex matter phase diagram

In addition to the vortex lattice occupying the main part of the  $H$ – $T$  vortex–matter phase diagram of borocarbide superconductors, several other vortex–matter phases have been identified in the non-magnetic borocarbides. Mun et al. (1996) found, by transport measurements on  $\text{YNi}_2\text{B}_2\text{C}$ , a vortex liquid between the vortex–lattice phase and the normal state, and a vortex-glass phase at low temperatures and high magnetic fields. A vortex glass transition is also suggested by results of Eskildsen et al. (1997a) who found, for  $\text{YNi}_2\text{B}_2\text{C}$  as well as  $\text{LuNi}_2\text{B}_2\text{C}$ , a static disorder of the square vortex lattice for  $H > 0.2H_{c2}$  where collective pinning of the flux lines breaks down. The change from vortex lattice through vortex glass to vortex liquid has also been seen by NMR measurements (Lee et al., 1999, 2000). A more complex phase diagram including a Bragg glass in a field range below the vortex-glass phase has been proposed recently for  $\text{YNi}_2\text{B}_2\text{C}$  and  $\text{LuNi}_2\text{B}_2\text{C}$  (Jaiswal-Nagar et al., 2006).

### 5.1.4 Vortex pinning

The symmetry changes of the vortex lattice in borocarbide superconductors affect the pinning of vortices as was shown for  $\text{YNi}_2\text{B}_2\text{C}$  (Silhanek et al., 2001). For the field orientation  $\mathbf{H}||c$ , the reorientation transition  $H_1(T)$  of the vortex lattice mentioned above was found to be associated with a significant kink in the volume pinning force  $F_p = \mathbf{j}_c \times \mu_0\mathbf{H}$  which is related to the critical current density  $\mathbf{j}_c$  and the applied field  $\mathbf{H}$ . Vortex pinning depends on the elastic properties of the vortex lattice and, in particular, on its shear modulus  $c_{66}$  which is strongly influenced by the reorientation of the vortex lattice at the transition field  $H_1(T)$  (Eskildsen et al., 1997b). For the field orientation  $\mathbf{H}\perp c$  the signature of non-local effects is a four-fold periodicity of  $F_p$  when the applied magnetic field is rotated within the basal plane. This in-plane anisotropy of  $F_p$  can be strongly suppressed by reducing the mean free path, showing that this anisotropy is a consequence of non-local effects. In contrast, the much larger out-of-plane anisotropy of  $F_p$  persisting for increasing impurity levels indicates bulk pinning due to the presence of some still unidentified anisotropic pinning centers (Silhanek et al., 2002).

Peculiarities of vortex pinning near  $H_{c2}$  and, in particular, the so-called peak effect in the critical current density  $j_c(H)$  observed in non-magnetic borocarbides (Eskildsen et al., 1997a; K.-J. Song et al., 1999) can be explained by the softening of the shear moduli of the vortex lattice near  $H_{c2}$  (Larkin and Ovchinnikov, 1979). Additionally, a pronounced dip anomaly in the  $ac$ -susceptibility response in the mixed state of  $\text{YNi}_2\text{B}_2\text{C}$  and  $\text{LuNi}_2\text{B}_2\text{C}$  single crystals was observed, which was found to be connected with the peak effect in  $j_c(H)$  (Narozhnyi et al., 2000b).

### 5.1.5 Dynamics of the vortex lattice

The dynamics of the vortex lattice in  $\text{YNi}_2\text{B}_2\text{C}$  thin films has been studied by high-resolution magneto-optical imaging (MOI; Wimbush et al., 2004a). The MOI technique is based on Faraday rotation. By placing a doped iron-garnet layer as a magneto-optically active sensing element on the top of the film, the normal component of the magnetic flux density distribution can be measured with a spatial resolution of up to  $1\ \mu\text{m}$ . A series of magneto-optical images obtained for  $\text{YNi}_2\text{B}_2\text{C}$  thin films prepared by pulsed laser deposition is shown in Figure 55. After zero-field cooling, a magnetic field of  $92.4\ \text{mT}$  was applied and gradually reduced. Down to  $\mu_0H = 26.4\ \text{mT}$ , a stable flux distribution with a typical roof-like pattern of trapped flux is visible (see Figure 55(a)). Upon further reduction of the applied field, the flux distribution becomes abruptly unstable below  $\approx 20\ \text{mT}$  showing a dendritic flux pattern as shown in panel (b) of Figure 55. This unusual flux pattern is found to remain unchanged as the applied magnetic field was reduced to zero. Interestingly, this flux pattern could be overridden by re-magnetizing the sample, and no instability was ever observed while increasing the applied magnetic field.

The stable flux pattern in Figure 55(a) forms due to the penetration of a magnetic flux front of pinned vortices from the sample surface. The joule heating arising from vortex motion can release global flux jumps and thermal quench instabilities under certain conditions which have to be avoided for stable operation of current-carrying superconductors (Mints and Rakhmanov, 1981). Dendritic flux patterns which have been observed in Nb disks (Goodman and Wertheimer,

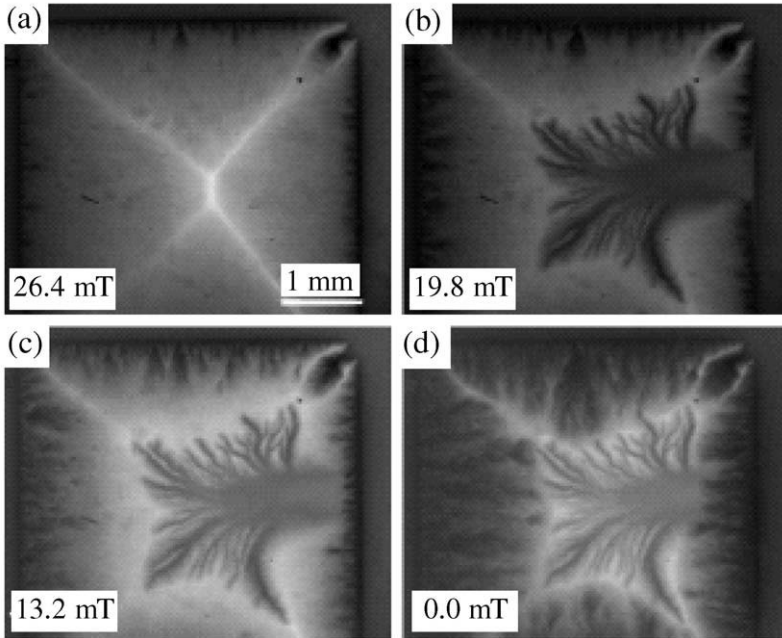


**FIGURE 55** Magneto-optical images of the flux distribution in an  $\text{YNi}_2\text{B}_2\text{C}$  thin film at 4 K under decreasing applied fields after zero-field cooling and applying a magnetic field  $\mu_0 H = 92.4$  mT. Field values are given in the figures. (a) Stable flux profile, (b)–(d) dendritic flux patterns. For details see the text. Reused with permission from Wimbush, S.C., Holzapfel, B., Jooss, Ch., *J. Appl. Phys.* 2004a, **96**, 3589.

© 2004 American Institute of Physics

1965),  $\text{MgB}_2$  thin films (Bobyly et al., 2002), and  $\text{YBa}_2\text{Cu}_3\text{O}_7$  thin films (Leiderer et al., 1993) represent a new class of instabilities of the critical state. They can be attributed to micro-avalanches of large bundles of vortices, which does not release a global flux-jump instability of the whole sample. The resulting local-temperature spikes leave behind frozen flux dendritic structures as shown in Figure 55(d).

It was shown by numerical simulations (Aranson et al., 2001) that the dendritic shape of the flux pattern can be explained by dynamic branching of a propagating hot spot in a flux-flow state in type-II superconductors triggered by a local heat pulse. Experimental investigations have shown that the dendritic instability can be also released by sweeping the magnetic field or by applying a transport current. A dendritic flux pattern forms within a surprisingly short time scale. The penetration velocity of the flux front of a dendritic instability in an  $\text{YNi}_2\text{B}_2\text{C}$  thin film triggered by a local heat pulse was measured with a magneto-optic pump-probe technique. Using a femtosecond laser system, a time resolution of 1 ns was achieved. A penetration velocity of the flux front of about 360 km/s was estimated, significantly exceeding the speed of sound  $c_s$ . The mechanism of this superfast flux propagation is not understood so far, because the velocity of the hot spot propagation was observed to be smaller than  $c_s$  (Aranson et al., 2001).

## 5.2 Magnetic borocarbides

In this section, the magnetic borocarbides  $R\text{Ni}_2\text{B}_2\text{C}$  with  $R = \text{Er}, \text{Ho}$  and  $\text{Tm}$  will be discussed. An interesting question is whether the subtle effects of non-locality on the vortex lattice will be preserved in these magnetic superconductors. Furthermore, the influence of the antiferromagnetic and ferromagnetic order on the vortex pinning will be considered. Up to now there is not much known about the vortex lattice in  $\text{DyNi}_2\text{B}_2\text{C}$ .

### 5.2.1 $\text{ErNi}_2\text{B}_2\text{C}$

In  $\text{ErNi}_2\text{B}_2\text{C}$  single crystals, the hexagonal-to-square transition of the vortex lattice was observed by SANS investigations and by magnetic decoration at temperatures above and below the Néel temperature,  $T_N \approx 6$  K. At  $T = 3.5$  K, i.e. in the antiferromagnetic state, the hexagonal-to-square transition occurs for the field orientation  $\mathbf{H}||\mathbf{c}$  at above  $H_2 \approx 500$  Oe (Eskildsen et al., 1997b). Whereas the square lattice was found to be aligned with the  $[110]$  direction of the host crystal, the hexagonal lattice has domains aligned along  $[100]$  (or  $[010]$ ). Of special interest is the question whether the vortex lattice is influenced by the magnetic order. For both symmetries of the vortex lattice, a significant coupling between the magnetic ordering and the flux lines was evidenced in the weakly ferromagnetic state below 2.5 K by a rotation of the flux lines away from the direction of the applied field  $\mathbf{H}||\mathbf{c}$ , whereas at higher temperatures the vortex lattice was found to be well aligned with the applied field (Yaron et al., 1996). The angle between the vortex lattice and the applied field increases with decreasing temperature up to about  $1^\circ$  at 1.5 K and 0.55 T.

Enhanced vortex pinning was found in  $\text{ErNi}_2\text{B}_2\text{C}$  for applied fields  $\mathbf{H}||\mathbf{c}$  (DeWhurst et al., 2001a, 2001b; James et al., 2001). Magneto-optical (Saha et al., 2001) and high-resolution Bitter decoration studies (Vinnikov et al., 2005) of the vortex lattice in  $\text{ErNi}_2\text{B}_2\text{C}$  single crystals for the field direction  $\mathbf{H}||\mathbf{c}$  provided evidence for the formation of antiferromagnetic domain walls at  $T < T_N$ . Instead of forming a vortex lattice, rows of vortices were found to be pinned at magnetic twin boundaries. Saha et al. (2001) observed an enhanced stray field near the domain walls by magneto-optical studies and concluded that localized ferromagnetic spin components at twin boundaries between antiferromagnetic domains cause enhanced flux pinning. However, recent data for  $\text{ErNi}_2\text{B}_2\text{C}$  with single-vortex resolution obtained by scanning Hall probe imaging (Bluhm et al., 2006) and Bitter decoration (Vinnikov et al., 2005) strongly suggest that the observed variation of the stray field is due to a high vortex density at the twin boundaries.

In contrast to  $\mathbf{H}||\mathbf{c}$ , no significant increase in pinning was found at  $T < T_N$  for the field direction  $\mathbf{H}\perp\mathbf{c}$  (James et al., 2001) where the vortices are aligned perpendicular to the  $c$ -axis. Because the planar domain boundaries are directed along  $[110]$  and  $[\bar{1}\bar{1}0]$  with the ferromagnetic moment parallel to the domain plane direction ( $c$ -axis), these planar pinning centers are expected to become ineffective when the vortices are tilted away from the  $c$ -axis (see also Section 4.10).

A typical Bitter decoration pattern for  $\text{ErNi}_2\text{B}_2\text{C}$  (Vinnikov et al., 2005) in the antiferromagnetic state is shown in Figure 56(a). Bands of vortices aligned along

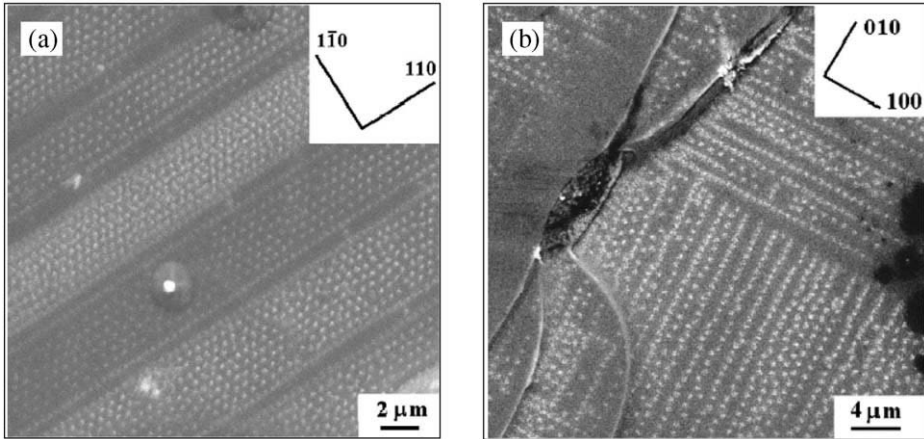


**FIGURE 56** Bitter decoration patterns showing vortices in the  $a$ - $b$ -plane of (a)  $\text{ErNi}_2\text{B}_2\text{C}$  at  $T = 5.8$  K and (b)  $\text{HoNi}_2\text{B}_2\text{C}$  at  $T = 4.3$  K as white spots. A magnetic field of (a) 72 Oe and (b) 17 Oe was applied along the  $c$ -axis of the single crystals. The magnetic domain structure in the antiferromagnetic state for  $T < T_N$  becomes visible by rows of vortices pinned at twin boundaries (reprinted figure with permission from Vinnikov, L.Ya., Andereg, J., Bud'ko, S.L., Canfield, P.C., Kogan, V.G., Phys. Rev. B 2005, **71**, 224513).

© 2005 American Physical Society

the  $[110]$  direction are visible. Due to strong pinning at the domain walls, the vortex spacing along the lines formed by the twin boundaries is much smaller than the vortex spacing in the middle of a twin. A regular hexagonal vortex lattice develops within the bands formed by the magnetic domains. The width of the magnetic domains shown in Figure 56(a) is about  $4 \mu\text{m}$ . The domain width was found to decrease with increasing magnetic field ranging between about 1 and  $10 \mu\text{m}$  (Vinnikov et al., 2005). The origin of the dependence is not understood so far. Another peculiarity that requires further studies is that always two lines of enhanced vortex density appear along the twin boundaries (see Figure 56(a)). For temperatures above  $T_N$  where the magnetic domains disappear the vortex distribution becomes hexagonal in the range of low applied magnetic fields used for the decoration experiments (Vinnikov et al., 2005).

In the temperature range below  $T_{\text{WFM}} \approx 2.3$  K where superconductivity was found to coexist with weak ferromagnetism, a strong increase in bulk pinning was observed in  $\text{ErNi}_2\text{B}_2\text{C}$  for both orientations  $\mathbf{H} \parallel c$  and  $\mathbf{H} \perp c$  (Gammel et al., 2000a; James et al., 2001). Local scanning Hall probe measurements on  $\text{ErNi}_2\text{B}_2\text{C}$  with single-vortex resolution have shown that a weak random magnetic signal appears below  $T_{\text{WFM}}$  instead of a spontaneous vortex lattice (Bluhm et al., 2006). This suggests that after cooling in zero-field the ferromagnetism has a domain-like or oscillatory structure characterized by a variation of the magnetization on sub-penetration-depth length scales. The strong, local pair breaking at these ferromagnetic features would result in significant vortex pinning and was proposed to explain the enhanced pinning below  $T_{\text{WFM}}$  (Bluhm et al., 2006).

### 5.2.2 HoNi<sub>2</sub>B<sub>2</sub>C

Early studies on vortex pinning in HoNi<sub>2</sub>B<sub>2</sub>C (Dewhurst et al., 1999) revealed significant bulk pinning for **H**||**c** only in the narrow temperature range between 5 and 6 K, where superconductivity is strongly suppressed due to the presence of incommensurate antiferromagnetic phases. It was suggested that the enhanced pinning in the same temperature range is caused by a direct interaction between the vortice lattice and the **a**\*-type magnetic states or domains thereof (Dewhurst et al., 1999).

However, recent investigations of HoNi<sub>2</sub>B<sub>2</sub>C single crystals prepared by the floating-zone technique with optical heating (Souptel et al., 2005a, 2005b) revealed bulk pinning in the entire region of the *H*-*T* phase diagram where superconductivity occurs (Krutzler et al., 2005; for the influence of neutron irradiation, see Fuger et al., 2007). Data for the temperature dependence of the critical current density *j<sub>c</sub>* are plotted for two field orientations in Figure 57 for the same field *H*/*H<sub>c2</sub>* = 0.05. With decreasing temperature, *j<sub>c</sub>* strongly increases for both orientations following the same temperature dependence between 6.5 K and *T<sub>c</sub>*. Due to the appearance of the incommensurate phases below 6 K, *j<sub>c</sub>* is suppressed, dropping to almost zero at *T<sub>N</sub>* ≈ 5 K. Note that the maximum of *j<sub>c</sub>* for applied fields within the **a**-**b**-plane is about two times lower than that for **H**||**c**. A similar ratio is observed for the maxima of *H<sub>c2</sub>* around 6 K (see Figure 42). As aforementioned, the stronger suppression of *H<sub>c2</sub>* for applied fields within the **a**-**b**-plane is attributed to enhanced pair breaking of Cooper pairs due to the magnetic Ho moments being oriented within the **a**-**b**-planes (see also Section 4.9).

Below *T<sub>N</sub>*, the critical current density *j<sub>c</sub>* starts increasing again with decreasing temperature, reaching values of about 15 kA/cm<sup>2</sup> at low temperatures. This rather high *j<sub>c</sub>* clearly indicates bulk pinning in that single crystal. Most likely, bulk pinning below *T<sub>N</sub>* arises from domain walls between the antiferromagnetic domains

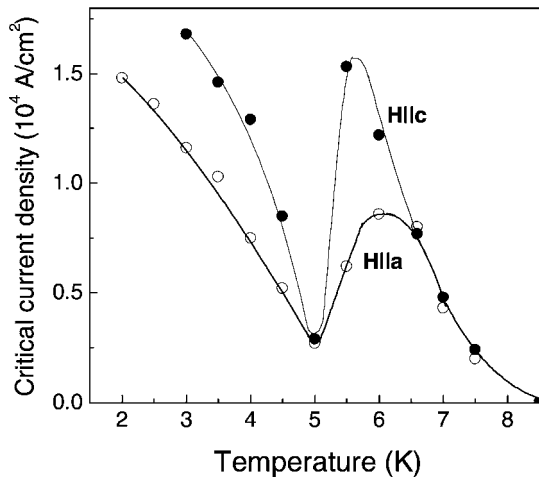


**FIGURE 57** Critical current density of HoNi<sub>2</sub>B<sub>2</sub>C as a function of temperature at the same reduced field of *H*/*H<sub>c2</sub>* = 0.05 for the two field orientations **H**||**c** and **H**||**a**. After Krutzler et al. (2005).

appearing as in  $\text{ErNi}_2\text{B}_2\text{C}$ . The domain structure was studied by a high-resolution Bitter decoration technique (Vinnikov et al., 2005). A typical decoration pattern with rows of vortices along the  $[100]$  and  $[010]$  direction, at  $T = 4.3$  K, is shown in Figure 56(b). For  $\text{HoNi}_2\text{B}_2\text{C}$ , the tetragonal-to-orthorhombic lattice distortion occurs along the  $[110]$  direction, which favors the formation of domains with domain walls parallel to the  $[100]$  (or  $[010]$ ) direction and the  $c$ -axis, as was demonstrated in Figure 8(b). In contrast, the tetragonal-to-orthorhombic distortion for  $\text{ErNi}_2\text{B}_2\text{C}$  occurs along the  $[100]$  direction (see Table 5). Therefore, there the domain walls are aligned along the  $[110]$  (or  $[1\bar{1}0]$ ) direction and the  $c$ -axis as shown in Figure 56(a).

### 5.2.3 $\text{TmNi}_2\text{B}_2\text{C}$

Detailed SANS studies of the magnetic structure and the vortex lattice were performed on  $\text{TmNi}_2\text{B}_2\text{C}$  single crystals for applied magnetic fields  $\mathbf{H}||c$  (Eskildsen et al., 1998, 2001a; Gammel et al., 2000b). The combined magnetic, vortex lattice, and superconducting phase diagram is shown in Figure 58.

At first, the temperature range below  $T_N \sim 1.5$  K will be considered in which superconductivity coexists with antiferromagnetism. In the low-field region ( $H < 0.2$  T), the same incommensurate modulated state (denoted in Figure 58 as  $\text{AFM}_1$ ) was observed as in zero magnetic field (Lynn et al., 1997). The Tm magnetic moments order into a squared-up spin-density wave with a modulation vector  $\tau_F = (0.093, 0.093, 0)$  and the moment parallel to the  $c$ -axis. In this field range,  $H < 0.2$  T, a square vortex lattice was found for all temperatures below  $T_N$ . Above 0.2 T, a magnetic transition into a more complex structure is observed with

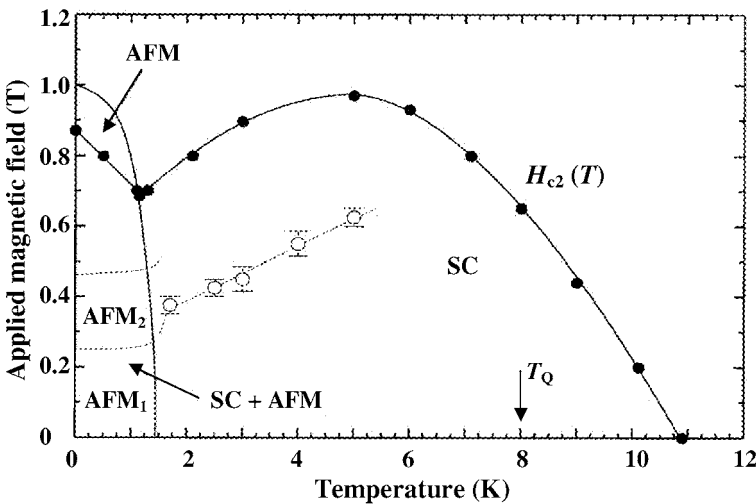


**FIGURE 58** Combined field (parallel to  $[001]$ )-vs.-temperature phase diagram for superconductivity (filled circles), antiferromagnetic order (thin lines without symbols) and the vortex-lattice symmetry (dashed line and open circles) in  $\text{TmNi}_2\text{B}_2\text{C}$ . For details see the text. Below  $T_Q$  the system develops long-range quadrupolar order (at least at small magnetic fields; see Figure 48; after Gammel et al., 2000b; Andersen et al., 2006b; Jensen and Hedegård, 2007).

additional peaks of the SANS signal appearing around the [100] and [010] directions (denoted as AFM<sub>2</sub>). Coincident with this magnetic transition at  $\approx 0.2$  T, the vortex lattice undergoes a rhombic distortion. Finally, the vortex lattice becomes hexagonal for fields above about 0.45 T. This transition is shown in Figure 58. Superconductivity vanishes above  $H_{c2}(T)$  and TmNi<sub>2</sub>B<sub>2</sub>C goes into a saturated paramagnetic state above  $\mu_0 H = 1.0$  T at low temperatures. The joint magnetic and vortex lattice transition at  $\approx 0.2$  T continues into the paramagnetic state above  $T_N \approx 1.5$  K as sole vortex lattice transition. This transition is shown in Figure 58 by the open circles.

These studies revealed an intimate coupling between the vortex lattice and the magnetic structure. It should be noted that TmNi<sub>2</sub>B<sub>2</sub>C is different from the other borocarbides with regard to the vortex lattice transitions: Starting from a square vortex lattice at low fields, the vortex lattice of TmNi<sub>2</sub>B<sub>2</sub>C becomes hexagonal at higher fields, whereas for YNi<sub>2</sub>B<sub>2</sub>C, LuNi<sub>2</sub>B<sub>2</sub>C and ErNi<sub>2</sub>B<sub>2</sub>C a hexagonal-to-square transition of the vortex lattice is observed as the applied magnetic field increases. The origin of this different behavior of TmNi<sub>2</sub>B<sub>2</sub>C in relation to its specific ground-state magnetic order (see Figure 28) and magnetic transitions is not understood so far. A further open question is how the quadrupolar order in TmNi<sub>2</sub>B<sub>2</sub>C recently discovered above  $T_N$  (see Section 4.11) affects the vortex lattice in this material.

## 6. SUPERCONDUCTIVITY IN R(Ni,T)<sub>2</sub>B<sub>2</sub>C AND (R,R')Ni<sub>2</sub>B<sub>2</sub>C

The pseudoquaternary compounds obtained from RNi<sub>2</sub>B<sub>2</sub>C by either partially substituting R by some other element R' (Kuznietz et al., 2002) or Ni by an other transition metal T represent a large class of materials with a rich variety of properties whose systematic investigation is expected to result in a better understanding of superconductivity and magnetism and their interplay in the RNi<sub>2</sub>B<sub>2</sub>C compounds. Here we present only a limited selection of results on this large class of materials.

### 6.1 Partial substitution of Ni by T = Co, Cu, Pd, Pt, etc.

As seen in Table 2, the LuNi<sub>2</sub>B<sub>2</sub>C-type structure is formed with many transition-metal T elements and it is natural to investigate series of mixed compounds R(Ni,T)<sub>2</sub>B<sub>2</sub>C in order to search for improved properties but also to get more insight into the microscopic mechanisms underlying the superconductivity and magnetism in these materials. Most work has been done in replacing Ni in RNi<sub>2</sub>B<sub>2</sub>C by its neighbors in the periodic table, i.e. Co, Cu, Pd, and Pt, but also by other transition metals, see, e.g., Hilscher and Michor (1999). The transition temperature  $T_c$  is reduced if Ni  $\rightarrow$  Cu (R = Y; Choi et al., 1998) as well as Ni  $\rightarrow$  Co (R = Y: Schmidt et al., 1994; Hoellwarth et al., 1996; R = Lu: Cheon et al., 1998; Kogan et al., 2006; R = Dy, Ho, Er, Tm, Lu: Schmidt and Braun, 1997; R = Ce: El Massalami et al., 1997; R = Gd: Bud'ko et al., 1995b, 1995c; R = Ho: Lynn et al., 1996; R = Er: Felner et al., 1997a; Bud'ko and Canfield, 2000b). In the case of

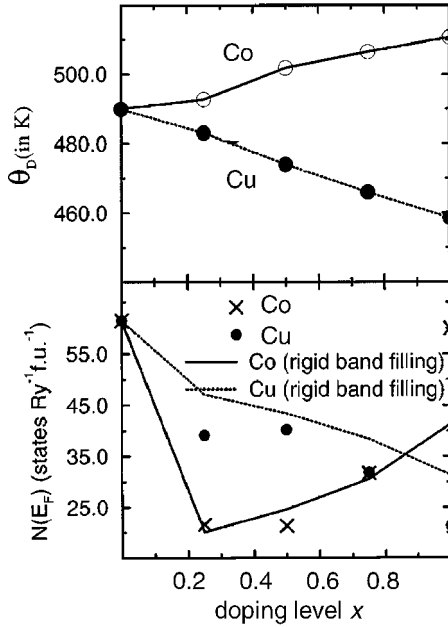


**FIGURE 59** Debye temperature,  $\theta_D$ , and density of states at the Fermi level,  $N(E_F)$ , for  $Y(Ni_{1-x}Co_x)_2B_2C$  and  $Y(Ni_{1-x}Cu_x)_2B_2C$  as functions of the Co or Cu substitution,  $x$ . The symbols are for results derived from relativistic band calculations in the atomic-sphere approximation; and the curves in the lower panel are from a rigid-band model (after Ravindran et al., 1998).

$Lu(Ni_{1-x}Co_x)_2B_2C$  the almost linear decrease of  $T_c$  is  $dT_c/dx \approx -74$  K. In both cases (Cu and Co substitutions) this can be qualitatively understood within the framework of a simple rigid-band picture assuming a more or less rigid band structure across the substitutional series and a varying degree of band filling due to the different number of conduction electrons in Co, Ni, and Cu. Thus the Fermi level  $E_F$  is shifted away from the local maximum of  $N(E_F)$  or from a state with optimum conditions for the occurrence of superconductivity which is found at  $T = Ni$ . More detailed electronic-structure calculations by Ravindran et al. (1998) have shown that the rigid-band model reproduces  $N(E_F)$  rather well (see Figure 59). However, above  $x \approx 0.2$ , the value of  $N(E_F)$  of  $Y(Ni_{1-x}Co_x)_2B_2C$  compounds again increases with increasing  $x$  and the two parent compounds for  $x = 0$  and  $x = 1$  do not much differ in their  $N(E_F)$ . Nevertheless  $YCo_2B_2C$  is neither a superconductor nor a magnetic system. Ravindran et al. (1998) have concluded that this difference is due to stiffening of the lattice with increasing  $x$ . These authors emphasize that, although both Co and Cu have an ionic radius of  $0.72 \text{ \AA}$ , which is larger than that of Ni ( $0.69 \text{ \AA}$ ), the substitution of Co for Ni in  $YNi_2B_2C$  results in a contraction of the lattice, whereas  $Ni \rightarrow Cu$  leads to lattice expansion. Also the ratio  $c/a$  of the lattice parameters depends on the doping level. Such local-structure aspects may affect the superconducting properties in addition to the simple effects of band filling. In

addition, we note the absence of B-derived states at the Fermi level and a missing contribution of boron vibrations to the electron–phonon coupling in  $\text{YCo}_2\text{B}_2\text{C}$ .

Suppression of superconductivity has also been investigated for Ni replaced in  $\text{YNi}_2\text{B}_2\text{C}$  by other d elements such as Fe and Ru (Bud'ko et al., 1995c). Different from the behavior of Co and Fe, Mn forms a magnetic moment in  $\text{Y}(\text{Ni}_{1-x}\text{Mn}_x)_2\text{B}_2\text{C}$ , with  $0 \leq x \leq 0.15$ , which has a maximum of its magnitude at  $x \approx 0.1$  (da Rocha et al., 2001, 2002a, 2002b). The maximum achievable value of  $x$  and details on the interplay of magnetism and superconductivity in this interesting system have still to be investigated. In  $\text{Er}(\text{Ni}_{1-x}\text{Fe}_x)_2\text{B}_2\text{C}$  with  $0 \leq x \leq 0.1$  the superconductivity is strongly suppressed ( $dT_c/dx \approx -300$  K) but the magnetic ordering temperatures  $T_N$  and  $T_{\text{WFM}}$  (see Section 4.10) only moderately decrease with iron doping, which has been explained by the modification of the electronic structure within a rigid-band model (Alleno et al., 2003, 2004b).

An interesting problem is how the properties of  $\text{RNi}_2\text{B}_2\text{C}$  change upon Ni replacement by the isoelectronic metals Pd or Pt. Modest decrease of  $T_c$  with increasing doping level has been reported for substitutions  $\text{Ni} \rightarrow \text{Pt}$  or  $\text{Pd}$  in  $\text{ErNi}_2\text{B}_2\text{C}$  and  $\text{TmNi}_2\text{B}_2\text{C}$  (Bonville et al., 1996; Felner et al., 1997b). Interestingly, the magnetic ordering temperature  $T_N$  decreases for these substitutions in the case of  $\text{TmNi}_2\text{B}_2\text{C}$  but it increases (even up to  $T_N > T_c$ ) for  $\text{ErNi}_2\text{B}_2\text{C}$ . This difference in the behavior of the Tm- and Er-based compounds is not yet understood (Felner et al., 1997b). The system  $\text{Y}(\text{Ni,Pt})_2\text{B}_2\text{C}$  will be discussed in Section 6.2.

In summary the change of  $T_c$  with varying  $x$  in  $\text{R}(\text{Ni}_{1-x}\text{T}_x)_2\text{B}_2\text{C}$  superconductors can rather well be understood taking into account the variation in the lattice structure and the band-filling levels which influence the electron density of states at the Fermi level. However there are properties as, e.g., the anisotropy of the superconducting gap (Yokoya et al., 2000) or the field dependence of the electronic specific heat (Lipp et al., 2001) or the vortex core radius (Nohara et al., 2000) in  $\text{Y}(\text{Ni}_{1-x}\text{Pt}_x)_2\text{B}_2\text{C}$ , which cannot be explained considering the mixed compounds as more or less homogeneous systems. It will be discussed in Section 6.2 that disorder on the lattice sites has a remarkable influence on the properties of such mixed-compound superconductors.

## 6.2 Effects of chemical pressure and disorder

Besides the primary effects of substitutional modification of  $\text{RNi}_2\text{B}_2\text{C}$  compounds, discussed in Section 6.1, namely changes in electron structure (with the rigid-band scenario as the simplest case) a further obvious effect is the emergence of internal stress and atomic disorder. Thus the low-temperature mean free path  $l$  of the conduction electrons in single-crystalline  $\text{Lu}(\text{Ni}_{1-x}\text{Co}_x)_2\text{B}_2\text{C}$  decreases nearly by a factor 10 if  $x$  increases from 0 to 9% and the ratio  $\xi_0/l$  increases from 1.1 to 17, indicating a change from a clean-limit to a dirty-limit superconductor as a consequence of disorder on a microscopic length scale (see Table 9; Cheon et al., 1998). In this section we will discuss pseudoquaternary  $\text{RNi}_2\text{B}_2\text{C}$  systems where (with respect to the conduction electrons) isoelectronic atoms are substituted for R or Ni. In such systems effects of disorder are expected to be dominating.

**TABLE 9** Experimental data for  $\text{Lu}(\text{Ni}_{1-x}\text{Co}_x)_2\text{B}_2\text{C}$  (after Cheon et al., 1998) with  $T_c$  determined from electrical resistivity  $\rho(T)$ ,  $\rho_0$ —the residual resistivity,  $H_{c2}(0)$ —the zero-temperature upper critical field,  $l$ —the mean free path, and  $\xi_0$ —the BCS coherence length

Nominal $x$	$T_c$ (K)	$\rho(300\text{ K})/\rho_0$	$H_{c2}(0)$ (kOe)	$l$ (Å)	$\xi_0$ (Å)	$\xi_0/l$
0	16.0	24.0	Not analyzed	270	310	1.1
0.015	15.0	9.4	60	100	330	3.3
0.030	14.2	7.4	55	70	350	5
0.045	12.9	5.5	43	50	390	7.8
0.060	11.4	4.1	33	40	440	11
0.090	9.5	3.5	22	30	520	17

Since  $R = \text{Sc}, \text{Y}, \text{La}$ , and most of the 4f elements form  $\text{RNi}_2\text{B}_2\text{C}$  compounds with the  $\text{LuNi}_2\text{B}_2\text{C}$ -type structure, it is relatively easy to prepare and investigate the pseudoquaternary compounds  $(\text{R}_x\text{R}'_{1-x})\text{Ni}_2\text{B}_2\text{C}$ . It should be noted, however, that for cases of large difference in the ionic radii of  $\text{R}^{3+}$  and  $\text{R}'^{3+}$ , such as  $(\text{Lu}, \text{La})$  and  $(\text{Y}, \text{La})$  there are large miscibility gaps for  $x$  around 0.5 (Freudenberger et al., 2001b). Therefore data on physical properties (e.g.,  $T_c$ ) measured for  $x$ -values within that gap (see, e.g., Lai et al., 1995) have only limited significance because the corresponding samples are two-phase. Furthermore, in such systems the superconducting properties are affected by internal stress (connected with strain, sometimes called chemical pressure) as observed for  $(\text{Y}_{1-x}\text{La}_x)\text{Ni}_2\text{B}_2\text{C}$  by Sánchez et al. (2000) and mixed magnetic  $(\text{R}_x\text{R}'_{1-x})\text{Ni}_2\text{B}_2\text{C}$  systems (Michor et al., 2000a, 2000b). Effects of chemical pressure are not yet systematically investigated and will not be further discussed in this review.

If the ionic radii of  $\text{R}^{3+}$  and  $\text{R}'^{3+}$  do not much differ the systems are miscible. Thus, Freudenberger et al. (1998a), Fuchs et al. (2001, 2002b), Lipp et al. (2002a), Zarestky et al. (2002), and Rathnayaka et al. (2003) have investigated compounds with both elements  $R$  and  $R'$  being non-magnetic, in particular  $(R, R') = (\text{Y}, \text{Lu})$ . The main problem is how the properties of such mixed systems deviate from those of the two parent systems and from a fictive ‘gray’ system with an ‘average’ or effective  $R$  ion in an average lattice. Zarestky et al. (2002) found an additional optical phonon mode in the mixed  $(\text{Lu}, \text{Y})\text{Ni}_2\text{B}_2\text{C}$  crystal, which is not present in the parent compounds. The influence of this mode on the superconductivity is not yet analyzed.

In the fictive ‘gray’ system the value of  $T_c$  would be on the upper curve in Figure 6 with a value between the values of both parent compounds. However, in the real pseudoquaternary system  $\text{Y}_x\text{Lu}_{1-x}\text{Ni}_2\text{B}_2\text{C}$ ,  $T_c$  has a considerably lower value than expected from a linear interpolation, i.e. the ‘gray’ system. As shown in Figure 60 the concentration dependence of  $T_c$  is non-monotonic with a minimum near  $x = 0.5$ . A similar behavior was found also for other quantities characterizing the electronic state of the system as the upper critical field  $H_{c2}^*$  and the parameter  $\alpha$  [from  $H_{c2}(T) = H_{c2}^*(1 - T/T_c)^{1+\alpha}$ ] which is a measure for the positive curvature of  $H_{c2}(T)$ , the residual resistance ratio  $\text{RRR} = \rho_n(300\text{ K})/\rho_n(T_c)$ , where  $\rho_n(T)$  is the normal-state resistivity, and the two parameters  $\gamma_N$  and  $\beta$  describing the field

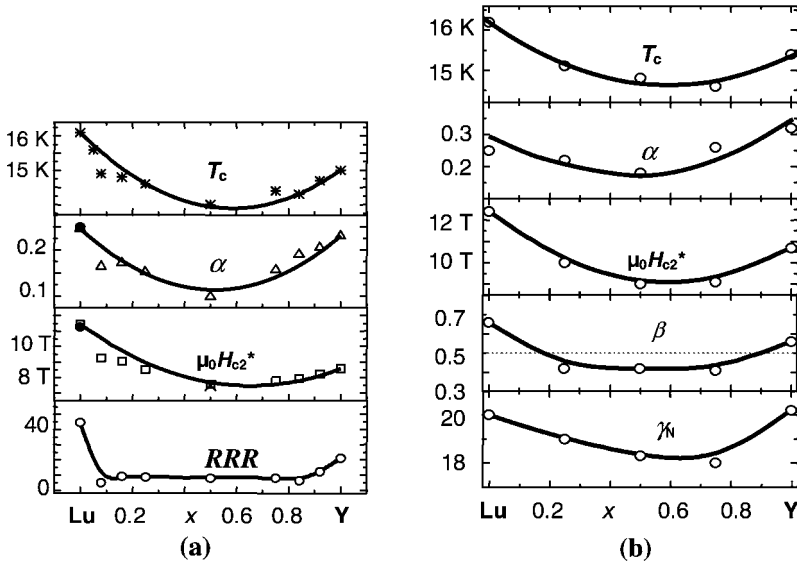


**FIGURE 60** Concentration dependence of various electronic properties of polycrystalline  $Y_xLu_{1-x}Ni_2B_2C$  obtained from measurements of (a) the resistivity and (b) the specific heat. The meaning of the parameters is explained in the text.

dependence of the electronic specific heat in the mixed state,  $C_e \sim \gamma(H)T$ , namely

$$\gamma(H) \sim \gamma_N (H/H_{c2}(0))^{1-\beta}, \quad (8)$$

where  $\gamma_N$  is the normal-state Sommerfeld constant (Fuchs et al., 2001; Lipp et al., 2001). These quantities have their highest values for the pure compounds and show a minimum near  $x = 0.5$ . This behavior has been attributed to disorder-induced local lattice distortions due to the different size of the ionic radii of Y and Lu. A quantitative analysis shows that the sensitivity to the site disorder is most pronounced for the magnitude of  $H_{c2}(0)$ , somewhat less for  $\alpha$  and weakest for  $T_c$ . Therefore, the parameter  $H_{c2}(0)$  can be considered as the most sensitive measure of the perfection of the clean-limit multiband superconductor.

The field dependence of the linear-in- $T$  electronic specific-heat contribution  $\gamma(H)T$  of the polycrystalline  $Y_xLu_{1-x}Ni_2B_2C$  samples of Figure 60 is shown in Figure 61.  $YNi_2B_2C$  and  $LuNi_2B_2C$  exhibit significant deviations from the usual linear  $\gamma(H)$  law, which are described in Eq. (8) by the parameter  $\beta$ . These deviations are even larger than those reported for an  $YNi_2B_2C$  single crystal and for a polycrystalline  $LuNi_2B_2C$  sample (Nohara et al., 1997) in which  $\beta = 0.5$  was found. In particular, a very strong sublinearity parameter from Eq. (8),  $\beta = 0.67$ , was observed for the polycrystalline  $LuNi_2B_2C$  sample in Figure 61. The origin for the observed  $\gamma(H) \sim H^{1-\beta}$  dependence will be discussed in more detail at the end of this section. The deviation from the linear  $\gamma(H)$  law is significantly reduced with increasing disorder, reaching values of  $\beta \approx 0.4$  in the range of Y concentrations between 0.25 and 0.75 (see also Figure 60).

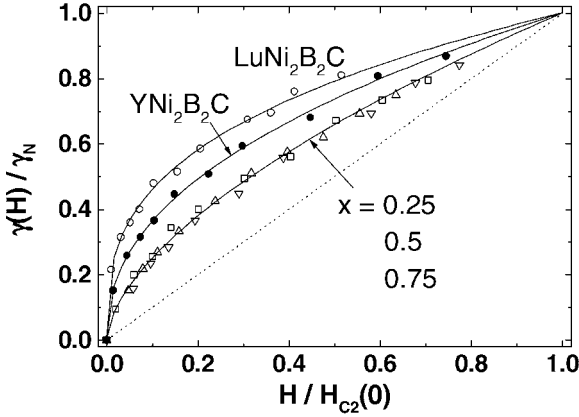


**FIGURE 61** Specific-heat contribution  $\gamma(H)$  of the vortex-core electrons in the mixed state (normalized by the Sommerfeld parameter  $\gamma_N$ ) of the  $Y_xLu_{1-x}Ni_2B_2C$  samples from Figure 60 as function of the applied magnetic field. The dotted straight line  $\gamma(H) \sim H$  corresponds to the usual s-wave behavior in the dirty limit.

A growing degree of substitutional disorder results in a reduction of the other above-mentioned quantities. However, the microscopic mechanism, which mediates disorder to  $T_c$  and to the other physical quantities, is not yet clarified. Typical scenarios for such disorder effects could be: the peak of the density of states at the Fermi level,  $N(E_F)$ , may be broadened or the phonon spectrum may be modified by disorder (Manalo et al., 2001) or the scattering rate of the conduction electrons may increase.

As already discussed in Section 3.6, the latter mechanism has been successfully treated using a two-band model for  $H_{c2}(T)$  taking into account the dispersion of the Fermi velocity in these clean-limit type-II superconductors (Shulga et al., 1998; see also in particular Figure 26). In this model two bands of electrons with different Fermi velocities are considered. The electrons with the low Fermi velocity have a strong electron–phonon coupling and are responsible for the superconductivity, whereas the values of  $H_{c2}(0)$  and  $T_c$  are reduced by the electrons with the large Fermi velocity, which have only a moderate el–ph coupling. The typical positive curvature of  $H_{c2}(T)$  near  $T_c$  is caused by interband coupling between the slow and fast electrons. This model predicts a transition from the clean to the quasi-dirty limit for increasing interband scattering rate of the conduction electrons on impurities (note that pure intra-band impurity scattering would enhance  $H_{c2}$ ). Within the clean limit,  $H_{c2}(0)$  and the parameter  $\alpha$  for the positive curvature of  $H_{c2}(T)$  near  $T_c$  decrease with increasing scattering rate (see Figure 60). In this way, the observed minimum of  $H_{c2}^*$  and  $\alpha$  for  $x \approx 0.5$  (see Figure 60) can be explained by the increased interband scattering rate in the samples with substitutional disorder at the rare-earth site. The comparison of the two-band model (Figure 26) with the experimental data for  $Y_xLu_{1-x}Ni_2B_2C$  (Figure 60) indicates that also the most disordered sample is not yet in the dirty limit because their curvature remains positive.

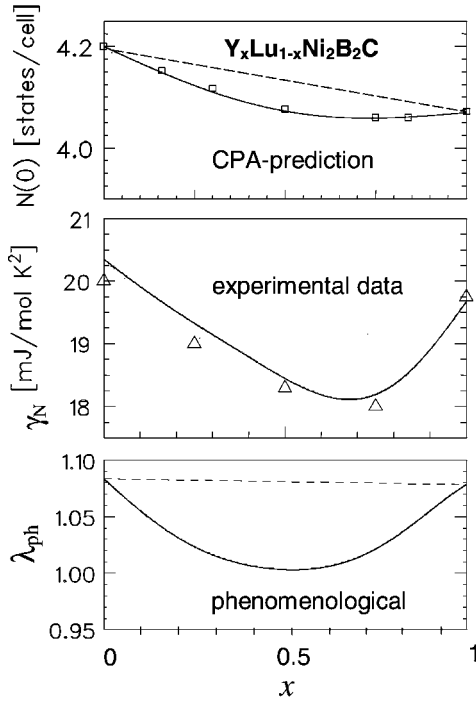


**FIGURE 62** Composition dependence of the density of states  $N(E_F)$  at the Fermi level of  $Y_xLu_{1-x}Ni_2B_2C$ —comparison of linear extrapolation with the CPA approach (squares); experimental data for the Sommerfeld parameter  $\gamma_N$  (triangles), and the phenomenologically extracted values of the electron–phonon coupling constant  $\lambda_{ph}$ , using Eq. (9).

From the experimental data for the Sommerfeld constant  $\gamma_N$  in Figure 60, conclusions concerning the influence of substitutional disorder on the rare-earth site of  $Y_xLu_{1-x}Ni_2B_2C$  compounds on their electronic structure can be drawn. According to the well known expression

$$\gamma_N \sim N(E_F)(1 + \lambda_{ph}), \quad (9)$$

the Sommerfeld constant  $\gamma_N$  is closely related to the density of states at the Fermi level  $N(E_F)$  and the electron–phonon coupling constant  $\lambda_{ph}$ . Calculations of  $N(E_F)$  within the coherent-potential approximation (CPA) revealed that  $N(E_F)$ , as function of the Y concentration, passes through a minimum which only slightly deviates from the linear interpolation between the values for the pure samples (Rosner et al., 2000; see upper panel of Figure 62).

The maximum deviation from this dashed line in Figure 62 is only about 1% and can not explain the observed 10% variation of the Sommerfeld constant. Therefore, taking into account Eq. (9), it was concluded that the local lattice distortions due to the different size of the Y and Lu ions in the  $Y_xLu_{1-x}Ni_2B_2C$  compounds mainly reduce the electron–phonon interaction (Rosner et al., 2000). The dependence of  $\lambda_{ph}$  on the Y concentration resulting from Eq. (9) and  $N(E_F)$  is

shown in the lower panel of Figure 62. With values for  $\lambda_{\text{ph}}$  between 1.0 and 1.1, medium coupling strengths are estimated for the  $\text{Y}_x\text{Lu}_{1-x}\text{Ni}_2\text{B}_2\text{C}$  compounds. An alternative (to the non-monotonic variation of electron-phonon interaction with increasing  $x$  as discussed above) interpretation of the minimum of  $\gamma_{\text{N}}(x)$  observed in  $\text{Y}_x\text{Lu}_{1-x}\text{Ni}_2\text{B}_2\text{C}$  was proposed by Michor et al. (2000b) and Manalo et al. (2001). Analyzing the thermodynamic properties of  $\text{Y}_x\text{Lu}_{1-x}\text{Ni}_2\text{B}_2\text{C}$  in the framework of the Eliashberg theory including anisotropy effects, they explained the minimum of  $\gamma_{\text{N}}(x)$  by a corresponding reduction of the density of states  $N(E_{\text{F}})$  at medium  $x$  values, whereas  $\lambda_{\text{ph}}$  was found to change monotonously between the  $\lambda_{\text{ph}}$  values of  $\text{YNi}_2\text{B}_2\text{C}$  and  $\text{LuNi}_2\text{B}_2\text{C}$ .

As noted above, the dirty limit is not reached in  $\text{Y}_x\text{Lu}_{1-x}\text{Ni}_2\text{B}_2\text{C}$ , even in the case of maximum disorder. Since the Ni-3d electrons participate much more in the Fermi surface than the R-4d and R-5d electrons, disorder on the Ni site is expected to have a stronger influence on the superconducting properties than disorder on the R site. As an example the anisotropy in the s-wave gap of  $\text{YNi}_2\text{B}_2\text{C}$  is nearly completely destroyed in  $\text{Y}(\text{Ni}_{0.8}\text{Pt}_{0.2})_2\text{B}_2\text{C}$  due to effects of disorder (see Figure 22; Yokoya et al., 2002; Takaki et al., 2002; Ohishi et al., 2003a, 2003b; Baba et al., 2006a, 2006b). The transition from clean- to dirty-limit superconductivity in this material had already been reported by Nohara et al. (1999). Systematic investigations of the influence of substitutional disorder on the properties of  $\text{Y}(\text{Ni}_{1-x}\text{Pt}_x)_2\text{B}_2\text{C}$  compounds were performed over a wide concentration range  $x \leq 0.75$  by Lipp et al. (2002b, 2003) and Fuchs et al. (2002b). It should be noted that the phase formation of compounds with larger Pt concentrations is much more complicated than of those with small Pt content because these  $\text{RPt}_2\text{B}_2\text{C}$  phases become metastable with decreasing atomic size of the rare-earth element R (Cava et al., 1994d). Therefore, no single-phase  $\text{YPt}_2\text{B}_2\text{C}$  could be synthesized. Improvement of the phase purity of  $\text{YPt}_2\text{B}_2\text{C}$  has been obtained in samples in which platinum had been partially replaced by gold (Cava et al., 1994e;

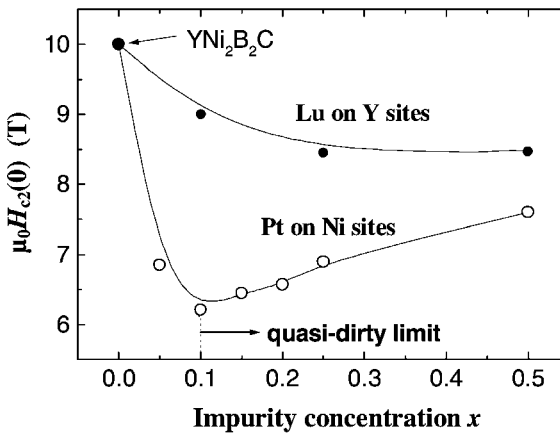


**FIGURE 63** Suppression of the upper critical field  $H_{c2}(0)$  in  $\text{Lu}_x\text{Y}_{1-x}\text{Ni}_2\text{B}_2\text{C}$  (filled circles) and  $\text{Y}(\text{Pt}_x\text{Ni}_{1-x})_2\text{B}_2\text{C}$  (open circles). After Lipp et al. (2002b).

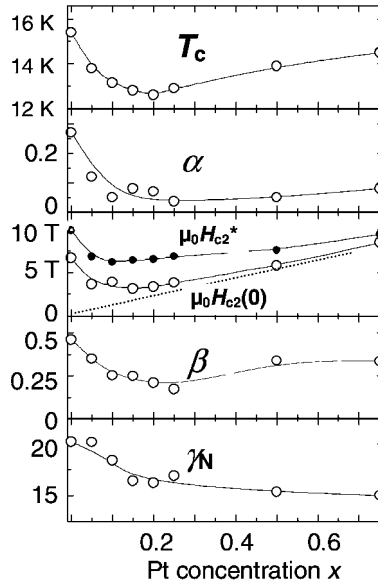


**FIGURE 64** Concentration dependence of various properties of polycrystalline  $\text{Y}(\text{Ni}_{1-x}\text{Pt}_x)_2\text{B}_2\text{C}$  obtained by specific-heat measurements: transition temperature  $T_c$ ; exponent  $\alpha$  and parameter  $H_{c2}^*$  from Eq. (6); upper critical field  $H_{c2}(0)$  at  $T = 0$ , where the dotted line schematically describes the dirty limit corresponding to the isotropic single-band case (in reality there is a finite intersection with the field-axis for the dotted asymptotic line, see Shulga and Drechsler, 2002); exponent  $\beta$  of Eq. (8) for the curvature of the electronic specific heat in the mixed state; and Sommerfeld constant  $\gamma_N$  (Lipp et al., 2002b).

© 2002 EDP Sciences

Buchgeister et al., 1995). In Figure 63, the effect of Pt (on Ni sites) and Lu impurities (on Y sites) on  $H_{c2}(0)$  of  $\text{Y}(\text{Ni}_{1-x}\text{Pt}_x)_2\text{B}_2\text{C}$  and  $\text{Y}_x\text{Lu}_{1-x}\text{Ni}_2\text{B}_2\text{C}$ , respectively is compared in the range of  $x \leq 0.5$ . It is clearly seen that  $H_{c2}(0)$  is much stronger suppressed by Pt impurities on Ni sites than by Lu impurities on Y sites. The quasi-dirty limit in the  $\text{Y}(\text{Ni}_{1-x}\text{Pt}_x)_2\text{B}_2\text{C}$  compounds is observed at a Pt concentration of  $x = 0.1$ , where  $H_{c2}(0)$  has its lowest value. The positive curvature of  $H_{c2}(T)$ , which is typical for the clean limit, practically disappears in the quasi-dirty limit. This is shown in Figure 64, where the influence of increasing disorder on the superconducting parameters of  $\text{Y}(\text{Ni}_{1-x}\text{Pt}_x)_2\text{B}_2\text{C}$  (Lipp et al., 2002b) is summarized.

An unexpected concentration dependence is found for the parameter  $\beta$  which describes, according to Eq. (8), the deviation of the field dependence of the electronic specific heat in the mixed state from the expected linear law (Nohara et al., 1997) for isotropic s-wave superconductors in the dirty limit. The large deviations from this linear  $\gamma(H)$  law observed for  $\text{YNi}_2\text{B}_2\text{C}$  become smaller in the quasi-dirty limit, however, they do not completely disappear. It has been pointed out by Lipp et al. (2001) that for intermediate deviations from linearity of  $\gamma(H)$ , i.e. for  $\beta = 0.15\text{--}0.3$ , the specific heat data of borocarbides at low magnetic fields can be discussed in the context of the conventional s-wave picture as well as within the

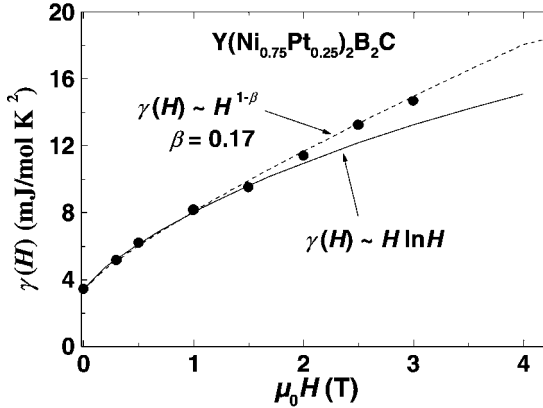


**FIGURE 65** Magnetic field dependence of the specific heat contribution  $\gamma(H)$  of the vortex core electrons in the mixed state for  $\text{Y}(\text{Ni}_{0.75}\text{Pt}_{0.25})_2\text{B}_2\text{C}$ . The dashed line is a fit according to Eq. (8) with  $\beta = 0.17$ , the solid line corresponds to the  $\gamma(H) \sim H \ln H$  dependence predicted by a d-wave model in the dirty limit.

framework of a d-wave model in the dirty limit. At low fields, the  $H \ln H$  dependence of  $\gamma(H)$  predicted for d-wave pairing in the dirty limit (Barash et al., 1997; Kübert and Hirschfeld, 1998) is not very distinct from the  $H^{1-\beta}$  behavior which favors s-wave superconductivity. This is illustrated in Figure 65.

Thus, considering results on  $\gamma(H)$  only, a possible unconventional pairing in borocarbides cannot be ruled out. Similarly it has been noted by Dobrosavljević-Grujić and Miranović (2003) that a sizable anisotropy of the s-wave gap function leads to strong deviations for the specific heat in the superconducting state from the predictions of the one-band isotropic BCS-Eliashberg theory. In particular, at low temperatures gap-node like dependencies may appear.

### 6.3 Magnetic impurities in a non-magnetic superconductor

In this section we will consider how the magnetic moment of a lanthanide  $R'$  influences the properties of  $(R,R')\text{Ni}_2\text{B}_2\text{C}$  compounds with  $R = \text{Y}$  or  $\text{Lu}$ . For such investigations of the interplay of local-moment magnetism with superconductivity the elements  $R'$  should not differ too much in its ionic size from  $R$  to avoid additional effects from the induced local pressure. Figure 66 shows the influence of dilution of  $R = \text{Lu}$  and  $\text{Y}$  by  $R' = \text{Ho}$ ,  $\text{Dy}$ , or  $\text{Gd}$  on the superconducting transition temperature  $T_c$ . For  $\text{Gd}_x\text{Y}_{1-x}\text{Ni}_2\text{B}_2\text{C}$  the dependence of  $T_c$  on  $x$ , or the effective de Gennes factor  $\overline{\text{DG}} = x\text{DG}[R'] + (1-x)\text{DG}[R]$  where  $\text{DG}[R]$  is the de Gennes factor of the free (Hund's rule)  $R^{3+}$  ion, can be well described (for the general case) by the expression

$$\ln\left(\frac{T_c^0}{T_c}\right) = \psi\left(\frac{N(E_F)I^2\overline{\text{DG}}}{2T_c}\right) - \psi\left(\frac{1}{2}\right) \quad (10)$$

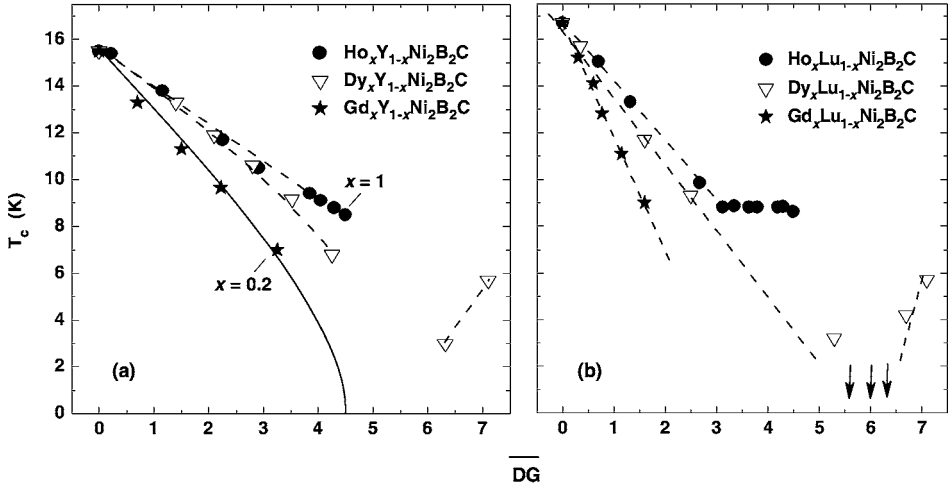


**FIGURE 66** Dependence of the superconducting transition temperature  $T_c$  on the effective de Gennes factor  $\overline{DG}$  for the non-magnetic superconductors (a)  $YNi_2B_2C$  and (b)  $LuNi_2B_2C$ , both diluted by the magnetic rare-earth elements Ho, Dy, Gd. The data for  $Dy_xY_{1-x}Ni_2B_2C$  are taken from Hossain et al. (1999). The solid line in (a) corresponds to the theory of Abrikosov and Gor'kov (1960); the dashed lines are guides for the eye, the arrows mark values of  $\overline{DG}$  (or  $x$ ) where no superconductivity has been observed down to 2 K.

of the classical theory of Abrikosov and Gor'kov (1960) for magnetic impurities in a non-magnetic superconductor (solid line in Figure 66(a); see also Section 1.3). In Eq. (10),  $T_c^0$  is the superconducting transition temperature without magnetic impurities,  $N(E_F)$  is the electron density of states at the Fermi level,  $I$  is a measure of the exchange coupling between conduction electrons and magnetic  $R^{3+}$  ions, and  $\psi$  is the digamma function. The solid line in Figure 66(a) was also found to describe the  $T_c$ -versus- $\overline{DG}$  dependence for  $Tb_xY_{1-x}Ni_2B_2C$  (Freudenberger et al., 2000). For Dy or Ho impurities in  $LuNi_2B_2C$  and  $YNi_2B_2C$ , the  $T_c$ -versus- $\overline{DG}$  curves in Figure 66 become more flat i.e. the pair-breaking effect of Dy and Ho is less pronounced than that of Gd (El-Hagary et al., 2000b; Freudenberger et al., 2001a). This is caused by the influence of crystalline electric fields acting on  $Dy^{3+}$  and  $Ho^{3+}$  thus reducing the magnetic degrees of freedom of these ions, i.e. the available space for fluctuations and scattering of their local moment (Cho et al., 1996c; Freudenberger et al., 1998b), as described by Fulde and Keller (1982) in a modified Abrikosov-Gor'kov theory. As can be seen in Figure 66, the decrease of  $T_c$  with increasing  $\overline{DG}$  is stronger for  $(Lu,R')Ni_2B_2C$  than for  $(Y,R')Ni_2B_2C$  ( $R' = Ho, Dy, Gd$ ). Obviously this observation is related to the smaller ionic radius of  $Lu^{3+}$  compared to that of  $Y^{3+}$ ,  $Ho^{3+}$ ,  $Dy^{3+}$  and  $Gd^{3+}$ . Thus in  $(Lu,R')Ni_2B_2C$  larger distortions in the rare-earth sublattice will occur than in  $(Y,R')Ni_2B_2C$ , which might result in enhanced pair breaking. The detailed mechanism for this effect is still unknown. The curves for  $(Y,Dy)Ni_2B_2C$  and  $(Lu,Dy)Ni_2B_2C$  in Figure 66 will be further discussed in Section 6.4.

Besides changes in the electronic properties caused by the change of average lattice constants and the effects of disorder on the electronic density of states and on the scattering rate, as discussed in the previous section, also the parameter  $I$  describing the exchange interaction between the 4f and the conduction electrons may be more strongly modified by the stronger lattice distortions (Michor et al., 2000a). Interestingly, El-Hagary et al. (2000b) found a correlation between the specific-heat jump associated with the superconducting transition,  $\Delta C_p$ , and the transition temperature  $T_c$ , i.e.  $\Delta C_p \sim T_c^2$  (compare BCS:  $\Delta C_p \sim T_c$ ), being valid for all superconducting  $Y_{1-x}R'_xNi_2B_2C$  compounds ( $R' = Gd, Dy, Ho, Er$ ) including the parent compounds  $DyNi_2B_2C$  (with  $T_N > T_c$ ) and  $HoNi_2B_2C, ErNi_2B_2C$  ( $T_N < T_c$ ). This comparison rests on the assumption of both the Sommerfeld parameter  $\gamma_N$  and the density of states  $N(E_F)$  being nearly constant within this series of heavy lanthanide solid solutions and their boundary compounds.

Lan et al. (2000, 2001) and Lan (2001) report on  $Y_{1-x}R'_xNi_2B_2C$  superconductors with  $R' = Gd, Dy, Ho, Er$ . They found that the positive curvature of  $H_{c2}(T)$  near  $T_c$  discussed in Section 6.2 for  $Y_xLu_{1-x}Ni_2B_2C$  also occurs in these compounds, i.e. the  $R'$  magnetic moments do not cause a strong interband impurity scattering which might weaken the multiband character being responsible for the positive curvature of  $H_{c2}(T)$  near  $T_c$ .

Specific-heat measurements showed that the ground state of Lu-rich (Lu,Gd)- $Ni_2B_2C$  is an RKKY spin glass (Bud'ko et al., 2003; see Figure 67), i.e. the long-

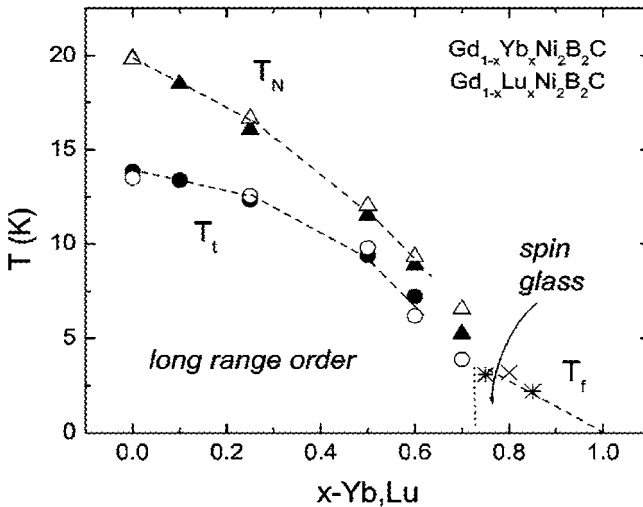


**FIGURE 67** Combined  $T$ - $x$  magnetic phase diagram of  $Lu_xGd_{1-x}Ni_2B_2C$  and  $Yb_xGd_{1-x}Ni_2B_2C$ ; symbols: triangles—magnetic ordering ( $T_N$ ), circles—spin reorientation ( $T_t$  corresponding to  $T_R$  in Figure 34), asterisks and crosses—spin-glass freezing ( $T_f$ ) (reprinted figure with permission from Bud'ko, S.L., Strand, J.D., Anderson, Jr., N.E., Ribeiro, R.A., Canfield, P.C., Phys. Rev. B 2003, **68**, 104417). The solid symbols (including the asterisks) and the open symbols (including the crosses) belong to the compounds based on Yb and Lu, respectively.

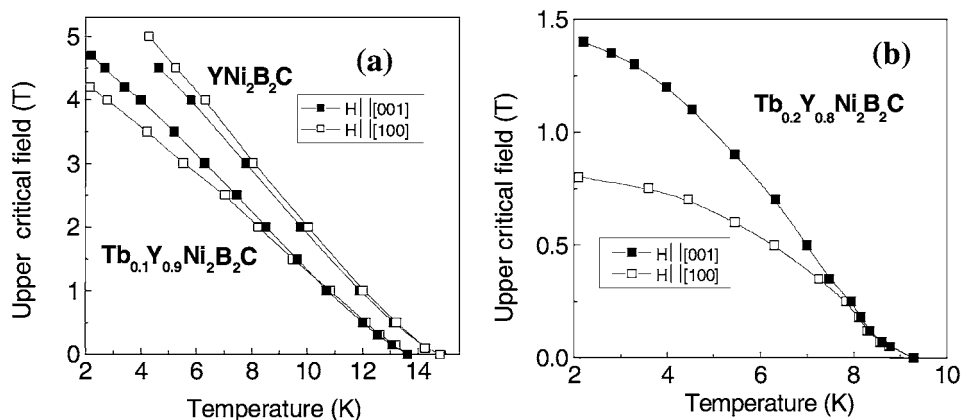


**FIGURE 68** Temperature dependence of the upper critical field,  $H_{c2}(T)$ , (a) of  $\text{YNi}_2\text{B}_2\text{C}$  and  $\text{Tb}_{0.1}\text{Y}_{0.9}\text{Ni}_2\text{B}_2\text{C}$  and (b) of  $\text{Tb}_{0.2}\text{Y}_{0.8}\text{Ni}_2\text{B}_2\text{C}$  single crystals for two directions of the applied magnetic field:  $H \parallel [001]$  (closed squares) and  $H \parallel [100]$  (open squares); after Bitterlich et al. (2001b, 2002a).

range RKKY exchange interaction (see Section 4) which oscillates in its sign, together with the disorder in the spatial positions of the Gd atoms, causes a frozen disorder of the Gd magnetic moments. From a comparison of Figures 66 and 67 it can be seen that for small Gd concentrations the superconductivity and the spin-glass state coexist in  $(\text{Lu,Gd})\text{Ni}_2\text{B}_2\text{C}$  compounds. Consequently, similar spin-glass ground states coexisting with superconductivity should also be present in other  $(\text{R,R}')\text{Ni}_2\text{B}_2\text{C}$  superconductors with diluted magnetic moments, in particular in all systems of Figure 66. This, however, has not yet been proven so far. (In  $\text{Y}_{0.75}\text{Er}_{0.25}\text{Ni}_2\text{B}_2\text{C}$  Hillier et al. (2001) could not detect spin freezing by  $\mu\text{SR}$  down to 1.5 K.)

The magnetic phase diagram of  $(\text{Gd,Y})\text{Ni}_2\text{B}_2\text{C}$  seems to be similar to that of  $(\text{Gd,Lu})\text{Ni}_2\text{B}_2\text{C}$  in Figure 67 (Drzazga et al., 2003). However these authors did not search for spin-glass states at low Gd concentrations. On the other hand Hilscher and Michor (1999) reported on a specific-heat anomaly in  $\text{Y}_{0.8}\text{Gd}_{0.2}\text{Ni}_2\text{B}_2\text{C}$  at about 3.5 K, well below  $T_c \approx 7.5$  K, which was attributed to antiferromagnetic ordering, but could also be due to spin-glass freezing. Interestingly the substitutions of Gd in  $\text{GdNi}_2\text{B}_2\text{C}$  by Lu and Yb have similar consequences on the Gd-moment ordering (see Figure 67), i.e. the hybridization of the Yb-4f electrons with the conduction electrons does not much modify the Gd magnetism of the mixed system. On the other hand this hybridization results in a 75 times stronger suppression of superconductivity in  $(\text{Lu,Yb})\text{Ni}_2\text{B}_2\text{C}$  compared to  $(\text{Lu,Gd})\text{Ni}_2\text{B}_2\text{C}$  (if the decrease in  $T_c$  is related to the change in the effective de Gennes factor; Bud'ko et al., 1997).

An interesting interplay of disorder and local-moment magnetism has been observed in  $\text{Tb}_x\text{Y}_{1-x}\text{Ni}_2\text{B}_2\text{C}$  single crystals with  $0 \leq x < 0.4$  (Bitterlich et al., 2001b, 2002a; see also Cho et al., 2001) with respect to the magnitude, anisotropy, and the shape of the  $H_{c2}(T)$  curves (see Figure 68). First, with increasing Tb con-

centration one observes the expected decrease of the general magnitude of  $H_{c2}$ . But this decrease develops rather differently for fields applied parallel or perpendicular to the basal plane ([100] direction; the maximum in-plane anisotropy is comparable in size with the out-of-plane anisotropy shown in Figure 68(a) for  $x = 0$  and, for  $x \geq 0.3$ , it becomes very small). There is a much steeper decrease for fields in in-plane direction. Hence the anisotropy of  $H_{c2}$  changes its sign already at the small Tb content of  $x < 0.1$ . The maximal anisotropy occurs near  $x \approx 0.2$  where macroscopic antiferromagnetism in the Tb subsystem does not yet develop. However, locally antiferromagnetically ordered cluster might occur. The shape of  $H_{c2}(T)$  changes, too. Deviations from Eq. (6) appear, although a positive curvature remains near  $T_c$  in spite of the disorder present. Compared with the non-magnetic borocarbides discussed above an even more pronounced curvature develops. Quite interestingly, the heavy-fermion superconductor URu<sub>2</sub>Si<sub>2</sub> (Brisson et al., 1995) exhibits nearly the same shape of  $H_{c2}(T)$  caused there by ordering of weak U-derived moments and possibly by a hidden order of still unknown nature. Kasahara et al. (2007) proposed a superconducting state with two distinct gaps having different nodal topology.

As expected a stronger suppression of superconductivity than extrapolated from the de Gennes-scaling curves in Figure 66 is observed in (Pr,Y)Ni<sub>2</sub>B<sub>2</sub>C and (Nd,Y)Ni<sub>2</sub>B<sub>2</sub>C (Freudenberger et al., 1999c; Mori et al., 2003) because Pr and Nd differ considerably from Y in their ionic size.

Strong magnetic pair-breaking effects have been reported for (Y,R)Pd<sub>2</sub>B<sub>2</sub>C. Also in these compounds the drop in  $T_c$  follows the de Gennes scaling, with the exception of R = Ce, Eu and Yb (Ghosh et al., 2001). This is supported by measurements of X-ray absorption near-edge structure (XANES) which showed that the total density of electron states at the Fermi level does not remarkably change if Y in YPd<sub>2</sub>B<sub>2</sub>C is substituted by Gd, Dy, Ho or Er (Wang et al., 2005).

## 6.4 Non-magnetic impurities in an antiferromagnetic superconductor

As can be seen in Figure 66, for medium and high concentrations of Dy in (Lu,Dy)Ni<sub>2</sub>B<sub>2</sub>C the  $T_c$ -versus- $\overline{DG}$  curve is strongly non-monotonic, i.e.  $T_c$  even increases with increasing  $\overline{DG}$  and possibly it goes to zero around  $\overline{DG} = 6$  although both parent compounds are superconductors (see also Cho et al., 1996c; Freudenberger et al., 2001a). The steep branches of this curve for high Dy concentrations can be interpreted as being based on electron scattering on non-magnetic Lu impurities in the antiferromagnetic superconductor DyNi<sub>2</sub>B<sub>2</sub>C. This strong depression of superconductivity has been interpreted as pair breaking due to creation of magnetic holes (Nagarajan, 2001). However it had been shown in the theoretical analyses presented by Morozov (1980), Zwicknagl and Fulde (1981), and Nass et al. (1982) that other types of non-magnetic impurities should also be efficient in suppression of superconductivity (see also Morosov, 2001). As a consequence of this phenomenon, the value of  $T_c$  of DyNi<sub>2</sub>B<sub>2</sub>C is very sensitive to the presence of non-magnetic impurities or, more generally, to the detailed metallurgical state of the samples. Possibly for that reason the identification

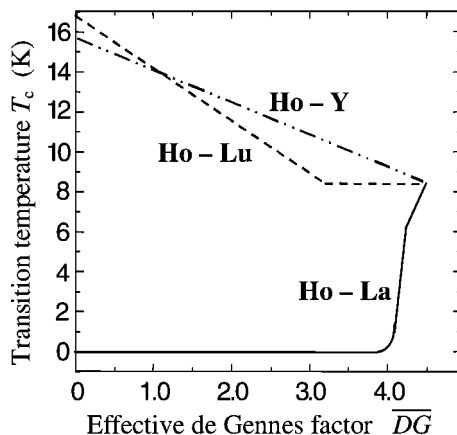


**FIGURE 69** Schematic curves showing the different influence of the non-magnetic R elements Y, Lu and La on the superconducting transition temperature  $T_c$  in the series  $\text{Ho}_x\text{R}_{1-x}\text{Ni}_2\text{B}_2\text{C}$  (after Freudenberger et al., 1999b).

of superconductivity in  $\text{DyNi}_2\text{B}_2\text{C}$  was delayed compared to the other borocarbide superconductors and the published experimental data on the properties of  $\text{DyNi}_2\text{B}_2\text{C}$  and of Dy-rich pseudoquaternary compounds  $(\text{Y,Dy})\text{Ni}_2\text{B}_2\text{C}$  exhibit much scatter (Hossain et al., 1999; Michor et al., 1999; El-Hagary et al., 2000b; Freudenberger et al., 2001a; Sánchez et al., 2005a). Therefore no data have been presented in Figure 66(a) for  $\text{Dy}_x\text{Y}_{1-x}\text{Ni}_2\text{B}_2\text{C}$  in the range  $5 < \overline{DG} < 6$  (i.e.  $0.7 < x < 0.85$ ). As has been pointed out by Levin et al. (1984) and Gupta (1998), the depression of superconductivity in antiferromagnetic superconductors by non-magnetic impurities may be the reason why not many antiferromagnetic superconductors with  $T_c < T_N$  are known. In principle there is no reason as to why many more such materials should not exist. However, in most such cases  $T_c$  may already have been suppressed, beyond observation, by non-magnetic impurities that are always present to some degree. In the scenario of coexistence of superconductivity and magnetism on different Fermi surface sheets as discussed above, this behavior is attributed to the local lattice deformations and the resulting symmetry breaking caused by the non-magnetic impurity ions. Consequently the formerly protected superconducting subsystem is coupled to the magnetic one and finally superconductivity is destroyed.

A strong decrease of  $T_c$  is observed if the Ho in  $\text{HoNi}_2\text{B}_2\text{C}$  is diluted by La (see Figure 69; Freudenberger et al., 1999b; Kreyssig et al., 2000). This observation is not completely understood and probably various mechanisms are in competition. Beyond doubt the La-rich mixed compounds do not superconduct because the Fermi surface of  $\text{LaNi}_2\text{B}_2\text{C}$  does not exhibit nesting features and the density of states at the Fermi level is not as high as in  $\text{LuNi}_2\text{B}_2\text{C}$  and  $\text{YNi}_2\text{B}_2\text{C}$  (see Sections 3.2 and 3.3). Also, La has a much larger ionic radius than Ho and, consequently, large distortions will occur around the La impurities. Furthermore, below 6 K  $\text{HoNi}_2\text{B}_2\text{C}$  is an antiferromagnetic superconductor. Therefore in a certain concentration range the La ions may act as non-magnetic impurities in an anti-

ferromagnetic superconductor (notice the kink in the Ho–La curve in Figure 69). The  $T_c$ -vs.- $\overline{DG}$  for (Ho,Y)Ni<sub>2</sub>B<sub>2</sub>C in Figure 69 obeys de Gennes scaling. However the substitution of Ho in HoNi<sub>2</sub>B<sub>2</sub>C by Y has also substantial consequences on the reentrant behavior (Zhao et al., 2006; Section 4.9.4), which is attributed to the multiband character of the coexistence of magnetism and superconductivity in this material.

### 6.5 (R,R')Ni<sub>2</sub>B<sub>2</sub>C superconductors with magnetic parent compounds

In this section we will consider examples of mixed systems where both parent compounds, RNi<sub>2</sub>B<sub>2</sub>C and R'Ni<sub>2</sub>B<sub>2</sub>C, develop long-range magnetic order on their lanthanide sublattices. Among them those with R and R' having similar atomic size and similar ionic magnetic properties are of particular interest. An example is Dy<sub>x</sub>Ho<sub>1-x</sub>Ni<sub>2</sub>B<sub>2</sub>C. According to Figure 28, both parent compounds have the same ground-state magnetic structure due to similar CEF-induced magnetic anisotropy (see Section 4). As shown in Figure 70 the expected overall de Gennes scaling of  $T_N$  observed in the RNi<sub>2</sub>B<sub>2</sub>C series with heavy lanthanides R (see Figure 5) continues to hold also in Dy<sub>x</sub>Ho<sub>1-x</sub>Ni<sub>2</sub>B<sub>2</sub>C. On the other hand, in the  $x$  range where both key temperatures,  $T_N(DG)$  and  $T_c(DG)$ , cross each other in the series Dy<sub>x</sub>Ho<sub>1-x</sub>Ni<sub>2</sub>B<sub>2</sub>C there is a total breakdown of the de Gennes scaling of  $T_c$ . This phenomenon has been analyzed by extending the phenomenological Ginzburg–Landau theory taking into account the multiband electronic structure of this material (as first done by Shulga et al., 1998 for YNi<sub>2</sub>B<sub>2</sub>C), in particular using two magnetic and two superconducting order parameters (Doh

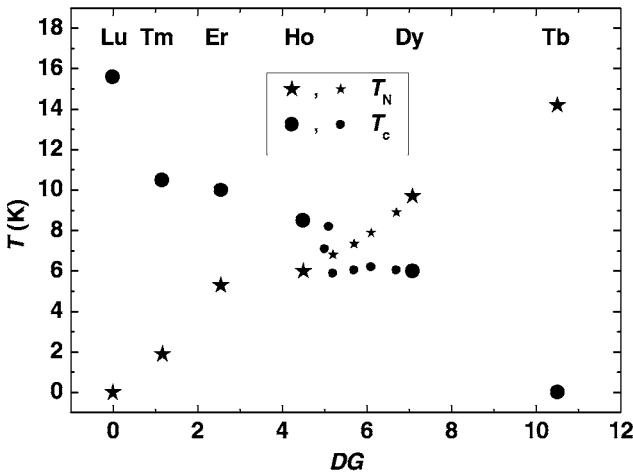


**FIGURE 70** Magnetic ordering temperature  $T_N$  and superconducting transition temperature  $T_c$  of various RNi<sub>2</sub>B<sub>2</sub>C compounds (large symbols) and Dy<sub>x</sub>Ho<sub>1-x</sub>Ni<sub>2</sub>B<sub>2</sub>C (small symbols for  $0 < x < 1$ ) as functions of the de Gennes factor DG of the corresponding R<sup>3+</sup> ions. For  $0 < x < 1$ , DG means the effective de Gennes factor  $\overline{DG}$  as defined in Section 6.3 (according to Figure 5 and Cho et al., 1996c).

et al., 1999). According to this model, the jump of  $T_c$  (at the crossing point in Figure 70) marks an intrinsic reentrant behavior, i.e. there the superconductivity with the higher (of the two)  $T_c$  values ceases to exist. This approach has been affirmed by experiments on pressure effects (J.-H. Choi et al., 2001; E.-M. Choi et al., 2003) as well as band-structure analysis (Drechsler et al., 2004; Shorikov et al., 2006).

Contrary to the behavior of  $\text{Dy}_x\text{Ho}_{1-x}\text{Ni}_2\text{B}_2\text{C}$ , the crossover from  $T_c > T_N$  to  $T_N > T_c$  in  $\text{Tb}_x\text{Er}_{1-x}\text{Ni}_2\text{B}_2\text{C}$  at  $x \approx 0.15$  does not affect the linear de Gennes scaling of  $T_c$  in the latter system but  $T_N$  remains constant below  $x \approx 0.5$  (Rustom et al., 1998). No analysis has been done so far to explain this behavior by (multiband) electron structure. Also the transition between the magnetic structures of the two parent compounds (see Figure 28) has not yet been studied: However there are results on the transition between the states of weak ferromagnetism (WFM) being present in both parent compounds. Kim and Cho (2002), Cho et al. (2003) and Sok and Cho (2004) found a nearly  $x$ -independent  $T_{\text{WFM}} \approx 2$  K for small Tb concentrations,  $x < 0.4$ , and a nearly  $x$ -independent  $T_{\text{WFM}} \approx 9$  K for  $x > 0.6$  but no continuous increase of  $T_{\text{WFM}}$  with  $x$ . On the other hand, Alleno et al. (2004a) report on reduced values of  $T_{\text{WFM}}$  in the concentration range  $0 < x < 0.25$ . This has been confirmed by Takeya et al. (2001), Takeya and El Massalami (2004), and El Massalami et al. (2005) who studied magnetization, magnetoresistance, and specific heat of  $\text{Tb}_{0.2}\text{Er}_{0.8}\text{Ni}_2\text{B}_2\text{C}$  single crystals and performed neutron-diffraction experiments on polycrystalline samples. These authors could not observe a transition to WFM in  $\text{Tb}_{0.2}\text{Er}_{0.8}\text{Ni}_2\text{B}_2\text{C}$  down to 1 K. Also, as expected, the squaring up of the spin-density wave (being considered as a prerequisite of the WFM in  $\text{ErNi}_2\text{B}_2\text{C}$ ; see Section 4.10.1) does not occur in the investigated temperature range, which has been attributed to a substitution-induced change of the crystalline electric fields (El Massalami et al., 2005).

A further interesting mixed system is  $\text{Dy}_x\text{Pr}_{1-x}\text{Ni}_2\text{B}_2\text{C}$  because, as in the case of  $\text{Dy}_x\text{Ho}_{1-x}\text{Ni}_2\text{B}_2\text{C}$ , both parent compounds have the same type of ground-state magnetic order shown in Figure 28. However the Dy and Pr parent compounds differ much more in their lattice constants than the Dy and Ho ones. Therefore a miscibility gap around  $x \approx 0.5$  is expected in the  $\text{Dy}_x\text{Pr}_{1-x}\text{Ni}_2\text{B}_2\text{C}$  series (see Freudenberger et al., 2001b) and it will be hard to find optimum heat-treatment conditions for obtaining the correct occupation of the lattice sites by the different atomic species (see also Section 3.1). In a series of papers on  $\text{Dy}_x\text{Pr}_{1-x}\text{Ni}_2\text{B}_2\text{C}$  (Takeya and Kuznietz, 1999; El Massalami et al., 2004; Takeya et al., 2005) a magnetic transition temperature  $T_0$  in addition to  $T_N$ , even for the  $x = 1$  parent compound  $\text{DyNi}_2\text{B}_2\text{C}$  has been found. In the latter case Takeya et al. (2005) report  $T_N = 16.3$  K and  $T_0 = 10.4$  K. Further work has to be done in order to clarify whether  $T_0$  is really an intrinsic property of the  $\text{Dy}_x\text{Pr}_{1-x}\text{Ni}_2\text{B}_2\text{C}$  compounds (see also Section 4.8). These authors also found that Pr strongly suppresses superconductivity, as  $\text{Dy}_{0.99}\text{Pr}_{0.01}\text{Ni}_2\text{B}_2\text{C}$  does not superconduct above 1.8 K. It is not yet clear whether this phenomenon is of similar nature as the suppression of superconductivity in  $\text{HoNi}_2\text{B}_2\text{C}$  by small amounts of La (see Section 6.4, Figure 69; also compare Section 4.3, Figure 30) or it is connected with certain magnetic ordering processes as proposed by Takeya et al. (2005).

## 7. CONCLUSIONS AND OUTLOOK

The rapid progress in the study of borocarbides is closely connected with the availability of high quality polycrystalline samples, single crystals, and thin films over a wide range of compositions. The main trends of superconducting properties and ordering of the lanthanide's magnetic moments have been elucidated. On the other hand many legitimate questions, e.g., why does  $\text{YPd}_2\text{B}_2\text{C}$  have the largest  $T_c$  (23 K) among the 1:2:2:1 superconductors, are still open. Much work has still to be done to establish the complete thermodynamic phase diagrams for the concerned quaternary systems and to prepare single-phase samples of metastable compounds such as  $\text{YPd}_2\text{B}_2\text{C}$  and  $\text{ScNi}_2\text{B}_2\text{C}$ . It has been particularly shown for  $\text{HoNi}_2\text{B}_2\text{C}$  that convenient low-temperature heat treatment is needed to reduce site disorder between boron and carbon.

One of the most interesting aspects of borocarbides is the possibility to observe both, coexistence and competition of superconductivity and magnetic order. Most of the zero-field magnetic structures have been determined, but a number of key questions remains to be clarified. A variety of both, commensurate and incommensurate magnetic structures were observed. To explain these structures theoretically a detailed understanding of the role of superexchange versus indirect exchange, combined with single-ion crystal field and hybridization effects, is needed. Inelastic neutron-scattering experiments giving the form of magnetic excitation spectra can provide a detailed picture of these interactions. Another significant aspect to be investigated is the coupling of the rare-earth ions to the conduction electrons. It would be interesting to know what is the extent of the Ni d-electron polarization in these materials. Additional experimental and theoretical efforts are necessary to understand magnetic phase diagrams of these compounds. The coupling of the magnetic and crystallographic structures through magnetoelastic interaction constitutes an additional complication for this study. Among the interesting problems that have to be solved in future is the question whether or not the (incommensurate) quadrupolar order reported to be present in  $\text{TmNi}_2\text{B}_2\text{C}$  in the magnetically non-ordered superconducting state can be confirmed and whether it also exists in other 1:2:2:1 superconductors. Also the correlation between this quadrupolar order and superconductivity is still unknown.

Superconducting and electronic properties of borocarbides exhibit rich and interesting behaviors. The band structure has been investigated in some detail for most of the materials. However the Fermi surface features have been investigated for a few systems only. As an important finding the Fermi surface of 1:2:2:1 superconductors shows a nesting feature at a wave vector  $\mathbf{q} \approx (0.55, 0, 0)$ , which has various consequences on the magnetic and superconducting properties of these materials. More work is needed to fully elucidate the electronic and itinerant-electron magnetic behavior. The superconductivity is thought to be phonon mediated. A direct manifestation of the electron-phonon coupling is observed in the remarkable, but quantitatively not yet fully understood boron isotope effect and in the softening of the phonon spectrum near the above mentioned nesting wave vector along the  $\mathbf{a}$ -axis, which is no doubt also related to some of the observed magnetic structures. The superconducting energy gap seems to be substantially of

s-wave character whereas the presence of a strong anisotropy or, alternatively, of gap point-nodes is controversially discussed. Most probably both, the proposed (s + g)-wave approach and the isotropic two-band model are too simple for a consistent description of the variety of measured properties. Seemingly, the influence of at least two different groups of electrons and also that of anisotropy within these bands has to be considered, taking into account the full multiband character and, furthermore, effects of additional anisotropy beyond the more or less anisotropic electron–phonon interaction. The multiband approach for strong-coupling systems firstly employed here, in the non-magnetic 1:2:2:1 superconductors, has been later successfully used to describe other novel superconductors such as MgB<sub>2</sub> and MgCNi<sub>3</sub>. In addition, the complex Fermi surface consisting of pieces with different orbital admixtures allows coexistence of ordinary extended s-wave superconductivity and commensurate antiferromagnetism in pure enough HoNi<sub>2</sub>B<sub>2</sub>C and DyNi<sub>2</sub>B<sub>2</sub>C samples on different Fermi surface pieces. The elucidation of the fate of the former electron group in the field of other magnetic structures realized in RNi<sub>2</sub>B<sub>2</sub>C with R = Er, Tm, etc., as well as in corresponding diluted magnetic mixed systems is an interesting problem, worth to be considered in more detail. The rather complex band character of superconductivity in HoNi<sub>2</sub>B<sub>2</sub>C is also evidenced by the complete disappearance of the out-of plane anisotropy of the upper critical field  $H_{c2}(T)$  in the commensurate antiferromagnetic phase below  $T_N$  whereas such anisotropy is observed in the paramagnetic and the incommensurate antiferromagnetic phases. The isotropy of  $H_{c2}(T)$  below  $T_N$  strongly supports that superconductivity survives at a special Fermi-surface sheet which is isolated from the influence of the lanthanide magnetism localized at the remaining Fermi-surface sheets. In non-magnetic borocarbides, in the temperature range from about  $T_c/3$  or  $T_c/2$  up to  $T_c$  there is probably a corresponding coexistence of uncondensed electrons with anisotropic multiband superconductivity on different Fermi-surface sheets (regions).

Another still unsolved problem is the relation of the **a**-axis modulated incommensurate magnetic structure to the superconductivity in HoNi<sub>2</sub>B<sub>2</sub>C. Even the details of this **a**-axis magnetic structure itself remain to be experimentally determined. Furthermore, the relation between incommensurate and metamagnetic structures appearing in this material for magnetic fields applied parallel to the basal plane has to be explored. The exact knowledge of the evolution of the magnetic structure for increasing applied magnetic field in the temperature range between 5 and 6 K is essential for better understanding of the anomalous decrease of  $H_{c2}(T)$  and the suppression of superconductivity in this range.

The absence of superconductivity for light lanthanide-based borocarbides has been understood to some extent but the reasons for this are not completely clear so far. Although YbNi<sub>2</sub>B<sub>2</sub>C is neither superconducting nor magnetically ordered, it reveals interesting properties at low temperatures where the formation of a heavy-fermion state was observed. Some indications of an anomalous behavior of PrNi<sub>2</sub>B<sub>2</sub>C were found, similar in some respects to that observed for YbNi<sub>2</sub>B<sub>2</sub>C. More work is necessary to understand these anomalies.

The investigation of pseudoquaternary compounds with two different rare earths on the R site in RNi<sub>2</sub>B<sub>2</sub>C revealed much insight into the pair-breaking

mechanisms in these materials, such as pair breaking by magnetic impurities in non-magnetic superconductors or by non-magnetic impurities in antiferromagnetic superconductors, the modification of both effects by crystal fields, as well as the influence of chemical pressure or disorder caused by the inhomogeneous (partially random) occupation of the R site.

A fundamental problem, which needs more exploration, is the interaction and coexistence of superconductivity and weak ferromagnetism discussed for  $\text{ErNi}_2\text{B}_2\text{C}$ . One of the important questions related to this problem is the possibility of the formation of a spontaneous vortex phase. The problem of coexistence of superconductivity and weak ferromagnetism in borocarbides is closely related to the similar issue for ruthenocuprates with typical compositions  $\text{RuSr}_2\text{GdCu}_2\text{O}_8$  or  $\text{RuSr}_2(\text{Gd,Ce})_2\text{Cu}_2\text{O}_{10}$ , for which the magnetic ordering temperatures are much higher than  $T_c$ .

The vortex lattice in non-magnetic  $\text{RNi}_2\text{B}_2\text{C}$  compounds ( $R = \text{Y, Lu}$ ) shows several unusual features. The most exciting one is a hexagonal-to-square transition found for increasing magnetic fields applied along the *c*-axis. The square vortex lattice is caused by the four-fold symmetry of the Fermi velocity. The resulting quasiparticle states localized around the cores of the vortices were imaged by scanning tunneling spectroscopy showing a star-shaped cross-section of the vortex cores. The structure, orientation, and field dependence of the vortex lattice have been successfully described by a non-local London model. At low applied magnetic fields, i.e. for large distances between the vortices, the hexagonal vortex lattice is not affected by the four-fold symmetry of the vortices. However, the square lattice becomes energetically favorable at higher fields, when the intervortex distance becomes comparable to the penetration depth. A square vortex lattice was found also in the magnetic borocarbides  $\text{ErNi}_2\text{B}_2\text{C}$  and  $\text{TmNi}_2\text{B}_2\text{C}$ . However, whereas for  $\text{YNi}_2\text{B}_2\text{C}$ ,  $\text{LuNi}_2\text{B}_2\text{C}$ , and  $\text{ErNi}_2\text{B}_2\text{C}$  a hexagonal-to-square transition of the vortex lattice was found as the applied magnetic field increases, the opposite transition is observed in  $\text{TmNi}_2\text{B}_2\text{C}$ . This surprising difference is not understood so far. Another open question is why all attempts to investigate the vortex lattice of  $\text{HoNi}_2\text{B}_2\text{C}$  by SANS experiments failed so far.

The open issues mentioned here should legitimate the assumption that this class of compounds will provide further substantial and general insight into mechanisms of superconductivity and its interplay with magnetism.

## ACKNOWLEDGEMENTS

In writing this article the authors had very close cooperation with G. Behr, J. Freudenberger, A. Kreyssig, V.N. Narozhnyi, L. Schultz, S. Shulga and A. Wälte.

The authors also would like to acknowledge many stimulating and important discussions with B. Bergk, H. Bitterlich, S. Borisenko, H.F. Braun, T. Cichorek, K. Dörr, Z. Drzazga, D. Eckert, J. Eckert, H. Eschrig, P. Fulde, J. Fink, P. Gegenwart, A. Gladun, L.C. Gupta, A. Gümbel, K. Häse, A. Handstein, B. Holzapfel, O. Ignatchik, M. Kulić, O. Kvitnitskaya, T. Leisegang, D. Lipp, W. Löser, M. Loewenhaupt, D.C. Meyer, Yu. Naidyuk, K. Nenkov, M. Nicklas, M. Nohara, I. Opahle,

P. Paufler, C. Ritter, H. Rosner, C. Sierks, D. Souptel, M. Weber, K. Winzer, S. Wimbush, M. Wolf and J. Wosnitza.

This report encloses many results and insights from discussions with the participants of the workshop on borocarbides, supported by NATO, held at Dresden in June 2000, in particular with E.M. Baggio-Saitovitch, P.C. Canfield, R.J. Cava, I. Felner, G. Hilscher, J.W. Lynn, K. Maki, A.I. Morozov, R. Nagarajan and I.K. Yanson.

This work has been supported by DFG (SFB463 and MU1015/4-2), RFBR (01-02-04002) and IFW Dresden.

## REFERENCES

- Abliz, M., Kindo, K., Kadowaki, K., Takeya, H. J. Phys. Soc. Jpn. 2003, **72**, 2599.
- Abrikosov, A.A. Zh. Eksp. Teor. Fiz. 1957, **32**, 1442 (engl. transl.: Sov. Phys. JETP 1957, **5**, 1174).
- Abrikosov, A.A. J. Phys.: Condens. Matter 2001, **13**, L943.
- Abrikosov, A.A., Gor'kov, L.P. Zh. Eksp. Teor. Fiz. 1960, **39**, 1781 (engl. transl.: Sov. Phys. JETP 1961, **12**, 1243).
- Adachi, H., Miranović, P., Ichioka, M., Machida, K. Phys. Rev. Lett. 2005, **94**, 067007.
- Aharony, A., Birgeneau, R.J., Coniglio, A., Kastner, M.A., Stanley, H.E. Phys. Rev. Lett. 1988, **60**, 1330.
- Akiyama, H., Kaji, S., Oomi, G., Cho, B.K., Canfield, P.C. J. Alloys Compd. 2006, **408–412**, 226.
- Allen, P.B., in: Lerner, R.G., Trigg, G.L., editors. Encyclopedia of Physics. New York: VCH Publishers; 1991, p. 1198.
- Alleno, E., Hossain, Z., Godart, C., Nagarajan, R., Gupta, L.C. Phys. Rev. B 1995a, **52**, 7428.
- Alleno, E., Neumeier, J.J., Thompson, J.D., Canfield, P.C., Cho, B.K. Physica C 1995b, **242**, 169.
- Alleno, E., Berger, P., Leroy, E., Godart, C., in: Müller, K.-H., Narozhnyi, V.N., editors. Rare Earth Transition Metal Borocarbides (Nitrides): Superconducting, Magnetic and Normal State Properties. Dordrecht: Kluwer Academic; 2001, p. 265.
- Alleno, E., Godart, C., André, G., Dhar, S.K., Pattalwar, S.M., Bonville, P., Nagarajan, R., Gupta, L.C. Phys. Rev. B 2003, **68**, 214518.
- Alleno, E., Talhaoui, M., Godart, C. J. Magn. Magn. Mater. 2004a, **272–276**, e159.
- Alleno, E., Vivet, S., Godart, C., Leroy, E. Physica C 2004b, **411**, 59.
- Allenspach, P., Gasser, U. J. Alloys Compd. 2000, **311**, 1.
- Amici, A., Thalmeier, P. Phys. Rev. B 1998, **57**, 10684.
- Amici, A., Thalmeier, P., Fulde, P. Phys. Rev. Lett. 2000, **84**, 1800.
- An, J.M., Pickett, W.E. Phys. Rev. Lett. 2001, **86**, 4366.
- Andersen, N.H., Jensen, J., Jensen, T.B.S., v. Zimmermann, M., Pinholt, R., Abrahamsen, A.B., Nørgaard Toft, K., Hedegård, P., Canfield, P.C. Phys. Rev. B 2006a, **73**, 020504(R).
- Andersen, N.H. et al., 2006b, unpublished result in Figure 48, to be published.
- Anderson, P.W. J. Phys. Chem. Solids 1959, **11**, 26.
- Anderson, P.W., Suhl, H. Phys. Rev. 1959, **116**, 898.
- Andreone, A., Iavarone, M., Vaglio, R., Manini, P., Cogliati, E. Appl. Phys. Lett. 1996, **69**, 118.
- Andreone, A., Aruta, C., Fontana, F., Iavarone, M., Russo, M.L., Vaglio, R., Crabtree, G.W., DeWilde, Y., in: Narlikar, A., editor. Studies of High Temperature Superconductors, vol. 26. New York: Nova Science; 1998, p. 79.
- Aoki, D., Huxley, A., Ressouche, E., Braithwaite, D., Flouquet, J., Brison, J.-P., Lhotel, E., Paulsen, C. Nature 2001, **413**, 613.
- Aranson, I., Gurevich, A., Vinokur, V. Phys. Rev. Lett. 2001, **87**, 067003.
- Arisawa, S., Hatano, T., Hirata, K., Mochiku, T., Kitaguchi, H., Fujii, H., Kumakura, H., Kadowaki, K., Nakamura, K., Togano, K. Appl. Phys. Lett. 1994, **65**, 1299.
- Ashcroft, N.W. Phys. Rev. Lett. 1968, **21**, 1748.
- Askerzade, I.N. Physica C 2003a, **397**, 99.
- Askerzade, I.N. J. Kor. Phys. Soc. 2003b, **43**, 111.

- Avila, M.A., Bud'ko, S.L., Canfield, P.C. *Phys. Rev. B* 2002, **66**, 132504.
- Avila, M.A., Wu, Y.Q., Condrón, C.L., Bud'ko, S.L., Kramer, M., Müller, G.J., Canfield, P.C. *Phys. Rev. B* 2004, **69**, 205107.
- Awana, V.P.S., in: Narlikar, A.V., editor. *Frontiers in Magnetic Materials*. Berlin: Springer; 2005, p. 531.
- Baba, T., Yokoya, T., Tsuda, S., Kiss, T., Shimojima, T., Shin, S., Togashi, T., Chen, C.T., Zhang, C.Q., Watanabe, S., Watanabe, T., Nohara, M., Takagi, H. *Physica C* 2006a, **445–448**, 46.
- Baba, T., Yokoya, T., Tsuda, S., Kiss, T., Shimojima, T., Shin, S., Togashi, T., Chen, C.T., Zhang, C.Q., Watanabe, S., Watanabe, T., Nohara, M., Takagi, H. *Physica B* 2006b, **378–380**, 469.
- Baggio-Saitovitch, E.M., Sánchez, D.R., Micklitz, H. *Physica C* 2000, **341–348**, 703.
- Baggio-Saitovitch, E.M., Sanchez, D.R., Micklitz, H., in: Müller, K.-H., Narozhnyi, V.N., editors. *Rare Earth Transition Metal Borocarbides (Nitrides): Superconducting, Magnetic and Normal State Properties*. Dordrecht: Kluwer Academic; 2001, p. 51.
- Baggio-Saitovitch, E.M., Sánchez, D.R., Fontes, M.B., Medeiros, S.N., Passamani, E., Micklitz, H. *Hyperfine Interact.* 2002a, **144/145**, 161.
- Baggio-Saitovitch, E.M., Sánchez, D.R., Micklitz, H. *Brazilian J. Phys.* 2002b, **32**, 739.
- Baltensperger, W., Strässler, S. *Phys. Kondens. Materie* 1963, **1**, 20.
- Barash, Yu.S., Svidzinskii, A.A., Mineev, V.P. *JETP Lett.* 1997, **65**, 638.
- Bardeen, J., in: Evetts, J., editor. *Concise Encyclopedia of Magnetic & Superconducting Materials*. Oxford: Pergamon Press; 1992, p. 554.
- Bardeen, J., Cooper, L.N., Schrieffer, J.R. *Phys. Rev.* 1957a, **106**, 162.
- Bardeen, J., Cooper, L.N., Schrieffer, J.R. *Phys. Rev.* 1957b, **108**, 1175.
- Bashlakov, D.L., Naidyuk, Yu.G., Yanson, I.K., Wimbush, S.C., Holzapfel, B., Fuchs, G., Drechsler, S.-L. *Supercond. Sci. Technol.* 2005, **18**, 1094.
- Bashlakov, D.L., Naidyuk, Yu.G., Yanson, I.K., Behr, G., Drechsler, S.-L., Fuchs, G., Schultz, L., Souptel, D. *J. Low Temp. Phys.* 2007, **147**, 335.
- Bauer, J., Bars, O. *Acta Crystallogr. B* 1980, **36**, 1540.
- Bauer, E.D., Dickey, R.P., Zapf, V.S., Maple, M.B. *J. Phys.: Condens. Matter* 2001, **13**, L759.
- Bauer, E.D., Frederick, N.A., Ho, P.-C., Zapf, V.S., Maple, M.B. *Phys. Rev. B* 2002, **65**, 100506(R).
- Bauernfeind, L., Widder, W., Braun, H.F. *Physica C* 1995, **254**, 151.
- Bednorz, J.G., Müller, K.A. *Z. Phys. B* 1986, **64**, 189.
- Behr, G., Löser, W. *Recent Res. Devel. Cryst. Growth* 2005, **4**, 129.
- Behr, G., Löser, W., Graw, G., Bitterlich, H., Freudenberger, J., Fink, J., Schultz, L. *J. Cryst. Growth* 1999a, **198/199**, 642.
- Behr, G., Löser, W., Graw, G., Nenkov, K., Krämer, U., Belger, A., Wehner, B. *J. Mater. Res.* 1999b, **14**, 16.
- Behr, G., Löser, W., Graw, G., Bitterlich, H., Fink, J., Schultz, L. *Cryst. Res. Technol.* 2000, **35**, 461.
- Belevtsev, B.I., Hennings, B.D., Rathnayaka, K.D.D., Naugle, D.G., in: Narlikar, A.V., editor. *Studies of High Temperature Superconductors*, vol. 46. New York: Nova Science; 2003, p. 99.
- Berger, P., Tominez, E., Godart, C., Alleno, E., Daudin, L., Gallien, J.-P. *J. Solid State Chem.* 2000, **154**, 301.
- Bergk, B. et al., 2007, to be published.
- Bernhard, C., Tallon, J.L., Niedermayer, Ch., Blasius, Th., Golnik, A., Brücher, E., Kremer, R.K., Noakes, D.R., Stronach, C.E., Ansaldo, E.J. *Phys. Rev. B* 1999, **59**, 14099.
- Beyermann, W.P., Lacerda, A.H., Canfield, P.C. *Physica B* 1999, **259–261**, 584.
- Bhatnagar, A.K., Rathnayaka, K.D.D., Naugle, D.G., Canfield, P.C. *Phys. Rev. B* 1997, **56**, 437.
- Bintley, D., Meeson, P.J. *Physica C* 2003, **388–389**, 181.
- Bitterlich, H., Löser, W., Behr, G., Nenkov, K., Fuchs, G., Gümbel, A., Schultz, L. *Physica C* 1999, **321**, 93.
- Bitterlich, H., Löser, W., Behr, G., Graw, G., Yang-Bitterlich, W., Krämer, U., Schultz, L. *J. Cryst. Growth* 2000, **213**, 319.
- Bitterlich, H., Löser, W., Lindenkreuz, H.-G., Schultz, L. *J. Alloys Compd.* 2001a, **325**, 285.
- Bitterlich, H., Löser, W., Behr, G., Drechsler, S.-L., Nenkov, K., Fuchs, G., Müller, K.-H., Schultz, L., in: Müller, K.-H., Narozhnyi, V.N., editors. *Rare Earth Transition Metal Borocarbides (Nitrides): Superconducting, Magnetic and Normal State Properties*. Dordrecht: Kluwer Academic; 2001b, p. 281.
- Bitterlich, H., Löser, W., Behr, G., Drechsler, S.-L., Nenkov, K., Fuchs, G., Müller, K.-H., Schultz, L. *Phys. Rev. B* 2002a, **65**, 224416.

- Bitterlich, H., Löser, W., Behr, G. *Mater. Lett.* 2002b, **57**, 59.
- Blackstead, H.A., Dow, J.D., Felner, I., Yelon, W.B. *Phys. Rev. B* 2001, **63**, 094517.
- Blaschkowski, B., Jing, H., Meyer, H.-J. *Angew. Chem. Int. Ed.* 2002, **41**, 3323.
- Blount, E.I., Varma, C.M. *Phys. Rev. Lett.* 1979, **42**, 1079.
- Bluhm, H., Sebastian, S.E., Guikema, J.W., Fisher, I.R., Moler, K.A. *Phys. Rev. B* 2006, **73**, 014514.
- Boaknin, E., Hill, R.W., Lupien, C., Taillefer, L., Canfield, P.C. *Physica C* 2000, **341–348**, 1845.
- Boaknin, E., Hill, R.W., Proust, C., Lupien, C., Taillefer, L., Canfield, P.C. *Phys. Rev. Lett.* 2001, **87**, 237001.
- Bobrov, N.L., Beloborod'ko, S.I., Tyutrina, L.V., Yanson, I.K., Naugle, D.G., Rathnayaka, K.D.D. *Phys. Rev. B* 2005, **71**, 014512.
- Bobrov, N.L., Beloborod'ko, S.I., Tyutrina, L.V., Chernobay, V.N., Yanson, I.K., Naugle, D.G., Rathnayaka, K.D.D. *Low Temp. Phys.* 2006, **32**, 489.
- Boby1, A.V., Shantsev, D.V., Johansen, T.H., Kang, W.N., Kim, H.J., Choi, E.M., Lee, S.I. *Appl. Phys. Lett.* 2002, **80**, 4588.
- Bommeli, F., Degiorgi, L., Wachter, P., Cho, B.K., Canfield, P.C., Chau, R., Maple, M.B. *Phys. Rev. Lett.* 1997, **78**, 547.
- Bonville, P., Hodges, J.A., Vaast, C., Alleno, E., Godart, C., Gupta, L.C., Hossain, Z., Nagarajan, R. *Physica B* 1996, **223&224**, 72.
- Bonville, P., Hodges, J.A., Hossain, Z., Nagarajan, R., Dhar, S.K., Gupta, L.C., Alleno, E., Godart, C. *Eur. Phys. J. B* 1999, **11**, 377.
- Boothroyd, A.T. *J. Alloys Compd.* 2000, **303–304**, 489.
- Boothroyd, A.T., Barratt, J.P., Lister, S.J.S., Wildes, A.R., Canfield, P.C., Bewley, R.I., in: Müller, K.-H., Narozhnyi, V.N., editors. *Rare Earth Transition Metal Borocarbides (Nitrides): Superconducting, Magnetic and Normal State Properties*. Dordrecht: Kluwer Academic; 2001, p. 163.
- Boothroyd, A.T., Barratt, J.P., Bonville, P., Canfield, P.C., Murani, A., Wildes, A.R., Bewley, R.I. *Phys. Rev. B* 2003, **67**, 104407.
- Bourdarot, F., Lynn, J.W., Baggio-Saitovitch, E., Huang, Q., Sanchez, D.R., Skanthakumar, S. *Phys. Rev. B* 2001, **64**, 104410.
- Brabers, J.H.V.J., Bakker, K., Nakotte, H., de Boer, F.R., Lenczowski, S.K.J., Buschow, K.H.J. *J. Alloys Compd.* 1993, **199**, L1.
- Brandow, B.H. *Philos. Mag.* 2003, **83**, 2487.
- Brandt, E.H. *Rep. Prog. Phys.* 1995, **58**, 1465.
- Braun, H.F., in: Müller, K.-H., Narozhnyi, V.N., editors. *Rare Earth Transition Metal Borocarbides (Nitrides): Superconducting, Magnetic and Normal State Properties*. Dordrecht: Kluwer Academic; 2001, p. 233.
- Braunisch, W., Knauf, N., Kataev, V., Neuhausen, S., Grütz, A., Kock, A., Roden, B., Khomskii, D., Wohlleben, D. *Phys. Rev. Lett.* 1992, **68**, 1908.
- van den Brink, J., Khaliullin, G., Khomskii, D., in: Chatterji, T., editor. *Colossal Magnetoresistive Magnetites*. Dordrecht: Kluwer Academic; 2004, p. 263.
- Brisson, J.P., Keller, N., Vernière, A., Lejay, P., Schmidt, L., Buzdin, A., Flouquet, J., Julian, S.R., Lonzarich, G.G. *Physica C* 1995, **250**, 128.
- Brown, S.P., Charalambous, D., Jones, E.C., Forgan, E.M., Kealey, P.G., Erb, A., Kohlbrecher, J. *Phys. Rev. Lett.* 2004, **92**, 067004.
- Buchgeister, M., Pitschke, W. *Physica C* 1996, **264**, 250.
- Buchgeister, M., Fuchs, G., Klosowski, J., Wiesner, U., Zawadzki, J. *Physica C* 1995, **255**, 19.
- Bud'ko, S.L., Canfield, P.C. *Phys. Rev. B* 2000a, **61**, R14932.
- Bud'ko, S.L., Canfield, P.C. *Physica B* 2000b, **280**, 356.
- Bud'ko, S.L., Canfield, P.C. *Phys. Rev. B* 2005, **71**, 024409.
- Bud'ko, S.L., Canfield, P.C. *C. R. Physique* 2006, **7**, 56.
- Bud'ko, S.L., Giordanengo, B., Sulpice, A., Fontes, M.B., Baggio-Saitovitch, E.M. *Solid State Commun.* 1995a, **94**, 119.
- Bud'ko, S.L., Fontes, M.B., Aliaga-Guerra, D., Baggio-Saitovitch, E.M. *Phys. Rev. B* 1995b, **52**, 305.
- Bud'ko, S.L., Elmassalami, M., Fontes, M.B., Mondragon, J., Vanoni, W., Giordanengo, B., Baggio-Saitovitch, E.M. *Physica C* 1995c, **243**, 183.
- Bud'ko, S.L., Demishev, G.B., Fontes, M.B., Baggio-Saitovitch, E. *J. Phys.: Condens. Matter* 1996, **8**, L159.

- Bud'ko, S.L., Canfield, P.C., Yatskar, A., Beyermann, W.P. *Physica B* 1997, **230–232**, 859.
- Bud'ko, S.L., Petrovic, C., Lapertot, G., Cunningham, C.E., Canfield, P.C., Jung, M.-H., Lacerda, A.H. *Phys. Rev. B* 2001a, **63**, 220503(R).
- Bud'ko, S.L., Kogan, V.G., Canfield, P.C. *Phys. Rev. B* 2001b, **64**, 180506(R).
- Bud'ko, S.L., Strand, J.D., Anderson Jr., N.E., Ribeiro, R.A., Canfield, P.C. *Phys. Rev. B* 2003, **68**, 104417.
- Bud'ko, S.L., Schmiedeshoff, G.M., Lapertot, G., Canfield, P.C. *J. Phys.: Condens. Matter* 2006a, **18**, 8353.
- Bud'ko, S.L., Schmiedeshoff, G.M., Canfield, P.C. *Solid State Commun.* 2006b, **140**, 281.
- Bulaevskii, L.N., Buzdin, A.I., Kulić, M.L., Panjukov, S.V. *Adv. Phys.* 1985, **34**, 175.
- Bullock, M., Zarestky, J., Stassis, C., Goldman, A., Canfield, P., Honda, Z., Shirane, G., Shapiro, S.M. *Phys. Rev. B* 1998, **57**, 7916.
- Buschow, K.H.J., in: Wohlfarth, E.P., editor. *Ferromagnetic Materials*, vol. 1. Amsterdam: North-Holland; 1980, p. 297.
- Campbell, A.J., Paul, D.McK., McIntyre, G.J. *Phys. Rev. B* 2000a, **61**, 5872.
- Campbell, A.J., Paul, D.McK., McIntyre, G.J. *Solid State Commun.* 2000b, **115**, 213.
- Canfield, P.C., Bud'ko, S.L. *J. Alloys Compd.* 1997, **262–263**, 169.
- Canfield, P.C., Bud'ko, S.L., in: Müller, K.-H., Narozhnyi, V.N., editors. *Rare Earth Transition Metal Borocarbides (Nitrides): Superconducting, Magnetic and Normal State Properties*. Dordrecht: Kluwer Academic; 2001, p. 33.
- Canfield, P.C., Fisher, I.R. *J. Cryst. Growth* 2001, **225**, 155.
- Canfield, P.C., Cho, B.K., Johnston, D.C., Finnemore, D.K., Hundley, M.F. *Physica C* 1994, **230**, 397.
- Canfield, P.C., Cho, B.K., Dennis, K.W. *Physica B* 1995, **215**, 337.
- Canfield, P.C., Bud'ko, S.L., Cho, B.K. *Physica C* 1996, **262**, 249.
- Canfield, P.C., Bud'ko, S.L., Cho, B.K., Lacerda, A., Farrell, D., Johnston-Halperin, E., Kalatsky, V.A., Pokrovsky, V.L. *Phys. Rev. B* 1997a, **55**, 970.
- Canfield, P.C., Bud'ko, S.L., Cho, B.K., Beyermann, W.P., Yatskar, A. *J. Alloys Compd.* 1997b, **250**, 596.
- Canfield, P.C., Gammel, P.L., Bishop, D.J. *Phys. Today* 1998, **51**, 40.
- Cao, G.H., Simon, P., Krämer, U., Wimbush, S.C., Holzapfel, B. *Chem. Mater.* 2004, **16**, 842.
- Cao, G.H., Skrotzki, W., Simon, P., Wimbush, S.C., Holzapfel, B. *Chem. Mater.* 2005, **17**, 3558.
- Cao, S., Sakai, S., Nishimura, K., Mori, K. *Physica C* 2000, **341–348**, 751.
- Cao, S., Sakai, S., Nishimura, K., Mori, K. *IEEE Trans. Appl. Supercond.* 2001, **11**, 3603.
- Cao, S., Zhang, J., Qin, X., Nishimura, K., Mori, K. *Physica C* 2003, **388–389**, 195.
- Cappannini, O.M., Rodríguez, C.O., Christensen, N.E. *Physica C* 1998, **306**, 101.
- Carbotte, J.P. *Rev. Mod. Phys.* 1990, **62**, 1027.
- Caroli, C., de Gennes, P.G., Matricon, J. *Phys. Lett.* 1964, **9**, 307.
- Carter, S.A., Batlogg, B., Cava, R.J., Krajewski, J.J., Peck Jr., W.F. *Phys. Rev. B* 1995a, **51**, 12829.
- Carter, S.A., Batlogg, B., Cava, R.J., Krajewski, J.J., Peck Jr., W.F. *Phys. Rev. B* 1995b, **51**, 12644.
- Cava, R.J., in: Müller, K.-H., Narozhnyi, V.N., editors. *Rare Earth Transition Metal Borocarbides (Nitrides): Superconducting, Magnetic and Normal State Properties*. Dordrecht: Kluwer Academic; 2001, p. 21.
- Cava, R.J., Takagi, H., Batlogg, B., Zandbergen, H.W., Krajewski, J.J., Peck Jr., W.F., van Dover, R.B., Felder, R.J., Siegrist, T., Mizuhashi, K., Lee, J.O., Eisaki, H., Carter, S.A., Uchida, S. *Nature* 1994a, **367**, 146.
- Cava, R.J., Takagi, H., Zandbergen, H.W., Krajewski, J.J., Peck Jr., W.F., Siegrist, T., Batlogg, B., van Dover, R.B., Felder, R.J., Mizuhashi, K., Lee, J.O., Eisaki, H., Uchida, S. *Nature* 1994b, **367**, 252.
- Cava, R.J., Zandbergen, H.W., Batlogg, B., Eisaki, H., Takagi, H., Krajewski, J.J., Peck Jr., W.F., Gyorgy, E.M., Uchida, S. *Nature* 1994c, **372**, 245.
- Cava, R.J., Batlogg, B., Siegrist, T., Krajewski, J.J., Peck Jr., W.F., Carter, S., Felder, R.J., Takagi, H., van Dover, R.B. *Phys. Rev. B* 1994d, **49**, 12384.
- Cava, R.J., Batlogg, B., Krajewski, J.J., Peck Jr., W.F., Siegrist, T., Fleming, R.M., Carter, S., Takagi, H., Felder, R.J., van Dover, R.B., Rupp Jr., L.W. *Physica C* 1994e, **226**, 170.
- Cavadini, N., Strässle, Th., Allenspach, P., Canfield, P.C., Bourges, Ph. *Eur. Phys. J. B* 2002, **29**, 377.
- Chakoumakos, B.C., Paranthaman, M. *Physica C* 1994, **227**, 143.
- Chang, L.J., Tomy, C.V., Paul, D.McK., Andersen, N.H., Yethiraj, M. *J. Phys.: Condens. Matter* 1996a, **8**, 2119.
- Chang, L.J., Tomy, C.V., Paul, D.McK., Ritter, C. *Phys. Rev. B* 1996b, **54**, 9031.

- Chen, Y., Liang, J.K., Chen, X.L., Liu, Q.L. *J. Alloys Compd.* 2000, **296**, L1.
- Cheon, K.O., Fisher, I.R., Kogan, V.G., Canfield, P.C., Miranović, P., Gammel, P.L. *Phys. Rev. B* 1998, **58**, 6463.
- Cheon, K.O., Fisher, I.R., Canfield, P.C. *Physica C* 1999, **312**, 35.
- Chia, E.E.M., Salamon, M.B., Park, T., Kim, H.-J., Lee, S.-I., Takeya, H. *Europhys. Lett.* 2006, **73**, 772.
- Chinchure, A.D., Nagarajan, R., Gupta, L.C. *Solid State Commun.* 1999, **110**, 691.
- Chinchure, A.D., Nagarajan, R., Gupta, L.C. *Physica B* 2000, **281&282**, 894.
- Cho, B.K. *Physica C* 1998, **298**, 305.
- Cho, B.K. *Physica C* 2000, **341–348**, 2025.
- Cho, B.K., Canfield, P.C., Johnston, D.C. *Phys. Rev. B* 1995a, **52**, R3844.
- Cho, B.K., Xu, M., Canfield, P.C., Miller, L.L., Johnston, D.C. *Phys. Rev. B* 1995b, **52**, 3676.
- Cho, B.K., Canfield, P.C., Miller, L.L., Johnston, D.C., Beyermann, W.P., Yatskar, A. *Phys. Rev. B* 1995c, **52**, 3684.
- Cho, B.K., Canfield, P.C., Johnston, D.C. *Phys. Rev. B* 1996a, **53**, 8499.
- Cho, B.K., Harmon, B.N., Johnston, D.C., Canfield, P.C. *Phys. Rev. B* 1996b, **53**, 2217.
- Cho, B.K., Canfield, P.C., Johnston, D.C. *Phys. Rev. Lett.* 1996c, **77**, 163.
- Cho, B.K., Kim, H.B., Lee, S.-I. *Phys. Rev. B* 2001, **63**, 144528.
- Cho, B.K., Kim, C.A., Ri, H.-C. *J. Appl. Phys.* 2003, **93**, 8662.
- Choi, C.K., Choi, E.S., Lee, J.H., Park, Y.W., Song, Y.S. *Phys. Rev. B* 1998, **57**, 126.
- Choi, E.-M., Choi, J.-H., Doh, H., Lee, S.-I., Ohashi, M., Mōri, N. *J. Low Temp. Phys.* 2003, **131**, 1181.
- Choi, J.-H., Doh, H., Choi, E.-M., Kim, H.-J., Lee, S.-I., Yamamoto, T., Kawae, T., Takeda, K. *J. Phys. Soc. Jpn.* 2001, **70**, 3037.
- Choi, J.-H., Doh, H., Choi, E.-M., Lee, S.-I., Ohashi, M., Mōri, N. *Phys. Rev. B* 2002, **65**, 024520.
- Choi, S.-M., Lynn, J.W., Lopez, D., Gammel, P.L., Canfield, P.C., Bud'ko, S.L. *Phys. Rev. Lett.* 2001, **87**, 107001.
- Christen, D.K., Kerchner, H.R., Sekula, S.T., Thorel, P. *Phys. Rev. B* 1980, **21**, 102.
- Christianson, A.D., Bud'ko, S.L., Schmiedeshoff, G.M., Beyermann, W.P., Canfield, P.C., Boebinger, G.S., Lacerda, A.H. *Physica B* 2001, **294–295**, 225.
- Chu, C.W., Lorenz, B., Meng, R.L., Xue, Y.Y., in: Narlikar, A.V., editor. *Frontiers in Superconducting Materials*. Berlin: Springer; 2005, p. 331.
- Chu, R.K., Chu, W.K., Chen, Q., Zhang, Z.H., Miller Jr, J.H. *J. Phys.: Condens. Matter* 2000, **12**, 275.
- Cimberle, M.R., Ferdeghini, C., Guasconi, P., Marrè, D., Putti, M., Siri, A.S., Canepa, F., Manfrinetti, P., Palenzona, A. *Physica C* 1997, **282–287**, 573.
- Civale, L., Silhanek, A.V., Thompson, J.R., Song, K.J., Tomy, C.V., Paul, D.McK. *Phys. Rev. Lett.* 1999, **83**, 3920.
- Coehoorn, R. *Physica C* 1994, **228**, 331.
- Cooper, A.S., Corenzwit, E., Longinotti, L.D., Matthias, B.T., Zachariasen, W.H. *Proc. Natl. Acad. Sci. USA* 1970, **67**, 313.
- Corcoran, R., Meeson, P., Onuki, Y., Probst, P.-A., Springford, M., Takita, K. *Physica B* 1994, **194–196**, 1573.
- Crespo, M., Suderow, H., Vieira, S., Bud'ko, S., Canfield, P.C. *Phys. Rev. Lett.* 2006, **96**, 027003.
- Cura, Ch., Schubert, R., Ewert, S. *Physica C* 2004, **408–410**, 140.
- Dagotto, E. *Rep. Prog. Phys.* 1999, **62**, 1525.
- Davidov, D., Baberschke, K., Mydosh, J.A., Nieuwenhuys, G.J. *J. Phys. F: Metal Phys.* 1977, **7**, L47.
- Dertinger, A. *Supraleitung und Magnetismus in Holmium-Nickel-Borocarbide vom Strukturtyp LuNi<sub>2</sub>B<sub>2</sub>C*, Thesis, Universität Bayreuth, Aachen: Shaker; 2001.
- Dertinger, A., Dinnebier, R.E., Kreyssig, A., Stephens, P.W., Pagola, S., Loewenhaupt, M., van Smaalen, S., Braun, H.F. *Phys. Rev. B* 2001, **63**, 184518.
- Dervenagas, P., Zarestky, J., Stassis, C., Goldman, A.I., Canfield, P.C., Cho, B.K. *Physica B* 1995a, **212**, 1.
- Dervenagas, P., Bullock, M., Zarestky, J., Canfield, P., Cho, B.K., Harmon, B., Goldman, A.I., Stassis, C. *Phys. Rev. B* 1995b, **52**, R9839.
- Dervenagas, P., Zarestky, J., Stassis, C., Goldman, A.I., Canfield, P.C., Cho, B.K. *Phys. Rev. B* 1996, **53**, 8506.
- Detlefs, C., Goldman, A.I., Stassis, C., Canfield, P.C., Cho, B.K., Hill, J.P., Gibbs, D. *Phys. Rev. B* 1996, **53**, 6355.

- Detlefs, C., Islam, A.H.M.Z., Gu, T., Goldman, A.I., Stassis, C., Canfield, P.C., Hill, J.P., Vogt, T. *Phys. Rev. B* 1997a, **56**, 7843.
- Detlefs, C., Islam, A.H.M.Z., Goldman, A.I., Stassis, C., Canfield, P.C., Hill, J.P., Gibbs, D. *Phys. Rev. B* 1997b, **55**, R680.
- Detlefs, C., Abernathy, D.L., Grübel, G., Canfield, P.C. *Europhys. Lett.* 1999, **47**, 352.
- Detlefs, C., Bourdarot, F., Burlet, P., Dervenagas, P., Bud'ko, S.L., Canfield, P.C. *Phys. Rev. B* 2000, **61**, R14916.
- Detlefs, C., Bourdarot, F., Burlet, P., Bud'ko, S.L., Canfield, P.C., in: Müller, K.-H., Narozhnyi, V.N., editors. *Rare Earth Transition Metal Borocarbides (Nitrides): Superconducting, Magnetic and Normal State Properties*. Dordrecht: Kluwer Academic; 2001, p. 155.
- Devereaux, T.P. *Phys. Rev. B* 2000, **62**, 682.
- Dewhurst, C.D., Doyle, R.A., Zeldov, E., Paul, D.McK. *Phys. Rev. Lett.* 1999, **82**, 827.
- Dewhurst, C.D., James, S.S., Doyle, R.A., Paltiel, Y., Shtrikman, H., Zeldov, E., Paul, McK.D. *Phys. Rev. B* 2001a, **63**, 060501(R).
- Dewhurst, C.D., James, S.S., Saha, N., Surdeanu, R., Paltiel, Y., Zeldov, E., Paul, D.McK., in: Müller, K.-H., Narozhnyi, V.N., editors. *Rare Earth Transition Metal Borocarbides (Nitrides): Superconducting, Magnetic and Normal State Properties*. Dordrecht: Kluwer Academic; 2001b, p. 347.
- Dewhurst, C.D., Levett, S.J., Paul, D.McK. *Phys. Rev. B* 2005, **72**, 014542.
- Dezaneti, L.M., Xue, Y.Y., Sun, Y.Y., Ross, K., Chu, C.W. *Physica C* 2000, **334**, 123.
- Dhar, S.K., Nagarajan, R., Hossain, Z., Tominez, E., Godart, C., Gupta, L.C., Vijayaraghavan, R. *Solid State Commun.* 1996, **98**, 985.
- Diviš, M., 2001, unpublished results.
- Diviš, M., Ruzs, J. *Appl. Phys. A* 2002, **74**, S772.
- Diviš, M., Schwarz, K., Blaha, P., Hilscher, G., Michor, H., Khmelevskiy, S. *Phys. Rev. B* 2000, **62**, 6774.
- Diviš, M., Michor, H., Khmelevskiy, S., Blaha, P., Hilscher, G., Schwarz, K., in: Müller, K.-H., Narozhnyi, V.N., editors. *Rare Earth Transition Metal Borocarbides (Nitrides): Superconducting, Magnetic and Normal State Properties*. Dordrecht: Kluwer Academic; 2001, p. 83.
- Diviš, M., Ruzs, J., Hilscher, G., Michor, H., Blaha, P., Schwarz, K. *Czech. J. Phys.* 2002, **52**, 283.
- Diviš, M., Ruzs, J., Michor, H., Hilscher, G., Blaha, P., Schwarz, K. *J. Alloys Compd.* 2005, **403**, 29.
- Dobrosavljević-Grujić, L., Miranović, P. *Physica C* 2003, **397**, 117.
- Doerr, M., Rotter, M., Lindbaum, A. *Adv. Phys.* 2005, **54**, 1.
- Doh, H., Sigríst, M., Cho, B.K., Lee, S.-I. *Phys. Rev. Lett.* 1999, **83**, 5350.
- Drechsler, S.-L., Mishonov, T., editors. *High- $T_c$  Superconductors and Related Materials*. Dordrecht: Kluwer Academic; 2001, pp. 1–559.
- Drechsler, S.-L., Shulga, S.V., Müller, K.-H., Fuchs, G., Freudenberger, J., Behr, G., Eschrig, H., Schultz, L., Golden, M.S., von Lips, H., Fink, J., Narozhnyi, V.N., Rosner, H., Zahn, P., Gladun, A., Lipp, D., Kreyssig, A., Loewenhaupt, M., Koepernik, K., Winzer, K., Krug, K. *Physica C* 1999a, **317–318**, 117.
- Drechsler, S.-L., Rosner, H., Shulga, S.V., Fuchs, G., von Lips, H., Freudenberger, J., Golden, M.S., Knapfer, M., Müller, K.-H., Schultz, L., Fink, J., Kaindl, G., Eschrig, H., Koepernik, K. *J. Low Temp. Phys.* 1999b, **117**, 1617.
- Drechsler, S.-L., Rosner, H., Shulga, S.V., Eschrig, H., Freudenberger, J., Fuchs, G., Nenkov, K., Müller, K.-H., Lipp, D., Gladun, A., Kreyssig, A., Koepernik, K., Gegenwart, P., Cichorek, T. *Physica C* 2000, **341–348**, 749.
- Drechsler, S.-L., Rosner, H., Shulga, S., Opahle, I., Eschrig, H., in: Müller, K.-H., Narozhnyi, V.N., editors. *Rare Earth Transition Metal Borocarbides (Nitrides): Superconducting, Magnetic and Normal State Properties*. Dordrecht: Kluwer Academic; 2001a, p. 403.
- Drechsler, S.-L., Rosner, H., Shulga, S.V., Opahle, I., Eschrig, H., Freudenberger, J., Fuchs, G., Nenkov, K., Müller, K.-H., Bitterlich, H., Löser, W., Behr, G., Lipp, D., Gladun, A. *Physica C* 2001b, **364–365**, 31.
- Drechsler, S.-L., Rosner, H., Shulga, S.V., Eschrig, H., in: Drechsler, S.-L., Mishonov, T., editors. *High- $T_c$  Superconductors and Related Materials*. Dordrecht: Kluwer Academic; 2001c, p. 167.
- Drechsler, S.-L., Opahle, I., Shulga, S.V., Eschrig, H., Fuchs, G., Müller, K.-H., Löser, W., Bitterlich, H., Behr, G., Rosner, H. *Physica B* 2003, **329–333**, 1352.
- Drechsler, S.-L., Rosner, H., Opahle, I., Shulga, S.V., Eschrig, H. *Physica C* 2004, **408–410**, 104.

- Drechsler, S.-L. et al., 2007, to be published.
- Drzazga, Z., Fuchs, G., Handstein, A., Nenkov, K., Müller, K.-H. *Physica C* 2003, **383**, 421.
- Dugdale, S.B., Alam, M.A., Wilkinson, I., Hughes, R.J., Fisher, I.R., Canfield, P.C., Jarlborg, T., Santi, G. *Phys. Rev. Lett.* 1999, **83**, 4824.
- Dukan, S., Powell, T.P., Tešanović, Z. *Phys. Rev. B* 2002, **66**, 014517.
- Du Mar, A.C., Rathnayaka, K.D.D., Naugle, D.G., Canfield, P.C. *Int. J. Mod. Phys. B* 1998, **12**, 3264.
- Dunlap, B.D., Slaski, M., Hinks, D.G., Soderholm, L., Beno, M., Zhang, K., Segre, C., Crabtree, G.W., Kwok, W.K., Malik, S.K., Schuller, I.K., Jorgensen, J.D., Sungaila, Z. *J. Magn. Magn. Mater.* 1987, **68**, L139.
- Dunlap, B.D., Slaski, M., Sungaila, Z., Hinks, D.G., Zhang, K., Segre, C., Malik, S.K., Alp, E.E. *Phys. Rev. B* 1988, **37**, 592(R).
- Durán, A., Muñoz, E., Bernès, S., Escudero, R. *J. Phys.: Condens. Matter* 2000, **12**, 7595.
- Durán, A., Bernès, S., Escudero, R. *Phys. Rev. B* 2002, **66**, 212510.
- Durán, A., Bernès, S., Falconi, R., Escudero, R., Laborde, O., Guillot, M. *Phys. Rev. B* 2006, **74**, 134513.
- Dzyaloshinsky, I.E. *Zh. Eksp. Teor. Fiz.* 1957, **33**, 1454 (engl. transl.: *Sov. Phys. JETP* 1958, **6**, 1120).
- Eibenstein, U., Jung, W. *J. Solid State Chem.* 1997, **133**, 21.
- Eisaki, H., Takagi, H., Cava, R.J., Batlogg, B., Krajewski, J.J., Peck Jr., W.F., Mizuhashi, K., Lee, J.O., Uchida, S. *Phys. Rev. B* 1994, **50**, 647(R).
- Ekimov, E.A., Sidorov, V.A., Bauer, E.D., Mel'nik, N.N., Curro, N.J., Thompson, J.D., Stishov, S.M. *Nature* 2004, **428**, 542.
- Ekino, T., Fujii, H., Kosugi, M., Zenitani, Y., Akimitsu, J. *Phys. Rev. B* 1996, **53**, 5640.
- El-Hagary, M., Michor, H., Jambrich, C., Hauser, R., Galli, M., Bauer, E., Hilscher, G. *J. Magn. Magn. Mater.* 1998, **177–181**, 551.
- El-Hagary, M., Michor, H., Hilscher, G. *Physica B* 2000a, **284–288**, 1489.
- El-Hagary, M., Michor, H., Hilscher, G. *Phys. Rev. B* 2000b, **61**, 11695.
- Eliashberg, G.M. *Zh. Eksp. Teor. Fiz.* 1960, **38**, 966 (engl. transl.: *Sov. Phys. JETP* 1960, **11**, 696).
- El Massalami, M., Baggio-Saitovitch, E., Sulpice, A. *J. Alloys Compd.* 1995a, **228**, 49.
- El Massalami, M., Giordanengo, B., Mondragon, J., Baggio-Saitovitch, E.M., Takeuchi, A., Voiron, J., Sulpice, A. *J. Phys.: Condens. Matter* 1995b, **7**, 10015.
- El Massalami, M., Bud'ko, S.L., Giordanengo, B., Baggio-Saitovitch, E.M. *Physica C* 1995c, **244**, 41.
- El Massalami, M., Amaral Jr., M.R., Ghivelder, L., Abrego Castillo, I., Nieuwenhuys, G.J., Snel, C.E. *J. Magn. Magn. Mater.* 1997, **172**, 139.
- El Massalami, M., Rapp, R.E., Nieuwenhuys, G.J. *Physica C* 1998a, **304**, 184.
- El Massalami, M., da Costa, M.S., Novak, M.A., Barthel, V. *J. Magn. Magn. Mater.* 1998b, **188**, 379.
- El Massalami, M., da Costa, M.S., Rapp, R.E., Chaves, F.A.B. *Phys. Rev. B* 2000, **62**, 8942.
- El Massalami, M., Takeya, H., Hirata, K., Amara, M., Galera, R.-M., Schmitt, D. *Phys. Rev. B* 2003a, **67**, 144421.
- El Massalami, M., Rapp, R.E., Chaves, F.A.B., Takeya, H., Chaves, C.M. *Phys. Rev. B* 2003b, **67**, 224407.
- El Massalami, M., Rapp, R.E., Takeya, H., in: Narlikar, A.V., editor. *Studies of High Temperature Superconductors*, vol. 46. New York: Nova Science; 2003c, p. 153.
- El Massalami, M., Borges, H.A., Takeya, H., Rapp, R.E., Chaves, F.A.B. *J. Magn. Magn. Mater.* 2004, **279**, 5.
- El Massalami, M., Galera, R.-M., Schmitt, D., Ouladdiaf, B., Takeya, H. *Phys. Rev. B* 2005, **72**, 144521.
- Eremets, M.I., Struzhkin, V.V., Mao, H.-K., Hemley, R.J. *Science* 2001, **293**, 272.
- Eskildsen, M.R., Gammel, P.L., Barber, B.P., Ramirez, A.P., Bishop, D.J., Andersen, N.H., Mortensen, K., Bolle, C.A., Lieber, C.M., Canfield, P.C. *Phys. Rev. Lett.* 1997a, **79**, 487.
- Eskildsen, M.R., Gammel, P.L., Barber, B.P., Yaron, U., Ramirez, A.P., Huse, D.A., Bishop, D.J., Bolle, C., Lieber, C.M., Oxx, S., Sridhar, S., Andersen, N.H., Mortensen, K., Canfield, P.C. *Phys. Rev. Lett.* 1997b, **78**, 1968.
- Eskildsen, M.R., Harada, K., Gammel, P.L., Abrahamsen, A.B., Andersen, N.H., Ernst, G., Ramirez, A.P., Bishop, D.J., Mortensen, K., Naugle, D.G., Rathnayaka, K.D.D., Canfield, P.C. *Nature* 1998, **393**, 242.
- Eskildsen, M.R., Harada, K., Gammel, P.L., Andersen, N.H., Ernst, G., Ramirez, A.P., Bishop, D.J., Mortensen, K., Canfield, P.C. *Physica B* 1999, **259–261**, 582.
- Eskildsen, M.R., Fisher, I.R., Gammel, P.L., Bishop, D.J., Andersen, N.H., Mortensen, K., Canfield, P.C. *Physica C* 2000, **332**, 320.

- Eskildsen, M.R., Nørgaard, K., Abrahamsen, A.B., Andersen, N.H., Mortensen, K., Gammel, P.L., Lopez, D., Bishop, D.J., Vorderwisch, P., Meissner, M., Canfield, P.C., in: Müller, K.-H., Narozhnyi, V.N., editors. Rare Earth Transition Metal Borocarbides (Nitrides): Superconducting, Magnetic and Normal State Properties. Dordrecht: Kluwer Academic; 2001a, p. 333.
- Eskildsen, M.R., Abrahamsen, A.B., Kogan, V.G., Gammel, P.L., Mortensen, K., Andersen, N.H., Canfield, P.C. Phys. Rev. Lett. 2001b, **86**, 5148.
- Eskildsen, M.R., Dewhurst, C.D., Hoogenboom, B.W., Petrovic, C., Canfield, P.C. Phys. Rev. Lett. 2003, **90**, 187001.
- Eversmann, K., Handstein, A., Fuchs, G., Cao, L., Müller, K.-H. Physica C 1996, **266**, 27.
- Falconi, R., Durán, A., Escudero, R. Phys. Rev. B 2002, **65**, 024505.
- Fay, D., Appel, J. Phys. Rev. B 1980, **22**, 3173.
- Fehrenbacher, R., Rice, T.M. Phys. Rev. Lett. 1993, **70**, 3471.
- Felner, I. Solid State Commun. 1984, **52**, 191.
- Felner, I., in: Narlikar, A., editor. Studies of High Temperature Superconductors, vol. 26. New York: Nova Science; 1998, p. 27.
- Felner, I., in: Müller, K.-H., Narozhnyi, V.N., editors. Rare Earth Transition Metal Borocarbides (Nitrides): Superconducting, Magnetic and Normal State Properties. Dordrecht: Kluwer Academic; 2001, p. 197.
- Felner, I., Godart, C., Alleno, E. Physica C 1997a, **282–287**, 1317.
- Felner, I., Schmitt, D., Barbara, B., Godart, C., Alleno, E. J. Solid State Chem. 1997b, **133**, 5.
- Felner, I., Asaf, U., Levi, Y., Millo, O. Phys. Rev. B 1997c, **55**, R3374.
- Felner, I., Asaf, U., Reich, S., Tsabba, Y. Physica C 1999, **311**, 163.
- Felner, I., Galstyan, E., Nowik, I. Phys. Rev. B 2005, **71**, 064510.
- Felner, C. J. Solid State Chem. 2001, **160**, 93.
- Ferdeghini, C., Grassano, G., Bellingeri, E., Marré, D., Ramadan, W., Ferrando, V., Beneduce, C. Int. J. Mod. Phys. B 2003, **17**, 824.
- Fernandez-Baca, J.A., Lynn, J.W. J. Appl. Phys. 1981, **52**, 2183.
- Fertig, W.A., Johnston, D.C., DeLong, L.E., McCallum, R.W., Maple, M.B., Matthias, B.T. Phys. Rev. Lett. 1977, **38**, 987.
- Fil, V.D., Knigavko, A., Zholobenko, A.N., Choi, E.-M., Lee, S.-I. Phys. Rev. B 2004, **70**, 220504(R).
- Fil, V.D., Fil, D.V., Zholobenko, A.N., Burma, N.G., Avramenko, Yu.A., Kim, J.D., Choi, S.M., Lee, S.I. Europhys. Lett. 2006, **76**, 484.
- Fink, H.J., Thorsen, A.C., Parker, E., Zackay, V.F., Toth, L. Phys. Rev. 1965, **138**, A1170.
- Fischer, Ø., in: Buschow, K.H.J., Wohlfarth, E.P., editors. Ferromagnetic Materials, vol. 5. Amsterdam: Elsevier; 1990, p. 466.
- Fischer, Ø., Maple, M.B., editors. Superconductivity in Ternary Compounds I, Structural, Electronic, and Lattice Properties. Berlin: Springer; 1982.
- Fisher, I.R., Cooper, J.R., Cava, R.J. Phys. Rev. B 1995, **52**, 15086.
- Fisher, I.R., Cooper, J.R., Canfield, P.C. Phys. Rev. B 1997, **56**, 10820.
- Fletcher, J.D., Carrington, A., Kazakov, S.M., Karpinski, J. Phys. Rev. B 2004, **70**, 144501.
- Fontes, M.B., Trochez, J.C., Giordanengo, B., Bud'ko, S.L., Sanchez, D.R., Baggio-Saitovitch, E.M., Continentino, M.A. Phys. Rev. B 1999, **60**, 6781.
- Foulkes, I.F., Gyorffy, B.L. Phys. Rev. B 1977, **15**, 1395.
- Freudenberger, J. Paarbrechung in Seltenerd-Übergangsmetall-Borocarbiden, Thesis, TU Dresden, 2000.
- Freudenberger, J., Drechsler, S.-L., Fuchs, G., Kreyssig, A., Nenkov, K., Shulga, S.V., Müller, K.-H., Schultz, L. Physica C 1998a, **306**, 1.
- Freudenberger, J., Fuchs, G., Nenkov, K., Handstein, A., Wolf, M., Kreyssig, A., Müller, K.-H., Loewenhaupt, M., Schultz, L. J. Magn. Magn. Mater. 1998b, **187**, 309.
- Freudenberger, J., Narozhnyi, V.N., Kochetkov, V.N., Nenkov, K.A., Fuchs, G., Handstein, A., Müller, K.-H., Schultz, L. J. Low Temp. Phys. 1999a, **117**, 1605.
- Freudenberger, J., Kreyssig, A., Ritter, C., Nenkov, K., Drechsler, S.-L., Fuchs, G., Müller, K.-H., Loewenhaupt, M., Schultz, L. Physica C 1999b, **315**, 91.
- Freudenberger, J., Fuchs, G., Müller, K.-H., Nenkov, K., Drechsler, S.-L., Kreyssig, A., Rosner, H., Koepf, K., Lipp, D., Schultz, L. J. Low Temp. Phys. 1999c, **117**, 1623.
- Freudenberger, J., Fuchs, G., Nenkov, K., Drechsler, S.-L., Müller, K.-H., Schultz, L. Physica C 2000, **339**, 195.

- Freudenberger, J., Fuchs, G., Nenkov, K., Drechsler, S.L., Müller, K.-H., Schultz, L., Kreyssidig, A., Loewenhaupt, M., in: Müller, K.-H., Narozhnyi, V.N., editors. Rare Earth Transition Metal Borocarbides (Nitrides): Superconducting, Magnetic and Normal State Properties. Dordrecht: Kluwer Academic; 2001a, p. 275.
- Freudenberger, J., Fuchs, G., Müller, K.-H., Schultz, L. Mater. Res. Bull. 2001b, **36**, 117.
- Fuchs, G., Müller, K.-H., Freudenberger, J., Nenkov, K., Drechsler, S.-L., Rosner, H., Shulga, S.V., Gladun, A., Lipp, D., Cichorek, T., Gegenwart, P., in: Müller, K.-H., Narozhnyi, V.N., editors. Rare Earth Transition Metal Borocarbides (Nitrides): Superconducting, Magnetic and Normal State Properties. Dordrecht: Kluwer Academic; 2001, p. 243.
- Fuchs, G., Drechsler, S.-L., Shulga, S.V., Handstein, A., Narozhnyi, V.N., Nenkov, K., Müller, K.-H., Rosner, H., in: Narlikar, A.V., editor. Studies of High Temperature Superconductors, vol. 41. New York: Nova Science; 2002a, p. 171.
- Fuchs, G., Müller, K.-H., Freudenberger, J., Nenkov, K., Drechsler, S.-L., Shulga, S.V., Lipp, D., Gladun, A., Cichorek, T., Gegenwart, P. Pramana – J. Phys. 2002b, **58**, 791.
- Fuchs, G., Müller, K.-H., Drechsler, S.-L., Shulga, S., Nenkov, K., Freudenberger, J., Behr, G., Souptel, D., Handstein, A., Wälte, A., Lipp, D., Gupta, L.C. Physica C 2004, **408–410**, 107.
- Fuger, R., Krutzler, C., Fuchs, G., Behr, G., Weber, H.W. Physica C 2007, **460–462**, 628.
- Fukazawa, H., Nomura, T., Ikeda, H., Yamada, K. J. Phys. Soc. Jpn. 2001, **70**, 3011.
- Fulde, P., Ferrell, R.A. Phys. Rev. 1964, **135**, A550.
- Fulde, P., Keller, J., in: Maple, M.B., Fischer, Ø., editors. Superconductivity in Ternary Compounds, Superconductivity and Magnetism. Berlin: Springer; 1982, p. 249.
- Fulde, P., Peschel, I. Adv. Phys. 1972, **21**, 1.
- Gabovich, A.M., Voitenko, A.I., Annett, J.F., Ausloos, M. Supercond. Sci. Technol. 2001, **14**, R1.
- Gammel, P.L., Barber, B.P., Ramirez, A.P., Varma, C.M., Bishop, D.J., Canfield, P.C., Kogan, V.G., Eskildsen, M.R., Andersen, N.H., Mortensen, K., Harada, K. Phys. Rev. Lett. 1999a, **82**, 1756.
- Gammel, P.L., Bishop, D.J., Eskildsen, M.R., Mortensen, K., Andersen, N.H., Fisher, I.R., Cheon, K.O., Canfield, P.C., Kogan, V.G. Phys. Rev. Lett. 1999b, **82**, 4082.
- Gammel, P.L., Barber, B., Lopez, D., Ramirez, A.P., Bishop, D.J., Bud'ko, S.L., Canfield, P.C. Phys. Rev. Lett. 2000a, **84**, 2497.
- Gammel, P.L., Lopez, D., Bishop, D.J., Eskildsen, M.R., Andersen, N.H., Mortensen, K., Fisher, I.R., Cheon, K.O., Canfield, P.C. J. Appl. Phys. 2000b, **87**, 5544.
- Gangopadhyay, A.K., Schilling, J.S. Phys. Rev. B 1996, **54**, 10107.
- Gao, L., Qiu, X.D., Cao, Y., Meng, R.L., Sun, Y.Y., Xue, Y.Y., Chu, C.W. Phys. Rev. B 1994, **50**, 9445.
- Gasparov, V.A., Sidorov, N.S., Zver'kova, I.I. Phys. Rev. B 2006, **73**, 094510.
- Gasser, U., 1999, Magnetic properties of the rare earth borocarbides  $RNi_2B_2C$ —A neutron scattering study, Thesis, ETH Zürich/PSI Villigen.
- Gasser, U., Allenspach, P., in: Müller, K.-H., Narozhnyi, V.N., editors. Rare Earth Transition Metal Borocarbides (Nitrides): Superconducting, Magnetic and Normal State Properties. Dordrecht: Kluwer Academic; 2001, p. 131.
- Gasser, U., Allenspach, P., Fauth, F., Henggeler, W., Mesot, J., Furrer, A., Rosenkranz, S., Vorderwisch, P., Buchgeister, M. Z. Phys. B 1996, **101**, 345.
- Gasser, U., Allenspach, P., Mesot, J., Furrer, A. Physica C 1997, **282–287**, 1327.
- Gasser, U., Allenspach, P., Furrer, A., 1998a, unpublished.
- Gasser, U., Allenspach, P., Furrer, A., Mulders, A.M. J. Alloys Compd. 1998b, **275–277**, 587.
- Gavaler, J.R., Janocko, M.A., Jones, C.K. J. Appl. Phys. 1974, **45**, 3009.
- de Gennes, P.-G. C. R. Acad. Sci. 1958, **247**, 1836.
- Ghosh, G., Chinchure, A.D., Nagarajan, R., Godart, C., Gupta, L.C. Phys. Rev. B 2001, **63**, 212505.
- Gilardi, R., Mesot, J., Drew, A., Divakar, U., Lee, S.L., Forgan, E.M., Zaharko, O., Conder, K., Aswal, V.K., Dewhurst, C.D., Cubitt, R., Momono, N., Oda, M. Phys. Rev. Lett. 2002, **88**, 217003.
- Gilardi, R., Mesot, J., Brown, S.P., Forgan, E.M., Drew, A., Lee, S.L., Cubitt, R., Dewhurst, C.D., Uefuji, T., Yamada, K. Phys. Rev. Lett. 2004, **93**, 217001.
- Ginzburg, V.L. Zh. Eksp. Teor. Fiz. 1956, **31**, 202 (engl. transl.: Sov. Phys. JETP 1957, **4**, 153).
- Ginzburg, V.L. Phys. Lett. 1964, **13**, 101.
- Ginzburg, V.L. Physics-Uspeski 2000, **43**, 573.
- Ginzburg, V.L., Landau, L.D. Zh. Eksp. Teor. Fiz. 1950, **20**, 1064.

- Giorgi, A.L., Szklarz, E.G., Krupka, M.C., Krikorian, N.H. *J. Less-Common Met.* 1969, **17**, 121.
- Godart, C., Gupta, L.C., Nagarajan, R., Dhar, S.K., Noel, H., Potel, M., Mazumdar, C., Hossain, Z., Levy-Clement, C., Schiffmacher, G., Padalia, B.D., Vijayaraghavan, R. *Phys. Rev. B* 1995, **51**, 489.
- Godart, C., Alleno, E., Tominez, E., Gupta, L.C., Nagarajan, R., Hossain, Z., Lynn, J.W., Bonville, P., Hodges, J.A., Sanchez, J.P., Felner, I. *J. Solid State Chem.* 1997, **133**, 169.
- Goldman, A.I., Stassis, C., Canfield, P.C., Zarestky, J., Dervenagas, P., Cho, B.K., Johnston, D.C., Sternlieb, B. *Phys. Rev. B* 1994, **50**, 9668(R).
- Goll, G., Heinecke, M., Jansen, A.G.M., Joss, W., Nguyen, L., Steep, E., Winzer, K., Wyder, P. *Phys. Rev. B* 1996, **53**, R8871.
- Gonnelli, R.S., Morello, A., Ummarino, G.A., Stepanov, V.A., Behr, G., Graw, G., Shulga, S.V., Drechsler, S.-L. *Int. J. Mod. Phys. B* 2000, **14**, 2840;
- Gonnelli, R.S., Morello, A., Ummarino, G.A., Stepanov, V.A., Behr, G., Graw, G., Shulga, S.V., Drechsler, S.-L. *Physica C* 2000, **341–348**, 1957.
- Goodenough, J.B. *Phys. Rev.* 1955, **100**, 564.
- Goodman, B.B., Wertheimer, M. *Phys. Lett.* 1965, **18**, 236.
- Goodrich, R.G., Young, D.P., Hall, D., Balicas, L., Fisk, Z., Harrison, N., Betts, J., Miglioro, A., Woodward, F.M., Lynn, J.W. *Phys. Rev. B* 2004, **69**, 054415.
- Gor'kov, L.P. *Zh. Eksp. Teor. Fiz.* 1959, **36**, 1918 (engl. transl.: *Sov. Phys. JETP* 1959, **9**, 1364) and *Zh. Eksp. Teor. Fiz.* 1959, **37**, 1407 (engl. transl.: *Sov. Phys. JETP* 1960, **10**, 998).
- Gor'kov, L.P., Rusinov, A.I. *Zh. Eksp. Teor. Fiz.* 1964, **46**, 1363 (engl. transl.: *Sov. Phys. JETP* 1964, **19**, 922).
- Grassano, G., Canepa, F., Marrè, D., Putti, M., Ramadan, W., Siri, A.S., Ferdeghini, C., in: Müller, K.-H., Narozhnyi, V.N., editors. *Rare Earth Transition Metal Borocarbides (Nitrides): Superconducting, Magnetic and Normal State Properties*. Dordrecht: Kluwer Academic; 2001a, p. 369.
- Grassano, G., Marrè, D., Pallecchi, I., Ricci, F., Siri, A.S., Ferdeghini, C. *Supercond. Sci. Technol.* 2001b, **14**, 117.
- Graw, G., Günther, K., Behr, G., Löser, W., Nenkov, K., Krämer, U. *J. Alloys Compd.* 2001, **319**, 162.
- Grewe, N., Steglich, F., in: Gschneidner Jr., K.A., Eyring, L., editors. *Handbook on the Physics and Chemistry of Rare Earths*, vol. 14. Amsterdam: Elsevier; 1991, p. 343.
- Grigereit, T.E., Lynn, J.W., Huang, Q., Santoro, A., Cava, R.J., Krajewski, J.J., Peck Jr., W.F. *Phys. Rev. Lett.* 1994, **73**, 2756.
- Gümbel, A., Eckert, J., Handstein, A., Schultz, L. *Physica B* 2000a, **284–288**, 1107.
- Gümbel, A., Eckert, J., Handstein, A., Skrotzki, W., Schultz, L. *Mater. Sci. Forum* 2000b, **343–346**, 924.
- Gulden, Th., Henn, R.W., Jepsen, O., Kremer, R.K., Schnelle, W., Simon, A., Felser, C. *Phys. Rev. B* 1997, **56**, 9021.
- Gunnarsson, O. *Rev. Mod. Phys.* 1997, **69**, 575.
- Gupta, L.C. *Philos. Mag. B* 1998, **77**, 717.
- Gupta, L.C. *J. Phys. Soc. Jpn.* 2000, **69**, A138.
- Gupta, L.C. *Adv. Phys.* 2006, **55**, 691.
- Gupta, L.C., Nagarajan, R., Hossain, Z., Mazumdar, C., Dhar, S.K., Godart, C., Levy-Clement, C., Padalia, B.D., Vijayaraghavan, R. *J. Magn. Magn. Mater.* 1995, **140–144**, 2053.
- Gurevich, A. *Phys. Rev. B* 2003, **67**, 184515.
- Gurevich, A., Kogan, V.G. *Phys. Rev. Lett.* 2001, **87**, 177009.
- Gusev, A.I., Rempel, A.A., Lipatnikov, V.N. *Phys. Status Solidi (b)* 1996, **194**, 467.
- Gygi, F., Schlüter, M. *Phys. Rev. B* 1991, **43**, 7609.
- Haas, St., Maki, K. *Phys. Rev. B* 2002, **65**, 020502(R).
- Häse, K., Holzapfel, B., Schultz, L. *Physica C* 1997, **288**, 28.
- Häse, K., Holzapfel, B., Schultz, L. *Physica C* 2000a, **341–348**, 761.
- Häse, K., Hough, D., Holzapfel, B., Schultz, L. *Physica B* 2000b, **284–288**, 1105.
- Häse, K., Wimbush, S.C., Eckert, D., Paschen, S., Holzapfel, B., Schultz, L., in: Müller, K.-H., Narozhnyi, V.N., editors. *Rare Earth Transition Metal Borocarbides (Nitrides): Superconducting, Magnetic and Normal State Properties*. Dordrecht: Kluwer Academic; 2001a, p. 363.
- Häse, K., Wimbush, S.C., Paschen, S., Holzapfel, B. *IEEE Trans. Appl. Supercond.* 2001b, **11**, 3836.
- Hamid, A.S. *Int. J. Mod. Phys. B* 2003, **17**, 5973.
- Hannay, N.B., Geballe, T.H., Matthias, B.T., Andres, K., Schmidt, P., MacNair, D. *Phys. Rev. Lett.* 1965, **14**, 225.

- Havinga, E.E., Damsma, H., Kanis, J.M. *J. Less-Common Met.* 1972, **27**, 281.
- He, T., Huang, Q., Ramirez, A.P., Wang, Y., Regan, K.A., Rogado, N., Hayward, M.A., Haas, M.K., Slusky, J.S., Inumara, K., Zandbergen, H.W., Ong, N.P., Cava, R.J. *Nature* 2001, **411**, 54.
- Heinecke, M., Winzer, K. *Z. Phys. B* 1995, **98**, 147.
- Henn, R.W., Bernhard, C., Kremer, R.K., Gulden, Th., Simon, A., Blasius, Th., Niedermayer, Ch. *Phys. Rev. B* 2000, **62**, 14469; and references cited therein.
- Hennings, B.D., Rathnayaka, K.D.D., Naugle, D.G., Canfield, P.C. *Physica C* 2001, **364–365**, 257.
- Hennings, B.D., Naugle, D.G., Canfield, P.C. *Phys. Rev. B* 2002, **66**, 214512.
- Hill, J.P., Sternlieb, B.J., Gibbs, D., Detlefs, C., Goldman, A.I., Stassis, C., Canfield, P.C., Cho, B.K. *Phys. Rev. B* 1996, **53**, 3487.
- Hillenbrand, B., Wilhelm, M. *Phys. Lett.* 1970, **31**, A448.
- Hillier, A.D., Preston, J.M., Stewart, J.R., Cywinski, R. *Hyperfine Interact.* 2001, **136/137**, 313.
- Hillier, A.D., Smith, R.I., Cywinski, R. *Appl. Phys. A* 2002, **74**, S823.
- Hilscher, G., Michor, H., in: Narlikar, A., editor. *Studies of High Temperature Superconductors*, vol. 28. New York: Nova Science; 1999, p. 241.
- Hilscher, G., Michor, H., Divis, M., in: Müller, K.-H., Narozhnyi, V.N., editors. *Rare Earth Transition Metal Borocarbides (Nitrides): Superconducting, Magnetic and Normal State Properties*. Dordrecht: Kluwer Academic; 2001, p. 187.
- Hilscher, G., Michor, H., El-Hagary, M., Divis, M. *Egypt. J. Sol.* 2002, **25**, 153.
- Hoellwarth, C.C., Klavins, P., Shelton, R.N. *Phys. Rev. B* 1996, **53**, 2579.
- Hohenberg, P.C., Werthamer, N.R. *Phys. Rev.* 1967, **153**, 493.
- Hossain, Z., Gupta, L.C., Mazumdar, C., Nagarajan, R., Dhar, S.K., Godart, C., Levy-Clement, C., Padalia, B.D., Vijayaraghavan, R. *Solid State Commun.* 1994, **92**, 341.
- Hossain, Z., Dhar, S.K., Nagarajan, R., Gupta, L.C., Godart, C., Vijayaraghavan, R. *IEEE Trans. Mag.* 1995, **31**, 4133.
- Hossain, Z., Nagarajan, R., Dhar, S.K., Gupta, L.C. *J. Magn. Magn. Mater.* 1998, **184**, 235.
- Hossain, Z., Nagarajan, R., Dhar, S.K., Gupta, L.C. *Physica B* 1999, **259–261**, 606.
- Hossain, Z., Geibel, C., Gupta, L.C., Nagarajan, R., Godart, C. *J. Phys.: Condens. Matter* 2002, **14**, 7045.
- Hotta, T. *Rep. Prog. Phys.* 2006, **69**, 2061.
- Hsu, Y.Y., Chiang, H.C., Ku, H.C. *J. Appl. Phys.* 1998, **83**, 6789.
- Huang, C.L., Lin, J.-Y., Sun, C.P., Lee, T.K., Kim, J.D., Choi, E.M., Lee, S.I., Yang, H.D. *Phys. Rev. B* 2006, **73**, 012502.
- Hüser, D., Rewiersma, M.J.F.M., Mydosh, J.A., Nieuwenhuys, G.J. *Phys. Rev. Lett.* 1983, **51**, 1290.
- Hutchings, M.T., in: Seitz, F., Turnbull, D., editors. *Solid State Physics*, vol. 16. New York: Academic Press; 1964, p. 227.
- Iavarone, M., Andreone, A., Cassinese, A., DiCapua, R., Gianni, L., Vaglio, R., de Wilde, Y., Crabtree, G.W., in: Müller, K.-H., Narozhnyi, V.N., editors. *Rare Earth Transition Metal Borocarbides (Nitrides): Superconducting, Magnetic and Normal State Properties*. Dordrecht: Kluwer Academic; 2001, p. 357.
- Ignatchik, O., Coffey, T., Hagel, J., Jäckel, M., Jobiliong, E., Souptel, D., Behr, G., Wosnitza, J. *J. Magn. Magn. Mater.* 2005, **290–291**, 424.
- Ishikawa, M., Fischer, Ø. *Solid State Commun.* 1977, **23**, 37.
- Ishikawa, M., Fischer, Ø., Müller, J., in: Maple, M.B., Fischer, Ø., editors. *Superconductivity in Ternary Compounds II, Superconductivity and Magnetism*. Berlin: Springer; 1982, p. 143.
- Isida, S., Matsushita, A., Takeya, H., Suzuki, M. *Physica C* 2001, **349**, 150.
- Iwamoto, Y., Ueda, K., Kohara, T. *Solid State Commun.* 2000, **113**, 615.
- Izawa, K., Shibata, A., Matsuda, Y., Kato, Y., Takeya, H., Hirata, K., van der Beek, C.J., Konczykowski, M. *Phys. Rev. Lett.* 2001, **86**, 1327.
- Izawa, K., Kamata, K., Nakajima, Y., Matsuda, Y., Watanabe, T., Nohara, M., Takagi, H., Thalmeier, P., Maki, K. *Phys. Rev. Lett.* 2002, **89**, 137006.
- Izawa, K., Nakajima, Y., Goryo, J., Matsuda, Y., Osaki, S., Sugawara, H., Sato, H., Thalmeier, P., Maki, K. *Phys. Rev. Lett.* 2003, **90**, 117001.
- Jacobs, T., Willemsen, B.A., Sridhar, S., Nagarajan, R., Gupta, L.C., Hossain, Z., Mazumdar, C., Canfield, P.C., Cho, B.K. *Phys. Rev. B* 1995, **52**, R7022.
- Jaenicke-Rössler, U., Zahn, G., Paufler, P., Bitterlich, H., Behr, G. *Physica C* 1998, **305**, 209.

- Jaiswal-Nagar, D., Thakur, A.D., Eskildsen, M.R., Canfield, P.C., Yusuf, S.M., Ramakrishnan, S., Grover, A.K. *Physica B* 2005, **359–361**, 476.
- Jaiswal-Nagar, D., Thakur, A.D., Ramakrishnan, S., Grover, A.K., Pal, D., Takeya, H. *Phys. Rev. B* 2006, **74**, 184514.
- James, S.S., Dewhurst, C.D., Doyle, R.A., Paul, D.McK., Paltiel, Y., Zeldov, E., Campbell, A.M. *Physica C* 2000, **332**, 173.
- James, S.S., Dewhurst, C.D., Field, S.B., Paul, D.McK., Paltiel, Y., Shtrikman, H., Zeldov, E., Campbell, A.M. *Phys. Rev. B* 2001, **64**, 092512.
- Jensen, A., Nørgaard Toft, K., Abrahamsen, A.B., McMorro, D.F., Eskildsen, M.R., Andersen, N.H., Jensen, J., Hedegård, P., Klenke, J., Danilkin, S., Prokes, K., Sikolenko, V., Smeibidl, P., Bud'ko, S.L., Canfield, P.C. *Phys. Rev. B* 2004, **69**, 104527.
- Jensen, J. *Phys. Rev. B* 2002, **65**, 140514(R).
- Jensen, J., Hedegård, P. *Phys. Rev. B* 2007, **76**, 094504.
- Jiang, P.J., Lin, M.S., Shieh, J.H., You, Y.B., Ku, H.C., Ho, J.C. *Phys. Rev. B* 1995, **51**, 16436.
- Jo, Y., Park, J.-G., Kim, C.A., Cho, B.K., Kim, H.C., Ri, H.-C., Doh, H., Lee, S.-I. *J. Korean Phys. Soc.* 2003, **43**, 263.
- Johnston-Halperin, E., Fiedler, J., Farrell, D.E., Xu, M., Cho, B.K., Canfield, P.C., Finnemore, D.K., Johnston, D.C. *Phys. Rev. B* 1995, **51**, 12852.
- Jones, T.E., Kwak, J.F., Chock, E.P., Chaikin, P.M. *Solid State Commun.* 1978, **27**, 209.
- Just, G., Paufler, P. *J. Alloys Compd.* 1996, **232**, 1.
- Kalatsky, V.A., Pokrovsky, V.L. *Phys. Rev. B* 1998, **57**, 5485.
- Kanamori, J. *J. Appl. Phys.* 1960, **31**, 14S.
- Kaneko, K., Onodera, H., Yamauchi, H., Sakon, T., Motokawa, M., Yamaguchi, Y. *Phys. Rev. B* 2003, **68**, 012401.
- Kasahara, Y., Iwasawa, T., Shishido, H., Shibauchi, T., Behnia, K., Haga, Y., Matsuda, T.D., Onuki, Y., Sigrist, M., Matsuda, Y. *Phys. Rev. Lett.* 2007, **99**, 116402.
- Kawano, H., Takeya, H., Yoshizawa, H., Kadowaki, K. *J. Phys. Chem. Solids* 1999, **60**, 1053.
- Kawano-Furukawa, H. *Physica C* 2004, **408–410**, 68.
- Kawano-Furukawa, H., Habuta, E., Nagata, T., Nagao, M., Yoshizawa, H., Furukawa, N., Takeya, H., Kadowaki, K. 2001; *cond-mat/0106273*.
- Kawano-Furukawa, H., Takeshita, H., Ochiai, M., Nagata, T., Yoshizawa, H., Furukawa, N., Takeya, H., Kadowaki, K. *Phys. Rev. B* 2002a, **65**, 180508(R).
- Kawano-Furukawa, H., Yoshizawa, H., Takeya, H., Kadowaki, K. *Phys. Rev. B* 2002b, **66**, 212503.
- Keller, J., Fulde, P. *J. Low Temp. Phys.* 1971, **4**, 289.
- Khomskii, D.I., Kugel, K.I. *Phys. Rev. B* 2003, **67**, 134401.
- Kim, C.-A., Cho, B.K. *Phys. Rev. B* 2002, **66**, 214501.
- Kim, H., Hwang, C.-D., Ihm, J. *Phys. Rev. B* 1995, **52**, 4592.
- Kim, H.-J., Choi, J.-H., Doh, H., Choi, E.-M., Lee, S.-I., Ohashi, M., Mōri, N. *Physica B* 2003, **327**, 438.
- Kiruthika, G.V.M., Behr, G., Kulkarni, R., Dhar, S.K., Gupta, L.C. *Physica C* 2004, **405**, 245.
- Kiruthika, G.V.M., Paulose, P.L., Patil, S., Gupta, L.C. *Physica C* 2005, **433**, 9.
- Kitō, H., Ikeda, S., Takekawa, S., Abe, H., Kitazawa, H. *Physica C* 1997, **291**, 332.
- Kobayashi, Y., Iwata, M., Okamoto, T., Takeya, H., Kuroki, K., Suzuki, M., Asai, K. *Physica B* 2006, **378–380**, 475.
- Kogan, V.G., Zhelezina, N.V. *Phys. Rev. B* 2005, **71**, 134505.
- Kogan, V.G., Miranović, P., Dobrosavljević-Grujić, Lj., Pickett, W.E., Christen, D.K. *Phys. Rev. Lett.* 1997a, **79**, 741.
- Kogan, V.G., Bullock, M., Harmon, B., Miranović, P., Dobrosavljević-Grujić, Lj., Gammel, P.L., Bishop, D.J. *Phys. Rev. B* 1997b, **55**, R8693.
- Kogan, V.G., Bud'ko, S.L., Canfield, P.C., Miranović, P. *Phys. Rev. B* 1999, **60**, R12577.
- Kogan, V.G., Bud'ko, S.L., Fisher, I.R., Canfield, P.C. *Phys. Rev. B* 2000, **62**, 9077.
- Kogan, V.G., Prozorov, R., Bud'ko, S.L., Canfield, P.C., Thompson, J.R., Karpinski, J., Zhigadlo, N.D., Miranović, P. *Phys. Rev. B* 2006, **74**, 184521.
- Kohgi, M., Iwasa, K., Nakajima, M., Metoki, N., Araki, S., Bernhoeft, N., Mignot, J.-M., Gukasov, A., Sato, H., Aoki, Y., Sugawara, H. *J. Phys. Soc. Jpn.* 2003, **72**, 1002.
- Kolesnichenko, Yu.A., Shevchenko, S.N. *Low Temp. Phys.* 2005, **31**, 137.

- Kontani, H. *Phys. Rev. B* 2004, **70**, 054507.
- Kortus, J., Mazin, I.I., Belashchenko, K.D., Antropov, V.P., Boyer, L.L. *Phys. Rev. Lett.* 2001, **86**, 4656.
- Kramer, L., Pesch, W. *Z. Physik* 1974, **269**, 59.
- Kramers, H.A. *Proc. Acad. Sci. (Amsterdam)* 1930, **33**, 959.
- Kremer, R.K., Kim, J.S., Simon, A., in: Bussmann-Holder, A., Keller, H., editors. *High  $T_c$  Superconductors and Related Transition Metal Oxides*. Berlin: Springer; 2007, p. 213.
- Kreyßig, A., Einfluß der magnetischen Ordnung auf Supraleitung und Kristallstruktur in Seltenerd-Nickel-Borborocarbide-Verbindungen, Thesis, TU Dresden; 2001.
- Kreyßig, A., Loewenhaupt, M., Müller, K.-H., Fuchs, G., Handstein, A., Ritter, C. *Physica B* 1997, **234–236**, 737.
- Kreyßig, A., Loewenhaupt, M., Freudenberger, J., Müller, K.-H., Ritter, C. *J. Appl. Phys.* 1999a, **85**, 6058.
- Kreyßig, A., Freudenberger, J., Sierks, C., Loewenhaupt, M., Müller, K.-H., Hoser, A., Stuesser, N. *Physica B* 1999b, **259–261**, 590.
- Kreyßig, A., Freudenberger, J., Ritter, C., Hoser, A., Hofmann, M., Fuchs, G., Müller, K.-H., Loewenhaupt, M. *Physica B* 2000, **276–278**, 554.
- Kreyßig, A., Schneidewind, A., Loewenhaupt, M., Ritter, C., Freudenberger, J., Fuchs, G., Müller, K.-H., in: Müller, K.-H., Narozhnyi, V.N., editors. *Rare Earth Transition Metal Borocarbides (Nitrides): Superconducting, Magnetic and Normal State Properties*. Dordrecht: Kluwer Academic; 2001, p. 181.
- Kreyßig, A., Stockert, O., Reznik, D., Woodward, F.M., Lynn, J.W., Reichardt, W., Souptel, D., Behr, G., Loewenhaupt, M. *Physica B* 2004, **350**, 69.
- Kreyßig, A. et al., 2005, unpublished result; see also (Souptel, 2005).
- Krupka, M.C., Giorgi, A.L., Krikorian, N.H., Szklarz, E.G. *J. Less-Common Met.* 1969, **19**, 113.
- Krutzler, C., Fuger, R., Eisterer, M., Fuchs, G., Behr, G., Weber, H.W. *Phys. Rev. B* 2005, **72**, 144508.
- Ku, H.C., Shelton, R.N. *Mater. Res. Bull.* 1980, **15**, 1441.
- Ku, H.C., Lai, C.C., You, Y.B., Shieh, J.H., Guan, W.Y. *Phys. Rev. B* 1994, **50**, 351.
- Kübert, C., Hirschfeld, P.J. *Solid State Commun.* 1998, **105**, 459.
- Kugel, K.I., Khomskii, D.I. *Sov. Phys. Usp.* 1982, **25**, 231.
- Kumari, K., Singhal, R.K., Garg, K.B., Heinonen, M., Leiro, J., Norblad, P., Gupta, L.C. *Int. J. Mod. Phys. B* 2003, **17**, 361.
- Kusunose, H. *J. Phys. Soc. Jpn.* 2005, **74**, 1119.
- Kuznietz, M., Gonçalves, A.P., Almeida, M. *J. Magn. Magn. Mater.* 2002, **248**, 423.
- Lacerda, A., Yatskar, A., Schmiedeshoff, G.M., Beyermann, W.P., Canfield, P.C. *Philos. Mag. B* 1996, **74**, 641.
- Lai, C.C., Lin, M.S., You, Y.B., Ku, H.C. *Phys. Rev. B* 1995, **51**, 420.
- Lan, M.D. *J. Phys. Chem. Solids* 2001, **62**, 1827.
- Lan, M.D., Chang, J.C., Lee, C.Y. *J. Phys. Chem. Solids* 2000, **61**, 2035.
- Lan, M.D., Chang, J.C., Lu, K.T., Lee, C.Y., Shih, H.Y., Jeng, G.Y. *IEEE Trans. Appl. Supercond.* 2001, **11**, 3607.
- Landau, I.L., Keller, H. *Physica C* 2007, doi:10.1016/j.physc.2007.07.003.
- Larkin, A.I., Ovchinnikov, Yu.N. *Zh. Eksp. Teor. Fiz.* 1964, **47**, 1136 (engl. transl.: *Sov. Phys. JETP* 1965, **20**, 762).
- Larkin, A.I., Ovchinnikov, Yu.N. *J. Low Temp. Phys.* 1979, **34**, 409.
- Lascialfari, A., Mishonov, T., Rigamonti, A., Zucca, I., Behr, G., Löser, W., Drechsler, S.-L. *Eur. Phys. J. B* 2003, **35**, 325.
- Lawrie, D.D., Franck, J.P. *Physica C* 1995, **245**, 159.
- Le, L.P., Heffner, R.H., Thompson, J.D., Nieuwenhuys, G.J., Maclaughlin, D.E., Canfield, P.C., Cho, B.K., Amato, A., Feyerherm, R., Gygax, F.N., Schenck, A. *Hyperfine Interact.* 1997, **104**, 49.
- Lee, H.C., Choi, H.-Y. *Phys. Rev. B* 2002, **65**, 174530.
- Lee, J.I., Zhao, T.S., Kim, I.G., Min, B.I., Youn, S.J. *Phys. Rev. B* 1994, **50**, 4030.
- Lee, K.H., Mean, B.J., Seo, S.W., Han, K.S., Kim, D.H., Lee, M., Lee, S.I., Cho, B.K. *Int. J. Mod. Phys. B* 1999, **13**, 3682.
- Lee, K.H., Mean, B.J., Go, G.S., Seo, S.W., Han, K.S., Kim, D.H., Lee, M., Cho, B.K., Lee, S.I. *Phys. Rev. B* 2000, **62**, 123.
- Lee, W.H., Zeng, H.K. *Solid State Commun.* 1997, **101**, 323.

- Lee, W.H., Appl, S., Shelton, R.N. *J. Low Temp. Phys.* 1987, **68**, 147.
- Lee, W.H., Zeng, H.K., Yao, Y.D., Chen, Y.Y. *Physica C* 1996, **266**, 138.
- Leiderer, P., Boneberg, J., Brüll, P., Bujok, V., Herminghaus, S. *Phys. Rev. Lett.* 1993, **71**, 2646.
- Leisegang, T., Meyer, D.C., Paufler, P., et al., 2006, unpublished results.
- Lejay, P., Chevalier, B., Etourneau, J., Hagenmuller, P., Peshev, P. *Synth. Met.* 1981, **4**, 139.
- Levett, S.J., Dewhurst, C.D., Paul, D.McK. *Phys. Rev. B* 2002, **66**, 014515.
- Levin, K., Nass, M.J., Ro, C., Grest, G.S., in: Matsubara, T., Kotani, A., editors. *Superconductivity in Magnetic and Exotic Materials*. Berlin: Springer; 1984, p. 104.
- Levy, P.M., Morin, P., Schmitt, D. *Phys. Rev. Lett.* 1979, **42**, 1417.
- Li, D.P., Lin, P.-J., Rosenstein, B., Shapiro, B.Ya., Shapiro, I. *Phys. Rev. B* 2006, **74**, 174518.
- Li, S., de Andrade, M.C., Freeman, E.J., Sirvent, C., Dickey, R.P., Amann, A., Frederick, N.A., Rathnayaka, K.D.D., Naugle, D.G., Bud'ko, S.L., Canfield, P.C., Beyermann, W.P., Maple, M.B. *Philos. Mag.* 2006, **86**, 3021.
- Lin, M.S., Shieh, J.H., You, Y.B., Hsu, Y.Y., Chen, J.W., Lin, S.H., Yao, Y.D., Chen, Y.Y., Ho, J.C., Ku, H.C. *Physica C* 1995, **249**, 403.
- Link, J.R., Loureiro, S.M., Kealhofer, C., Zandbergen, H.W., Cava, R.J. *J. Solid State Chem.* 2002, **164**, 246.
- Lipp, D., Gladun, A., Bartkowski, K., Belger, A., Paufler, P., Behr, G. *Physica B* 2000, **284–288**, 1103.
- Lipp, D., Schneider, M., Gladun, A., Drechsler, S.-L., Freudenberger, J., Fuchs, G., Nenkov, K., Müller, K.-H., Cichorek, T., Gegenwart, P., in: Müller, K.-H., Narozhnyi, V.N., editors. *Rare Earth Transition Metal Borocarbides (Nitrides): Superconducting, Magnetic and Normal State Properties*. Dordrecht: Kluwer Academic; 2001, p. 89.
- Lipp, D., Drechsler, S.-L., Schneider, M., Gladun, A., Freudenberger, J., Fuchs, G., Nenkov, K., Müller, K.-H., in: Annett, J.F., Kruchinin, S., editors. *New Trends in Superconductivity*, vol. 67. Dordrecht: Kluwer Academic; 2002a, p. 245.
- Lipp, D., Schneider, M., Gladun, A., Drechsler, S.-L., Freudenberger, J., Fuchs, G., Nenkov, K., Müller, K.-H., Cichorek, T., Gegenwart, P. *Europhys. Lett.* 2002b, **58**, 435.
- Lipp, D., Drechsler, S.-L., Freudenberger, J., Fuchs, G., Nenkov, K., Müller, K.-H., Schneider, M., Gladun, A. *Physica C* 2003, **388–389**, 183.
- von Lips, H., Hu, Z., Grazioli, C., Drechsler, S.-L., Behr, G., Knupfer, M., Golden, M.S., Fink, J., Rosner, H., Kaindl, G. *Phys. Rev. B* 1999, **60**, 11444.
- Loewenhaupt, M., Kreyssig, A., Sierks, C., Müller, K.-H., Freudenberger, J., Ritter, C., Schober, H., in: Büttner H.G., Leadbetter A.J., editors. *ILL Annual Report*, Grenoble; 1997, p. 37.
- London, F., London, H. *Proc. Roy. Soc. (London) A* 1935a, **149**, 71.
- London, F., London, H. *Physica* 1935b, **2**, 341.
- Looney, C., Gangopadhyay, A.K., Klehe, A.-K., Schilling, J.S. *Physica C* 1995, **252**, 199.
- Loureiro, S.M., Kealhofer, C., Felser, C., Cava, R.J. *Solid State Commun.* 2001, **119**, 675.
- Luke, G.M., Le, L.P., Sternlieb, B.J., Uemura, Y.J., Brewer, J.H., Kadono, R., Kiefl, R.F., Kreitzman, S.R., Riseman, T.M., Stronach, C.E., Davis, M.R., Uchida, S., Takagi, H., Tokura, Y., Hidaka, Y., Murakami, T., Gopolarishnan, J., Sleight, A.W., Subramanian, M.A., Early, E.A., Markert, J.T., Maple, M.B., Seaman, C.L. *Phys. Rev. B* 1990, **42**, 7981.
- Lynn, J.W. *J. Alloys Compd.* 1992, **181**, 419.
- Lynn, J.W. *J. Alloys Compd.* 1997, **250**, 552.
- Lynn, J.W., in: Müller, K.-H., Narozhnyi, V.N., editors. *Rare Earth Transition Metal Borocarbides (Nitrides): Superconducting, Magnetic and Normal State Properties*. Dordrecht: Kluwer Academic; 2001, p. 121.
- Lynn, J.W., Moncton, D.E., Passell, L., Thomlinson, W. *Phys. Rev. B* 1980, **21**, 70.
- Lynn, J.W., Gotaas, J.A., Erwin, R.W., Ferrell, R.A., Bhattacharjee, J.K., Shelton, R.N., Klavins, P. *Phys. Rev. Lett.* 1984, **52**, 133.
- Lynn, J.W., Huang, Q., Santoro, A., Cava, R.J., Krajewski, J.J., Peck Jr, W.F. *Phys. Rev. B* 1996, **53**, 802.
- Lynn, J.W., Skanthakumar, S., Huang, Q., Sinha, S.K., Hossain, Z., Gupta, L.C., Nagarajan, R., Godart, C. *Phys. Rev. B* 1997, **55**, 6584.
- Lynn, J.W., Keimer, B., Ulrich, C., Bernhard, C., Tallon, J.L. *Phys. Rev. B* 2000, **61**, R14964.
- Machida, K., Nokura, K., Matsubara, T. *Phys. Rev. Lett.* 1980a, **44**, 821.
- Machida, K., Nokura, K., Matsubara, T. *Phys. Rev. B* 1980b, **22**, 2307.

- Mailhiot, C., Grant, J.B., McMahan, A.K. *Phys. Rev. B* 1990, **42**, 9033.
- Maki, K., Thalmeier, P., Won, H. *Phys. Rev. B* 2002, **65**, 140502.
- Maki, K., Won, H., Haas, St. *Phys. Rev. B* 2004, **69**, 012502.
- Manalo, S., Schachinger, E. J. *Low Temp. Phys.* 2001, **123**, 149.
- Manalo, S., Michor, H., El-Hagary, M., Hilscher, G., Schachinger, E. *Phys. Rev. B* 2001, **63**, 104508.
- Mandal, P., Winzer, K. *Solid State Commun.* 1997, **103**, 679.
- Maniv, T., Zhuravlev, V., Wosnitza, J., Ignatchik, O., Bergk, B., Canfield, P.C. *Phys. Rev. B* 2006, **73**, 134521.
- Maple, M.B. *Physica B* 1995, **215**, 110.
- Maple, M.B., Fischer, Ø., editors. *Superconductivity in Ternary Compounds II, Superconductivity and Magnetism*. Berlin: Springer; 1982.
- Martínez-Samper, P., Suderow, H., Vieira, S., Brison, J.P., Luchier, N., Lejay, P., Canfield, P.C. *Phys. Rev. B* 2003, **67**, 014526.
- Maška, M.M., Mierzejewski, M. *Phys. Rev. B* 2001, **64**, 064501.
- Matsuda, N., Setoguchi, H., Kagayama, T., Oomi, G., Cho, B.K., Canfield, P.C. *Physica B* 2000, **281&282**, 1001.
- Matsuda, Y., Izawa, K., Vekhter, I. J. *Phys.: Condens. Matter* 2006, **18**, R705.
- Matsumoto, H., Umezawa, H., Tachiki, M. *Solid State Commun.* 1979, **31**, 157.
- Mattheiss, L.F. *Phys. Rev. B* 1994, **49**, 13279(R).
- Mattheiss, L.F., Siegrist, T., Cava, R.J. *Solid State Commun.* 1994, **91**, 587.
- Matthias, B.T., Bozorth, R.M. *Phys. Rev.* 1958, **109**, 604.
- Matthias, B.T., Suhl, H., Corenzwit, E. *Phys. Rev. Lett.* 1958a, **1**, 92.
- Matthias, B.T., Suhl, H., Corenzwit, E. *Phys. Rev. Lett.* 1958b, **1**, 449.
- Matthias, B.T., Geballe, T.H., Andres, K., Corenzwit, E., Hull, G.W., Maita, J.P. *Science* 1968, **159**, 530.
- Mazumdar, Ch., Nagarajan, R. *Curr. Sci.* 2005, **88**, 83.
- Mazumdar, Ch., Nagarajan, R., Godart, C., Gupta, L.C., Latroche, M., Dhar, S.K., Levy-Clement, C., Padalia, B.D., Vijayaraghavan, R. *Solid State Commun.* 1993, **87**, 413.
- Mazumdar, Ch., Hossain, Z., Radha, S., Nigam, A.K., Nagarajan, R., Gupta, L.C., Godart, C., Padalia, B.D., Chandra, G., Vijayaraghavan, R. *Physica B* 1996, **223&224**, 102.
- Mazumdar, Ch., Hu, Z., von Lips, H., Golden, M.S., Fink, J., Canfield, P.C., Kaindl, G. *Phys. Rev. B* 2001, **64**, 020504(R).
- Mazumdar, Ch., Alleno, E., Sologub, O., Salamakha, P., Noel, H., Potel, M., Chinchure, A.D., Nagarajan, R., Gupta, L.C., Godart, C. *J. Alloys Compd.* 2002, **339**, 18.
- Measson, M.-A., Braithwaite, D., Flouquet, J., Seyfarth, G., Brison, J.P., Lhotel, E., Paulsen, C., Sugawara, H., Sato, H. *Phys. Rev. B* 2004, **70**, 064516.
- Meenakshi, S., Vijayakumar, V., Rao, R.S., Godwal, B.K., Sikka, S.K., Hossain, Z., Nagarajan, R., Gupta, L.C., Vijayaraghavan, R. *Physica B* 1996, **223&224**, 93.
- Meenakshi, S., Vijayakumar, V., Rao, R.S., Godwal, B.K., Sikka, S.K., Ravindran, P., Hossain, Z., Nagarajan, R., Gupta, L.C., Vijayaraghavan, R. *Phys. Rev. B* 1998, **58**, 3377.
- Meiklejohn, W.H., Bean, C.P. *Phys. Rev.* 1957, **105**, 904.
- Metlushko, V., Welp, U., Koshelev, A., Aranson, I., Crabtree, G.W., Canfield, P.C. *Phys. Rev. Lett.* 1997, **79**, 1738.
- Miao, X.Y., Bud'ko, S.L., Canfield, P.C. *J. Alloys Compd.* 2002, **338**, 13.
- Michor, H., Holubar, T., Dusek, C., Hilscher, G. *Phys. Rev. B* 1995, **52**, 16165.
- Michor, H., Krendelsberger, R., Hilscher, G., Bauer, E., Dusek, C., Hauser, R., Naber, L., Werner, D., Rogl, P., Zandbergen, H.W. *Phys. Rev. B* 1996, **54**, 9408.
- Michor, H., Hilscher, G., Krendelsberger, R., Rogl, P., Bourée, F. *Phys. Rev. B* 1998, **58**, 15045.
- Michor, H., El-Hagary, M., Hauser, R., Bauer, E., Hilscher, G. *Physica B* 1999, **259–261**, 604.
- Michor, H., El-Hagary, M., Naber, L., Bauer, E., Hilscher, G. *Phys. Rev. B* 2000a, **61**, R6487.
- Michor, H., Manalo, S., El-Hagary, M., Hilscher, G. *Physica B* 2000b, **283–284**, 491.
- McMillan, W.L. *Phys. Rev.* 1968, **167**, 331.
- Mints, R.G., Rakhmanov, A.L. *Rev. Mod. Phys.* 1981, **53**, 551.
- Miranović, P., Ichioka, M., Machida, K., Nakai, N. *J. Phys.: Condens. Matter* 2005, **17**, 7971.
- Mitrović, B., Samokhin, K.V. *Phys. Rev. B* 2006, **74**, 144510.
- Mori, K., Nishimura, K., Cao, S. *Physica C* 2003, **388–389**, 187.

- Morin, P., Schmitt, D., in: Buschow, K.H.J., Wohlfarth, E.P., editors. *Ferromagnetic Materials*, vol. 5. Amsterdam: Elsevier; 1990, p. 1.
- Moriya, T. *Phys. Rev.* 1960, **117**, 635.
- Morozov, A.I. *Sov. Solid State Phys.* 1977, **19**, 1486.
- Morozov, A.I. *Sov. Phys. Solid State* 1980, **22**, 1974.
- Morosov, A.I., in: Müller, K.-H., Narozhnyi, V.N., editors. *Rare Earth Transition Metal Borocarbides (Nitrides): Superconducting, Magnetic and Normal State Properties*. Dordrecht: Kluwer Academic; 2001, p. 287.
- Movshovich, R., Hundley, M.F., Thompson, J.D., Canfield, P.C., Cho, B.K., Chubukov, A.V. *Physica C* 1994, **227**, 381.
- Müller, K.-H., Narozhnyi, V.N. *Rep. Prog. Phys.* 2001a, **64**, 943.
- Müller, K.-H., Narozhnyi, V.N., editors. *Rare Earth Transition Metal Borocarbides (Nitrides): Superconducting, Magnetic and Normal State Properties*. Dordrecht: Kluwer Academic; 2001b, pp. 1–445.
- Müller, K.-H., Kreyssig, A., Handstein, A., Fuchs, G., Ritter, C., Loewenhaupt, M. *J. Appl. Phys.* 1997, **81**, 4240.
- Müller, K.-H., Handstein, A., Eckert, D., Fuchs, G., Nenkov, K., Freudenberger, J., Richter, M., Wolf, M. *Physica B* 1998, **246–247**, 226.
- Müller, K.-H., Freudenberger, J., Fuchs, G., Nenkov, K., Kreyssig, A., Loewenhaupt, M., in: Müller, K.-H., Narozhnyi, V.N., editors. *Rare Earth Transition Metal Borocarbides (Nitrides): Superconducting, Magnetic and Normal State Properties*. Dordrecht: Kluwer Academic; 2001a, p. 255.
- Müller, K.-H., Fuchs, G., Handstein, A., Nenkov, K., Narozhnyi, V.N., Eckert, D. *J. Alloys Compd.* 2001b, **322**, L10.
- Müller, K.-H., Fuchs, G., Drechsler, S.-L., Narozhnyi, V.N., in: Buschow, K.H.J., editor. *Handbook of Magnetic Materials*, vol. 14. Amsterdam: Elsevier; 2002, p. 199.
- Müller, K.-H., Fuchs, G., Drechsler, S.-L., Opahle, I., Eschrig, H., Schultz, L., Behr, G., Löser, W., Souptel, D., Wälte, A., Nenkov, K., Naidyuk, Yu., Rosner, H. *Physica C* 2007, **460–462**, 99.
- Müller-Hartmann, E., Zittartz, J. *Phys. Rev. Lett.* 1971, **26**, 428.
- Mukhopadhyay, S., Sheet, G., Raychaudhuri, P., Takeya, H. *Phys. Rev. B* 2005, **72**, 014545.
- Mulder, F.M., Brabers, J.H.V.J., Coehoorn, R., Thiel, R.C., Buschow, K.H.J., de Boer, F.R. *J. Alloys Compd.* 1995, **217**, 118.
- Mulders, A.M., Gubbens, P.C.M., Gasser, U., Baines, C., Buschow, K.H.J. *J. Magn. Magn. Mater.* 1998, **177–181**, 555.
- Mulders, A.M., Staub, U., Scagnoli, V., Tanaka, Y., Kikkawa, A., Katsumata, K., Tonnerre, J.M. *Phys. Rev. B* 2007, **75**, 184438.
- Mun, M.-O., Lee, S.-I., Lee, W.C., Canfield, P.C., Cho, B.K., Johnston, D.C. *Phys. Rev. Lett.* 1996, **76**, 2790.
- Mun, M.-O., Kim, M.-S., Lee, S.-I., Cho, B.K., Yang, I.-S., Lee, W.C., Canfield, P.C. *Physica C* 1998, **303**, 57.
- Mun, M.-O., Kim, Y.J., Yoon, Y.K., Paik, H., Kim, J.H., Lee, S.-I., Cho, B.K. *J. Korean Phys. Soc.* 2001, **39**, 406.
- Murakami, Y., Hill, J.P., Gibbs, D., Blume, M., Koyama, I., Tanaka, M., Kawata, H., Arima, T., Tokura, Y., Hirota, K., Endoh, Y. *Phys. Rev. Lett.* 1998, **81**, 582.
- Murayama, C., Mori, N., Takagi, H., Eisaki, H., Mizuhashi, K., Uchida, S., Cava, R.J. *Physica C* 1994, **235–240**, 2545.
- Murdoch, J., Salamati, H., Quirion, G., Razavi, F.S. *Physica C* 1999, **321**, 108.
- Nagamatsu, J., Nakagawa, N., Muranaka, T., Zenitani, Y., Akimitsu, J. *Nature* 2001, **410**, 63.
- Nagarajan, R., in: Müller, K.-H., Narozhnyi, V.N., editors. *Rare Earth Transition Metal Borocarbides (Nitrides): Superconducting, Magnetic and Normal State Properties*. Dordrecht: Kluwer Academic; 2001, p. 1.
- Nagarajan, R., Gupta, L.C., in: Narlikar, A., editor. *Studies of High Temperature Superconductors*, vol. 26. New York: Nova Science; 1998, p. 1.
- Nagarajan, R., Mazumdar, Ch., Hossain, Z., Dhar, S.K., Gopalakrishnan, K.V., Gupta, L.C., Godart, C., Padalia, B.D., Vijayaraghavan, R. *Phys. Rev. Lett.* 1994, **72**, 274.
- Nagarajan, R., Gupta, L.C., Mazumdar, Ch., Hossain, Z., Dhar, S.K., Godart, C., Padalia, B.D., Vijayaraghavan, R. *J. Alloys Compd.* 1995, **225**, 571.

- Nagarajan, R., Alleno, E., Blundell, S.J., Mazumdar, Ch., Cooke, D.W., Cottrell, S.P., Cox, S.F.J., Godart, C., Gupta, L.C., Hossain, Z., Hults, W.L., Jestadt, Th., Peterson, E.J., Pratt, F.L., Smith, J.L. *Physica B* 1999, **259–261**, 588.
- Nagarajan, R., Mazumdar, Ch., Hossain, Z., Gupta, L.C., in: Narlikar, A.V., editor. *Frontiers in Superconducting Materials*. Berlin: Springer; 2005, p. 393.
- Naidyuk, Yu.G., Bashlakov, D.L., Bobrov, N.L., Chernobay, V.N., Kvitnitskaya, O.E., Yanson, I.K., Behr, G., Drechsler, S.-L., Fuchs, G., Souptel, D., Naugle, D.G., Rathnayaka, K.D.D., Ross Jr., J.F. *Physica C* 2007a, **460–462**, 107.
- Naidyuk, Yu.G., Kvitnitskaya, O.E., Yanson, I.K., Fuchs, G., Nenkov, K., Wälte, A., Behr, G., Souptel, D., Drechsler, S.-L. *Phys. Rev. B* 2007b, **76**, 014520.
- Nakai, N., Miranović, P., Ichioka, M., Machida, K. *Phys. Rev. Lett.* 2002, **89**, 237004.
- Nakai, N., Miranović, P., Ichioka, M., Hess, H.F., Uchiyama, K., Nishimori, H., Kaneko, S., Nishida, N., Machida, K. *Phys. Rev. Lett.* 2006, **97**, 147001.
- Nakane, H., Motoyama, G., Nishioka, T., Sato, N.K. *J. Phys. Soc. Jpn.* 2005, **74**, 855.
- Narozhnyi, V.N., Drechsler, S.-L. *Phys. Rev. Lett.* 1999, **82**, 461.
- Narozhnyi, V.N., Kochetkov, V.N., Tsvyashchenko, A.V., Fomicheva, L.N. *J. Low Temp. Phys.* 1996, **105**, 1647.
- Narozhnyi, V.N., Freudenberger, J., Kochetkov, V.N., Nenkov, K.A., Fuchs, G., Handstein, A., Müller, K.-H. *Phys. Rev. B* 1999a, **59**, 14762.
- Narozhnyi, V.N., Kochetkov, V.N., Tsvyashchenko, A.V., Fomicheva, L.N. *Solid State Commun.* 1999b, **111**, 259.
- Narozhnyi, V.N., Freudenberger, J., Fuchs, G., Nenkov, K.A., Eckert, D., Czopnik, A., Müller, K.-H. *J. Low Temp. Phys.* 1999c, **117**, 1599.
- Narozhnyi, V.N., Fuchs, G., Freudenberger, J., Nenkov, K., Müller, K.-H. *Physica B* 2000a, **284–288**, 535.
- Narozhnyi, V.N., Fuchs, G., Nenkov, K., Eckert, D., Teresiak, A., Müller, K.-H., Canfield, P.C. *Physica C* 2000b, **341–348**, 1141.
- Narozhnyi, V.N., Fuchs, G., Freudenberger, J., Nenkov, K.A., Eckert, D., Teresiak, A., Czopnik, A., Müller, K.-H., in: Müller, K.-H., Narozhnyi, V.N., editors. *Rare Earth Transition Metal Borocarbides (Nitrides): Superconducting, Magnetic and Normal State Properties*. Dordrecht: Kluwer Academic; 2001a, p. 171.
- Narozhnyi, V.N., Fuchs, G., Freudenberger, J., Nenkov, K., Müller, K.-H. *Physica C* 2001b, **364–365**, 571.
- Nass, M.J., Levin, K., Grest, G.S. *Phys. Rev. B* 1982, **25**, 4541.
- Naugle, D.G., Rathnayaka, K.D.D., Canfield, P.C. *Int. J. Mod. Phys. B* 1998, **12**, 3174.
- Naugle, D.G., Rathnayaka, K.D.D., Bhatnagar, A.K., in: Narlikar, A., editor. *Studies of High Temperature Superconductors*, vol. 28. New York: Nova Science; 1999a, p. 189.
- Naugle, D.G., Rathnayaka, K.D.D., Clark, K., Canfield, P.C. *Int. J. Mod. Phys. B* 1999b, **13**, 3715.
- Naugle, D.G., Rathnayaka, K.D.D., Parasiris, A., Canfield, P.C. *Physica C* 2000, **341–348**, 1959.
- Naugle, D.G., Rathnayaka, K.D.D., Hennings, B.D., Eyhorn, J.M., in: Müller, K.-H., Narozhnyi, V.N., editors. *Rare Earth Transition Metal Borocarbides (Nitrides): Superconducting, Magnetic and Normal State Properties*. Dordrecht: Kluwer Academic; 2001, p. 115.
- Naugle, D.G., Belevtsev, B.I., Rathnayaka, K.D.D., Adegbenro, S.A., Canfield, P.C., Lee, S.-I. *J. Appl. Phys.* 2006, **99**, 08F701.
- Ng, T.K., Varma, C.M. *Phys. Rev. Lett.* 1997, **78**, 330.
- Nguyen, L.H., Goll, G., Steep, E., Jansen, A.G.M., Wyder, P., Jepsen, O., Heinecke, M., Winzer, K. *J. Low Temp. Phys.* 1996, **105**, 1653.
- Nicol, E.J., Carbotte, J.P. *Phys. Rev. B* 2005, **71**, 054501.
- Nishimori, H., Uchiyama, K., Kaneko, S.-I., Tokura, A., Takeya, H., Hirata, K., Nishida, N. *J. Phys. Soc. Jpn.* 2004, **73**, 3247.
- Nohara, M., Isshiki, M., Takagi, H., Cava, R.J. *J. Phys. Soc. Jpn.* 1997, **66**, 1888.
- Nohara, M., Isshiki, M., Sakai, F., Takagi, H. *J. Phys. Soc. Jpn.* 1999, **68**, 1078.
- Nohara, M., Suzuki, H., Mangkorntong, N., Takagi, H. *Physica C* 2000, **341–348**, 2177.
- Nørgaard, K., Eskildsen, M.R., Andersen, N.H., Jensen, J., Hedegård, P., Klausen, S.N., Canfield, P.C. *Phys. Rev. Lett.* 2000, **84**, 4982.
- Nørgaard, T.K., Abrahamsen, A.B., Eskildsen, M.R., Lefmann, K., Andersen, N.H., Vorderwisch, P., Smeibidl, P., Meissner, M., Canfield, P.C. *Phys. Rev. B* 2004, **69**, 214507.

- Obst, B. *Phys. Lett.* 1969, **28A**, 662.
- Oertel, C.-G., Ledig, L., Eckert, J., Skrotzki, W. *Cryst. Res. Technol.* 2000, **35**, 427.
- Ohishi, K., Kakuta, K., Akimitsu, J., Koda, A., Higemoto, W., Kadono, R., Sonier, J.E., Price, A.N., Miller, R.I., Kiefl, R.F., Nohara, M., Suzuki, H., Takagi, H. *Physica C* 2003a, **388–389**, 197.
- Ohishi, K., Kakuta, K., Akimitsu, J., Koda, A., Higemoto, W., Kadono, R., Sonier, J.E., Price, A.N., Miller, R.I., Kiefl, R.F., Nohara, M., Suzuki, H., Takagi, H. *Physica B* 2003b, **326**, 364.
- Onimaru, T., Sakakibara, T., Aso, N., Yoshizawa, H., Suzuki, H.S., Takeuchi, T. *Phys. Rev. Lett.* 2005, **94**, 197201.
- Onodera, H., Yamauchi, H., Yamaguchi, Y. *J. Phys. Soc. Jpn.* 1999, **68**, 2526.
- Oomi, G., Matsuda, N., Honda, F., Kagayama, T., Honda, K., Cho, B.K., Canfield, P.C. *Physica B* 1999, **259–261**, 601.
- Oomi, G., Kagayama, T., Mitamura, H., Goto, T., Cho, B.K., Canfield, P.C. *Physica B* 2001, **294–295**, 229.
- Oomi, G., Minamitake, I., Ohashi, M., Eto, T., Cho, B.K., Canfield, P.C. *High Pressure Res.* 2002, **22**, 195.
- Oomi, G., Masaoka, D., Kagayama, T., Kuroda, N., Cho, B.K., Canfield, P.C. *Physica C* 2003a, **388–389**, 177.
- Oomi, G., Matsuda, N., Kagayama, T., Cho, B.K., Canfield, P.C. *Int. J. Mod. Phys. B* 2003b, **17**, 3664.
- Oomi, G., Akiyama, H., Sakigawa, Y., Kaji, S., Uwatoko, Y., Cho, B.K. *Physica B* 2006, **378–380**, 473.
- Ovchinnikov, Y.N., Kresin, V.Z. *Eur. Phys. J. B* 2000, **14**, 203.
- Pairor, P., Smith, M.F. *J. Phys.: Condens. Matter* 2003, **15**, 4457.
- Paranthaman, M., Chakoumakos, B.C., in: Narlikar, A., editor. *Studies of High Temperature Superconductors*, vol. 26. New York: Nova Science; 1998, p. 97.
- Park, T., Salamon, M.B., Choi, E.M., Kim, H.J., Lee, S.-I. *Phys. Rev. Lett.* 2003, **90**, 177001.
- Park, T., Salamon, M.B., Choi, E.M., Kim, H.J., Lee, S.-I. *Phys. Rev. B* 2004a, **69**, 054505.
- Park, T., Chia, E.E.M., Salamon, M.B., Bauer, E.D., Vekhter, I., Thompson, J.D., Choi, E.M., Kim, H.J., Lee, S.-I., Canfield, P.C. *Phys. Rev. Lett.* 2004b, **92**, 237002.
- Parker, D., Haas, St. *Phys. Rev. B* 2007, **75**, 052501.
- Paul, D.McK., Mook, H.A., Hewat, A.W., Sales, B.C., Boatner, L.A., Thompson, J.R., Mostoller, M. *Phys. Rev. B* 1988, **37**, 2341.
- Paul, D.McK., Bancroft, N.J., Tomy, C.V., Dewhurst, C.D., Cubitt, R., Yethiraj, M., Aegerter, C.M., Lee, S.L., Lloyd, S.H., Kealey, P.G., Forgan, E.M., in: Müller, K.-H., Narozhnyi, V.N., editors. *Rare Earth Transition Metal Borocarbides (Nitrides): Superconducting, Magnetic and Normal State Properties*. Dordrecht: Kluwer Academic; 2001, p. 323.
- Paulose, P.L., Dhar, S.K., Chinchure, A.D., Alleno, E., Godart, C., Gupta, L.C., Nagarajan, R. *Physica C* 2003, **399**, 165.
- Peng, Z.Q., Krug, K., Winzer, K. *Phys. Rev. B* 1998, **57**, R8123.
- Peter, M., Donzé, P., Fischer, O., Junod, A., Ortelli, J., Treyvaud, A., Walker, E., Wilhelm, M., Hillenbrand, B. *Helv. Phys. Acta* 1971, **44**, 345.
- Pickett, W.E. *Physica B* 2001, **296**, 112.
- Pickett, W.E., Singh, D.J. *Phys. Rev. Lett.* 1994, **72**, 3702.
- Prassides, K., Lappas, A., Buchgeister, M., Verges, P. *Europhys. Lett.* 1995, **29**, 641.
- Price, A.N., Miller, R.I., Kiefl, R.F., Chakhalian, J.A., Dunsiger, S.R., Morris, G.D., Sonier, J.E., Canfield, P.C. *Phys. Rev. B* 2002, **65**, 214520.
- Prozorov, R., Yakoby, E.R., Felner, I., Yeshurun, Y. *Physica C* 1994, **233**, 367.
- Radzihovsky, L., Ettouhami, A.M., Saunders, K., Toner, J. *Phys. Rev. Lett.* 2001, **87**, 027001.
- Rams, M., Królas, K., Bonville, P., Hodges, J.A., Hossain, Z., Nagarajan, R., Dhar, S.K., Gupta, L.C., Alleno, E., Godart, C. *J. Magn. Mater.* 2000, **219**, 15.
- Rapp, R.E., El Massalami, M. *Phys. Rev. B* 1999, **60**, 3355.
- Rathnayaka, K.D.D., Naugle, D.G., Cho, B.K., Canfield, P.C. *Phys. Rev. B* 1996, **53**, 5688.
- Rathnayaka, K.D.D., Bhatnagar, A.K., Parasiris, A., Naugle, D.G., Canfield, P.C., Cho, B.K. *Phys. Rev. B* 1997, **55**, 8506.
- Rathnayaka, K.D.D., Naugle, D.G., Li, S., de Andrade, M.C., Dickey, R.P., Amann, A., Maple, M.B., Bud'ko, S.L., Canfield, P.C., Beyermann, W.P. *Int. J. Mod. Phys. B* 1999, **13**, 3725.
- Rathnayaka, K.D.D., Naugle, D.G., Dumar, A.C., Anatska, M.P., Canfield, P.C. *Int. J. Mod. Phys. B* 2003, **17**, 3493.
- Rauchschwalbe, U., Lieke, W., Steglich, F., Godart, C., Gupta, L.C., Parks, R.D. *Phys. Rev. B* 1984, **30**, 444.

- Ravindran, P., Johansson, B., Eriksson, O. *Phys. Rev. B* 1998, **58**, 3381.
- Raychaudhuri, P., Jaiswal-Nagar, D., Sheet, G., Ramakrishnan, S., Takeya, H. *Phys. Rev. Lett.* 2004, **93**, 156802.
- Raychaudhuri, P., Sheet, G., Mukhopadhyay, S., Takeya, H. *Physica C* 2007, **460–462**, 95.
- Reibold, M., Wimbush, S.C., Holzapfel, B., Krämer, U. *J. Alloys Compd.* 2002, **347**, 24.
- Reichardt, W., Heid, R., Bohnen, K.P. *J. Supercond.* 2005, **18**, 159.
- Rhee, J.Y., Harmon, B.N. *Phys. Rev. B* 2002, **66**, 153102.
- Rhee, J.Y., Wang, X., Harmon, B.N. *Phys. Rev. B* 1995, **51**, 15585.
- Rho, H., Klein, M.V., Canfield, P.C. *Phys. Rev. B* 2004, **69**, 144420.
- Ribeiro, R.A., Bud'ko, S.L., Canfield, P.C. *J. Magn. Magn. Mater.* 2003, **267**, 216.
- Riblet, G., Winzer, K. *Solid State Commun.* 1971, **9**, 1663.
- Richardson, C.F., Ashcroft, N.W. *Phys. Rev. Lett.* 1997, **78**, 118.
- Riseman, T.M., Kealey, P.G., Forgan, E.M., Mackenzie, A.P., Galvin, L.M., Tyler, A.W., Lee, S.L., Ager, C., Paul, D.McK., Aegerter, C.M., Cubitt, R., Mao, Z.Q., Akima, T., Maeno, Y. *Nature* 1998, **396**, 242.
- da Rocha, F.S., Fraga, G.L.F., Brandão, D.E., Gomes, A.A. *Physica C* 2001, **363**, 41.
- da Rocha, F.S., Fraga, G.L.F., Brandão, D.E., Gomes, A.A. *Physica C* 2002a, **371**, 57.
- da Rocha, F.S., Fraga, G.L.F., Brandão, D.E., Granada, C.M., da Silva, C.M., Gomes, A.A. *Eur. Phys. J. B* 2002b, **25**, 307.
- da Rocha, F.S., Granada, C.M., da Silva, C.M., Gomes, A.A., in: Narlikar, A.V., editor. *Studies of High Temperature Superconductors*, vol. 46. New York: Nova Science; 2003, p. 171.
- Röhler, J., in: Gschneidner Jr., K.A., Eyring, L., Hufner, S., editors. *Handbook on the Physics and Chemistry of Rare Earths*, vol. 10. Amsterdam: Elsevier Science; 1987, p. 453.
- Rogl, P., in: Gschneidner Jr., K.A., Eyring, L., editors. *Handbook on the Physics and Chemistry of Rare Earths*, vol. 6. Amsterdam: Elsevier Science; 1984, p. 335.
- Rosner, H., Drechsler, S.-L., Shulga, S.V., Koepernik, K., Opahle, I., Eschrig, H., in: Kramer, B., editor. *Adv. Solid State Physics*, vol. 40. Braunschweig: Vieweg & Sohn; 2000, p. 713.
- Rosner, H., Drechsler, S.-L., Koepernik, K., Opahle, I., Eschrig, H., in: Müller, K.-H., Narozhnyi, V.N., editors. *Rare Earth Transition Metal Borocarbides (Nitrides): Superconducting, Magnetic and Normal State Properties*. Dordrecht: Kluwer Academic; 2001, p. 71.
- Rosseinsky, M.J., Ramirez, A.P., Glarum, S.H., Murphy, D.W., Haddon, R.C., Hebard, A.F., Palstra, T.T.M., Kortan, A.R., Zahurak, S.M., Makhija, A.V. *Phys. Rev. Lett.* 1991, **66**, 2830.
- Roth, S. *Appl. Phys.* 1978, **15**, 1.
- Rotter, M., Sierks, C., Loewenhaupt, M., Freudenberger, J., Schober, H., in: Müller, K.-H., Narozhnyi, V.N., editors. *Rare Earth Transition Metal Borocarbides (Nitrides): Superconducting, Magnetic and Normal State Properties*. Dordrecht: Kluwer Academic; 2001, p. 137.
- Rotter, M., Loewenhaupt, M., Doerr, M., Lindbaum, A., Sassik, H., Ziebeck, K., Beuneu, B. *Phys. Rev. B* 2003, **68**, 144418.
- Rotter, M., Lindbaum, A., Barcza, A., El Massalami, M., Doerr, M., Loewenhaupt, M., Michor, H., Beuneu, B. *Europhys. Lett.* 2006, **75**, 160.
- Ruiz, D., Garland, M.T., Saillard, J.-Y., Halet, J.-F., Bohn, M., Bauer, J. *Solid State Sci.* 2002, **4**, 1173.
- Rukang, L., Chaoshui, X., Hong, Z., Bin, L., Li, Y. *J. Alloys Compd.* 1995, **223**, 53.
- Rupp, B., Rogl, P., Hulliger, F. *J. Less-Common Met.* 1987, **135**, 113.
- Russell, V., Hirst, R., Kanda, F.A., King, A.J. *Acta Crystallogr.* 1953, **6**, 870.
- Rustom, A., Hillier, A.D., Cywinski, R. *J. Magn. Magn. Mater.* 1998, **177–181**, 1153.
- Rybaltchenko, L.F., Jansen, A.G.M., Wyder, P., Tjutrina, L.V., Canfield, P.C., Tomy, C.V., Paul, D.McK. *Physica C* 1999, **319**, 189.
- Saha, N., Surdeanu, R., Marchevsky, M., Nieuwenhuys, G.J., Dewhurst, C.D., Wijngaarden, R.J., Paul, D.McK., Kes, P.H. *Phys. Rev. B* 2001, **63**, 020502(R).
- Saito, T., Koyama, K., Magishi, K.-I., Endo, K. *J. Magn. Magn. Mater.* 2007, **310**, 681.
- Sakai, T., Adachi, G., Shiokawa, J. *Solid State Commun.* 1981, **40**, 445.
- Sakai, T., Adachi, G., Shiokawa, J. *J. Less-Common Met.* 1982, **84**, 107.
- Sala, R., Borsa, F., Lee, E., Canfield, P.C. *Phys. Rev. B* 1997, **56**, 6195.
- Sales, B.C., in: Gschneidner Jr., K.A., Bünzli, J.-C.G., Pecharsky, V.K., editors. *Handbook on the Physics and Chemistry of Rare Earths*, vol. 33. Amsterdam: Elsevier; 2003, p. 1.
- Sales, B.C., Wohlleben, D.K. *Phys. Rev. Lett.* 1975, **35**, 1240.

- Sánchez, D.R., Micklitz, H., Fontes, M.B., Bud'ko, S.L., Baggio-Saitovitch, E. *Phys. Rev. Lett.* 1996, **76**, 507.
- Sánchez, D.R., de Melo, M.A.C., Fontes, M.B., Bud'ko, S.L., Baggio-Saitovitch, E., Hillberg, M., Wagnener, W., Klauß, H.-H., Walf, G.H., Litterst, F.J. *Phys. Rev. B* 1998, **57**, 10268.
- Sánchez, D.R., Bud'ko, S.L., Baggio-Saitovitch, E.M. *J. Phys.: Condens. Matter* 2000, **12**, 9941.
- Sánchez, D.R., Baggio-Saitovitch, E.M., Micklitz, H., Lee, S.-I. *Phys. Rev. B* 2005a, **71**, 024508.
- Sánchez, D.R., Micklitz, H., Baggio-Saitovitch, E.M. *Phys. Rev. B* 2005b, **71**, 024509.
- Sánchez, J.P., Vulliet, P., Godart, C., Gupta, L.C., Hossain, Z., Nagarajan, R. *Phys. Rev. B* 1996, **54**, 9421.
- Sarrao, J.L., de Andrade, M.C., Herrmann, J., Han, S.H., Fisk, Z., Maple, M.B., Cava, R.J. *Physica C* 1994, **229**, 65.
- Savitskii, E.M., Baron, V.V., Efimov, Yu.V., Bychkova, M.I., Myzenkova, L.F. *Superconducting Materials*, New York: Plenum Press; 1973.
- Saxena, S.S., Littlewood, P.B. *Nature* 2001, **412**, 290.
- Saxena, S.S., Agarwal, P., Ahilan, K., Grosche, F.M., Haselwimmer, R.K.W., Steiner, M.J., Pugh, E., Walker, I.R., Julian, S.R., Monthoux, P., Lonzarich, G.G., Huxley, A., Sheikin, I., Braithwaite, D., Flouquet, J. *Nature* 2000, **406**, 587.
- Schenck, A., Solt, G. *J. Phys.: Condens. Matter* 2004, **16**, S4639.
- Schmidt, H. Wechselwirkung von Supraleitung und Magnetismus in quaternären Borocarbidgebindungen, Thesis, Universität Bayreuth; 1997.
- Schmidt, H., Braun, H.F. *Physica C* 1994, **229**, 315.
- Schmidt, H., Braun, H.F. *Phys. Rev. B* 1997, **55**, 8497.
- Schmidt, H., Braun, H.F., in: Narlikar, A., editor. *Studies of High Temperature Superconductors*, vol. 26. New York: Nova Science; 1998, p. 47.
- Schmidt, H., Müller, M., Braun, H.F. *Physica C* 1994, **235–240**, 779.
- Schmidt, H., Weber, M., Braun, H.F. *Physica C* 1995, **246**, 177.
- Schmidt, H., Dertinger, A., Ernstberger, B., Braun, H.F. *J. Alloys Compd.* 1997, **262–263**, 459.
- Schmiedeshoff, G.M., De Boer, C., Tompkins, M.V., Beyermann, W.P., Lacerda, A.H., Smith, J.L., Canfield, P.C. *J. Supercond.* 2000, **13**, 847.
- Schmiedeshoff, G.M., Detwiler, J.A., Beyermann, W.P., Lacerda, A.H., Canfield, P.C., Smith, J.L. *Phys. Rev. B* 2001, **63**, 134519.
- Schmiedeshoff, G.M., Touton, S., Beyermann, W.P., Lacerda, A.H., Bud'ko, S.L., Canfield, P.C. *Int. J. Mod. Phys. B* 2002, **16**, 3212.
- Schneider, M., Thermische Tieftemperatureigenschaften von Magnesium-Diborid und Seltenerd-Nickel-Borocarbiden, Thesis, TU Dresden; 2005.
- Schneider, M., Lipp, D., Gladun, A., Zahn, P., Handstein, A., Fuchs, G., Drechsler, S.-L., Richter, M., Müller, K.-H., Rosner, H. *Physica C* 2001, **363**, 6.
- Schneider, M., Gladun, A., Kreyssig, A., Wosnitzer, J., Souptel, D., Behr, G. *J. Magn. Magn. Mater.* 2007, **311**, 489.
- Schneider, M., Zaharko, O., Gasser, U., Kreyssig, A., Brown, P.J., Canfield, P.C. *Phys. Rev. B* 2006, **74**, 104426.
- Schubnikow, L.W., Chotkewitsch, W.I., Schepelew, J.D., Rjabinin, J.N. *Phys. Z. Sowjet.* 1936, **10**, 165 (russ. transl.: *Zh. Eksp. Teor. Fiz.* 1937, **7**, 221).
- Sera, M., Kobayash, S., Hiroi, M., Kobayashi, N., Takeya, H., Kadowaki, K. *Phys. Rev. B* 1996, **54**, 3062.
- Seyfarth, G., Brison, J.P., Méasson, M.-A., Flouquet, J., Izawa, K., Matsuda, Y., Sugawara, H., Sato, H. *Phys. Rev. Lett.* 2005, **95**, 107004.
- Seyfarth, G., Brison, J.P., Méasson, M.-A., Braithwaite, D., Lapertot, G., Flouquet, J. *J. Magn. Magn. Mater.* 2007, **310**, 703.
- Shelton, R.N., Hausermann-Berg, L.S., Johnson, M.J., Klavins, P., Yang, H.D. *Phys. Rev. B* 1986, **34**, 199.
- Shimizu, K., Kimura, T., Furomoto, S., Takeda, K., Kontani, K., Onuki, Y., Amaya, K. *Nature* 2001, **412**, 316.
- Shiraishi, J., Kohmoto, M., Maki, K. *Phys. Rev. B* 1999, **59**, 4497.
- Shorikov, A.O., Anisimov, V.I., Sigrist, M. *J. Phys.: Condens. Matter* 2006, **18**, 5973.
- Shulga, S.V., Drechsler, S.-L., in: Müller, K.-H., Narozhnyi, V.N., editors. *Rare Earth Transition Metal Borocarbides (Nitrides): Superconducting, Magnetic and Normal State Properties*. Dordrecht: Kluwer Academic; 2001, p. 393.

- Shulga, S.V., Drechsler, S.-L. 2002; cond-mat/0202172.
- Shulga, S.V., Drechsler, S.-L., Fuchs, G., Müller, K.-H., Winzer, K., Heinecke, M., Krug, K. Phys. Rev. Lett. 1998, **80**, 1730.
- Shulga, S.V., Drechsler, S.-L., Eschrig, H., Rosner, H., Pickett, W. 2001; cond-mat/0103154.
- Sieberer, M., Michor, H., Manalo, S., Della Mea, M., Hilscher, G., Grytsiv, A., Rogl, P. Physica B 2006, **378–380**, 904.
- Siegrist, T., Zandbergen, H.W., Cava, R.J., Krajewski, J.J., Peck Jr., W.F. Nature 1994a, **367**, 254.
- Siegrist, T., Cava, R.J., Krajewski, J.J., Peck Jr., W.F. J. Alloys Compd. 1994b, **216**, 135.
- Sierks, C., Loewenhaupt, M., Tils, P., Freudenberger, J., Müller, K.-H., Loong, C.-K., Schober, H. Physica B 1999, **259–261**, 592.
- Sierks, C., Loewenhaupt, M., Freudenberger, J., Müller, K.-H., Schober, H. Physica B 2000, **276–278**, 630.
- Silhanek, A.V., Thompson, J.R., Civale, L., Paul, D.McK., Tomy, C.V. Phys. Rev. B 2001, **64**, 012512.
- Silhanek, A.V., Civale, L., Thompson, J.R., Canfield, P.C., Bud'ko, S.L., Paul, D.McK., Tomy, C.V., in: Annett, J.F., Kruchinin, S., editors. New Trends in Superconductivity, vol. 67. Dordrecht: Kluwer Academic; 2002, p. 255.
- Simon, A., Mattausch, H., Eger, R., Kremer, R.K. Angew. Chem. 1991, **103**, 1210.
- Singh, D.J. Phys. Rev. B 1994, **50**, 6486.
- Sinha, S.K., Lynn, J.W., Grigereit, T.E., Hossain, Z., Gupta, L.C., Nagarajan, R., Godart, C. Phys. Rev. B 1995, **51**, 681.
- Skanthakumar, S., Lynn, J.W. Physica B 1999, **259–261**, 576.
- Skanthakumar, S., Lynn, J.W., Rosov, N., Cao, G., Crow, J.E. Phys. Rev. B 1997, **55**, R3406.
- Sok, J., Cho, B.K. Physica C 2004, **408–410**, 142.
- Sok, J., Cho, B.K. J. Korean Phys. Soc. 2005, **47**, 318.
- Sologubenko, A.V., Jun, J., Kazakov, S.M., Karpinski, J., Ott, H.R. Phys. Rev. B 2002, **66**, 014504.
- Song, C., Islam, Z., Lottermoser, L., Goldman, A.I., Canfield, P.C., Detlefs, C. Phys. Rev. B 1999, **60**, 6223.
- Song, C., Wermeille, D., Goldman, A.I., Canfield, P.C., Rhee, J.Y., Harmon, B.N. Phys. Rev. B 2001a, **63**, 104507.
- Song, C., Lang, J.C., Detlefs, C., Létoublon, A., Good, W., Kim, J., Wermeille, D., Bud'ko, S.L., Canfield, P.C., Goldman, A.I. Phys. Rev. B 2001b, **64**, 020403(R).
- Song, K.-J., Thompson, J.R., Yethiraj, M., Christen, D.K., Tomy, C.V., Paul, D.McK. Phys. Rev. B 1999, **59**, R6620.
- Song, K.-J., Park, C., Oh, S.S., Kwon, Y.K., Thompson, J.R., Mandrus, D.G., Paul, D.McK., Tomy, C.V. Physica C 2003, **398**, 107.
- Sonier, J.E. J. Phys.: Condens. Matter 2004, **16**, S4499.
- Souptel D. Crystal growth and perfection of selected intermetallic and oxide compounds, Thesis, TU Dresden; 2005.
- Souptel, D., Behr, G., Löser, W., Nenkov, K., Fuchs, G. J. Crystal Growth 2005a, **275**, e91.
- Souptel, D., Behr, G., Kreyssig, A., Löser, W. J. Crystal Growth 2005b, **276**, 652.
- Souptel, D., Behr, G., Löser, W., Teresiak, A. J. Alloys Compd. 2007, doi:10.1016/j.jallcom.2007.01.090.
- Stanley, H.B., Lynn, J.W., Shelton, R.N., Klavins, P. J. Appl. Phys. 1987, **61**, 3371.
- Stassis, C., Bullock, M., Zarestky, J., Canfield, P., Goldman, A.I., Shirane, G., Shapiro, S.M. Phys. Rev. B 1997, **55**, R8678.
- Staub, U., Mulders, A.M., Zaharko, O., Janssen, S., Nakamura, T., Lovesey, S.W. Phys. Rev. Lett. 2005, **94**, 036408.
- Steglich, F. Physica C 2007, **460–462**, 7.
- Steglich, F., Geibel, Chr., Modler, R., Lang, M., Hellmann, P., Gegenwart, Ph. J. Low Temp. Phys. 1995, **99**, 267.
- Sternlieb, B., Stassis, C., Goldman, A.I., Canfield, P., Shapiro, S. J. Appl. Phys. 1997, **81**, 4937.
- Ström, V., Kim, K.S., Grishin, A.M., Rao, K.V. J. Appl. Phys. 1996, **79**, 5860.
- Subba Rao, K., Tamm, R., Wimbush, S.C., Cao, G.H., Oertel, C.-G., Skrotzki, W., Holzapfel, B. Mater. Sci. Forum 2005, **495–497**, 1425.
- Suderow, H., Martínez-Samper, P., Luchier, N., Brison, J.P., Vieira, S., Canfield, P.C. Phys. Rev. B 2001, **64**, 020503(R).
- Suderow, H., Rodrigo, J.G., Martínez-Samper, P., Vieira, S., Brison, J.P., Lejay, P., Canfield, P.C., Lee, S.I., Tajima, S. Int. J. Mod. Phys. B 2003, **17**, 3300.

- Suderow, H., Tissen, V.G., Brison, J.P., Martínez, J.L., Vieira, S., Lejay, P., Lee, S., Tajima, S. *Phys. Rev. B* 2004, **70**, 134518.
- Suderow, H., Tissen, V.G., Brison, J.P., Martínez, J.L., Vieira, S. *Phys. Rev. Lett.* 2005, **95**, 117006.
- Sudhakar Rao, G.V., Reedyk, M., Kikugawa, N., Maeno, Y. *Phys. Rev. B* 2006, **73**, 052507.
- Suh, B.J., Borsari, F., Torgeson, D.R., Cho, B.K., Canfield, P.C., Johnston, D.C., Rhee, J.Y., Harmon, B.N. *Phys. Rev. B* 1996, **53**, R6022.
- Suhl, H. *Phys. Rev. Lett.* 2001, **87**, 167007.
- Suzuki, M., Kimura, T., Suetake, M., Takahashi, Y., Asai, K., Isida, S., Takeya, H. *J. Magn. Magn. Mater.* 2004, **272–276**, e467.
- Szymczak, R., Szymczak, H., Gladczuk, L., Baran, M. *J. Magn. Magn. Mater.* 1996, **157/158**, 706.
- Takagi, H., Cava, R.J., Eisaki, H., Lee, J.O., Mizuhashi, K., Batlogg, B., Uchida, S., Krajewski, J.J., Peck Jr., W.F. *Physica C* 1994, **228**, 389.
- Takagi, H., Nohara, M., Cava, R.J. *Physica B* 1997, **237–238**, 292.
- Takaki, K., Koizumi, A., Hanaguri, T., Nohara, M., Takagi, H., Kitazawa, K., Kato, Y., Tsuchiya, Y., Kitano, H., Maeda, A. *Phys. Rev. B* 2002, **66**, 184511.
- Takeya, H., El Massalami, M. *Phys. Rev. B* 2004, **69**, 024509.
- Takeya, H., Kuznietz, M. *J. Magn. Magn. Mater.* 1999, **195**, 366.
- Takeya, H., Hirano, T., Kadowaki, K. *Physica C* 1996, **256**, 220.
- Takeya, H., Habuta, E., Kawano-Furukawa, H., Ooba, T., Hirata, K. *J. Magn. Magn. Mater.* 2001, **226–230**, 269.
- Takeya, H., Kuznietz, M., Hirata, K. *Physica B* 2005, **359–361**, 473.
- Terashima, T., Haworth, C., Takeya, H., Uji, S., Aoki, H., Kadowaki, K. *Phys. Rev. B* 1997, **56**, 5120.
- Thalmeier, P., Maki, K. *Acta Phys. Pol. B* 2003, **34**, (557 and) 2843.
- Thalmeier, P., Zwicky, G., in: Gschneidner Jr., K.A., Bünzli, J.-C.G., Pecharsky, V.K., editors. *Handbook on the Physics and Chemistry of Rare Earths*, vol. 34. Amsterdam: Elsevier; 2005, p. 135.
- Thomlinson, W., Shirane, G., Lynn, J.W., Moncton, D.E., in: Maple, M.B., Fischer, Ø., editors. *Superconductivity in Ternary Compounds II, Superconductivity and Magnetism*. Berlin: Springer; 1982, p. 229.
- Thompson, J.R., Silhanek, A.V., Civale, L., Song, K.J., Tomy, C.V., Paul, D.McK. *Phys. Rev. B* 2001, **64**, 024510.
- Tinkham, M. *Physica C* 1994, **235–240**, 3.
- Togano, K., Badica, P., Nakamori, Y., Orimo, S., Takeya, H., Hirata, K. *Phys. Rev. Lett.* 2004, **93**, 247004.
- Tokura, Y., Nagaosa, N. *Science* 2000, **288**, 462.
- Tomala, K., Sanchez, J.P., Vulliet, P., Canfield, P.C., Drzazga, Z., Winiarska, A. *Phys. Rev. B* 1998, **58**, 8534.
- Tomilo, Zh., Molchan, P., Ustinovich, S., Finskaya, V., Prytkova, N. *J. Low Temp. Phys.* 1999, **117**, 1629.
- Tomilo, Zh.M., Molchan, P.V., Shestak, A.S., Finskaya, V.M., Prytkova, N.A., in: Müller, K.-H., Narozhnyi, V.N., editors. *Rare Earth Transition Metal Borocarbides (Nitrides): Superconducting, Magnetic and Normal State Properties*. Dordrecht: Kluwer Academic; 2001a, p. 375.
- Tomilo, Zh.M., Molchan, P.V., Shestak, A.S., Finskaya, V.M., Prytkova, N.A., Ustinovich, S.N. *Physica C* 2001b, **361**, 95.
- Tominez, E., Berger, P., Alleno, E., Décamps, B., Schiffmacher, G., Bohn, M., Godart, C. *J. Alloys Compd.* 1998, **275–277**, 123.
- Tominez, E., Alleno, E., Berger, P., Bohn, M., Mazumdar, Ch., Godart, C. *J. Solid State Chem.* 2000, **154**, 114.
- Tomy, C.V., Lees, M.R., Afalfiz, L., Balakrishnan, G., Paul, D.McK. *Phys. Rev. B* 1995, **52**, 9186.
- Tomy, C.V., Afalfiz, L.A., Lees, M.R., Martin, J.M., Paul, D.McK., Adroja, D.T. *Phys. Rev. B* 1996a, **53**, 307.
- Tomy, C.V., Lees, M.R., Balakrishnan, G., Adroja, D.T., Paul, D.McK. *Physica B* 1996b, **223&224**, 62.
- Tomy, C.V., Martin, J.M., Paul, D.McK. *Physica B* 1996c, **223&224**, 116.
- Udagawa, M., Yanase, Y., Ogata, M. *Phys. Rev. B* 2005, **71**, 024511.
- Uehara, M., Nagata, T., Akimitsu, J., Takahashi, H., Mōri, N., Kinoshita, K. *J. Phys. Soc. Jpn.* 1996, **65**, 2764.
- Uwatoko, Y., Oomi, G., Canfield, P.C., Cho, B.K. *Physica B* 1996, **216**, 329.
- Veremchuk, I., Chaban, N., Kuzma, Y.B. *J. Alloys Compd.* 2006, **413**, 127.

- Verma, A.K., Modak, P., Gaitonde, D.M., Rao, R.S., Godwal, B.K., Gupta, L.C. *Solid State Commun.* 2005, **134**, 329.
- Vinnikov, L.Ya., Anderegg, J., Bud'ko, S.L., Canfield, P.C., Kogan, V.G. *Phys. Rev. B* 2005, **71**, 224513.
- Volkova, L.M., Polyshchuk, S.A., Magarill, S.A., Herbeck, F.E. *J. Supercond.* 2002, **15**, 663.
- Wälte, A., Fuchs, G., Müller, K.-H., Handstein, A., Nenkov, K., Narozhnyi, V.N., Drechsler, S.-L., Shulga, S., Schultz, L., Rosner, H. *Phys. Rev. B* 2004, **70**, 174503.
- Wälte, A., Fuchs, G., Müller, K.-H., Drechsler, S.-L., Nenkov, K., Schultz, L. *Phys. Rev. B* 2005, **72**, 100503(R).
- Wälte, A., Drechsler, S.-L., Fuchs, G., Müller, K.-H., Nenkov, K., Hinz, D., Schultz, L. *Phys. Rev. B* 2006, **73**, 064501.
- Wagner, T.A., Dertinger, A., Ettig, W., Krause, A., Schmidt, H., Braun, H.F. *Physica C* 1999, **323**, 71.
- Walker, M.B., Detlefs, C. *Phys. Rev. B* 2003, **67**, 132407.
- Wang, G., Maki, K. *Phys. Rev. B* 1998, **58**, 6493.
- Wang, X., Amoruso, S., Bruzzese, R., Spinelli, N., Tortora, A., Velotta, R., Ferdeghini, C., Grassano, G., Ramadan, W. *Chem. Phys. Lett.* 2002a, **353**, 1.
- Wang, X., Amoruso, S., Tortora, A., Armenante, M., Bruzzese, R., Velotta, R., Spinelli, N. *Appl. Surf. Sci.* 2002b, **186**, 303.
- Wang, Y., Plackowski, T., Junod, A. *Physica C* 2001, **355**, 179.
- Wang, Y.K., Hsu, L.-S., Lan, M.-D. *J. Alloys Compd.* 2005, **389**, 1.
- Watanabe, T., Kitazawa, K., Hasegawa, T., Hossain, Z., Nagarajan, R., Gupta, L.C. *J. Phys. Soc. Jpn.* 2000, **69**, 2708.
- Watanabe, T., Nohara, M., Hanaguri, T., Takagi, H. *Phys. Rev. Lett.* 2004, **92**, 147002.
- Weht, R., Cappannini, O.M., Rodríguez, C.O., Christensen, N.E. *Physica C* 1996, **260**, 125.
- Weller, Th.E., Ellerby, M., Saxena, S.S., Smith, R.P., Skipper, N.T. *Nature Phys.* 2005, **1**, 39.
- Wijngaarden, R.J., Griessen, R., in: Evetts, J., editor. *Concise Encyclopedia of Magnetic & Superconducting Materials.* Oxford: Pergamon; 1992, p. 583.
- De Wilde, Y., Iavarone, M., Welp, U., Metlushko, V., Koshelev, A.E., Aranson, I., Crabtree, G.W., Canfield, P.C. *Phys. Rev. Lett.* 1997, **78**, 4273.
- Williams, A.J., Attfield, J.P. *Phys. Rev. B* 2005, **72**, 024436.
- Williams, G.V.M. *Phys. Rev. B* 2006, **73**, 064510.
- Williams, J.M., Shultz, A.J., Geiser, U., Carlson, K.D., Kini, A.M., Wang, H.H., Kwok, W.-K., Whangbo, M.-H., Schirber, J.E. *Science* 1991, **252**, 1501.
- Willis, J.O., Erickson, D.J., Olsen, C.E., Taylor, R.D. *Phys. Rev. B* 1980, **21**, 79.
- Wills, A.S., Detlefs, C., Canfield, P.C. *Philos. Mag.* 2003, **83**, 1227.
- Wimbush, S.C., Holzapfel, B. *phys. status solidi (c)* 2006, **3**, 3007.
- Wimbush, S.C., Häse, K., Schultz, L., Holzapfel, B. *J. Phys.: Condens. Matter* 2001, **13**, L355.
- Wimbush, S.C., Schultz, L., Holzapfel, B. *Physica C* 2003, **388–389**, 191.
- Wimbush, S.C., Holzapfel, B., Jooss, Ch. *J. Appl. Phys.* 2004a, **96**, 3589.
- Wimbush, S.C., Schultz, L., Holzapfel, B. *Physica C* 2004b, **408–410**, 83.
- Winzer, K., Krug, K., in: Müller, K.-H., Narozhnyi, V.N., editors. *Rare Earth Transition Metal Borocarbides (Nitrides): Superconducting, Magnetic and Normal State Properties.* Dordrecht: Kluwer Academic; 2001, p. 63.
- Winzer, K., Peng, Z., Krug, K. *Physica B* 1999, **259–261**, 586.
- Winzer, K., Krug, K., Peng, Z.Q. *J. Magn. Magn. Mater.* 2001, **226–230**, 321.
- Wohlfarth, E.P. *J. Appl. Phys.* 1968, **39**, 1061.
- Wohlfarth, E.P. *Phys. Lett.* 1979, **75A**, 141.
- Won, H., Maki, K. *Physica C* 2004, **408–410**, 386.
- Won, H., Yuan, Q., Thalmeier, P., Maki, K. *Brazilian J. Phys.* 2003, **33**, 675.
- Won, H., Jang, H., Parker, D., Haas, St., Maki, K. 2004; *cond-mat/0405099*.
- Wu, M.K., Ashburn, J.R., Torng, C.J., Hor, P.H., Meng, R.L., Gao, L., Huang, Z.J., Wang, Y.Q., Chu, C.W. *Phys. Rev. Lett.* 1987, **58**, 908.
- Xu, M., Canfield, P.C., Ostenson, J.E., Finnemore, D.K., Cho, B.K., Wang, Z.R., Johnston, D.C. *Physica C* 1994, **227**, 321.
- Yamaguchi, T., Akatsu, M., Nakano, Y., Washizawa, T., Nemoto, Y., Goto, T., Dönni, A., Nakamura, S., Kunii, S. *Physica B* 2003, **329–333**, 622.

- Yamauchi, H., Onodera, H., Ohoyama, K., Onimaru, T., Kosaka, M., Ohashi, M., Yamaguchi, Y. *J. Phys. Soc. Jpn.* 1999, **68**, 2057.
- Yamauchi, K., Harima, H. *Physica B* 2005, **359–361**, 597.
- Yamauchi, K., Katayama-Yoshida, H., Yanase, A., Harima, H. *Physica C* 2004, **412–414**, 225.
- Yang, I.-S., Klein, M.V., Cooper, S.L., Canfield, P.C., Cho, B.K., Lee, S.-I. *Phys. Rev. B* 2000, **62**, 1291.
- Yang, I.-S., Klein, M.V., Bud'ko, S., Canfield, P.C. *J. Phys. Chem. Solids* 2002, **63**, 2195.
- Yang-Bitterlich, W., Krämer, U. *Cryst. Res. Technol.* 2000, **35**, 369.
- Yang-Bitterlich, W., Bitterlich, H., Zahn, G., Krämer, U. *J. Alloys Compd.* 2002, **347**, 131.
- Yanson, I.K., in: Müller, K.-H., Narozhnyi, V.N., editors. *Rare Earth Transition Metal Borocarbides (Nitrates): Superconducting, Magnetic and Normal State Properties*. Dordrecht: Kluwer Academic; 2001, p. 95.
- Yanson, I.K., Fisun, V.V., Jansen, A.G.M., Wyder, P., Canfield, P.C., Cho, B.K., Tomy, C.V., Paul, D.McK. *Phys. Rev. Lett.* 1997, **78**, 935.
- Yanson, I.K., Bobrov, N.L., Tomy, C.V., Paul, D.McK. *Physica C* 2000a, **334**, 33.
- Yanson, I.K., Bobrov, N.L., Tomy, C.V., Paul, D.McK. *Physica C* 2000b, **334**, 152.
- Yaron, U., Gammel, P.L., Ramirez, A.P., Huse, D.A., Bishop, D.J., Goldman, A.I., Stassis, C., Canfield, P.C., Mortensen, K., Eskildsen, M.R. *Nature* 1996, **382**, 236.
- Yatskar, A., Budraa, N.K., Beyermann, W.P., Canfield, P.C., Bud'ko, S.L. *Phys. Rev. B* 1996, **54**, R3772.
- Yatskar, A., Mielke, C.H., Canfield, P.C., Lacerda, A.H., Beyermann, W.P. *Phys. Rev. B* 1999, **60**, 8012.
- Yelland, E.A., Hayden, S.M., Yates, S.J.C., Pfeleiderer, C., Uhlarz, M., Vollmer, R., v. Löhneysen, H., Bernhoeft, N.R., Smith, R.P., Saxena, S.S., Kimura, N. *Phys. Rev. B* 2005, **72**, 214523.
- Yethiraj, M., Paul, D.McK., Tomy, C.V., Forgan, E.M. *Phys. Rev. Lett.* 1997, **78**, 4849.
- Yethiraj, M., Paul, D.McK., Tomy, C.V., Thompson, J.R. *Phys. Rev. B* 1998, **58**, R14767.
- Yethiraj, M., Christen, D.K., Paul, D.McK., Miranovic, P., Thompson, J.R. *Phys. Rev. Lett.* 1999, **82**, 5112.
- Yokoya, T., Kiss, T., Watanabe, T., Shin, S., Nohara, M., Takagi, H., Oguchi, T. *Phys. Rev. Lett.* 2000, **85**, 4952.
- Yokoya, T., Kiss, T., Chainani, A., Shin, S. *J. Electron Spectrosc. Relat. Phenom.* 2002, **124**, 99.
- Yokoya, T., Baba, T., Tsuda, S., Kiss, T., Chainani, A., Shin, S., Watanabe, T., Nohara, M., Hanaguri, T., Takagi, H., Takano, Y., Kito, H., Itoh, J., Harima, H., Oguchi, T. *J. Phys. Chem. Solids* 2006, **67**, 277.
- Yosida, K. *Theory of Magnetism*, Berlin: Springer; 1996.
- Youn, S.J., Min, B.I., Freeman, A.J. *Phys. Rev. B* 2002, **66**, 052512.
- Yuan, Q., Thalmeier, P. *Phys. Rev. B* 2003, **68**, 174501.
- Yuan, Q., Chen, H.-Y., Won, H., Lee, S., Maki, K., Thalmeier, P., Ting, C.S. *Phys. Rev. B* 2003, **68**, 174510.
- Zandbergen, H.W., Jansen, J., Cava, R.J., Krajewski, J.J., Peck Jr., W.F. *Nature* 1994a, **372**, 759.
- Zandbergen, H.W., Gortenmulder, T.J., Sarrac, J.L., Harrison, J.C., de Andrade, M.C., Hermann, J., Han, S.H., Fisk, Z., Maple, M.B., Cava, R.J. *Physica C* 1994b, **232**, 328.
- Zandbergen, H.W., Cava, R.J., Krajewski, J.J., Peck Jr., W.F. *J. Solid State Chem.* 1994c, **110**, 196.
- Zarestky, J., Stassis, C., Goldman, A.I., Canfield, P.C., Dervenagas, P., Cho, B.K., Johnston, D.C. *Phys. Rev. B* 1995, **51**, 678(R).
- Zarestky, J., Stassis, C., Goldman, A., Canfield, P., Shirane, G., Shapiro, S. *Phys. Rev. B* 1999, **60**, 11932.
- Zarestky, J.L., Stassis, C., Goldman, A.I., Canfield, P.C., Shirane, G., Shapiro, S.M. *J. Phys. Chem. Solids* 2002, **63**, 811.
- Zhao, S.R., Xu, Z.A., Takeya, H., Hirata, K., Luo, J.L. *J. Phys.: Condens. Matter* 2006, **18**, 8533.
- Zou, Z., Ye, J., Oka, K., Nishihara, Y. *Phys. Rev. Lett.* 1998, **80**, 1074.
- Zwicknagl, G., Fulde, P. *Z. Phys. B: Condens. Matter* 1981, **43**, 23.

## Polyoxometalates

Michael T. Pope\*

Contents		
	1. Introduction	338
	2. Structural Types and Features	340
	2.1 Dodecamolybdocrates and related species	340
	2.2 The Peacock–Weakley anions	342
	2.2.1 Bis(pentatungsto)metalates, $[R(W_5O_{18})_2]^{8,9-}$	343
	2.2.2 $[R(XM_{11}O_{39})_x]^{n-}$ , $[R(X_2M_{17}O_{61})_x]^{n-}$ and related anions	344
	2.2.2.1 1:2 complexes ( $x = 2$ ): trivalent lanthanides	344
	2.2.2.2 1:2 complexes: tetravalent lanthanides	348
	2.2.2.3 1:1 complexes ( $x = 1$ )	351
	2.2.2.4 Derivatives of 1:1 complexes	354
	2.3 Complexes of multivacant lacunary anions	355
	2.4 Polyoxotungstate “cryptate” derivatives	362
	2.5 Polyoxomolybdates	366
	2.5.1 Anderson-type hexamolybdate complexes	367
	2.5.2 $R_4Mo_{29}$ complexes	368
	2.5.3 Reduced molybdate complexes	369
	2.6 Niobates and vanadates	371
	3. Properties and Applications	372
	3.1 Photophysical properties	372
	3.2 Other reported potential applications	373
	4. Perspectives	374
	Acknowledgements	375
	References	375

\* Department of Chemistry, Georgetown University, Washington, DC 20057-1227, USA  
E-mail: [popem@georgetown.edu](mailto:popem@georgetown.edu)

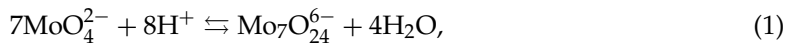
### Abbreviations

1-D	one-dimensional	HL-60	human promyelocytic leukemia cell-line
3-D	three-dimensional	HSV	herpes simplex virus
a.c.	alternating current	IR	infrared
ESI	electrospray ionization	LMCT	ligand to metal charge transfer
ESR	electron spin resonance	n.d.	not determined
EXAFS	extended X-ray absorption fine structure	NMR	nuclear magnetic resonance spectroscopy
<i>fac</i>	facial (configuration of three ligands on an octahedral metal center)	POM	polyoxometalate
h	hour	SCE	saturated calomel electrode
HIV	human immunodeficiency virus	UV-vis	ultraviolet-visible
		XANES	X-ray absorption near edge spectroscopy

## 1. INTRODUCTION

Polyoxometalates, formerly and still occasionally known as heteropoly- and isopolyanions (or “acids”), comprise an immense and expanding class of oxoanions of the early transition metal elements, molybdenum(VI), tungsten(VI) and vanadium(V), and to a much lesser extent, pentavalent niobium and tantalum. The major characteristics of these elements that distinguish them from other polyoxoanion formers such as chromium(VI), silicon and phosphorus are (1) the ability of the metal atom to increase its coordination by oxide from 4 to (commonly) 6 or 7, and (2) a consequence of the metal’s vacant and accessible d-orbitals, the ability to engage in multiple bonding with “terminal” oxygen atoms. As we shall see in this chapter, by far the commonest environment of the metal atom in polyoxometalates (POMs) is quasi-octahedral with either one or two (mutually *cis*) unshared or terminal oxygens. In 1965, based upon the handful of POM structures that were known at that time, Lipscomb noted that no structure contained metal atoms with *three* terminal oxygens, and proposed that this would prove to be a general restriction (Lipscomb, 1965). Since then some POM structures that violate the so-called Lipscomb criterion have been reported with three terminal oxygens occupying a face of an  $MO_6$  octahedron. However in most cases which have been examined closely one of the three terminal oxygens has been found to be protonated or is a water ligand. The Lipscomb rule is of course a consequence of the strong trans influences of the  $M-O_{\text{terminal}}$  multiple bonds. This leads, in the “octahedral” *fac*- $MO_3$  case, to long and therefore weak bonds attaching M to the remainder of the polyoxometalate structure.

In a formal sense, POMs are produced via Brønsted acid–base condensation–addition processes, e.g.



However, Eqs. (1) and (2) are oversimplifications since the stoichiometry of such reactions can be strongly influenced by the nature of the counter-cations present and by the total ionic strength of the medium (Pope, 1991; Sasaki and Sillén, 1968; Yagasaki et al., 1987; Tytko et al., 1985; Knoth and Harlow, 1981).

It has been known for well over 150 years that other positive-valent elements can be incorporated into POM structures as “heteroatoms” (hence the term “heteropoly acids”). Most elements of the Periodic Table have been incorporated, some such as phosphorus yielding dozens of compositions and structures. At the present time the field of POMs appears to be limitless.

Although it is always possible, once the formula of a specific POM is known, to write an equation analogous to Eq. (1) describing its formation, this is often not the appropriate synthetic procedure. In addition to variation of counter-cation, ionic strength and pH in aqueous media, syntheses may be carried out in non-aqueous solvents, via hydro- or solventothermal methods, and by solid state reactions. The starting material may even be a pre-formed stable or metastable POM; this is especially the case for tungstates. While in some cases the preparation of a specific POM may be rationally designed, in the majority of systems the synthesis has to be described simply as “self assembly.”

From the viewpoint of a heteroatom the polyoxometalate framework that immediately surrounds it can be regarded as a multidentate “ligand.” Such a ligand has some special properties: (1) it is fully oxidized and therefore can in principle accommodate heteroatoms in high oxidation states, (2) it is a “hard” sigma donor via the oxygen atoms, but can also act as a  $\pi$  acceptor as a result of the availability of appropriate vacant d-orbitals of the adjacent metal atoms (Rong and Pope, 1992), and (3) it has high thermal stability, and the oxometalate framework has stability to ionizing radiation.

A general introduction to the chemistry of POMs (Pope, 1983; Pope and Müller, 1991) and more recent reviews (Pope, 2004; Hill, 1998, 2004) illustrate the broad range and potential scope of this field. By far the commonest heteroatoms in POMs demand “tetrahedral” or “octahedral” sites. Such a requirement cannot exist for the rare-earth cations which generally exhibit larger and more variable coordination environments. With the relatively few exceptions to be noted below, rare-earth cations act as linking groups between two or more POM fragments, leading to large anion assemblies or to extended one-, two- or three-dimensional lattices.

The present chapter reviews the structural chemistry (Section 2) and properties and applications (Section 3) of polyoxometalates that incorporate one or more rare-earth elements. In most cases these are discrete anionic entities within the crystal and in solution, but there are also extended lattices in which POM groups are linked by rare-earth cations. Solids which can best be described as mixed oxides, or which appear to be salts of common polyoxometalate architectures such as the

**TABLE 1** Reviews of aspects of polyoxometalate rare-earth chemistry

Title	Reference
Nonradiative transitions in europium polytungstates	Blasse (1991)
Intramolecular energy transfer in polyoxometaloeuropate lattices and their application to a.c. electroluminescence device	Naruke and Yamase (1991)
Spectroscopic studies of polyoxometalates and their complexes with lanthanide(III) ions in solution	Lis (1996)
Condensed heteropoly anions and their complexes with lanthanide(III) ions. Spectroscopic studies	Lis (1998)
Photo- and electrochromism of polyoxometalates and related materials	Yamase (1998)
Complexes of f elements with heteropolyanions	Yusov and Shilov (1999)
Applications of spectroscopic methods in studies of polyoxometalates and their complexes with lanthanide(III) ions	Lis (2000)
Spectroscopic studies of heteropolyanions and their complexes with lanthanide(III) ions	Lis and But (2001)
Complexation of 4f and 5f cations with polyoxometalates	Choppin (2002)
Preparation and structural chemistry of polyoxometalates containing rare-earth ions	Naruke (2003a)
Synthesis and structural chemistry of polyoxometalates containing rare-earth ions	Naruke (2003b)
Photoluminescence properties of rare-earth polyoxometalates as molecular phosphors	Naruke and Yamase (2004)

Keggin anions, in which the rare-earth element functions as a counter-cation, will in general not be considered.

Previous reviews focusing on certain aspects of the chemistry of POM-rare-earth complexes are listed in Table 1.

## 2. STRUCTURAL TYPES AND FEATURES

### 2.1 Dodecamolybdocerates and related species

The first example of a polyoxometalate that contained a rare-earth heteroatom, cerium(IV), was reported almost a century ago (Barbieri, 1914). Formulated at the time as  $4(\text{NH}_4)_2\text{O}\cdot\text{CeO}_2\cdot 12\text{MoO}_3$ , the yellow salt was later converted into the free acid by ion-exchange (Baker et al., 1953) and was shown to be octabasic. An X-ray structural investigation of  $(\text{NH}_4)_2\text{H}_6[\text{CeMo}_{12}\text{O}_{42}]\cdot n\text{H}_2\text{O}$  revealed the anion structure shown in Figure 1 (Dexter and Silvertown, 1968). The anion structure has been reconfirmed for  $\text{H}_8[\text{CeMo}_{12}\text{O}_{42}]\cdot 18\text{H}_2\text{O}$  (Tat'yana et al., 1982a) and for

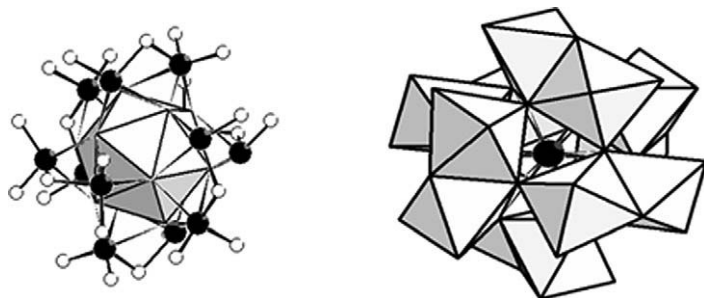


**FIGURE 1** Two views of the structure of  $[\text{CeMo}_{12}\text{O}_{42}]^{8-}$  emphasizing the central  $\text{CeO}_{12}$  icosahedron (left) and the pairs of face-sharing  $\text{MoO}_6$  octahedra (right).

some tetravalent actinide analogues. The 12-coordinate cerium heteroatom occupies a central site of nominal icosahedral symmetry, although the overall anion has only  $D_{3d}$  point symmetry. The surrounding polymolybdate shell is generally described in terms of face-sharing pairs of  $\text{MoO}_6$  octahedra, although if the longest (and weakest)  $\text{Mo}-\text{O}$  bonds that are trans to the short  $\text{Mo}-\text{O}_{\text{terminal}}$  bonds are “deleted,” the anion structure can be viewed as six ditetrahedral  $\text{Mo}_2\text{O}_7^{2-}$  ligands surrounding an “octahedral” cerium heteroatom (Day et al., 1977; Day and Klemperer, 1987). The cyclic voltammogram of a solution of  $[\text{CeMo}_{12}\text{O}_{42}]^{8-}$  shows a reversible  $\text{Ce}^{4+/3+}$  redox process at 0.49 V vs SCE in 1 M sulfuric acid (McKean and Pope, 1974). At more negative potentials the anion undergoes a multielectron irreversible reduction resulting in anion decomposition. Solutions of the electrolytically-generated  $\text{Ce}^{\text{III}}$  anion are metastable, and  $[\text{CeMo}_{12}\text{O}_{42}]^{9-}$  has yet to be isolated in a crystalline salt. A  $\text{Gd}^{\text{III}}$  analog has recently been reported as a component of a hydrothermally-produced three-dimensional network solid,  $[\text{Gd}(\text{H}_2\text{O})_3]_3[\text{GdMo}_{12}\text{O}_{42}] \cdot 3\text{H}_2\text{O}$  (Wu et al., 2002). The only other examples of the structure contain tetravalent actinide heteroatoms (U, Np, Pu). Rare-earth adducts of the uranium anion,  $[\text{UMo}_{12}\text{O}_{42}\{\text{R}(\text{H}_2\text{O})_6\}_2]^{2-}$  ( $\text{R} = \text{Sc}, \text{Nd}, \text{Er}$ ), see Figure 2, have been reported and structurally characterized (Samokhvalova et al., 1989a, 1989b, 1990a, 1990c; Tat’yanina et al., 1982b). Analogous chemistry undoubtedly exists for  $[\text{CeMo}_{12}\text{O}_{42}]^{8-}$  based on  $^{95}\text{Mo}$ -,  $^{17}\text{O}$ - and  $^{139}\text{La}$ -NMR studies with first row transition metal and trivalent rare-earth cations (Petrukhina et al., 1989; Samokhvalova et al., 1990b). Based on these studies yttrium and the heavy rare earths form complexes which are labile on the NMR time scale, whereas the lighter rare earths form inert complexes.

The 9-molybdate anions  $[\text{MMo}_9\text{O}_{32}]^{6-}$  ( $\text{M} = \text{Mn}^{\text{IV}}, \text{Ni}^{\text{IV}}$ ) have been shown to form analogous labile adducts with  $\text{La}(\text{III})$  and  $\text{Pr}(\text{III})$  according to  $^{95}\text{Mo}$ -NMR of the diamagnetic nickel complex (Gavrilova et al., 1990). Structures of  $[(\text{CH}_3)_4\text{N}]_2[(\text{H}_2\text{O})_6\text{LaHMnMo}_9\text{O}_{32}]$  (Gavrilova et al., 1991) and of  $\{[(\text{H}_2\text{O})_6\text{La}]_2\text{-MnMo}_9\text{O}_{32}\}$  (Gavrilova and Molchanov, 2005) confirm the mode of attachment of the lanthanum cation, see Figure 3. Formation constants for 1:1 complexes of  $[\text{MnMo}_9\text{O}_{32}]^{6-}$  with La, Nd, Gd and Yb have been reported (Saito et al., 1997).

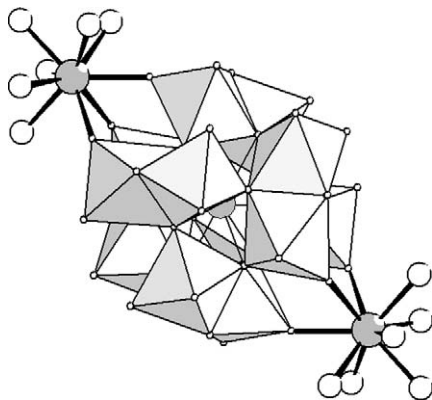


**FIGURE 2**  $[\text{UMo}_{12}\text{O}_{42}\{\text{R}(\text{H}_2\text{O})_6\}_2]^{2-}$  ( $\text{R} = \text{Sc}, \text{Nd}, \text{Er}$ ).

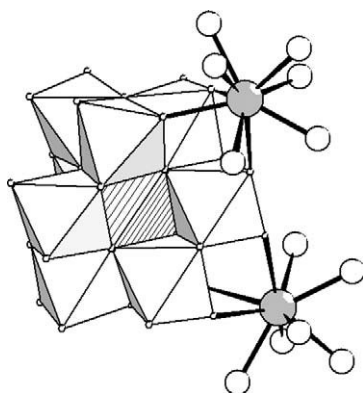


**FIGURE 3**  $[\{(\text{H}_2\text{O})_6\text{La}\}_2\text{MnMo}_9\text{O}_{32}]$ .

## 2.2 The Peacock–Weakley anions

The first systematic studies of polyoxometalate—rare-earth complexes were published in 1971 (Peacock and Weakley, 1971a, 1971b). Two classes of polytungstate complexes were described and these can now be seen to have common structural features. The complexes of Y, La, Ce(III and IV), Pr, Nd, Sm, Ho, Er, and Yb in which  $\text{R}:\text{W} = 1:10$  were readily formed by reaction of  $\text{WO}_4^{2-}$  with the appropriate rare-earth salt, but are stable only within the pH range 5.5–8.5. More recent  $^{183}\text{W}$ -NMR studies (Inoue et al., 2003) indicate that *in solution* the anions containing the heaviest R (Tm, Yb and Lu) are partially decomposed.

An early structure determination of the sodium salt of the Ce(IV) complex revealed the anion  $[\text{CeW}_{10}\text{O}_{36}]^{8-}$  with a nominally square-antiprismatic Ce cation sandwiched between two  $[\text{W}_5\text{O}_{18}]^{6-}$  anions as shown in Figure 4 (Iball et al., 1974; Rosu and Weakley, 1998). The  $\{\text{W}_5\text{O}_{18}\}$  fragments observed in Figure 4 are formally derived from the hexatungstate anion  $[\text{W}_6\text{O}_{19}]^{2-}$  by “removal” of a  $\{\text{WO}_{\text{terminal}}\}^{4+}$

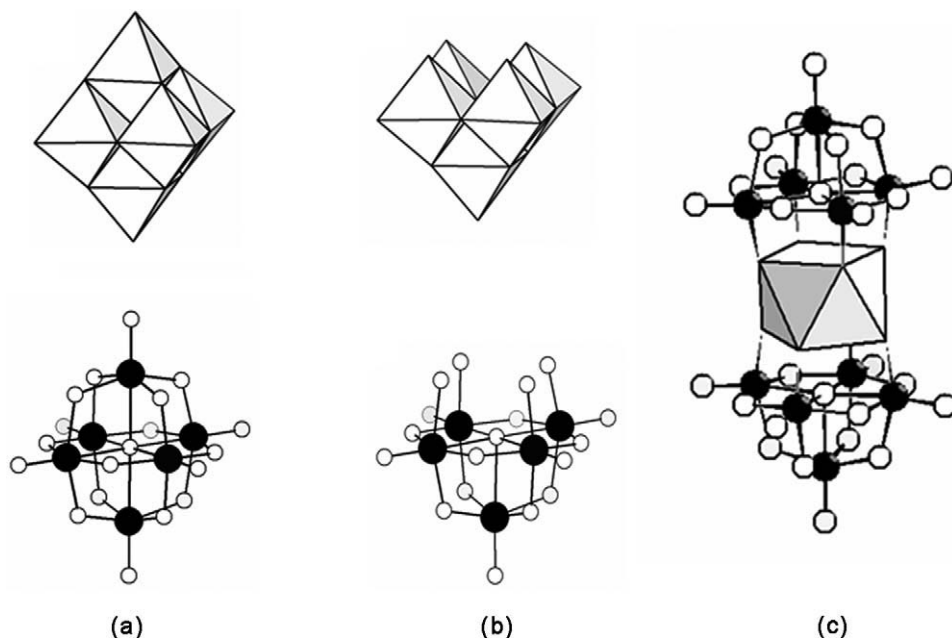


**FIGURE 4** Polyhedral and ball-and-stick representations of the structures of (a)  $[W_6O_{19}]^{2-}$ , (b) lacunary  $[W_5O_{18}]^{6-}$ , and (c)  $[R(W_5O_{18})_2]^{9-}$ .

group. Such derivatives are known as *lacunary* structures, many examples of which are known in polyoxometalate chemistry. Although the pentatungsto group is seen in the  $RW_{10}$  anions and in a few other structures to be discussed below, the lacunary anion itself has not been isolated in stable form. This behavior stands in contrast to the numerous examples of stable lacunary versions of the well-known Keggin ( $[XW_{12}O_{40}]^{n-}$ ) and Wells–Dawson ( $[X_2W_{18}O_{62}]^{n-}$ ) structures. Peacock and Weakley (1971a) also reported 1:1 and 1:2 complexes of rare-earth cations with the lacunary anions  $[SiW_{11}O_{39}]^{8-}$  and  $[P_2W_{17}O_{61}]^{10-}$  (the latter subsequently identified as the  $\alpha_2$ -isomer), although only the 1:2 complexes were isolated. The proposed general features of the structures for the 1:2 complexes were initially confirmed for the  $U^{IV}$  analog  $Cs_{12}[U(\alpha\text{-Ge}W_{11}O_{39})_2]13\text{--}14H_2O$  (Tourné et al., 1980) and for  $K_{16}[Ce^{IV}(\alpha_2\text{-P}_2W_{17}O_{61})_2]\text{--}ca.50H_2O$  (Molchanov et al., 1979), see Figure 5. A considerable body of literature, including structure determinations of higher quality, has accumulated for this particular class of complexes, and this will be discussed in more detail below.

### 2.2.1 Bis(pentatungsto)metalates, $[R(W_5O_{18})_2]^{8,9-}$

The anion structure originally reported by Iball et al. for the  $Ce^{IV}$  derivative has been confirmed in numerous subsequent determinations, see Table 2.

As shown in Figure 4, the anions have nominal  $D_{4d}$  symmetry in the solid state, and NMR studies are consistent with the same structure in solution. Tungsten-183 NMR spectra (Fedotov et al., 1989a, 1989b, 1996; Shiozaki et al., 1996a; Bartis et al.,

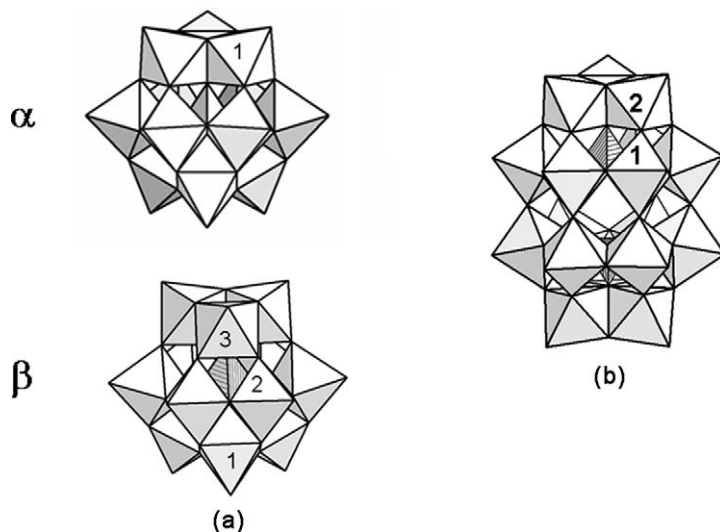


**FIGURE 5** (a)  $\alpha$ -( $T_d$ ) and  $\beta$ -( $C_{3v}$ ) isomers of the Keggin anion  $[\text{SiW}_{12}\text{O}_{40}]^{4-}$  and (b) the Dawson anion  $\alpha$ - $[\text{P}_2\text{W}_{18}\text{O}_{62}]^{6-}$ . The six monovacant lacunary derivatives ( $\alpha_n, \beta_n$ ) are formed by “removal” of the numbered  $\text{WO}_6$  octahedra (stoichiometric loss of  $\{\text{WO}\}^{4+}$ ).

**TABLE 2** Structure determinations of salts containing  $[\text{R}(\text{W}_5\text{O}_{18})_2]^{8,9-}$  anions

R	Reference(s)
La	Almeida Paz et al. (2005)
Ce(IV)	Iball et al. (1974); Rosu and Weakley (1998)
Pr, Nd, Dy	Ozeki and Yamase (1994a)
Sm, Gd, Tb	Ozeki and Yamase (1993a)
Sm	Ozeki and Yamase (1993b, 1994b)
Eu	Sugeta and Yamase (1993); Yamase et al. (1993)
Gd	Yamase and Ozeki (1993); Yamase et al. (1994)
Tb	Ozeki et al. (1992)

1997a; Inoue et al., 2003) show two lines in a 1:4 ratio corresponding to the apical ( $W_A$ ) and equatorial ( $W_B$ ) sites, see Table 3. The Fedotov et al. (1996) and Inoue et al. (2003) papers also report fully-resolved 6-line  $^{17}\text{O}$ -NMR data and an analysis of the contact and dipolar contributions to the chemical shifts of the oxygen and tungsten atoms adjacent to paramagnetic rare-earth cations.

### 2.2.2 $[\text{R}(\text{XM}_{11}\text{O}_{39})_x]^{n-}$ , $[\text{R}(\text{X}_2\text{M}_{17}\text{O}_{61})_x]^{n-}$ and related anions

**2.2.2.1 1:2 complexes ( $x = 2$ ): trivalent lanthanides** Complexes of this type, first reported by Peacock and Weakley (1971a), have received considerable attention in the subsequent decades. The possibilities are virtually endless—variability of

**TABLE 3**  $^{183}\text{W}$ -NMR data<sup>a</sup> for  $[\text{R}(\text{W}_5\text{O}_{18})_2]^{8,9-}$ 

R	Temperature (K)	$\delta(\text{W}_A)$	$\Delta\nu(\text{W}_A)$ (Hz)	$\delta(\text{W}_B)$	$\Delta\nu(\text{W}_B)$ (Hz)
Y	293	-28	15	-11	15
La	293	-19	11	2	11
Ce(III)	299	51	16	155	16
Ce(IV)	<sup>b</sup>	-13		-18	
Pr	298	53	30	376	30
Nd	299	17	25	444	22
Sm	299	-31		-10	17
Eu	<sup>b</sup>	-18		-611	
Gd	313	-108	200		
Tb	313	-185	100	-1567	220
Dy	313	-122	90	-1061	160
Ho	313	-118	34	-754	160
Er	313	-34	150	-382	100
Tm <sup>c</sup>	<sup>b</sup>	-90		-86	
Yb <sup>c</sup>	<sup>b</sup>	82		8	
Lu <sup>c</sup>	<sup>b</sup>	20		-4	

<sup>a</sup> Fedotov et al. (1996); Inoue et al. (2003). Chemical shifts for the paramagnetic complexes are temperature sensitive and account for differences between literature reports.

<sup>b</sup> Not reported.

<sup>c</sup> Solutions of these anions also show resonances for  $[\text{W}_7\text{O}_{24}]^{6-}$  as a result of partial decomposition.

R, X and M (=Mo, W and mixtures) coupled with different structural isomers of the lacunary  $\text{XM}_{11}$  and  $\text{X}_2\text{M}_{17}$  "ligands," which are illustrated in Figure 5. By far the commonest examples are based on the (mono)lacunary derivatives of the  $\alpha$ -(Keggin) isomer of  $\text{XM}_{12}\text{O}_{40}^{7-}$  and the  $\alpha_2$ -isomer of  $[\text{P}_2\text{W}_{17}\text{O}_{61}]^{10-}$ . Reported structure determinations of such 1:2 complexes are summarized in Table 4, the last two entries of which (17, 18) are examples of mixed-ligand type species. Structures of complexes of the  $\beta_2$ -isomer of  $[\text{SiW}_{11}\text{O}_{39}]^{8-}$  (Figure 5) have recently been reported (entry 10 in Table 4).

The  $\beta_2$ -isomer is chiral and the crystal structures show a trend from complexes of  $C_i$  symmetry with the rare-earth cation bound to both enantiomers of the lacunary anion (100% for R = La and Ce) to those of  $C_1$  symmetry with a single enantiomer bound to the central cation (100% for R = Yb, Lu). For R = Sm–Tb both conformations were present in the crystals. Tungsten-NMR spectra for the La and Lu complexes, 11 and 22 lines, respectively, illustrate that the conformational differences survive dissolution (Bassil et al., 2007). Isolated examples of 1:2 complexes of rare-earth cations incorporating the  $\alpha_1$ -isomer (also chiral) of  $[\text{P}_2\text{W}_{17}\text{O}_{61}]^{10-}$  (Table 4, entry 11) are rare,<sup>1</sup> an observation consistent with unfavorable formation constants (see data reported in Table 7 below) that have been attributed to steric crowding (Zhang et al., 2005b). Strong alkali metal counter-

<sup>1</sup> This generalization may not apply to the analogous complexes of tetravalent actinide cations (Ostuni et al., 2003).

**TABLE 4** Confirmed structures of 1:2 complexes with monolacunary derivatives of  $\text{XM}_{12}$  and  $\text{X}_2\text{M}_{18}$  anions

Anion	Reference(s)	Notes
1 $[\text{Dy}(\alpha\text{-SiMo}_{11}\text{O}_{39})_2]^{13-}$	Shan et al. (1990); Wang et al. (1991f); Liu et al. (1991a)	
2 $[\text{Pr}(\alpha\text{-SiMo}_{11}\text{O}_{39})_2]^{13-}$	Shan et al. (1991)	
3 $[\text{Nd}(\alpha\text{-GeMo}_{11}\text{O}_{39})_2]^{13-}$	Shan et al. (1992a, 1992b)	
4 $[\text{R}(\alpha\text{-PMo}_{11}\text{O}_{39})_2]^{11-}$	Gaunt et al. (2003)	R = Ce, Sm, Dy, Lu
5 $[\text{La}(\alpha\text{-SiMo}_9\text{W}_2\text{O}_{39})_2]^{13-}$	Zhou et al. (1992); Lu et al. (1996)	Mo,W disordered
6 $[\text{Dy}(\alpha\text{-SiMo}_6\text{W}_5\text{O}_{39})_2]^{13-}$	Wang et al. (1997)	Mo,W disordered
7 $[\text{Ce}(\alpha\text{-SiW}_{11}\text{O}_{39})_2]^{12-}$	Sun et al. (2001)	Ce(IV)
8 $[\text{Ce}(\alpha\text{-SiW}_{11}\text{O}_{39})_2]^{13-}$	Zhao et al. (2004)	Ce(III)
9 $[\text{Pr}(\alpha\text{-SiW}_{11}\text{O}_{39})_2]^{13-}$	Mialane et al. (2004)	
10 $[\text{R}(\beta_2\text{-SiW}_{11}\text{O}_{39})_2]^{13-}$	Bassil et al. (2007)	R = La, Ce, Sm–Tb, Yb, Lu
11 $[\text{R}(\alpha_1\text{-P}_2\text{W}_{17}\text{O}_{61})_2]^{17-}$	Zhang et al. (2005b)	R = La, Nd, Eu
12 $[\text{Ce}(\alpha_2\text{-P}_2\text{W}_{17}\text{O}_{61})_2]^{16-}$	Molchanov et al. (1979)	Ce(IV)
13 $[\text{Lu}(\alpha_2\text{-P}_2\text{W}_{17}\text{O}_{61})_2]^{17-}$	Luo et al. (2001)	
14 $[\text{Yb}(\alpha_2\text{-P}_2\text{W}_{17}\text{O}_{61})_2]^{17-}$	Niu et al. (2004a)	
15 $[\text{R}(\alpha_2\text{-P}_2\text{W}_{17}\text{O}_{61})_2]^{17-}$	Zhang et al. (2006)	R = Gd, Eu
16 $[\text{Ce}\{\text{X}(\text{H}_4)\text{W}_{17}\text{O}_{61}\}_2]^{19-}$	Belai et al. (2005)	Ce(III); X = P, As
17 $[\text{R}(\text{BW}_{11}\text{O}_{39})(\text{W}_5\text{O}_{18})]^{12-}$	Naruke and Yamase (2000)	R = Ce(III), Eu
18 $[\text{Ce}(\alpha_1\text{-P}_2\text{W}_{17}\text{O}_{61})(\alpha_2\text{-P}_2\text{W}_{17}\text{O}_{61})]^{17-}$	Ostuni et al. (2003)	Ce(III)

cation binding to the free ligand is also a factor, see Figure 6. As a consequence of the nominal square antiprismatic coordination geometry of the rare-earth cation the global symmetry of the complexes with identical polyoxoanion ligands is  $C_2$ . Since these ligands have only  $C_s$  symmetry at most (in contrast to the  $C_{4v}$  symmetry of the  $\{\text{W}_5\text{O}_{18}\}$  group in the decatungstates of Figure 4 and complex 17 in Table 4) the resultant polyoxoanion can adopt *syn* or *anti* conformations (each of which exists as a pair of enantiomers). Only the *syn* conformers shown in Figure 7 have yet been observed in the solid state structures of Table 4, except for the last entry (18), the *anti* structure of which is shown in Figure 8. The anion  $[(\text{H}_4)\text{PW}_{17}\text{O}_{61}]^{11-}$  (Contant et al., 2000), was shown in compound 16 to have a structure analogous to that of  $\alpha_2\text{-}[\text{P}_2\text{W}_{17}\text{O}_{61}]^{10-}$  but with a missing phosphorus atom. The four non-acidic protons appear to “occupy” the vacant  $\text{O}_4$  tetrahedron.

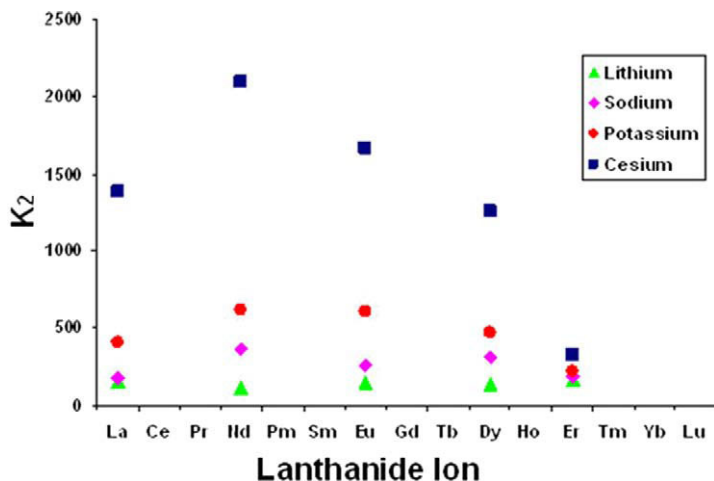


**FIGURE 6** Dependence of the conditional equilibrium constants for  $[(\text{H}_2\text{O})_4\text{-R}(\alpha_1\text{-P}_2\text{W}_{17}\text{O}_{61})]^{7+} + [\alpha_1\text{-P}_2\text{W}_{17}\text{O}_{61}]^{10-} \rightleftharpoons [\text{R}(\alpha_1\text{-P}_2\text{W}_{17}\text{O}_{61})_2]^{17-}$  upon R and the counteranion. See Table 7 for conditions. Reproduced with permission from Zhang et al. (2005b).

© 2005 American Chemical Society.

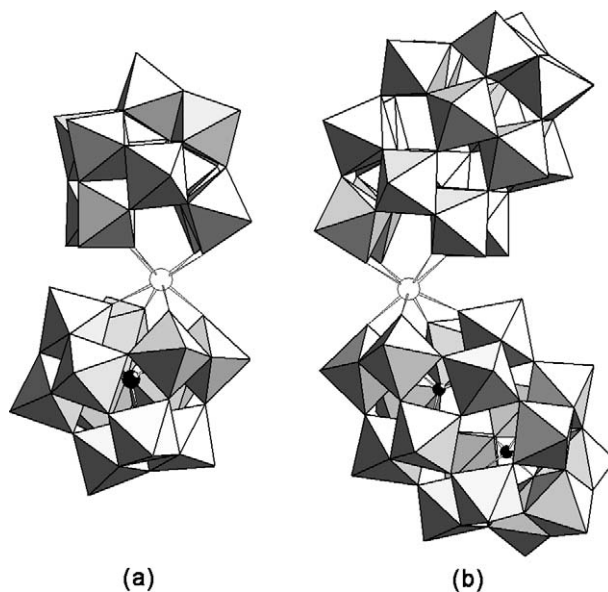


**FIGURE 7** (a)  $[\text{R}(\alpha\text{-SiW}_{11}\text{O}_{39})_2]^{13-}$  and (b)  $[\text{R}(\alpha_2\text{-P}_2\text{W}_{17}\text{O}_{61})_2]^{17-}$ .

Since the solid-state anion structures, shown in Figure 7 both have overall  $C_2$  symmetry the  $^{183}\text{W}$ -NMR spectra should show 11 (or 17) lines if the same structures are retained in solution. A multinuclear NMR (P, W, O) study of

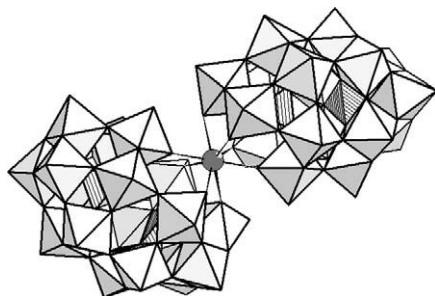


**FIGURE 8** The *anti* conformation of  $[\text{Ce}(\alpha_1\text{-P}_2\text{W}_{17}\text{O}_{61})(\alpha_2\text{-P}_2\text{W}_{17}\text{O}_{61})]^{17-}$ .

$[\text{R}(\text{PW}_{11}\text{O}_{39})_2]^{11-}$  (Fedotov et al., 1990a, 1990b, 1991) showed that for  $\text{R} = \text{La-Eu}$  only 6  $^{183}\text{W}$ -NMR lines were observed compared with 11 lines for the complexes with  $\text{R} = \text{Tb-Lu}$ . This result suggested a structure of  $\text{C}_{2v}$  symmetry (quasi-cubic coordination of the R-cation) for complexes of the early rare earths. Similar results were subsequently observed (Bartis et al., 1997a) for  $^{183}\text{W}$ -NMR spectra of  $[\text{R}(\text{SiW}_{11}\text{O}_{39})_2]^{13-}$  and  $[\text{R}(\alpha_2\text{-P}_2\text{W}_{17}\text{O}_{61})_2]^{17-}$ ,  $\text{R} = \text{La}$  (6 and 9 lines, respectively),  $\text{Yb}$  and  $\text{Lu}$  (11 and 17 lines, respectively). Variable temperature  $^{183}\text{W}$ -NMR measurements on the lutetium complexes showed broadening and partial coalescence of the multiline spectra (Figure 9) consistent with dynamic processes in solution, most probably intramolecular “rotation” of the polyoxotungstate ligands, that ultimately could have led to time-averaged structures of  $\text{C}_{2v}$  symmetry. Spectra of  $[\text{La}(\text{SiW}_{11}\text{O}_{39})_2]^{13-}$  at lower temperatures showed only broadened lines and no confirmable evidence for slow ligand rotation. Since it seems probable that the magnitude of the barrier to ligand rotation is determined by the radius of the lanthanide cation, it seems likely that complete transformation between 6- and 11-line spectra could best be observed for complexes on both sides of the “divide” observed by Fedotov et al. (1990b), i.e. for the  $\text{Eu}$  and  $\text{Tb}$  complexes (owing to slow electron spin relaxation for the  $\text{Gd}^{3+}$  complex, some tungsten lines could not be observed).

Numerous reports of other examples of 1:2 Peacock–Weakley complexes are summarized in Table 5. Whereas some of these species have subsequently been confirmed by structural crystallography, many of the cited references report only non structure-specific data such as elemental analyses, IR spectra, magnetic moments, and electrochemistry.

Among the compounds listed in Table 5 that would benefit from additional investigation are those involving lacunary anion isomers known to be metastable (entries 13–15, 22, 24, but see entries 10 and 11 in Table 4) and complexes of transition metal-centered lacunary anions (17–21). Mixed metal species (3, 10) even if homogeneous, inevitably exist as complex mixtures of isomers, as revealed by observation of multiple NMR signals (Shan et al., 1995).

**2.2.2.2 1:2 complexes: tetravalent lanthanides** The stabilization of  $\text{Ce(IV)}$  complexes is noteworthy (formal redox potentials are shown in Table 6) and this observation has spurred attempts to access other tetravalent lanthanide species

**TABLE 5** Reported examples of 1:2 Peacock–Weakley complexes,  $[\text{RL}_2]^{n-}$ 

	L	R	References
1	$\text{PMo}_{11}$	Y, La–Lu	Xiao et al. (1986); Wang et al. (1991f); Fedoseev and Yusov (1992); Copping et al. (2005)
2	$\text{SiMo}_{11}$	Y, La–Tb, Er, Yb	Chen et al. (1986); Wang et al. (1991f); Liu et al. (1999)
3	$\text{SiMo}_{11-n}\text{W}_n$	La–Gd, Dy, Yb	Zhou et al. (1991, 1992); Fedoseev and Yusov (1992)
4	$\text{GeMo}_{11}$	La–Dy, Yb	Wang et al. (1991f)
5	$\text{P}_2\text{Mo}_{17}$	La–Nd, Sm–Tb, Yb	Wang et al. (1991c, 1991e)
6	$\text{As}_2\text{Mo}_{17}$	Y, La–Er, Yb	Wang et al. (1990)
7	$\text{BW}_{11}$	La–Yb	Wang et al. (1991b); Jiang et al. (2000)
8	$\text{GaW}_{11}$	La–Yb	Liu et al. (1989)
9	$\text{PW}_{11}$	Y, La–Lu	Fedotov et al. (1990a, 1990b, 1991); Griffith et al. (2000)
10	$\text{PW}_{10}\text{V}$	La, Pr–Gd, Dy, Yb	Shan et al. (1992c)
11	$\text{AsW}_{11}$	La–Er	Liu et al. (1986, 1994); Wang et al. (1998)
12	$\alpha\text{-SiW}_{11}$	Y, La–Lu	Peacock and Weakley (1971a); Qu et al. (1991); Bartis et al. (1997a, 1997b); Zhou et al. (2002)
13	$\beta_1\text{-SiW}_{11}$	La–Sm, Gd, Er	Niu et al. (1992)
14	$\beta_2\text{-SiW}_{11}$	La–Sm, Gd, Er	Qu et al. (1991); Bassil et al. (2007)
15	$\beta_3\text{-SiW}_{11}$	La–Sm, Gd, Er	Niu et al. (1992)
16	$\text{GeW}_{11}$	Ce–Yb	Rong et al. (1987)
17	$\text{TiW}_{11}$	La–Yb	Zhu et al. (1990); Liu et al. (1991b)
18	$\text{ZrW}_{11}$	La–Eu	Wang et al. (1993a)
19	$\text{Cr}^{\text{III}}\text{W}_{11}$	La–Yb	Wang et al. (1991d)
20	$\text{Mn}^{\text{IV}}\text{W}_{11}$	La, Nd, Eu–Tb, Dy	Wu et al. (1990); Wang et al. (1991a)
21	$\text{Cu}^{\text{II}}\text{W}_{11}$	La–Yb	Wu et al. (1993)
22	$\alpha_1\text{-P}_2\text{W}_{17}$	La–Gd, Dy	Qu et al. (1992)
23	$\alpha_2\text{-P}_2\text{W}_{17}$		Peacock and Weakley (1971a); Wang et al. (1991c, 1993b); Bartis et al. (1997a); Luo et al. (2001)
24	$\beta\text{-P}_2\text{W}_{17}$	La, Pr–Gd, Dy	Qu et al. (1993)
25	$\alpha_2\text{-As}_2\text{W}_{17}$	La–Gd, Dy	Liu et al. (1993b); Wang and Liu (1995)

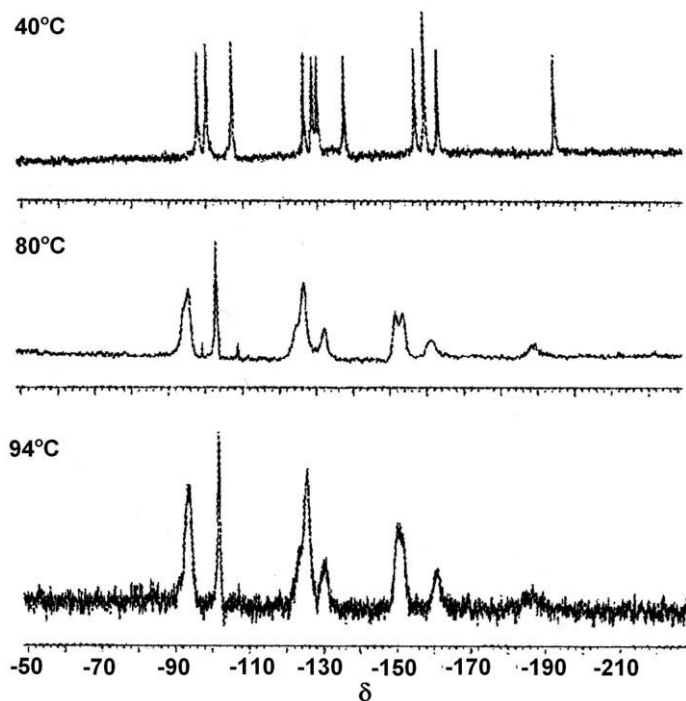


**FIGURE 9** Variable-temperature  $^{183}\text{W}$ -NMR spectra of  $\text{K}_{13}[\text{Lu}(\text{SiW}_{11}\text{O}_{39})_2]$ . Reproduced from Bartis et al. (1997a) with permission of the Royal Society of Chemistry.

**TABLE 6** Cerium(III/IV) redox potentials, V vs NHE

L	CeL	CeL <sub>2</sub>	Reference and medium
$[\text{PW}_{11}\text{O}_{39}]^{7-}$	0.90 (0.962)	0.67 (0.645)	a,b
$[\text{SiW}_{11}\text{O}_{39}]^{8-}$	0.84 (0.812)	0.59 (0.545)	a,b
$[\text{GeW}_{11}\text{O}_{39}]^{8-}$	0.854	n.d.	b
$\alpha_1\text{-}[\text{P}_2\text{W}_{17}\text{O}_{61}]^{10-}$	0.85 (0.822)	0.57	a,c
$\alpha_2\text{-}[\text{P}_2\text{W}_{17}\text{O}_{61}]^{10-}$	0.89 (0.873)	0.62 (0.587)	a,b

a Ciabrini and Contant (1993); 1 M  $\text{LiNO}_3$ .

b Haraguchi et al. (1994); 0.1 M  $\text{Na}_2\text{SO}_4$ , pH 4.5.

c Sadakane et al. (2001); 0.1 M  $\text{Na}_2\text{SO}_4$ , pH 4.5.

in a similar manner. Terbium(III) in the presence of  $[\text{PW}_{11}\text{O}_{39}]^{7-}$ ,  $[\text{SiW}_{11}\text{O}_{39}]^{8-}$ ,  $[\text{BW}_{11}\text{O}_{39}]^{9-}$  or  $\alpha_2\text{-}[\text{P}_2\text{W}_{17}\text{O}_{61}]^{10-}$  is reported to be partially or completely oxidized by  $\text{S}_2\text{O}_8^{2-}$  to a Tb(IV) species, kinetically stable at pH 7 (Saprykin et al., 1976a, 1976b; Shilov, 1981; Haraguchi et al., 1991). Partial oxidation of Pr(III) under similar conditions has also been reported (Saprykin et al., 1976a), and chemi-

**TABLE 7** Some reported conditional formation constants for Peacock–Weakley complexes

L	R	log $\beta_1$	log $\beta_2$	Reference and medium
[PW <sub>11</sub> O <sub>39</sub> ] <sup>7-</sup>	Ce(III)	8.7	15.4	a
	Ce(IV)	22.9	33.5	a
[SiW <sub>11</sub> O <sub>39</sub> ] <sup>8-</sup>	Ce(III)	9.4	15.6	a
	Ce(IV)	24.6	35.0	a
$\alpha_1$ -[P <sub>2</sub> W <sub>17</sub> O <sub>61</sub> ] <sup>10-</sup>	Ce(III)	6.6	8.1	a
	Ce(IV)	21.7	27.9	a
	La	8.00	10.19–11.14	b
	Nd	8.63	10.70–11.95	b
	Eu	10.35	12.53–13.57	b
	Dy	11.08	13.21–14.18	b
	Er	11.62	13.85–14.14	b
	Yb	12.01	14.08–14.72	b
	Lu	12.50	14.37–14.68	b
$\alpha_2$ -[P <sub>2</sub> W <sub>17</sub> O <sub>61</sub> ] <sup>10-</sup>	La	7.53 (5.70)	12.97	c,d
	Ce(III)	7.85 (8.8)	12.64 (14.8)	c,a
	Ce(IV)	23.1	33.6	a
	Pr	8.28	12.75	c
	Nd	7.92 (6.75)	12.42	c,d
	Sm	7.16	12.64	c
	Eu	8.05 (7.36)	14.59 (13.2)	c,d
	Gd	7.84	13.44	c
	Tb	8.03	14.07	c
	Dy	8.25 (7.05)	14.99	c,d
	Ho	9.03	14.37	c
	Er	7.00		d
	Yb	7.93 (7.04)	14.31	c,d

a Ciabrini and Contant (1993); 1 M LiNO<sub>3</sub>.

b Zhang et al. (2005b); 0.5 M LiNO<sub>3</sub> for  $\beta_1$ , 0.02 M M acetate (M = Li, Na, K, Cs) for  $\beta_2$ ; pH 4.75.

c Lu et al. (2004); 0.1 M Na<sup>+</sup>, pH 3.5 (chloroacetate buffer).

d Van Pelt et al. (2003); 1 M NaClO<sub>4</sub>, pH 6.

luminescence during the reduction of Tb(IV) and Pr(IV) in the presence of  $\alpha_2$ -[P<sub>2</sub>W<sub>17</sub>O<sub>61</sub>]<sup>10-</sup> has been examined (Yusov et al., 1986).

**2.2.2.3 1:1 complexes ( $x = 1$ )** Peacock and Weakley (1971a) noted that complexes of this type were formed in solution but were unable to isolate stable crystalline forms. Subsequent electrochemical and spectroscopic investigations have allowed estimates of the formation constants of both 1:1 and 1:2 complexes. Some relevant data are summarized in Table 7.

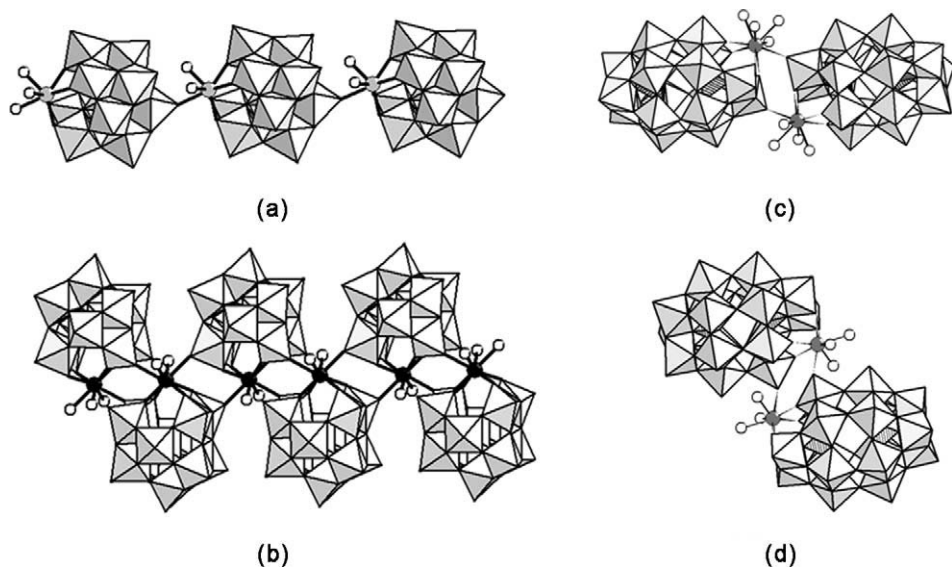


**FIGURE 10** Solid state structures of some 1:1 Peacock-Weakley complexes:

(a)  $\{[(\text{H}_2\text{O})_2\text{Yb}(\text{SiW}_{11}\text{O}_{39})]^{5-}\}_x$ , (b)  $\{[(\text{H}_2\text{O})_2\text{Eu}(\text{SiW}_{11}\text{O}_{39})]^{5-}\}_x$ , (c)  $\{[(\text{H}_2\text{O})_4\text{Ce}(\alpha_2\text{-P}_2\text{W}_{17}\text{O}_{61})_2]^{14-}\}$ , (d)  $\{[(\text{H}_2\text{O})_3\text{Eu}(\alpha_2\text{-P}_2\text{W}_{17}\text{O}_{61})_2]^{14-}\}$ .

Crystallization of the 1:1 complexes derived from the  $[\text{XW}_{11}\text{O}_{39}]^{n-}$  and  $\alpha_2\text{-}[\text{P}_2\text{W}_{17}\text{O}_{61}]^{10-}$  anions yields polymeric or dimeric species as shown in Figure 10. It would be rash to generalize with conviction from the limited number of experimental data so far available (Table 8), but it appears that 1:1 complexes of the  $\text{W}_{11}$  ligands crystallize as one-dimensional polymers, and the corresponding complexes of the  $\text{W}_{17}$  ligands form dimers [but see Kholdeeva et al. (2005)]. As illustrated in Figure 10 the exact structural features of polymers and dimers vary, depending upon the identity of the rare-earth cation involved and its preferred coordination number. Only three structures (see Table 8) have been reported for 1:1 complexes of the  $\alpha_1$ -isomer of  $[\text{P}_2\text{W}_{17}\text{O}_{61}]^{10-}$ . Two of these ( $\text{R} = \text{La}, \text{Ce}$ ) are non-identical dimers (one is shown in Figure 11), but the  $\text{Lu}$  complex is a monomer. It has been suggested that the smaller coordination number favored by the later rare-earth cations would have yielded dimeric structures that are sterically overcrowded (Zhang et al., 2005b).

The complexes listed in Table 8 yield solutions containing the monomeric anions. Such solutions exhibit  $^{183}\text{W}$ -NMR spectra consistent with the expected symmetry ( $\text{C}_1$  or  $\text{C}_s$ ) of a monomer and with chemical shifts distinct from those of the 1:2 complexes.

Measurement of luminescence lifetimes of the complexes in  $\text{H}_2\text{O}$  and  $\text{D}_2\text{O}$  solutions permits an estimate of the number of aqua ligands attached to the rare-earth cations. This was first carried out for complexes of  $\text{Eu}, \text{Dy}, \text{Sm},$  and  $\text{Tb}$  with  $[\text{SiW}_{11}\text{O}_{39}]^{8-}$  and  $[\text{PW}_{11}\text{O}_{39}]^{7-}$  and indicated ca. 4–6  $\text{H}_2\text{O}$  for the 1:1 complexes and 0.1–0.5  $\text{H}_2\text{O}$  for the 1:2 complexes (Yusov and Fedoseev, 1988). More recent measurements have been reported for the 1:1 complexes of  $\text{Eu}$  with the  $\alpha_1$ - and

**TABLE 8** Structure reports for “1:1” Peacock–Weakley complexes

	Formula	Structure type	RO <sub>n</sub>	Reference
1	{[La(SiW <sub>11</sub> O <sub>39</sub> )(H <sub>2</sub> O) <sub>3</sub> ] <sup>5-</sup> } <sub>x</sub>		LaO <sub>9</sub>	a
2	{[Ce(SiW <sub>11</sub> O <sub>39</sub> )(H <sub>2</sub> O) <sub>3</sub> ] <sup>5-</sup> } <sub>x</sub>		CeO <sub>9</sub>	a
3	{[Eu(SiW <sub>11</sub> O <sub>39</sub> )(H <sub>2</sub> O) <sub>2</sub> ] <sup>5-</sup> } <sub>x</sub>	Figure 10b	EuO <sub>8</sub>	a
4	{[Yb(SiW <sub>11</sub> O <sub>39</sub> )(H <sub>2</sub> O) <sub>2</sub> ] <sup>5-</sup> } <sub>x</sub>	Figure 10a	YbO <sub>7</sub>	b
5	[[R(α <sub>2</sub> -P <sub>2</sub> W <sub>17</sub> O <sub>61</sub> )(H <sub>2</sub> O) <sub>4</sub> ] <sub>2</sub> ] <sup>14-</sup>	Figure 10c	RO <sub>9</sub>	(Ce) <sup>c</sup> ; (La, Pr) <sup>d</sup>
6	[[R(α <sub>2</sub> -P <sub>2</sub> W <sub>17</sub> O <sub>61</sub> )(H <sub>2</sub> O) <sub>3</sub> ] <sub>2</sub> ] <sup>14-</sup>	Figure 10d	RO <sub>8</sub>	(Nd) <sup>d,e</sup> ; (Lu) <sup>d</sup> ; (Eu) <sup>f,g</sup> ; (Tb, Ho) <sup>h</sup>
7	[[R(α <sub>1</sub> -P <sub>2</sub> W <sub>17</sub> O <sub>61</sub> )(H <sub>2</sub> O) <sub>4</sub> ] <sub>2</sub> ] <sup>14-</sup>	Figure 11	RO <sub>9</sub>	(Ce) <sup>i</sup> ; (La) <sup>j</sup>
8	[Lu(α <sub>1</sub> -P <sub>2</sub> W <sub>17</sub> O <sub>61</sub> )(H <sub>2</sub> O) <sub>4</sub> ] <sup>7-</sup>		LuO <sub>8</sub>	k

a Sadakane et al. (2000).

b Mialane et al. (2003).

c Sadakane et al. (2002).

d Zhang et al. (2006).

e Kortz (2003).

f Luo et al. (2002).

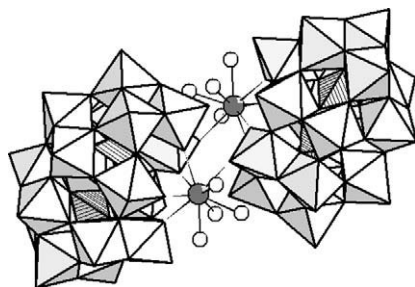
g Zhang et al. (2004).

h Drewes and Krebs (2006).

i Sadakane et al. (2001).

j Boglio et al. (2006).

k Luo et al. (2001).

**FIGURE 11** [Ce(H<sub>2</sub>O)<sub>4</sub>(α<sub>1</sub>-P<sub>2</sub>W<sub>17</sub>O<sub>61</sub>)]<sup>7-</sup> dimer.

α<sub>2</sub>-isomers of [P<sub>2</sub>W<sub>17</sub>O<sub>61</sub>]<sup>10-</sup> and these confirm the attachment of four H<sub>2</sub>O ligands as noted in the crystal structure of the monomeric lutetium complex of the α<sub>1</sub>-isomer (Bartis et al., 1999; Luo et al., 2001, 2002).

The existence of the dimeric (“2:2”) complexes in solution has been detected for complexes of Ce<sup>III</sup> with both α<sub>1</sub>- and α<sub>2</sub>-[P<sub>2</sub>W<sub>17</sub>O<sub>61</sub>]<sup>10-</sup> (Sadakane et al., 2001, 2002). Based upon concentration-dependent <sup>31</sup>P-NMR data the dimerization constant for the α<sub>1</sub> system is 20 ± 4 M<sup>-1</sup> at 22 °C. The corresponding value for the

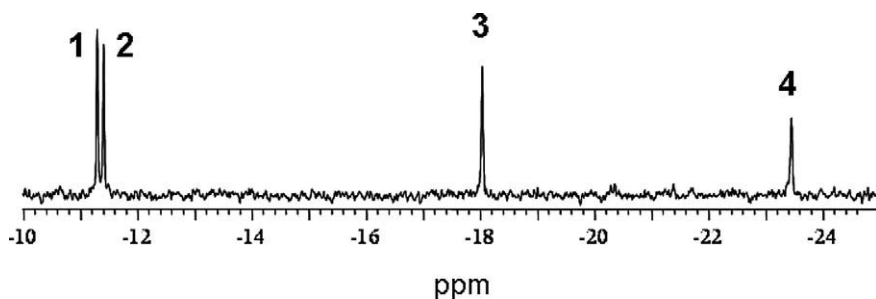


**FIGURE 12**  $^{31}\text{P}$ -NMR spectrum of an equimolar mixture of  $[\text{La}(\text{W}_5\text{O}_{18})_2]^{9-}$  and  $[\text{Ce}(\text{PW}_{11}\text{O}_{39})_2]^{11-}$  showing signals for  $\{\text{La}(\text{PW}_{11})_2\}$  (1),  $\{\text{La}(\text{PW}_{11})(\text{W}_5)\}$  (2),  $\{\text{Ce}(\text{PW}_{11})_2\}$  (3), and  $\{\text{Ce}(\text{PW}_{11})(\text{W}_5)\}$  (4).

$\alpha_2$ -isomer is  $1.46 \pm 0.04 \text{ M}^{-1}$  at  $23^\circ\text{C}$ , but in this case there is a more complicated solution behavior owing to equilibria involving the 1:2 complex.

The isolation of the “mixed ligand” complex (entry 17, Table 4) raises the question of the existence of 1:1 complexes of  $[\text{W}_5\text{O}_{18}]^{6-}$ . Evidence for the kinetic stability of such complexes is provided by the  $^{31}\text{P}$ -NMR spectrum (Figure 12) of an equimolar mixture of  $[\text{La}(\text{W}_5\text{O}_{18})_2]^{9-}$  and  $[\text{Ce}(\text{PW}_{11}\text{O}_{39})_2]^{11-}$  which also shows signals for  $[\text{La}(\text{W}_5\text{O}_{18})(\text{PW}_{11}\text{O}_{39})]^{10-}$  and  $[\text{Ce}(\text{W}_5\text{O}_{18})(\text{PW}_{11}\text{O}_{39})]^{10-}$  (Belai et al., 2001).

**2.2.2.4 Derivatives of 1:1 complexes** As a result of the chirality of  $\alpha_1$ - $[\text{P}_2\text{W}_{17}\text{O}_{61}]^{10-}$  (Figure 5) solutions of  $[\{\text{Ce}(\alpha_1\text{-P}_2\text{W}_{17}\text{O}_{61})(\text{H}_2\text{O})_4\}_2]^{14-}$  contain enantiomeric pairs of monomers in equilibrium with the *meso* dimer. Addition of chiral amino acids to such solutions causes a doubling of the  $^{31}\text{P}$ -NMR resonances as a result of diastereomer formation presumably caused by coordination of the amino acid to the rare-earth cation (Sadakane et al., 2001). No splitting was observed when similar experiments were carried out with complexes of the achiral  $\alpha_2$  isomer. Formation constants for the two diastereomers of the complexes with L-proline were estimated as  $7.3 \pm 1.3$  and  $9.8 \pm 1.4 \text{ M}^{-1}$ . The corresponding proline complex of achiral  $[\text{Ce}(\alpha_2\text{-P}_2\text{W}_{17}\text{O}_{61})]^{7-}$  has a formation constant of  $4.5 \pm 0.1 \text{ M}^{-1}$  (Sadakane et al., 2002).

In acetonitrile solution the luminescence of  $[\text{Eu}(\text{H}_2\text{O})_4(\alpha_1\text{-P}_2\text{W}_{17}\text{O}_{61})]^{7-}$  increases with the addition of 1,10-phenanthroline or 2,2-bipyridine and reaches a limiting value with a 2:1 ratio of the bidentate ligand to polyoxometalate complex, consistent with the replacement of the four aqua ligands of the Eu cation (Boglio et al., 2006).

Crystallization of 1:1 complexes in the presence of acetate buffer has led to the acetate-bridged dimeric species  $[\{\text{La}(\alpha_2\text{-P}_2\text{W}_{17}\text{O}_{61})(\text{H}_2\text{O})_2\}_2(\mu\text{-CH}_3\text{COO})_2]^{16-}$  (Kortz et al., 2003) and  $[\{\text{Yb}(\alpha\text{-SiW}_{11}\text{O}_{39})(\text{H}_2\text{O})_2\}_2(\mu\text{-CH}_3\text{COO})_2]^{12-}$  (Mialane et al., 2004). Addition of oxalate anions generates a tetrameric species  $[\{\text{Yb}(\alpha_2\text{-P}_2\text{W}_{17}\text{O}_{61})\}_4(\text{C}_2\text{O}_4)_3(\text{H}_2\text{O})_4]^{34-}$  (Figure 13) which dissociates in solution (Mialane et al., 2005).

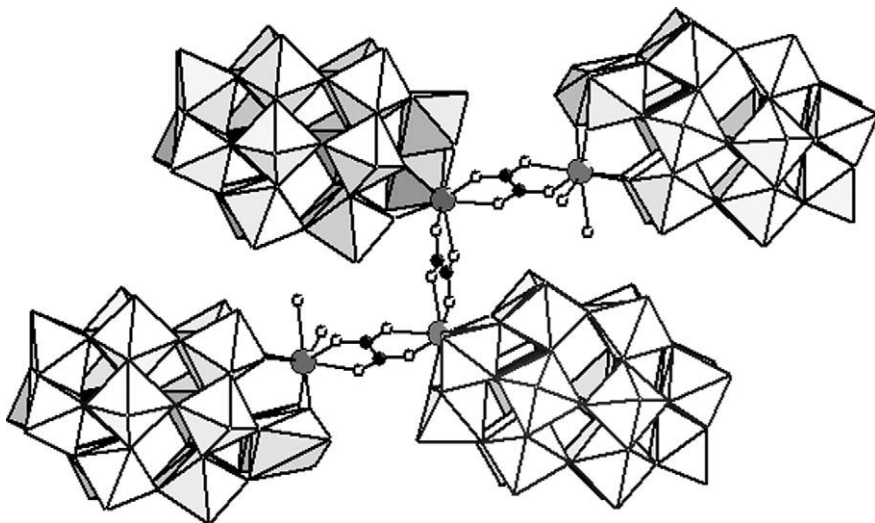


**FIGURE 13** Structure of anion in  $(\text{NH}_4)_{29}\text{K}_5[\{\text{Yb}(\text{P}_2\text{W}_{17}\text{O}_{61})\}_4(\text{C}_2\text{O}_4)_3(\text{H}_2\text{O})_4]\cdot 95\text{H}_2\text{O}$ . Reproduced with permission from Mialane et al. (2005). © 2005 Elsevier B.V.

A more elaborate, but so far not structurally identified complex, formulated as  $(\text{Bu}_4\text{N})_8\text{K}_3[\text{Yb}(\alpha_1\text{-YbP}_2\text{W}_{17}\text{O}_{61})_2]$ , has been reported and characterized by elemental analysis,  $^{31}\text{P}$ -NMR and ESI mass spectra (Boglio et al., 2006).

Polymeric solid-state structures incorporating 1:1  $\{\text{R}(\alpha\text{-SiW}_{11}\text{O}_{39})\}$  subunits but with different overall R:POM stoichiometries have been reported, and more will undoubtedly be discovered. The structure of the anion in  $\text{K}_{0.5}\text{Nd}_{0.5}[\text{Nd}_2(\alpha\text{-SiW}_{11}\text{O}_{39})(\text{H}_2\text{O})_{11}]\cdot 17\text{H}_2\text{O}$  consists of chains of polymeric 1:1 complexes linked by the additional Nd cations into two-dimensional layers (Mialane et al., 2003). Two different types of chain structures have been reported for the Pr complexes  $\text{K}_{3n}[(\text{Pr}(\text{H}_2\text{O})_4\text{SiW}_{11}\text{O}_{39})(\text{NaPr}_2(\text{H}_2\text{O})_{12})(\text{Pr}(\text{H}_2\text{O})_4\text{SiW}_{11}\text{O}_{39})]_n\cdot 13.5n\text{H}_2\text{O}$  (Niu et al., 2004c) and  $\text{Cs}_{6n}\text{K}_{2n}[\{(\text{Pr}(\text{H}_2\text{O})_7)(\text{Pr}(\text{H}_2\text{O})_2)(\alpha\text{-SiW}_{11}\text{O}_{39})\}_4]_n\cdot 33n\text{H}_2\text{O}$  (Drewes and Krebs, 2006) and the erbium complex  $\text{K}_2\text{H}_2\{\text{Er}(\text{H}_2\text{O})_6[\text{Er}(\text{H}_2\text{O})_3\text{SiW}_{11}\text{O}_{39}]\}_2\cdot 22\text{H}_2\text{O}$  has yet a different stoichiometry and chain structure (Niu et al., 2004b).

### 2.3 Complexes of multivacant lacunary anions

In addition to the monolacunary derivatives of the Keggin and Wells–Dawson structures illustrated in Figure 5, several other multivacant structures are known, either as discrete entities or as identifiable building blocks in larger polyoxometalate assemblies. Three well-established trivacant structures derived from the  $\alpha$ -isomers of the Keggin and Wells–Dawson structures are shown in Figure 14, together with a divacant derivative of the  $\gamma$ -isomer of the Keggin anion. “Removal” of a corner-shared group of three  $\text{WO}_6$  octahedra from, for example  $\alpha\text{-}[\text{PW}_{12}\text{O}_{40}]^{3-}$  generates  $\text{A-}\alpha\text{-}[\text{PW}_9\text{O}_{34}]^{9-}$  whereas removal of an edge-shared group of octahedra generates the B-isomer in which the  $\text{PO}_4$  tetrahedron now has

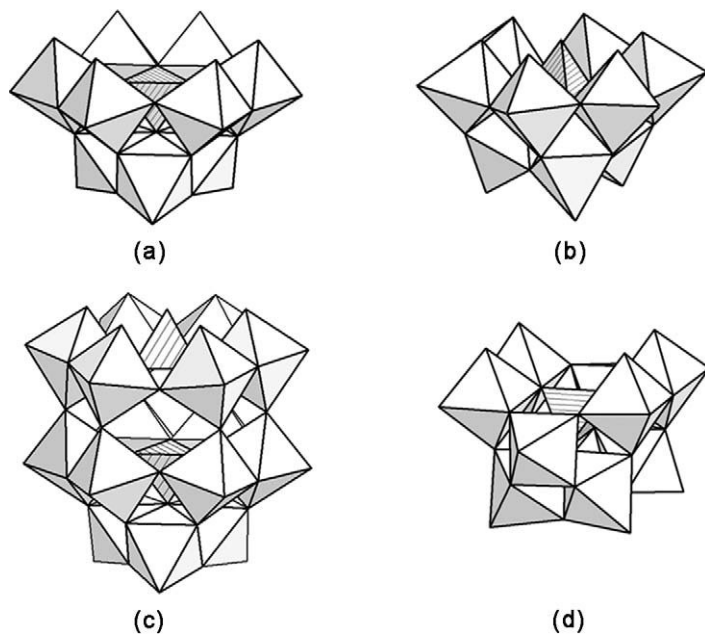


**FIGURE 14** Some multivalent lacunary structures derived from Keggin and Dawson anions. (a) A- $\alpha$ -[PW<sub>9</sub>O<sub>34</sub>]<sup>9-</sup>, (b) B- $\alpha$ -[PW<sub>9</sub>O<sub>34</sub>]<sup>9-</sup>, (c)  $\alpha$ -[P<sub>2</sub>W<sub>15</sub>O<sub>56</sub>]<sup>12-</sup>, (d)  $\gamma$ -[SiW<sub>10</sub>O<sub>36</sub>]<sup>8-</sup>.

one terminal oxygen atom, a structural feature shared by [P<sub>2</sub>W<sub>15</sub>O<sub>56</sub>]<sup>12-</sup>. The B-XW<sub>9</sub> structures in particular have very limited stability in solution, in contrast to a series of isotypical structures ([XW<sub>9</sub>O<sub>33</sub>]<sup>n-</sup>) in which the central atom X has a stereochemically-active lone pair of electrons (trivalent As, Sb, Bi; tetravalent Se, Te).

The tendency of all the trivalent lacunary anions is to form sandwich-type structures, most commonly with divalent transition metal cations. The first example of a structure incorporating rare-earth cations was the Ce(IV) derivative, [(Ce<sub>3</sub>O<sub>3</sub>)(H<sub>2</sub>O)<sub>2</sub>(A- $\alpha$ -PW<sub>9</sub>O<sub>34</sub>)<sub>2</sub>]<sup>12-</sup> reported by Knoth (Knoth et al., 1986), Figure 15. The coordinated water molecules are labile on the NMR timescale, and a recent structure determination of the AsW<sub>9</sub> analog of this complex contains an anion with a water molecule on each of the three Ce atoms (Alizadeh et al., 2004). Presumed analogous complexes with trivalent rare earths, K<sub>15</sub>[(R<sub>3</sub>O<sub>3</sub>)(PW<sub>9</sub>O<sub>34</sub>)<sub>2</sub>] $\cdot$ nH<sub>2</sub>O (R = La–Gd) were reported in 1991 (Liu et al., 1991c). Corresponding complexes (R = Ce<sup>IV</sup> and trivalent La–Gd, Er) with A-[SiW<sub>9</sub>O<sub>34</sub>]<sup>10-</sup> and A-[GeW<sub>9</sub>O<sub>34</sub>]<sup>10-</sup> (both  $\alpha$ - and  $\beta$ -isomers in each case) have been synthesized and characterized by elemental analysis and spectroscopic methods, including <sup>183</sup>W-NMR (Meng and Liu, 1995, 1997; Liu et al., 1996a). Reports of similar sandwich-type complexes with rare-earth cations and [P<sub>2</sub>W<sub>15</sub>O<sub>56</sub>]<sup>12-</sup> (Figure 14c) and  $\gamma$ -[SiW<sub>10</sub>O<sub>36</sub>]<sup>8-</sup> (Figure 14d) have appeared (Bi et al., 1999; Yue et al., 2004) but structural confirmation for these is lacking at present. Complexes in which {Y<sub>4</sub>(OH)<sub>4</sub>} and {Yb<sub>6</sub>O(OH)<sub>6</sub>} clusters are sandwiched between two

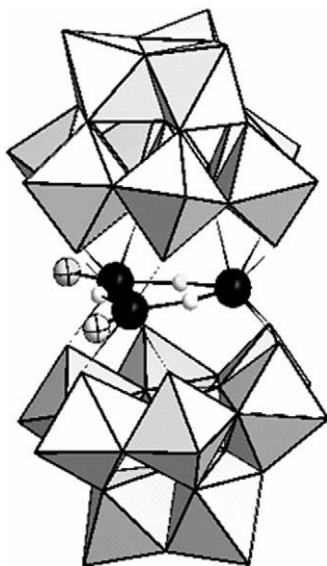


**FIGURE 15**  $[(\text{Ce}_3^{\text{IV}}\text{O}_3)(\text{H}_2\text{O})_2(\text{A-}\alpha\text{-PW}_9\text{O}_{34})_2]^{12-}$ .

$[\text{P}_2\text{W}_{15}\text{O}_{56}]^{12-}$  anions have recently been structurally and magnetically characterized (Fang et al., 2005).

Reaction of rare-earth cations with B-type  $\text{XW}_9$  anions, or with solutions containing tungstate and the appropriate  $\text{X}^{\text{III}}$  or  $\text{X}^{\text{IV}}$  source leads to larger, more complex structures, which sometimes incorporate extra tungstate groups in addition to the B- $\text{XW}_9$  building blocks. The possibilities appear to be endless based upon the variety of structures so far reported. Complexes incorporating only  $\text{AsW}_9$  units include the cyclic cryptate assemblies  $[\text{Cs} \subset \{\text{Eu}(\text{H}_2\text{O})_2(\alpha\text{-AsW}_9\text{O}_{33})\}_4]^{23-}$  and  $[\text{K} \subset \{\text{Eu}(\text{H}_2\text{O})_2(\alpha\text{-AsW}_9\text{O}_{33})\}_6]^{35-}$  (Fukaya and Yamase, 2003), Figure 16. Anions containing 2, 3, 4, 6, and 12  $\text{AsW}_9$  units are represented by the sandwich-type anion  $[\{(\text{H}_2\text{O})\text{Yb}(\text{OW}(\text{H}_2\text{O})_2)\}(\text{AsW}_9\text{O}_{33})_2]^{7-}$  (Kortz et al., 2003),  $[\text{R}_2(\text{H}_2\text{O})_7\text{As}_3\text{W}_{29}\text{O}_{103}]^{17-}$  ( $\equiv[\text{R}_2(\text{H}_2\text{O})_7(\text{AsW}_9\text{O}_{33})_3(\text{WO}_2)_2]^{17-}$ ,  $\text{R} = \text{La}, \text{Ce}$ ), Figure 17,  $[\text{Ce}_4(\text{H}_2\text{O})_4\text{As}_5\text{W}_{39}\text{O}_{143}]^{25-}$  (Pope et al., 1998),  $[\text{Ho}_5(\text{H}_2\text{O})_{16}(\text{OH})_2\text{As}_6\text{W}_{64}\text{O}_{220}]^{25-}$ , Figure 18 (Drewes et al., 2006), and  $[\text{Ce}_{16}(\text{H}_2\text{O})_{36}\text{As}_{12}\text{W}_{148}\text{O}_{524}]^{76-}$ , Figure 19 (Wassermann et al., 1997). The last of these complexes (including the lanthanum analog) is the largest discrete polytungstate structure known to date. Its stability in solution has been revealed by  $^{183}\text{W}$ -NMR spectroscopy (Figure 20) and by concentration-dependent conductivity measurements (Liu et al., 2006).

A notable feature of the structure of  $\{\text{As}_{12}\text{W}_{148}\}$  is the presence of  $\{\text{Ce}(\text{W}_5\text{O}_{18})\}$  groups analogous to those observed in the  $[\text{R}(\text{W}_5\text{O}_{18})_2]^{n-}$  anions discussed in Section 2.2.1. A similar feature is observed in a family of complexes containing the  $\{\text{B-}\alpha\text{-Sb}^{\text{III}}\text{W}_9\text{O}_{33}\}$  structural unit, all of which, like the  $\text{W}_{148}$  anion are synthesized by “self assembly” from the monomeric components. As shown in Figure 21a  $\{\text{R}(\text{W}_5\text{O}_{18})\}^{3-}$  groups are found to be attached to the  $\text{SbW}_9$  anion at two possi-

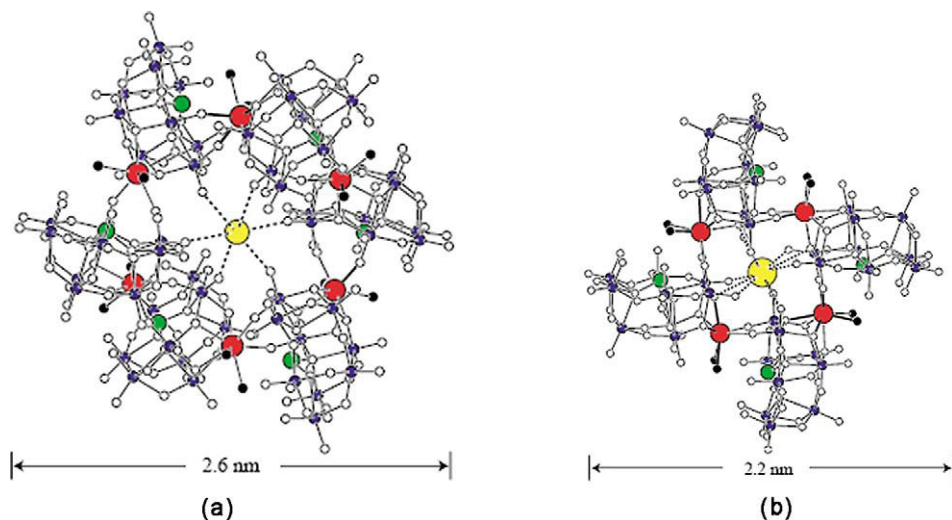


**FIGURE 16** (a)  $[K \subset \{Eu(H_2O)_2(\alpha\text{-AsW}_9\text{O}_{33})\}_6]^{35-}$ ; (b)  $[Cs \subset \{Eu(H_2O)_2(\alpha\text{-AsW}_9\text{O}_{33})\}_4]^{23-}$ . Color scheme: As (green), Eu (red), K, Cs (yellow). Reproduced with permission from Fukaya and Yamase (2003). © 2003 Wiley–Interscience.

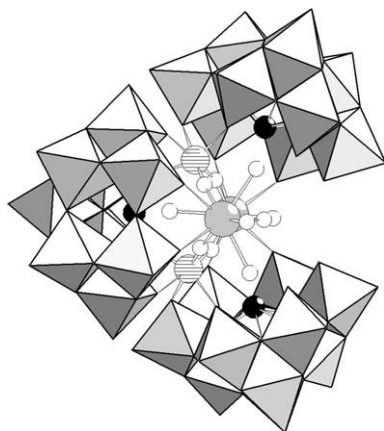


**FIGURE 17**  $[R_2(H_2O)_7(AsW_9O_{33})_3(WO_2)_2]^{17-}$ , R = La, Ce.

ble sites (I and II). In  $[(SbW_9O_{33})\{R(W_5O_{18})\}\{R(H_2O)_2(W_5O_{18})\}]^{15-}$  (R = Er, Y, Dy, Eu, Sm) both sites are occupied. From luminescence and crystallographic investigations of mixed Eu/Y and Eu/Lu complexes, it was shown that the smaller rare earth cation was preferentially bound to site II. With lutetium alone two  $\{SbW_9O_{33}\}(LuW_5O_{18})$  groups are linked by  $[Lu(H_2O)_4]^{3+}$  into an assembly of  $C_2$  symmetry (Naruke and Yamase, 2001, 2002a). Two complexes of  $C_{3v}$  symmetry,  $[(SbW_9O_{33})\{Eu(H_2O)(W_5O_{18})\}_3]^{18-}$ , Figure 21b (Yamase et al., 1990) and  $[(SbW_9O_{33})\{(\mu_3\text{-CO}_3)(CeW_5O_{18})\}_3]^{20-}$  (Naruke and Yamase, 1998), involve bind-

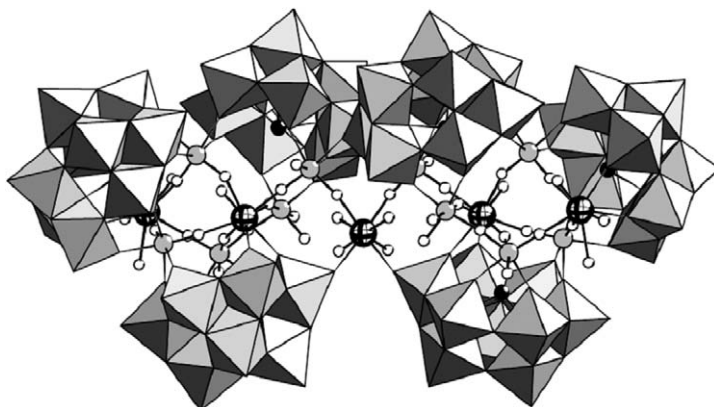


**FIGURE 18**  $[\text{Ho}_5(\text{H}_2\text{O})_{16}(\text{OH})_2\text{As}_6\text{W}_{64}\text{O}_{220}]^{25-}$  ( $\equiv\{[(\text{Ho}(\text{H}_2\text{O})_4)(\text{Ho}(\text{H}_2\text{O}))(\text{Ho}(\text{H}_2\text{O})_3)^-(\text{W}_2\text{O}_5(\text{H}_2\text{O})_2)(\text{WO}_2)_2(\text{WO}_2(\text{OH}))(\text{AsW}_9\text{O}_{33})_3]_2\}^{25-}$ ) with six  $\text{AsW}_9\text{O}_{33}$  groups in polyhedral form and additional tungsten atoms (gray). Reproduced with permission from Drewes et al. (2006). © 2006 Wiley–Interscience.

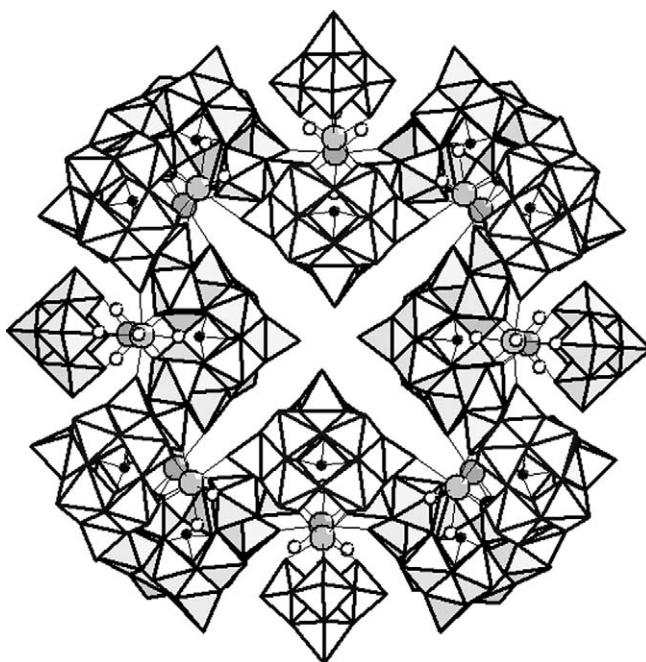


**FIGURE 19**  $[\text{Ce}_{16}(\text{H}_2\text{O})_{36}\text{As}_{12}\text{W}_{148}\text{O}_{524}]^{76-}$  ( $\equiv\{[\text{Ce}(\text{H}_2\text{O})_5]_4[\text{Ce}(\text{H}_2\text{O})_2]_8^-(\text{AsW}_9\text{O}_{33})_{12}(\text{WO}_2)_4(\text{W}_2\text{O}_6)_8[\text{Ce}(\text{W}_5\text{O}_{18})]_4\}^{76-}$ ).

ing to Site II regions of  $\text{SbW}_9$  only. The three rare-earth cations are linked either by bridging aqua ligands or by the oxygen atoms of an enclosed carbonate anion, a novel feature subsequently observed in an yttrium sandwich complex, see below.

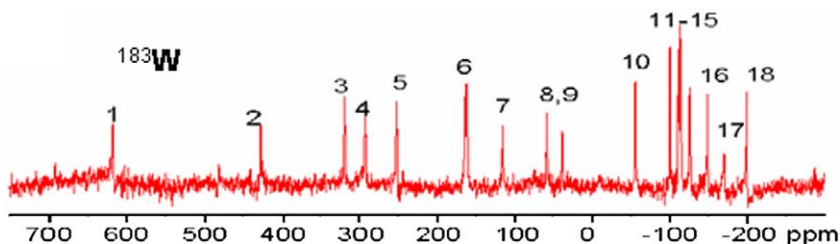


**FIGURE 20**  $^{183}\text{W}$ -NMR spectrum of  $[\text{Ce}_{16}(\text{H}_2\text{O})_{36}\text{As}_{12}\text{W}_{148}\text{O}_{524}]^{76-}$ . Based upon the  $D_{2d}$  symmetry of the anion 21 resonances are expected.

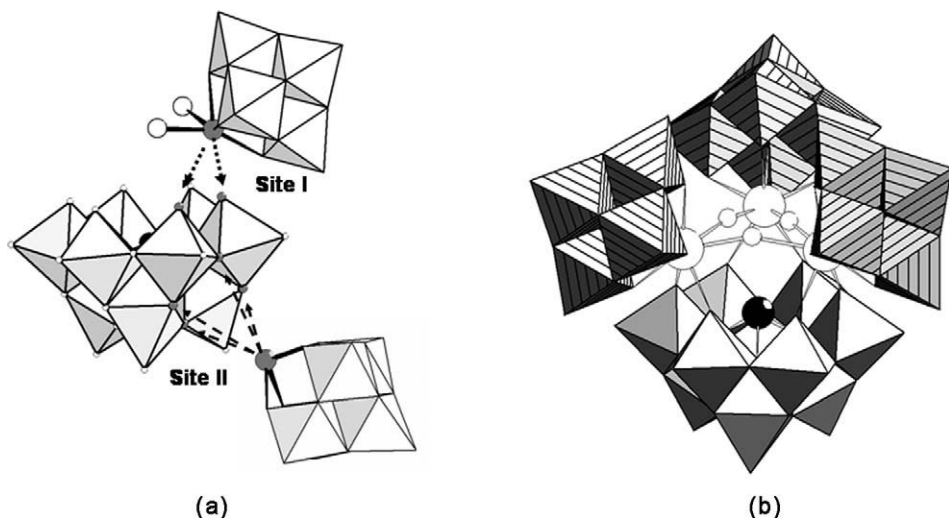


**FIGURE 21** (a) Two attachment sites for  $\{\text{R}(\text{W}_5\text{O}_{18})\}^{3-}$  groups in  $[(\text{SbW}_9\text{O}_{33})\{\text{R}(\text{W}_5\text{O}_{18})\}-\{\text{R}(\text{H}_2\text{O})_2(\text{W}_5\text{O}_{18})\}]^{15-}$ ; (b)  $[(\text{SbW}_9\text{O}_{33})(\text{Eu}(\text{H}_2\text{O})(\text{W}_5\text{O}_{18}))_3]^{18-}$ ; Eu (large spheres),  $\mu\text{-H}_2\text{O}$  (small spheres).

Addition of solid  $\text{Na}_9[\text{PW}_9\text{O}_{34}] \cdot n\text{H}_2\text{O}$  (either A- or B-form) to solutions of  $\text{YCl}_3$  or  $\text{EuCl}_3$  in the presence of  $\text{K}^+$  cations, yields salts of  $[(\text{PR}_2\text{W}_{10}\text{O}_{38})_4\{\text{W}_3\text{O}_8(\text{H}_2\text{O})_2(\text{OH})_4\}]^{22-}$ ,  $\text{R} = \text{Y}, \text{Eu}$ . The anion structure (Figure 22) shows four A-PW<sub>9</sub> groups bound to an  $\{\text{R}_8\text{W}_7\text{O}_{30}\}^{6+}$  core with overall  $C_2$  symmetry. The anions are stable in aqueous solution at pH 7–9 according to  $^{31}\text{P}$ -NMR (2 signals expected and observed for each) and  $^{183}\text{W}$ -NMR of the Y anion (22 signals expected, 19 observed, three with double intensity). The excitation spectrum of the Eu anion in aqueous solution showed four transitions at ca. 580 nm corresponding to the  $^7\text{F}_0$  to  $^5\text{D}_0$  transitions of the four structurally distinct Eu sites (Howell et al., 2001; Zhang et al., 2004). In the presence of sodium carbonate the reaction of  $\text{YCl}_3$  with  $\text{Na}_9[\text{PW}_9\text{O}_{34}]$  yields the sandwich structure anion  $[(\text{YOH}_2)_3(\text{CO}_3)(\text{A-}\alpha\text{-PW}_9\text{O}_{34})_2]^{11-}$  (Fang et al., 2003) in which the enclosed carbonate anion bridges

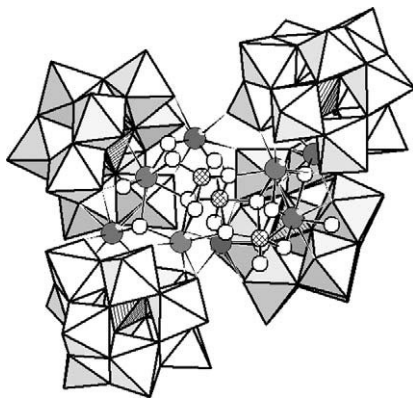


**FIGURE 22**  $[(PR_2W_{10}O_{38})_4(W_3O_8(H_2O)_2(OH)_4)]^{22-}$ , R = Y, Eu. Showing arrangement of A-[PW<sub>9</sub>O<sub>34</sub>] groups augmented by an additional WO<sub>6</sub> octahedron. R (gray spheres), W (cross-hatched spheres) and O, OH, H<sub>2</sub>O (white spheres).

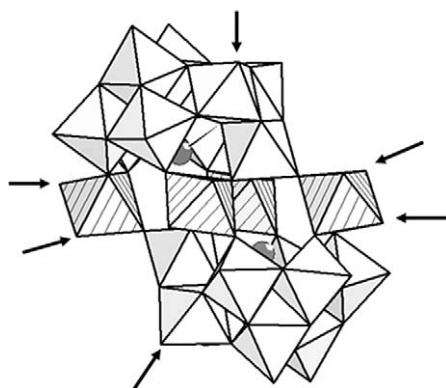


**FIGURE 23** The structure of  $[Bi_2W_{22}O_{76}]^{14-}$  as an assembly of four WO<sub>6</sub> octahedra sandwiched by  $\{B\text{-}\beta\text{-}BiW_9O_{33}\}$  groups. The arrows identify the binding sites of aquated Eu<sup>3+</sup> cations that link the polytungstates into a 3-D network  $\{[Eu_3(H_2O)_{18}(Bi_2W_{22}O_{76})]^{5-}\}_x$ .

the three Y cations in a fashion identical to that observed for the three Ce atoms in  $[Ce_3(CO_3)(SbW_9O_{33})(W_5O_{18})_3]^{20-}$  (Naruke and Yamase, 1998).

Several sandwich-type polyoxotungstates incorporating  $\{B\text{-}\beta\text{-}X^{III}W_9O_{33}\}$  X = Sb, Bi, have been structurally characterized by Krebs and coworkers. To date one example involving a rare-earth cation has been reported (Krebs et al., 1998). The structure of  $Na_3H_2[Eu_3(H_2O)_{18}(Bi_2W_{22}O_{76})]\cdot 29H_2O$  contains the anion  $[(BiW_9O_{33})_2(W_4O_{10})]^{14-}$  (Figure 23) linked into a 3-D network by 8-coordinate Eu<sup>3+</sup> cations.

The anion  $[Ce_4(OH)_2(H_2O)_9(P_2W_{16}O_{59})_2]^{14-}$  (Figure 24) is isolated in good yield from reaction of  $Ce(NO_3)_3$  with  $K_{12}H_2P_2W_{12}O_{48}\cdot nH_2O$ , a hexavacant derivative of the Wells–Dawson anion  $[P_2W_{18}O_{62}]^{6-}$ , and  $Na_2WO_4$ . The anion has

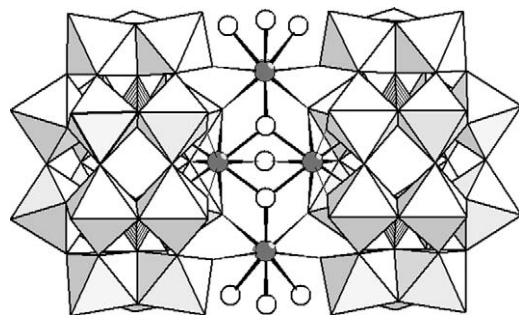


**FIGURE 24**  $[\text{Ce}_4(\text{OH})_2(\text{H}_2\text{O})_9(\text{P}_2\text{W}_{16}\text{O}_{59})_2]^{14-}$ .

nominal  $C_{2v}$  symmetry with a cluster of four  $\text{Ce}^{3+}$  cations (two 9-coordinate and two 10-coordinate) sandwiched between two  $\text{P}_2\text{W}_{16}$  groups. The structure remains intact in solution according to  $^{31}\text{P}$ - ( $\delta = +4.0$  ppm) and fully-resolved 8-line  $^{183}\text{W}$ -NMR ( $\delta = +296$  to  $-188$  ppm) (Ostuni and Pope, 2000).

## 2.4 Polyoxotungstate “cryptate” derivatives

Four large polytungstate anions have cyclic or hollow structures that contain encapsulated alkali metal cations:  $[\text{Na} \subset \text{Sb}_9\text{W}_{21}\text{O}_{86}]^{18-}$  (1),  $[\text{Na} \subset \text{As}_4\text{W}_{40}\text{O}_{140}]^{27-}$  (2),  $[(\text{NaOH}_2) \subset \text{P}_5\text{W}_{30}\text{O}_{110}]^{14-}$  (3), and  $[\text{K}_8 \subset \text{P}_8\text{W}_{48}\text{O}_{184}]^{40-}$  (4) (Figures 25–28). There have been several attempts to incorporate trivalent rare-earth cations within these structures owing to the similarity of the ionic radii of  $\text{Na}^+$  and  $\text{R}^{3+}$ .

Nine derivatives of 1,  $[\text{RSb}_9\text{W}_{21}\text{O}_{86}]^{16-}$  ( $\text{R} = \text{La-Gd}, \text{Dy}, \text{Yb}$ ), have been isolated and characterized by elemental analysis, magnetic susceptibility, and infrared spectra. The four-line  $^{183}\text{W}$ -NMR spectrum of the lanthanum derivative is consistent with the  $D_{3h}$  symmetry of the parent structure, but the emission spectrum of the europium derivative suggests a lower symmetry in the solid state (Liu et al., 1992). No structural determinations of these derivatives have yet been reported.

Anion 2 has two types of site where additional cations can be incorporated, and these are shown in Figure 26. In the original structure determination (Robert et al., 1980) an ammonium cation occupies the central  $S_1$  site and  $\{\text{CoOH}_2\}^{2+}$  occupy two of the four  $S_2$  sites. Several lanthanum complexes  $[\text{LaAs}_4\text{W}_{40}\text{O}_{140}]^{23-}$  and  $[\text{LaAs}_4\text{W}_{40}\text{O}_{140}\text{M}_2]^{20,21-}$  ( $\text{M} = \text{Cr}^{3+}, \text{Fe}^{3+}$ , divalent  $\text{Mn}, \text{Fe}, \text{Co}, \text{Ni}, \text{Cu}, \text{Zn}$ ) were prepared and characterized by elemental analysis, IR and UV-vis spectroscopy (Liu et al., 1993a). Other rare-earth derivatives ( $\text{Ce-Dy}, \text{Yb}$ ) were later described (Liu et al., 1998). It was presumed that the rare-earth cation occupied the  $S_1$  site ( $^{183}\text{W}$ -NMR of the M-cation-free La complex gave the expected six lines), and the M cations occupied the  $S_2$  sites. This conclusion was later confirmed by a structure determination of the gadolinium complex  $[\text{Gd}(\text{H}_2\text{O})_5\text{As}_4\text{W}_{40}\text{O}_{140}(\text{NiOH}_2)_2]^{21-}$  (Xue et al., 2004). The same paper reports the preparation of analogs with  $\text{R} = \text{Y}, \text{Ce-Eu}$ .

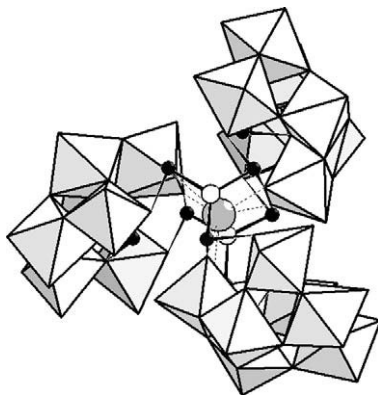


**FIGURE 25**  $[\text{Na} \subset \text{Sb}_9\text{W}_{21}\text{O}_{86}]^{18-}$ .

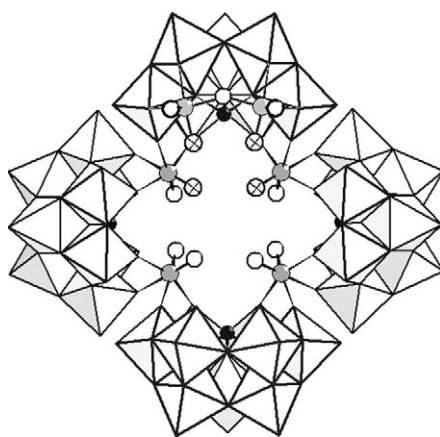


**FIGURE 26** Framework of  $[\text{Na} \subset \text{As}_4\text{W}_{40}\text{O}_{140}]^{27-}$  as an assembly of four  $\{\text{AsW}_9\text{O}_{33}\}$  groups linked by  $\{\text{WO}_2\}$  groups (gray spheres). The sodium cation occupies the nominal 8-coordinate  $S_1$  site at the center of the structure. The cross-hatched oxygen atoms identify one of the four  $S_2$  sites.

If the  $S_2$  sites are not occupied by transition metal cations more than one rare-earth cation can be taken up by **2**. Complexes with three and four rare-earth cations (La, Ce, Nd–Gd) have been isolated and structurally characterized. In  $\{\text{R}_3\text{As}_4\text{W}_{40}\}$  species two R cations occupy  $S_2$  sites and are linked by bridging OH; the third R cation occupies a site below  $S_1$ . In  $\{\text{R}_4\text{As}_4\text{W}_{40}\}$  all four  $S_2$  sites are occupied by  $\text{R}^{3+}$  and the  $S_1$  site contains  $\text{K}^+$  or  $\text{Ba}^{2+}$  or is vacant (Wassermann and Pope, 2001). In crystals the R-cations occupying the  $S_2$  sites link the polyanions into dimers  $\{\text{R}_3\text{As}_4\text{W}_{40}\}_2$  or 1-D chains  $\{\text{R}_4\text{As}_4\text{W}_{40}\}_x$ , see Figure 29. According to  $^{183}\text{W}$ -NMR dissociation to monomers occurs in solution.

In the initial structure report of anion **3** it was noted that the internal non-labile  $\text{Na}^+$  cation could be replaced by  $\text{Ca}^{2+}$  under vigorous conditions (120 °C, several

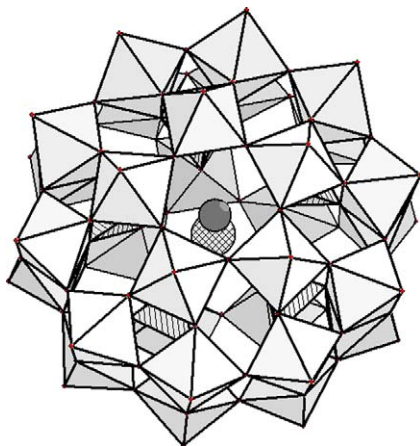


**FIGURE 27**  $[(\text{NaOH}_2) \subset \text{P}_5\text{W}_{30}\text{O}_{110}]^{14-}$  showing location of  $\text{Na}^+$  (gray sphere) and encrypted  $\text{H}_2\text{O}$  (cross-hatched sphere).

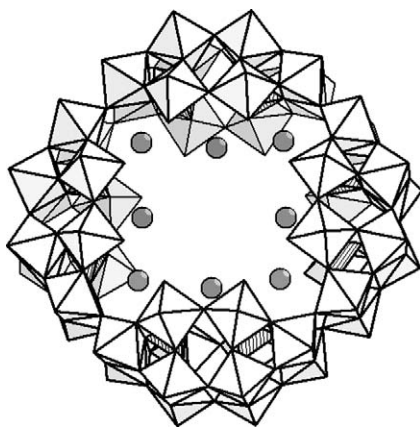


**FIGURE 28**  $[\text{K}_8 \subset \text{P}_8\text{W}_{48}\text{O}_{184}]^{40-}$  as an assembly of four  $\{\text{P}_2\text{W}_{12}\}$  lacunary derivatives of the Wells–Dawson structure enclosing eight potassium cations (gray).

hours) (Alizadeh et al., 1985). It was later shown that at 160–180 °C trivalent Nd–Lu, Y could also be inserted and the products were characterized by  $^{31}\text{P}$ -NMR (see Table 9) electrochemistry and other methods (Creaser et al., 1993). The ESR spectrum of the gadolinium complex has also been reported (Szytczewski et al., 1996). No reaction was observed under similar conditions with  $\text{Ce}^{3+}$  and  $\text{Pr}^{3+}$ , but reaction proceeded with  $\text{Ce}^{4+}$ . It was subsequently demonstrated by EXAFS that the product of this reaction contained the  $\text{Ce}^{3+}$  derivative (Antonio and Soderholm, 1994). Successful direct synthesis of the  $\text{Ce}^{3+}$  and  $\text{Pr}^{3+}$  complexes has been achieved under more extreme conditions of temperature and time (Antonio et al., 1995).

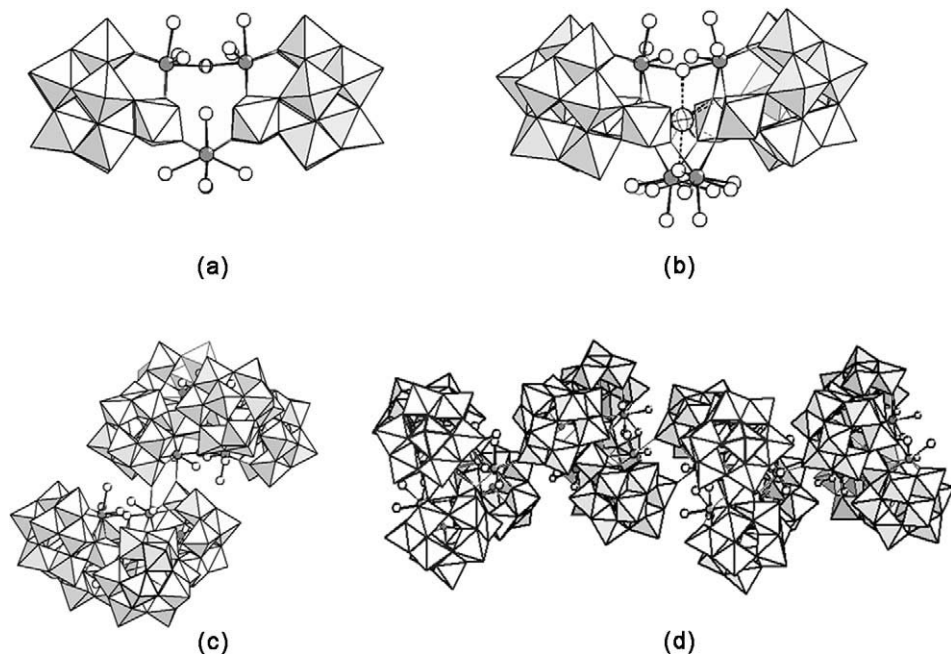


**FIGURE 29** (a) Central section of  $\{R_3As_4W_{40}\}$  structure showing two (OH-bridged) R cations occupying  $S_2$  sites and the third R cation occupying a site *below*  $S_1$ . (b) Section of  $\{R_4As_4W_{40}\}$  structure showing all four  $S_2$  sites occupied by R cations, and  $S_1$  occupied by  $K^+$  or  $Ba^{2+}$  (cross-hatched sphere). (c and d) Linkage of  $R_3$  and  $R_4$  complexes in crystals into dimers and extended chains, respectively.

Cyclic voltammetry of solutions containing the rare-earth-exchanged anions reveals multiple tungsten reductions ( $W^{VI}/W^V$ ) as anticipated but no evidence for  $Ce^{III}/Ce^{IV}$  (Creaser et al., 1993; Antonio et al., 1999). Based on anomalies in the cyclic voltammogram of the europium derivative, it has been suggested that  $Eu(III)$  is reduced to  $Eu(II)$  at potentials within the tungsten reduction manifold. This conclusion is supported by  $Eu$   $L_3$ -XANES of a solution reduced at  $-0.55$  V (Antonio and Soderholm, 1996) which stands in contrast to analogous measurements made on reduced solutions of  $[Eu(As_2W_{17}O_{61})_2]^{17-}$  and  $[Eu(W_5O_{18})_2]^{9-}$  (Antonio et al., 1998) that reveal only  $Eu^{III}$ .

Structure determinations of salts containing  $[R \subset P_5W_{30}O_{110}]^{12-}$ ,  $R = Y, Eu$ , and a redetermination of the sodium derivative, showed that the central cavity also contained a water molecule coordinated to the encrypted cation (Dickman et al., 1996; Kim et al., 1999). This observation, also noted for the  $Ca$  and  $U^{IV}$  structures, provides an explanation for the fact that the encrypted cation does not lie in the pseudo-equatorial mirror plane of the polytungstate framework. Luminescence lifetime measurements on the europium complex have led to ambiguous conclusions regarding the number of coordinated water molecules (Soderholm et al., 1995; Lis et al., 1996). As shown in Table 9 the  $^{31}P$  chemical shifts are significantly affected by the acidity of the solution. Remarkably, at intermediate acidities

**TABLE 9** P-NMR data for rare-earth derivatives [R C P<sub>5</sub>W<sub>30</sub>O<sub>110</sub>]<sup>12-</sup>; pH ca. 4<sup>a</sup>

R	$\delta$ (ppm)	Linewidth (Hz)
Ce	-16.1 (-10.5) <sup>a</sup>	4.5
Nd	-21.6 (-12.5)	8.8
Sm	-9.6 (-7.4)	4.6
Eu	+0.6 (-9.1)	5.0
Gd	<sup>b</sup>	<sup>b</sup>
Tb	-27.2 (+24.1)	175
Dy	-68.1	241
Ho	-40.0	222
Er	+1.8	151
Tm	+17.0 (-9.9)	68
Yb	+9.1	16
Lu	-10.1	
Y	-10.2 <sup>c</sup>	

<sup>a</sup> Values in parentheses are for solutions in 2 M HCl.

<sup>b</sup> Not observed.

<sup>c</sup> Doublet, <sup>2</sup>J(P-O-<sup>89</sup>Y) = 1.6 Hz.

two <sup>31</sup>P-NMR signals are observed indicating slow proton exchange on the NMR timescale. A detailed examination of the Eu derivative has been made and reveals that protonation of the anion increases the rate of H/D exchange on the encrypted water molecule. At pH ca. 3.6 the exchange rates are slow enough to permit being determined by monitoring the <sup>31</sup>P-NMR signals of the three isotopomers containing EuOH<sub>2</sub>, EuOHD, and EuOD<sub>2</sub>. It was concluded that the slow proton exchange between the +0.6 ppm and -9.1 ppm species involved the relatively inaccessible internal phosphate oxygens (see Figure 30) (Kim et al., 1999).

To date, the only rare-earth derivatives of anion **4** are the network solids {R<sub>4</sub>(H<sub>2</sub>O)<sub>28</sub>[K C P<sub>8</sub>W<sub>48</sub>O<sub>184</sub>(H<sub>4</sub>W<sub>4</sub>O<sub>12</sub>)<sub>2</sub>R<sub>2</sub>(H<sub>2</sub>O)<sub>10</sub>]<sup>13-</sup>}<sub>x</sub>, R = La, Ce, Pr, Nd, that contain both internal and linking rare-earth cations. Additional polytungstate groups are also incorporated within the large central cavity, Figure 31 (Zimmermann et al., 2007).

## 2.5 Polyoxomolybdates

In addition to the 12-molybdocerate complexes described in Section 2.1, and the Peacock-Weakley analogs listed in Table 4, there have been other attempts to synthesize rare-earth complexes of molybdates. In view of the inadequacies of <sup>95</sup>Mo-NMR caused by low sensitivity and quadrupolar relaxation, and the ambiguities of other spectroscopic methods, it has so far been impossible to confirm whether those compounds that reveal discrete polyoxoanions in crystal structure analysis yield solutions that retain the same structures.

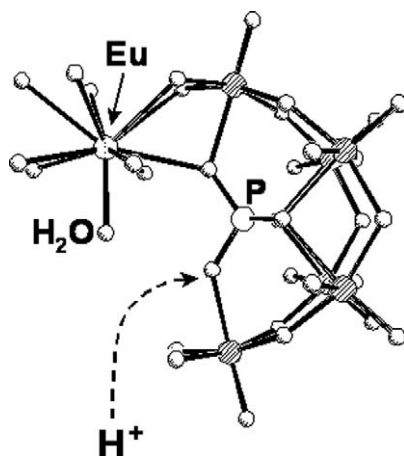


**FIGURE 30** Local environment of the Eu cation and encrypted water molecule in  $[(\text{EuOH}_2) \subset \text{P}_5\text{W}_{30}\text{O}_{110}]^{12-}$ . Protonation of the indicated phosphate oxygen atom (one of five in the complete anion) results in slow intermolecular proton exchange, but rapid H/D exchange with the internal water.

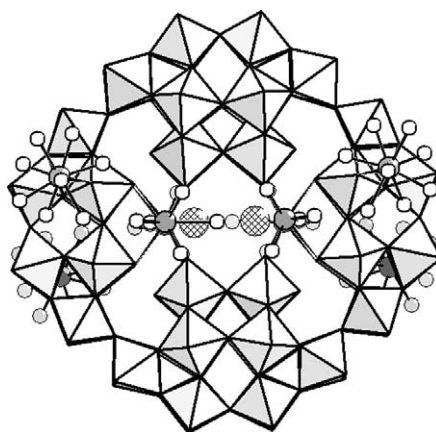


**FIGURE 31** Repeat unit of  $\{\text{R}_4(\text{H}_2\text{O})_{28}[\text{K} \subset \text{P}_8\text{W}_{48}\text{O}_{184}(\text{H}_4\text{W}_4\text{O}_{12})_2\text{R}_2(\text{H}_2\text{O})_{10}]^{13-}\}_x$ . The four interior R-cations and two  $\text{K}^+$  (cross-hatched) have 50% occupancy.

### 2.5.1 Anderson-type hexamolybdate complexes

Apart from spectroscopic evidence for the formation of 1:1 complexes of  $[\text{Cr}(\text{OH})_6\text{Mo}_6\text{O}_{18}]^{3-}$  and  $[\text{TeO}_6\text{Mo}_6\text{O}_{18}]^{6-}$  with  $\text{Eu}^{3+}$  (Saito and Choppin, 1995) the chemistry of these complexes is based upon isolation of solid materials and examination of photophysical properties.

Many compounds containing various rare-earth cations and the hexamolybdate anions  $[\text{M}^{\text{III}}(\text{OH})_6\text{Mo}_6\text{O}_{18}]^{3-}$  ( $\text{M} = \text{Al}, \text{Cr}, \text{Fe}$ ),  $[\text{I}^{\text{VII}}\text{O}_6\text{Mo}_6\text{O}_{18}]^{5-}$  and  $[\text{Te}^{\text{VI}}\text{O}_6\text{Mo}_6\text{O}_{18}]^{6-}$  have been synthesized and in many cases crystal structures have

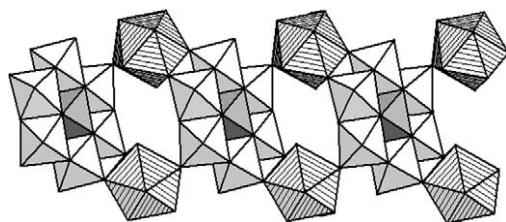


**FIGURE 32**  $\{(H_2O)_6Nd(TeMo_6O_{24})\}_x$ . Redrawn from Grigor'ev et al. (1992).

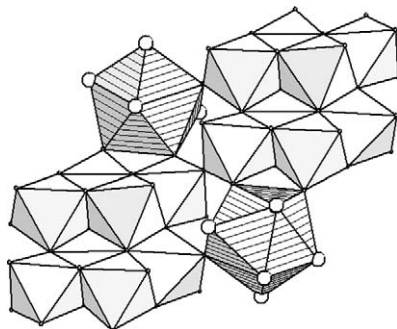


**FIGURE 33** Repeat unit of 1-D chain observed for  $\{R_2(H_2O)_{12}Mo_8O_{27}\}_x$ , R = Eu, Sm.

been reported (Grigor'ev et al., 1992; Krebs et al., 1998; Fedoseev et al., 2000; Andreev et al., 2002; Yusov et al., 2002; Zhou et al., 2002; An et al., 2004, 2005a, 2005b; Ma et al., 2004; Drewes et al., 2004a, 2004b; Drewes and Krebs, 2005; Charushnikova et al., 2005). These substances may be considered to be salts or mixed salts of the heteropolymolybdate anions rather than new polyoxomolybdate species. In most structures so far reported the rare-earth cations link unmodified hexamolybdate anions into 1-D chains. An example is illustrated in Figure 32. Only in two cases,  $\{[(H_2O)_6R]_2TeO_6Mo_6O_{18}\}$ , R = Ho and Yb, are discrete neutral complexes observed in the crystal structure (Drewes and Krebs, 2005).

A related complex is the chain polymer  $\{R_2(H_2O)_{12}Mo_8O_{27}\}_x$  (R = Eu, Sm) shown in Figure 33 (Yamase and Naruke, 1991b; Yamase et al., 1995). Thermal decomposition of these complexes leads to new mixed-oxide phases  $R_2Mo_5O_{18}$  and  $R_6Mo_{12}O_{45}$  (R = Eu and Gd) (Naruke and Yamase, 2002b).

### 2.5.2 $R_4Mo_{29}$ complexes

The remarkable assembly shown in Figure 34 was first reported as a weakly-linked dimer in the structure of " $(NH_4)_{28}[Pr_8Mo_{58}O_{200}] \cdot 40H_2O$ " (Fedoseev et al., 1987). A monomeric example  $[(MoO_4)Ce^{III}(H_2O)_{16}(Mo_7O_{24})_4]^{14-}$  was subsequently reported (Samokhvalova et al., 1989c). The structure consists of a central  $MoO_4^{2-}$  anion surrounded by four 9-coordinate  $R^{3+}$  cations and four heptamolybdate anions forming an assembly of  $D_{2d}$  symmetry. Yamase later prepared and structurally characterized the Eu analog for the purpose of exploring its photophysical prop-

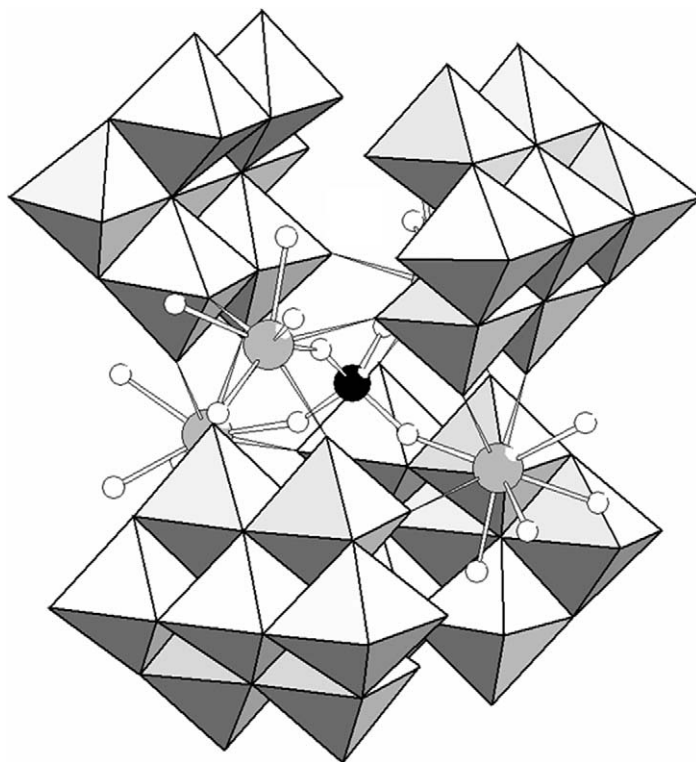


**FIGURE 34**  $[(\text{MoO}_4)\text{Ce}_4(\text{H}_2\text{O})_{16}(\text{Mo}_7\text{O}_{24})_4]^{14-}$  Ce (gray), central Mo(O<sub>4</sub>) (black), O, H<sub>2</sub>O (white).

erties (see below) (Naruke et al., 1991) and the structures of the La, Ce, Pr, Nd, Sm and Gd complexes have also been reported (Cai et al., 1997a, 1997b; Huang et al., 2000; Burgemeister et al., 2004). It is notable that both monomolybdate and heptamolybdate anions, which are stable under different conditions of acidity, coexist in the structure. There have been no reports of the solution stability of the composite anion, although this is a case where <sup>95</sup>Mo-NMR could prove useful since the central Mo atom should produce a narrow signal, at least with the La complex. Analogs with different central tetrahedra (SO<sub>4</sub><sup>2-</sup>, etc.) do not seem to have been explored.

### 2.5.3 Reduced molybdate complexes

Inclusion of rare-earth cations in the synthetic procedures for the remarkable “giant wheel” mixed-valence polymolybdate structures {Mo<sub>154</sub>} and {Mo<sub>176</sub>} based on tetradecameric and hexadecameric assemblies of {Mo<sub>1</sub> + Mo<sub>2</sub> + Mo<sub>3</sub>} building blocks (Müller and Serain, 2000), has the effect of modifying the size and curvature of the rings. In Na<sub>6</sub>[Mo<sub>120</sub>O<sub>366</sub>(H<sub>2</sub>O)<sub>48</sub>H<sub>12</sub>{Pr(H<sub>2</sub>O)<sub>5</sub>]<sub>6</sub>·aq. the hypothetical {Mo<sub>132</sub>} dodecamer is modified by the replacement of six of the {Mo<sub>2</sub><sup>V</sup>}<sup>2+</sup> building blocks by {Pr(H<sub>2</sub>O)<sub>5</sub>}<sup>3+</sup> thereby introducing a twist to an otherwise “planar” ring

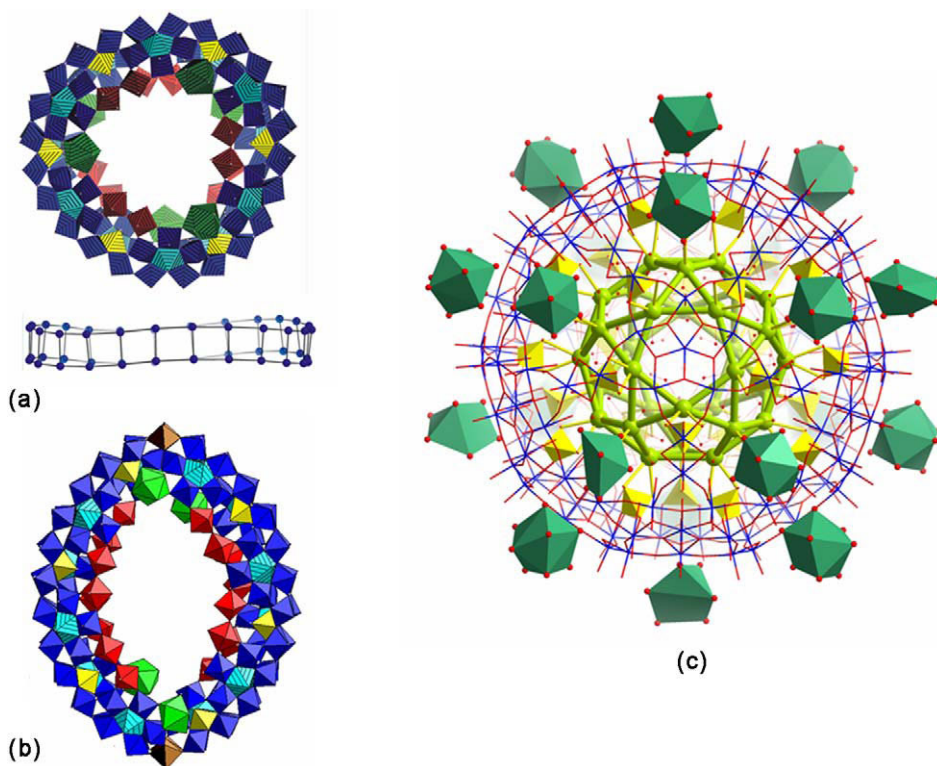


**FIGURE 35** (a, upper) Structure of  $[\text{Mo}_{120}\text{O}_{366}(\text{H}_2\text{O})_{48}\text{H}_{12}\{\text{Pr}(\text{H}_2\text{O})_5\}_6]^{6-}$  with  $\text{MoO}_n$  polyhedra shown in red, yellow, and blue;  $\text{PrO}_n$  polyhedra in green. (a, lower) Distortion of ring planarity induced by the attachment of Pr cations. Reproduced with permission from Müller et al. (2000). © 2000 American Chemical Society. (b) Half unit of dimer  $[\{(\text{Mo}_{128}\text{Eu}_4\text{O}_{388}\text{H}_{10}(\text{H}_2\text{O})_{81})_2\}^{20+}]^{20-}$  showing placement of  $\text{EuO}_n$  polyhedra (green). Reproduced with permission from Cronin et al. (2002). © 2002 Wiley–Interscience. (c) Representation of the  $\text{Pr}^{3+}$ -decorated capsule anion  $[\{(\text{Mo}^{\text{VI}})\text{Mo}_6^{\text{VI}}\text{O}_{21}(\text{H}_2\text{O})_6\}_{12}\{\text{Mo}_2^{\text{V}}\text{O}_4(\text{SO}_4)\}_{30}\}^{72-}]^{72-}$  shown as blue and red wire model with yellow  $\text{SO}_4^{2-}$  tetrahedra. Five internal  $\text{Pr}^{3+}$  are disordered over sites defined by the vertices of the green icosidodecahedron, and external  $[\text{Pr}(\text{H}_2\text{O})_9]^{3+}$  are shown as green polyhedra. Reproduced with permission from Müller et al. (2006). © 2006 Wiley–Interscience.

(Müller et al., 2000), Figure 35a. With the smaller  $\text{Eu}^{3+}$  cation the effect is more drastic and the product is  $[\{(\text{Mo}_{128}\text{Eu}_4\text{O}_{388}\text{H}_{10}(\text{H}_2\text{O})_{81})_2\}^{20+}]^{20+}$  a dimer of two elliptically-shaped rings (which may be viewed as fragments of  $\{\text{Mo}_{154}\}$ ) linked by  $\text{Eu–O–Mo}$  bonds (Cronin et al., 2002), Figure 35b. Similar elliptical ring mixed-valent molybdates incorporating  $\text{La}^{3+}$  cations, 28-electron reduced  $\{\text{Mo}_{150}\text{La}_2\}$  and 24-electron reduced  $\{\text{Mo}_{120}\text{La}_6\}$  have been generated by prolonged photolysis of acidic solutions containing  $[\text{Mo}_{36}\text{O}_{112}(\text{H}_2\text{O})_{16}]^{8-}$  and  $\text{LaCl}_3$  (Yamase et al., 2006).

Recently Müller et al. (2006) have studied the interaction of praseodymium cations with the polymolybdate capsule  $[\{(\text{Mo}^{\text{VI}})\text{Mo}_6^{\text{VI}}\text{O}_{21}(\text{H}_2\text{O})_6\}_{12}\{\text{Mo}_2^{\text{V}}\text{O}_4(\text{SO}_4)\}_{30}\}^{72-}]^{72-}$  which has 20 surface pores and a central cavity linked by 20 channels,

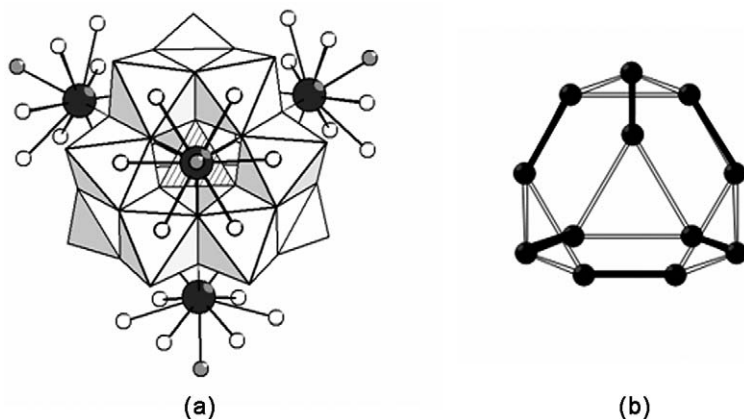


**FIGURE 36** (a)  $[\epsilon\text{-PMo}_8^{\text{V}}\text{Mo}_4^{\text{VI}}\text{O}_{36}(\text{OH})_4\{\text{La}(\text{H}_2\text{O})_4\}_4]^{5+}$ , La (large black spheres),  $\text{H}_2\text{O}$  (white and gray spheres). All  $\text{H}_2\text{O}$  molecules shown in white have half-occupancy. (b)  $\text{Mo}_{12}^{\text{VI}}$  framework crystallographically constrained to cubic symmetry, all Mo...Mo distances equal. Reproduced with permission from Mialane et al. (2002). © 2002 Wiley-Interscience.

and which has been used to model cation uptake by cells. As shown in Figure 35c, under high concentrations of  $\text{Pr}^{3+}$ , 5 cations are taken up within the capsule (disordered over sites represented by the 30 vertices of an icosidodecahedron) and additional  $[\text{Pr}(\text{H}_2\text{O})_9]^{3+}$  are bound at the surface of the capsule at sites above the pores.

A curious polyoxometal cation  $[\epsilon\text{-PMo}_8^{\text{V}}\text{Mo}_4^{\text{VI}}\text{O}_{36}(\text{OH})_4\{\text{La}(\text{H}_2\text{O})_4\}_4]^{5+}$  has been structurally characterized in three compounds (Mialane et al., 2002). The core of the structure is the hypothetical  $\epsilon$ -isomer of the Keggin anion, in which all  $\text{MoO}_6$  octahedra are linked by shared edges. Although four of the Mo atoms are hexavalent, crystallographic disorder or valence electron delocalization equalizes the arrangements of these atoms as  $\text{Mo}_2$  pairs with  $d_{\text{Mo-Mo}} \approx 2.7 \text{ \AA}$ , typical of diamagnetic  $\text{Mo}^{\text{V}}$  dimers. Each of the triangular faces of the truncated tetrahedral  $\text{PMo}_{12}$  cluster is capped by  $[\text{La}(\text{H}_2\text{O})_4]^{3+}$  as shown in Figure 36.  $^{31}\text{P}$ -NMR spectroscopy reveals an equilibrium involving  $\text{La}_4$  and  $\text{La}_3$  derivatives.

## 2.6 Niobates and vanadates

Yamase and colleagues have reported the only examples of rare-earth complexes of niobates (Ozeki et al., 1994; Naruke and Yamase, 1996b, 1997). These complexes,  $[\{\text{R}_3\text{O}(\text{OH})_3(\text{H}_2\text{O})_3\}_2\text{Al}_2(\text{Nb}_6\text{O}_{19})_5]^{26-}$ , are assemblies of two  $\{\text{R}_3\text{O}(\text{OH})_3(\text{H}_2\text{O})_3\}^{4+}$  cores ( $\text{R} = \text{Eu}, \text{Tb}, \text{Er}, \text{Lu}$ ) surrounded by five  $[\text{Nb}_6\text{O}_{19}]^{8-}$  anions and two  $\text{Al}^{3+}$  cations as shown in Figure 37.

Apart from the derivatives of the tungstovanadates mentioned in Table 5, there appear no examples of polyoxovanadates that incorporate rare-earth cations as heteroatoms, although several salts, e.g.,  $\text{R}_2\text{H}[\text{MV}_{13}\text{O}_{38}] \cdot n\text{H}_2\text{O}$  ( $\text{M} = \text{Mn}^{\text{IV}}$ ,

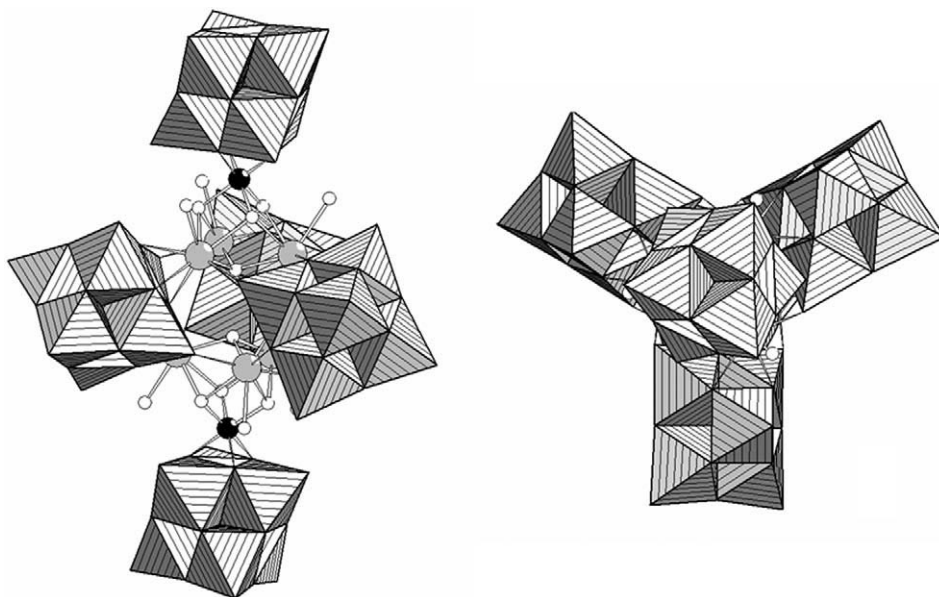


**FIGURE 37** Two views of  $[(R_3O(OH)_3(H_2O)_3)_2Al_2(Nb_6O_{19})_5]^{26-}$  R (gray), Al (black), O, OH, H<sub>2</sub>O (white).

Ni<sup>IV</sup>) and  $R_2[V_{10}O_{28}] \cdot nH_2O$  have been reported (Liu et al., 1996b; Rigotti et al., 1981).

### 3. PROPERTIES AND APPLICATIONS

#### 3.1 Photophysical properties

Interest in polyoxometalate complexes of the rare earths has been driven to a large extent by their photophysical and photochemical properties. Table 1 lists several reviews. In general, photoexcitation into LMCT (O → W, O → Mo) bands results in intramolecular energy transfer to the rare earth with subsequent emission and luminescence.

The luminescence properties of the decatungstolanthanate anions, especially  $[Eu(W_5O_{18})_2]^{9-}$ , have attracted considerable attention, both in the solid state and solution (Blasse et al., 1981a, 1981b; Blasse and Zonnevijlle, 1982; Ballardini et al., 1983; Darwent et al., 1986; Blasse, 1988; Sugeta and Yamase, 1993; Ozeki and Yamase, 1993c; Lis et al., 2003). Electroluminescence cells based on alkaline earth metal salts of the europium anion have been described (Yamase and Ueda, 1993) and the results of pulse- and continuous-radiolysis of solutions of the europium and neodymium anions have been reported (Mulazzani et al., 1985).

The Peacock-Weakley complexes  $[R(PW_{11}O_{39})_2]^{11-}$  and  $[R(P_2W_{17}O_{61})_2]^{17-}$  are reported to give higher luminescence intensities than the corresponding decatungsto complexes when R = Nd or Yb, but no energy transfer to the rare-earth

cation occurred when R = Sm–Dy (Yusov and Fedoseev, 1991). From a comparison of the emission lifetimes and quantum yields of the tungstoeuropates  $[\text{Eu}(\text{W}_5\text{O}_{18})_2]^{9-}$ ,  $[\text{Eu}(\text{SiW}_{11}\text{O}_{39})_2]^{13-}$  and  $[\text{Eu}_3(\text{H}_2\text{O})_3(\text{SbW}_9\text{O}_{33})(\text{W}_5\text{O}_{18})_3]^{18-}$  it was shown that the predominant channel for deactivation of the LMCT levels involves hopping of the  $d^1$  electron between corner-shared  $\text{WO}_6$  octahedra, thereby reducing communication with the excited levels of  $\text{Eu}^{3+}$  (Yamase et al., 1990).

The molybdate complexes  $[(\text{MoO}_4)\text{Ce}_4^{\text{III}}(\text{H}_2\text{O})_{16}(\text{Mo}_7\text{O}_{24})_4]^{14-}$  and  $\{\text{R}_2(\text{H}_2\text{O})_{12}\text{Mo}_8\text{O}_{27}\}_x$  (R = Sm, Eu) have also received attention (Yusov and Fedoseev, 1987; Naruke and Yamase, 1991; Yamase and Naruke, 1991a, 1991b; Yamase et al., 1994, 1997). With the mixed rare-earth complexes  $[\text{Tb}_x\text{Eu}_{3-x}(\text{H}_2\text{O})_3(\text{SbW}_9\text{O}_{33})(\text{W}_5\text{O}_{18})_3]^{18-}$  ( $x = 2$ ),  $[\text{Tb}_x\text{Eu}_{6-x}\text{Al}_2\text{O}_3(\text{OH})_6(\text{H}_2\text{O})_6(\text{Nb}_6\text{O}_{19})_5]^{26-}$  ( $x = 5$ ), and  $[\text{Tb}_x\text{Eu}_{4-x}(\text{MoO}_4)(\text{H}_2\text{O})_{16}(\text{Mo}_7\text{O}_{24})_4]^{14-}$  ( $x = 1$ ) with different mean Tb=Eu distances of 3.75, 5.02 and 6.12 Å, respectively, excitation into the  $^7\text{F}_6 \rightarrow ^5\text{D}_4$  transition of  $\text{Tb}^{3+}$  (~488 nm) led to both  $\text{Tb}^{3+}$  and  $\text{Eu}^{3+}$  emission (Naruke and Yamase, 1996a). Photoexcitation of the undoped nioboeuropate anion  $[\{\text{Eu}_3(\text{OH})_3(\text{H}_2\text{O})_3\}_2\text{Al}_2(\text{Nb}_6\text{O}_{18})_5]^{26-}$ , in the O  $\rightarrow$  Nb LMCT bands leads to low yield of  $\text{Eu}^{3+}$  emission as a result of radiationless deactivation via linear Nb–O–Nb linkages (Yamase and Kobayashi, 1995).

The presence of coordinated aqua ligands on  $\text{Eu}^{3+}$  centers in polyoxometalates decreases the lifetime of the  $^5\text{D}_0$  emitting state as a result of vibronic coupling with the OH oscillators. Titration of an acetonitrile solution of the tetra-*n*-butylammonium salt of  $[\text{Eu}(\text{H}_2\text{O})_4\text{PW}_{11}\text{O}_{39}]^{4-}$  with *o*-phenanthroline or 2,2'-*N*-bipyridine leads to a marked increase in emission intensity that reaches a maximum at a 1:2 ratio of polyoxometalate to organic ligand as would be expected for complete replacement of coordinated water. In related work the luminescence of a methanolic suspension of a crystalline solid containing an extended polymer of the dimeric anion  $[\{\text{Eu}(\text{H}_2\text{O})_3(\alpha_2\text{-P}_2\text{W}_{17}\text{O}_{61})\}_2]^{14-}$  linked by two additional surface-attached aquated  $\text{Eu}^{3+}$  cations was sensitized by addition of a variety of bidentate ligands (Zhang et al., 2005c).

There has been considerable recent activity in the investigation of extended materials assembled from luminescent rare-earth polyoxometalates using Langmuir–Blodgett (Wang et al., 2002c, 2003, 2004a, 2004b, 2004c; Ito et al., 2006), sol–gel (Wang et al., 2002a, 2004d) and layer-by-layer techniques (Liu et al., 2002; Wang et al., 2002b, 2004e; Zhang et al., 2003, 2005a; Sousa et al., 2004; Zhai et al., 2004; Jiang et al., 2005).

Thermal decomposition of the mixed erbium–ytterbium complexes  $\text{Na}_6\text{H}_{18}\text{-}[\text{Er}_x\text{Yb}_{6-x}(\text{H}_2\text{O})_6(\text{OH})_6\text{O}_2\text{Al}_2(\text{Nb}_6\text{O}_{19})_5]\cdot n\text{H}_2\text{O}$  ( $x = 1\text{--}6$ ) at 700 °C for 2 h yields new  $\text{NaNbO}_3$ -based up-conversion phosphors doped with  $\text{Yb}^{3+}$ ,  $\text{Er}^{3+}$  and  $\text{Al}^{3+}$ . Excitation in the near IR (980 nm) generates variable red and green emission intensities depending upon the amount of Yb-doping and the excitation pulse-width (Naruke and Yamase, 2005).

### 3.2 Other reported potential applications

Several of the decatungsto anions have been investigated as catalysts for  $\text{H}_2\text{O}_2$  oxidations, e.g., alkene epoxidations and oxidation of primary and secondary alco-

hols, generally under biphasic conditions (Shiozaki et al., 1993, 1995, 1996b, 1997a, 1997b; Inagaki et al., 1997a, 1997b; Yasuhara et al., 1999; Kera et al., 2002). Growing evidence suggests that the active catalysts are peroxotungstates generated from the lanthanide-containing anions (Griffith et al., 1996, 2000; Kera et al., 2002).

More recently ammonium decatungstocerate(IV) has been shown to act as an efficient catalyst for esterification of primary and sterically-hindered secondary or tertiary alcohols with acetic anhydride (Mirkhani et al., 2004) and for ring opening of oxiranes with aromatic amines (Mirkhani et al., 2005). Other Ce<sup>IV</sup> polyoxometalates have been investigated as oxidation catalysts. Aerobic oxidation of formaldehyde to formic acid under mild conditions is catalysed by NaH<sub>3</sub>[SiW<sub>11</sub>Ce<sup>IV</sup>O<sub>39</sub>] via autoxidation and Haber–Weiss radical chain processes (Kholdeeva et al., 2005). The compound K<sub>16</sub>[Ce(P<sub>2</sub>W<sub>15</sub>Mo<sub>2</sub>O<sub>61</sub>)<sub>2</sub>] was found to be an efficient catalyst both for oxidation of glyoxal by hydrogen peroxide and for condensation of urea with glyoxalic acid in the two-step synthesis of allantoin (Xin et al., 2002) and Na<sub>12</sub>[(CeO)<sub>3</sub>(H<sub>2</sub>O)<sub>2</sub>(PW<sub>9</sub>O<sub>34</sub>)<sub>2</sub>].45H<sub>2</sub>O and K<sub>16</sub>[Ce(P<sub>2</sub>MoW<sub>16</sub>O<sub>61</sub>)<sub>2</sub>].42H<sub>2</sub>O have been tested as potential catalysts for the oxidation of sabinene by air (Ratiu et al., 2004).

Several rare-earth Peacock–Weakley complexes with [SiW<sub>11</sub>O<sub>39</sub>]<sup>8-</sup> ligands have been investigated for catalysis of methanol conversion and showed enhanced activity over H<sub>4</sub>SiW<sub>12</sub>O<sub>40</sub> (Wu et al., 1985, 1986).

The antihypertensive activity of 3,6-bis(dimethylamino)dibenzoiodinium salts of [R(W<sub>5</sub>O<sub>18</sub>)<sub>2</sub>]<sup>9-</sup> (R = Y, La–Lu) has been compared with that of 3,6-bis(dimethylamino)dibenzoiodohexacycloformate (Liao et al., 1993). Antitumor and anti-HIV activity of [TbAs<sub>4</sub>W<sub>40</sub>O<sub>140</sub>]<sup>27-</sup> and [PrSb<sub>9</sub>W<sub>21</sub>O<sub>86</sub>]<sup>16-</sup> have been reported. The complexes display inhibitory action to HL-60 cancers and rectum—as well as breast cancer cells. The terbium complex displays *in vivo* murine leukemia virus activity (Liu et al., 1998, 2000). The molybdate complex (NH<sub>4</sub>)<sub>12</sub>H<sub>2</sub>(Eu<sub>4</sub>(MoO<sub>4</sub>)(H<sub>2</sub>O)<sub>16</sub>(Mo<sub>7</sub>O<sub>24</sub>)<sub>4</sub>).13H<sub>2</sub>O (“PM-104”) has been found to be associated with potent anti-HIV-1 activity. PM-104 also blocks the replication of herpes simplex virus type 1 (HSV-1) and type 2 (HSV-2) (Inouye et al., 1993).

Lacunary polytungstates, especially  $\alpha_2$ -{P<sub>2</sub>W<sub>17</sub>O<sub>61</sub>}<sup>10-</sup> have been used to facilitate the solvent extraction of rare-earth cations (and trivalent actinides) with primary amines (Milyukova et al., 1986, 1988, 1990). Thermal decomposition of ammonium salts of several rare-earth (and actinide) POM complexes under nitrogen or hydrogen atmospheres generates cubic tungsten bronzes, R<sub>x</sub>WO<sub>3</sub>, under relatively mild conditions and offers a potential process for storage of radioactive waste (Wassermann et al., 2000; Bessonov et al., 2002). Gadolinium POM complexes have been evaluated as potential magnetic resonance imaging contrast agents, and in some cases have been tested *in vivo* (Crooks, 1995; Gilbert et al., 1995; Li et al., 2000; Feng et al., 2002a, 2002b; Sun et al., 2004a, 2004b).

#### 4. PERSPECTIVES

As this chapter has shown, the oxophilic (hard acid) nature and high- and variable-coordination requirements of the rare-earth cations can frequently be satisfied by

highly-charged polyoxometalate anions and fragments to yield very large discrete polyanion assemblies (see, for example, [Figures 18, 19, 22](#)) or extended lattices (e.g., [Figures 10, 32, 33](#)). Much current attention is focused on photophysical properties and applications, on potential new catalytic systems, and on magnetic properties, especially the (albeit weak) cooperative behavior between multiple rare-earth centers. Clearly this type of research will continue, and new structures and solid-state materials will be identified. The possibilities are virtually unlimited, even for polytungstates which have so far received the most attention. Nevertheless there remain areas in which there has been little or no systematic investigation. Some examples are: (1) Complexes incorporating reduced or mixed-valent polyoxometalate components. The vanadates(IV,V) would seem to be especially appropriate, although even polytungstates(V,VI) might stabilize lower-valent rare-earth cations as has been observed for the {Eu-P<sub>5</sub>W<sub>30</sub>} system ([Antonio and Soderholm, 1997](#)). Such combinations, especially those with extended lattices, would produce solid-state materials with unusual electronic structures exhibiting valuable magnetic and electronic properties; (2) Rare-earth derivatives of polyoxometalates with paramagnetic transition metal heteroatoms. Those with adjacent paramagnetic metal centers, e.g. [R(Co<sup>III</sup>W<sub>11</sub>O<sub>39</sub>)<sub>2</sub>]<sup>15-</sup>, will exhibit magnetic interactions between unpaired d- and f-electrons and yield materials with potentially unprecedented magnetic properties; (3) The recent blossoming of a more extensive polyoxoniobate chemistry ([Nyman et al., 2002, 2004](#)) suggests many possibilities for new rare-earth-based materials, including high oxidation state cations; (4) Further development of non-aqueous chemistry of POM-rare-earth complexes ([Boglio et al., 2006](#)) can be anticipated. This opens up many avenues; to new catalytic processes, e.g., Lewis acid activity, to the coupling of POMs to substrates of biological interest, and especially to the large realm of organometallic rare-earth chemistry.

## ACKNOWLEDGEMENTS

This review was initially planned during a visit to the University of Bielefeld supported by the Alexander von Humboldt Foundation. I am grateful to Professor Achim Müller for his hospitality, and to Professors Lynn Francesconi, Uli Kortz, Bernt Krebs, Pierre Mialane, and Achim Müller, for preprints and copies of figures.

## REFERENCES

- Alizadeh, M.H., Harmalkar, S.P., Jeannin, Y., Martin-Frère, J., Pope, M.T. *J. Am. Chem. Soc.* 1985, **107**, 2662–9.
- Alizadeh, M.H., Eshtiagh-Hosseini, H., Khoshnavazi, R. *J. Mol. Struct.* 2004, **688**, 33–9.
- Almeida Paz, F.A., Balula, M.S.S., Cavaleiro, A.M.W., Klinowski, J., Nogueira, H.I.S. *Acta Crystallogr., Sect. E: Struct. Rep. E* 2005, **61**, i28–31.
- An, H., Lan, Y., Li, Y., Wang, E., Hao, N., Xiao, D., Duan, L., Xu, L. *Inorg. Chem. Commun.* 2004, **7**, 356–8.
- An, H., Xiao, D., Wang, E., Li, Y., Wang, X., Xu, L. *Eur. J. Inorg. Chem.* 2005a, 854–9.
- An, H., Xiao, D., Wang, E., Li, Y., Xu, L. *New J. Chem.* 2005b, **29**, 667–72.

- Andreev, G.B., Fedoseev, A.M., Budantseva, N.A., Antipin, M.Y. *Crystallogr. Rep.* 2002, **47**, 394–6.
- Antonio, M.R., Soderholm, L. *Inorg. Chem.* 1994, **33**, 5988–93.
- Antonio, M.R., Soderholm, L. *J. Cluster Sci.* 1996, **7**, 585–91.
- Antonio, M.R., Soderholm, L. *J. Alloys Compd.* 1997, **250**, 541–3.
- Antonio, M.R., Malinsky, J., Soderholm, L. *Mater. Res. Soc. Symp. Proc.* 1995, **368**, 223–8.
- Antonio, M.R., Soderholm, L., Jennings, G., Francesconi, L.C., Dankova, M., Bartis, J. *J. Alloys Compd.* 1998, **275–277**, 827–30.
- Antonio, M.R., Soderholm, L., Williams, C.W., Ullah, N., Francesconi, L.C. *Dalton Trans.* 1999, 3825–30.
- Baker, L.C.W., Gallagher, G.A., McCutcheon, T.P. *J. Am. Chem. Soc.* 1953, **75**, 2493–5.
- Ballardini, R., Mulazzani, Q.G., Venturi, M., Bolletta, F., Balzani, V. *Congr. Naz. Chim. Inorg. [Atti]* 1983, **16**, 363–4.
- Barbieri, G.A. *Atti Accad. Naz. Lincei* 1914, **23**, 805–12.
- Bartis, J., Sukal, S., Dankova, M., Kraft, E., Kronzon, R., Blumenstein, M., Francesconi, L.C. *J. Chem. Soc. Dalton Trans.* 1997a, 1937–44.
- Bartis, J., Dankova, M., Blumenstein, M., Francesconi, L.C. *J. Alloys Compd.* 1997b, **249**, 56–68.
- Bartis, J., Dankova, M., Lessmann, J.J., Luo, Q.-H., De Horrocks Jr., W., Francesconi, L.C. *Inorg. Chem.* 1999, **38**, 1042–53.
- Bassil, B.S., Dickman, M.H., von der Kammer, B., Kortz, U. *Inorg. Chem.* 2007, **46**, 2452–8.
- Belai, N., Sadakane, M., Pope, M.T. *J. Am. Chem. Soc.* 2001, **123**, 2087–8.
- Belai, N., Dickman, M.H., Pope, M.T., Contant, R., Keita, B., Mbomekalle, I.-M., Nadjio, L. *Inorg. Chem.* 2005, **44**, 169–71.
- Bessonov, A.A., Fedosseev, A.M., Krupa, J.C., Shirokova, I.B., Budantseva, N.A. *J. Solid State Chem.* 2002, **169**, 182–8.
- Bi, L.-H., Liu, J.-H., Wang, E.-B., Huang, R.-D., Yu, P.-S. *Chem. Res. Chin. Univ.* 1999, **15**, 364–6.
- Blasse, G. *Inorg. Chim. Acta* 1988, **142**, 153–4.
- Blasse, G. *Eur. J. Solid State Inorg. Chem.* 1991, **28**, 719–26.
- Blasse, G., Zonnevijlle, F. *Recl.: J.R. Neth. Chem. Soc.* 1982, **101**, 434–7.
- Blasse, G., Dirksen, G.J., Zonnevijlle, F. *Chem. Phys. Lett.* 1981a, **83**, 449–51.
- Blasse, G., Dirksen, G.J., Zonnevijlle, F. *J. Inorg. Nucl. Chem.* 1981b, **43**, 2847–53.
- Boglio, C., Lenoble, G., Duhayon, C., Hasenknopf, B., Thouvenot, R., Zhang, C., Howell, R.C., Burton-Pye, B.P., Francesconi, L.C., Lacote, E., Thorimbert, S., Malacria, M., Afonso, C., Tabet, J.-C. *Inorg. Chem.* 2006, **45**, 1389–98.
- Burgemeister, K., Drewes, D., Limanski, E.M., Kueper, I., Krebs, B. *Eur. J. Inorg. Chem.* 2004, 2690–4.
- Cai, X.-Z., Wang, S.-M., Guan, H.-M., Huang, J., Feng, Lin, Y.-H., Xing, Y. *Jiegou Huaxue* 1997a, **16**, 239–46. [Chem. Abs. 127:89723].
- Cai, X.-Z., Wang, S.-M., Huang, J.-F., Guan, H., Min, Lin, X. *Jiegou Huaxue* 1997b, **16**, 328–34. [Chem. Abs. 127:184826].
- Charushnikova, I.A., Fedoseev, A.M., Yusov, A.B., Den Auwer, C. *Crystallogr. Rep.* 2005, **50**, 191–3.
- Chen, H., Chen, Q., Chen, C. *Fujian Shifan Daxue Xuebao, Ziran Kexueban* 1986, **2**, 69–76. [Chem. Abs. 106:226257].
- Choppin, G.R. *J. Nucl. Sci. Technol.* 2002, 229–32.
- Ciabrin, J.P., Contant, R. *J. Chem. Res.* 1993, 391 (S), 2720 (M).
- Contant, R., Piro-Sellem, S., Canny, J., Thouvenot, R. *C. R. Acad. Sci., Ser. IIC: Chim.* 2000, **3**, 157–61.
- Copping, R., Gaunt, A.J., May, I., Sarsfield, M.J., Collison, D., Helliwell, M., Denniss, I.S., Apperley, D.C. *Dalton Trans.* 2005, 1256–62.
- Creaser, I., Heckel, M.C., Neitz, R.J., Pope, M.T. *Inorg. Chem.* 1993, **32**, 1573–8.
- Cronin, L., Beugholt, C., Krickemeyer, E., Schmidtmann, M., Bögge, H., Kögerler, P., Luong, T.K.K., Müller, A. *Angew. Chem. Int. Ed. Engl.* 2002, **41**, 2805–8.
- Crooks III, W.J. *Diss. Abstr. Int., B* 1995, **56**, 2008.
- Darwent, J.R., Flint, C.D., O'Grady, P.J. *Chem. Phys. Lett.* 1986, **127**, 547–50.
- Day, V.W., Klemperer, W.G. *Science* 1987, **228**, 533–41.
- Day, V.W., Fredrich, M.F., Klemperer, W.G., Shum, W. *J. Am. Chem. Soc.* 1977, **99**, 952–3.
- Dexter, D.D., Silverton, J.V. *J. Am. Chem. Soc.* 1968, **90**, 3589–90.
- Dickman, M.H., Gama, G.J., Kim, K.-C., Pope, M.T. *J. Cluster Sci.* 1996, **7**, 567–83.
- Drewes, D., Krebs, B. *Z. Anorg. Allg. Chem.* 2005, **631**, 2591–4.

- Drewes, D., Krebs, B. *Z. Naturforsch.* 2006, **61b**, 637–43.
- Drewes, D., Limanski, E.M., Krebs, B. *Dalton Trans.* 2004a, 2087–91.
- Drewes, D., Limanski, E.M., Krebs, B. *Eur. J. Inorg. Chem.* 2004b, 4849–53.
- Drewes, D., Piepenbrink, M., Krebs, B. *Z. Anorg. Allg. Chem.* 2006, **632**, 534–6.
- Fang, X., Anderson, T.M., Neiwert, W.A., Hill, C.L. *Inorg. Chem.* 2003, **42**, 8600–2.
- Fang, X., Anderson, T.M., Benelli, C., Hill, C.L. *Chem. Eur. J.* 2005, **11**, 712–8.
- Fedoseev, A.M., Yusov, A.B. *Sov. Radiochem.* 1992, **34**, 560–2.
- Fedoseev, A.M., Grigor'ev, M.S., Yanovskii, A.I., Struchkov, Y.T., Spitsyn, V.I. *Dokl. Chem.* 1987, **297**, 477.
- Fedoseev, A.M., Grigor'ev, M.S., Budantseva, N.A., Shirokova, I.B., Antic-Fidancev, E., Krupa, J.-C. *J. Lumin.* 2000, **87–89**, 1065–8.
- Fedotov, M.A., Samokhvalova, E.P., Torchenkova, F.A. *Izv. Sib. Otd. Akad. Nauk SSSR Ser. Khim. Nauk* 1989a, 42–5. [Chem. Abs. 112:244625].
- Fedotov, M.A., Samokhvalova, E.P., Maksimov, G.M., Torchenkova, E.A. *Zh. Strukt. Khim.* 1989b, **30**, 174. [Chem. Abs. 112:209601].
- Fedotov, M.A., Maksimov, G.M., Matveev, K.I. *Sov. J. Coord. Chem.* 1990a, **16**, 117–20.
- Fedotov, M.A., Pertsikov, B.Z., Danovich, D.K. *Polyhedron* 1990b, **9**, 1249–56.
- Fedotov, M.A., Pertsikov, B.Z., Danovich, D.K. *Sov. J. Coord. Chem.* 1991, **17**, 117–25.
- Fedotov, M.A., Samokhvalova, E.P., Kazansky, L. *Polyhedron* 1996, **15**, 3341–51.
- Feng, J., Sun, G., Pei, F., Liu, M. *J. Inorg. Biochem.* 2002a, **92**, 193–9.
- Feng, J., Li, X., Pei, F., Sun, G., Zhang, X., Liu, M. *Magn. Reson. Imag.* 2002b, **20**, 407–12.
- Fukaya, K., Yamase, T. *Angew. Chem., Int. Ed.* 2003, **42**, 654–8.
- Gaunt, A.J., May, I., Sarsfield, M.J., Collison, D., Helliwell, M., Denniss, I.S. *Dalton Trans.* 2003, 2767–71.
- Gavrilova, L.O., Molchanov, V.N. *Russ. J. Coord. Chem.* 2005, **31**, 401–9.
- Gavrilova, L.O., Fedotov, M.A., Tat'yanina, I.V., Torchenkova, E.A. *Russ. J. Inorg. Chem.* 1990, **35**, 1197–200.
- Gavrilova, L.O., Golubev, A.M., Tat'yanina, I.V., Torchenkova, E.A. *Vestn. Mosk. Univ., Ser. 2: Khim.* 1991, **32**, 261–4. [Chem. Abs. 116:14787].
- Gilbert, J., Kassab, D., Pawlow, J.H., Santora, B.P., Fiel, R.J., Joshi, V.N., Kozik, M. *Inorg. Chem.* 1995, **34**, 924–7.
- Griffith, W.P., Moreau, R.G.H., Nogueira, H. *Polyhedron* 1996, **15**, 3493–500.
- Griffith, W.P., Morley-Smith, N., Nogueira, H.I.S., Shoair, A.G.F., Suriaatmaja, M., White, A.J.P., Williams, D.J. *J. Organomet. Chem.* 2000, **607**, 146–55.
- Grigor'ev, M.S., Struchkov, Y.T., Fedoseev, A.M., Yusova, A.B., Yanovskii, A.I. *Russ. J. Inorg. Chem.* 1992, **37**, 1293–7.
- Haraguchi, N., Nagatomo, S., Okaue, Y., Isobe, T., Matsuda, Y. *Kidorui* 1991, **18**, 84–5.
- Haraguchi, N., Okaue, Y., Isobe, T., Matsuda, Y. *Inorg. Chem.* 1994, **33**, 1015–20.
- Hill, C.L. *Chem. Rev.* 1998, **98**, 1–390.
- Hill, C.L., in: McCleverty, J.A., Meyer, T.J., editors. *Comprehensive Coordination Chemistry II*, vol. 4. Oxford: Elsevier; 2004, pp. 679–759.
- Howell, R.C., Perez, F.G., Jain, S., Horrocks Jr., W.D., Rheingold, A.L., Francesconi, L.C. *Angew. Chem., Int. Ed.* 2001, **40**, 4031–4.
- Huang, J.-F., Wang, S.-M., Lin, S., Cai, X.-Z., Lin, X. *Jiegou Huaxue* 2000, **19**, 432–9. [Chem. Abs. 134:172322].
- Iball, J., Low, J.N., Weakley, T.J.R. *J. Chem. Soc., Dalton Trans.* 1974, 2021–4.
- Inagaki, A., Satoh, K., Kominami, H., Kera, Y., Yamaguchi, S., Ichihara, J. *Kidorui* 1997a, **30**, 288–9.
- Inagaki, A., Satoh, K., Kominami, H., Kera, Y., Yamaguchi, S., Ichihara, J. *Kidorui* 1997b, **30**, 286–7.
- Inoue, M., Yamase, T., Kazansky, L.P. *Polyhedron* 2003, **22**, 1183–9.
- Inouye, Y., Tokutake, Y., Yoshida, T., Seto, Y., Hujita, H., Dan, K., Yamamoto, A., Nishiya, S., Yamase, T., Nakamura, S. *Antiviral Res.* 1993, **20**, 317–31.
- Ito, T., Yashito, H., Yamase, T. *J. Cluster Sci.* 2006, **17**, 375–87.
- Jiang, H., Li, Z., Li, X. *Beihua Daxue Xuebao, Ziran Kexueban* 2000, **1**, 112–4. [Chem. Abs. 134:260436].
- Jiang, M., Zhai, X., Liu, M. *Langmuir* 2005, **21**, 11128–35.
- Kera, Y., Inagaki, A., Mochizuki, Y., Kominami, H., Yamaguchi, S., Ichihara, J. *J. Mol. Catal. A: Chem.* 2002, **184**, 413–29.

- Kholdeeva, O.A., Timofeeva, M.N., Maksimov, G.M., Maksimovskaya, R.I., Neiwert, W.A., Hill, C.L. *Inorg. Chem.* 2005, **44**, 666–72.
- Kim, K.-C., Pope, M.T., Gama, G.J., Dickman, M.H. *J. Am. Chem. Soc.* 1999, **121**, 11164–70.
- Knuth, W.H., Harlow, R.L. *J. Am. Chem. Soc.* 1981, **103**, 1865–7.
- Knuth, W.H., Domaille, P.J., Harlow, R.L. *Inorg. Chem.* 1986, **25**, 1577–84.
- Kortz, U. *J. Cluster Sci.* 2003, **14**, 205–14.
- Kortz, U., Holzapfel, C., Reicke, M. *J. Mol. Struct.* 2003, **656**, 93–100.
- Krebs, B., Loose, I., Bosing, M., Noh, A., Droste, E. *C. R. Acad. Sci., Ser. IIc* 1998, **1**, 351–60.
- Li, J.-X., Chen, Y.-G., Liu, Q., Sun, Z.-G., Liu, J.-F. *Gaodeng Xuexiao Huaxue Xuebao* 2000, **21**, 520–1. [Chem. Abs. 133:25849].
- Liao, C., Chen, S., Hou, Z., Weng, Z., Qiu, P. *Lanzhou Daxue Xuebao, Ziran Kexueban* 1993, **29**, 295–7. [Chem. Abs. 122:280560].
- Lipscomb, W.N. *Inorg. Chem.* 1965, **4**, 132–4.
- Lis, S. *Acta Phys. Pol. A* 1996, **90**, 275–83.
- Lis, S. *Wiadomosci Chemiczne (Volume Date 1997)* 1998, 27–39. [Chem. Abs. 130:46501].
- Lis, S. *J. Alloys Compd.* 2000, **300–301**, 88–94.
- Lis, S., But, S. *Wiadomosci Chemiczne* 2001, **55**, 1029–46. [Chem. Abs. 137:256724].
- Lis, S., Elbanowski, M., But, S. *Acta Phys. Pol. A* 1996, **90**, 361–6.
- Lis, S., But, S., Klonski, A.M., Grobelna, B. *Int. J. Photoenergy* 2003, **5**, 233–8.
- Liu, J., Rong, C., Wang, E. *Gaodeng Xuexiao Huaxue Xuebao* 1986, **7**, 565–8. [Chem. Abs. 106:112528].
- Liu, J., Zu, Z., Zhao, B., Liu, Z. *Inorg. Chim. Acta* 1989, **164**, 179–83.
- Liu, Z., Shan, Y., Wang, E., Jin, Z., Wei, G., Liu, Y. *Gaodeng Xuexiao Huaxue Xuebao* 1991a, **12**, 1–5. [Chem. Abs. 115:221719].
- Liu, J., Wang, W., Zhu, Z., Wang, E., Wang, Z. *Transition Met. Chem. (London)* 1991b, **16**, 169–72.
- Liu, J., Liu, Z., Wang, E., Qu, L. *Huaxue Xuebao* 1991c, **49**, 782–7. [Chem. Abs. 115:269230].
- Liu, J., Liu, S., Qu, L., Pope, M.T., Rong, C. *Transition Met. Chem. (London)* 1992, **17**, 311–3.
- Liu, J., Guo, J., Zhao, B., Xu, G., Li, M. *Transition Met. Chem. (London)* 1993a, **18**, 205–8.
- Liu, J., Wang, G., Zhao, B. *Chem. Res. Chin. Univ.* 1993b, **9**, 175–80. [Chem. Abs. 121:67927].
- Liu, J., Wang, W., Wang, G., Zhao, B., Sun, S. *Polyhedron* 1994, **13**, 1057–61.
- Liu, J.-F., Wang, W.-Q., Meng, L., Liu, Y. *Gaodeng Xuexiao Huaxue Xuebao* 1996a, **17**, 179–82.
- Liu, S.-X., Liu, Y.-Y., Wang, E.-B. *Huaxue Xuebao* 1996b, **54**, 673–8. [Chem. Abs. 125:291497].
- Liu, J.-F., Chen, Y.-G., Meng, L., Guo, J., Liu, Y., Pope, M.T. *Polyhedron* 1998, **17**, 1541–6.
- Liu, J., Xin, M., Li, J., Huang, R., Bu, L. *Dongbei Shida Xuebao, Ziran Kexueban* 1999, 92–7. [Chem. Abs. 132:202189].
- Liu, J.-f., Chen, Y.-g., Ma, J.-f., Wang, X.-h., Liu, Y. *Zhongguo Xitu Xuebao* 2000, **18**, 282–5. [Chem. Abs. 134:320578].
- Liu, J., Liu, B., Dong, S. *Fenzi Huaxue* 2002, **30**, 129–33. [Chem. Abs. 137:12251].
- Liu, G.K., Kistler, M.L., Li, T., Bhatt, A., Liu, T. *J. Cluster Sci.* 2006, **17**, 427–43.
- Lu, B., Shan, Y., Wu, Y., Xing, Y., Lin, Y.-H., Bai, S. *Chin. J. Struct. Chem.* 1996, **15**, 301–6.
- Lu, Y.-W., Keita, B., Nadjro, L. *Polyhedron* 2004, **23**, 1579–86.
- Luo, Q.-H., Howell, R.C., Dankova, M., Bartis, J., Williams, C.W., Horrocks Jr., W.D., Young, V.G., Rheingold, A.L., Francesconi, L.C., Antonio, M.R. *Inorg. Chem.* 2001, **40**, 1894–901.
- Luo, Q., Howell, R.C., Bartis, J., Dankova, M., Horrocks Jr., W.D., Rheingold, A.L., Francesconi, L.C. *Inorg. Chem.* 2002, **41**, 6112–7.
- Ma, J., Zhou, B., Ma, H., Guo, Y., Wei, Y. *Fenzi Kexue Xuebao* 2004, **20**, 18–23. [Chem. Abs. 143:338424].
- McKean, L., Pope, M.T. *Inorg. Chem.* 1974, **13**, 747–9.
- Meng, L., Liu, J.-F. *Chem. Res. Chin. Univ.* 1995, **11**, 64–6.
- Meng, L., Liu, J.-F. *Huaxue Xuebao* 1997, **55**, 1077–83. [Chem. Abs. 128:83598].
- Mialane, P., Dolbecq, A., Lisnard, L., Mallard, A., Marrot, J., Secheresse, F. *Angew. Chem., Int. Ed.* 2002, **41**, 2398–401.
- Mialane, P., Lisnard, L., Mallard, A., Marrot, J., Antic-Fidancev, E., Aschehoug, P., Vivien, D., Secheresse, F. *Inorg. Chem.* 2003, **42**, 2102–8.
- Mialane, P., Dolbecq, A., Riviere, E., Marrot, J., Secheresse, F. *Eur. J. Inorg. Chem.* 2004, 33–6.
- Mialane, P., Dolbecq, A., Marrot, J., Secheresse, F. *Inorg. Chem. Commun.* 2005, **8**, 740–2.
- Milyukova, M.S., Varezhkina, N.S., Myasoedov, B.F. *J. Radioanal. Nucl. Chem.* 1986, **105**, 249–56.

- Milyukova, M.S., Varezhkina, N.S., Myasoedov, B.F. *J. Radioanal. Nucl. Chem.* 1988, **121**, 403–8.
- Milyukova, M.S., Varezhkina, N.S., Myasoedov, B.F. *Sov. Radiochem.* 1990, **32**, 361–7.
- Mirkhani, V., Tangestaninejad, S., Moghadam, M., Yadollahi, B., Alipanah, L. *Monatsh. Chem.* 2004, **135**, 1257–63.
- Mirkhani, V., Tangestaninejad, S., Yadollahi, B., Alipanah, L. *Catal. Lett.* 2005, **101**, 93–7.
- Molchanov, V.N., Kazanskii, L.P., Torchenkova, E.A., Simonov, V.I. *Sov. Phys. Crystallogr.* 1979, **24**, 96–7.
- Müller, A., Serain, C. *Acc. Chem. Res.* 2000, **33**, 2–10.
- Müller, A., Beugholt, C., Bögge, H., Schmidtmann, M. *Inorg. Chem.* 2000, **39**, 3112–3.
- Müller, A., Zhou, Y., Bögge, H., Schmidtmann, M., Mitra, T., Haupt, E.T.K., Berkle, A. *Angew. Chem. Int. Ed.* 2006, **45**, 460–5.
- Mulazzani, Q.G., Venturi, M., Ballardini, R., Gandolfi, M.T., Balzani, V. *Isr. J. Chem.* 1985, **25**, 183–8.
- Naruke, H. *Kidorui* 2003a, **43**, 1–11. [Chem. Abs. 141:166618].
- Naruke, H. *Kidorui* 2003b, **42**, 120–1. [Chem. Abs. 140:262960].
- Naruke, H., Yamase, T. *J. Lumin.* 1991, **50**, 55–60.
- Naruke, H., Yamase, T. *Kidorui* 1996a, **30**, 252–3. [Chem. Abs. 127:142685].
- Naruke, H., Yamase, T. *Acta Crystallogr. Sect. C* 1996b, **52**, 2655–60.
- Naruke, H., Yamase, T. *J. Alloys Compd.* 1997, **255**, 183–9.
- Naruke, H., Yamase, T. *J. Alloys Compd.* 1998, **268**, 100–6.
- Naruke, H., Yamase, T. *Bull. Chem. Soc. Jpn.* 2000, **73**, 375–82.
- Naruke, H., Yamase, T. *Bull. Chem. Soc. Jpn.* 2001, **74**, 1289–94.
- Naruke, H., Yamase, T. *Bull. Chem. Soc. Jpn.* 2002a, **75**, 1275–82.
- Naruke, H., Yamase, T. *Inorg. Chem.* 2002b, **41**, 6514–20.
- Naruke, H., Yamase, T. *Mater. Integ.* 2004, **17**, 21–5. [Chem. Abs. 140:396686].
- Naruke, H., Yamase, T. *J. Alloys Compd.* 2005, **391**, 302–6.
- Naruke, H., Ozeki, T., Yamase, T. *Acta Crystallogr. Sect. C: Cryst. Struct. Commun.* 1991, **C47**, 489–92.
- Niu, Z., Qu, L., Chen, Y., Peng, J., Liu, J. *Yingyong Huaxue* 1992, **9**, 46–50. [Chem. Abs. 117:183639].
- Niu, J., Zhao, J., Guo, D., Wang, J. *J. Mol. Struct.* 2004a, **692**, 223–9.
- Niu, J., Zhao, J., Wang, J. *J. Mol. Struct.* 2004b, **701**, 19–24.
- Niu, J.-Y., Zhao, J.-W., Wang, J.-P. *Inorg. Chem. Commun.* 2004c, **7**, 876–9.
- Nyman, M., Bonhomme, F., Alam, T.M., Rodriguez, M.A., Cherry, B.R., Krumhansl, J.L., Nenoff, T.M., Sattler, A.M. *Science* 2002, **297**, 996–8.
- Nyman, M., Bonhomme, F., Alam, T.M., Paire, J.B., Vaughan, G.M.B. *Angew. Chem., Int. Ed.* 2004, **43**, 2787–92.
- Ostuni, A., Pope, M.T. *C. R. Acad. Sci. Paris, Ser. IIc* 2000, **3**, 199–204.
- Ostuni, A., Bachman, R.E., Pope, M.T. *J. Cluster Sci.* 2003, **14**, 431–46.
- Ozeki, T., Yamase, T. *Kidorui* 1993a, **22**, 14–5. [Chem. Abs. 122:278605].
- Ozeki, T., Yamase, T. *Acta Crystallogr. Sect. C: Cryst. Struct. Commun.* 1993b, **C49**, 1574–7.
- Ozeki, T., Yamase, T. *J. Alloys Compd.* 1993c, **192**, 28–9.
- Ozeki, T., Yamase, T. *Acta Crystallogr. Sect. B: Struct. Sci.* 1994a, **B50**, 128–34.
- Ozeki, T., Yamase, T. *Acta Crystallogr. Sect. C: Cryst. Struct. Commun.* 1994b, **C50**, 327–30.
- Ozeki, T., Takahashi, M., Yamase, T. *Acta Crystallogr. Sect. C: Cryst. Struct. Commun.* 1992, **C48**, 1370–4.
- Ozeki, T., Yamase, T., Naruke, H., Sasaki, Y. *Inorg. Chem.* 1994, **33**, 409–10.
- Peacock, R.D., Weakley, T.J.R. *J. Chem. Soc. A* 1971a, 1836–9.
- Peacock, R.D., Weakley, T.J.R. *J. Chem. Soc. A* 1971b, 1937–40.
- Petrukhina, M.A., Fedotov, M.A., Tat'yanina, I.V., Torchenkova, E.A. *Russ. J. Inorg. Chem.* 1989, **34**, 1782–5.
- Pope, M.T. *Heteropoly and Isopoly Oxometalates*, New York: Springer; 1983.
- Pope, M.T. *Prog. Inorg. Chem.* 1991, **39**, 181–254.
- Pope, M.T., in: McCleverty, J.A., Meyer, T.J., editors. *Comprehensive Coordination Chemistry II*, vol. 4. Oxford: Elsevier; 2004, pp. 635–78.
- Pope, M.T., Müller, A. *Angew. Chem. Int. Ed. Engl.* 1991, **30**, 34–48.
- Pope, M.T., Wei, X., Wassermann, K., Dickman, M.H. *C. R. Acad. Sci., Ser. IIc* 1998, **1**, 297–304.
- Qu, L., Niu, Z., Liu, J., Chen, Y., Zhao, B., Peng, J. *Gaodeng Xuexiao Huaxue Xuebao* 1991, **12**, 1434–6. [Chem. Abs. 118:159754].

- Qu, L., Wang, S., Peng, J., Chen, Y., Wang, G. *Polyhedron* 1992, **11**, 2645–9.
- Qu, L., Wang, S., Peng, J., Chen, Y., Yu, M. *Chin. Sci. Bull.* 1993, **38**, 1087–91. [Chem. Abs. 121:270258].
- Ratiu, C., Oprean, I., Gabrus, R., Ciocan-Tarta, I., Budiu, T. *Rev. Chim. (Bucharest)* 2004, **55**, 106–7.
- Rigotti, G., Punte, G., Rivero, B.E., Escobar, M.E., Baran, E.J. *J. Inorg. Nucl. Chem.* 1981, **43**, 2811–4.
- Robert, F., Leyrie, M., Hervé, G., Tézé, A., Jeannin, Y. *Inorg. Chem.* 1980, **19**, 1746–52.
- Rong, C., Pope, M.T. *J. Am. Chem. Soc.* 1992, **114**, 2932–8.
- Rong, C., Liu, J., Chen, X., Wang, E. *Inorg. Chim. Acta* 1987, **130**, 265–9.
- Rosu, C., Weakley, T.J.R. *Acta Crystallogr., Sect. C: Cryst. Struct. Commun. Online* 1998, **C54**, IUC9800047.
- Sadakane, M., Dickman, M.H., Pope, M.T. *Angew. Chem., Int. Ed.* 2000, **39**, 2914–6.
- Sadakane, M., Dickman, M.H., Pope, M.T. *Inorg. Chem.* 2001, **40**, 2715–9.
- Sadakane, M., Ostuni, A., Pope, M.T. *J. Chem. Soc. Dalton Trans.* 2002, 63–7.
- Saito, A., Choppin, G.R. *Radiochim. Acta* 1995, **68**, 221–5.
- Saito, A., Tomari, H., Choppin, G.R. *Inorg. Chim. Acta* 1997, **258**, 145–53.
- Samokhvalova, E.P., Fedotov, M.A., Tat'yanina, I.V., Torchenkova, E.A. *Russ. J. Inorg. Chem.* 1989a, **34**, 367–9.
- Samokhvalova, E.P., Borisova, A.P., Fedotov, M.A., Tat'yanina, I.V., Torchenkova, E.A. *Russ. J. Inorg. Chem.* 1989b, **34**, 1451–4.
- Samokhvalova, E.P., Borisova, A.P., Tat'yanina, I.V., Torchenkova, E.A. *Vestn. Mosk. Univ., Ser.* 1989c, **2**, 408. [Chem. Abs. 109:177663].
- Samokhvalova, E.P., Molchanov, V.N., Tat'yanina, I.V., Torchenkova, E.A. *Sov. J. Coord. Chem.* 1990a, **16**, 683–7.
- Samokhvalova, E.P., Fedotov, M.A., Tat'yanina, I.V., Torchenkova, E.A. *Russ. J. Inorg. Chem.* 1990b, **35**, 1200–3.
- Samokhvalova, E.P., Molchanov, V.N., Tat'yanina, I.V., Torchenkova, E.A. *Koord. Khim.* 1990c, **16**, 207–11. [Chem. Abs. 112:169579n].
- Saprykin, A.S., Spitsyn, V.I., Krot, N.N. *Dokl. Chem.* 1976a, **226**, 114–6.
- Saprykin, A.S., Spitsyn, V.I., Krot, N.N. *Dokl. Phys. Chem.* 1976b, **231**, 1038–9.
- Sasaki, Y., Sillén, L.G. *Arkiv Kemi* 1968, **29**, 253.
- Shan, Y., Liu, Z., Wang, E., Jin, Z., Wei, G., Liu, Y. *Jiegou Huaxue* 1990, **9**, 159–63. [Chem. Abs. 114:239243].
- Shan, Y., Liu, Z., Jin, Z., Wei, G., Liu, Y., Wang, E. *Sci. China, Ser. B* 1991, **34**, 513–21. [Chem. Abs. 115:293496].
- Shan, Y., Liu, Z., Jin, Z., Wei, G. *Jiegou Huaxue* 1992a, **11**, 90–5. [Chem. Abs. 118:91353].
- Shan, Y., Liu, Z., Jin, Z., Wei, G. *Huaxue Xuebao* 1992b, **50**, 357–64. [Chem. Abs. 117:61562].
- Shan, Y., Liu, Z., Cai, Q. *Eur. J. Solid State Inorg. Chem.* 1992c, **29**, 1065–77.
- Shan, Y., Ye, X., Wu, Y. *Yingyong Huaxue* 1995, **12**, 42–6.
- Shilov, V.P. *Koord. Khim.* 1981, **7**, 1654–8. [Chem. Abs. 96:12075y].
- Shiozaki, R., Goto, H., Kera, Y. *Bull. Chem. Soc. Jpn.* 1993, **66**, 2790–6.
- Shiozaki, R., Inagaki, A., Nishino, A., Kominami, H., Kera, Y. *Kidorui* 1995, **26**, 274–5. [Chem. Abs. 123:240509].
- Shiozaki, R., Inagaki, A., Nishino, A., Nishio, E., Maekawa, M., Kominami, H., Kera, Y. *J. Alloys Compd.* 1996a, **234**, 193–8.
- Shiozaki, R., Kominami, H., Kera, Y. *Synth. Commun.* 1996b, **26**, 1663–8.
- Shiozaki, R., Inagaki, A., Ozaki, A., Kominami, H., Yamaguchi, S., Ichihara, J., Kera, Y. *J. Alloys Compd.* 1997a, **261**, 132–9.
- Shiozaki, R., Inagaki, A., Kominami, H., Yamaguchi, S., Ichihara, J., Kera, Y. *J. Mol. Catal. A: Chem.* 1997b, **124**, 29–37.
- Soderholm, L., Liu, G.K., Muntean, J., Malinsky, J., Antonio, M.R. *J. Phys. Chem.* 1995, **99**, 9611–6.
- Sousa, F.L., Ferreira, A.C.A.S., Ferreira, R.A.S., Cavaleiro, A.M.V., Carlos, L.D., Nogueira, H.I.S., Rocha, J., Trindade, T. *J. Nanosci. Nanotechnol.* 2004, **4**, 214–20.
- Sugeta, M., Yamase, T. *Bull. Chem. Soc. Jpn.* 1993, **66**, 444–9.
- Sun, R.-Q., Zhang, H.-H., Zhao, S.-L., Huang, C.-C., Zheng, X.-L. *Jiegou Huaxue* 2001, **20**, 413–7. [Chem. Abs. 136:63163].
- Sun, G., Feng, J., Wu, H., Pei, F., Fang, K., Lei, H. *J. Magn. Magn. Mater.* 2004a, **281**, 405–9.

- Sun, G., Feng, J., Wu, H., Pei, F., Fang, K., Lei, H. *Magn. Reson. Imag.* 2004b, **22**, 421–6.
- Szytczewski, A., Lis, S., Kruczynski, Z., Pietrzak, J., But, S., Elbanowski, M. *Acta Phys. Pol. A* 1996, **90**, 345–51.
- Tat'yanina, I.V., Molchanov, V.N., Ionov, V.M., Torchenkova, E.A., Spitsyn, V.I. *Izv. Akad. Nauk SSSR, Ser. Khim.* 1982a, 803–7. [Chem. Abs. 96:208780].
- Tat'yanina, I.V., Fomicheva, E.B., Molchanov, V.N., Zavodnik, V.E., Bel'skii, V.K., Torchenkova, E.A. *Sov. Phys., Crystallogr.* 1982b, **27**, 142.
- Tourné, C.M., Tourné, G.F., Brianso, M.C. *Acta Crystallogr., Sect. B: Struct. Sci.* 1980, **B36**, 2012–8.
- Tytko, K.H., Baethe, G., Cruywagen, J.J. *Inorg. Chem.* 1985, **24**, 3132–6.
- Van Pelt, C.E., Crooks, W.J., Choppin, G.R. *Inorg. Chim. Acta* 2003, **346**, 215–22.
- Wang, E., Hu, C., Zhou, Y., Liu, J. *Gaodeng Xuexiao Huaxue Xuebao* 1990, **11**, 340–4. [Chem. Abs. 113:203791].
- Wang, E., Wu, Q., Wang, Z., Shen, E. *Yingyong Huaxue* 1991a, **8**, 13–6. [Chem. Abs. 115:269111].
- Wang, E., Liu, L., Shen, E., Wang, Z. *Gaodeng Xuexiao Huaxue Xuebao* 1991b, **12**, 1576–8. [Chem. Abs. 118:159753].
- Wang, E., Zhang, L., Wang, Z., Shen, E., Zhang, S., Zhan, R., Liu, Y. *Chin. Chem. Lett.* 1991c, **2**, 877–80. [Chem. Abs. 116:226908].
- Wang, E., Wa, Q., Huang, R. *Zhongguo Xitu Xuebao* 1991d, **9**, 174–6. [Chem. Abs. 116:247247].
- Wang, E., Yu, W., Liu, J., Hu, C. *Gaodeng Xuexiao Huaxue Xuebao* 1991e, **12**, 1279–83. [Chem. Abs. 118:159752].
- Wang, E., Shan, Y., Liu, Z., Liu, J., Zhang, B. *Huaxue Xuebao* 1991f, **49**, 774–81. [Chem. Abs. 116:119632].
- Wang, W., Liu, J. *Zhongguo Xitu Xuebao* 1995, **13**, 365–7. [Chem. Abs. 124:271035].
- Wang, W., Zhu, X., You, W., Liu, J. *Wuji Huaxue Xuebao* 1993a, **9**, 347–51. [Chem. Abs. 121:72334].
- Wang, S., Peng, J., Yu, M., Chen, Y., Qu, L. *Wuji Huaxue Xuebao* 1993b, **9**, 364–8. [Chem. Abs. 121:194146].
- Wang, X.-G., Shan, Y.-K., Chu, W.-L., Wu, Y., Xing, Y., Lin, Y.-H., Bai, S.-Y. *Jiegou Huaxue* 1997, **16**, 233–8. [Chem. Abs. 127:59793].
- Wang, X., Wang, E., Huang, R., Wang, Z. *Dongbei Shida Xuebao, Ziran Kexueban* 1998, 114–8. [Chem. Abs. 131:178850].
- Wang, J., Liu, F., Fu, L., Zhang, H. *Mater. Lett.* 2002a, **56**, 300–4.
- Wang, Y., Wang, X., Hu, C. *J. Colloid Interface Sci.* 2002b, **249**, 307–15.
- Wang, J., Wang, H.S., Fu, L.S., Liu, F.Y., Zhang, H.J. *Thin Solid Films* 2002c, **414**, 256–61.
- Wang, J., Wang, H., Fu, L., Liu, F., Zhang, H. *Mater. Sci. Eng., B* 2003, **B97**, 83–6.
- Wang, Z., Liu, S., Du, Z., Hu, Z., Zhang, H. *Mater. Sci. Eng., C* 2004a, **C24**, 459–62.
- Wang, Z., Liu, S., Du, Z., Zhang, H. *Mater. Lett.* 2004b, **58**, 1642–5.
- Wang, Z., Liu, S.-Z., Du, Z.-L., Hu, Z.-G., Zhang, H.-J. *Gaodeng Xuexiao Huaxue Xuebao* 2004c, **25**, 401–4. [Chem. Abs. 141:148742].
- Wang, Z., Wang, J., Zhang, H. *Mater. Chem. Phys.* 2004d, **87**, 44–8.
- Wang, J., Wang, Z., Wang, H., Liu, F., Fu, L., Zhang, H. *J. Alloys Compd.* 2004e, **376**, 68–72.
- Wassermann, K., Pope, M.T. *Inorg. Chem.* 2001, **40**, 2763–8.
- Wassermann, K., Dickman, M.H., Pope, M.T. *Angew. Chem. Int. Ed. Engl.* 1997, **36**, 1445–8.
- Wassermann, K., Pope, M.T., Salmen, M., Dann, J.N., Lunk, H.-J. *J. Solid State Chem.* 2000, **149**, 378–83.
- Wu, Z., Zhao, Z., Jiang, M., Li, K., Zhang, Q., in: Xu, G., Xiao, J., editors. *Proc. Int. Conf. Rare Earth Dev. Appl.*, vol. 1. Beijing, People's Republic of China: Science Press; 1985, pp. 630–3. [Chem. Abs. 106:32144].
- Wu, Z., Zhao, Z., Jiang, M., Li, K., Zhang, Q. *Zhongguo Xitu Xuebao* 1986, **4**, 25–30. [Chem. Abs. 106:198085].
- Wu, Q., Wang, E., Zhou, Y. *Zhongguo Xitu Xuebao* 1990, **8**, 209–12. [Chem. Abs. 115:269075].
- Wu, Q., Wang, E., Liu, J. *Polyhedron* 1993, **12**, 2563–8.
- Wu, C.-D., Lu, C.-Z., Zhuang, H.-H., Huang, J.-S. *J. Am. Chem. Soc.* 2002, **124**, 3836–7.
- Xiao, Z., Chen, Q., Chen, C. *Fujian Shifan Daxue Xuebao, Ziran Kexueban* 1986, **2**, 77–84. [Chem. Abs. 106:130622].
- Xin, X.-l., Gao, L.-h., Wen, L.-l. *Jingxi Huagong* 2002, **19**, 68–70, 82. [Chem. Abs. 137:156382].
- Xue, G., Liu, B., Hu, H., Yang, J., Wang, J., Fu, F. *J. Mol. Struct.* 2004, **690**, 95–103.
- Yagasaki, A., Andersson, I., Pettersson, L. *Inorg. Chem.* 1987, **26**, 3926–33.

- Yamase, T. *Chem. Rev.* 1998, **98**, 307–25.
- Yamase, T., Kobayashi, T. *Kidorui* 1995, **26**, 120–1. [Chem. Abs. 123:240687].
- Yamase, T., Naruke, H. *Coord. Chem. Rev.* 1991a, **111**, 83–90.
- Yamase, T., Naruke, H. *J. Chem. Soc. Dalton Trans.* 1991b, 285–92.
- Yamase, T., Ozeki, T. *Acta Crystallogr., Sect. C: Cryst. Struct. Commun.* 1993, **C49**, 1577–80.
- Yamase, T., Ueda, K. *Kidorui* 1993, **22**, 190–1. [Chem. Abs. 122:145828].
- Yamase, T., Naruke, H., Sasaki, Y. *J. Chem. Soc. Dalton Trans.* 1990, 1687.
- Yamase, T., Ozeki, T., Ueda, K. *Acta Crystallogr., Sect. C: Cryst. Struct. Commun.* 1993, **C49**, 1572–4.
- Yamase, T., Ozeki, T., Tosaka, M. *Acta Crystallogr., Sect. C: Cryst. Struct. Commun.* 1994, **C50**, 1849–52.
- Yamase, T., Ozeki, T., Kawashima, I. *Acta Crystallogr., Sect. C: Cryst. Struct. Commun.* 1995, **C51**, 545–7.
- Yamase, T., Kobayashi, T., Sugeta, M., Naruke, H. *J. Phys. Chem. A* 1997, **101**, 5046–53.
- Yamase, T., Ishikawa, E., Abe, Y., Yano, Y. *J. Alloys Compd.* 2006, **408–412**, 693–700.
- Yasuhara, Y., Kominami, H., Kera, Y. *Kidorui* 1999, **34**, 108–9. [Chem. Abs. 131:63922].
- Yue, B., Jiang, L., Kong, Z.-P., Jiao, F., Lin, X.-R., Jin, S.-L. *Gaodeng Xuexiao Huaxue Xuebao* 2004, **25**, 199–203. [Chem. Abs. 141:252917].
- Yusov, A.B., Fedoseev, A.M. *Zh. Prikl. Spektrosk.* 1987, **47**, 40–5. [Chem. Abs. 107:186376].
- Yusov, A.B., Fedoseev, A.M. *Zh. Prikl. Spektrosk.* 1988, **49**, 929–35. [Chem. Abs. 111:67023].
- Yusov, A.B., Fedoseev, A.M. *Zh. Prikl. Spektrosk.* 1991, **55**, 334–6. [Chem. Abs. 116:12654].
- Yusov, A.B., Shilov, V.P. *Radiochemistry* 1999, **41**, 1–23.
- Yusov, A.B., Fedoseev, A.M., Spitsyn, V.I., Krot, N.N. *Dokl. Akad. Nauk SSSR (Phys. Chem.)* 1986, **289**, 1441–4.
- Yusov, A.B., Yin, M., Fedoseev, A.M., Andreev, G.B., Shirokova, I.B., Krupa, J.C. *J. Alloys Compd.* 2002, **344**, 289–92.
- Zhai, S., Chen, Y., Wang, S., Jiang, J., Dong, S., Li, J. *Talanta* 2004, **63**, 927–31.
- Zhang, T.R., Lu, R., Zhang, H.Y., Xue, P.C., Feng, W., Liu, X.L., Zhao, B., Zhao, Y.Y., Li, T.J., Yao, J.N. *J. Mater. Chem.* 2003, **13**, 580–4.
- Zhang, C., Howell, R.C., Scotland, K.B., Perez, F.G., Todaro, L., Francesconi, L.C. *Inorg. Chem.* 2004, **43**, 7691–701.
- Zhang, T., Spitz, C., Antonietti, M., Faul, C.F.J. *Chem. Eur. J.* 2005a, **11**, 1001–9.
- Zhang, C., Howell, R.C., Luo, Q.-H., Fieselmann, H.L., Todaro, L.J., Francesconi, L.C. *Inorg. Chem.* 2005b, **44**, 3569–78.
- Zhang, C., Howell, R.C., McGregor, D., Bensaid, L., Rahyab, S., Nayshtut, M., Lekperic, S., Francesconi, L.C. *Comptes Rend. Chim.* 2005c, **8**, 1035–44.
- Zhang, C., Bensaid, L., McGregor, D., Fang, X., Howell, R.C., Burton-Pye, B., Luo, Q., Todaro, L., Francesconi, L.C. *J. Cluster Sci.* 2006, **17**, 389–425.
- Zhao, J., Wen, Y., Wang, J. *Henan Daxue Xuebao, Ziran Kexueban* 2004, **34**, 47–51. [Chem. Abs. 142:366066].
- Zhou, B., Shan, Y., Liu, Z., Zhang, X. *Gaodeng Xuexiao Huaxue Xuebao* 1991, **12**, 1425–9. [Chem. Abs. 118:93136].
- Zhou, B., Shan, Y., Liu, Z., Zhang, X. *Wuji Huaxue Xuebao* 1992, **8**, 315–20. [Chem. Abs. 118:246257].
- Zhou, B., Ma, H., Li, S., Xu, X., Wei, Y. *Fenzi Kexue Xuebao* 2002, **18**, 156–61. [Chem. Abs. 140:11995].
- Zhu, Z., Liu, J., Zhao, B. *Gaodeng Xuexiao Huaxue Xuebao* 1990, **11**, 322–4. [Chem. Abs. 113:183593].
- Zimmermann, M., Belai, N., Butcher, R.J., Pope, M.T., Chubarova, E.V., Dickman, M.H., Kortz, U. *Inorg. Chem.* 2007, **46**, 1737–40.

## AUTHOR INDEX

- Abe, H., see Kitô, H. 200, 201  
 Abe, H., see Mori, T. 122, 130, 143  
 Abe, S., see Wang, Y. 113  
 Abe, Y., see Yamase, T. 370  
 Abernathy, D.L., see Detlefs, C. 199, 200  
 Abliz, M. 265  
 Abrahamsen, A.B., see Andersen, N.H. 200, 276  
 Abrahamsen, A.B., see Eskildsen, M.R. 277, 280, 284, 292  
 Abrahamsen, A.B., see Jensen, A. 272  
 Abrahamsen, A.B., see Nørgaard, T.K. 276  
 Abrego Castillo, I., see El Massalami, M. 293  
 Abrikosov, A.A. 186, 191, 279, 303  
 Abrikosov, I.A., see Skorodumova, N.V. 7  
 Adachi, G.-y., see Sakai, T. 184, 203  
 Adachi, G.-y. 8, 56  
 Adachi, H. 223  
 Adams, J.B., see Jiang, Y. 7, 33, 34  
 Adegbenro, S.A., see Naugle, D.G. 270  
 Adroja, D.T., see Tomy, C.V. 193, 257–260  
 Aegerter, C.M., see Paul, D.McK. 277  
 Aegerter, C.M., see Riseman, T.M. 280  
 Afalfiz, L.A., see Tomy, C.V. 193, 197, 242, 257–259  
 Afonso, C., see Boglio, C. 353–355, 375  
 Agarwal, P., see Saxena, S.S. 191  
 Ager, C., see Riseman, T.M. 280  
 Aharony, A. 185  
 Ahilan, K., see Saxena, S.S. 191  
 Akatsu, M., see Yamaguchi, T. 246  
 Akima, T., see Riseman, T.M. 280  
 Akimitsu, J., see Ekino, T. 240  
 Akimitsu, J., see Nagamatsu, J. 114, 184, 185  
 Akimitsu, J., see Ohishi, K. 300  
 Akimitsu, J., see Uehara, M. 182  
 Akiyama, H. 238, 267  
 Akiyama, H., see Oomi, G. 239  
 Aksel'rud, L.G., see Kalychak, Ya.M. 86, 87  
 Alam, M.A., see Dugdale, S.B. 210  
 Alam, T.M., see Nyman, M. 375  
 Alberigi-Quaranta, A., see Prudenziati, M. 138  
 Alexander, M.G., see Gordon, R.A. 67, 86, 93, 98  
 Aliaga-Guerra, D., see Bud'ko, S.L. 293  
 Alipanah, L., see Mirkhani, V. 374  
 Alizadeh, M.H. 356, 364  
 Allen, P.B. 214  
 Alleno, E. 203–205, 207, 238, 242, 249, 261, 266, 295, 309  
 Alleno, E., see Berger, P. 206  
 Alleno, E., see Bonville, P. 278, 295  
 Alleno, E., see Felner, I. 293, 295  
 Alleno, E., see Godart, C. 195  
 Alleno, E., see Mazumdar, C. 249  
 Alleno, E., see Nagarajan, R. 277  
 Alleno, E., see Paulose, P.L. 197  
 Alleno, E., see Rams, M. 278  
 Alleno, E., see Tominez, E. 184, 193, 197, 202  
 Allenspach, P. 245  
 Allenspach, P., see Cavadini, N. 246  
 Allenspach, P., see Gasser, U. 198, 241, 244–246, 276, 278  
 Almeida, M., see Kuznietz, M. 293  
 Almeida Paz, F.A. 344  
 Alp, E.E., see Dunlap, B.D. 190  
 Amann, A., see Li, S. 278  
 Amann, A., see Rathnayaka, K.D.D. 278  
 Amara, M., see El Massalami, M. 255  
 Amaral Jr., M.R., see El Massalami, M. 293  
 Amato, A., see Le, L.P. 241  
 Amaya, K., see Shimizu, K. 182, 186  
 Amici, A. 262, 265, 268  
 Amoruso, S., see Wang, X. 208  
 An, H. 368  
 An, J.M. 185  
 Anatska, M.P., see Rathnayaka, K.D.D. 219, 236, 296  
 Anderegg, J., see Vinnikov, L.Ya. 275, 289, 290, 292  
 Anderico, C.Z. 147  
 Andersen, N.H. 200, 276, 277, 292  
 Andersen, N.H., see Chang, L.J. 200  
 Andersen, N.H., see Eskildsen, M.R. 276, 277, 280, 284–287, 289, 292

- Andersen, N.H., see Gammel, P.L. 275, 285, 292
- Andersen, N.H., see Jensen, A. 272
- Andersen, N.H., see Nørgaard, T.K. 276
- Anderson, P.W. 188, 191
- Anderson, T.M., see Fang, X. 357, 360
- Anderson Jr., N.E., see Bud'ko, S.L. 304
- Andersson, I., see Yagasaki, A. 339
- Andersson, S., see Hyde, B.G. 91
- André, G., see Alleno, E. 295
- Andreev, G.B. 368
- Andreev, G.B., see Yusov, A.B. 368
- Andreone, A. 207, 208, 227
- Andreone, A., see Iavarone, M. 208
- Andres, K., see Hannay, N.B. 182
- Andres, K., see Matthias, B.T. 112–115, 184
- Anisimov, V.I., see Shorikov, A.O. 210, 259, 309
- Annett, J.F., see Gabovich, A.M. 192
- Ansaldò, E.J., see Bernhard, C. 191
- Antic-Fidancev, E., see Fedoseev, A.M. 368
- Antic-Fidancev, E., see Mialane, P. 353, 355
- Antipin, M.Y., see Andreev, G.B. 368
- Antonietti, M., see Zhang, T. 373
- Antonio, M.R. 364, 365, 375
- Antonio, M.R., see Luo, Q.-H. 346, 349, 353
- Antonio, M.R., see Soderholm, L. 365
- Antropov, V.P., see Kortus, J. 185
- Aoki, D. 191
- Aoki, H., see Terashima, T. 230
- Aoki, Y., see Kohgi, M. 246
- Appel, J., see Fay, D. 186, 191
- Apperley, D.C., see Copping, R. 349
- Appl, S., see Lee, W.H. 184
- Araki, S., see Kohgi, M. 246
- Aranson, I. 288
- Aranson, I., see De Wilde, Y. 280
- Aranson, I., see Metlushko, V. 215, 232, 233, 237, 285
- Arima, T., see Murakami, Y. 248
- Arisawa, S. 207, 208
- Armenante, M., see Wang, X. 208
- Aronsson, B. 88
- Arpe, P.E. 70, 81, 82, 94
- Arpe, P.E., see Pöttgen, R. 57, 63, 77, 81, 95
- Aruta, C., see Andreone, A. 208, 227
- Asaf, U., see Felner, I. 190, 191
- Asai, K., see Kobayashi, Y. 239, 267
- Asai, K., see Suzuki, M. 198
- Aschehoug, P., see Mialane, P. 353, 355
- Aselage, T.L. 107, 158, 159, 165
- Ashburn, J.R., see Wu, M.K. 185
- Ashcroft, N.W. 182
- Ashcroft, N.W., see Richardson, C.F. 182
- Askerzade, I.N. 235
- Aso, N., see Onimaru, T. 246, 247
- Asulin, I., see Tsindlekht, M.I. 113, 115
- Aswal, V.K., see Gilardi, R. 280
- Attfield, J.P., see Williams, A.J. 248
- Auer, J. 113
- Ausloos, M., see Gabovich, A.M. 192
- Avila, M.A. 206, 279
- Avramenko, Yu.A., see Fil, V.D. 217
- Awana, V.P.S. 191
- Baba, T. 227, 228, 274, 300
- Baba, T., see Yokoya, T. 227
- Baberschke, K., see Davidov, D. 187
- Bachman, R.E., see Ostuni, A. 345, 346
- Badica, P., see Togano, K. 184
- Baenziger, N.C. 4, 5
- Baenziger, N.C., see Duwell, E.J. 81
- Baenziger, N.C., see Guth, E.D. 2, 3
- Baenziger, N.C., see Nielsen, J.W. 80
- Baethe, G., see Tytko, K.H. 339
- Baggio-Saitovitch, E.M. 196, 200, 242, 255
- Baggio-Saitovitch, E.M., see Bourdarot, F. 200
- Baggio-Saitovitch, E.M., see Bud'ko, S.L. 198, 238, 293, 295
- Baggio-Saitovitch, E.M., see El Massalami, M. 200, 242
- Baggio-Saitovitch, E.M., see Fontes, M.B. 200
- Baggio-Saitovitch, E.M., see Sánchez, D.R. 196, 239, 242, 257, 268, 296, 307
- Bai, S., see Lu, B. 346
- Bai, S.-Y., see Wang, X.-G. 346
- Baines, C., see Mulders, A.M. 276
- Baker, L.C.W. 340
- Bakker, K., see Brabers, J.H.V.J. 195
- Balakrishnan, G., see Tomy, C.V. 197, 242, 259, 260
- Balicas, L., see Goodrich, R.G. 276
- Ballardini, R. 372
- Ballardini, R., see Mulazzani, Q.G. 372
- Baltensperger, W. 188, 189
- Balula, M.S.S., see Almeida Paz, F.A. 344
- Balzani, V., see Ballardini, R. 372
- Balzani, V., see Mulazzani, Q.G. 372
- Bambakidis, G. 109, 110
- Bancroft, N.J., see Paul, D.McK. 277
- Baran, E.J., see Rigotti, G. 372
- Baran, M., see Szymczak, R. 271
- Baranyak, V.M., see Kalychak, Ya.M. 87
- Barash, Yu.S. 302
- Barbara, B., see Felner, I. 295

- Barber, B.P., see Eskildsen, M.R. 276, 286, 287, 289
- Barber, B.P., see Gammel, P.L. 275, 290
- Barbieri, G.A. 340
- Barcza, A., see Rotter, M. 256
- Bardeen, J. 181, 212
- Baron, V.V., see Savitskii, E.M. 184
- Barratt, J.P., see Boothroyd, A.T. 278, 279
- Bars, O., see Bauer, J. 203
- Barthem, V., see El Massalami, M. 200
- Bartis, J. 343, 348–350, 353
- Bartis, J., see Antonio, M.R. 365
- Bartis, J., see Luo, Q. 353
- Bartis, J., see Luo, Q.-H. 346, 349, 353
- Bartkowski, K., see Lipp, D. 206
- Bartram, S.F. 4, 5
- Bashlakov, D.L. 229, 241
- Bashlakov, D.L., see Naidyuk, Yu.G. 227
- Bassil, B.S. 345, 346, 349
- Bat'ko, I., see Gabani, S. 112–115
- Batko, I., see Kohout, A. 114–116
- Batko, I., see Paderno, Yu.B. 111, 112, 114, 115
- Batlogg, B., see Carter, S.A. 238, 249
- Batlogg, B., see Cava, R.J. 180, 181, 184, 197, 200–202, 240, 242, 300
- Batlogg, B., see Eisaki, H. 197, 242, 261
- Batlogg, B., see Takagi, H. 216, 240
- Baudin, M., see Yang, Z. 7, 33
- Bauer, E.D. 192, 246
- Bauer, E.D., see Ekimov, E.A. 182, 184
- Bauer, E.D., see El-Hagary, M. 271
- Bauer, E.D., see Gabani, S. 116
- Bauer, E.D., see Michor, H. 200, 296, 304, 307
- Bauer, E.D., see Park, T. 227
- Bauer, J. 140, 203
- Bauer, J., see Ruiz, D. 204
- Bauernfeind, L. 190
- Bean, C.P., see Meiklejohn, W.H. 243
- Becher, H.J. 63
- Bednorz, J.G. 182
- Behnia, K., see Kasahara, Y. 306
- Behr, G. 202, 204, 205, 261, 266
- Behr, G., see Bashlakov, D.L. 229
- Behr, G., see Bitterlich, H. 202, 206, 207, 305
- Behr, G., see Drechsler, S.-L. 193, 209, 210, 212, 213, 259
- Behr, G., see Fuchs, G. 240
- Behr, G., see Fuger, R. 291
- Behr, G., see Gonnelli, R.S. 215
- Behr, G., see Graw, G. 206
- Behr, G., see Ignatchik, O. 210, 230
- Behr, G., see Jaenicke-Rössler, U. 239
- Behr, G., see Kiruthika, G.V.M. 203
- Behr, G., see Kreyssig, A. 215
- Behr, G., see Krutzler, C. 208, 263, 291
- Behr, G., see Lascialfari, A. 206
- Behr, G., see Lipp, D. 206
- Behr, G., see Müller, K.-H. 207, 232, 247, 248, 267, 269, 270
- Behr, G., see Naidyuk, Yu.G. 213, 227, 269
- Behr, G., see Schneider, Ma. 239, 267
- Behr, G., see Souptel, D. 205, 206, 240, 291
- Behr, G., see von Lips, H. 210
- Belai, N. 346, 354
- Belai, N., see Zimmermann, M. 366
- Belashchenko, K.D., see Kortus, J. 185
- Belevtsev, B.I. 219
- Belevtsev, B.I., see Naugle, D.G. 270
- Belger, A., see Behr, G. 204
- Belger, A., see Lipp, D. 206
- Bellingeri, E., see Ferdeghini, C. 208
- Beloborod'ko, S.I., see Bobrov, N.L. 228, 229, 240
- Belogolovskii, M., see Khasanov, R. 113
- Belogolovskii, M.A., see Tsindlekht, M.I. 113, 115
- Bel'skii, V.K., see Tat'yanina, I.V. 341
- Beneduce, C., see Ferdeghini, C. 208
- Benelli, C., see Fang, X. 357
- Benesovsky, F., see Rieger, W. 63, 87, 88
- Beno, M., see Dunlap, B.D. 190
- Bensaid, L., see Zhang, C. 346, 353, 373
- Berger, P. 206
- Berger, P., see Alleno, E. 203, 204, 261, 266
- Berger, P., see Tominez, E. 184, 193, 197, 202
- Berger, S., see Gabani, S. 116
- Bergk, B. 230
- Bergk, B., see Maniv, T. 230
- Berkle, A., see Müller, A. 370
- Bernal, S. 18, 30, 49
- Bernès, S., see Durán, A. 198, 205, 250
- Bernhard, C. 191
- Bernhard, C., see Henn, R.W. 184
- Bernhard, C., see Lynn, J.W. 190
- Bernhoeft, N., see Kohgi, M. 246
- Bernhoeft, N.R., see Yelland, E.A. 191
- Bertaut, F. 111
- Bessonov, A.A. 374
- Betts, J., see Goodrich, R.G. 276
- Beugholt, C., see Cronin, L. 370
- Beugholt, C., see Müller, A. 370
- Beuneu, B., see Rotter, M. 255, 256
- Bevan, D.J.M. 3, 8
- Bevan, D.J.M., see Hyde, B.G. 3, 5, 8, 37
- Bevan, D.J.M., see Thornber, M.R. 5
- Bevan, D.J.M., see Schweda, E.D. 4
- Bewley, R.I., see Boothroyd, A.T. 278, 279
- Beyermann, W.P. 278
- Beyermann, W.P., see Bud'ko, S.L. 278, 305

- Beyermann, W.P., see Canfield, P.C. 192  
 Beyermann, W.P., see Cho, B.K. 242, 245, 274  
 Beyermann, W.P., see Christianson, A.D. 279  
 Beyermann, W.P., see Lacerda, A. 278, 279  
 Beyermann, W.P., see Li, S. 278  
 Beyermann, W.P., see Rathnayaka, K.D.D. 278  
 Beyermann, W.P., see Schmiedeshoff, G.M. 193, 232, 240, 274  
 Beyermann, W.P., see Yatskar, A. 194, 242, 278, 279  
 Bhatnagar, A.K. 215, 218, 219  
 Bhatnagar, A.K., see Naugle, D.G. 218  
 Bhatnagar, A.K., see Rathnayaka, K.D.D. 215, 216, 218, 219, 232  
 Bhatt, A., see Liu, G.K. 357  
 Bhattacharjee, J.K., see Lynn, J.W. 188  
 Bi, L.-H. 356  
 Bilc, D., see Salvatore, J.R. 150, 152  
 Bin, L., see Rukang, L. 201  
 Binder, K., see Kinzel, W. 147  
 Bintley, D. 230, 240  
 Birgeneau, R.J., see Aharony, A. 185  
 Bishop, D.J., see Canfield, P.C. 180, 192, 274  
 Bishop, D.J., see Eskildsen, M.R. 276, 277, 280, 285–287, 289, 292  
 Bishop, D.J., see Gammel, P.L. 275, 285, 290, 292  
 Bishop, D.J., see Kogan, V.G. 215, 282  
 Bishop, D.J., see Yaron, U. 280, 289  
 Bitterlich, H. 202, 204, 206, 207, 305  
 Bitterlich, H., see Behr, G. 205  
 Bitterlich, H., see Drechsler, S.-L. 193, 209, 210, 213, 259  
 Bitterlich, H., see Jaenicke-Rössler, U. 239  
 Bitterlich, H., see Yang-Bitterlich, W. 201  
 Blackstead, H.A. 190  
 Blaha, P., see Diviš, M. 210, 212, 240–242, 251–254  
 Blaha, P., see Principi, G. 89  
 Blanco, G., see Bernal, S. 18, 30, 49  
 Blaschkowski, B. 200, 201  
 Blasius, Th., see Bernhard, C. 191  
 Blasius, Th., see Henn, R.W. 184  
 Blasse, G. 340, 372  
 Blount, E.I. 188  
 Bluhm, H. 275, 289, 290  
 Blum, P., see Bertaut, F. 111  
 Blume, M., see Murakami, Y. 248  
 Blumenstein, M., see Bartis, J. 343, 348–350  
 Blundell, S.J., see Nagarajan, R. 277  
 Boaknin, E. 215, 220, 221, 224  
 Boatner, L.A., see Paul, D.McK. 189  
 Bobrov, N.L. 228, 229, 240  
 Bobrov, N.L., see Naidyuk, Yu.G. 227  
 Bobrov, N.L., see Yanson, I.K. 259, 260  
 Bobyl, A.V. 288  
 Bockelmann, W. 79, 80  
 Bodak, O.I., see Gladyshevsky, E.I. 56  
 Bodak, O.I., see Kalychak, Ya.M. 87  
 Bodak, O.I., see Salamakha, P.S. 56, 58, 68, 69  
 Boebinger, G.S., see Christianson, A.D. 279  
 Bögge, H., see Cronin, L. 370  
 Bögge, H., see Müller, A. 370  
 Boglio, C. 353–355, 375  
 Bohn, M., see Ruiz, D. 204  
 Bohn, M., see Tominez, E. 184, 193, 197, 202  
 Bohnen, K.P., see Reichardt, W. 214  
 Bojin, M.D. 82  
 Bolle, C., see Eskildsen, M.R. 276, 287, 289  
 Bolle, C.A., see Eskildsen, M.R. 286, 287  
 Bolletta, F., see Ballardini, R. 372  
 Bommeli, F. 211  
 Boneberg, J., see Leiderer, P. 288  
 Bonhomme, F., see Nyman, M. 375  
 Bonville, P. 278, 295  
 Bonville, P., see Alleno, E. 295  
 Bonville, P., see Boothroyd, A.T. 278, 279  
 Bonville, P., see Godart, C. 195  
 Bonville, P., see Rams, M. 278  
 Boothroyd, A.T. 190, 278, 279  
 Borges, H.A., see El Massalami, M. 250, 309  
 Boring, A.M., see Koelling, D.D. 7  
 Borisova, A.P., see Samokhvalova, E.P. 341, 368  
 Borsa, F., see Sala, R. 278  
 Borsa, F., see Suh, B.J. 209  
 Borzone, G., see Mazzone, D. 66, 67, 69–71, 73, 75, 77  
 Bosing, M., see Krebs, B. 361, 368  
 Boulesteix, C. 14  
 Bourdarot, F. 200  
 Bourdarot, F., see Detlefs, C. 263–265  
 Bourée, F., see Michor, H. 200  
 Bourgeois, L., see Leithe-Jasper, A. 140, 142, 157  
 Bourges, Ph., see Cavadini, N. 246  
 Bowman, A.L., see Von Dreele, R.B. 4, 5  
 Boyer, L.L., see Kortus, J. 185  
 Boysen, H., see Landrum, G.A. 82  
 Bozorth, R.M., see Matthias, B.T. 191  
 Brabers, J.H.V.J. 195  
 Brabers, J.H.V.J., see Mulder, F.M. 196, 198, 255  
 Braithwaite, D., see Aoki, D. 191  
 Braithwaite, D., see Measson, M.-A. 238  
 Braithwaite, D., see Saxena, S.S. 191  
 Braithwaite, D., see Seyfarth, G. 224  
 Brandão, D.E., see da Rocha, F.S. 295

- Brandow, B.H. 223  
 Brandt, E.H. 280  
 Brandt, N.B., see Korsukova, M.M. 136, 138–140, 152  
 Brauer, G. 4  
 Braun, H.F. 191  
 Braun, H.F., see Bauernfeind, L. 190  
 Braun, H.F., see Dertinger, A. 206, 261, 266  
 Braun, H.F., see Schmidt, H. 192, 193, 206, 238, 266, 293  
 Braun, H.F., see Wagner, T.A. 206, 261, 266  
 Braunisch, W. 260  
 Brewer, J.H., see Luke, G.M. 185  
 Brianso, M.C., see Tourné, C.M. 343  
 Brison, J.P. 306  
 Brison, J.P., see Aoki, D. 191  
 Brison, J.P., see Martínez-Samper, P. 215, 229  
 Brison, J.P., see Measson, M.-A. 238  
 Brison, J.P., see Seyfarth, G. 224  
 Brison, J.P., see Suderow, H. 229, 236–238, 277  
 Britton, D., see Lipscomb, W.N. 109, 110  
 Brower, G.D., see Oliver, D.W. 117  
 Brower, G.D., see Slack, G.A. 119  
 Brown, P.J., see Schneider, Mi. 264  
 Brown, S.P. 280  
 Brown, S.P., see Gilardi, R. 280  
 Brücher, E., see Bernhard, C. 191  
 Brüll, P., see Leiderer, P. 288  
 Brüttsch, R., see Khasanov, R. 113  
 Bruzzese, R., see Wang, X. 208  
 Bu, L., see Liu, J. 349  
 Bucher, E. 113  
 Buchgeister, M. 197, 205, 301  
 Buchgeister, M., see Gasser, U. 245, 246, 276, 278  
 Buchgeister, M., see Prassides, K. 242, 253  
 Budantseva, N.A., see Andreev, G.B. 368  
 Budantseva, N.A., see Bessonov, A.A. 374  
 Budantseva, N.A., see Fedoseev, A.M. 368  
 Budiu, T., see Ratiu, C. 374  
 Bud'ko, S.L. 193, 198, 206, 215, 231, 232, 237–240, 272, 274, 275, 278, 293, 295, 304, 305  
 Bud'ko, S.L., see Avila, M.A. 206, 279  
 Bud'ko, S.L., see Canfield, P.C. 192, 242, 257–259, 263, 264, 268, 271, 272, 274  
 Bud'ko, S.L., see Choi, S.-M. 273  
 Bud'ko, S.L., see Christianson, A.D. 279  
 Bud'ko, S.L., see Crespo, M. 275  
 Bud'ko, S.L., see Detlefs, C. 263–265  
 Bud'ko, S.L., see El Massalami, M. 242  
 Bud'ko, S.L., see Fontes, M.B. 200  
 Bud'ko, S.L., see Gammel, P.L. 275, 290  
 Bud'ko, S.L., see Jensen, A. 272  
 Bud'ko, S.L., see Kogan, V.G. 215, 223, 293  
 Bud'ko, S.L., see Li, S. 278  
 Bud'ko, S.L., see Miao, X.Y. 206  
 Bud'ko, S.L., see Rathnayaka, K.D.D. 278  
 Bud'ko, S.L., see Ribeiro, R.A. 206, 250, 258  
 Bud'ko, S.L., see Sánchez, D.R. 239, 257, 268, 296  
 Bud'ko, S.L., see Schmiedeshoff, G.M. 274  
 Bud'ko, S.L., see Silhanek, A.V. 287  
 Bud'ko, S.L., see Song, C. 257  
 Bud'ko, S.L., see Vinnikov, L.Ya. 275, 289, 290, 292  
 Bud'ko, S.L., see Yang, I.-S. 213  
 Bud'ko, S.L., see Yatskar, A. 194, 242, 278, 279  
 Budnyk, S., see Mori, T. 168  
 Budraa, N.K., see Yatskar, A. 194, 242, 278, 279  
 Bujok, V., see Leiderer, P. 288  
 Bulaevskii, L.N. 185  
 Bullett, D.W. 109, 110, 136  
 Bullock, M. 214  
 Bullock, M., see Dervenagas, P. 214  
 Bullock, M., see Kogan, V.G. 215, 282  
 Bullock, M., see Stassis, C. 214  
 Burgemeister, K. 369  
 Burkhardt, U., see Mori, T. 168  
 Burlet, P., see Detlefs, C. 263–265  
 Burma, N.G., see Fil, V.D. 217  
 Bursill, L.A. 20  
 Burton-Pye, B.P., see Zhang, C. 346, 353  
 Burton-Pye, B.P., see Boglio, C. 353–355, 375  
 Buschow, K.H.J. 204  
 Buschow, K.H.J., see Brabers, J.H.V.J. 195  
 Buschow, K.H.J., see Mulder, F.M. 196, 198, 255  
 Buschow, K.H.J., see Mulders, A.M. 276  
 Buseck, P.R. 5, 20  
 But, S., see Lis, S. 340, 365, 372  
 But, S., see Szyzewski, A. 364  
 Butcher, R.J., see Zimmermann, M. 366  
 Buzdin, A., see Brison, J.P. 306  
 Buzdin, A.I., see Bulaevskii, L.N. 185  
 Bychkova, M.I., see Savitskii, E.M. 184  
 Cahill, D.G. 158, 159, 164  
 Cai, Q., see Shan, Y. 349  
 Cai, X.-Z. 369  
 Cai, X.-Z., see Huang, J.-F. 369  
 Calvert, L.D., see Villars, P. 62  
 Calzolari, A., see Daghero, D. 113, 115  
 Campbell, A.J. 263, 264, 271  
 Campbell, A.M., see James, S.S. 208, 289, 290  
 Canepa, F., see Cimberle, M.R. 207  
 Canepa, F., see Grassano, G. 208, 232

- Canepa, F., see Manfrinetti, P. 89  
 Canepa, F., see Moze, O. 89  
 Canfield, P.C. 180, 192, 197, 204, 242, 255, 257–259, 261, 263, 264, 268, 271, 272, 274  
 Canfield, P.C., see Akiyama, H. 238, 267  
 Canfield, P.C., see Alleno, E. 238  
 Canfield, P.C., see Andersen, N.H. 200, 276  
 Canfield, P.C., see Avila, M.A. 206, 279  
 Canfield, P.C., see Beyermann, W.P. 278  
 Canfield, P.C., see Bhatnagar, A.K. 215, 218, 219  
 Canfield, P.C., see Boaknin, E. 215, 220, 221, 224  
 Canfield, P.C., see Bommeli, F. 211  
 Canfield, P.C., see Boothroyd, A.T. 278, 279  
 Canfield, P.C., see Bud'ko, S.L. 193, 206, 215, 231, 232, 237, 239, 240, 272, 274, 275, 278, 293, 304, 305  
 Canfield, P.C., see Bullock, M. 214  
 Canfield, P.C., see Cavadini, N. 246  
 Canfield, P.C., see Cheon, K.O. 212, 213, 285, 293, 295, 296  
 Canfield, P.C., see Cho, B.K. 197, 242, 243, 245, 254, 257, 259, 262, 263, 274, 277, 303, 306, 308  
 Canfield, P.C., see Choi, S.-M. 273  
 Canfield, P.C., see Christianson, A.D. 279  
 Canfield, P.C., see Crespo, M. 275  
 Canfield, P.C., see De Wilde, Y. 280  
 Canfield, P.C., see Dervenagas, P. 197, 214, 242, 257  
 Canfield, P.C., see Detlefs, C. 198–200, 241, 242, 245, 253–255, 263–265  
 Canfield, P.C., see Du Mar, A.C. 232, 240  
 Canfield, P.C., see Dugdale, S.B. 210  
 Canfield, P.C., see Eskildsen, M.R. 276, 277, 280, 284–287, 289, 292  
 Canfield, P.C., see Fisher, I.R. 210, 215, 216, 241, 266  
 Canfield, P.C., see Gammel, P.L. 275, 285, 290, 292  
 Canfield, P.C., see Goldman, A.I. 197, 242, 262  
 Canfield, P.C., see Hennings, B.D. 215, 218–221  
 Canfield, P.C., see Hill, J.P. 262  
 Canfield, P.C., see Hundley, M.F. 114  
 Canfield, P.C., see Jacobs, T. 261  
 Canfield, P.C., see Jaiswal-Nagar, D. 232  
 Canfield, P.C., see Jensen, A. 272  
 Canfield, P.C., see Johnston-Halperin, E. 212  
 Canfield, P.C., see Kogan, V.G. 215, 223, 293  
 Canfield, P.C., see Lacerda, A. 278, 279  
 Canfield, P.C., see Le, L.P. 241  
 Canfield, P.C., see Li, S. 278  
 Canfield, P.C., see Maniv, T. 230  
 Canfield, P.C., see Martínez-Samper, P. 215, 229  
 Canfield, P.C., see Matsuda, N. 238  
 Canfield, P.C., see Mazumdar, C. 278  
 Canfield, P.C., see Metlushko, V. 215, 232, 233, 237, 285  
 Canfield, P.C., see Miao, X.Y. 206  
 Canfield, P.C., see Movshovich, R. 242  
 Canfield, P.C., see Mun, M.-O. 232, 286  
 Canfield, P.C., see Narozhnyi, V.N. 287  
 Canfield, P.C., see Naugle, D.G. 218, 259, 270, 277  
 Canfield, P.C., see Nørgaard, T.K. 276  
 Canfield, P.C., see Oomi, G. 215, 236, 238, 239, 266  
 Canfield, P.C., see Park, T. 227  
 Canfield, P.C., see Price, A.N. 286  
 Canfield, P.C., see Rathnayaka, K.D.D. 197, 215, 216, 218, 219, 232, 236, 242, 263, 278, 296  
 Canfield, P.C., see Rho, H. 244  
 Canfield, P.C., see Ribeiro, R.A. 206, 250, 258  
 Canfield, P.C., see Rybaltchenko, L.F. 270  
 Canfield, P.C., see Sala, R. 278  
 Canfield, P.C., see Schmiedeshoff, G.M. 193, 232, 240, 274  
 Canfield, P.C., see Schneider, Mi. 264  
 Canfield, P.C., see Silhanek, A.V. 287  
 Canfield, P.C., see Song, C. 198, 256, 257  
 Canfield, P.C., see Stassis, C. 214  
 Canfield, P.C., see Sternlieb, B.J. 242  
 Canfield, P.C., see Suderow, H. 229, 277  
 Canfield, P.C., see Suh, B.J. 209  
 Canfield, P.C., see Tomala, K. 255, 256  
 Canfield, P.C., see Uwatoko, Y. 238, 266  
 Canfield, P.C., see Vinnikov, L.Ya. 275, 289, 290, 292  
 Canfield, P.C., see Wills, A.S. 193, 246  
 Canfield, P.C., see Xu, M. 181, 204, 232  
 Canfield, P.C., see Yang, I.-S. 213, 223  
 Canfield, P.C., see Yanson, I.K. 214  
 Canfield, P.C., see Yaron, U. 280, 289  
 Canfield, P.C., see Yatskar, A. 194, 242, 278, 279  
 Canfield, P.C., see Zarestky, J. 197, 242, 271  
 Canfield, P.C., see Zarestky, J.L. 214, 296  
 Canny, J., see Contant, R. 346  
 Cao, G., see Skanthakumar, S. 190  
 Cao, G.H. 208  
 Cao, G.H., see Subba Rao, K. 208  
 Cao, L., see Eversmann, K. 269  
 Cao, S. 220, 221, 232  
 Cao, S., see Mori, K. 306  
 Cao, Y., see Gao, L. 200, 201, 238

- Cappannini, O.M. 239  
 Cappannini, O.M., see Weht, R. 239  
 Carbotte, J.P. 214, 235  
 Carbotte, J.P., see Nicol, E.J. 235  
 Carlos, L.D., see Sousa, F.L. 373  
 Carlson, K.D., see Williams, J.M. 184  
 Caro, P.E. 5  
 Caroli, C. 282  
 Carrington, A., see Fletcher, J.D. 230  
 Carter, S.A. 238, 249  
 Carter, S.A., see Cava, R.J. 180, 184, 197, 202, 300  
 Cassinese, A., see Iavarone, M. 208  
 Catlow, C.R.A., see Hill, S.E. 7  
 Catlow, C.R.A., see Sayle, T.X. 33  
 Cauqui, M.A., see Bernal, S. 18  
 Cava, R.J. 180, 181, 184, 197, 200–202, 240, 242, 300  
 Cava, R.J., see Carter, S.A. 238, 249  
 Cava, R.J., see Eisaki, H. 197, 242, 261  
 Cava, R.J., see Fisher, I.R. 215, 217–219, 239  
 Cava, R.J., see Grigereit, T.E. 197, 242, 262  
 Cava, R.J., see He, T. 184  
 Cava, R.J., see Link, J.R. 203  
 Cava, R.J., see Loureiro, S.M. 196  
 Cava, R.J., see Lynn, J.W. 293  
 Cava, R.J., see Mattheiss, L.F. 196, 210, 212, 243, 250, 252  
 Cava, R.J., see Murayama, C. 238  
 Cava, R.J., see Nohara, M. 222, 226, 297, 301  
 Cava, R.J., see Sarrao, J.L. 197, 202  
 Cava, R.J., see Siegrist, T. 195, 200, 249, 250, 252, 278  
 Cava, R.J., see Takagi, H. 192, 216, 240  
 Cava, R.J., see Zandbergen, H.W. 200–202  
 Cavadini, N. 246  
 Cavaleiro, A.M.V., see Sousa, F.L. 373  
 Cavaleiro, A.M.V., see Almeida Paz, F.A. 344  
 Cella, A.A., see Honig, J.M. 43  
 Chaban, N.F., see Korsukova, M.M. 136, 138–140, 152  
 Chaban, N.F., see Veremchuk, I. 204  
 Chabot, B., see Hovestreydt, E. 83  
 Chabot, B., see Parthé, E. 56  
 Chaikin, P.M., see Jones, T.E. 187  
 Chainani, A., see Yokoya, T. 227, 300  
 Chakhalian, J.A., see Price, A.N. 286  
 Chakoumakos, B.C. 206  
 Chakoumakos, B.C., see Paranthaman, M. 193  
 Chakoumakos, B.C., see Sales, B.C. 164  
 Chandra, G., see Mazumdar, C. 216  
 Chang, J.C., see Lan, M.D. 236, 304  
 Chang, L.J. 200, 242  
 Chaoshui, X., see Rukang, L. 201  
 Charalambous, D., see Brown, S.P. 280  
 Charushnikova, I.A. 368  
 Chau, R., see Bommeli, F. 211  
 Chaves, C.M., see El Massalami, M. 255, 257, 272  
 Chaves, F.A.B., see El Massalami, M. 198, 250, 255, 257, 272, 309  
 Chen, C., see Chen, H. 349  
 Chen, C., see Xiao, Z. 349  
 Chen, C.T., see Baba, T. 227, 228, 274, 300  
 Chen, H. 349  
 Chen, H.-Y., see Yuan, Q. 223, 227  
 Chen, J.W., see Lin, M.S. 259  
 Chen, Q., see Chen, H. 349  
 Chen, Q., see Chu, R.K. 216  
 Chen, Q., see Xiao, Z. 349  
 Chen, S., see Liao, C. 374  
 Chen, X., see Rong, C. 349  
 Chen, X.L., see Chen, Y. 204  
 Chen, Y. 204  
 Chen, Y., see Niu, Z. 349  
 Chen, Y., see Qu, L. 349  
 Chen, Y., see Wang, S. 349  
 Chen, Y., see Zhai, S. 373  
 Chen, Y.-G., see Li, J.-X. 374  
 Chen, Y.-G., see Liu, J.-F. 362  
 Chen, Y.-G., see Liu, J.-F. 374  
 Chen, Y.Y., see Lee, W.H. 184  
 Chen, Y.Y., see Lin, M.S. 259  
 Chenavas, J., see Hodeau, J.L. 90  
 Cheon, K.O. 212, 213, 285, 293, 295, 296  
 Cheon, K.O., see Gammel, P.L. 285, 292  
 Chernobay, V.N., see Bobrov, N.L. 228, 229, 240  
 Chernobay, V.N., see Naidyuk, Yu.G. 227  
 Cherry, B.R., see Nyman, M. 375  
 Cheung, T.T.P. 132  
 Chevalier, B., see Lejay, P. 184  
 Chia, E.E.M. 188, 207, 275  
 Chia, E.E.M., see Park, T. 227  
 Chiang, H.C., see Hsu, Y.Y. 197  
 Chinchure, A.D. 57, 64, 71, 72, 74, 75, 95–97, 200  
 Chinchure, A.D., see Ghosh, G. 306  
 Chinchure, A.D., see Mazumdar, C. 249  
 Chinchure, A.D., see Muñoz-Sandoval, E. 96  
 Chinchure, A.D., see Paulose, P.L. 197  
 Chinchure, A.D., see Prokeš, K. 63, 96  
 Cho, B.K. 57, 86, 93, 98, 197, 209, 241–243, 245, 254, 257, 259, 262, 263, 274, 277, 303, 305, 306, 308, 309  
 Cho, B.K., see Akiyama, H. 238, 267  
 Cho, B.K., see Alleno, E. 238  
 Cho, B.K., see Bommeli, F. 211

- Cho, B.K., see Canfield, P.C. 192, 197, 242, 255, 261, 263, 272
- Cho, B.K., see Dervenagas, P. 197, 214, 242, 257
- Cho, B.K., see Detlefs, C. 242, 245, 255
- Cho, B.K., see Doh, H. 259, 308
- Cho, B.K., see Goldman, A.I. 197, 242, 262
- Cho, B.K., see Hill, J.P. 262
- Cho, B.K., see Jacobs, T. 261
- Cho, B.K., see Jo, Y. 238, 267
- Cho, B.K., see Johnston-Halperin, E. 212
- Cho, B.K., see Jones, C.D.W. 67, 93, 99
- Cho, B.K., see Kim, C.A. 309
- Cho, B.K., see Le, L.P. 241
- Cho, B.K., see Lee, K.H. 286
- Cho, B.K., see Matsuda, N. 238
- Cho, B.K., see Movshovich, R. 242
- Cho, B.K., see Mun, M.-O. 211, 232, 286
- Cho, B.K., see Oomi, G. 215, 236, 238, 239, 266
- Cho, B.K., see Rathnayaka, K.D.D. 197, 215, 216, 218, 219, 232, 242, 263
- Cho, B.K., see Sok, J. 242, 309
- Cho, B.K., see Suh, B.J. 209
- Cho, B.K., see Uwatoko, Y. 238, 266
- Cho, B.K., see Xu, M. 181, 204, 232
- Cho, B.K., see Yang, I.-S. 223
- Cho, B.K., see Yanson, I.K. 214
- Cho, B.K., see Zarestky, J. 197, 242, 271
- Chock, E.P., see Jones, T.E. 187
- Choi, C.K. 293
- Choi, E.M. 309
- Choi, E.M., see Bobyl, A.V. 288
- Choi, E.M., see Choi, J.-H. 238, 264, 309
- Choi, E.M., see Fil, V.D. 198
- Choi, E.M., see Huang, C.L. 226, 227, 232
- Choi, E.M., see Kim, H.-J. 238
- Choi, E.M., see Park, T. 227, 264, 269, 270, 284
- Choi, E.S., see Choi, C.K. 293
- Choi, H.-Y., see Lee, H.C. 222, 223
- Choi, J.-H. 238, 264, 309
- Choi, J.-H., see Choi, E.-M. 309
- Choi, J.-H., see Kim, H.-J. 238
- Choi, S.M. 273
- Choi, S.M., see Fil, V.D. 217
- Choppin, G.R. 340
- Choppin, G.R., see Saito, A. 341, 367
- Choppin, G.R., see Van Pelt, C.E. 351
- Chotkewitsch, W.I., see Schubnikow, L.W. 239
- Christen, D.K. 280
- Christen, D.K., see Kogan, V.G. 282
- Christen, D.K., see Song, K.-J. 287
- Christen, D.K., see Yethiraj, M. 280
- Christensen, N.E., see Cappannini, O.M. 239
- Christensen, N.E., see Weht, R. 239
- Christianson, A.D. 279
- Chu, C.W. 113, 191
- Chu, C.W., see Dezaneti, L.M. 180, 184, 197, 202
- Chu, C.W., see Gao, L. 200, 201, 238
- Chu, C.W., see Wu, M.K. 185
- Chu, R.K. 216
- Chu, W.-L., see Wang, X.-G. 346
- Chu, W.K., see Chu, R.K. 216
- Chubarova, E.V., see Zimmermann, M. 366
- Chubukov, A.V., see Movshovich, R. 242
- Chykhrii, S.I., see Korsukova, M.M. 136, 138–140, 152
- Chykhrij, S., see Kuz'ma, Yu. 56
- Ciabrin, J.P. 350, 351
- Cichorek, T., see Drechsler, S.-L. 236
- Cichorek, T., see Fuchs, G. 236, 296, 297, 300
- Cichorek, T., see Lipp, D. 295, 297, 300, 301
- Cimberle, M.R. 207
- Ciocan-Tarta, I., see Ratiu, C. 374
- Civale, L. 223
- Civale, L., see Silhanek, A.V. 287
- Civale, L., see Thompson, J.R. 215
- Clark, K., see Naugle, D.G. 277
- Coehoorn, R. 210, 251
- Coehoorn, R., see Mulder, F.M. 196, 198, 255
- Coey, J.M.D., see Leithe-Jasper, A. 67, 68, 89, 97
- Coffey, T., see Ignatchik, O. 210, 230
- Cogliati, E., see Andreone, A. 207, 208
- Cohn, J.L., see Nolas, G.S. 164
- Cole, K.S. 145
- Cole, R.H., see Cole, K.S. 145
- Collison, D., see Copping, R. 349
- Collison, D., see Gaunt, A.J. 346
- Conder, K., see Gilardi, R. 280
- Condron, C.L., see Avila, M.A. 206, 279
- Coniglio, A., see Aharony, A. 185
- Conner Jr., R.A., see Dwight, A.E. 82
- Contant, R. 346
- Contant, R., see Belai, N. 346
- Contant, R., see Ciabrin, J.P. 350, 351
- Continentino, M.A., see Fontes, M.B. 200
- Cooke, D.W., see Nagarajan, R. 277
- Cooper, A.S. 184
- Cooper, J.R., see Fisher, I.R. 210, 215–219, 239, 241, 266
- Cooper, L.N., see Bardeen, J. 212
- Cooper, S.L., see Yang, I.-S. 223
- Copping, R. 349
- Corbett, J.D., see Guloy, A.M. 65, 66, 88
- Corchado, P., see Bernal, S. 18
- Corcoran, R. 230

- Corenzwit, E., see Cooper, A.S. 184  
 Corenzwit, E., see Fisk, Z. 113–115  
 Corenzwit, E., see Matthias, B.T. 112–115,  
 184, 186, 187  
 Cornwell, J.C., see Honig, J.M. 43  
 Corrucini, L.R., see Tang, J. 87  
 Cottrell, S.P., see Nagarajan, R. 277  
 Cowley, J.M. 5, 20  
 Cowley, J.M., see Buseck, P.R. 5, 20  
 Cox, D.E., see Ray, S.P. 4  
 Cox, S.F.J., see Nagarajan, R. 277  
 Crabtree, G.W., see Andreone, A. 208, 227  
 Crabtree, G.W., see De Wilde, Y. 280  
 Crabtree, G.W., see Dunlap, B.D. 190  
 Crabtree, G.W., see Iavarone, M. 208  
 Crabtree, G.W., see Metlushko, V. 215, 232,  
 233, 237, 285  
 Creaser, I. 364, 365  
 Crespo, M. 275  
 Cromer, D.T., see Larson, A.C. 81  
 Cronin, L. 370  
 Cronin, S.B., see Dresselhaus, M.S. 165  
 Crooks, W.J., see Van Pelt, C.E. 351  
 Crooks III, W.J. 374  
 Crow, J.E., see Skanthakumar, S. 190  
 Crozier, P., see Sharma, R. 30  
 Crozier, P.A., see Jiang, Y. 7, 33, 34  
 Cruywagen, J.J., see Tytco, K.H. 339  
 Cubitt, R., see Gilardi, R. 280  
 Cubitt, R., see Paul, D.McK. 277  
 Cubitt, R., see Riseman, T.M. 280  
 Cunningham, C.E., see Bud'ko, S.L. 237  
 Cura, Ch. 239  
 Curro, N.J., see Ekimov, E.A. 182, 184  
 Cywinski, R., see Hillier, A.D. 206, 305  
 Cywinski, R., see Rustom, A. 309  
 Czopnik, A. 112, 115  
 Czopnik, A., see Kohout, A. 114–116  
 Czopnik, A., see Murasik, A. 115, 116  
 Czopnik, A., see Narozhnyi, V.N. 252  
  
 da Costa, M.S., see El Massalami, M. 198,  
 200  
 da Rocha, F.S. 215, 295  
 da Silva, C.M., see da Rocha, F.S. 215, 295  
 Daane, A.H., see Gschneidner Jr, K.A. 128  
 Daane, A.H., see Johnson, R.W. 111, 112  
 Daghero, D. 113, 115  
 Dagotto, E. 182  
 Damsma, H., see Havinga, E.E. 184  
 Dan, K., see Inouye, Y. 374  
 Danilkin, S., see Jensen, A. 272  
 Dankova, M., see Antonio, M.R. 365  
 Dankova, M., see Bartis, J. 343, 348–350, 353  
 Dankova, M., see Luo, Q. 353  
  
 Dankova, M., see Luo, Q.-H. 346, 349, 353  
 Dann, J.N., see Wassermann, K. 374  
 Danovich, D.K., see Fedotov, M.A. 348, 349  
 Darby, M.I., see Taylor, K.N.R. 113  
 Darwent, J.R. 372  
 Daudin, L., see Berger, P. 206  
 Davidov, D. 187  
 Davis, M.R., see Luke, G.M. 185  
 Day, V.W. 341  
 de Andrade, M.C., see Li, S. 278  
 de Andrade, M.C., see Rathnayaka, K.D.D.  
 278  
 de Andrade, M.C., see Sarrao, J.L. 197, 202  
 de Andrade, M.C., see Zandbergen, H.W.  
 202  
 De Boer, C., see Schmiedeshoff, G.M. 193  
 de Boer, F.R., see Brabers, J.H.V.J. 195  
 de Boer, F.R., see Mulder, F.M. 196, 198, 255  
 de Gennes, P.G. 114, 127, 133, 193  
 de Gennes, P.G., see Caroli, C. 282  
 De Horrocks Jr, W., see Bartis, J. 353  
 de Melo, M.A.C., see Sánchez, D.R. 257  
 De Wilde, Y. 280  
 De Wilde, Y., see Iavarone, M. 208  
 Décamps, B., see Tominez, E. 184, 197  
 Degiorgi, L. 114  
 Degiorgi, L., see Bommeli, F. 211  
 deGroot, K., see Werheit, H. 158, 159, 163,  
 166  
 Della Mea, M., see Sieberer, M. 200  
 Dellarocca, V., see Daghero, D. 113, 115  
 DeLong, L.E., see Fertig, W.A. 188  
 Demchenko, P., see Salamakha, P.S. 58, 68  
 Demishev, G.B., see Bud'ko, S.L. 238  
 Den Auwer, C., see Charushnikova, I.A. 368  
 Dennis, K.W., see Canfield, P.C. 255  
 Denniss, I.S., see Copping, R. 349  
 Denniss, I.S., see Gaunt, A.J. 346  
 Dertinger, A. 206, 238, 239, 261, 266–268  
 Dertinger, A., see Schmidt, H. 206, 266  
 Dertinger, A., see Wagner, T.A. 206, 261, 266  
 Dervenagas, P. 197, 214, 242, 257  
 Dervenagas, P., see Detlefs, C. 263–265  
 Dervenagas, P., see Goldman, A.I. 197, 242,  
 262  
 Dervenagas, P., see Zarestky, J. 197, 242, 271  
 Detlefs, C. 198–200, 241, 242, 245, 253–255,  
 263–265  
 Detlefs, C., see Hill, J.P. 262  
 Detlefs, C., see Song, C. 198, 257  
 Detlefs, C., see Walker, M.B. 257, 274  
 Detlefs, C., see Wills, A.S. 193, 246  
 Detwiler, J.A., see Schmiedeshoff, G.M. 232,  
 240

- Devereaux, T.P. 229  
 Dewhurst, C.D. 268, 283, 284, 289, 291  
 Dewhurst, C.D., see Eskildsen, M.R. 280  
 Dewhurst, C.D., see Gilardi, R. 280  
 Dewhurst, C.D., see James, S.S. 208, 289, 290  
 Dewhurst, C.D., see Levett, S.J. 281  
 Dewhurst, C.D., see Paul, D.McK. 277  
 Dewhurst, C.D., see Saha, N. 275, 289  
 DeWilde, Y., see Andreone, A. 208, 227  
 Dexter, D.D. 340  
 Dezaneti, L.M. 180, 184, 197, 202  
 Dhar, S.K. 65, 66, 71, 94, 242, 278  
 Dhar, S.K., see Alleno, E. 295  
 Dhar, S.K., see Bonville, P. 278  
 Dhar, S.K., see Godart, C. 204  
 Dhar, S.K., see Gupta, L.C. 242, 253, 255  
 Dhar, S.K., see Hossain, Z. 180, 200, 202, 242, 253, 303, 307  
 Dhar, S.K., see Kiruthika, G.V.M. 203  
 Dhar, S.K., see Mazumdar, C. 180  
 Dhar, S.K., see Nagarajan, R. 180, 203, 242, 253  
 Dhar, S.K., see Paulose, P.L. 197  
 Dhar, S.K., see Rams, M. 278  
 Di Castro, D., see Khasanov, R. 113  
 Díaz-Ortiz, A., see Muñoz-Sandoval, E. 96  
 DiCapua, R., see Iavarone, M. 208  
 Dickey, R.P., see Bauer, E.D. 192  
 Dickey, R.P., see Li, S. 278  
 Dickey, R.P., see Rathnayaka, K.D.D. 278  
 Dickman, M.H. 365  
 Dickman, M.H., see Bassil, B.S. 345, 346, 349  
 Dickman, M.H., see Belai, N. 346  
 Dickman, M.H., see Kim, K.-C. 365, 366  
 Dickman, M.H., see Pope, M.T. 357  
 Dickman, M.H., see Sadakane, M. 350, 353, 354  
 Dickman, M.H., see Wassermann, K. 357  
 Dickman, M.H., see Zimmermann, M. 366  
 Dietz, R.E., see Cheung, T.T.P. 132  
 Dinnebier, R.E., see Dertinger, A. 206, 261, 266  
 Dirksen, G.J., see Blasse, G. 372  
 DiSalvo, F.J., see Cho, B.K. 57, 86, 93, 98  
 DiSalvo, F.J., see Gordon, R.A. 57, 67, 86, 93, 95, 98  
 DiSalvo, F.J., see Jones, C.D.W. 67, 93, 99  
 DiSalvo, F.J., see Niewa, R. 56  
 Divakar, U., see Gilardi, R. 280  
 Diviš, M. 210, 212, 240–242, 251–254  
 Divis, M., see Hilscher, G. 193, 214  
 Dmytrakh, O.V., see Kalychak, Ya.M. 87  
 Dobrosavljević-Grujić, L. 302  
 Dobrosavljević-Grujić, L.J., see Kogan, V.G. 215, 282  
 Doerr, M. 239, 256  
 Doerr, M., see Rotter, M. 255, 256  
 Doh, H. 259, 308  
 Doh, H., see Choi, E.M. 309  
 Doh, H., see Choi, J.-H. 238, 264, 309  
 Doh, H., see Jo, Y. 238, 267  
 Doh, H., see Kim, H.-J. 238  
 Dolbecq, A., see Mialane, P. 346, 354, 355, 371  
 Domaille, P.J., see Knoth, W.H. 356  
 Dong, S., see Liu, J. 373  
 Dong, S., see Zhai, S. 373  
 Dönni, A., see Yamaguchi, T. 246  
 Donohue, J. 87, 88, 92  
 Donzé, P., see Peter, M. 187  
 Dow, J.D., see Blackstead, H.A. 190  
 Downey, J.W., see Dwight, A.E. 82  
 Doyle, R.A., see Dewhurst, C.D. 268, 289, 291  
 Doyle, R.A., see James, S.S. 208  
 Drechsler, S.-L. 193, 209, 210, 212–214, 229, 235, 236, 259, 260, 270, 309  
 Drechsler, S.-L., see Bashlakov, D.L. 229, 241  
 Drechsler, S.-L., see Bitterlich, H. 305  
 Drechsler, S.-L., see Freudenberger, J. 234, 296, 303, 306, 307  
 Drechsler, S.-L., see Fuchs, G. 235, 236, 240, 296, 297, 300  
 Drechsler, S.-L., see Gonnelli, R.S. 215  
 Drechsler, S.-L., see Lascialfari, A. 206  
 Drechsler, S.-L., see Lipp, D. 295–297, 300, 301  
 Drechsler, S.-L., see Müller, K.-H. 193, 207, 222, 232, 247, 248, 267, 269, 270  
 Drechsler, S.-L., see Naidyuk, Yu.G. 213, 227, 269  
 Drechsler, S.-L., see Narozhnyi, V.N. 190  
 Drechsler, S.-L., see Rosner, H. 210, 211, 214, 235, 299  
 Drechsler, S.-L., see Schneider, M. 219  
 Drechsler, S.-L., see Shulga, S.V. 180, 214, 222, 232, 234–237, 240, 241, 259, 298, 301, 308  
 Drechsler, S.-L., see von Lips, H. 210  
 Drechsler, S.-L., see Wälte, A. 182, 185  
 Drechsler, S.-L., see Freudenberger, J. 303, 306, 307  
 Dresselhaus, G., see Dresselhaus, M.S. 165  
 Dresselhaus, M.S. 165  
 Drew, A., see Gilardi, R. 280  
 Drewes, D. 353, 355, 357, 359, 368  
 Drewes, D., see Burgemeister, K. 369  
 Droste, E., see Krebs, B. 361, 368  
 Drzazga, Z. 305  
 Drzazga, Z., see Tomala, K. 255, 256

- Du, Z., see Wang, Z. 373  
 Du, Z.-L., see Wang, Z. 373  
 Du Mar, A.C. 232, 240  
 Duan, L., see An, H. 368  
 Dugdale, S.B. 210  
 Duhayon, C., see Boglio, C. 353–355, 375  
 Dukan, S. 224  
 Dumar, A.C., see Rathnayaka, K.D.D. 219, 236, 296  
 Dunlap, B.D. 190  
 Dunsiger, S.R., see Price, A.N. 286  
 Durán, A. 198, 205, 250  
 Durán, A., see Falconi, R. 238, 260  
 Dusek, C., see Michor, H. 200, 240  
 Duwell, E.J. 81  
 Dwight, A.E. 82  
 Dyck, J.S., see Nolas, G.S. 164  
 Dzevenko, M.V., see Zaremba, V.I. 84  
 Dzyaloshinsky, I.E. 272
- Early, E.A., see Luke, G.M. 185  
 Eckart, M., see Wong, J. 119  
 Eckert, D., see Häse, K. 232  
 Eckert, D., see Müller, K.-H. 237, 258  
 Eckert, D., see Narozhnyi, V.N. 252, 287  
 Eckert, H., see Sebastian, C.P. 80  
 Eckert, J., see Gumbel, A. 202, 205  
 Eckert, J., see Oertel, C.-G. 205  
 Economy, J., see Matkovich, V.I. 107, 109, 136, 138  
 Efimov, Yu.V., see Savitskii, E.M. 184  
 Efros, A.L. 119, 129  
 Eger, R., see Simon, A. 184  
 Egorov, A.I., see Sovestnov, A.E. 41  
 Eibenstein, U. 184  
 Eick, H.A., see Baenziger, N.C. 4, 5  
 Eick, H.A., see Kang, Z.C. 50  
 Eisaki, H. 197, 242, 261  
 Eisaki, H., see Cava, R.J. 180, 181, 184, 197, 200–202, 240, 242  
 Eisaki, H., see Murayama, C. 238  
 Eisaki, H., see Takagi, H. 216, 240  
 Eisenmann, B. 90  
 Eisterer, M., see Krutzler, C. 208, 263, 291  
 Ekimov, E.A. 182, 184  
 Ekino, T. 240  
 El Massalami, M. 194, 197, 198, 200, 242, 250, 255, 257, 272, 293, 309  
 El Massalami, M., see Bud'ko, S.L. 293, 295  
 El Massalami, M., see Rapp, R.E. 198  
 El Massalami, M., see Rotter, M. 256  
 El Massalami, M., see Takeya, H. 216, 236, 309  
 El-Hagary, M. 245, 253, 271, 303, 304, 307  
 El-Hagary, M., see Hilscher, G. 193
- El-Hagary, M., see Manalo, S. 240, 298, 300  
 El-Hagary, M., see Michor, H. 296, 300, 304, 307  
 Elbanowski, M., see Lis, S. 365  
 Elbanowski, M., see Szczyzewski, A. 364  
 Eliashberg, G.M. 234  
 Ellerby, M., see Weller, Th.E. 184  
 Emin, D. 107, 109, 163, 166  
 Emin, D., see Aselage, T.L. 107, 158, 159, 165  
 Emin, D., see Wood, C. 158, 163, 164, 166  
 Emsley, J. 82, 87, 88  
 Endo, K., see Saito, T. 224  
 Endoh, Y., see Murakami, Y. 248  
 Engel, N., see Hovestreydt, E. 83  
 Erb, A., see Brown, S.P. 280  
 Eremets, M.I. 182, 184  
 Erickson, D.J., see Willis, J.O. 187  
 Eriksson, O., see Ravindran, P. 210, 294  
 Ernst, G., see Eskildsen, M.R. 277, 280, 292  
 Ernstberger, B., see Schmidt, H. 206, 266  
 Erwin, R.W., see Lynn, J.W. 188  
 Eschen, M., see Fickscher, Th. 63  
 Eschrig, H., see Drechsler, S.-L. 193, 209, 210, 212–214, 229, 235, 236, 259, 270, 309  
 Eschrig, H., see Müller, K.-H. 207, 232, 247, 248, 267, 269, 270  
 Eschrig, H., see Rosner, H. 210, 211, 214, 235, 299  
 Eschrig, H., see Shulga, S.V. 237, 241  
 Escobar, M.E., see Rigotti, G. 372  
 Escudero, R., see Durán, A. 198, 205, 250  
 Escudero, R., see Falconi, R. 238, 260  
 Eshtiagh-Hosseini, H., see Alizadeh, M.H. 356  
 Eskildsen, M.R. 276, 277, 280, 284–287, 289, 292  
 Eskildsen, M.R., see Gammel, P.L. 275, 285, 292  
 Eskildsen, M.R., see Jaiswal-Nagar, D. 232  
 Eskildsen, M.R., see Jensen, A. 272  
 Eskildsen, M.R., see Nørgaard, T.K. 276  
 Eskildsen, M.R., see Yaron, U. 280, 289  
 Eto, T., see Oomi, G. 239  
 Etourneau, J. 107, 108  
 Etourneau, J., see Lejay, P. 184  
 Ettig, W., see Wagner, T.A. 206, 261, 266  
 Ettouhami, A.M., see Radzihovsky, L. 275  
 Evers, J., see Landrum, G.A. 82  
 Evers, J., see Nuspl, G. 82  
 Eversmann, K. 269  
 Ewert, S., see Cura, Ch. 239  
 Eyhorn, J.M., see Naugle, D.G. 219  
 Eyring, L. 2, 5, 8, 13, 26  
 Eyring, L., see Baenziger, N.C. 4, 5

- Eyring, L., see Boulesteix, C. 14  
 Eyring, L., see Buseck, P.R. 5, 20  
 Eyring, L., see Ferguson, R.E. 2, 3  
 Eyring, L., see Guth, E.D. 2, 3  
 Eyring, L., see Haire, R.G. 8, 9  
 Eyring, L., see Hyde, B.G. 3, 5, 6, 8, 37  
 Eyring, L., see Inaba, H. 43, 44  
 Eyring, L., see Kang, Z.C. 4, 6, 17, 18, 24, 33, 38, 39, 41, 49, 50  
 Eyring, L., see Knappe, P. 4  
 Eyring, L., see Kunzmann, P. 4–6  
 Eyring, L., see Sawyer, J.O. 4  
 Eyring, L., see Schweda, E.D. 4  
 Eyring, L., see Sharma, R. 30  
 Eyring, L., see Skarnulis, A.J. 4  
 Eyring, L., see Summerville, E. 4  
 Eyring, L., see Tuenge, R.T. 4, 10, 37  
 Eyring, L., see Turcotte, R.A. 10  
 Eyring, L., see Turcotte, R.P. 16, 37  
 Eyring, L., see Von Dreele, R.B. 4, 5  
 Eyring, L., see Zhang, J.R. 4, 5
- Fagg, D.P. 45  
 Falconi, R. 238, 260  
 Falconi, R., see Durán, A. 198  
 Fang, K., see Sun, G. 374  
 Fang, X. 357, 360  
 Fang, X., see Zhang, C. 346, 353  
 Farrell, D., see Canfield, P.C. 263  
 Farrell, D.E., see Johnston-Halperin, E. 212  
 Fässler, Th.F., see Schreyer, M. 90  
 Faul, C.F.J., see Zhang, T. 373  
 Fauth, F., see Gasser, U. 245, 246, 276, 278  
 Fay, D. 186, 191  
 Fedoseev, A.M. 349, 368  
 Fedoseev, A.M., see Andreev, G.B. 368  
 Fedoseev, A.M., see Bessonov, A.A. 374  
 Fedoseev, A.M., see Charushnikova, I.A. 368  
 Fedoseev, A.M., see Grigor'ev, M.S. 368  
 Fedoseev, A.M., see Yusov, A.B. 351, 352, 368, 373  
 Fedotov, M.A. 343–345, 348, 349  
 Fedotov, M.A., see Gavrilova, L.O. 341  
 Fedotov, M.A., see Petrukchina, M.A. 341  
 Fedotov, M.A., see Samokhvalova, E.P. 341  
 Fehrenbacher, R. 190  
 Felder, R.J., see Cava, R.J. 180, 181, 184, 197, 202, 240, 242, 300  
 Felner, I. 190–192, 196, 198, 241, 255, 293, 295  
 Felner, I., see Blackstead, H.A. 190  
 Felner, I., see Godart, C. 195  
 Felner, I., see Prozorov, R. 240  
 Felner, I., see Tsindlekht, M.I. 113, 115  
 Felser, C. 210  
 Felser, C., see Gulden, T. 184
- Felser, C., see Loureiro, S.M. 196  
 Felser, C., see Pöttgen, R. 57, 63, 77, 81, 95  
 Feng, , see Cai, X.-Z. 369  
 Feng, J. 374  
 Feng, J., see Sun, G. 374  
 Feng, W., see Zhang, T.R. 373  
 Ferdeghini, C. 208  
 Ferdeghini, C., see Cimberle, M.R. 207  
 Ferdeghini, C., see Grassano, G. 208, 232  
 Ferdeghini, C., see Wang, X. 208  
 Ferguson, R.E. 2, 3  
 Fernandez, J.F., see Anderico, C.Z. 147  
 Fernandez-Baca, J.A. 187  
 Ferrando, V., see Ferdeghini, C. 208  
 Ferreira, A.C.A.S., see Sousa, F.L. 373  
 Ferreira, R.A.S., see Sousa, F.L. 373  
 Ferrell, R.A., see Fulde, P. 188  
 Ferrell, R.A., see Lynn, J.W. 188  
 Ferro, R., see Marazza, R. 65–75, 83, 90  
 Ferro, R., see Mazzone, D. 65–71, 73–78, 80  
 Fertig, W.A. 188  
 Feyerherm, R., see Le, L.P. 241  
 Fickenscher, Th. 63  
 Fickenscher, Th., see Kraft, R. 96  
 Fiedler, J., see Johnston-Halperin, E. 212  
 Fiel, R.J., see Gilbert, J. 374  
 Field, S.B., see James, S.S. 289, 290  
 Fieselmann, H.L., see Zhang, C. 345–347, 351, 352  
 Fil, D.V., see Fil, V.D. 217  
 Fil, V.D. 198, 217  
 Filippov, V., see Khasanov, R. 113  
 Filippov, V., see Wang, Y. 113  
 Filippov, V.B., see Daghero, D. 113, 115  
 Filippov, V.B., see Tsindlekht, M.I. 113, 115  
 Filoti, G., see Principi, G. 89  
 Fink, H.J. 184  
 Fink, J., see Behr, G. 205  
 Fink, J., see Drechsler, S.-L. 193, 212, 214  
 Fink, J., see Mazumdar, C. 278  
 Fink, J., see von Lips, H. 210  
 Finnemore, D.K., see Canfield, P.C. 197, 242, 261  
 Finnemore, D.K., see Johnston-Halperin, E. 212  
 Finnemore, D.K., see Xu, M. 181, 204, 232  
 Finskaya, V., see Tomilo, Zh.M. 202  
 Finskaya, V.M., see Tomilo, Zh.M. 202  
 Fischer, H.E., see Cahill, D.G. 158, 159, 164  
 Fischer, Ø. 184, 185, 188, 190, 194  
 Fischer, Ø., see Ishikawa, M. 188, 189  
 Fischer, Ø., see Maple, M.B. 184, 185, 188, 189  
 Fischer, O., see Peter, M. 187  
 Fisher, I.R. 210, 215–219, 239, 241, 266

- Fisher, I.R., see Bluhm, H. 275, 289, 290  
 Fisher, I.R., see Canfield, P.C. 204  
 Fisher, I.R., see Cheon, K.O. 212, 213, 285, 293, 295, 296  
 Fisher, I.R., see Dugdale, S.B. 210  
 Fisher, I.R., see Eskildsen, M.R. 285  
 Fisher, I.R., see Gammel, P.L. 285, 292  
 Fisher, I.R., see Kogan, V.G. 215  
 Fisk, Z. 112–115  
 Fisk, Z., see Goodrich, R.G. 276  
 Fisk, Z., see Hundley, M.F. 114  
 Fisk, Z., see Movshovich, R. 57, 66, 67, 94  
 Fisk, Z., see Sarrao, J.L. 197, 202  
 Fisk, Z., see Zandbergen, H.W. 202  
 Fisun, V.V., see Yanson, I.K. 214  
 Fitzgerald, R.W., see Fisk, Z. 112  
 Flachbart, K. 112, 115  
 Flachbart, K., see Gabani, S. 112–116  
 Flachbart, K., see Kohout, A. 114–116  
 Flachbart, K., see Paderno, Y.B. 111, 112, 114, 115  
 Flachbart, K., see Siemensmeyer, K. 114–116  
 Fleming, R.M., see Cava, R.J. 300  
 Fletcher, J.D. 230  
 Flint, C.D., see Darwent, J.R. 372  
 Flouquet, J., see Aoki, D. 191  
 Flouquet, J., see Brison, J.P. 306  
 Flouquet, J., see Measson, M.-A. 238  
 Flouquet, J., see Saxena, S.S. 191  
 Flouquet, J., see Seyfarth, G. 224  
 Fomicheva, E.B., see Tat'yanina, I.V. 341  
 Fomicheva, L.N., see Narozhnyi, V.N. 217, 279  
 Foner, S., see Shapira, Y. 155  
 Fontana, F., see Andreone, A. 208, 227  
 Fontes, M.B. 200  
 Fontes, M.B., see Baggio-Saitovitch, E.M. 200, 255  
 Fontes, M.B., see Bud'ko, S.L. 198, 238, 293, 295  
 Fontes, M.B., see Sánchez, D.R. 257, 268  
 Forgan, E.M., see Brown, S.P. 280  
 Forgan, E.M., see Gilardi, R. 280  
 Forgan, E.M., see Paul, D.McK. 277  
 Forgan, E.M., see Riseman, T.M. 280  
 Forgan, E.M., see Yethiraj, M. 280  
 Fornasini, M.L. 57, 63, 76, 77, 81  
 Fornasini, M.L., see Manfrinetti, P. 89  
 Fornasini, M.L., see Merlo, F. 70, 76, 77, 79–81  
 Fornasini, M.L., see Moze, O. 89  
 Foulkes, I.F. 191  
 Fournier, J.M. 113  
 Frade, J.R., see Fagg, D.P. 45  
 Fraga, G.L.F., see da Rocha, F.S. 295  
 Francesconi, L.C., see Antonio, M.R. 365  
 Francesconi, L.C., see Bartis, J. 343, 348–350, 353  
 Francesconi, L.C., see Boglio, C. 353–355, 375  
 Francesconi, L.C., see Howell, R.C. 360  
 Francesconi, L.C., see Luo, Q. 353  
 Francesconi, L.C., see Luo, Q.-H. 346, 349, 353  
 Francesconi, L.C., see Zhang, C. 345–347, 351–353, 360, 373  
 Franck, J.P., see Lawrie, D.D. 212, 213  
 Frederick, N.A., see Bauer, E.D. 246  
 Frederick, N.A., see Li, S. 278  
 Fredrich, M.F., see Day, V.W. 341  
 Freeman, A.J., see Youn, S.J. 210, 211  
 Freeman, E.J., see Li, S. 278  
 Freudenberger, J. 202, 205, 207, 217, 234, 268, 296, 303, 306, 307, 309  
 Freudenberger, J., see Behr, G. 205  
 Freudenberger, J., see Drechsler, S.-L. 193, 209, 212–214, 236, 259  
 Freudenberger, J., see Fuchs, G. 236, 240, 296, 297, 300  
 Freudenberger, J., see Kreyszig, A. 198, 199, 264, 307  
 Freudenberger, J., see Lipp, D. 295–297, 300, 301  
 Freudenberger, J., see Loewenhaupt, M. 263  
 Freudenberger, J., see Müller, K.-H. 258, 266  
 Freudenberger, J., see Narozhnyi, V.N. 216, 217, 252  
 Freudenberger, J., see Rotter, M. 244, 246, 278  
 Freudenberger, J., see Sierks, C. 244, 278  
 Fu, F., see Xue, G. 362  
 Fu, L., see Wang, J. 373  
 Fu, L.S., see Wang, J. 373  
 Fuchs, G. 235, 236, 240, 296, 297, 300  
 Fuchs, G., see Bashlakov, D.L. 229, 241  
 Fuchs, G., see Bitterlich, H. 207, 305  
 Fuchs, G., see Buchgeister, M. 197, 301  
 Fuchs, G., see Drechsler, S.-L. 193, 209, 210, 212–214, 236, 259  
 Fuchs, G., see Drzazga, Z. 305  
 Fuchs, G., see Eversmann, K. 269  
 Fuchs, G., see Freudenberger, J. 205, 207, 217, 234, 268, 296, 303, 306, 307, 309  
 Fuchs, G., see Fuger, R. 291  
 Fuchs, G., see Kreyszig, A. 198, 199, 264, 269, 307  
 Fuchs, G., see Krutzler, C. 208, 263, 291  
 Fuchs, G., see Lipp, D. 295–297, 300, 301  
 Fuchs, G., see Müller, K.-H. 193, 207, 222, 232, 237, 247, 248, 258, 266–270  
 Fuchs, G., see Naidyuk, Yu.G. 213, 227, 269

- Fuchs, G., see Narozhnyi, V.N. 216, 217, 252, 287
- Fuchs, G., see Schneider, M. 219
- Fuchs, G., see Shulga, S.V. 180, 214, 222, 232, 234, 235, 240, 241, 259, 298, 308
- Fuchs, G., see Souptel, D. 240, 291
- Fuchs, G., see Wälte, A. 182, 185
- Fuger, R. 291
- Fuger, R., see Krutzler, C. 208, 263, 291
- Fugmann, A., see Pöttgen, R. 67
- Fujii, H., see Arisawa, S. 207, 208
- Fujii, H., see Ekino, T. 240
- Fukaya, K. 357, 358
- Fukazawa, H. 222
- Fulde, P. 186, 188, 303
- Fulde, P., see Amici, A. 268
- Fulde, P., see Keller, J. 186
- Fulde, P., see Zwicknagl, G. 189, 191, 306
- Furomoto, S., see Shimizu, K. 182, 186
- Furrer, A., see Gasser, U. 198, 241, 244–246, 276, 278
- Furukawa, N., see Kawano-Furukawa, H. 273–275
- Gabani, S. 112–116
- Gabani, S., see Flachbart, K. 112, 115
- Gabani, S., see Siemensmeyer, K. 114–116
- Gabovich, A.M. 192
- Gabus, R., see Ratiu, C. 374
- Gaitonde, D.M., see Verma, A.K. 200
- Galadzhun, Ya.V. 90
- Galadzhun, Ya.V., see Kalychak, Ya.M. 86, 87
- Galera, R.-M., see El Massalami, M. 255, 309
- Gallagher, G.A., see Baker, L.C.W. 340
- Galli, M., see El-Hagary, M. 271
- Gallien, J.-P., see Berger, P. 206
- Galstyan, E., see Felner, I. 191
- Galvin, L.M., see Riseman, T.M. 280
- Gama, G.J., see Dickman, M.H. 365
- Gama, G.J., see Kim, K.-C. 365, 366
- Gammel, P.L. 275, 285, 290, 292
- Gammel, P.L., see Canfield, P.C. 180, 192, 274
- Gammel, P.L., see Cheon, K.O. 285, 293, 295, 296
- Gammel, P.L., see Choi, S.M. 273
- Gammel, P.L., see Eskildsen, M.R. 276, 277, 280, 284–287, 289, 292
- Gammel, P.L., see Kogan, V.G. 215, 282
- Gammel, P.L., see Yaron, U. 280, 289
- Gandolfi, M.T., see Mulazzani, Q.G. 372
- Gangopadhyay, A.K. 200, 206
- Gangopadhyay, A.K., see Looney, C. 238
- Gao, L. 200, 201, 238
- Gao, L., see Wu, M.K. 185
- Gao, L.-h., see Xin, X.-l. 374
- Garbauskas, M., see Slack, G.A. 138, 158, 159, 163, 166
- Garg, K.B., see Kumari, K. 210
- Garland, M.T., see Ruiz, D. 204
- Gasparov, V.A. 113, 115, 237
- Gasser, U. 198, 241, 244–246, 276, 278
- Gasser, U., see Allenspach, P. 245
- Gasser, U., see Mulders, A.M. 276
- Gasser, U., see Schneider, M. 264
- Gatica, J.M., see Bernal, S. 30, 49
- Gaunt, A.J. 346
- Gaunt, A.J., see Copping, R. 349
- Gavaler, J.R. 185
- Gavrilova, L.O. 341
- Geballe, T.H., see Hannay, N.B. 182
- Geballe, T.H., see Matthias, B.T. 112–115, 184
- Gegenwart, P., see Drechsler, S.-L. 236
- Gegenwart, P., see Fuchs, G. 236, 296, 297, 300
- Gegenwart, P., see Lipp, D. 295, 297, 300, 301
- Geibel, C., see Hossain, Z. 249
- Geibel, C., see Steglich, F. 195
- Geiser, U., see Williams, J.M. 184
- Gelato, M.L. 82
- Gelato, M.L., see Parthé, E. 82
- Ghivelder, L., see El Massalami, M. 293
- Ghosh, G. 306
- Gianni, L., see Iavarone, M. 208
- Giannini, E., see Manfrinetti, P. 89
- Gibbs, D., see Detlefs, C. 241, 242, 245, 253–255
- Gibbs, D., see Hill, J.P. 262
- Gibbs, D., see Murakami, Y. 248
- Gignoux, D. 107, 108
- Gilardi, R. 280
- Gilbert, J. 374
- Gingerich, K., see Brauer, G. 4
- Ginzburg, V.L. 185, 187, 232
- Giordanengo, B., see Bud'ko, S.L. 198, 293, 295
- Giordanengo, B., see El Massalami, M. 200, 242
- Giordanengo, B., see Fontes, M.B. 200
- Giorgi, A.L. 184
- Giorgi, A.L., see Krupka, M.C. 184
- Gippius, A.A., see Korsukova, M.M. 136, 138–140, 152
- Gladczuk, L., see Szymczak, R. 271
- Gladun, A., see Drechsler, S.-L. 193, 209, 212, 213, 236, 259
- Gladun, A., see Fuchs, G. 236, 296, 297, 300
- Gladun, A., see Lipp, D. 206, 295–297, 300, 301
- Gladun, A., see Schneider, M. 219

- Gladun, A., see Schneider, Ma. 239, 267  
 Gladyshevskii, E.I. 56, 84  
 Gladyshevskii, R.E., see Grin, Yu.N. 56  
 Gladyshevsky, R.E. 83  
 Glarum, S.H., see Rosseinsky, M.J. 182, 184  
 Gloos, K., see Flachbart, K. 112, 115  
 Go, G.S., see Lee, K.H. 286  
 Godart, C. 195, 204  
 Godart, C., see Alleno, E. 203–205, 207, 242, 249, 261, 266, 295, 309  
 Godart, C., see Berger, P. 206  
 Godart, C., see Bonville, P. 278, 295  
 Godart, C., see Dhar, S.K. 242, 278  
 Godart, C., see Felner, I. 293, 295  
 Godart, C., see Ghosh, G. 306  
 Godart, C., see Gupta, L.C. 242, 253, 255  
 Godart, C., see Hossain, Z. 180, 202, 242, 249, 253  
 Godart, C., see Lynn, J.W. 197, 209, 242, 244, 245, 249, 250, 253, 257, 292  
 Godart, C., see Mazumdar, C. 180, 216, 249  
 Godart, C., see Nagarajan, R. 180, 203, 242, 253, 277  
 Godart, C., see Paulose, P.L. 197  
 Godart, C., see Rams, M. 278  
 Godart, C., see Rauchschalbe, U. 250  
 Godart, C., see Sanchez, J.P. 209, 243  
 Godart, C., see Sinha, S.K. 197, 242, 271  
 Godart, C., see Tominez, E. 184, 193, 197, 202  
 Godwal, B.K., see Meenakshi, S. 239  
 Godwal, B.K., see Verma, A.K. 200  
 Golden, M.S., see Drechsler, S.-L. 193, 212, 214  
 Golden, M.S., see Mazumdar, C. 278  
 Golden, M.S., see von Lips, H. 210  
 Goldman, A.I. 197, 242, 262  
 Goldman, A.I., see Bullock, M. 214  
 Goldman, A.I., see Dervenagas, P. 197, 214, 242, 257  
 Goldman, A.I., see Detlefs, C. 198, 241, 242, 245, 253–255  
 Goldman, A.I., see Hill, J.P. 262  
 Goldman, A.I., see Song, C. 198, 256, 257  
 Goldman, A.I., see Stassis, C. 214  
 Goldman, A.I., see Sternlieb, B.J. 242  
 Goldman, A.I., see Yaron, U. 280, 289  
 Goldman, A.I., see Zarestky, J. 197, 214, 242, 271  
 Goldman, A.I., see Zarestky, J.L. 296  
 Goldschmidt, V.M. 3  
 Goldsmid, H.J., see Nolas, G.S. 158  
 Goldstein, W., see Wong, J. 119  
 Golikova, O.A. 107, 109, 119, 159  
 Goll, G. 235  
 Goll, G., see Nguyen, L.H. 210  
 Golnik, A., see Bernhard, C. 191  
 Golubev, A.M., see Gavrilova, L.O. 341  
 Gomes, A.A., see da Rocha, F.S. 215, 295  
 Gonçalves, A.P., see Kuznietz, M. 293  
 Gonnelli, R.S. 215  
 Gonnelli, R.S., see Daghero, D. 113, 115  
 Gonnelli, R.S., see Gonnelli, R.S. 215  
 Good, W., see Song, C. 257  
 Goodenough, J.B. 248  
 Goodman, B.B. 287  
 Goodrich, R.G. 276  
 Goodwin, T.J., see Tang, J. 87  
 Gopalakrishnan, K.V., see Nagarajan, R. 180  
 Gopalakrishnan, J., see Luke, G.M. 185  
 Gordon, R.A. 57, 67, 86, 93, 95, 98  
 Gordon, R.A., see Cho, B.K. 57, 86, 93, 98  
 Gordon, R.A., see Jones, C.D.W. 67, 93, 99  
 Gor'kov, L.P. 187, 232, 285  
 Gor'kov, L.P., see Abrikosov, A.A. 186, 303  
 Gortenmulder, T.J., see Chinchure, A.D. 64, 71, 72, 74, 75, 95, 96  
 Gortenmulder, T.J., see Zandbergen, H.W. 202  
 Goryo, J., see Izawa, K. 224  
 Gotaas, J.A., see Lynn, J.W. 188  
 Goto, H., see Shiozaki, R. 374  
 Goto, T., see Oomi, G. 238  
 Goto, T., see Watanuki, R. 115  
 Goto, T., see Yamaguchi, T. 246  
 Gradinger, H., see Brauer, G. 4  
 Graham, J., see Thornber, M.F. 5  
 Granada, C.M., see da Rocha, F.S. 215, 295  
 Grant, J.B., see Mailhiot, C. 182  
 Grassano, G. 208, 232  
 Grassano, G., see Ferdeghini, C. 208  
 Grassano, G., see Wang, X. 208  
 Gratz, E., see Fournier, J.M. 113  
 Graw, G. 206  
 Graw, G., see Behr, G. 204, 205  
 Graw, G., see Bitterlich, H. 206  
 Graw, G., see Gonnelli, R.S. 215  
 Gray, P.E., see Wood, C. 163, 164  
 Grazioli, C., see von Lips, H. 210  
 Greenblatt, M., see Shuk, P. 44  
 Grest, G.S., see Levin, K. 307  
 Grest, G.S., see Nass, M.J. 306  
 Grewe, N. 279  
 Griese, R.F., see Matkovich, V.I. 107  
 Griessen, R., see Wijngaarden, R.J. 182  
 Griffith, W.P. 349, 374  
 Grigereit, T.E. 197, 242, 262  
 Grigereit, T.E., see Sinha, S.K. 197, 242, 271  
 Grigor'ev, M.S. 368  
 Grigor'ev, M.S., see Fedoseev, A.M. 368  
 Grin, Yu.N. 56

- Grin, Yu.N., see Gladyshevsky, R.E. 83  
 Grin, Yu.N., see Mori, T. 140, 168  
 Grin, Yu.N., see Sichevich, O.M. 88  
 Grishin, A.M., see Ström, V. 202, 205  
 Grobelna, B., see Lis, S. 372  
 Grosche, F.M., see Saxena, S.S. 191  
 Grover, A.K., see Jaiswal-Nagar, D. 232, 286  
 Grübel, G., see Detlefs, C. 199, 200  
 Gruen, D.M. 3  
 Grütz, A., see Braunisch, W. 260  
 Grytsiv, A., see Sieberer, M. 200  
 Gschneidner Jr., K.A. 117, 128  
 Gschneidner Jr., K.A., see Tang, J. 87  
 Gu, T., see Detlefs, C. 198  
 Guan, H., see Cai, X.-Z. 369  
 Guan, H.-M., see Cai, X.-Z. 369  
 Guan, W.Y., see Ku, H.C. 184, 197, 202  
 Guasconi, P., see Cimberle, M.R. 207  
 Gubbens, P.C.M., see Mulders, A.M. 276  
 Guette, A., see Naslain, R. 107, 109, 110  
 Guikema, J.W., see Bluhm, H. 275, 289, 290  
 Guillot, M., see Durán, A. 198  
 Gukasov, A., see Kohgi, M. 246  
 Gulay, L.D. 57, 58, 62–84, 86, 87, 91, 93, 95  
 Gulay, L.D., see Kaczorowski, D. 65–67, 98  
 Gulay, L.D., see Melnyk, G. 63, 64, 66–77  
 Gulay, L.D., see Tran, V.H. 73, 99  
 Gulden, T. 184  
 Gulden, T., see Henn, R.W. 184  
 Gulden, T., see Pöttgen, R. 57  
 Guloy, A.M. 65, 66, 88  
 Gümbel, A. 202, 205  
 Gümbel, A., see Bitterlich, H. 207  
 Gunnarsson, O. 182  
 Günther, K., see Graw, G. 206  
 Guo, D., see Niu, J. 346  
 Guo, J., see Liu, J. 362  
 Guo, J., see Liu, J.-F. 362, 374  
 Guo, Y., see Ma, J. 368  
 Gupta, A., see Kirfel, A. 142  
 Gupta, L.C. 192, 193, 242, 253, 255, 307  
 Gupta, L.C., see Alleno, E. 242, 249, 295  
 Gupta, L.C., see Bonville, P. 278, 295  
 Gupta, L.C., see Chinchure, A.D. 200  
 Gupta, L.C., see Dhar, S.K. 242, 278  
 Gupta, L.C., see Fuchs, G. 240  
 Gupta, L.C., see Ghosh, G. 306  
 Gupta, L.C., see Godart, C. 195, 204  
 Gupta, L.C., see Hossain, Z. 180, 200, 202, 242, 249, 253, 303, 307  
 Gupta, L.C., see Jacobs, T. 261  
 Gupta, L.C., see Kiruthika, G.V.M. 203, 206  
 Gupta, L.C., see Kumari, K. 210  
 Gupta, L.C., see Lynn, J.W. 197, 209, 242, 244, 245, 249, 250, 253, 257, 292  
 Gupta, L.C., see Mazumdar, C. 180, 216, 249  
 Gupta, L.C., see Meenakshi, S. 239  
 Gupta, L.C., see Nagarajan, R. 180, 192, 193, 203, 242, 253, 277  
 Gupta, L.C., see Paulose, P.L. 197  
 Gupta, L.C., see Rams, M. 278  
 Gupta, L.C., see Rauchschalbe, U. 250  
 Gupta, L.C., see Sanchez, J.P. 209, 243  
 Gupta, L.C., see Sinha, S.K. 197, 242, 271  
 Gupta, L.C., see Verma, A.K. 200  
 Gupta, L.C., see Watanabe, T. 274  
 Gurevich, A. 215, 236, 284  
 Gurevich, A., see Aranson, I. 288  
 Gurin, V.N., see Korsukova, M.M. 136, 138–140, 152  
 Gurin, V.N., see Tanaka, T. 157  
 Gusev, A.I. 184  
 Guth, E.D. 2, 3  
 Guth, E.D., see Ferguson, R.E. 2, 3  
 Gygax, F.N., see Le, L.P. 241  
 Gygi, F. 282  
 Gyorffy, B.L., see Foulkes, I.F. 191  
 Gyorgy, E.M., see Cava, R.J. 200, 201  
 Haas, M.K., see He, T. 184  
 Haas, St. 224  
 Haas, St., see Maki, K. 223  
 Haas, St., see Parker, D. 223  
 Haas, St., see Won, H. 223  
 Habuta, E., see Kawano-Furukawa, H. 275  
 Habuta, E., see Takeya, H. 309  
 Haddon, R.C., see Rosseinsky, M.J. 182, 184  
 Haga, Y., see Kasahara, Y. 306  
 Hagel, J., see Ignatchik, O. 210, 230  
 Hagenmuller, P., see Lejay, P. 184  
 Hagenmuller, P., see Naslain, R. 107, 109, 110  
 Haire, R.G. 8, 9  
 Haldane, F.D.M. 130  
 Halet, J.-F., see Ruiz, D. 204  
 Halet, J.F., see Bauer, J. 140  
 Hall, D., see Goodrich, R.G. 276  
 Hamada, K. 111, 113  
 Hamid, A.S. 210  
 Han, K.S., see Lee, K.H. 286  
 Han, S.H., see Sarrao, J.L. 197, 202  
 Han, S.H., see Zandbergen, H.W. 202  
 Hanaguri, T., see Takaki, K. 223, 300  
 Hanaguri, T., see Watanabe, T. 223  
 Hanaguri, T., see Yokoya, T. 227  
 Handstein, A., see Drzazga, Z. 305  
 Handstein, A., see Eversmann, K. 269  
 Handstein, A., see Freudenberger, J. 217, 268, 303  
 Handstein, A., see Fuchs, G. 235, 240

- Handstein, A., see Gumbel, A. 202, 205  
Handstein, A., see Kreyssig, A. 264, 269  
Handstein, A., see Müller, K.-H. 237, 258, 268, 269  
Handstein, A., see Narozhnyi, V.N. 216, 217  
Handstein, A., see Schneider, M. 219  
Handstein, A., see Wälte, A. 182  
Hannay, N.B. 182  
Hanzawa, K. 114  
Hao, N., see An, H. 368  
Harada, K., see Eskildsen, M.R. 277, 280, 292  
Harada, K., see Gammel, P.L. 275  
Haraguchi, N. 350  
Harima, H., see Yamauchi, K. 210, 211, 231  
Harima, H., see Yokoya, T. 227  
Harlow, R.L., see Knoth, W.H. 339, 356  
Harmalker, S.P., see Alizadeh, M.H. 364  
Harmon, B.N., see Cho, B.K. 243, 262, 263  
Harmon, B.N., see Dervenagas, P. 214  
Harmon, B.N., see Kogan, V.G. 215, 282  
Harmon, B.N., see Rhee, J.Y. 210, 211, 285  
Harmon, B.N., see Song, C. 198, 256  
Harmon, B.N., see Suh, B.J. 209  
Harris, I.R. 86  
Harrison, J.C., see Zandbergen, H.W. 202  
Harrison, N., see Goodrich, R.G. 276  
Häse, K. 207, 208, 232  
Häse, K., see Wimbush, S.C. 208  
Hasegawa, T., see Watanabe, T. 274  
Haselwimmer, R.K.W., see Saxena, S.S. 191  
Hasenknopf, B., see Boglio, C. 353–355, 375  
Hatano, M., see Otsuka, K. 46, 47  
Hatano, T., see Arisawa, S. 207, 208  
Haupt, E.T.K., see Müller, A. 370  
Hauser, R., see El-Hagary, M. 271  
Hauser, R., see Michor, H. 200, 307  
Hausermann-Berg, L.S., see Shelton, R.N. 191  
Havinga, E.E. 184  
Haworth, C., see Terashima, T. 230  
Hayden, S.M., see Yelland, E.A. 191  
Hayward, M.A., see He, T. 184  
He, T. 184  
Hebard, A.F., see Rosseinsky, M.J. 182, 184  
Heckel, M.C., see Creaser, I. 364, 365  
Hedegård, P., see Andersen, N.H. 200, 276  
Hedegård, P., see Jensen, A. 272  
Hedegård, P., see Jensen, J. 277, 292  
Hedegård, P., see Nørgaard, T.K. 276  
Heffner, R.H., see Le, L.P. 241  
Heid, R., see Reichardt, W. 214  
Heinecke, M. 240  
Heinecke, M., see Goll, G. 235  
Heinecke, M., see Nguyen, L.H. 210  
Heinecke, M., see Shulga, S.V. 180, 214, 222, 232, 234, 235, 240, 241, 259, 298, 308  
Heinonen, M., see Kumari, K. 210  
Hejna, C., see Slack, G.A. 138, 158, 159, 163, 166  
Helliwell, M., see Copping, R. 349  
Helliwell, M., see Gaunt, A.J. 346  
Hellmann, P., see Steglich, F. 195  
Hemley, R.J., see Eremets, M.I. 182, 184  
Hendrikx, R.W.A., see Chinchure, A.D. 64, 71, 72, 74, 75, 95, 96  
Hendrikx, R.W.A., see Muñoz-Sandoval, E. 96  
Henggeler, W., see Gasser, U. 245, 246, 276, 278  
Henn, R.W. 184  
Henn, R.W., see Gulden, T. 184  
Hennings, B.D. 215, 218–221  
Hennings, B.D., see Belevtsev, B.I. 219  
Hennings, B.D., see Naugle, D.G. 219  
Herbeck, F.E., see Volkova, L.M. 196  
Hermann, J., see Zandbergen, H.W. 202  
Hermansson, K., see Yang, Z. 7, 33  
Herminghaus, S., see Leiderer, P. 288  
Herrmann, J., see Sarrao, J.L. 197, 202  
Herrmannsdoerfer, T., see Gabani, S. 112–115  
Hervé, G., see Robert, F. 362  
Hess, H.F., see Nakai, N. 229  
Heusler, O. 89  
Hewat, A.W., see Paul, D.McK. 189  
Hidaka, Y., see Luke, G.M. 185  
Hiebl, K., see Gulay, L.D. 63, 64, 69, 71–76, 93, 95  
Hiebl, K., see Weitzer, F. 65, 67–69, 88, 93, 96  
Higashi, I. 107, 118, 122, 123, 125, 126, 136, 159  
Higemoto, W., see Ohishi, K. 300  
Hill, C.L. 339  
Hill, C.L., see Fang, X. 357, 360  
Hill, C.L., see Kholdeeva, O.A. 352, 374  
Hill, H.H., see Chu, C.W. 113  
Hill, J.P. 262  
Hill, J.P., see Detlefs, C. 198, 241, 242, 245, 253–255  
Hill, J.P., see Murakami, Y. 248  
Hill, R.W., see Boaknin, E. 215, 220, 221, 224  
Hill, S.E. 7  
Hillberg, M., see Sánchez, D.R. 257  
Hillenbrand, B. 187  
Hillenbrand, B., see Peter, M. 187  
Hillier, A.D. 206, 305  
Hillier, A.D., see Rustom, A. 309  
Hilscher, G. 193, 214, 240, 241, 293, 305

- Hilscher, G., see Diviš, M. 210, 212, 240–242, 251–254
- Hilscher, G., see El-Hagary, M. 245, 253, 271, 303, 304, 307
- Hilscher, G., see Manalo, S. 240, 298, 300
- Hilscher, G., see Michor, H. 200, 240, 296, 300, 304, 307
- Hilscher, G., see Sieberer, M. 200
- Hinks, D.G., see Dunlap, B.D. 190
- Hinz, D., see Wälte, A. 185
- Hirano, T., see Takeya, H. 204, 205
- Hirata, K., see Arisawa, S. 207, 208
- Hirata, K., see El Massalami, M. 255
- Hirata, K., see Izawa, K. 227
- Hirata, K., see Nishimori, H. 229, 280–282, 284
- Hirata, K., see Takeya, H. 258, 309
- Hirata, K., see Togano, K. 184
- Hirata, K., see Zhao, S.R. 308
- Hiroi, M., see Sera, M. 219–221, 261
- Hirota, K., see Murakami, Y. 248
- Hirschfeld, P.J., see Kübert, C. 302
- Hirst, R., see Russell, V. 182
- Ho, J.C., see Jiang, P.J. 197
- Ho, J.C., see Lin, M.S. 259
- Ho, P.-C., see Bauer, E.D. 246
- Hoard, J.L. 107, 109, 110
- Hodeau, J.L. 90, 91
- Hodges, J.A., see Bonville, P. 278, 295
- Hodges, J.A., see Godart, C. 195
- Hodges, J.A., see Rams, M. 278
- Hoellwarth, C.C. 293
- Hoffmann, R., see Bojin, M.D. 82
- Hoffmann, R., see Johnston, R.L. 85
- Hoffmann, R., see Landrum, G.A. 82
- Hoffmann, R., see Nuspl, G. 82
- Hoffmann, R.-D. 80, 81
- Hoffmann, R.-D., see Kalychak, Ya.M. 56, 93
- Hoffmann, R.-D., see Kraft, R. 96
- Hoffmann, R.-D., see Kußmann, D. 57
- Hoffmann, R.-D., see Pöttgen, R. 57, 67, 87
- Hoffmann, R.-D., see Sebastian, C.P. 80
- Hoffmann, R.-D., see Zaremba, V.I. 84
- Hoffmann, R.-D., see Zumdick, M.F. 82
- Hofmann, M., see Kreyssig, A. 264, 307
- Hohenberg, P.C. 232, 285
- Holden, J.R., see Guth, E.D. 2, 3
- Holubar, T., see Michor, H. 240
- Holzapfel, B., see Bashlakov, D.L. 229, 241
- Holzapfel, B., see Cao, G.H. 208
- Holzapfel, B., see Häse, K. 207, 208, 232
- Holzapfel, B., see Reibold, M. 208
- Holzapfel, B., see Subba Rao, K. 208
- Holzapfel, B., see Wimbush, S.C. 208, 232, 233, 271, 287
- Holzapfel, C., see Kortz, U. 354, 357
- Honda, F., see Oomi, G. 238
- Honda, K., see Oomi, G. 238
- Honda, Z., see Bullock, M. 214
- Hong, Z., see Rukang, L. 201
- Honig, J.M. 43
- Hoogenboom, B.W., see Eskildsen, M.R. 280
- Hor, P.H., see Wu, M.K. 185
- Horn, F.H., see Slack, G.A. 158, 159
- Horrocks Jr., W.D., see Howell, R.C. 360
- Horrocks Jr., W.D., see Luo, Q. 353
- Horrocks Jr., W.D., see Luo, Q.-H. 346, 349, 353
- Hoser, A., see Kreyssig, A. 264, 307
- Hoskins, B.F. 5
- Hossain, Z. 180, 200, 202, 242, 249, 253, 303, 307
- Hossain, Z., see Alleno, E. 242, 249
- Hossain, Z., see Bonville, P. 278, 295
- Hossain, Z., see Dhar, S.K. 242, 278
- Hossain, Z., see Godart, C. 195, 204
- Hossain, Z., see Gupta, L.C. 242, 253, 255
- Hossain, Z., see Jacobs, T. 261
- Hossain, Z., see Lynn, J.W. 197, 209, 242, 244, 245, 249, 250, 253, 257, 292
- Hossain, Z., see Mazumdar, C. 216
- Hossain, Z., see Meenakshi, S. 239
- Hossain, Z., see Nagarajan, R. 180, 193, 203, 242, 253, 277
- Hossain, Z., see Rams, M. 278
- Hossain, Z., see Sanchez, J.P. 209, 243
- Hossain, Z., see Sinha, S.K. 197, 242, 271
- Hossain, Z., see Watanabe, T. 274
- Hotta, T. 248
- Hou, Z., see Liao, C. 374
- Hough, D., see Häse, K. 208
- Hovestreydt, E. 83
- Howell, R.C. 360
- Howell, R.C., see Boglio, C. 353–355, 375
- Howell, R.C., see Luo, Q. 353
- Howell, R.C., see Luo, Q.-H. 346, 349, 353
- Howell, R.C., see Zhang, C. 345–347, 351–353, 360, 373
- Hsu, L.-S., see Wang, Y.K. 306
- Hsu, Y.Y. 197
- Hsu, Y.Y., see Lin, M.S. 259
- Hu, C., see Wang, E. 349
- Hu, C., see Wang, Y. 373
- Hu, H., see Xue, G. 362
- Hu, Z., see Mazumdar, C. 278
- Hu, Z., see von Lips, H. 210
- Hu, Z., see Wang, Z. 373
- Hu, Z.-G., see Wang, Z. 373
- Huang, C.-C., see Sun, R.-Q. 346
- Huang, C.L. 226, 227, 232

- Huang, J.-F. 369  
Huang, J.-F., see Cai, X.-Z. 369  
Huang, J.-S., see Wu, C.-D. 341  
Huang, Q., see Bourdarot, F. 200  
Huang, Q., see Grigereit, T.E. 197, 242, 262  
Huang, Q., see He, T. 184  
Huang, Q., see Lynn, J.W. 197, 209, 242, 244, 245, 249, 250, 253, 257, 292, 293  
Huang, R., see Liu, J. 349  
Huang, R., see Wang, E. 349  
Huang, R., see Wang, X. 349  
Huang, R.-D., see Bi, L.-H. 356  
Huang, Z.J., see Wu, M.K. 185  
Hughes, R.E., see Hoard, J.L. 107, 109, 110  
Hughes, R.J., see Dugdale, S.B. 210  
Hujita, H., see Inouye, Y. 374  
Hull, G.W., see Matthias, B.T. 112–115, 184  
Hulliger, F., see Rupp, B. 198  
Hults, W.L., see Nagarajan, R. 277  
Hundley, M.F. 114  
Hundley, M.F., see Canfield, P.C. 197, 242, 261  
Hundley, M.F., see Movshovich, R. 57, 66, 67, 94, 242  
Huse, D.A., see Eskildsen, M.R. 276, 287, 289  
Huse, D.A., see Yaron, U. 280, 289  
Huser, D. 145  
Hüser, D. 187  
Hutchings, M.T. 245  
Huxley, A., see Aoki, D. 191  
Huxley, A., see Saxena, S.S. 191  
Hwang, C.-D., see Kim, H. 210  
Hyde, B.G. 3, 5, 6, 8, 37, 91  
Hyde, B.G., see Bursill, L.A. 20  
Hyde, B.G., see Sawyer, J.O. 4
- Iandelli, A. 57, 64, 66–68, 70, 71, 73, 75, 78  
Iavarone, M. 208  
Iavarone, M., see Andreone, A. 207, 208, 227  
Iavarone, M., see De Wilde, Y. 280  
Iball, J. 342, 344  
Ichihara, J., see Inagaki, A. 374  
Ichihara, J., see Kera, Y. 374  
Ichihara, J., see Shiozaki, R. 374  
Ichioka, M., see Adachi, H. 223  
Ichioka, M., see Miranović, P. 227  
Ichioka, M., see Nakai, N. 229, 284, 285  
Iga, F. 114, 127, 128  
Iga, F., see Kasaya, M. 114, 127, 128  
Iga, F., see Michimura, S. 115  
Ignatchik, O. 210, 230  
Ignatchik, O., see Maniv, T. 230  
Ihm, J., see Kim, H. 210  
Ijiri, Y., see Gordon, R.A. 57, 67, 95  
Ikeda, H., see Fukazawa, H. 222  
Ikeda, K., see Otsuka-Yao-Matsuo, S. 18, 47  
Ikeda, S., see Kitō, H. 200, 201  
Imanaka, N., see Adachi, G.-y. 8, 56  
Inaba, H. 43, 44  
Inagaki, A. 374  
Inagaki, A., see Kera, Y. 374  
Inagaki, A., see Shiozaki, R. 343, 374  
Inoue, M. 342, 344, 345  
Inouye, Y. 374  
Inumara, K., see He, T. 184  
Ionov, V.M., see Tat'yanina, I.V. 340  
Ishihara, M., see Watanuki, R. 115  
Ishii, T., see Higashi, I. 125, 126  
Ishii, Y., see Mori, T. 134, 135  
Ishikawa, E., see Yamase, T. 370  
Ishikawa, M. 188, 189  
Ishizawa, Y. 161  
Ishizawa, Y., see Higashi, I. 118, 122, 123, 159  
Ishizawa, Y., see Tanaka, T. 120, 122, 123, 135, 136, 138  
Isida, S. 214  
Isida, S., see Suzuki, M. 198  
Islam, A.H.M.Z., see Detlefs, C. 198, 241, 242, 245, 253, 254  
Islam, Z., see Song, C. 198  
Isobe, T., see Haraguchi, N. 350  
Isshiki, M., see Nohara, M. 222, 226, 297, 300, 301  
Ito, T. 373  
Ito, T., see Higashi, I. 136  
Itoh, J., see Yokoya, T. 227  
Iwamoto, Y. 223  
Iwasa, K., see Kohgi, M. 246  
Iwasawa, T., see Kasahara, Y. 306  
Iwata, M., see Kobayashi, Y. 239, 267  
Izawa, K. 220, 224, 227, 284  
Izawa, K., see Matsuda, Y. 224, 226  
Izawa, K., see Seyfarth, G. 224  
Izu, N., see Otsuka-Yao-Matsuo, S. 18, 47  
Izumi, F., see Mori, T. 134, 135
- Jäckel, M., see Ignatchik, O. 210, 230  
Jacobs, H., see Bockelmann, W. 79, 80  
Jacobs, H., see Niewa, R. 56  
Jacobs, T. 261  
Jaenicke-Rössler, U. 239  
Jain, S., see Howell, R.C. 360  
Jaiswal-Nagar, D. 232, 286  
Jaiswal-Nagar, D., see Raychaudhuri, P. 227, 284  
Jambrich, C., see El-Hagary, M. 271  
James, S.S. 208, 289, 290  
James, S.S., see Dewhurst, C.D. 289

- Jang, H., see Won, H. 223  
Janocko, M.A., see Gavalier, J.R. 185  
Jansen, A.G.M., see Goll, G. 235  
Jansen, A.G.M., see Nguyen, L.H. 210  
Jansen, A.G.M., see Rybaltchenko, L.F. 270  
Jansen, A.G.M., see Yanson, I.K. 214  
Jansen, J., see Zandbergen, H.W. 200  
Janssen, S., see Staub, U. 247  
Jarlborg, T., see Dugdale, S.B. 210  
Jeannin, Y., see Alizadeh, M.H. 364  
Jeannin, Y., see Robert, F. 362  
Jeitschko, W., see Kanatzidis, M.G. 57  
Jeng, G.Y., see Lan, M.D. 236, 304  
Jenkins, M.S., see Turcotte, R.P. 16, 37  
Jennings, G., see Antonio, M.R. 365  
Jensen, A. 272  
Jensen, J. 272, 277, 292  
Jensen, J., see Andersen, N.H. 200, 276  
Jensen, J., see Jensen, A. 272  
Jensen, J., see Nørgaard, T.K. 276  
Jensen, T.B.S., see Andersen, N.H. 200, 276  
Jepsen, O., see Gulden, T. 184  
Jepsen, O., see Nguyen, L.H. 210  
Jestadt, Th., see Nagarajan, R. 277  
Jezowski, A., see Paderno, Y.B. 111, 112, 114, 115  
Jiang, H. 349  
Jiang, J., see Zhai, S. 373  
Jiang, L., see Yue, B. 356  
Jiang, M. 373  
Jiang, M., see Wu, Z. 374  
Jiang, P.J. 197  
Jiang, Y. 7, 33, 34  
Jiao, F., see Yue, B. 356  
Jin, S.-L., see Yue, B. 356  
Jin, Z., see Liu, Z. 346  
Jin, Z., see Shan, Y. 346  
Jing, H., see Blaschkowski, B. 200, 201  
Jo, Y. 238, 267  
Jobiliong, E., see Ignatchik, O. 210, 230  
Johansen, T.H., see Bobyl, A.V. 288  
Johansson, B., see Ravindran, P. 210, 294  
Johansson, B., see Skorodumova, N.V. 7  
Johnson, M.J., see Shelton, R.N. 191  
Johnson, R.W. 111, 112  
Johnston, D.C., see Canfield, P.C. 197, 242, 261  
Johnston, D.C., see Cho, B.K. 197, 242, 243, 245, 254, 257, 259, 262, 263, 274, 277, 303, 306, 308  
Johnston, D.C., see Fertig, W.A. 188  
Johnston, D.C., see Goldman, A.I. 197, 242, 262  
Johnston, D.C., see Johnston-Halperin, E. 212  
Johnston, D.C., see Mun, M.-O. 286  
Johnston, D.C., see Suh, B.J. 209  
Johnston, D.C., see Xu, M. 181, 204, 232  
Johnston, D.C., see Zarestky, J. 197, 242, 271  
Johnston, R.L. 85  
Johnston-Halperin, E. 212  
Johnston-Halperin, E., see Canfield, P.C. 263  
Johrendt, D., see Pöttgen, R. 94  
Jones, C.D.W. 67, 93, 99  
Jones, C.D.W., see Cho, B.K. 57, 86, 93, 98  
Jones, C.D.W., see Gordon, R.A. 67, 86, 93, 98  
Jones, C.K., see Gavalier, J.R. 185  
Jones, E.C., see Brown, S.P. 280  
Jones, T.E. 187  
Jooss, Ch., see Wimbush, S.C. 208, 287  
Jorgensen, J.D., see Dunlap, B.D. 190  
Joshi, V.N., see Gilbert, J. 374  
Joss, W., see Goll, G. 235  
Julian, S.R., see Brison, J.P. 306  
Julian, S.R., see Saxena, S.S. 191  
Jun, J., see Mironov, A. 142, 143  
Jun, J., see Sologubenko, A.V. 224  
Jung, M.-H., see Bud'ko, S.L. 237  
Jung, W., see Eibenstein, U. 184  
Junod, A., see Peter, M. 187  
Junod, A., see Wang, Y. 113, 237  
Just, G. 195, 198  
Kaczorowski, D. 65–67, 98  
Kadono, R., see Luke, G.M. 185  
Kadono, R., see Ohishi, K. 300  
Kadowaki, K., see Abliz, M. 265  
Kadowaki, K., see Arisawa, S. 207, 208  
Kadowaki, K., see Kawano, H. 242, 273  
Kadowaki, K., see Kawano-Furukawa, H. 214, 273–275  
Kadowaki, K., see Sera, M. 219–221, 261  
Kadowaki, K., see Takeya, H. 204, 205  
Kadowaki, K., see Terashima, T. 230  
Kagayama, T., see Matsuda, N. 238  
Kagayama, T., see Oomi, G. 215, 236, 238, 239, 266  
Kaindl, G., see Drechsler, S.-L. 214  
Kaindl, G., see Mazumdar, C. 278  
Kaindl, G., see von Lips, H. 210  
Kaji, S., see Akiyama, H. 238, 267  
Kaji, S., see Oomi, G. 239  
Kakuta, K., see Ohishi, K. 300  
Kalatsky, V.A. 265  
Kalatsky, V.A., see Canfield, P.C. 263  
Kalychak, Ya.M. 56, 86, 87, 93  
Kalychak, Ya.M., see Gulay, L.D. 63–65, 67–77, 81, 86, 87  
Kalychak, Ya.M., see Zaremba, R.I. 84  
Kalychak, Ya.M., see Zaremba, V.I. 84

- Kamata, K., see Izawa, K. 220, 224, 227, 284  
 Kamiya, K., see Tanaka, T. 159  
 Kamta, M., see Venturini, G. 64, 66–70, 76, 90, 91  
 Kanamori, J. 248  
 Kanatzidis, M.G. 57, 158  
 Kanatzidis, M.G., see Salvatore, J.R. 150, 152  
 Kanda, F.A., see Russell, V. 182  
 Kandpal, H.C., see Melnyk, G. 63, 64, 66–77  
 Kaneko, K. 248  
 Kaneko, S., see Nakai, N. 229  
 Kaneko, S.-I., see Nishimori, H. 229, 280–282, 284  
 Kang, W.N., see Bobyl, A.V. 288  
 Kang, Z.C. 4, 6, 14, 17, 18, 24, 33, 38, 39, 41, 49, 50  
 Kang, Z.C., see Adachi, G.-y. 8  
 Kang, Z.C., see Eyring, L. 26  
 Kang, Z.C., see Sharma, R. 30  
 Kanis, J.M., see Havinga, E.E. 184  
 Karpinski, J., see Fletcher, J.D. 230  
 Karpinski, J., see Kogan, V.G. 215, 293  
 Karpinski, J., see Mironov, A. 142, 143  
 Karpinski, J., see Sologubenko, A.V. 224  
 Kasahara, Y. 306  
 Kasaya, M. 114, 127, 128  
 Kasaya, M., see Iga, F. 114, 127, 128  
 Kasper, J.S., see Richards, S.M. 117  
 Kasper, J.S., see Slack, G.A. 138, 158, 159, 163, 166  
 Kassab, D., see Gilbert, J. 374  
 Kastner, M.A., see Aharony, A. 185  
 Kasuya, T. 114, 115, 127, 128, 133  
 Kasuya, T., see Iga, F. 114, 127, 128  
 Kasuya, T., see Kasaya, M. 114, 127, 128  
 Kataev, V., see Braunisch, W. 260  
 Katayama-Yoshida, H., see Yamauchi, K. 210, 231  
 Kato, Y., see Izawa, K. 227  
 Kato, Y., see Takaki, K. 223, 300  
 Katsumata, K., see Mulders, A.M. 207, 232, 247, 248, 267, 269, 270  
 Katz, J.J., see Gruen, D.M. 3  
 Kawae, T., see Choi, J.-H. 264, 309  
 Kawano, H. 242, 273  
 Kawano-Furukawa, H. 214, 273–275  
 Kawano-Furukawa, H., see Takeya, H. 309  
 Kawashima, I., see Yamase, T. 368  
 Kawata, H., see Murakami, Y. 248  
 Kazakov, S., see Mironov, A. 142, 143  
 Kazakov, S.M., see Fletcher, J.D. 230  
 Kazakov, S.M., see Sologubenko, A.V. 224  
 Kazanskii, L.P., see Molchanov, V.N. 343, 346  
 Kazansky, L., see Fedotov, M.A. 343–345  
 Kazansky, L.P., see Inoue, M. 342, 344, 345  
 Kealey, P.G., see Brown, S.P. 280  
 Kealey, P.G., see Paul, D.McK. 277  
 Kealey, P.G., see Riseman, T.M. 280  
 Kealhofer, C., see Link, J.R. 203  
 Kealhofer, C., see Loureiro, S.M. 196  
 Keimer, B., see Lynn, J.W. 190  
 Keita, B., see Belai, N. 346  
 Keita, B., see Lu, Y.-W. 351  
 Keller, H., see Khasanov, R. 113  
 Keller, H., see Landau, I.L. 224  
 Keller, J. 186  
 Keller, J., see Fulde, P. 188, 303  
 Keller, L., see Murasik, A. 115, 116  
 Keller, N., see Brison, J.P. 306  
 Keppens, V., see Sales, B.C. 164  
 Kera, Y. 374  
 Kera, Y., see Inagaki, A. 374  
 Kera, Y., see Shiozaki, R. 343, 374  
 Kera, Y., see Yasuhara, Y. 374  
 Kerchner, H.R., see Christen, D.K. 280  
 Kes, P.H., see Saha, N. 275, 289  
 Khaliullin, G., see van den Brink, J. 247, 248  
 Kharton, V.V., see Fagg, D.P. 45  
 Khasanov, R. 113  
 Khmelevskiy, S., see Diviš, M. 210, 212, 240–242, 251, 252  
 Kholdeeva, O.A. 352, 374  
 Khomskii, D., see Braunisch, W. 260  
 Khomskii, D., see van den Brink, J. 247, 248  
 Khomskii, D.I. 248  
 Khomskii, D.I., see Kugel, K.I. 247, 248  
 Khoshnavazi, R., see Alizadeh, M.H. 356  
 Kido, G., see Mori, T. 122, 130, 143  
 Kiefl, R.F., see Luke, G.M. 185  
 Kiefl, R.F., see Ohishi, K. 300  
 Kiefl, R.F., see Price, A.N. 286  
 Kikkawa, A., see Mulders, A.M. 207, 232, 247, 248, 267, 269, 270  
 Kikugawa, N., see Sudhakar Rao, G.V. 191  
 Kim, C.A. 309  
 Kim, C.A., see Cho, B.K. 309  
 Kim, C.A., see Jo, Y. 238, 267  
 Kim, D.H., see Lee, K.H. 286  
 Kim, H. 210  
 Kim, H.-J. 238  
 Kim, H.-J., see Chia, E.E.M. 188, 207, 275  
 Kim, H.-J., see Choi, J.-H. 264, 309  
 Kim, H.B., see Cho, B.K. 305  
 Kim, H.C., see Jo, Y. 238, 267  
 Kim, H.J., see Bobyl, A.V. 288  
 Kim, H.J., see Park, T. 227, 264, 269, 270, 284  
 Kim, I.G., see Lee, J.I. 210  
 Kim, J.D., see Song, C. 257  
 Kim, J.D., see Fil, V.D. 217  
 Kim, J.D., see Huang, C.L. 226, 227, 232

- Kim, J.H., see Mun, M.-O. 211  
 Kim, J.S., see Cho, B.K. 57, 86, 93, 98  
 Kim, J.S., see Jones, C.D.W. 67, 93, 99  
 Kim, J.S., see Kremer, R.K. 182  
 Kim, K.-C. 365, 366  
 Kim, K.-C., see Dickman, M.H. 365  
 Kim, K.S., see Ström, V. 202, 205  
 Kim, M.-S., see Mun, M.-O. 232  
 Kim, Y.J., see Mun, M.-O. 211  
 Kimura, N., see Yelland, E.A. 191  
 Kimura, T., see Shimizu, K. 182, 186  
 Kimura, T., see Suzuki, M. 198  
 Kindo, K., see Abliz, M. 265  
 King, A.J., see Russell, V. 182  
 Kini, A.M., see Williams, J.M. 184  
 Kinoshita, K., see Uehara, M. 182  
 Kinzel, W. 147  
 Kirfel, A. 142  
 Kiruthika, G.V.M. 203, 206  
 Kiss, T., see Baba, T. 227, 228, 274, 300  
 Kiss, T., see Yokoya, T. 222, 227, 284, 295, 300  
 Kistler, M.L., see Liu, G.K. 357  
 Kitaguchi, H., see Arisawa, S. 207, 208  
 Kitano, H., see Takaki, K. 223, 300  
 Kitazawa, H., see Kitô, H. 200, 201  
 Kitazawa, H., see Mori, T. 122, 130, 143  
 Kitazawa, K., see Takaki, K. 223, 300  
 Kitazawa, K., see Watanabe, T. 274  
 Kitô, H. 200, 201  
 Kito, H., see Yokoya, T. 227  
 Kittel, C., see Ruderman, M.A. 133  
 Klausen, S.N., see Nørgaard, T.K. 276  
 Klauß, H.-H., see Sánchez, D.R. 257  
 Klavins, P., see Hoellwarth, C.C. 293  
 Klavins, P., see Lynn, J.W. 188  
 Klavins, P., see Shelton, R.N. 191  
 Klavins, P., see Stanley, H.B. 191  
 Klehe, A.-K., see Looney, C. 238  
 Klein, M.V., see Rho, H. 244  
 Klein, M.V., see Yang, I.-S. 213, 223  
 Klemperer, W.G., see Day, V.W. 341  
 Klenke, J., see Jensen, A. 272  
 Klepp, K., see Hovestreydt, E. 83  
 Klinowski, J., see Almeida Paz, F.A. 344  
 Klonkowski, A.M., see Lis, S. 372  
 Klosowski, J., see Buchgeister, M. 197, 301  
 Knappe, P. 4  
 Knauf, N., see Braunisch, W. 260  
 Knigavko, A., see Fil, V.D. 198  
 Knoth, W.H. 339, 356  
 Knott, H., see Dwight, A.E. 82  
 Knupfer, M., see Drechsler, S.-L. 214  
 Knupfer, M., see von Lips, H. 210  
 Kobayash, S., see Sera, M. 219–221, 261  
 Kobayashi, K., see Higashi, I. 118, 122, 123, 159  
 Kobayashi, N., see Sera, M. 219–221, 261  
 Kobayashi, T., see Yamase, T. 373  
 Kobayashi, Y. 239, 267  
 Kochetkov, V.N., see Freudenberger, J. 217  
 Kochetkov, V.N., see Narozhnyi, V.N. 216, 217, 279  
 Kock, A., see Braunisch, W. 260  
 Koda, A., see Ohishi, K. 300  
 Koehler, W.C., see Gruen, D.M. 3  
 Koelling, D.D. 7  
 Koenig, Y., see Gabani, S. 112–115  
 Koepernik, K., see Drechsler, S.-L. 193, 212, 214, 236  
 Koepernik, K., see Freudenberger, J. 306  
 Koepernik, K., see Rosner, H. 210, 211, 214, 235, 299  
 Koga, T., see Dresselhaus, M.S. 165  
 Kogan, V.G. 215, 223, 282, 286, 293  
 Kogan, V.G., see Bud'ko, S.L. 232  
 Kogan, V.G., see Cheon, K.O. 285, 293, 295, 296  
 Kogan, V.G., see Eskildsen, M.R. 284  
 Kogan, V.G., see Gammel, P.L. 275, 285  
 Kogan, V.G., see Gurevich, A. 215, 284  
 Kogan, V.G., see Vinnikov, L.Ya. 275, 289, 290, 292  
 Kögerler, P., see Cronin, L. 370  
 Kohara, T., see Iwamoto, Y. 223  
 Kohgi, M. 246  
 Kohlbrecher, J., see Brown, S.P. 280  
 Kohmoto, M., see Shiraishi, J. 233  
 Kohout, A. 114–116  
 Koizumi, A., see Takaki, K. 223, 300  
 Kolesnichenko, Yu.A. 231  
 Kominami, H., see Inagaki, A. 374  
 Kominami, H., see Kera, Y. 374  
 Kominami, H., see Shiozaki, R. 343, 374  
 Kominami, H., see Yasuhara, Y. 374  
 Konczykowski, M., see Izawa, K. 227  
 Kong, Z.-P., see Yue, B. 356  
 Kontani, H. 223  
 Kontani, K., see Shimizu, K. 182, 186  
 Kordis, J., see Bevan, D.J.M. 3, 8  
 Korsukova, M.M. 136, 138–140, 152  
 Kortan, A.R., see Rosseinsky, M.J. 182, 184  
 Kortus, J. 185  
 Kortz, U. 353, 354, 357  
 Kortz, U., see Bassil, B.S. 345, 346, 349  
 Kortz, U., see Zimmermann, M. 366  
 Kosaka, M., see Yamauchi, H. 203, 247  
 Koshelev, A., see Metlushko, V. 215, 232, 233, 237, 285  
 Koshelev, A.E., see De Wilde, Y. 280

- Kosugi, M., see Ekino, T. 240  
 Kotzyba, G., see Kraft, R. 96  
 Kotzyba, G., see Pöttgen, R. 57, 63, 77, 81, 95  
 Koyama, I., see Murakami, Y. 248  
 Koyama, K., see Saito, T. 224  
 Kozik, M., see Gilbert, J. 374  
 Kraft, E., see Bartis, J. 343, 348–350  
 Kraft, R. 96  
 Krajewski, J.J., see Carter, S.A. 238, 249  
 Krajewski, J.J., see Cava, R.J. 180, 181, 184, 197, 200–202, 240, 242, 300  
 Krajewski, J.J., see Eisaki, H. 197, 242, 261  
 Krajewski, J.J., see Grigereit, T.E. 197, 242, 262  
 Krajewski, J.J., see Lynn, J.W. 293  
 Krajewski, J.J., see Siegrist, T. 195, 200, 249, 250, 252, 278  
 Krajewski, J.J., see Takagi, H. 216, 240  
 Krajewski, J.J., see Zandbergen, H.W. 200, 201  
 Kramer, L. 286  
 Kramer, M., see Avila, M.A. 206, 279  
 Krämer, U., see Behr, G. 204  
 Krämer, U., see Bitterlich, H. 206  
 Krämer, U., see Cao, G.H. 208  
 Krämer, U., see Graw, G. 206  
 Krämer, U., see Reibold, M. 208  
 Krämer, U., see Yang-Bitterlich, W. 201, 206  
 Kramers, H.A. 244  
 Krause, A., see Wagner, T.A. 206, 261, 266  
 Krebs, B. 361, 368  
 Krebs, B., see Burgemeister, K. 369  
 Krebs, B., see Drewes, D. 353, 355, 357, 359, 368  
 Kritzman, S.R., see Luke, G.M. 185  
 Kremer, R.K. 182  
 Kremer, R.K., see Bernhard, C. 191  
 Kremer, R.K., see Gulden, T. 184  
 Kremer, R.K., see Henn, R.W. 184  
 Kremer, R.K., see Pöttgen, R. 87  
 Kremer, R.K., see Simon, A. 184  
 Krendelsberger, R., see Michor, H. 200  
 Kresin, V.Z., see Ovchinnikov, Y.N. 237  
 Kreyssig, A. 198, 199, 215, 262, 264, 269, 307  
 Kreyßig, A. 199, 262, 263  
 Kreyssig, A., see Dertinger, A. 206, 261, 266  
 Kreyssig, A., see Drechsler, S.-L. 193, 212, 236  
 Kreyssig, A., see Freudenberger, J. 234, 268, 296, 303, 306, 307  
 Kreyssig, A., see Loewenhaupt, M. 263  
 Kreyssig, A., see Müller, K.-H. 266, 268, 269  
 Kreyssig, A., see Schneider, Ma. 239, 267  
 Kreyssig, A., see Schneider, Mi. 264  
 Kreyssig, A., see Souptel, D. 206, 291  
 Krickemeyer, E., see Cronin, L. 370  
 Krikorian, N.H., see Giorgi, A.L. 184  
 Krikorian, N.H., see Krupka, M.C. 184  
 Kripiakevich, P.I., see Gladyshevskii, E.I. 84  
 Krishnamurthy, H.R., see Vidhyadhiraja, N.S. 114  
 Krivchikov, A., see Czopnik, A. 112, 115  
 Krivovichev, S.V. 25  
 Krogmann, K., see Becher, H.J. 63  
 Królas, K., see Rams, M. 278  
 Kronzon, R., see Bartis, J. 343, 348–350  
 Krot, N.N., see Saprykin, A.S. 350  
 Krot, N.N., see Yusov, A.B. 351  
 Kruczynski, Z., see Szczyzewski, A. 364  
 Krug, K., see Drechsler, S.-L. 193, 212  
 Krug, K., see Peng, Z.Q. 259  
 Krug, K., see Shulga, S.V. 180, 214, 222, 232, 234, 235, 240, 241, 259, 298, 308  
 Krug, K., see Winzer, K. 229, 259  
 Krumhansl, J.L., see Nyman, M. 375  
 Krupa, J.-C., see Bessonov, A.A. 374  
 Krupa, J.-C., see Fedoseev, A.M. 368  
 Krupa, J.-C., see Yusov, A.B. 368  
 Krupka, M.C. 184  
 Krupka, M.C., see Giorgi, A.L. 184  
 Krutzler, C. 208, 263, 291  
 Krutzler, C., see Fuger, R. 291  
 Krypyakevich, P.I. 82  
 Ku, H.C. 184, 197, 202  
 Ku, H.C., see Hsu, Y.Y. 197  
 Ku, H.C., see Jiang, P.J. 197  
 Ku, H.C., see Lai, C.C. 184, 194, 197, 296  
 Ku, H.C., see Lin, M.S. 259  
 Kübert, C. 302  
 Kubo, K., see Hamada, K. 111, 113  
 Kueper, I., see Burgemeister, K. 369  
 Kugel, K.I. 247, 248  
 Kugel, K.I., see Khomskii, D.I. 248  
 Kuhlmann, U., see Werheit, H. 119  
 Kulić, M.L., see Bulaevskii, L.N. 185  
 Kulkarni, R., see Kiruthika, G.V.M. 203  
 Kumakura, H., see Arisawa, S. 207, 208  
 Kumari, K. 210  
 Kuncser, V., see Principi, G. 89  
 Kunii, S., see Yamaguchi, T. 246  
 Kunitomi, M., see Otsuka, K. 4  
 Künnen, B., see Pöttgen, R. 57, 63, 77, 81, 95  
 Kunzmann, P. 4–6  
 Kuroda, N., see Oomi, G. 215, 236  
 Kuroki, K., see Kobayashi, Y. 239, 267  
 Kußmann, D. 57  
 Kußmann, D., see Pöttgen, R. 57, 63, 77, 81, 95  
 Kusunose, H. 223

- Kuzma, B.Yu., see Korsukova, M.M. 136,  
 138–140, 152  
 Kuzma, Y.B., see Veremchuk, I. 204  
 Kuz'ma, Yu. 56  
 Kuznietz, M. 293  
 Kuznietz, M., see Takeya, H. 250, 258, 309  
 Kvitnitskaya, O.E., see Naidyuk, Yu.G. 213,  
 227, 269  
 Kwak, J.F., see Jones, T.E. 187  
 Kwok, W.K., see Dunlap, B.D. 190  
 Kwon, Y.K., see Song, K.-J. 240  
 Kwok, W.K., see Williams, J.M. 184
- Laborde, O., see Durán, A. 198  
 Lacerda, A.H. 278, 279  
 Lacerda, A.H., see Beyermann, W.P. 278  
 Lacerda, A.H., see Bud'ko, S.L. 237  
 Lacerda, A.H., see Canfield, P.C. 263  
 Lacerda, A.H., see Christianson, A.D. 279  
 Lacerda, A.H., see Movshovich, R. 57, 66,  
 67, 94  
 Lacerda, A.H., see Schmiedeshoff, G.M. 193,  
 232, 240, 274  
 Lacerda, A.H., see Yatskar, A. 279  
 Lacote, E., see Boglio, C. 353–355, 375  
 Lai, C.C. 184, 194, 197, 296  
 Lai, C.C., see Ku, H.C. 184, 197, 202  
 Lan, M.-D., see Wang, Y.K. 306  
 Lan, M.D. 236, 304  
 Lan, Y., see An, H. 368  
 Landau, I.L. 224  
 Landau, L.D., see Ginzburg, V.L. 232  
 Landrum, G.A. 82  
 Landrum, G.A., see Nuspl, G. 82  
 Lang, A., see Pöttgen, R. 57  
 Lang, J.C., see Song, C. 257  
 Lang, M., see Steglich, F. 195  
 Lapertot, G., see Bud'ko, S.L. 231, 237, 239,  
 240  
 Lapertot, G., see Seyfarth, G. 224  
 Lappas, A., see Prassides, K. 242, 253  
 Lapunova, R.V., see Sichevich, O.M. 88  
 Larkin, A.I. 188, 287  
 Larson, A.C. 81  
 Lascialfari, A. 206  
 Latroche, M., see Mazumdar, C. 180  
 Lawrence, J.M., see Hundley, M.F. 114  
 Lawrence, J.M., see Movshovich, R. 57, 66,  
 67, 94  
 Lawrie, D.D. 212, 213  
 Lawson, A.C., see Fisk, Z. 112, 113, 115  
 Le, L.P. 241  
 Le, L.P., see Luke, G.M. 185  
 Le Bihan, T., see Remschnig, K. 63  
 Ledig, L., see Oertel, C.-G. 205
- Lee, C.Y., see Lan, M.D. 236, 304  
 Lee, E., see Sala, R. 278  
 Lee, H.C. 222, 223  
 Lee, J.H., see Choi, C.K. 293  
 Lee, J.I. 210  
 Lee, J.O., see Cava, R.J. 180, 181, 184, 197,  
 202, 240, 242  
 Lee, J.O., see Eisaki, H. 197, 242, 261  
 Lee, J.O., see Takagi, H. 216, 240  
 Lee, K.H. 286  
 Lee, M., see Lee, K.H. 286  
 Lee, S.-I., see Bobyl, A.V. 288  
 Lee, S.-I., see Chia, E.E.M. 188, 207, 275  
 Lee, S.-I., see Cho, B.K. 305  
 Lee, S.-I., see Choi, E.M. 309  
 Lee, S.-I., see Choi, J.-H. 238, 264, 309  
 Lee, S.-I., see Doh, H. 259, 308  
 Lee, S.-I., see Fil, V.D. 198, 217  
 Lee, S.-I., see Huang, C.L. 226, 227, 232  
 Lee, S.-I., see Jo, Y. 238, 267  
 Lee, S.-I., see Kim, H.-J. 238  
 Lee, S.-I., see Lee, K.H. 286  
 Lee, S.-I., see Mun, M.-O. 211, 232, 286  
 Lee, S.-I., see Naugle, D.G. 270  
 Lee, S.-I., see Park, T. 227, 264, 269, 270, 284  
 Lee, S.-I., see Sánchez, D.R. 307  
 Lee, S.-I., see Suderow, H. 229, 236–238  
 Lee, S.-I., see Yang, I.-S. 223  
 Lee, S.-I., see Yuan, Q. 223, 227  
 Lee, S.L., see Gilardi, R. 280  
 Lee, S.L., see Paul, D.McK. 277  
 Lee, S.L., see Riseman, T.M. 280  
 Lee, T.K., see Huang, C.L. 226, 227, 232  
 Lee, W.C., see Mun, M.-O. 232, 286  
 Lee, W.H. 184  
 Lees, M.R., see Tomy, C.V. 193, 197, 242,  
 257–260  
 Lefmann, K., see Nørgaard, T.K. 276  
 Lei, H., see Sun, G. 374  
 Leiderer, P. 288  
 Leiro, J., see Kumari, K. 210  
 Leisegang, T. 206, 207  
 Leithe-Jasper, A. 67, 68, 89, 97, 140, 142, 157  
 Leithe-Jasper, A., see Mori, T. 134, 135, 143,  
 144, 148, 149, 165  
 Leithe-Jasper, A., see Tanaka, T. 159  
 Leithe-Jasper, A., see Weitzer, F. 65, 67–69,  
 88, 93, 96  
 Leithe-Jasper, A., see Zhang, F.X. 142  
 Lejay, P. 184  
 Lejay, P., see Brison, J.P. 306  
 Lejay, P., see Martínez-Samper, P. 215, 229  
 Lejay, P., see Suderow, H. 229, 236–238  
 Lekperic, S., see Zhang, C. 373  
 Lenczowski, S.K.J., see Brabers, J.H.V.J. 195

- Lenoble, G., see Boglio, C. 353–355, 375  
Leroy, E., see Alleno, E. 203–205, 261, 266, 295  
Lessmann, J.J., see Bartis, J. 353  
Létoublon, A., see Song, C. 257  
Levett, S.J. 281  
Levett, S.J., see Dewhurst, C.D. 283, 284  
Levi, Y., see Felner, I. 190  
Leviev, G.I., see Tsindlekht, M.I. 113, 115  
Levin, K. 307  
Levin, K., see Nass, M.J. 306  
Levy, P.M. 247  
Levy-Clement, C., see Godart, C. 204  
Levy-Clement, C., see Gupta, L.C. 242, 253, 255  
Levy-Clement, C., see Hossain, Z. 180, 202  
Levy-Clement, C., see Mazumdar, C. 180  
Leyrie, M., see Robert, F. 362  
Lhotel, E., see Aoki, D. 191  
Lhotel, E., see Measson, M.-A. 238  
Li, D.P. 284  
Li, J., see Liu, J. 349  
Li, J., see Zhai, S. 373  
Li, J.-X. 374  
Li, K., see Wu, Z. 374  
Li, M., see Liu, J. 362  
Li, S. 278  
Li, S., see Rathnayaka, K.D.D. 278  
Li, S., see Zhou, B. 349, 368  
Li, T., see Liu, G.K. 357  
Li, T.J., see Zhang, T.R. 373  
Li, X., see Feng, J. 374  
Li, X., see Jiang, H. 349  
Li, Y., see An, H. 368  
Li, Y., see Rukang, L. 201  
Li, Z., see Jiang, H. 349  
Liang, J.K., see Chen, Y. 204  
Liao, C. 374  
Lieber, C.M., see Eskildsen, M.R. 276, 286, 287, 289  
Lieke, W., see Rauchschtalbe, U. 250  
Limanski, E.M., see Burgemeister, K. 369  
Limanski, E.M., see Drewes, D. 368  
Lin, J.-Y., see Huang, C.L. 226, 227, 232  
Lin, M.S. 259  
Lin, M.S., see Jiang, P.J. 197  
Lin, M.S., see Lai, C.C. 184, 194, 197, 296  
Lin, P.-J., see Li, D.P. 284  
Lin, S., see Huang, J.-F. 369  
Lin, S.H., see Inaba, H. 43, 44  
Lin, S.H., see Lin, M.S. 259  
Lin, X., see Cai, X.-Z. 369  
Lin, X., see Huang, J.-F. 369  
Lin, X.-R., see Yue, B. 356  
Lin, Y.-H., see Cai, X.-Z. 369  
Lin, Y.-H., see Lu, B. 346  
Lin, Y.-H., see Wang, X.-G. 346  
Lindbaum, A., see Doerr, M. 239, 256  
Lindbaum, A., see Rotter, M. 255, 256  
Lindenkreuz, H.-G., see Bitterlich, H. 204  
Link, J.R. 203  
Lipatnikov, V.N., see Gusev, A.I. 184  
Lipp, D. 206, 295–297, 300, 301  
Lipp, D., see Drechsler, S.-L. 193, 209, 212, 213, 236, 259  
Lipp, D., see Freudenberger, J. 306  
Lipp, D., see Fuchs, G. 236, 240, 296, 297, 300  
Lipp, D., see Schneider, M. 219  
Lipscomb, W.N. 109, 110, 338  
Lis, S. 340, 365, 372  
Lis, S., see Szyzewski, A. 364  
Lisnard, L., see Mialane, P. 353, 355, 371  
Lister, S.J.S., see Boothroyd, A.T. 278  
Litterst, F.J., see Sánchez, D.R. 257  
Littlewood, P.B., see Saxena, S.S. 186  
Liu, B., see Liu, J. 373  
Liu, B., see Xue, G. 362  
Liu, F.Y., see Wang, J. 373  
Liu, G.K. 357  
Liu, G.K., see Soderholm, L. 365  
Liu, J. 349, 356, 362, 373  
Liu, J., see Niu, Z. 349  
Liu, J., see Qu, L. 349  
Liu, J., see Rong, C. 349  
Liu, J., see Wang, E. 346, 349  
Liu, J., see Wang, W. 349  
Liu, J., see Wu, Q. 349  
Liu, J., see Zhu, Z. 349  
Liu, J.-F. 356, 362, 374  
Liu, J.-F., see Li, J.-X. 374  
Liu, J.-F., see Meng, L. 356  
Liu, J.-H., see Bi, L.-H. 356  
Liu, L., see Wang, E. 349  
Liu, M., see Feng, J. 374  
Liu, M., see Jiang, M. 373  
Liu, Q., see Li, J.-X. 374  
Liu, Q.L., see Chen, Y. 204  
Liu, Q.L., see Zhang, F.X. 142  
Liu, S.-X. 372  
Liu, S.-Z., see Liu, J. 362  
Liu, S.-Z., see Wang, Z. 373  
Liu, T., see Liu, G.K. 357  
Liu, X.L., see Zhang, T.R. 373  
Liu, Y., see Liu, J.-F. 356, 362, 374  
Liu, Y., see Liu, Z. 346  
Liu, Y., see Shan, Y. 346  
Liu, Y., see Wang, E. 349  
Liu, Y.-Y., see Liu, S.-X. 372  
Liu, Y.H., see Owen, E.A. 84  
Liu, Z. 346

- Liu, Z., see Liu, J. 349, 356  
 Liu, Z., see Shan, Y. 346, 349  
 Liu, Z., see Wang, E. 346, 349  
 Liu, Z., see Zhou, B. 346, 349  
 Lloyd, S.H., see Paul, D.McK. 277  
 Loewenhaupt, M. 263  
 Loewenhaupt, M., see Dertinger, A. 206, 261, 266  
 Loewenhaupt, M., see Drechsler, S.-L. 193, 212  
 Loewenhaupt, M., see Freudenberger, J. 268, 303, 306, 307  
 Loewenhaupt, M., see Kreyszig, A. 198, 199, 215, 264, 269, 307  
 Loewenhaupt, M., see Müller, K.-H. 266, 268, 269  
 Loewenhaupt, M., see Rotter, M. 244, 246, 255, 256, 278  
 Loewenhaupt, M., see Sierks, C. 244, 278  
 Logan, D.E., see Vidhyadhiraja, N.S. 114  
 London, F. 282  
 London, H., see London, F. 282  
 Longinotti, L.D., see Cooper, A.S. 184  
 Longuet, H.C. 109, 110  
 Lonzarich, G.G., see Brison, J.P. 306  
 Lonzarich, G.G., see Saxena, S.S. 191  
 Looney, C. 238  
 Loong, C.-K., see Sierks, C. 278  
 Loose, I., see Krebs, B. 361, 368  
 Lopez, D., see Choi, S.M. 273  
 Lopez, D., see Eskildsen, M.R. 277, 292  
 Lopez, D., see Gammel, P.L. 275, 290, 292  
 Lorenz, B., see Chu, C.W. 191  
 Lortz, R., see Wang, Y. 113  
 Löser, W., see Behr, G. 202, 204, 205, 261, 266  
 Löser, W., see Bitterlich, H. 202, 204, 206, 207, 305  
 Löser, W., see Drechsler, S.-L. 193, 209, 210, 213, 259  
 Löser, W., see Graw, G. 206  
 Löser, W., see Lascialfari, A. 206  
 Löser, W., see Müller, K.-H. 207, 232, 247, 248, 267, 269, 270  
 Löser, W., see Souptel, D. 205, 206, 240, 291  
 Lottermoser, L., see Song, C. 198  
 Loureiro, S.M. 196  
 Loureiro, S.M., see Link, J.R. 203  
 Lovesey, S.W., see Staub, U. 247  
 Low, J.N., see Iball, J. 342, 344  
 Lu, B. 346  
 Lu, C.-Z., see Wu, C.-D. 341  
 Lu, K.T., see Lan, M.D. 236, 304  
 Lu, R., see Zhang, T.R. 373  
 Lu, Y.-W. 351  
 Luchier, N., see Martínez-Samper, P. 215, 229  
 Luchier, N., see Suderow, H. 277  
 Lukachuk, M. 78  
 Lukachuk, M., see Kalychak, Ya.M. 56, 93  
 Łukaszewicz, K., see Gulay, L.D. 64, 65, 67–77, 81, 86, 87  
 Luke, G.M. 185  
 Lundqvist, B.I., see Skorodumova, N.V. 7  
 Lundstrom, T., see Korsukova, M.M. 136  
 Lundstrom, T., see Werheit, H. 158, 159, 163, 166  
 Lunk, H.-J., see Wassermann, K. 374  
 Luo, J.L., see Zhao, S.R. 308  
 Luo, Q. 353  
 Luo, Q., see Zhang, C. 346, 353  
 Luo, Q.-H. 346, 349, 353  
 Luo, Q.-H., see Bartis, J. 353  
 Luo, Q.-H., see Zhang, C. 345–347, 351, 352  
 Luong, T.K.K., see Cronin, L. 370  
 Lupien, C., see Boaknin, E. 215, 220, 221, 224  
 Lynn, J.W. 187, 188, 190–192, 197, 209, 242, 244, 245, 249, 250, 252, 253, 257, 292, 293  
 Lynn, J.W., see Bourdarot, F. 200  
 Lynn, J.W., see Choi, S.M. 273  
 Lynn, J.W., see Fernandez-Baca, J.A. 187  
 Lynn, J.W., see Godart, C. 195  
 Lynn, J.W., see Goodrich, R.G. 276  
 Lynn, J.W., see Grigereit, T.E. 197, 242, 262  
 Lynn, J.W., see Kreyszig, A. 215  
 Lynn, J.W., see Sinha, S.K. 197, 242, 271  
 Lynn, J.W., see Skanthakumar, S. 190, 241, 242, 245, 252, 276  
 Lynn, J.W., see Stanley, H.B. 191  
 Lynn, J.W., see Thomlinson, W. 188, 189  
 Ma, H., see Ma, J. 368  
 Ma, H., see Zhou, B. 349, 368  
 Ma, J. 368  
 Ma, J.-f., see Liu, J.-f. 374  
 Machesky, L., see Kang, Z.C. 50  
 Machida, K. 189, 194, 268  
 Machida, K., see Adachi, H. 223  
 Machida, K., see Miranović, P. 227  
 Machida, K., see Nakai, N. 229, 284, 285  
 Mackenzie, A.P., see Riseman, T.M. 280  
 MacLaughlin, D.E., see Le, L.P. 241  
 MacNair, D., see Hannay, N.B. 182  
 Maddalena, A., see Principi, G. 89  
 Maeda, A., see Takaki, K. 223, 300  
 Maekawa, M., see Shiozaki, R. 343  
 Maeno, Y., see Riseman, T.M. 280  
 Maeno, Y., see Sudhakar Rao, G.V. 191  
 Magarill, S.A., see Volkova, L.M. 196  
 Magishi, K.-I., see Saito, T. 224  
 Mahanti, S.D., see Salvadore, J.R. 150, 152  
 Mailhot, C. 182

- Maita, J.P., see Matthias, B.T. 112–115, 184  
 Majni, G., see Prudenziati, M. 138  
 Makhija, A.V., see Rosseinsky, M.J. 182, 184  
 Maki, K. 222, 223, 284  
 Maki, K., see Haas, St. 224  
 Maki, K., see Izawa, K. 220, 224, 227, 284  
 Maki, K., see Shiraiishi, J. 233  
 Maki, K., see Thalmeier, P. 223  
 Maki, K., see Wang, G. 222  
 Maki, K., see Won, H. 223  
 Maki, K., see Yuan, Q. 223, 227  
 Maksimov, G.M., see Fedotov, M.A. 343, 348, 349  
 Maksimov, G.M., see Kholdeeva, O.A. 352, 374  
 Maksimovskaya, R.I., see Kholdeeva, O.A. 352, 374  
 Malacria, M., see Boglio, C. 353–355, 375  
 Malaman, B., see Venturini, G. 64, 66–70, 76, 90, 91  
 Malik, S.K., see Dunlap, B.D. 190  
 Malinsky, J., see Antonio, M.R. 364  
 Malinsky, J., see Soderholm, L. 365  
 Malkemper, W., see Werheit, H. 158, 159, 163, 166  
 Mallard, A., see Mialane, P. 353, 355, 371  
 Mamiya, H., see Mori, T. 143, 145–147, 149, 165  
 Manalo, S. 235, 240, 298, 300  
 Manalo, S., see Michor, H. 296, 300  
 Manalo, S., see Sieberer, M. 200  
 Mandal, P. 217  
 Mandrus, D., see Sales, B.C. 164  
 Mandrus, D.G., see Song, K.-J. 240  
 Manes, L. 6  
 Manfrinetti, P. 89  
 Manfrinetti, P., see Cimberle, M.R. 207  
 Manfrinetti, P., see Dhar, S.K. 65, 66, 71, 94  
 Manfrinetti, P., see Moze, O. 89  
 Manfrinetti, P., see Principi, G. 89  
 Mangkorntong, N., see Nohara, M. 295  
 Manini, P., see Andreone, A. 207, 208  
 Maniv, T. 230  
 Mao, H.-K., see Eremets, M.I. 182, 184  
 Mao, Z.Q., see Riseman, T.M. 280  
 Maple, M.B. 184, 185, 188, 189  
 Maple, M.B., see Bauer, E.D. 192, 246  
 Maple, M.B., see Bommeli, F. 211  
 Maple, M.B., see Fertig, W.A. 188  
 Maple, M.B., see Fischer, Ø. 184, 185, 188  
 Maple, M.B., see Li, S. 278  
 Maple, M.B., see Luke, G.M. 185  
 Maple, M.B., see Rathnayaka, K.D.D. 278  
 Maple, M.B., see Sarrao, J.L. 197, 202  
 Maple, M.B., see Zandbergen, H.W. 202  
 Mar, A. 56  
 Marazza, R. 64–77, 83, 89, 90  
 Marazza, R., see Mazzone, D. 65, 66, 68, 69, 71, 73–76, 78, 80  
 Marchevsky, M., see Saha, N. 275, 289  
 Marêché, J.F., see Venturini, G. 64, 66–70, 76, 90, 91  
 Marezio, M., see Hodeau, J.L. 90, 91  
 Mari, C.M., see Manes, L. 6  
 Markert, J.T., see Luke, G.M. 185  
 Markiv, V.Ya., see Kryptayevich, P.I. 82  
 Marozau, I.P., see Fagg, D.P. 45  
 Marré, D., see Cimberle, M.R. 207  
 Marré, D., see Ferdeghini, C. 208  
 Marré, D., see Grassano, G. 208, 232  
 Marrot, J., see Mialane, P. 346, 353–355, 371  
 Martin, J., see Mori, T. 164  
 Martin, J.M., see Tomy, C.V. 193, 256–259  
 Martin, R.L. 5  
 Martin, R.L., see Hoskins, B.F. 5  
 Martin-Frère, J., see Alizadeh, M.H. 364  
 Martínez, J.L., see Suderow, H. 236–238  
 Martínez-Samper, P. 215, 229  
 Martínez-Samper, P., see Suderow, H. 229, 277  
 Masaoka, D., see Oomi, G. 215, 236  
 Maška, M.M. 233  
 Massalski, T.B. 58  
 Mat'as, S., see Kohout, A. 114–116  
 Mat'as, S., see Siemensmeyer, K. 114–116  
 Matkovich, V.I. 107, 109, 136, 138  
 Matricon, J., see Caroli, C. 282  
 Matsubara, T., see Machida, K. 189, 194, 268  
 Matsuda, N. 238  
 Matsuda, N., see Oomi, G. 238, 239, 266  
 Matsuda, T.D., see Kasahara, Y. 306  
 Matsuda, Y. 224, 226  
 Matsuda, Y., see Haraguchi, N. 350  
 Matsuda, Y., see Izawa, K. 220, 224, 227, 284  
 Matsuda, Y., see Kasahara, Y. 306  
 Matsuda, Y., see Seyfarth, G. 224  
 Matsuda, Y., see Takasu, Y. 45  
 Matsui, Y., see Zhang, F.X. 142  
 Matsumoto, H. 188  
 Matsushita, A., see Isida, S. 214  
 Matsuura, K., see Hamada, K. 111, 113  
 Mattausch, H., see Simon, A. 184  
 Mattheiss, L.F. 196, 210, 212, 213, 232, 243, 250, 252, 285  
 Matthias, B.T. 112–115, 184, 186, 187, 191  
 Matthias, B.T., see Cooper, A.S. 184  
 Matthias, B.T., see Fertig, W.A. 188  
 Matthias, B.T., see Fisk, Z. 113–115  
 Matthias, B.T., see Hannay, N.B. 182  
 Matveev, K.I., see Fedotov, M.A. 348, 349

- May, I., see Copping, R. 349  
 May, I., see Gaunt, A.J. 346  
 Mazin, I.I., see Kortus, J. 185  
 Mazumdar, C. 180, 193, 196, 205, 216, 249, 278  
 Mazumdar, C., see Godart, C. 204  
 Mazumdar, C., see Gupta, L.C. 242, 253, 255  
 Mazumdar, C., see Hossain, Z. 180, 202  
 Mazumdar, C., see Jacobs, T. 261  
 Mazumdar, C., see Nagarajan, R. 180, 193, 203, 242, 253, 277  
 Mazumdar, C., see Tominez, E. 193, 202  
 Mazzone, D. 65–71, 73–78, 80  
 Mazzone, D., see Marazza, R. 64, 66–77, 89  
 Mbomekalle, I.-M., see Belai, N. 346  
 McCallum, R.W., see Fertig, W.A. 188  
 McCutcheon, T.P., see Baker, L.C.W. 340  
 McGregor, D., see Zhang, C. 346, 353, 373  
 McIntyre, G.J., see Campbell, A.J. 263, 264, 271  
 McKean, L. 341  
 McMahan, A.K., see Mailhot, C. 182  
 McMillan, W.L. 214  
 McMorrow, D.F., see Jensen, A. 272  
 McRae, E., see Venturini, G. 64, 66–70, 76, 90, 91  
 Mean, B.J., see Lee, K.H. 286  
 Measson, M.-A. 238  
 Méasson, M.-A., see Seyfarth, G. 224  
 Medeiros, S.N., see Baggio-Saitovitch, E.M. 200, 255  
 Meenakshi, S. 239  
 Meeson, P., see Corcoran, R. 230  
 Meeson, P.J., see Bintley, D. 230, 240  
 Mehrotra, P.N., see Rao, G.V.R. 43  
 Meiklejohn, W.H. 243  
 Meissner, H.G., see Schubert, K. 88  
 Meissner, M., see Eskildsen, M.R. 277, 292  
 Meissner, M., see Flachbart, K. 112, 115  
 Meissner, M., see Kohout, A. 114–116  
 Meissner, M., see Nørgaard, T.K. 276  
 Melekh, B.T., see Sovestnov, A.E. 41  
 Mel'nik, N.N., see Ekimov, E.A. 182, 184  
 Melnyk, E.V., see Krypyakevich, P.I. 82  
 Melnyk, G. 63, 64, 66–77  
 Meng, L. 356  
 Meng, L., see Liu, J.-F. 356, 362, 374  
 Meng, R.L., see Chu, C.W. 191  
 Meng, R.L., see Gao, L. 200, 201, 238  
 Meng, R.L., see Wu, M.K. 185  
 Merlo, F. 70, 76, 77, 79–81  
 Merlo, F., see Fornasini, M.L. 57, 63, 76, 77, 81  
 Merritt, F.R., see Cheung, T.T.P. 132  
 Mesot, J., see Gasser, U. 241, 244–246, 276, 278  
 Mesot, J., see Gilardi, R. 280  
 Metlushko, V. 215, 232, 233, 237, 285  
 Metlushko, V., see De Wilde, Y. 280  
 Metoki, N., see Kohgi, M. 246  
 Mewis, A., see Wenski, G. 78, 80  
 Meyer, D.C., see Leisegang, T. 206, 207  
 Meyer, H.-J., see Blaschkowski, B. 200, 201  
 Mialane, P. 346, 353–355, 371  
 Miao, X.Y. 206  
 Michimura, S. 115  
 Michiue, Y., see Leithe-Jasper, A. 157  
 Michiue, Y., see Leithe-Jasper, A. 140, 142  
 Michor, H. 200, 240, 296, 300, 304, 307  
 Michor, H., see Diviš, M. 210, 212, 240–242, 251–254  
 Michor, H., see El-Hagary, M. 245, 253, 271, 303, 304, 307  
 Michor, H., see Hilscher, G. 193, 214, 240, 241, 293, 305  
 Michor, H., see Manalo, S. 240, 298, 300  
 Michor, H., see Rotter, M. 256  
 Michor, H., see Sieberer, M. 200  
 Micklitz, H., see Baggio-Saitovitch, E.M. 196, 200, 242, 255  
 Micklitz, H., see Sánchez, D.R. 196, 242, 268, 307  
 Mielke, C.H., see Yatskar, A. 279  
 Mierzejewski, M., see Maška, M.M. 233  
 Miglioro, A., see Goodrich, R.G. 276  
 Mignot, J.-M., see Kohgi, M. 246  
 Miller, G.J., see Avila, M.A. 206, 279  
 Miller, G.J., see Nesper, R. 85  
 Miller, L.L., see Cho, B.K. 197, 242, 245, 274, 277  
 Miller, R.I., see Ohishi, K. 300  
 Miller, R.I., see Price, A.N. 286  
 Miller Jr., J.H., see Chu, R.K. 216  
 Millo, O., see Felner, I. 190  
 Millo, O., see Tsindlekht, M.I. 113, 115  
 Milyukova, M.S. 374  
 Min, , see Cai, X.-Z. 369  
 Min, B.I., see Lee, J.I. 210  
 Min, B.I., see Youn, S.J. 210, 211  
 Minamitake, I., see Oomi, G. 239  
 Mineev, V.P., see Barash, Yu.S. 302  
 Mints, R.G. 287  
 Miranović, P. 227  
 Miranović, P., see Adachi, H. 223  
 Miranović, P., see Cheon, K.O. 285, 293, 295, 296  
 Miranović, P., see Dobrosavljević-Grujić, L. 302

- Miranović, P., see Kogan, V.G. 215, 223, 282, 293
- Miranović, P., see Nakai, N. 229, 284, 285
- Miranovic, P., see Yethiraj, M. 280
- Mirkhani, V. 374
- Mironov, A. 142, 143
- Misch, L. 84
- Mishonov, T., see Drechsler, S.-L. 193
- Mishonov, T., see Lascialfari, A. 206
- Mishra, R., see Fickenscher, Th. 63
- Misiorek, H., see Paderno, Y.B. 111, 112, 114, 115
- Mitamura, H., see Oomi, G. 238
- Mitra, T., see Müller, A. 370
- Mitrović, B. 223
- Mizuhashi, K., see Cava, R.J. 180, 181, 184, 197, 202, 240, 242
- Mizuhashi, K., see Eisaki, H. 197, 242, 261
- Mizuhashi, K., see Murayama, C. 238
- Mizuhashi, K., see Takagi, H. 216, 240
- Mochiku, T., see Arisawa, S. 207, 208
- Mochizuki, Y., see Kera, Y. 374
- Modak, P., see Verma, A.K. 200
- Modler, R., see Steglich, F. 195
- Moghadam, M., see Mirkhani, V. 374
- Moiseenko, L.L. 113
- Molchan, P.V., see Tomilo, Zh.M. 202
- Molchanov, V.N. 343, 346
- Molchanov, V.N., see Gavrilova, L.O. 341
- Molchanov, V.N., see Samokhvalova, E.P. 341
- Molchanov, V.N., see Tat'yanina, I.V. 340, 341
- Moler, K.A., see Bluhm, H. 275, 289, 290
- Momono, N., see Gilardi, R. 280
- Moncton, D.E., see Lynn, J.W. 187
- Moncton, D.E., see Thomlinson, W. 188, 189
- Mondragon, J., see Bud'ko, S.L. 293, 295
- Mondragon, J., see El Massalami, M. 200
- Monthoux, P., see Saxena, S.S. 191
- Moodie, A.F., see Cowley, J.M. 5, 20
- Mook, H.A., see Paul, D.McK. 189
- Moreea, R.G.H., see Griffith, W.P. 374
- Morello, A., see Gonnelli, R.S. 215
- Mori, K. 306
- Mori, K., see Cao, S. 220, 221, 232
- Môri, N., see Choi, E.M. 309
- Môri, N., see Choi, J.-H. 238
- Môri, N., see Kim, H.-J. 238
- Mori, N., see Murayama, C. 238
- Môri, N., see Uehara, M. 182
- Mori, T. 120–124, 127–140, 143–150, 152–156, 159–168
- Mori, T., see Leithe-Jasper, A. 140, 142
- Mori, T., see Tanaka, T. 159
- Mori, T., see Zhang, F.X. 142
- Morikawa, A., see Otsuka, K. 46, 47
- Morin, P. 199
- Morin, P., see Levy, P.M. 247
- Moriya, T. 272
- Morley-Smith, N., see Griffith, W.P. 349, 374
- Morosov, A.I. 306
- Morozov, A.I. 189, 191, 213, 306
- Morris, G.D., see Price, A.N. 286
- Mortensen, K., see Eskildsen, M.R. 276, 277, 280, 284–287, 289, 292
- Mortensen, K., see Gammel, P.L. 275, 285, 292
- Mortensen, K., see Yaron, U. 280, 289
- Mosel, B.D., see Pöttgen, R. 57, 63, 77, 81, 95
- Moshchalkov, V.V., see Korsukova, M.M. 136, 138–140, 152
- Mostoller, M., see Paul, D.McK. 189
- Motokawa, M., see Kaneko, K. 248
- Motoyama, G., see Nakane, H. 191
- Mott, N.F. 119, 129
- Movshovich, R. 57, 66, 67, 94, 242
- Moze, O. 89
- Mucha, J., see Paderno, Y.B. 111, 112, 114, 115
- Mueller, M.H., see Dwight, A.E. 82
- Mukhopadhyay, S. 228, 241, 284
- Mukhopadhyay, S., see Raychaudhuri, P. 228, 284
- Mulazzani, Q.G. 372
- Mulazzani, Q.G., see Ballardini, R. 372
- Mulder, F.M. 196, 198, 255
- Mulders, A.M. 207, 232, 247, 248, 267, 269, 270, 276
- Mulders, A.M., see Gasser, U. 276
- Mulders, A.M., see Staub, U. 247
- Müller, A. 369, 370
- Müller, A., see Cronin, L. 370
- Müller, A., see Pope, M.T. 339
- Muller, B.R., see Wong, J. 120
- Muller, J., see Bucher, E. 113
- Muller, J., see Ishikawa, M. 189
- Müller, K.-H. 179, 193, 207, 222, 232, 237, 247, 248, 258, 266–270
- Müller, K.-H., see Bitterlich, H. 305
- Müller, K.-H., see Drechsler, S.-L. 193, 209, 210, 212–214, 236, 259
- Müller, K.-H., see Drzazga, Z. 305
- Müller, K.-H., see Eversmann, K. 269
- Müller, K.-H., see Freudenberger, J. 205, 207, 217, 234, 268, 296, 303, 306, 307, 309
- Müller, K.-H., see Fuchs, G. 235, 236, 240, 296, 297, 300
- Müller, K.-H., see Kreyssig, A. 198, 199, 264, 269, 307
- Müller, K.-H., see Lipp, D. 295–297, 300, 301

- Müller, K.-H., see Loewenhaupt, M. 263  
Müller, K.-H., see Narozhnyi, V.N. 216, 217, 252, 287  
Müller, K.-H., see Schneider, M. 219  
Müller, K.-H., see Shulga, S.V. 180, 214, 222, 232, 234, 235, 240, 241, 259, 298, 308  
Müller, K.-H., see Sierks, C. 244, 278  
Müller, K.-H., see Wälte, A. 182, 185  
Müller, K.A., see Bednorz, J.G. 182  
Müller, M., see Schmidt, H. 293  
Müller, U. 84  
Müller, W. 79, 80  
Müller-Hartmann, E. 186, 278  
Müllmann, R., see Pöttgen, R. 57, 63, 77, 81, 95  
Mun, M.-O. 211, 232, 286  
Muñoz, E., see Durán, A. 205, 250  
Muñoz-Sandoval, E. 96  
Muñoz-Sandoval, E., see Chinchure, A.D. 57, 64, 71, 72, 74, 75, 95–97  
Muñoz-Sandoval, E., see Prokeš, K. 63, 96  
Muntean, J., see Soderholm, L. 365  
Murakami, T., see Luke, G.M. 185  
Murakami, Y. 248  
Murakami, Y., see Osamura, K. 84  
Muranaka, T., see Nagamatsu, J. 114, 184, 185  
Murani, A., see Boothroyd, A.T. 278, 279  
Murasik, A. 115, 116  
Muratov, L.A., see Zaplatinskii, O.V. 69  
Murayama, C. 238  
Murdoch, J. 238  
Murphy, D.W., see Rosseinsky, M.J. 182, 184  
Myasoedov, B.F., see Milyukova, M.S. 374  
Mydosh, J.A. 146  
Mydosh, J.A., see Chinchure, A.D. 57, 64, 71, 72, 74, 75, 95–97  
Mydosh, J.A., see Davidov, D. 187  
Mydosh, J.A., see Huser, D. 145  
Mydosh, J.A., see Hüser, D. 187  
Mydosh, J.A., see Muñoz-Sandoval, E. 96  
Mydosh, J.A., see Prokeš, K. 63, 96  
Myzenkova, L.F., see Savitskii, E.M. 184
- Naber, L., see Michor, H. 200, 296, 304  
Nadjo, L., see Belai, N. 346  
Nadjo, L., see Lu, Y.-W. 351  
Nagamatsu, J. 114, 184, 185  
Nagao, M., see Kawano-Furukawa, H. 275  
Nagaosa, N., see Tokura, Y. 248  
Nagarajan, R. 180, 192, 193, 203, 242, 253, 277, 306  
Nagarajan, R., see Alleno, E. 242, 249, 295  
Nagarajan, R., see Bonville, P. 278, 295  
Nagarajan, R., see Chinchure, A.D. 200  
Nagarajan, R., see Dhar, S.K. 242, 278  
Nagarajan, R., see Ghosh, G. 306  
Nagarajan, R., see Godart, C. 195, 204  
Nagarajan, R., see Gupta, L.C. 242, 253, 255  
Nagarajan, R., see Hossain, Z. 180, 200, 202, 242, 249, 253, 303, 307  
Nagarajan, R., see Jacobs, T. 261  
Nagarajan, R., see Lynn, J.W. 197, 209, 242, 244, 245, 249, 250, 253, 257, 292  
Nagarajan, R., see Mazumdar, C. 180, 193, 196, 205, 216, 249  
Nagarajan, R., see Meenakshi, S. 239  
Nagarajan, R., see Paulose, P.L. 197  
Nagarajan, R., see Rams, M. 278  
Nagarajan, R., see Sanchez, J.P. 209, 243  
Nagarajan, R., see Sinha, S.K. 197, 242, 271  
Nagarajan, R., see Watanabe, T. 274  
Nagata, T., see Kawano-Furukawa, H. 273–275  
Nagata, T., see Uehara, M. 182  
Nagatomo, S., see Haraguchi, N. 350  
Naidyuk, Yu.G. 213, 227, 269  
Naidyuk, Yu.G., see Bashlakov, D.L. 229, 241  
Naidyuk, Yu.G., see Müller, K.-H. 207, 232, 247, 248, 267, 269, 270  
Naito, K., see Inaba, H. 43  
Nakagawa, N., see Nagamatsu, J. 114, 184, 185  
Nakai, N. 229, 284, 285  
Nakai, N., see Miranović, P. 227  
Nakai, S., see Kasaya, M. 114, 127, 128  
Nakajima, M., see Kohgi, M. 246  
Nakajima, Y., see Izawa, K. 220, 224, 227, 284  
Nakamatsu, H., see Shirai, K. 109, 110  
Nakamori, Y., see Togano, K. 184  
Nakamura, K., see Arisawa, S. 207, 208  
Nakamura, S., see Inouye, Y. 374  
Nakamura, S., see Yamaguchi, T. 246  
Nakamura, T., see Staub, U. 247  
Nakane, H. 191  
Nakano, Y., see Yamaguchi, T. 246  
Nakotte, H., see Brabers, J.H.V.J. 195  
Narozhnyi, V.N. 190, 216, 217, 252, 279, 287  
Narozhnyi, V.N., see Drechsler, S.-L. 193, 212  
Narozhnyi, V.N., see Freudenberger, J. 217  
Narozhnyi, V.N., see Fuchs, G. 235  
Narozhnyi, V.N., see Müller, K.-H. 179, 193, 222, 237  
Narozhnyi, V.N., see Wälte, A. 182  
Naruke, H. 340, 346, 358, 361, 368, 369, 371, 373  
Naruke, H., see Ozeki, T. 371  
Naruke, H., see Yamase, T. 358, 368, 373  
Naslain, R. 107, 109, 110  
Nass, M.J. 306

- Nass, M.J., see Levin, K. 307  
 Naugle, D.G. 218, 219, 259, 270, 277  
 Naugle, D.G., see Belevtsev, B.I. 219  
 Naugle, D.G., see Bhatnagar, A.K. 215, 218, 219  
 Naugle, D.G., see Bobrov, N.L. 228, 229, 240  
 Naugle, D.G., see Du Mar, A.C. 232, 240  
 Naugle, D.G., see Eskildsen, M.R. 277, 280, 292  
 Naugle, D.G., see Hennings, B.D. 215, 218–221  
 Naugle, D.G., see Li, S. 278  
 Naugle, D.G., see Naidyuk, Yu.G. 227  
 Naugle, D.G., see Rathnayaka, K.D.D. 197, 215, 216, 218, 219, 232, 236, 242, 263, 278, 296  
 Navrotsky, A., see Inaba, H. 43, 44  
 Nayshtut, M., see Zhang, C. 373  
 Negishi, K., see Kasaya, M. 114, 127, 128  
 Neitz, R.J., see Creaser, I. 364, 365  
 Neiwert, W.A., see Fang, X. 360  
 Neiwert, W.A., see Kholdeeva, O.A. 352, 374  
 Nemoto, Y., see Watanuki, R. 115  
 Nemoto, Y., see Yamaguchi, T. 246  
 Nenkov, K., see Behr, G. 204  
 Nenkov, K., see Bitterlich, H. 207, 305  
 Nenkov, K., see Drechsler, S.-L. 193, 209, 213, 236, 259  
 Nenkov, K., see Drzazga, Z. 305  
 Nenkov, K., see Freudenberger, J. 234, 268, 296, 303, 306, 307  
 Nenkov, K., see Fuchs, G. 235, 236, 240, 296, 297, 300  
 Nenkov, K., see Graw, G. 206  
 Nenkov, K., see Lipp, D. 295–297, 300, 301  
 Nenkov, K., see Müller, K.-H. 207, 232, 237, 247, 248, 258, 266, 267, 269, 270  
 Nenkov, K., see Naidyuk, Yu.G. 213, 269  
 Nenkov, K., see Narozhnyi, V.N. 252, 287  
 Nenkov, K., see Souptel, D. 240, 291  
 Nenkov, K., see Wälte, A. 182, 185  
 Nenkov, K.A., see Freudenberger, J. 217  
 Nenkov, K.A., see Narozhnyi, V.N. 216, 217, 252  
 Nenoff, T.M., see Nyman, M. 375  
 Nesper, R. 85  
 Neuhausen, S., see Braunisch, W. 260  
 Neumeier, J.J., see Alleno, E. 238  
 Neumeier, J.J., see Movshovich, R. 57, 66, 67, 94  
 Ng, T.K. 275  
 Nguyen, L., see Goll, G. 235  
 Nguyen, L.H. 210  
 Nicol, E.J. 235  
 Niedermayer, Ch., see Bernhard, C. 191  
 Niedermayer, Ch., see Henn, R.W. 184  
 Nielsen, J.W. 80  
 Niepmann, D., see Fickenscher, Th. 63  
 Niepmann, D., see Pöttgen, R. 67  
 Nieuwenhuys, G.J., see Davidov, D. 187  
 Nieuwenhuys, G.J., see El Massalami, M. 194, 197, 242, 250, 293  
 Nieuwenhuys, G.J., see Huser, D. 145  
 Nieuwenhuys, G.J., see Hüser, D. 187  
 Nieuwenhuys, G.J., see Le, L.P. 241  
 Nieuwenhuys, G.J., see Saha, N. 275, 289  
 Niewa, R. 56  
 Nigam, A.K., see Mazumdar, C. 216  
 Nishida, N., see Nakai, N. 229  
 Nishida, N., see Nishimori, H. 229, 280–282, 284  
 Nishihara, Y., see Zou, Z. 190  
 Nishimori, H. 229, 280–282, 284  
 Nishimori, H., see Nakai, N. 229  
 Nishimura, K., see Cao, S. 220, 221, 232  
 Nishimura, K., see Mori, K. 306  
 Nishimura, T., see Mori, T. 165–168  
 Nishino, A., see Shiozaki, R. 343, 374  
 Nishio, E., see Shiozaki, R. 343  
 Nishioka, T., see Nakane, H. 191  
 Nishiya, S., see Inouye, Y. 374  
 Niu, J.-Y. 346, 355  
 Niu, Z. 349  
 Niu, Z., see Qu, L. 349  
 Noakes, D.R., see Bernhard, C. 191  
 Noel, H., see Godart, C. 204  
 Noel, H., see Mazumdar, C. 249  
 Noël, H., see Remschnig, K. 63  
 Noël, H., see Weitzer, F. 65, 67–69, 88, 93, 96  
 Nogueira, H., see Griffith, W.P. 374  
 Nogueira, H.I.S., see Almeida Paz, F.A. 344  
 Nogueira, H.I.S., see Griffith, W.P. 349, 374  
 Nogueira, H.I.S., see Sousa, F.L. 373  
 Noh, A., see Krebs, B. 361, 368  
 Nohara, M. 222, 226, 295, 297, 300, 301  
 Nohara, M., see Baba, T. 227, 228, 274, 300  
 Nohara, M., see Izawa, K. 220, 224, 227, 284  
 Nohara, M., see Ohishi, K. 300  
 Nohara, M., see Takagi, H. 192  
 Nohara, M., see Takaki, K. 223, 300  
 Nohara, M., see Watanabe, T. 223  
 Nohara, M., see Yokoya, T. 222, 227, 284, 295  
 Nokura, K., see Machida, K. 189, 194, 268  
 Nolas, G., see Mori, T. 164  
 Nolas, G.S. 158, 164  
 Nölting, J., see Ricken, J. 3  
 Nomura, T., see Fukazawa, H. 222  
 Norblad, P., see Kumari, K. 210  
 Nørgaard, T.K. 276  
 Nørgaard, T.K., see Andersen, N.H. 200, 276  
 Nørgaard, T.K., see Eskildsen, M.R. 277, 292

- Nørgaard, T.K., see Jensen, A. 272  
 Norman, M., see Harris, I.R. 86  
 Novak, M.A., see El Massalami, M. 200  
 Nowick, A.S., see Ray, S.P. 4  
 Nowik, I., see Felner, I. 191  
 Nowotny, H. 90  
 Nowotny, H., see Rieger, W. 63, 87, 88  
 Numazawa, T., see Tanaka, T. 159  
 Nuspl, G. 82  
 Nyan, K.K., see Korsukova, M.M. 136, 138–140, 152  
 Nyman, M. 375
- Obst, B. 280  
 Ochiai, M., see Kawano-Furukawa, H. 273, 274  
 Oda, M., see Gilardi, R. 280  
 Odintsov, V.V., see Moiseenko, L.L. 113  
 Oertel, C.-G. 205  
 Oertel, C.-G., see Subba Rao, K. 208  
 Ogata, M., see Udagawa, M. 224, 229  
 O'Grady, P.J., see Darwent, J.R. 372  
 Oguchi, T., see Yokoya, T. 222, 227, 284, 295  
 Oh, S.S., see Song, K.-J. 240  
 Ohashi, M., see Choi, E.M. 309  
 Ohashi, M., see Choi, J.-H. 238  
 Ohashi, M., see Kim, H.-J. 238  
 Ohashi, M., see Oomi, G. 239  
 Ohashi, M., see Yamauchi, H. 203, 247  
 Ohishi, K. 300  
 Ohoyama, K., see Michimura, S. 115  
 Ohoyama, K., see Yamauchi, H. 203, 247  
 Oka, K., see Zou, Z. 190  
 Okabe, Y., see Michimura, S. 115  
 Okada, S., see Tanaka, T. 120, 122, 123, 135, 136, 138, 157  
 Okada, S., see Zhang, F.X. 142  
 Okamoto, T., see Kobayashi, Y. 239, 267  
 Okaue, Y., see Haraguchi, N. 350  
 Oliver, D.W. 117  
 Oliver, D.W., see Slack, G.A. 119, 158, 159  
 Olsen, C.E., see Willis, J.O. 187  
 Olsen, J.L., see Bucher, E. 113  
 Omata, T., see Otsuka-Yao-Matsuo, S. 18, 47  
 Öner, Y. 94  
 Ong, N.P., see He, T. 184  
 Onimaru, T. 246, 247  
 Onimaru, T., see Yamauchi, H. 203, 247  
 Onodera, H. 203, 247  
 Onodera, H., see Kaneko, K. 248  
 Onodera, H., see Yamauchi, H. 203, 247  
 Onuki, Y., see Corcoran, R. 230  
 Onuki, Y., see Czopnik, A. 112, 115  
 Onuki, Y., see Kasahara, Y. 306  
 Onuki, Y., see Shimizu, K. 182, 186
- Ooba, T., see Takeya, H. 309  
 Oomi, G. 215, 236, 238, 239, 266  
 Oomi, G., see Akiyama, H. 238, 267  
 Oomi, G., see Matsuda, N. 238  
 Oomi, G., see Uwatoko, Y. 238, 266  
 Opahle, I., see Drechsler, S.-L. 193, 209, 210, 213, 214, 229, 259, 270, 309  
 Opahle, I., see Müller, K.-H. 207, 232, 247, 248, 267, 269, 270  
 Opahle, I., see Rosner, H. 210, 211, 214, 235, 299  
 Opel, M., see Flachbart, K. 112, 115  
 Oprean, I., see Ratiu, C. 374  
 Orimo, S., see Togano, K. 184  
 Ortelli, J., see Peter, M. 187  
 Osaki, S., see Izawa, K. 224  
 Osamura, K. 84  
 Ostenson, J.E., see Xu, M. 181, 204, 232  
 Ostuni, A. 345, 346, 362  
 Ostuni, A., see Sadakane, M. 353, 354  
 Otsuka, K. 4, 46, 47  
 Otsuka-Yao-Matsuo, S. 18, 47  
 Ott, H.R., see Sologubenko, A.V. 224  
 Ouladdiaf, B., see El Massalami, M. 309  
 Ovchinnikov, Yu.N. 237  
 Ovchinnikov, Yu.N., see Larkin, A.I. 188, 287  
 Owen, E.A. 84  
 Oxx, S., see Eskildsen, M.R. 276, 287, 289  
 Ozaki, A., see Shiozaki, R. 374  
 Ozeki, T. 344, 371, 372  
 Ozeki, T., see Naruke, H. 369  
 Ozeki, T., see Yamase, T. 344, 368, 373
- Pack, S.P., see Inaba, H. 43, 44  
 Padalia, B.D., see Godart, C. 204  
 Padalia, B.D., see Gupta, L.C. 242, 253, 255  
 Padalia, B.D., see Hossain, Z. 180, 202  
 Padalia, B.D., see Mazumdar, C. 180, 216  
 Padalia, B.D., see Nagarajan, R. 180, 203, 242, 253  
 Paderno, R., see Gabani, S. 112–115  
 Paderno, Yu.B. 111, 112, 114, 115  
 Paderno, Yu.B., see Czopnik, A. 112, 115  
 Paderno, Yu.B., see Daghero, D. 113, 115  
 Paderno, Yu.B., see Flachbart, K. 112, 115  
 Paderno, Yu.B., see Gabani, S. 116  
 Paderno, Yu.B., see Khasanov, R. 113  
 Paderno, Yu.B., see Kohout, A. 114–116  
 Paderno, Yu.B., see Murasik, A. 115, 116  
 Paderno, Yu.B., see Siemensmeyer, K. 114–116  
 Paderno, Yu.B., see Tsindlekht, M.I. 113, 115  
 Paderno, Yu.B., see Wang, Y. 113  
 Pagola, S., see Dertinger, A. 206, 261, 266

- Paik, H., see Mun, M.-O. 211  
 Pairor, P. 229  
 Pairese, J.B., see Nyman, M. 375  
 Pal, D., see Jaiswal-Nagar, D. 286  
 Palenzona, A., see Cimberle, M.R. 207  
 Palenzona, A., see Dhar, S.K. 65, 66, 71, 94  
 Palenzona, A., see Manfrinetti, P. 89  
 Palenzona, A., see Moze, O. 89  
 Palenzona, A., see Principi, G. 89  
 Pallecchi, I., see Grassano, G. 208  
 Palmy, C., see Bucher, E. 113  
 Palstra, T.T.M., see Rosseinsky, M.J. 182, 184  
 Paltiel, Y., see Dewhurst, C.D. 289  
 Paltiel, Y., see James, S.S. 208, 289, 290  
 Pani, M., see Fornasini, M.L. 57, 63, 76, 77, 81  
 Pani, M., see Merlo, F. 70, 76, 77, 79–81  
 Panjukov, S.V., see Bulaevskii, L.N. 185  
 Paranthaman, M. 193  
 Paranthaman, M., see Chakoumakos, B.C. 206  
 Parasiris, A., see Naugle, D.G. 218  
 Parasiris, A., see Rathnayaka, K.D.D. 215, 216, 218, 219, 232  
 Park, C., see Song, K.-J. 240  
 Park, J.-G., see Jo, Y. 238, 267  
 Park, T. 227, 264, 269, 270, 284  
 Park, T., see Chia, E.E.M. 188, 207, 275  
 Park, Y.W., see Choi, C.K. 293  
 Parker, D. 223  
 Parker, D., see Won, H. 223  
 Parker, E., see Fink, H.J. 184  
 Parker, T.S.C., see Sayle, T.X. 33  
 Parks, R.D., see Rauchschalbe, U. 250  
 Parthé, E. 56, 82  
 Parthé, E., see Gelato, M.L. 82  
 Parthé, E., see Hovestreydt, E. 83  
 Parthé, E., see Rieger, W. 66, 67  
 Paschen, S., see Häse, K. 208, 232  
 Passamani, E., see Baggio-Saitovitch, E.M. 200, 255  
 Passell, L., see Lynn, J.W. 187  
 Patil, S., see Kiruthika, G.V.M. 206  
 Pattalwar, S.M., see Alleno, E. 295  
 Paufler, P., see Jaenicke-Rössler, U. 239  
 Paufler, P., see Just, G. 195, 198  
 Paufler, P., see Leisegang, T. 206, 207  
 Paufler, P., see Lipp, D. 206  
 Paul, C., see Gabani, S. 116  
 Paul, D.McK. 189, 277  
 Paul, D.McK., see Campbell, A.J. 263, 264, 271  
 Paul, D.McK., see Chang, L.J. 200, 242  
 Paul, D.McK., see Civale, L. 223  
 Paul, D.McK., see Dewhurst, C.D. 268, 283, 284, 289, 291  
 Paul, D.McK., see James, S.S. 208, 289, 290  
 Paul, D.McK., see Levett, S.J. 281  
 Paul, D.McK., see Riseman, T.M. 280  
 Paul, D.McK., see Rybaltchenko, L.F. 270  
 Paul, D.McK., see Saha, N. 275, 289  
 Paul, D.McK., see Silhanek, A.V. 287  
 Paul, D.McK., see Song, K.-J. 240, 287  
 Paul, D.McK., see Thompson, J.R. 215  
 Paul, D.McK., see Tomy, C.V. 193, 197, 242, 256–260  
 Paul, D.McK., see Yanson, I.K. 214, 259, 260  
 Paul, D.McK., see Yethiraj, M. 280, 281  
 Paul, McK.D., see Dewhurst, C.D. 289  
 Paulose, P.L. 197  
 Paulose, P.L., see Kiruthika, G.V.M. 206  
 Paulsen, C., see Aoki, D. 191  
 Paulsen, C., see Measson, M.-A. 238  
 Pavlik, V., see Flachbart, K. 112, 115  
 Pavlik, V., see Gabani, S. 116  
 Pawlow, J.H., see Gilbert, J. 374  
 Peacock, R.D. 342–344, 349, 351  
 Pecharsky, V.K., see Gladyshevsky, E.I. 56  
 Peck Jr., W.F., see Carter, S.A. 238, 249  
 Peck Jr., W.F., see Cava, R.J. 180, 181, 184, 197, 200–202, 240, 242, 300  
 Peck Jr., W.F., see Eisaki, H. 197, 242, 261  
 Peck Jr., W.F., see Grigereit, T.E. 197, 242, 262  
 Peck Jr., W.F., see Lynn, J.W. 293  
 Peck Jr., W.F., see Siegrist, T. 195, 200, 249, 250, 252, 278  
 Peck Jr., W.F., see Takagi, H. 216, 240  
 Peck Jr., W.F., see Zandbergen, H.W. 200, 201  
 Pei, F., see Feng, J. 374  
 Pei, F., see Sun, G. 374  
 Peisker, E., see Becher, H.J. 63  
 Peng, J., see Niu, Z. 349  
 Peng, J., see Qu, L. 349  
 Peng, J., see Wang, S. 349  
 Peng, Z.Q. 259  
 Peng, Z.Q., see Winzer, K. 259  
 Perez, F.G., see Howell, R.C. 360  
 Perez, F.G., see Zhang, C. 353, 360  
 Pérez Omil, J.A., see Bernal, S. 30, 49  
 Pertsikov, B.Z., see Fedotov, M.A. 348, 349  
 Pesch, W., see Kramer, L. 286  
 Peschel, I., see Fulde, P. 186  
 Peshev, P., see Lejay, P. 184  
 Peter, M. 187  
 Peterson, E.J., see Nagarajan, R. 277  
 Petrovic, C., see Bud'ko, S.L. 237  
 Petrovic, C., see Eskildsen, M.R. 280  
 Petrukhina, M.A. 341  
 Pettersson, L., see Yagasaki, A. 339  
 Pfleiderer, C., see Yelland, E.A. 191

- Pickett, W.E. 180, 210  
Pickett, W.E., see An, J.M. 185  
Pickett, W.E., see Kogan, V.G. 282  
Pickett, W.E., see Shulga, S.V. 237, 241  
Piepenbrink, M., see Drewes, D. 357, 359  
Pietrzak, J., see Szyzewski, A. 364  
Pinholt, R., see Andersen, N.H. 200, 276  
Pintado, J.M., see Bernal, S. 18, 30, 49  
Piro-Sellem, S., see Contant, R. 346  
Pitschke, W., see Buchgeister, M. 205  
Plackowski, T., see Wang, Y. 237  
Pluzhnikov, V., see Czopnik, A. 112, 115  
Pohl, R.O., see Cahill, D.G. 158, 159, 164  
Pokrovsky, V.L., see Canfield, P.C. 263  
Pokrovsky, V.L., see Kalatsky, V.A. 265  
Polborn, K., see Nuspl, G. 82  
Polyschuk, S.A., see Volkova, L.M. 196  
Pope, M.T. 339, 357  
Pope, M.T., see Alizadeh, M.H. 364  
Pope, M.T., see Belai, N. 346, 354  
Pope, M.T., see Creaser, I. 364, 365  
Pope, M.T., see Dickman, M.H. 365  
Pope, M.T., see Kim, K.-C. 365, 366  
Pope, M.T., see Liu, J. 362  
Pope, M.T., see Liu, J.-F. 362, 374  
Pope, M.T., see McKean, L. 341  
Pope, M.T., see Ostuni, A. 345, 346, 362  
Pope, M.T., see Rong, C. 339  
Pope, M.T., see Sadakane, M. 350, 353, 354  
Pope, M.T., see Wassermann, K. 357, 363, 374  
Pope, M.T., see Zimmermann, M. 366  
Potel, M., see Godart, C. 204  
Potel, M., see Mazumdar, C. 249  
Pöttgen, R. 57, 63, 67, 77, 78, 81, 87, 94, 95  
Pöttgen, R., see Fickenscher, Th. 63  
Pöttgen, R., see Galadzhun, Ya.V. 90  
Pöttgen, R., see Hoffmann, R.-D. 80, 81  
Pöttgen, R., see Kalychak, Ya.M. 56, 93  
Pöttgen, R., see Kanatzidis, M.G. 57  
Pöttgen, R., see Kraft, R. 96  
Pöttgen, R., see Kußmann, D. 57  
Pöttgen, R., see Lukachuk, M. 78  
Pöttgen, R., see Sebastian, C.P. 80  
Pöttgen, R., see Zarembo, R.I. 84  
Pöttgen, R., see Zarembo, V.I. 84  
Pöttgen, R., see Zumtick, M.F. 82, 83  
Pötzschke, M. 88  
Pötzschke, M., see Schubert, K. 88  
Powell, T.P., see Dukan, S. 224  
Prassides, K. 242, 253  
Pratt, F.L., see Nagarajan, R. 277  
Preston, J.M., see Hillier, A.D. 305  
Price, A.N. 286  
Price, A.N., see Ohishi, K. 300  
Principi, G. 89  
Probst, P.-A., see Corcoran, R. 230  
Prokeš, K. 63, 96  
Prokes, K., see Jensen, A. 272  
Proust, C., see Boaknin, E. 215, 224  
Prozorov, R. 240  
Prozorov, R., see Kogan, V.G. 215, 293  
Prudenziati, M. 138  
Prytkova, N.A., see Tomilo, Zh.M. 202  
Pugh, E., see Saxena, S.S. 191  
Punte, G., see Rigotti, G. 372  
Putti, M., see Cimberle, M.R. 207  
Putti, M., see Grassano, G. 208, 232  
Qin, X., see Cao, S. 221, 232  
Qiu, P., see Liao, C. 374  
Qiu, X.D., see Gao, L. 200, 201, 238  
Qu, L. 349  
Qu, L., see Liu, J. 356, 362  
Qu, L., see Niu, Z. 349  
Qu, L., see Wang, S. 349  
Qui, Q., see Leithe-Jasper, A. 67, 68, 89, 97  
Quirion, G., see Murdoch, J. 238  
Radha, S., see Mazumdar, C. 216  
Radzihovsky, L. 275  
Rahyab, S., see Zhang, C. 373  
Rakhmanov, A.L., see Mints, R.G. 287  
Ramadan, W., see Ferdeghini, C. 208  
Ramadan, W., see Grassano, G. 208, 232  
Ramadan, W., see Wang, X. 208  
Ramakrishnan, S., see Jaiswal-Nagar, D. 232, 286  
Ramakrishnan, S., see Raychaudhuri, P. 227, 284  
Ramdas, S., see Rao, G.V.R. 43  
Ramirez, A.P., see Eskildsen, M.R. 276, 277, 280, 286, 287, 289, 292  
Ramirez, A.P., see Gammel, P.L. 275, 290  
Ramirez, A.P., see He, T. 184  
Ramirez, A.P., see Rosseinsky, M.J. 182, 184  
Ramirez, A.P., see Yaron, U. 280, 289  
Rams, M. 278  
Rao, C.N.R., see Rao, G.V.R. 43  
Rao, G.V.R. 43  
Rao, K.V., see Ström, V. 202, 205  
Rao, R.S., see Meenakshi, S. 239  
Rao, R.S., see Verma, A.K. 200  
Rapp, R.E. 198  
Rapp, R.E., see El Massalami, M. 194, 197, 198, 242, 250, 255, 257, 272, 309  
Rathnayaka, K.D.D. 197, 215, 216, 218, 219, 232, 236, 242, 263, 278, 296  
Rathnayaka, K.D.D., see Belevtsev, B.I. 219  
Rathnayaka, K.D.D., see Bhatnagar, A.K. 215, 218, 219

- Rathnayaka, K.D.D., see Bobrov, N.L. 228, 229, 240
- Rathnayaka, K.D.D., see Du Mar, A.C. 232, 240
- Rathnayaka, K.D.D., see Eskildsen, M.R. 277, 280, 292
- Rathnayaka, K.D.D., see Hennings, B.D. 220, 221
- Rathnayaka, K.D.D., see Li, S. 278
- Rathnayaka, K.D.D., see Naidyuk, Yu.G. 227
- Rathnayaka, K.D.D., see Naugle, D.G. 218, 219, 259, 270, 277
- Ratiu, C. 374
- Rauchschwalbe, U. 250
- Ravindran, P. 210, 294
- Ravindran, P., see Meenakshi, S. 239
- Ray, S.P. 4
- Rayaprol, S., see Sebastian, C.P. 80
- Raychaudhuri, P. 227, 228, 284
- Raychaudhuri, P., see Mukhopadhyay, S. 228, 241, 284
- Razavi, F.S., see Murdoch, J. 238
- Reedyk, M., see Sudhakar Rao, G.V. 191
- Regan, K.A., see He, T. 184
- Reibold, M. 208
- Reich, S., see Felner, I. 191
- Reichardt, W. 214
- Reichardt, W., see Kreyssig, A. 215
- Reicke, M., see Kortz, U. 354, 357
- Rek, Z.U., see Wong, J. 119, 120
- Remeika, J.P., see Hodeau, J.L. 90, 91
- Rempel, A.A., see Gusev, A.I. 184
- Remshnig, K. 63
- Ressouche, E., see Aoki, D. 191
- Rewiersma, M.J.F.M., see Hüser, D. 187
- Reznik, D., see Kreyssig, A. 215
- Rhee, J.Y. 210, 211, 285
- Rhee, J.Y., see Song, C. 198, 256
- Rhee, J.Y., see Suh, B.J. 209
- Rheingold, A.L., see Howell, R.C. 360
- Rheingold, A.L., see Luo, Q. 353
- Rheingold, A.L., see Luo, Q.-H. 346, 349, 353
- Rho, H. 244
- Ri, H.-C., see Cho, B.K. 309
- Ri, H.-C., see Jo, Y. 238, 267
- Riani, P., see Marazza, R. 64, 66–77, 89
- Ribeiro, R.A. 206, 250, 258
- Ribeiro, R.A., see Bud'ko, S.L. 304
- Riblet, G. 186
- Ricci, F., see Grassano, G. 208
- Rice, T.M., see Fehrenbacher, R. 190
- Richards, S.M. 117
- Richardson, C.F. 182
- Richter, M., see Müller, K.-H. 258
- Richter, M., see Schneider, M. 219
- Ricken, J. 3
- Rieger, W. 63, 66, 67, 87, 88
- Riess, I., see Ricken, J. 3
- Rigamonti, A., see Lascialfari, A. 206
- Rigotti, G. 372
- Riseman, T.M. 280
- Riseman, T.M., see Luke, G.M. 185
- Ritter, C., see Chang, L.J. 242
- Ritter, C., see Freudenberger, J. 307
- Ritter, C., see Kreyssig, A. 198, 199, 264, 269, 307
- Ritter, C., see Loewenhaupt, M. 263
- Ritter, C., see Müller, K.-H. 268, 269
- Rivero, B.E., see Rigotti, G. 372
- Riviere, E., see Mialane, P. 346, 354
- Rjabinin, J.N., see Schubnikow, L.W. 239
- Ro, C., see Levin, K. 307
- Robert, F. 362
- Roberts, M. De V., see Longuet, H.C. 109, 110
- Rocha, J., see Sousa, F.L. 373
- Roden, B., see Braunisch, W. 260
- Rodewald, U.Ch., see Fickenschler, Th. 63
- Rodewald, U.Ch., see Pöttgen, R. 67
- Rodewald, U.Ch., see Zarembo, R.I. 84
- Rodewald, U.Ch., see Zarembo, V.I. 84
- Rodrigo, J.G., see Suderow, H. 229
- Rodríguez, C.O., see Cappannini, O.M. 239
- Rodríguez, C.O., see Weht, R. 239
- Rodríguez, M.A., see Nyman, M. 375
- Rodríguez-Carvajal, J.R., see Moze, O. 89
- Rodríguez-Izquierdo, J.M., see Bernal, S. 18
- Rodríguez-Izquierdo, J.M., see Bernal, S. 30, 49
- Rogado, N., see He, T. 184
- Rogl, P. 56, 140, 184
- Rogl, P., see Leithe-Jasper, A. 67, 68, 89, 97
- Rogl, P., see Michor, H. 200
- Rogl, P., see Remshnig, K. 63
- Rogl, P., see Rupp, B. 198
- Rogl, P., see Sieberer, M. 200
- Rogl, P., see Weitzer, F. 65, 67–69, 88, 93, 96
- Röhler, J. 249
- Rong, C. 339, 349
- Rong, C., see Liu, J. 349, 362
- Roques, B., see Venturini, G. 64, 66–70, 76, 90, 91
- Rosenhahn, C., see Pöttgen, R. 57
- Rosenkranz, S., see Gasser, U. 245, 246, 276, 278
- Rosenstein, B., see Li, D.P. 284
- Roser, M.R., see Tang, J. 87
- Rosner, H. 210, 211, 214, 235, 299
- Rosner, H., see Drechsler, S.-L. 193, 209, 210, 212–214, 229, 235, 236, 259, 270, 309
- Rosner, H., see Freudenberger, J. 306

- Rosner, H., see Fuchs, G. 235, 236, 296, 297  
 Rosner, H., see Müller, K.-H. 207, 232, 247, 248, 267, 269, 270  
 Rosner, H., see Schneider, M. 219  
 Rosner, H., see Shulga, S.V. 237, 241  
 Rosner, H., see von Lips, H. 210  
 Rosner, H., see Wälte, A. 182  
 Rosolowski, J.H., see Slack, G.A. 138, 158, 159, 163, 166  
 Rosov, N., see Skanthakumar, S. 190  
 Ross, K., see Dezaneti, L.M. 180, 184, 197, 202  
 Ross Jr., J.F., see Naidyuk, Yu.G. 227  
 Rosseinsky, M.J. 182, 184  
 Rossi, D., see Marazza, R. 65–75, 83, 90  
 Rossi, D., see Mazzone, D. 65–71, 73–78, 80  
 Rossteutscher, W., see Schubert, K. 88  
 Rosu, C. 342, 344  
 Roth, S. 187  
 Rotter, M. 244, 246, 255, 256, 278  
 Rotter, M., see Doerr, M. 239, 256  
 Rowe, D.M. 158  
 Rowen, M., see Wong, J. 120  
 Roy, I., see Manes, L. 6  
 Ruderman, M.A. 133  
 Ruiz, D. 204  
 Rukang, L. 201  
 Rupp, B. 198  
 Rupp Jr., L.W., see Cava, R.J. 300  
 Rusinov, A.I., see Gor'kov, L.P. 187  
 Russell, V. 182  
 Russo, M.L., see Andreone, A. 208, 227  
 Rustom, A. 309  
 Ruzs, J., see Diviš, M. 253, 254  
 Rybaltchenko, L.F. 270
- Sadakane, M. 350, 353, 354  
 Sadakane, M., see Belai, N. 354  
 Sagawa, T., see Iga, F. 114, 127, 128  
 Saha, N. 275, 289  
 Saha, N., see Dewhurst, C.D. 289  
 Saillard, J.-Y., see Ruiz, D. 204  
 Saillard, J.V., see Bauer, J. 140  
 Saito, A. 341, 367  
 Saito, T. 224  
 Saito, T., see Otsuka, K. 4  
 Sakai, F., see Nohara, M. 222, 226, 300  
 Sakai, S., see Cao, S. 220, 221  
 Sakai, T. 184, 203  
 Sakakibara, T., see Onimaru, T. 246, 247  
 Sakigawa, Y., see Oomi, G. 239  
 Sakon, T., see Kaneko, K. 248  
 Sala, R. 278  
 Salamakha, P.S. 56–58, 68, 69  
 Salamakha, P.S., see Mazumdar, C. 249  
 Salamakha, P.S., see Öner, Y. 94  
 Salamakha, P.S., see Sologub, O.L. 56  
 Salamakha, P.S., see Zaplatinskii, O.V. 69  
 Salamati, H., see Murdoch, J. 238  
 Salamon, M.B., see Chia, E.E.M. 188, 207, 275  
 Salamon, M.B., see Park, T. 227, 264, 269, 270, 284  
 Sales, B.C. 91, 164, 246, 249  
 Sales, B.C., see Paul, D.McK. 189  
 Salmen, M., see Wassermann, K. 374  
 Salvadore, J.R. 150, 152  
 Samokhin, K.V., see Mitrović, B. 223  
 Samokhvalova, E.P. 341, 368  
 Samokhvalova, E.P., see Fedotov, M.A. 343–345  
 Samuely, P., see Flachbart, K. 112, 115  
 Sánchez, D.R. 196, 239, 242, 257, 268, 296, 307  
 Sánchez, D.R., see Baggio-Saitovitch, E.M. 196, 200, 242, 252  
 Sanchez, D.R., see Baggio-Saitovitch, E.M. 200, 242  
 Sanchez, D.R., see Bourdarot, F. 200  
 Sanchez, D.R., see Fontes, M.B. 200  
 Sanchez, J.P. 209, 243  
 Sanchez, J.P., see Godart, C. 195  
 Sanchez, J.P., see Tomala, K. 255, 256  
 Santi, G., see Dugdale, S.B. 210  
 Santora, B.P., see Gilbert, J. 374  
 Santoro, A., see Grigereit, T.E. 197, 242, 262  
 Santoro, A., see Lynn, J.W. 293  
 Saprykin, A.S. 350  
 Sarrac, J.L., see Zandbergen, H.W. 202  
 Sarrao, J.L. 197, 202  
 Sarsfield, M.J., see Copping, R. 349  
 Sarsfield, M.J., see Gaunt, A.J. 346  
 Sasakawa, T., see Shigetoh, K. 66, 98  
 Sasaki, Y. 339  
 Sasaki, Y., see Ozeki, T. 371  
 Sasaki, Y., see Yamase, T. 358, 373  
 Sassik, H., see Rotter, M. 255  
 Sato, A., see Tanaka, T. 157, 159  
 Sato, A., see Zhang, F. 150  
 Sato, A., see Zhang, F.X. 142  
 Sato, G., see Watanuki, R. 115  
 Sato, H., see Izawa, K. 224  
 Sato, H., see Kohgi, M. 246  
 Sato, H., see Measson, M.-A. 238  
 Sato, H., see Seyfarth, G. 224  
 Sato, N.K., see Nakane, H. 191  
 Satoh, K., see Inagaki, A. 374  
 Sattler, A.M., see Nyman, M. 375  
 Saunders, K., see Radzihovsky, L. 275  
 Savitskii, E.M. 184  
 Sawyer, J.O. 4

- Saxena, S.S. 186, 191  
 Saxena, S.S., see Weller, Th.E. 184  
 Saxena, S.S., see Yelland, E.A. 191  
 Sayle, T.X. 33  
 Scagnoli, V., see Mulders, A.M. 207, 232, 247, 248, 267, 269, 270  
 Schachinger, E., see Manalo, S. 235, 240, 298, 300  
 Schäfer, H., see Eisenmann, B. 90  
 Schafers, F., see Wong, J. 120  
 Schenck, A. 247  
 Schenck, A., see Le, L.P. 241  
 Schepelew, J.D., see Schubnikow, L.W. 239  
 Schiffmacher, G., see Godart, C. 204  
 Schiffmacher, G., see Tominez, E. 184, 197  
 Schilling, J.S., see Gangopadhyay, A.K. 200, 206  
 Schilling, J.S., see Looney, C. 238  
 Schirber, J.E., see Williams, J.M. 184  
 Schlüter, M., see Gygi, F. 282  
 Schmidt, H. 192, 193, 206, 238, 266, 267, 293  
 Schmidt, H., see Wagner, T.A. 206, 261, 266  
 Schmidt, L., see Brison, J.P. 306  
 Schmidt, P., see Hannay, N.B. 182  
 Schmidtman, M., see Cronin, L. 370  
 Schmidtman, M., see Müller, A. 370  
 Schmiedeshoff, G.M. 193, 232, 240, 274  
 Schmiedeshoff, G.M., see Bud'ko, S.L. 231, 239, 240, 272  
 Schmiedeshoff, G.M., see Christianson, A.D. 279  
 Schmiedeshoff, G.M., see Lacerda, A. 278, 279  
 Schmitt, D., see El Massalami, M. 255, 309  
 Schmitt, D., see Felner, I. 295  
 Schmitt, D., see Gignoux, D. 107, 108  
 Schmitt, D., see Levy, P.M. 247  
 Schmitt, D., see Morin, P. 199  
 Schneider, M. 215, 218–221  
 Schneider, M., see Lipp, D. 295–297, 300, 301  
 Schneider, Ma. 239, 267  
 Schneider, Mi. 264  
 Schneidewind, A., see Kreyszig, A. 198, 199  
 Schnelle, W., see Gulden, T. 184  
 Schnelle, W., see Pöttgen, R. 87  
 Schober, H., see Loewenhaupt, M. 263  
 Schober, H., see Rotter, M. 244, 246, 278  
 Schober, H., see Sierks, C. 244, 278  
 Schreyer, M. 90  
 Schrieffer, J.R., see Bardeen, J. 212  
 Schubert, K. 88  
 Schubert, K., see Pötzschke, M. 88  
 Schubert, R., see Cura, Ch. 239  
 Schubert, E., see Flachbart, K. 112, 115  
 Schubnikow, L.W. 239  
 Schuld, H.S., see Baenziger, N.C. 4, 5  
 Schuller, I.K., see Dunlap, B.D. 190  
 Schultz, L., see Bashlakov, D.L. 229  
 Schultz, L., see Behr, G. 205  
 Schultz, L., see Bitterlich, H. 204, 206, 207, 305  
 Schultz, L., see Drechsler, S.-L. 193, 212, 214  
 Schultz, L., see Freudenberger, J. 205, 207, 217, 234, 268, 296, 303, 306, 307, 309  
 Schultz, L., see Gumbel, A. 202, 205  
 Schultz, L., see Häse, K. 207, 208, 232  
 Schultz, L., see Müller, K.-H. 207, 232, 247, 248, 267, 269, 270  
 Schultz, L., see Wälte, A. 182, 185  
 Schultz, L., see Wimbush, S.C. 208, 232, 233  
 Schuster, H.-U., see Bockelmann, W. 79, 80  
 Schwarz, K., see Diviš, M. 210, 212, 240–242, 251–254  
 Schwarz, K., see Principi, G. 89  
 Schweda, E.D. 4  
 Scotland, K.B., see Zhang, C. 353, 360  
 Seaman, C.L., see Luke, G.M. 185  
 Sebastian, C.P. 80  
 Sebastian, S.E., see Bluhm, H. 275, 289, 290  
 Secheresse, F., see Mialane, P. 346, 353–355, 371  
 Segre, C., see Dunlap, B.D. 190  
 Sekula, S.T., see Christen, D.K. 280  
 Sendlinger, B. 70  
 Senoussi, S., see Öner, Y. 94  
 Seo, S.W., see Lee, K.H. 286  
 Sera, M. 219–221, 261  
 Sera, M., see Michimura, S. 115  
 Serain, C., see Müller, A. 369  
 Seto, Y., see Inouye, Y. 374  
 Setoguchi, H., see Matsuda, N. 238  
 Seyboldt, A.U. 116  
 Seyfarth, G. 224  
 Seyfarth, G., see Measson, M.-A. 238  
 Shaburov, V.A., see Sovestnov, A.E. 41  
 Shan, Y. 346, 348, 349  
 Shan, Y., see Liu, Z. 346  
 Shan, Y., see Lu, B. 346  
 Shan, Y., see Wang, E. 346, 349  
 Shan, Y., see Zhou, B. 346, 349  
 Shan, Y.-K., see Wang, X.-G. 346  
 Shantsev, D.V., see Bobyl, A.V. 288  
 Shapira, Y. 155  
 Shapiro, B.Ya., see Li, D.P. 284  
 Shapiro, I., see Li, D.P. 284  
 Shapiro, S.M., see Bullock, M. 214  
 Shapiro, S.M., see Stassis, C. 214  
 Shapiro, S.M., see Sternlieb, B.J. 242  
 Shapiro, S.M., see Zarestky, J. 214  
 Shapiro, S.M., see Zarestky, J.L. 296

- Sharma, R. 30  
 Sharma, R., see Jiang, Y. 7, 33, 34  
 Sharoni, A., see Tsindlekht, M.I. 113, 115  
 Sharp, J., see Nolas, G.S. 158  
 Shaula, A., see Fagg, D.P. 45  
 Sheet, G., see Mukhopadhyay, S. 228, 241, 284  
 Sheet, G., see Raychaudhuri, P. 227, 228, 284  
 Sheikin, I., see Saxena, S.S. 191  
 Shelton, R.N. 191  
 Shelton, R.N., see Hoellwarth, C.C. 293  
 Shelton, R.N., see Ku, H.C. 184  
 Shelton, R.N., see Lee, W.H. 184  
 Shelton, R.N., see Lynn, J.W. 188  
 Shelton, R.N., see Stanley, H.B. 191  
 Shen, E., see Wang, E. 349  
 Shestak, A.S., see Tomilo, Zh.M. 202  
 Shevchenko, S.N., see Kolesnichenko, Yu.A. 231  
 Shi, Y., see Leithe-Jasper, A. 157  
 Shi, Y., see Tanaka, T. 159  
 Shibata, A., see Izawa, K. 227  
 Shibauchi, T., see Kasahara, Y. 306  
 Shieh, J.H., see Jiang, P.J. 197  
 Shieh, J.H., see Ku, H.C. 184, 197, 202  
 Shieh, J.H., see Lin, M.S. 259  
 Shigekawa, A., see Michimura, S. 115  
 Shigetoh, K. 66, 98  
 Shih, H.Y., see Lan, M.D. 236, 304  
 Shilov, V.P. 350  
 Shilov, V.P., see Yusov, A.B. 340  
 Shimizu, K. 182, 186  
 Shimkaveg, G., see Wong, J. 119  
 Shimojima, T., see Baba, T. 227, 228, 274, 300  
 Shin, S., see Baba, T. 227, 228, 274, 300  
 Shin, S., see Yokoya, T. 222, 227, 284, 295, 300  
 Shiokawa, J., see Sakai, T. 184, 203  
 Shiozaki, R. 343, 374  
 Shirai, K. 109, 110  
 Shiraishi, J. 233  
 Shirane, G., see Bullock, M. 214  
 Shirane, G., see Stassis, C. 214  
 Shirane, G., see Thomlinson, W. 188, 189  
 Shirane, G., see Zarestky, J. 214  
 Shirane, G., see Zarestky, J.L. 296  
 Shirokova, I.B., see Bessonov, A.A. 374  
 Shirokova, I.B., see Fedoseev, A.M. 368  
 Shirokova, I.B., see Yusov, A.B. 368  
 Shishido, H., see Kasahara, Y. 306  
 Shitsevalova, N., see Czopnik, A. 112, 115  
 Shitsevalova, N., see Flachbart, K. 112, 115  
 Shitsevalova, N., see Gabani, S. 112–116  
 Shitsevalova, N., see Kohout, A. 114–116  
 Shitsevalova, N., see Murasik, A. 115, 116  
 Shitsevalova, N., see Paderno, Y.B. 111, 112, 114, 115  
 Shitsevalova, N., see Siemensmeyer, K. 114–116  
 Shklovskii, B.I., see Efros, A.L. 119, 129  
 Shoair, A.G.F., see Griffith, W.P. 349, 374  
 Shoemaker, C.B. 81  
 Shoemaker, D.P., see Shoemaker, C.B. 81  
 Shorikov, A.O. 210, 259, 309  
 Shtrikman, H., see Dewhurst, C.D. 289  
 Shtrikman, H., see James, S.S. 289, 290  
 Shuk, P. 44  
 Shulga, S.V. 180, 214, 222, 232, 234–237, 240, 241, 259, 298, 301, 308  
 Shulga, S.V., see Drechsler, S.-L. 193, 209, 210, 212–214, 229, 235, 236, 259, 270, 309  
 Shulga, S.V., see Freudenberger, J. 234, 296  
 Shulga, S.V., see Fuchs, G. 235, 236, 240, 296, 297, 300  
 Shulga, S.V., see Gonnelli, R.S. 215  
 Shulga, S.V., see Rosner, H. 299  
 Shulga, S.V., see Wälte, A. 182  
 Shultz, A.J., see Williams, J.M. 184  
 Shum, W., see Day, V.W. 341  
 Sibert, W., see Nowotny, H. 90  
 Sichevich, O.M. 88  
 Sidorov, N.S., see Gasparov, V.A. 113, 115, 237  
 Sidorov, V.A., see Ekimov, E.A. 182, 184  
 Sieberer, M. 200  
 Siegrist, T. 195, 200, 249, 250, 252, 278  
 Siegrist, T., see Cava, R.J. 180, 181, 184, 197, 202, 240, 242, 300  
 Siegrist, T., see Mattheiss, L.F. 196, 210, 212, 243, 250, 252  
 Siemensmeyer, K. 114–116  
 Siemensmeyer, K., see Flachbart, K. 112, 115  
 Siemensmeyer, K., see Kohout, A. 114–116  
 Sierks, C. 244, 278  
 Sierks, C., see Kreyssig, A. 264  
 Sierks, C., see Loewenhaupt, M. 263  
 Sierks, C., see Rotter, M. 244, 246, 278  
 Sigrist, M., see Doh, H. 259, 308  
 Sigrist, M., see Kasahara, Y. 306  
 Sigrist, M., see Shorikov, A.O. 210, 259, 309  
 Sigrist, M., see Tsunetsugu, H. 114  
 Sikka, S.K., see Meenakshi, S. 239  
 Sikolenko, V., see Jensen, A. 272  
 Silhanek, A.V. 287  
 Silhanek, A.V., see Civale, L. 223  
 Silhanek, A.V., see Thompson, J.R. 215  
 Sillén, L.G., see Sasaki, Y. 339  
 Silverton, J.V., see Dexter, D.D. 340  
 Simak, S.I., see Skorodumova, N.V. 7  
 Simon, A. 85, 184

- Simon, A., see Gulden, T. 184  
 Simon, A., see Henn, R.W. 184  
 Simon, A., see Kremer, R.K. 182  
 Simon, A., see Pöttgen, R. 57  
 Simon, P., see Cao, G.H. 208  
 Simonov, V.I., see Molchanov, V.N. 343, 346  
 Singh, D.J. 212  
 Singh, D.J., see Pickett, W.E. 210  
 Singhal, R.K., see Kumari, K. 210  
 Sinha, S.K. 197, 242, 271  
 Sinha, S.K., see Lynn, J.W. 197, 209, 242, 244, 245, 249, 250, 253, 257, 292  
 Siri, A.S., see Cimberle, M.R. 207  
 Siri, A.S., see Grassano, G. 208, 232  
 Sirvent, C., see Li, S. 278  
 Skanthakumar, S. 190, 241, 242, 245, 252, 276  
 Skanthakumar, S., see Bourdarot, F. 200  
 Skanthakumar, S., see Lynn, J.W. 197, 209, 242, 244, 245, 249, 250, 253, 257, 292  
 Skarnulis, A.J. 4  
 Skipper, N.T., see Weller, Th.E. 184  
 Skolozdra, R.V. 56, 58, 62, 93  
 Skomski, R., see Leithe-Jasper, A. 67, 68, 89, 97  
 Skorodumova, N.V. 7  
 Skrotzki, W., see Cao, G.H. 208  
 Skrotzki, W., see Gümbel, A. 202, 205  
 Skrotzki, W., see Oertel, C.-G. 205  
 Skrotzki, W., see Subba Rao, K. 208  
 Slack, G.A. 119, 138, 158, 159, 163, 164, 166  
 Slack, G.A., see Cahill, D.G. 158, 159, 164  
 Slaski, M., see Dunlap, B.D. 190  
 Sleight, A.W., see Luke, G.M. 185  
 Slusky, J.S., see He, T. 184  
 Smeibidl, P., see Jensen, A. 272  
 Smeibidl, P., see Nørgaard, T.K. 276  
 Smirnov, I.A., see Sovestnov, A.E. 41  
 Smirnov, Yu.P., see Sovestnov, A.E. 41  
 Smith, D.J., see Kang, Z.C. 33  
 Smith, J.L., see Nagarajan, R. 277  
 Smith, J.L., see Schmiedeshoff, G.M. 193, 232, 240  
 Smith, M.F., see Pairor, P. 229  
 Smith, R.I., see Hillier, A.D. 206  
 Smith, R.P., see Weller, Th.E. 184  
 Smith, R.P., see Yelland, E.A. 191  
 Smith, V.E., see Vidhyadhiraja, N.S. 114  
 Snel, C.E., see El Massalami, M. 293  
 Sobolev, A.N., see Sichevich, O.M. 88  
 Soderholm, L. 365  
 Soderholm, L., see Antonio, M.R. 364, 365, 375  
 Soderholm, L., see Dunlap, B.D. 190  
 Sok, J. 242, 309  
 Sologub, O.L. 56  
 Sologub, O.L., see Mazumdar, C. 249  
 Sologub, O.L., see Öner, Y. 94  
 Sologub, O.L., see Salamakha, P.S. 56, 58, 68, 69  
 Sologubenko, A.V. 224  
 Solt, G., see Schenck, A. 247  
 Song, C. 198, 256, 257  
 Song, K.-J. 240, 287  
 Song, K.J., see Civale, L. 223  
 Song, K.J., see Thompson, J.R. 215  
 Song, Y.S., see Choi, C.K. 293  
 Sonier, J.E. 286  
 Sonier, J.E., see Ohishi, K. 300  
 Sonier, J.E., see Price, A.N. 286  
 Soos, Z.G., see Cheung, T.T.P. 132  
 Sorensen, O.T. 6  
 Sørensen, O.T., see Manes, L. 6  
 Souptel, D. 205–207, 240, 291, 325  
 Souptel, D., see Bashlakov, D.L. 229  
 Souptel, D., see Fuchs, G. 240  
 Souptel, D., see Ignatchik, O. 210, 230  
 Souptel, D., see Kreyssig, A. 215  
 Souptel, D., see Müller, K.-H. 207, 232, 247, 248, 267, 269, 270  
 Souptel, D., see Naidyuk, Yu.G. 213, 227, 269  
 Souptel, D., see Schneider, Ma. 239, 267  
 Sousa, F.L. 373  
 Sovestnov, A.E. 41  
 Spataru, T., see Principi, G. 89  
 Spencer, C.M., see Gordon, R.A. 57, 67, 95  
 Spinelli, N., see Wang, X. 208  
 Spitsyn, V.I., see Fedoseev, A.M. 368  
 Spitsyn, V.I., see Saprykin, A.S. 350  
 Spitsyn, V.I., see Tat'yanina, I.V. 340  
 Spitsyn, V.I., see Yusov, A.B. 351  
 Spitz, C., see Zhang, T. 373  
 Springford, M., see Corcoran, R. 230  
 Sridhar, S., see Eskildsen, M.R. 276, 287, 289  
 Sridhar, S., see Jacobs, T. 261  
 Stanley, H.B. 191  
 Stanley, H.E., see Aharony, A. 185  
 Stassis, C. 214  
 Stassis, C., see Bullock, M. 214  
 Stassis, C., see Dervenagas, P. 197, 214, 242, 257  
 Stassis, C., see Detlefs, C. 198, 241, 242, 245, 253–255  
 Stassis, C., see Goldman, A.I. 197, 242, 262  
 Stassis, C., see Hill, J.P. 262  
 Stassis, C., see Sternlieb, B.J. 242  
 Stassis, C., see Yaron, U. 280, 289  
 Stassis, C., see Zarestky, J. 197, 214, 242, 271  
 Stassis, C., see Zarestky, J.L. 296  
 Staub, U. 247

- Staub, U., see Mulders, A.M. 207, 232, 247, 248, 267, 269, 270  
 Steep, E., see Goll, G. 235  
 Steep, E., see Nguyen, L.H. 210  
 Steglich, F. 192, 195  
 Steglich, F., see Grewe, N. 279  
 Steglich, F., see Rauchschalbe, U. 250  
 Steiner, M.J., see Saxena, S.S. 191  
 Steiner, W., see Weitzer, F. 65, 67–69, 88, 93, 96  
 Stepanov, V.A., see Daghero, D. 113, 115  
 Stepanov, V.A., see Gonnelli, R.S. 215  
 Stephens, P.W., see Dertinger, A. 206, 261, 266  
 Stepień-Damm, J., see Gulay, L.D. 64–66, 68, 69, 71–77, 79, 80  
 Stepień-Damm, J., see Kalychak, Ya.M. 86, 87  
 Sternlieb, B.J. 242  
 Sternlieb, B.J., see Goldman, A.I. 197, 242, 262  
 Sternlieb, B.J., see Hill, J.P. 262  
 Sternlieb, B.J., see Luke, G.M. 185  
 Stewart, G.R., see Cho, B.K. 57, 86, 93, 98  
 Stewart, G.R., see Jones, C.D.W. 67, 93, 99  
 Stewart, J.R., see Hillier, A.D. 305  
 Stishov, S.M., see Ekimov, E.A. 182, 184  
 Stockert, O., see Kreyszig, A. 215  
 Stolz, E., see Schubert, K. 88  
 Strand, J.D., see Bud'ko, S.L. 304  
 Strässle, Th., see Cavadini, N. 246  
 Strässler, S., see Baltensperger, W. 188, 189  
 Streit, T.S.J., see Anderico, C.Z. 147  
 Ström, V. 202, 205  
 Stronach, C.E., see Bernhard, C. 191  
 Stronach, C.E., see Luke, G.M. 185  
 Struchkov, Y.T., see Fedoseev, A.M. 368  
 Struchkov, Y.T., see Grigor'ev, M.S. 368  
 Struzhkin, V.V., see Eremets, M.I. 182, 184  
 Strydom, A.M. 66, 95  
 Stuesser, N., see Kreyszig, A. 264  
 Subba Rao, K. 208  
 Subramanian, M.A., see Luke, G.M. 185  
 Suderow, H. 229, 236–238, 277  
 Suderow, H., see Crespo, M. 275  
 Suderow, H., see Martínez-Samper, P. 215, 229  
 Sudhakar Rao, G.V. 191  
 Suetake, M., see Suzuki, M. 198  
 Sugawara, H., see Izawa, K. 224  
 Sugawara, H., see Kohgi, M. 246  
 Sugawara, H., see Measson, M.-A. 238  
 Sugawara, H., see Seyfarth, G. 224  
 Sugeta, M. 344, 372  
 Sugeta, M., see Yamase, T. 373  
 Sugii, N., see Hamada, K. 111, 113  
 Sugino, T., see Takasu, Y. 45  
 Suh, B.J. 209  
 Suhl, H. 191  
 Suhl, H., see Anderson, P.W. 188  
 Suhl, H., see Matthias, B.T. 186, 187  
 Sukal, S., see Bartis, J. 343, 348–350  
 Sulpice, A., see Bud'ko, S.L. 198  
 Sulpice, A., see El Massalami, M. 200  
 Summerville, E. 4  
 Summerville, E., see Skarmulis, A.J. 4  
 Sun, C.P., see Huang, C.L. 226, 227, 232  
 Sun, G. 374  
 Sun, G., see Feng, J. 374  
 Sun, R.-Q. 346  
 Sun, S., see Liu, J. 349  
 Sun, X., see Dresselhaus, M.S. 165  
 Sun, Y.Y., see Dezaneti, L.M. 180, 184, 197, 202  
 Sun, Y.Y., see Gao, L. 200, 201, 238  
 Sun, Z.-G., see Li, J.-X. 374  
 Sungaila, Z., see Dunlap, B.D. 190  
 Surdeanu, R., see Dewhurst, C.D. 289  
 Surdeanu, R., see Saha, N. 275, 289  
 Suriaatmaja, M., see Griffith, W.P. 349, 374  
 Suzuki, H., see Nohara, M. 295  
 Suzuki, H., see Ohishi, K. 300  
 Suzuki, H.S., see Onimaru, T. 246, 247  
 Suzuki, K., see Watanuki, R. 115  
 Suzuki, M. 198  
 Suzuki, M., see Isida, S. 214  
 Suzuki, M., see Kobayashi, Y. 239, 267  
 Svidzinskii, A.A., see Barash, Yu.S. 302  
 Szabo, P., see Flachbart, K. 112, 115  
 Szklarz, E.G., see Giorgi, A.L. 184  
 Szklarz, E.G., see Krupka, M.C. 184  
 Szyzewski, A. 364  
 Szymczak, H., see Szymczak, R. 271  
 Szymczak, R. 271  
 Tabet, J.-C., see Boglio, C. 353–355, 375  
 Tachiki, M., see Matsumoto, H. 188  
 Taillefer, L., see Boaknin, E. 215, 220, 221, 224  
 Tajima, S., see Suderow, H. 229, 236–238  
 Takabatake, T., see Michimura, S. 115  
 Takabatake, T., see Shigetoh, K. 66, 98  
 Takagi, H. 192, 216, 240  
 Takagi, H., see Baba, T. 227, 228, 274, 300  
 Takagi, H., see Cava, R.J. 180, 181, 184, 197, 200–202, 240, 242, 300  
 Takagi, H., see Eisaki, H. 197, 242, 261  
 Takagi, H., see Izawa, K. 220, 224, 227, 284  
 Takagi, H., see Luke, G.M. 185  
 Takagi, H., see Murayama, C. 238

- Takagi, H., see Nohara, M. 222, 226, 295, 297, 300, 301
- Takagi, H., see Ohishi, K. 300
- Takagi, H., see Takaki, K. 223, 300
- Takagi, H., see Watanabe, T. 223
- Takagi, H., see Yokoya, T. 222, 227, 284, 295
- Takahashi, H., see Uehara, M. 182
- Takahashi, M., see Ozeki, T. 344
- Takahashi, Y., see Iga, F. 114, 127, 128
- Takahashi, Y., see Suzuki, M. 198
- Takaki, K. 223, 300
- Takakuwa, Y., see Iga, F. 114, 127, 128
- Takami, M., see Higashi, I. 122, 123
- Takano, Y., see Yokoya, T. 227
- Takasu, Y. 45
- Takayama-Muromachi, E., see Mori, T. 168
- Takeda, K., see Choi, J.-H. 264, 309
- Takeda, K., see Shimizu, K. 182, 186
- Takekawa, S., see Kitô, H. 200, 201
- Takenouchi, S., see Tanaka, T. 159
- Takeshita, H., see Kawano-Furukawa, H. 273, 274
- Takeuchi, A., see El Massalami, M. 200
- Takeuchi, T., see Onimaru, T. 246, 247
- Takeya, H. 204, 205, 216, 236, 250, 258, 309
- Takeya, H., see Abliz, M. 265
- Takeya, H., see Chia, E.E.M. 188, 207, 275
- Takeya, H., see El Massalami, M. 250, 255, 257, 272, 309
- Takeya, H., see Isida, S. 214
- Takeya, H., see Izawa, K. 227
- Takeya, H., see Jaiswal-Nagar, D. 286
- Takeya, H., see Kawano, H. 242, 273
- Takeya, H., see Kawano-Furukawa, H. 214, 273–275
- Takeya, H., see Kobayashi, Y. 239, 267
- Takeya, H., see Mukhopadhyay, S. 228, 241, 284
- Takeya, H., see Nishimori, H. 229, 280–282, 284
- Takeya, H., see Raychaudhuri, P. 227, 228, 284
- Takeya, H., see Sera, M. 219–221, 261
- Takeya, H., see Suzuki, M. 198
- Takeya, H., see Terashima, T. 230
- Takeya, H., see Togano, K. 184
- Takeya, H., see Zhao, S.R. 308
- Takimoto, T., see Mori, T. 140
- Takita, K., see Corcoran, R. 230
- Talhaoui, M., see Alleno, E. 207, 309
- Tallon, J.L., see Bernhard, C. 191
- Tallon, J.L., see Lynn, J.W. 190
- Tamm, R., see Subba Rao, K. 208
- Tanaka, M., see Murakami, Y. 248
- Tanaka, T. 120, 122, 123, 135, 136, 138, 157, 159
- Tanaka, T., see Higashi, I. 118, 122, 123, 125, 126, 159
- Tanaka, T., see Ishizawa, Y. 161
- Tanaka, T., see Leithe-Jasper, A. 140, 142, 157
- Tanaka, T., see Mori, T. 120–124, 127, 128, 130, 134–139, 143, 159–161
- Tanaka, T., see Werheit, H. 119
- Tanaka, T., see Wong, J. 119, 120
- Tanaka, T., see Zhang, F. 150
- Tanaka, T., see Zhang, F.X. 142
- Tanaka, Y., see Mulders, A.M. 207, 232, 247, 248, 267, 269, 270
- Tang, J. 87
- Tangestaninejad, S., see Mirkhani, V. 374
- Tat'yanina, I.V. 340, 341
- Tat'yanina, I.V., see Gavrilova, L.O. 341
- Tat'yanina, I.V., see Petrukhina, M.A. 341
- Tat'yanina, I.V., see Samokhvalova, E.P. 341, 368
- Taylor, K.N.R. 113
- Taylor, R.D., see Willis, J.O. 187
- Terashima, T. 230
- Teresiak, A., see Narozhnyi, V.N. 252, 287
- Teresiak, A., see Souptel, D. 205
- Tergenius, L.E., see Korsukova, M.M. 136
- Tešanović, Z., see Dukan, S. 224
- Tesliuk, M.J., see Gladyshevskii, E.I. 84
- Tézé, A., see Robert, F. 362
- Thakur, A.D., see Jaiswal-Nagar, D. 232, 286
- Thalmeier, P. 193, 223
- Thalmeier, P., see Amici, A. 262, 265, 268
- Thalmeier, P., see Izawa, K. 220, 224, 227, 284
- Thalmeier, P., see Maki, K. 222, 284
- Thalmeier, P., see Won, H. 223
- Thalmeier, P., see Yuan, Q. 223, 227
- Thiel, R.C., see Mulder, F.M. 196, 198, 255
- Thomassen, L., see Goldschmidt, V.M. 3
- Thomlinson, W. 188, 189
- Thomlinson, W., see Lynn, J.W. 187
- Thompson, J.D., see Alleno, E. 238
- Thompson, J.D., see Ekimov, E.A. 182, 184
- Thompson, J.D., see Hundley, M.F. 114
- Thompson, J.D., see Le, L.P. 241
- Thompson, J.D., see Movshovich, R. 57, 66, 67, 94, 242
- Thompson, J.D., see Park, T. 227
- Thompson, J.R. 215
- Thompson, J.R., see Civile, L. 223
- Thompson, J.R., see Kogan, V.G. 215, 293
- Thompson, J.R., see Paul, D.McK. 189
- Thompson, J.R., see Sales, B.C. 164
- Thompson, J.R., see Silhanek, A.V. 287
- Thompson, J.R., see Song, K.-J. 240, 287

- Thompson, J.R., see Yethiraj, M. 280, 281  
 Thorel, P., see Christen, D.K. 280  
 Thorimbert, S., see Boglio, C. 353–355, 375  
 Thornber, M.R. 5  
 Thorsen, A.C., see Fink, H.J. 184  
 Thouvenot, R., see Boglio, C. 353–355, 375  
 Thouvenot, R., see Contant, R. 346  
 Tilley, R.J.D., see Turcotte, R.A. 10  
 Tils, P., see Sierks, C. 278  
 Timofeeva, M.N., see Kholdeeva, O.A. 352, 374  
 Ting, C.S., see Yuan, Q. 223, 227  
 Tinkham, M. 237  
 Tissen, V.G., see Suderow, H. 236–238  
 Tjutrina, L.V., see Rybaltchenko, L.F. 270  
 Todaro, L., see Zhang, C. 346, 353, 360  
 Todaro, L.J., see Zhang, C. 345–347, 351, 352  
 Togano, K. 184  
 Togano, K., see Arisawa, S. 207, 208  
 Togashi, T., see Baba, T. 227, 228, 274, 300  
 Tokura, A., see Nishimori, H. 229, 280–282, 284  
 Tokura, Y. 248  
 Tokura, Y., see Luke, G.M. 185  
 Tokura, Y., see Murakami, Y. 248  
 Tokutake, Y., see Inouye, Y. 374  
 Tomala, K. 255, 256  
 Tomari, H., see Saito, A. 341  
 Tomilo, Zh.M. 202  
 Tominez, E. 184, 193, 197, 202  
 Tominez, E., see Berger, P. 206  
 Tominez, E., see Dhar, S.K. 242, 278  
 Tominez, E., see Godart, C. 195  
 Tompkins, H., see Wong, J. 119  
 Tompkins, M.V., see Schmiedeshoff, G.M. 193  
 Tomy, C.V. 193, 197, 242, 256–260  
 Tomy, C.V., see Chang, L.J. 200, 242  
 Tomy, C.V., see Civale, L. 223  
 Tomy, C.V., see Paul, D.McK. 277  
 Tomy, C.V., see Rybaltchenko, L.F. 270  
 Tomy, C.V., see Silhanek, A.V. 287  
 Tomy, C.V., see Song, K.-J. 240, 287  
 Tomy, C.V., see Thompson, J.R. 215  
 Tomy, C.V., see Yanson, I.K. 214, 259, 260  
 Tomy, C.V., see Yethiraj, M. 280, 281  
 Toner, J., see Radzihovsky, L. 275  
 Tonnerre, J.M., see Mulders, A.M. 207, 232, 247, 248, 267, 269, 270  
 Torchenkova, E.A., see Fedotov, M.A. 343  
 Torchenkova, E.A., see Gavrilova, L.O. 341  
 Torchenkova, E.A., see Molchanov, V.N. 343, 346  
 Torchenkova, E.A., see Petrukhina, M.A. 341  
 Torchenkova, E.A., see Samokhvalova, E.P. 341, 368  
 Torchenkova, E.A., see Tat'yanina, I.V. 340, 341  
 Torgeson, D.R., see Suh, B.J. 209  
 Torng, C.J., see Wu, M.K. 185  
 Tortora, A., see Wang, X. 208  
 Tosaka, M., see Yamase, T. 344, 373  
 Toth, L., see Fink, H.J. 184  
 Tourné, C.M. 343  
 Tourné, G.F., see Tourné, C.M. 343  
 Touton, S., see Schmiedeshoff, G.M. 274  
 Iran, V.H. 73, 99  
 Tremel, W., see Melnyk, G. 63, 64, 66–77  
 Treyvaud, A., see Peter, M. 187  
 Trindade, T., see Sousa, F.L. 373  
 Trochez, J.C., see Fontes, M.B. 200  
 Trovarelli, A. 8  
 Tsabba, Y., see Felner, I. 191  
 Tsindlekht, M.I. 113, 115  
 Tsoukala, V., see Slack, G.A. 164  
 Tsuchiya, Y., see Takaki, K. 223, 300  
 Tsuda, S., see Baba, T. 227, 228, 274, 300  
 Tsuda, S., see Yokoya, T. 227  
 Tsujii, N., see Mori, T. 122, 130, 143  
 Tsunetsugu, H. 114  
 Tsvyashchenko, A.V., see Narozhnyi, V.N. 217, 279  
 Tuenge, R.T. 4, 10, 37  
 Tuenge, R.T., see Summerville, E. 4  
 Turcotte, R.A. 10  
 Turcotte, R.P. 16, 37  
 Tutsch, U., see Wang, Y. 113  
 Tyler, A.W., see Riseman, T.M. 280  
 Tytko, K.H. 339  
 Tyunis, A.V., see Sovestnov, A.E. 41  
 Tyutrina, L.V., see Bobrov, N.L. 228, 229, 240  
 Uchida, S., see Cava, R.J. 180, 181, 184, 197, 200–202, 240, 242  
 Uchida, S., see Eisaki, H. 197, 242, 261  
 Uchida, S., see Luke, G.M. 185  
 Uchida, S., see Murayama, C. 238  
 Uchida, S., see Takagi, H. 216, 240  
 Uchiyama, K., see Nakai, N. 229  
 Uchiyama, K., see Nishimori, H. 229, 280–282, 284  
 Udagawa, M. 224, 229  
 Ueda, K., see Iwamoto, Y. 223  
 Ueda, K., see Tsunetsugu, H. 114  
 Ueda, K., see Yamase, T. 344, 372  
 Uefuji, T., see Gilardi, R. 280  
 Uehara, M. 182  
 Uemura, Y.J., see Luke, G.M. 185  
 Uher, C., see Nolas, G.S. 164

- Uhlarz, M., see Yelland, E.A. 191  
 Uji, S., see Terashima, T. 230  
 Ullah, N., see Antonio, M.R. 365  
 Ullmaier, H., see Auer, J. 113  
 Ulrich, C., see Lynn, J.W. 190  
 Umeo, K., see Shigetoh, K. 66, 98  
 Umezawa, H., see Matsumoto, H. 188  
 Ummarino, G.A., see Daghero, D. 113, 115  
 Ummarino, G.A., see Gonnelli, R.S. 215  
 Ustinovich, S.N., see Tomilo, Zh.M. 202  
 Uwatoko, Y. 238, 266  
 Uwatoko, Y., see Oomi, G. 239
- v. Löhneysen, H., see Yelland, E.A. 191  
 v. Zimmermann, M., see Andersen, N.H. 200, 276  
 Vaast, C., see Bonville, P. 295  
 Vaglio, R., see Andreone, A. 207, 208, 227  
 Vaglio, R., see Iavarone, M. 208  
 van den Brink, J. 247, 248  
 van der Beek, C.J., see Izawa, K. 227  
 van Dover, R.B., see Cava, R.J. 180, 181, 184, 197, 202, 240, 242, 300  
 van Duynveldt, A.J., see Huser, D. 145  
 Van Pelt, C.E. 351  
 Van Schilfgaarde, M., see Jiang, Y. 7, 33, 34  
 van Smaalen, S., see Dertinger, A. 206, 261, 266  
 Vandenberg, J.M. 91  
 Vanoni, W., see Bud'ko, S.L. 293, 295  
 Varezhkina, N.S., see Milyukova, M.S. 374  
 Varma, C.M., see Blount, E.I. 188  
 Varma, C.M., see Gammel, P.L. 275  
 Varma, C.M., see Ng, T.K. 275  
 Vaughan, G.M.B., see Nyman, M. 375  
 Vekhter, I., see Matsuda, Y. 224, 226  
 Vekhter, I., see Park, T. 227  
 Velotta, R., see Wang, X. 208  
 Venturi, M., see Ballardini, R. 372  
 Venturi, M., see Mulazzani, Q.G. 372  
 Venturini, G. 64, 66–70, 76, 90, 91  
 Veremchuk, I. 204  
 Verges, P., see Prassides, K. 242, 253  
 Verma, A.K. 200  
 Vernière, A., see Brison, J.P. 306  
 Vidal, H., see Bernal, S. 30, 49  
 Vidhyadhiraja, N.S. 114  
 Vieira, S., see Crespo, M. 275  
 Vieira, S., see Martínez-Samper, P. 215, 229  
 Vieira, S., see Suderow, H. 229, 236–238, 277  
 Vijayakumar, V., see Meenakshi, S. 239  
 Vijayaraghavan, R., see Dhar, S.K. 242, 278  
 Vijayaraghavan, R., see Godart, C. 204  
 Vijayaraghavan, R., see Gupta, L.C. 242, 253, 255  
 Vijayaraghavan, R., see Hossain, Z. 180, 202, 242, 253  
 Vijayaraghavan, R., see Mazumdar, C. 180, 216  
 Vijayaraghavan, R., see Meenakshi, S. 239  
 Vijayaraghavan, R., see Nagarajan, R. 180, 203, 242, 253  
 Villars, P. 62  
 Vinnikov, L.Ya. 275, 289, 290, 292  
 Vinokur, V., see Aranson, I. 288  
 Vivet, S., see Allen, E. 205, 295  
 Vivien, D., see Mialane, P. 353, 355  
 Vogt, T., see Detlefs, C. 198  
 Voiron, J., see El Massalami, M. 200  
 Voitenko, A.I., see Gabovich, A.M. 192  
 Volkova, L.M. 196  
 Vollmer, R., see Yelland, E.A. 191  
 Voltz, R., see Müller, W. 79, 80  
 von der Kammer, B., see Bassil, B.S. 345, 346, 349  
 Von Dreele, R.B. 4, 5  
 Von Dreele, R.B., see Zhang, J.R. 4, 5  
 von Lips, H. 210  
 von Lips, H., see Drechsler, S.-L. 193, 212, 214  
 von Lips, H., see Mazumdar, C. 278  
 Vorderwisch, P., see Eskildsen, M.R. 277, 292  
 Vorderwisch, P., see Gasser, U. 245, 246, 276, 278  
 Vorderwisch, P., see Nørgaard, T.K. 276  
 Vulliet, P., see Sanchez, J.P. 209, 243  
 Vulliet, P., see Tomala, K. 255, 256
- Wa, Q., see Wang, E. 349  
 Wachter, P. 7  
 Wachter, P., see Bommeli, F. 211  
 Wagener, W., see Sánchez, D.R. 257  
 Wagner, R.P., see Bambakidis, G. 109, 110  
 Wagner, T.A. 206, 261, 266  
 Wakata, M., see Hamada, K. 111, 113  
 Walf, G.H., see Sánchez, D.R. 257  
 Walker, E., see Peter, M. 187  
 Walker, I.R., see Saxena, S.S. 191  
 Walker, M.B. 257, 274  
 Wälte, A. 182, 185  
 Wälte, A., see Fuchs, G. 240  
 Wälte, A., see Müller, K.-H. 207, 232, 247, 248, 267, 269, 270  
 Wälte, A., see Naidyuk, Yu.G. 213, 269  
 Wang, E. 346, 349  
 Wang, E., see An, H. 368  
 Wang, E., see Liu, J. 349, 356  
 Wang, E., see Liu, Z. 346  
 Wang, E., see Rong, C. 349

- Wang, E., see Shan, Y. 346  
 Wang, E., see Wang, X. 349  
 Wang, E., see Wu, Q. 349  
 Wang, E.-B., see Bi, L.-H. 356  
 Wang, E.-B., see Liu, S.-X. 372  
 Wang, G. 222  
 Wang, G., see Liu, J. 349  
 Wang, G., see Qu, L. 349  
 Wang, H.H., see Williams, J.M. 184  
 Wang, H.S., see Wang, J. 373  
 Wang, J. 373  
 Wang, J., see Niu, J. 346, 355  
 Wang, J., see Wang, Z. 373  
 Wang, J., see Xue, G. 362  
 Wang, J., see Zhao, J. 346  
 Wang, J.-P., see Niu, J.-Y. 355  
 Wang, S. 349  
 Wang, S., see Qu, L. 349  
 Wang, S., see Zhai, S. 373  
 Wang, S.-M., see Cai, X.-Z. 369  
 Wang, S.-M., see Huang, J.-F. 369  
 Wang, W. 349  
 Wang, W., see Liu, J. 349  
 Wang, W.-Q., see Liu, J.-F. 356  
 Wang, X. 208, 349  
 Wang, X., see An, H. 368  
 Wang, X., see Rhee, J.Y. 285  
 Wang, X., see Wang, Y. 373  
 Wang, X.-G. 346  
 Wang, X.-h., see Liu, J.-f. 374  
 Wang, Y. 113, 237, 373  
 Wang, Y., see He, T. 184  
 Wang, Y.K. 306  
 Wang, Y.Q., see Wu, M.K. 185  
 Wang, Z. 373  
 Wang, Z., see Liu, J. 349  
 Wang, Z., see Wang, E. 349  
 Wang, Z., see Wang, J. 373  
 Wang, Z., see Wang, X. 349  
 Wang, Z.R., see Xu, M. 181, 204, 232  
 Warmkessel, J.M., see Turcotte, R.A. 10  
 Washizawa, T., see Yamaguchi, T. 246  
 Wassermann, K. 357, 363, 374  
 Wassermann, K., see Pope, M.T. 357  
 Watanabe, S., see Baba, T. 227, 228, 274, 300  
 Watanabe, T. 223, 274  
 Watanabe, T., see Baba, T. 227, 228, 274, 300  
 Watanabe, T., see Izawa, K. 220, 224, 227, 284  
 Watanabe, T., see Yokoya, T. 222, 227, 284, 295  
 Watanuki, R. 115  
 Watson, S.K., see Cahill, D.G. 158, 159, 164  
 Weakley, T.J.R., see Iball, J. 342, 344  
 Weakley, T.J.R., see Peacock, R.D. 342–344, 349, 351  
 Weakley, T.J.R., see Rosu, C. 342, 344  
 Weber, H.W., see Fuger, R. 291  
 Weber, H.W., see Krutzler, C. 208, 263, 291  
 Weber, M., see Schmidt, H. 266  
 Wehner, B., see Behr, G. 204  
 Weht, R. 239  
 Wei, G., see Liu, Z. 346  
 Wei, G., see Shan, Y. 346  
 Wei, X., see Pope, M.T. 357  
 Wei, Y., see Ma, J. 368  
 Wei, Y., see Zhou, B. 349, 368  
 Weitzer, F. 65, 67–69, 88, 93, 96  
 Weitzer, F., see Leithe-Jasper, A. 67, 68, 89, 97  
 Weller, Th.E. 184  
 Wells, A.F. 84  
 Welp, U., see De Wilde, Y. 280  
 Welp, U., see Metlushko, V. 215, 232, 233, 237, 285  
 Wen, L.-l., see Xin, X.-l. 374  
 Wen, Y., see Zhao, J. 346  
 Weng, Z., see Liao, C. 374  
 Wenski, G. 78, 80  
 Werheit, H. 107, 119, 158, 159, 163, 166  
 Wermeille, D., see Song, C. 198, 256, 257  
 Werner, D., see Michor, H. 200  
 Werthamer, N.R., see Hohenberg, P.C. 232, 285  
 Wertheimer, M., see Goodman, B.B. 287  
 Whangbo, M.-H., see Williams, J.M. 184  
 White, A.J.P., see Griffith, W.P. 349, 374  
 White, S.J., see Tang, J. 87  
 Widder, W., see Bauernfeind, L. 190  
 Wiesinger, G., see Weitzer, F. 65, 67–69, 88, 93, 96  
 Wiesner, U., see Buchgeister, M. 197, 301  
 Wijngaarden, R.J. 182  
 Wijngaarden, R.J., see Saha, N. 275, 289  
 Wildes, A.R., see Boothroyd, A.T. 278, 279  
 Wilhelm, M., see Hillenbrand, B. 187  
 Wilhelm, M., see Peter, M. 187  
 Wilkinson, I., see Dugdale, S.B. 210  
 Will, G., see Kirfel, A. 142  
 Willemsen, B.A., see Jacobs, T. 261  
 Williams, A.J. 248  
 Williams, C.W., see Antonio, M.R. 365  
 Williams, C.W., see Luo, Q.-H. 346, 349, 353  
 Williams, D.J., see Griffith, W.P. 349, 374  
 Williams, G.V.M. 191  
 Williams, J.M. 184  
 Willis, J.O. 187  
 Wills, A.S. 193, 246  
 Wimbush, S.C. 208, 232, 233, 271, 287  
 Wimbush, S.C., see Bashlakov, D.L. 229, 241  
 Wimbush, S.C., see Cao, G.H. 208  
 Wimbush, S.C., see Häse, K. 208, 232

- Wimbush, S.C., see Reibold, M. 208  
 Wimbush, S.C., see Subba Rao, K. 208  
 Winiarska, A., see Tomala, K. 255, 256  
 Winzer, K. 229, 259  
 Winzer, K., see Drechsler, S.-L. 193, 212  
 Winzer, K., see Goll, G. 235  
 Winzer, K., see Heinecke, M. 240  
 Winzer, K., see Mandal, P. 217  
 Winzer, K., see Nguyen, L.H. 210  
 Winzer, K., see Peng, Z.Q. 259  
 Winzer, K., see Riblet, G. 186  
 Winzer, K., see Shulga, S.V. 180, 214, 222,  
 232, 234, 235, 240, 241, 259, 298, 308  
 Wohlfarth, E.P. 186, 191, 272  
 Wohlleben, D.K., see Braunisch, W. 260  
 Wohlleben, D.K., see Sales, B.C. 249  
 Wolcyrz, M., see Gulay, L.D. 57, 63–77,  
 79–81, 83, 84, 86, 87  
 Wolf, M., see Freudenberg, J. 268, 303  
 Wolf, M., see Müller, K.-H. 258  
 Won, H. 223  
 Won, H., see Maki, K. 222, 223, 284  
 Won, H., see Yuan, Q. 223, 227  
 Wong, J. 119, 120  
 Woo, T.K., see Yang, Z. 7, 33  
 Wood, C. 158, 163, 164, 166  
 Wood, J.H., see Koelling, D.D. 7  
 Woodward, F.M., see Goodrich, R.G. 276  
 Woodward, F.M., see Kreyssig, A. 215  
 Wosnitza, J., see Ignatchik, O. 210, 230  
 Wosnitza, J., see Maniv, T. 230  
 Wosnitza, J., see Schneider, Ma. 239, 267  
 Wu, C.-D. 341  
 Wu, H., see Sun, G. 374  
 Wu, M.K. 185  
 Wu, Q. 349  
 Wu, Q., see Wang, E. 349  
 Wu, Y., see Lu, B. 346  
 Wu, Y., see Shan, Y. 348  
 Wu, Y., see Wang, X.-G. 346  
 Wu, Y.Q., see Avila, M.A. 206, 279  
 Wu, Z. 374  
 Wyder, P., see Goll, G. 235  
 Wyder, P., see Nguyen, L.H. 210  
 Wyder, P., see Rybaltchenko, L.F. 270  
 Wyder, P., see Yanson, I.K. 214  
  
 Xiao, D., see An, H. 368  
 Xiao, Z. 349  
 Xin, M., see Liu, J. 349  
 Xin, X.-I. 374  
 Xing, Y., see Cai, X.-Z. 369  
 Xing, Y., see Lu, B. 346  
 Xing, Y., see Wang, X.-G. 346  
 Xu, F.F., see Zhang, F.X. 142  
 Xu, G., see Liu, J. 362  
 Xu, J., see Zhang, F.X. 142  
 Xu, L., see An, H. 368  
 Xu, M. 181, 204, 232  
 Xu, M., see Cho, B.K. 197, 242, 277  
 Xu, M., see Johnston-Halperin, E. 212  
 Xu, X., see Zhou, B. 349, 368  
 Xu, Z.A., see Zhao, S.R. 308  
 Xue, G. 362  
 Xue, P.C., see Zhang, T.R. 373  
 Xue, Y.Y., see Chu, C.W. 191  
 Xue, Y.Y., see Dezaneti, L.M. 180, 184, 197,  
 202  
 Xue, Y.Y., see Gao, L. 200, 201, 238  
  
 Yadollahi, B., see Mirkhani, V. 374  
 Yagasaki, A. 339  
 Yakoby, E.R., see Prozorov, R. 240  
 Yamada, K., see Fukazawa, H. 222  
 Yamada, K., see Gilardi, R. 280  
 Yamaguchi, S., see Inagaki, A. 374  
 Yamaguchi, S., see Kera, Y. 374  
 Yamaguchi, S., see Shiozaki, R. 374  
 Yamaguchi, T. 246  
 Yamaguchi, Y., see Kaneko, K. 248  
 Yamaguchi, Y., see Onodera, H. 203, 247  
 Yamaguchi, Y., see Yamauchi, H. 203, 247  
 Yamamoto, A., see Inouye, Y. 374  
 Yamamoto, A., see Tanaka, T. 157  
 Yamamoto, T., see Choi, J.-H. 264, 309  
 Yamase, T. 340, 344, 358, 368, 370, 372, 373  
 Yamase, T., see Fukaya, K. 357, 358  
 Yamase, T., see Inoue, M. 342, 344, 345  
 Yamase, T., see Inouye, Y. 374  
 Yamase, T., see Ito, T. 373  
 Yamase, T., see Naruke, H. 340, 346, 358,  
 361, 368, 369, 371, 373  
 Yamase, T., see Ozeki, T. 344, 371, 372  
 Yamase, T., see Sugeta, M. 344, 372  
 Yamauchi, H. 203, 247  
 Yamauchi, H., see Hamada, K. 111, 113  
 Yamauchi, H., see Kaneko, K. 248  
 Yamauchi, H., see Onodera, H. 203, 247  
 Yamauchi, K. 210, 211, 231  
 Yamaura, K., see Mori, T. 168  
 Yanagisawa, T., see Watanuki, R. 115  
 Yanase, A., see Yamauchi, K. 210, 231  
 Yanase, Y., see Udagawa, M. 224, 229  
 Yang, H.D., see Huang, C.L. 226, 227, 232  
 Yang, H.D., see Shelton, R.N. 191  
 Yang, I.-S. 213, 223  
 Yang, I.-S., see Mun, M.-O. 232  
 Yang, J., see Nolas, G.S. 164  
 Yang, J., see Xue, G. 362

- Yang, Z. 7, 33  
 Yang-Bitterlich, W. 201, 206  
 Yang-Bitterlich, W., see Bitterlich, H. 206  
 Yano, Y., see Yamase, T. 370  
 Yanovskii, A.I., see Fedoseev, A.M. 368  
 Yanovskii, A.I., see Grigor'ev, M.S. 368  
 Yanson, I.K. 214, 227, 259, 260  
 Yanson, I.K., see Bashlakov, D.L. 229, 241  
 Yanson, I.K., see Bobrov, N.L. 228, 229, 240  
 Yanson, I.K., see Naidyuk, Yu.G. 213, 227, 269  
 Yao, J.N., see Zhang, T.R. 373  
 Yao, Y.D., see Lee, W.H. 184  
 Yao, Y.D., see Lin, M.S. 259  
 Yarmolyuk, Ya.P., see Gladyshevsky, R.E. 83  
 Yarmolyuk, Ya.P., see Sichevich, O.M. 88  
 Yarnell, J.L., see Von Dreele, R.B. 4, 5  
 Yaron, U. 280, 289  
 Yaron, U., see Eskildsen, M.R. 276, 287, 289  
 Yashito, H., see Ito, T. 373  
 Yasuhara, Y. 374  
 Yates, S.J.C., see Yelland, E.A. 191  
 Yatskar, A. 194, 242, 278, 279  
 Yatskar, A., see Bud'ko, S.L. 278, 305  
 Yatskar, A., see Canfield, P.C. 192  
 Yatskar, A., see Cho, B.K. 242, 245, 274  
 Yatskar, A., see Lacerda, A. 278, 279  
 Ye, J., see Zou, Z. 190  
 Ye, X., see Shan, Y. 348  
 Yelland, E.A. 191  
 Yelon, W.B., see Blackstead, H.A. 190  
 Yeshurun, Y., see Prozorov, R. 240  
 Yeste, M.P., see Bernal, S. 30, 49  
 Yethiraj, M. 280, 281  
 Yethiraj, M., see Chang, L.J. 200  
 Yethiraj, M., see Paul, D.McK. 277  
 Yethiraj, M., see Song, K.-J. 287  
 Yin, M., see Yusov, A.B. 368  
 Yokoya, T. 222, 227, 284, 295, 300  
 Yokoya, T., see Baba, T. 227, 228, 274, 300  
 Yoon, Y.K., see Mun, M.-O. 211  
 Yoshida, K. 133  
 Yoshida, T., see Inouye, Y. 374  
 Yoshizawa, H., see Kawano, H. 242, 273  
 Yoshizawa, H., see Kawano-Furukawa, H. 214, 273-275  
 Yoshizawa, H., see Onimaru, T. 246, 247  
 Yosida, K. 243  
 You, W., see Wang, W. 349  
 You, Y.B., see Jiang, P.J. 197  
 You, Y.B., see Ku, H.C. 184, 197, 202  
 You, Y.B., see Lai, C.C. 184, 194, 197, 296  
 You, Y.B., see Lin, M.S. 259  
 Youn, S.J. 210, 211  
 Youn, S.J., see Lee, J.I. 210  
 Young, A.P. 147  
 Young, D.P., see Goodrich, R.G. 276  
 Young, J.D., see Slack, G.A. 119  
 Young, V.G., see Luo, Q.-H. 346, 349, 353  
 Yu, M., see Qu, L. 349  
 Yu, M., see Wang, S. 349  
 Yu, P.-S., see Bi, L.-H. 356  
 Yu, W., see Wang, E. 349  
 Yu, Y., see Tanaka, T. 136  
 Yuan, Q. 223, 227  
 Yuan, Q., see Won, H. 223  
 Yue, B. 356  
 Yusov, A.B. 340, 351, 352, 368, 373  
 Yusov, A.B., see Charushnikova, I.A. 368  
 Yusov, A.B., see Fedoseev, A.M. 349  
 Yusov, A.B., see Grigor'ev, M.S. 368  
 Yusuf, S.M., see Jaiswal-Nagar, D. 232  
 Zachariasen, W.H. 63  
 Zachariasen, W.H., see Cooper, A.S. 184  
 Zackay, V.F., see Fink, H.J. 184  
 Zaharko, O., see Gilardi, R. 280  
 Zaharko, O., see Schneider, Mi. 264  
 Zaharko, O., see Staub, U. 247  
 Zahn, G., see Jaenicke-Rössler, U. 239  
 Zahn, G., see Yang-Bitterlich, W. 201  
 Zahn, P., see Drechsler, S.-L. 193, 212  
 Zahn, P., see Schneider, M. 219  
 Zahurak, S.M., see Rosseinsky, M.J. 182, 184  
 Zandbergen, H.W. 200-202  
 Zandbergen, H.W., see Cava, R.J. 180, 181, 184, 197, 200-202, 240, 242  
 Zandbergen, H.W., see He, T. 184  
 Zandbergen, H.W., see Link, J.R. 203  
 Zandbergen, H.W., see Michor, H. 200  
 Zandbergen, H.W., see Siegrist, T. 195, 200, 249  
 Zanicchi, G., see Marazza, R. 64, 66-77, 89  
 Zapf, V.S., see Bauer, E.D. 192, 246  
 Zaplatinskii, O.V. 69  
 Zaplatynsky, O., see Salamakha, P.S. 57, 58, 68, 69  
 Zaremba, R.I. 84  
 Zaremba, V.I. 84  
 Zaremba, V.I., see Kalychak, Ya.M. 56, 86, 87, 93  
 Zaremba, V.I., see Zaremba, R.I. 84  
 Zarestky, J. 197, 214, 242, 271  
 Zarestky, J., see Bullock, M. 214  
 Zarestky, J., see Dervenagas, P. 197, 214, 242, 257  
 Zarestky, J., see Goldman, A.I. 197, 242, 262  
 Zarestky, J., see Stassis, C. 214  
 Zarestky, J.L. 296  
 Zavaliy, Yu.P., see Kalychak, Ya.M. 87

- Zavodnik, V.E., see Tat'yanina, I.V. 341  
Zawadzki, J., see Buchgeister, M. 197, 301  
Zeldov, E., see Dewhurst, C.D. 268, 289, 291  
Zeldov, E., see James, S.S. 208, 289, 290  
Zeng, H.K., see Lee, W.H. 184  
Zenitani, Y., see Ekino, T. 240  
Zenitani, Y., see Nagamatsu, J. 114, 184, 185  
Zhai, S. 373  
Zhai, X., see Jiang, M. 373  
Zhan, R., see Wang, E. 349  
Zhang, B., see Wang, E. 346, 349  
Zhang, C. 345–347, 351–353, 360, 373  
Zhang, C., see Boglio, C. 353–355, 375  
Zhang, C.Q., see Baba, T. 227, 228, 274, 300  
Zhang, F. 150  
Zhang, F., see Adachi, G.-y. 56  
Zhang, F., see Mori, T. 120, 122, 134–139,  
143, 148–150, 152–154, 165  
Zhang, F.X. 142  
Zhang, H.-H., see Sun, R.-Q. 346  
Zhang, H.J., see Wang, Z. 373  
Zhang, H.J., see Wang, J. 373  
Zhang, H.Y., see Zhang, T.R. 373  
Zhang, J., see Cao, S. 221, 232  
Zhang, J., see Kang, Z.C. 4, 6, 24  
Zhang, J.R. 4, 5  
Zhang, K., see Dunlap, B.D. 190  
Zhang, L., see Wang, E. 349  
Zhang, Q., see Wu, Z. 374  
Zhang, S., see Wang, E. 349  
Zhang, T.R. 373  
Zhang, X., see Feng, J. 374  
Zhang, X., see Zhou, B. 346, 349  
Zhang, Z., see Dresselhaus, M.S. 165  
Zhang, Z.H., see Chu, R.K. 216  
Zhao, B., see Liu, J. 349, 362  
Zhao, B., see Qu, L. 349  
Zhao, B., see Zhang, T.R. 373  
Zhao, B., see Zhu, Z. 349  
Zhao, J.-W. 346  
Zhao, J.-W., see Niu, J.-Y. 346, 355  
Zhao, S.-L., see Sun, R.-Q. 346  
Zhao, S.R. 308  
Zhao, T.S., see Lee, J.I. 210  
Zhao, Y.Y., see Zhang, T.R. 373  
Zhao, Z., see Wu, Z. 374  
Zhelezina, N.V., see Kogan, V.G. 286  
Zheng, X.-L., see Sun, R.-Q. 346  
Zhigadlo, N.D., see Kogan, V.G. 215, 293  
Zholobenko, A.N., see Fil, V.D. 198, 217  
Zhou, B. 346, 349, 368  
Zhou, B., see Ma, J. 368  
Zhou, Y., see Müller, A. 370  
Zhou, Y., see Wang, E. 349  
Zhou, Y., see Wu, Q. 349  
Zhu, X., see Wang, W. 349  
Zhu, Z. 349  
Zhu, Z., see Liu, J. 349  
Zhuang, H.-H., see Wu, C.-D. 341  
Zhuravlev, V., see Maniv, T. 230  
Ziebeck, K., see Rotter, M. 255  
Zimmermann, M. 366  
Zittartz, J., see Müller-Hartmann, E. 186, 278  
Zolliker, M., see Murasik, A. 115, 116  
Zonnevillage, F., see Blasse, G. 372  
Zou, Z. 190  
Zu, Z., see Liu, J. 349  
Zucca, I., see Lascialfari, A. 206  
Zumdick, M.F. 82, 83  
Zver'kova, I.I., see Gasparov, V.A. 113, 115,  
237  
Zwicknagl, G. 189, 191, 306  
Zwicknagl, G., see Thalmeier, P. 193, 223

# SUBJECT INDEX

- <sup>57</sup>Fe Mössbauer 97
- 1D dimer-like transition 108, 169
- 2D long range order 169
- 2D spin glass 108, 147, 149, 169
- 3D long range order 108, 153, 156
- $\alpha$ -[P<sub>2</sub>W<sub>15</sub>O<sub>56</sub>]<sup>12-</sup> 356
- $\alpha_1$ -[P<sub>2</sub>W<sub>17</sub>O<sub>61</sub>]<sup>10-</sup> 345
- $\alpha$ -phase 9, 13, 14, 20
- $\alpha_2$ -[P<sub>2</sub>W<sub>17</sub>O<sub>61</sub>]<sup>10-</sup> 345, 346
- $\alpha$  (CeO<sub>1.98</sub>) 9
- $\beta_2$ -[SiW<sub>11</sub>O<sub>39</sub>]<sup>8-</sup> 345
- $\delta$  (CeO<sub>1.818</sub>) 9
- $\gamma$ -[SiW<sub>10</sub>O<sub>36</sub>]<sup>8-</sup> 356, 357
- $\mu$ SR 224, 241, 247, 253, 257, 276, 277, 286, 305
- $[\varepsilon\text{-PMo}_8^V\text{Mo}_4^VI\text{O}_{36}(\text{OH})_4\{\text{La}(\text{H}_2\text{O})_4\}_4]^{5+}$   
371
- A- $\alpha$ -[PW<sub>9</sub>O<sub>34</sub>]<sup>9-</sup> 356
- a\*** structure 262–269
- absorption spectroscopy 210, 249, 278
- ac susceptibility
- HoB<sub>22</sub>C<sub>2</sub>N 145
- amorphous behavior 159
- anisotropic exchange 232, 243, 255
- anisotropy in borides 154, 170
- anisotropy in borocarbides
- in the critical current 208, 287
  - in the magnetic properties 223, 260, 264, 274
  - in the transport properties 215, 216, 218, 279
  - of the effective mass 232, 237
  - of the electronic structure 210, 214, 232, 233, 240, 241, 271, 280, 282, 285
  - of the Fermi velocity 211, 212, 222, 237, 282–285
  - of the upper critical field 208, 231–234, 237, 240, 270, 271, 274, 284, 285, 305, 311
- antiferromagnetic coupled pairs 131
- antiferromagnetic interaction 143, 148, 149
- antiferromagnetic order 192, 193, 197–199, 206, 209, 242, 249, 250, 252, 255, 257–259, 263, 264, 268, 273, 274, 276, 277, 289–293, 305, 306, 308
- and quadrupolar order 247, 248
  - and superconductivity 188–191
  - in cuprates 189–191
- antiferromagnetic order in RNi<sub>2</sub>B<sub>2</sub>C 192
- antiferromagnetic structure in borocarbides  
231, 242, 244, 262–265, 267–270, 276, 311
- antiferromagnetic structure of RNi<sub>2</sub>B<sub>2</sub>C 231
- antiferromagnetic transition
- GdB<sub>18</sub>Si<sub>5</sub> 152
  - RB<sub>12</sub> 113
  - RB<sub>44</sub>Si<sub>2</sub> 130, 132
  - RB<sub>50</sub> 127, 130
  - TbB<sub>25</sub> 139
  - TbB<sub>44</sub>Si<sub>2</sub> 131
  - TbB<sub>50</sub> 120, 121
- antiferromagnetic transition temperature
- GdB<sub>18</sub>Si<sub>5</sub> 154
  - RB<sub>12</sub> 114, 115
  - RB<sub>44</sub>Si<sub>2</sub> 133
  - RB<sub>50</sub> 127
- antiferromagnetism in borocarbides 190,  
192, 193, 195, 271, 272, 275, 276, 306, 311
- antiferroquadrupolar order 246–248
- antiphase boundaries 273, 274
- ARPES 227
- Arrhenius law 147
- average valence state 29
- B- $\alpha$ -[PW<sub>9</sub>O<sub>34</sub>]<sup>9-</sup> 356
- B- $\beta$ -X<sup>III</sup>W<sub>9</sub>O<sub>33</sub> 361
- B<sub>12</sub> icosahedra chains 132
- B<sub>4</sub>C 142
- band-structure calculations 210, 218, 219,  
229, 231, 232, 282, 285, 294, 309
- barocarbide 283
- BCS theory 181, 185, 188, 191, 212–214, 223,  
228, 232, 234, 241, 260, 261, 269, 270, 277,  
282, 286, 302, 304
- BCS superconductor 112, 113
- beta-boron 138, 158, 159
- binary compounds 182, 203, 204

- bis(pentatungsto)metalates,  $[R(W_5O_{18})_2]^{8,9-}$  343
- Bloch–Grüneisen relation 94
- bond alternating chain 132, 135
- boride structures, building block of 107–110
- borides 106–169, 175–312
- borocarbide superconductors 180, 185, 197, 204, 214, 232, 233, 260, 263, 264, 287, 307
- borocarbides 180, 183, 195, 200–204, 207, 209, 210, 212, 214, 219, 221, 222, 224, 227, 229, 231, 232, 235, 237–239, 241, 243, 252, 268, 279, 280, 285–287, 289, 293, 301, 306, 310–312
- boron carbide 141, 143, 158, 159, 164–166
- boron icosahedra chains 123, 126, 136, 139
- boron isotope effect 212, 213, 310
- boron–carbon disorder 203, 206, 207, 229, 259, 276
- boron-based superconductors 181, 183, 185
- Bragg glass 286
- $c^*$  structure 262, 264, 265, 268
- CaAgPb 79, 81
- CaC<sub>6</sub> 182
- carbides 182, 183
- carbon-based superconductors 181, 183, 185
- Ce ( $[Xe]4f^{15}d^{16}s^2$ ) 7
- Ce–Cu–Pb phase diagram 61
- Ce–Ni–Pb phase diagram 59
- Ce<sub>0.6</sub>Tb<sub>0.2</sub>Zr<sub>0.2</sub>O<sub>x</sub> 17
- $[Ce_{16}(H_2O)_{36}As_{12}W_{148}O_{524}]^{76-}$  357, 359
- Ce<sub>19</sub>O<sub>34</sub> 6, 39, 43
- Ce<sub>24</sub>O<sub>44</sub> 43
- Ce<sub>24</sub>O<sub>44</sub> (CeO<sub>1.833</sub>) 35
- Ce<sub>2</sub>Au<sub>2</sub>Pb 67
- Ce<sub>2</sub>Pd<sub>2</sub>Pb 67, 95
- Ce<sub>2</sub>Pt<sub>2</sub>Pb 67
- Ce<sub>2</sub>Rh<sub>2</sub>Pb 66
- $[Ce_3(CO_3)(SbW_9O_{33})(W_5O_{18})_3]^{20-}$  361
- $[(Ce_3O_3)(H_2O)_2(A-\alpha-PW_9O_{34})_2]^{12-}$  356
- Ce<sub>3</sub>Rh<sub>4</sub>Pb<sub>13</sub> 66, 67, 90, 91
- Ce<sub>4</sub>Ni<sub>3</sub>Pb<sub>4</sub> 66, 98
- $[Ce_4(OH)_2(H_2O)_9(P_2W_{16}O_{59})_2]^{14-}$  361, 362
- Ce<sub>5</sub>AgPb<sub>3</sub> 67
- Ce<sub>5</sub>CuPb<sub>3</sub> 66
- Ce<sub>5</sub>NiPb<sub>3</sub> 66
- Ce<sub>7</sub>O<sub>12</sub> 35, 43
- Ce<sub>7</sub>O<sub>12</sub> (CeO<sub>1.714</sub>) 35
- Ce<sub>8</sub>Pd<sub>24</sub>Pb 67, 93, 99
- Ce<sub>8</sub>Pd<sub>24</sub>Sb 86
- $[(Ce_3^{IV}O_3)(H_2O)_2(A-\alpha-PW_9O_{34})_2]^{12-}$  357
- CeAgPb 67
- CeAuPb 67
- CeCuPb 66, 94
- CEF 249, 250, 253, 254, 265, 278, 308
- Ce(III/IV) redox potentials 341
- $[CeMo_{12}O_{42}]^{8-}$  340
- CeNi<sub>2</sub>B<sub>2</sub>C 194–197, 242, 244, 249, 250
- CeO<sub>1.714</sub> 39
- CeO<sub>1.818</sub> 37
- CeO<sub>1.895</sub> 39
- CeO<sub>2- $\delta$</sub>  34
- CeO<sub>2- $\delta$</sub>  electrolyte 36, 43
- CePdPb 67
- CePtPb 67, 94
- cerium(III/IV) redox potentials 350
- CeRu<sub>2</sub> 187, 250, 286
- $[CeW_{10}O_{36}]^{8-}$  342
- characteristic temperature 129, 130, 138, 150, 159
- RB<sub>44</sub>Si<sub>2</sub> 129
- chemical and physical properties of plumbides 93–99
- Chevrel phases 188
- clean limit 233, 235, 236, 240, 282, 285, 295, 297, 298, 300, 301
- coexistence 185–188, 190–192, 195, 221, 231, 258–260, 262, 268, 274, 290, 292, 305, 307, 308, 310–312
- coherence length 188, 224, 233, 240, 280, 282, 284–286, 296
- coherent-potential approximation 299
- collective phenomena 185, 195
- collective pinning 286
- commensurate 199, 200, 231, 242–244, 246, 250, 257, 262–268, 273, 310, 311
- composition domains 29, 30
- $\alpha$ -phase and  $\beta$ (1) phase 32
- RO<sub>2</sub>, RO<sub>1.833</sub>, RO<sub>1.80</sub>, RO<sub>1.778</sub> 31
- compositional formula 27
- conductivity and catalytic properties 42
- conductivity of  $\alpha$ -phase of PrO<sub>x</sub> 43, 44
- cooperative Jahn–Teller effect 247
- cooperative phenomena 185, 187, 192, 246
- coordination number 27–29
- coupling strength 213, 214, 231, 232, 235, 236, 241, 284, 300
- covalent bonds 185, 203, 243
- critical current 208, 275, 287, 291
- critical field 113, 121, 131
- RB<sub>50</sub> 127
- crystal chemistry
- plumbides 57
- R<sub>x</sub>T<sub>y</sub>Pb<sub>z</sub> plumbides 62
- crystal field excitations 276
- crystal growth 109, 114
- RB<sub>12</sub> 111
- RB<sub>44</sub>Si<sub>2</sub> 120–122
- RB<sub>50</sub> 120–122
- RB<sub>66</sub> 117

- YbB<sub>44</sub>Si<sub>2</sub> 127
- crystalline electric field (CEF) 186, 199, 242–250, 252–256, 258, 262, 265, 271, 272, 274, 278, 303, 308, 309
- [Cs<sub>2</sub>[Eu(H<sub>2</sub>O)<sub>2</sub>( $\alpha$ -AsW<sub>9</sub>O<sub>33</sub>)]<sub>4</sub>]<sup>23-</sup> 357, 358
- cuprates 182, 185, 189, 191–193, 208, 209, 219, 231, 252, 260, 280
- Curie–Weiss temperature 134, 154
- RAlB<sub>14</sub> 139
- R–B–C(N) homologous compounds 148
- RB<sub>44</sub>Si<sub>2</sub> 133
- R<sub>1.8</sub>B<sub>36</sub>C<sub>2</sub>Si<sub>8</sub> 152
- RB<sub>50</sub> 127
  
- d-wave 222, 226, 227, 231, 280, 302
- de Gennes factor 121, 127, 133, 134, 193, 219, 242, 245, 302, 303, 305, 308
- de Gennes scaling 193, 194, 219, 242, 252, 254, 278, 306, 308, 309
- de Haas–van Alphen effect 210, 222, 229, 230, 231, 235, 240
- Debye temperature 159, 181, 212, 240, 294
- decoration of superconductors 275, 289, 290, 292
- delocalized quasiparticles 224, 227, 286
- dendritic flux pattern 208, 287, 288
- density of states 129, 181, 186, 194, 206, 209–212, 214, 219, 224, 229, 235, 238, 240–242, 250–254, 256, 294, 295, 298–300, 303, 304, 306, 307
- diamagnetism 209
- diamond 182
- diffraction patterns of the  $\alpha$ -phase 22
- dimer-like behavior 131, 132
- dimerization constant 353
- Dingle temperature 235, 240
- dipole interaction 116, 133
- dipoles of the fluorite-type modules 25
- dirty limit 226, 236, 240, 285, 286, 295, 298, 300–302
- disorder 130, 143, 149, 152, 164
- disorder effects 203, 204, 207, 226, 229, 232, 236, 240, 258, 259, 266, 267, 276, 284, 286, 295–301, 304–306, 310, 312
- dispersion of the Fermi velocity 235, 240, 298
- dodecaboride *see* RB<sub>12</sub>
- domains
  - antiferromagnetic 275, 289, 290–292
  - ferromagnetic 275
- doping
  - carbon 161
  - non-magnetic dilution 130, 131
  - transition metal 159, 163, 168
- Doppler shift 223, 227
  
- double occupancy 118
- double-layer borocarbides 200, 201, 205
- Dy–Cu–Pb phase diagram 62
- Dy–Ni–Pb phase diagram 60
- Dy<sub>12</sub>Ni<sub>6</sub>Pb 72
- Dy<sub>2</sub>Ni<sub>2</sub>Pb 72, 96, 97
- Dy<sub>2</sub>Pd<sub>2</sub>Pb 73
- Dy<sub>5</sub>CuPb<sub>3</sub> 73
- Dy<sub>5</sub>NiPb<sub>3</sub> 73
- Dy<sub>6</sub>Co<sub>2.37</sub>Pb<sub>0.53</sub> 72
- Dy<sub>6</sub>Ni<sub>2.39</sub>Pb<sub>0.55</sub> 72
- Dy(Ag<sub>0.30(9)</sub>Pb<sub>0.70(9)</sub>)<sub>3</sub> 73
- DyAgPb 73
- DyAlB<sub>14</sub> 138
- DyAuPb 73
- DyB<sub>12</sub> 112–115
- DyB<sub>25</sub> 138
- DyB<sub>44</sub>Si<sub>2</sub> 123, 133
- DyB<sub>50</sub> 123, 127
- DyCu<sub>5–4.47</sub>Pb<sub>0–0.53</sub> 73
- DyCuPb 73, 79
- DyNi<sub>2</sub>B<sub>2</sub>C 193–195, 197–200, 206, 209, 215, 216, 218, 220, 221, 231, 238, 242–244, 246, 248, 250, 258–260, 268, 289, 304, 306, 307, 309, 311
- DyNiPb 73
- DyPd<sub>2</sub>Pb 73
- DyPdPb 73
  
- effective magnetic moments
  - R–B–C(N) homologous compounds 148
  - RB<sub>44</sub>Si<sub>2</sub> 133
  - RB<sub>50</sub> 127
- electrical properties
  - RAlB<sub>14</sub> 138, 139
  - RB<sub>12</sub> 111–113
  - RB<sub>18</sub>Si<sub>5</sub> 150–152
  - RB<sub>25</sub> 138, 139
  - RB<sub>50</sub>-type compounds 129, 130
  - RB<sub>66</sub> 119
  - RNiPb 93
  - R<sub>2</sub>Ni<sub>2</sub>Pb 95
- electrical resistivity 180, 202, 206, 209, 215, 219, 221, 232, 239, 252, 257, 296
- electrolyte 34
- electron configurations 6
- electron crystal phonon glass 158
- electron deficient 107, 110, 111, 136
- electron diffraction pattern
  - Ce<sub>19</sub>O<sub>34</sub> phase 40
  - pyrochlore-type phase 41
  - Ce<sub>11</sub>O<sub>20</sub>, Pr<sub>88</sub>O<sub>160</sub>, and Tb<sub>11</sub>O<sub>20</sub> 38
  - homologous series phases 21
- electron–magnon interaction 219

- electron-phonon coupling 213, 214, 229,  
231, 235, 240, 241, 295, 298, 299, 310
- electron-phonon interaction 181, 212–215,  
219, 222, 223, 229, 231, 235, 299, 310, 311  
– spectral function 235
- electronic density of states of  $\text{CeO}_2$  and  
 $\text{Ce}_2\text{O}_3$  7, 8
- electronic specific heat 226, 297, 235, 295,  
297, 301
- electronic structure 109, 110, 136, 182, 185,  
196, 200, 209–216, 229, 232, 233, 235, 240,  
243, 246, 250, 252, 255, 268, 294, 295, 299,  
308
- electronic structures of  $\text{CeO}_2$ ,  $\text{PrO}_2$ , and  
 $\text{Ce}_2\text{O}_3$  7
- Eliashberg theory 189, 214, 234, 240, 300, 302
- encapsulated alkali metal cations 362
- energy gap 221–231, 237, 238, 240, 269, 270,  
282, 284, 310
- entropy 154
- equilibrium constants 347
- $\text{Er}_2\text{Ni}_2\text{Pb}$  63, 75, 95–97
- $\text{Er}_2\text{Pd}_2\text{Pb}$  75
- $\text{Er}_5\text{CuPb}_3$  75
- $\text{Er}_5\text{NiPb}_3$  74
- $\text{Er}_6\text{Co}_{2.08}\text{Pb}_{0.63}$  74
- $\text{Er}_6\text{Ni}_{2.22}\text{Pb}_{0.54}$  74
- $\text{Er}(\text{Ag}_{0.24(9)}\text{Pb}_{0.76(9)})_3$  75
- $\text{Er}(\text{Ag}_{0.35}\text{Pb}_{0.65})_2$  75
- $\text{ErAg}_{0.70}\text{Pb}_{1.30}$  80
- $\text{ErAgPb}$  75
- $\text{ErAlB}_{14}$  138, 152
- $\text{ErAuPb}$  75
- $\text{ErB}_{12}$  111, 113, 115
- $\text{ErB}_{15.5}\text{CN}$  142, 148
- $\text{ErB}_{22}\text{C}_2\text{N}$  142, 148, 167
- $\text{ErB}_{25}$  138
- $\text{ErB}_{28.5}\text{C}_4$  142, 148
- $\text{ErB}_{44}\text{Si}_2$  123, 133
- $\text{ErB}_{50}$  123, 127
- $\text{ErCu}_{5-4.34}\text{Pb}_{0-0.66}$  75
- $\text{ErCuPb}$  75
- $\text{ErNi}_2\text{B}_2\text{C}$  180, 191–195, 197–200, 207,  
214–216, 220, 221, 236, 238, 242, 244, 245,  
251, 255, 257, 264, 271–277, 280, 289, 290,  
292, 293, 295, 304, 309, 311, 312
- $\text{ErNiPb}$  75, 93
- $\text{ErPd}_2\text{Pb}$  75
- $\text{ErPdPb}$  75
- ESR 132, 364
- $[(\text{Eu}_3(\text{OH})_3(\text{H}_2\text{O})_3)_2\text{Al}_2(\text{Nb}_6\text{O}_{18})_5]^{26-}$  373
- $\text{Eu}_3\text{Rh}_4\text{Pb}_{13}$  70
- $\text{EuAgPb}$  70
- $\text{EuAuPb}$  70, 81, 82, 94
- $\text{EuCdPb}$  70
- $\text{EuHgPb}$  70
- $\text{EuMgPb}$  70
- $\text{EuNi}_2\text{B}_2\text{C}$  241
- $\text{EuPdPb}$  70
- $\text{EuZnPb}$  70
- EXAFS 364
- exchange 180, 185, 187, 188, 190, 193, 194,  
242, 243, 247, 248, 255, 256, 258, 259, 262,  
272, 277, 303–305, 310
- excitation spectrum 360
- f-electron dependence 132, 133, 135
- Fermi level 181, 194, 209–212, 214, 221, 240,  
242, 250–252, 254, 256, 272, 294, 295, 298,  
299, 303, 306, 307
- Fermi surface 211, 214, 216, 217, 219,  
221–224, 226–233, 235–237, 239, 240, 241,  
255, 259, 269, 275, 280, 282, 284, 300, 307,  
310, 311
- Fermi surface nesting 195, 211, 212, 215, 222,  
226, 227, 231, 235, 250, 258, 263–265, 268,  
274, 310
- Fermi velocity 211, 214, 222, 231, 233,  
235–237, 240, 282–285, 298, 312
- ferromagnet 186, 187, 200, 203, 204, 266, 290
- ferromagnetic 139, 149, 188
- ferromagnetic order 182, 186, 188, 189, 191,  
197, 198, 263, 265, 271, 273–275, 289  
– in  $\text{LaMnO}_3$  248  
– in  $\text{UGe}_2$  191  
– in  $\text{ZrZn}_2$  191  
– short-range 187
- ferromagnetism 191, 192, 274, 275
- ferroquadrupolar order 200, 246–248
- figure of merit 159, 167  
–  $\text{ErB}_{44}\text{Si}_2$  164, 165
- floating zone growth 122
- floating zone method 109, 122, 127
- floating-zone melting 205, 206, 264, 267, 282,  
291
- fluorite structure and oxygen centered  
tetrahedron 23
- fluorite-type module theory 6, 23
- flux line 279, 286, 289
- flux line lattice 195, 227, 277, 280
- flux method 109
- flux penetration 208, 279, 287, 288
- flux pinning 208, 275, 289
- formation constants 341, 345, 351  
– diastereomers of the complexes with  
L-proline 354  
– Peacock–Weakley complexes 351
- frustration 116, 143, 144, 149

- gap anisotropy 221–233, 241, 277, 280, 282, 284, 285, 295, 300, 302, 311
- gap nodes 221–231, 241, 277, 302, 311
- gap symmetry 212, 221–232, 280, 284
- gapless superconductivity 220, 221, 270, 271
- Gd–Cu–Pb phase diagram 62
- Gd–Ni–Pb phase diagram 59
- Gd–Ni–Sn system 62
- Gd<sub>12</sub>Co<sub>6</sub>Pb 70
- Gd<sub>12</sub>Ni<sub>6</sub>Pb 70
- Gd<sub>2</sub>Ni<sub>2</sub>Pb 71, 96
- Gd<sub>2</sub>Pd<sub>2</sub>Pb 71
- Gd<sub>5</sub>CuPb<sub>3</sub> 71
- Gd<sub>5</sub>NiPb<sub>3</sub> 71, 87, 88
- Gd<sub>6</sub>Co<sub>2.37</sub>Pb<sub>0.56</sub> 70
- Gd<sub>6</sub>Ni<sub>2.5</sub>Pb<sub>0.5</sub> 71
- Gd(Ag<sub>0.26(7)</sub>Pb<sub>0.74(7)</sub>)<sub>3</sub> 71
- GdAgPb 71
- GdAuPb 71, 90
- GdB<sub>18</sub>Si<sub>5</sub> 150, 153, 154, 156
- GdB<sub>25</sub> 138, 154
- GdB<sub>44</sub>Si<sub>2</sub> 120, 123, 132–134
- GdB<sub>50</sub> 121
- GdB<sub>66</sub> 152
- GdCu<sub>4.60</sub>Pb<sub>0.40</sub> 71
- GdCuPb 71, 94
- GdMo<sub>6</sub>S<sub>8</sub> 189, 261
- GdNi<sub>2</sub>B<sub>2</sub>C 193, 215, 217–220, 238, 242, 245, 246, 254–256, 264, 271, 305
- GdNiPb 71, 93, 94
- GdPd<sub>2</sub>Pb 71
- GdPdPb 71
- Ginzburg–Landau parameter 240, 282
- [[ $(\text{H}_2\text{O})_6\text{La}$ ]<sub>2</sub>MnMo<sub>9</sub>O<sub>32</sub>] 341
- [[ $(\text{H}_2\text{O})_6\text{R}$ ]<sub>2</sub>TeO<sub>6</sub>Mo<sub>6</sub>O<sub>18</sub>] 368
- [(H<sub>4</sub>)PW<sub>17</sub>O<sub>61</sub>]<sup>11-</sup> 346
- H<sub>c2</sub> 189, 195, 214, 221, 222, 228, 230–238, 240, 267–271, 274, 277, 283, 285–287, 291, 293, 296, 298, 300, 301, 304–306, 311
- Haldane compounds 130
- Hall coefficient 206, 215, 217, 279
- Hall effect 211, 215, 217, 218
- heat capacity 226
- heat treatment 204, 206, 250, 266, 267, 309, 310
- heavy-fermion 192, 195, 206, 215, 239, 242, 246, 249, 278–280, 306, 311
- Hebel–Slichter peak 223
- heteroatoms 339
- cerium(IV) 340
- europium(II) 365
- praseodymium(IV) 351
- terbium(IV) 350
- heteropoly anions 338
- Heusler type structure 90
- hexaboride *see* RB<sub>6</sub>
- hexagonal vortex lattice 195, 275, 280–283, 285, 286, 289–293, 312
- high pressure 183, 186, 238, 239
- high-temperature superconductors (high-*T<sub>c</sub>*) 180, 181, 182, 185, 189, 191–193, 260, 280
- Ho<sub>12</sub>Ni<sub>6</sub>Pb 74
- Ho<sub>2</sub>Ni<sub>2</sub>Pb 63, 74, 78, 96, 97
- Ho<sub>2</sub>Pd<sub>2</sub>Pb 74
- Ho<sub>5</sub>CuPb<sub>3</sub> 74
- [Ho<sub>5</sub>(H<sub>2</sub>O)<sub>16</sub>(OH)<sub>2</sub>As<sub>6</sub>W<sub>64</sub>O<sub>220</sub>]<sup>25-</sup> 357, 359
- Ho<sub>5</sub>NiPb<sub>3</sub> 73
- Ho<sub>6</sub>Co<sub>2.20</sub>Pb<sub>0.59</sub> 73
- Ho<sub>6</sub>Ni<sub>2.41</sub>Pb<sub>0.53</sub> 73, 83, 84, 93
- Ho(Ag<sub>0.26(6)</sub>Pb<sub>0.74(6)</sub>)<sub>3</sub> 74
- HoAgPb 74
- HoAlB<sub>14</sub> 138
- HoAuPb 74
- HoB<sub>12</sub> 111, 113, 115
- HoB<sub>15.5</sub>CN 142, 148, 167
- HoB<sub>22</sub>C<sub>2</sub>N 142, 145–148
- HoB<sub>25</sub> 138
- HoB<sub>28.5</sub>C<sub>4</sub> 142, 148
- HoB<sub>44</sub>Si<sub>2</sub> 123, 129, 133
- HoB<sub>50</sub> 123, 127
- HoCu<sub>5-4.50</sub>Pb<sub>0-0.50</sub> 74
- HoCuPb 74
- homologous phases, space groups, and transformation matrix 37
- homologous R–B–C(N) compounds – lattice parameters 142
- HoNi<sub>2</sub>B<sub>2</sub>C 180, 193–195, 197–200, 205–208, 213, 215–221, 231, 232, 238, 239, 242–244, 246, 248, 250, 259–271, 274, 276, 289–292, 304, 307, 309–312
- HoNiPb 74, 93
- HoPd<sub>2</sub>Pb 74
- HoPdPb 74
- hot press 165, 167
- Hund’s rule 189, 193, 204, 243, 245, 302
- hybridization 187, 190, 194, 244, 249–252, 256, 278, 305, 310
- hysteresis 12, 14, 29, 250, 257, 259
- ID dimer-like transition 135
- impurity 186, 198, 203, 204, 208, 221, 223, 235, 236, 250, 254, 259, 278, 286, 287, 298, 304, 307
- incommensurate 200, 242–244, 246, 255, 256, 262–268, 271, 273, 276, 291, 292, 310, 311
- incommensurate magnetic structure 190, 246, 263, 268, 274, 310, 311

- induced magnetic moment 190, 242, 244,  
 247, 250, 276  
 inelastic neutron scattering 241, 244, 248,  
 253, 276, 278, 310  
 infrared spectroscopy 119  
 interband coupling 235, 241, 298  
 intergrowth variants 63  
 interplay of superconductivity and  
 magnetism 180, 185–192, 212, 218, 237,  
 238, 268, 269, 293, 295, 302, 312  
 iron cluster unit 89  
 isobaric data  
 –  $\text{Ce}_{0.6}\text{Tb}_{0.2}\text{Zr}_{0.2}\text{O}_x$  18  
 –  $\text{CeO}_x\text{--O}_2$  system 11  
 –  $\text{PrO}_x$  9  
 –  $\text{PrO}_x\text{--O}_2$  system 11  
 isobaric hysteresis loop of the  $\text{TbO}_x$  system  
 13  
 isomer shift 209, 243  
 isopolyanions 338  
 isothermal remanent magnetization 143, 144  
 isotope effect 212, 213, 235, 310  
 IT-SOFC 34, 43  
 itinerant ferromagnet 191  
 itinerant-electron antiferromagnetism 192  
  
 Josephson effect 231  
  
 $[\text{Kc}\{\text{Eu}(\text{H}_2\text{O})_2(\alpha\text{-AsW}_9\text{O}_{33})_6\}]^{35-}$  357, 358  
 Keggin anion 340, 343, 344, 371  
 –  $\alpha$ -isomer 355  
 –  $\gamma$ -isomer 355  
 –  $\varepsilon$ -isomer 371  
 Kohler's rule 216  
 Kondo effect 187, 239, 278  
 Kramer–Pesch effect 286  
 Kramers doublet 127  
 Kramers ions 244, 249, 252, 253  
  
 La–Cu–Pb phase diagram 60  
 La–Ni–Pb phase diagram 58  
 $\text{La}_{12}\text{Co}_6\text{Pb}$  65  
 $\text{La}_{12}\text{Ni}_6\text{Pb}$  65  
 $\text{La}_2\text{Pd}_2\text{Pb}$  66  
 $\text{La}_3\text{Rh}_4\text{Pb}_{13}$  66  
 $\text{La}_4\text{Ni}_3\text{Pb}_4$  65, 92, 98  
 $\text{La}_5\text{AgPb}_3$  66  
 $\text{La}_5\text{CoPb}_3$  65  
 $\text{La}_5\text{CrPb}_3$  65  
 $\text{La}_5\text{CuPb}_3$  65  
 $\text{La}_5\text{FePb}_3$  65  
 $\text{La}_5\text{MnPb}_3$  65  
 $\text{La}_5\text{NiPb}_3$  65  
 $\text{La}_5\text{RuPb}_3$  66  
  
 $\text{La}_5\text{ZnPb}_3$  65  
 $\text{La}_6\text{Co}_{13}\text{Pb}$  65, 96, 97  
 $\text{La}_6\text{Fe}_{13}\text{Pb}$  65, 96  
 $[\{\text{La}(\alpha_2\text{-P}_2\text{W}_{17}\text{O}_{61})(\text{H}_2\text{O})_2\}_2(\mu\text{-CH}_3\text{COO})_2]^{16-}$  354  
 $\text{LaAgPb}$  66  
 $[\text{LaAs}_4\text{W}_{40}\text{O}_{140}]^{23-}$  362  
 $[\text{LaAs}_4\text{W}_{40}\text{O}_{140}\text{M}_2]^{20,21-}$  362  
 $\text{LaAuPb}$  66  
 lacunary anions 343, 345  
 – chiral isomers 345  
 – complexes of multivacant lacunary anions  
 355  
 –  $[\text{P}_2\text{W}_{17}\text{O}_{61}]^{10-}$  343  
 –  $[\text{SiW}_{11}\text{O}_{39}]^{8-}$  343  
 $\text{LaCuPb}$  65, 79, 94  
 $\text{LaNi}_2\text{B}_2\text{C}$  194, 196, 211, 212, 214, 217, 235,  
 307  
 lanthanide higher oxides 1–51  
 $\text{LaPd}_2\text{B}_2\text{C}$  197  
 $\text{LaPdPb}$  66  
 $\text{LaPt}_2\text{B}_2\text{C}$  197, 212, 214  
 $\text{LaPtPb}$  66, 94  
 lattice 238, 239, 243, 246, 247, 252, 259, 266,  
 282, 285, 294–296, 309  
 lattice constant 194–196, 198, 202, 205, 238,  
 239, 249, 250, 252, 254, 273, 278, 294, 304,  
 309  
 lattice distortion 195, 198, 199, 200, 247, 248,  
 256, 264, 292, 297, 299, 304, 307  
 lattice oxygen 49  
 lattice parameters  
 – homologous R–B–C(N) compounds 142  
 –  $\text{RAlB}_{14}$  138  
 –  $\text{RB}_{25}$  138  
 –  $\text{RB}_{44}\text{Si}_2$  123  
 –  $\text{RB}_{50}$  123  
 – scandium higher borides 157  
 lattice symmetry 200, 256, 272  
 layered structure 142, 182, 201, 209  
 leaching 49  
 lead flux 57  
 level crossing 265  
 ligand disorder 206, 279  
 line node 222, 224–227, 229  
 Lipscomb criterion 338  
 local-density approximation 209, 210, 214,  
 230, 239  
 local-moment magnetism 187, 256, 269, 302,  
 305  
 localization length 129, 130, 139, 159  
 localized magnetic moment 187–189, 192,  
 209, 237, 262, 263, 272, 275, 289, 303, 306  
 locking-in 257, 273, 274  
 long-range order 188, 246, 276, 277, 308

- lower critical field 188, 221, 240, 275  
 Lu<sub>2</sub>Ni<sub>2</sub>Pb 77  
 Lu<sub>2</sub>Pd<sub>2</sub>Pb 77  
 Lu<sub>5</sub>CuPb<sub>3</sub> 77  
 Lu<sub>5</sub>NiPb<sub>3</sub> 77  
 Lu<sub>6</sub>Co<sub>2.07</sub>Pb<sub>0.61</sub> 77  
 Lu<sub>6</sub>Ni<sub>2.10</sub>Pb<sub>0.56</sub> 77  
 LuAgPb 77, 82, 83  
 LuAlB<sub>14</sub> 138  
 LuB<sub>12</sub> 111, 112, 115  
 LuB<sub>15.5</sub>CN 142  
 LuB<sub>22</sub>C<sub>2</sub>N 142  
 LuCu<sub>5-4.42</sub>Pb<sub>0-0.58</sub> 77  
 LuCuPb 77  
 luminescence 354, 358  
 luminescence lifetime 352, 365  
 luminescence polyoxometalate materials  
 – Langmuir–Blodgett 373  
 – layer-by-layer 373  
 – sol-gel 373  
 LuNi<sub>2</sub>B<sub>2</sub>C 180, 181, 193, 196, 197, 204,  
 208–217, 219–224, 227–229, 231–236,  
 238–241, 252, 260, 263, 264, 269, 278–281,  
 284–287, 293, 297, 300, 302, 303, 307, 312  
 LuNi<sub>2</sub>B<sub>2</sub>C-type structure 194–198, 202, 293,  
 296  
 LuNiPb 77  
  
 magnetic anisotropy 122, 153, 155, 247, 255,  
 308  
 magnetic entropy 127, 128, 153  
 magnetic excitation 310  
 magnetic fluctuations 186, 189, 191, 216, 223,  
 231, 250, 264, 271, 303  
 magnetic impurities 186, 187, 221, 254,  
 302–306, 312  
 magnetic interaction mechanism 120, 121,  
 132–135, 139, 143, 145, 148, 149, 153, 157,  
 169, 170  
 magnetic order in borocarbides 180, 192,  
 195–200, 209, 215, 216, 218, 220, 221, 231,  
 237, 238, 242–247, 252–259, 261–272,  
 276–278, 289, 291–293, 295, 304, 308, 309  
 – in Chevrel phases 188  
 – in cuprates 189–191  
 – in RNi<sub>4</sub>B compounds 203  
 – in RRu<sub>2</sub> compounds 187  
 – in UGe<sub>2</sub> 191  
 – Mn in Y(Ni<sub>1-x</sub>Mn<sub>x</sub>)<sub>2</sub>B<sub>2</sub>C 295  
 – RNi<sub>2</sub>B<sub>2</sub>C 192  
 magnetic pair breaking 221, 236, 251, 254,  
 274, 306, 312  
 magnetic parameters  
 – R–B–C(N) homologous compounds 148  
 – RB<sub>44</sub>Si<sub>2</sub> 133  
 magnetic phase diagram  
 – of RNi<sub>2</sub>B<sub>2</sub>C compounds 257, 259, 263, 264,  
 271, 304, 305, 310  
 magnetic phase transition  
 – in RNi<sub>2</sub>B<sub>2</sub>C compounds 258  
 magnetic properties of borocarbides 192,  
 195, 197, 209, 238, 241–279, 308, 310  
 – of free R<sup>3+</sup> ions 245  
 – R–B–(CN) homologous compounds  
 143–149  
 – R<sub>1.8</sub>B<sub>36</sub>C<sub>2</sub>Si<sub>8</sub> 152–157  
 – RAlB<sub>14</sub> 139, 140  
 – RB<sub>12</sub> 113–116  
 – RB<sub>18</sub>Si<sub>5</sub> 152–157  
 – RB<sub>25</sub> 139  
 – RB<sub>44</sub>Si<sub>2</sub> 135  
 – RB<sub>50</sub> 127, 128, 135  
 – TbB<sub>50</sub> 120  
 magnetic properties  
 – Ce<sub>8</sub>Pd<sub>24</sub>Pb 98  
 – Dy<sub>5</sub>CuPb<sub>3</sub> 99  
 – R<sub>2</sub>T<sub>2</sub>Pb 95  
 – R<sub>4</sub>Ni<sub>3</sub>Pb<sub>4</sub> 98  
 – R<sub>6</sub>T<sub>13</sub>Pb 96  
 – RNi<sub>2</sub>B<sub>2</sub>C 192  
 – RTPb 93  
 magnetic superconductor 180, 191, 193, 195,  
 243, 278, 289, 306, 308, 312  
 magnetic susceptibility 180, 181, 202, 209,  
 241, 249, 250, 253, 255, 277, 278  
 – GdB<sub>18</sub>Si<sub>5</sub> 153, 155, 156  
 – HoB<sub>15.5</sub>CN 148  
 – HoB<sub>22</sub>C<sub>2</sub>N 148  
 – HoB<sub>28.5</sub>C<sub>4</sub> 148  
 – TbB<sub>25</sub> 139  
 – TbB<sub>50</sub> 121  
 magnetism 185–192, 195, 201, 221, 237, 238,  
 241, 243, 252, 259, 268, 270, 274, 293, 305,  
 307, 308, 311, 312  
 magnetization 121, 130, 131, 156, 191, 213,  
 223, 229, 231, 232, 241, 243, 246, 247, 255,  
 257–259, 263–265, 268, 271, 272, 275, 277,  
 283, 290, 309  
 magnetoelastic effects 199, 200, 267, 310  
 magnetoresistance 96, 138, 195, 215–217,  
 241, 252, 258, 259, 263, 265, 266, 274, 277,  
 279, 309  
 – Dy<sub>5</sub>CuPb<sub>3</sub> 99  
 magnetoresistivity 98  
 magnetostriction 231, 239, 256  
 material design 120  
 mean free path 192, 233, 240, 285, 287, 295,  
 296  
 melting point 107, 158, 163, 165  
 metal flux 57

- metamagnetic state 246, 258, 259, 263, 264, 311  
 metamagnetic transition 98, 120, 121, 131, 195, 257–259, 263–266, 270–272  
 metastable phase 202–205, 209, 300, 310  
 metastable state 275  
 methane oxidization by  
 – CeO<sub>2</sub> and a reduced cerium higher oxide 46  
 – Ce<sub>0.7</sub>Tb<sub>0.05</sub>Zr<sub>0.25</sub>O<sub>2-δ</sub> oxide 47  
 – Ce<sub>0.8</sub>Tb<sub>0.2</sub>O<sub>2-δ</sub> oxide 47  
 MgAlB<sub>14</sub> 136, 138  
 MgB<sub>2</sub> 180, 182, 185, 219, 224, 228, 230, 237, 241, 288, 311  
 MgB<sub>9</sub>CN 142  
 MgB<sub>9</sub>N 143  
 MgCNi<sub>3</sub> 311  
 MgNi<sub>3</sub>C 182  
 microanalysis 180, 206, 266  
 microwave 261  
 microwave surface impedance 227  
 miscibility gaps 296  
 mixed state 217, 224, 287, 297, 298, 301, 302  
 mixed valency 111, 114, 128  
 [MMo<sub>9</sub>O<sub>32</sub>]<sup>6-</sup> 341  
 [Mo<sub>120</sub>O<sub>366</sub>(H<sub>2</sub>O)<sub>48</sub>H<sub>12</sub>[Pr(H<sub>2</sub>O)<sub>5</sub>]<sub>6</sub>]<sup>6-</sup> 370  
 [(Mo<sub>128</sub>Eu<sub>4</sub>O<sub>388</sub>H<sub>10</sub>(H<sub>2</sub>O)<sub>81</sub>]<sub>2</sub>]<sup>20-</sup> 370  
 [(Mo<sup>VI</sup>)<sub>6</sub>Mo<sup>VI</sup><sub>6</sub>O<sub>21</sub>(H<sub>2</sub>O)<sub>6</sub>]<sub>12</sub>[Mo<sup>V</sup>O<sub>4</sub>(SO<sub>4</sub>)<sub>30</sub>]<sup>72-</sup> 370  
 moderate coupling 235, 241, 298  
 molecular field 189  
 molecular orbital calculation 110  
 [(MoO<sub>4</sub>)Ce<sup>III</sup>(H<sub>2</sub>O)<sub>16</sub>(Mo<sup>7</sup>O<sub>24</sub>)<sub>4</sub>]<sup>14-</sup> 368, 369  
 Mössbauer effect in borocarbides 187, 209, 241, 242, 255, 257, 268, 276, 278  
 multiband superconductivity 185, 214, 222, 224, 228, 229, 231, 235, 239, 240, 259, 268, 271, 275, 280, 297, 304, 308, 309, 311  
 multilayer compounds 201  
 multivacant lacunary structures 356  
  
 n-type behavior 108, 113, 165–169  
 Nb-doped YB<sub>6</sub> 159  
 NbSe<sub>2</sub> 230, 237, 286  
 Nd–Ag–Pb phase diagram 58  
 Nd–Cu–Pb phase diagram 61  
 Nd–Zn–Pb system 58  
 Nd<sub>0.35</sub>Th<sub>0.65</sub>Ru<sub>2</sub> 187  
 Nd<sub>12</sub>Co<sub>6</sub>Pb 68  
 Nd<sub>12</sub>Ni<sub>6</sub>Pb 68  
 Nd<sub>2</sub>Ni<sub>2</sub>Pb 68  
 Nd<sub>2</sub>Pd<sub>2</sub>Pb 69  
 Nd<sub>5</sub>CuPb<sub>3</sub> 68  
 Nd<sub>5</sub>NiPb<sub>3</sub> 68  
 Nd<sub>6</sub>Fe<sub>13</sub>Pb 68, 89, 96, 97  
 Nd<sub>6</sub>Fe<sub>13</sub>PbH<sub>13.1</sub> 97  
 Nd<sub>~4</sub>Rh<sub>6</sub>Pb<sub>~19</sub> (623 K) 69  
 Nd<sub>~4</sub>Rh<sub>6</sub>Pb<sub>~19</sub> (723 K) 69  
 NdAgPb 69, 94  
 NdAuPb 69, 94  
 NdCuPb 68, 94  
 NdNi<sub>2</sub>B<sub>2</sub>C 242, 251–254  
 NdNiPb 68, 81  
 NdPdPb 69  
 NdPt<sub>2</sub>B<sub>2</sub>C 197  
 NdZnPb 68  
 nesting 211, 222, 223, 226, 231, 235, 307, 310  
 nesting vector 195, 211, 214, 237, 246, 255, 256, 259, 263, 264, 271, 276, 310  
 neutron diffraction 116, 134, 135, 153, 190, 199, 200, 206, 247, 249, 250, 253, 255, 257, 262–264, 266, 269, 271, 273, 276, 278, 309  
 neutron scattering 187, 189, 198, 262, 266, 277  
 Ni<sub>2</sub> dumb-bells 84  
 NMR 209, 223, 278, 286  
 NMR spectra  
 – <sup>31</sup>P 354  
 nomenclature of borides 116, 136, 150  
 non-Kramers ions 244, 247  
 non-local effects 215, 223, 227, 232–234, 240, 282, 284, 285, 287, 289, 312  
 non-magnetic impurities 191, 306, 307, 312  
 normal state magnetoresistance 215  
  
 one dimensional chains 130, 132, 135  
 one-dimensional antiferromagnet *see also* 1D dimer-like transition 132  
 open orbits 216  
 orbital ordering 198–200, 243, 246–248  
 organic compounds 182  
 oxidization of carbon monoxide by cerium dioxide and a reduced cerium higher oxide 46  
 oxygen migration 29, 35  
 oxygen partial pressure swing 18, 19  
 oxygen releasing 14  
 – of Ce<sub>x</sub>Tb<sub>1-x</sub>O<sub>2-δ</sub> oxides (x = 0.2, 0.4, 0.6, 0.8) 16  
 – of Pr<sub>x</sub>Tb<sub>1-x</sub>O<sub>2-δ</sub> oxides (x = 0.25, 0.5, 0.75) 16  
 – of PrO<sub>x</sub> 15  
 – of TbO<sub>x</sub> 15  
 – of CeO<sub>2</sub> 14  
 oxygen-deficient fluorite-related lanthanide higher oxides of the R<sub>n</sub>O<sub>2n-2m</sub> series 4

- p-type behavior 113, 119, 138, 158, 159, 163, 165, 166, 170
- p-wave 191, 280
- pair breaking 186, 190, 191, 195, 221, 231, 251, 278, 290, 291, 303, 306, 311
- paramagnetic moment 245, 253, 255, 274, 278
- partial occupancy 116, 118, 122, 124, 136, 142, 143, 149, 150, 152, 157, 164
- Pauli paramagnetism 198, 209
- Pb<sub>2</sub> pairs 81
- Pb<sub>3</sub>O<sub>4</sub> 50
- PbO<sub>2</sub> 50
- PCS 227–229
- Peacock–Weakley anions 342
- *syn* and *anti* conformations 346
- Peacock–Weakley complexes 372
- peak effect 230, 287
- penetration depth 188, 240, 275, 280, 281, 283, 290, 312
- phase diagram 186, 194, 204
- of RNi<sub>2</sub>B<sub>2</sub>C compounds 202, 277, 283, 286, 291, 292, 310
- CeO<sub>x</sub>–O<sub>2</sub> system 9
- PrO<sub>x</sub>–O<sub>2</sub> system 10
- TbO<sub>x</sub>–O<sub>2</sub> system 10
- R–T–Pb systems 57
- phase transition, 247, 248
- in RNi<sub>2</sub>B<sub>2</sub>C compounds 255, 261
- in RNi<sub>2</sub>B<sub>2</sub>C compounds 198, 220, 255, 264, 272, 276
- phonon softening 195, 214, 264, 310
- phonon spectrum 206, 212, 214, 215, 298, 310
- RNi<sub>2</sub>B<sub>2</sub>C 195, 206
- phonon-drag 219
- phonon-mediated superconductivity 189, 212–214, 310
- photoemission spectroscopy (PES) 227, 228, 274, 284
- photophysical properties 372
- plumbides
- chemical properties 93–99
- crystal chemistry 57–93
- physical properties 93–99
- pinning 208, 217, 275, 287, 289–291
- PmNi<sub>2</sub>B<sub>2</sub>C 241
- point nodes 222–227, 229, 241, 311
- point-contact spectroscopy (PCS) 208, 213, 214, 222, 227–229, 241, 259, 260, 269, 270, 284
- polymolybdate complexes 366
- Anderson-type hexamolybdates 367
- dodecamolybdocerates and related species 340
- “giant wheel” mixed-valence polymolybdate structures 369
- R<sub>4</sub>Mo<sub>29</sub> complexes 368
- polyniobate complexes 371
- up-conversion phosphors 373
- polyoxometalate complexes
- biological activity 374
- catalysis 373
- electroluminescence cells 372
- emission lifetimes and quantum yields 373
- luminescence 372
- perspectives 374
- properties and applications 372
- reviews 340
- polyoxometalate NMR 347
- <sup>139</sup>La 341
- <sup>17</sup>O 341, 344
- <sup>183</sup>W 342, 343, 345, 347, 352, 357, 360, 362, 363
- <sup>31</sup>P 353–355, 360, 362, 366
- <sup>95</sup>Mo 341
- intramolecular “rotation” of polyoxotungstate ligands 348
- [RCP<sub>5</sub>W<sub>30</sub>O<sub>110</sub>]<sup>12-</sup> data 366
- [R(W<sub>5</sub>O<sub>18</sub>)<sub>2</sub>]<sup>8,9-</sup> 345
- variable temperature <sup>183</sup>W 350
- polyoxotungstate “cryptate” derivatives 362
- [K<sub>8</sub>CP<sub>8</sub>W<sub>48</sub>O<sub>184</sub>]<sup>40-</sup> 362, 364
- [NaCAs<sub>4</sub>W<sub>40</sub>O<sub>140</sub>]<sup>27-</sup> 362, 363
- [NaCSb<sub>9</sub>W<sub>21</sub>O<sub>86</sub>]<sup>18-</sup> 362, 363
- [(NaOH)<sub>2</sub>CP<sub>5</sub>W<sub>30</sub>O<sub>110</sub>]<sup>14-</sup> 362, 364
- positive curvature 195, 234–237, 240, 296, 298, 301, 304, 306
- power factor 168
- Nb-doped YB<sub>66</sub> 159, 161
- RB<sub>44</sub>Si<sub>2</sub> 163
- RB<sub>66</sub> 159
- Pr ([Xe]4f<sup>3</sup>6s<sup>2</sup>) 7
- Pr<sub>12</sub>Co<sub>6</sub>Pb 67
- Pr<sub>12</sub>Ni<sub>6</sub>Pb 67
- Pr<sub>12</sub>O<sub>22</sub> 6
- Pr<sub>24</sub>O<sub>44</sub> 6, 38
- Pr<sub>24</sub>O<sub>44</sub> (1.833) 38
- Pr<sub>2</sub>Pd<sub>2</sub>Mg 96
- Pr<sub>2</sub>Pd<sub>2</sub>Pb 68
- [(Pr<sub>2</sub>W<sub>10</sub>O<sub>38</sub>)<sub>4</sub>{W<sub>3</sub>O<sub>8</sub>(H<sub>2</sub>O)<sub>2</sub>(OH)<sub>4</sub>]<sup>22-</sup> 360
- Pr<sub>3</sub>Rh<sub>4</sub>Pb<sub>13</sub> 68
- Pr<sub>40</sub>O<sub>72</sub> 6, 38, 39
- Pr<sub>4</sub>Ni<sub>3</sub>Pb<sub>4</sub> 67, 98

- $\text{Pr}_5\text{CuPb}_3$  68  
 $\text{Pr}_5\text{Ni}_6\text{In}_{11}$  87  
 $\text{Pr}_5\text{NiPb}_3$  67  
 $\text{Pr}_6\text{Fe}_{13}\text{Pb}$  67, 88, 89, 93, 96, 97  
 $\text{Pr}_6\text{Fe}_{13}\text{PbH}_{13.1}$  97  
 $\text{Pr}_7\text{O}_{12}$  5, 6, 29, 43  
 $\text{Pr}_7\text{O}_{12}$  ( $\text{PrO}_{1.714}$ ) 38  
 $\text{Pr}_{88}\text{O}_{160}$  38  
 $\text{Pr}_9\text{O}_{16}$  ( $\text{PrO}_{1.778}$ ) 6, 38  
 $\text{PrAgPb}$  68  
 $\text{PrAuPb}$  68  
 $\text{PrCuPb}$  68  
 pressure 182, 186, 191, 192, 215, 236–239,  
 250, 260, 266–268, 295, 296, 302, 309, 312  
 pressure-induced superconductivity 182,  
 191  
 $\text{PrNi}_2\text{B}_2\text{C}$  216, 242, 244, 250–252, 309, 311  
 $\text{PrO}_{1.778}$  37  
 $\text{PrO}_{1.818}$  37, 38  
 $\text{PrO}_{1.833}$  37, 38  
 $\text{PrO}_2$  49  
 $\text{PrO}_x$  43  
 propagation vector 199, 243, 244, 246, 253,  
 255, 256, 259, 262–264, 271, 273, 276, 277,  
 292  
 proposal structure of the  
 –  $\text{Ce}_{19}\text{O}_{34}$  phase 39, 40  
 –  $\text{Pr}_{88}\text{O}_{160}$  37, 39  
 $\text{PrOs}_4\text{Sb}_{12}$  224, 238, 246  
 $\text{PrPd}_2\text{Pb}$  68  
 $\text{PrPdPb}$  68  
 $\text{PrPt}_2\text{B}_2\text{C}$  197  
 pseudo-isostructure 120, 135  
 pseudopotential 214, 235, 240  
 pseudoquaternary borocarbides 195, 202,  
 207, 216, 226, 236, 293–311  
 pulsed laser deposition 207, 208, 287  
  
 quadrupolar interactions 203  
 quadrupolar order 199, 203, 243, 246–248,  
 276, 277, 292, 293, 306, 310  
 quadrupole moment 199, 200, 245–248  
 quantum critical point 186, 192, 279  
 quasiparticles 190, 221, 282, 312  
 – density of states 227, 280, 282, 284, 312  
 quaternary borocarbide superconductors  
 179, 195, 203, 215, 256  
 quaternary borocarbides 180, 185, 193, 195,  
 201, 209, 212, 214, 264  
  
 R–B–C(N) homologous compounds 140, 153  
 – magnetic parameters 148  
 – magnetic properties 143–149  
 – structure 142, 143  
  
 – thermoelectric properties 165–168  
 R–Ni(Cu)–Pb systems 62  
 $\text{R}_{0.62}\text{Al}_{0.73}\text{B}_{14}$  136, 138  
 $\text{R}_{1.8}\text{B}_{36}\text{C}_2\text{Si}_8$  149, 150  
 – magnetic properties 152–157  
 – structure 150  
 $\text{R}_{11}\text{O}_{20}$  6  
 $\text{R}_{12}\text{O}_{22}$  5  
 $\text{R}_{24}\text{O}_{44}$  6, 29  
 $\{\text{R}_2(\text{H}_2\text{O})_{12}\text{Mo}_8\text{O}_{27}\}_x$  368  
 $[\text{R}_2(\text{H}_2\text{O})_7\text{As}_3\text{W}_{29}\text{O}_{103}]^{17-}$  357  
 $\{\text{R}_3\text{As}_4\text{W}_{40}\}$  363  
 $[\{\text{R}_3\text{O}(\text{OH})_3(\text{H}_2\text{O})_3\}_2\text{Al}_2(\text{Nb}_6\text{O}_{19})_5]^{26-}$  372  
 $\text{R}_{40}\text{O}_{72}$  6  
 $\text{R}_{48}\text{O}_{88}$  6  
 $\{\text{R}_4\text{As}_4\text{W}_{40}\}$  363  
 $\{\text{R}_4(\text{H}_2\text{O})_{28}[\text{KCP}_8\text{W}_{48}\text{O}_{184}(\text{H}_4\text{W}_4\text{O}_{12})_2\text{-}$   
 $\text{R}_2(\text{H}_2\text{O})_{10}]^{13-}\}_x$  366  
 $\text{R}_{4n}\text{O}_{8n-8m}$  27  
 $\text{R}_7\text{O}_{12}$  ( $\text{RO}_{1.714}$ ) 5, 6, 29  
 $\text{R}_9\text{O}_{16}$  6, 29  
 $\text{R}_{-4}\text{Rh}_6\text{Pb}_{-19}$  91  
 $\text{R}_n\text{O}_{2n-2}$  6, 39  
 $\text{R}_n\text{O}_{2n-2m}$  6, 27  
 $\text{R}_x\text{B}_{12}\text{Si}_3$  150  
 $[\text{R}(\alpha_2\text{-P}_2\text{W}_{17}\text{O}_{61})_2]^{17-}$  348  
 $[\text{RCP}_5\text{W}_{30}\text{O}_{110}]^{12-}$  365  
 – slow proton exchange 366  
 $\text{RAlB}_{14}$  150, 152, 169  
 – electrical properties 138, 139  
 – lattice parameters 138  
 – magnetic properties 139, 140  
 – resistivity 138, 139  
 – structure 136  
 Raman scattering 213, 223, 244  
 rare earth existence diagram for borides 110,  
 168, 169  
 rattlers 164  
 $\text{RB}_{12}$  111, 169  
 – antiferromagnetic transition temperature  
 115  
 – crystal growth 111  
 – electrical properties 111–113  
 – magnetic properties 113–116  
 – resistivity 111–113  
 – structure 111  
 – superconducting transition temperature  
 115  
 $\text{RB}_{15.5}\text{CN}$  108, 116, 128, 140–143, 147, 165,  
 168, 169  
 $\text{RB}_{18}\text{Si}_5$  108, 149, 150, 152, 169  
 – electrical properties 150–152  
 – magnetic properties 152–157  
 – resistivity 150

- structures 150
- RB<sub>22</sub>C<sub>2</sub>N 108, 116, 128, 140–143, 147, 150, 165, 168, 169
- RB<sub>25</sub> 107, 136, 138, 154, 169
  - electrical properties 138, 139
  - lattice parameters 138
  - magnetic properties 139
  - resistivity 138, 139
  - structure 136
- RB<sub>28,5</sub>C<sub>4</sub> 108, 116, 128, 140–143, 147, 165, 169
- Rb<sub>3</sub>C<sub>60</sub> 182
- RB<sub>4</sub> 108, 111, 114, 168
- RB<sub>44</sub>Si<sub>2</sub> 120, 138, 151, 152, 158, 169
  - crystal growth 120–122
  - electrical properties 129, 130
  - lattice parameters 123
  - magnetic parameters 133
  - magnetic properties 135
  - resistivity 129, 130
  - structure 123–126
  - thermoelectric properties 161–165
- RB<sub>50</sub> 107, 120, 169
  - crystal growth 120–122
  - electrical properties 129, 130
  - resistivity 129, 130
  - lattice parameters 123
  - magnetic properties 127, 128, 135
  - structure 123–126
- RB<sub>50</sub>-type *see* RB<sub>50</sub>, RB<sub>44</sub>Si<sub>2</sub>
- RB<sub>6</sub> 108, 111, 115, 168
- RB<sub>66</sub> 107, 116, 129, 138, 152, 158, 169
  - electrical properties 119
  - resistivity 119
  - structure 117, 118
  - thermoelectric properties 158–161
- reduced molybdate complexes 369
- reentrant superconductivity 187–189, 203, 206, 259–261, 266–269, 274, 275, 308, 309
- relaxation time 145–147
- reorientation transition 253, 255, 256, 266, 283, 287, 304
- residual resistivity ratio 240, 282, 296
- resistance 201
- resistivity 189, 211, 215–217, 221, 223, 233, 235, 241, 250, 259–261, 269, 278, 279, 296, 297
  - GdB<sub>18</sub>Si<sub>5</sub> 152
  - RAlB<sub>14</sub> 138, 139
  - RB<sub>12</sub> 111–113
  - RB<sub>1815</sub> 150–152
  - RB<sub>25</sub> 138, 139
  - RB<sub>44</sub>Si<sub>2</sub> 129
  - RB<sub>50</sub>-type compounds 129, 130
  - RB<sub>66</sub> 119
  - rhombic vortex lattice 281–284, 293
  - RKKY interaction 116, 188, 190, 242–244, 246, 247, 255, 262, 265, 273, 274, 304
  - RKKY mechanism 127, 133
    - [R(PW<sub>11</sub>O<sub>39</sub>)<sub>2</sub>]<sup>11-</sup> 348
    - [RSb<sub>9</sub>W<sub>21</sub>O<sub>86</sub>]<sup>16-</sup> 362
    - [R(SiW<sub>11</sub>O<sub>39</sub>)<sub>2</sub>]<sup>13-</sup> 348
  - ruthenocuprates 190, 258, 272, 312
    - [R(W<sub>5</sub>O<sub>18</sub>)<sub>2</sub>]<sup>8,9-</sup> 344
    - [R(W<sub>5</sub>O<sub>18</sub>)<sub>3</sub>]<sup>3-</sup> 357
    - [R(XM<sub>11</sub>O<sub>39</sub>)<sub>x</sub>]<sup>m-</sup>, [R(X<sub>2</sub>M<sub>17</sub>O<sub>61</sub>)<sub>x</sub>]<sup>m-</sup> and related anions
      - 1:1 complex derivatives 354
      - 1:1 complex polymers and dimers 352
      - 1:1 complexes (x = 1) 351
      - 1:2 complexes (x = 2): tetravalent lanthanides 348
      - 1:2 complexes (x = 2): trivalent lanthanides 344
    - structure reports of 1:1 complexes 353
    - structure reports of 1:2 complexes 346
  - (s + g)-wave 222–228, 231, 284, 311
  - s-wave 191, 192, 222–224, 227–229, 231 280, 298, 300–302, 311
  - sandwich-type polyoxometalate structures 356, 361
  - saturation moment 245
    - [(SbW<sub>9</sub>O<sub>33</sub>)(μ<sub>3</sub>-CO<sub>3</sub>)(CeW<sub>5</sub>O<sub>18</sub>)<sub>3</sub>]<sup>20-</sup> 358
    - [(SbW<sub>9</sub>O<sub>33</sub>)(Eu(H<sub>2</sub>O)(W<sub>5</sub>O<sub>18</sub>)<sub>3</sub>)<sup>18-</sup> 358, 360
    - [(SbW<sub>9</sub>O<sub>33</sub>)(R(W<sub>5</sub>O<sub>18</sub>))<sub>3</sub>(H<sub>2</sub>O)<sub>2</sub>(W<sub>5</sub>O<sub>18</sub>)]<sup>15-</sup> 358, 360
  - Sc higher borides 157, 158
    - lattice parameters 157
  - Sc<sub>1-x</sub>M<sub>x</sub>B<sub>12</sub> 111, 114
  - Sc<sub>15.5</sub>CN 142
  - Sc<sub>3.67-x</sub>B<sub>41.4-y-z</sub>C<sub>0.67+z</sub>Si<sub>0.33-w</sub> 157
  - Sc<sub>4.5-x</sub>B<sub>57-y+z</sub>C<sub>3.5-z</sub> 157
  - scattering rate 235, 236, 298, 304
  - ScB<sub>12</sub> 111, 115
  - ScB<sub>15.5</sub>CN 143
  - ScB<sub>17</sub>C<sub>0.25</sub> 157
  - ScB<sub>19</sub> 157
  - ScNi<sub>2</sub>B<sub>2</sub>C 197, 202, 204, 205, 252, 310
  - Seebeck coefficient (also *see* thermoelectric) 43
    - HoB<sub>15.5</sub>CN 166
    - Nb-doped YB<sub>66</sub> 160
    - R-B-C(N) homologous compounds 165
    - RB<sub>22</sub>C<sub>2</sub>N 166
    - RB<sub>44</sub>Si<sub>2</sub> 162, 163
    - RB<sub>66</sub> 159
    - Nb-doped YB<sub>66</sub> 159

- seeding 168  
 shear modulus 287  
 short range order 127, 134, 187, 258, 264,  
     266, 276, 277  
 shrinking of the vortex core 226, 286  
 single-ion anisotropy 244, 265  
 single-layer borocarbides 200, 201  
 singlet pairing 185, 221, 275  
 Sm–Cu–Pb phase diagram 61  
 Sm–Ni–Pb phase diagram 59  
 Sm<sub>12</sub>Co<sub>6</sub>Pb 69  
 Sm<sub>12</sub>Ni<sub>6</sub>Pb 69  
 Sm<sub>2</sub>Ni<sub>2</sub>Pb 69, 95  
 Sm<sub>2</sub>Pd<sub>2</sub>Pb 63, 70, 78  
 Sm<sub>5</sub>CuPb<sub>3</sub> 69  
 Sm<sub>5</sub>NiPb<sub>3</sub> 69  
 Sm<sub>6</sub>Fe<sub>13</sub>Pb 69, 96  
 Sm<sub>~4</sub>Rh<sub>6</sub>Pb<sub>~19</sub> (623 K) 69  
 Sm<sub>~4</sub>Rh<sub>6</sub>Pb<sub>~19</sub> (723 K) 69  
 Sm(Ag<sub>0.29(8)</sub>Pb<sub>0.71(8)</sub>)<sub>3</sub> 70  
 SmAgPb 70  
 small-angle neutron scattering 275, 277,  
     280–282, 284, 289, 292, 312  
 SmAuPb 70  
 SmCuPb 69  
 SmNi<sub>2</sub>B<sub>2</sub>C 242, 245, 251–254  
 SmNiPb 69, 93, 94  
 SmPd<sub>2</sub>Pb 70  
 SmPdPb 70  
 solvolytic disproportionation 49  
 Sommerfeld constant 240, 278, 297–299, 301,  
     304  
 spark plasma synthesis 167, 168  
 specific heat 127, 128, 153, 154, 164, 187, 206,  
     209, 214, 219, 222–224, 226, 227, 231, 232,  
     237, 241, 247, 249, 250, 252, 253, 255, 257,  
     261, 264, 266, 269–272, 276, 278, 284, 297,  
     298, 301, 302, 304, 305, 309  
 specific heat jump 240, 261, 270, 271, 304  
 spectral function 215, 222, 235  
 spin canting 191, 247, 272  
 spin density wave 192, 242, 244, 256, 257,  
     271, 273, 274, 276, 292, 306, 309  
 spin flip 155  
 spin glass 143, 145, 147, 153  
 spin reorientations 95  
 spin scattering 113  
 spin–orbit coupling 199, 200, 221, 243, 247,  
     248, 272  
 spontaneous magnetization 188, 203  
 spontaneous vortex state 275, 290, 312  
 square vortex lattice 195, 276, 280–283, 285,  
     286, 289–293, 312  
 staggered magnetic moment 189, 200,  
     243–246, 253–255, 257, 271, 272, 276  
 Stevens coefficient 245, 254, 258, 271  
 strong magnetic coupling 108, 120, 135  
 structure  
   – principles 110  
   – R–B–(CN) homologous compounds 142,  
     143  
   – R<sub>1.8</sub>B<sub>36</sub>C<sub>2</sub>Si<sub>8</sub> 150  
   – RAlB<sub>14</sub> 136  
   – RB<sub>12</sub> 111, 112  
   – RB<sub>18</sub>Si<sub>5</sub> 151  
   – RB<sub>25</sub> 136, 137  
   – RB<sub>44</sub>Si<sub>2</sub> 123–126  
   – RB<sub>50</sub> 123–126  
   – RB<sub>66</sub> 117, 118  
   – size requirement of the rare earth site 110,  
     111, 128, 140, 168  
   – YB<sub>66</sub> 119  
 structure of quaternary borocarbides 195,  
     197, 200–204  
 structure type  
   – AuBe<sub>5</sub> 84  
   – CaIn<sub>2</sub> 78  
   – CaLiSn 79  
   – Ce<sub>8</sub>Pd<sub>24</sub>Sb 86  
   – Cu<sub>3</sub>Au 84  
   – Er<sub>2</sub>Au<sub>2</sub>Sn 63  
   – Hf<sub>5</sub>CuSn<sub>3</sub> 87  
   – Ho<sub>6</sub>Co<sub>2</sub>Ga 83  
   – KHg<sub>2</sub> 81  
   – La<sub>4</sub>Ni<sub>3</sub>Pb<sub>4</sub> 91  
   – La<sub>6</sub>Co<sub>11</sub>Ga<sub>3</sub> 88  
   – LiGaGe 79  
   – MgAgAs 90  
   – Mn<sub>2</sub>AlB<sub>2</sub> 63  
   – MnCu<sub>2</sub>Al 89  
   – Mo<sub>2</sub>FeB<sub>2</sub> 63  
   – NdPtSb 78  
   – Sm<sub>12</sub>Ni<sub>6</sub>In 86  
   – TiNiSi 81  
   – Yb<sub>3</sub>Rh<sub>4</sub>Sn<sub>13</sub> 90  
   – YbAgPb 80  
   – ZrBeSi 80  
   – ZrNiAl 82  
   – Mo<sub>2</sub>FeB<sub>2</sub>, Er<sub>2</sub>Au<sub>2</sub>Sn and Mn<sub>2</sub>AlB<sub>2</sub> 63  
 structure–property relationships of  
   plumbides 57  
 structures  
   – Pr<sub>7</sub>O<sub>12</sub>, Pr<sub>9</sub>O<sub>16</sub>, Tb<sub>11</sub>O<sub>20</sub>, Pr<sub>40</sub>O<sub>72</sub>, and  
     Pr<sub>24</sub>O<sub>44</sub> phases 22  
   – R–B–C(N) homologous compounds 141  
   – RB<sub>18</sub>Si<sub>5</sub> 150  
 STS 229  
 substitutional disorder 236, 240, 295–300

- super-icosahedra 118, 119, 126  
 superconducting fluctuations 206, 230  
 superconducting gap 185, 208, 212, 213,  
     221–231, 260, 270, 271, 274, 277, 280, 282,  
     285, 295, 308  
 superconducting transition 217, 220, 221,  
     261, 278, 304  
 superconducting transition temperature  
     180, 181, 183, 185, 186, 188, 189, 191–194,  
     196, 197, 200–202, 204–207, 212–215,  
     218–222, 228, 234, 235, 238–243, 249–252,  
     254, 258, 260–262, 266–269, 272, 276–278,  
     293, 295–298, 301–312  
 – RB<sub>12</sub> 112, 115  
 superconductivity 180, 191–197, 201, 202,  
     205, 206, 211–213, 218, 221–224, 231, 235,  
     237, 240–243, 250–254, 256, 258–260, 266,  
     268–271, 274, 275, 277, 278, 284, 285,  
     290–296, 298, 300, 302, 303, 305, 306,  
     308–312  
 – LuB<sub>12</sub> 112  
 – MgB<sub>2</sub> 114  
 – ScB<sub>12</sub> 112  
 – YB<sub>12</sub> 112  
 – ZrB<sub>12</sub> 112, 113  
 superconductivity and magnetic order 180,  
     185–192, 238, 310  
 superconductivity in RNi<sub>2</sub>B<sub>2</sub>C 192  
 superparamagnet 146  
 superstructures 63, 80, 82, 86  
 surface character and oxygen migration 33  
 surface with steps of the {111} facet 33  
 synthesis of metal–plumbides 57  
  
 TB-LMTO-ASA band structure calculations  
     81  
 Tb<sub>1-x</sub>Lu<sub>x</sub>B<sub>44</sub>Si<sub>2</sub> 131  
 (Tb<sub>1-x</sub>Lu<sub>x</sub>)B<sub>44</sub>Si<sub>2</sub> 131  
 Tb<sub>1.8</sub>B<sub>36</sub>C<sub>2</sub>Si<sub>8</sub> 152  
 Tb<sub>11</sub>O<sub>20</sub> 6, 38, 43  
 Tb<sub>12</sub>Ni<sub>6</sub>Pb 72  
 Tb<sub>24</sub>O<sub>44</sub> 6  
 Tb<sub>2</sub>Ni<sub>2</sub>Pb 72, 96  
 Tb<sub>2</sub>O<sub>3</sub> 43  
 Tb<sub>2</sub>Pd<sub>2</sub>Pb 72  
 Tb<sub>48</sub>O<sub>88</sub> 6  
 Tb<sub>5</sub>CuPb<sub>3</sub> 72  
 Tb<sub>5</sub>NiPb<sub>3</sub> 72  
 Tb<sub>62</sub>O<sub>112</sub> 6  
 Tb<sub>6</sub>Co<sub>2.35</sub>Pb<sub>0.61</sub> 71  
 Tb<sub>6</sub>Ni<sub>2.38</sub>Pb<sub>0.63</sub> 71  
 Tb<sub>7</sub>O<sub>12</sub> 5, 43  
 Tb<sup>11</sup>B<sub>44</sub>Si<sub>2</sub> 134, 135  
 Tb(Ag<sub>0.23(9)</sub>Pb<sub>0.77(9)</sub>)<sub>3</sub> 72  
 TbAgPb 72  
  
 TbAlB<sub>14</sub> 138  
 TbAuPb 72  
 TbB<sub>12</sub> 111, 112, 114, 115  
 TbB<sub>25</sub> 136, 138, 139, 154  
 TbB<sub>44</sub>Si<sub>2</sub> 123, 129, 133  
 TbB<sub>50</sub> 123, 127, 139, 154  
 TbCu<sub>5-4.44</sub>Pb<sub>0-0.56</sub> 72  
 TbCuPb 72  
 TbNi<sub>2</sub>B<sub>2</sub>C 193, 198–200, 206, 215, 216, 218,  
     220, 239, 242, 244, 256–259, 263, 264, 271,  
     272  
 TbNiPb 72, 93, 94  
 TbO<sub>1.714</sub> 12  
 TbO<sub>1.806</sub> 6, 13  
 TbO<sub>1.818</sub> 12, 13, 37  
 TbO<sub>1.833</sub> steps surface profile 33  
 TbO<sub>2</sub> 49  
 TbO<sub>x</sub> 43  
 TbPd<sub>2</sub>Pb 72  
 TbPdPb 72  
 Tb([Xe]4f<sup>9</sup>6s<sup>2</sup>) 7  
 temperature swing 18  
 ternary oxides 14  
 tetraboride *see* RB<sub>4</sub>  
 Th<sub>4</sub>Fe<sub>13</sub>Sn<sub>5</sub> 89  
 thermal conductivity 158, 163, 164, 215, 219,  
     220, 223–226, 231, 232, 247, 261, 284  
 – ErB<sub>22</sub>C<sub>2</sub>N 167  
 – ErB<sub>44</sub>Si<sub>2</sub> 164  
 – HoB<sub>15.5</sub>CN 167  
 – Nb-doped YB<sub>66</sub> 159  
 – R–B–C(N) homologous compounds 167  
 – RB<sub>66</sub> 158  
 – YB<sub>28.5</sub>C<sub>4</sub> 167  
 thermal diffusivity constant 163  
 thermal expansion 239, 247, 267, 272  
 thermal conductivity 221, 227  
 thermodynamic properties 214, 229, 235, 300  
 – higher oxides 8  
 thermoelectric power 206, 215, 217–219, 239  
 thermoelectric properties 158  
 – Ce<sub>3</sub>Pd<sub>24</sub>Pb 99  
 – R–B–C(N) homologous compounds  
     165–168  
 – RB<sub>44</sub>Si<sub>2</sub> 161–165  
 – RB<sub>66</sub> 158–161  
 thermopower *see* Seebeck coefficient  
 thin films 179, 204, 207–209, 229, 232, 233,  
     271, 287, 288, 310  
 thirteen fluorite-type modules 24, 27  
 ThNi<sub>2</sub>B<sub>2</sub>C 197, 209, 252  
 ThPd<sub>2</sub>B<sub>2</sub>C 197, 202  
 ThPt<sub>2</sub>B<sub>2</sub>C 197  
 Tm<sub>2</sub>Ni<sub>2</sub>Pb 76  
 Tm<sub>2</sub>Pd<sub>2</sub>Pb 76

- $\text{Tm}_5\text{CuPb}_3$  76  
 $\text{Tm}_5\text{NiPb}_3$  76  
 $\text{Tm}_6\text{Co}_{2.17}\text{Pb}_{0.59}$  75  
 $\text{Tm}_6\text{Ni}_{2.22}\text{Pb}_{0.57}$  75  
 $\text{Tm}(\text{Ag}_{0.22(8)}\text{Pb}_{0.78(8)})_3$  76  
 $\text{Tm}(\text{Ag}_{0.31}\text{Pb}_{0.69})_2$  76  
 $\text{TmAg}_{0.62}\text{Pb}_{1.38}$  80  
 $\text{TmAgPb}$  76  
 $\text{TmB}_{12}$  111, 113, 115  
 $\text{TmB}_{15.5}\text{CN}$  142  
 $\text{TmB}_{22}\text{C}_2\text{N}$  142  
 $\text{TmB}_{28.5}\text{C}_4$  142  
 $\text{TmB}_{44}\text{Si}_2$  122, 123, 129, 133  
 $\text{TmCu}_{5-4.55}\text{Pb}_{0-0.45}$  76  
 $\text{TmCuPb}$  76  
 $\text{TmNi}_2\text{B}_2\text{C}$  180, 193, 194, 197, 200, 215, 216, 220, 236, 238, 242, 244, 248, 251, 264, 274, 276, 277, 280, 289, 292, 293, 295, 310–312  
 $\text{TmNiPb}$  76, 93  
 $\text{TmPdPb}$  76  
torque magnetometry 212  
total conductivity of  $\text{Ce}_{0.8}\text{Pr}_{0.2}\text{O}_{2-\delta}$ ,  $\text{Ce}_{0.7}\text{Pr}_{0.3}\text{O}_{2-\delta}$ ,  $\text{Ce}_{0.6}\text{Pr}_{0.3}\text{Zr}_{0.1}\text{O}_{2-\delta}$ , and  $\text{Ce}_{0.7}\text{Pr}_{0.2}\text{Zr}_{0.1}\text{O}_{2-\delta}$  under one atmosphere pressure 45  
transition of the vortex lattice 280  
transition of the vortex structure 276, 280–283, 285, 286, 289–293, 312  
triangular lattice 142, 143, 145, 147, 149, 150, 151, 154  
triple-layer borocarbides 200, 201  
triplet pairing 191, 192  
trivalent ytterbium 128  
tunneling microscopy 215, 280, 282  
tunneling spectroscopy (STS) 208, 215, 222, 227, 229, 274, 277, 280, 281, 282, 312  
two dimensional networks of clusters 126, 150  
two-band model 180, 182, 214, 220–224, 226–231, 234–238, 240, 241, 277, 284, 298, 311  
two-dimensional metal layers 166  
two-gap superconductivity 113  
type-II superconductors 188, 232, 233, 239, 279, 280, 285, 288, 298  
  
 $\text{UGe}_2$  191, 192  
ultrasound 223, 247  
 $[\text{UMo}_{12}\text{O}_{42}\{\text{R}(\text{H}_2\text{O})_6\}_2]^{2-}$  341  
unconventional superconductivity 191, 223, 231, 235, 280, 302  
unconventional superconductor 186, 212, 221, 224, 238  
  
upper critical field (also see  $H_{c2}$ ) 180, 189, 195, 208, 222, 228, 231–238, 240, 259, 267, 268, 274, 283, 285, 296, 300, 301, 305, 311  
 $\text{UPt}_3$  224  
 $\text{UY}_6\text{O}_{12}$  5  
  
 $\text{V}_3\text{Si}$  224, 280, 286  
valence determination 128  
valence ratio of  $\text{Ce}_x\text{Tb}_{1-x}\text{O}_{2-\delta}$  oxides ( $x = 0.1, 0.2, 0.3, 0.4$ ) 17  
van Vleck paramagnetism 209, 253  
variable range hopping 119, 129, 138, 150, 159  
vector potential 215, 282  
vortex 280–282, 289, 290, 312  
vortex core 223, 227, 229, 280–284, 286, 295, 298, 302, 312  
vortex lattice 215, 224, 233, 275, 279–283, 285–293, 312  
vortex liquid 286  
vortex pinning 268, 275, 284, 286, 287, 289–291  
vortex-glass 286  
  
 $[\text{W}_5\text{O}_{18}]^{6-}$  342  
 $[\text{W}_6\text{O}_{19}]^{2-}$  342  
weak ferromagnetism 191, 192, 195, 203, 207, 218, 220, 242, 257, 258, 272–274, 289, 290, 309, 312  
weak itinerant ferromagnetism 185, 191, 192, 272  
weak-coupling limit 214  
Wells–Dawson anion 343, 344  
  
X-ray absorption near-edge structure (XANES) 278, 306  
X-ray diffraction 198, 206, 208, 248, 266  
X-ray photo-electron spectroscopy 210  
X-ray resonant exchange scattering (XRES) 241, 253, 254  
 $[\text{X}_2\text{W}_{18}\text{O}_{62}]^{n-}$  343  
 $[\text{XW}_{12}\text{O}_{40}]^{n-}$  343  
  
Y–Cu–Pb phase diagram 60  
Y–Ni–Pb phase diagram 58  
Y–Pd–B–C 180, 202  
 $\text{Y}_{12}\text{Co}_6\text{Pb}$  64  
 $\text{Y}_{12}\text{Ni}_6\text{Pb}$  64, 86–88, 93  
 $\text{Y}_2\text{Ni}_2\text{Pb}$  64, 95  
 $\text{Y}_2\text{Pd}_2\text{Pb}$  64  
 $\text{Y}_5\text{CuPb}_3$  64  
 $\text{Y}_5\text{NiPb}_3$  64  
 $\text{Y}_6\text{Co}_{2.23}\text{Pb}_{0.57}$  64  
 $\text{Y}_6\text{Ni}_{2.5}\text{Pb}_{0.5}$  64

- $Y_{\sim 4}Rh_6Pb_{\sim 19}$  64  
 $Y(Ag_{0.23(8)}Pb_{0.77(8)})_3$  65  
 $Y(Ag_{0.23}Pb_{0.77})_3$  85  
 $Y(Ag_{0.39}Pb_{0.61})_2$  65  
 $YAg_{0.78}Pb_{1.22}$  80  
 $YAgPb$  64  
 $YAlB_{14}$  136, 138  
 $YAuPb$  65  
 $YB_{12}$  111, 115  
 $YB_{15.5}CN$  142  
 $YB_{17.6}Si_{4.6}$  150  
 $YB_{22}C_2N$  142, 143  
 $YB_{25}$  136, 138  
 $YB_{28.5}C_4$  142, 143, 167  
 $Yb_2Au_2Pb$  77  
 $Yb_2Pt_2Pb$  63, 77, 78, 95  
 $YB_{44}Si_2$  123  
 $YB_{50}$  123  
 $YB_6$  112  
 $YB_{66}$  117, 124  
 $Yb_{\sim 4}Rh_6Pb_{\sim 19}$  76  
 $[[Yb(\alpha-SiW_{11}O_{39})(H_2O)]_2(\mu-CH_3COO)_2]^{12-}$   
 354  
 $[[Yb(\alpha_2-P_2W_{17}O_{61})_4(C_2O_4)_3(H_2O)_4]^{34-}$   
 354  
 $YbAgPb$  77, 79–81  
 $YbAlB_{14}$  138  
 $YbB_{12}$  108, 111, 114, 127, 128  
 $YbB_{18}Si_5$  128  
 $YbB_{44}Si_2$  123, 127–129, 133  
 $YbB_{66}$  128  
 $YbCdPb$  77  
 $YbCuPb$  76, 79  
 $YbHgPb$  77, 79, 80  
 $YbLiPb$  76, 81  
 $YbMgPb$  76  
 $YbNi_2B_2C$  194, 195, 206, 215, 241, 242, 244,  
 278, 279, 311  
 $YbPd_2Pb$  77  
 $YbZnPb$  76  
 $YCu_{4.74-4.11}Pb_{0.26-0.89}$  64  
 $YCu_{4.74}Pb_{0.26}$  85  
 $YCuPb$  64  
 $YNi_2B_2C$  180, 181, 197, 201, 204–230,  
 232–235, 237–241, 252, 260, 263, 264, 269,  
 271, 280–283, 285–288, 293–295, 297,  
 300–303, 305, 307, 308, 312  
 $YNiPb$  64, 93, 95  
 $[(YOH_2)_3(CO_3)(A-\alpha-PW_9O_{34})_2]^{11-}$  360  
 $YPd_2B_2C$  180, 197, 202, 205, 209, 211, 238,  
 306, 310  
 $YPd_2Pb$  64, 89, 90  
 $YPdPb$  64  
 $YPt_2B_2C$  197, 300  
 $YRu_2B_2C$  197  
 $Zr_{0.5}Ce_{0.5}O_{2-\delta}$  41  
 $Zr_3Sc_4O_{12}$  5  
 $ZrB_{12}$  113, 115